11 The Analysis of the Regulation of Gene Expression

Learning outcomes:

By the end of this chapter you will have an understanding of:

- *the various methods that can be used to map the transcription start site for a gene*
- *how regulation of gene expression can be investigated*
- *the different approaches that can be used to identify the DNA sequences required for proper regulation of gene expression*
- *the strategies that can be used to identify and then clone the gene for a transcription factor*
- *the techniques that can be used to study the transcriptome and proteome*

11.1 Introduction

The regulation of gene transcription is an essential process in all living organisms and viruses. Even for bacteria and viruses not all genes are expressed at any one time. At its simplest, regulation of gene expression is required for the response to a changing environment, so that nutrients can be efficiently utilized and so that biomolecules not present can be synthesized when required. Complex gene regulation patterns are required for the growth and development of multicellular organisms from a single cell, the fertilized egg. An example of the importance of gene regulation in development is the observation that mice and men have virtually the same "set of genes" and it is therefore how the expression of these genes is regulated that is responsible for correct development, rather than the genes themselves. Regulation of gene transcription is therefore a very active field of research and many techniques involving gene cloning and analysis have been developed. In this chapter you will learn about a range of techniques that can be used to characterize the regulation of expression of a gene. Initially most techniques that will be discussed are used to study regulation of expression of a single gene, but in the latter part of the chapter we will discuss how techniques have been developed to help us exploit the

genomic sequences that are available and allow us to monitor gene transcription and translation on a genomic scale. For most of the questions that you might want to ask about gene regulation the experimental techniques are essentially the same for prokaryotic and eukaryotic organisms with only minor modifications.

The co-ordinated expression of a gene involves DNA elements in the vicinity of the gene and many protein factors. The level of complexity is somewhat different between prokaryotes and eukaryotes. In bacteria, all the DNA sequences required for correct control of transcription are located within a few hundred base pairs of the transcription start (see Figure 8.1). Immediately upstream from the transcription start is the RNA polymerase binding site and then upstream from this there may be activator binding sites. Repressor binding sites may be located at different positions within the promoter; they may overlap, be upstream of or downstream of the RNA polymerase binding site. Figure 11.1a shows the sequence elements required for the regulation of the *lac* operon from *E. coli*.

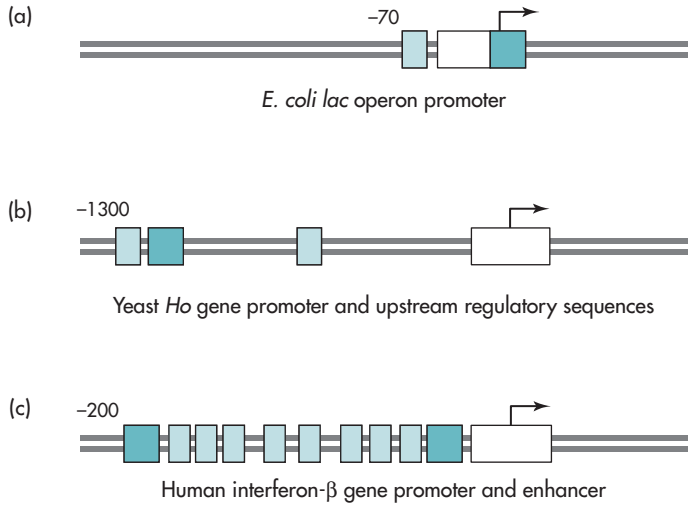


Figure 11.1 Schematic representations of the regulatory regions for three genes. The upstream limit of regulatory sequences is indicated. Regions responsible for binding RNA polymerase and general transcription factors are shown as white boxes, activator and repressor binding sites are shown as gray and blue boxes respectively. a) The *E. coli lac* operon contains the binding sites for RNA polymerase, for one activator protein and for one repressor protein. b) The yeast *HO* gene contains the core promoter responsible for recruiting the general transcription machinery, two sites that bind two different activator proteins and a repressor binding site. c) The human interferon-β gene contains the core promoter responsible for recruiting the general transcription machinery, several binding sites for activator proteins and two sites that bind proteins involved in repression.

In eukaryotes the core promoter, where the transcription machinery assembles, is normally upstream from the first exon. Some genes have several core promoters that drive transcription from different start points, maybe even from within an intron. Immediately upstream from the core promoter is the proximal promoter, which typically contains binding sites for several transcription factors. In addition most genes have associated enhancer elements. Enhancers are regions of DNA that contain binding sites for transcription factors, they do not contain binding sites for RNA polymerase or the general transcription factors and therefore function by activating transcription from a core promoter. Enhancers can be several kilobases upstream or downstream from the core promoter. A gene may have several enhancers that can be utilized at different times, by different signals or in different cell types. Examples of two eukaryotic promoters are shown in Figure 11.1b and c. It is beyond the scope of this book to discuss the complexities of transcription, but you should be aware that in eukaryotes these DNA elements drive the assembly of more than fifty protein components including RNA polymerase, and that many activators work by not only interacting with the transcription machinery but by altering the chromatin environment to make it more suitable for transcription. Despite the differences in the mechanisms for control of transcription in prokaryotes and eukaryotes the experimental techniques used to investigate these processes in the two groups of organisms are essentially the same with only minor modifications.

This chapter is organized into five sections, each of which deals with one aspect of gene expression, each one answering a particular question regarding the transcription process. The types of questions you may have when you first start to investigate a particular gene are:

- Where does transcription start?
- Is the gene subject to regulation?
- When is the gene switched on and when is it off?
- Where are the important regulatory elements in the DNA sequence?
- What protein factors bind the DNA elements identified?
- How do these protein factors interact with each other and with other proteins involved in transcription?

Normally, the cloned gene is the starting point for any study of the regulation of a gene's expression. In prokaryotes, most regulatory elements are within the first 200 bp upstream from the transcription start; therefore if studying a bacterial promoter you would require a clone spanning the 5′ end of the coding region and approximately 200–300 bp of sequence upstream from the translation start codon. In eukaryotes, since enhancer sequences can be several kilobases away from the transcription start you would ideally have a genomic clone that, in addition to containing at least

the first exon of the transcribed region, would contain several kb of upstream sequence. Even so, this may not encompass all the elements required for proper regulation. The DNAse I hypersensitivity assay can be used to help identify and determine the position of distant enhancers (see Section 11.4).

11.2 Determining the Transcription Start of a Gene

One of the first questions that needs to be answered when studying the transcriptional regulation of a gene is the location of the transcription start, i.e the point on the DNA template at which mRNA synthesis begins. One of the reasons that this is important is that once you have located the transcription start it is often possible to deduce possible promoter elements based on their location with respect to the start point. For example, most genes in *E. coli* are transcribed by RNA polymerase that is directed to the transcription start by a transcription factor, called σ^{70}, which recognizes and binds sequence elements positioned 10 and 35 bases upstream from the transcription start. In eukaryotes the core promoter may contain conserved sequences overlapping the transcription start, 25 bases upstream or 30 bases downstream.

There are several techniques that can be used to map the transcription start point. We will discuss three approaches: primer extension, nuclease protection, and rapid amplification of cDNA ends (RACE). All three approaches require that you have some sequence information within the 5′ end of the transcript.

Primer extension

Primer extension is a relatively easy way to determine the transcription start point of a gene (Figure 11.2). All that is required is a source of cells in which the gene is actively transcribed and a radiolabeled oligonucleotide primer complementary to a region within the 5′ end of the target transcript, reverse transcriptase and nucleoside triphosphates. How to radiolabel the 5′ end of an oligonucleotide is discussed in Box 11.1.

The technique can use either total RNA or mRNA, which is purified from cells isolated in conditions when the gene is expressed. How you purify mRNA away from the abundant rRNA and tRNA was discussed in Chapter 4 (Section 4.18 and Figure 4.12). The RNA population is used as template for a reverse transcription reaction primed by the radiolabeled oligonucleotide. The oligonucleotide, which is specific to the gene of interest, should hybridize only to the mRNA of interest. Reverse transcriptase (see Box 4.2) can then be used to synthesize a DNA copy of the mRNA using, as a primer, the labeled oligonucleotide. DNA synthesis will continue until reverse transcriptase reaches the 5′ end of the transcript when it will "fall off" the mRNA template. Assuming that all the original transcripts started from the same point, i.e. had the same 5′ end, the product of this reaction will be a labeled

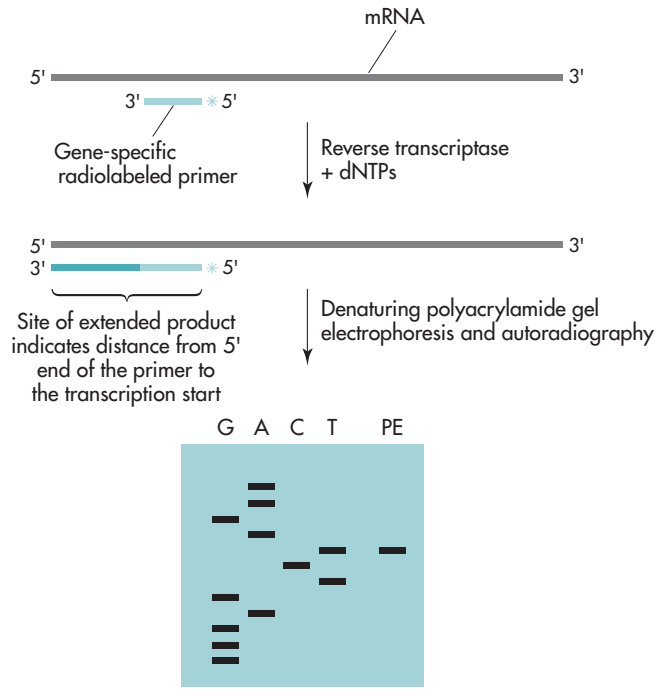


Figure 11.2 Transcription start site mapping: primer extension. RNA is purified, a gene-specific radiolabeled (*) primer is hybridized to the RNA for the gene of interest and the primer extended by reverse transcriptase in the presence of dNTPs. The size of the extended product (PE) is determined by denaturing polyacrylamide gel electrophoresis. A sequencing reaction (G, A, C and T), using the same primer and the cloned gene as template, is used to calibrate the gel and determine the length of the extended product.

DNA fragment of one specific size. The size of the fragment, relative to the position where the primer hybridized, allows you to map the transcription start point. You should note that if you are mapping the start point for a eukaryotic gene, your primer should anneal within exon 1.

Q11.1. You are mapping the transcription start for a eukaryotic gene using primer extension and the intron/exon boundaries are not known. What effect would using a primer that anneals to a sequence in exon 2 have on the predicted transcription start?

Nuclease protection

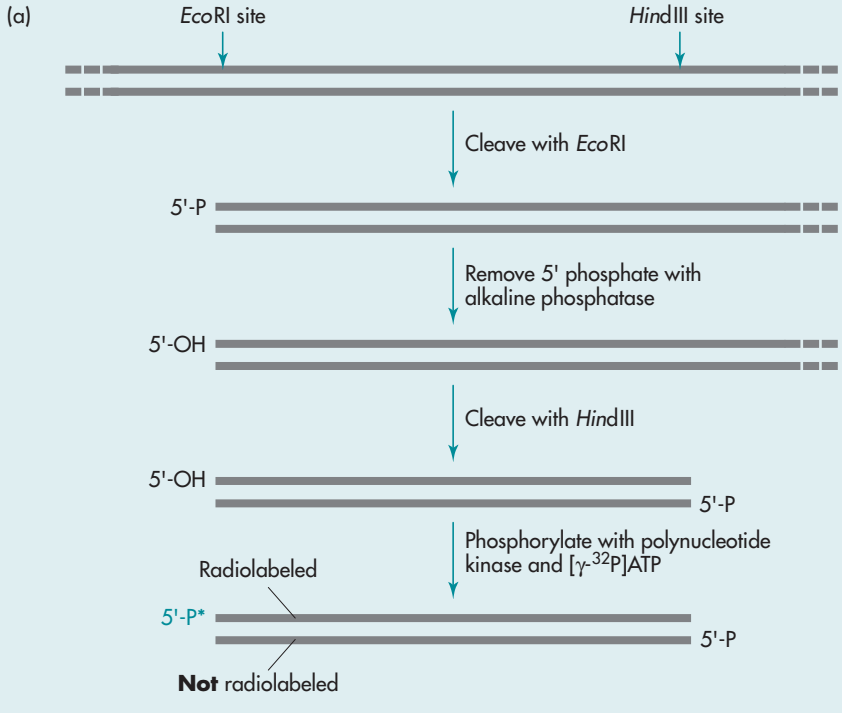
An alternative approach to primer extension that is more robust, but technically slower to complete, is nuclease protection mapping (Figure 11.3). Two alternative nucleases can be used (S1 nuclease or RNAse), but the

Box 11.1 End Labeling

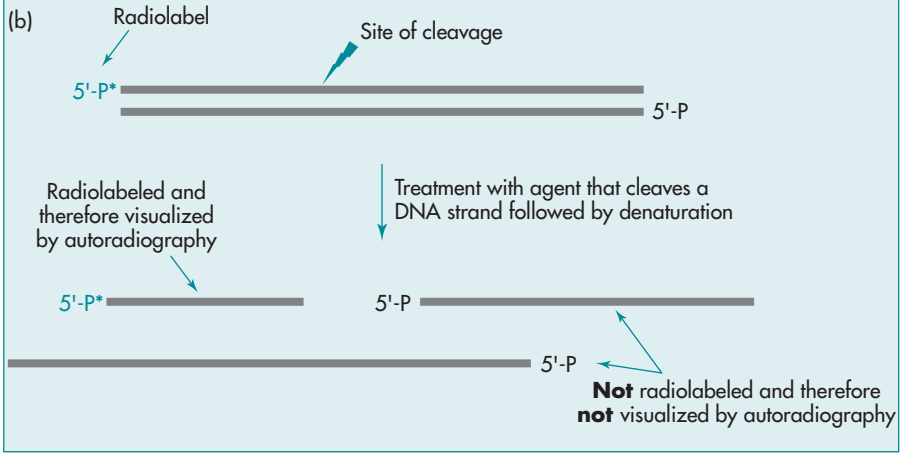
In end labeling, an enzyme such as T4 polynucleotide kinase is used to add a radioactive phosphate on to the 5′ end of a DNA molecule. This technique can be used to label both oligonucleotides and double-stranded DNA fragments.

Preparing a DNA fragment that is radiolabeled at one 5′ end

For some assays, such as primer extension and footprinting, it is important that one specific 5′ end is labeled. In (a) in the figure below, the DNA is cleaved with a restriction enzyme that cuts adjacent to the region to be analyzed. The cut DNA is then treated with the DNA modifying enzyme alkaline phosphatase (Section 3.8). Alkaline phosphatase removes the 5′ phosphate that is present on the ends of the restriction fragments. The enzyme is inactivated and the DNA cleaved with a second restriction enzyme downstream from the region to be sequenced. You do not treat with alkaline phosphatase after the second restriction enzyme digest and therefore the second cut site will still have the 5′ phosphate. So at this point you have a DNA fragment with the 5′ phosphate removed from one end but not the other. This allows you to add a radiolabeled phosphate to the dephosphorylated end by treating with polynucleotide kinase, in the presence of ATP that contains ^{32}P at the gamma position, [γ-^{32}P]ATP (Box 5.3). The product of this procedure is a DNA fragment with a ^{32}P-labeled phosphate on only one of the 5′ ends.



In (b), the strand that is radiolabeled is now cleaved and the DNA is denatured, this generates three single-stranded DNA molecules, one full length and the other two from the strand that was cleaved. The one fragment upstream from the cleavage site will be radiolabeled, whereas, the fragment downstream from the cleavage point and the full length complementary fragment will not be. The important outcome of this procedure is that only the radiolabeled DNA is visualized.



principles of the two approaches are essentially the same. A synthetic DNA or RNA probe is hybridized to the 5′ end of the mRNA. The region of the probe that is hybridized to the mRNA is protected from the action of enzymes which cleave single-stranded nucleic acid molecules, the size of the heteroduplex is determined and the transcription start mapped relative to the 5′ end of the probe. The S1 nuclease mapping procedure was the first to be developed, but has since been superseded by the RNAse protection assay. Both approaches rely on the generation of a probe of known length covering the transcription start and complementary to the mRNA transcript, this is labeled using a technique such as random prime labeling (Box 5.4). S1 nuclease mapping requires a single-stranded DNA probe, whereas RNAse mapping requires a single-stranded RNA probe. Since the RNAse protection assay is used more routinely this will be discussed in more detail. How a single-stranded labeled RNA probe is generated is discussed in Box 11.2. The labeled RNA probe is hybridized to the mRNA to form a double-stranded RNA–RNA duplex. The two ends of the duplex are determined by the 5′ end of the mRNA (the transcription start) and the 5′ end of the labeled probe. Since the probe is generated specifically for this experiment the position of the 5′ end is known. By determining the length of the duplex you will know how far the 5′ end of the probe is from the transcription start. The length of the duplex is determined by digesting any single-stranded RNA probe by RNAse. RNAse will not digest the RNA–RNA duplex.

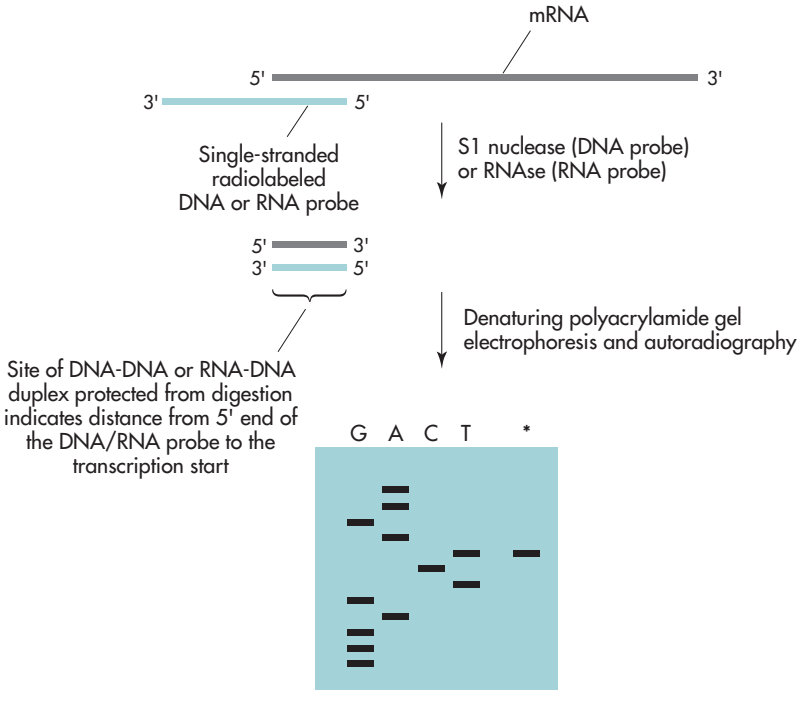
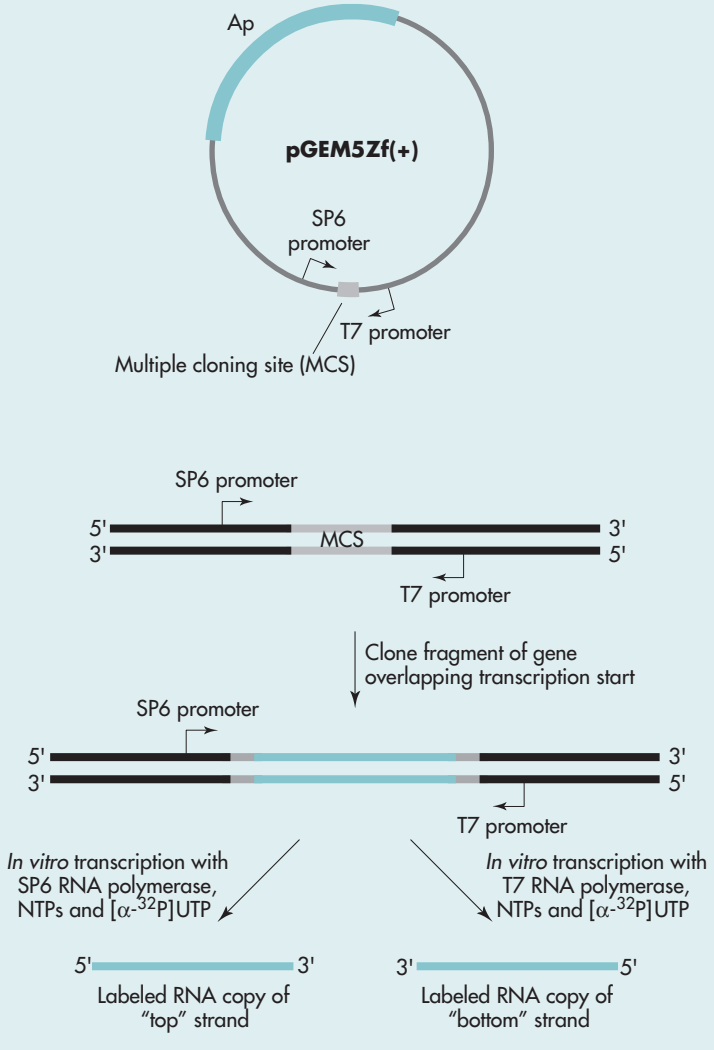


Figure 11.3 Transcription start site mapping: Nuclease protection. RNA is purified and a labeled RNA probe complementary to the 5′ end of the mRNA hybridized. The probe extends from within the gene near the 5′ end to past the likely transcription start site. A duplex forms that extends from the 5′ end of the probe to the transcription start. The size of the duplex is determined by digesting the single-stranded part of the probe with S1 nuclease or RNAse. The size of the protected DNA/RNA probe (*) is then determined by denaturing polyacrylamide gel electrophoresis. A sequencing reaction (G, A, C and T) is used to calibrate the gel.

Box 11.2. Production of Labeled RNA Probes for Use in the RNAse Protection Assay

It is possible to purchase a number of different plasmids which allow you to make RNA probes from a cloned DNA template. One example is the pGEM5Zf(+) plasmid. This plasmid contains a multiple cloning site that is flanked by an SP6 promoter and a T7 promoter on either side. The SP6 and T7 promoters are recognized by RNA polymerase encoded by the phages SP6 and T7, respectively. For an RNAse protection assay a fragment covering the transcription start of your gene is cloned into the multiple cloning site of pGEM5Zf(+). Depending on the orientation of cloning, either SP6 RNA polymerase or T7 RNA polymerase is used to generate an RNA probe that is complementary to the mRNA for the gene and overlaps the transcription start. Plasmid DNA can be purified and used as template by one

of the bacteriophage RNA polymerases in the presence of nucleoside triphosphates (GTP, CTP, ATP and UTP) and one labeled nucleoside triphosphate (typically [α-^{32}P]UTP). This labeled RNA probe can then be used in an RNAse protection assay.



Following digestion the length of the labeled probe protected from digestion is determined by analysis on a denaturing polyacrylamide sequencing gel.

Rapid amplification of cDNA ends

Rapid amplification of cDNA ends (RACE) is a technique that is designed to facilitate the cloning of the 5′ end of a cDNA which should include the region where transcription starts (Figure 11.4). In addition to being a

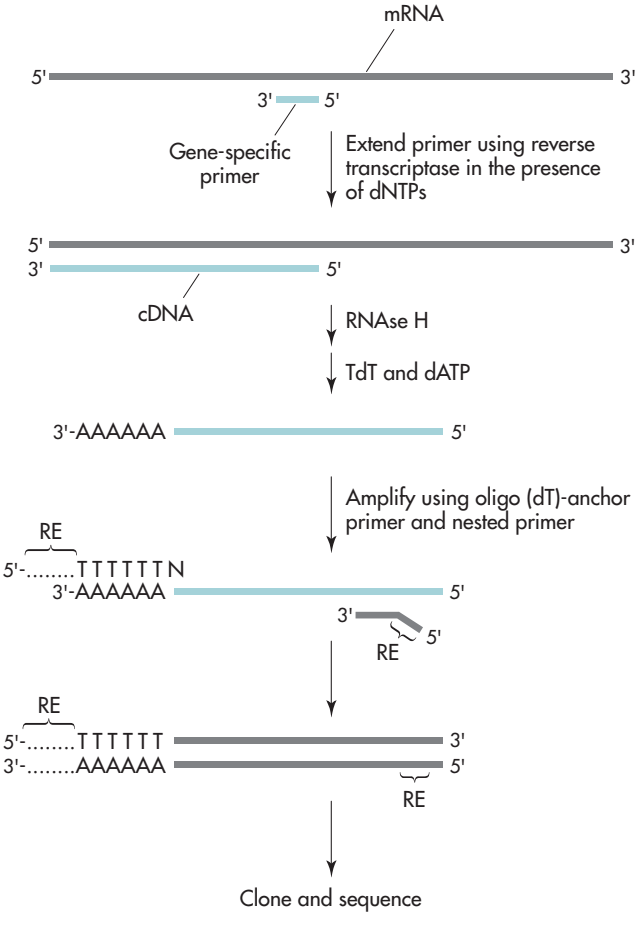


Figure 11.4. Transcription start site mapping – rapid amplification of cDNA ends (RACE). RNA is purified, a gene-specific primer is hybridised to the RNA of the gene of interest and the primer extended by reverse transcriptase in the presence of dNTPs. The RNA template is degraded by RNAse H and the 3′ end of the cDNA extended using terminal transferase in the presence of a single deoxynucleotide (dATP in this example). The cDNA is amplified using a "nested" primer upstream to the primer used for cDNA synthesis and a second primer complementary to the 3′ extension. Both primers contain sites for a restriction enzyme at their 5′ end (RE). In this example an oligo (dT)-anchor primer is used, the "primer" is in fact a mixture of four primers which, in addition to having a run of Ts, have either G, A, C or T (shown as N in the diagram) at their 3′ end (the anchor), this ensures that the primer anneals to the cDNA at the junction of the polyA tract and the original extension product. The amplification product is cloned and sequenced. The transcription start site is adjacent to the poly T tract in the sequence.

technique often employed to generate full-length cDNA clones, it can also be used to map transcription start points. The technique has some advantages over primer extension and nuclease mapping. Firstly, it involves a PCR step and is therefore very sensitive, requiring only a small amount of mRNA from the gene of interest. Secondly, the RACE product is normally sequenced and therefore the actual sequence of the 5′ end of the transcript is confirmed, rather than obtaining a relative distance from a fixed point within the gene. This can therefore avoid problems that can arise due to the presence of unknown intron sequences (see Question 11.1).

The initial step in the RACE protocol is a primer extension but in the absence of label. This yields a single-stranded cDNA where the 3′ end represents the transcription start. The next part of the procedure is to use PCR to amplify the cDNA. PCR requires two primers flanking the region to be amplified. One primer could be the same as used for primer extension, but rather than using the same primer, one just internal to the original is used to help reduce non-specific amplification. The sequence at the 3′ end of the cDNA is not known and so a specific primer cannot be used. Instead, a sequence is added to the 3′ end to which a primer can hybridized. Two methods are generally used to do this. One method is to extend the 3′ end by the addition of a short single-stranded oligonucleotide using RNA ligase, an enzyme that can be used to ligate single-stranded nucleic acids. Alternatively, a homopolymer can be added to the 3′ end using a terminal deoxynucleotidyl transferase (TdT) and one deoxynucleoside triphosphate, e.g. dATP. In this case a polyA tail will be added to the 3′ end and therefore a polyT primer can be used in the PCR reaction. PCR is then used to amplify a DNA fragment containing the 5′ end of the transcript and this is cloned into a plasmid vector. Several independent clones are then sequenced to determine the transcription start point.

Q11.2. In the final PCR step of the RACE protocol, rather than use the same primer that was used for the original primer extension step, one just internal ("upstream") is used. Why does this help reduce non-specific amplification?

You may wonder which of the three techniques discussed above would be best for determining the transcription start. Each approach has different advantages and disadvantages and best practice would be to use at least two different techniques so that the transcription start site is mapped with more confidence. Primer extension is the easiest technique to do, but is often prone to artefacts. Primer extensions also require more RNA template because the product of the extension reaction is only labeled once, at the 5′ end. RNAse protection is more sensitive because the RNA probe is labeled several times during synthesis, but generating the RNA probe requires a

cloning step. RACE is very sensitive because it includes a PCR amplification step, although reverse transcriptase is prone to pausing before the end of the RNA template is reached and can give rise to a truncated cDNA product, which results in the transcription start being mapped incorrectly.

11.3 Determining the Level of Gene Expression

Gene regulation is of course not an all-or-nothing phenomenon, with genes either being "on" or "off"; rather, individual genes can display a huge range of levels of expression relative to one another, and the level of expression of a single gene can also vary considerably under different conditions or at different developmental phases. One of the most important pieces of data that you require if you wish to study the transcriptional regulation of a gene is to know under what conditions the gene is transcribed, and the amount of transcription which takes place. In many cases you will determine the level of gene regulation before you map the transcription start. The techniques described below for determining the level of gene regulation do not require the precise transcription start to be known, but they do require sequence information for at least part of the gene. Three of the techniques that will be discussed below (northern analysis and dot blots, QRT-PCR and nuclear run-ons) are used predominantly to determine the level of the wild-type promoter in its normal genetic context. However, when you want to characterize regulatory elements, for instance by mutagenesis, you would normally use reporter gene assays. In addition to the techniques described in this section it is also possible to use primer extension and nuclease protection assays to measure not only the transcription start but also the level of transcription if the products of the primer extension or nuclease protection assay are quantified. However, these techniques are not as robust as northern blots and QRT-PCR.

Northern analysis and dot blots

Northern analysis and dot blots can be used to determine the level of a particular RNA species in a population of RNA that has been purified from either cells in culture or from a tissue sample. The technique is very similar to Southern analysis which was described in Chapter 6 (Box 5.2). When using Southern analysis a labeled DNA probe is hybridized to its complementary DNA sequence, which allows the detection of this "target" sequence, following agarose gel electrophoresis and transfer of the DNA to a membrane. Northern analysis (also called northern blotting) is essentially the same, with the main difference being that a labeled DNA probe is hybridized to RNA that has been separated by gel electrophoresis, rather than DNA.

Northern analysis involves first purifying RNA from tissue samples or cells growing in culture. It is important that the sample contains no DNA contamination (see Question 11.3). Once the RNA has been purified the

RNA molecules are separated according to size on an agarose gel before being transferred to a nitrocellulose or nylon membrane. The membrane is than placed in a sealed container with a labeled probe complementary to the gene of interest. The probe will hybridize to complementary mRNA. The probe that has not hybridized to the target is washed from the membrane and hybridization detected by autoradiography or phosphor-imager analysis. Separating the RNA population by gel electrophoresis means that you obtain information about the length of the mRNA as well as its abundance; for example, if the mRNA is cleaved or transcription starts from a different start point then the size of the transcript detected will differ from that predicted.

However, often the mRNA has been previously characterized and you simply need to determine the amount of mRNA for a particular gene. In this case a modified version of northern analysis, called dot blots, can be used. The dot blot procedure is shown in Figure 11.5. For dot blots, rather than separating the RNA sample on an agarose gel, the sample is applied directly as a single spot to the membrane. Many RNA samples can be applied to the same membrane; these samples may be from different cell types, from cells growing under different conditions or cells at different stages of development. The membrane with the RNA samples bound is placed in a sealed container with a labeled probe complementary to the gene of interest. If a spot on the membrane contains mRNA for the gene of interest the probe will hybridize. Probe that has not hybridized to its target mRNA is washed off the membrane. The presence of hybridized probe is then detected by autoradiography or phosphor-imager analysis. A spot on your autoradiograph or phosphor-image tells you that the transcript from the gene was present in the RNA samples and therefore the gene was being transcribed in the cell from which the RNA was purified. If, as is normally the case, the labeled probe is in excess, the amount of probe that hybridizes to the RNA sample will be proportional to the amount of RNA for that gene in the sample. Since the probe is labeled we can quantify the amount of probe that has hybridized which gives a readout for the amount of RNA in the starting sample.

Q11.3. Why is it essential to remove all DNA from the RNA sample before northern analysis?

Quantitative real-time reverse transcriptase–polymerase chain reaction

Quantitative real-time reverse transcriptase–polymerase chain reaction (QRT–PCR) is now a common method for determining the amount of a particular mRNA (Figure 11.6). The protocol has essentially two steps. In the first, a single-stranded cDNA is made from the mRNA using reverse transcriptase (Section 4.18) and then the amount of this cDNA is determined using quantitative real-time PCR (see Section 3.18).

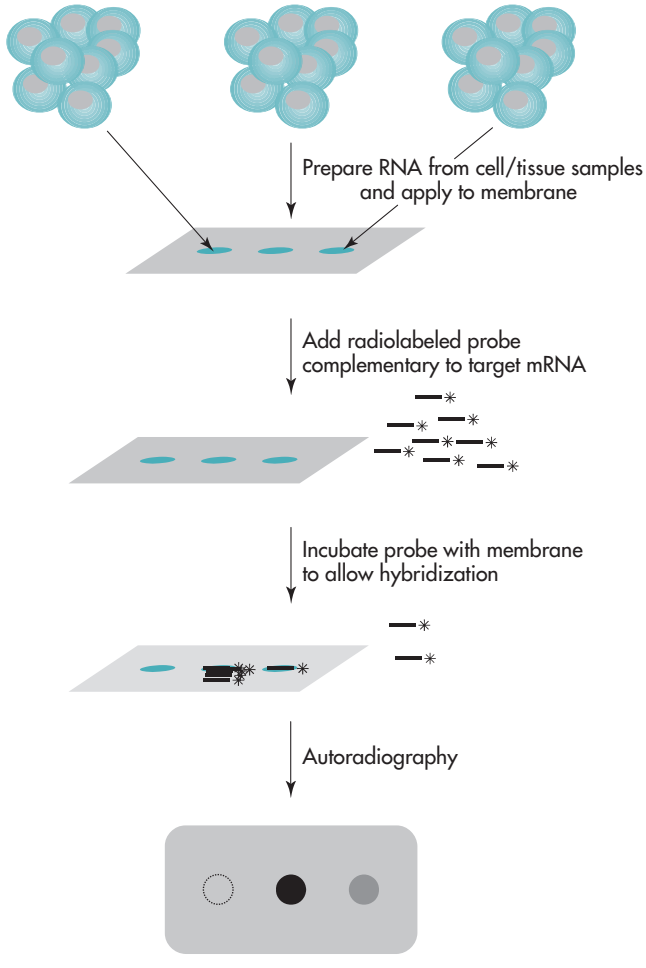


Figure 11.5 Northern analysis. RNA is prepared from different test cells or tissues; it can either be separated by electrophoresis or, as in this example, spotted onto a nylon or nitrocellulose membrane. A labeled (*) probe specific for the gene of interest is incubated with the membrane and will hybridize to its complementary RNA. Hybridization can be detected by autoradiography if using a radiolabeled probe or chemiluminescence if the probe is labeled with biotin. The intensities of the spots can be quantified to give an estimate of the amount of probe hybridization to each spot, which in turn indicates the amount of the corresponding mRNA in each of the starting samples.

The cDNA synthesis step can use a primer that is specific for a single gene, if so reverse transcriptase will only copy the gene of interest into cDNA. Alternatively, random hexanucleotides can be used to prime the reverse transcription reaction. Random hexanucleotides are a population of oligonucleotides representing all possible six base sequences. Using

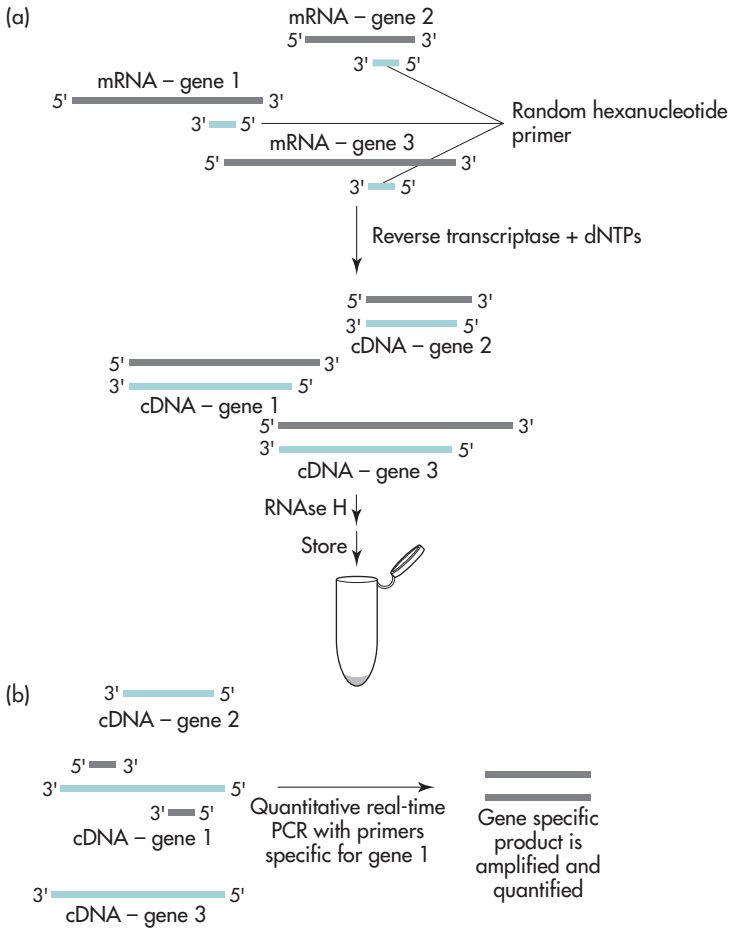


Figure 11.6 Quantitative real-time reverse transcriptase-PCR. a) RNA is purified and random hexanucleotides are used to prime the synthesis of cDNAs by reverse transcriptase for all RNAs present in the starting sample. RNA is removed by RNAse H and the samples stored. b) The amount of any one particular cDNA in the sample can be quantified by quantitative real-time PCR using gene-specific primers.

random hexanucleotides means that all RNA molecules should be reverse-transcribed into cDNA. For the subsequent QRT–PCR reaction gene-specific primers are used. These primers direct the amplification of a short segment of the cDNA. How QRT–PCR is used to quantify the amount of DNA, in this case cDNA, is described in Section 3.18.

Q11.4. The QRT–PCR protocol utilizes random hexanucleotide primers to generate the cDNA prior to QRT–PCR. What is the advantage of using random hexanucleotides rather that a gene-specific primer?

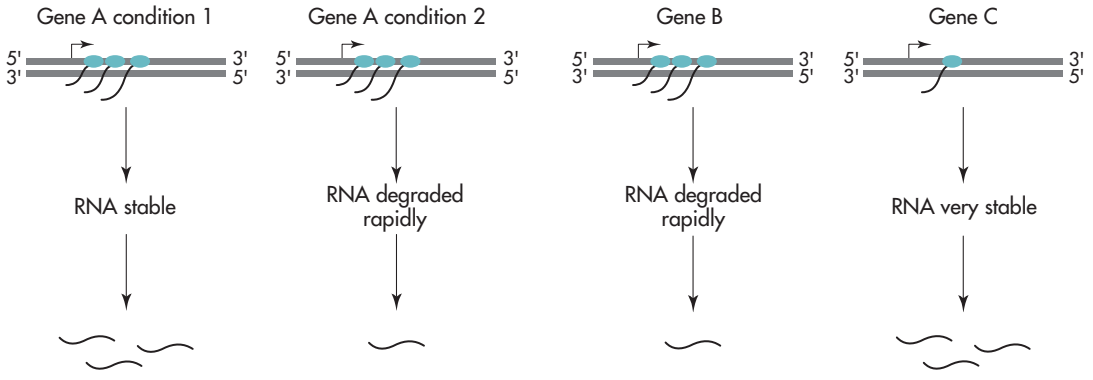


Figure 11.7 RNA stability as well as the rate of transcription initiation can affect the steady-state levels of a mRNA. Genes A (condition 1) and B are transcribed at the same rate, however, the mRNA for gene B is rapidly degraded leading to a difference in the steady-state mRNA levels of the two genes. Gene C is transcribed at low levels, but its mRNA is very stable and therefore it has the same steady-state mRNA levels as gene A. Altering the rate of mRNA degradation can alter the steady-state mRNA levels (gene A conditions 1 and 2).

Nuclear run-on

Although the expression of many, if not most, genes is controlled at the level of transcription initiation, many are regulated at later steps such as elongation, termination and RNA stability, and in eukaryotes by splicing, polyadenylation and mRNA transport (e.g. Figure 11.7). Using both northern blots and QRT–PCR you can determine the steady-state level of an RNA transcript. However, these techniques will not provide any information as to whether it is transcription initiation or one of the other steps that is being regulated. One technique that does provide some evidence that the level of mRNA is regulated at the point of transcription initiation is the nuclear run-on (Figure 11.8). This procedure is normally used when studying regulation of a eukaryotic gene. The nuclear run-on assay indicates the number of RNA polymerase molecules transcribing a gene at the time of the assay. It can therefore be used to differentiate between regulation due to changes in transcription initiation or changes in another step in gene expression. Changes in the rate of initiation will result in an altered nuclear run-on readout, whereas regulation of a subsequent step, for example control due to changes in RNA stability, will not result in a difference in the nuclear run-on readout.

The nuclear run-on assay is shown in Figure 11.8. Cells are isolated at different times or under different conditions when levels of expression of the gene of interest are thought to change. The cells are cooled on ice, the cells lysed and nuclei isolated by centrifugation. The nuclei are then warmed to 37°C in the presence of all four nucleoside triphosphates

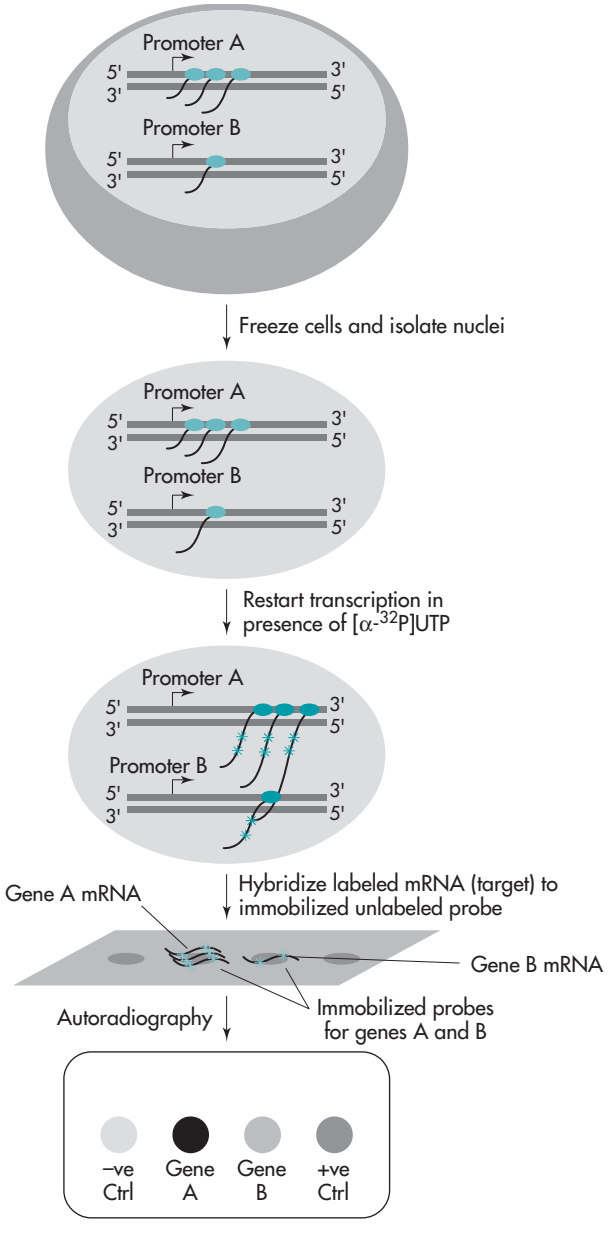


Figure 11.8 The nuclear run-on assay. Cells are isolated and cooled on ice to pause transcription and nuclei are isolated. The cells are warmed in the presence of [α-^{32}P]UTP (*) and transcription of genes that were being transcribed when the cells were cooled resumes; there is no new initiation of transcription. The radiolabeled mRNA produced is incubated with a membrane containing an immobilized probe. The probe is a single-stranded DNA complementary to the mRNA for the gene of interest. Several probes for different genes can be spotted onto the membrane. Following hybridization and autoradiography the intensities of each spot can be quantified to give the amount of labeled target hybridized to each probe, which indicates the level of transcription of each gene when the cells were isolated.

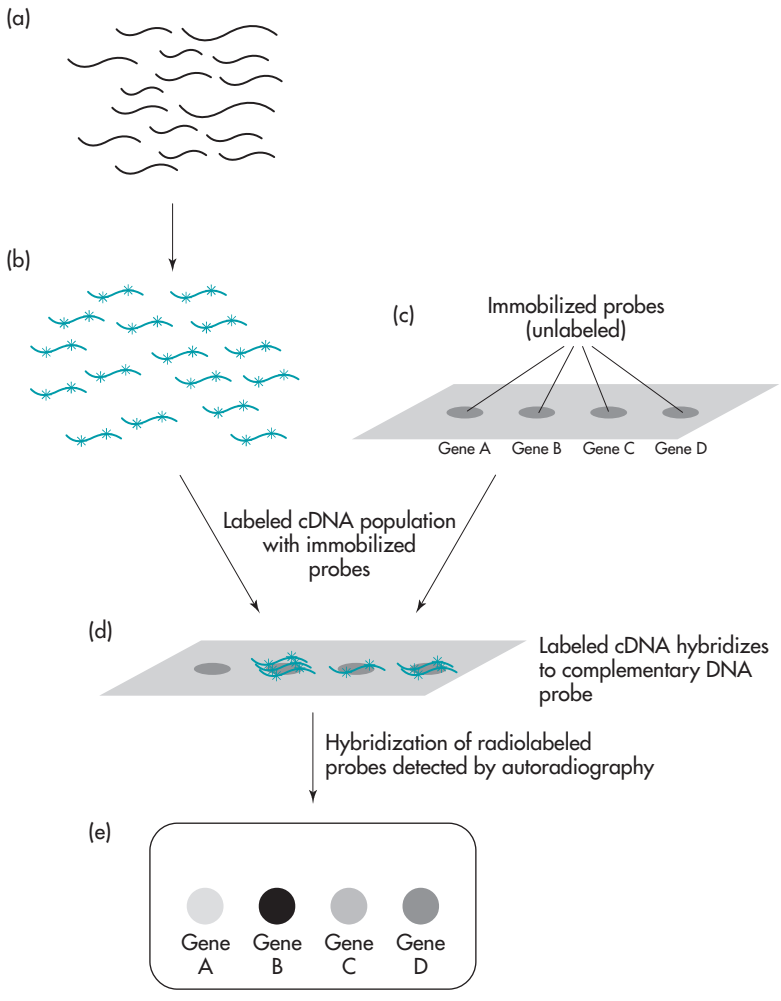


Figure 11.9 Reverse northern dot-blot analysis. a) RNA is purified and random hexanucleotides used to prime cDNA synthesis by reverse transcriptase in the presence of dNTPs and a labeled deoxynucleoside triphosphate (*) to give labeled cDNAs b). Unlabeled DNA probe(s) complementary to the gene(s) of interest are immobilized on a membrane c). The labeled cDNA is incubated with the membrane d) and hybridization quantified by autoradiography e).

including radiolabeled [α-^{32}P]UTP. The paused RNA polymerase molecules that were transcribing the gene when the cells were isolated and cooled now resume transcription and generate a radiolabeled product. The labeled product for the gene of interest is quantified by using "reverse" northern analysis (Figure 11.9). In this method, a DNA probe complementary to the gene of interest is immobilized on a nylon or nitrocellulose membrane (Figure 11.9c) and the labeled products from the nuclear run-on (Figure 11.9b) are hybridized to the immobilized probe. Since the

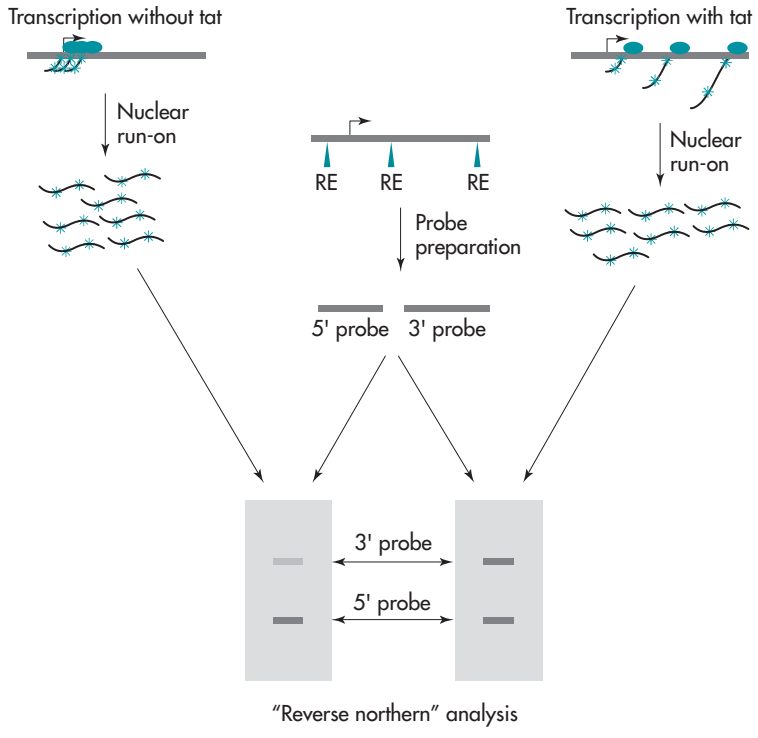


Figure 11.10 Using the nuclear run-on assay to study regulation of gene expression by the HIV-1 activator, tat. A plasmid containing the HIV-1 DNA was cut with two restriction enzymes, the fragments (probes) separated by gel electrophoresis and transferred to a nylon membrane. One probe was complementary to the 5′ end of the transcript including the TAR sequence and one probe was complementary to the 3′ end. Labeled (*) RNA was hybridized to the immobilized probes on the nylon membrane and the level of hybridization quantified by autoradiography. (See Kao *et al.* 1987 for further details.)

mRNA is labeled we can quantify the amount of mRNA that has hybridized to the immobilized probe, which gives a readout for the level of transcription of the gene at the time the cells were isolated.

The nuclear run-on assay can often provide information about which step, post-initiation, is being regulated. The nuclear run-on assay has been used to study activation of HIV-1 gene expression by the virally encoded activator, tat (Figure 11.10). Tat increases the steady-state levels of full length mRNA, not by increasing the rate of transcription, but by stopping RNA polymerase from terminating transcription prematurely while transcribing the gene. Following termination, any truncated transcripts are degraded to a 59-base RNA species called TAR. A slightly modified nuclear run-on protocol to that described above was used. The experiments were completed in tissue culture using two strains, one producing the activator

tat and one in which tat was not produced. The assays were started by addition of radiolabeled [α-^{32}P]UTP to permeabilized cells and the amount of labeled RNA produced determined following a 15-min incubation. The RNA was purified and quantified by "reverse" northern analysis. A plasmid containing the HIV-1 DNA was cut with two restriction enzymes which generated several DNA fragments; these were separated by gel electrophoresis and transferred to a nylon membrane, as discussed for Southern analysis. Two of the restriction fragments (immobilized DNA probes) covered the tat regulated transcript. One probe was complementary to the 5′ end of the transcript including the TAR sequence and one probe was complementary to the 3′ end. The labeled RNA was hybridized to the immobilized probes on the nylon membrane and the level of hybridization quantified by autoradiography. The results showed that the amount of RNA complementary to the 5′ end of the HIV-1 transcript was the same in the presence or absence of tat, so the level of transcription initiation is the same in both cases. The amount of RNA complementary to the 3′ end of the transcript was increased in the presence of tat. This indicates that transcription can initiate at high levels in the presence or absence of tat, but in the absence of tat transcription terminates before a full-length message is produced.

Q11.5. Which technique, standard northern or reverse northern analysis would be best to study (a) the levels of mRNA for the same gene in several RNA samples (e.g. from different cell types) or (b) the levels of mRNA for several genes in the same RNA sample?

Reporter gene assays

If you want to determine the level of expression of a particular gene you might think it possible to simply measure the level of the protein product directly. However, most gene products are difficult or impossible to assay. Even more importantly, the promoter of interest may be one for an essential gene, so if you want to subsequently study the promoter by introducing mutations and studying the effect on transcription any loss of activity would lead to the death of the cell. By cloning the promoter alone, fusing it to a reporter gene, and introducing the fusion into the organism, the regulation of the promoter can be studied without any effect on the endogenous gene from which the promoter was originally isolated.

Promoter probes are specialized vectors that contain a promoter-less gene, upstream from which is a cloning site into which potential promoters can be cloned. Promoter probes rely on a simple concept, which is that a promoter can be fused to any other gene, and that gene will now be regulated by that promoter. This is an enormously useful idea, since it means that any promoter can be isolated and fused to a gene which produces a protein which is simple to assay (Figure 11.11). Promoters can then be

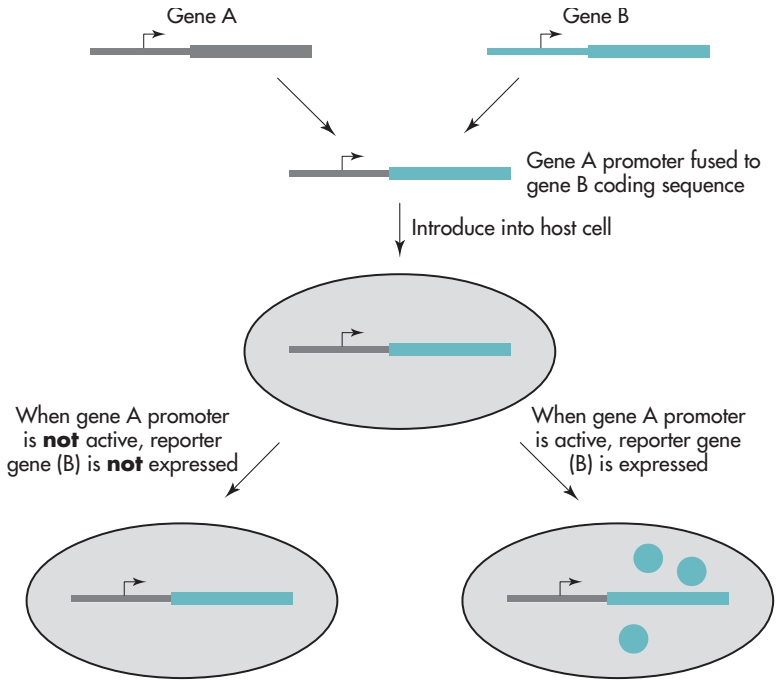


Figure 11.11 Reporter gene assays. Gene A is subject to regulation in different cell types or under different environmental or developmental signals. Regulation is due to the properties of the promoter. Gene B is a gene which expresses a protein with an easily detectable or assayable property. Fusing the coding sequence of gene B with the promoter for gene A produces a reporter gene construct in which the regulation of the gene A promoter can be studied by measuring or detecting the gene B product.

examined to see how their activity varies in specific tissues or cell types, over time as an organism grows and develops, or in response to external effects such as hormones or stresses. Also, mutations can be made in the promoter (still fused to the gene which produces the easily assayable protein) and the effects of these mutations on levels of the protein can be studied. Mutations which alter DNA bases which are essential for promoter function will result in the loss of the protein, whereas mutations in non-essential bases will have no effect. Thus by using such assays, a picture of the entire promoter can be built up. The proteins which are assayed are referred to as reporter proteins, and the genes which encode them are called reporter genes.

An effective reporter protein needs a number of properties, listed below. It is probably true to say that no one reporter protein has all of these properties fully optimized, and the choice of reporter used depends on the particular organism under study and the particular study being done.

Box 11.3 Examples of Reporter Proteins and their Assays

β-galactosidase

This protein, originally from *E. coli*, is encoded by the *lacZ* gene; there are a variety of assays used for this protein. The presence of β-galactosidase can be revealed using the dye X-gal, which is cleaved to form a blue product when β-galactosidase is present. This has already been discussed in the context of blue–white selection (Chapter 2) but can also be used for staining tissue sections of transgenic organisms. This gives a quick indication of where the gene is expressed, and can be used very accurately to look at expression in individual cells. In addition, the substrate ONPG is cleaved by β-galactosidase to give a yellow product that can be measured in a spectrophotometer, and this is widely used to quantitate the level of β-galactosidase.

Green fluorescent protein (GFP)

This protein from the jelly fish *Aequorea victoria* is naturally fluorescent, emitting green light when excited with blue or UV light. The fluorescence can be measured to determine the amount of protein expressed. A great advantage of this reporter is that it is active in cells without any need for fixing or adding co-factors or substrates, and so can be used to monitor gene expression in living tissue. This includes monitoring gene expression in "real time"; for example, following the change in expression from a given promoter during tumor development. Variants have been also produced which fluoresce at different wavelengths, enabling two different promoters to be monitored in the same cell at the same time.

Luciferase

The luciferase protein, from the firefly *Photinus pyralis*, is luminescent; it converts chemical energy to light energy (unlike GFP, which absorbs light energy in one wavelength and emits it in a different one). When supplied with its substrate (luciferin) in the presence of oxygen and ATP, luciferase emits yellow–green light, which can be detected in a variety of ways. If the luciferase is in a crude cell-free extract, light is measured using a photomultiplier to measure the intensity of the light. If the luciferase is in a whole organism, a video camera (which has to be fitted with appropriate devices to detect low light intensity) can be used to detect the luminescent signal.

A reporter protein should:

- Be easy to assay. Ideally the assay will be fully quantitative, so that a precise measure of the level of the protein (and hence by inference the extent to which the promoter is active) can be obtained.

- Be non-toxic to the cell. There is no point in inducing the expression of a protein which will kill the cells that you wish to study!
- Be stable under the conditions of the experiment. You need to be sure that any variation in level of the protein that you see is due to changes in expression from the promoter, rather than the reporter protein itself varying in stability under different conditions.
- Not be present in the organism under study. It is important that there is no background activity produced by the organism, so that the level of activity assayed is due solely to that produced from the promoter of interest.

Many reporter genes producing a variety of proteins are now in common use, some of these are listed in Box 11.3.

An example of the use of a reporter gene assay is a study completed on the *nirB* promoter from *E. coli*. This promoter is controlled in response to anaerobiosis and nitrite. This can be demonstrated by cloning the *nirB* promoter upstream from the *lacZ* gene in a promoter probe vector; transcription from the *nirB* promoter will lead to the expression of the *lacZ* gene product, β-galactosidase. *E. coli* was transformed with the recombinant plasmid and the transformant grown in four conditions: aerobically, aerobically with nitrite, anaerobically, and anaerobically with nitrite. The promoter was shown to be turned on only during anaerobiosis, and that nitrite could drive increased rates of transcription during anaerobic growth (Figure 11.12).

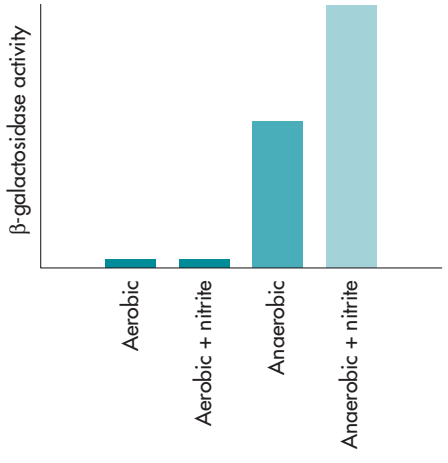


Figure 11.12 Analysis of the *E. coli nirB* promoter using the reporter gene assay. The levels of β-galactosidase expressed under each growth condition is shown in the graph. (See Jayaraman *et al.* 1988 for further details.)

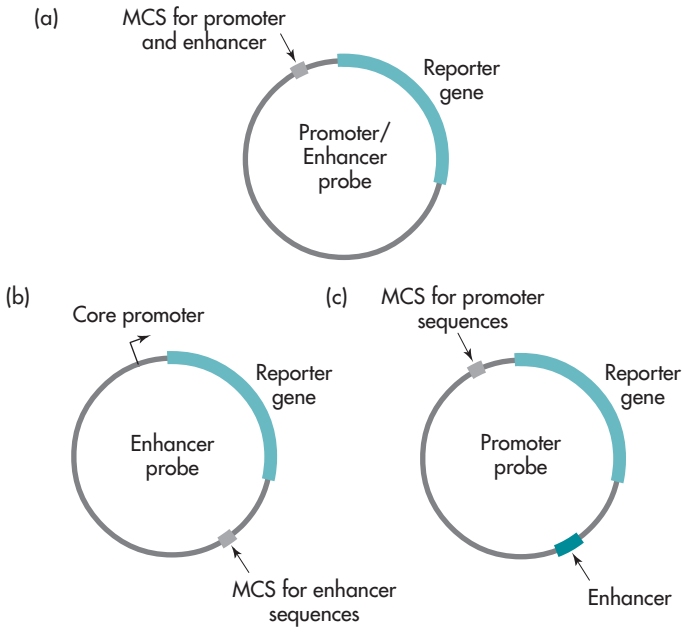


Figure 11.13 Vectors for reporter gene assays. a) Basic promoter probe vector; promoter regions, with associated enhancer regions when present, can be cloned upstream from the reporter gene using the multiple cloning site (MCS). b) Enhancer probe vector contains a core promoter upstream from the reporter gene; downstream from the reporter gene is a MCS into which potential enhancers can be cloned and studied. c) Promoter probe vector contains a generic enhancer downstream from the reporter gene and a MCS upstream into which a potential core promoter can be cloned and studied.

When studying regulation of a eukaryotic gene, a family of promoter and/or enhancer probes can be exploited (Figure 11.13). An enhancer probe vector contains a "generic" core promoter and a multiple cloning site into which potential enhancer can be cloned, so that enhancer dependent activation of the core promoter can be studied. A promoter probe vector contains a "generic" enhancer and a multiple cloning site immediately upstream from the reporter gene into which potential core promoters can be cloned. A third vector that contains neither a promoter nor enhancer can be used to study genome fragments that encompass all the regulatory elements, promoter and enhancers, required for proper regulation. Reporter gene assays in eukaryotes require a method for introducing the recombinant constructs into cells in culture (Box 11.4), using protocols analogous to transformation of bacteria cells.

11.4 Identifying the Important Regulatory Regions

Once you have determined the transcription start site for a gene and shown that changes in gene expression are due to regulation of transcription

Box 11.4 Methods for Introducing DNA into Eukaryotic Cells

Introduction of DNA into eukaryotic cells is termed transfection. There are several transfection procedures.

- Calcium phosphate, DEAE-dextran and polycations

The DNA is mixed with either calcium phosphate, DEAE-dextran or polycations and then applied to eukaryotic cells resulting in the uptake of the DNA via endocytosis.

- Electroporation

In a similar procedure to transformation of bacterial cells, the application of a high voltage to cells in the presence of DNA results in the uptake of the DNA by the cells.

- Liposome-mediated transfer (lipofection)

The DNA is treated with a cationic lipid which binds the DNA. This complex then fuses with the cell membrane allowing entry of the DNA into the cell.

initiation, the next task is to identify the sequences within the DNA that are responsible for this control. In prokaryotes these sequences are normally the RNA polymerase binding sites and sites for activator and repressor sequences. The RNA polymerase binding site is within 35 base pairs of the transcription start and in most cases activator and repressors will normally bind within a few hundred base pairs upstream and/or downstream of the transcription start. It is therefore relatively straightforward to identify these sites using a combination of approaches including sequence analysis (see Chapter 8), deletion analysis, site-directed mutagenesis (Section 10.6) and footprinting (see below). In eukaryotes, although the core promoter and proximal promoter element are within a few hundred base pairs of the transcription start site, identification of all the sequence elements required for the correct regulation of gene transcription is much more difficult because enhancer elements can be many thousands of base pairs away. Added complexity arises because in many cases a single gene may be controlled by multiple enhancers and there are often other function elements such as locus control regions (LCRs) and matrix attachment regions (MARs). One approach to identify regulatory elements would be to clone a large (about 100 kb) genomic fragment containing the gene of interest and create a reporter gene construct which can be used to create transgenic mice or be introduced into a cell line by transfection. Once proper regulation had been demonstrated deletion analysis could be used to map

important regulatory sequences. This approach would be very time consuming and involve a large amount of cloning in order to characterize such a large fragment. An alternative approach is to use the DNAse I hypersensitivity assay.

DNAse I hypersensitivity assay

In eukaryotes the DNA is tightly packaged into chromatin and therefore protected from cleavage by endonucleases such as DNAse I. However, *in vivo* promoter and enhancer elements tend to be either nucleosome-free or have altered nucleosome structure. These regions may be more accessible to nucleases and are therefore cleaved when the chromatin is treated with DNAse I, i.e. they are DNAse I hypersensitive. The DNAse I hypersensitivity assay if often used to identify possible enhancer elements (Figure 11.14). The assay is essentially a modified Southern blot, in which nuclei are prepared and treated with DNAse I prior to purification of the genomic DNA and Southern analysis. The important point is that the chromatin structure should not be disrupted prior to the DNAse I treatment so that the nuclease only cleaves DNA that would be accessible in the normal living cell. Cells should also be isolated when the gene of interest is being expressed.

If you were completing a standard Southern analysis you would expect your DNA probe to hybridize to a genomic fragment of precise size as determined by the distance between the sites of cleavage of the restriction enzyme used. If the DNA is cleaved by DNAse I, however, the fragment that is bound by the labeled probe will be shorter than expected. This difference in size between DNAse I treated and an untreated control can be used to map the DNAse I hypersensitive site and therefore the possible location of potential enhancers and other regulatory elements. The DNA is digested with different restriction enzymes and several different probes used so that the whole region in the vicinity of the gene can be analyzed and the location of each hypersensitive site mapped. If the genome of interest has been sequenced it is relatively simple to design PCR primers to amplify the DNAse I hypersensitive region and hence clone the potential enhancer or promoter region. If sequence information is not available and the enhancer is upstream or downstream of your cloned gene you can use inverse PCR to clone the DNA sequences flanking your gene, which should include the region identified by the DNAse I hypersensitivity assay. Once cloned the region can be further characterized e.g. using EMSAs (see below) and reporter gene assays.

Electromobility shift assay

The electromobility shift assay (EMSA) can be used to identify important regions of a promoter and/or enhancer as discussed below. The assay involves observing the migration of a DNA fragment during polyacrylamide gel electrophoresis (PAGE) in the presence or absence of one or

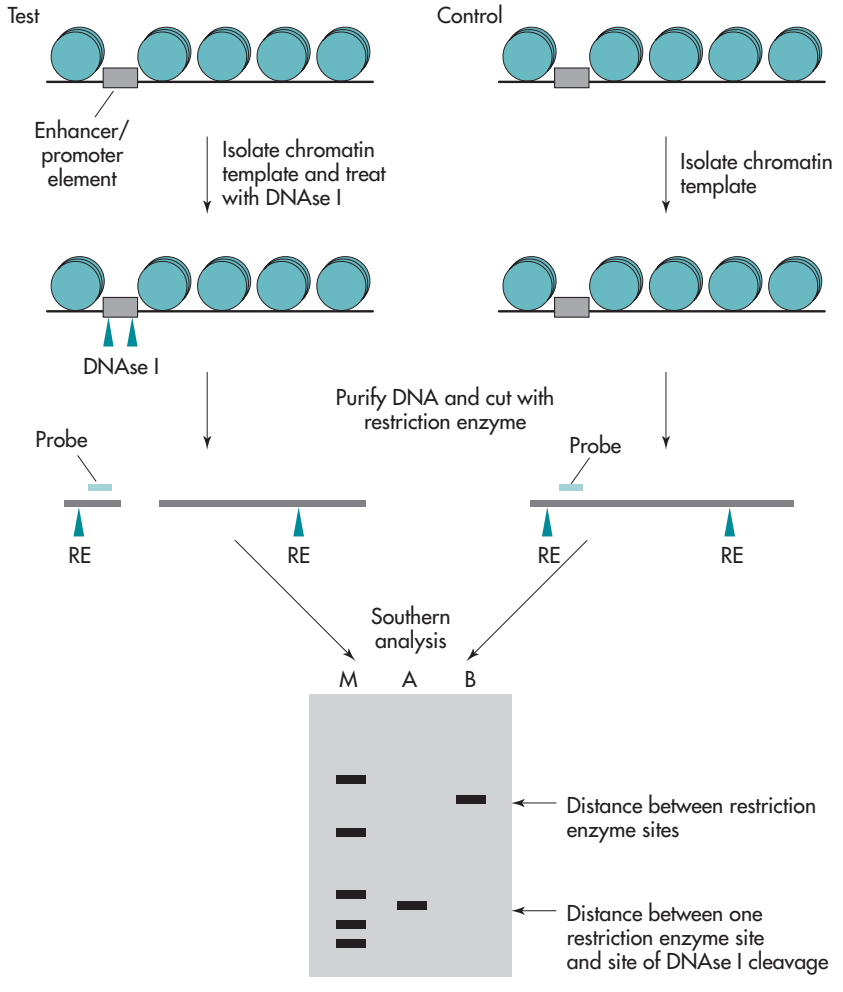


Figure 11.14 DNAse I hypersensitivity assay. Intact chromatin is isolated from cells expressing the gene of interest and treated with DNAse I, which cleaves the DNA where there are no nucleosomes or where the nucleosome structure is altered. The DNA is purified and analyzed by Southern analysis using DNA that has not been treated with DNAse I as a control (lane B). DNAse I cleavage results in detection of a shorter fragment in the Southern blot (lane A), the difference in size can be used to map the position of the DNAse I hypersensitive site relative to the position of the restriction enzyme recognition sites. DNA standards are used to calibrate the gel (M).

more transcription factors (Figure 11.15a). As you will be aware, the migration of a linear DNA fragment during gel electrophoresis is mainly dependent on the length of the DNA fragment. It is possible to analyze DNA–protein complexes using gel electrophoresis and, since these complexes have a higher mass than the free DNA, they will migrate at a slower rate

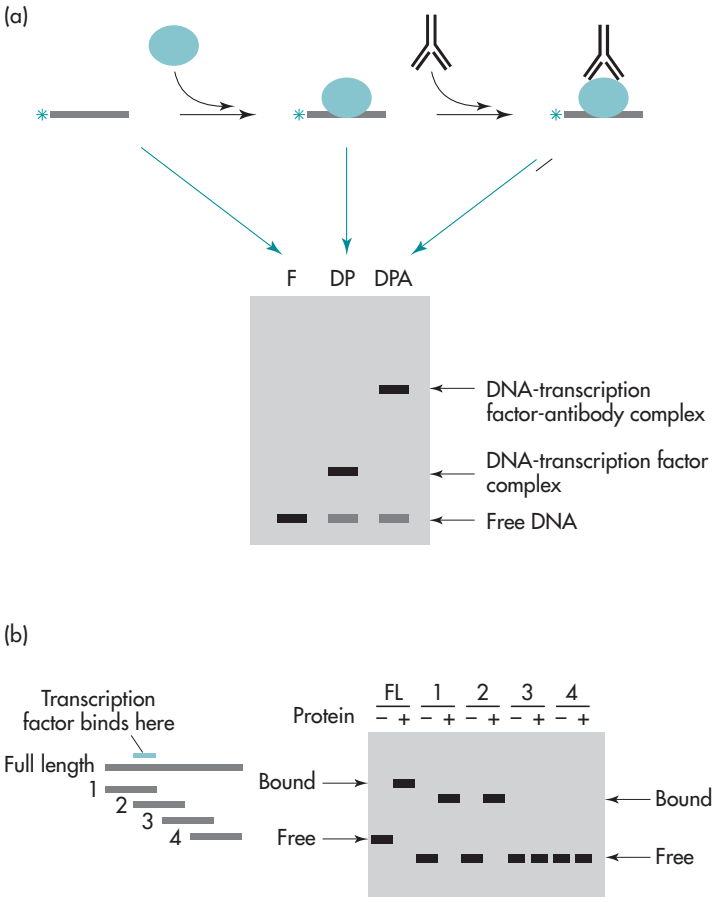


Figure 11.15 The electromobility shift assay (EMSA). a) A labeled (*) DNA fragment migrates according to its size during gel electrophoresis (lane F). When bound by a protein the DNA fragment's mobility during electophoresis is reduced and therefore protein binding to DNA can be detected as a shift in mobility (lane DP). Increasing the mass of the complex further by binding of a second protein, in this case an antibody, results in another shift, often called a supershift. Binding of the antibody to the complex is used to help confirm the identity of the protein present in the original complex. b) The full length fragment binds the transcription factor (lane FL). Four shorter overlapping fragments are used to map the position of the transcription factor binding site. The transcription factor binds to fragments 1 and 2, but not 3 and 4. The binding site on the DNA must be within the common sequence between fragments 1 and 2.

compared with the free DNA. When visualized the position of the DNA–protein complex will have shifted compared with the free DNA hence the term electromobility shift assay. The assay normally requires the formation of the DNA–protein complex *in vitro* with a radiolabeled DNA fragment.

Once separated on a polyacrylamide gel, the free DNA and DNA–protein complex are detected by autoradiography. You may wonder why you cannot visualize the DNA using standard staining such as ethidium bromide. The reason is that the concentration of the DNA used in most EMSAs is too low to be detected by conventional staining; low DNA concentrations are required because the amount of protein is often limiting because you are either using purified proteins and do not have large quantities or you are using a cell extract in which the protein will be present at low concentrations. Although the EMSA will tell you if the DNA fragment contains a binding site for a transcription factor, it will not tell you where on the fragment the protein binds. To map where proteins bind to a large DNA fragment a set of smaller overlapping fragments can be used (Figure 11.15b).

The assay requires a source of the transcription factors thought to bind the DNA. These can be either purified proteins or cell extracts from cells where the gene is thought to be regulated. When using cell extracts, the identity of the transcription factor may not be known, in which case the EMSA may be the starting point for the purification of the factor and then the cloning of its gene.

In other cases once a potential transcription factor binding site has been identified, sequence analysis may provide insight into which transcription factor binds. In this case the EMSA can again be used to help confirm which transcription factor binds the promoter/enhancer region. To do this, an antibody specific for the transcription factor suspected to bind the DNA can be added to the DNA–protein complex, forming a tertiary DNA–protein–antibody complex. This tertiary complex will have a larger mass than the transcription factor–DNA complex and therefore will migrate even more slowly during gel electrophoresis. The antibody is said to "supershift" the complex. So a supershift after addition of an antibody specific to a transcription factor helps confirm that the factor is present in the DNA–protein complex and therefore binds the promoter and/or enhancer fragment. Antibodies specific for a large number of transcription factors can be bought from commercial suppliers.

Q11.6. Figure 11.15b shows how a series of overlapping fragments can be used to map where a transcription factor binds within a large DNA fragment. Why would you use overlapping fragments rather than a series of non-overlapping fragments?

Footprinting

The EMSA is a relatively easy technique that can be used to study DNA–protein interactions and, although it will confirm that a protein binds to a DNA fragment, it gives no direct information about the position on the DNA where the protein binds. As described above, this can be deduced

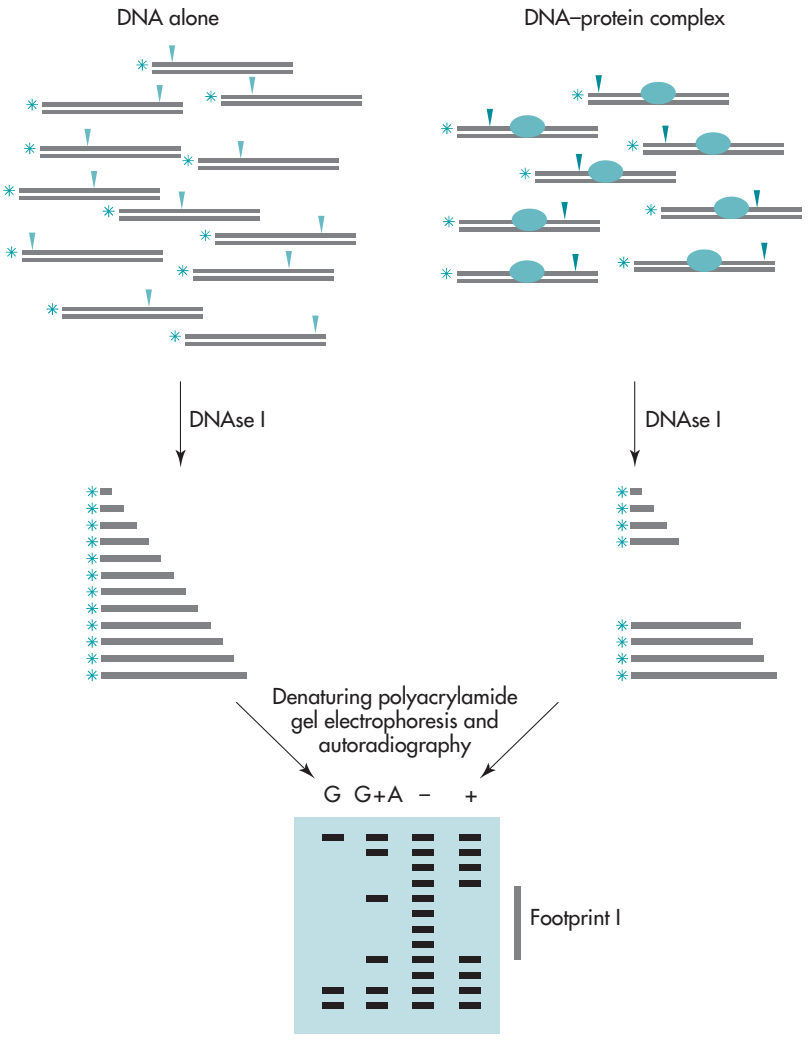


Figure 11.16 DNAse I footprinting. A DNA fragment labeled (*) at one end of one strand is treated with a limiting amount of DNAse I, such that each molecule is cleaved once, the position of cleavage being random (▼). When analyzed by denaturing polyacrylamide gel electrophoresis followed by autoradiography, only the labeled DNA fragments are visualized (one from each cleavage reaction). This produces a ladder (lane –). If a DNA–protein complex is treated with DNAse I, the DNA will be protected from cleavage where the protein is bound and a population of fragments will be missing (lane +). Mapping where the DNA is protected from cleavage indicates where the protein is bound. Sequencing reactions are used to calibrate the gel.

using the EMSA by characterizing several overlapping fragments. A more direct way to determine where a protein binds on a DNA fragment is to use a footprinting protocol. In a footprinting experiment we exploit the ability of a protein bound to DNA to protect the DNA from cleavage. There are several enzymes and chemical reactions that can be used to cleave DNA at random points. Determining which region of the DNA is protected from cleavage tells us where the protein was bound (Figure 11.16). We will discuss footprinting using DNAse I as an example.

All footprinting protocols require an end-labeled DNA fragment labeled only at one end of one strand (Box 11.1). This end-labeled fragment is then subject to cleavage by DNAse I at a very low concentration of DNAse I such that each molecule is cleaved just once. This will generate a population of cleavage products which in theory contains DNA fragments representing cleavage at every base in the sequence. When these are separated by denaturing polyacrylamide electrophoresis and analyzed by autoradiography a ladder will be produced. If the same DNAse I cleavage reaction is done in the presence of a DNA–protein complex, the DNA will be protected from cleavage where the protein binds the DNA, and therefore fragments of a certain length will be missing. Mapping where the DNAse I fails to cleave the DNA will tell us where the transcription factor was bound to the DNA. In addition, the binding of the protein to the DNA may change the conformation of the DNA which results in certain positions within the sequence being more readily cleaved by DNAse I than in the unprotected fragment, and therefore giving more intense, hypersensitive, bands in the footprint. These too can thus be used as a way of mapping the binding site of the protein. An example of a DNAse I footprint is shown in Figure 11.17.

Because DNAse I is a large protein it generates a low resolution footprint; all the DNA in the region that is bound by the protein is protected rather than individual nucleotides that are in close contact with the protein. An alternative to DNAse I footprinting which has better resolution is hydroxyl radical footprinting. This is a chemical based approach, in which a transcription factor–DNA complex is formed and then a chemical reaction started that will generate hydroxyl radicals. Hydroxyl radicals cleave DNA, but because they are very small molecules, you only see protection from cleavage where the protein comes into close proximity with the DNA. Hydroxyl radical footprinting, therefore, generates a high resolution footprint.

Footprinting experiments not only tell you whether a protein binds to a DNA fragment but they also tell you where they bind. It would therefore appear that they would be the preferred choice over EMSAs for studying DNA–protein interactions. However, EMSAs are more straightforward and more robust, and they can be done using crude cell extracts or partially purified proteins, whereas footprinting normally requires purified proteins. Another advantage of EMSAs is discussed in Question 11.8.

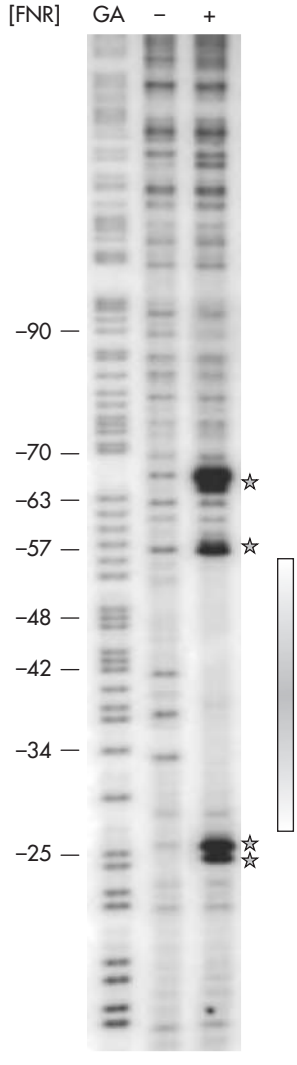


Figure 11.17 DNAse I footprint of the transcription factor FNR bound to the *E. coli nirB* promoter. The DNAse I cleavage pattern in the absence (–) and presence (+) of FNR is shown. The gray bar indicates the region of the promoter protected from cleavage by FNR and stars indicate the positions of enhanced cleavage. Enhanced cleavage is due to FNR bending the DNA and therefore giving DNAse I better assess. A G+A sequencing reaction was used to calibrate the gel. (Courtesy of Dr D. Browning, University of Birmingham.)

Q11.7. You have a limiting amount of protein or cell extract which you use in an EMSA or footprinting experiment which results in only 10% of the fragments being bound by the protein. Would you be able to detect the DNA–protein complex using either the EMSA or footprinting protocol?

Deletion analysis and site-directed mutagenesis

So far, we have discussed using reporter gene assays, EMSAs and footprinting to characterize DNA containing promoters and/or enhancer regions. Footprinting allows us to map the precise position of binding sites for transcription factors within a DNA fragment, but it is not a robust technique and normally requires purified protein. If you do not have a purified system, you need another strategy to try and map the important elements within a larger genomic fragment. Deletion analysis and site-directed mutagenesis combined with reporter gene assays and EMSAs provide a relatively robust strategy to further characterize a promoter or enhancer region.

As an example of deletion analysis we will look at how you might analyze the promoter region of a prokaryotic gene. The first task is to clone the promoter region into a promoter probe vector to generate a reporter gene construct as discussed in Section 11.3 and to determine the conditions in which proper transcriptional regulation is observed in the reporter gene assay. You would then construct a series of derivatives in which sequences are deleted from the promoter region and the activity of these promoter derivatives would then be determined. You could use a reporter gene assay and/or EMSAs to study the different promoter derivatives. For example, if you wished to determine the upstream limit of your promoter, you would create a set of nested deletions where the 5′ limit of your promoter is successively closer to the transcription start (Figure 11.18a) and analyze the deletions using a reporter gene assay. Deletion of sequences that are not important for regulation would not affect promoter activity, but deletion of an important region will lead to deregulation. The deletions can either be made by exploiting sites for restriction enzymes or more typically by PCR. If using PCR you would use a common 3′ primer in all PCR reactions and then use a set of 5′ primers to generate the series of nested deletions. The primers would incorporate a recognition site for a restriction enzyme to facilitate cloning (see Section 3.17).

In addition to making nested deletions you can use site-directed mutagenesis to create specific deletions or change specific base sequences within a promoter region (Figure 11.18b and c). This would allow you to map more precisely any important sites within the DNA. These defined deletions or sequence changes can be characterized in a reporter gene assay or EMSAs.

Deletion analysis was used to investigate the *nirB* promoter discussed above (Figure 11.19). Six promoter constructs were cloned in which successively larger regions of the upstream promoter sequence was deleted. A promoter that extends to 208 base pairs upstream from the transcription start (–208) has normal regulation, as does a promoter that extends to –149. Promoters that extend to –87 or –73 have slightly higher activity under anaerobic conditions but can no longer respond to nitrite. A promoter that only extends to –47 shows limited activation, and one that extends to –19 is

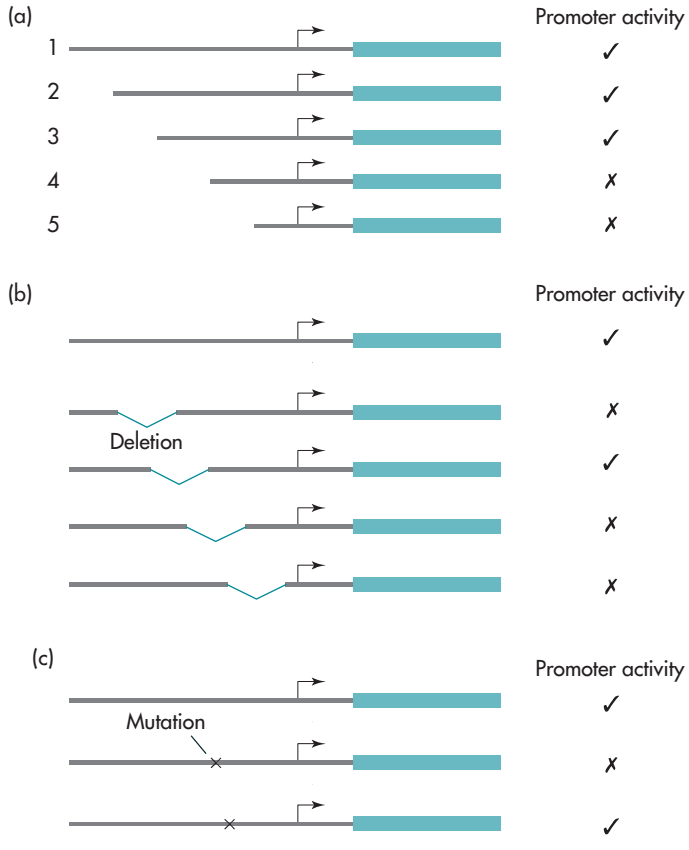


Figure 11.18 Deletion and site-directed mutagenesis analysis of promoter regions. a) A set of nested deletions where the 5′ limit of your promoter is successively closer to the transcription start. Construct 3 contains all sequences required for activity, whereas construct 4 is missing sequences essential for promoter activity. b) Deleting different regions and checking promoter activity helps identify DNA sequences important for activity. c) Changing individual bases helps confirm which bases are important for promoter activity.

inactive. This information was used to develop a model for the regulation of this promoter. The sequence between –87 and –149 contains elements vital for an activator that responds to nitrite and also contains a site for a repressor that reduces the anaerobic activity of the promoter in the absence of nitrite. Sequences between –47 and –73 contain elements that bind an activator that turns on transcription in response to anaerobiosis. Having identified important regions, site-directed mutagenesis was used to identify which individual bases are important for regulation.

Creating a large number of deletion and site-directed mutants and cloning them into a promoter probe vector is a major undertaking. To then

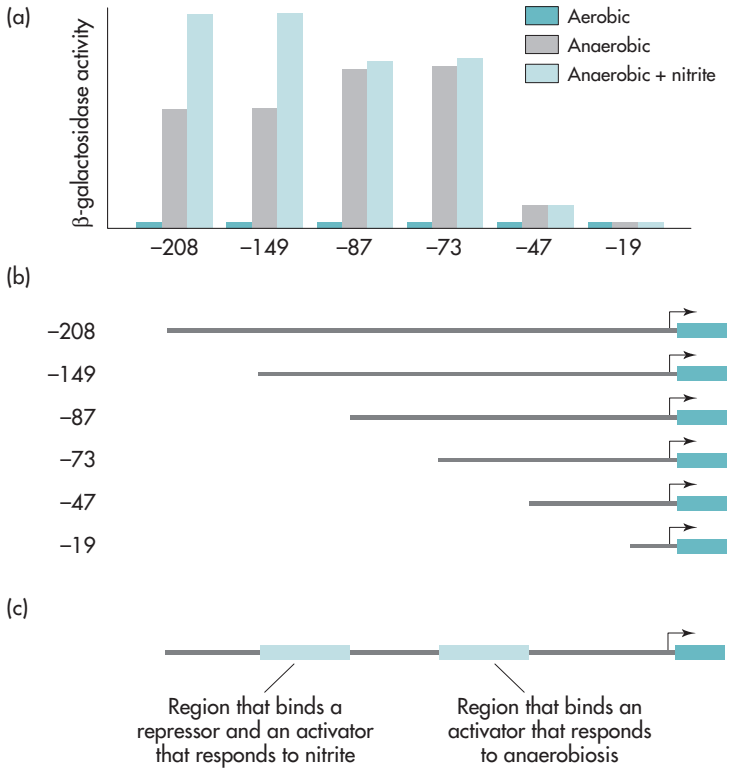


Figure 11.19 Deletion analysis of the *E. coli nirB* promoter. The graph a) shows the levels of β-galactosidase, during various growth conditions, expressed from each of the deletion constructs shown in b). This allowed the identification of important regulatory regions c). (See Jayaraman *et al.* 1988 for further details.)

isolate and label each derivative for EMSA analysis also requires a large amount of effort. However, the effect of mutations on protein binding can be characterized using the EMSA, without the need to prepare a labeled fragment for each mutant, by looking at how well they compete for binding with the wild-type fragment. In an EMSA, autoradiography is used to detect the DNA fragments following electrophoresis and therefore you only visualize the radiolabeled fragment. If you add a large excess of unlabeled fragment this will bind the transcription factor and stop it binding the labeled copies of the fragment and so the shift will be lost. The ability of a large excess of unlabeled fragment to specifically compete for binding can be exploited to analyze promoter mutants. Rather than having to prepare labeled fragments for each mutant, you simply prepare a labeled fragment carrying the wild-type promoter. This labeled "wild-type" fragment is used in EMSAs in which unlabeled, "cold", fragments carrying mutations are added. If the mutations do not affect binding the mutant fragment will still

bind the transcription factor and no shift will be observed. If, however, the mutation stops the transcription factor binding, the unlabeled fragment will not be able to compete and you will get a shift of the labeled "wild-type" fragment.

Q11.8. Are laboratory-based techniques, such as deletion analysis, the only approach to identify possible binding sites for transcription factors?

11.5 Identifying Protein Factors

Techniques such as reporter gene assays and EMSAs in combination with deletion analysis and site-directed mutagenesis can identify sites within promoter/enhancer regions that are important for proper regulation of gene transcription. However, often you do not know the identity of the protein factor(s) that bind these sites. In order to fully characterize the promoter it is vital that the transcription factors responsible for regulation are identified. In the following section we will discuss three techniques – affinity purification, the yeast one-hybrid screen and expression library screening – that can be used to identify the transcription factors that bind a specific sequence.

Affinity purification

One strategy that can be used to purify and identify a transcription factor is to use its ability to bind specifically to a DNA sequence as an aid to protein purification (Figure 11.20). Once the site on the DNA which is bound has been defined using deletion or site-directed mutagenesis as described above, this DNA can be synthesized as an oligonucleotide which is then attached to a matrix that is packed into a chromatography column. If a crude cell extract prepared from cells that are known to contain the active transcription factor is now passed down the column, the target factor will bind to its DNA site and will therefore be retained on the column. The column can be flushed with buffer to remove all proteins that are interacting non-specifically before a different buffer is applied that results in the transcription factor being washed from the column and collected. The transcription factor is thus purified based on its affinity for its target DNA sequence. The purification process can be monitored using EMSAs and SDS PAGE, a technique designed to analyze proteins (Box 5.1) which provides information about the subunit composition of the transcription factor, i.e. whether it contains more than one different protein component, and can also be used to measure the size of the protein components. Affinity purification can be used in conjunction with more conventional protein purification techniques such as size exclusion chromatography and ion exchange chromatography. Once any protein factors have been purified you can determine the amino acid sequence of the N terminus of the protein and then design an oligonucleotide probe that can be used to

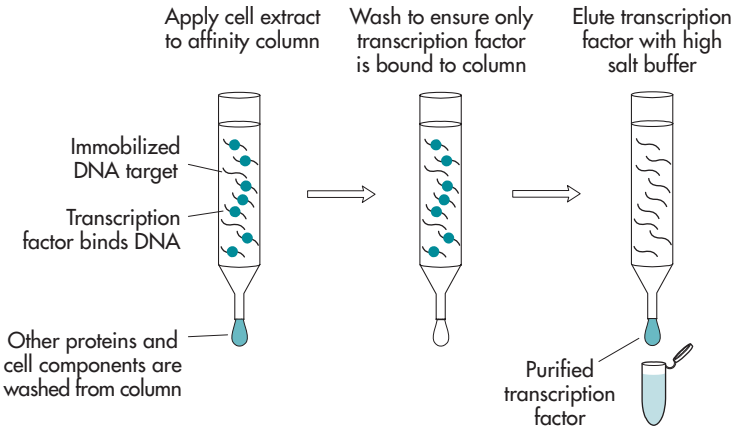


Figure 11.20 Affinity purification of a transcription factor. The DNA sequence that the transcription factor binds is immobilized on a matrix. A cell extract containing the factor is passed over the column; the factor binds its target DNA sequence whereas other proteins are washed from the column. The transcription factor is eluted by washing the column with a high salt buffer.

screen a cDNA library and so clone the gene(s) for the transcription factor, as discussed in more detail in Section 5.8.

Yeast one-hybrid screen

An alternative approach to affinity purification is to attempt to clone the gene for the transcription factor that recognizes a DNA site within your promoter/enhancer regions using a functional screen. The yeast one-hybrid screen (Figure 11.21 and Question 10.8) exploits the fact that the product of the gene you are trying to clone binds to a specific DNA sequence. It relies on the fact that in eukaryotes many transcription factors have a modular design with the DNA binding function present on one domain of the protein and the activation function present on another domain. Importantly, it is possible to "pick and mix" activation domains and DNA binding domains. In the yeast one-hybrid screen you first clone multiple tandem copies of your DNA binding site (target sequence) upstream of a reporter gene and then integrate the reporter gene construct into the yeast genome. Transcription of the reporter gene is dependent upon a transcriptional activator recognizing the target sequence. The integrated reporter gene can be used to screen a special cDNA library. The cDNA library is cloned into a specialized vector such that the cDNAs are cloned upstream of a sequence of DNA that codes for a strong activation domain from a yeast transcription factor. The cDNA and activation domain coding sequence are transcribed and translated into a single polypeptide, a translational fusion (see Box 9.1). Your cDNA library will therefore consist

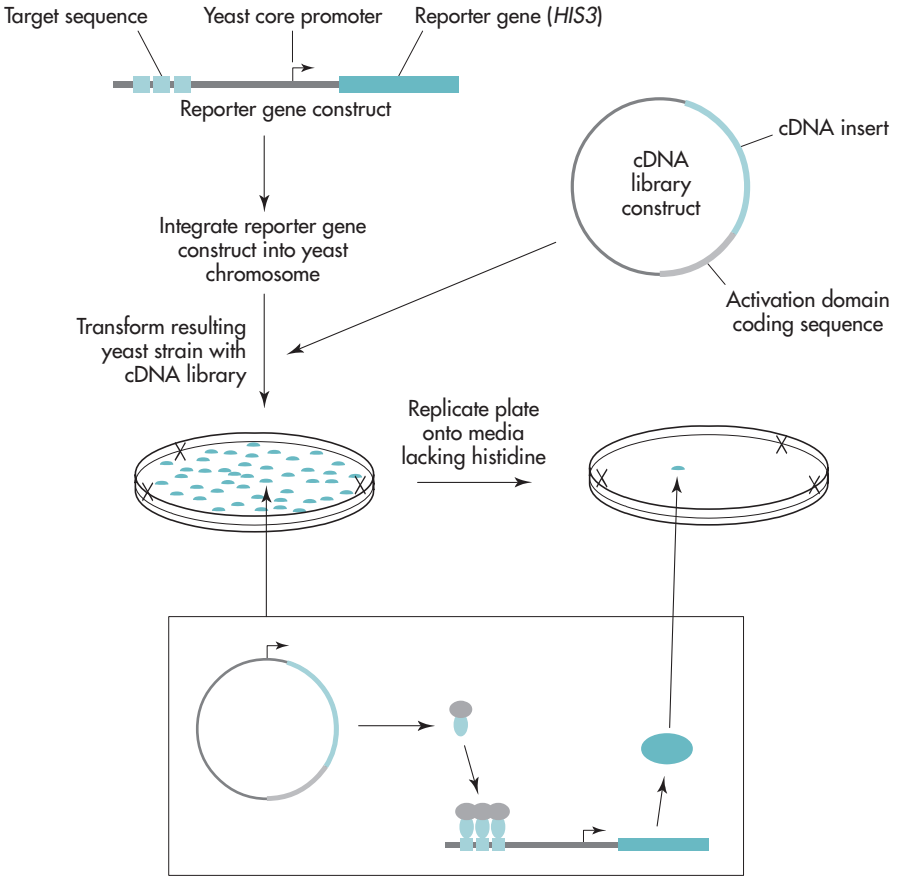


Figure 11.21 The yeast one-hybrid assay. Several copies of the DNA sequence that the transcription factor binds are cloned in tandem upstream from a yeast core promoter and reporter gene (in this example *HIS3*). The construct is integrated into the yeast genome. The resulting yeast strain is used to screen a cDNA library in which the cDNA (blue) is cloned upstream from a coding sequence for a strong activation domain from a yeast activator (gray). The cDNA and activation domain coding sequence are transcribed and translated into a single polypeptide, a translation fusion. If a cDNA clone codes for a DNA binding domain that recognizes the target sequence, this translational fusion will drive the transcription of the integrated reporter gene construct. Colonies expressing the reporter protein can be selected by their ability to grow in the absence of histidine.

of a very large collection of genes coding for translation fusions. Any cDNA clones that contain a DNA binding domain will encode an artificial yeast transcription factor, because the DNA binding domain will be fused to a yeast activation domain. If the DNA binding domain recognizes your target sequence, this artificial activator will drive the transcription of the reporter gene construct.

An example of a reporter gene that can be used in the assay is the yeast *HIS3* gene. This gene is required for the biosynthesis of histidine, so cells that lack *HIS3* cannot grow on media that lack histidine. The yeast strain used in the one-hybrid screen lacks the *HIS3* gene. Integration of the reporter gene construct has the *HIS3* gene downstream of the target DNA binding sequence The cDNA library containing the cDNA-activation domain translation fusions is used to transform the yeast strain with the integrated reporter gene construct and the transformants are plated on a medium lacking histidine. A cDNA that codes for a DNA binding domain that recognizes the target sequence will therefore generate an artificial activator that will drive transcription of the reporter gene and support growth on the medium lacking histidine. The advantage of this technique is that it enables the direct selection of the cDNA for the transcription factor of interest. There are limitations to this technique, however, that are discussed in Question 11.10.

Expression library screening

In Section 5.4 we discussed the construction of a cDNA expression library and the immunological screening of this library. This procedure can be modified to allow screening of an expression library with a labeled DNA probe rather than an antibody. The DNA probe should contain multiple tandem copies of your DNA binding site (target sequence). Rather than binding an antibody to the nitrocellulose filter to which the "plaques" have been transferred, the labeled DNA probe is hybridized. This will identify which plaque contains the cDNA clone encoding the transcription factor that binds the target sequence.

Q11.9. Which approach would you use to clone the genes for a transcription factor that you suspect contains two different protein subunits and where neither subunit can bind the DNA target on its own?

Further analysis

Once a transcription factor has been purified and/or its gene cloned a large number of techniques can be used to further characterize the transcription factor, including some strategies already discussed in this chapter (e.g. footprinting) and other chapters. For example, interacting partners can be identified using the yeast two-hybrid system or the pull-down assay, described in Section 10.5.

11.6 Global Studies of Gene Expression

Until recently most scientists interested in the regulation of gene expression would study a single gene or operon. However, with the advent of genomics and the availability of whole genome sequences, techniques

have been developed which allow us to study the regulation of expression of all, or a very large number of, genes from an organism in a single experiment. These are very powerful techniques that can provide a large amount of information including an insight into the function of genes of unknown function. We will look at techniques that allow us to monitor the level of RNA transcription and protein expression.

Transcriptomics

Transcriptomics is a term that has been coined to describe the study of global gene expression at the level of RNA. The transcriptome is the complete set of RNA transcripts produced by a cell or organism at any one time. Since different genes are being transcribed at different times and in different cell types, the transcriptome is very dynamic (unlike the genome of an organism which is always the same). We discussed northern analysis in Section 11.3 as a method to determine the level of an RNA transcript and how this technique is used to study a single gene. During northern analysis you immobilize your RNA sample on a nylon or nitrocellulose filter; you then incubate a labeled probe with the filter, and the level of probe hybridization gives you a readout of the level of RNA for that gene in the original sample. Transcriptomics exploits a technique that is essentially "reverse" northern analysis (Figure 11.9). In this technique, rather than immobilizing the RNA sample, the DNA probe is immobilized, for example applied to a nylon filter; the DNA probe is not labeled. RNA is then isolated from your sample cells and labeled cDNA prepared representing all the RNA in the sample; this is then incubated with the immobilized DNA probe. The level of probe hybridization gives a readout of the level of RNA for the gene represented by the probe. If you immobilize several probes on the same nylon filter you can determine the RNA levels for each gene, based on the level of hybridization to each probe, since the labeled RNA will only hybridize to its complementary probe on the membrane. It is possible to array thousands of probes onto a single nylon membrane just a few centimeters square, for example a commercial array that is readily available contains probes for nearly 3000 cancer-related human genes on an 8 cm $\times$ 24 cm nylon membrane. So by using this array you are in essence doing northern analysis of nearly 3000 genes in a single experiment. Rather than using nylon membranes to immobilize your probe it is possible to use glass slides. The glass slides are high quality microscope slides that have been chemically treated so that they can bind the DNA probes. The glass slides have some advantages, the main one being that they allow the detection of fluorescently labeled cDNA. This permits independent detection of two samples because each sample can be labeled with different fluorescent dyes (Box 5.3) and hybridized to the same array, facilitating direct comparison of the two samples. Arrays are printed on glass slides at a very high density with tens of thousands of probes arrayed on a single glass slide and

are often termed DNA micro-arrays (nylon based arrays are often called macro-arrays). DNA micro-arrays are printed by specialized machines that deposit a single spot of each probe at a mapped position on the glass slide so that, following hybridization, you know which spot corresponds to each gene.

The DNA probes bound to the slide can be either oligonucleotides or PCR fragments. PCR fragments can either contain the whole coding sequence (ORF) or a shorter region within the gene. The PCR products need to be denatured to give single-stranded DNA when spotted onto the glass slide or nylon membrane in order to allow hybridization of the labeled cDNA. One disadvantage of using the complete ORF is that it may lead to cross-hybridization between cDNAs and probes for homologous genes leading to incorrect readout for the homologous genes. PCR primers could be designed that direct the amplification of a unique region for each gene, however this would require a large amount of bioinformatic analysis. Whether you amplify the whole ORF or a section of the gene, probe preparation requires a large number of PCR reactions; for example, a yeast array would require more than 6000 reactions. This has led to automation of many procedures with laboratory robots being used to set up reactions. In addition, if gene specific primers are being used you need to synthesize a large number of oligonucleotides; 12,000 are required to amplify the 6000 yeast genes. In many cases the DNA probes are amplified from an existing library of clones. If this is the case it may be possible to use the same primers, derived from the vector sequence, to amplify all the probes. For example, a library containing every *E. coli* gene cloned into the same vector has been constructed and so it is possible to use primers that anneal to the vector sequence on either side of the insert. However, you still need to set up thousands of PCR reactions and, as the library was originally created by using gene specific primer pairs to amplify each ORF, if starting from scratch it would not save time or money. The alternative is to use oligonucleotide probes. Oligonucleotide probes are normally 40 to 70 bases in length and are designed so that they are unique for each gene to avoid cross-hybridization with homologous genes. Gene chips are another type of array. These are created by synthesizing oligonucleotides *de novo* directly on the array using photolithographic technology, the same technology that is used to make electronic chips. The oligonucleotides are approximately 25 bases in length and normally several oligonucleotides are synthesized for each gene.

Once an array has been constructed, the basic experimental procedure for doing a transcriptomic analysis is the same whether you are using a nylon-, glass- or gene chip-based array. RNA is isolated from test and control cells. Labeled cDNA is then synthesized from this RNA and hybridized to the array, and the amount of cDNA bound to each spot is quantified. If using a nylon-based array the cDNA can be labeled with a radioisotope and

detected by autoradiography or labeled with biotin and detected by chemiluminescence (Box 5.3). When using a glass-based array or gene chip the cDNA is labeled with a fluorescent dye and detected by a specialized machine, called a micro-array scanner, which uses a laser to scan the slide. The laser excites the dyes at their respective excitation wavelengths and a detector measures the emission signal from the excited dyes as the laser passes each spot.

Figure 11.22 is a schematic representation of a glass-based array experiment. RNA is isolated from control and test cells, and the RNA is used as template for cDNA synthesis using random hexanucleotide primers in the presence of dUTP labeled with one of two fluorescent dyes, Cy3 and Cy5. Cy3 is used to label the control sample and Cy5 is used to label the test sample. Random hexanucleotides are a population of oligonucleotides six bases in length with random sequence; using random hexanucleotides means that all RNA molecules should be reverse-transcribed into cDNA. The samples are combined and the mixture of labeled cDNAs is hybridized to the glass array. The array is then scanned using a micro-array scanner. Transcript levels in the control and test samples are measured as Cy3 or Cy5 fluorescence respectively. By comparing the relative Cy3 and Cy5 fluorescence it is possible to determine if genes are up-regulated, down-regulated, constitutively expressed or not expressed under the two conditions tested. If the Cy3 signal is represented as green and the Cy5 signal as red, overlaying the fluorescent scans gives different colored spots. Spots corresponding to genes expressed in both conditions will be yellow (i.e. green + red), genes induced or upregulated in the control conditions will appear as green spots, and genes induced or upregulated in the test conditions will appear as red spots. Spots that give no signal from either dye after scanning represent genes that are not transcribed under either condition.

Q11.10. In a micro-array constructed with oligonucleotides, should the oligonucleotide probes be sense or antisense, i.e. the same sequence as the RNA or the template strand of the DNA?

Q11.11. Could an oligonucleotide array be used to analyze the labeled RNA from a nuclear run-on experiment?

Proteomics

Proteomics is a term that has been coined to describe the analysis of all proteins present in the cell. The proteome is the complete set of proteins produced by a cell or organism at any one time. The proteome, like the transcriptome, is very dynamic, since different genes are being transcribed, translated and subject to different post-translational modification at any given time in a cell. As you will learn, proteomics techniques cannot pro-

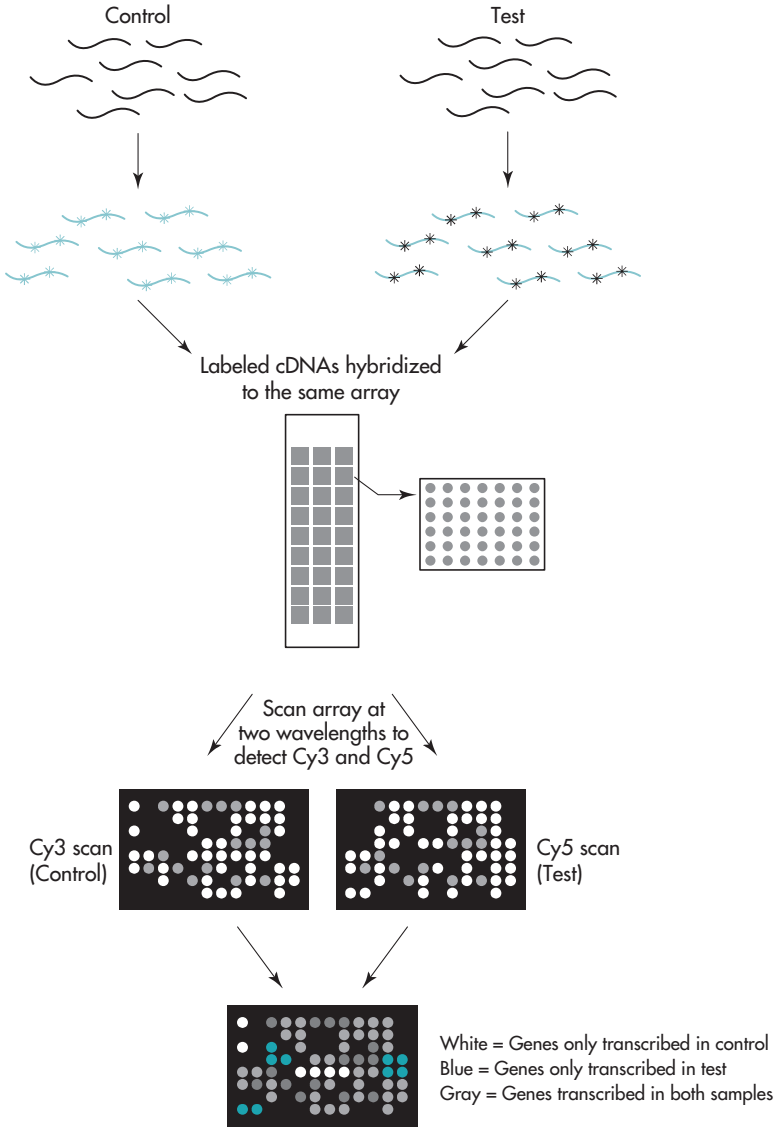


Figure 11.22. Using microarrays to analyse the transcriptome. RNA is purified and random hexanucleotides used to prime cDNA synthesis by reverse transcriptase in the presence of dNTPs and a labeled deoxynucleoside triphosphate (*). Two samples can be prepared, control and test, and labeled with the fluorescent dyes Cy3 and Cy5 respectively. The labeled DNAs are combined and hybridised to an array containing thousands of probes immobilised on a glass slide. The array is scanned with a laser which excites the dyes and fluorescent emission from each spot is detected and quantified. The figure shows the Cy3 and Cy5 scans (different levels of signal are shown as gray and white spots). Often the Cy3 output is depicted as green and the Cy5 as red, when overlaid the colour of the spot is determined by the expression pattern of the gene. Green spots represent genes only transcribed in the control sample, red spots gene only transcribed in the test sample, yellow spots represent gene transcribed in both samples.

vide a complete list of all proteins present in a cell. This therefore begs the question, why study the proteome when transcriptomics can provide what appears to be detailed information about every gene? The main reason is that gene activity is not regulated solely by changes in the amount of mRNA, especially in eukaryotes. Many genes are transcribed but not translated, and once translated many proteins are not active unless post-translationally modified. Turn-over levels for different proteins also vary dramatically and for many proteins differ depending on the conditions. Ultimately, the consequence of gene expression is not whether a mRNA is made, but rather whether an active protein is made. Transcriptomics provides an indirect readout of gene activity, whereas proteomics has the potential to give more definitive information. Transcriptomic techniques are more straightforward and can provide information about every gene, whereas proteomics gives less coverage but the information is probably more relevant to understanding the cell and the organism. Moreover, proteomic techniques not only have the potential to tell you if the protein has been translated and how much is around in the cell, but can also tell you whether it has been covalently modified.

The most common protocol used for analyzing the proteome is two-dimensional gel electrophoresis (Box 5.1) followed by mass spectrometry of the separated proteins (Figure 11.23). Current two-dimensional gel protocols allow the separation of up to 3000 proteins in a single gel but you cannot separate and detect all the proteins present in a complex sample such as a cell extract. Once the proteins have been visualized you are presented with an image containing up to 3000 spots of varying intensity, and unlike with DNA micro-arrays you do not have a map of which spot represents which protein. To identify the protein in each spot, the spot is cut out and the protein treated with a proteolytic enzyme to fragment it. The sizes of the fragments are then determined by mass spectrometry (MS) which can determine molecular masses with a very high degree of accuracy. Each protein will generate a unique proteolytic "fingerprint" because the probability of two proteins being cleaved into the same number of fragments, with each fragment having the same mass, is extremely small. The proteolytic fingerprint can be compared with a database of theoretical fingerprints generated by computer cleavage of all entries in a protein database (see Box 8.2). Various proteolytic enzymes are used. A common example is trypsin, an enzyme found in the gastrointestinal tract of animals; trypsin specifically cleaves proteins after lysines or arginines. The proteolysis products are normally analyzed by a specialized mass spectrometry method called MALDI-TOF MS (matrix-assisted laser desorption/ionization time-of-flight mass spectrometry), which can measure the mass of each fragment to a very high degree of accuracy. MALDI-TOF MS allows high throughput analysis of several hundred samples in a few hours. This approach is only of use if a database of theoretical fingerprints is available.

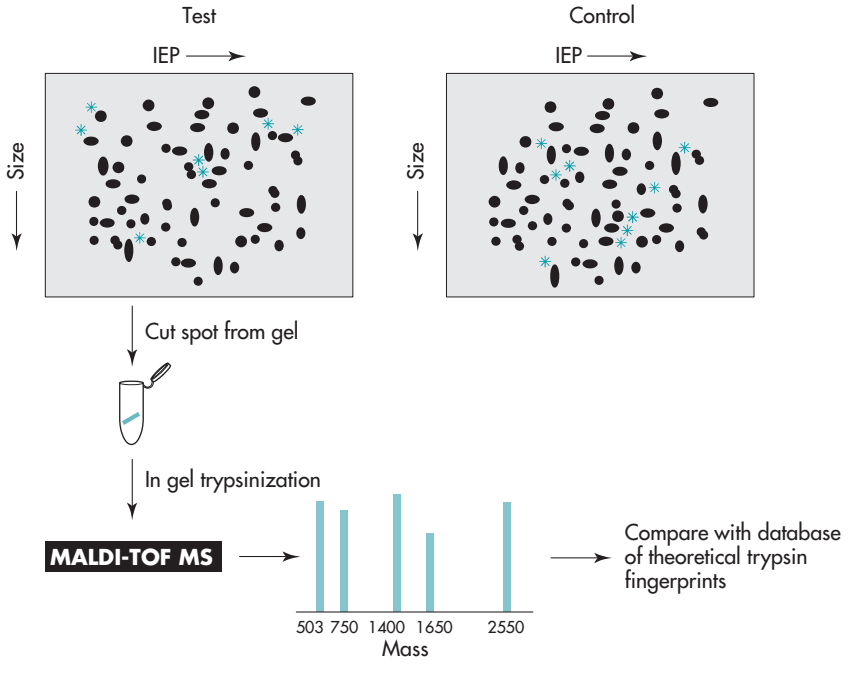


Figure 11.23 Analysis of the proteome using two-dimensional gel electrophoresis and mass spectrometry (MS). The proteins present in a cell extract are separated first by electrophoresis on an immobilized pH gradient which separates proteins according to charge (IEP) and then by traditional SDS polyacrylamide gel electrophoresis which separates proteins according to size. Differences in the proteome between two sample (test and control) are visualized as missing or additional spots, indicated by *. Individual spots can be analyzed by mass spectrometry, a spot is treated with the proteolytic enzyme trypsin and the mass of the tryptic fragments determined by MS. The MS fingerprint can be compared with a database of theoretical trypsin fingerprints.

An alternative mass spectrometry approach, tandem mass spectrometry (MS/MS), can be used to sequence a protein fragment and can therefore be used to identify proteins that cannot be identified by MALDI-TOF MS (Figure 11.24). In this approach, following proteolytic cleavage, the peptide fragments are separated by MALDI-TOF MS and then each fragment is passed through a collision chamber that breaks the fragments into a series of random smaller daughter fragments. These daughter fragments are analyzed by a second round of MS. The collision breaks each individual molecule just once; this generates two populations of fragments. In one population the fragments have a common N terminus and vary in size by one amino acid, whereas in the second they have a common C terminus and also vary in size by one amino acid. The characteristics of the N-terminal fragments are different to the C-terminal fragments and so the data from the second MS can be separated into two ladders. Each ladder starts from

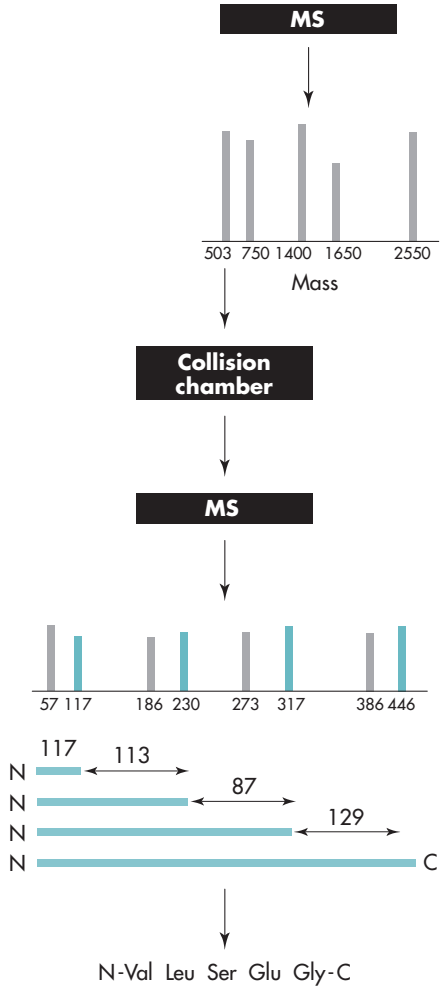


Figure 11.24 Protein sequencing by MS/MS. A protein is first digested with trypsin and the tryptic fragments separated by MS. One of the fragments is selected during the first MS and passed through a "collision" chamber which fragments the peptide into two populations of fragments. One set have a common N terminus and vary in size by one amino acid, whereas the second have a common C terminus and also vary in size by one amino acid. The mass of each fragment is determined by a second MS procedure. The N-terminal and C-terminal fragments can be differentiated. The fragments can be arranged by size giving two ladders, the N-terminal (blue) and the C-terminal (gray). The difference in size between the two adjacent fragments indicates the identity of the residue.

one end of the original proteolytic fragment, the individual "rungs" of the ladder representing the mass of one peptide fragment, and the difference in mass between two adjacent fragments is determined by which amino acid is present at that position. It is therefore relatively straightforward to determine the amino acid sequence of each proteolytic fragment. Each

protein spot can be digested with at least two proteolytic enzymes, in separate experiments, to generate overlapping fragments that can be sequenced by MS/MS and assembled into a complete protein sequence.

Proteomics can be used to identify which genes are regulated in test and control conditions. Comparison of the two two-dimensional gels reveals which proteins are subject to regulation. In many cases only spots representing genes subject to regulation are picked and analyzed by MS (Figure 11.23).

Q11.12. You are interested in the major differences in gene expression between cells grown in two different conditions. Which approach (transcriptomics or proteomics) would be easier to implement for an organism for which the genome has not been sequenced?

Questions and Answers

Q11.1. You are mapping the transcription start for a eukaryotic gene using primer extension and the intron/exon boundaries are not known. What effect would using a primer that anneals to a sequence in exon 2 have on the predicted transcription start?

A11.1. *It is not possible to sequence the primer extension product without using an extended protocol such as RACE (see below). If the primer hybridized to a sequence within exon 2, the intron will be missing from the mRNA but not the genome sequence, and therefore the start site will not be mapped correctly. The length of the primer extension product represents the distance from where the primer hybridizes to the 5′ end of the mRNA. If you only have the genomic sequence, and don't know where the introns are, you would map the transcription start as the distance on the genomic sequence as defined by the length of the primer extension product.*

Q11.2. In the final PCR step of the RACE protocol, rather than use the same primer that was used for the original primer extension step, one just internal ("upstream") is used. Why does this help reduce non-specific amplification?

A11.2. *If in the original primer extension step the primer annealed to RNA from somewhere else on the genome and produced a second cDNA, this cDNA would not have the same sequence as the target cDNA. If PCR was done with the same primer as was used in the initial step, this cDNA would still be amplified even though it does not correspond to a transcript. However, if a primer slightly upstream of the first one is used, it would be very unlikely to have any homology to this second cDNA which would not be amplified in the final PCR reaction.*

Q11.3. Why is it essential to remove all DNA from the RNA sample before northern analysis?

A11.3. *The labeled probe used to detect the RNA during northern analysis will also hybridize to any contaminating DNA as all genes, expressed or otherwise, will be present in the genomic DNA; this can give you a false positive for transcription of the gene.*

Q11.4. The QRT–PCR protocol utilizes random hexanucleotide primers to generate the cDNA prior to QRT–PCR. What is the advantage of using random hexanucleotides rather that a gene-specific primer?

A11.4. *Random hexanucleotides will generate a population of cDNAs reflecting the range of RNA molecules in the starting sample. It is therefore possible to subsequently use quantitative real-time PCR on the same mixture of cDNAs to determine the levels of mRNA for any gene for which the DNA sequence is known.*

Q11.5. Which technique, standard northern or reverse northern analysis would be best to study (a) the levels of mRNA for the same gene in several RNA samples (e.g. from different cell types) or (b) the levels of mRNA for several genes in the same RNA sample?

A11.5. (*a*) *Standard northern analysis is best suited to determining the mRNA levels for the same gene from several samples, because each RNA sample can be immobilized on the same membrane and the same labeled probe hybridized and the level of hybridization quantified. You cannot use two different probes in the same hybridization, so cannot analyze more than one gene at a time.*

(*b*) *Reverse northern would be best for determining the mRNA levels of several genes within the same sample because the probes are immobilized on the membrane, so several probes can be immobilized on the same membrane. The labeled cDNA will then hybridize to the immobilized probe and the level of hybridization of each mRNA can be quantified.*

Q11.6. Figure 11.15b shows how a series of overlapping fragments can be used to map where a transcription factor binds within a large DNA fragment. Why would you use overlapping fragments rather than a series of non-overlapping fragments?

A11.6. *If you used a series of non-overlapping fragments, the DNA binding site may be spilt between two adjacent fragments and therefore no binding would be detected. For example, if you have two fragments 1–40 and 40–80, the protein may require sequences from 35 to 50 to bind, and so would bind neither fragment. Overlapping fragments are used to ensure that any potential site is present on at least one fragment. For example, if you have three fragments 1–40, 20–60 and 40–80, a protein that binds from 35 to 50 could bind to the 20–60 fragment.*

Q11.7. You have a limiting amount of protein or cell extract which you use in an EMSA or footprinting experiment which results in only 10% of the fragments being bound by the protein. Would you be able to detect the protein–DNA complex using either the EMSA or footprinting protocol?

A11.7. *EMSA would still detect the small percentage of labeled DNA fragments that have bound protein because you would see the appearance of a shifted band. You would have difficulty detecting the bound protein using footprinting protocols because the 90% of unbound fragments in the "+ protein" lane would give rise to a ladder almost identical to the "– protein" lane.*

Q11.8. Are laboratory-based techniques, such as deletion analysis, the only approach to identify possible binding sites for transcription factors?

A11.8. *No, you can also use a bioinformatics approach. It is possible that your promoter or enhancer contains binding sites for known transcription factors. Therefore, you can search the DNA sequence for potential target sequences for known transcription factors. Although this approach may help you identify potential regulators for your gene, experimental work is still required to confirm that the transcription factors identified by bioinformatics really are involved in regulation.*

Q11.9. Which approach would you use to clone the genes for a transcription factor that you suspect contains two different protein subunits and where neither subunit can bind the DNA target on its own?

A11.9. *The only approach that you can use is affinity purification, because both the one-hybrid assay and an expression library screen a single clone in each colony or plaque.*

Q11.10. In a micro-array constructed with oligonucleotides, should the oligonucleotide probes be sense or antisense, i.e. the same sequence as the RNA or the template strand of the DNA?

A11.10. *The probes are sense, i.e. have the same sequence as the RNA. This is because the RNA is purified and then labeled cDNA, that is complementary to the RNA, prepared. The oligonucleotides need to hybridize to the labeled cDNA, so like the RNA, are complementary to the cDNA.*

Q11.11. Could an oligonucleotide array be used to analyze the labeled RNA from a nuclear run-on experiment?

A11.11. *No, in the nuclear run-on experiment the RNA is directly labeled and hybridized to the immobilized probe. The immobilized probe therefore needs to be complementary to the RNA (see answer to Q11.10 for more detail).*

Q11.12. You are interested in the major differences in gene expression between cells grown in two different conditions. Which approach

(transcriptomics or proteomics) would be easier to implement for an organism for which the genome has not been sequenced?

A11.12. *A proteomic approach would be the easiest to implement, since it would be difficult to obtain the sequence information to generate the probes required to print the array for a transcriptomics approach. With a proteomics based approach, you would need to optimize the two-dimensional gel electrophoresis for your sample, but once this has been done you should be able to visualize differences in the protein complement of the cells grown in the two conditions, isolate individual proteins form the gels and obtain sequence information using mass spectrometry. Bioinformatics can then be used to attempt to identify the proteins due to similarity to sequences in a protein database.*

Further Reading

The *nirB* promoter of *Escherichia coli*: location of nucleotide sequences essential for regulation by oxygen, the FNR protein and nitrite (1988) Jayaraman PS, Gaston KL, Cole JA and Busby SJW, Molecular Microbiology, Volume 2 Pages 527–530.
This paper describes a study that used reporter gene assays and deletion analysis to investigate regulation of gene transcription

Anti-termination of transcription within the long terminal repeat of HIV-1 by *tat* gene product (1987) Kao SY, Calman AF, Luciw PA and Peterlin BM, Nature, Volume 330 Pages 489–493.
This paper describes a study that used the nuclear run-on assay to investigate the regulation of gene transcription

Marker proteins for gene expression (1995) Wood KV, Current Opinion in Biotechnology, Volume 6 Pages 50–58.
This is a review of reporter gene assays

Three functional classes of transcriptional activation domains (1996) Blau J, Xiao H, McCracken S, O'Hare P, Greenblatt J and Bentley D, Molecular and Cellular Biology, Volume 16 Pages 2044–2055.
This paper describes a study that used nuclease protection and reporter gene assays to investigate the regulation of gene transcription

DNAse footprinting: a simple method for the detection of protein–DNA binding specificity (1978) Galas DJ and Schmitz A, Nucleic Acids Research, Volume 5 Pages 3157–3170.
This paper describes the use of DNAse footprinting in studying protein–DNA interactions

Applications of DNA microarrays in biology (2005) Stoughton RB, Annual Review of Biochemistry, Volume 74 Pages 53–82.
This is a detailed review of DNA microarrays used in transcriptomic studies

From genomic to proteomics (2003) Tyers M and Mann M, Nature, Volume 422 Pages 193–197.
This is a review of proteomics

Synthesis and Patterning Methods for Nanostructures Useful for Biological Applications

Chiara Daraio and Sungho Jin

1 Introduction

The importance and benefits of nanotechnology in biology and medicine are now well-recognized by scientists, technologists, as well as various governmental and private research funding agencies. The basis that enables the application of nanotechnology is the availability of nanostructured materials. Therefore, it is essential to provide an insight on the state-of-the-art methods to manufacture various nanostructures.

Nanotechnology has exploded onto the scientific scene in the last 20 years or so after the discovery, followed by a Nobel Prize recognition, of novel forms of carbon as the fullerenes molecules or buckyballs (Kroto et al. 1985), and the rediscovery of carbon nanotubes (CNTs) (Iijima 1991). The subsequent development has impacted nearly every field of scientific research. The infancy of nanotechnology began in materials science laboratories and has now matured at the forefront of several other disciplines, including chemistry, physics, various engineering fields, and, of course, biology and biomedical engineering. Nanotechnology is now rapidly being expanded for improved biotechnology to the extent that it can now be called as a subfield of "nanobiotechnology." The research and development on synthesis of nanowires and nanoparticles, nanopatterning, as well as nanoscale phenomena and properties literally exploded in the past several years developing a large variety of nanostructures extending to a myriad of other physical or chemical components. Some of the biological applications of the nanostructures, such as nanopatterns, nanochannels, nanotubes, and nanoparticles, synthesized using the

C. Daraio
Division of Engineering and Applied Science, California Institute of Technology, Pasadena, CA, USA

S. Jin (✉)
Materials Science & Engineering Program, Mechanical and Aerospace Engineering Department, University of California, San Diego, La Jolla, CA, USA

G.A. Silva and V. Parpura (eds.), *Nanotechnology for Biology and Medicine: At the Building Block Level*, Fundamental Biomedical Technologies,
DOI 10.1007/978-0-387-31296-5_2, © Springer Science+Business Media, LLC 2012

methods described in this chapter include nanoparticles for fluorescent biological labeling and tagging, drug and gene delivery, biodetection of pathogens and proteins, nanotubes and nanochannels for probing the structure of DNA, tissue engineering, magnetic nanoparticles for tumor destruction via heating (hyperthermia) and magnetic resonance imaging contrast enhancement, separation and purification of biological molecules and cells, and many others that are still currently under investigation (Salata 2004).

The methods for synthesis and patterning for many of these nanostructures are founded on basic, well-known techniques and their modifications, as is described in this chapter. The nanofabrication processes can be divided into the two well-known approaches: "top-down" and "bottom-up." The "top-down" approach uses traditional methods to guide the synthesis of nanoscale materials. The paradigm proper of its definition generally dictates that in the "top-down" approach it all begins from a bulk piece of material, which is then gradually or step-by-step removed to form objects in the nanometer-size regime (~1 billionth of a meter or 10^{-9} m). Well-known techniques, such as photo lithography and electron beam lithography, anodization, and ion- and plasma etching (PE), that are later described, all belong to this type of approach. The top-down approach for nanofabrication is the one first suggested by Feynman in his famous American Physical Society lecture in 1959, "There is plenty of room at the bottom" (Feynman 1959):

> Now comes the interesting question: How do we make such a tiny mechanism? I leave that to you. However, let me suggest one weird possibility. You know, in the atomic energy plants they have materials and machines that they can't handle directly because they have become radioactive. To unscrew nuts and put on bolts and so on, they have a set of master and slave hands, so that by operating a set of levers here, you control the "hands" there, and can turn them this way and that so you can handle things quite nicely.
>
> Most of these devices are actually made rather simply, in that there is a particular cable, like a marionette string, that goes directly from the controls to the "hands." But, of course, things also have been made using servo motors, so that the connection between the one thing and the other is electrical rather than mechanical. When you turn the levers, they turn a servo motor, and it changes the electrical currents in the wires, which repositions a motor at the other end.
>
> Now, I want to build much the same device – a master-slave system which operates electrically. But I want the slaves to be made especially carefully by modern large-scale machinists so that they are one-fourth the scale of the "hands" that you ordinarily maneuver. So you have a scheme by which you can do things at one-quarter scale anyway – the little servo motors with little hands play with little nuts and bolts; they drill little holes; they are four times smaller. Aha! So I manufacture a quarter-size lathe; I manufacture quarter-size tools; and I make, at the one-quarter scale, still another set of hands again relatively one-quarter size! This is one-sixteenth size, from my point of view. And after I finish doing this I wire directly from my large-scale system, through transformers perhaps, to the one-sixteenth-size servo motors. Thus I can now manipulate the one-sixteenth size hands. Well, you get the principle from there on. It is rather a difficult program, but it is a possibility …

The "bottom-up" approach on the other hand takes the idea of "top-down" approach and flips it right over. In this case, instead of starting with large materials and chipping them away to reveal small bits of them, it all begins from atoms and molecules that get rearranged and assembled to larger nanostructures. It is the new paradigm for synthesis in the nanotechnology world as the "bottom-up" approach allows a creation of diverse

types of nanomaterials, and it is likely to revolutionize the way we make materials. It requires a thorough understanding of the short-range forces of attraction, such as Van der Waals forces, electrostatic forces, and a variety of interatomic or intermolecular forces. Since it is not possible to have various minute things come together without some attractive force or active field of force in the region, having the fundamental forces "doing all the work" for us is the key principle underlying this approach.

Some examples of such a synthesis route starting from atoms and molecules are methods like self-assembly of nanoparticles or monomer/polymer molecules, chemical or electrochemical reactions for precipitation of nanostructures, sol–gel processing, laser pyrolysis, chemical vapor deposition (CVD), plasma or flame spraying synthesis, and atomic or molecular condensation. The bio-assisted synthesis of nanomaterials also belongs to this approach (Sarikaya et al. 2003). However, despite being so promising and inviting, our ability to build things from the bottom up is fairly limited in scope. While we can assemble relatively simple structures, we cannot produce complex, integrated devices using the bottom-up approach. Any kind of overall ordered arrangement aside from repeating regular patterns cannot be done without some sort of top-down influence, like lithographic patterning. Until we have fully mastered the bottom-up synthesis approach, we will not be able to fully exploit its speed and accuracy. The important factor is that they are two different approaches to creating nanostructures which can be applied according to the specific needs for each application, often in a complementary way.

1.1 Nanofabrication by Top-Down Methods

Top-down methods were originally introduced as a new set of manufacturing tools to solve specific industrial problems in micromachining, such as the microelectromechanical systems (MEMS) devices. At the nanoscale though, these methods are generally not suitable for production on a very large scale because they presently encounter technological limitation and require extremely long and costly processes. Nonetheless, they represent some of the most common approaches now used to pattern surfaces and create three-dimensional (3-D) features on substrates. Over the past decades, there has been a wide variety of top-down manufacturing techniques that have been implemented using different media that span from chemical and electrochemical means to photofabrication, laser machining, electron- and ion-beam milling (IBM), plasma etching and powder blasting. Here, we describe only the most common techniques used for nano- or nanobio-related applications.

1.1.1 Nanolithography

Nanolithography is one of the most established techniques for making nanostructured materials and patterns. Nanolithography derives its name from the Greek words *nanos* (dwarf), *lithos* (rock), and *grapho* (to write), which literally means "small writing on rocks." This technique is based on depositing, etching, or writing

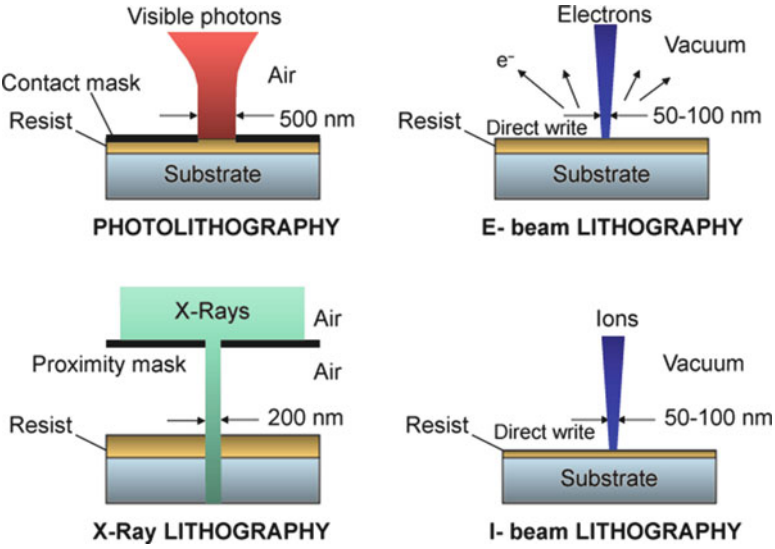


Fig. 1 Comparison of the available lithography techniques (image adapted from Brodie and Muray 1982)

on a surface features with dimensions on the order of nanometers. Lithography (Madou 2002) can be performed using light (optical- or photolithography), electrons (e-beam lithography), ions (i-beam lithography), or X-ray (X-ray lithography, LIGA) depending on the desired minimum feature size of the outputs (Fig. 1).

Photolithography is the most common and widely used technique in applications requiring micron and submicron feature sizes, like electronic, integrated circuits manufacturing, and microfluidic devices. It finds a lot of applications in bio-MEMS devices for its applicability to patterning of organic and inorganic materials, hydrogels, membranes, and ion-selective electrodes (Lambrechts 1992). With this technique, a design or pattern can be transferred at once on the surface of a device by exposure with light. Similarly, e-beam, i-beam, and X-ray lithography use the exposure to beams of electrons, ions, or X-ray for the design transfer.

All the lithographic techniques are multistep processes. As an example, we describe the steps followed in the specific case of photolithography of a Si/SiO_2 substrate (Fig. 2), keeping in mind that other techniques follow a very similar path. The first step is to coat the surface of the desired substrate with a thin polymer layer of a positive or negative photoresist (Fig. 2a), which is then covered by a predesigned, light-blocking mask and exposed to UV light (Fig. 2b). After exposure, the cured photoresist remains on the substrate as a protective coating, and the uncured portions are removed by the developer (Fig. 2c). This step is then followed by the etching of the substrate and the final removing of the photoresist (Fig. 2d). The type of resist chosen allows having a direct duplication of the mask used (as in the case of positive resist) or inverse of it (negative resist) exactly like in the case of film photography developing.

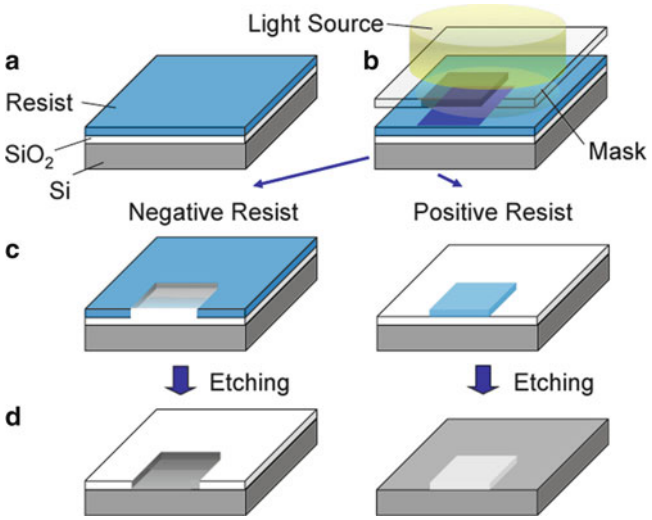


Fig. 2 Photolithography steps of surface patterning

The technical limits of photolithography are related to the wavelength of light used, which also determines the smallest feature sizes achievable. A limitation is dictated by the lens characteristics: if the used wavelength is made too small, the lens simply absorbs the light in its entirety and do not allow curing of the photoresist. This implies that photolithography cannot reach the superfine sizes of some other technologies, such as electron beam lithography, as the wavelength of typical light, even UV lasers, is somewhat limited. Small-wavelength UV light (deep UV techniques) can now be employed to obtain finer nanostructures.

A technology that allows for fabrication of much smaller nanostructures than photolithography is that of electron beam (e-beam) lithography. The use of an electron beam to draw a pattern nanometer by nanometer and expose an e-beam resist layer (usually made of a polymer) allows achieving incredibly small sizes (on the order of 20 nm). This technique, though, is much more expensive and time consuming than photolithography, as the e-beam exposure is carried out line-by-line or dot-by-dot, unlike the photolithography by which the whole area of, e.g., 12-in. diameter Si wafer can be exposed all at once. It takes orders of magnitude longer to complete the patterning with e-beam, so it is therefore difficult to sell the e-beam lithography for large-scale industry applications.

New nanolithography technologies are continued to being researched, leading to smaller possible sizes and access to more complex surface geometries and properties. Extreme ultraviolet (EUV) lithography, for example, is capable of using light at wavelengths of 13.5 nm and fabricating ~30-nm regime features. While hurdles still exist in this new field, it promises the possibility of sizes far below those produced by current industry standards. Another lithography technique proposed for the realization of nanoscale features is the direct-write, “dip-pen” nanolithography

(DPN) method. This technique relies on the use of a small tip to deposit molecules on a surface in a positive printing mode (Piner et al. 1999). It can achieve relatively small sizes, but currently it cannot go below 40 nm.

Similarly, scanning probe microscopes (SPMs) and atomic force microscopes (AFMs) are often used in relation to nanolithography. They allow imaging the fine details on surfaces without necessarily modifying it or inducing undesired damage. However, SPM and AFM can also be used to achieve precise etch, write, or print on surfaces obtaining nanometer or even single-atom resolution.

1.1.2 Dry Etching Techniques

In addition to the commonly used wet chemical etching for nanostructure fabrication, dry etching techniques (Lehmann 1991) are also used in the processing of semiconductor wafers in which the material is immersed in plasmas or discharges containing etching species. Dry etching is a process to remove material carried out in the gas phase that uses no aqueous solutions, such as an acid or base, hence the name "dry etching." Dry etching techniques can be either purely chemical (plasma etching), purely physical (ion beam milling, IBM), or a combination of both (reactive ion etching, RIE). The dry etch reactions are generally isotropic, taking place with equal rate in any direction. They can be very selective etching techniques for removal of one material relative to another, generally used in those applications in which directionality (anisotropy) of etching in not required, e.g., in resist stripping.

Plasma etching, like most dry etching techniques, is carried out in chambers in which high-energy electric and magnetic fields rapidly dissociate suitable feeding gasses, forming a plasma. When the surface of a material gets in contact with the plasma, it gets bombarded by molecules, ions, electrons, and photons which stimulate the expulsion of material from the surface, leading to atomically precise removal of materials. Commonly, plasmas can be created in different ways: using direct current (DC) electric fields, applying a radio frequency (RF) voltage source or using a microwave source. One of the most common plasma etching techniques used is RIE because of its relative simplicity and versatility. The RIE method requires process pressures varying between 10^{-3} and 10^{-1} Torr. A schematic diagram summarizing the differences between some of the dry etching methods is shown in Fig. 3 (Madou 2002).

Another common dry etching technique is IBM. In this case, the plasma source is decoupled from the substrate, which is placed on a separate third electrode in a triode setup. IBM can be employed to cover relatively large areas. A commonly used IBM method is focused ion beam (FIB), usually coupled to a high-resolution scanning electron microscope (SEM) to provide visual guidance during the writing process. FIB uses a beam of ions (usually Ga^{2+}) that gets narrowed in a very small area and it is employed as a direct writing tool for patterning holes, thinning samples, and depositing insulating or conductive material almost atom by atom. FIB milling is a powerful technique, now commonly considered a "mechanical" machining technique in which the classical metal drill bit used in all machine shops is

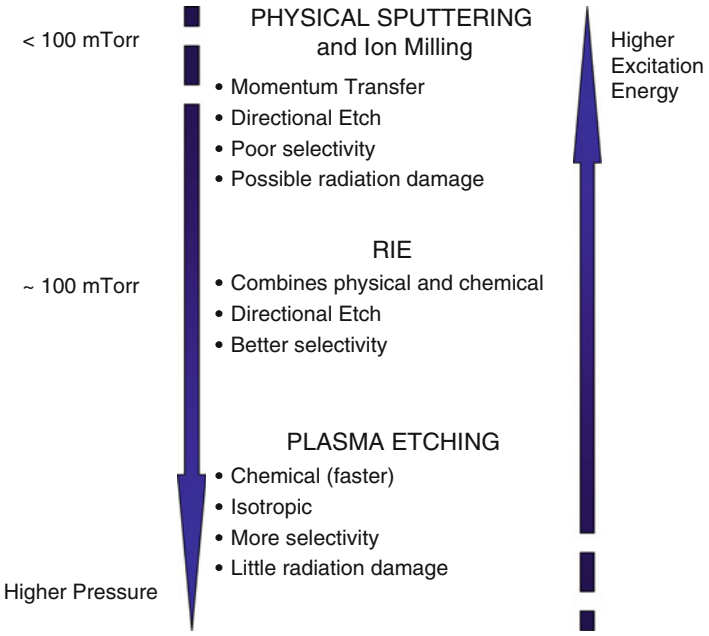


Fig. 3 Schematic diagram of the dry etching techniques spectrum (modified from Madou 2002)

replaced by the focused beam of highly energetic ions. However, the disadvantages of FIB are long processing time, the risk of undesired ion implantation, or damage to the sample.

1.1.3 Anodization

Anodization is a term that stands for anodic oxidation and it is "the process of growth of an oxide on the surface of a biased conductive solid (e.g., semiconductor wafer) immersed in a liquid electrolyte or gas. With this method, under specific process conditions, a thin, dense, barrier oxide of uniform thickness can be grown on several different metals" (Alwitt 2002). The properties of the grown oxide layer vary as a function of the materials selected and the process conditions. The commercial application of anodic oxidation extends to different surface coatings, mostly based on aluminum, tantalum, niobium, and zirconium. Recently, titanium has been also receiving increasing attention in bio-related applications (Oh et al. 2005). Aluminum in particular is commonly used because of its ease and versatility of processing. In addition to the creation of a thin barrier oxide, the anodization of aluminum, under specific conditions, can produce a thick oxide coating with a high density of vertically oriented nanopores (see Fig. 4) (Asoh et al. 2001). This porous substrate can then function as template for other assisted

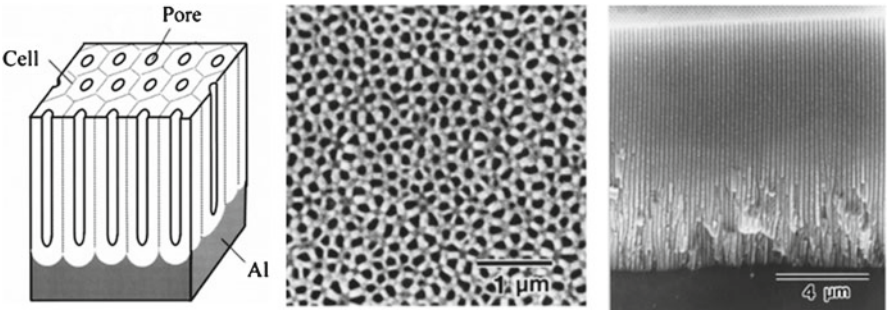


Fig. 4 Porous-anodized aluminum with neighboring cells of aluminum oxide merges together to form the matrix supporting the aligned nanopores. *Left*, scheme; *center*, top view transmission EM; *right*, side view SEM (Reproduced from Asoh et al. 2001 with permission from The Electrochemical Society, Inc.)

growth of CNTs or other nanomaterials or as substrate for several different applications, like corrosion prevention for automobile and aerospace structures or electrical insulation.

The anodization process takes place in a processing cell containing a cathode and an anode. Usually, the metallic sample of choice functions as the anode, and it is connected to the positive terminal of a DC power supply. A different conductive material, inert in the anodizing bath, functions as the cathode (some example materials used as cathodes are carbon, lead, nickel, or stainless steel), and it is connected to the negative terminal of the supply. When this circuit is closed, electrons are allowed to move, being attracted by the positive terminal, and permit the reaction between the ions present on the surface of the metal with the water molecules that forms the oxide layer.

1.2 Nanofabrication by Bottom-Up Methods

With the first decades of the new millennium, standard top-down techniques for nanomanufacturing have approached a critical limit in the ability to miniaturize components. Further size reduction has required innovative chemical routes. Eric Drexler, a pioneer in nanotechnology, in 1986 said, “our ability to arrange atoms lies at the foundation of technology.” From this point on, several bottom-up approaches have blossomed, trying to build nanostructures one atom at a time, in the most efficient and precise way possible. On this aspect, nature is well-ahead of human engineering: proteins build structures quickly and effectively mastering the self-assembly of molecules as the basic building blocks of life. Nanoengineering is today putting a lot of effort in combining old, well-known chemical methods with new systems, even looking for inspiration from nature in bio-inspired structures and bio-assisted synthesis of nanodevices (Madou 2002).

One of the basic bottom-up techniques used to fabricate nanomaterials is chemical precipitation. This method allows producing nanoparticles of metals, alloys, oxides, etc. from aqueous or organic solutions following relatively simple and cost-effective steps. The drawback of this synthesis method, however, is the difficulty in the ability to control the distribution of particle size and shape, which limits the use of the produced nanomaterials in applications where a random particle distribution is undesired. Nanoscale precipitates can be obtained with various techniques, for example by a controlled phase transformation guided by the free energy diagrams or by controlling the solid-state diffusion, following a composite route approach, for example mixing two different materials and stirring them mechanically. Other approaches can be found in exploiting internal oxidation of materials, in thin film deposition of coatings, or sputtering.

The phase transformation approaches rely mostly on the rapid cooling of a solution that, not given enough time to reestablish equilibrium transformations, becomes supersaturated and precipitates into more stable and fine solid states. Common methods for rapidly cooling a solution (achieving cooling rates between 10^5 and 10^8 degrees per second) are splat cooling, quenching in salt baths, or melt spinning. These techniques are often used to obtain thin films and bulk materials with an extremely fine microstructure that influences positively its mechanical and electrical properties. Another common example of nanofabrication of nanoparticles or nanostructured films based on phase transformation of materials is called "spinodal decomposition." It is a spontaneous reaction driven by the free energy minimization of the material that guarantees the formation of a periodic structure of nanoparticles of equal sizes.

In order to control or limit the growth of nanomaterials produced with bottom-up methods, two techniques are conventionally used: arrested precipitation and physical restriction. Arrested precipitation relies on the exhaustion of one of the reactants or on the introduction of chemicals that would block the reaction. The physical restriction method relies on the confinement of the volume available during growth of the individual nanoparticles. Example of physical restriction includes using the micelle-reverse-micelle reactions or using templates (like, for example, the porous alumina described in the Sect. 1.1.3 above).

There are numerous bottom-up methods used to produce nanomaterials; we limit the rest of the chapter to the description of a few: sol–gel processing, CVD, self-assembly and bio-assisted synthesis, laser pyrolysis, electroplating, plasma or flame spraying synthesis, atomic or molecular condensation, and supercritical fluid synthesis.

1.2.1 Sol–Gel Processing

The sol–gel process in general is based on the transition of a system from a liquid "sol" (mostly a colloidal suspension of particles) into a gelatinous network "gel" phase. With this, it is possible to create at low temperature ceramic or glass materials in a wide variety of forms. It is a long-established industrial process that is

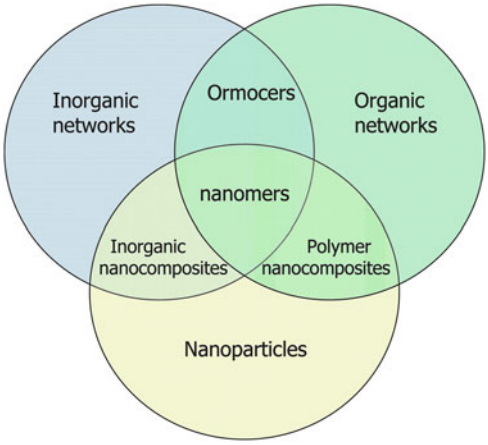


Fig. 5 System model for nanocomposites produced by sol–gel (modified from Luther 2004)

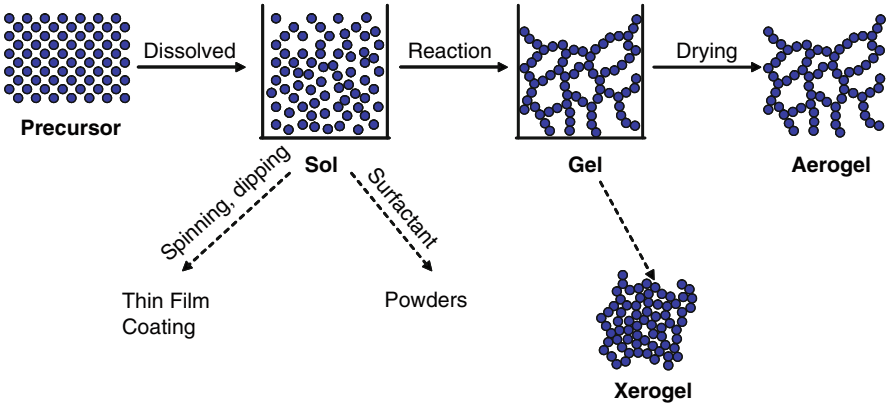


Fig. 6 Basic flow of a sol–gel process (modified from Madou 2002)

very cost-effective and versatile. It has been further developed in last year for the production of advanced nanomaterials and coatings but also in bio-MEMS application for the production of piezoelectrics, such as lead–zirconium–titanate (PZT) (Madou 2002) or membranes (Guizard et al. 1992). Sol–gel processes are well-adapted for oxide nanoparticles (Lakshmi et al. 1997) and composite nanopowder synthesis as well as for access to organic–inorganic materials. A summary of all the possible interlinked combination of organic and inorganic nanocomposites that are produced by the sol–gel method is provided in Fig. 5.

The basic flow of the sol–gel process is described in Fig. 6. The "sol" is prepared by mechanically mixing a liquid alkoxide precursor (such as tetramethoxysilane, TMOS, or tetraethoxysilane, TEOS), water, a cosolvent, and an acid or base catalyst at room temperature. During this step, the alkoxide groups are removed by the acid- or

base-catalyzed hydrolysis reactions, and networks of O–Si–O linkages are formed in subsequent condensation reactions. After this step, the treatment of the sol is varied depending on the final products desired. For example, spinning or dipping techniques can create thin film coating, and the exposure of the sol to a surfactant can lead to powders. Depending on the water–alkoxide molar ratio *R*, the pH, the temperature, and the type of solvent chosen, additional condensation steps can lead to different polymeric structures, such as linear, entangled chains, clusters, and colloidal particles. In some cases, the resulting sol is cast into a mold and dried to remove the solvent. This leads to the formation of a solid structure in the shape of the mold (e.g., aerogels and xerogels) with large surface-to-volume ratios, high pore connectivity, and narrow pore size distribution. They can be doped with a variety of organic/inorganic materials during the mixing stage to target specific applications.

1.2.2 Chemical Vapor Deposition

The CVD process is now probably the most common of all bottom-up approaches. It is used today to grow structures, like nanotubes, nanowires, and nanoparticles aided by several different types of chambers and growth-enhancing methods. The process consists of decomposing a gaseous precursor that adheres and accumulates onto a substrate (i.e., a silicon wafer or a quartz slide) (Jensen 1989). The presence of a catalyst, either predeposited on the substrate or provided in the gas feedstock, activates the chemical reaction between the substrate surface and the gaseous precursor. The CVD reaction can be achieved either with temperature (thermal CVD) or with plasma (PECVD). Plasmas can be obtained with DC electric fields, RF fields, or microwave fields, and their presence allows decreasing significantly the process temperature compared to the thermal CVD process. The presence of plasma also enables a more aligned or directional growth of the desired nanomaterials. A number of forms of CVD systems are in wide use and are frequently referenced in the literature. Some examples include atomic-layer CVD (ALCVD) in which two complementary precursors [e.g., $Al(CH_3)_3$ and H_2O] are alternatively introduced into the reaction chamber; metal-organic CVD (MOCVD) in which metal-organic precursors are used to obtain specific crystalline structures [e.g., tantalum ethoxide, $Ta(OC_2H_5)_5$, to create TaO nanostructures, and tetra dimethyl amino titanium (TDMAT) to create TiN]; laser-assisted CVD (LCVD); rapid thermal CVD (RTCVD) that uses heating lamps or other methods to rapidly heat the wafer substrate; ultrahigh vacuum CVD (UHVCVD); and more (Adams 1988; Jensen 1989).

The CVD process is widely used to produce CNTs and semiconductor nanowires, such as Si, GaN, and ZnO. CNTs have received much attention in the recent years for their potential application in several fields of bioengineering, from enhanced cell growth to biosensing, biomanipulation, and drug delivery. The most common synthesis routes for CNTs are CVD processes because they allow large-scale production of CNTs with high purity and good yield. To clarify how the CVD process works, we show a schematic diagram of a thermal CVD growth system used for the synthesis of CNTs (Fig. 7). In this example, a carbon-containing precursor is

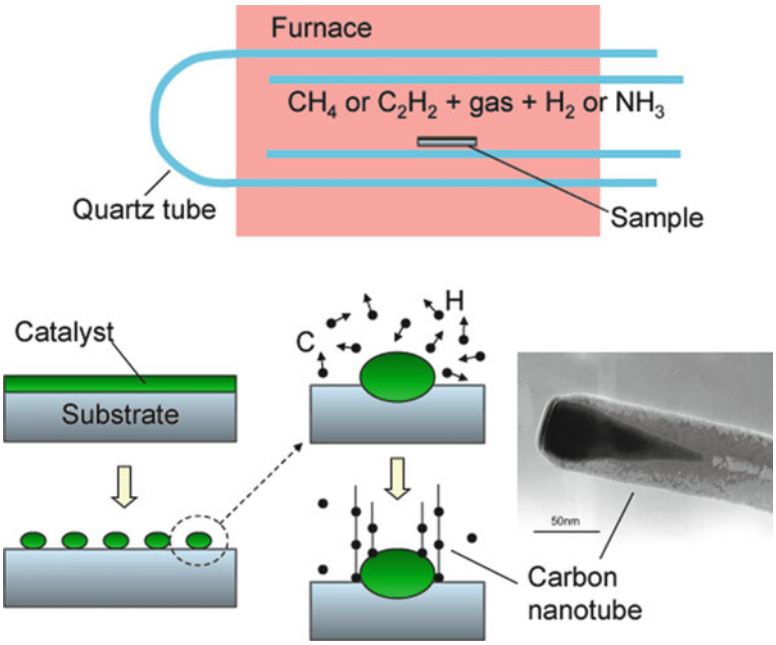


Fig. 7 Schematics of a thermal CVD furnace (*top*) and basic flow of a carbon nanotube growth process (*bottom*)

decomposed in the furnace at high temperature. The growth reaction is activated by the presence of a catalyst that can be deposited on the sample's surface (as in the figure) or in the gas mixture fed to the reactor (e.g., injecting ferrocene $C_{10}H_{10}Fe$). The most common carbon sources used in thermal CVD growth of CNTs are mixtures of ammonia (NH_3) and acetylene (C_2H_2) while the catalyst metal can be cobalt, iron, or nickel. The growth proceeds through several steps: first, the catalyst metal breaks up into islands at high temperatures and forms metal seeds for the reaction; then, the hydrocarbon gas supplied in the quartz tube decomposes creating floating C and H atoms; the floating atoms are then attracted by the catalyst seeds that become supersaturated and condensate forming ordered tube-shaped graphene sheets. The catalyst particle can then either stay attached to the substrate (base growth) or get pushed to the tip of the formed nanotube (tip growth) conferring different properties to the final structure. This type of growth process, although being relatively inexpensive, forms a randomly distributed array of CNTs with a complex hierarchical microstructure. Bundles of tubes grow vertically, but the tubes are intertwined and partially curled at small scales. This lack of complete alignment is normally overcome by the use of PECVD systems, which are a bit more complex and expensive, since they need additional constituents like electrodes, pumps, voltage supplies, etc.

1.2.3 Self-Assembly and Bio-Assisted Synthesis

As mentioned in the earlier section for the case of CNT growth, the assembly of nanostructures or nanoparticles in a periodically aligned fashion or in a functionally engineered geometry is often desired over random or disordered structures. Approaches for ordering or assembling nanostructures in a desired geometry have been widely investigated in the past and are still pursued in many different laboratories. Self-assembly provides the most convenient way for alignment, especially considering that at such small scales, single-structure manipulation and postgrowth rearrangement appear to be very expensive if not at all impractical. Chemistry and molecular biomimetics are the dominant fields leading the design of hybrid technologies combining the tools of molecular biology and nanotechnology. Molecular biomimetics combines the physical and biological fields to assemble nanomaterials using the recognition properties of proteins.

Researchers have found ways to process nanoparticles of a wide range of materials – including organic and biological compounds, inorganic oxides, metals, and semiconductors – using chemical self-assembly techniques. In these cases, molecules are attached, patterned, or clustered on specific substrates or to themselves using chemical and biomolecular recognition (e.g., the preferential docking of DNA strands with complementary base pairs). Other techniques, like micelle, reverse micelle, and photochemical and sonochemical synthesis, are also employed to realize one-, two-, and three-dimensional self-assembled nanostructures. Lately, viruses have also been used to assemble specific nanostructures (Mao et al. 2004). A review of the path to nanotechnology through biology is provided in (Sarikaya et al. 2003). It was shown that proteins, through their specific interactions with inorganic and other macromolecules, could be used in nanotechnology to control structures and functions just like they do biological tissues in organisms. Taking lessons from nature, polypeptides can be genetically engineered to specifically bind to selected inorganic compounds for specific applications, as outlined in Fig. 8 (Sarikaya et al. 2003).

The use of organic molecules is also a powerful technique in the synthesis and arrangement of semiconducting nanoparticles, for example quantum dots, used in biological labeling and tagging. One of the major issues in the synthesis of these isolated islands of materials is to prevent particles' agglomeration and coarsening. Micelle processes and organic ligands capping (TOPO) are synthesis methods based on the simple mixing of surfactant with desired materials' sources. With these methods, it is possible to synthesize and/or align a wide range of nanomaterials spanning from magnetic nanoparticles (i.e., Fe_3O_4 particles found in magnetotactic bacteria) to the bright CdS quantum dots used for bioimaging. Micelles are employed as small chemical-reacting chambers in which nanomaterials are synthesized in fixed-sized cells (Fig. 9). One of the first examples of nanoparticle synthesis using a reverse-micelle process was for fabrication of FePt nanoparticles (Sun et al. 2000) using a combination of oleic acids and oleyl amine to stabilize the monodisperse FePt colloids and to prevent oxidation. With this method, the authors showed that it is also possible to control the size of the synthesized nanoparticles and their composition,

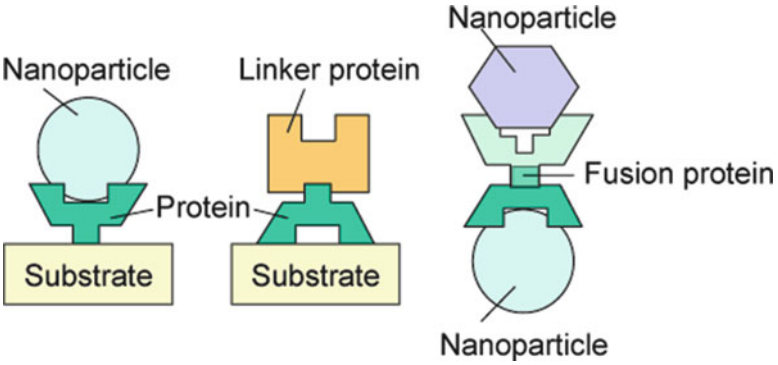


Fig. 8 Examples of molecular biomimetics (adapted from Sarikaya et al. 2003). Proteins can be used, for example, to bind nanoparticles to a functionalized substrate, to create linkers onto a specific substrate, or to connect different nanoparticles with each other

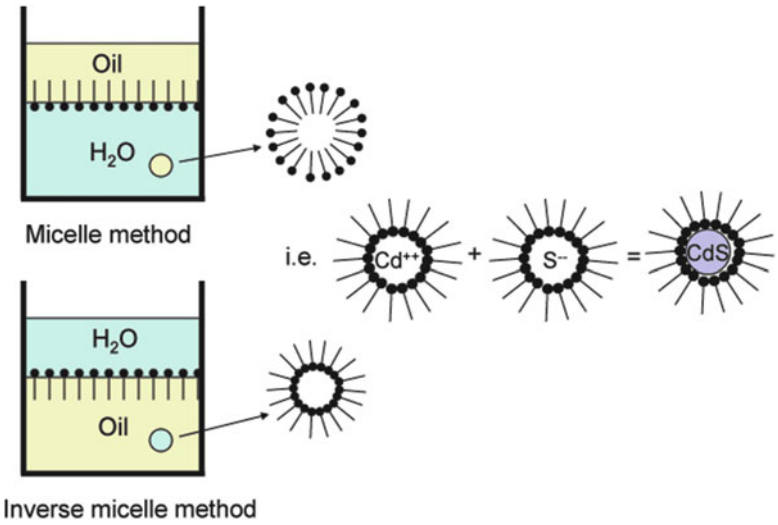


Fig. 9 Micelle and reverse micelle processing for synthesis of nanoparticles. On the *right*, it is shown the schematic for the synthesis of CdS quantum dots via reverse (inverse) micelle method

simply tuning the molar ratio of the solvents. Upon drying, the particles could self-assemble into three-dimensional superlattices that are chemically and mechanically robust and can, for example, support high-density magnetization reversal transitions.

The micelle process is also commonly used in the synthesis of semiconducting quantum dots. For example, CdSe nanoparticles capped with ZnS coating offer significant advantages as bioimaging agents as compared to the commonly used organic

fluorescent dye materials. Quantum dots are ~20 times brighter than the typical organic dye molecules, and their emission is ~100 times more stable to photobleaching than conventional fluorescent dyes (e.g., rhodamine). They can be made water soluble by chemical functionalization and can also be made specific cell- or organ-targetable via chemical or biological conjugation (Chan and Nie 1998; Akerman 2002). They can be imaged with a conventional fluorescence microscope. Besides the visible-emitting quantum dots, both near-IR and UV-emitting dots can also be synthesized.

The essence of bottom-up processing of nanotechnologies is mastered by nature in biological systems. For example, cells function on similar length scales to those of synthetic nanosystems. The molecules that operate and react in living cells are similar to the devices imagined for building nanosystems. Rather than using biological elements for the assembling of inorganic nanostructures, another way proposed for the synthesis of nanomaterials relies on incorporating the biological components themselves into artificial nanoscale structures and devices. Biological molecular motors, for example, have been incorporated into artificial structures, and the light harvesting complexes of plants or photosynthetic bacteria have been incorporated into synthetic membranes. From this point on, a vast array of applications that combine artificial structures with biological components can be envisioned and investigated, defining the future of nanobiotechnology.

1.2.4 Laser Pyrolysis

Laser pyrolysis is a technique that uses IR laser energy to decompose materials by heating gas-phase reactants in an oxygen-deprived environment. This method is used to produce extremely pure spherical nanoparticles with small-diameter, small-size distribution and with a low agglomeration level (Herlin-Boime et al. 2004). Such particles are used, for example, as precursors for surface treatments of ceramics. A similar technique, called laser ablation, is also used for the production of CNTs and nanowires.

1.2.5 Electrochemical Deposition/Electroplating

Electrochemical deposition is a technique used for manufacturing ordered arrays of nanomaterials, like quantum dots on a flat surface, for coating different surfaces or for patterning thin films (Allred et al. 2005). It represents one of the most powerful techniques that allow obtaining high-density and high-aspect ratio designs, with excellent reproducibility of the process and with great precision of the final products. Similarly to lithographic techniques, electrochemical deposition requires a polymer mask through which metal is deposited. Differently from other mask-based techniques like isotropic etching, ion milling, and RIE, electrochemical deposition avoids the problem of shadowing near edges or interfaces and builds structures atom by atom. The techniques rely on the presence of an electric field in a solution, which allows metal ions to discharge and conform to the smallest features of a mold.

Metal deposition can be carried on under two major techniques (Madou 2002): with current (pulsed or DC) or electroless (via catalytic, exchange, or electrophoretic reactions). The first method takes place in an electrolytic cell and involves a reaction under an imposed bias and current flow. In this case, important process parameters to control are pH, current density, temperature, agitation, and solution composition. The second technique, the electroless deposition, is based on a substantial oxidation reaction that replaces the dissolution of a sacrificial substrate.

1.2.6 Spraying Synthesis

Spraying processes are a viable technology for coating large area devices, and represent a simple and inexpensive alternative to produce sensing devices and nanosized coating of surfaces (Mooney and Radding 1982). Spraying processes take place in a chamber containing a high-energy flame produced, for example, using plasma spraying equipment or using a carbon dioxide laser. A flow of reactants (gas or liquid in form of aerosols or a mixture of both) is forced into the flame and decomposes, forming particles by homogeneous nucleation and growth. The subsequent rapid cooling of the material completes the formation of nanoscale particles. In its simplest form, the reagent is simply dissolved in a carrier liquid and sprayed on a hot surface in the form of tiny droplet of ~100-nm diameter. In this case, the spray is formed from a liquid pressurized by compressed air or mechanically compressed through a small nozzle.

1.2.7 Atomic or Molecular Condensation

Condensation is a well-known technique used to produce primarily metal-based nanoparticles. The process takes place in a vacuum chamber: first, a bulk piece of metallic material is heated, melted, and vaporized to produce a stream of atomized matter. A gas flow (either inert or reactive) is then introduced into the reaction chamber to rapidly cool the metallic vapor. The cooled metallic atoms form condensed liquid nanoparticles, which then coalesce in a controlled environment, preserving a spherical shape with smooth surfaces. As the liquid particles are further cooled, they solidify and stop growing. The so-formed nanoparticles are very reactive and sensitive to agglomeration, which is prevented by adding coating or surfactants to keep them separated. If oxygen is present in the gaseous stream of the second chamber, the reaction results in the formation of metal oxide nanoparticles.

1.2.8 Supercritical Fluid Synthesis

Supercritical fluids are materials forced in a state above their critical point by regulating their pressure and temperature. They are obtained by vaporizing a liquid in a closed chamber, until the vapor phase becomes as dense as the liquid phase.

This supercritical state is very sensitive to the process' parameters and tunable. Methods using fluids in such a unique state are now used for the synthesis of nanoparticles, exploiting the rapid expansion of the supercritical solution, and they are also used for coating and filling nanostructures (Ye et al. 2004). The most common reaction media used in this process are supercritical carbon dioxide ($scCO_2$) and water (scH_2O) because they are nontoxic, nonflammable, inexpensive, and environmentally benign. In addition, they ensure much higher reaction rates and an increased selectivity. Although it has many advantages, supercritical fluid synthesis remains technically demanding, and it is still being adapted for large-scale production.

2 Conclusions

Top-down and bottom-up approaches are complementary in nanofabrication and comprise a numerous set of techniques. Their use and development have been at the center of material research for the past few decades, promising a wide range of applications in (non)biologically related nanotechnology fields. The use of a particular approach is often dictated by the specific need for a particular characteristic, shape, or composition of the nanomaterials for the different applications. Often, methods are used in combination to complement each other.

This chapter presented a brief overview of the most common techniques used for the fabrication of nanostructured bulk materials and nanomaterials with potential applications in biology and bioengineering fields. Most of the techniques described are continuously evolving even as we write and they represent a wide and active area of research in physics, chemistry, and engineering fields. A deep understanding of the mechanisms behind all the nanofabrication methods requires a broad and profound knowledge of the interdisciplinary aspects that regulate the properties of the materials and of the processes used. The details of the chemistry, physics, and mechanics of these methods go beyond the scope of this chapter and can be found in the related technical literature.

References

Adams A (1988) In VLSI Technology. New York: McGraw-Hill.

Akerman M (2002) Nanocrystal targeting in vivo. Proc Natl Acad Sci 99:12617–12621.

Allred D, Sarikaya M, Baneyx F, Schwartz D (2005) Electrochemical Nanofabrication Using Crystalline Protein Masks. Nano Letters 5,4,:609–613.

Alwitt RS (2002) Electrochemistry Encyclopedia. In. Cleveland Ohio (http://electrochem.cwru.edu/encycl/).

Asoh H NK, Nakao M, Tamamura T and Masuda H (2001) Conditions for Fabrication of Ideally Ordered Anodic Porous Alumina Using Pretextured Al. Journal of the Electrochemical Society 148:B152-B156.

Brodie I, Muray, J J (1982) The Physics of Microfabrication, Plenum Press, New York.

Chan W, Nie S (1998) Quantum dot bioconjugates for ultrasensitive nonisotopic detection. Science 281:2016–2018.

Feynman R (1959) Plenty of Room at the Bottom. In. Pasadena: Caltech.

Guizard C, Julbe A, Larbot A, Cot L (1992) Nanostructures in sol-gel derived materials: application to the elaboration of nanofiltration membranes. Journal of Alloys and Compounds 188:8–13.
Herlin-Boime N, Mayne-L'Hermite M, Reynaud C (2004) Synthesis of covalent nanoparticles by CO2 laser. Encyclopedia of Nanoscience and Nanotechnology 10:301–326.
Iijima S (1991) Helical Microtubules of Graphitic Carbon. Nature 354:56–58.
Jensen K, ed (1989) Chemical Vapor Deposition, in Microelectronics Processing: Chemical Engineering Aspects. Washington DC: American Chemical Society.
Kroto H, Heath J, O'Brien S, Curl R, Smalley R (1985) C60: Buckminsterfullerene. Nature 318:162–163.
Lakshmi BB, Dorhout PK, Martin CR (1997) Sol-Gel Template Synthesis of Semiconductor Nanostructures. Chemistry of Materials 9, 3:857–862.
Lambrechts M SW (1992) Biosensors: Microelectrochemical Devices. Phildelphia: The Institute of Physics Publishing.
Lehmann H (1991) Plasma Assisted Etching, in Thin Film Processes II. Boston: Academic Press.
Luther W (2004) System model for nanocomposites produced by sol-gel. Published by Future Technologies Division of VDI Technologiezentrum GmbH, Dusseldorf, Germany.
Madou M (2002) Fundamentals of Microfabrication: the science of miniaturization. BocaRaton: CRC Press.
Mao C, et al. (2004) Virus-Based Toolkit for the Directed Synthesis of Magnetic and Semiconducting Nanowires, Science, Vol. 303 no. 5655 pp. 213–217.
Mooney J, Radding S (1982) Spray Pyrolysis Processing. Ann Rev Mat Science 12:81–101.
Oh S, Finones R, Daraio C, Chen L-H, Jin S (2005) Growth of Nano-scale Hydroxyapatite using chemically treated Titanium oxide nanotubes. Biomater 26:4938–4943.
Piner, R.D. et al, (1999) "Dip pen" nanolythography, Science 283, 661.
Salata O (2004) Applications of Nanoparticles in Biology and Medicine. Journal of Nanobiotechnology 2:3.
Sarikaya M, Tamerler C, Jen A-Y, Schulten K, Baneyx F (2003) Molecular Biomimetics: Nanotechnology through Biology. Nature Materials 2:577–585.
Sun S, Murray C, Weller D, Folks L, Moser A (2000) Monodisperse FePt Nanoparticles and Ferromagnetic FePt Nanocrystal superlattices. Science 287:1989–1992.
Ye X-R, Lin Y, Wang C, Engelhard MH, Wang Y, Wai CM (2004) Supercritical fluid synthesis and characterization of catalytic metal nanoparticles on carbon nanotubes. Journal of Materials of Chemistry 14:908–913.

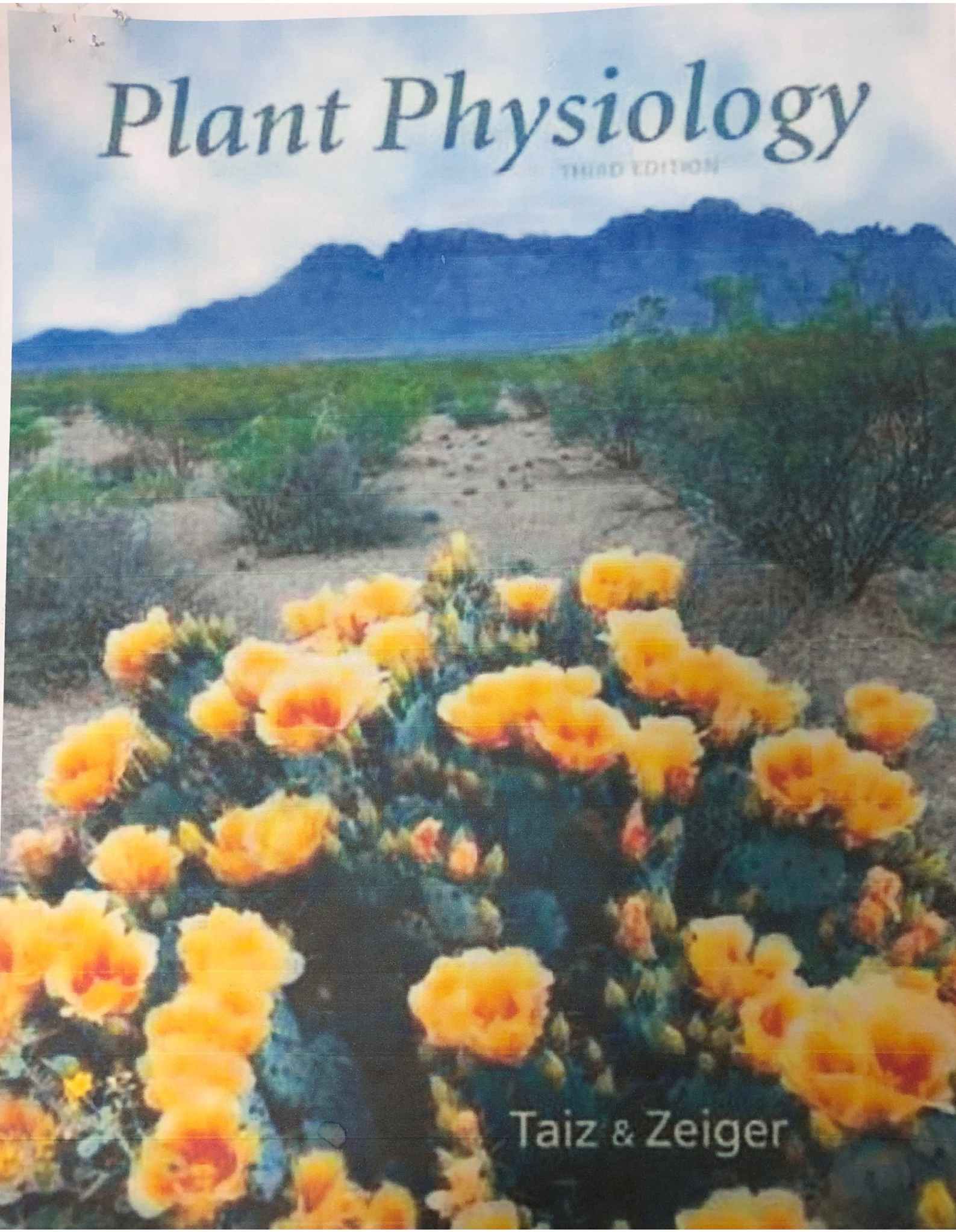


http://www.springer.com/978-0-387-31282-8

Nanotechnology for Biology and Medicine
At the Building Block Level
Silva, G.A.; Parpura, V. (Eds.)
2012, XVI, 236 p., Hardcover
ISBN: 978-0-387-31282-8

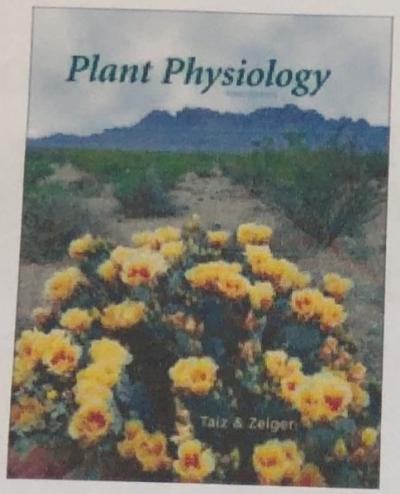
Plant Physiology

THIRD EDITION



Taiz & Zeiger

Scanned with CamScanner



Plant Physiology, 3rd ed

by Lincoln Taiz and Eduardo Zeiger

Hardcover: 690 pages
Publisher: Sinauer Associates; 3 edition (Aug 30 2002)
Language: English
ISBN: 0878938230

Book Description

With this Third Edition, the authors and contributors set a new standard for textbooks in the field by tailoring the study of plant physiology to virtually every student—providing the basics for introductory courses without sacrificing the more challenging material sought by upper-division and graduate-level students.

Key pedagogical changes to the text will result in a shorter book. Material typically considered prerequisite for plant physiology courses, as well as advanced material from the Second Edition, will be removed and posted at an affiliated Web site, while many new or revised figures and photographs (now in full color), study questions, and a glossary of key terms will be added. Despite the streamlining of the text, the new edition incorporates all the important new developments in plant physiology, especially in cell, molecular, and developmental biology.

The Third Edition's interactive Web component is keyed to textbook chapters and referenced from the book. It includes WebTopics (elaborating on selected topics discussed in the text), WebEssays (discussions of cutting-edge research topics, written by those who did the work), additional study questions (by chapter), additional references, and suggestions for further reading.

Book Info

Plant Physiology textbook covers the transport and translocation of water and solutes, biochemistry and metabolism, and growth and development. Twenty-three scientists contributed to the text.

Scanned with CamScanner

Chapter

8 Photosynthesis: Carbon Reactions

IN CHAPTER 5 WE DISCUSSED plants' requirements for mineral nutrients and light in order to grow and complete their life cycle. Because living organisms interact with one another and their environment, mineral nutrients cycle through the biosphere. These cycles involve complex interactions, and each cycle is critical in its own right. Because the amount of matter in the biosphere remains constant, energy must be supplied to keep the cycles operational. Otherwise increasing entropy dictates that the flow of matter would ultimately stop.

Autotrophic organisms have the ability to convert physical and chemical sources of energy into carbohydrates in the absence of organic substrates. Most of the external energy is consumed in transforming CO_2 to a reduced state that is compatible with the needs of the cell (—CHOH—).

Recent estimates indicate that about 200 billion tons of CO_2 are converted to biomass each year. About 40% of this mass originates from the activities of marine phytoplankton. The bulk of the carbon is incorporated into organic compounds by the carbon reduction reactions associated with photosynthesis.

In Chapter 7 we saw how the photochemical oxidation of water to molecular oxygen is coupled to the generation of ATP and reduced pyridine nucleotide (NADPH) by reactions taking place in the chloroplast thylakoid membrane. The reactions catalyzing the reduction of CO_2 to carbohydrate are coupled to the consumption of NADPH and ATP by enzymes found in the stroma, the soluble phase of chloroplasts.

These stroma reactions were long thought to be independent of light and, as a consequence, were referred to as the *dark reactions*. However, because these stroma-localized reactions depend on the products of the photochemical processes, and are also directly regulated by light, they are more properly referred to as the *carbon reactions of photosynthesis*.

In this chapter we will examine the cyclic reactions that accomplish fixation and reduction of CO_2, then consider how the phenomenon of photorespiration catalyzed by the carboxylating enzyme alters the effi-

Scanned with CamScanner

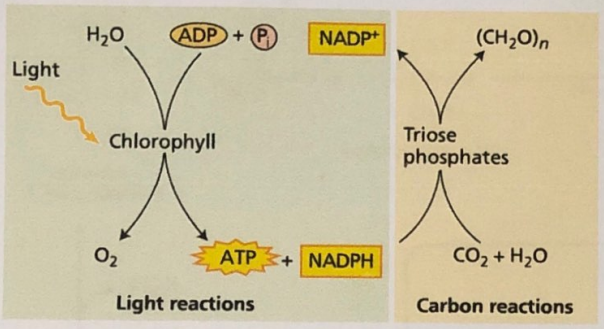


FIGURE 8.1 The light and carbon reactions of photosynthesis. Light is required for the generation of ATP and NADPH. The ATP and NADPH are consumed by the carbon reactions, which reduce CO_2 to carbohydrate (triose phosphates).

ciency of photosynthesis. This chapter will also describe biochemical mechanisms for concentrating carbon dioxide that allow plants to mitigate the impact of photorespiration: CO_2 pumps, C_4 metabolism, and crassulacean acid metabolism (CAM). We will close the chapter with a consideration of the synthesis of sucrose and starch.

THE CALVIN CYCLE

All photosynthetic eukaryotes, from the most primitive alga to the most advanced angiosperm, reduce CO_2 to carbohydrate via the same basic mechanism: the photosynthetic carbon reduction cycle originally described for C_3 species (the **Calvin cycle**, or **reductive pentose phosphate [RPP] cycle**). Other metabolic pathways associated with the photosynthetic fixation of CO_2, such as the C_4 photosynthetic carbon assimilation cycle and the photorespiratory carbon oxidation cycle, are either auxiliary to or dependent on the basic Calvin cycle.

In this section we will examine how CO_2 is fixed by the Calvin cycle through the use of ATP and NADPH generated by the light reactions (Figure 8.1), and how the Calvin cycle is regulated.

The Calvin Cycle Has Three Stages: Carboxylation, Reduction, and Regeneration

The Calvin cycle was elucidated as a result of a series of elegant experiments by Melvin Calvin and his colleagues in the 1950s, for which a Nobel Prize was awarded in 1961 (see **Web Topic 8.1**). In the Calvin cycle, CO_2 and water from the environment are enzymatically combined with a five-carbon acceptor molecule to generate two molecules of a three-carbon intermediate. This intermediate (3-phosphoglycerate) is reduced to carbohydrate by use of the ATP and NADPH generated photochemically. The cycle is completed by regeneration of the five-carbon acceptor (ribulose-1,5-bisphosphate, abbreviated RuBP).

The Calvin cycle proceeds in three stages (Figure 8.2):

1. *Carboxylation* of the CO_2 acceptor ribulose-1,5-bisphosphate, forming two molecules of 3-phosphoglycerate, the first stable intermediate of the Calvin cycle
2. *Reduction* of 3-phosphoglycerate, forming gyceraldehyde-3-phosphate, a carbohydrate
3. *Regeneration* of the CO_2 acceptor ribulose-1,5-bisphosphate from glyceraldehyde-3-phosphate

The carbon in CO_2 is the most oxidized form found in nature (+4). The carbon of the first stable intermediate, 3-phosphoglycerate, is more reduced (+3), and it is further reduced in the glyceraldehyde-3-phosphate product (+1). Overall, the early reactions of the Calvin cycle complete the reduction of atmospheric carbon and, in so doing, facilitate its incorporation into organic compounds.

The Carboxylation of Ribulose Bisphosphate Is Catalyzed by the Enzyme Rubisco

CO_2 enters the Calvin cycle by reacting with ribulose-1,5-bisphosphate to yield two molecules of 3-phosphoglycerate (Figure 8.3 and Table 8.1), a reaction catalyzed by the chloroplast enzyme ribulose bisphosphate carboxylase/oxygenase, referred to as **rubisco** (see **Web Topic 8.2**). As indi-

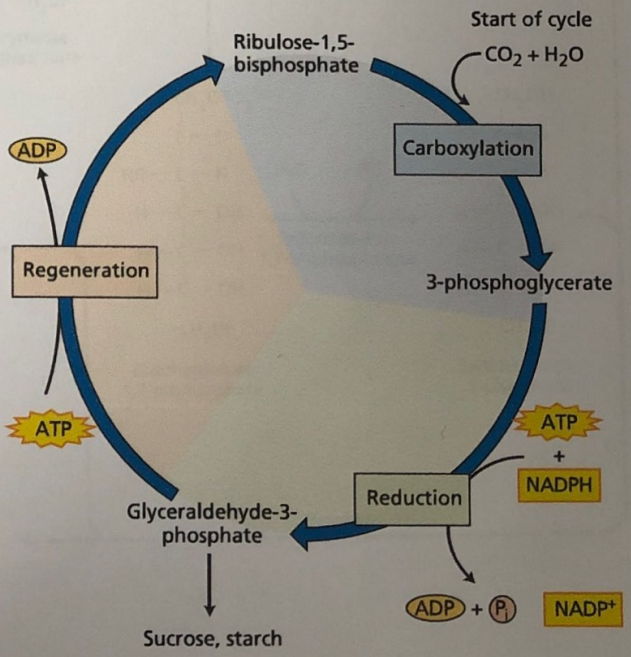


FIGURE 8.2 The Calvin cycle proceeds in three stages: (1) carboxylation, during which CO_2 is covalently linked to a carbon skeleton; (2) reduction, during which carbohydrate is formed at the expense of the photochemically derived ATP and reducing equivalents in the form of NADPH; and (3) regeneration, during which the CO_2 acceptor ribulose-1,5-bisphosphate re-forms.

Scanned with CamScanner

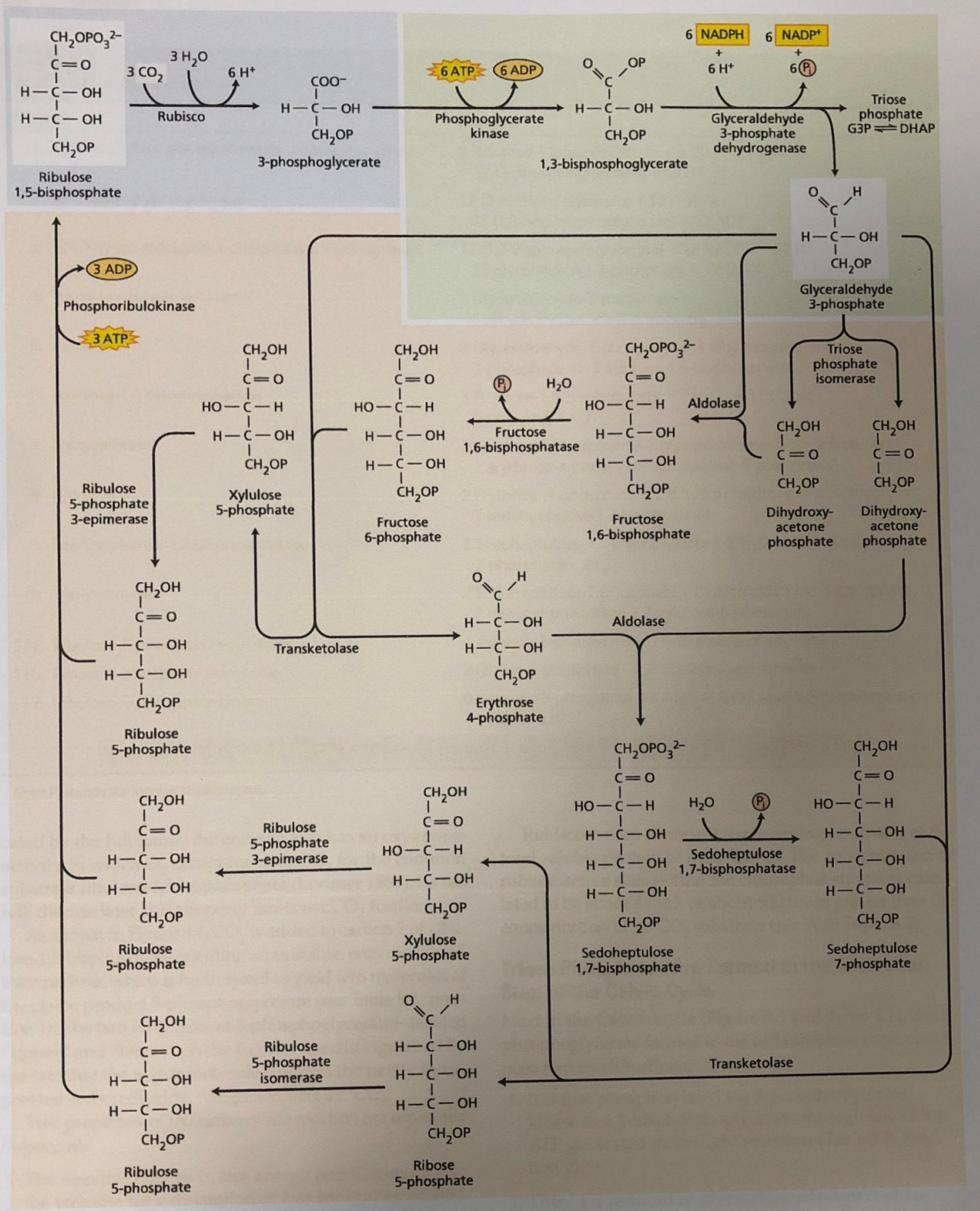


FIGURE 8.3 The Calvin cycle. The carboxylation of three molecules of ribulose-1,5-bisphosphate leads to the *net* synthesis of one molecule of glyceraldehyde-3-phosphate and the regeneration of the three molecules of starting material. This process starts and ends with three molecules of ribulose-1,5-bisphosphate, reflecting the cyclic nature of the pathway.

Scanned with CamScanner

TABLE 8.1
Reactions of the Calvin cycle

Enzyme	Reaction
1. Ribulose-1,5-bisphosphate carboxylase/oxygenase	6 Ribulose-1,5-bisphosphate + 6 CO_2 + 6 H_2O → 12 (3-phosphoglycerate) + 12 H^+
2. 3-Phosphoglycerate kinase	12 (3-Phosphoglycerate) + 12 ATP → 12 (1,3-bisphosphoglycerate) + 12 ADP
3. NADP:glyceraldehyde-3-phosphate dehydrogenase	12 (1,3-Bisphosphoglycerate) + 12 NADPH + 12 H^+ → 12 glyceraldehye-3-phosphate + 12 $NADP^+$ + 12 P_i
4. Triose phosphate isomerase	5 Glyceraldehyde-3-phosphate → 5 dihydroxyacetone-3-phosphate
5. Aldolase	3 Glyceraldehyde-3-phosphate + 3 dihydroxyacetone-3-phosphate → 3 fructose-1,6-bisphosphate
6. Fructose-1,6-bisphosphatase	3 Fructose-1,6-bisphosphate + 3 H_2O → 3 fructose-6-phosphate + 3 P_i
7. Transketolase	2 Fructose-6-phosphate + 2 glyceraldehyde-3-phosphate → 2 erythrose-4-phosphate + 2 xylulose-5-phosphate
8. Aldolase	2 Erythrose-4-phosphate + 2 dihydroxyacetone-3-phosphate → 2 sedoheptulose-1,7-bisphosphate
9. Sedoheptulose-1,7,bisphosphatase	2 Sedoheptulose-1,7-bisphosphate + 2 H_2O → 2 sedoheptulose-7-phosphate + 2 P_i
10. Transketolase	2 Sedoheptulose-7-phosphate + 2 glyceraldehyde-3-phosphate → 2 ribose-5-phosphate + 2 xylulose-5-phosphate
11a. Ribulose-5-phosphate epimerase	4 Xylulose-5-phosphate → 4 ribulose-5-phosphate
11b. Ribose-5-phosphate isomerase	2 Ribose-5-phosphate → 2 ribulose-5-phosphate
12. Ribulose-5-phosphate kinase	6 Ribulose-5-phosphate + 6 ATP → 6 ribulose-1,5-bisphosphate + 6 ADP + 6 H^+
	Net: 6 CO_2 + 11 H_2O + 12 NADPH + 18 ATP → Fructose-6-phosphate + 12 $NADP^+$ + 6 H^+ + 18 ADP + 17 P_i

Note: P_i stands for inorganic phosphate.

cated by the full name, the enzyme also has an oxygenase activity in which O_2 competes with CO_2 for the common substrate ribulose-1,5-bisphosphate (Lorimer 1983). As we will discuss later, this property limits net CO_2 fixation.

As shown in Figure 8.4, CO_2 is added to carbon 2 of ribulose-1,5-bisphosphate, yielding an unstable, enzyme-bound intermediate, which is hydrolyzed to yield two molecules of the stable product 3-phosphoglycerate (see Table 8.1, reaction 1). The two molecules of 3-phosphoglycerate—labeled "upper" and "lower" on the figure—are distinguished by the fact that the upper molecule contains the newly incorporated carbon dioxide, designated here as $*CO_2$.

Two properties of the carboxylase reaction are especially important:

1. The negative change in free energy (see Chapter 2 on the web site for a discussion of free energy) associated with the carboxylation of ribulose-1,5-bisphosphate is large; thus the forward reaction is strongly favored.
2. The affinity of rubisco for CO_2 is sufficiently high to ensure rapid carboxylation at the low concentrations of CO_2 found in photosynthetic cells.

Rubisco is very abundant, representing up to 40% of the total soluble protein of most leaves. The concentration of rubisco active sites within the chloroplast stroma is calculated to be about 4 m*M*, or about 500 times greater than the concentration of its CO_2 substrate (see **Web Topic 8.3**).

Triose Phosphates Are Formed in the Reduction Step of the Calvin Cycle

Next in the Calvin cycle (Figure 8.3 and Table 8.1), the 3-phosphoglycerate formed in the carboxylation stage undergoes two modifications:

1. It is first phosphorylated via 3-phosphoglycerate kinase to 1,3-bisphosphoglycerate through use of the ATP generated in the light reactions (Table 8.1, reaction 2).
2. Then it is reduced to glyceraldehyde-3-phosphate through use of the NADPH generated by the light reactions (Table 8.1, reaction 3). The chloroplast enzyme NADP:glyceraldehyde-3-phosphate dehydrogenase catalyzes this step. Note that the enzyme is similar to that of glycolysis (which will be dis-

Scanned with CamScanner

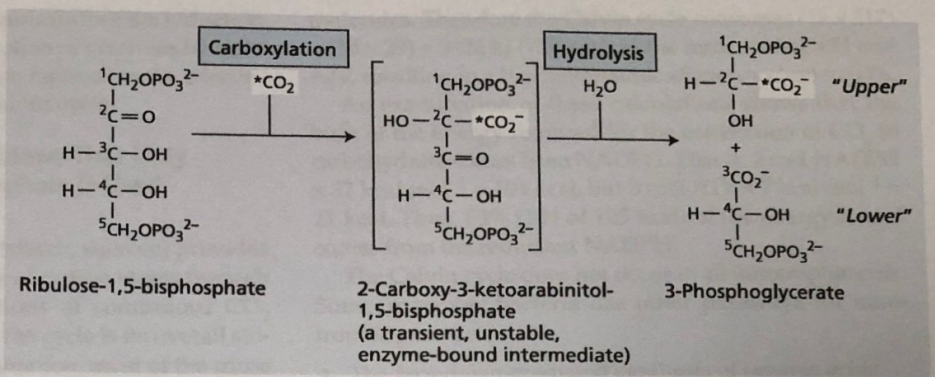


FIGURE 8.4 The carboxylation of ribulose-1,5-bisphosphate by rubisco.

cussed in Chapter 11), except that NADP rather than NAD is the coenzyme. An NADP-linked form of the enzyme is synthesized during chloroplast development (greening), and this form is preferentially used in biosynthetic reactions.

Operation of the Calvin Cycle Requires the Regeneration of Ribulose-1,5-Bisphosphate

The continued uptake of CO_2 requires that the CO_2 acceptor, ribulose-1,5-bisphosphate, be constantly regenerated. To prevent depletion of Calvin cycle intermediates, three molecules of ribulose-1,5-bisphosphate (15 carbons total) are formed by reactions that reshuffle the carbons from the five molecules of triose phosphate ($5 \times 3 = 15$ carbons). This reshuffling consists of reactions 4 through 12 in Table 8.1 (see also Figure 8.3):

1. One molecule of glyceraldehyde-3-phosphate is converted via triose phosphate isomerase to dihydroxyacetone-3-phosphate in an isomerization reaction (reaction 4).
2. Dihydroxyacetone-3-phosphate then undergoes aldol condensation with a second molecule of glyceraldehyde-3-phosphate, a reaction catalyzed by aldolase to give fructose-1,6-bisphosphate (reaction 5).
3. Fructose-1,6-bisphosphate occupies a key position in the cycle and is hydrolyzed to fructose-6-phosphate (reaction 6), which then reacts with the enzyme transketolase.
4. A two-carbon unit (C-1 and C-2 of fructose-6-phosphate) is transferred via transketolase to a third molecule of glyceraldehyde-3-phosphate to give erythrose-4-phosphate (from C-3 to C-6 of the fructose) and xylulose-5-phosphate (from C-2 of the fructose and the glyceraldehyde-3-phosphate) (reaction 7).
5. Erythrose-4-phosphate then combines via aldolase with a fourth molecule of triose phosphate (dihydroxyacetone-3-phosphate) to yield the seven-carbon sugar sedoheptulose-1,7-bisphosphate (reaction 8).
6. This seven-carbon bisphosphate is then hydrolyzed by way of a specific phosphatase to give sedoheptulose-7-phosphate (reaction 9).
7. Sedoheptulose-7-phosphate donates a two-carbon unit to the fifth (and last) molecule of glyceraldehyde-3-phosphate via transketolase and produces ribose-5-phosphate (from C-3 to C-7 of sedoheptulose) and xylulose-5-phosphate (from C-2 of the sedoheptulose and the glyceraldehyde-3-phosphate) (reaction 10).
8. The two molecules of xylulose-5-phosphate are converted to two molecules of ribulose-5-phosphate sugars by a ribulose-5-phosphate epimerase (reaction 11a). The third molecule of ribulose-5-phosphate is formed from ribose-5-phosphate by ribose-5-phosphate isomerase (reaction 11b).
9. Finally, ribulose-5-phosphate kinase catalyzes the phosphorylation of ribulose-5-phosphate with ATP, thus regenerating the three needed molecules of the initial CO_2 acceptor, ribulose-1,5-bisphosphate (reaction 12).

The Calvin Cycle Regenerates Its Own Biochemical Components

The Calvin cycle reactions regenerate the biochemical intermediates that are necessary to maintain the operation of the cycle. But more importantly, the rate of operation of the Calvin cycle can be enhanced by increases in the concentration of its intermediates; that is, the cycle is **autocatalytic**. As a consequence, the Calvin cycle has the metabolically desirable feature of producing more substrate than is consumed, as long as triose phosphate is not being diverted elsewhere:

$$5\ RuBP^{4-} + 5\ CO_2 + 9\ H_2O + 16\ ATP^{4-} + 10\ NADPH \rightarrow 6\ RuBP^{4-} + 14\ P_i + 6\ H^+ + 16\ ADP^{3-} + 10\ NADP^+$$

The importance of this autocatalytic property is shown by experiments in which previously darkened leaves or isolated chloroplasts are illuminated. In such experiments, CO_2 fixation starts only after a lag, called the *induction period*, and the rate of photosynthesis increases with time in the first few minutes after the onset of illumination. The

Scanned with CamScanner

increase in the rate of photosynthesis during the induction period is due in part to the activation of enzymes by light (discussed later), and in part to an increase in the concentration of intermediates of the Calvin cycle.

Calvin Cycle Stoichiometry Shows That Only One-Sixth of the Triose Phosphate Is Used for Sucrose or Starch

The synthesis of carbohydrates (starch, sucrose) provides a sink ensuring an adequate flow of carbon atoms through the Calvin cycle under conditions of continuous CO_2 uptake. An important feature of the cycle is its overall stoichiometry. At the onset of illumination, most of the triose phosphates are drawn back into the cycle to facilitate the buildup of an adequate concentration of metabolites. When photosynthesis reaches a steady state, however, five-sixths of the triose phosphate contributes to regeneration of the ribulose-1,5-bisphosphate, and one-sixth is exported to the cytosol for the synthesis of sucrose or other metabolites that are converted to starch in the chloroplast.

An input of energy, provided by ATP and NADPH, is required in order to keep the cycle functioning in the fixation of CO_2. The calculation at the end of Table 8.1 shows that in order to synthesize the equivalent of 1 molecule of hexose, 6 molecules of CO_2 are fixed at the expense of 18 ATP and 12 NADPH. In other words, the Calvin cycle consumes two molecules of NADPH and three molecules of ATP for every molecule of CO_2 fixed into carbohydrate.

We can compute the maximal overall thermodynamic efficiency of photosynthesis if we know the energy content of the light, the minimum quantum requirement (moles of quanta absorbed per mole of CO_2 fixed; see Chapter 7), and the energy stored in a mole of carbohydrate (hexose).

Red light at 680 nm contains 175 kJ (42 kcal) per quantum mole of photons. The minimum quantum requirement is usually calculated to be 8 photons per molecule of CO_2 fixed, although the number obtained experimentally is 9 to 10 (see Chapter 7). Therefore, the minimum light energy needed to reduce 6 moles of CO_2 to a mole of hexose is approximately $6 \times 8 \times 175$ kJ = 8400 kJ (2016 kcal). However, a mole of a hexose such as fructose yields only 2804 kJ (673 kcal) when totally oxidized.

Comparing 8400 and 2804 kJ, we see that the maximum overall thermodynamic efficiency of photosynthesis is about 33%. However, most of the unused light energy is lost in the generation of ATP and NADPH by the light reactions (see Chapter 7) rather than during operation of the Calvin cycle.

We can calculate the efficiency of the Calvin cycle more directly by computing the changes in free energy associated with the hydrolysis of ATP and the oxidation of NADPH, which are 29 and 217 kJ (7 and 52 kcal) per mole, respectively. We saw in the list summarizing the Calvin cycle reactions that the synthesis of 1 molecule of fructose-6-phosphate from 6 molecules of CO_2 uses 12 NADPH and 18 ATP molecules. Therefore the Calvin cycle consumes $(12 \times 217) + (18 \times 29) = 3126$ kJ (750 kcal) in the form of NADPH and ATP, resulting in a thermodynamic efficiency close to 90%.

An examination of these calculations shows that the bulk of the energy required for the conversion of CO_2 to carbohydrate comes from NADPH. That is, 2 mol NADPH $\times$ 52 kcal mol^{-1} = 104 kcal, but 3 mol ATP $\times$ 7 kcal mol^{-1} = 21 kcal. Thus, 83% (104 of 125 kcal) of the energy stored comes from the reductant NADPH.

The Calvin cycle does not occur in all autotrophic cells. Some anaerobic bacteria use other pathways for autotrophic growth:

- The ferredoxin-mediated synthesis of organic acids from acetyl– and succinyl– CoA derivatives via a reversal of the citric acid cycle (the reductive carboxylic acid cycle of green sulfur bacteria)
- The glyoxylate-producing cycle (the hydroxypropionate pathway of green nonsulfur bacteria)
- The linear route (acetyl-CoA pathway) of acetogenic, methanogenic bacteria

Thus although the Calvin cycle is quantitatively the most important pathway of autotrophic CO_2 fixation, others have been described.

REGULATION OF THE CALVIN CYCLE

The high energy efficiency of the Calvin cycle indicates that some form of regulation ensures that all intermediates in the cycle are present at adequate concentrations and that the cycle is turned off when it is not needed in the dark. In general, variation in the concentration or in the specific activity of enzymes modulates catalytic rates, thereby adjusting the level of metabolites in the cycle.

Changes in gene expression and protein biosynthesis regulate enzyme concentration. Posttranslational modification of proteins contributes to the regulation of enzyme activity. At the genetic level the amount of each enzyme present in the chloroplast stroma is regulated by mechanisms that control expression of the nuclear and chloroplast genomes (Maier et al. 1995; Purton 1995).

Short-term regulation of the Calvin cycle is achieved by several mechanisms that optimize the concentration of intermediates. These mechanisms minimize reactions operating in opposing directions, which would waste resources (Wolosiuk et al. 1993). Two general mechanisms can change the kinetic properties of enzymes:

1. The transformation of covalent bonds such as the reduction of disulfides and the carbamylation of amino groups, which generate a chemically modified enzyme.
2. The modification of noncovalent interactions, such as the binding of metabolites or changes in the composi-

Scanned with CamScanner

tion of the cellular milieu (e.g., pH). In addition, the binding of the enzymes to the thylakoid membranes enhances the efficiency of the Calvin cycle, thereby achieving a higher level of organization that favors the channeling and protection of substrates.

Light-Dependent Enzyme Activation Regulates the Calvin Cycle

Five light-regulated enzymes operate in the Calvin cycle:

1. Rubisco
2. NADP:glyceraldehyde-3-phosphate dehydrogenase
3. Fructose-1,6-bisphosphatase
4. Sedoheptulose-1,7-bisphosphatase
5. Ribulose-5-phosphate kinase

The last four enzymes contain one or more disulfide (—S—S—) groups. Light controls the activity of these four enzymes via the **ferredoxin–thioredoxin system**, a covalent thiol-based oxidation–reduction mechanism identified by Bob Buchanan and colleagues (Buchanan 1980; Wolosiuk et al. 1993; Besse and Buchanan 1997; Schürmann and Jacquot 2000). In the dark these residues exist in the oxidized state (—S—S—), which renders the enzyme inactive or subactive. In the light the —S—S— group is reduced to the sulfhydryl state (—SH HS—). This redox change leads to activation of the enzyme (Figure 8.5). The resolution of the crystal structure of each member of the ferredoxin–thioredoxin system and of the target enzymes fructose-1,6-bisphosphatase and NADP:malate dehydrogenase (Dai et al. 2000) have provided valuable information about the mechanisms involved.

This sulfhydryl (also called dithiol) signal of the regulatory protein thioredoxin is transmitted to specific target enzymes, resulting in their activation (see **Web Topic 8.4**). In some cases (such as fructose-1,6-bisphosphatase), the thioredoxin-linked activation is enhanced by an effector (e.g., fructose-1,6-bisphosphate substrate).

Inactivation of the target enzymes observed upon darkening appears to take place by a reversal of the reduction (activation) pathway. That is, oxygen converts the thioredoxin and target enzyme from the reduced state (—SH HS—) to the oxidized state (—S—S—) and, in so doing, leads to inactivation of the enzyme (see Figure 8.5; see also **Web Topic 8.4**). The last four of the enzymes listed here are regulated directly by thioredoxin; the first, rubisco, is regulated indirectly by a thioredoxin accessory enzyme, rubisco activase (see the next section).

Rubisco Activity Increases in the Light

The activity of rubisco is also regulated by light, but the enzyme itself does not respond to thioredoxin. George Lorimer and colleagues found that rubisco is activated when activator CO_2 (a different molecule from the substrate CO_2 that becomes fixed) reacts slowly with an uncharged ε-NH_2 group of lysine within the active site of the enzyme. The resulting carbamate derivative (a new anionic site) then rapidly binds Mg^{2+} to yield the activated complex (Figure 8.6).

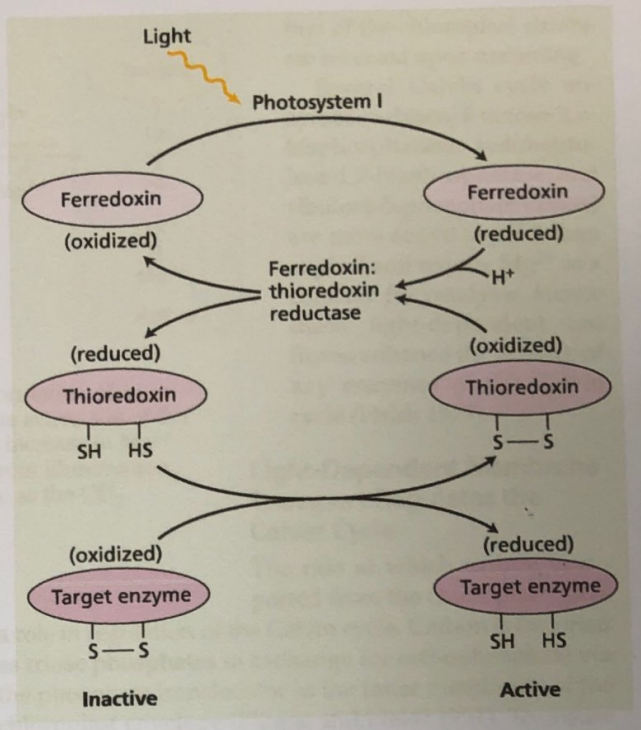


FIGURE 8.5 The ferredoxin–thioredoxin system reduces specific enzymes in the light. Upon reduction, biosynthetic enzymes are converted from an inactive to an active state. The activation process starts in the light by a reduction of ferredoxin by photosystem I (see Chapter 7). The reduced ferredoxin plus two protons are used to reduce a catalytically active disulfide (—S—S—) group of the iron–sulfur enzyme ferredoxin:thioredoxin reductase, which in turn reduces the highly specific disulfide (—S—S—) bond of the small regulatory protein thioredoxin (see Web Topic 8.4 for details). The reduced form (—SH HS—) of thioredoxin then reduces the critical disulfide bond (converts —S—S— to —SH HS—) of a target enzyme and thereby leads to activation of that enzyme. The light signal is thus converted to a sulfhydryl, or —SH, signal via ferredoxin and the enzyme ferredoxin:thioredoxin reductase.

Two protons are released during the formation of the ternary complex rubisco–CO_2–Mg^{2+}, so activation is promoted by an increase in both pH and Mg^{2+} concentration. Thus, light-dependent stromal changes in pH and Mg^{2+} (see the next section) appear to facilitate the observed activation of rubisco by light.

In the active state, rubisco binds another molecule of CO_2, which reacts with the 2,3-enediol form of ribulose-1,5-bisphosphate (P—O—CH_2—COH=COH—CHOH—CH_2O—P) yielding 2-carboxy-3-ketoribitol 1,5-bisphos-

Scanned with CamScanner

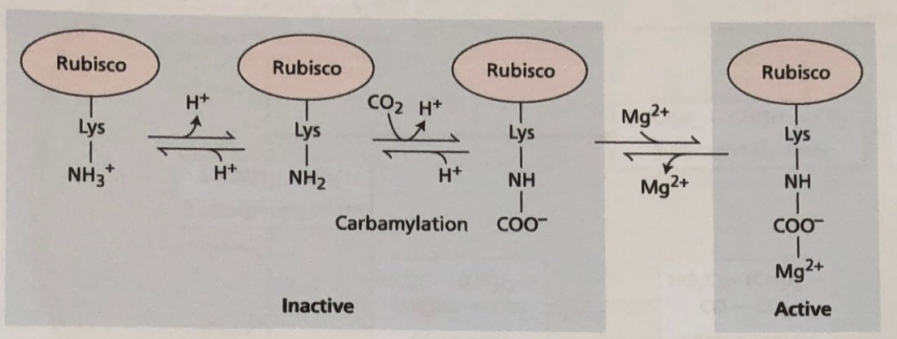


FIGURE 8.6 One way in which rubisco is activated involves the formation of a carbamate–Mg^{2+} complex on the ε-amino group of a lysine within the active site of the enzyme. Two protons are released. Activation is enhanced by the increase in Mg^{2+} concentration and higher pH (low H^+ concentration) that result from illumination. The CO_2 involved in the carbamate–Mg^{2+} reaction is not the same as the CO_2 involved in the carboxylation of ribulose-1,5-bisphosphate.

phate. The extreme instability of the latter intermediate leads to the cleavage of the bond that links carbons 2 and 3 of ribulose-1,5-bisphosphate, and as a consequence, rubisco releases two molecules of 3-phosphoglycerate.

The binding of sugar phosphates, such as ribulose-1,5-bisphosphate, to rubisco prevents carbamylation. The sugar phosphates can be removed by the enzyme rubisco activase, in a reaction that requires ATP. The primary role of rubisco activase is to accelerate the release of bound sugar phosphates, thus preparing rubisco for carbamylation (Salvucci and Ogren 1996, see also **Web Topic 8.5**).

Rubisco is also regulated by a natural sugar phosphate, carboxyarabinitol-1-phosphate, that closely resembles the six-carbon transition intermediate of the carboxylation reaction. This inhibitor is present at low concentrations in leaves of many species and at high concentrations in leaves of legumes such as soybean and bean. Carboxyarabinitol-1-phosphate binds to rubisco at night, and it is removed by the action of rubisco activase in the morning, when photon flux density increases.

Recent work has shown that in some plants rubisco activase is regulated by the ferredoxin–thioredoxin system (Zhang and Portis 1999). In addition to connecting thioredoxin to all five regulatory enzymes of the Calvin cycle, this finding provides a new mechanism for linking light to the regulation of enzyme activity.

Light-Dependent Ion Movements Regulate Calvin Cycle Enzymes

Light causes reversible ion changes in the stroma that influence the activity of rubisco and other chloroplast enzymes. Upon illumination, protons are pumped from the stroma into the lumen of the thylakoids. The proton efflux is coupled to Mg^{2+} uptake into the stroma. These ion fluxes decrease the stromal concentration of H^+ (pH 7 → 8) and increase that of Mg^{2+}. These changes in the ionic composition of the chloroplast stroma are reversed upon darkening.

Several Calvin cycle enzymes (rubisco, fructose-1,6-bisphosphatase, sedoheptulose-1,7-bisphosphatase, and ribulose-5-phosphate kinase) are more active at pH 8 than at pH 7 and require Mg^{2+} as a cofactor for catalysis. Hence these light-dependent ion fluxes enhance the activity of key enzymes of the Calvin cycle (Heldt 1979).

Light-Dependent Membrane Transport Regulates the Calvin Cycle

The rate at which carbon is exported from the chloroplast plays a role in regulation of the Calvin cycle. Carbon is exported as triose phosphates in exchange for orthophosphate via the phosphate translocator in the inner membrane of the chloroplast envelope (Flügge and Heldt 1991). To ensure continued operation of the Calvin cycle, at least five-sixths of the triose phosphate must be recycled (see Table 8.1 and Figure 8.3). Thus, at most one-sixth can be exported for sucrose synthesis in the cytosol or diverted to starch synthesis within the chloroplast. The regulation of this aspect of photosynthetic carbon metabolism will be discussed further when the syntheses of sucrose and starch are considered in detail later in this chapter.

THE C_2 OXIDATIVE PHOTOSYNTHETIC CARBON CYCLE

An important property of rubisco is its ability to catalyze both the carboxylation and the oxygenation of RuBP. Oxygenation is the primary reaction in a process known as **photorespiration**. Because photosynthesis and photorespiration work in diametrically opposite directions, photorespiration results in loss of CO_2 from cells that are simultaneously fixing CO_2 by the Calvin cycle (Ogren 1984; Leegood et al. 1995).

In this section we will describe the C_2 oxidative photosynthetic carbon cycle—the reactions that result in the partial recovery of carbon lost through oxidation.

Photosynthetic CO_2 Fixation and Photorespiratory Oxygenation Are Competing Reactions

The incorporation of one molecule of O_2 into the 2,3-enediol isomer of ribulose-1,5-bisphosphate generates an unstable intermediate that rapidly splits into 2-phosphoglycolate and 3-phosphoglycerate (Figure 8.7 and Table 8.2, reaction 1). The ability to catalyze the oxygenation of ribulose-1,5-bisphosphate is a property of all rubiscos, regard-

Scanned with CamScanner

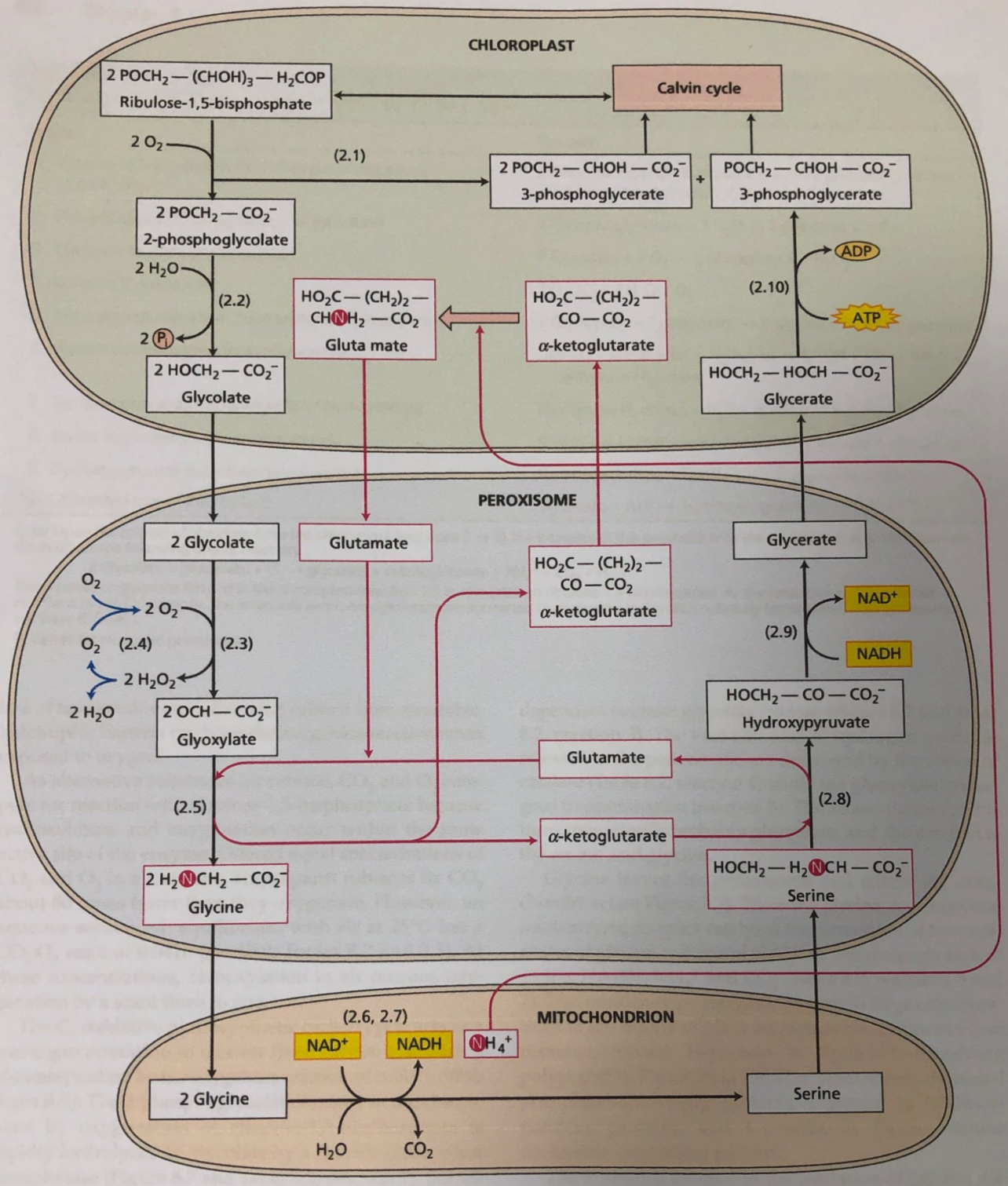


FIGURE 8.7 The main reactions of the photorespiratory cycle. Operation of the C_2 oxidative photosynthetic cycle involves the cooperative interaction among three organelles: chloroplasts, mitochondria, and peroxisomes. Two molecules of glycolate (four carbons) transported from the chloroplast into the peroxisome are converted to glycine, which in turn is exported to the mitochondrion and transformed to serine (three carbons) with the concurrent release of carbon dioxide (one carbon). Serine is transported to the peroxisome and transformed to glycerate. The latter flows to the chloroplast where it is phosphorylated to 3-phosphoglycerate and incorporated into the Calvin cycle. Inorganic nitrogen (ammonia) released by the mitochondrion is captured by the chloroplast for the incorporation into amino acids by using appropiate skeletons (α-ketoglutarate). The heavy arrow in red marks the assimilation of ammonia into glutamate catalyzed by glutamine synthetase. In addition, the uptake of oxygen in the peroxisome supports a short oxygen cycle coupled to oxidative reactions. The flow of carbon, nitrogen and oxygen are indicated in black, red and blue, respectively. See Table 8.2 for a description of each numbered reaction.

Scanned with CamScanner

TABLE 8.2
Reactions of the C_2 oxidative photosynthetic carbon cycle

Enzyme	Reaction
1. Ribulose-1,5-bisphosphate carboxylase/oxygenase (chloroplast)	2 Ribulose-1,5-bisphosphate + 2 O_2 → 2 phosphoglycolate + 2 3-phosphoglycerate + 4 H^+
2. Phosphoglycolate phosphatase (chloroplast)	2 Phosphoglycolate + 2 H_2O → 2 glycolate + 2 P_i
3. Glycolate oxidase (peroxisome)	2 Glycolate + 2 O_2 → 2 glyoxylate + 2 H_2O_2
4. Catalase (peroxisome)	2 H_2O_2 → 2 H_2O + O_2
5. Glyoxylate:glutamate aminotransferase (peroxisome)	2 Glyoxylate + 2 glutamate → 2 glycine + 2 α-ketoglutarate
6. Glycine decarboxylase (mitochondrion)	Glycine + NAD^+ + H^+ + H_4-folate → NADH + CO_2 + NH_4^+ + methylene-H_4-folate
7. Serine hydroxymethyltransferase (mitochondrion)	Methylene-H_4-folate + H_2O + glycine → serine + H_4-folate
8. Serine aminotransferase (peroxisome)	Serine + α-ketoglutarate → hydroxypyruvate + glutamate
9. Hydroxypyruvate reductase (peroxisome)	Hydroxypyruvate + NADH + H^+ → glycerate + NAD^+
10. Glycerate kinase (chloroplast)	Glycerate + ATP → 3-phosphoglycerate + ADP + H^+

Note: Upon the release of glycolate from the chloroplast (reactions 2 → 3), the interplay of this organelle with the peroxisome and the mitochondrion drives the following overall reaction:

2 Glycolate + glutamate + O_2 → glycerate + α-ketoglutarate + NH_4^+ + CO_2 + H_2O

The 3-phosphoglycerate formed in the chloroplast (reaction 10) is converted to ribulose-1,5-bisphosphate via the reductive and regenerative reactions of the Calvin cycle. The ammonia and α-ketoglutarate are converted to glutamate in the chloroplast by ferrodoxin-linked glutamate synthase (GOGAT).

P_i stands for inorganic phosphate.

less of taxonomic origin. Even the rubisco from anaerobic, autotrophic bacteria catalyzes the oxygenase reaction when exposed to oxygen.

As alternative substrates for rubisco, CO_2 and O_2 compete for reaction with ribulose-1,5-bisphosphate because carboxylation and oxygenation occur within the same active site of the enzyme. Offered equal concentrations of CO_2 and O_2 in a test tube, angiosperm rubiscos fix CO_2 about 80 times faster than they oxygenate. However, an aqueous solution in equilibrium with air at 25°C has a CO_2:O_2 ratio of 0.0416 (see **Web Topics 8.2 and 8.3**). At these concentrations, carboxylation in air outruns oxygenation by a scant three to one.

The C_2 oxidative photosynthetic carbon cycle acts as a scavenger operation to recover fixed carbon lost during photorespiration by the oxygenase reaction of rubisco (**Web Topic 8.6**). The 2-phosphoglycolate formed in the chloroplast by oxygenation of ribulose-1,5-bisphosphate is rapidly hydrolyzed to glycolate by a specific chloroplast phosphatase (Figure 8.7 and Table 8.2, reaction 2). Subsequent metabolism of the glycolate involves the cooperation of two other organelles: peroxisomes and mitochondria (see Chapter 1) (Tolbert 1981).

Glycolate leaves the chloroplast via a specific transporter protein in the envelope membrane and diffuses to the peroxisome. There it is oxidized to glyoxylate and hydrogen peroxide (H_2O_2) by a flavin mononucleotide-dependent oxidase: glycolate oxidase (Figure 8.7 and Table 8.2, reaction 3). The vast amounts of hydrogen peroxide released in the peroxisome are destroyed by the action of catalase (Table 8.2, reaction 4) while the glyoxylate undergoes transamination (reaction 5). The amino donor for this transamination is probably glutamate, and the product is the amino acid glycine.

Glycine leaves the peroxisome and enters the mitochondrion (see Figure 8.7). There the glycine decarboxylase multienzyme complex catalyzes the conversion of two molecules of glycine and one of NAD^+ to one molecule each of serine, NADH, NH_4^+ and CO_2 (Table 8.2, reactions 6 and 7). This multienzyme complex, present in large concentrations in the matrix of plant mitochondria, comprises four proteins, named H-protein (a lipoamide-containing polypeptide), P-protein (a 200 kDa, homodimer, pyridoxal phosphate-containing protein), T-protein (a folate-dependent protein), and L-protein (a flavin adenine nucleotide–containing protein).

The ammonia formed in the oxidation of glycine diffuses rapidly from the matrix of mitochondria to chloroplasts, where glutamine synthetase combines it with carbon skeletons to form amino acids. The newly formed serine leaves the mitochondria and enters the peroxisome, where it is converted first by transamination to hydroxypyruvate (Table 8.2, reaction 8) and then by an NADH-dependent reduction to glycerate (reaction 9).

Scanned with CamScanner

A malate-oxaloacetate shuttle transfers NADH from the cytoplasm into the peroxisome, thus maintaining an adequate concentration of NADH for this reaction. Finally, glycerate reenters the chloroplast, where it is phosphorylated to yield 3-phosphoglycerate (Table 8.2, reaction 10).

In photorespiration, various compounds are circulated in concert through two cycles. In one of the cycles, carbon exits the chloroplast in two molecules of glycolate and returns in one molecule of glycerate. In the other cycle, nitrogen exits the chloroplast in one molecule of glutamate and returns in one molecule of ammonia (together with one molecule of α-ketoglutarate) (see Figure 8.7).

Thus overall, two molecules of phosphoglycolate (four carbon atoms), lost from the Calvin cycle by the oxygenation of RuBP, are converted into one molecule of 3-phosphoglycerate (three carbon atoms) and one CO_2. In other words, 75% of the carbon lost by the oxygenation of ribulose-1,5-bisphosphate is recovered by the C_2 oxidative photosynthetic carbon cycle and returned to the Calvin cycle (Lorimer 1981).

On the other hand, the total organic nitrogen remains unchanged because the formation of inorganic nitrogen (NH_4^+) in the mitochondrion is balanced by the synthesis of glutamine in the chloroplast. Similarly, the use of NADH in the peroxisome (by hydroxypyruvate reductase) is balanced by the reduction of NAD^+ in the mitochondrion (by glycine decarboxylase).

Competition between Carboxylation and Oxygenation Decreases the Efficiency of Photosynthesis

Because photorespiration is concurrent with photosynthesis, it is difficult to measure the rate of photorespiration in intact cells. Two molecules of 2-phosphoglycolate (four carbon atoms) are needed to make one molecule of 3-phosphoglycerate, with the release of one molecule of CO_2; so theoretically one-fourth of the carbon entering the C_2 oxidative photosynthetic carbon cycle is released as CO_2.

Measurements of CO_2 release by sunflower leaves support this calculated value. This result indicates that the actual rate of photosynthesis is approximately 120 to 125% of the measured rate. The ratio of carboxylation to oxygenation in air at 25°C is computed to be between 2.5 and 3. Further calculations indicate that photorespiration lowers the efficiency of photosynthetic carbon fixation from 90% to approximately 50%.

This decreased efficiency can be measured as an increase in the quantum requirement for CO_2 fixation under photorespiratory conditions (air with high O_2 and low CO_2) as opposed to nonphotorespiratory conditions (low O_2 and high CO_2).

Carboxylation and Oxygenation Are Closely Interlocked in the Intact Leaf

Photosynthetic carbon metabolism in the intact leaf reflects the integrated balance between two mutually opposing and interlocking cycles (Figure 8.8). The Calvin cycle can operate independently, but the C_2 oxidative photosynthetic carbon cycle depends on the Calvin cycle for a supply of ribulose-1,5-bisphosphate. The balance between the two cycles is determined by three factors: the kinetic properties of rubisco, the concentrations of the substrates CO_2 and O_2, and temperature.

As the temperature increases, the concentration of CO_2 in a solution in equilibrium with air decreases more than the concentration of O_2 does (see **Web Topic 8.3**). Consequently, the concentration ratio of CO_2 to O_2 decreases as the temperature rises. As a result of this property, photorespiration (oxygenation) increases relative to photosynthesis (carboxylation) as the temperature rises. This effect is enhanced by the kinetic properties of rubisco, which also result in a relative increase in oxygenation at higher temperatures (Ku and Edwards 1978). Overall, then, increasing temperatures progressively tilt the balance away from the Calvin cycle and toward the oxidative photosynthetic carbon cycle (see Chapter 9).

The Biological Function of Photorespiration Is Unknown

Although the C_2 oxidative photosynthetic carbon cycle recovers 75% of the carbon originally lost from the Calvin cycle as 2-phosphoglycolate, why does 2-phosphoglycolate form at all? One possible explanation is that the formation

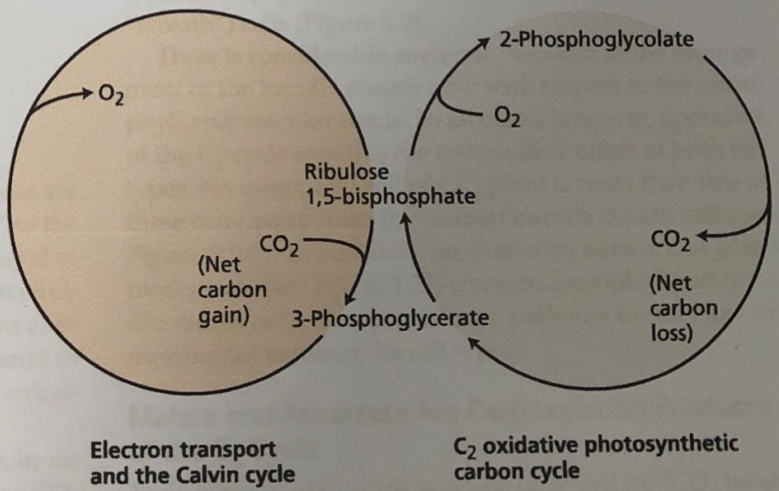


FIGURE 8.8 The flow of carbon in the leaf is determined by the balance between two mutually opposing cycles. Whereas the Calvin cycle is capable of independent operation in the presence of adequate substrates generated by photosynthetic electron transport, the C_2 oxidative photosynthetic carbon cycle requires continued operation of the Calvin cycle to regenerate its starting material, ribulose-1,5-bisphosphate.

Scanned with CamScanner

of 2-phosphoglycolate is a consequence of the chemistry of the carboxylation reaction, which requires an intermediate that can react with both CO_2 and O_2.

Such a reaction would have had little consequence in early evolutionary times if the ratio of CO_2 to O_2 in air were higher than it is today. However, the low CO_2:O_2 ratios prevalent in modern times are conducive to photorespiration, with no other function than the recovery of some of the carbon present in 2-phosphoglycolate.

Another possible explanation is that photorespiration is important, especially under conditions of high light intensity and low intercellular CO_2 concentration (e.g., when stomata are closed because of water stress), to dissipate excess ATP and reducing power from the light reactions, thus preventing damage to the photosynthetic apparatus. *Arabidopsis* mutants that are unable to photorespire grow normally under 2% CO_2, but they die rapidly if transferred to normal air. There is evidence from work with transgenic plants that photorespiration protects C_3 plants from photooxidation and photoinhibition (Kozaki and Takeba 1996). Further work is needed to improve our understanding of the function of photorespiration.

CO_2-CONCENTRATING MECHANISMS I: ALGAL AND CYANOBACTERIAL PUMPS

Many plants either do not photorespire at all, or they do so to only a limited extent. These plants have normal rubiscos, and their lack of photorespiration is a consequence of mechanisms that concentrate CO_2 in the rubisco environment and thereby suppress the oxygenation reaction.

In this and the two following sections we will discuss three mechanisms for concentrating CO_2 at the site of carboxylation:

1. C_4 photosynthetic carbon fixation (C_4)
2. Crassulacean acid metabolism (CAM)
3. CO_2 pumps at the plasma membrane

The first two of these CO_2-concentrating mechanisms are found in some angiosperms and involve "add-ons" to the Calvin cycle. Plants with C_4 metabolism are often found in hot environments; CAM plants are typical of desert environments. We will examine each of these two systems after we consider the third mechanism: a CO_2 pump found in aquatic plants that has been studied extensively in unicellular cyanobacteria and algae.

When algal and cyanobacterial cells are grown in air enriched with 5% CO_2 and then transferred to a low-CO_2 medium, they display symptoms typical of photorespiration (O_2 inhibition of photosynthesis at low concentration of CO_2). But if the cells are grown in air containing 0.03% CO_2, they rapidly develop the ability to concentrate inorganic carbon (CO_2 plus HCO_3^-) internally. Under these low-CO_2 conditions, the cells no longer photorespire.

At the concentrations of CO_2 found in aquatic environments, rubisco operates far below its maximal specific activity. Marine and freshwater organisms overcome this drawback by accumulating inorganic carbon by the use of CO_2 and HCO_3^- pumps at the plasma membrane. ATP derived from the light reactions provides the energy necessary for the active uptake of CO_2 and HCO_3^-. Total inorganic carbon inside some cyanobacterial cells can reach concentrations of 50 m*M* (Ogawa and Kaplan 1987). Recent work indicates that a single gene encoding a transcription factor can regulate the expression of genes that encode the components of the CO_2-concentrating mechanism in algae (Xiang et al. 2001).

The proteins that function as CO_2–HCO_3^- pumps are not present in cells grown in high concentrations of CO_2 but are induced upon exposure to low concentrations of CO_2. The accumulated HCO_3^- is converted to CO_2 by the enzyme carbonic anhydrase, and the CO_2 enters the Calvin cycle.

The metabolic consequence of this CO_2 enrichment is suppression of the oxygenation of ribulose bisphosphate and hence also suppression of photorespiration. The energetic cost of this adaptation is the additional ATP needed for concentrating the CO_2.

CO_2-CONCENTRATING MECHANISMS II: THE C_4 CARBON CYCLE

There are differences in leaf anatomy between plants that have a C_4 carbon cycle (called *C_4 plants*) and those that photosynthesize solely via the Calvin photosynthetic cycle (*C_3 plants*). A cross section of a typical C_3 leaf reveals one major cell type that has chloroplasts, the **mesophyll**. In contrast, a typical C_4 leaf has two distinct chloroplast-containing cell types: mesophyll and **bundle sheath** (or *Kranz*, German for "wreath") cells (Figure 8.9).

There is considerable anatomic variation in the arrangement of the bundle sheath cells with respect to the mesophyll and vascular tissue. In all cases, however, operation of the C_4 cycle requires the cooperative effort of both cell types. No mesophyll cell of a C_4 plant is more than two or three cells away from the nearest bundle sheath cell (see Figure 8.9A). In addition, an extensive network of plasmodesmata (see Figure 1.27) connects mesophyll and bundle sheath cells, thus providing a pathway for the flow of metabolites between the cell types.

Malate and Aspartate Are Carboxylation Products of the C_4 Cycle

Early labeling of C_4 acids was first observed in $^{14}CO_2$ labeling studies of sugarcane by H. P. Kortschack and colleagues and of maize by Y. Karpilov and coworkers. When leaves were exposed for a few seconds to $^{14}CO_2$ in the light, 70 to 80% of the label was found in the C_4 acids malate and aspartate—a pattern very different from the one observed in leaves that photosynthesize solely via the Calvin cycle.

Scanned with CamScanner

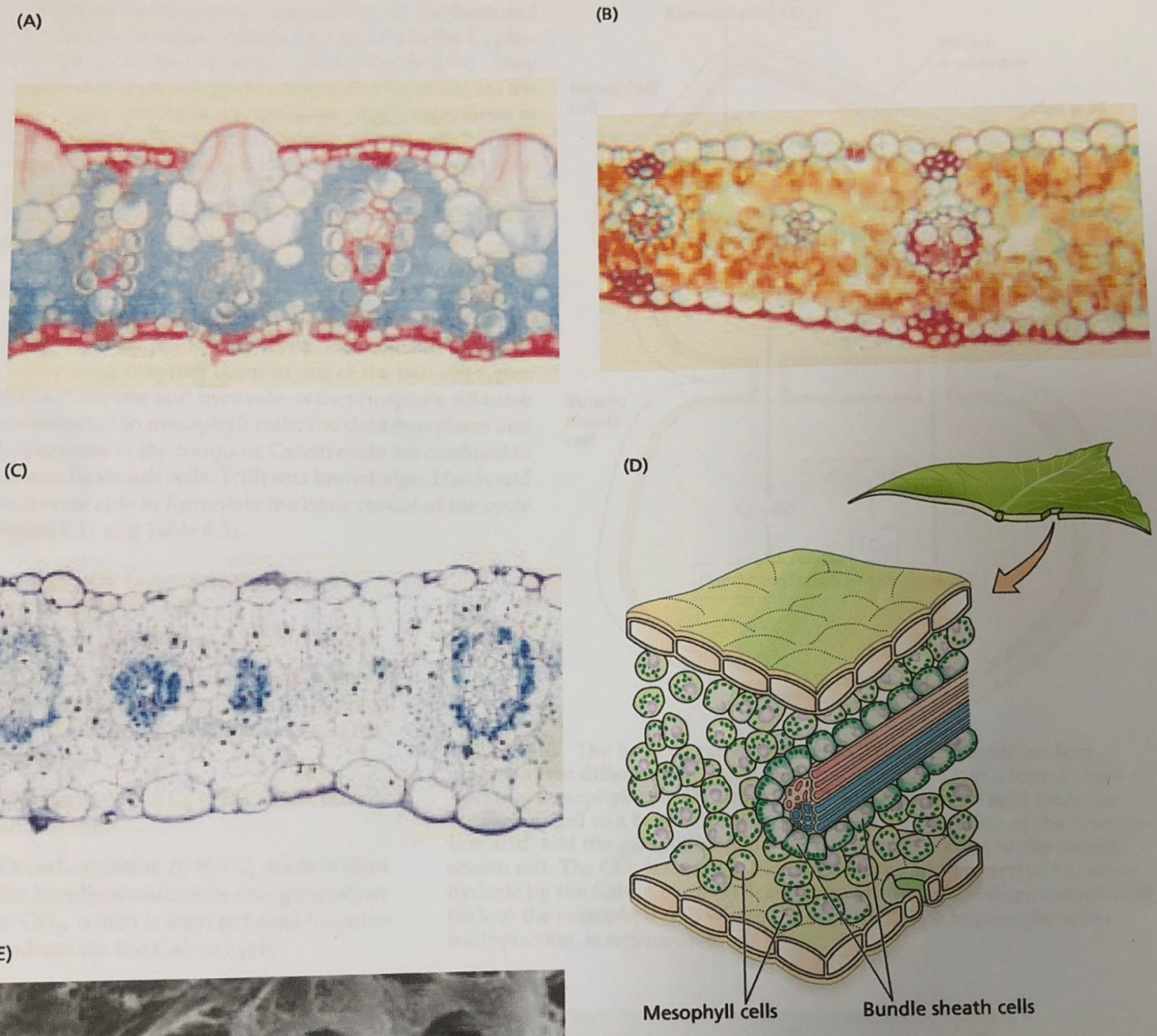


FIGURE 8.9 Cross-sections of leaves, showing the anatomic differences between C_3 and C_4 plants. (A) A C_4 monocot, *saccharum officinarum* (sugarcane). (135×) (B) A C_3 monocot, Poa sp. (a grass). (240×) (C) A C_4 dicot, *Flaveria australasica* (Asteraceae). (740×) The bundle sheath cells are large in C_4 leaves (A and C), and no mesophyll cell is more than two or three cells away from the nearest bundle sheath cell. These anatomic features are absent in the C_3 leaf (B). (D) Three-dimensional model of a C_4 leaf. (A and B © David Webb; C courtesy of Athena McKown; D after Lüttge and Higinbotham; E from Craig and Goodchild 1977.) (E) Scanning electon micrograph of a C_4 leaf from *Triodia irritans*, showing the plasmodesmata pits in the bundle sheath heath cell walls through which metabolites of the C_4 carbon cycle are thought to be transported.

Scanned with CamScanner

In pursuing these initial observations, M. D. Hatch and C. R. Slack elucidated what is now known as the C_4 photosynthetic carbon cycle (C_4 cycle) (Figure 8.10). They established that the C_4 acids malate and aspartate are the first stable, detectable intermediates of photosynthesis in leaves of sugarcane and that carbon atom 4 of malate subsequently becomes carbon atom 1 of 3-phosphoglycerate (Hatch and Slack 1966). The primary carboxylation in these leaves is catalyzed not by rubisco, but by PEP (phosphoenylpyruvate) carboxylase (Chollet et al. 1996).

The manner in which carbon is transferred from carbon atom 4 of malate to carbon atom 1 of 3-phosphoglycerate became clear when the involvement of mesophyll and bundle sheath cells was elucidated. The participating enzymes occur in one of the two cell types: PEP carboxylase and pyruvate–orthophosphate dikinase are restricted to mesophyll cells; the decarboxylases and the enzymes of the complete Calvin cycle are confined to the bundle sheath cells. With this knowledge, Hatch and Slack were able to formulate the basic model of the cycle (Figure 8.11 and Table 8.3).

The C_4 Cycle Concentrates CO_2 in Bundle Sheath Cells

The basic C_4 cycle consists of four stages:

1. Fixation of CO_2 by the carboxylation of phosphoenolpyruvate in the mesophyll cells to form a C_4 acid (malate and/or aspartate)
2. Transport of the C_4 acids to the bundle sheath cells
3. Decarboxylation of the C_4 acids within the bundle sheath cells and generation of CO_2, which is then reduced to carbohydrate via the Calvin cycle

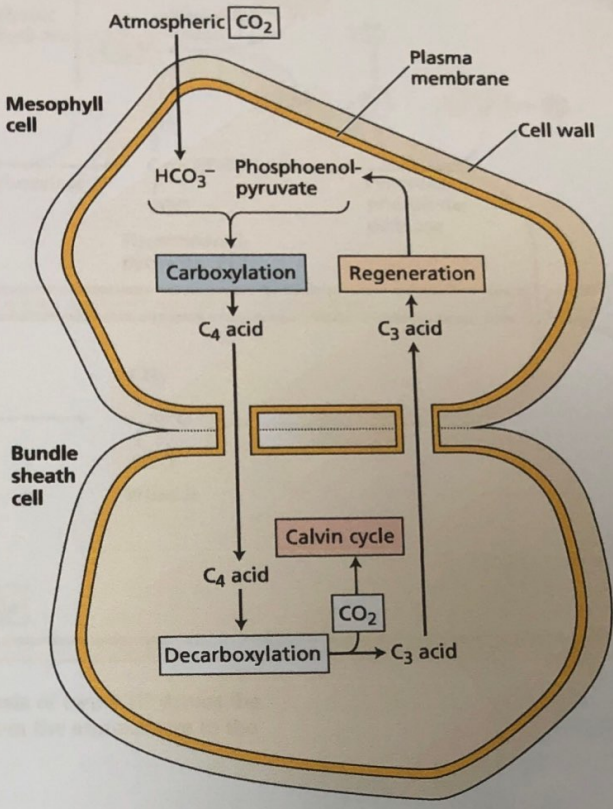


FIGURE 8.10 The basic C_4 photosynthetic carbon cycle involves four stages in two different cell types: (1) Fixation of CO_2 into a four-carbon acid in a mesophyll cell; (2) Transport of the four-carbon acid from the mesophyll cell to a bundle sheath cell; (3) Decarboxylation of the four-carbon acid, and the generation of a high CO_2 concentration in the bundle sheath cell. The CO_2 released is fixed by rubisco and converted to carbohydrate by the Calvin cycle.(4) Transport of the residual three-carbon acid back to the mesophyll cell, where the original CO_2 acceptor, phosphoenolpyruvate, is regenerated.

TABLE 8.3
Reactions of the C_4 photosynthetic carbon cycle

Enzyme	Reaction
1. Phosphoenolpyruvate (PEP) carboxylase	Phosphoenolpyruvate + HCO_3^- → oxaloacetate + P_i
2. NADP:malate dehydrogenase	Oxaloacetate + NADPH + H^+ → malate + $NADP^+$
3. Aspartate aminotransferase	Oxaloacetate + glutamate → aspartate + α-ketoglutarate
4. NAD(P) malic enzyme	Malate + $NAD(P)^+$ → pyruvate + CO_2 + NAD(P)H + H^+
5. Phosphoenolpyruvate carboxykinase	Oxaloacetate + ATP → phosphoenolpyruvate + CO_2 + ADP
6. Alanine aminotransferase	Pyruvate + glutamate ↔ alanine + α-ketoglutarate
7. Adenylate kinase	AMP + ATP → 2 ADP
8. Pyruvate–orthophosphate dikinase	Pyruvate + P_i + ATP → phosphoenolpyruvate + AMP + PP_i
9. Pyrophosphatase	PP_i + H_2O → 2 P_i

Note: P_i and PP_i stand for inorganic phosphate and pyrophosphate, respectively.

Scanned with CamScanner

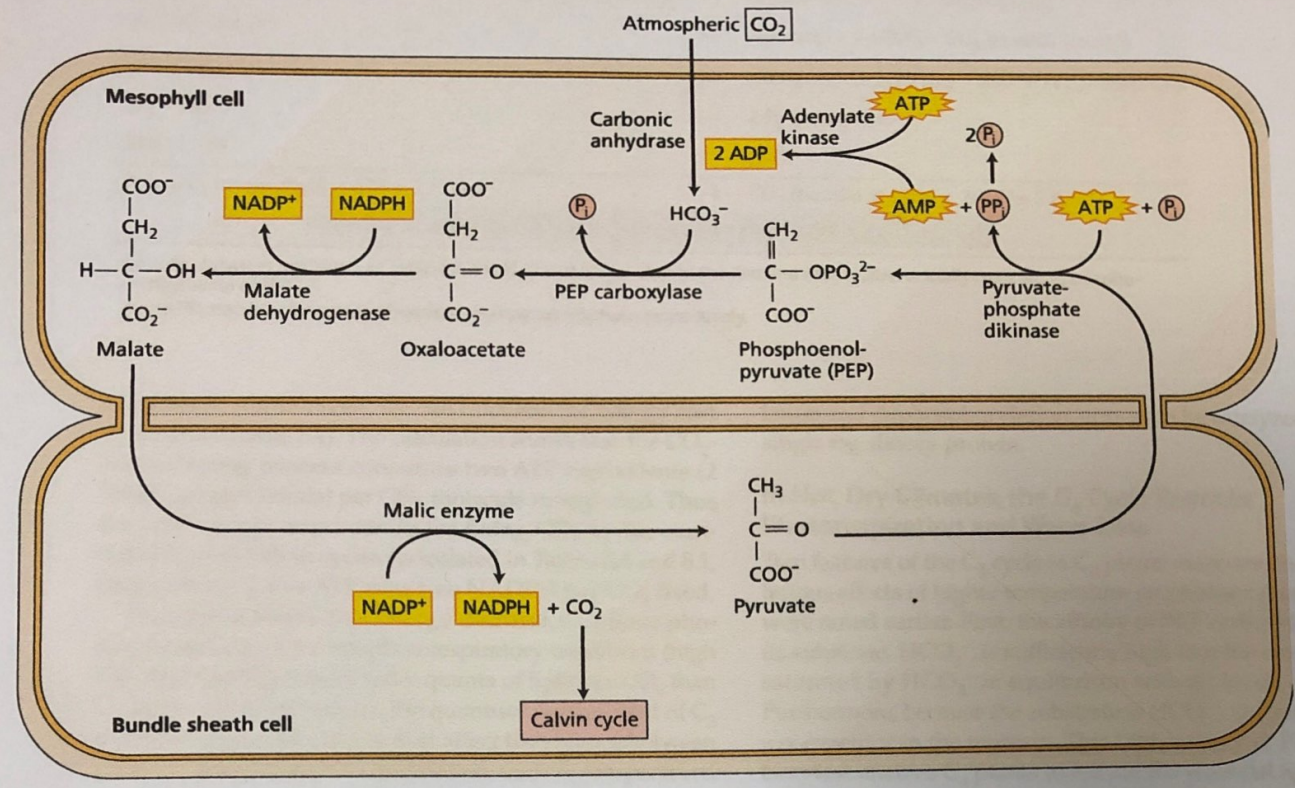


FIGURE 8.11 The C_4 photosynthetic pathway. The hydrolysis of two ATP drives the cycle in the direction of the arrows, thus pumping CO_2 from the atmosphere to the Calvin cycle of the chloroplasts from bundle sheath cells.

4. Transport of the C_3 acid (pyruvate or alanine) that is formed by the decarboxylation step back to the mesophyll cell and regeneration of the CO_2 acceptor phosphoenolpyruvate

One interesting feature of the cycle is that regeneration of the primary acceptor—phosphoenolpyruvate—consumes two "high-energy" phosphate bonds: one in the reaction catalyzed by pyruvate–orthophosphate dikinase (Table 8.3, reaction 8) and another in the conversion of PP_i to $2P_i$ catalyzed by pyrophosphatase (reaction 9; see also Figure 8.11).

Shuttling of metabolites between mesophyll and bundle sheath cells is driven by diffusion gradients along numerous plasmodesmata, and transport within the cells is regulated by concentration gradients and the operation of specialized translocators at the chloroplast envelope. The cycle thus effectively shuttles CO_2 from the atmosphere into the bundle sheath cells. This transport process generates a much higher concentration of CO_2 in the bundle sheath cells than would occur in equilibrium with the external atmosphere. This elevated concentration of CO_2 at the carboxylation site of rubisco results in suppression of the oxygenation of ribulose-1,5-bisphosphate and hence of photorespiration.

Discovered in the tropical grasses, sugarcane, and maize, the C_4 cycle is now known to occur in 16 families of both monocotyledons and dicotyledons, and it is particularly prominent in Gramineae (corn, millet, sorghum, sugarcane), Chenopodiaceae (*Atriplex*), and Cyperaceae (sedges). About 1% of all known species have C_4 metabolism (Edwards and Walker 1983).

There are three variations of the basic C_4 pathway that occur in different species (see **Web Topic 8.7**). The variations differ principally in the C_4 acid (malate or aspartate) transported into the bundle sheath cells and in the manner of decarboxylation.

The Concentration of CO_2 in Bundle Sheath Cells Has an Energy Cost

The net effect of the C_4 cycle is to convert a dilute solution of CO_2 in the mesophyll cells into a concentrated CO_2 solution in cells of the bundle sheath. Studies of a PEP carboxylase–deficient mutant of *Amaranthus edulis* clearly showed that the lack of an effective mechanism for concentrating CO_2 in the bundle sheath markedly enhances photorespiration in a C_4 plant (Dever et al. 1996).

Thermodynamics tells us that work must be done to establish and maintain the CO_2 concentration gradient in the bundle sheath (for a detailed discussion of theomodynamics, see Chapter 2 on the web site). This principle also applies to the operation of the C_4 cycle. From a summation

Scanned with CamScanner

TABLE 8.4
Energetics of the C_4 photosynthetic carbon cycle

Phosphoenolpyruvate + H_2O + NADPH + CO_2 (mesophyll)	→	malate + $NADP^+$ + P_i (mesophyll)
Malate + $NADP^+$	→	pyruvate + NADPH + CO_2 (bundle sheath)
Pyruvate + P_i + ATP	→	phosphoenolpyruvate + AMP + PP_i (mesophyll)
PP_i + H_2O	→	2 P_i (mesophyll)
AMP + ATP	→	2ADP
Net: CO_2 (mesophyll) + ATP + 2 H_2O	→	CO_2 (bundle sheath) + 2ADP + 2 P_i
Cost of concentrating CO_2 within the bundle sheath cell = 2 ATP per CO_2		

Note: As shown in reaction 1 of Table 8.3, the H_2O and CO_2 shown in the first line of this table actually react with phosphoenolpyruvate as HCO_3^-.
P_i and PP_i stand for inorganic phosphate and pyrophosphate, respectively.

of the reactions involved, we can calculate the energy cost to the plant (Table 8.4). The calculation shows that the CO_2-concentrating process consumes two ATP equivalents (2 "high-energy" bonds) per CO_2 molecule transported. Thus the total energy requirement for fixing CO_2 by the combined C_4 and Calvin cycles (calculated in Tables 8.4 and 8.1, respectively) is five ATP plus two NADPH per CO_2 fixed.

Because of this higher energy demand, C_4 plants photosynthesizing under nonphotorespiratory conditions (high CO_2 and low O_2) require more quanta of light per CO_2 than C_3 leaves do. In normal air, the quantum requirement of C_3 plants changes with factors that affect the balance between photosynthesis and photorespiration, such as temperature. By contrast, owing to the mechanisms built in to avoid photorespiration, the quantum requirement of C_4 plants remains relatively constant under different environmental conditions (see Figure 9.23).

Light Regulates the Activity of Key C_4 Enzymes

Light is essential for the operation of the C_4 cycle because it regulates several specific enzymes. For example, the activities of PEP carboxylase, NADP:malate dehydrogenase, and pyruvate–orthophosphate dikinase (see Table 8.3) are regulated in response to variations in photon flux density by two different processes: reduction–oxidation of thiol groups and phosphorylation–dephosphorylation.

NADP:malate dehydrogenase is regulated via the thioredoxin system of the chloroplast (see Figure 8.5). The enzyme is reduced (activated) upon illumination of leaves and is oxidized (inactivated) upon darkening. PEP carboxylase is activated by a light-dependent phosphorylation–dephosphorylation mechanism yet to be characterized.

The third regulatory member of the C_4 pathway, pyruvate–orthophosphate dikinase, is rapidly inactivated by an unusual ADP-dependent phosphorylation of the enzyme when the photon flux density drops (Burnell and Hatch 1985). Activation is accomplished by phosphorolytic cleavage of this phosphate group. Both reactions, phosphorylation and dephosphorylation, appear to be catalyzed by a single regulatory protein.

In Hot, Dry Climates, the C_4 Cycle Reduces Photorespiration and Water Loss

Two features of the C_4 cycle in C_4 plants overcome the deleterious effects of higher temperature on photosynthesis that were noted earlier. First, the affinity of PEP carboxylase for its substrate, HCO_3^-, is sufficiently high that the enzyme is saturated by HCO_3^- in equlibrium with air levels of CO_2. Furthermore, because the substrate is HCO_3^-, oxygen is not a competitor in the reaction. This high activity of PEP carboxylase enables C_4 plants to reduce the stomatal aperture and thereby conserve water while fixing CO_2 at rates equal to or greater than those of C_3 plants. The second beneficial feature is the suppression of photorespiration resulting from the concentration of CO_2 in bundle sheath cells (Marocco et al. 1998).

These features enable C_4 plants to photosynthesize more efficiently at high temperatures than C_3 plants, and they are probably the reason for the relative abundance of C_4 plants in drier, hotter climates. Depending on their natural environment, some plants show properties intermediate between strictly C_3 and C_4 species.

CO_2-CONCENTRATING MECHANISMS III: CRASSULACEAN ACID METABOLISM

A third mechanism for concentrating CO_2 at the site of rubisco is found in crassulacean acid metabolism (CAM). Despite its name, CAM is not restricted to the family Crassulaceae (*Crassula, Kalanchoe, Sedum*); it is found in numerous angiosperm families. Cacti and euphorbias are CAM plants, as well as pineapple, vanilla, and agave.

The CAM mechanism enables plants to improve water use efficiency. Typically, a CAM plant loses 50 to 100 g of water for every gram of CO_2 gained, compared with values of 250 to 300 g and 400 to 500 g for C_4 and C_3 plants,

Scanned with CamScanner

respectively (see Chapter 4). Thus, CAM plants have a competitive advantage in dry environments.

The CAM mechanism is similar in many respects to the C_4 cycle. In C_4 plants, formation of the C_4 acids in the mesophyll is spatially separated from decarboxylation of the C_4 acids and from refixation of the resulting CO_2 by the Calvin cycle in the bundle sheath. In CAM plants, formation of the C_4 acids is both temporally and spatially separated. At night, CO_2 is captured by PEP carboxylase in the cytosol, and the malate that forms from the oxaloacetate product is stored in the vacuole (Figure 8.12). During the day, the stored malate is transported to the chloroplast and decarboxylated by NADP-malic enzyme, the released CO_2 is fixed by the Calvin cycle, and the NADPH is used for converting the decarboxylated triose phosphate product to starch.

The Stomata of CAM Plants Open at Night and Close during the Day

CAM plants such as cacti achieve their high water use efficiency by opening their stomata during the cool, desert nights and closing them during the hot, dry days. Closing the stomata during the day minimizes water loss, but because H_2O and CO_2 share the same diffusion pathway, CO_2 must then be taken up at night.

CO_2 is incorporated via carboxylation of phosphoenolpyruvate to oxaloacetate, which is then reduced to malate. The malate accumulates and is stored in the large vacuoles that are a typical, but not obligatory, anatomic feature of the leaf cells of CAM plants (see Figure 8.12). The accumulation of substantial amounts of malic acid, equivalent to the amount of CO_2 assimilated at night, has long been recognized as a nocturnal acidification of the leaf (Bonner and Bonner 1948).

With the onset of day, the stomata close, preventing loss of water and further uptake of CO_2. The leaf cells deacidify as the reserves of vacuolar malic acid are consumed. Decarboxylation is usually achieved by the action of NADP-malic enzyme on malate (Drincovich et al. 2001). Because the stomata are closed, the internally released CO_2 cannot escape from the leaf and instead is fixed and converted to carbohydrate by the Calvin cycle.

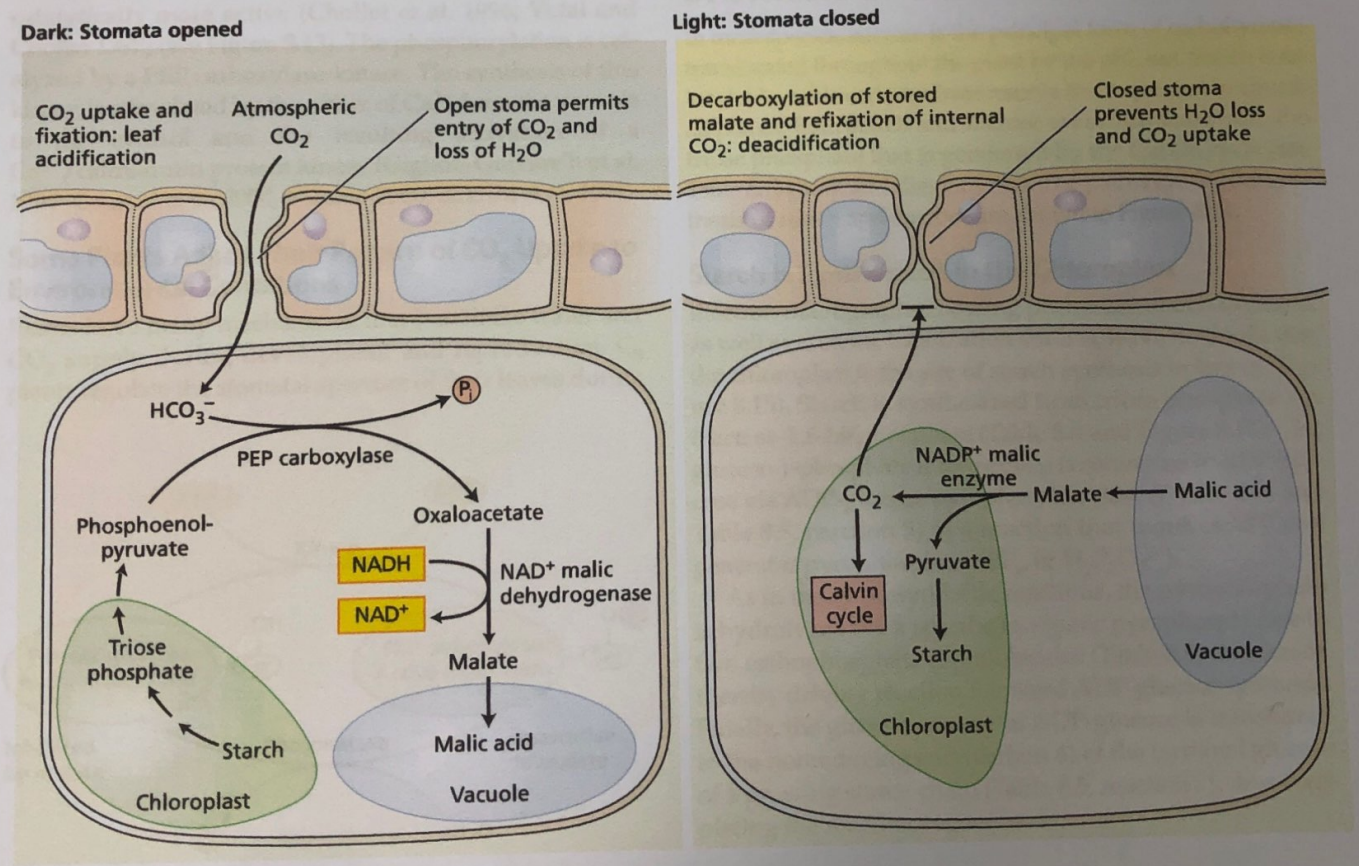


FIGURE 8.12 Crassulacean acid metabolism (CAM). Temporal separation of CO_2 uptake from photosynthetic reactions: CO_2 uptake and fixation take place at night, and decarboxylation and refixation of the internally released CO_2 occur during the day. The adaptive advantage of CAM is the reduction of water loss by transpiration, achieved by the stomatal opening during the night.

Scanned with CamScanner

The elevated internal concentration of CO_2 effectively suppresses the photorespiratory oxygenation of ribulose bisphosphate and favors carboxylation. The C_3 acid resulting from the decarboxylation is thought to be converted first to triose phosphate and then to starch or sucrose, thus regenerating the source of the original carbon acceptor.

Phosphorylation Regulates the Activity of PEP Carboxylase in C_4 and CAM Plants

The CAM mechanism that we have outlined in this discussion requires separation of the initial carboxylation from the subsequent decarboxylation, to avoid a futile cycle. In addition to the spatial and temporal separation exhibited by C_4 and CAM plants, respectively, a futile cycle is avoided by the regulation of PEP carboxylase (Figure 8.13). In C_4 plants the carboxylase is "switched on," or active, during the day and in CAM plants during the night. In both C_4 and CAM plants, PEP carboxylase is inhibited by malate and activated by glucose-6-phosphate (see **Web Essay 8.1** for a detailed discussion of the regulation of PEP carboxylase).

Phosphorylation of a single serine residue of the CAM enzyme diminishes the malate inhibition and enhances the action of glucose-6-phosphate so that the enzyme becomes catalytically more active (Chollet et al. 1996; Vidal and Chollet 1997) (see Figure 8.13). The phosphorylation is catalyzed by a PEP carboxylase-kinase. The synthesis of this kinase is stimulated by the efflux of Ca^{2+} from the vacuole to the cytosol and the resulting activation of a Ca^{2+}/calmodulin protein kinase (Giglioli-Guivarc'h et al. 1996; Coursol et al. 2000; Nimmo 2000; Bakrim et al. 2001).

Some Plants Adjust Their Pattern of CO_2 Uptake to Environmental Conditions

Plants have many mechanisms that maximize water and CO_2 supply during development and reproduction. C_3 plants regulate the stomatal aperture of their leaves during the day, and stomata close during the night. C_4 and CAM plants utilize PEP carboxylase to fix CO_2, and they separate that enzyme from rubisco either spatially (C_4 plants) or temporally (CAM plants).

Some CAM plants show longer-term regulation and are able to adjust their pattern of CO_2 uptake to environmental conditions. Facultative CAM plants such as the ice plant (*Mesembryanthemum crystallinum*) carry on C_3 metabolism under unstressed conditions, and they shift to CAM in response to heat, water, or salt stress. This form of regulation requires the expression of numerous CAM genes in response to stress signals (Adams et al. 1998; Cushman 2001).

In aquatic environments, cyanobacteria and green algae have abundant water but find low CO_2 concentrations in their surroundings and actively concentrate inorganic CO_2 intracellularly. In diatoms, which abound in the phytoplankton, a CO_2-concentrating mechanism operates simultaneously with a C_4 pathway (Reinfelder et al. 2000). Diatoms are a fine example of photosynthetic organisms that have the capacity to use different CO_2-concentrating mechanisms in response to environmental fluctuations.

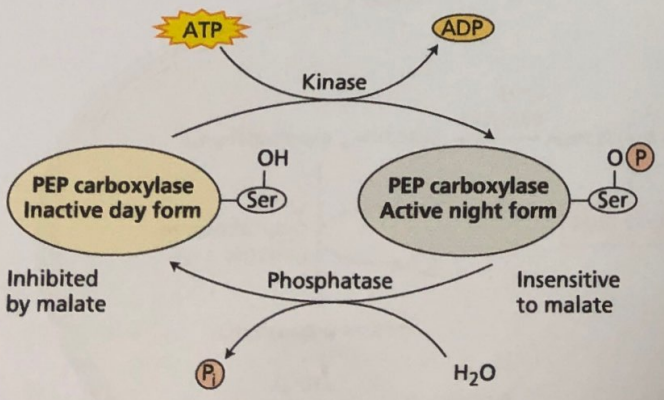


FIGURE 8.13 Diurnal regulation of CAM phosphoenolpyruvate (PEP) carboxylase. Phosphorylation of the serine residue (Ser-OP) yields a form of the enzyme which is active during the night and relatively insensitive to malate. During the day, dephosphorylation of the serine (Ser-OH) gives a form of the enzyme which is inhibited by malate.

SYNTHESIS OF STARCH AND SUCROSE

In most species, sucrose is the principal form of carbohydrate translocated throughout the plant by the phloem. Starch is an insoluble stable carbohydrate reserve that is present in almost all plants. Both starch and sucrose are synthesized from the triose phosphate that is generated by the Calvin cycle (see Table 8.1) (Beck and Ziegler 1989). The pathways for the synthesis of starch and sucrose are shown in Figure 8.14.

Starch Is Synthesized in the Chloroplast

Electron micrographs showing prominent starch deposits, as well as enzyme localization studies, leave no doubt that the chloroplast is the site of starch synthesis in leaves (Figure 8.15). Starch is synthesized from triose phosphate via fructose-1,6-bisphosphate (Table 8.5 and Figure 8.14). The glucose-1-phosphate intermediate is converted to ADP-glucose via ADP-glucose pyrophosphorylase (Figure 8.14 and Table 8.5, reaction 5) in a reaction that requires ATP and generates pyrophosphate (PP_i, or $H_2P_2O_7^{2-}$).

As in many biosynthetic reactions, the pyrophosphate is hydrolyzed via a specific inorganic pyrophosphatase to two orthophosphate (P_i) molecules (Table 8.5, reaction 6), thereby driving reaction 5 toward ADP-glucose synthesis. Finally, the glucose moiety of ADP-glucose is transferred to the nonreducing end (carbon 4) of the terminal glucose of a growing starch chain (Table 8.5, reaction 7), thus completing the reaction sequence.

Sucrose Is Synthesized in the Cytosol

The site of sucrose synthesis has been studied by cell fractionation, in which the organelles are isolated and separated from one another. Enzyme analyses have shown that sucrose is synthesized in the cytosol from triose phosphates

Scanned with CamScanner

Scanned with CamScanner

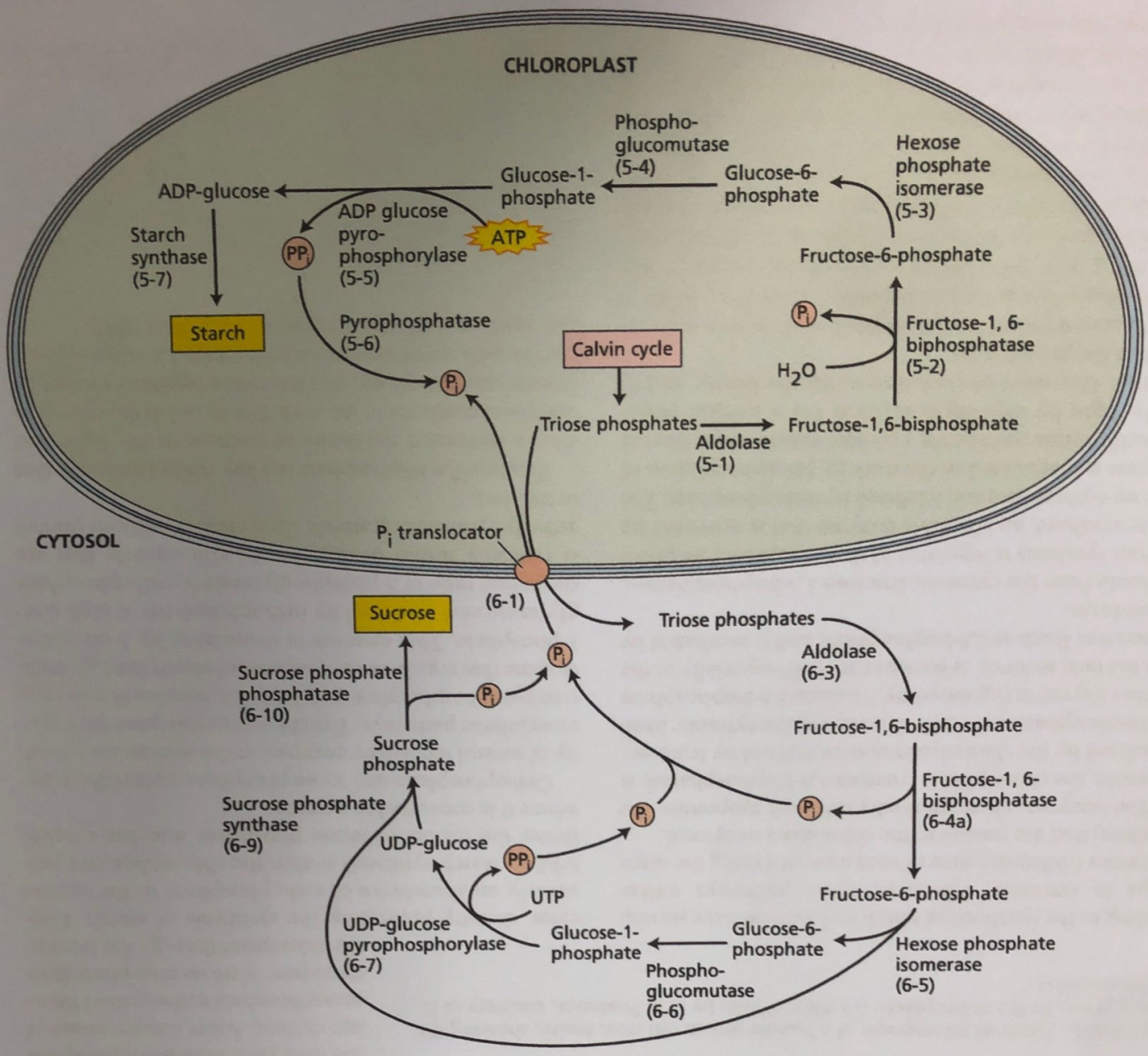


FIGURE 8.14 The syntheses of starch and sucrose are competing processes that occur in the chloroplast and the cytosol, respectively. When the cytosolic P_i concentration is high, chloroplast triose phosphate is exported to the cytosol via the P_i in exchange for P_i, and sucrose is synthesized. When the cytosolic P_i concentration is low, triose phosphate is retained within the chloroplast, and starch is synthesized. The numbers facing the arrows are keyed to Tables 8.5 and 8.6.

by a pathway similar to that of starch—that is, by way of fructose-1,6-bisphosphate and glucose-1-phosphate (Figure 8.14 and Table 8.6, reactions 2–6).

In sucrose synthesis, the glucose-1-phosphate is converted to UDP-glucose via a specific UDP-glucose pyrophosphorylase (Table 8.6, reaction 7) that is analogous to the ADP-glucose pyrophosphorylase of chloroplasts. At this stage, two consecutive reactions complete the synthesis of sucrose (Huber and Huber 1996). First, sucrose-6-phosphate synthase catalyzes the reaction of UDP-glucose with fructose-6-phosphate to yield sucrose-6-phosphate and UDP (Table 8.6, reaction 9). Second, the sucrose-6-phosphate phosphatase (phosphohydrolase) cleaves the phosphate from sucrose-6-phosphate, yielding sucrose (Table 8.6, reaction 10). The latter reaction, which is essentially irreversible, pulls the former in the direction of sucrose synthesis.

As in starch synthesis, the pyrophosphate formed in the reaction catalyzed by UDP-glucose pyrophosphorylase (Table 8.6, reaction 7) is hydrolyzed, but not immediately as in the chloroplasts. Because of the absence of an inorganic pyrophosphatase, the pyrophosphate can be used by other enzymes, in transphosphorylation reactions. One example is fructose-6-phosphate phosphotransferase, an enzyme that catalyzes a reaction like the one catalyzed by phosphofructokinase (Table 8.6, reaction 4a) except that pyrophosphate replaces ATP as the phosphoryl donor.

A comparison of the reactions in Tables 8.5 and 8.6 (as illustrated in Figure 8.14) reveals that the conversion of triose phosphates to glucose-1-phosphate in the pathways

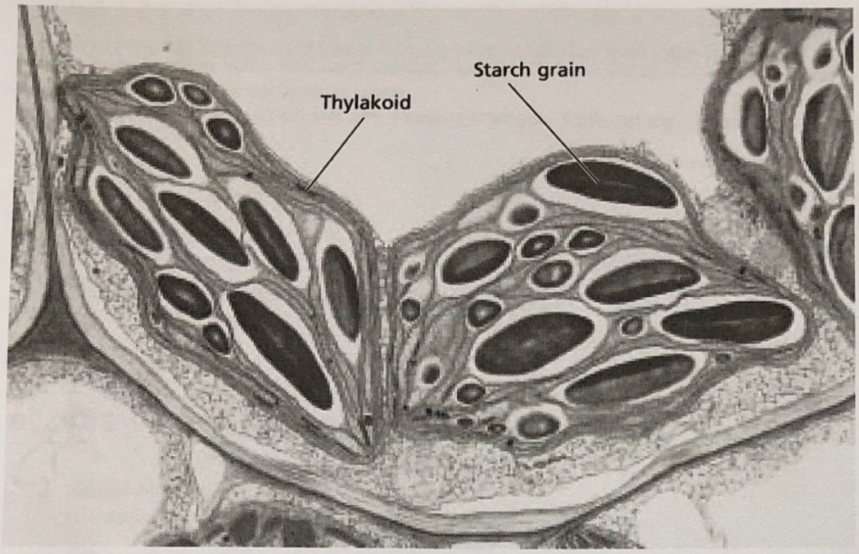


FIGURE 8.15 Electron micrograph of a bundle sheath cell from maize, showing the starch grains in the chloroplasts. (15,800×) (Photo by S. E. Frederick, courtesy of E. H. Newcomb.)

leading to the synthesis of starch and sucrose have several steps in common. However, these pathways utilize isozymes (different forms of enzymes catalyzing the same reaction) that are unique to the chloroplast or cytosol.

The isozymes show markedly different properties. For example, the chloroplastic fructose-1,6-bisphosphatase is regulated by the thioredoxin system but not by fructose-2,6-bisphosphate and AMP. Conversely, the cytosolic form of the enzyme is regulated by fructose-2,6-bisphosphate (see the next section), is sensitive to AMP especially in the presence of fructose-2,6-bisphosphate, and is unaffected by thioredoxin.

Aside from the cytosolic fructose-1,6-bisphosphatase, sucrose synthesis is regulated at the level of sucrose phosphate synthase, an allosteric enzyme that is activated by glucose-6-phosphate and inhibited by orthophosphate. The enzyme is inactivated in the dark by phosphorylation of a specific serine residue via a protein kinase and activated in the light by dephosphorylation via a protein phosphatase. Glucose-6-phosphate inhibits the kinase, and P_i inhibits the phosphatase.

The recent purification and cloning of sucrose-6-phosphate phosphatase from rice leaves (Lund et al. 2000) is providing new information on the molecular and functional properties of this enzyme. These studies indicate that sucrose-6-phosphate synthase and sucrose-6-phosphatase exist as a supramolecular complex showing an enzymatic activity that is higher than that of the isolated constituent enzymes (Salerno et al. 1996). This noncovalent interaction of the two enzymes involved in the last two steps of sucrose synthesis points to a novel regulatory feature of carbohydrate metabolism in plants.

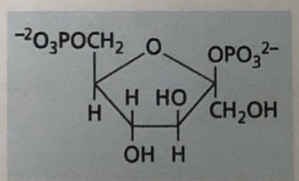
The Syntheses of Sucrose and Starch Are Competing Reactions

The relative concentrations of orthophosphate and triose phosphate are major factors that control whether photosynthetically fixed carbon is partitioned as starch in the chloroplast or as sucrose in the cytosol. The two compartments communicate with one another via the phosphate/triose phosphate translocator, also called the phosphate translocator (see Table 8.6, reaction 1), a strict stoichiometric antiporter.

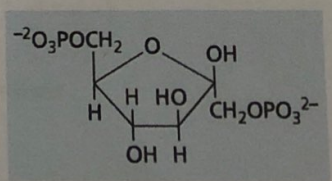
The phosphate translocator catalyzes the movement of orthophosphate and triose phosphate in opposite directions between chloroplast and cytosol. A low concentration of orthophosphate in the cytosol limits the export of triose phosphate from the chloroplast through the translocator, thereby promoting the synthesis of starch. Conversely, an abundance of orthophosphate in the cytosol inhibits starch synthesis within the chloroplast and promotes the export of triose phosphate into the cytosol, where it is converted to sucrose.

Orthophosphate and triose phosphate control the activity of several regulatory enzymes in the sucrose and starch biosynthetic pathways. The chloroplast enzyme ADP-glucose pyrophosphorylase (see Table 8.5, reaction 5) is the key enzyme that regulates the synthesis of starch from glucose-1-phosphate. This enzyme is stimulated by 3-phosphoglycerate and inhibited by orthophosphate. A high concentration ratio of 3-phosphoglycerate to orthophosphate is typically found in illuminated chloroplasts that are actively synthesizing starch. Reciprocal conditions prevail in the dark.

Fructose-2,6-bisphosphate is a key control molecule that allows increased synthesis of sucrose in the light and decreased synthesis in the dark. It is found in the cytosol in minute concentrations, and it exerts a regulatory effect on the cytosolic interconversion of fructose-1,6-bisphosphate and fructose-6-phosphate (Huber 1986; Stitt 1990):



Fructose-2,6-bisphosphate
(a regulatory metabolite)

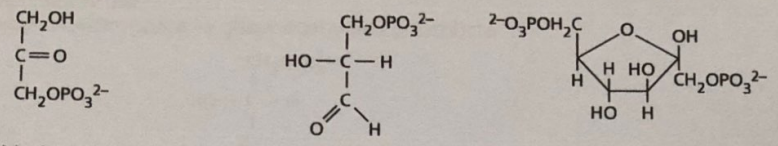


Fructose-1,6-bisphosphate
(an intermediary metabolite)

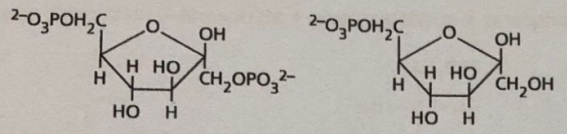
Scanned with CamScanner

TABLE 8.5
Reactions of starch synthesis from triose phosphate in chloroplasts

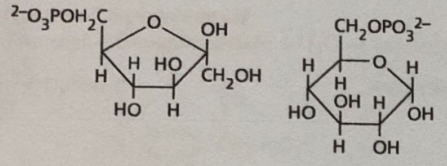
1. *Fructose-1,6,bisphosphate aldolase*
   Dihydroxyacetone-3-phosphate + glyceraldehyde-3-phosphate→ fructose-1,6-bisphosphate



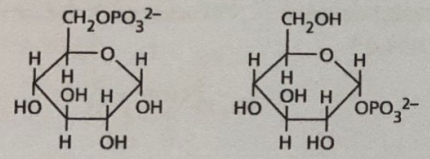
2. *Fructose-1,6-bisphosphatase*
   Fructose-1,6-bisphosphate + $H_2O \rightarrow$ fructose-6-phosphate + P_i



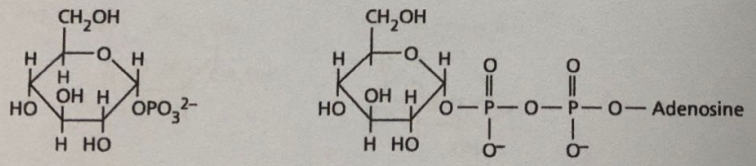
3. *Hexose phosphate isomerase*
   Fructose-6-phosphate → glucose-6-phosphate



4. *Phosphoglucomutase*
   Glucose-6-phosphate → glucose-1-phosphate



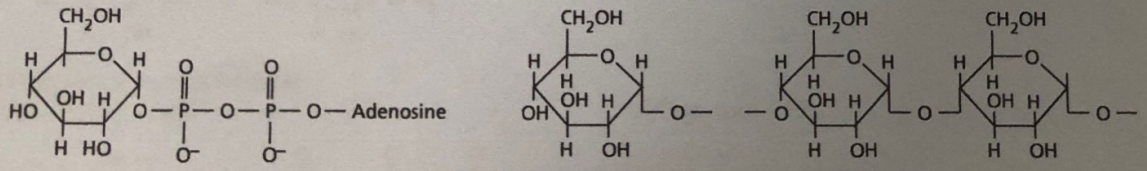
5. *ADP-glucose pyrophosphorylase*
   Glucose-1-phosphate + ATP → ADP-glucose + PP_i



6. *Pyrophosphatase*

   $PP_i + H_2O \rightarrow 2\,P_i + 2H^+$

7. *Starch synthase*
   ADP-glucose + $(1,4\text{-}\alpha\text{-D-glucosyl})_n \rightarrow$ ADP + $(1,4\text{-}\alpha\text{-D-glucosyl})_{n+1}$



Nonreducing end of a starch chain with *n* residues

Elongated starch with *n* + 1 residues

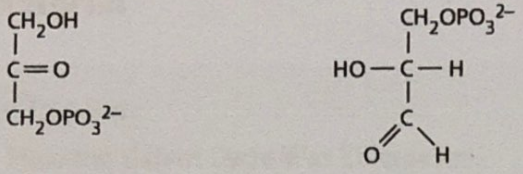
Note: Reaction 6 is irreversible and "pulls" the preceding reaction to the right.
P_i and PP_i stand for inorganic phosphate and pyrophosphate, respectively.

Scanned with CamScanner

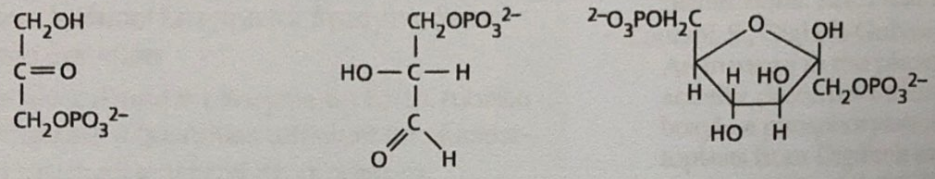
TABLE 8.6
Reactions of sucrose synthesis from triose phosphate in the cytosol

1. *Phosphate/triose phosphate translocator*
   Triose phosphate (chloroplast) + P_i (cytosol) → triose phosphate (cytosol) + P_i (chloroplast)

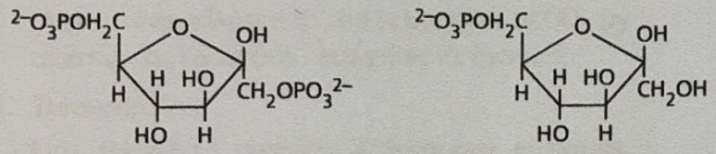
2. *Triose phosphate isomerase*
   Dihydroxyacetone-3-phosphate → glyceraldehyde-3-phosphate



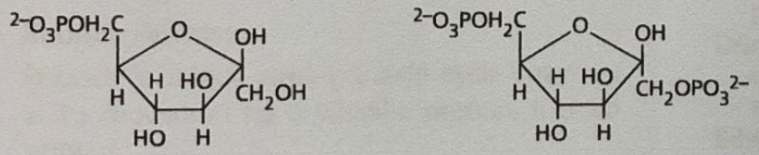
3. *Fructose-1,6-bisphosphate aldolase*
   Dihydroxyacetone-3-phosphate + glyceraldehyde-3-phosphate → fructose-1,6-bisphosphate



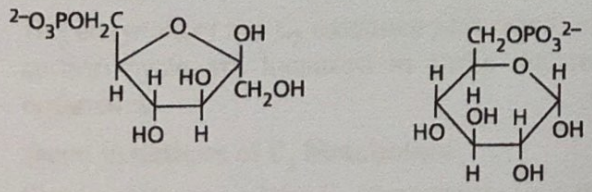
4a. *Fructose-1,6-phosphatase*
   Fructose-1,6-bisphosphate + H_2O → fructose-6-phosphate + P_i



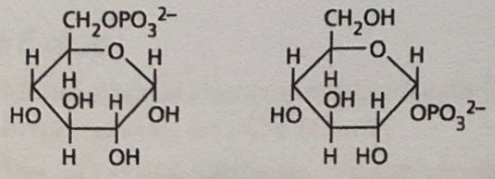
4b. *PP_i-linked phosphofructokinase*
   Fructose-6-phosphate + PP_i → fructose-1,6-bisphosphate + P_i



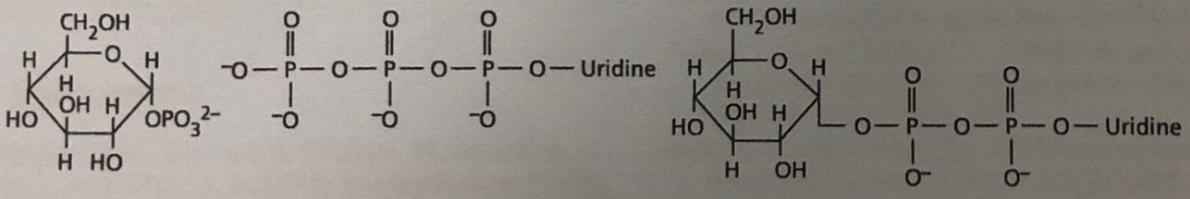
5. *Hexose phosphate isomerase*
   Fructose-6-phosphate → glucose-6-phosphate



6. *Phosphoglucomutase*
   Glucose-6-phosphate → glucose-1-phosphate



7. *UDP-glucose pyrophosphorylase*
   Glucose-1-phosphate + UTP → UDP-glucose + PP_i



Scanned with CamScanner

starch synthesis in the chloroplast by allosterically regulating the activity of ADP-glucose pyrophosphorylase. In this way the synthesis of starch from triose phosphates during the day can be separated from its breakdown, which is required to provide energy to the plant at night.

Web Material

Web Topics

8.1 How the Calvin Cycle Was Elucidated
Experiments carried out in the 1950s led to the discovery of the path of CO_2 fixation.

8.2 Rubisco: A Model Enzyme for Studying Structure and Function
As the most abundant enzyme on Earth, rubisco was obtained in quantities sufficient for elucidating its structure and catalytic properties.

8.3 Carbon Dioxide: Some Important Physicochemical Properties
Plants have adapted to the properties of CO_2 by altering the reactions catalyzing its fixation.

8.4 Thioredoxins
First found to regulate chloroplast enzymes, thioredoxins are now known to play a regulatory role in all types of cells.

8.5 Rubisco Activase
Rubisco is unique among Calvin cycle enzymes in its regulation by a specific protein, rubisco activase.

8.6 Operation of the C_2 Oxidative Photosynthetic Carbon Cycle
The enzymes of the C_2 oxidative photosynthetic carbon cycle are localized in three different organelles.

8.7 Three Variations of C_4 Metabolism
Certain reactions of the C_4 photosynthetic pathway differ among plant species.

Web Essay

8.1 Modulation of Phosphoenolpyruvate Carboxylase in C_4 and CAM Plants
The CO_2-fixing enzyme, phosphoenolpyruvate carboxylase is regulated differently in C_4 and CAM species.

Chapter References

Adams, P., Nelson, D. E., Yamada, S., Chmara, W., Jensen, R. G., Bohnert, H. J., and Griffiths, H. (1998) Tansley Review No. 97; Growth and development of *Mesembryanthemum crystallinum*. *New Phytol.* 138:171–190.

Bakrim, N., Brulfert, J., Vidal, J., and Chollet, R. (2001) Phosphoenolpyruvate carboxylase kinase is controlled by a similar signaling cascade in CAM and C_4 plants. *Biochem. Biophys. Res. Commun.* 286: 1158–1162.

Beck, E., and Ziegler, P. (1989) Biosynthesis and degradation of starch in higher plants. *Annu. Rev. Plant Physiol. Plant Mol. Biol.* 40: 95–118.

Besse, I., and Buchanan, B. B. (1997) Thioredoxin-linked plant and animal processes: The new generation. *Bot. Bull. Acad. Sinica* 38: 1–11.

Bonner, W., and Bonner, J. (1948) The role of carbon dioxide in acid formation by succulent plants. *Am. J. Bot.* 35: 113–117.

Buchanan, B. B. (1980) Role of light in the regulation of chloroplast enzymes. *Annu. Rev. Plant Phsyiol.* 31: 341–394.

Burnell, J. N., and Hatch, M. D. (1985) Light–dark modulation of leaf pyruvate, P_i dikinase. *Trends Biochem. Sci.* 10: 288–291.

Chollet, R., Vidal, J., and O'Leary, M. H. (1996) Phosphoenolpyruvate carboxylase: A ubiquitous, highly regulated enzyme in plants. *Annu. Rev. Plant Physiol. Plant Mol. Biol.* 47: 273–298.

Coursol, S., Giglioli-Guivarc'h, N., Vidal, J., and Pierre J.-N. (2000) An increase in the phosphoinositide-specific phospholipase C activity precedes induction of C_4 phosphoenolpyruvate carboxylase phosphorylation in illuminated and NH_4Cl-treated protoplasts from *Digitaria sanguinalis*. *Plant J.* 23: 497–506.

Craig, S., and Goodchild, D. J. (1977) Leaf ultrastructure of *Triodia irritans*: A C_4 grass possessing an unusual arrangement of photosynthetic tissues. *Aust. J. Bot.* 25: 277–290.

Cushman, J. C. (2001) Crassulacean acid metabolism: A plastic photosynthetic adaptation to arid environments. *Plant Physiol.* 127: 1439–1448.

Dai, S., Schwendtmayer, C., Schürmann, P., Ramaswamy, S., and Eklund, H. (2000) Redox signaling in chloroplasts: Cleavage of disulfides by an iron-sulfur cluster. *Science* 287: 655–658.

Dever, L. V., Bailey, K. J., Lacuesta, M., Leegood, R. C., and Lea P. J. (1996) The isolation and characterization of mutants of the C_4 plant *Amaranthus edulis*. *Comp. Rend. Acad. Sci., III.* 919–959.

Drincovich, M. F., Casati, P., and Andreo, C. S. (2001) NADP-malic enzyme from plants: A ubiquitous enzyme involved in different metabolic pathways. *FEBS Lett.* 490: 1–6.

Edwards, G. E., and Walker, D. (1983) C_3, C_4: *Mechanisms and Cellular and Environmental Regulation of Photosynthesis*. University of California Press, Berkeley.

Flügge, U. I., and Heldt,. H. W. (1991) Metabolite translocators of the chloroplast envelope. *Annu. Rev. Plant Physiol. Plant Mol. Biol.* 42: 129–144.

Frederick, S. E., and Newcomb, E. H. (1969) Cytochemical localization of catalase in leaf microbodies (peroxisomes). *J. Cell Biol.* 43: 343–353.

Giglioli-Guivarc'h, N., Pierre, J.-N., Brown, S., Chollet, R., Vidal, J., and Gadal, P. (1996) The light-dependent transduction pathway controlling the regulatory phosphorylation of C_4 phosphoenolpyruvate carboxylase in protoplasts from *Digitaria sanguinalis*. *Plant Cell* 8: 573–586.

Hatch, M. D., and Slack, C. R. (1966) Photosynthesis by sugarcane leaves. A new carboxylation reaction and the pathway of sugar formation. *Biochem. J.* 101: 103–111.

Heldt, H. W. (1979) Light-dependent changes of stromal H^+ and Mg^{2+} concentrations controlling CO_2 fixation. In *Photosynthesis II (Encyclopedia of Plant Physiology*, New Series, vol. 6) M. Gibbs and E. Latzko, eds. Springer, Berlin, pp. 202–207.

Huber, S. C. (1986) Fructose-2,6-bisphosphate as a regulatory metabolite in plants. *Annu. Rev. Plant Physiol.* 37: 233–246.

Huber, S. C., and Huber, J. L. (1996) Role and regulation of sucrose-phosphate synthase in higher plants. *Annu. Rev. Plant Physiol. Plant Mol. Biol.* 47: 431–444.

Kozaki, A., and Takeba, G. (1996) Photorespiration protects C_3 plants from photooxidation. *Nature* 384: 557–560.

Scanned with CamScanner

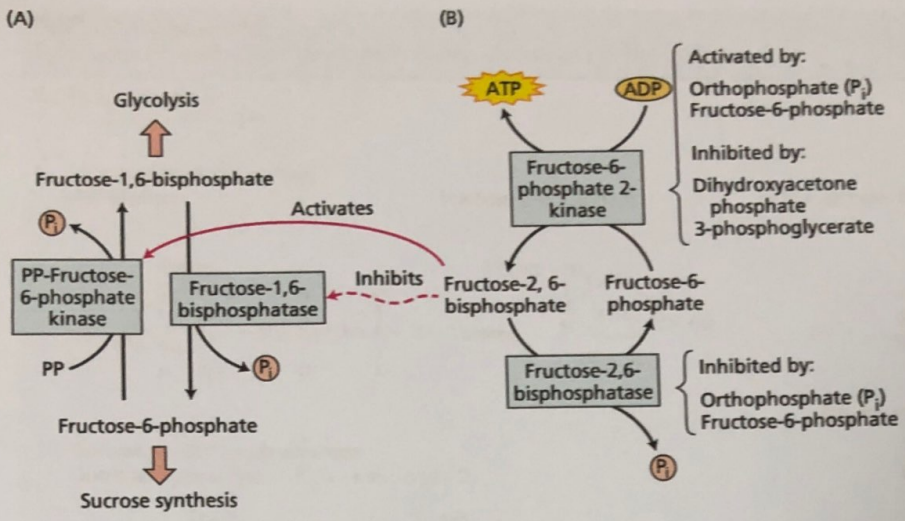


FIGURE 8.16 Regulation of the cytosolic interconversion of fructose-6-phosphate and fructose-1,6-bisphosphate. (A) The key metabolites in the allocation between glycolysis and sucrose synthesis. The regulatory metabolite fructose 2,6-bisphosphate regulates the interconversion by inhibiting the phosphatase and activating the kinase, as shown. (B) The synthesis of fructose-2,6-bisphosphate itself is under strict regulation by the activators and inhibitors shown in the figure.

SUMMARY

The reduction of CO_2 to carbohydrate via the carbon-linked reactions of photosynthesis is coupled to the consumption of NADPH and ATP synthesized by the light reactions of thylakoid membranes. Photosynthetic eukaryotes reduce CO_2 via the Calvin cycle that takes place in the stroma, or soluble phase, of chloroplasts. Here, CO_2 and water are combined with ribulose-1,5-bisphosphate to form two molecules of 3-phosphoglycerate, which are reduced and converted to carbohydrate. The continued operation of the cycle is ensured by the regeneration of ribulose-1,5-bisphosphate. The Calvin cycle consumes two molecules of NADPH and three molecules of ATP for every CO_2 fixed and, provided these substrates, has a thermodynamic efficiency close to 90%.

Several light-dependent systems act jointly to regulate the Calvin cycle: changes in ions (Mg^{2+} and H^+), effector metabolites (enzyme substrates), and protein-mediated systems (rubisco activase, ferredoxin–thioredoxin system).

The ferredoxin–thioredoxin control system plays a versatile role by linking light to the regulation of other chloroplast processes, such as carbohydrate breakdown, photophosphorylation, fatty acid biosynthesis, and mRNA translation. Control of these reactions by light separates opposing biosynthetic from degradative processes and thereby minimizes the waste of resources that would occur if the processes operated concurrently.

Rubisco, the enzyme that catalyzes the carboxylation of ribulose-1,5-bisphosphate, also acts as an oxygenase. In both cases the enzyme must be carbamylated to be fully active. The carboxylation and oxygenation reactions take place at the active site of rubisco. When reacting with oxygen, rubisco produces 2-phosphoglycolate and 3-phosphoglycerate from ribulose-1,5-bisphosphate rather than two 3-phosphoglycerates as with CO_2, thereby decreasing the efficiency of photosynthesis.

The C_2 oxidative photosynthetic carbon cycle rescues the carbon lost as 2-phosphoglycolate by rubisco oxygenase activity. The dissipative effects of photorespiration are avoided in some plants by mechanisms that concentrate CO_2 at the carboxylation sites in the chloroplast. These mechanisms include a C_4 photosynthetic carbon cycle, CAM metabolism, and "CO_2 pumps" of algae and cyanobacteria.

The carbohydrates synthesized by the Calvin cycle are converted into storage forms of energy and carbon: sucrose and starch. Sucrose, the transportable form of carbon and energy in most plants, is synthesized in the cytosol, and its synthesis is regulated by phosphorylation of sucrose phosphate synthase. Starch is synthesized in the chloroplast. The balance between the biosynthetic pathways for sucrose and starch is determined by the relative concentrations of metabolite effectors (orthophosphate, fructose-6-phosphate, 3-phosphoglycerate, and dihydroxyacetone phosphate).

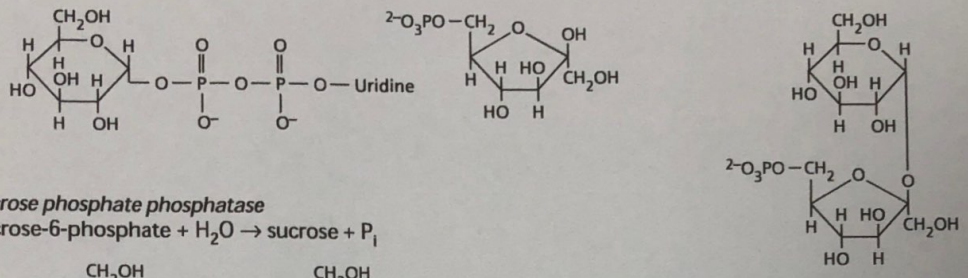
These metabolite effectors function in the cytosol by way of the enzymes synthesizing and degrading fructose-2,6-bisphosphate, the regulatory metabolite that plays a primary role in controlling the partitioning of photosynthetically fixed carbon between sucrose and starch. Two of these effectors, 3-phosphoglycerate and orthophosphate, also act on

Scanned with CamScanner

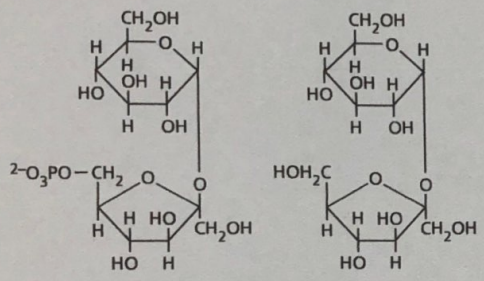
TABLE 8.6 (continued)
Reactions of sucrose synthesis from triose phosphate in the cytosol

8. *Pyrophosphatase*
$PP_i + H_2O \rightarrow 2\,P_i + 2\,H^+$

9. *Sucrose phosphate synthase*
UDP-glucose + fructose-6-phosphate → UDP + sucrose-6-phosphate



10. *Sucrose phosphate phosphatase*
Sucrose-6-phosphate + H_2O → sucrose + P_i



Note: Reaction 1 takes place on the chloroplast inner envelope membrane. Reactions 2 through 10 take place in the cytosol. Reaction 8 is irreversible and "pulls" the preceding reaction to the right.
P_i and PP_i stand for inorganic phosphate and pyrophosphate, respectively.

Increased cytosolic fructose-2,6-bisphosphate is associated with decreased rates of sucrose synthesis because fructose-2,6-bisphosphate is a powerful inhibitor of cytosolic fructose-1,6-bisphosphatase (see Table 8.6, reaction 4a) and an activator of the pyrophosphate-dependent (PP_i-linked) phosphofructokinase (reaction 4b). But what, in turn, controls the cytosolic concentration of fructose-2,6-bisphosphate?

Fructose-2,6-bisphosphate is synthesized from fructose-6-phosphate by a special fructose-6-phosphate 2-kinase (not to be confused with the fructose-6-phosphate 1-kinase of glycolysis) and is degraded specifically by fructose-2,6-bisphosphatase (not to be confused with fructose-1,6-bisphosphatase of the Calvin cycle). Recent evidence suggests that, as in animal cells, both plant activities reside on a single polypeptide chain.

The kinase and phosphatase activities are controlled by orthophosphate and triose phosphate. Orthophosphate stimulates fructose-6-phosphate 2-kinase and inhibits fructose-2,6-bisphosphatase; triose phosphate inhibits the 2-kinase (Figure 8.16). Consequently, a low cytosolic ratio of triose phosphate to orthophosphate promotes the formation of fructose-2,6-bisphosphate, which in turn inhibits the hydrolysis of cytosolic fructose-1,6-bisphosphate and slows the rate of sucrose synthesis. A high cytosolic ratio of triose phosphate to orthophosphate has the opposite effect.

Light regulates the concentration of these activators and inhibitors through the reactions associated with photosynthesis and thereby controls the concentration of fructose-2,6-bisphosphate in the cytosol. The glycolytic enzyme phosphofructokinase also functions in the conversion of fructose-6-phosphate to fructose-1,6-bisphosphate, but in plants it is not appreciably affected by fructose-2,6-bisphosphate.

The activity of phosphofructokinase in plants appears to be regulated by the relative concentrations of ATP, ADP, and AMP. The remarkable plasticity of plants was once again illustrated by recent gene deletion experiments with transformed tobacco plants. This experiment shows that the transformed plants can grow without a functional pyrophosphate-dependent fructose-6-phosphate kinase enzyme. In this case the conversion of fructose-6-phosphate to fructose-1,6-bisphosphate is apparently catalyzed exclusively by phosphofructokinase (Paul et al. 1995).

Scanned with CamScanner

Introduction to Endocrinology

Chapter 64

INTRODUCTION
CELL-TO-CELL SIGNALING
CHEMICAL MESSENGERS
ENDOCRINE GLANDS
METHODS OF STUDY
STUDY OF ENDOCRINE GLANDS
STUDY OF HORMONES
STUDY OF ENDOCRINE DISORDERS

INTRODUCTION

All the physiological activities of the body are regulated by two major systems:

1. Nervous system
2. Endocrine system.

These two systems interact with one another and regulate the body functions. This section deals with endocrine system and Section 10 deals with nervous system. Endocrine system functions by secreting some chemical substances called hormones.

CELL-TO-CELL SIGNALING

Celltocell signaling refers to the transfer of information from one cell to another. It is also called **cell signaling** or intercellular communication. The cells of the body communicate with each other through some chemical substances called chemical messengers.

CHEMICAL MESSENGERS

Chemical messengers are the substances involved in cell signaling. These messengers are mainly secreted from endocrine glands. Some chemical messengers are secreted by nerve endings and the cells of several other tissues also.

All these chemical messengers carry the message (signal) from the **signaling cells (controlling cells)** to the **target cells.** The messenger substances may be the hormones or hormonelike substances.

Classification of Chemical Messengers

Generally the chemical messengers are classified into two types:

1. Classical hormones secreted by endocrine glands
2. Local hormones secreted from other tissues.

However, recently chemical messengers are classified into four types:

1. Endocrine messengers
2. Paracrine messengers
3. Autocrine messengers
4. Neurocrine messengers.

1. *Endocrine Messengers*

Endocrine messengers are the classical hormones. A hormone is defined as a chemical messenger, synthesized by endocrine glands and transported by blood to the target organs or tissues (site of action).

Examples are growth hormone and insulin.

2. *Paracrine Messengers*

Paracrine messengers are the chemical messengers, which diffuse from the control cells to the target cells through the interstitial fluid. Some of these substances directly enter the neighboring target cells through gap junctions. Such substances are also called **juxtacrine messengers** or **local hormones.**

Examples are prostaglandins and histamine.

3. *Autocrine Messengers*

Autocrine messengers are the chemical messengers that control the source cells which secrete them. So, these messengers are also called **intracellular chemical mediators.**

Examples are leukotrienes.

4. *Neurocrine or Neural Messengers*

Neurocrine or neural messengers are neurotransmitters and neurohormones (Fig. 64.1).

Neurotransmitter

Neurotransmitter is an endogenous signaling molecule that carries information form one nerve cell to another nerve cell or muscle or another tissue.

Examples are acetylcholine and dopamine.

Neurohormone

Neurohormone is a chemical substance that is released by the nerve cell directly into the blood and transported to the distant target cells.

Examples are oxytocin, antidiuretic hormone and hypothalamic releasing hormones.

Some of the chemical mediators act as more than one type of chemical messengers. For example, noradrenaline and dopamine function as classical hormones as well as neurotransmitters. Similarly, histamine acts as neurotransmitter and paracrine messenger.

④ ENDOCRINE GLANDS

Endocrine glands are the glands which synthesize and release the classical hormones into the blood. Endocrine glands are also called **ductless glands** because the

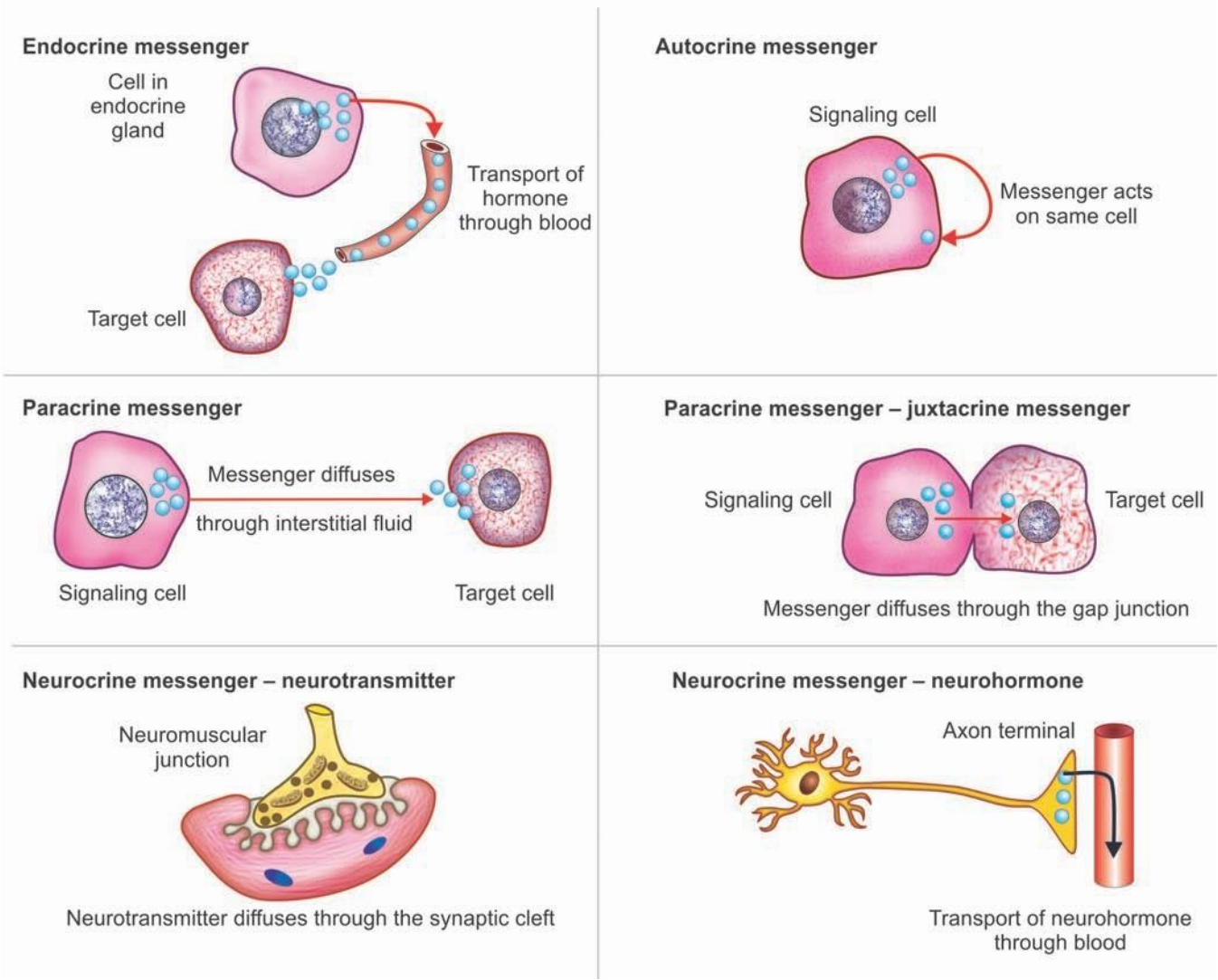


FIGURE 64.1: Chemical messengers

hormones secreted by them are released directly into blood without any duct. Endocrine glands are distinct from exocrine glands which release their secretions through ducts.

Endocrine glands play an important role in homeostasis and control of various other activities in the body through their hormones. Hormones are transported by blood to target organs or tissues in different parts of the body, where the actions are executed.

Major endocrine glands: Fig. 64.2.

Hormones secreted by endocrine glands: Table 64.1.

Hormones secreted by gonads: Table 64.2.

Hormones secreted by other organs: Table 64.3.

Local hormones: Table 64.4.

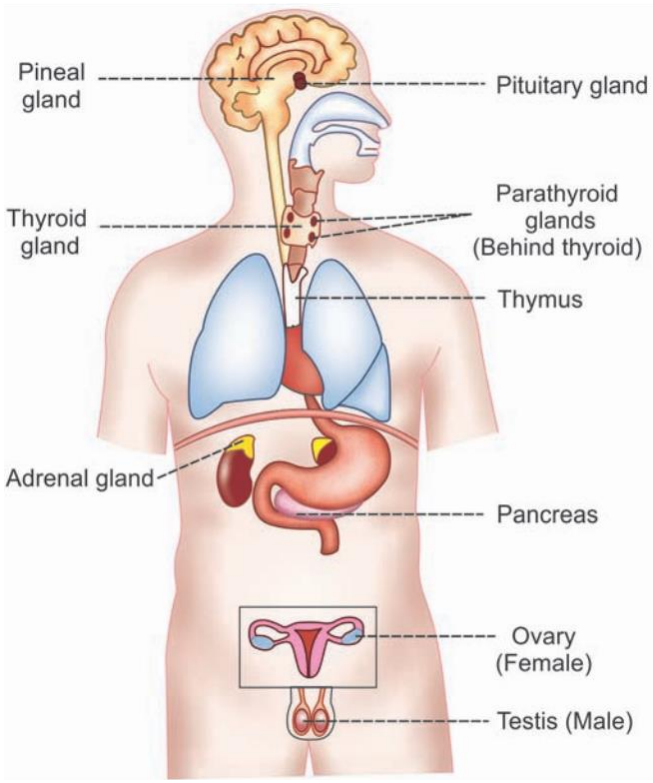


FIGURE 64.2: Diagram showing major endocrine glands

¶ METHODS OF STUDY

④ STUDY OF ENDOCRINE GLANDS

Methods followed to study an endocrine gland:

1. *Functional Anatomy*

i. Situation
ii. Divisions or parts
iii. Histology
Blood supply
iv. Nerve supply.
v.

2. *Functions*

i. Hormones secreted by the gland
ii. Actions of each hormone.

3. *Evidences to Support the Functions of the Gland*

i. Effects of **extirpation** (removal) of the gland
ii. Effects of administration of extract or the hormone of the gland
iii. Clinical observation.

TABLE 64.1: Hormones secreted by major endocrine glands

Anterior pituitary	1. Growth hormone (GH) 2. Thyroidstimulating hormone (TSH) 3. Adrenocorticotropic hormone (ACTH) 4. Follicle stimulating hormone (FSH) 5. Luteinizing hormone (LH) 6. Prolactin	Adrenal cortex	*Mineralocorticoids* 1. Aldosterone 2. 11deoxycorticosterone
			Glucocorticoids 1. Cortisol 2. Corticosterone
Posterior pituitary	1. Antidiuretic hormone (ADH) 2. Oxytocin		*Sex hormones* 1. Androgens 2. Estrogen 3. Progesterone
Thyroid gland	1. Thyroxine (T_4) 2. Triiodothyronine (T_3) 3. Calcitonin		
Parathyroid gland	Parathormone	Adrenal medulla	1. Catecholamines 2. Adrenaline (Epinephrine) 3. Noradrenaline (Norepinephrine) 4. Dopamine
Pancreas – Islets of Langerhans	1. Insulin 2. Glucagon 3. Somatostatin 4. Pancreatic polypeptide		

TABLE 64.2: Hormones secreted by gonads

Testis	1. Testosterone 2. Dihydrotestosterone 3. Androstenedion
Ovary	1. Estrogen 2. Progesterone

TABLE 64.3: Hormones secreted by other organs

Pineal gland	Melatonin
Thymus	1. Thymosin 2. Thymin
Kidney	1. Erythropoietin 2. Thrombopoietin 3. Renin 4. 1,25dihydroxycholecalcifero (calcitriol) 5. Prostaglandins
Heart	1. Atrial natriuretic peptide 2. Brain natriuretic peptide 3. Ctype natriuretic peptide
Placenta	1. Human chorionic gonadotropin (HCG) 2. Human chorionic somatomammotropin 3. Estrogen 4. Progesterone

TABLE 64.4: Local hormones

1. Prostaglandins	7. Serotonin
2. Thromboxanes	8. Histamine
3. Prostacyclin	9. Substance P
4. Leukotrienes	10. Heparin
5. Lipoxins	11. Bradykinin
6. Acetylcholine	12. Gastrointestinal hormones

4. *Regulation of Activity of the Gland*

i. By other endocrine glands
ii. By other factors
iii. By feedback mechanism.

5. *Applied Physiology*

i. Disorders due to hyperactivity of the gland
ii. Disorders due to hypoactivity of the gland.

④ STUDY OF HORMONES

A hormone is usually studied as follows:

1. Source of secretion (gland as well as the cell that secretes the hormone)
2. Chemistry
3. Halflife
4. Synthesis and metabolism
5. Actions
6. Mode of action
7. Regulation of secretion
8. Applied physiology
   i. Disorders due to hypersecretion of the hormone
   ii. Disorders due to hyposecretion of the hormone.

Half-life of the Hormones

Halflife is defined as the time during which half the quantity of a hormone, drug or any substance is metabolized or eliminated from circulation by biological process. It is also defined as the time during which the activity or potency of a substance is decreased to half of its initial value.

Halflife is also called biological halflife. Halflife of a hormone denotes the elimination of that hormone from circulation.

④ STUDY OF ENDOCRINE DISORDERS

An endocrine disorder is studied by analyzing:

1. Causes
2. Signs and symptoms
3. Syndrome.

1. *Causes*

Endocrine disorder may be due to the hyperactivity or hypoactivity of the concerned gland. Secretion of hormones increases during hyperactivity and decreases during hypoactivity.

2. *Signs and Symptoms*

A sign is the feature of a disease as detected by the doctor during the physical examination. So, it is the **objective physical evidence** of disease found by the examiner.

Examples of signs are yellow coloration of skin and mucous membrane in jaundice, paleness in anemia, enlargement of liver, etc.

A symptom is the feature of a disease felt by the patient. So, it is the **subjective evidence** perceived by the patient. In simple words, it is a noticeable change in the body, experienced by the patient.

Examples of symptoms are fever, itching, swelling, tremor, etc.

3. *Syndrome*

Syndrome is the combination of signs and symptoms (associated with a disease), which occur together and suggest the presence of a certain disease or the possibility of developing the disease.

Examples are **Stoke-Adams syndrome** and syndrome of inappropriate antidiuretic hormone hyper secretion **(SIADH).**

Hormones

Chapter 65

- CHEMISTRY OF HORMONES
  - STEROID HORMONES
  - PROTEIN HORMONES
  - TYROSINE DERIVATIVES
- HORMONAL ACTION
  - INTRODUCTION
  - HORMONE RECEPTORS
- MECHANISM OF HORMONAL ACTION
  - BY ALTERING PERMEABILITY OF CELL MEMBRANE
  - BY ACTIVATING INTRACELLULAR ENZYME
  - BY ACTING ON GENES

CHEMISTRY OF HORMONES

Hormones are **chemical messengers,** synthesized by endocrine glands. Based on chemical nature, hormones are classified into three types (Table 65.1):

1. Steroid hormones
2. Protein hormones
3. Derivatives of the amino acid called tyrosine.

STEROID HORMONES

Steroid hormones are the hormones synthesized from cholesterol or its derivatives. Steroid hormones are secreted by adrenal cortex, gonads and placenta.

TABLE 65.1: Classification of hormones depending upon chemical nature

Steroids	Proteins	Derivatives of tyrosine
Aldosterone	Growth hormone (GH)	Thyroxine (T_4)
11-deoxycorticosterone	Thyroid-stimulating hormone (TSH)	Triiodothyronine (T_3)
Cortisol Corticosterone	Adrenocorticotropic hormone (ACTH)	Adrenaline (Epinephrine)
Testosterone	Follicle-stimulating hormone (FSH)	Noradrenaline (Norepinephrine)
Dihydrotestosterone	Luteinizing hormone (LH)	Dopamine.
Dehydroepiandrosterone	Prolactin	
Androstenedione	Antidiuretic hormone (ADH)	
Estrogen	Oxytocin	
Progesterone	Parathormone	
	Calcitonin	
	Insulin	
	Glucagon	
	Somatostatin	
	Pancreatic polypeptide	
	Human chorionic gonadotropin (HCG)	
	Human chorionic somatomammotropin.	

④ PROTEIN HORMONES

Protein hormones are large or small peptides. Protein hormones are secreted by pituitary gland, parathyroid glands, pancreas and placenta ('P's).

④ TYROSINE DERIVATIVES

Two types of hormones, namely thyroid hormones and adrenal medullary hormones are derived from the amino acid tyrosine.

¶ HORMONAL ACTION

④ INTRODUCTION

Hormone does not act directly on target cells. First it combines with receptor present on the target cells and forms a **hormone-receptor complex.** This hormone-receptor complex induces various changes or reactions in the target cells.

④ HORMONE RECEPTORS

Hormone receptors are the large proteins present in the target cells. Each cell has thousands of receptors. Important characteristic feature of the receptors is that, each receptor is specific for one single hormone, i.e. each receptor can combine with only one hormone. Thus, a hormone can act on a target cell, only if the target cell has the receptor for that particular hormone.

Situation of the Hormone Receptors

Hormone receptors are situated either in cell membrane or cytoplasm or nucleus of the target cells as follows:

1. *Cell membrane:* Receptors of protein hormones and adrenal medullary hormones (catecholamines) are situated in the cell membrane (Fig. 65.1)
2. *Cytoplasm:* Receptors of steroid hormones are situated in the cytoplasm of target cells
3. *Nucleus:* Receptors of thyroid hormones are in the nucleus of the cell.

Regulation of Hormone Receptors

Receptor proteins are not static components of the cell. Their number increases or decreases in various conditions.

Generally, when a hormone is secreted in excess, the number of receptors of that hormone decreases due to binding of hormone with receptors. This process is called **down regulation.** During the deficiency of the hormone, the number of receptor increases, which is called **upregulation.**

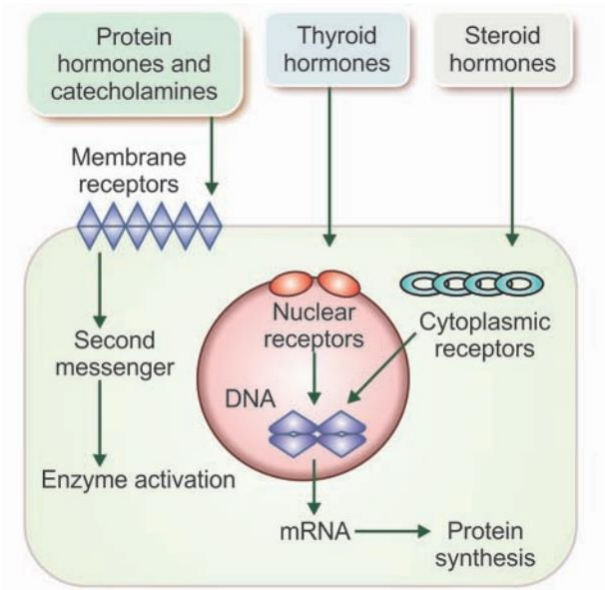


FIGURE 65.1: Situation of hormonal receptors

Hormone in the form of hormone-receptor complex enters the target cell by means of endocytosis and executes the actions. The whole process is called **internalization.**

After internalization, some receptors are recycled, whereas many of them are degraded and new receptors are formed. Formation of new receptors takes a long time. So, the number of receptors decreases when hormone level increases.

¶ MECHANISM OF HORMONAL ACTION

Hormone does not act on the target cell directly. It combines with receptor to form hormone-receptor complex. This complex executes the hormonal action by any one of the following mechanisms:

1. By altering permeability of cell membrane
2. By activating intracellular enzyme
3. By acting on genes.

④ BY ALTERING PERMEABILITY OF CELL MEMBRANE

Neurotransmitters in synapse or neuromuscular junction act by changing the permeability of postsynaptic membrane.

For example, in a neuromuscular junction, when an impulse (action potential) reaches the axon terminal of the motor nerve, acetylcholine is released from the vesicles. Acetylcholine increases the permeability of the postsynaptic membrane for sodium, by opening the

ligand-gated sodium channels. So, sodium ions enter the neuromuscular junction from ECF through the channels and cause the development of endplate potential. Refer Chapter 32 for details.

④ BY ACTIVATING INTRACELLULAR ENZYME

Protein hormones and the catecholamines act by activating the intracellular enzymes.

First Messenger

The hormone which acts on a target cell, is called first messenger or **chemical mediator.** It combines with the receptor and forms hormone-receptor complex.

Second Messenger

Hormone-receptor complex activates the enzymes of the cell and causes the formation of another substance called the second messenger or **intracellular hormonal mediator.**

Second messenger produces the effects of the hormone inside the cells. Protein hormones and the catecholamines act through second messenger. Most common second messenger is cyclic AMP.

Cyclic AMP

Cyclic AMP, cAMP or cyclic adenosine 3'5'-monophosphate acts as a second messenger for protein hormones and catecholamines.

Formation of cAMP – Role of G proteins

G proteins or **guanosine nucleotide-binding proteins** are the membrane proteins situated on the inner surface of cell membrane. These proteins play an important role in the formation of cAMP

Each G protein molecule is made up of trimeric (three) subunits called α, β and γ subunits. The α-subunit is responsible for most of the biological actions. It is bound with **guanosine diphosphate** (GDP) and forms α-GDP unit. The α-subunit is also having the intrinsic enzyme activity called **GTPase** activity. The β and γ subunits always bind together to form the β-γ dimmer. It can also bring about some actions. In the inactivated G protein, both α-GDP unit and β-γ dimmer are united (Fig. 65.2: Stage 1).

Sequence of events in the formation of cAMP

i. Hormone binds with the receptor in the cell membrane and forms the hormone-receptor complex
ii. It activates the G protein
iii. G protein releases GDP from α-GDP unit

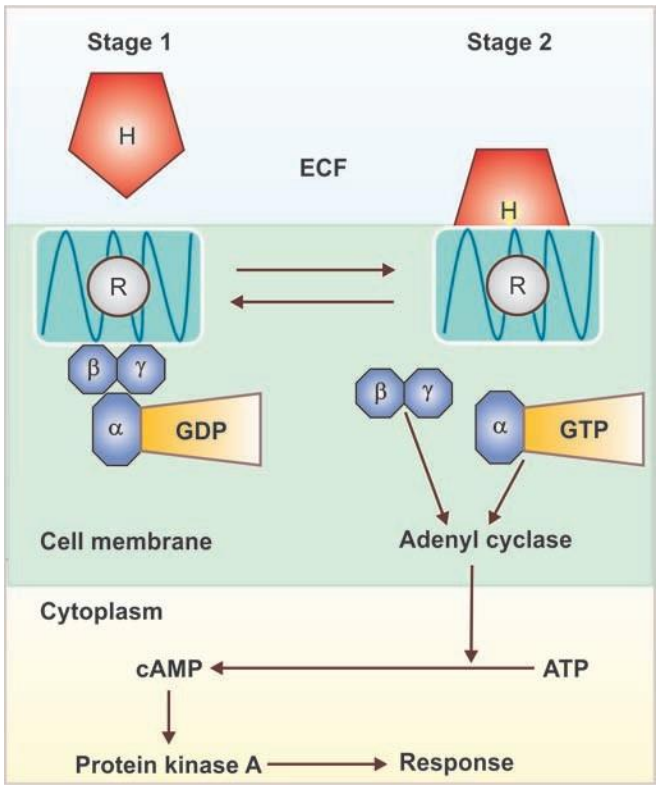


FIGURE 65.2: Mode of action of protein hormones and catecholamines. H = Hormone. R = Receptor, α, β, γ = G protein, GDP = Guanosine diphosphate, GTP = Guanosine triphosphate, ECF = Extracellular fluid, cAMP = Cyclic adenosine 3'5'-monophosphate, ATP = Adenosine triphosphate.

iv. The α-subunit now binds with a new molecule of GTP, i.e. the GDP is exchanged for GTP
v. This exchange triggers the dissociation of α-GTP unit and β-γ dimmer from the receptor
vi. Both α-GTP unit and β-γ dimmer now activate the second messenger pathways (Fig. 65.2: Stage 2)
vii. The α-GTP unit activates the enzyme adenyl cyclase, which is also present in the cell membrane. Most of the adenyl cyclase protrudes into the cytoplasm of the cell from inner surface of the cell membrane
viii. Activated adenyl cyclase converts the adenosine triphosphate of the cytoplasm into cyclic adenosine monophosphate (cAMP)

When the action is over, α-subunit hydrolyzes the attached GTP to GDP by its GTPase activity. This allows the reunion of α-subunit with β-γ dimmer and commencing a new cycle (Fig. 65.2: Stage 1).

Actions of cAMP

Cyclic AMP executes the actions of hormone inside the cell by stimulating the enzymes like protein kinase A.

Cyclic AMP produces the response, depending upon the function of the target cells through these enzymes.

Response produced by cAMP

Cyclic AMP produces one or more of the following responses:

i. Contraction and relaxation of muscle fibers
ii. Alteration in the permeability of cell membrane
Synthesis of substances inside the cell
iii. Secretion or release of substances by target cell
iv. Other physiological activities of the target cell.
v.

Other Second Messengers

In addition to cAMP, some other substances also act like second messengers for some of the hormones in target cells.

i. *Calcium ions and calmodulin*

Many hormones act by increasing the calcium ion, which fucntions as second messenger along with another protein called calmodulin or troponin C. Calmodulin is present in smooth muscles and troponin C is present in skeletal muscles. Calcium-calmodulin complex activates various enzymes in the cell, which cause the physiological responses. Common enzyme activated by calcium-calmodulin complex is the **myosin kinase** in smooth muscle. Myosin kinase catalyses the reactions, resulting in muscular contraction (Chapter 33).
In the skeletal muscle, calcium ions bind with troponin C, which is similar to calmodulin (Chapter 31).

ii. *Inositol triphosphate*

Inositol triphosphate (IP_3) is formed from phosphatidylinositol biphosphate (PIP_2). Hormone-receptor complex activates the enzyme phospholipase, which converts PIP_2 into IP_3. IP_3 acts on protein kinase C and causes the physiological response by the release of calcium ions into the cytoplasm of target cell.

iii. *Diacylglycerol*

Diacylglycerol (DAG) is also produced from PIP_2. It acts via protein kinase C.

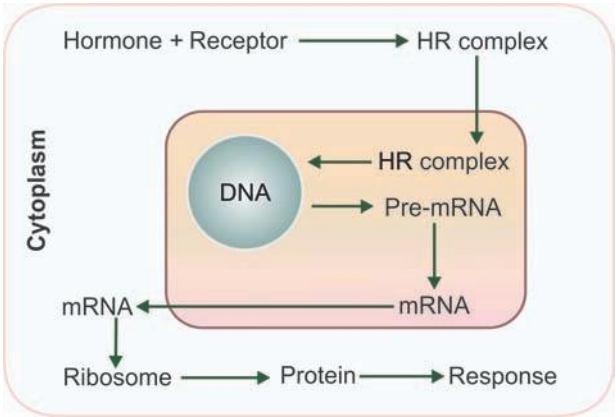


FIGURE 65.3: Mode of action of steroid hormones. Thyroid hormones also act in the similar way but their receptors are in the nucleus. HR = Hormone-receptor complex

iv. *Cyclic guanosine monophosphate*

Cyclic guanosine monophosphate (cGMP) functions like cAM P by acting on protein kinase A.

④ BY ACTING ON GENES

Thyroid and steroid hormones execute their function by acting on genes in the target cells (Fig. 65.3).

Sequence of Events during Activation of Genes

i. Hormone enters the interior of cell and binds with receptor in cytoplasm (steroid hormone) or in nucleus (thyroid hormone) and forms hormone-receptor complex
ii. Hormone-receptor complex moves towards the DNA and binds with DNA
iii. This increases transcription of mRNA
iv. The mRNA moves out of nucleus and reaches ribosomes and activates them
v. Activated ribosomes produce large quantities of proteins
vi. These proteins produce physiological responses in the target cells.

Pituitary Gland

Chapter 66

- ¶ INTRODUCTION
  - ④ DIVISIONS
  - ④ DEVELOPMENT
  - ④ REGULATION OF SECRETIONS
- ¶ ANTERIOR PITUITARY OR ADENOHYPOPHYSIS
  - ④ PARTS
  - ④ HISTOLOGY
  - ④ REGULATION
  - ④ HORMONES
  - ④ GROWTH HORMONE
  - ④ OTHER HORMONES
- ¶ POSTERIOR PITUITARY OR NEUROHYPOPHYSIS
  - ④ PARTS
  - ④ HISTOLOGY
  - ④ HORMONES
  - ④ ANTIDIURETIC HORMONE
  - ④ OXYTOCIN
- ¶ APPLIED PHYSIOLOGY – DISORDERS OF PITUITARY GLAND
  - ④ HYPERACTIVITY OF ANTERIOR PITUITARY
  - ④ HYPOACTIVITY OF ANTERIOR PITUITARY
  - ④ HYPERACTIVITY OF POSTERIOR PITUITARY
  - ④ HYPOACTIVITY OF POSTERIOR PITUITARY
  - ④ HYPOACTIVITY OF ANTERIOR AND POSTERIOR PITUITARY

¶ INTRODUCTION

Pituitary gland or **hypophysis** is a small endocrine gland with a diameter of 1 cm and weight of 0.5 to 1 g. It is situated in a depression called '**sella turcica',** present in the sphenoid bone at the base of skull. It is connected with the hypothalamus by the **pituitary stalk** or **hypophyseal stalk.**

④ DIVISIONS OF PITUITARY GLAND

Pituitary gland is divided into two divisions:

1. Anterior pituitary or adenohypophysis
2. Posterior pituitary or neurohypophysis.

Both the divisions are situated close to each other. Still both are entirely different in their development, structure and function.

Between the two divisions, there is a small and relatively avascular structure called **pars intermedia.** Actually, it forms a part of anterior pituitary.

④ DEVELOPMENT OF PITUITARY GLAND

Both the divisions of pituitary glands develop from different sources.

Anterior pituitary is **ectodermal** in origin and arises from the **pharyngeal epithelium** as an upward growth known as **Rathke pouch.**

Posterior pituitary is **neuroectodermal** in origin and arises from hypothalamus as a downward **diverticulum.** Rathke pouch and the downward diverticulum from hypothalamus grow towards each other and meet in the midway between the roof of the buccal cavity and base of brain. There, the two structures lie close together.

④ REGULATION OF SECRETION

Hypothalamo-hypophyseal Relationship

The relationship between hypothalamus and pituitary gland is called hypothalamo-hypophyseal relationship. Hormones secreted by hypothalamus are transported to anterior pituitary and posterior pituitary. But the mode of transport of these hormones is different. Hormones from hypothalamus are transported to anterior pituitary through hypothalamo-hypophysial portal blood vessels. But, the hormones from hypothalamus to posterior pituitary are transported by nerve fibers of hypothalamo-hypophyseal tract (see below for details).

ANTERIOR PITUITARY OR ADENOHYPOPHYSIS

Anterior pituitary is also known as the **master gland** because it regulates many other endocrine glands through its hormones.

④ PARTS

Anterior pituitary consists of three parts (Fig. 66.1):

1. Pars distalis
2. Pars tuberalis
3. Pars intermedia.

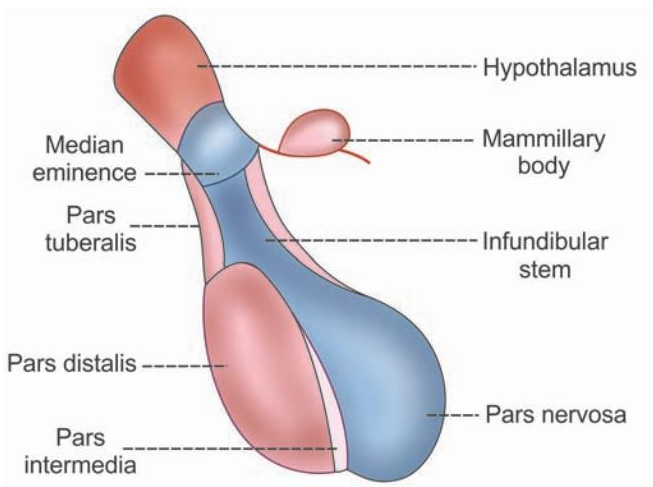


FIGURE 66.1: Parts of pituitary gland
Adenohypophysis Neurohypophysis

④ HISTOLOGY

Anterior pituitary has two types of cells, which have different staining properties:

1. Chromophobe cells
2. Chromophil cells.

Chromophobe Cells

Chromophobe cells do not possess granules and stain poorly. These cells form 50% of total cells in anterior pituitary. Chromophobe cells are not secretory in nature, but are the precursors of chromophil cells.

Chromophil Cells

Chromophil cells contain large number of granules and are darkly stained.

Types of chromophil cells

Chromophil cells are classified by two methods.

1. Classification on the basis of staining property: Chromophil cells are divided into two types:
   i. **Acidophilic cells** or **alpha cells,** which form 35%
   ii. **Basophilic cells** or **beta cells,** which form 15%.
2. Classification on the basis of secretory nature: Chromophil cells are classified into five types:
   i. **Somatotropes,** which secrete growth hormone
   ii. **Corticotropes,** which secrete adrenocorticotropic hormone
   iii. **Thyrotropes,** which secrete thyroid-stimulating hormone (TSH)
   iv. **Gonadotropes,** which secrete follicle-stimulating hormone (FSH) and luteinizing hormone (LH)
   v. **Lactotropes,** which secrete prolactin.

Somatotropes and lactotropes are acidophilic cells, whereas others are basophilic cells. Somatotropes form about 30% to 40% of the chromophil cells. So, pituitary tumors that secrete large quantities of human growth hormone are called acidophilic tumors.

④ REGULATION OF ANTERIOR PITUITARY SECRETION

Hypothalamus controls anterior pituitary by secreting the releasing and inhibitory hormones (factors), which are called **neurohormones.** These hormones from hypothalamus are transported anterior pituitary through hypothalamo-hypophyseal **portal vessels.** Some special nerve cells present in various parts hypothalamus send their nerve fibers (axons) to median eminence and tuber cinereum. These nerve cells synthesize the hormones and release them into median

eminence and tuber cinereum. From here, the hormones are transported by blood via hypothalamo-hypophyseal portal vessels to anterior pituitary (Fig. 66.2).

Releasing and Inhibitory Hormones Secreted by Hypothalamus

1. Growth hormone-releasing hormone (GHRH): Stimulates the release of growth hormone
2. Growth hormone-releasing polypeptide (GHRP): Stimulates the release of GHRH and growth hormone
3. Growth hormone-inhibitory hormone (GHIH) or
4. somatostatin: Inhibits the growth hormone release
5. Thyrotropic-releasing hormone (TRH): Stimulates the release of thyroid stimulating hormone
6. Corticotropin-releasing hormone (CRH): Stimulates the release of adrenocorticotropin
7. Gonadotropin-releasing hormone (GnRH): Stimulates the release of gonadotropins, FSH and LH
8. Prolactin inhibitory hormone (PIH): Inhibits prolactin secretion. It is believed that PIH is dopamine.

③ HORMONES SECRETED BY ANTERIOR PITUITARY

Six hormones are secreted by the anterior pituitary:

1. Growth hormone (GH) or somatotropic hormone (STH)
2. Thyroid-stimulating hormone (TSH) or thyrotropic hormone
3. Adrenocorticotropic hormone (ACTH)
4. Follicle-stimulating hormone (FSH)
5. Luteinizing hormone (LH) in females or interstitial-cell-stimulating hormone (ICSH) in males
6. Prolactin.

Recently, the hormone β-lipotropin is found to be secreted by anterior pituitary.

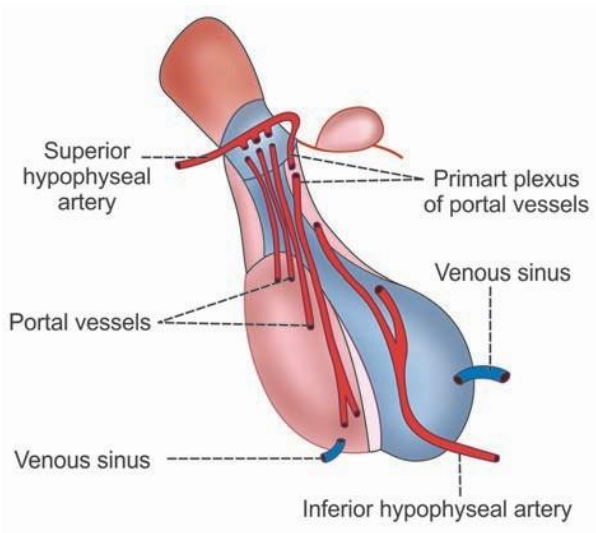


FIGURE 66.2: Blood supply to pituitary gland

Tropic Hormones

First five hormones of anterior pituitary stimulate the other endocrine glands. Growth hormone also stimulates the secretory activity of liver and other tissues. Therefore, these five hormones are called **tropic hormones.** Prolactin is concerned with milk secretion.

Gonadotropic Hormones

Follicle-stimulating hormone and the luteinizing hormone are together called **gonadotropic hormones** or **gonadotropins** because of their action on gonads.

④ GROWTH HORMONE

Source of Secretion

Growth hormone is secreted by somatotropes which are the acidophilic cells of anterior pituitary.

Chemistry, Blood Level and Daily Output

GH is protein in nature, having a single-chain polypeptide with 191 amino acids. Its molecular weight is 21,500. Basal level of GH concentration in blood of normal adult is up to 300 g/dL and in children, it is up to 500 ng/dL. Its daily output in adults is 0.5 to1.0 mg.

Transport

Growth hormone is transported in blood by GH-binding proteins (GHBPs).

Half-life and Metabolism

Half-life of circulating growth hormone is about 20 minutes. It is degraded in liver and kidney.

Actions of Growth Hormone

GH is responsible for the general growth of the body. Hypersecretion of GH causes enormous growth of the body, leading to **gigantism.** Deficiency of GH in children causes stunted growth, leading to **dwarfism.**

GH is responsible for the growth of almost all tissues of the body, which are capable of growing. It increases the size and number of cells by mitotic division. GH also causes specific differentiation of certain types of cells like bone cells and muscle cells.

GH also acts on the metabolism of all the three major types of foodstuffs in the body, viz. proteins, lipids and carbohydrates.

1. *On metabolism*

GH increases the synthesis of proteins, mobilization of lipids and conservation of carbohydrates.

a. On protein metabolism

GH accelerates the synthesis of proteins by:

i. *Increasing amino acid transport through cell membrane:* The concentration of amino acids in the cells increases and thus, the synthesis of proteins is accelerated.

ii. *Increasing ribonucleic acid (RNA) translation:* GH increases the translation of RNA in the cells (Refer Chapter 1 for details of translation). Because of this, ribosomes are activated and more proteins are synthesized.
GH can increase the RNA translation even without increasing the amino acid transport into the cells.

iii. *Increasing transcription of DNA to RNA:* It also stimulates the transcription of DNA to RNA. RNA, in turn accelerates the synthesis of proteins in the cells (Refer Chapter 1 for details of transcription).

iv. *Decreasing catabolism of protein:* GH inhibits the breakdown of cellular protein. It helps in the building up of tissues.

v. *Promoting anabolism of proteins indirectly:* GH increases the release of insulin (from β-cells of islets in pancreas), which has anabolic effect on proteins.

b. *On fat metabolism*

GH mobilizes fats from adipose tissue. So, the concentration of fatty acids increases in the body fluids. These fatty acids are used for the production of energy by the cells. Thus, the proteins are spared. During the utilization of fatty acids for energy production, lot of acetoacetic acid is produced by liver and is released into the body fluids, leading to ketosis. Sometimes, excess mobilization of fat from the adipose tissue causes accumulation of fat in liver, resulting in **fatty liver.**

c. *On carbohydrate metabolism*

Major action of GH on carbohydrates is the conservation of glucose.

Effects of GH on carbohydrate metabolism:

i. Decrease in the **peripheral utilization** of glucose for the production of energy: GH reduces the peripheral utilization of glucose for energy production. It is because of the formation of acetyl-CoA during the metabolism of fat, influenced by GH. The acetyl-CoA inhibits the glycolytic pathway. Moreover, since the GH increases the mobilization of fat, more fatty acid is available for the production of energy. By this way, GH reduces the peripheral utilization of glucose for energy production.

ii. Increase in the deposition of glycogen in the cells: Since glucose is not utilized for energy production by the cells, it is converted into glycogen and deposited in the cells.

iii. Decrease in the uptake of glucose by the cells: As glycogen deposition increases, the cells become saturated with glycogen. Because of this, no more glucose can enter the cells from blood. So, the blood glucose level increases.

iv. Diabetogenic effect of GH: Hypersecretion of GH increases blood glucose level enormously. It causes continuous stimulation of the β-cells in the islets of Langerhans in pancreas and increase in secretion of insulin. In addition to this, the GH also stimulates β-cells directly and causes secretion of insulin. Because of the excess stimulation, β-cells are burnt out at one stage. This causes deficiency of insulin, leading to **true diabetes mellitus** or **full-blown diabetes mellitus.** This effect of GH is called the **diabetogenic effect.**

2. *On bones*

In embryonic stage, GH is responsible for the differentiation and development of bone cells. In later stages, GH increases the growth of the skeleton. It increases both the length as well as the thickness of the bones.

In bones, GH increases:

i. Synthesis and deposition of proteins by chondrocytes and osteogenic cells

ii. Multiplication of **chondrocytes** and **osteogenic cells** by enhancing the intestinal calcium absorption

iii. Formation of new bones by converting chondrocytes into osteogenic cells

iv. Availability of calcium for mineralization of bone matrix.

GH increases the length of the bones, until epiphysis fuses with shaft, which occurs at the time of puberty. After the **epiphyseal fusion,** length of the bones cannot be increased. However, it stimulates the **osteoblasts** strongly. So, the bone continues to grow in thickness throughout the life. Particularly, the membranous bones

such as the jaw bone and the skull bones become thicker under the influence of GH.

Hypersecretion of GH before the fusion of epiphysis with the shaft of the bones causes enormous growth of the skeleton, leading to a condition called **gigantism.** Hypersecretion of GH after the fusion of epiphysis with the shaft of the bones leads to a condition called **acromegaly.**

Mode of Action of GH – Somatomedin

GH acts on bones, growth and protein metabolism through somatomedin secreted by liver. GH stimulates the liver to secrete somatomedin. Sometimes, in spite of normal secretion of GH, growth is arrested (dwarfism) due to the absence or deficiency of somatomedin.

Somatomedin

Somatomedin is defined as a substance through which growth hormone acts. It is a polypeptide with the molecular weight of about 7,500.

Types of somatomedin

Somatomedins are of two types:

i. Insulin-like growth factor-I (IGF-I), which is also called somatomedin C
ii. Insulin-like growth factor-II.

Somatomedin C (IGF-I) acts on the bones and protein metabolism. Insulin-like growth factor-II plays an important role in the growth of fetus.

Duration of action of GH and somatomedin C

GH is transported in blood by loose binding with plasma protein. So, at the site of action, it is released from plasma protein rapidly. Its action also lasts only for a short duration of 20 minutes. But, the somatomedin C binds with plasma proteins very strongly. Because of this, the molecules of somatomedin C are released slowly from the plasma proteins. Thus, it can act continuously for a longer duration. The action of somatomedin C lasts for about 20 hours.

Mode of action of somatomedin C

Somatomedin C acts through the second messenger called cyclic AMP (refer previous Chapter).

Growth hormone receptor

GH receptor is called **growth hormone secretagogue** (GHS) receptor. It is a transmembrane receptor, belonging to cytokine receptor family. GH binds with the receptor situated mainly in liver cells and forms the hormone-receptor complex. Hormone-receptor complex induces various intracellular enzyme pathways, resulting in somatomedin secretion. Somatomedin in turn, executes the actions of growth hormone.

Regulation of GH Secretion

Growth hormone secretion is altered by various factors. However, hypothalamus and feedback mechanism play an important role in the regulation of GH secretion

GH secretion is stimulated by:

1. Hypoglycemia
2. Fasting
3. Starvation
4. Exercise
5. Stress and trauma
6. Initial stages of sleep.

GH secretion is inhibited by:

1. Hyperglycemia
2. Increase in free fatty acids in blood
3. Later stages of sleep.

Role of hypothalamus in the secretion of GH

Hypothalamus regulates GH secretion via three hormones:

1. Growth hormone-releasing hormone (GHRH): It increases the GH secretion by stimulating the somatotropes of anterior pituitary
2. Growth hormone-releasing polypeptide (GHRP): It increases the release of GHRH from hypothalamus and GH from pituitary
3. Growth hormone-inhibitory hormone (GHIH) or somatostatin: It decreases the GH secretion. Somatostatin is also secreted by delta cells of islets of Langerhans in pancreas.

These three hormones are transported from hypothalamus to anterior pituitary by hypothalamo-hypophyseal portal blood vessels.

Feedback control

GH secretion is under **negative feedback** control (Chapter 4). Hypothalamus releases GHRH and GHRP, which in turn promote the release of GH from anterior pituitary. GH acts on various tissues. It also activates the liver cells to secrete somatomedin C (IGF-I). Now, the somatomedin C increases the release of GHIH from hypothalamus. GHIH, in turn inhibits the release of GH from pituitary. Somatomedin also inhibits release of GHRP from hypothalamus. It acts on pituitary directly and inhibits the secretion of GH (Fig. 66.3). GH inhibits its own secretion by stimulating the release of GHIH from hypothalamus. This type of feedback is called **short-loop feedback** control. Similarly, GHRH inhibits its own release by short-loop feedback control.

Whenever, the blood level of GH decreases, the GHRH is secreted from the hypothalamus. It in turn causes secretion of GH from pituitary.

Role of ghrelin in the secretion of GH

Ghrelin is a peptide hormone synthesized by epithelial cells in the fundus of stomach. It is also produced in smaller amount in hypothalamus, pituitary, kidney and placenta (Chapter 44). Ghrelin promotes secretion of GH by stimulating somatotropes directly.

④ OTHER HORMONES OF ANTERIOR PITUITARY

Thyroid-stimulating Hormone (TSH)

TSH is necessary for the growth and secretory activity of the thyroid gland. It has many actions on the thyroid gland. Refer Chapter 67 for details of TSH.

Adrenocorticotropic Hormone (ACTH)

ACTH is necessary for the structural integrity and the secretory activity of adrenal cortex. It has other functions also. Refer Chapter 70 for details of ACTH.

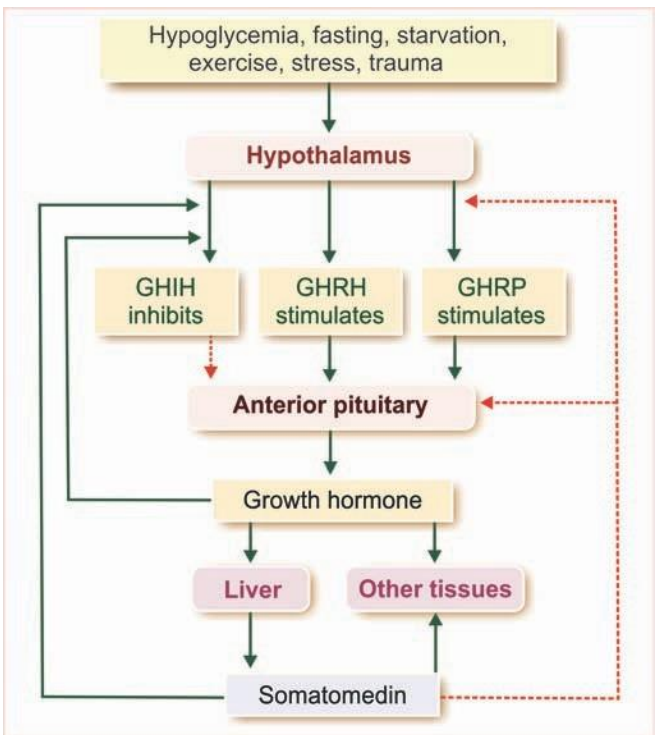


FIGURE 66.3: Regulation of GH secretion. GHIH = Growth hormone-inhibiting hormone, GHRH = Growth hormone-releasing hormone, GHRP = Growth hormone-releasing polypeptide. Growth hormone and somatomedin stimulate hypothalamus to release GHIH . Somatomedin inhibits anterior pituitary directly. Solid green line = Stimulation/secretion, Dashed red line = Inhibition.

Follicle-stimulating Hormone (FSH)

Follicle-stimulating hormone is a glycoprotein made up of one α-subunit and a β-subunit. The α-subunit has 92 amino acids and β-subunit has 118 amino acids. The half-life of FSH is about 3 to 4 hours.

Actions of FSH

In males, FSH acts along with testosterone and accelerates the process of **spermeogenesis** (refer Chapter 74 for details).

In females FSH:

1. Causes the development of **graafian follicle** from primordial follicle
2. Stimulates the theca cells of graafian follicle and causes secretion of estrogen (refer Chapter 79 for details)
3. Promotes the **aromatase activity** in granulosa cells, resulting in conversion of androgens into estrogen (Chapter 80).

Luteinizing Hormone (LH)

LH is a glycoprotein made up of one α-subunit and one β-subunit. The α-subunit has 92 amino acids and β-subunit has 141 amino acids. The half-life of LH is about 60 minutes.

Actions of LH

In males, LH is known as **interstitial cell-stimulating hormone** (ICSH) because it stimulates the interstitial cells of Leydig in testes. This hormone is essential for the secretion of testosterone from Leydig cells (Chapter 74).

In females, LH:

1. Causes maturation of vesicular follicle into graafian follicle along with follicle-stimulating hormone
2. Induces synthesis of androgens from theca cells of growing follicle
3. Is responsible for **ovulation**
4. Is necessary for the formation of corpus luteum
5. Activates the secretory functions of corpus luteum.

Prolactin

Prolactin is a single chain polypeptide with 199 amino acids. Its half-life is about 20 minutes. Prolactin is necessary for the final preparation of mammary glands for the production and secretion of milk. Prolactin acts directly on the epithelial cells of mammary glands and causes localized **alveolar hyperplasia.** Refer Chapter 87 for details.

β-lipotropin

β-lipotropin is a polypeptide hormone with 31 amino acids. It mobilizes fat from adipose tissue and promotes lipolysis. It also forms the precursor of endorphins. This hormone acts through the adenyl cyclase.

POSTERIOR PITUITARY OR NEUROHYPOPHYSIS

④ PARTS

Posterior pituitary consists of three parts:

1. Pars nervosa or infundibular process
2. Neural stalk or infundibular stem
3. Median eminence.

Pars tuberalis of anterior pituitary and the neural stalk of posterior pituitary together form the **hypophyseal stalk.**

④ HISTOLOGY

Posterior pituitary is made up of neural type of cells called pituicytes and unmyelinated nerve fibers.

Pituicytes

Pituicytes are the fusiform cells derived from glial cells. These cells have several processes and brown pigment granules. Pituicytes act as supporting cells and do not secrete any hormone.

Unmyelinated Nerve Fibers

Unmyelinated nerve fibers come from supraoptic and paraventricular nuclei of the hypothalamus through the pituitary stalk.

Other Structures

Posterior pituitary also has numerous blood vessels, hyaline bodies, neuroglial cells and mast cells.

④ HORMONES OF POSTERIOR PITUITARY

Posterior pituitary hormones are:

1. Antidiuretic hormone (ADH) or vasopressin
2. Oxytocin.

Source of Secretion of Posterior Pituitary Hormones

Actually, the posterior pituitary does not secrete any hormone. ADH and oxytocin are synthesized in the hypothalamus. From hypothalamus, these two hormones are transported to the posterior pituitary through the nerve fibers of **hypothalamo-hypophyseal tract** (Fig. 66.4), by means of axonic flow. Proteins involved in transport of these hormones are called neurophysins (see below).

In the posterior pituitary, these hormones are stored at the nerve endings. Whenever, the impulses from hypothalamus reach the posterior pituitary, these hormones are released from the nerve endings into the circulation. Hence, these two hormones are called **neurohormones.**

Experimental Evidence

Secretion of posterior pituitary hormones in hypothalamus and their transport to posterior pituitary are proved by experimental evidences. When the pituitary stalk is cut above the pituitary gland, by leaving the entire hypothalamus intact, the hormones drip through the cut end of the nerves in the pituitary stalk. This proves the fact that the hormones are secreted by hypothalamus.

Neurophysins

Neurophysins are the binding proteins which transport ADH and oxytocin from hypothalamus to posterior pituitary via hypothalamo-hypophyseal tract and storage of these hormones in posterior pituitary. Neurophysin I or oxytocin-neurophysin is the binding protein for oxytocin and neurophysin II or ADH-neurophysin is the binding protein for ADH.

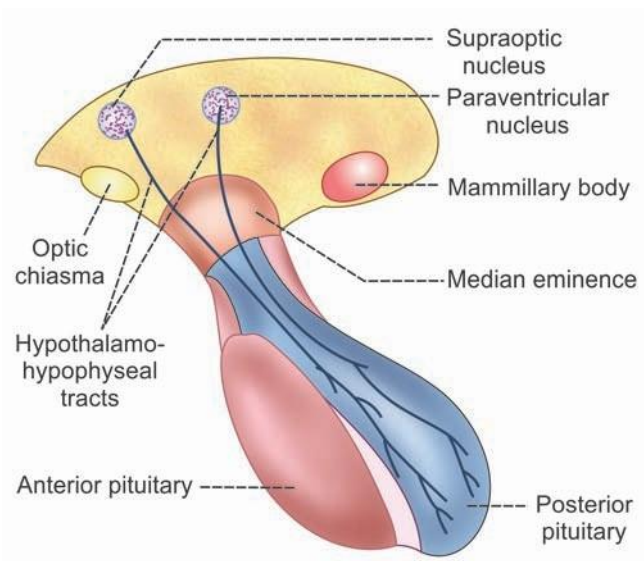


FIGURE 66.4: Hypothalamo-hypophyseal tracts

④ ANTIDIURETIC HORMONE

Source of Secretion

Antidiuretic hormone (ADH) is secreted mainly by **supraoptic nucleus** of hypothalamus. It is also secreted by **paraventricular nucleus** in small quantity. From here, this hormone is transported to posterior pituitary through the nerve fibers of hypothalamo-hypophyseal tract, by means of axonic flow.

Chemistry and Half-life

Antidiuretic hormone is a polypeptide containing 9 amino acids. Its half-life is 18 to 20 minutes.

Actions

Antidiuretic hormone has two actions:
1. Retention of water
2. Vasopressor action.

1. Retention of water

Major function of ADH is retention of water by acting on kidneys. It increases the **facultative reabsorption** of water from distal convoluted tubule and collecting duct in the kidneys (Chapter 52). In the absence of ADH, the distal convoluted tubule and collecting duct are totally impermeable to water. So, reabsorption of water does not occur in the renal tubules and dilute urine is excreted. This leads to loss of large amount of water through urine. This condition is called **diabetes insipidus** and the excretion of large amount of water is called diuresis.

Mode of action on renal tubules

ADH increases water reabsorption in tubular epithelial membrane by regulating the **water channel proteins** called **aquaporins** through **V2 receptors** (Chapter 52).

2. Vasopressor action

In large amount, ADH shows vasoconstrictor action. Particularly, causes constriction of the arteries in all parts of the body. Due to vasoconstriction, the blood pressure increases. ADH acts on blood vessels through V_{1A} receptors. However, the amount of ADH required to cause the vasopressor effect is greater than the amount required to cause the **antidiuretic effect.**

Regulation of Secretion

ADH secretion depends upon the volume of body fluid and the osmolarity of the body fluids.

Potent stimulants for ADH secretion are:
1. Decrease in the extracellular fluid (ECF) volume
2. Increase in osmolar concentration in the ECF.

Role of osmoreceptors

Osmoreceptors are the receptors which give response to change in the osmolar concentration of the blood. These receptors are situated in the hypothalamus near supraoptic and paraventricular nuclei. When osmolar concentration of blood increases, the osmoreceptors are activated. In turn, the osmoreceptors stimulate the supraoptic and paraventricular nuclei which send motor impulses to posterior pituitary through the nerve fibers and cause release of ADH. ADH causes reabsorption of water from the renal tubules. This increases ECF volume and restores the normal osmolarity.

④ OXYTOCIN

Source of Secretion

Oxytocin is secreted mainly by **paraventricular nucleus** of hypothalamus. It is also secreted by **supraoptic nucleus** in small quantity and it is transported from hypothalamus to posterior pituitary through the nerve fibers of hypothalamo-hypophyseal tract. In the posterior pituitary, the oxytocin is stored in the nerve endings of hypothalamo-hypophyseal tract. When suitable stimuli reach the posterior pituitary from hypothalamus, oxytocin is released into the blood. Oxytocin is secreted in both males and females.

Chemistry and Half-life

Oxytocin is a polypeptide having 9 amino acids. It has a half-life of about 6 minutes.

Actions in Females

In females, oxytocin acts on mammary glands and uterus.

Action of oxytocin on mammary glands

Oxytocin causes ejection of milk from the mammary glands. Ducts of the mammary glands are lined by myo-epithelial cells. Oxytocin causes contraction of the myo-epithelial cells and flow of milk from alveoli of mammary glands to the exterior through duct system and nipple. The process by which the milk is ejected from alveoli of mammary glands is called milk ejection reflex or milk let-down reflex. It is one of the **neuroendocrine reflexes.**

Milk ejection reflex

Plenty of touch receptors are present on the mammary glands, particularly around the nipple. When the

infant suckles mother nipple, the touch receptors are stimulated. The impulses discharged from touch receptors are carried by the somatic afferent nerve fibers to paraventricular and supraoptic nuclei of hypothalamus.

Now hypothalamus, in turn sends impulses to the posterior pituitary through hypothalamo-hypophyseal tract. Afferent impulses cause release of oxytocin into the blood. When the hormone reaches the mammary gland, it causes contraction of myoepithelial cells, resulting in ejection of milk from mammary glands (Fig. 66.5).

As this reflex is initiated by the nervous factors and completed by the hormonal action, it is called a **neuroendocrine reflex.** During this reflex, large amount of oxytocin is released by **positive feedback mechanism.**

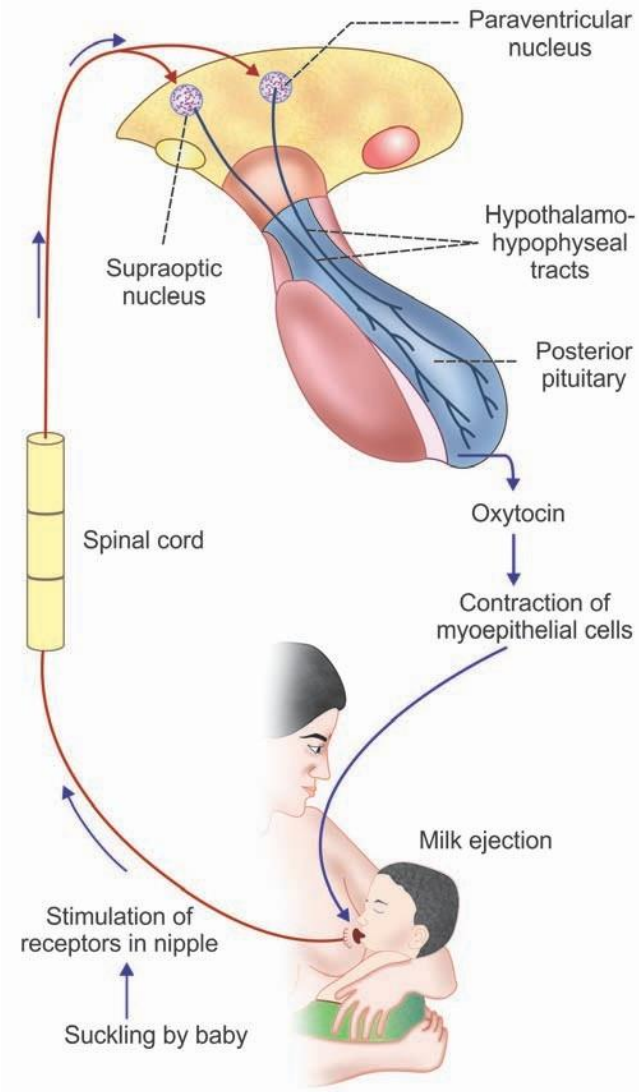


FIGURE 66.5: Milk ejection reflex

Action on uterus

Oxytocin acts on pregnant uterus and also non-pregnant uterus.

On pregnant uterus

Throughout the period of pregnancy, oxytocin secretion is inhibited by estrogen and progesterone. At the end of pregnancy, the secretion of these two hormones decreases suddenly and the secretion of oxytocin increases. Oxytocin causes contraction of uterus and helps in the expulsion of fetus.

During the later stages of pregnancy, the number of receptors for oxytocin increases in the wall of the uterus. Because of this, the uterus becomes more sensitive to oxytocin.

Oxytocin secretion increases during **labor.** At the onset of labor, the cervix dilates and the fetus descends through the birth canal. During the movement of fetus through cervix, the receptors on the cervix are stimulated and start discharging large number of impulses. These impulses are carried to the paraventricular and supraoptic nuclei of hypothalamus by the somatic afferent nerve fibers. Now, these two hypothalamic nuclei secrete large quantity of oxytocin, which enhances labor by causing contraction of uterus (Chapter 84).

Throughout labor, large quantity of oxytocin is released by means of **positive feedback mechanism,** i.e. oxytocin induces contraction of uterus, which in turn causes release of more amount of oxytocin (Fig. 4.5).

The contraction of uterus during labor is also a neuroendocrine reflex. Oxytocin also stimulates the release of prostaglandins in the placenta. Prostaglandins intensify the uterine contraction induced by oxytocin.

On non-pregnant uterus

The action of oxytocin on non-pregnant uterus is to facilitate the transport of sperms through female genital tract up to the fallopian tube, by producing the uterine contraction during sexual intercourse.

During the sexual intercourse, the receptors in the vagina are stimulated. Vaginal receptors generate the impulses, which are transmitted by somatic afferent nerves to the paraventricular and supraoptic nuclei of hypothalamus. When, these two nuclei are stimulated, oxytocin is released and transported by blood. While reaching the female genital tract, the hormone causes antiperistaltic contractions of uterus towards the fallopian tube. It is also a **neuroendocrine reflex.**

Sensitivity of uterus to oxytocin is accelerated by estrogen and decreased by progesterone.

Action in Males

In males, the release of oxytocin increases during ejaculation. It facilitates release of sperm into urethra by causing contraction of smooth muscle fibers in reproductive tract, particularly vas deferens.

Mode of Action of Oxytocin

Oxytocin acts on mammary glands and uterus by activating **G-protein coupled oxytocin receptor.**

⚕ APPLIED PHYSIOLOGY – DISORDERS OF PITUITARY GLAND

Disorders of pituitary gland are given in Table 66.1.

④ HYPERACTIVITY OF ANTERIOR PITUITARY

1. *Gigantism*

Gigantism is the pituitary disorder characterized by excess growth of the body. The subjects look like the giants with average height of about 7 to 8 feet.

Causes

Gigantism is due to hypersecretion of GH in childhood or in pre-adult life before the **fusion of epiphysis** of bone with shaft. Hypersecretion of GH is because of tumor of acidophil cells in the anterior pituitary.

Signs and symptoms

i. General overgrowth of the person leads to the development of a huge stature, with a height of more than 7 or 8 feet. The limbs are disproportionately long
ii. Giants are hyperglycemic and they develop glycosuria and pituitary diabetes. Hyperglycemia causes constant stimulation of β-cells of islets of Langerhans in the pancreas and release of insulin. However, the overactivity of β-cells of Langerhans in pancreas leads to degeneration of these cells and deficiency of insulin and ultimately, diabetes mellitus is developed
iii. Tumor of the pituitary gland itself causes constant headache
iv. Pituitary tumor also causes **visual disturbances.** It compresses the lateral fibers of optic chiasma, leading to **bitemporal hemianopia** (Chapter 168)

2. *Acromegaly*

Acromegaly is the disorder characterized by the enlargement, thickening and broadening of bones, particularly in the extremities of the body.

Causes

Acromegaly is due to hypersecretion of GH in adults after the fusion of epiphysis with shaft of the bone. Hypersecretion of GH is because of tumor of acidophil cells in the anterior pituitary.

Signs and symptoms

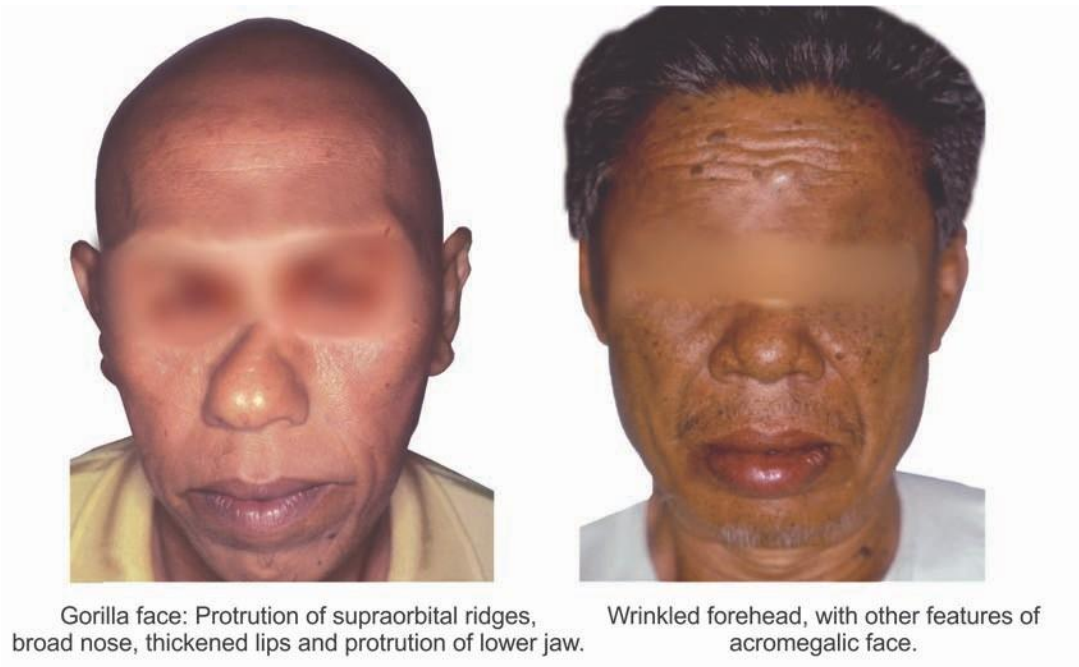
i. Acromegalic or **gorilla face:** Face with rough features such as protrusion of supraorbital ridges, broadening of nose, thickening of lips, thickening and wrinkles formation on forehead and **prognathism** (protrusion of lower jaw) (Fig. 66.6)
ii. Enlargement of hands and feet (Fig. 66.7)
iii. Kyphosis (extreme curvature of upper back – thoracic spine)
iv. Thickening of scalp. Scalp is also thrown into folds or wrinkles like **bulldog scalp**
v. Overgrowth of body hair
vi. Enlargement of visceral organs such as lungs, thymus, heart, liver and spleen
vii. Hyperactivity of thyroid, parathyroid and adrenal glands
viii. Hyperglycemia and glucosuria, resulting in diabetes mellitus
ix. Hypertension
x. Headache
xi. Visual disturbance **(bitemporal hemianopia).**

3. *Acromegalic Gigantism*

Acromegalic gigantism is a rare disorder with symptoms of both gigantism and acromegaly. Hypersecretion of GH

TABLE 66.1: Disorders of pituitary gland

Parts involved	Hyperactivity	Hypoactivity
Anterior pituitary	Gigantism Acromegaly Acromegalic gigantism Cushing disease	Dwarfism Acromicria Simmond disease
Posterior pituitary	Syndrome of inappropriate hypersecretion of ADH (SIADH)	Diabetes insipidus
Anterior and posterior pituitary	–	Dystrophia adiposogenitalis



Gorilla face: Protrution of supraorbital ridges, broad nose, thickened lips and protrution of lower jaw.

Wrinkled forehead, with other features of acromegalic face.

FIGURE 66.6: Acromegaly (*Courtesy:* Prof Mafauzy Mohamad)

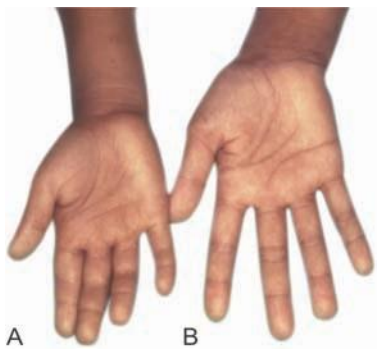


FIGURE 66.7: A. Normal hand; B. Acromegalic hand (*Courtesy:* Prof Mafauzy Mohamad)

in children, before the fusion of epiphysis with shaft of the bones causes gigantism and if hypersecretion of GH is continued even after the fusion of epiphysis, the symptoms of acromegaly also appear.

4. *Cushing Disease*

It is also a rare disease characterized by obesity.

Causes

Cushing disease develops by basophilic adenoma of adenohypophysis. It increases the secretion of adrenocorticotropic hormone, which in turn stimulates the adrenal cortex to release cortisol. Cushing disease also develops by hyperplasia or tumor of adrenal cortex.

Usually, the disorder due to the pituitary cause is called **Cushing disease** and when it is due to the adrenal cause, it is called **Cushing syndrome.**

Details of this condition are given in Chapter 70.

④ HYPOACTIVITY OF ANTERIOR PITUITARY

1. *Dwarfism*

Dwarfism is a pituitary disorder in children, characterized by the stunted growth.

Causes

Reduction in GH secretion in infancy or early childhood causes dwarfism. It occurs because of the following reasons:

i. Tumor of chromophobes: It is a non-functioning tumor, which compresses and destroys the normal cells secreting GH. It is the most common cause for hyposecretion of GH, leading to dwarfism
ii. Deficiency of GH-releasing hormone secreted by hypothalamus
iii. Deficiency of somatomedin C
iv. Atrophy or degeneration of acidophilic cells in the anterior pituitary
iv. **Panhypopituitarism:** In this condition, there is reduction in the secretion of all the hormones of anterior pituitary gland. This type of dwarfism is associated with other symptoms due to the deficiency of other anterior pituitary hormones.

Signs and symptoms

i. Primary symptom of hypopituitarism in children is the stunted skeletal growth. The maximum height of anterior pituitary dwarf at the adult age is only about 3 feet
ii. But the proportions of different parts of the body are almost normal. Only the head becomes slightly larger in relation to the body
iii. Pituitary dwarfs do not show any deformity and their mental activity is normal with no mental retardation
iv. Reproductive function is not affected, if there is only GH deficiency. However, during panhypopituitarism, the dwarfs do not obtain puberty due to the deficiency of gonadotropic hormones.

Laron dwarfism

Laron dwarfism is a genetic disorder. It is also called **GH insensitivity.** It occurs due to the presence of abnormal growth hormone **secretagogue** (GHS) receptors in liver. GHS receptors become abnormal because of the mutation of genes for the receptors.

GH secretion is normal or high. But the hormone cannot stimulate growth because of the abnormal GHS receptors. So, dwarfism occurs.

Psychogenic dwarfism

Dwarfism occurs if the child is exposed to extreme emotional deprivation or stress. The short stature is because of deficiency of GH. This type of dwarfism is called psychogenic dwarfism, **psychosocial dwarfism** or **stress dwarfism.**

Dwarfism in dystrophia adiposogenitalis

Dystrophia adiposogenitalis or **Fröhlich syndrome** is a pituitary disorder (see below). Dwarfism occurs if it develops in children.

Dwarfism in panhypopituitarism

Panhypopituitarism is the pituitary disorder due to reduction in secretion of all anterior pituitary hormones. These dwarfs do not attain puberty.

2. *Acromicria*

Acromicria is a rare disease in adults characterized by the atrophy of the extremities of the body.

Causes

Deficiency of GH in adults causes acromicria. The secretion of GH decreases in the following conditions:

i. Deficiency of GH-releasing hormone from hypothalamus
ii. Atrophy or degeneration of acidophilic cells in the anterior pituitary
iii. Tumor of chromophobes: It is a non-functioning tumor, which compresses and destroys the normal cells secreting the GH. This is the most common cause for hyposecretion of GH leading to acromicria
iv. Panhypopituitarism: In this condition, there is a reduction in secretion of all the hormones of anterior pituitary gland. Acromicria is associated with other symptoms due to the deficiency of other anterior pituitary hormones.

Signs and symptoms

i. Atrophy and thinning of extremities of the body, (hands and feet) are the major symptoms in acromicria
ii. Acromicria is mostly associated with hypothyroidism
iii. Hyposecretion of adrenocortical hormones also is common in acromicria
iv. The person becomes lethargic and obese
v. There is loss of sexual functions.

3. *Simmond Disease*

Simmond disease is a rare pituitary disease. It is also called **pituitary cachexia.**

Causes

It occurs mostly in panhypopituitarism, i.e. hyposecretion of all the anterior pituitary hormones due to the atrophy or degeneration of anterior pituitary.

Symptoms

i. A major feature of Simmond disease is the rapidly developing **senile decay.** Thus, a 30-years-old person looks like a 60-years-old person. The senile decay is mainly due to deficiency of hormones from target glands of anterior pituitary, i.e. the thyroid gland, adrenal cortex and the gonads
ii. There is loss of hair over the body and loss of teeth
iii. Skin on face becomes dry and wrinkled. So, there is a shrunken appearance of facial features. It is the most common feature of this disease.

④ HYPERACTIVITY OF POSTERIOR PITUITARY

Syndrome of Inappropriate Hypersecretion of Antidiuretic Hormone (SIADH)

SIADH is the disease characterized by loss of sodium through urine due to hypersecretion of ADH.

Causes

SIADH occurs due to cerebral tumors, lung tumors and lung cancers because the **tumor cells** and **cancer cells** secrete ADH.

In normal conditions, ADH decreases the urine output by facultative reabsorption of water in distal convoluted tubule and the collecting duct. Urine that is formed is concentrated with sodium and other ions. Loss of sodium decreases the osmalarity of plasma, making it hypotonic. Hypotonic plasma inhibits ADH secretion resulting in restoration of plasma osmolarity.

However, in SIADH, secretion of ADH from tumor or cancer cells is not inhibited by hypotonic plasma. So there is continuous loss of sodium, resulting in persistent plasma hypotonicity.

Signs and symptoms

1. Loss of appetite
2. Weight loss
3. Nausea and vomiting
4. Headache
5. Muscle weakness, spasm and cramps
6. Fatigue
7. Restlessness and irritability.

In severe conditions, the patients die because of convulsions and coma.

④ HYPOACTIVITY OF POSTERIOR PITUITARY

Diabetes Insipidus

Diabetes insipidus is a posterior pituitary disorder characterized by excess excretion of water through urine.

Causes

This disorder develops due to the deficiency of ADH, which occurs in the following conditions:

i. Lesion (injury) or degeneration of supraoptic and paraventricular nuclei of hypothalamus
ii. Lesion in hypothalamo-hypophyseal tract
iii. Atrophy of posterior pituitary
iv. Inability of renal tubules to give response to ADH hormone. Such condition is called nephrogenic diabetes insipidus (see below).

Signs and symptoms

i. *Polyuria:* Excretion of large quantity of dilute urine, with increased frequency of voiding is called polyuria. Daily output of urine varies between 4 to 12 liter. In the absence of ADH, the epithelial cells of distal convoluted tubule in the nephron and the collecting duct of the kidney become impermeable to water. So, water is not reabsorbed from the renal tubule and collecting duct, leading to loss of water through urine.
ii. *Polydipsia:* Intake of excess water is called polydipsia. Because of polyuria, lot of water is lost from the body. It stimulates the thirst center in hypothalamus, resulting in intake of large quantity of water.
iii. *Dehydration:* In some cases, the thirst center in the hypothalamus is also affected by the lesion. Water intake decreases in these patients and loss of water through urine is not compensated. So, dehydration develops which may lead to death.

Nephrogenic diabetes insipidus

Nephrogenic diabetes insipidus is a genetic disorder due to inability of renal tubules to give response to ADH. It is caused by mutations of genes of V_2 receptors or aquaporin 2.

④ HYPOACTIVITY OF ANTERIOR AND POSTERIOR PITUITARY

Dystrophia Adiposogenitalis

Dystrophia adiposogenitalis is a disease characterized by **obesity** and **hypogonadism,** affecting mainly the adolescent boys. It is also called **Fröhlich syndrome** or **hypothalamic eunuchism.**

Causes

Dystrophia adiposogenitalis is due to hypoactivity of both anterior pituitary and posterior pituitary. Common cause of this disease is the tumor in pituitary gland and hypothalamic regions, concerned with food intake and gonadal development. Other causes are injury or atrophy of pituitary gland and genetic inability of hypothalamus to secrete luteinizing hormone-releasing hormone.

Symptoms

Obesity is the common feature of this disorder. Due to the abnormal stimulation of feeding center, the person overeats and consequently becomes obese. Obesity is accompanied by **sexual infantilism** (failure to develop secondary sexual characters) or eunuchism. **Dwarfism** occurs if the disease starts in growing age. In children, it is called infantile or prepubertal type of Fröhlich syndrome.

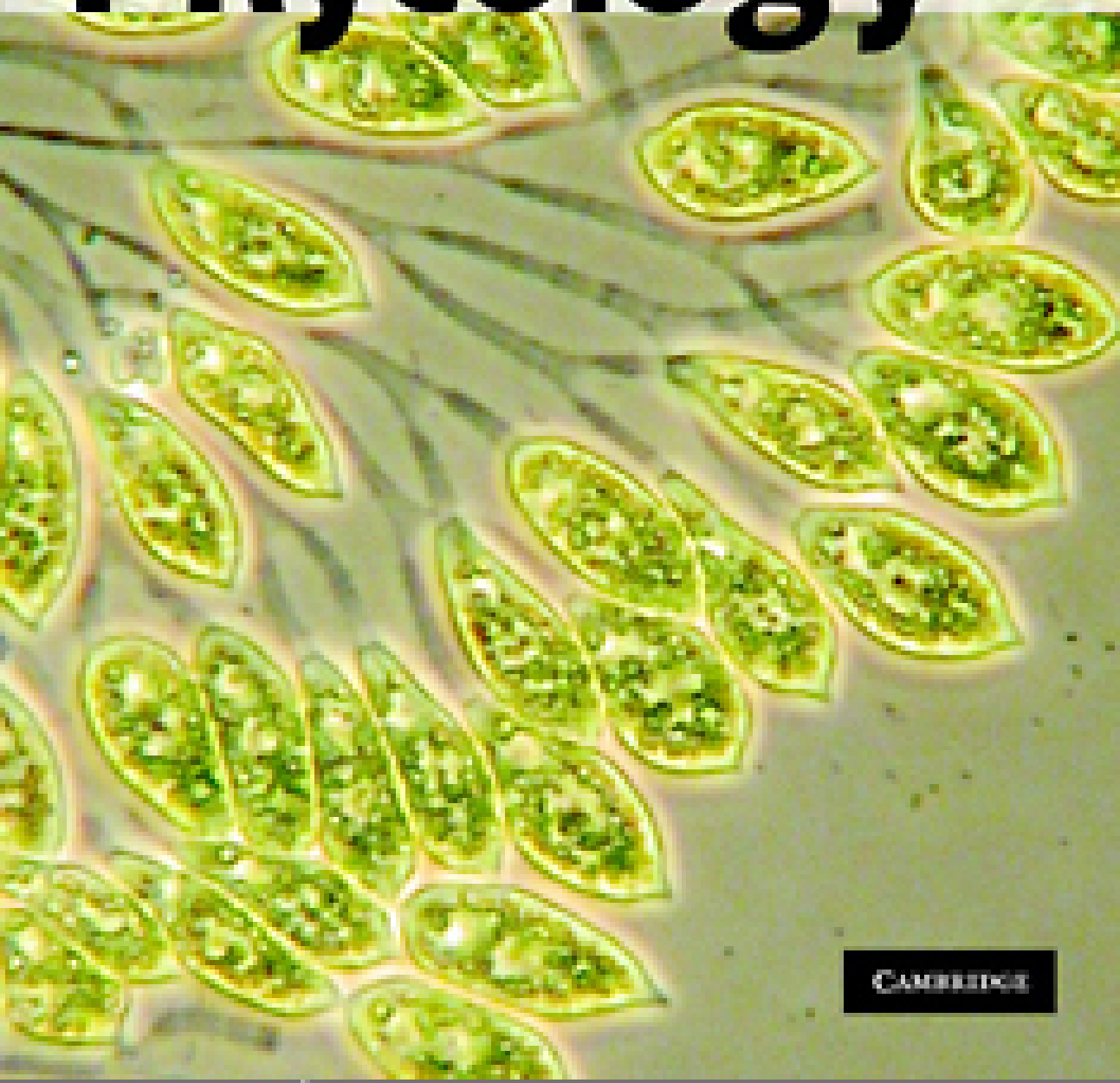
This disease develops in adults also. When it occurs in adults, it is called adult type of Fröhlich syndrome. In adults, the major symptoms are obesity and atrophy of sex organs.

Other features of this disorder are behavioral changes and loss of vision. Some patients develop diabetes insipidus.

Fourth Edition

Robert Edward Lee

Phycology



CAMBRIDGE

CAMBRIDGE www.cambridge.org/9780521864084

This page intentionally left blank

Phycology

Phycology is the study of algae, the primary photosynthetic organisms in freshwater and marine food chains. As a food source for zooplankton and filter-feeding shellfish, the algae are an extremely important group.

Since the publication of the first edition in 1980, this textbook has established itself as a classic resource on phycology. This revised edition maintains the format of previous editions, whilst incorporating the latest information from nucleic acid sequencing studies. Detailed life-history drawings of algae are presented alongside information on the cytology, ecology, biochemistry, and economic importance of selected genera.

Phycology is suitable for upper-level undergraduate and graduate students following courses in phycology, limnology or biological oceanography. Emphasis is placed on those algae that are commonly covered in phycology courses, and encountered by students in marine and freshwater habitats.

ROBERT LEE has had a long and varied career, teaching worldwide in countries including South Africa and Iran, as well as at Harvard Medical School, and Colorado State University, where he currently works as a Teaching Coordinator in the Department of Biomedical Sciences.

Phycology

Fourth edition

Robert Edward Lee
Colorado State University, USA

CAMBRIDGE
UNIVERSITY PRESS

CAMBRIDGE UNIVERSITY PRESS
Cambridge, New York, Melbourne, Madrid, Cape Town, Singapore, São Paulo

Cambridge University Press
The Edinburgh Building, Cambridge CB2 8RU, UK
Published in the United States of America by Cambridge University Press, New York
www.cambridge.org
Information on this title: www.cambridge.org/9780521864084

© R. E. Lee 2008

This publication is in copyright. Subject to statutory exception and to the provision of relevant collective licensing agreements, no reproduction of any part may take place without the written permission of Cambridge University Press.

First published in print format 2008

ISBN-13 978-0-511-38669-5 eBook (EBL)

ISBN-13 978-0-521-86408-4 hardback

ISBN-13 978-0-521-68277-0 paperback

Cambridge University Press has no responsibility for the persistence or accuracy of urls for external or third-party internet websites referred to in this publication, and does not guarantee that any content on such websites is, or will remain, accurate or appropriate.

To Patricia, Nicole, Alana, and Christian

Contents

Preface to the first edition *page ix*

Part I Introduction 1
1 Basic characteristics of the algae 3
Structure of the algal cell 3
Nutrition 23
Gene sequencing and algal systematics 24
Classification 24
Algae and the fossil record 26
References 27

Part II The prokaryotic algae 31
2 Cyanobacteria 33
Morphology 33
Cell wall and gliding 33
Pili and twitching 36
Sheaths 37
Protoplasmic structure 38
Gas vacuoles 41
Pigments and photosynthesis 43
Akinetes 45
Heterocysts 46
Nitrogen fixation 49
Circadian rhythms 52
Asexual reproduction 53
Growth and metabolism 55
Symbiosis 56
Ecology of cyanobacteria 59
Cyanotoxins 65
Cyanobacteria and the quality of drinking water 66
Utilization of cyanobacteria as food 67
Cyanophages 67
Secretion of antibiotics and siderophores 68
Calcium carbonate deposition and fossil record 69
Classification 71
References 74

Part III Evolution of the chloroplast 81
3 Glaucophyta 85
References 88

4 Rhodophyta 89
Cell structure 89
Calcification 93

Secretory cells 95
Iridescence 96
Epiphytes and parasites 96
Defense mechanisms of the red algae 98
Commercial utilization of red algal mucilages 99
Reproductive structures 101
Spore motility 106
Classification 107
References 132

5 Chlorophyta 139
Cell structure 139
Phototaxis and eyespots 141
Asexual reproduction 143
Sexual reproduction 143
Classification 144
Prasinophyceae 150
Charophyceae 154
Classification 155
Ulvophyceae 168
Classification 168
Chlorophyceae 189
Classification 191
References 226

Part IV Evolution of one membrane of chloroplast endoplasmic reticulum 239
6 Euglenophyta 245
Nucleus and nuclear division 248
Eyespot, paraflagellar swelling, and phototaxis 250
Muciferous bodies and extracellular structures 253
Chloroplasts and storage products 255
Nutrition 255
Classification 256
References 259

7 Dinophyta 262
Cell structure 263
Resting spores or cysts or hypnospores and fossil Dinophyceae 277
Toxins 279
Dinoflagellates and oil and coal deposits 284
Bioluminescence 285
Rhythms 287
Heterotrophic dinoflagellates 291
Symbiotic dinoflagellates 295
Classification 296
References 303

8 Apicomplexa 310
References 313

Part V Evolution of two membranes of chloroplast endoplasmic reticulum and the Chlorarachniophyta 315
9 Cryptophyta 321
Cell structure 321
Ecology 325
Symbiotic associations 326
Classification 326
References 330

10 Heterokontophyta, Chrysophyceae 333
Cell structure 333
Statospores 337
Nutrition 339
Ecology 339
Classification 341
References 346

11 Heterokontophyta, Synurophyceae 349
Classification 350
References 353

12 Heterokontophyta, Eustigmatophyceae 354
References 356

13 Heterokontophyta, Pinguiophyceae 357
References 358

14 Heterokontophyta, Dictyochophyceae 359
Classification 359
References 364

15 Heterokontophyta, Pelagophyceae 365
References 366

16 Heterokontophyta, Bolidophyceae 368
References 368

17 Heterokontophyta, Bacillariophyceae 369
Cell structure 369
Motility 378
Resting spores and resting cells 382
Auxospores 383
Rhythmic phenomena 386
Physiology 387
Chemical defense against predation 390
Ecology 391

Fossil diatoms 395
Classification 398
References 404

18 Heterokontophyta, Raphidophyceae 409
References 412

19 Heterokontophyta, Xanthophyceae 413
Cell structure 413
Asexual reproduction 415
Sexual reproduction 416
References 422

20 Heterokontophyta, Phaeothamniophyceae 424
References 425

21 Heterokontophyta, Phaeophyceae 426
Cell structure 427
Life history 431
Classification 433
References 475

22 Prymnesiophyta 484
Cell structure 484
Scales and coccoliths 490
Toxins 496
Classification 498
References 500

23 Algae and the environment 504
Toxic algae 504
Toxic algae and the end-Permian extinction 510
Cooling of the Earth, cloud condensation nuclei, and DMSP 511
Chemical defense mechanisms of algae 511
The Antarctic and Southern Ocean 513
The grand experiment 514
Antarctic lakes as a model for life on the planet Mars or Jupiter's moon Europa 515
Ultraviolet radiation, the ozone hole and sunscreens produced by algae 517
Hydrogen fuel cells and hydrogen gas production by algae 517
References 519

Glossary 521
Index 534

Preface to the first edition

It was that eccentric British soldier of fortune Col. Meinertzhagen, in his *Birds of Arabia*, who expressed the sentiment that prefaces should be kept short because few people ever read them. Accordingly, I would like to take a brief opportunity to express my gratitude to the people who offered encouragement and assistance during the preparation of this book. I would like to thank Adele Strauss Wolbarst, Robert Cnoops, Charmaine Slack, Sophia Skiordis, Caroline Mondel, Jill Keetley-Smith, Heather Edwards, Gail Arbeter, and the Lending Library at Boston Spa, England, for help while most of this manuscript was being prepared at the University of the Witwatersrand. For general encouragement while at Pahlavi (Shiraz) University and for providing assistance during the last turbulent and chaotic year of imperial rule in Iran, while the manuscript was being finished, I would like to thank Mark Gettner, Brian Coad, and Mumtaz Bokhari.

When photographs or drawings have been taken directly from the original material, this is indicated by stating in the legend that it is *from* the original work. Most of the drawings have been redrawn to suit my tastes, and these drawings are indicated by stating that the work is *after* the original. In some cases I have made drawings from photographs or have incorporated a number of drawings in one, in which case I state that the finished drawing is *adapted* from the original work or works.

I have used the metric system in this book, and the fine-structural illustrations are expressed in micrometers (μm) and nanometers (nm).

Part I

Introduction

Chapter 1

Basic characteristics of the algae

Phycology or algology is the study of the algae. The word **phycology** is derived from the Greek word *phykos*, which means "seaweed." The term **algology**, described in Webster's dictionary as the study of the algae, has fallen out of favor because it resembles the term *algogenic* which means "producing pain." The algae are **thallophytes** (plants lacking roots, stems, and leaves) that have chlorophyll *a* as their primary photosynthetic pigment and lack a sterile covering of cells around the reproductive cells. This definition encompasses a number of plant forms that are not necessarily closely related, for example, the cyanobacteria which are closer in evolution to the bacteria than to the rest of the algae.

Algae most commonly occur in water, be it freshwater, marine, or brackish. However, they can also be found in almost every other environment on earth, from the algae growing in the snow of some American mountains to algae living in lichen associations on bare rocks, to unicellular algae in desert soils, to algae living in hot springs. In most habitats they function as the primary producers in the food chain, producing organic material from sunlight, carbon dioxide, and water. Besides forming the basic food source for these food chains, they also form the oxygen necessary for the metabolism of the consumer organisms. In such cases humans rarely directly consume the algae as such, but harvest organisms higher up in the food chain (i.e., fish, crustaceans, shellfish). Some algae, particularly the reds and browns, are harvested and eaten as a vegetable, or the mucilages are extracted from the thallus for use as gelling and thickening agents.

Structure of the algal cell

There are two basic types of cells in the algae, **prokaryotic** and **eukaryotic**. Prokaryotic cells lack membrane-bounded organelles (plastids, mitochondria, nuclei, Golgi bodies, and flagella) and occur in the cyanobacteria (Fig. 2.11). The remainder of the algae are eukaryotic and have organelles.

A eukaryotic cell (Fig. 1.1) is often surrounded by a cell wall composed of polysaccharides that are partially produced and secreted by the Golgi body. The plasma membrane (plasmalemma) surrounds the remaining part of the cell; this membrane is a living structure responsible for controlling the influx and outflow of substances in the protoplasm. Locomotory organs, the flagella, propel the cell through the medium by their beating. The flagella are enclosed in the plasma membrane and have a specific number and orientation of microtubules. The nucleus, which contains the genetic material of the cell, is surrounded by a double membrane with pores in it. The contents of the nucleus are a nucleolus, chromosomes, and the background material or karyolymph. The chloroplasts have membrane sacs called thylakoids that carry out the light reactions of photosynthesis. The thylakoids are embedded in the stroma where the dark reactions of carbon fixation take place. The stroma has small 70S ribosomes, DNA, and in some cases the storage product. Chloroplasts are surrounded by the two membranes of the chloroplast envelope. Sometimes chloroplasts have a dense proteinaceous area, the pyrenoid, which is associated with storage-product formation.

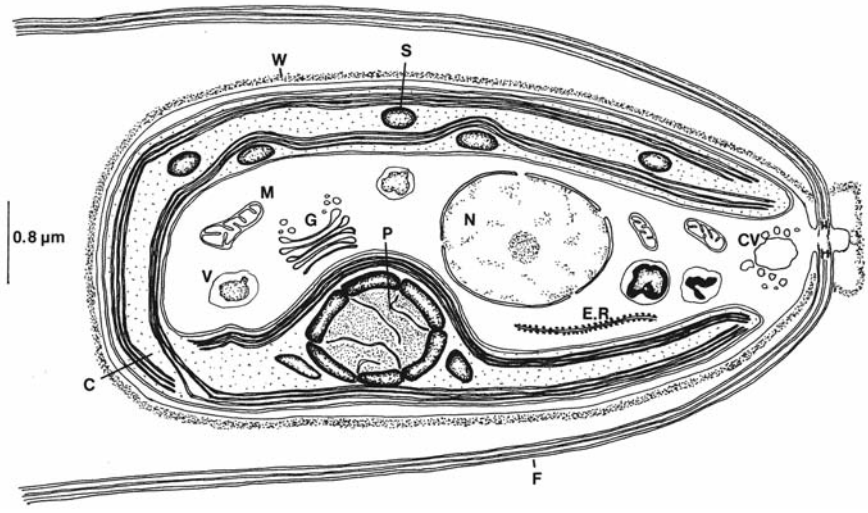


Fig. 1.1 Drawing of a cell of the green alga *Chlamydomonas* showing the organelles present in a eukaryotic algal cell. (C) Chloroplast; (CV) contractile vacuole; (E.R.) endoplasmic reticulum; (F) flagella; (G) Golgi body; (M) mitochondrion; (N) nucleus; (P) pyrenoid; (S) starch; (V) vacuole; (W) wall.

Double-membrane-bounded mitochondria have 70S ribosomes and DNA, and contain the respiratory apparatus. The Golgi body consists of a number of membrane sacs, called cisternae, stacked on top of one another. The Golgi body functions in the production and secretion of polysaccharides. The cytoplasm also contains large 80S ribosomes and lipid bodies.

Flagella

The flagella of the green alga *Chlamydomonas* have been used as a model of flagellar structure. Flagella structure has been highly conserved throughout evolution, images from *Chlamydomonas* are virtually indistinguishable from flagella (or **cilia** – a term for a short flagellum) of mammalian cells including human sperm and certain epithelia (Johnson, 1995). *Chlamydomonas* has been chosen because of the ease of growing the organism and because the flagella can be detached from the cells by pH shock or blending. Since the flagella are not essential for viability of the cell, it is relatively easy to isolate mutations affecting flagella synthesis by the cells.

A flagellum consists of an **axoneme** of nine doublet microtubules that surround two central microtubules, with all of the microtubules encased in the plasma membrane (Figs. 1.2, 1.3). On entering the cell body, the two central microtubules end at a dense plate, whereas the nine peripheral doublets continue into the cell, usually picking up an additional structure that transforms them into triplets. The flagellum passes through a tunnel in the cell wall called the **flagellar collar**.

The central pair of microtubules are single microtubules with 13 protofilaments while the outer microtubules are doublets with the A-tubule consisting of 13 protofilaments and the B-tubule having 11 protofilaments. The central-pair microtubules resemble cytoplasmic microtubules, in that they are more labile than the outer doublet microtubules. The axoneme microtubules are composed of α- and β-tubulin which make up 70% of the protein mass of the axoneme (Dutcher, 1995). **Radial spokes**, each consisting of a thin stalk and head, project from the A-tubule of the outer microtubule doublets (Figs. 1.2, 1.3).

Inner and outer **dynein arms** attach to the A-tubule of the outer microtubule doublet and extend to the B-tubule of the adjacent outer microtubule doublet. Dynein is a mechanoenzyme that hydrolyzes ATP with the resulting energy used by dynein to move along the B-tubule of the adjacent outer microtubule doublet (Fig. 1.3). In this action, the B-tubule is called the **track** while the A-tubule is called the **cargo**. The resulting displacement of outer microtubule

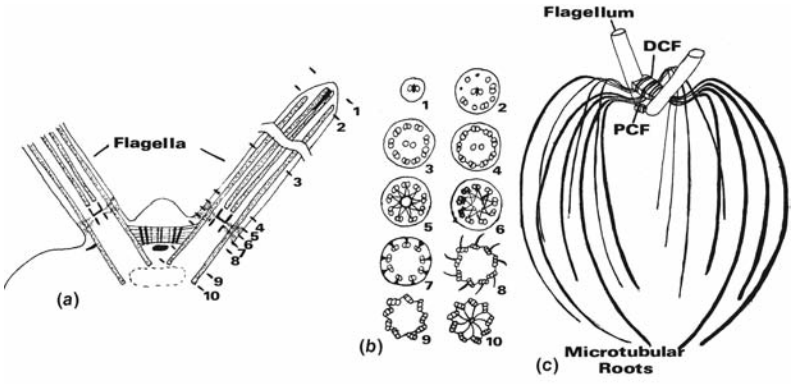


Fig. 1.2 The flagellar system in the green alga *Chlamydomonas*. (*a*) A diagrammatic drawing of a section of the flagellar system. The numbers refer to cross sections of the flagellar system in (*b*). (*c*) Diagrammatic drawing of the whole flagellar apparatus. The two flagella are joined by the proximal connecting fiber (PCF) and distal connecting fiber (DCF). (After Ringo, 1967.)

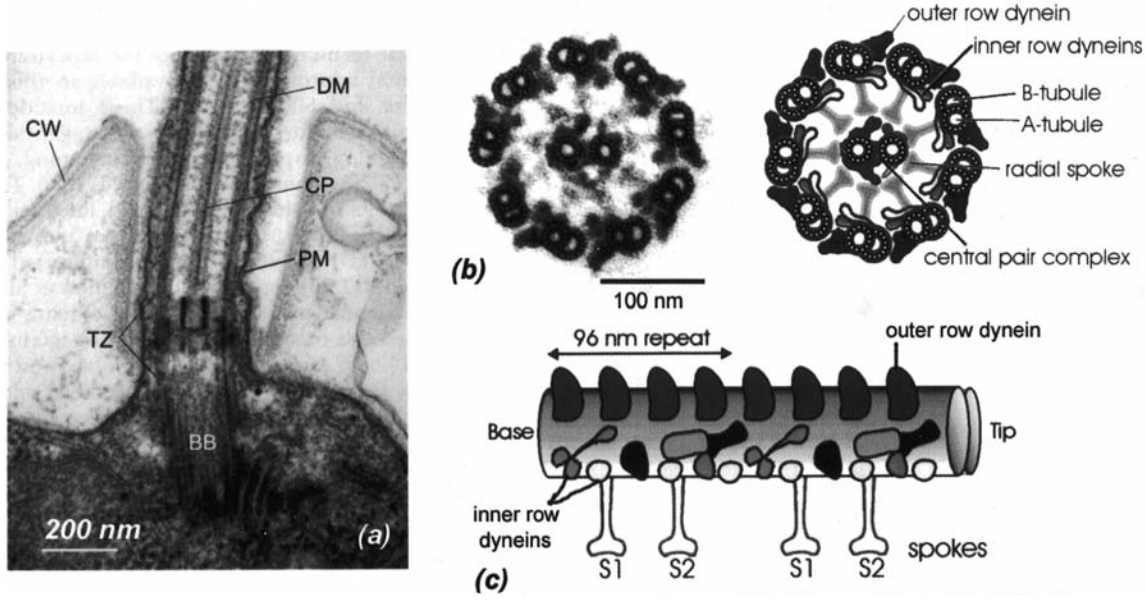


Fig. 1.3 *Chlamydomonas* flagella. (*a*) Transmission electron micrograph through the anterior region of a *Chlamydomonas reinhardtii* cell including the cell wall (CW), double microtubules (DM), central pair microtubules (CP), plasma membrane (PM), transition zone (TZ), and basal body (BB). (*b*) Thin section through an isolated demembranated flagellar axoneme showing the main components. (*c*) Diagrams of dyneins and related structures seen along the A-tubule of each doublet. (From Mitchell, 2000.)

doublets in relation to each other causes bending of the flagellum (Mitchell, 2000). Kinesin proteins cause the central pair of microtubules to rotate within the axoneme (Fig. 1.4). As the central pair of microtubules rotates, the microtubules interact with the individual radial spokes inducing sliding between adjacent microtubule doublets, asymmetric bending of the flagellum and propagation of flagellar waves (Johnson, 1995).

There are also other structures between the microtubules in the basal region of the flagellum (**basal body**). Attached to the basal body there can be either microtubular roots or striated fibrillar roots. The former type of root consists of a group of microtubules running from the basal body into the protoplasm (Figs. 1.2, 1.4), whereas the latter consists of groups of fibers that have striations along their length (Figs. 1.4, 1.6) The gamete of the green seaweed *Ulva lactuca* (sea lettuce) has both types of flagellar roots (Fig. 1.5) (Melkonian, 1980; Andersen et al., 1991). There are four **microtubular roots** composed of microtubules arranged in a cruciate pattern, and **fibrous roots** (**rhizoplasts**) composed of a bundle

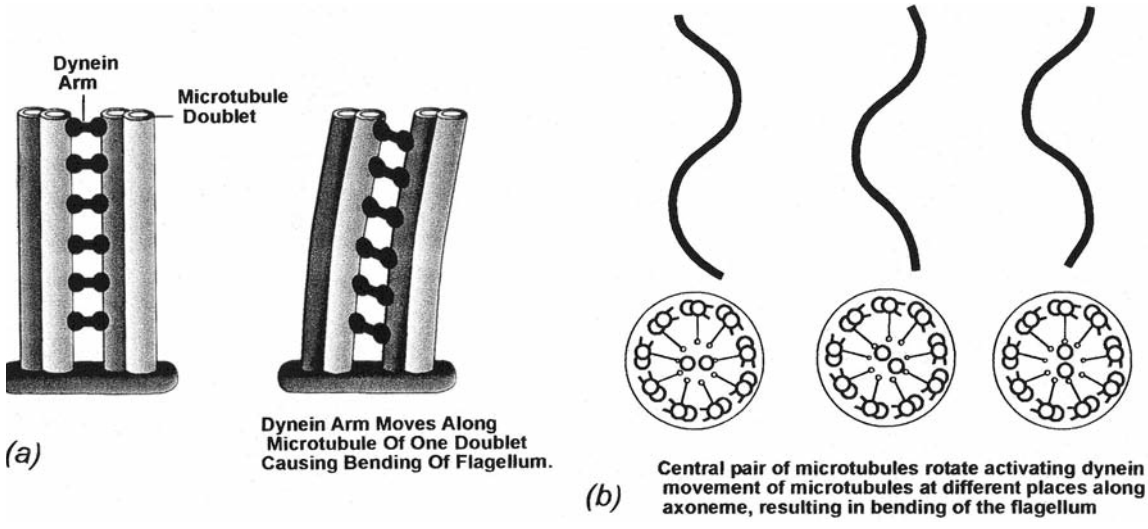


Fig. 1.4 Bending of flagella occurs by the rotating central pair of microtubules activating dynein movement of specific outer doublet microtubules.

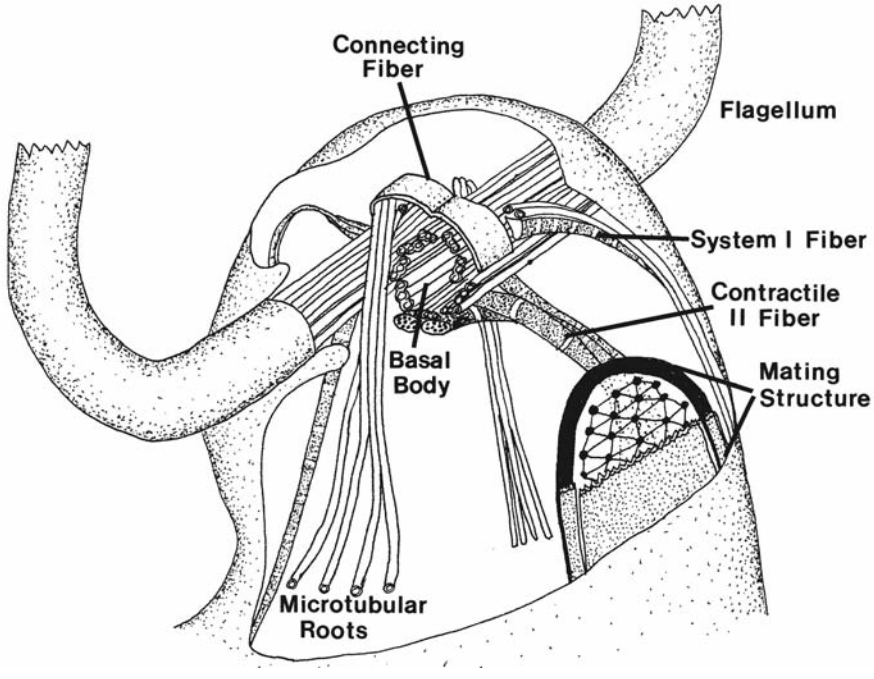


Fig. 1.5 Schematic three-dimensional reconstruction of the flagellar apparatus of a female gamete of *Ulva lactuca* showing the four cruciately arranged microtubular roots and the fibrous contractile roots. (Adapted from Melkonian, 1980.)

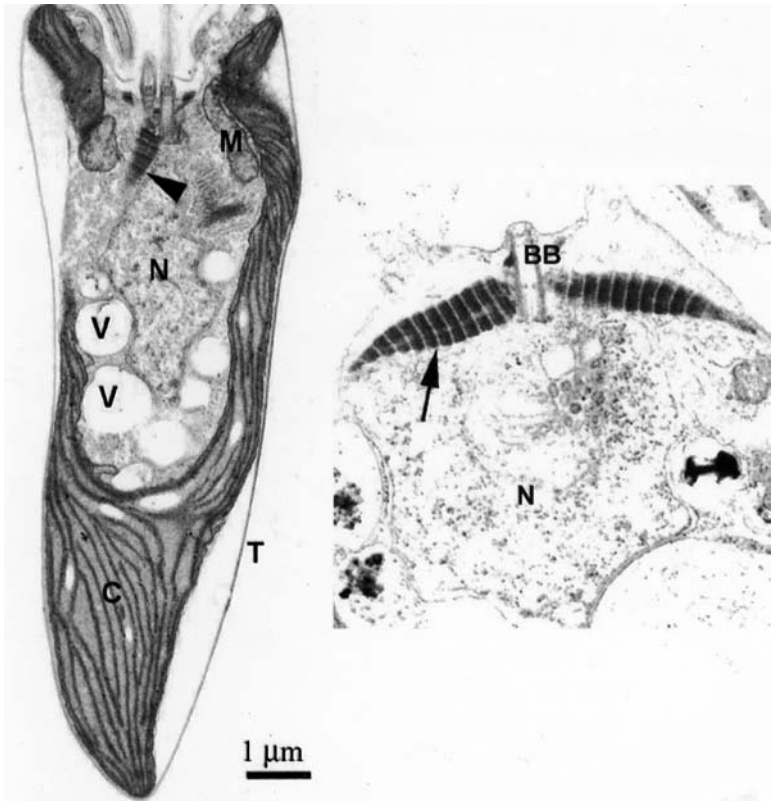


Fig. 1.6 Transmission electron micrographs of striated roots (rhizoplasts) in the green alga *Scherffelia dubia* (Chlorophyta). Arrow and arrowhead point to a striated root. (BB) Basal body; (C) chloroplast; (M) mitochondrion; (N) nucleus; (V) vacuole. (From Vierkotten et al., 2004.)

of filaments (Fig. 1.6). There are two types of fibrous roots: (1) **system I fibrous roots** composed of 2 nm filaments cross-striated with a periodicity of approximately 30 nm and (2) **system II fibrous roots** composed of 4–8 nm filaments usually cross-striated with a periodicity greater than 80 nm. System I fibrous roots are non-contractile while system II fibrous roots are contractile when appropriately stimulated (Moestrup, 2000; Brugerolle and Mignot, 2003).

The flagellar membrane may have no **hairs** (**mastigonemes**) on its surface (**whiplash** or **acronematic** flagellum) or it may have hairs on its surface (**tinsel** or **hairy** or **pantonematic** or **Flimmergeissel**). There are two types of flagellar hair (Fig. 1.7):

1 **Non-tubular flagellar hairs** made up of solid fibrils 5–10 nm wide and 1–3 μm long that are composed of glycoproteins. These hairs are flexible and wrap around the flagellum increasing the surface area and efficiency of propulsion.

2 **Tubular flagellar hairs** about 2 μm long composed of three regions: (1) a tapering basal region 200 nm long attached to the flagellar membrane, (2) a micotubular shaft 1 μm long, and (3) a few 0.52 μm-long terminal filaments (Andersen et al., 1991).

The bases of the hairs do not penetrate the flagellar membrane but are stuck to it. Development of the tubular hairs begins in the space between the inner and outer membrane of the nuclear envelope (perinuclear continuum) where the basal and microtubular regions are assembled. These then pass to the Golgi apparatus, where the terminal filaments are added. Finally the hairs are carried to the plasma membrane in Golgi vesicles, where they are discharged and attached to the flagellar membrane. Tripartite tubular hairs occur in the Heterokontophyta. The term **stramenopile** (straw hair) has been used to include all protists with tubular hairs (van der Auwera and deWachter, 1997). In addition to the algae in the Heterokontophyta, the

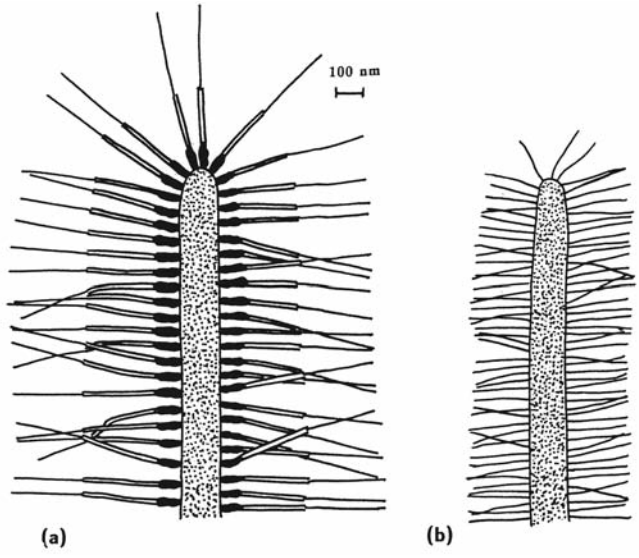


Fig. 1.7 Drawings of the types of hairs on algal flagella. (*a*) Tripartite hairs (example *Ascophyllum* sperm). Each hair is composed of a basal region attached to the flagellar membrane, the microtubular shaft, and a terminal hair. (*b*) Non-tubular hairs (example *Chlamydomonas* gamete). ((*a*) adapted from Bouck, 1969; (*b*) from Snell, 1976.)

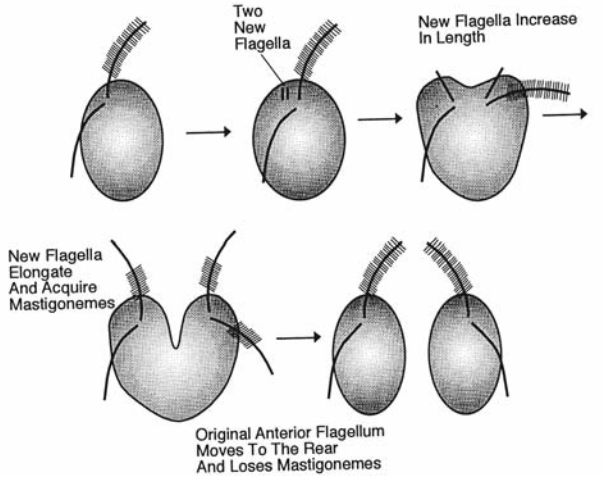


Fig. 1.8 The sequence of flagellar transformation during cell division.

stramenopiles include the fungal oomycetes, hyphochytridomycetes, thraustochytrids, and the bicosoecids and labyrinthulids.

The remainder of the algae have non-tubular hairs if hairs occur on the flagella (Moestrup, 1982). In addition to hairs, a number of different scale types occur on the surface of the flagella. These will be discussed in the chapters on the individual algal groups.

Flagella progress through a set of developmental cycles during cell division (Fig. 1.8). A biflagellate cell with an anterior flagellum covered with tubular hairs (tinsel flagellum), and a posterior smooth flagellum (whiplash flagellum), will be used as an example. Before the onset of cell division, two new flagella appear next to the anterior flagellum. These two new flagella elongate while the original anterior flagellum moves toward the posterior of the cell and loses its tubular hairs, to become the posterior smooth flagellum of one of the daughter cells. The two new flagella at the anterior end of the cell acquire tubular hairs and become the tinsel flagella of the daughter cells. Thus, each daughter cell has one new anterior tinsel flagellum, and one posterior smooth whiplash flagellum that was originally a flagellum in the parent cell (Beech and Wetherbee, 1990; Melkonian et al., 1987).

Algal cells can have different arrangements of flagella (Fig. 1.9). If the flagella are of equal length,

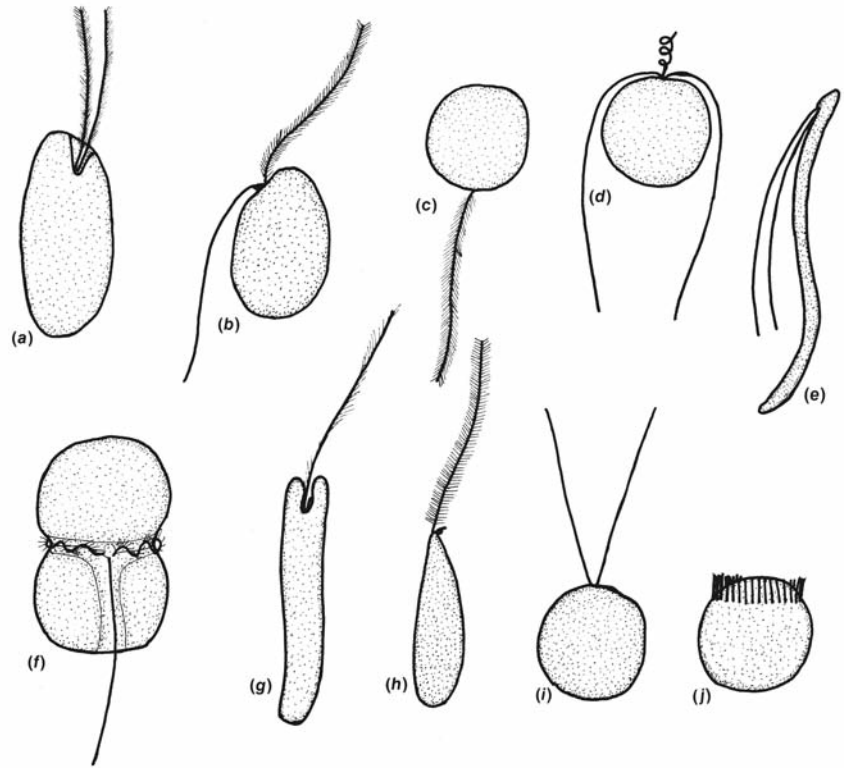


Fig. 1.9 The shape of eukaryotic motile algal cells and their flagella. The drawings represent the common arrangement of flagella in the groups. There are a number of modifications in structure that are not included here. (*a*) Cryptophyta; (*b*) most of the Heterokontophyta; (*c*) Bacillariophyceae of the Heterokontophyta; (*d*) Prymnesiophyta; (e) Chlorophyta; (*f*) Dinophyta; (*g*) Euglenophyta; (*h*) Eustigmatophyceae of the Heterokontophyta; (*i, j*) Chlorophyta.

they are called **isokont** flagella; if they are of unequal length, they are called **anisokont flagella**; and if they form a ring at one end of the cell, they are called **stephanokont** flagella. **Heterokont** refers to an organism with a hairy and a smooth flagellum (Moestrup, 1982).

Flagella can be of different length in the same cell. This is controlled by **intraflagellar transport**, defined as the *bi-directional movement of particles along the length of the flagellum between the axoneme and the flagellar membrane* (Beech, 2003). A mature flagellum that is not elongating has a steady disassembly of the flagellum that is countered by an equally steady assembly provided by intraflagellar transport (Fig. 1.10). A change in length of the flagellum is produced by an imbalance in the assembly or disassembly of flagellar components (Rosenbaum and Witman, 2002). Thus, disassembly occurs faster than assembly in flagellar retraction. The opposite occurs during flagellar growth. The differences in length of flagella arise from the shorter flagellum being delayed in the initial stages of construction. The assembly rate of the shorter flagellum is the same as the longer flagellum. There may be a gate at the base of the flagellum that regulates the passage of flagellar precursors into the basal body and the flagellum (Schoppmeier and Lechtreck, 2003).

Cell walls and mucilages

In general, algal cell walls are made up of two components: (1) the fibrillar component, which forms the skeleton of the wall, and (2) the amorphous component, which forms a matrix within which the fibrillar component is embedded.

The most common type of fibrillar component is **cellulose**, a polymer of 1,4 linked β-D-glucose. Cellulose is replaced by a **mannan**, a polymer of 1,4 linked β-D-mannose, in some siphonaceous

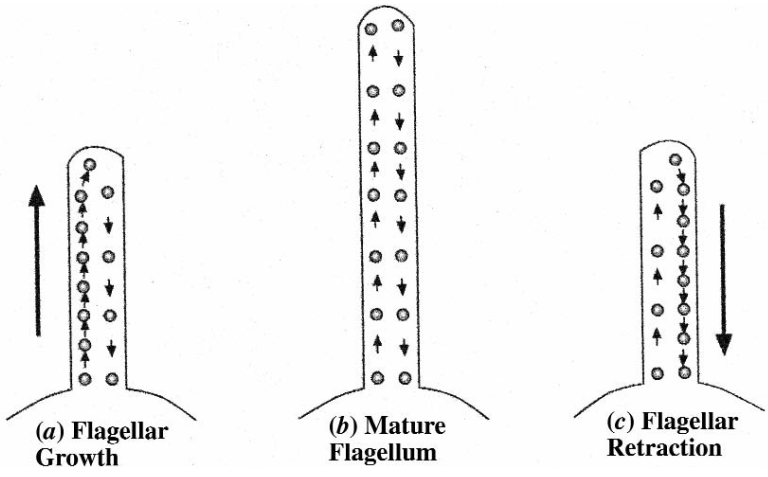


Fig. 1.10 (*a*) Intraflagellar transport results in more assembly of flagellar subunits than disassembly during flagellar growth. (*b*) A mature flagellum has an equal amount of assembly and disassembly of flagellar subunits. (*c*) There is more disassembly of flagellar subunits during flagellar retraction.

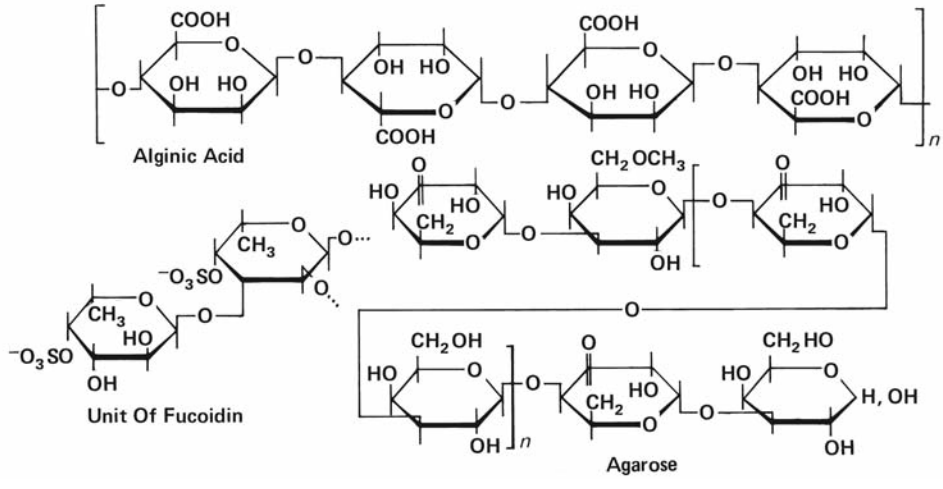


Fig. 1.11 Structural units of alginic acid, fucoidin, and agarose. (After Percival and McDowell, 1967.)

greens, and in *Porphyra* and *Bangia* in the Rhodophyta. In some siphonaceous green algae and some Rhodophyta (*Porphyra, Rhodochorton, Laurencia*, and *Rhodymenia*), fibrillar **xylans** of different polymers occur.

The amorphous mucilaginous components occur in the greatest amounts in the Phaeophyceae and Rhodophyta, the polysaccharides of which are commercially exploited. **Alginic acid** (Fig. 1.11) is a polymer composed mostly of β-1,4 linked D-mannuronic acid residues with variable amounts of L-guluronic acid. Alginic acid is present in the intercellular spaces and cell walls of the Phaeophyceae. **Fucoidin** (Fig. 1.11) also occurs in the Phaeophyceae and is a polymer of α-1, 2, α-1, 3, and α-1, 4 linked residues of L-fucose sulfated at C-4. In the Rhodophyta the amorphous component of the wall is composed of galactans or polymers of galactose, which are alternatively β-1,3 and β-1,4 linked. These galactans include **agar** (made up of **agaropectin** and **agarose**, Fig. 1.11) and **carrageenan** (Fig. 4.15).

Plastids

The basic type of plastid in the algae is a **chloroplast**, a plastid capable of photosynthesis. **Chromoplast** is synonymous with chloroplast; in the older literature a chloroplast that has a color other than green is often called a chromoplast. A **proplastid** is a reduced plastid with few if any

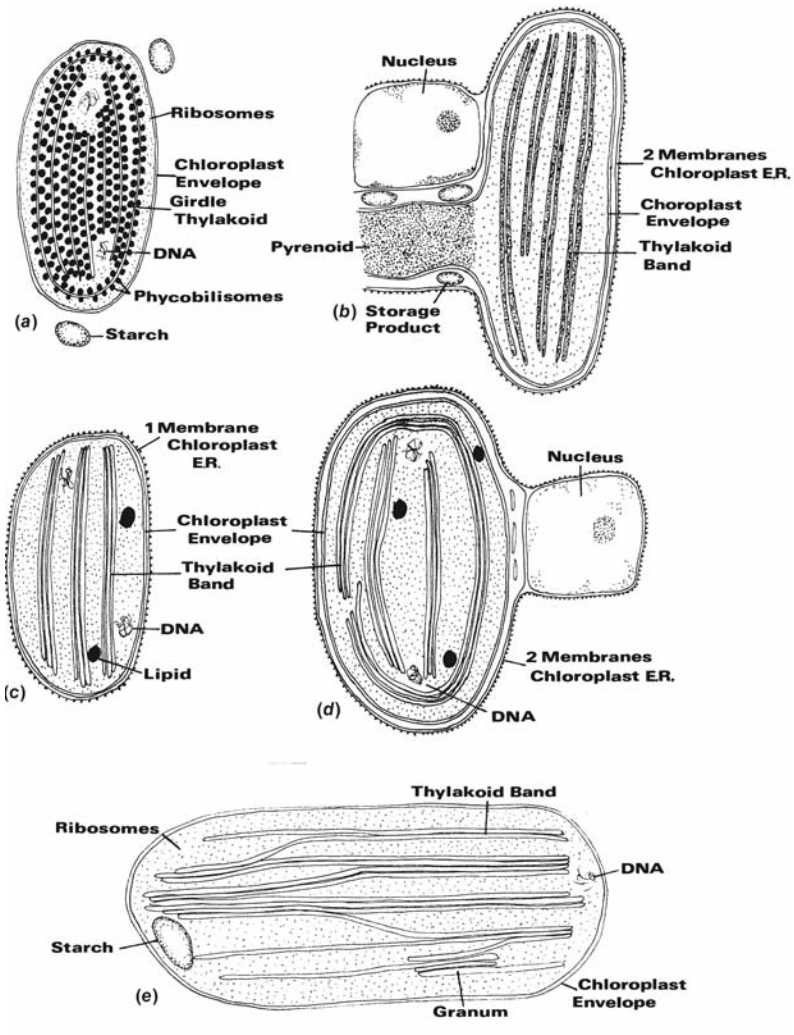


Fig. 1.12 Types of chloroplast structure in eukaryotic algae. (*a*) One thylakoid per band , no chloroplast endoplasmic reticulum (Rhodophyta). (*b*) Two thylakoids per band, two membranes of chloroplast E.R. (Cryptophyta). (*c*) Three thylakoids per band, one membrane of chloroplast E.R. (Dinophyta, Euglenophyta). (*d*) Three thylakoids per band, two membranes of chloroplast E.R. (Prymnesiophyta and Heterokontophyta). (*e*) Two to six thylakoids per band, no chloroplast E.R. (Chlorophyta).

thylakoids. A proplastid will usually develop into a chloroplast although in some heterotrophic algae it remains a proplastid. A **leucoplast** or **amyloplast** is a colorless plastid that has become adapted for the accumulation of storage product.

In the Rhodophyta and Chlorophyta, the chloroplasts are bounded by the double membrane of the chloroplast envelope (Fig. 1.12(*a*), (*e*)). In the other eukaryotic algae, the chloroplast envelope is surrounded by one of two membranes of **chloroplast endoplasmic reticulum** (chloroplast E.R.), which has ribosomes attached to the outer face of the membrane adjacent to the cytoplasm. The chloroplast E.R. is the remnant of the food vacuole membrane and/or the plasma membrane involved in the original endosymbiosis leading to the chloroplasts in a secondary endosymbiosis. In the Euglenophyta and Dinophyta, there is one membrane of chloroplast E.R. (Fig. 1.12(*c*). In the Cryptophyta, Prymnesiophyta, and Heterokontophyta, there are two membranes of chloroplast E.R., with the outer membrane of chloroplast E.R. usually continuous with the outer membrane of the nuclear envelope, especially if the chloroplast number is low (Fig. 1.12 (*b*), (*d*)).

The basic structure of the photosynthetic apparatus in a plastid consists of a series of flattened membranous vesicles called **thylakoids** or **discs**, and a surrounding matrix or **stroma**. The thylakoids contain the chlorophylls and are the sites of the photochemical reactions; carbon dioxide fixation occurs in the stroma. The thylakoids can

be free from one another or grouped to form **thylakoid bands**. In the cyanobacteria and Rhodophyta (Fig. 1.12(*a*)), the thylakoids are usually free from one another, with **phycobilisomes** (containing the phycobiliproteins) on the surface of the thylakoids. The phycobilisomes on the surface of one thylakoid alternate with those on the surface of an adjacent thylakoid. The phycobilisomes appear as 35-nm granules when phycoerythin predominates, or as discs when phycocyanin predominates. In the more primitive members of the Rhodophyta the thylakoids terminate close to the chloroplast envelope, whereas in advanced members of the Rhodophyta peripheral thylakoids are present, which enclose the rest of the thylakoids. In the Cryptophyta, the chloroplasts contain bands of two thylakoids (Fig. 1.12(*b*)); the phycobiliproteins are dispersed within the thylakoids. In the Euglenophyta and Heterokontophyta the thylakoids are grouped in bands of three with a girdle or peripheral band running parallel to the chloroplast envelope. In the Dinophyta, Prymnesiophyta, and Eustigmatophyceae, the thylakoids are also in bands of three, but there is no girdle band (Fig. 1.12(*c*), (*d*)). In the Chlorophyta, the thylakoids occur in bands of two to six, with thylakoids running from one band to the next. The above grouping of algal thylakoids into bands occurs under normal growth conditions. Abnormal growth conditions commonly cause lumping of thylakoids and other variations in structure.

A pyrenoid (Fig. 1.12(*b*)) is a differentiated region within the chloroplast that is denser than the surrounding stroma and may or may not be traversed by thylakoids. A pyrenoid is frequently associated with storage product. Pyrenoids contain ribulose-1, 5-bisphosphate carboxylase/oxygenase (Rubisco), the enzyme that fixes carbon dioxide (Jenks and Gibbs, 2000; Nagasato et al., 2003). Consequently, the size of the pyrenoid will vary depending on how much Rubisco is present.

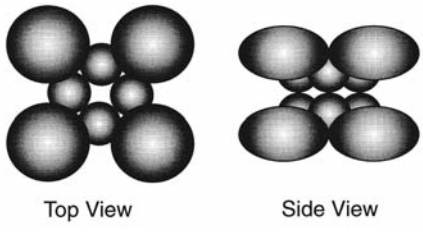


Fig. 1.13 The structure of Form I variation of Rubisco showing the eight large subunits and eight small subunits.

Rubisco exists in two forms (Jenks and Gibbs, 2000; Zhang and Lin, 2003):

1. Form I occurs in some bacteria, the cyanobacteria, in all green plants and non-green plants. Form I is composed of eight large subunits and eight small subunits (Fig. 1.13). Form I has a high affinity for CO_2 and a low catalytic efficiency (low rate of CO_2 fixation). In green algae, euglenoids, and green plants, the large subunit is coded by chloroplast DNA and the small subunit by nuclear DNA. In the cyanelle (endosymbiotic cyanobacterium) of *Cyanophora paradoxa* and in some non-green algae, both subunits are coded by chloroplast DNA.
2. Form II occurs in some eubacteria and in the dinoflagellates and is composed of two large subunits. Form II has a low affinity for CO_2 and a high catalytic efficiency.

The common ancestor of all ribulose-1,5-bisphosphate carboxylase was probably similar to Form II and was adapted to the anaerobic conditions and high CO_2 concentrations prevailing in the ancient earth (Haygood, 1996). Form I evolved as the earth's atmosphere became oxygenated, and CO_2 concentration declined and with it the need for a greater affinity for CO_2. The greater affinity for CO_2 in Form I, however, came at the price of reduced catalytic efficiency.

Chloroplasts contain small (30–100 nm), spherical lipid droplets between the thylakoids (Fig. 1.12 (*c*), (*d*)). These lipid droplets serve as a pool of lipid reserve within the chloroplast.

Many motile algae have groups of tightly packed carotenoid lipid-globules that constitute an orange-red eyespot or stigma (Fig. 5.2) that is involved in response to light. Motile algae exhibit three types of responses to light (Kawai and Kreimer, 2000): phototaxis, photophobia, and gliding (Fig. 1.14).

1. **Phototaxis.** In phototaxis, the orientation of cell movement is effected by the **direction** and

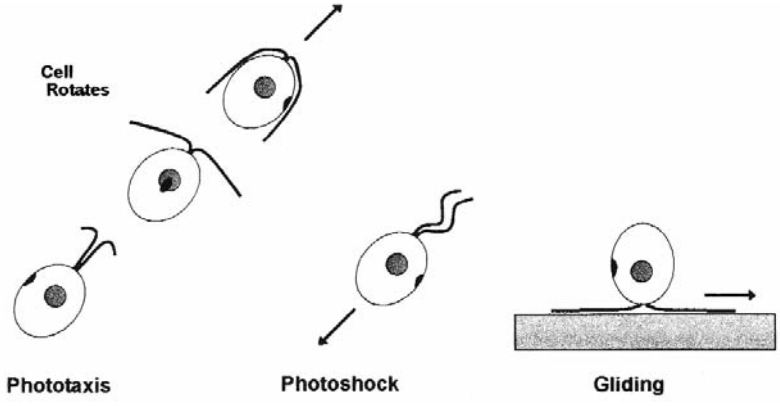


Fig. 1.14 Three types of flagellar orientation in *Chlamydomonas*. In **phototaxis**, the cells swim forward and rotate. Phototaxis requires that cells swim forward in a spiral path that causes rotation of the symmetrically placed eyespot. In **photoshock**, the cell has a transient avoidance response that causes the cell to swim backwards. In **gliding**, the leading flagellum and passive flagellum are 180° apart.

intensity of **light**. The cells move toward the light in **positive phototaxis** and away from the light in **negative phototaxis**. The photoreceptor in the green alga *Chlamydomonas* is **chlamyrhodopsin** (Fig. 1.15) in the plasma membrane over the eyespot. Chlamyrhodopsin contains an all-*trans*, 6-S-*trans* retinal chromophore that undergoes a 13-*trans* to *cis* isomerization during illumination (Hegemann, 1997). The eyespot periodically shades the photoreceptor as the cell rotates during swimming. The eyespot has a different structure in the different groups of algae and will be covered in the appropriate chapters. Eyespots have certain basic characteristics (Kawai and Kreimer, 2000): (1) Eyespots usually have carotenoid-rich lipid globules packed in a highly ordered hexagonal arrangement. (2) Eyespots are usually single structures in peripheral positions, most often oriented perpendicular to the axis of the swimming path.

Phototaxis in *Chlamydomonas* is controlled by the beating of each flagellum. The flagellum closest to the eyespot is the cis flagellum while the trans flagellum is furthest from the eyespot. The light is received by the photoreceptor which controls the opening and closing of calcium channels, and the level of intraflagellar calcium concentration. The calcium concentration within the flagellum effects the interactions of the radial spokes with the central pair of microtubules (Mitchell, 2000). When the plasma membrane of *Chlamydomonas* is made permeable, *Chlamydomonas* cells swim normally at 10^{-8} M calcium in the medium. Decreasing the calcium to 10^{-9} M reduces the stroke velocity of the trans flagellum, while increasing the calcium to 10^{-7} M reduces the stroke velocity of the cis flagellum.

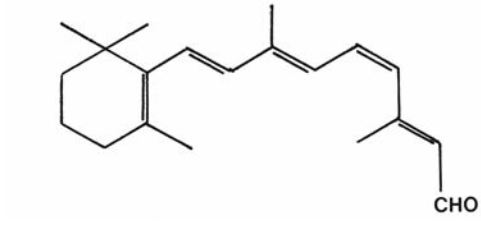


Fig. 1.15 The structure of chlamyrhodopsin, the photoreceptor in *Chlamydomonas*.

2 **Photophobia (photoshock).** Photophobia is a change in direction of movement of the cell caused by a rapid change in light intensity, **irrespective of the direction of the light**. Swimming cells stop and change the beat pattern from the normal asymmetric flagellar stroke to a symmetrical stroke that propels the cell backward (Fig. 1.14). At the end of the photophobic response, the cells tumble and resume swimming in a new direction. Laboratory experiments with *Chlamydomonas* link photophobic responses to increases in calcium above 10^{-6} M (Mitchell, 2000). Unlike phototaxis, interactions between radial spokes and central-pair microtubules are not necessary for a photophobic reaction.

3 **Gliding (quiesence).** In gliding, the flagella stop beating and adhere to a surface or an

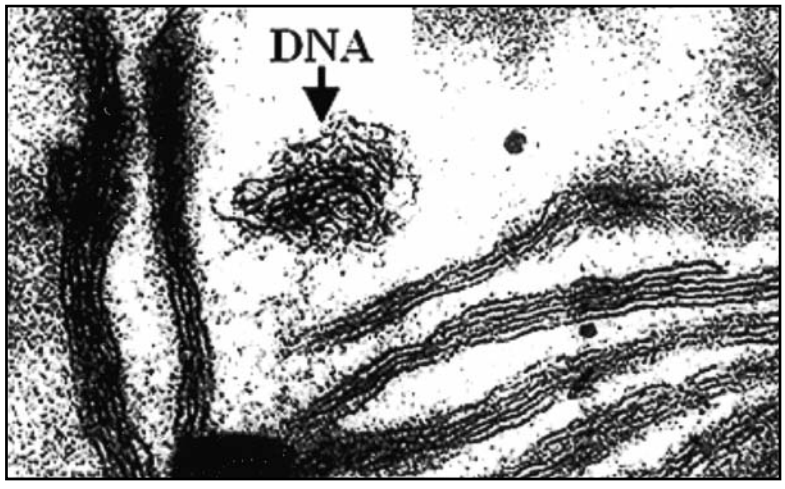


Fig. 1.16 Transmission electron micrograph of DNA in the chloroplast of the dinoflagellate *Prorocentrum micans*. (From Laatsch et al., 2004.)

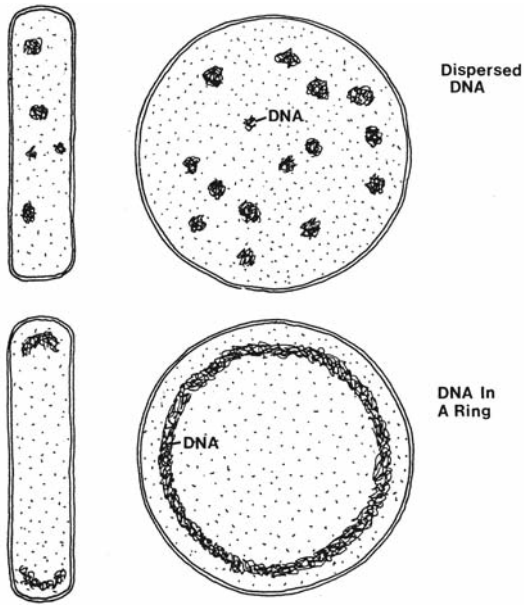


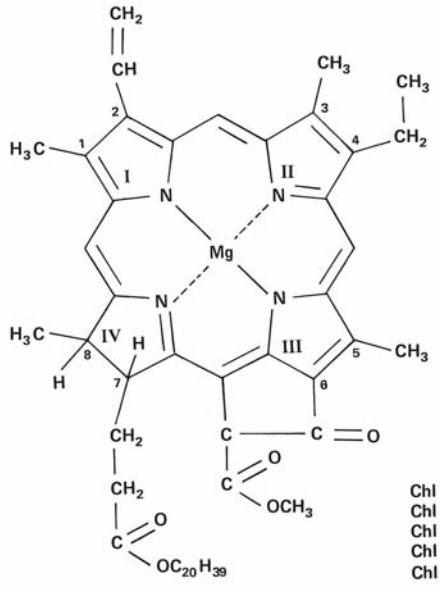
Fig. 1.17 Semidiagrammatic drawing of the two types of distribution of DNA in algal chloroplasts. Side and face views of the plastids are drawn. (Adapted from Coleman, 1985.)

air/water interface (Mitchell, 2000). The cells can glide over the surface with one flagellum actively leading and the other passively trailing (Fig. 1.14). Cells may switch direction by changing which flagellum is active. Gliding motility may be a common phenomenon among organisms that live in the thin film of water on soil particles.

In the Chlorophyta (Fig. 5.2), Cryptophyta (Fig. 9.4) and most of the Heterokontophyta (Fig. 10.1), the eyespot occurs as lipid droplets in the chloroplast. In the Euglenophyta (Fig. 6.2), Eustigmatophyceae (Fig. 12.1), and Dinophyta (Figs. 7.21, 7.22, 7.23), the eyespot occurs as a group of membrane-bounded lipid droplets, free of the chloroplast.

Most chloroplasts contain prokaryotic DNA in an area of the chloroplast devoid of 70S ribosomes (Figs. 1.16 and 1.17). The DNA is an evolutionary remnant of the cyanobacterium involved in the endosymbiosis leading to the chloroplast. The individual DNA microfibrils are circular, are attached to the chloroplast membranes, and lack basic proteins (**histones**). The algae can be divided into two general groups according to the distribution of DNA in the plastids (Coleman, 1985). In the first group, the clumps of DNA (**nucleoids**) are scattered throughout the plastids. This group includes the Cryptophyta, Dinophyta, Prymnesiophyta, Eustigmatophyceae, Rhodophyta, and Chlorophyta. In the second group, the DNA occurs in a ring just within the girdle lamella. This group includes the Chrysophyceae, Bacillariophyceae, Raphidophyceae, and Xanthophyceae (with the exception of *Vaucheria* and three genera known to lack girdle lamellae – *Bumilleria*, *Bumilleriopsis*, and *Pseudobumilleriopsis*). The Euglenophyta fit into neither group, showing a variable distribution of chloroplast DNA.

The photosynthetic algae have chlorophyll in their chloroplasts. **Chlorophyll** is composed of a



Chl *a*: as shown in structure
Chl *b*: II-3 = CHO
Chl *d*: I -2 = CHO
Chl c_1: IV-7 = CH=CHCOOH; double bond at IV-7, 8
Chl c_2: IV-7 = CH=CHCOOH; double bond at IV-7, 8
II-4 = $CH=CH_2$

Fig. 1.18 The structure of the chlorophylls. (From Meeks, 1974.)

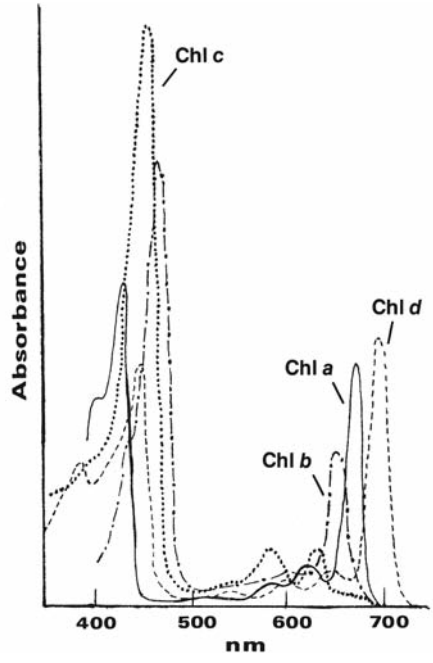


Fig. 1.19 The absorption spectra of chlorophylls *a*, *b*, *c*, and *d*.

porphyrin-ring system that is very similar to that of hemoglobin but has a magnesium atom instead of an iron atom (Fig. 1.18). The algae have four types of chlorophyll, *a*, *b*, *c* (c_1 and c_2), and *d*. Chlorophyll *a* is the primary photosynthetic pigment (the light receptor in photosystem I of the light reaction) in all photosynthetic algae and ranges from 0.3% to 3.0% of the dry weight. Chlorophyll *a* is insoluble in water and petroleum ether but soluble in alcohol, diethyl ether, benzene, and acetone. The pigment has two main absorption bands in vitro, one band in the red light region at 663 nm and the other at 430 nm (Fig. 1.19).

Whereas chlorophyll *a* is found in all photosynthetic algae, the other algal chlorophylls have a more limited distribution and function as accessory photosynthetic pigments. Chlorophyll *b* is found in the Euglenophyta and Chlorophyta (Fig. 1.18). Chlorophyll *b* functions photosynthetically as a light-harvesting pigment transferring absorbed light energy to chlorophyll *a*. The ratio of chlorophyll *a* to chlorophyll *b* varies from 2:1 to 3:1. The solubility characteristics of chlorophyll *a* are similar to chlorophyll *b*, and in vitro chlorophyll *b* has two main absorption maxima in acetone or methanol, one at 645 nm and the other at 435 nm (Fig. 1.19).

Chlorophyll *c* (Fig. 1.18) is found in the Dinophyta, Cryptophyta, and most of the Heterokontophyta. Chlorophyll *c* has two spectrally different components: chlorophyll c_1 and c_2. Chlorophyll c_2 is always present, but chlorophyll c_1 is absent in the Dinophyta and Cryptophyta. The ratio of chlorophyll *a* to chlorophyll *c* ranges from

1.2:2 to 5.5:1. Chlorophyll *c* probably functions as an accessory pigment to photosystem II. The pigment is soluble in ether, acetone, methanol, and ethyl acetate, but is insoluble in water and petroleum ether. Extracted chlorophyll c_1 has main absorption maxima at 634, 583, and 440 nm in methanol, whereas chlorophyll c_2 has maxima at 635, 586, and 452 nm.

Chlorophyll *d* (Fig. 1.18) occurs in some cyanobacteria (Murakami et al., 2004). It has three main absorption bands at 696, 456, and 400 nm.

The photosynthetically active pigments of algae are gathered in discrete pigment–protein complexes which can be divided functionally into two groups (Grossman et al., 1990):

1 the **photochemical reaction center** containing chlorophyll *a*, where light energy is converted into chemical energy;
2 the **light-harvesting complexes** that serve as antennae to collect and transfer available light energy to the reaction center.

The light-harvesting complexes use different antennae pigment complexes to capture light energy. All of the light-harvesting complexes are composed of three-membrane spanning helices (Fig. 1.20).

1 Green algae and higher plants use chlorophyll *a/b* binding proteins.
2 Brown and golden-brown algae, (diatoms, chrysophytes, dinoflagellates, brown algae, and related groups) use a fucoxanthin chlorophyll *a/c* complex that is an integral part of the thylakoid membrane. The ratio of fucoxanthin to chlorophyll in this complex is approximately 2:1 and the characteristic brown or golden-brown color of these algae is due to the high level of fucoxanthin in these cells. Due to chlorophyll *c* and special xanthophylls, these organisms are especially suited to harvest blue and green light, which are the most abundant at increasing ocean depths. This light-harvesting complex also is composed of three membrane-spanning helices and is closely related to the light-harvesting complex in the first group (Caron et al., 1996).
3 Cyanobacteria, cryptophytes and red algae use the phycobilisome as the major light-harvesting complex.

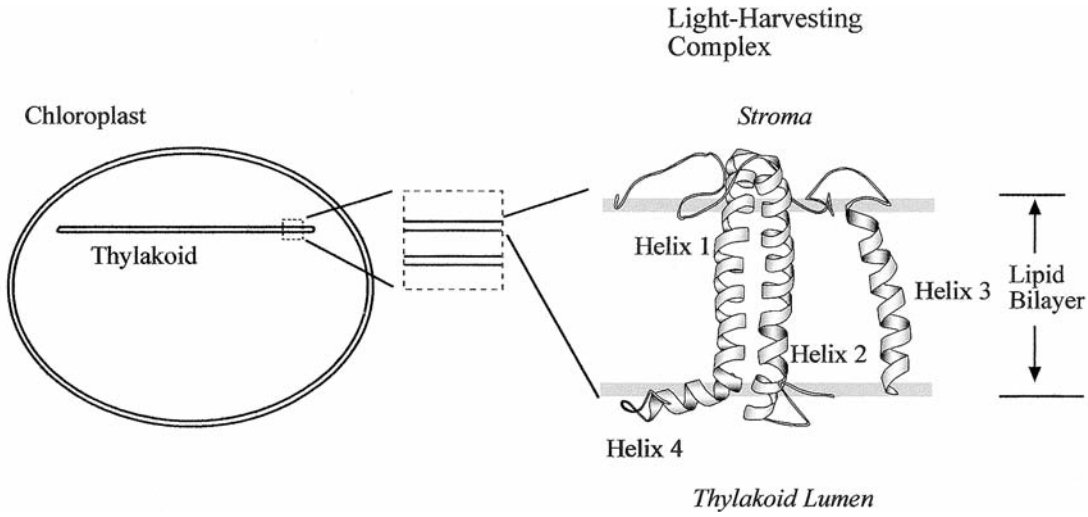


Fig. 1.20 The basic structure of the light-harvesting complex in all eukaryotic plants. Three transmembrane helices traverse the membrane. The similarity of the light-harvesting complex in all eukaryotic plants is an argument for the chloroplast arising from a single endosymbiotic event. (Modified from Kuhlbrandt et al., 1994.)

Carotenoids are yellow, orange, or red pigments that usually occur inside the plastid but may be outside in certain cases. In general, naturally occurring carotenoids can be divided into two classes: (1) oxygen-free hydrocarbons, the **carotenes**; and (2) their oxygenated derivatives, the **xanthophylls**. The most widespread carotene in the algae is β-carotene (Fig. 1.21). There are a large number of different xanthophylls, with the Chlorophyta having xanthophylls that most closely resemble those in higher plants. Fucoxanthin (Fig. 1.21) is the principal xanthophyll in the golden-brown algae (Chrysophyceae, Bacillariophyceae, Prymnesiophyceae, and Phaeophyceae), giving these algae their characteristic color. Like the chlorophylls, the carotenoids are soluble in alcohols, benzene, and acetone but insoluble in water.

The cyanobacteria and chloroplasts of the Rhodophyta and Cryptophyta have evolved membrane-peripheral antenna complexes containing phycobiliproteins that transfer light energy to photosytem II reaction centers. Like chlorophyll *b*/*c*/*d*, the phycobiliproteins expand the range of light energy that can be utilized in photosynthesis. Light tends to become blue-green as it courses down the water column, and this light is better absorbed by the biliproteins than chlorophyll *a*.

Phycobiliproteins are water-soluble blue or red pigments located *on* (Cyanophyta, Rhodophyta) or *inside* (Cryptophyta) thylakoids of algal chloroplasts (Glazer, 1982). They are described as **chromoproteins** (colored proteins) in which the **prosthetic group** (non-protein part of the molecule) or **chromophore** is a tetrapyrole (bile pigment) known as **phycobilin**. The prosthetic group is tightly bound by covalent linkages to its **apoprotein** (protein part of the molecule) (see Fig. 1.21). Because it is difficult to separate the pigment from the apoprotein, the term **phycobiliprotein** is used. There are two different apoproteins, α and β, which together form the basic unit of the phycobiliproteins. To either α or β are attached the colored chromophores. The major "blue" chromophore occurring in **phycocyanin** and **allophycocyanin** is **phycocyanobilin**, and the major "red" chromophore occurring in **phycoerythrin** is **phycoerythrobilin** (Fig. 1.22).

The general classification of phycobiliproteins is based on their absorption spectra. There are three types of phycoerythrin: R-phycoerythrin and B-phycoerythrin in the Rhodophyta, and C-phycoerythrin in the Cyanophyta. There are also three types of phycocyanin: R-phycocyanin from the Rhodophyta and C-phycocyanin and allophycocyanin from the Cyanophyta. In addition, in the Cryptophyta there are three spectral types of phycoerythrin and three spectral types of phycocyanin.

The basic subunit of a phycobilisome consists of apoproteins α and β, each of which is attached to a chromophore (Anderson and Toole,

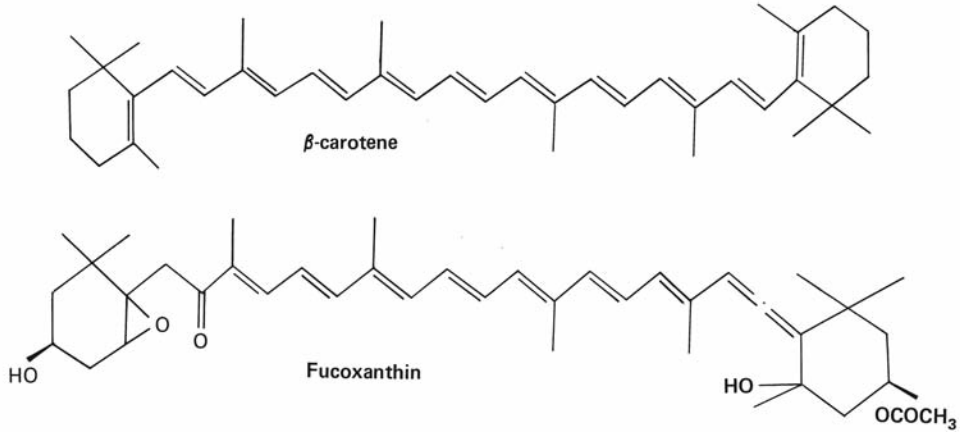


Fig. 1.21 The structure of β-carotene and fucoxanthin.

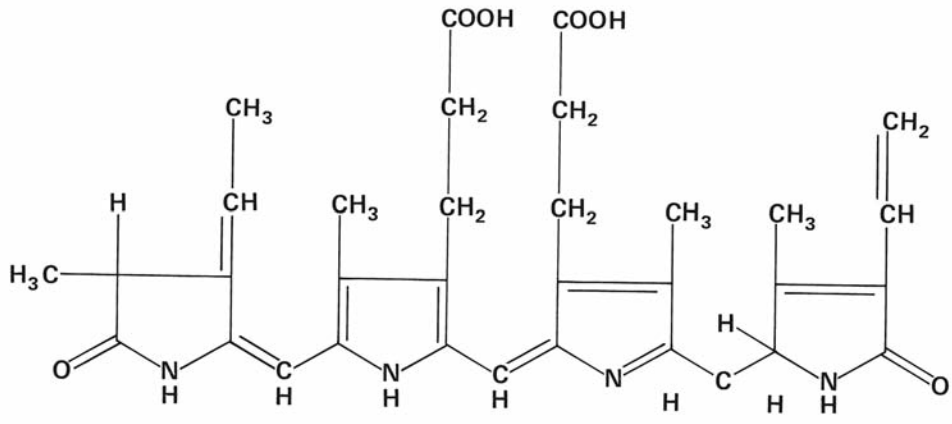


Fig. 1.22 The structure of phycoerythrobilin.

1998; Samsonoff and MacColl, 2001) (Fig. 1.23). In the core of the phycobilisome α and β are attached to allophycocyanins, which are closest to chlorophyll in the energy transfer pathway. In the outer rods, α and β are attached to phycocyanin or phycocyanin. In the core of the phycobilisome α and β are attached to allophycocyanin. The α, β molecules are assembled into hexamers (α_1, β_1) cylindrical in shape. The hexamers that make up the core of the phycobilisome are assembled in pairs, with the hexamers of the rods radiating from the core. The hexamers are joined together by linker polypeptides. The linker polypeptides are basic whereas the hexamers are acidic; this suggests that electrostatic interactions are important in assembling phycobiliproteins. There are high-molecular-weight polypeptides that anchor the phycobilisome to the area of the thylakoid membrane that contains the reaction center and associated chlorophylls.

The pathway of energy transfer (Glazer et al., 1985) is

phycoerythrin ($\lambda_{max} = 565$) or phycoerythrocyanin ($\lambda_{max} = 568$) → phycocyanin ($\lambda_{max} = 620$–638) → allophycocyanin ($\lambda_{max} = 650$) → allophycocyanin B ($\lambda_{max} = 670$) or high-molecular-weight polypeptide ($\lambda_{max} = 665$) → chlorophyll *a*

In intact cells, the overall efficiency of energy transfer from the phycobilisome to chlorophyll *a* in the thylakoids exceeds 90% (Porter et al., 1978).

Chromatic adapters change their pigment components under different light wavelengths (Fig. 1.24). For example, the cyanobacterium *Synechocystis* grown in green light produces phycoerythrin (red in color), phycocyanin (blue), and allophycocyanin (blue-green) in a molar ratio of about 2:2:1; when it is grown in red light, the ratio is about 0.4:2:1. The phycobilisome structure changes appropriately, with the peripheral rods having more phycoerythrin hexamers under green light, and less phycocyanin hexamers. The allophycocyanin core hexamers stay the same.

Depriving cells of nitrogen results in an ordered degradation of phycobilisomes (Fig. 1.25). There is a progressive degradation of hexamer rod and linker polypeptides followed by the core peptides. New phycobilisomes are rapidly synthesized on the addition of nitrogen to the medium. Phycobilisomes are, thus, an important source of internal nitrogen and offer the algae that have

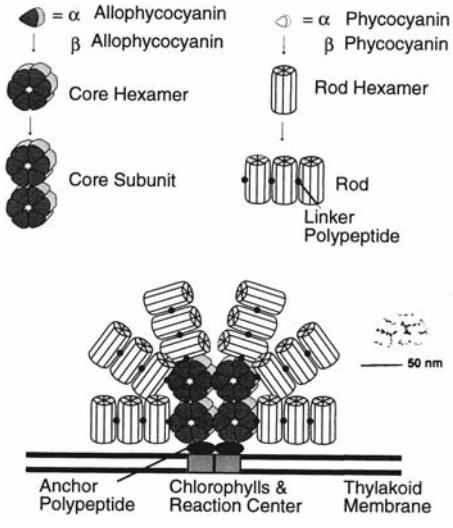


Fig. 1.23 Drawing of a phycobilisome from the cyanobacterium *Synechococcus*. (Adapted from Grossman et al., 1993.)

phycobilisomes (cyanobacteria, cryptophytes, and red algae) an important ecological advantage in the open ocean, which is predominantly nitrogen limited (Vergara and Niell, 1993).

Mitochondria and peroxisomes

There are two types of mitochondria in algal cells (Leipe et al., 1994). Mitochondria with **flat lamellae cristae** occur in the red algae, green algae, euglenoids, and cryptophytes (Fig. 1.26). Mitochondria with **tubular cristae** occur in heterokonts and haptophytes.

Glycolate, the major substrate of photorespiration, can be broken down by either **glycolate dehydrogenase** in the mitochondria, or by **glycolate oxidase** in **peroxisomes**, single membrane-bounded bodies in the cytoplasm (for the reactions, see the chapter on Chlorophyta). The distribution of the two enzymes is as follows (Betsche et al., 1992; Iwamoto et al., 1996):

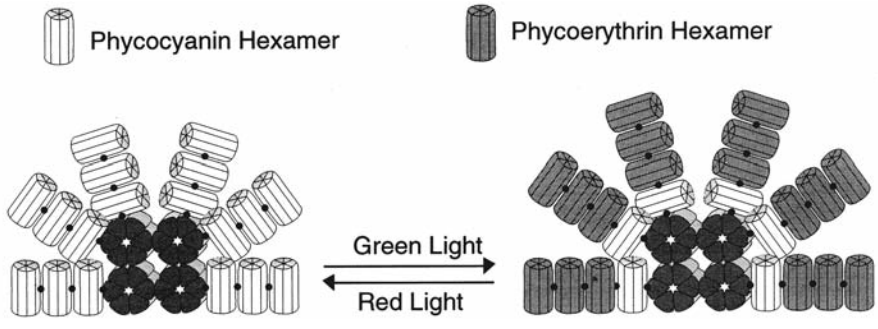


Fig. 1.24 Chromatic adaptation in a phycobilisome of a cyanobacterium.

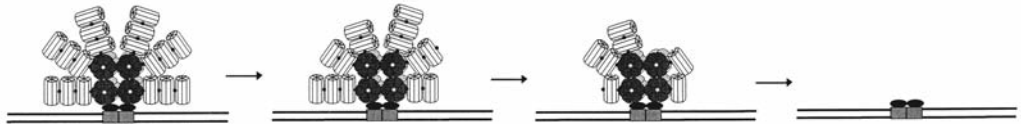


Fig. 1.25 Phycobilisome breakdown under conditions of nitrogen deprivation. (Adapted from Grossman et al., 1993.)

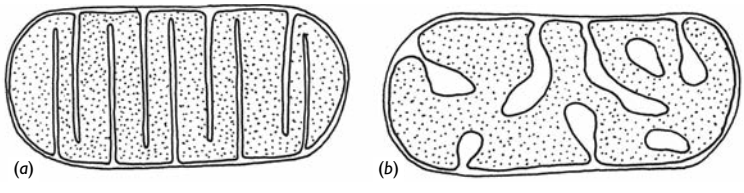


Fig. 1.26 Drawings of the two types of mitochondria that occur in the algae. (*a*) Mitochondrion with flat lamellar cristae. (*b*) Mitochondrion with tubular cristae.

1 Glycolate dehydrogenase occurs in the cyanobacteria, cryptophytes, euglenoids, diatoms, and the green algae with the exception of the Charophyceae.
2 Glycolate oxidase occurs in the glaucophytes, red algae, brown algae, and the Charophyceae in the green algae and higher plants.

Division of chloroplasts and mitochondria

Chloroplasts and mitochondria divide by pinching in half to form two new organelles. A plastid-dividing (PD) ring or mitochondrion-dividing (MD) ring surrounds the organelle in the area of fission (Fig. 1.27) (Miyagishima et al., 2003; Osteryoung and Nunnari, 2003). Each ring is composed of two parts, an outer ring in the protoplasm outside of the chloroplast and an inner ring in the stroma inside the inner membrane of the chloroplast. These rings are also called FtsZ (filamentous temperature-sensitive) rings after a counterpart that is present when bacteria divide. The similarity is indicative of the endosymbiotic origin of chloroplasts and mitochondria from bacteria. The plastid-dividing ring appears in the area of division and begins to contract after a microbody has migrated to the plastid-dividing ring (Fig. 1.27). The plastid-dividing ring contracts around the area of plastid fission in association with GTPase proteins called dynamins. The PD ring disappears after fission is completed.

Storage products

The storage products that occur in the algae are as follows:

High-molecular-weight compounds

1 α-1,4 Linked glucans
   a **Floridean starch** (Fig. 1.28): This substance occurs in the Rhodophyta and is similar to the amylopectin of higher plants. It stains red-violet with iodine, giving a color similar to that of the stain reaction of animal glycogen. Floridean starch occurs as bowl-shaped grains from 0.5 to 25 μm outside the chloroplast, inferring the host in the original endosymbiosis took over formation of storage product. This differs from the Chlorophyta where starch is produced in the chloroplast. Despite the differing locations of starch synthesis, the Rhodophyta and Chlorophyta use a common pathway in the synthesis of starch (Patron and Keeling, 2005).

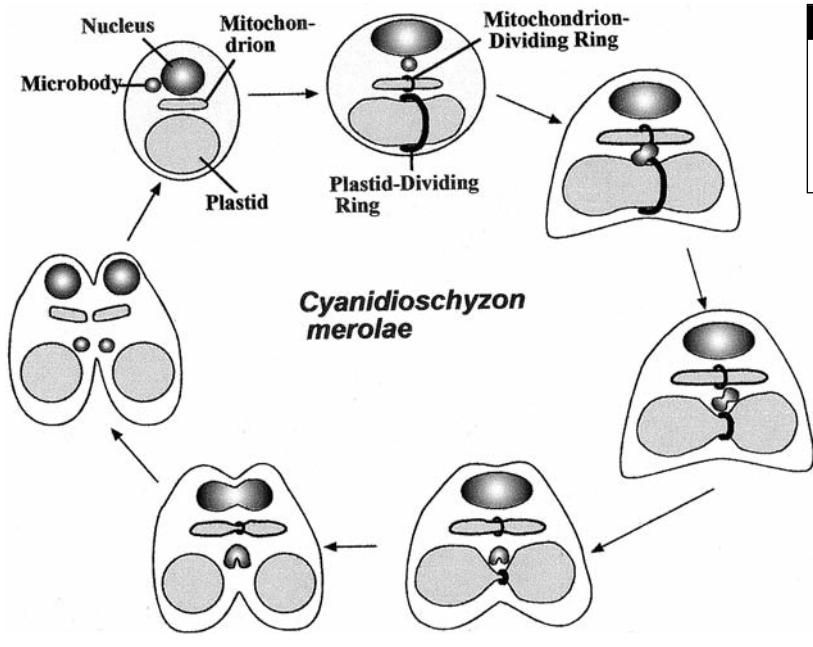


Fig. 1.27 Diagrammatic representation of the behavior of the plastid-dividing ring and mitochondrion-dividing ring in the unicellular red alga *Cyanidioschyzon merolae*.

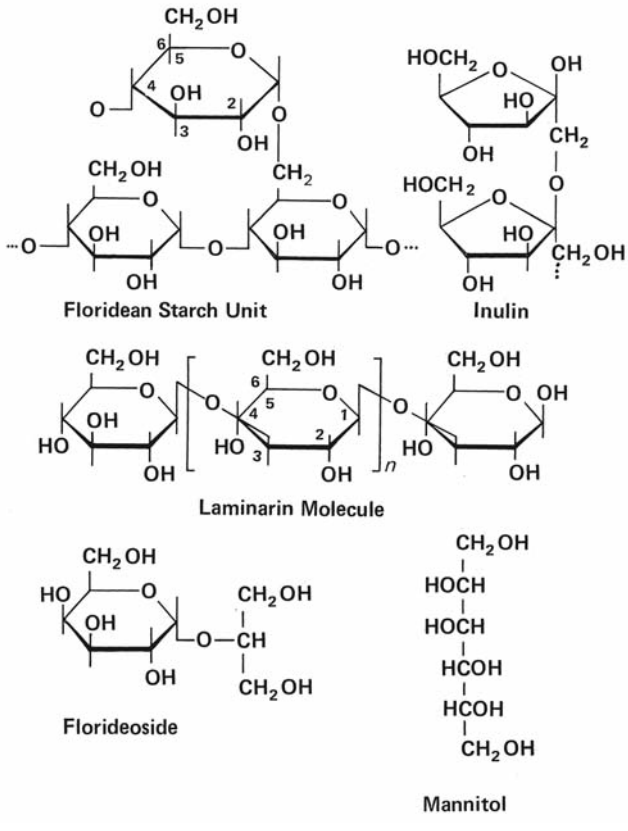


Fig. 1.28 The structure of floridean starch, inulin, laminarin, and floridoside. (After Percival and McDowell, 1967.)

b **Myxophycean starch:** Found in the Cyanophyta, myxophycean starch has a similar structure to glycogen. This reserve product occurs as granules (α-granules), the shape varying between species from rod-shaped granules to 25-nm particles to elongate 31- to 67-nm bodies.

c **Starch:** In the Chlorophyta, starch is composed of amylose and amylopectin. It occurs inside the chloroplast in the form of starch grains (Fig. 1.12(*e*)). In the Cryptophyta, starch has an unusually high content of amylose and occurs as grains between the chloroplast envelope and the chloroplast E.R. (Fig. 1.12(*b*)). In the Dinophyta also, starch occurs in the cytoplasm outside of the chloroplast, but its structure is not known.

2 β-1,3 Linked glucans

a **Laminarin** (Fig. 1.28): In the Phaeophyceae, laminarin consists of a related group of predominantly β-1,3 linked glucans containing 16 to 31 residues. Variation in the molecule is introduced by the number of $1\rightarrow6$ linkages, the degree of branching, and the occurrence of a terminal mannitol molecule. The presence of a high proportion of C-6 interresidue linkages and of branch points seems to determine the solubility of the polysaccharide in cold water: the greater the number of linkages, the higher the solubility. Laminarin occurs as an oil-like liquid outside of the chloroplasts, commonly in a vesicle surrounding the pyrenoid.

b **Chrysolaminarin (leucosin):** In the Chrysophyceae, Prymnesiophyta, and Bacillariophyceae, chrysolaminarin consists of β-1,3 linked D-glucose residues with two $1\rightarrow6$ glycosidic bonds per molecule. Chrysolaminarin occurs in vesicles outside of the chloroplast and has more glucose residues per molecule than laminarin.

c **Paramylon:** In the Euglenophyta, Xanthophyceae, and Prymnesiophyta (*Pavlova mesolychnon*), paramylon occurs as

water-soluble, single-membrane-bounded inclusions of various shapes and dimensions outside of the chloroplast (Fig. 6.2). Paramylon consists solely of β-1,3 linked glucose residues, and the molecule is about as large as that of chrysolaminarin.

3 **Fructosans:** *Acetabularia* (Chlorophyta) has an inulin-like storage product consisting of a series of 1,2 linked fructose units terminated by a glucose end group (Fig. 1.28).

Low-molecular-weight compounds

1 **Sugars:** Chlorophyta and Euglenophyta form sucrose as a reserve product; trehalose is found in the Cyanophyta and at low levels in the Rhodophyta.
2 **Glycosides**: The glycerol glycosides, floridoside (Fig. 1.28) and isofloridoside, are widely distributed in the Rhodophyta.
3 **Polyols**: Mannitol (Figs. 1.28, 4.4) occurs in Rhodophyta and Phaeophyceae. It is also present in lower green algae, where it replaces sucrose as a photosynthetic product. Free glycerol occurs widely in the algae and is an important photosynthetic product in several zooxanthellae (endosymbiotic algae in animals) and in some marine Volvocales, especially *Dunaliella*.

Contractile vacuoles

The ability of algal cells to adjust to changes in the salinity of the medium is an important aspect of the physiology of these cells. In cells with walls, this osmoregulation is accomplished with the aid of turgor pressure, whereas in naked cells it is accomplished by means of contractile vacuoles and/or regulation of the solutes present in the cells. In the latter case, cells increase the internal concentration of osmotically active molecules and ions when the concentration of dissolved solutes increases in the external medium. Likewise, the internal concentration of such molecules decreases when the concentration of dissolved salts in the external medium decreases.

Most algal flagellates have two contractile vacuoles in the anterior end of a cell (Fig. 1.1). A contractile vacuole will fill with an aqueous solution (**diastole**) and then expel the solution outside of the cell and contract (**systole**). The contractile vacuole rhythmically repeats this procedure. If there are two contractile vacuoles, they usually fill and empty alternately. Contractile vacuoles occur more frequently in freshwater than marine algae, a phenomenon that gives credence to the theory that the contractile vacuoles maintain a water balance in the cells. The algal cells in freshwater have a higher concentration of dissolved substances in their protoplasm than in the surrounding medium so that there is a net increase of water in the cells. The contractile vacuoles act to expel this excess water. An alternate theory on the function of the contractile vacuoles is that they remove waste products from the cells. The Dinophyta have a structure similar to a contractile vacuole, called a pusule, which may have a similar function but is more complex.

The contractile vacuoles of the Cryptophyta are characteristic of the algae (Fig. 1.29). In the Cryptophyta, the contractile vacuole occurs in a fixed anterior position next to the flagellar depression (Patterson and Hausmann, 1981). At the beginning of the filling phase (**diastole**), there is no distinct contractile vacuole, only a region filled with small (*ca*. 0.5-μm diameter) contributory vacuoles. These vacuoles fuse to form a large irregular vacuole which subsequently rounds up. The contributory vacuoles destined to form the next contractile vacuole now appear around the rounded contractile vacuole. The contractile vacuole fuses with the plasma membrane of the flagellar pocket and discharges its contents outside the cell. The area of the plasma membrane that fuses with the contractile vacuole does not have a periplast (specialized plates within the plasma membrane). This area is, instead, bounded by microtubules. The membrane of the contractile vacuole is recovered by the cell as small vesicles with an electron-dense coat, and the membrane components are reutilized by the cell. These vesicles plus the contractile vacuole occur in the **spongiome** or area around the contractile vacuole. In freshwater algae the contractile vacuole cycle lasts for 4 to 16 seconds, whereas in marine species the cycle can last for up to 40 seconds.

Algal flagellates use a combination of contractile vacuoles and osmoregulation to control the water content of their cells. In the chrysophyte

Table 1.1 | Types of nutrition found in the algae

Type of nutrition	Principle source of energy for growth	Principal source of carbon for growth
Autotrophic		
Photoautotrophic	Light	Carbon dioxide
Chemoautotrophic	Oxidation of organic compounds	Carbon dioxide
Heterotrophic		
Photoheterotrophic	Light	Organic compounds
Chemoheterotrophic	Oxidation of organic compounds	Organic compounds

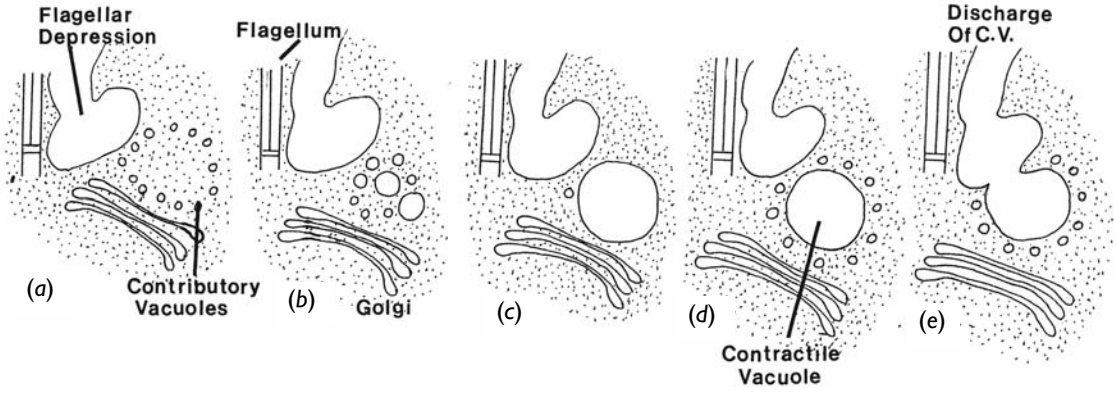


Fig. 1.29 Semidiagrammatic illustration of the behavior of the contractile vacuole (C.V.) complex during filling and discharge in the Cryptophyta. (Adapted from Patterson and Hausmann, 1981.)

Poterioochromonas malhamensis (Ochromonas malhamensis), the internal level of isofloridoside (*O*-α-D-galactopyranosyl-1→1-glycerol) is proportional to the external osmotic value as long as the external solute concentration exceeds 75 mOsm (Wessel and Robinson, 1979). Below this external solute concentration, the influx of water into the cytoplasm is counterbalanced by means of the contractile vacuoles (Kauss, 1974).

Nutrition

Algae can be either **autotrophic** (**lithotrophic** or **holophytic**) or **heterotrophic** (**organotrophic**) (Table 1.1). If they are **autotrophic**, they use inorganic compounds as a source of carbon. Autotrophs can be **photoautotrophic** (**photolithotrophic**), using light as a source of energy, or **chemoautotrophic** (**chemolithotrophic**), oxidizing inorganic compounds for energy. If they are **heterotrophic**, the algae use organic compounds for growth. Heterotrophs can be **photoheterotrophs** (**photoorganotrophs**), using light as a source of energy, or **chemoheterotrophs** (**chemoorganotrophs**), oxidizing organic compounds for energy. Heterotrophic algae may be **phagocytotic** (**holozoic**), absorbing food particles whole into food vesicles for digestion, or they may be **osmotrophic**, absorbing nutrients in a soluble form through the plasma membrane. If the algae live heterotrophically on dead material, they are **saprophytic**; if they live off a live host, they are **parasitic**. Some algae, particularly the flagellates, are **auxotrophic**, requiring a small amount of an organic compound, but not as an energy source. These algae usually require a vitamin. Some photosynthetic algae are **mixotrophic** (**facultatively heterotrophic**), capable of also using organic compounds supplied in the medium.

Gene sequencing and algal systematics

Specific sequences of nucleotides in DNA of the cell code for cell constituents. It is possible to isolate DNA from cells, multiply certain DNA segments and determine the nucleotide sequences of that DNA. Each species has differences in the nucleotides that make up the DNA and differences in nucleotides that can be used to produce an evolutionary history of the cell. The DNA nucleotides that are most commonly sequenced to produce phylogenies are those of ribosomal DNAs (rDNAs). These rDNA nucleotides make up the genes that code for the rRNAs. rRNAs occur in ribosomes and there are three types of ribosomes, each made up of a large and small subunit:

1 **Prokaryotic ribosomes.** The large 70S subunit contains 5S and 23S rRNAs as well as 34 ribosomal proteins. The small 30S subunit contains a single 16S rRNA and 21 proteins.
2 **Eukaryotic ribosomes** (Fig. 1.30). The large 60S subunit contains 28S, 5.8S, and 5S rRNAs, and 49 proteins. The small 40S subunit contains 18S RNA and 33 proteins.
3 **Mitochondrial ribosomes.** These are similar, although not the same, as prokaryotic ribosomes. They are not used to produce algal phylogenies, mostly because mitochondria have been transferred between eukaryotic hosts and, therefore, do not reflect the evolutionary history of the organism (Stiller and Hall, 1997).

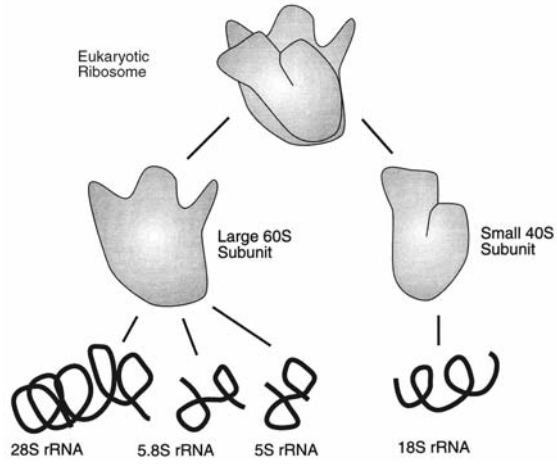


Fig. 1.30 The components of a eukaryotic ribosome.

The **rDNA** for the **18S rRNA** of the small subunit of the eukaryotic ribosome is the form of rDNA usually sequenced to determine the phylogeny of eukaryotic organisms. The nucleotides coding for all of the ribosomal subunits are encompassed within a single operon and transcribed by a single RNA polymerase (Kawai et al., 1997). The procedure for determining the nucleotide sequences is available in any basic biochemistry book.

The **rDNA** for the **5S rRNA** has been also used in phylogeny studies. Although less nucleotides are in the rDNA coding for 5S rRNA, making it easier to sequence, the data have been suspect because of large deviations in the nucleotides (Ragan, 1994). The DNA coding for other molecules, such as ribulose bisphosphate carboxylase/oxygenase (Freshwater et al., 1994; Fujiwara et al., 1994) and actin (Bhattacharya and Ehlting, 1995), have also been used in determining phylogeny.

Gene sequencing has been the most active field of phycological systematics in the last decade and has provided important new information on the relationships between algae. However, as stated by Manhart and McCourt (1992):

> . . . molecular data are not a magic bullet for species problems. They are data, no more, no less. Some molecular data are informative, and others are misleading. Molecular data are fraught with many of the same difficulties as morphological data . . .

Classification

There are four distinct groups within the algae. The remainder of the text is divided into four parts based on these four groups.

1 Prokaryotes. The cyanobacteria are the only prokaryotic algae.
2 Eukaryotic algae with chloroplasts surrounded by the two membranes of the chloroplast envelope.

3 Eukaryotic algae with the chloroplast surrounded by one membrane of chloroplast endoplasmic reticulum.
4 Eukaryotic algae with the chloroplast surrounded by two membranes of chloroplast endoplasmic reticulum.

The standard botanical classification system is used in the systematics of the algae:

Phylum – phyta
  Class – phyceae
    Order – ales
      Family – aceae
        Genus
          Species

Group 1 Prokaryotic algae
Cyanophyta (cyanobacteria) (Chapter 2): chlorophyll *a*; phycobiliproteins.

Group 2 Eukaryotic algae with chloroplasts surrounded only by the two membranes of the chloroplast envelope.
Glaucophyta (Chapter 3): algae that represent an intermediate position in the evolution of chloroplasts; photosynthesis is carried out by modified endosymbiotic cyanobacteria.
Rhodophyta (red algae) (Chapter 4): chlorophyll *a*; phycobiliproteins; no flagellated cells; storage product is floridean starch.
Chlorophyta (green algae) (Chapter 5): chlorophylls *a* and *b*; storage product, starch, is found inside the chloroplast.

Group 3 Eukaryotic algae with chloroplasts surrounded by one membrane of chloroplast endoplasmic reticulum.
Euglenophyta (euglenoids) (Chapter 6): chlorophylls *a* and *b*; one flagellum with a spiraled row of fibrillar hairs; proteinaceous pellicle in strips under the plasma membrane; storage product is paramylon; characteristic type of cell division.
Dinophyta (dinoflagellates) (Chapter 7): mesokaryotic nucleus; chlorophylls *a* and c_1; cell commonly divided into an epicone and a hypocone by a girdle; helical transverse flagellum; thecal plates in vesicles under the plasma membrane.
Apicompexa (Chapter 8): heterotrophic flagellates with colorless plastids.

Group 4 Eukaryotic algae with chloroplasts surrounded by two membranes of chloroplast endoplasmic reticulum.
Cryptophyta (cryptophytes) (Chapter 9): nucleomorph present between inner and outer membrane of chloroplast endoplasmic reticulum; starch formed as grains between inner membrane of chloroplast endoplasmic reticulum and chloroplast envelope; chlorophyll *a* and *c*; phycobiliproteins; periplast inside plasma membrane.
Heterokontophyta (heterokonts) (Chapters 10–21): anterior tinsel and posterior whiplash flagellum; chlorophyll *a* and *c*; fucoxanthin; storage product usually chrysolaminarin occurring in vesicles.
Chrysophyceae (golden-brown algae) (Chapter10)
Synurophyceae (Chapter 11)
Eustigmatophyceae (Chapter 12)
Pinguiophyceae (Chapter 13)
Dictyochophyceae (silicoflagellates) (Chapter 14)
Pelagophyceae (Chapter 15)
Bolidophyceae (Chapter 16)
Bacillariophyceae (diatoms) (Chapter 17)
Raphidophyceae (chloromonads) (Chapter 18)
Xanthophyceae (yellow-green algae) (Chapter 19)
Phaeothamniophyceae (Chapter 20)
Phaeophyceae (brown algae) (Chapter 21)
Prymnesiophyta (haptophytes) (Chapter 22): two whiplash flagella; haptonema present; chlorophyll *a* and *c*; fucoxanthin; scales common outside cell; storage product chrysolaminarin occurring in vesicles.

Data from molecular studies indicate that the red algae diverged about 1400 million years ago from the common line leading to higher plants (Saunders and Hommersand, 2004). This was followed by divergence of the green algae and, then, multiple independent secondary endosymbioses evolving to those algae with chloroplast endoplasmic reticulum. The host phagocytic organisms leading to the euglenoids was probably a kinetoplastid, that leading to the dinoflagellates was probably an apicomplexan, and that leading to the photosynthetic cryptophytes and haptophytes was a colorless cryptophyte and haptophyte,

Table 1.2 | First appearance of algae in the geological time scale

Era	Period	Epoch	Millions of years ago	First appearance of algal fossil
Cenozoic	Quaternary	Holocene		
		Pleistocene	1.8	
	Tertiary	Pliocene	5.5	
		Miocene	25.0	Xanthophyta
		Oligocene	36.0	
		Eocene	53.5	Euglenophyta
		Palaeocene	65.0	
Mesozoic	Cretaceous		135	Chrysophyta
	Jurassic		191–205	
	Triassic		235–245	Bacillariophyta
Paleozoic	Permian		275–290	Prymnesiophyta
	Carboniferous		360–380	
	Devonian		405–430	
	Silurian		435–460	Stoneworts (Chlorophyta)
	Ordovician		500–530	
	Cambrian		570–610	
Proterozoic	Precambrian		3000	Cyanophyta, Rhodophyta, Chlorophyta

respectively. The host organisms leading to the heterokonts have not been identified.

Algae and the fossil record

The cyanobacteria are the oldest group of algae with definite fossil remains in the form of stromatolites (Fig. 2.53), dating back about 2700 million years. When the cyanobacteria evolved, the atmosphere contained little or no oxygen and was composed primarily of methane (CH_4), ammonia (NH_3), and other reduced compounds. Photosynthesis by the cyanobacteria eventually built up the oxygen content of the atmosphere to what it is today (20%). The first eukaryotic algae appeared in a form similar to the extant Glaucophyta, with endosymbiotic cyanobacteria instead of chloroplasts (see Chapter 3). It is difficult to fix this date exactly because these first algae were composed of soft tissues and would not have been preserved. In order to appear in the fossil record, algae would usually have to be large or to have some calcified ($CaCO_3$) or silicified (SiO_2) structures, which are preserved in sedimentary rocks. The appearance of fossil members of the algal classes in the geological timetable is presented in Table 1.2. This table does not purport to show when the algal groups first evolved, but shows only where fossil specimens appear in the geological timetable. The fossil members of each of the algal classes are discussed in the chapter on the particular class.



Fig. 1.31 Two prominent phycologists of the twentieth century, Felix Eugen Fritsch (*left*) and Gilbert Morgan Smith (*right*). Photograph taken by Ralph Lewin.
Felix Eugen Fritsch Born April 26, 1879, in Hampstead, United Kingdom, died May 23, 1954. Dr. Fritsch was educated at the University of London and the University of Munich where he received his Ph.D. From 1902 to 1911, he was an assistant professor at University College London; from 1905 to 1906, a lecturer at Birkbeck College; and from 1907 to 1911, a lecturer at East London College. In 1911, he became head of the Department of Botany at Queen Mary College, University of London, where he stayed until retirement in 1948. Dr. Fritsch was the author of a number of books, by far the best known being *The Structure and Reproduction of the Algae*, which today is still the most comprehensive treatise on the algae as a whole.
Gilbert Morgan Smith Born January 6, 1885 in Beloit, Wisconsin. Died July 11, 1959. Dr. Smith received his BS from Beloit College (1907) and his Ph.D. from the University of Wisconsin (1913). From 1913 to 1925, he was at the University of Wisconsin, ultimately as an associate professor. From 1925 until his retirement, he was a professor at Stanford University. Dr. Smith is best known for his books on algae, which include *Phytoplankton of the Inland Lakes of Wisconsin*, *The Freshwater Algae of the United States*, *Cryptogamic Botany*, and *Marine Algae of the Monterey Peninsula*.

REFERENCES

Andersen, R. A., Barr, D. J. S., Lynn, D. H., Melkonian, M., Moestrup, O., and Sleigh, M. A. (1991). Terminology and nomenclature of the cytoskeletal elements associated with the flagellar/ciliary apparatus in protists. *Protoplasma* 164:1–8.

Anderson, L. K., and Toole, C. M. (1998). A model for early events in the assembly pathway of cyanobacterial phycobilisomes. *Mol. Microbiol.* 30:467–74.

Beech, P. L. (2003). The long and short of flagellar length control. *J. Phycol*. 39:837–39.

Beech, P. L., and Wetherbee, R. (1990). Direct observations on flagellar transformation in *Mallomonas splendens* (Synurophyceae). *J. Phycol*. 26:90–5.

Betsche, T., Schaller, D., and Melkonian, M. (1992). Identification and characterization of glycolate oxidase and related enzymes from the endocynotic alga *Cyanophora paradoxa* and from pea leaves. *Plant Physiol*. 98:887–93.

Bhattacharya, D., and Ehlting, J. (1995). Actin coding regions: gene family evolution and use as a phylogenetic marker. *Arch. Protistenkd*. 145:155–64.

Bouck, G. B. (1969). Extracellular microtubules. The origin, structure, and attachment of flagellar hairs in *Fucus* and *Ascophyllum* antherozoids. *J. Cell Biol*. 40:446–60.

Brugerolle, G., and Mignot, J.-P. (2003). The rhizoplast of chrysomonads, a basal body-nucleus connector that polarises the dividing spindle. *Protoplasma* 222:13–21.

Caron, L., Douady, D., Quinet-Szely, M., deGoër, S., and Berkaloff, C. (1996). Gene structure of a chlorophyll *a/c*-binding protein from a brown alga: Presence of an intron and phylogenetic implications. *J. Mol. Evol*. 43:270–80.

Coleman, A. W. (1985). Diversity of plastid DNA configuration among classes of eukaryote algae. *J. Phycol*. 21:1–16.

Dutcher, S. K. (1995). Flagellar assembly in two hundred and fifty easy-to-follow steps. *Trends Genet*. 11:398–404.

Freshwater, D. W., Fredericq, S., Butler, B. S., Hommersand, M. H., and Chase, M. W. (1994). A gene phylogeny of the red algae (Rhodophyta) based on plastid *rbc*L. *Proc. Natl. Acad. Sci., USA* 91:7281–5.

Fujiwara, S., Sawada, M., Someya, J., Minaka, N., Kawachi, M., and Inouye, I. (1994). Molecular phylogenetic analysis of *rbc*L in the Prymnesiophyta. *J. Phycol*. 30:863–71.

Glazer, A. N. (1982). Phycobilisomes: Structure and dynamics. *Annu. Rev. Microbiol*. 36:173–98.

Glazer, A. N., Yeh, S. W., Webb, S. P., and Clark, J. H. (1985). Disk-to-disk transfer as the rate-limiting step for energy flow in phycobilisomes. *Science* 227:419–23.

Grossman, A., Manodori, A., and Snyder, D. (1990). Light-harvesting proteins of diatoms: Their relationship to the chlorophyll *a/b* binding protein of higher plants and their mode of transport into plastids. *Mol. Gen. Genetics* 224:91–100.

Grossman, A. R., Schaffer, M. R., Chiang, G. G., and Collier, J. L. (1993). The phycobilisome, a light-harvesting complex response to environmental conditions. *Microbiol Rev*. 57:725–49.

Hegemann, P. (1997). Vision in microalgae. *Planta* 203:265–74.

Jenks, A., and Gibbs, S. P. (2000). Immunolocalization and distribution of Form II RUBISCO in the pyrenoid and chloroplast stroma of *Amphidinium carterae* and Form I RUBISCO in the symbiont-derived plastids of *Peridinium foliaceum* (Dinophyceae). *J. Phycol*. 36:127–38.

Johnson, K. A. (1995). Keeping the beat: form meets function in the *Chlamydomonas* flagellum. *BioEssays* 17:847–54.

Iwamoto, K., Suzuki, K., and Ikawa, T. (1996). Purification and characterization of glycolate oxidase from the brown alga *Spatoglossum pacificum* (Phaeophyta). *J. Phycol*. 32:790–8.

Kauss, H. (1974). Osmoregulation in *Ochromonas*. In *Membrane Transport in Plants*, ed. U. Zimmermann, and J. Daintz, pp. 90–4. Berlin: Springer-Verlag.

Kawai, H., and Kreimer, G. (2000). Sensory mechanisms. Phototaxes and light perception in algae. In *The Flagellates*, ed. B. S. C. Leadbeater, and J. C. Green, pp.124–46. London:Taylor and Francis.

Kawai, H., Nakayama, T., Inouye, I., and Kato, A. (1997). Linkage of 5S ribosomal DNA to other rDNAs in the chromophytic algae and related taxa. *J. Phycol*. 33:505–11.

Kuhlbrandt, W., Wang, D. N., and Fujiyoshi, Y. (1994). Atomic model of plant light-harvesting complex by electron crystallography. *Nature* 367:614–21.

Laatsch, T., Zauner, S., Stoebe-Maier, B., Kowallik, K. V., and Maier, U.-G. (2004). Plastid-derived single gene minicircles of the dinoflagellate *Ceratium horridum* are located in the nucleus. *Mol. Biol.* and *Evol*. 21:1318–22.

Lee, R. E. (1977). Evolution of algal flagellates with chloroplast endoplasmic reticulum from the ciliates. *S. Afr. J. Sci*. 73:179–82.

Leipe, D. D., Wainright, P. O., Gunderson, J. H., Porter, D., Patterson, D. J., Valois, F., Himmerich, S., and Sogin, M. L. (1994). The stramenopiles from a molecular perspective: 16S-like rRNA sequences from *Labyrinthuloides minuta* and *Cafeteria roenbergensis. Phycologia* 33:369–77.

Manhart, J. R., and McCourt, R. M. (1992). Molecular data and species concepts in the algae. *J. Phycol*. 28:730–7.

Meeks, J. C. (1974). Chlorophylls. In *Algal Physiology and Biochemistry*, ed. W. D. P. Stewart, pp. 161–75. Berkeley: Univ. Calif. Press.

Melkonian, M. (1980). Flagellar roots, mating structure and gametic fusion in the green alga *Ulva lactuca* (Ulvales). *J. Cell Sci*. 46:149–69.

Melkonian, M., Reize, I. B., and Preisig, H. R. (1987). Maturation of a flagellum/basal body requires more than one cell cycle in algal flagellates: studies on *Nephroselmis olivaea* (Prasinophyceae). In *Algal Development, Molecular and Cellular Aspects*, ed. W. Wiessner, D. G. Robinson, and R. C. Starr, pp. 102–13. Heidelberg: Springer.

Mitchell, D. R. (2000). *Chlamydomonas* flagella. *J. Phycol*. 36:261–73.

Miyagishima, S., Nishida, K., and Kuriowa, T. (2003). An evolutionary puzzle: chloroplast and mitochondrial division rings. *Trends Plant Sci.* 8:432–8.

Moestrup, Ø. (1982). Flagellar structure in algae: A review, with new observations particularly on the Chrysophyceae. Phaeophyceae (Fucophyceae), Euglenophyceae, and *Reckertia. Phycologia* 21:427–528.

Moestrup, O. (2000). The flagellate cytoskeleton. In *The Flagellates*, ed. B. S. C. Leadbeater, and J. C. Green, pp.69–94. London:Taylor and Francis.

Murakami, A., Miyashita, H., Iseki, M., Adachi, K., and Mimuro, M. (2004). Chlorophyll *d* in an epiphytic cyanobacterium of red algae. *Science* 303:1633.

Nagasato, C, Yoshikawa, S., Yamashita, M., Kawai, H., and Motomura, T. (2003). Pyrenoid formation associated with the cell cycle in the brown alga, *Scytosiphon lomentaria* (Scytosiphonales, Phaeophyceae). *J. Phycol*. 39:1172–80.

Osteryoung, K. W., and Nunnari, J. (2003). The division of endosymbiotic organelles. *Science* 302:1698–1704.

Patron, N. J., and Keeling, P. J. (2005). Common evolutionary origin of starch biosynthesis enzymes in green and red algae. *J. Phycol*. 41:1131–41.

Patterson, D. J., and Hausmann, K. (1981). The behavior of contractile vacuole complexes of cryptophycean flagellates. *Br. Phycol. J.* 16:429–39.

Percival, E., and McDowell, R. H. (1967). *Chemistry and Enzymology of Marine Algal Polysaccharides*. New York: Academic Press.

Porter, G., Tredwell, C. J., Searle, G. F. W., and Barber, J. (1978). Picosecond time-resolved energy transfer in *Porphyridium cruentum*. *Biochim. Biophys. Acta* 501:232–45.

Ragan, M. A. (1994). 18S ribosomal DNA sequences indicate a monophyletic origin of Charophyceae. *J. Phycol*. 30:490–500.

Raven, J. (1997). CO_2 concentrating mechanisms: a direct role for thylakoid lumen acidification? *Plant Cell and Environ*. 20:147–54.

Ringo, D. L. (1967). Flagellar motion and fine structure of the flagellar apparatus in *Chlamydomonas*. *J. Cell Biol*. 33:543–71.

Rosenbaum, J. L., and Witman, G. B. (2002). Intraflagellar transport. *Nat. Rev. Mol. Cell Biol*. 3:815–25.

Samsonoff, W. A., and MacColl, R. (2001). Biliproteins and phycobilisomes from cyanobacteria and red algae at extremes of habitat. *Arch. Microbiol*. 176:402–5.

Saunders, G. W., and Hommersand, M. H. (2004). Assessing red algal supraordinal diversity and taxonomy in the context of contemporary systematic data. *Amer. J. Bot*. 91:1494–1507.

Schoppmeier, J., and Lechtreck, K.-F. (2003). Flagellar regeneration in *Spermatozopsis similes* (Chlorophyta). *J. Phycol*. 39:918–22.

Snell, W. J. (1976). Mating in *Chlamydomonas:* A system for the study of specific cell adhesion. I. Ultrastructural and electrophoretic analyses of flagellar surface components involved in adhesion. *J. Cell Biol*. 68:48–69.

Stiller, J. W., and Hall, B. D. (1997). The origin of red algae: implication for plastid evolution. *Proc. Natl. Acad. Sci. USA* 94:4520–5.

Sukenik, A., Tchernov, D., Kaplan, A., Huertas, E., Lubian, L. M., and Livne, A. (1997). Uptake, efflux, and photosynthetic utilization of inorganic carbon by the marine eustigmatophyte *Nannochloropsis* sp. *J. Phycol*. 33:969–74.

van der Auwera, G., and deWachter, R. (1997). Complete large subunit ribosomal RNA sequences from the heterokont algae *Ochromonas danica*, *Nannochloropsis salina*, and *Tribonema aequale*, and phylogenetic analysis. *J. Mol. Evol*. 45:84–90.

Vergara, J. J., and Niell, F. X. (1993). Effects of nitrate availability and irradiance on internal nitrogen constituents in *Corallina elongata* (Rhodophyta). *J. Phycol*. 29:285–93.

Vierkotten, L., Simon, A., and Becker, B. (2004). Preparation and characterization of protoplasts from the prasinophyte *Scherffelia dubia* (Chlorophyta). *J. Phycol*. 40:1106–11.

Wessel, D., and Robinson, D. G. (1979). Studies on the contractile vacuole of *Poterioochromonas malhamensis* Peterfi. I. The structure of the alveolate vesicles. *Eur. J. Cell Biol*. 19:60–6.

Zhang, H., and Lin, S. (2003). Complex structure of the Form II RUBISCO in the dinoflagellate *Prorocentrum minimum* (Dinophyceae). *J. Phycol*. 38:1160–71.

Part II

The prokaryotic algae

The cyanobacteria or blue-green algae form a natural group by virtue of being the only prokaryotic algae. Prokaryotic algae have an outer plasma membrane enclosing protoplasm containing photosynthetic thylakoids, 70S ribosomes, and DNA fibrils not enclosed within a separate membrane. Chlorophyll *a* is the main photosynthetic pigment, and oxygen is evolved during photosynthesis.

Chapter 2

Cyanobacteria

CYANOPHYCEAE

The Cyanophyceae or **blue-green algae** are, today, usually referred to as the **cyanobacteria** (blue-green bacteria). The term cyanobacteria acknowledges that these prokaryotic algae are more closely related to the prokaryotic bacteria than to eukaryotic algae. For the last quarter century, cyanobacteria were thought to have evolved about 3.5 billion years ago. These reports were based on interpretation of microfossils, difficult at best with such small organisms. It now appears that these investigators selected specimens that fit the assumptions of the authors, with most phycologists now rejecting their claims. Based on other reports, the actual time of evolution of cyanobacteria is thought to be closer to 2.7 billion years ago (Buick, 1992; Brasier et al., 2002; Dalton, 2002).

Cyanobacteria have chlorophyll *a* (some also have chlorophyll *b* or *d*), phycobiliproteins, glycogen as a storage product, and cell walls containing amino sugars and amino acids.

At one time, the occurrence of chlorophyll *b* in cyanobacteria was used as a criterion to place the organisms in a separate group, the **Prochlorophyta**. Modern nucleic-acid sequencing, however, has shown that chlorophyll *b* evolved a number of times within the cyanobacteria and the term Prochlorophyta has been discarded (Palenik and Haselkorn, 1992; Urback et al., 1992).

Morphology

The simplest morphology in the cyanobacteria is that of unicells, free-living (see Figs. 2.19(*c*), 2.20) or enclosed within a mucilaginous envelope (Figs. 2.48, 2.56(*a*), (*b*)). Subsequent evolution resulted in the formation of a row of cells called a **trichome** (Fig. 2.16). When the trichome is surrounded by a sheath, it is called a **filament** (Fig. 2.10). It is possible to have more than one trichome in a filament (Figs. 2.56(*e*), 2.58(*b*)). The most complex thallus is the branched filament (Fig. 2.58(*a*)). Such a branched filament can be **uniseriate** (composed of a single row of cells) or **multiseriate** (composed of one or more rows of cells).

Cell wall and gliding

The cell wall of cyanobacteria is basically the same as the cell wall of Gram-negative bacteria (Fig. 2.1). A **peptidoglycan layer** is outside of the **cell membrane**. The peptidoglycan is an enormous polymer composed of two sugar derivatives, *N*-acetylglucosamine and *N*-acetylmuramic acid, and several different amino acids (Fig. 2.2). Outside of the peptidoglycan is a **periplasmic space**, probably filled with a loose network of peptidoglycan fibrils. An **outer membrane** surrounds the periplasmic space.

Some cyanobacteria are capable of gliding, that is, *the active movement of an organism on a solid*

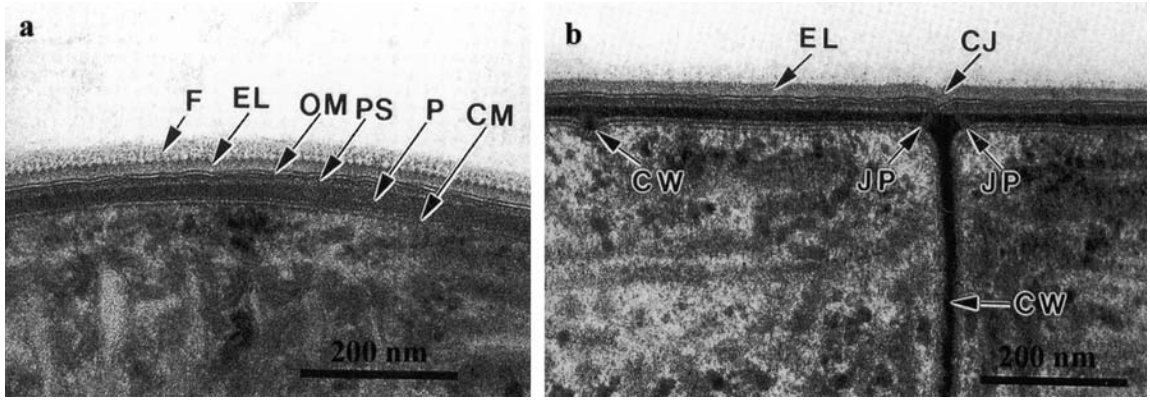


Fig. 2.1 Transmission electron micrographs of sections of the wall of the cyanobacterium *Phormidium uncinatum*. The cell wall (CW) contains layers similar to those of a Gram-negative bacterium, e.g., the cytoplasmic membrane (CM), peptidoglycan layers (P), periplasmic space (PS) and outer membrane (OM). In addition, the cyanobacterium contains the additional two external layers typical of a motile cell, the serrated external layer (EL) and hair-like fibers (F). (CJ) Circumferential junction; (JP) junctional pore. (From Hoiczyk and Baumeister, 1995.)

substrate where there is neither a visible organ responsible for the movement nor a distinct change in the shape of the organism (Jarosch, 1962). Gliding is a slow uniform motion (up to 600 μm s^{-1} in *Oscillatoria*; Bhaya, 2004) at a direction parallel to the long axis of the cell and is occasionally interrupted by reversals in direction. Gliding is accompanied by a steady secretion of slime, which is left behind as a mucilaginous trail. Some cyanobacteria (*Phormidium, Oscillatoria*) rotate during gliding while other cyanobacteria (*Anabaena*) do not rotate.

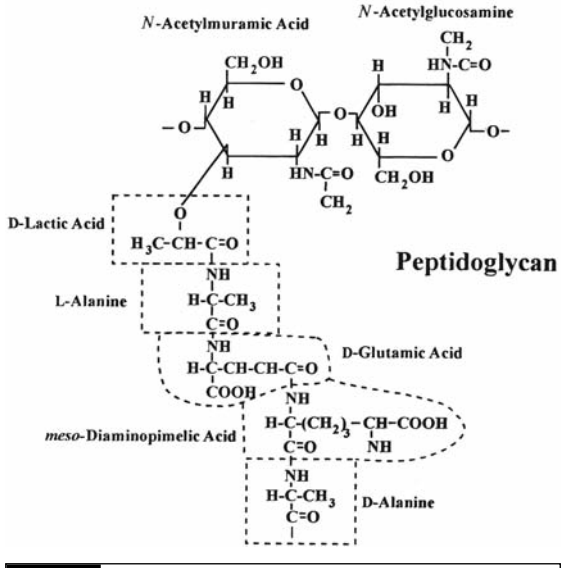


Fig. 2.2 The structure of a peptidoglycan molecule in the cell wall of cyanobacteria.

The cell wall of gliding bacteria has two additional layers outside of the cell wall (Figs. 2.1, 2.3, 2.4). A **serrated external layer (S-layer)** and a layer of **hair-like fibers** occur outside of the outer membrane of the cell wall of gliding cyanobacteria. The hair-like fibers of the outermost layer are composed of a rod-like glycoprotein called **oscillin** (Hoiczyk and Baumeister, 1998; Hoiczyk, 2000).

The cross walls of neighboring cells of gliding cyanobacteria contain **junctional pores** that are 15 nm in diameter and radiate outward from the cytoplasm at an angle of about 30–40° relative to the plane of each septum (Figs. 2.1, 2.5, 2.6). The number of rows of junctional pores around each side of the septum varies from one circumferential ring in *Phormidium* to several rows of pores that girdle the septum in *Anabaena*. The junctional pore is 70–80 nm long and spans the entire multilayered cell wall. The junctional pore is composed of a tube-like base and an outer pore complex.

Gliding occurs by slime secretion through the circumferential junctional pores on one side of the septum (Hoiczyk and Baumeister, 1998; Hoiczyk, 2000). The slime passes along the surface of the oscillin fibers of the outer layer of the cell wall and onto the adjacent substrate, propelling the filament forward. The orientation of the

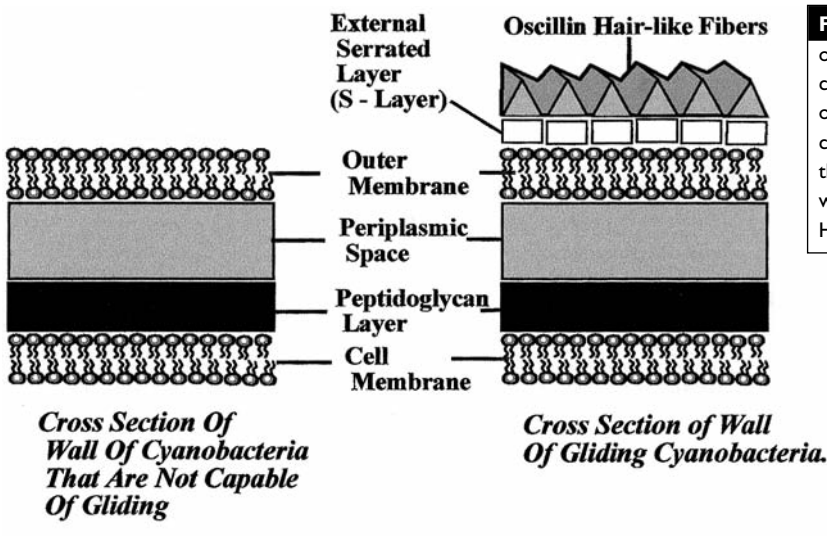


Fig. 2.3 Cross sections of a wall of a cyanobacterium that is not capable of gliding and a cross section of a wall of a cyanobacterium that is capable of gliding. Cyanobacteria that can glide have an additional two wall layers on the outside. (From Hoiczyk and Baumeister, 1995.)

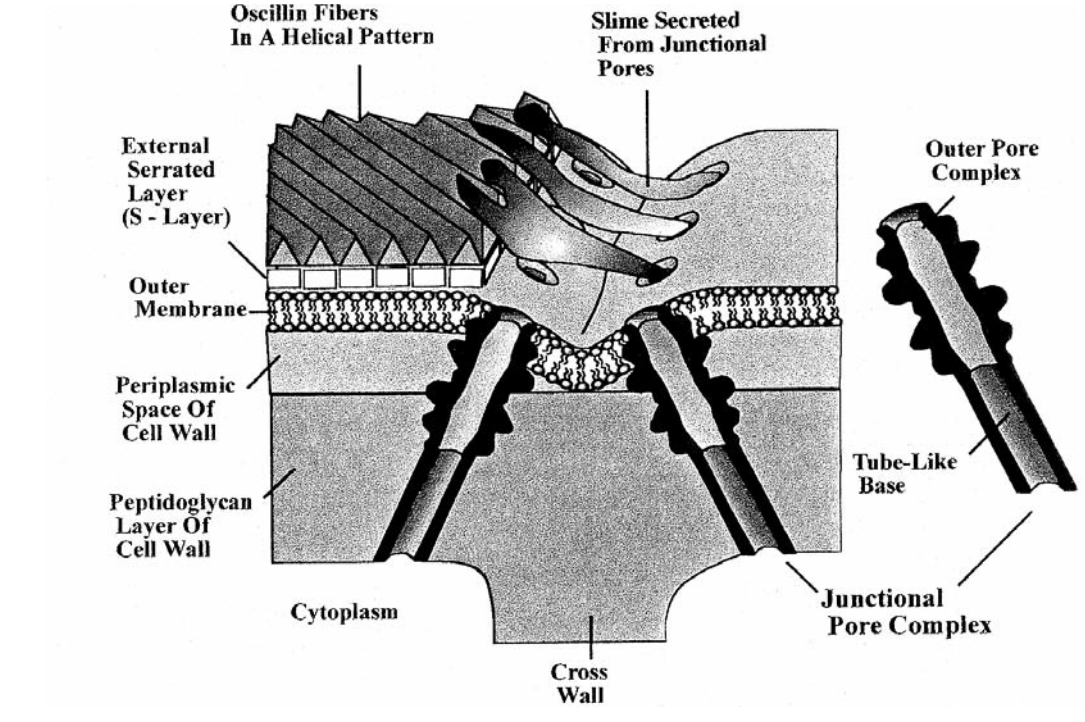


Fig. 2.4 A model of the junctional pore complex of a cyanobacterium. Extrusion of slime through the circumferentially arranged junctional pores on one side of the cross wall results in forward movement of the filament in contact with the substrate. The arrangement of the oscillin fibers in the outer layer of the cell wall determines whether the filament rotates as it glides over the surface. In the drawing, the oscillin fibers are spiraled so the filament rotates as it glides. (Modified from Hoiczyk and Baumeister, 1998.)

oscillin fibers of the outer layer determines whether the filament rotates during gliding. In *Anabaena*, the spiral oscillin fibers produce a clockwise rotation while in *Oscillatoria princeps* and *Lyngbya aeruginosa* the oscillin fibers are spiraled in the opposite direction and produce a counterclockwise rotation during gliding

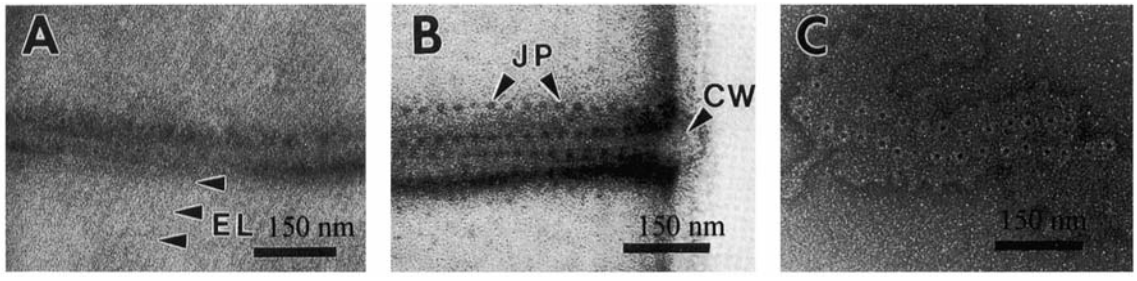


Fig. 2.5 Transmission electron micrographs of *Phormidium uncinatum*. (*A*) Isolated cell wall with the outer membrane and external layer (EL) still attached. On both sides of the cross wall, the ring-shaped counterpart of the junctional pores with their central pores are visible. (*B*) Negatively stained isolated wall showing the junctional pores (JP) filled with slime. (CW) cross wall. (*C*) Isolated outer membrane with the ring-shaped parts of the junctional pores. (From Hoiczyk and Baumeister, 1995.)

(Hoiczyk and Baumeister, 1995) (Fig. 2.7). In *Phormidium*, the oscillin fibers are not spiraled and the filament does not rotate during gliding.

The arrangement of hair-like fibers thus serves as a passive screw as the slime passes over their surface in gliding. Reversal of gliding occurs when slime stops coming out of the ring of junctional pores on one side of the septum, and when slime begins coming out of the ring of junctional pores on the other side of the septum.

Pili and twitching

Pili are proteinaceous appendages that project from the surface of cyanobacterial cells (Fig. 2.8). There are two types of pili in the unicellular cyanobacterium *Synechocystis* (Bhaya, 2004). The cell is covered uniformly with a layer of thin-brush-like pili with an average diameter of 3–4 nm and a length of 1 μm. Cells also have thick flexible pili with a diameter of 6–8 nm and length of 4–5 μm that often make connections with other cells. The pili are composed of 500 to 1000 units of the polypeptide **pilin**. Each pilin unit consists of between 145 and 170 amino acids (Bhaya et al., 1999). The pilin molecule is similar to the oscillin molecule involved in gliding. *Synechocystis* is able to move across a surface at 1 to 2 μm s^{-1} using a mechanism called twitching that utilizes change in configuration of the pili (Wall and Kaiser, 1999). The pili probably move the cell body along a sur-

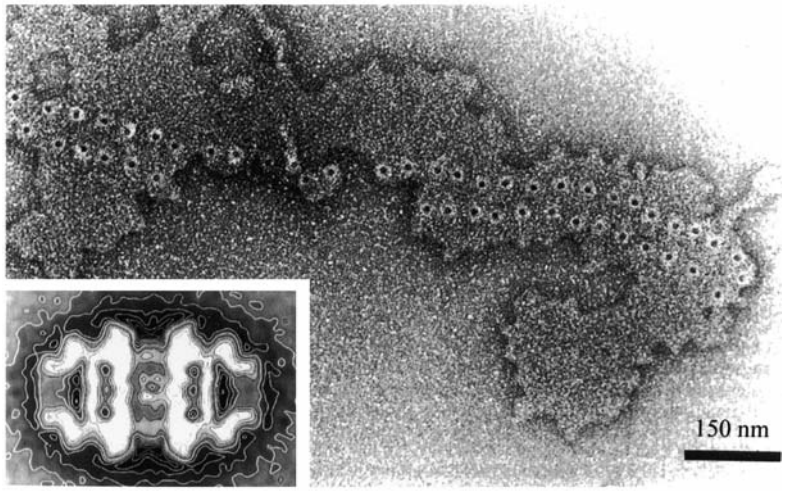


Fig. 2.6 Structure of the organelles of the junctional-pore complex in *Phormidium uncinatum*. Transmission electron micrograph of a negatively stained isolated outer membrane patch showing the ring-shaped orifices of the junctional pores that would be circumferentially arranged in the cross wall in the cell. Inset shows a number of superimposed images of junctional-pore complexes. (From Hoiczyk, 2000.)

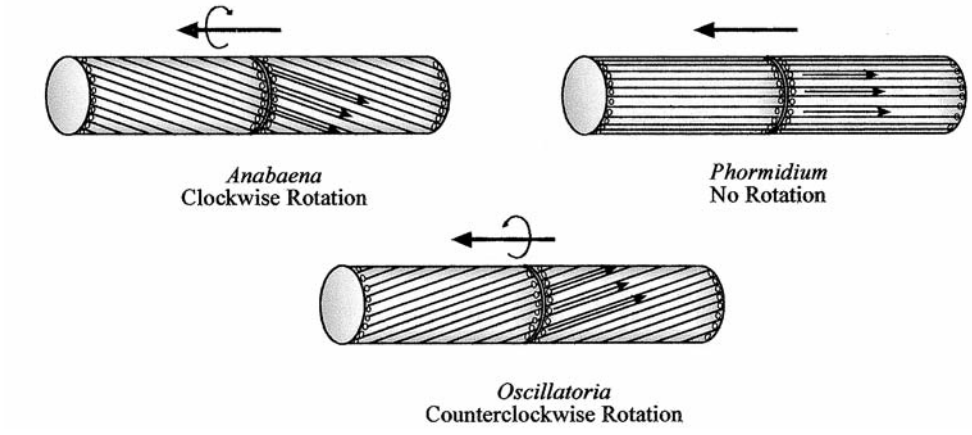


Fig. 2.7 Rotation of the cyanobacterial filament depends on the orientation of the oscillin protein. Mucilage is secreted from the pores near the cross walls. The mucilage flows along the oscillin fibers causing rotation if the oscillin is helically oriented. There is no rotation if the oscillin is not helically oriented.

face by a reiterative process of pili extension, adhesion, and retraction (Bhaya, 2004).

Synechocystis exhibits both positive and negative phototaxis in blue light (450 nm wavelength) but not in red or far-red light (Terauchi and Ohmori, 2004). Blue light stimulates the production of cyclic adenosine monophosphate (cAMP), a common second messenger in biological systems (Fig. 2.9).

Sheaths

A sheath (**capsule** or **extracellular polymeric substances** (**EPS**)) composed of mucilage and a small amount of cellulose is commonly present in cyanobacteria (Nobles et al., 2001) (Figs. 2.10, 2.11). The sheath protects cells from drying. Active growth appears necessary for sheath formation, a fact that may explain its sometimes poor development around spores and akinetes. The sheath of *Gloeothece* sp. is composed of polysaccharides with neutral sugars and uronic acids including galactose, glucose, mannose, rhamnose, 2-*O*-methyl-D-xylose, glucuronic acid and galacturonic acids (Weckesser et al., 1987). The

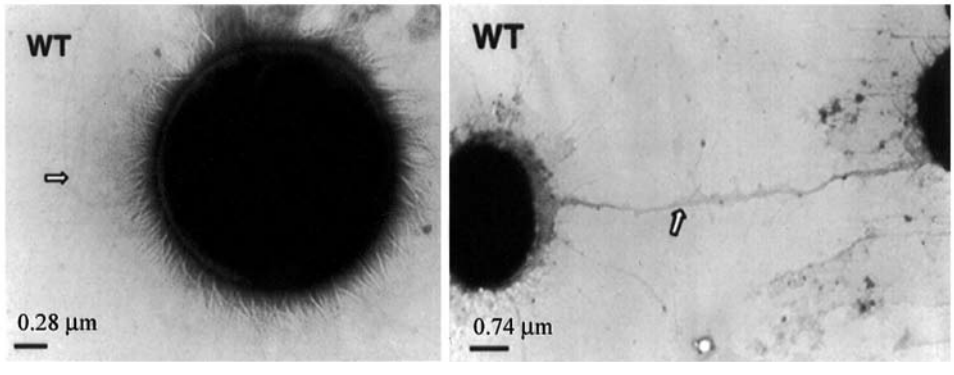


Fig. 2.8 Transmission electron micrographs of negatively stained whole cells of *Synechocystis* showing pili. (WT) Wild type. (From Bhaya et al., 1999.)

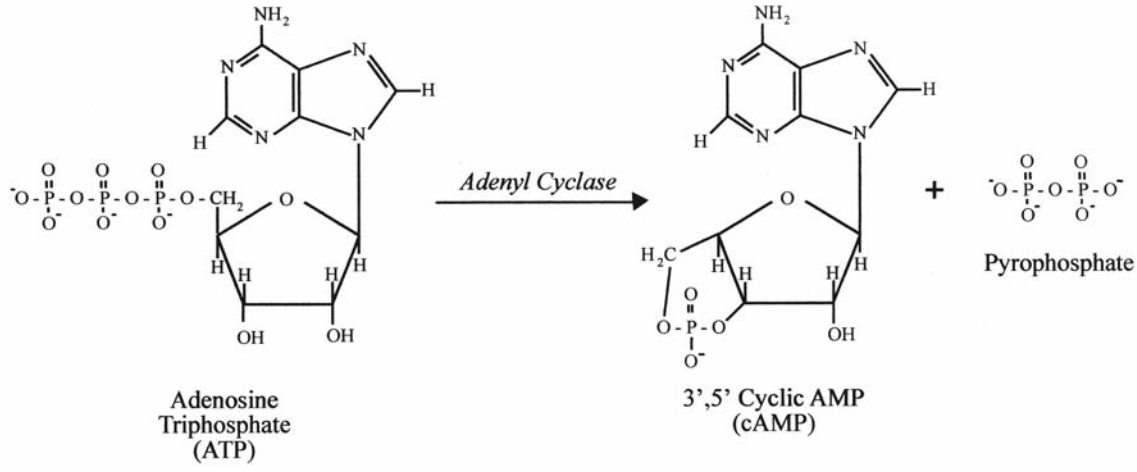


Fig. 2.9. The enzyme adenyl cyclase catalyzes the formation of cAMP from ATP.

sheath of *Gloeothece* contains only 2% protein and a trace of fatty acids and phosphate. The commercial applications of cyanobacterial EPS have been reviewed by De Philippis and Vincenzini (1998). Sheaths are often colored, with red sheaths found in algae from highly acid soils and blue sheaths characteristic of algae from basic soils (Drouet, 1978). Yellow and brown sheaths are common in specimens from habitats of high salt content, particularly after the algae dry out.

The sheath excludes India ink so the easiest way to visualize the sheath is to place a small amount of India ink in the water (Fig. 2.10). Production of a sheath is dependent on environmental conditions. A shortage of CO_2 results in cessation of sheath production and release of the sheath. An excess of fixed carbon results in formation of a sheath (Otero and Vincenzini, 2004).

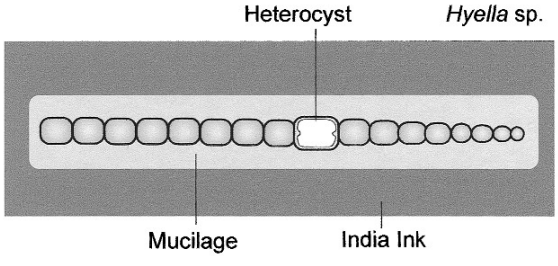


Fig. 2.10 A drawing of a filament of *Hyella* sp. in India ink. This method clearly shows the sheath around the filament.

Protoplasmic structure

Many of the protoplasmic structures found in the bacteria occur in the cyanobacteria. In the central protoplasm are the **circular fibrils of DNA** which are not associated with basic proteins (**histones**) (Figs. 2.11 and 2.14). The amount of DNA in unicellular cyanobacteria varies from 1.6×10^9 to 8.6×10^9 daltons. This is similar to the genome size in bacteria (1.0×10^9 to 3.6×10^9 daltons) and is larger than the genome size in mycoplasmas (0.4×10^9 to 0.5×10^9 daltons) (Herdman et al., 1979). The peripheral protoplasm is composed principally of **thylakoids** and their associated structures, the **phycobilisomes** (on the thylakoids, containing the phycobiliproteins) and **glycogen granules**. The **70S ribosomes** are dispersed throughout the cyanobacterial cell but are present in the highest density in the central region around the nucleoplasm (Allen, 1984).

Cyanophycin is a non-ribosomally synthesized protein-like polymer that occurs in the cytoplasm in structured granules that are not surrounded by a membrane (Fig. 2.13) (Aboulmagd et al., 2000; Sherman et al., 2000). Cyanophycin is a polymer that consists of equimolar amounts of arginine and aspartic acid arranged as a polyaspartate

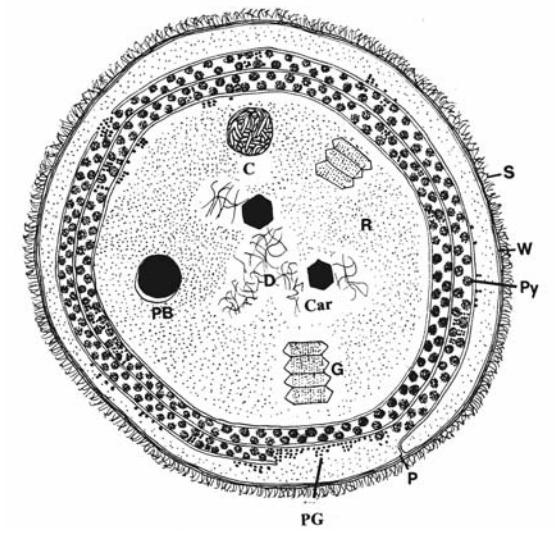


Fig. 2.11 Drawing of the fine-structural features of a cyanobacterial cell. (C) Cyanophycin body (structured granule); (Car) carboxysome (polyhedral body); (D) DNA fibrils; (G) gas vesicles; (P) plasmalemma; (PB) polyphosphate body; (PG) polyglucan granules; (Py) phycobilisomes; (R) ribosomes; (S) sheath; (W) wall.

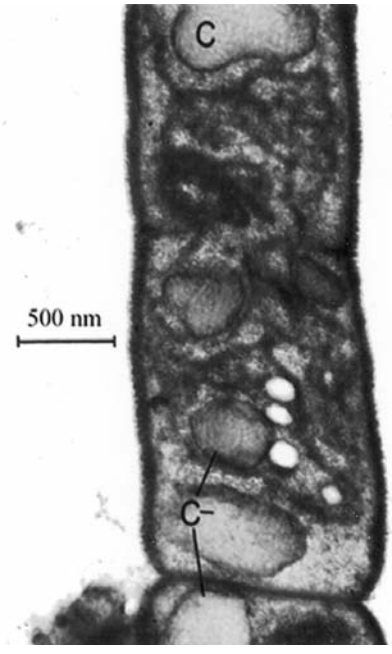


Fig. 2.13 Transmission electron micrograph of a section of a cell of *Plectonema boryanum* showing cyanophycin bodies (C). (From Lawry and Simon, 1982.)

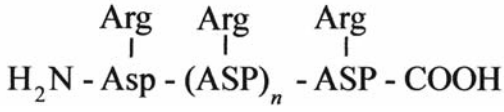


Fig. 2.12 Cyanophycin is composed of equimolar amounts of arginine (Arg) and aspartic acid (Asp) arranged as a polyaspartate backbone.

backbone (Fig. 2.12). Cyanophycin functions as a temporary nitrogen reserve in nitrogen-fixing cyanobacteria, accumulating during the transition from the exponential to the stationary phase and disappearing when balanced growth resumes. Nitrogen is stored in phycobilisomes in cyanobacteria that do not fix nitrogen (Li et al., 2001a).

Carboxysomes (polyhedral bodies) (Fig. 2.14) are similar to the carboxysomes in bacteria and contain the carbon dioxide-fixing enzyme **ribulose-1,5-bisphosphate carboxylase/oxygenase (Rubisco)**. There are two types of carboxysomes, α-carboxysomes and β-carboxysomes, which differ in their protein composition. Cyanobacteria with ***α*-carboxysomes** occur in environments where dissolved carbon is not limiting (e.g., oligotrophic oceanic waters), whereas cyanobacteria with ***β*-carboxysomes** occur in environments where dissolved carbon is limiting (e.g., mats, films, estuaries, and alkaline lakes with higher densities of photosynthetic organisms) (Badger et al., 2002).

Carboxysomes also contain the enzyme **carbonic anhydrase** that converts HCO_3^- into carbon dioxide, the only form of carbon that is fixed by Rubisco (Fig. 2.15). Bicarbonate (HCO_3^-) is transported into the cell and carboxysome. Carbonic anhydrase in the carboxysome converts HCO_3^- into CO_2 which is fixed by Rubisco into carbohydrates. The amount of a cell occupied by carboxysomes increases as the inorganic carbon (HCO_3^-, CO_2) in the medium decreases (Turpin et al., 1984). Heterocysts (Fig. 2.4) lack ribulose-1,5-bisphosphate carboxylase/oxygenase and the ability to fix carbon dioxide. Heterocysts also lack carboxysomes (Winkenbach and Wolk, 1973).

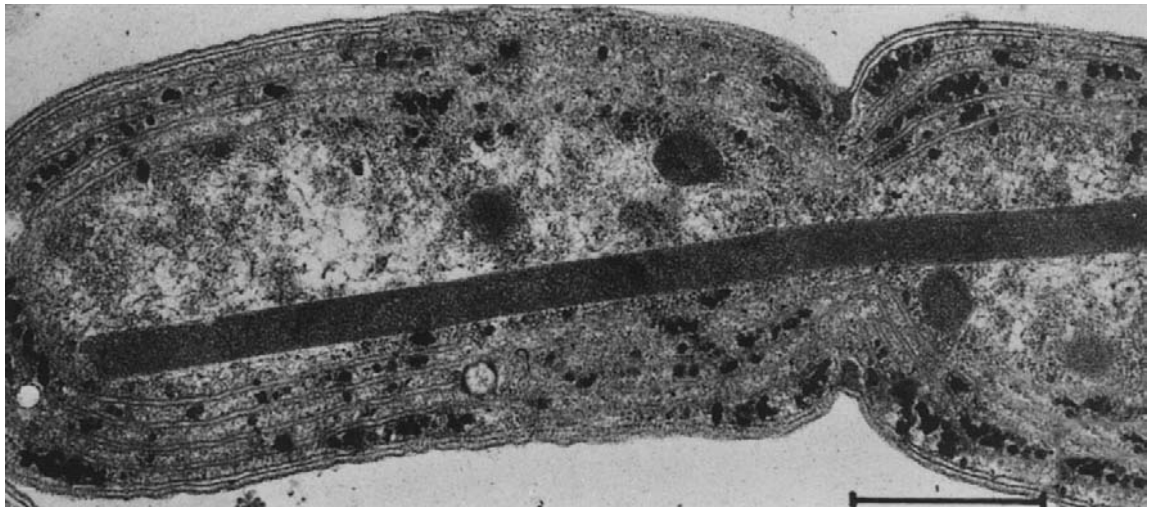


Fig. 2.14 Transmission electron micrograph of a section of a dividing cell of *Anacystis nidulans* showing thylakoids in the peripheral cytoplasm, DNA microfibrils, ribosomes, and a long carboxysome in the central cytoplasm. Bar = 0.5 μm. (From Gantt and Conti, 1969.)

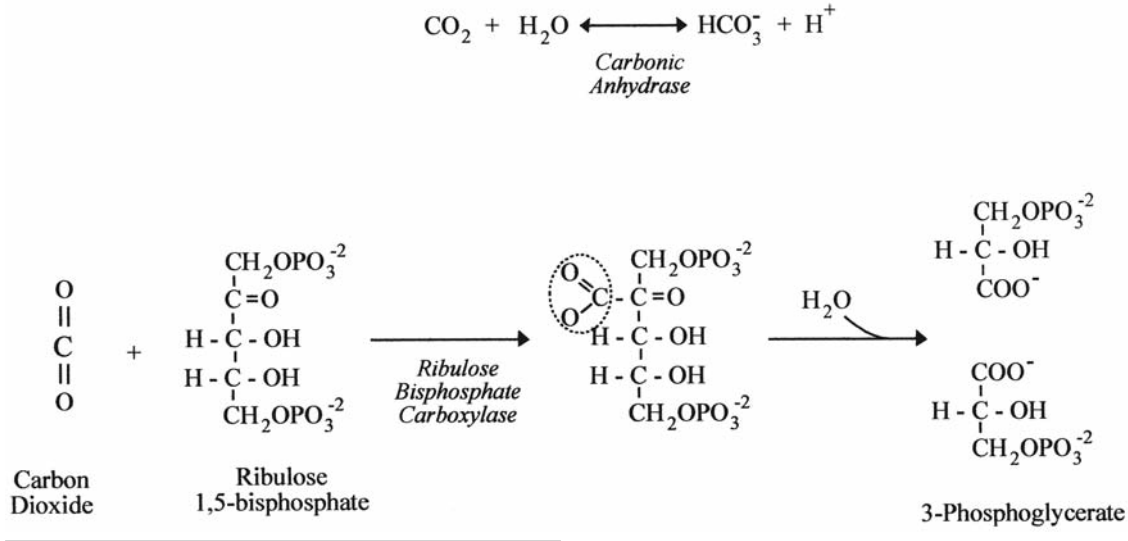


Fig. 2.15 Carboxysomes contain the enzymes carbonic anhydrase and ribulose-1,5-bisphosphate carboxylase/oxygenase. Carbonic anhydrase in the carboxysome converts HCO_3^- into CO_2 which is fixed by ribulose-1,5-bisphosphate carboxylase/oxygenase into carbohydrates.

Polyphosphate bodies (**metachromatic** or **volutin granules**) (Fig. 2.11) are spherical and appear similar to lipid bodies of eukaryotic cells in the electron microscope. Polyphosphate bodies contain stored phosphate, the bodies being absent in young growing cells or cells grown in a phosphate-deficient medium, but present in older cells (Tischer, 1957).

Polyglucan granules (**α-granules**) (Fig. 2.11) are common in the space between the thylakoids in actively photosynthesizing cells. These granules contain a carbohydrate, composed of 14 to 16

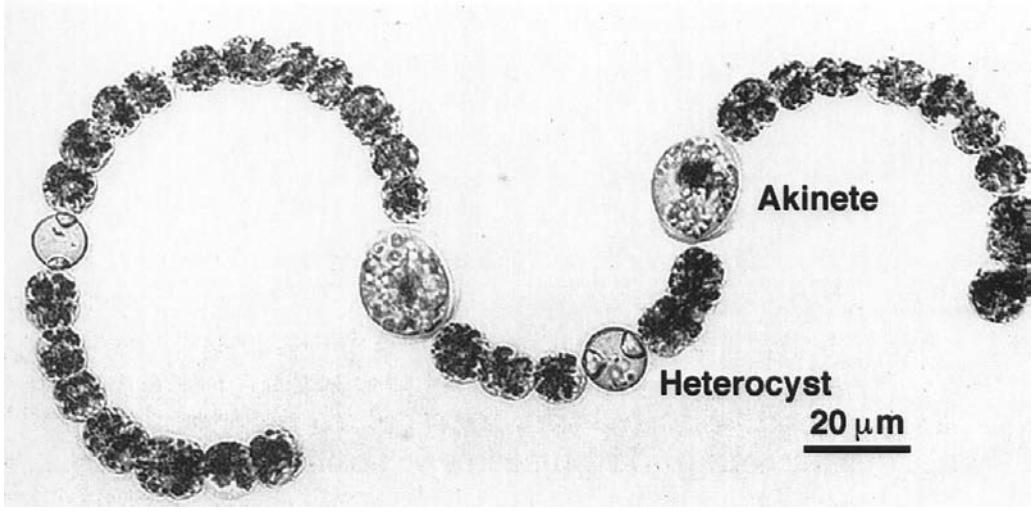


Fig. 2.16 Light micrograph of *Anabaena crassa* showing vegetative cells, akinetes, and heterocysts. (From Li et al., 1997.)

glucose molecules, that is similar to amylopectin (Hough et al., 1952; Frederick, 1951).

Gas vacuoles

A gas vacuole is composed of gas vesicles, or hollow cylindrical tubes with conical ends, in the cytoplasm of cyanobacteria (Figs. 2.11, 2.17) (Walsby, 1994; Oliver, 1994). Gas vesicles do not have true protein-lipid membranes, being composed exclusively of protein ribs or spirals arranged similarly to the hoops on a barrel. It is possible to collapse the gas vesicles by applying pressure to the cells, the collapsed vesicles having the two halves stuck together. The membrane of the gas vesicle is quite rigid, with the gas inside it at a pressure of 1 atm. The membrane is permeable to gases, allowing the contained gas to equilibrate with gases in the surrounding solution. The membrane must, however, be able to exclude water. It has been postulated that the inner surface must be **hydrophobic**, thereby preventing condensation on it of water droplets, and restraining, by surface tension, water creeping through the pores. At the same time these molecules must present a **hydrophilic** surface at the outer (water-facing) surface in order to minimize the interfacial tension, which would otherwise result in the collapse of the gas vacuole.

Cyanobacteria possessing gas vacuoles can be divided into two physiological-ecological groups. In the first group are those algae having vacuoles only at certain stages of their life cycle, or only in certain types of cells. In *Gloeotrichia ghosei* and in certain

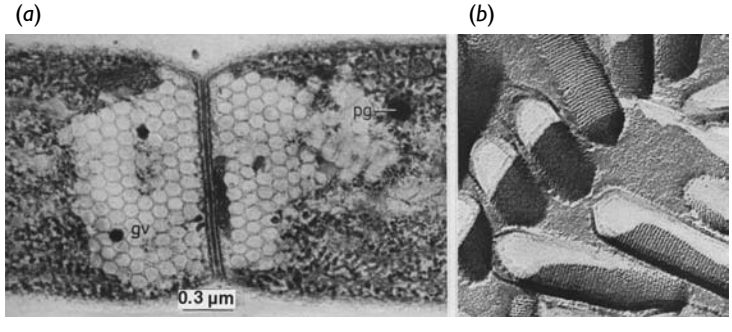


Fig. 2.17 (*a*) Transmission electron micrograph of two cells of *Oscillatoria redekei* showing a cross wall separating areas of gas vacuoles (gv); (pg) lipid droplet. (From Whitton and Peat, 1969.) (*b*) Freeze-etch preparation of gas vacuoles. (From Jones and Jost, 1970.)

species of *Tolypothrix* and *Calothrix*, gas vesicles appear only in hormogonia. The hormogonia float when they are released, and it is possible that the buoyancy provided is of significance in dispersal of these stages. The second group consists of planktonic cyanobacteria, including species of *Anabaena* (Figs. 2.16, 2.18(*d*), 2.57(*b*)), *Gloeotrichia* (Fig. 2.18(a)), *Microcystis* (Figs. 2.48, 2.56(*b*)), *Aphanizomenon* (Fig. 2.18(*b*)), *Oscillatoria* (Figs. 2.19(*a*), (*b*), 2.34(*a*), (*b*)), *Trichodesmium* (Figs. 2.31, 2.56(*g*)), and *Phormidium* (Figs. 2.18(*c*), 2.56(*c*)). These algae derive positive buoyancy from their gas vesicles, and as a consequence form blooms floating near the water surface. The loss of buoyancy, and subsequent sinking of these algae in the water column, can be due to different factors. In *Anabaena flos-aquae* (Fig. 2.18(*d*)), the loss of buoyancy is caused by the loss of gas vesicles owing to increased turgor pressure, whereas in *Oscillatoria agardhii* (Fig. 2.19(*a*)), buoyancy is lost through cessation of gas vesicle production and an increase in cell mass. In *Microcystis aeruginosa* (Fig. 2.56(*b*)), loss of buoyancy can be due to entrapment of whole colonies in a colloidal precipitate composed of organic material and iron salts. The colloidal precipitate is formed in certain lakes when dissolved iron in the anoxic water of the hypolimnion in stratified lakes becomes oxidized on mixing with aerated water of the epilimnion (Oliver et al., 1985).

There is a direct relationship between buoyancy and light quantity in nitrogen-fixing cyanobacteria such as *Anabaena flos-aquae* (Fig. 2.18(*d*)) (Spencer and King, 1985). The relationship is complex and also involves the concentration of ammonium ions (NH_4^+) in the water. Buoyancy in *Anabaena flos-aquae* increases under low irradiance (less than 10 $\mu E\, m^{-2}$

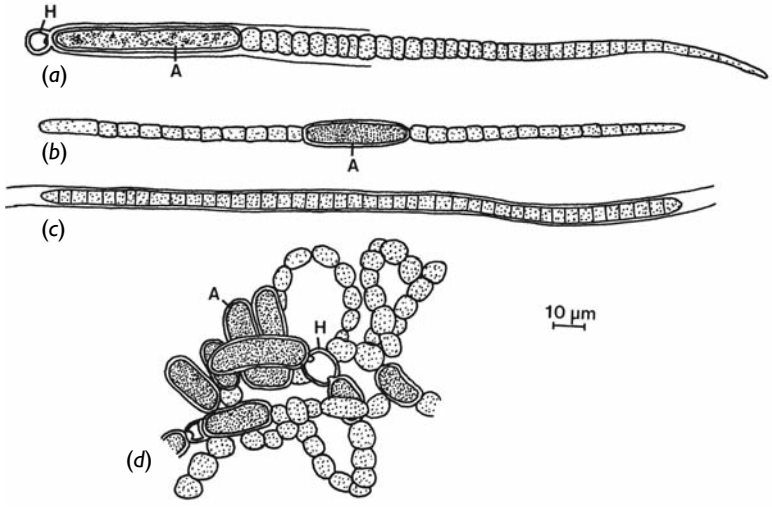


Fig. 2.18 (*a*) *Gloeotrichia echinulata*. (*b*) *Aphanizomenon flos-aquae*. (*c*) *Phormidium inundatum*. (*d*) *Anabaena flos-aquae*. (A) Akinete; (H) heterocyst. (After Prescott,1962.)

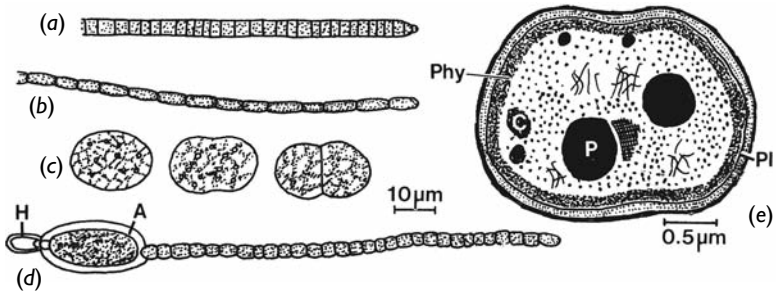


Fig. 2.19 (*a*) *Oscillatoria agardhii*. (*b*) *O. limnetica*. (*c*) *Synechococcus aeruginosus*. (*d*) *Cylindrospermum majus*. (A) Akinete; (H) heterocyst. (*e*) Drawing of the fine structure of *Gloeobacter violaceus*. (C) Cyanophycin granule; (P) polyphosphate body; (Phy) probable layer of phycobiliproteins; (Pl) plasmalemma. ((*c*),(*d*) after Prescott, 1962; (e) after Rippka et al., 1974.)

s^{-1}), absence of NH_4^+, and low CO_2 concentrations. Such conditions occur in many stagnant eutrophic lakes during the summer. In these lakes, rapid growth of algae has depleted the NH_4^+ and CO_2. The water transmits little light because of the large standing crop of algae. Under these conditions, *A. flos-aquae* and other nitrogen-fixing cyanobacteria having gas vacuoles increase their buoyancy and rise close to the surface of the water. Here they are able to outcompete other algae because of their ability to fix nitrogen in water that has little available nitrogen. Cyanobacteria that do not fix nitrogen have reduced growth, and therefore reduced buoyancy, and sink in the water column. Once established, a bloom of buoyant, nitrogen-fixing, cyanobacteria tends to be self-perpetuating in that increased mass of the bloom maintains the reduced light and CO_2 levels required for maximum buoyancy.

Structures other than gas vesicles can cause significant variation in cell density, and therefore buoyancy (Konopka et al., 1987). Polyphosphate granules may have a density of 2 g cm^{-3} or greater, and glycogen (which is accumulated under high light intensities) has a density of about 1.5 cm^{-3}. Both have a higher density than water (1 g cm^{-3}) and can cause cells to sink (Booker and Walsby, 1981; McCausland et al., 2005).

Pigments and photosynthesis

The major components of the photosynthetic light-harvesting system of the cyanobacteria are **chlorophyll** *a* in the thylakoid membrane, and the **phycobiliproteins**, which are water-soluble chromoproteins assembled into macromolecular aggregates (phycobilisomes) attached to the outer surface of the thylakoid membranes. Some cyanobacteria contain chlorophyll *b* and the cyanobacterium *Acaryochloris marina* (Fig. 2.20) contains chlorophyll *d*. At one time those cyanobacteria containing chlorophyll *b* (*Prochlorococcus* (Fig. 2.20), *Prochlorothrix*, *Prochloron*) were thought to be a distinct evolutionary group and they were placed in the Prochlorophyta. Evolutionary trees based on nucleic acid sequencing have shown that chlorophyll *b* arose a number of times and that these cyanobacteria are spread throughout the group (Palenik and Haselkorn, 1992; Urback et al., 1992). In contrast, *Acaryochloris marina* (Fig. 2.20), the only cyanobacterium known to have chlorophyll *d*, appears to be only distantly related to other cyanobacteria (Miller et al., 2005; Miyashita et al., 2003). The absorption spectrum of chlorophyll *d* (Fig. 1.19) is shifted toward far-red wavelengths and *A. marina* exists in environments where there is an abundance of these wavelengths of light (e.g., under red algae).

The carotenoids of the cyanobacteria differ from those of the eukaryotic algae in having **echineone** (4-keto-β-carotene) and **myxoxanthophyll**, which eukaryotic algae do not have; in lacking **lutein**, the major xanthophyll of chloroplasts; and in having much higher proportions of β-carotene than are found in eukaryotic algae (Goodwin, 1974).

The Cyanophyceae have four phycobiliproteins: **C-phycocyanin** (absorption maximum at a wavelength [λ] of 620 nm), **allophycocyanin** (λ_{max} at 650 nm), **C-phycoerythrin** (λ_{max} at 565 nm), and **phycoerythrocyanin** (λ_{max} at 568 nm). All cyanobacteria contain the first two, whereas C-phycoerythrin and phycoerythrocyanin occur only in some species. The phycobiliproteins of the cyanobacteria change in concentration in response to light quality and growth conditions. Cyanobacteria that produce the red phycoerythrin and the blue phycocyanin in white light, suppress phycoerythrin synthesis in red light and phycocyanin synthesis in green light (**complementary chromatic adaptation**; see Tandeau de Marsac, 1977).

In the evolution of the cyanobacteria, the thylakoids probably originated by invaginations of the plasmalemma; some cyanobacteria today have thylakoids that are continuous with the plasmalemma. An example of the primitive condition may be *Gloeobacter violaceus* (Fig. 2.19(*e*)), a unicellular cyanobacteria that lacks thylakoids but has chlorophyll *a*, carotenoids, and phycobiliproteins. In this alga the pigments, and presumably photosynthesis, are associated with the plasmalemma (Rippka et al., 1974).

Many cyanobacteria have the ability to photosynthesize under aerobic or anaerobic conditions. Under aerobic conditions, electrons for photosystem I are derived from photosystem II. Under

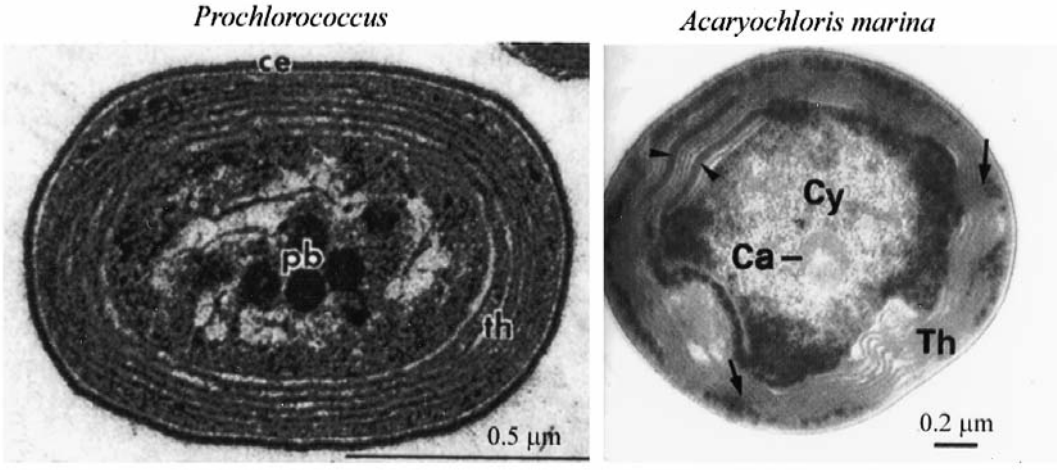


Fig. 2.20 Transmission electron micrographs of a section of *Prochlorococcus*, a chlorophyll *b* containing cyanobacterium, and of *Acaryochloris marina*, a chlorophyll *d* containing cyanobacterium. *Prochlorococcus* is the smallest known photosynthetic organism. (Ca) Carboxysome (polyhedral body); (Cy) cytoplasm; (pb) polyhedral body; (th) thylakoids. (Arrow) channel-like structures perforating thlyakoids. (Arrowheads) areas of accumulation of phycobiliproteins. (*Prochlorococcus* micrograph from Partensky, Hess and Vaulot, 1999; *Acaryochloris* micrograph is from Marquardt et al., 2000.)

anaerobic conditions, in the presence of sulfur, electrons are derived by the reduction of sulfur:

$$CO_2 + 2H_2S \xrightarrow[\text{chlorophyll}]{\text{light}} (CH_2O) + H_2O + S$$
sugar

These cyanobacteria are **facultative phototrophic anaerobes** and fill an important ecological niche in aquatic systems (Padan, 1979). Eukaryotic algae are restricted to photoaerobic habitats, whereas photosynthetic bacteria are restricted to photoanaerobic habitats. In habitats that fluctuate between the above conditions, cyanobacteria with facultative anaerobic photosynthesis have a clear selective advantage. An example of this is the Solar Lake, Elat, Israel, where in the winter high levels of sulfide are found in the anaerobic bottom layers of water of the thermally stratified lake. *Oscillatoria limnetica* (Fig. 2.19(*b*)) occurs in these highly anaerobic bottom layers, where sulfide functions as an electron donor for photosynthesis. In the spring, the lake overturns, with all of the water becoming aerobic, *Oscillatoria limnetica* activates aerobic photosystem II (Fig. 2.28) and carries out photosynthesis aerobically. Thus *O. limnetica*, by utilizing combined anoxygenic and oxygenic photosynthesis, is the dominant phototroph of the Solar Lake, with its fluctuating photoaerobic and photoanaerobic conditions. The interlinking position of the cyanobacteria in the phototropic world is compatible with the fact that they are among the oldest organisms, dating back to the Precambrian Period. Significantly, two of the sulfide-rich ecosystems containing high numbers of cyanobacteria – that is, hot sulfur springs and the marine littoral sediments – may represent old ecosystems that may predate the oxidized biosphere.

Photosynthesis in many cyanobacteria is stimulated by lowered oxygen concentration, the oxygen competing with carbon dioxide for the enzyme ribulose-1, 5-bisphosphate carboxylase/oxygenase (Fig. 2.21) (Stewart and Pearson, 1970; Weller et al., 1975). This phenomenon probably reflects an adaptation to the absence of free oxygen in the atmosphere of Precambrian times when the cyanobacteria first evolved. After the evolution of the oxygen-evolving cyanobacteria, the oxygen in the atmosphere gradually built up, creating a protective ozone (O_3) layer in the atmosphere at the same time. The ozone layer removed most of the harmful ultraviolet radiation from the sun and allowed the evolution of more radiation-sensitive organisms. The cyanobacteria are relatively insensitive to radiation, having a system that repairs radiation damage (Bhattacharjee, 1977).

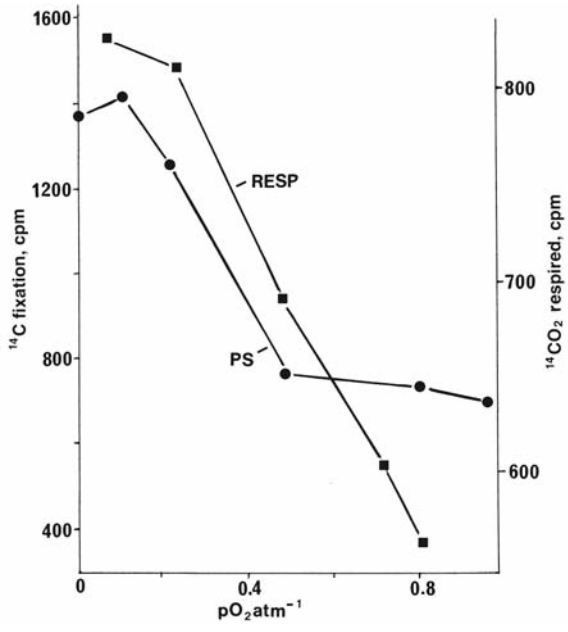


Fig. 2.21 Graph showing stimulation of photosynthesis (●-●) and respiration (■-■) by low concentrations of atmospheric O_2 in *Anabaena flos-aquae*. (After Stewart and Pearson, 1970.)

Akinetes

Akinetes are generally recognized by their larger size relative to vegetative cells and conspicuous granulation due to high concentrations of glycogen and cyanophycin (Figs. 2.22, 2.23) (Meeks et al., 2002). The most consistent property of akinetes is their greater resistance to cold compared with vegetative cells. Akinetes have often been compared to endospores in Gram-positive bacteria. Akinetes, however, are neither as metabolically quiescent nor as resistant to various environmental extremes. Akinetes only occur in cyanobacteria that form heterocysts.

In *Aphanizomenon* (Fig. 2.18(*b*)) (Wildman et al., 1975), the development of akinetes from vegetative cells involves an increase in cell size, the gradual disappearance of gas vacuoles, and an increase in cytoplasmic density and number of ribosomes and cyanophycin granules. Akinetes of *Nostoc* lose 90% of their photosynthetic and respiratory capabilities, as compared with vegetative cells. The loss occurs even though there is little change in phycocyanin and chlorophyll, the main photosynthetic pigments (Chauvat et al., 1982). Mature akinetes are usually considerably larger than vegetative cells, contain protoplasm full of food reserves, and have a normal cell wall surrounded by a wide three-layered coat (Jensen and Clark, 1969; Cmiech et al., 1986) (Figs. 2.16, 2.18, 2.19(*d*), 2.22, 2.23). Loss of flotation by an increase in cytoplasmic density causes filaments with akinetes to sink and overwinter in bottom sediments. In akinete germination, there is a reverse of the above events (Fig. 2.24).

A wide range of physicochemical factors have been reported to stimulate akinete differentiation; for example, phosphate deficiency, low temperature, carbon limitation and reduction in the availability of light energy (Li et al., 1997; van Dok and Hart, 1995).

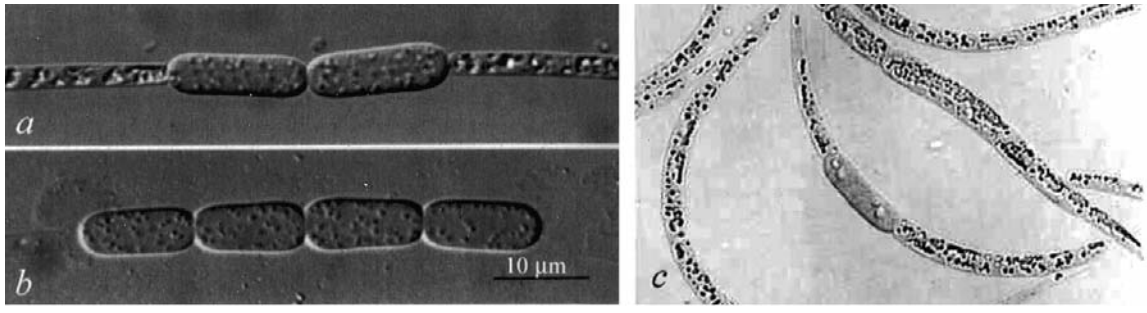


Fig. 2.22 Light micrographs of akinetes in *Raphidiopsis mediterranea* (*a*),(*b*) and *R. curvata* (*c*). ((*a*),(*b*) from Watanabe et al., 2003; (*c*) from Li et al., 2001a.)

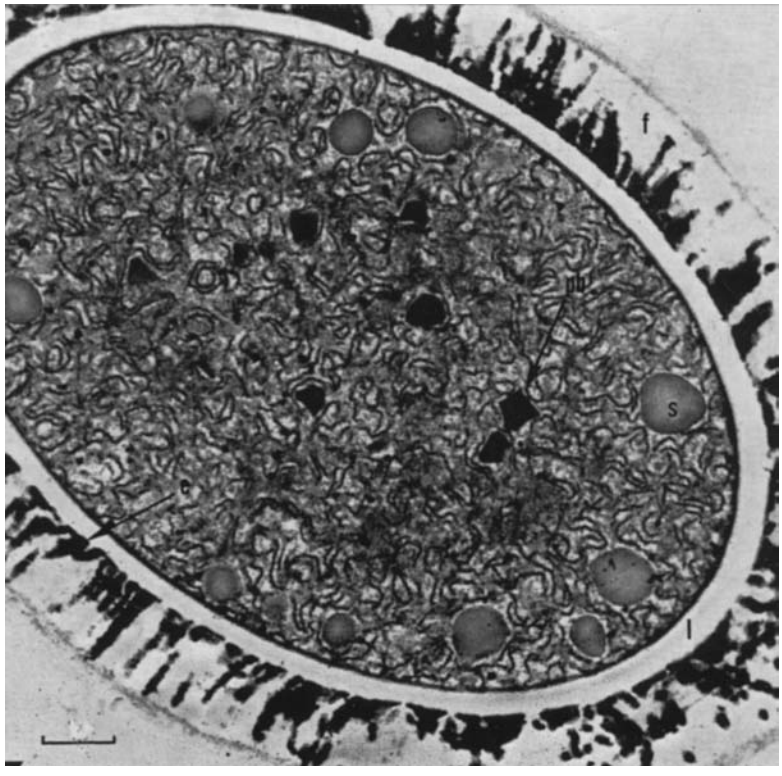


Fig. 2.23 Electron micrograph of a mature akinete of *Cylindrospermum* sp. with a thick layered wall (f,l) and cytoplasm full of proteinaceous cyanophycin (structured) granules (s), polyhedral bodies, and ribosomes. (From Clark and Jensen, 1969.)

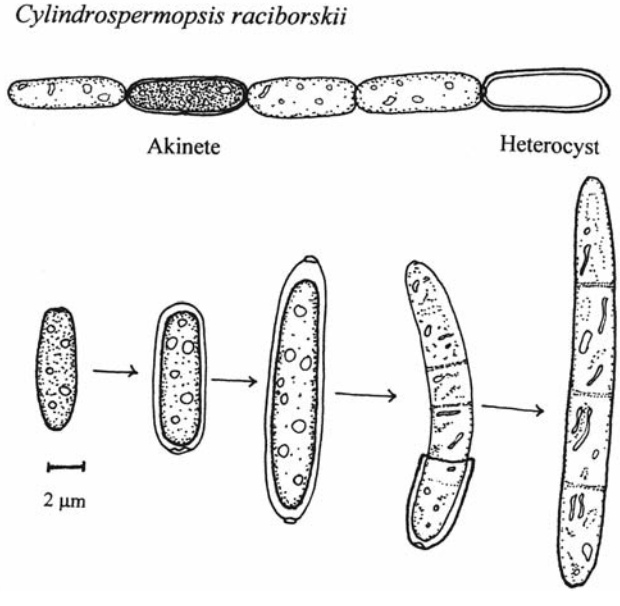


Fig. 2.24 The germination of an akinete of *Cylindrospermopsis raciborskii*. (Modified from Moore et al., 2004.)

Heterocysts

Heterocysts are larger than vegetative cells and appear empty in the light microscope (whereas akinetes appear full of storage products) (Figs. 2.16, 2.18(*a*), 2.19(*d*), 2.25, 2.35). Heterocysts are photosynthetically inactive, they do not fix CO_2, nor do they produce O_2. They also exhibit a high rate of respiratory O_2 consumption and are

surrounded by a thick, laminated cell wall that limits ingress of atmospheric gases, including O_2. The internal environment of heterocysts is, therefore, virtually anoxic, which is ideal for nitrogenase, a notoriously O_2 sensitive enzyme.

Heterocysts are formed at regular intervals from vegetative cells by the dissolution of storage granules, the deposition of a multilayered envelope outside of the cell wall, the breakdown of photosynthetic thylakoids, and the formation of new membranous structures (Fig. 2.25) (Kulasooriya et al., 1972).

The differentiation of heterocysts in *Anabaena* is triggered by nitrogen deprivation (ammonia, nitrate, nitrite) in two steps: the first step is reversible and the second step is irreversible (Adams, 2000; El-Shehawy and Kleiner, 2003).

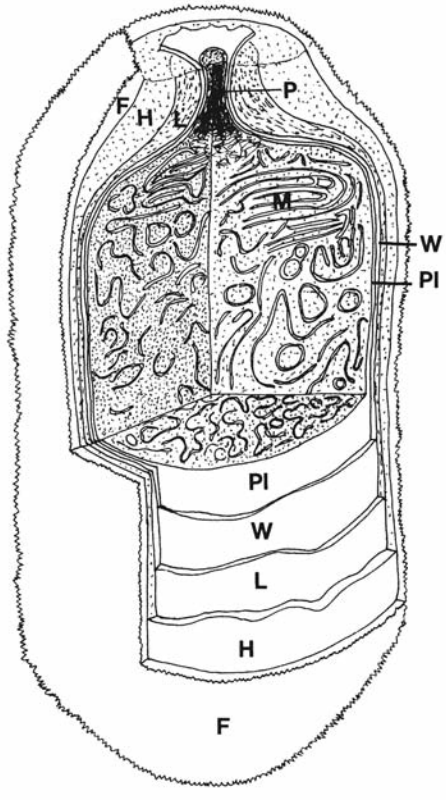


Fig. 2.25 Three-dimensional view of a heterocyst. The envelope has homogeneous (H), fibrous (F), and laminated (L) layers. (M) Membranes; (P) pore channel; (Pl) plasmalemma; (W) cell wall. (After Lang and Fay, 1971.)

Commitment point 1. 2-oxoglutarate (α-ketoglutarate) (Fig. 2.26) is the substrate used for incorporation of ammonium in cyanobacteria. The absence of combined nitrogen leads to an increase in intracellular 2-oxoglutarate since cyanobacteria lack 2-oxoglutarate dehydrogenase and the ability to breakdown 2-oxoglutarate. The increase in intracellular 2-oxoglutarate activates the **protein NtcA** and results in a drop in the amount of the calcium-binding protein CcbP, and a rise in Ca^{2+} in the cells (Zhao et al., 2005). Heterocysts have 10 times more Ca^{2+} than vegetative cells. The rise in Ca^{2+} up-regulates the *hetR* gene that forms **hetR**, a serine-type protease, which induces the vegetative cell to change into a heterocyst. *The hetR protein is considered the "master switch" in heterocyst development*. The production of hetR protein constitutes *commitment point 1*. A lack of combined nitrogen over a period of about 10 hours results in continued production of hetR protein and the cell becoming a **proheterocyst**, which under the light microscope appears less granulated than vegetative cells but still lacks a thick cell wall. The hetR protein also induces the production of an **oligopeptide** called **PatS**. This oligopeptide diffuses to adjacent cells where it prohibits the formation of hetR protein in the cells and assures that the adjacent cells do not transform into proheterocysts. This sets up the spacing seen in *Anabaena* where heterocysts are formed equidistant from each other. Commitment point 1 is reversible. A proheterocyst will revert back to a vegetative cell if combined nitrogen is added to the medium, causing a switch "off" of the *hetR* gene and formation of hetR protein. Differentiation of a vegetative cell to a proheterocyst also involves loss of photosystem II activity, thus eliminating photosynthetic generation of O_2 (which inhibits nitrogen fixation).

Commitment point 2. The second stage can not be reversed by the addition of combined nitrogen and comprises the transformation of a proheterocyst into a mature heterocyst. This involves the formation of a thick cell wall containing glycolipids and polysaccharides to reduce diffusion of O_2. The nitrogen-fixing enzyme **nitrogenase** is activated when 11 kilobases are removed between repeat sequences flanking nitrogenase (*nif*) genes.

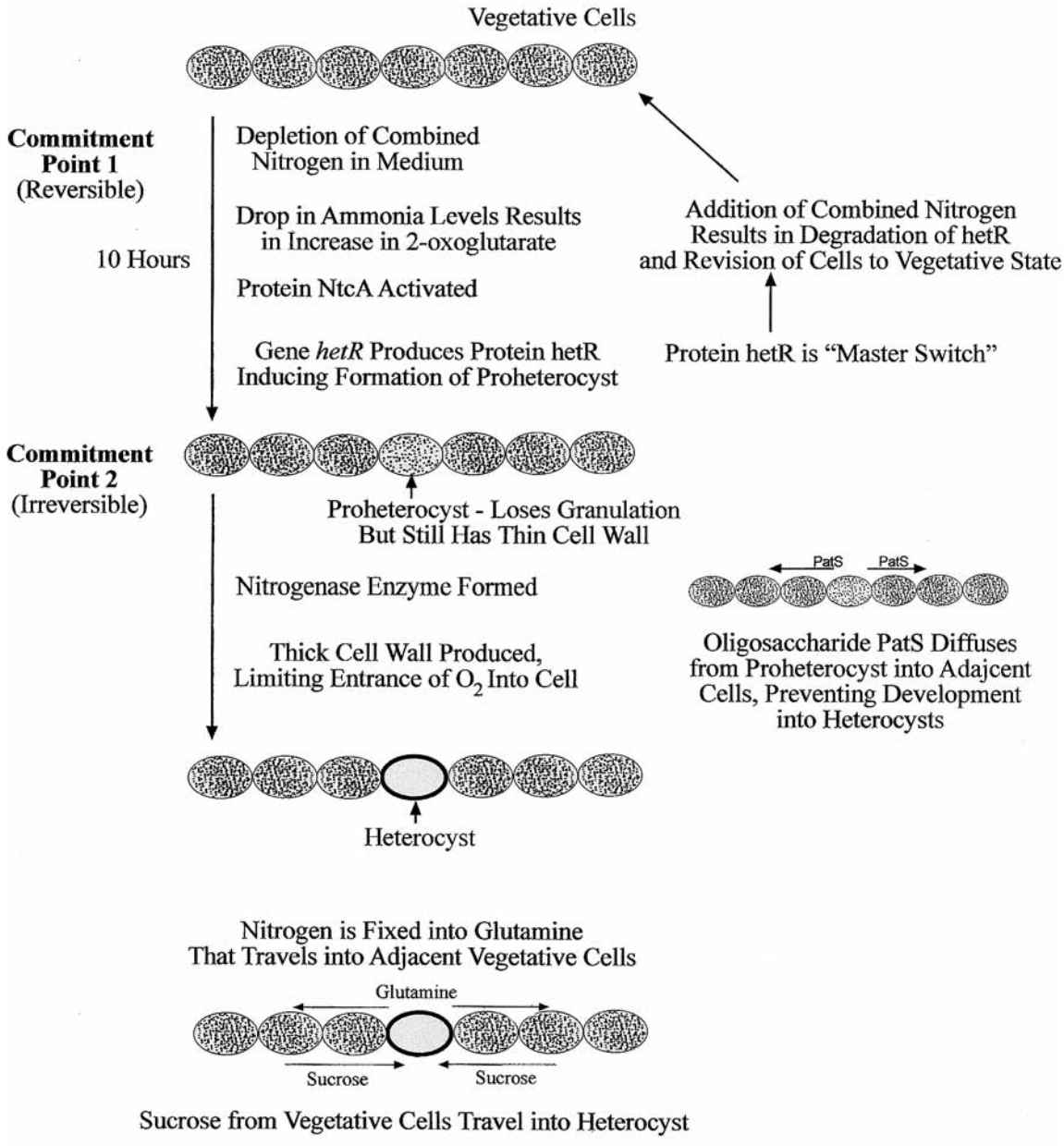


Fig. 2.26 Summation of events leading to the formation of heterocysts.

This process of heterocyst development is interesting in that it may represent one of the earliest examples of pattern formation in evolution. It is probable that akinetes were the evolutionary precursors in heterocysts (Meeks et al., 2002). Akinetes are only seen in heterocyst-forming cyanobacteria, akinetes contain glycolipids characteristic of heterocysts, and the cell wall of heterocysts is identical to that of akinetes (and unlike that of vegetative cells). Heterocyst differentiation is a terminal event and is a basic form of programmed cell death or **apotosis**.

Apart from the exceptional cases of germination, heterocysts are unable to divide. Heterocysts

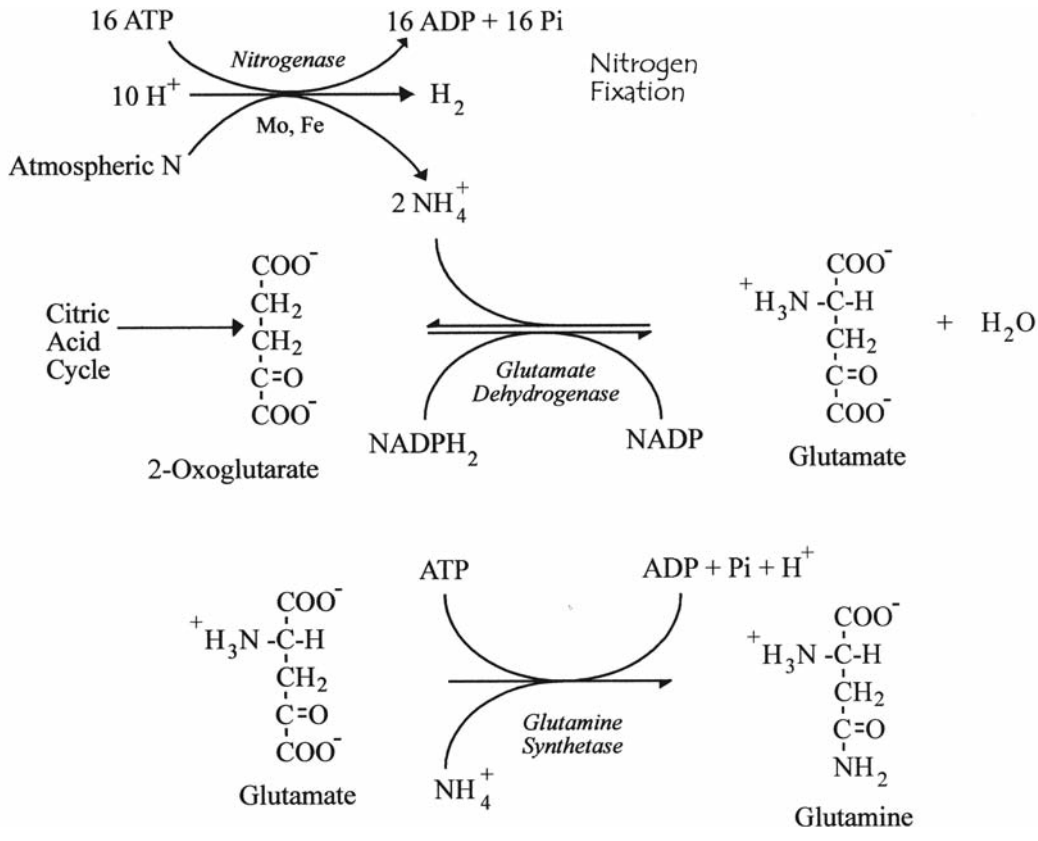


Fig. 2.27 The chemistry of nitrogen fixation and the subsequent incorporation of the fixed nitrogen into glutamate and glutamine.

have a limited period of physiological activity and appear to have a limited life. Senescent heterocysts undergo vacuolation and usually break off from the filament, causing fragmentation of the filament.

Heterocysts are dependent on a supply of substrates from adjacent vegetative cells through cytoplasmic connections (**microplasmodesmata**). These cytoplasmic connections probably convey nitrogen fixed in the form of glutamine (Fig. 2.27) by the heterocysts to vegetative cells. The vegetative cells transfer photosynthate to the heterocysts since the heterocysts are incapable of carbon fixation.

Nitrogen fixation

Cyanobacteria are **diazotrophs** (able to fix atmospheric nitrogen). All known nitrogen-fixing organisms are prokaryotes. In nitrogen fixation, N_2 from the atmosphere is fixed by the enzyme **nitrogenase** into ammonium using ATP as a source of energy (Fig. 2.27). The process is one of the most metabolically expensive processes in biology, requiring 16 ATP for each molecule of N_2 fixed. The amount of biologically fixed nitrogen produced is in excess of 2×10^{13} g year^{-1}. In contrast, lightning discharge, the primary abiotic source of fixed nitrogen, accounts for 5×10^{12} g year^{-1} (Raymond et al., 2004).

The ammonium fixed by nitrogen fixation is added to **2-oxoglutarate** (from the citric acid cycle) by the enzyme glutamate dehydrogenase to form **glutamate** (glutamic acid) (Fig. 2.27). Addition of a second ammonium to glutamate produces **glutamine**, the molecule that is transferred from one cyanobacterial cell to another.

In bacteria, nitrogenase is composed of two components, dinitrogenase reductase (iron protein) and dinitrogenase (molybdenum-iron protein) encoded by the *nif* HDK operon (Henson et al.,

2004). The situation is probably similar in the cyanobacteria.

Hydrogen gas is also produced in nitrogen fixation (Fig. 2.27) and has drawn interest as a renewable energy source as hydrogen fuel-cell technology for motor vehicles becomes more of a practical reality (Schutz et al., 2004).

Nitrogenase, the nitrogen-fixing enzyme, is very sensitive to inactivation by oxygen. Cyanobacteria have evolved three different mechanisms designed to exclude oxygen from the area of the cells containing nitrogenase:

1 *Heterocystous cyanobacteria*: These cyanobacteria occur primarily in fresh and brackish water and fix nitrogen in heterocysts. Heterocysts are surrounded by a glycolipid layer which is impermeable to O_2 (Staal et al., 2003). Heterocysts lack photosystem II (Fig. 2.28) and, therefore, the ability to evolve O_2. Heterocysts do have cyclic photophosphorulation (Fig. 2.29) and can produce the ATP necessary for nitrogen fixation. Heterocysts also have a form of myoglobin called **cyanoglobin** that scavenges oxygen, preventing inhibition of nitrogenase (Potts et al., 1992). Under anaerobic conditions, in an atmosphere of nitrogen and carbon dioxide, both vegetative cells and heterocysts can fix nitrogen.
2 *Non-filamentous cyanobacteria that fix nitrogen in the dark but not in the light*: These cyanobacteria fix nitrogen in the dark when photosynthesis is not producing nitrogenase-inhibiting oxygen. If *Synechococcus* is grown under a 12-hour light: 12-hour dark cycle, most of the nitrogen fixation occurs during the dark period (Fig. 2.30). If the cells are subjected to continuous illumination, an endogenous timing cycle entrained by cell division continues to alternate the level of photosynthesis and nitrogen fixation (Mitsui et al., 1986; Chen et al., 1996). Nitrogenase activity peaks at the same time that it had in the previous dark period

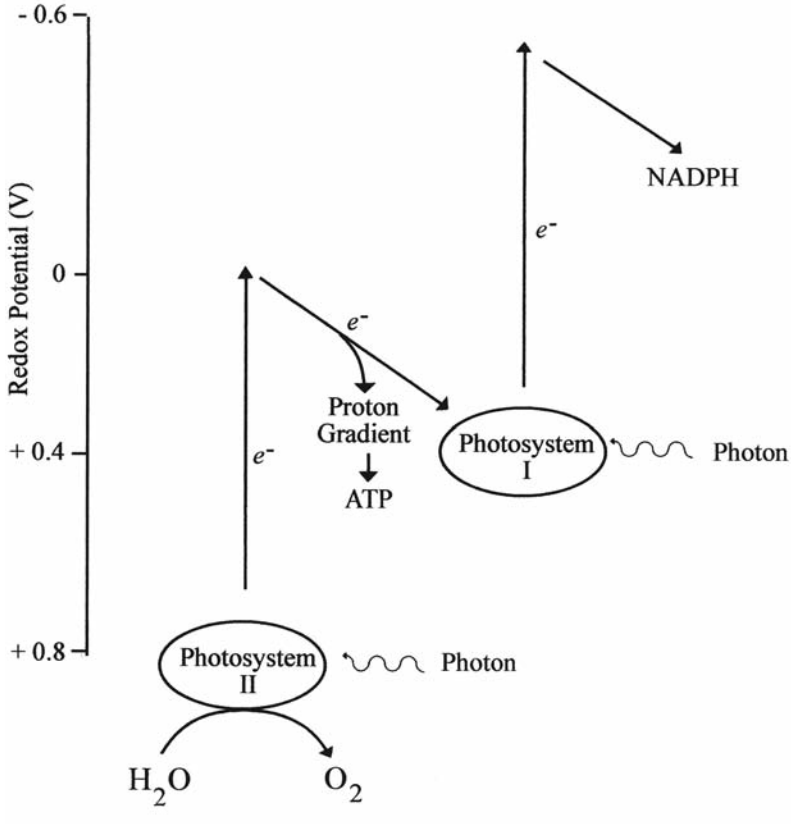


Fig. 2.28 Non-cyclic photophosphorulation. Heterocysts in cyanobacteria lack photosystem II and do not produce oxygen.

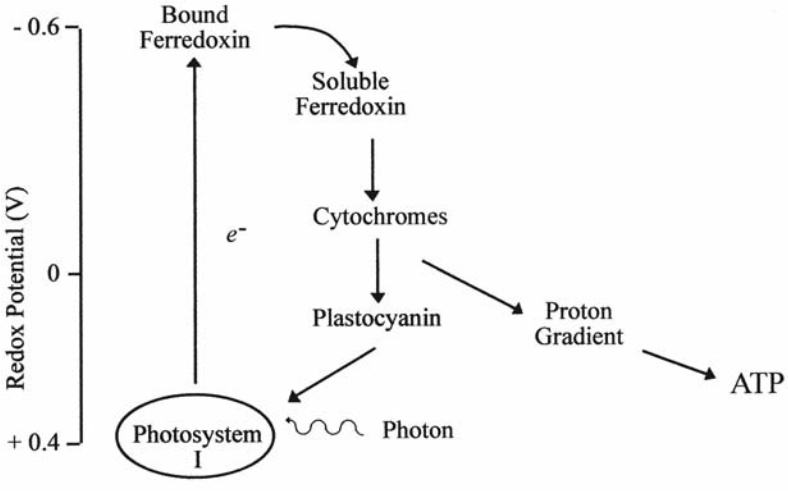


Fig. 2.29 Cyclic photophosphorulation. Heterocysts in cyanobacteria produce ATP by cyclic photophosphorulation.

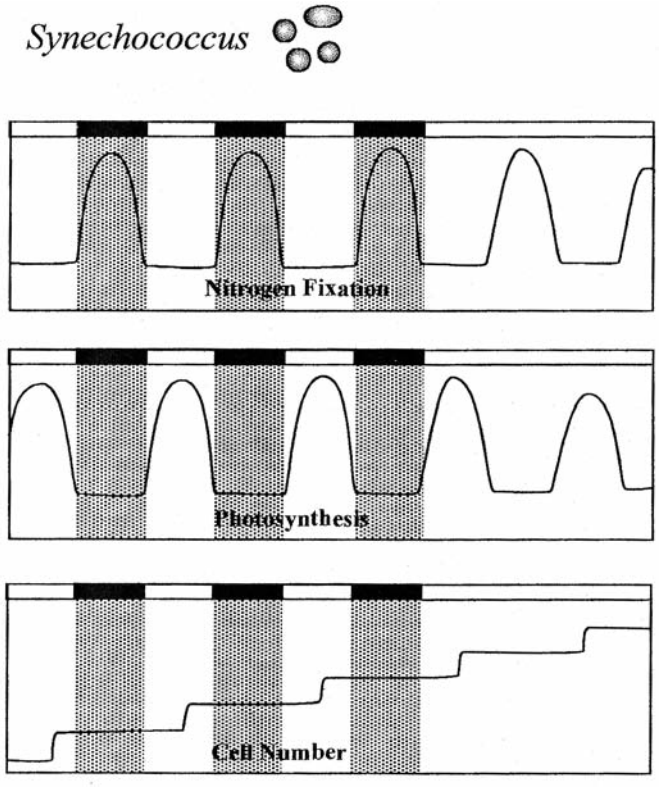


Fig. 2.30 Illustration of the relationship between photosynthesis and nitrogen fixation in a culture of *Synechococcus* sp. growing under a 12-hour light: 12-hour dark photoperiod. Under continuous illumination, an endogenous clock maintains the cycles. (After Mitsui et al., 1986.)

(Fig. 2.30). At the beginning of the next light period, oxygen is produced by photosynthesis and the nitrogenase is inactivated. New nitrogenase must be synthesized at the beginning of the next dark period for nitrogen fixation to occur.

3 *Trichodesmium* (Figs. 2.31, 2.56(*g*)) and *Katagnymene* (Fig. 2.31): These cyanobacteria

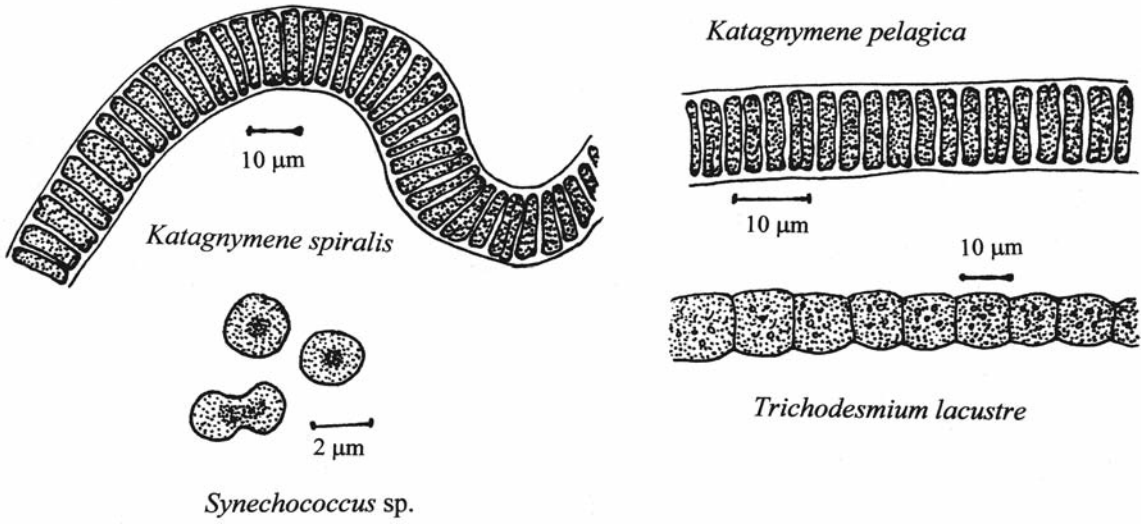


Fig. 2.31 Some nitrogen-fixing cyanobacteria that lack heterocysts.

are the major bloom-forming, nitrogen-fixing, organisms in the oceans, responsible for fixing one-quarter of the total nitrogen in the oceans of the world (Bergman and Carpenter, 1991). These filamentous cyanobacteria do not have heterocysts yet fix nitrogen in the light under aerobic conditions (Bergman et al., 1997). Within the filaments, 10 to 15% of the cells (called **diazocytes**) are specialized to fix nitrogen, while the others do not (Lundgren et al., 2001). Cells that fix nitrogen are adjacent to one another and have a denser thylakoid network with fewer gas vacuoles and cyanophycin granules (Fredriksson and Bergman, 1997). The tropical seas where *Trichodesmium* and *Katagnymene* live are relatively low in dissolved oxygen and this may assist the nitrogen-fixing cells in maintaining anaerobic conditions in the protoplasm where nitrogenase is present (Staal, Meysman and Stal, 2003).

Trichodesmium and *Katagnymene* represent the most ancient type of nitrogen-fixing cyanobacteria (Berman-Frank et al., 2001).

Circadian rhythms

The cyanobacteria have circadian rhythms in photosynthesis, nitrogen fixation, and cell division similar to those in eukaryotic organisms (Fig. 2.30). The requirements of a circadian rhythm are: (1) approximate 24-hour cycles in biological processes even in the absence of an environmental cycle; (2) synchronization with the environment through light or environmental cues; and (3) maintenance of a nearly constant period over a range of physiologically relevant temperatures (Golden, 2003).

The details of the cyanobacterial circadian rhythm have been elucidated in *Synechococcus elongatus* (Williams et al., 2002). The key components of the timekeeping complex are the proteins KaiA, KaiB, and KaiC coded by the genes *KaiA, KaiB*, and *KaiC* (Figs. 2.32, 2.33). Interactions between these three proteins maintain the rhythm at about 24 hours. In the real world, the clock is reset daily by cycles of light and darkness, temperature and humidity. The major portal into the clock is the protein kinase CikA. Environmental change to CikA changes the configuration of the protein KaiA which causes phosphorulation of the protein KaiC (Fig. 2.32), resetting the clock. The output that sets cycles of nitrogen fixation, photosynthesis, etc. begins when KaiC interacts with the protein SasA (*Synechococcus* **a**daptive **s**ensor). This results in information being relayed downstream to produce the observed effect.

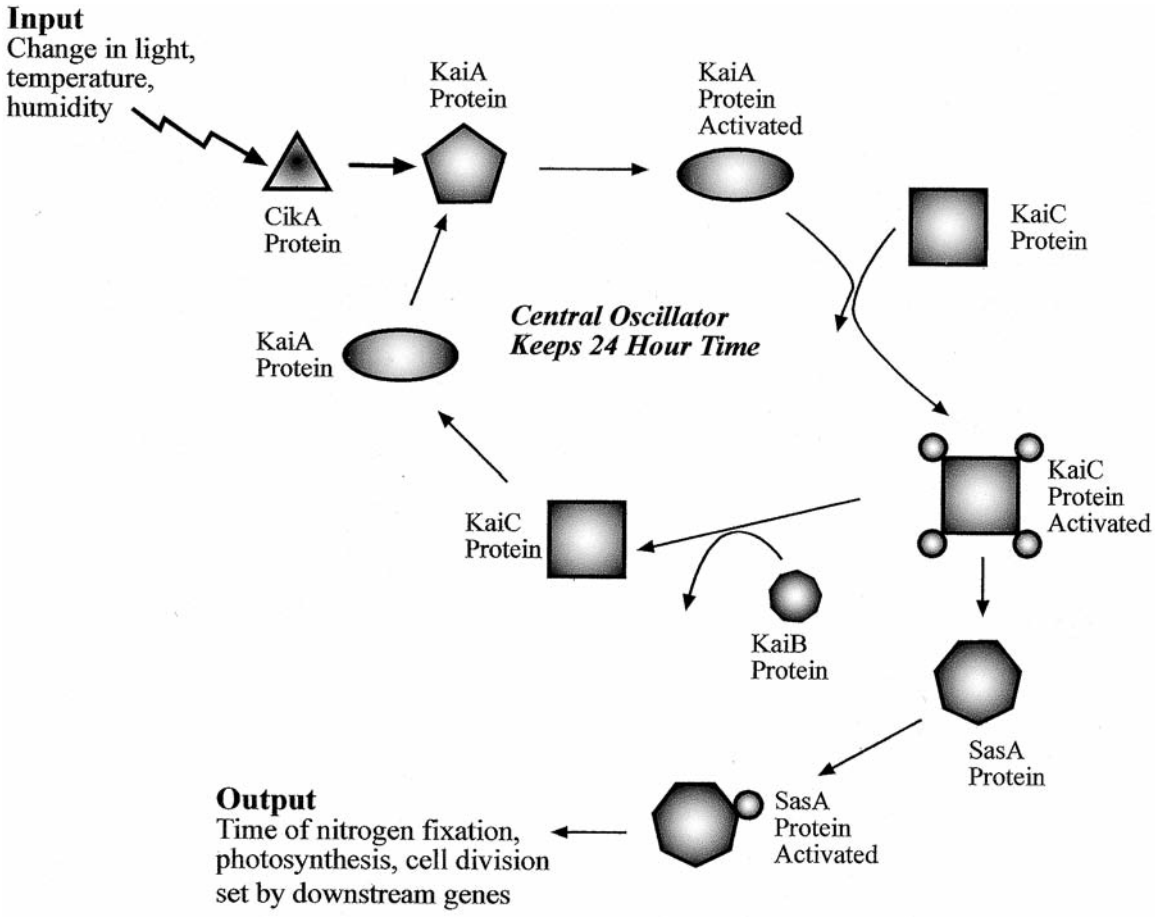


Fig. 2.32 Diagrammatic representation of the cyanobacterial circadian clock.

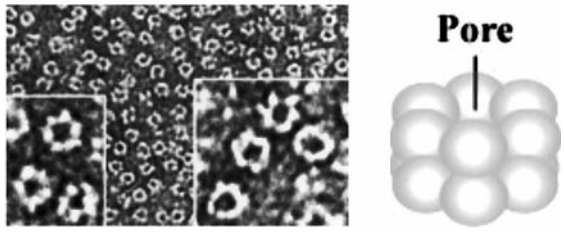


Fig. 2.33 KaiC protein from *Synechococcus elongatus*, one of the circadian clock proteins in cyanobacteria. *Left*: Transmission electron micrograph of negatively stained KaiC protein showing the hexamer formed in an ATP-containing solution. *Right*: Model of a KaiC hexamer. (From Mori et al., 2002.)

Asexual reproduction

Asexual reproduction occurs by the formation of hormogonia or baeocytes or fragmentation of colonies (Fig. 2.34).

Hormogonia (or hormogones), which are characteristic of all truly filamentous cyanobacteria, are *short pieces of trichome that become detached from the parent filament and move away by gliding, eventually developing into a separate filament*. Hormogonia are distinguished from vegetative filaments by their gliding motility, the small size of their cells (Figs. 2.34(*a*), (*b*), 2.35), and the absence of heterocysts (Meeks and Elhai, 2002). In some species, hormogonia contain gas vacuoles, which control buoyancy. In some filamentous algae, such as *Oscillatoria* and *Cylindrospermum*, the entire filament may break

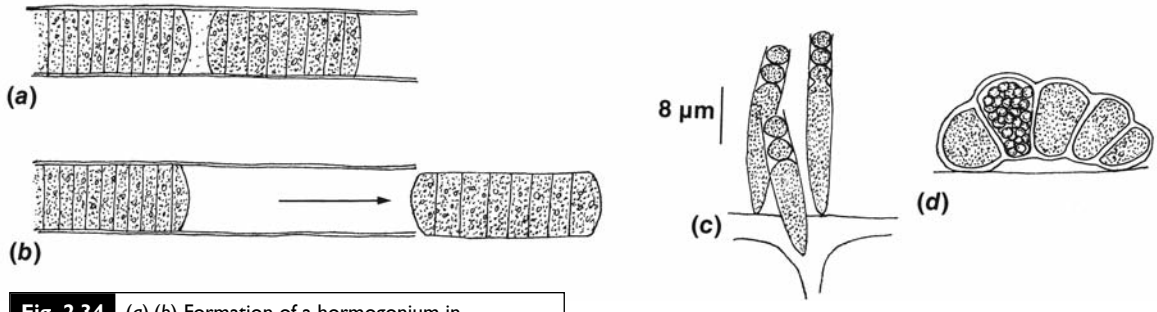


Fig. 2.34 (*a*),(*b*) Formation of a hormogonium in *Oscillatoria*. (*c*) Baeocyte formation in *Chamaesiphon incrustans*. (*d*) Baeocyte formation in *Dermocarpa pacifica*. (After Smith, 1950.)

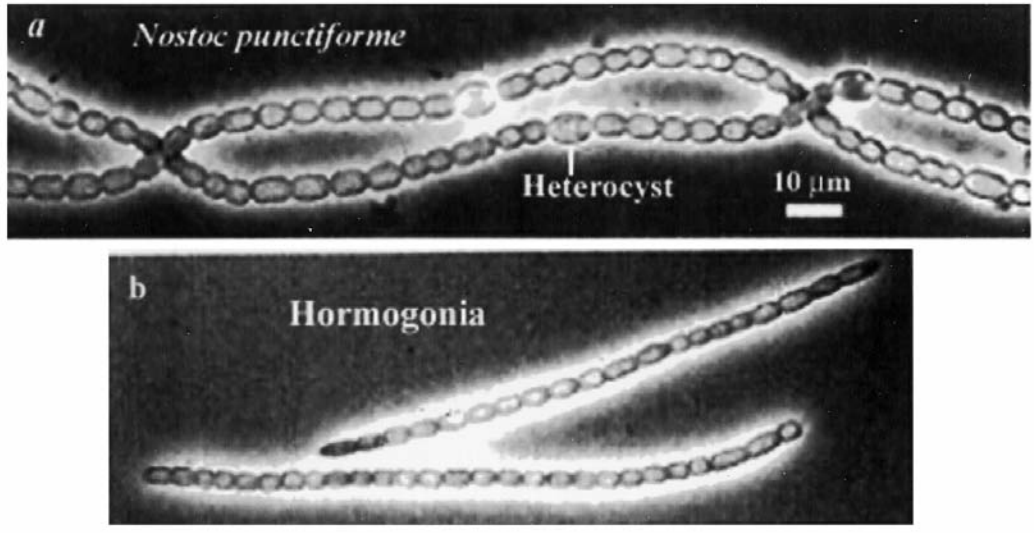


Fig. 2.35 *Nostoc punctiforme*. (*a*) Vegetative cells. (*b*) Hormogonia. The hormogonia lack heterocysts and are smaller than vegetative cells. (From Meeks and Elhai, 2002.)

up (Fig. 2.34(*a*), (*b*)), whereas in others the hormogonia are produced at the tips of special branches. In some algae, specialized separation discs or necridia (Fig. 2.34) are involved in the breaking of the hormogone from the parent filament, whereas in others, the filament just fractures.

The one common factor in initiation of hormogonium differentiation appears to be a change in some environmental parameter such as an increase or decrease of a nutrient or a change in the quantity of light.

Hormogonia of many strains display positive phototaxis, which is important in the colonization of illuminated portions of the habitats by these photoautotrophic organisms (Meeks and Elhai, 2002). The acquisition of motility in hormogonia comes at a price. Hormogonia lack heterocysts and are unable to fix nitrogen. Phycobiliprotein synthesis ceases, leading to an attrition in light gathering. Hormogonia cells continue to photosynthesize and assimilate exogenous ammonium, although the rates of CO_2 fixation and NH_4^+ incorporation are only 70% and 62%, respectively, of those of vegetative cells. Much of the metabolic output is devoted to the synthesis and secretion of mucilage required for gliding motility. Hormogonia remain in the

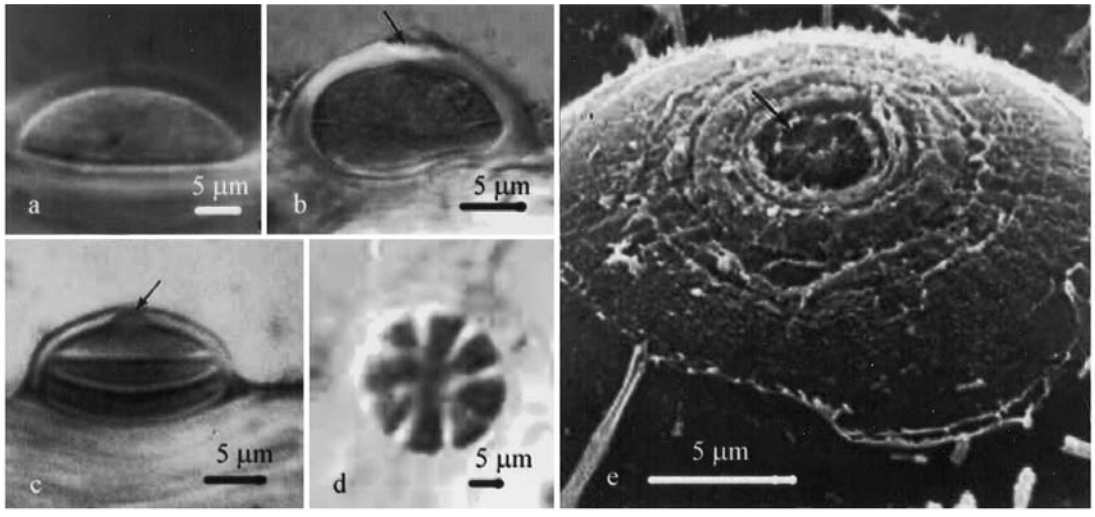


Fig. 2.36 Baeocyte formation in *Dermocarpella gardneri*. (*a*)–(*c*). Light micrographs of lateral views showing parallel divisions. (*d*) Top view showing radial divisions. (*e*) Scanning electron micrograph showing apical pore through which baeocytes escape. (From Montejano and Leon-Tejera, 2002.)

gliding stage for 36 to 48 hours. Heterocysts begin to develop at this stage in the absence of combined nitrogen. Conversion to vegetative filaments is complete after 96 hours.

Baeocytes (endospores) are formed by some coccoid (spherical) cyanobacteria (Figs. 2.34, 2.36). The protoplasm divides several times in different planes without growth between successive divisions. The resulting baeocytes are smaller than the original cell. Baeocytes are similar to bacterial endospores. In *Dermocarpella*, the baeocytes are released through an apical pore and enlarge to mature organisms (Fig. 2.36) (Montejano and Leon-Tejera, 2002).

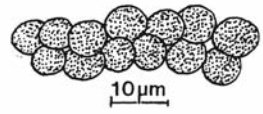
Growth and metabolism

In the cyanobacteria there are three nutritional types: (1) **facultative chemoheterotrophs**, or those organisms capable of growing in the dark on an organic carbon source and of growing phototrophically in the light (only a portion of the cyanobacteria exhibit this condition); (2) **obligate phototrophs**, or organisms that can grow only in the light on an inorganic medium (some of these are actually **auxotrophs**, requiring a small amount of an organic compound that is not used as a source of carbon, invariably meaning a vitamin); (3) **photoheterotrophs**, or those cells that are able to use organic compounds as a source of carbon in the light but not in the dark (Stanier, 1973).

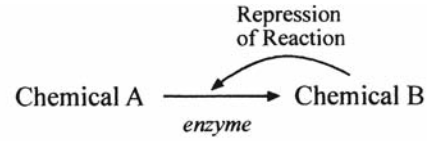
Facultative chemoheterotrophs are able to grow in the dark on a very narrow range of substrates, being confined to glucose, fructose, and one or two disaccharides. This range of substrates is so small because the pentose phosphate pathway is the sole energy-yielding dissimilatory pathway. The tricarboxylic acid cycle lacks the enzyme α-ketoglutarate (2-oxoglutarate) dehydrogenase and succinyl CoA synthetase, rendering it incomplete, and glycolysis likewise appears to be incomplete. Although the tricarboxylic acid cycle does not provide energy, it does provide carbon skeletons from the portions of it that are functional.

The pentose phosphate pathway does not operate in the *light* in the Cyanophyceae (although it is highly operational in the dark), being inhibited by ribulose-1,5-diphosphate, a product of light metabolism.

Even though some cyanobacteria grow in the dark, they grow very slowly. It is probable that the rate of chemoheterotrophic growth is always limited by the rate of dark ATP synthesis through oxidation of glucose-6-phosphate in the pentose phosphate pathway, a rate that is evidently not very great.



Chlorogloea fritschii



Feedback Repression of Enzyme Activity

Fig. 2.37 Cyanobacteria, such as *Chlorogloea fritschii* (*left*), lack feedback inhibition of enzyme activity (*right*).

Lack of feedback control of enzyme biosynthesis

Cyanobacteria, such as *Chlorogloea fritschii* (Fig. 2.37), lack metabolic control of many pathways by repression and derepression of enzyme biosynthesis as occurs in many other organisms. In other organisms, as an end product of a pathway builds up to excess, the end product represses an enzyme involved in its synthesis, thereby directing precursors to other parts of the cell's metabolism, where they can be better used. When the amount of end product falls, the enzyme is derepressed, allowing manufacture of the end product again.

Cyanobacteria often release considerable quantities of nitrogenous and organic substances into the medium, with most of the compounds being excreted as peptides (Fogg, 1942, 1952; Walsby, 1974). The secretion of nitrogenous substances represents a considerable waste of potential metabolites which have been formed from carbon dioxide with an expenditure of ATP and reducing potential (e.g., NADH). Such an excretion, however, could well be a necessary consequence of ill-controlled amino acid biosynthesis. Unable accurately to adjust the synthesis of each amino acid to the needs of protein synthesis, the cells would inevitably have to synthesize an excess of amino acids to ensure that protein synthesis would proceed smoothly. This excess would then form the basis of the extracellular peptide material associated with the cyanobacteria.

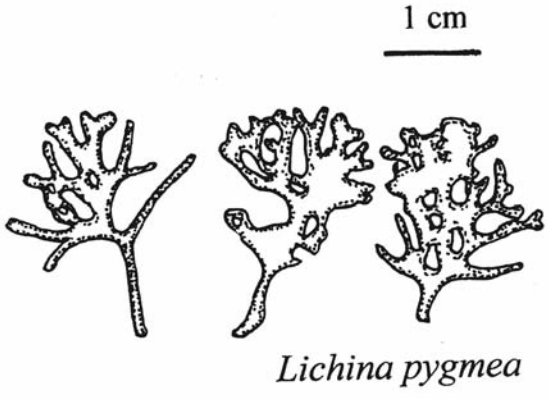
The general lack of repression and derepression of enzyme synthesis in the cyanobacteria implies that the algal metabolic pathways developed before the control systems responsible for their regulation. The failure to develop transcriptional or regulatory control places the cyanobacteria under a selective disadvantage relative to other organisms possessing such metabolic regulators. They would be unable to divert biosynthetic capacity away from surplus synthesis to more necessary activity. Such a selective advantage would survive only in microorganisms less open to competition than most, or, in other words, in organisms in a particular ecological niche or in an environment with an abundant energy source. Autotrophic microorganisms such as the cyanobacteria fall into this category. Their source of energy (light) is at times more than sufficient, and in certain cases they occur in eccentric ecological situations that extremes of temperature or pH make relatively inhospitable.

Symbiosis

The cyanobacteria occur in basically two types of associations: those in which the cyanobacterium is *extracellular* and those in which it is *intracellular*.

Extracellular associations

Cyanobacteria in extracellular associations all show a decrease in growth, assimilation of CO_2 and assimilation of NH_4^+ (Meeks and Elhai, 2002). Conversely, there is an increase in the rate of N_2 fixation that accompanies the increased numbers of heterocysts. The heterocysts and vegetative cells of *Nostoc* within leaf cavities of *Azolla* are up to fourfold larger than the vegetative cells of free-living cyanobacteria. In the symbiosis, *Nostoc* receives hexose sugars from the host, while *Nostoc* provides fixed nitrogen to the host. There is also a five- to ten-fold increase in the production of



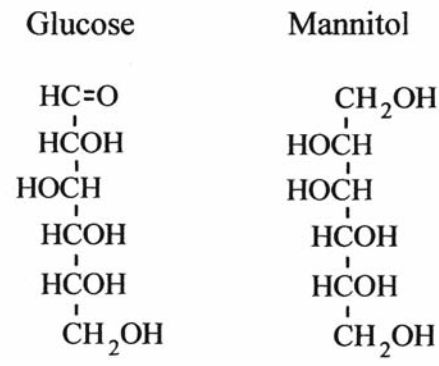


Fig. 2.38 *Lichina pygmea* is a lichen containing a cyanobacteria as the phycobiont. *Lichina* occurs on rocks near the high-tide mark and looks like a stubby seaweed with its club-shaped branches making a sward of uniform height. The cyanobacterial phycobiont transfers glucose to the mycobiont which converts the glucose to mannitol.

motile hormogonia that serve as infective units in the establishment of the symbioses (Meeks, 1998).

The most common type of extracellular association is that with fungi to form **lichens**. In most lichens, there is a single algal component (**phycobiont**), which is a green alga, cyanobacterium, or, as in species of *Verrucaria*, a member of the Xanthophyceae. Cyanobacteria occur in about 8% of the species of lichens (Fig. 2.38). Almost all of the fungal partners (**mycobionts**) are ascomycetes, but certain imperfect fungi and basidiomycetes also occur in lichens (Ahmadjian and Hale, 1973). Because the mycobionts frequently reproduce sexually whereas the phycobionts usually do not, the lichens are classified with the fungi. In the symbiotic association, the phycobiont fixes carbon in photosynthesis and liberates it as glucose, which the mycobiont converts into mannitol and assimilates (Fig. 2.38). Approximately 40% of the photosynthate of the alga is secreted as glucose in the lichen association (Smith et al., 1970). Whereas the benefits to the fungus in the association are obvious, the benefits to the alga are probably limited to some protection against desiccation.

The water fern *Azolla* (Fig. 2.40(*a*), (*b*)) has cavities in the dorsal lobe of the leaf that are occupied by *Anabaena azollae* (Fig. 2.39(*c*), (*d*)). This cyanobacterium fixes nitrogen (Peters and Mayne, 1974), some of which is excreted into the cavity and taken up by the cells of the *Azolla*. It is possible to obtain alga-free *Azolla* plants by treating them with antibiotic or subjecting them to growth conditions that allow the fern to outgrow the alga. The *Anabaena* is apparently unable to live outside of the host. The heterocyst frequency (compared to vegetative cells) in *A. azollae* is about 30%, which is very high, the highest for free-living *Anabaena* being about 8% (Hill, 1975). The host *Azolla* somehow modifies the surface properties of the *Anabaena*. The alga in the fern cavity has different surface antigens, as compared to when it is growing free in culture (Gates et al., 1980). Nitrogen fixation by the cyanobacterial symbionts of *Azolla* has for many years been utilized to advantage in the Far East; here the water fern has been used as a green manure in rice fields, where about 3 kg of atmospheric nitrogen per hectare per day is fixed by *Azolla* symbionts (Swaminathan, 1984; Canini et al., 1992).

Cycad roots are frequently infected with cyanobacteria that cause distortions of the roots (coralloid roots) (Figs. 2.39(*a*), (*b*), 2.40(*c*)). In these roots the cyanobacteria occupy a clearly defined cortical zone midway between the pericycle and the epidermis. The cyanobacteria occur in the intercellular spaces and are surrounded by a

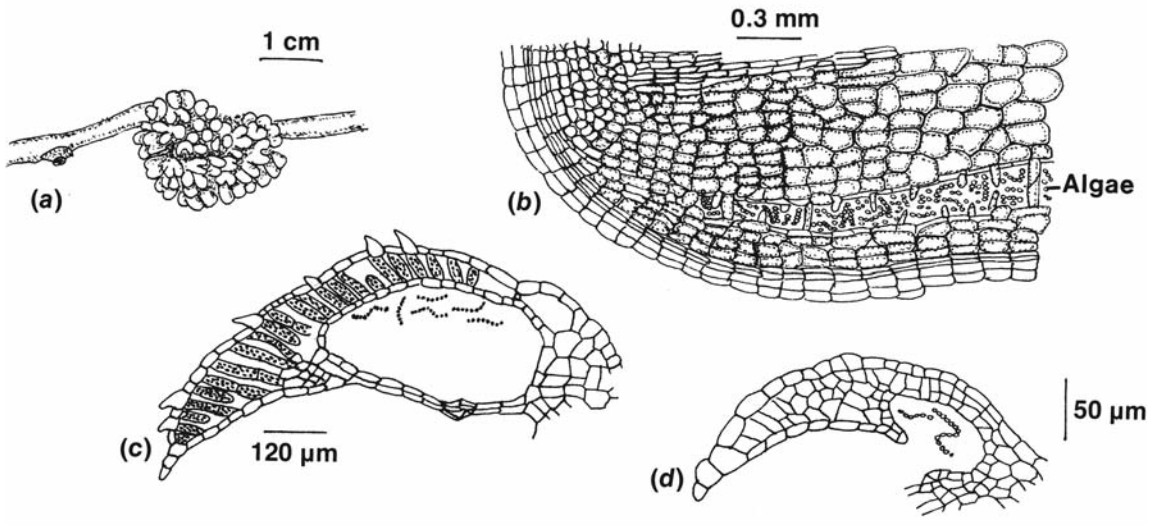


Fig. 2.39 (*a*) Root nodules of the cycad *Dioon spinulosum*. (*b*) Part of a longitudinal section of a nodule of *Encephalartos* with an algal zone. Longitudinal sections through the dorsal lobe of a mature (*c*) and an immature (*d*) leaf of the water fern *Azolla* illustrating filaments of *Anabaena* in leaf cavities. ((*a*),(*b*) after Spratt, 1915; (*c*),(*d*) after Smith, 1955.)

sheath and a multilayered wall, whereas the adjacent cycad cells have a reduced chromosome number and secrete slime (Storey, 1968; Caiola, 1975). These cyanobacteria are able to fix nitrogen and contribute a portion of the fixed nitrogen to the cycad cells (Watanabe and Kiyohara, 1963).

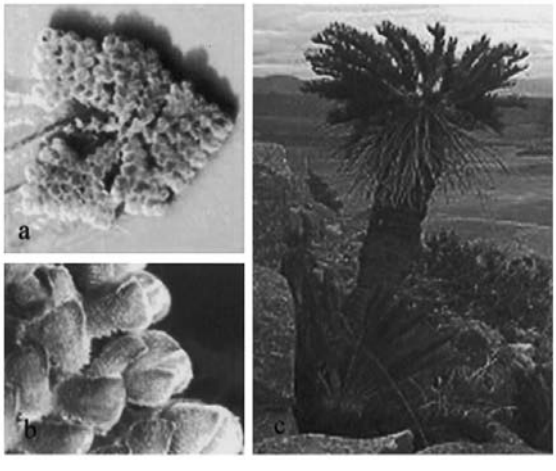


Fig. 2.40 Plants that have symbiotic cyanobacteria. (*a*,*b*) The water fern *Azolla* (*c*) The cycad *Encephalartos*.

Intracellular associations

Intracellular associations involving cyanobacteria are usually more specialized than extracellular associations, and it is not possible to culture the cyanobacteria away from the host. Pascher (1914) coined the term **cyanelle** for intracellular cyanobacteria in symbioses, and the term **cyanome** for the host cell. Cyanelles are present in a variety of cyanomes; such a variety that it is apparent that they are the result of a number of different symbiotic establishments and are not derived from a single event. It is probable that one of these endosymbiotic associations led to the development of chloroplasts in some of the algal groups. This line of evolution is considered under Glaucophyta (see beginning of Chapter 3).

Colonies of the coral *Montastraea cavernosa* contain endosymbiotic coccoid cyanobacteria in vacuoles in the epithelial cells of the coral (Lesser et al., 2004). The cyanobacteria are capable of nitrogen fixation. Anaerobic conditions (necessary for function of the nitrogen-fixing enzyme nitrogenase) are created by the Mehler reaction (Fig. 2.41) where glycerol provided by dinoflagellate zooxanthellae is reduced.

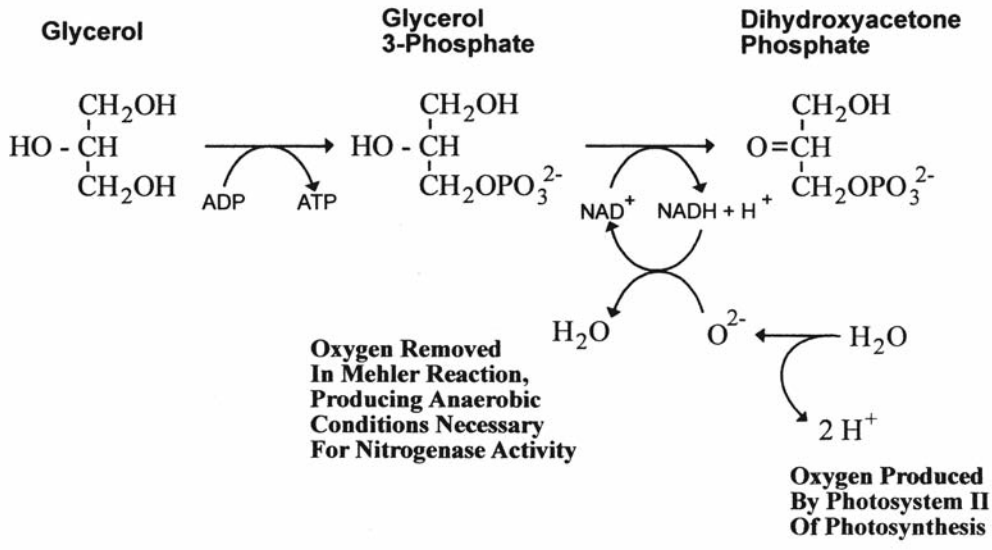


Fig. 2.41 Cyanobacteria in an endosymbiotic relationship with corals are able to maintain anaerobic conditions necessary for nitrogenase activity by the Mehler reaction. The dinoflagellate zooxanthellae produce glycerol which is transferred to the cyanobacteria. Glycolytic breakdown of glycerol produces hydrogen atoms that reduce oxygen molecules produced in photosynthesis. This creates the hypoxia necessary for nitrogenase activity and nitrogen fixation.

Ecology of cyanobacteria

Marine environment

Littoral zone

Cyanobacteria in the littoral zone occur as a black encrusting film on rocks at the upper limit of the high-tide mark. This zone is sandwiched between the lower barnacle zone (the grazing of the molluscs in this zone limits the cyanobacteria) and a higher zone of maritime lichens such as *Verrucaria* and *Lichina* (Fig. 2.38), the latter containing the cyanobacterium *Calothrix* (Fig. 2.42(*d*)) as the phycobiont. The brackish cyanobacterial zone is composed of various species of *Calothrix* (Fig. 2.42(*d*)), *Phormidium* (Figs. 2.18(*c*), 2.56(*c*)), *Nodularia* (Fig. 2.42(*a*)), *Gloeothece* (Fig. 2.56(*a*)), and *Rivularia* (Fig. 2.57(*d*)) (Little, 1973). The vertical extent of this zone tends to be greater with increasing exposure of the shore; the greater the spray, the wider the zone. In most exposed areas it forms a thin, adhering film, but in sheltered areas the growth may be much thicker, up to 5 mm. The nature of the rock is of some importance, with soft or granular rocks such as chalk

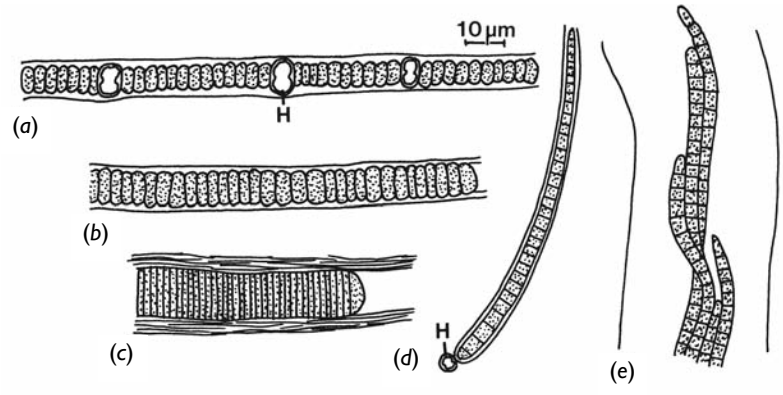


Fig. 2.42 (*a*) *Nodularia spumigena.* (*b*) *Lynbya sordida.* (*c*) *L. majuscula.* (*d*) *Calothrix scopulorum.* (e) *Microcoleus chthonoplastes.* (H) Heterocyst. ((*b*),(c),(e), after Desikachary, 1959.)

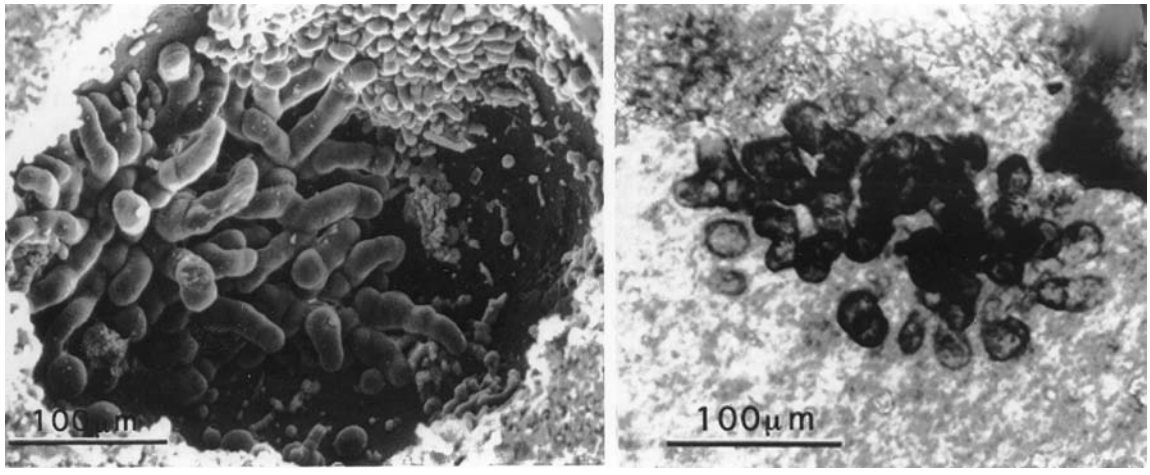


Fig. 2.43 *Left*: The endolith *Hyella immanis* inside a carbonate ooid sand grain. *Right*: The fossil endolith *Eohyella dichotoma* penetrating an ooid sand grain from the Late Proterozoic. (From Al-Thukair and Golubic, 1991.)

and sandstones, respectively, sustaining the greatest growth. Most of the cyanobacteria in the littoral zone are nitrogen fixing, and they make a significant contribution to the productivity of rocky shores and coral reefs (Mague and Holm-Hansen, 1975).

Ooids are spherical (0.2–2.0 mm in diameter), concentrically laminated, carbonate grains that form by carbonate accretion in agitated, shallow tropical marine environments. *Hyella* spp. are cyanobacterial endoliths that bore into, and live in, ooids (Fig. 2.43) (Al-Thukair and Golubic, 1991). Extant *Hyella* spp. are similar to extinct *Eohyella* in 800 million-year-old ooids (Fig. 2.43).

Open ocean cyanobacteria

In the open ocean, most of the total photosynthetic capacity is made up of **picophytoplankton** (*phytoplankton cells unable to pass through a filter with 2-µm-diameter holes*). The picophytoplankton is made up principally of tiny coccoid cyanobacteria at concentrations of around 10000 cells per milliliter (Glover et al., 1986). The coccoid cyanobacteria *Synechococcus* (Figs. 2.19(*c*), 2.31), *Synechocystis* (Fig. 2.8), and *Prochlorococcus* are the major organisms present (Ferris and Palenik, 1998). Although these cyanobacteria are small, they can be easily seen because their phycobiliproteins undergo autofluorescence in a fluorescence microscope. The picophytoplankton cyanobacteria have negligible sinking rates; thus they are ideally suited for planktonic life. The high surface:volume ratios, combined with steep diffusion gradients that are set up around small cells, allow them to take up nutrients at a high rate. Furthermore, a given amount of photosynthetic pigment dispersed in small cells absorbs more light than an equivalent amount of pigment packaged in large cells. Therefore, these cells grow best at low light intensities of less than 1/50 of full sunlight. The picophytoplanktonic cyanobacteria are more evident in nutrient-poor offshore waters where larger phytoplankton are less successful, because the larger phytoplankton are less able to utilize low concentrations of nutrients. Although the picophytoplanktonic cyanobacteria occur throughout the euphotic zone, they are concentrated at the bottom of the zone, not because they sediment out, but because they grow best under these conditions; they use the low irradiance efficiently to support growth and benefit from nutrients transported up from richer waters below. These algae contain large amounts of phycoerythrin that allows them to absorb the blue-green light penetrating into deep water (Fogg, 1986).

Cyanobacteria larger than picophytoplankton often form a significant part of oceanic phytoplankton. Massive development of filaments of the nitrogen-fixing *Trichodesmium* (Figs. 2.31,

2.56(*g*)) (Carpenter et al., 1992) occurs in certain tropical waters. Each colony of *Trichodesmium* consists of a mass of filaments that secrete a flocculent mucilage which supports bacterial colonies; these in turn are fed on by different protozoa. The large surface area produced by the algal filaments forms a miniature ecosystem (Andersen, 1977). *Trichodesmium* is a major component of the Caribbean Sea plankton, comprising 60% of the total chlorophyll *a* in the upper 50 m and about 20% of the primary production. It is also an important source of nitrogen, fixing 1.3 mg of nitrogen per square meter per day (Carpenter and Price, 1977). The cells produce gas vacuoles which, under calm conditions, cause the cells to accumulate at the water surface, giving rise to the phenomenon known to sailors as "**sea sawdust**," or long orange or gray windrows of algae. One such bloom stretched 1600 km along the Queensland coast of Australia, extending from the shore to the Great Barrier Reef, and occupying an area of 52 000 km^2 (Ferguson-Wood, 1965). *Trichodesmium* also occurs in the Red Sea and it was probably the color produced by blooms of the alga that gave the Red Sea its name (Hoffman, 1999).

Trichodesmium moves up in the water column by means of gas vesicles, and moves down in the water column by carbohydrate ballasting (Romans et al., 1994). The cells become progressively heavier from morning to evening as carbohydrates and polyphosphate bodies are produced. In the Caribbean, *Trichodesmium* cells have been found down to 200 m. The gas vesicles of this cyanobacterium are much stronger and more difficult to collapse than those found in any freshwater alga (Walsby, 1978). The gas vesicles are able to stand up to 20 atm of pressure, enabling *Trichodesmium* to rise from great depths.

Freshwater environment

Freshwater blooms of cyanobacteria are common. Most freshwater blooms of cyanobacteria consist of *Microcystis* (Figs. 2.48, 2.56(*b*)), *Anabaena* (Figs. 2.16, 2.18(*d*), 2.57(*b*)), *Aphanizomenon* (Fig. 2.57(*b*)), *Gloeotrichia* (Fig. 2.18(*a*)), *Lyngbya* (Fig. 2.42(*b*), (*c*)) or *Oscillatoria* (Fig. 2.19(*a*), (*b*)). Although they occur in lakes over the whole year, it is usually only in late summer and early autumn that they reach bloom proportions.

This because of (Tang et al., 1997):

1. the superior light-capturing abilities of cyanobacteria when self-shading is the greatest.
2. their high affinity for nitrogen and phosphorus when nutrient limitation is most severe.
3. their ability to regulate their position in the water column by gas vacuoles to take advantage of areas richer in nutrients and/or light.
4. their higher temperature optima for growth and photosynthesis (greater than 20 °C).

Similar to marine environments, freshwater plankton is dominated by the picoplankton cyanobacteria, particularly species of *Synechococcus* (Fig. 2.31) (Postius and Ernst, 1999).

Even in the Arctic and Antarctic, cyanobacteria dominate the algal flora in the late summer. These cyanobacteria are **psychrotrophs**, able to tolerate the severe conditions during the winter and then grow in the warmer summer months (as contrasted to **psychrophiles** that are able to grow at temperatures less than 15 °C; (Tang et al., 1997; Nadeau and Castenholz, 2000).

Hot-spring cyanobacteria

Cyanobacteria are important in the colonization of non-acidic hot springs throughout the world. Some cyanobacteria have the ability to grow at temperatures as high as 70 to 73 °C, a much higher temperature tolerance than occurs in eukaryotic algae. In thermal environments above 56 to 60 °C, both photosynthetic and non-photosynthetic eukaryotic algae are always absent. In acid springs (pH less than 4), no cyanobacteria are present, and at temperatures above 56 °C in these springs there are no photosynthetic organisms at all (Brock, 1973). *Mastigocladus laminosus* (Fig. 2.44(*a*)) is a cyanobacterium that occurs in thermal springs throughout the world, whereas other cyanobacteria such as *Synechococcus lividus* and *Oscillatoria terebriformis* have more restricted ranges (Castenholz, 1973). The cyanobacteria normally occur as mats mixed with flexibacteria, the cyanobacteria usually being more prevalent in the upper portion of the mat. The **thermophilic** cyanobacteria are especially adapted to live at elevated temperatures.

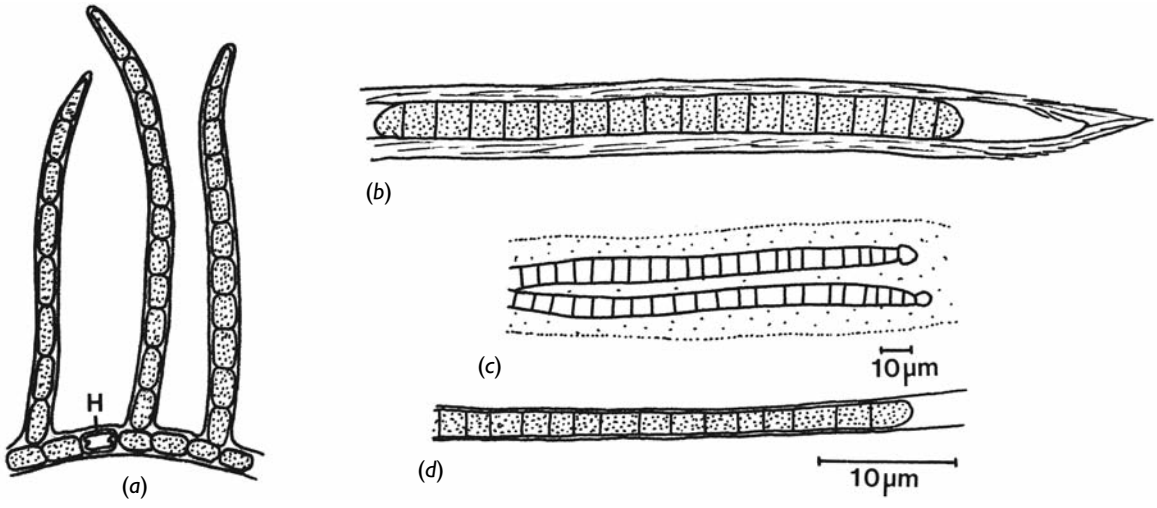


Fig. 2.44 (*a*) *Mastigocladus laminosus.* (H) Heterocyst. (*b*) *Porphyrosiphon notarisii.* (*c*) *Microcoleus vaginatus.* (*d*) *Plectonema notatum.* ((*c*),(*d*) after Prescott, 1962.)

Synechococcus lividus can grow at temperatures up to 73 °C but ceases to grow in culture when the temperature is lowered to 54 °C, with optimum growth occurring from 60 to 63 °C (Meeks and Castenholz, 1971); the cells will die if kept at 30 °C for 10 days. Enzymes isolated from thermal algae are more stable at higher temperatures than those from other organisms. For example, $NADPH_2$-cytochrome *c* reductase extracted from the thermal alga *Aphanocapsa thermalis* showed unimpaired activity after heating to 85 °C for 5 minutes, whereas that from *Anabaena cylindrica* was completely inactivated by a similar treatment.

Terrestrial environment

Terrestrial cyanobacteria play a major role as primary colonizers in the establishment of a soil flora and in the accumulation of humus. They do this in four main ways:

1 They bind sand and soil particles and prevent erosion. They do this with their gelatinous sheaths and by their growth pattern which produces closely intertwined rope-like bundles in and among soil particles. Genera that commonly perform this function are *Porphyrosiphon* (Fig. 2.44(*b*)) which covers large eroded areas in Brazil (Drouet, 1937), *Microcoleus* (Figs. 2.44(*c*), 2.45), *Plectonema* (Fig. 2.44(*d*)), *Schizothrix* and *Scytonema* (Figs. 2.58(*c*), (*d*), 2.59).
2 They help to maintain moisture in the soil. Booth (1941), in studies in Oklahoma, found that soil with an algal covering had a moisture content of 8.9% compared to 1.3% in the absence of algae.
3 They are important as contributors of combined nitrogen through nitrogen fixation. In grasslands, the soil surface between crowns of grasses may support extensive zones of cyanobacteria and lichens that include cyanobacteria as their phycobiont constituting up to 20% of the ground cover (Kapustka and DuBois, 1987).
4 It has been suggested that cyanobacteria assist higher plant growth by supplying growth substances.

Anhydrobiotics are organisms that can withstand the removal of the bulk of their intracellular water for extended periods of time. The cosmopolitan terrestrial cyanobacterium *Nostoc commune* is able to tolerate acute water stress and can survive in the air-dry state for many years. Approximately 0.1 g of blackened air-dried colonies becomes an olive-green rubbery mass of more than 20 g wet weight within 30 min of rehydration. In *Nostoc commune* (Fig. 2.46), rehydration rather than desiccation appears to be the fatal event. To protect the cells during rehydration, a water stress protein and large amounts of the sugar trehalose are

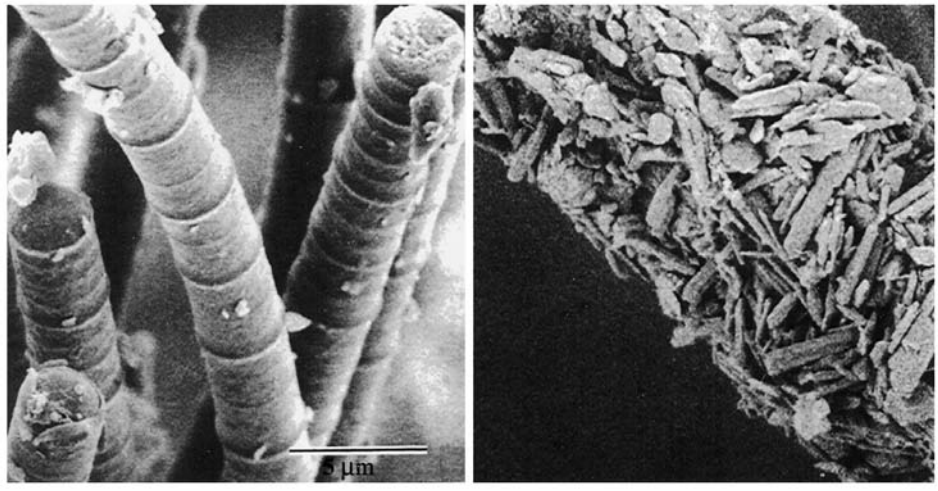


Fig. 2.45 Scanning electron micrographs of *Microcoleus vaginatus*. *Left*: Filament. *Right*: Filament with clay particles and sand grains embedded in the slime surrounding the cell walls. (From Belnap and Gardner, 1993.)

synthesized that stabilize the phospholipid bilayers of cellular membranes (Potts, 1996, 1999; Qiu et al., 2004).

Cyanobacteria comprise the dominant component of the soil photosynthetic community in hot and cold arid regions where higher plant vegetation is absent or restricted. Desert **cryptobiotic crusts** are initiated by the growth of cyanobacteria in the soil during episodic events of available moisture. The only cyanobacteria that are initial colonizers are those that have heterocysts, and are therefore able to fix nitrogen; and those cyanobacteria that produce **scytonemin**, a sunscreen that accumulates in the cyanobacterial sheaths and absorbs some of the strong sunlight in the near ultraviolet (370–384 nm) (Dillon and Castenholz, 1999). *Microcoleus vaginatus* (Fig. 2.45) makes up over 90% of cryptobiotic crusts in the arid soil of the Colorado Plateau in the United States (Belnap and Gardner, 1993). Filaments of *M. vaginatus* are surrounded by thick mucilaginous sheaths that can absorb eight times their weight in water, increasing the water capacity of sandy soils. Clay particles and sand grains become trapped in the cyanobacterial sheaths (Fig. 2.45). The clay particles are negatively charged and bind positive cationic nutrients (e.g., K^+, Ca^{2+}) preventing them from leaching into the subsoil. Subsequently, lichens, fungi and moss establish themselves in the crust, enriching and stabilizing the soil.

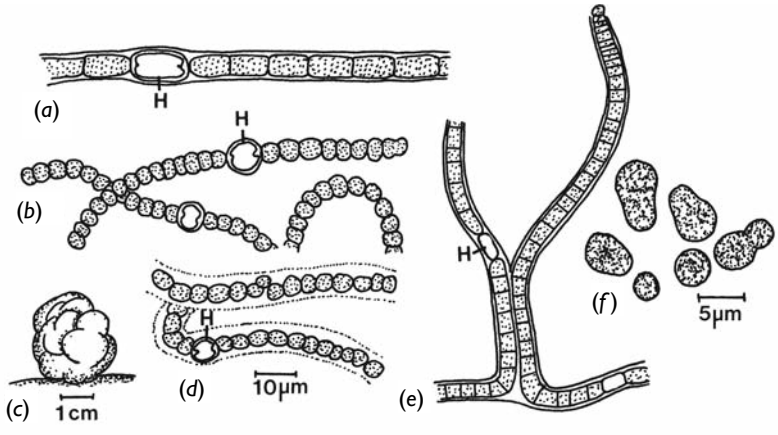


Fig. 2.46 (*a*) *Aulosira fertilissima*. (H) Heterocyst. (*b*) *Nostoc commune*. (*c,d*) *N. verrucosum*. (e) *Scytonema hofmanni*. (*f*) *Chamaesiphon* sp., showing formation of exospores. ((*a*),(e) after Desikachary, 1959; (*b*) after Prescott, 1962; (*f*) after Waterbury and Stanier, 1977.)

Nitrogen-fixing cyanobacteria make a major contribution to the fertility of paddy fields (Vaishampayan et al., 2001). In many Eastern countries, peasant farmers do not fertilize their fields; the nitrogen is fixed by cyanobacteria, thus permitting a moderate harvest when in their absence there would be a poor one. There are about 100 million km^2 of paddy fields, of which some are in southern Europe and the United States, but about 95% are in India and the Far East. Usually rice is grown on land that is submerged under 10 cm or so of water for 60 to 90 days during the growing season, and then allowed to dry to facilitate harvest. The warm conditions demanded by the rice, the availability of nutrients, the reducing conditions in the soil, and the cyanobacterial ability to withstand desiccation all favor growth of cyanobacteria. Over 70% of algal species in Indian paddy soils are cyanobacteria (Pandey, 1965). In paddy soils in India there is a succession of cyanobacteria over the growing season of the rice (Singh, 1961). Early in the rainy season (starting at the end of June), the soil becomes covered with a thick patchy growth composed of a variety of algae. In July, the fields are flooded, and the top 20 cm of soil and algae are mixed to form a muddy suspension. The rice seedlings are transplanted, and after about a fortnight the soil and algae have settled. By the middle of September, there is an extensive brownish-yellow gelatinous growth on the soil, composed primarily of *Aulosira fertilissima* (Fig. 2.46(*a*)), the most important nitrogen-fixing species in the fields. This species is dominant for about 3 months and forms a papery growth on the soil surface when the fields are dry.

From the above discussion, it is plain that cyanobacteria occur in most environments on earth. There is, however, one important exception: cyanobacteria are usually absent in waters or soils with a pH below 5, and they are uncommon between pH 5 and 6 (Brock, 1973).

Adaption to silting and salinity

In salt marshes and mud flats, felts of cyanobacteria, particularly *Microcoleus chthonoplastes* (Fig. 2.42(*e*)) are important in stabilizing mud surfaces. Filaments of *M. chthonoplastes* are phototactic and chemotactic, resulting in migration to the surface of the mud at a rate of about 7 mm per 24 h. The movement of the filaments is an adaption that allows the cyanobacterium to survive during silting (Whale and Walsby, 1984). *M. chthonoplastes* is **euryhaline**, it is able to survive in a wide range of salinities in the estuarine environment by producing glycosylglycerol (Fig. 2.47) as an osmolyte to counteract the osmolarity of the surrounding environment. It also synthesizes trehalose to stabilize the phospholipid membrane bilayers of the cell (Karsten, 1996).

In **hypersaline** environments, such as the Great Salt Lake in Utah, **halotolerant** and **halophilic** cyanobacteria can adapt to the high salinity in three ways (Fulda et al., 1999):

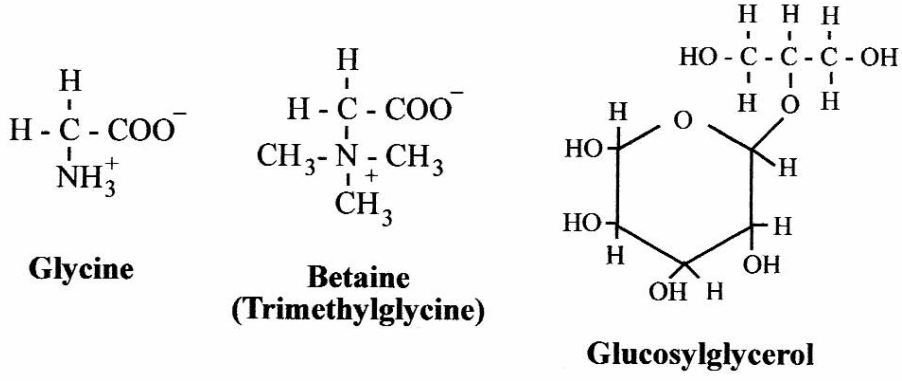


Fig. 2.47 The chemical structure of three osmoregulatory compounds in cyanobacteria.

1 Active export of inorganic ions in the protoplasm leading to relatively unchanged internal salt concentrations.
2 Accumulation of organic osmoprotective compounds, such as glucosylglycerol, glycine, and betaine (trimethylglycine) (Fig. 2.47), to maintain the osmotic equilibrium (Ferjani et al., 2003).
3 Expression of a set of salt-stress proteins such as the protein flavodoxin.

Cyanotoxins

Some of the cyanobacteria produce toxins (cyanotoxins). Physiologically, there are basically two types of cyanotoxins: neurotoxins and hepatotoxins (Carmichael, 1992; Bell and Cobb, 1994; Codd et al., 1999).

Neurotoxins – The neurotoxins are alkaloids (nitrogen-containing compounds of low molecular weight) that block transmission of the signal from neuron to neuron and neuron to muscle in animals and man. Symptoms include staggering, muscle twitching, gasping and convulsions. The neurotoxins can be fatal at high concentrations due to respiratory arrest caused by failure of the muscular diaphragm. The two neurotoxins produced by cyanobacteria are **anatoxin** and **saxitoxin** (Fig. 23.3). Anatoxins are synthesized by species of *Anabaena* (Figs. 2.16, 2.18(*d*), 2.57(*b*)), *Aphanizomenon* (Fig. 2.18(*b*)), *Oscillatoria* (Figs. 2.19(*a*), (*b*), 2.34(*a*), (*b*)) and *Trichodesmium* (Figs. 2.31, 2.56(*g*)) (Negri et al., 1997).

Hepatotoxins – The heptatotoxins are inhibitors of protein phosphatases 1 and 2A (Arment and Carmichael, 1996) and affect the animal by causing bleeding in the liver. Clinical signs include weakness, vomiting, diarrhea, and cold extremities. Cyanobacteria produce two types of hepatotoxins, the **microcystins** and **nodularins** (Fig. 23.2), that are produced along a similar pathway (Rinehart et al., 1994). Microcystins are synthesized by species of *Microcystis* (Figs. 2.48, 2.56(*b*)), *Anabaena* (Figs. 2.16, 2.18(*d*), 2.57(*b*)), *Nostoc* (Figs. 2.35, 2.46(*b*)–(*d*), 2.57(*a*)), *Nodularia* (2.42(*a*)), and *Oscillatoria* (Figs. 2.19(*a*), (*b*), 2.34(a), (b)) while the nodularins are produced by species of *Nodularia* (Fig. 2.42(*a*)) (Kotak et al., 1995; Bolch et al., 1999).

The cyanotoxins are mostly important in freshwaters where the cyanobacteria are ingested in drinking water by animals, with the algae dying and releasing their toxins in the intestinal tracts. The cyanotoxins are responsible for the loss of

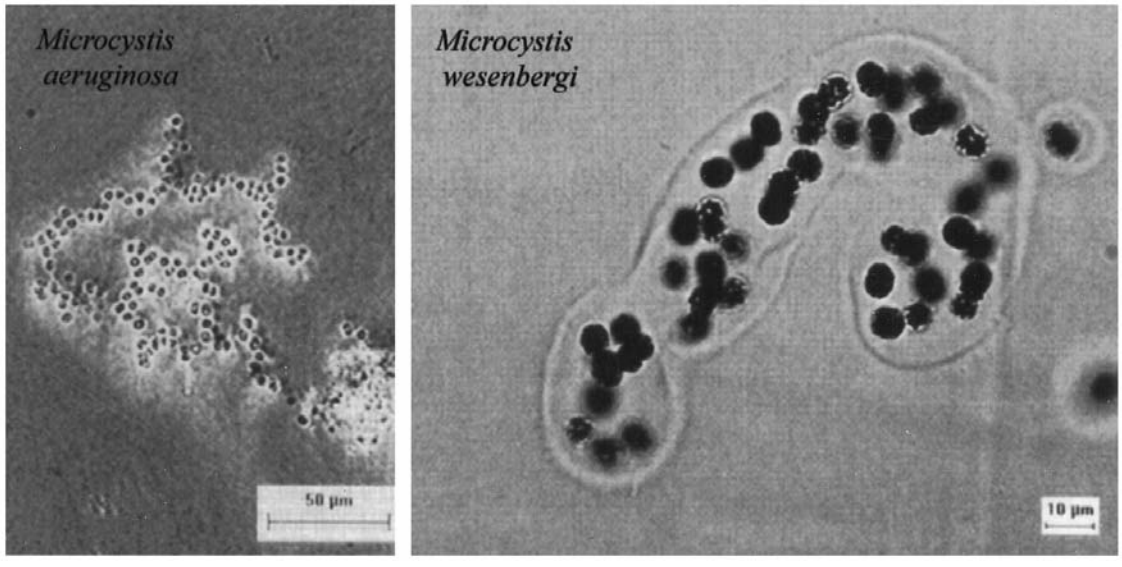


Fig. 2.48 Light micrographs of two species of *Microcystis*. (From Bittencourt-Oliveira et al., 2001.)

large numbers of stock each year throughout the world, usually in the warm summer months when the blooms of cyanobacteria are visible in the water. Seldom will man drink from such an unattractive water source. As such, poisoning of man by cyanotoxins is relatively rare, partly because of the odor from geosmin and MIB (Fig. 2.50) produced by cyanobacteria.

The cyanotoxins function as anti-herbivore chemicals by inhibiting invertebrate grazers in the aquatic environment. Grazing by invertebrates causes *Microcystis aeroginosa* (Figs. 2.48, 2.56(*b*)) to increase production of cyanotoxin (Jang et al., 2003). Cyanotoxins also can inhibit the growth of other algae. This is called an **allelopathic interaction** where one organism affects the growth of a second organism. An example of this is the inhibition of the freshwater dinoflagellate *Peridinium gatunense* by the microcystin produced by the cyanobacterium *Microcystis* (Figs. 2.48, 2.56) in Lake Kinneret (Sea of Galilee), Israel. The *Microcystis* cyanotoxins abolish carbonic anhydrase activity in the dinoflagellate and inhibit growth (Sukenik et al., 2002). The microcystin is classified as an **allelochemical** and acts as an **algicide**.

Another allelopathic interaction involves the zebra mussel (*Dreissena polymorpha*) (Fig. 2.49) and the cyanobacterium *Microcystis*. Zebra mussels, native to the Black and Caspian seas, were discovered in the United States near Detroit in 1988. Since then zebra mussels have spread throughout the Great Lakes of North America, displacing native shellfish. The zebra mussel has been beneficial in low-nutrient lakes (but not in lakes high in nutrients) because they graze on *Microcystis*, probably because the mussels have nothing else to eat (Raikow et al., 2004).



Fig. 2.49 Zebra mussels; each mussel is about the size of a pistachio nut.

Cyanobacteria and the quality of drinking water

Geosmin (E-1,10-dimethyl-E-9-decalol) and **MIB** (2-methylisoborneol) (Fig. 2.50) are two terpenoids (isoprenoids) that are produced by some cyanobacteria (Watson, 2003). These terpenoids are called **volatile organic compounds** (VOCs), have a highly potent earthy, musty or muddy aroma and account for most of the odors in drinking water. They have odor threshold concentrations of ~10 ng l^{-1}. Terpenoids as a class have extensive olfactory properties, which are exploited commercially in the food, beverage, and perfume industries. Both geosmin and MIB resist conventional water treatment, and their bioaccumulation in fish and shellfish causes off-flavor in farmed and wild stocks. Neither geosmin nor MIB are toxic to vertebrates (including humans). The low incidence of human

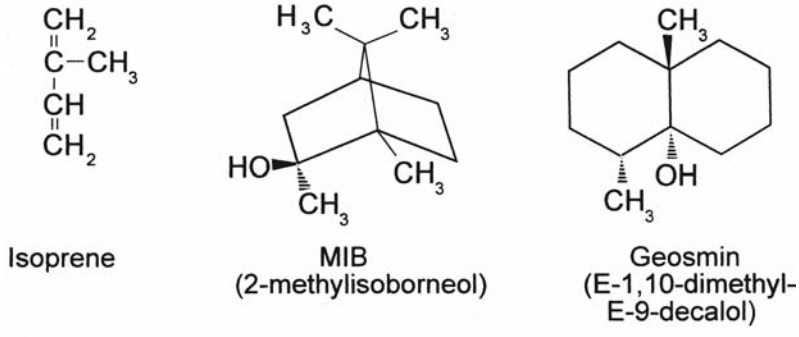


Fig. 2.50 The chemical structure of the terpenoids MIB and geosmin. The terpenoids are constructed of multiples of 5-carbon isoprene or 2-methyl-1,3 butadiene. Terpenoids containing three isoprene units (e.g., MIB and geosmin) are called sesquiterpenoids.

poisonings by cyanotoxins has been attributed to the avoidance of water containing cyanobacteria because of the odors produced by geosmin and MIB. Both compounds are commonly found in freshwater and solid habitats, but are rare in offshore marine environments, and can be used as landmass indicators. These volatile organic compounds produced by cyanobacteria act as infochemicals by attracting nematodes to cyanobacterial colonies where the nematodes feed and deposit eggs (Hockelmann et al., 2004).

Utilization of cyanobacteria as food

Cyanobacteria are used as human food and animal food supplements (Belay et al., 1966). In China, the *Spirulina* (Figs. 2.51, 2.56(*f*)) industry is supported by the State Science and Technology Commission as a natural strategic program (Li and Qi, 1997). In 1996 there were more than 90 *Spirulina* factories with a total production of 400 tons of *Spirulina* dry powder and a total production area of 1 million square meters. Besides *Spirulina* pills and capsules, there are also pastries, blocks, and *Spirulina*-filled chocolate blocks.

Nostoc (Figs. 2.46(*b*), (*c*), (*d*)) is a cyanobacterium that has been gathered for food for over two thousand years in China (Gao and Ye, 2003). It is called "hair vegetable" because of its hair-like appearance. The Chinese word for "hair vegetable" (Facai) sounds like another Chinese word that means fortunate and get rich, adding a spiritual value to the cyanobacterial food.

In Japan, *Aphanothece sacrum*, *Nostoc verrucosum* (Fig. 2.46(*d*)), *N. commune* (Fig. 2.46(*b*), (*c*)), and *Brachytrichia* have been used as side dishes since ancient time. Bernal Diaz del Castillo, who accompanied Cortez to Mexico, described in 1521 how people living in the area of Mexico City "sell some small cakes made from a sort of ooze which they get out of a great lake, which curdles and from which they make bread having a flavor something like cheese."

Aphanizomenon flos-aquae (Fig. 2.18(*b*)) has been harvested from Klamath Lake in California since the early 1980s and sold as a food and health supplement. In 1998, 10×10^6 kg (dry weight) was marketed with a value of $100 million (Carmichael et al., 2000). Other cyanobacteria, such as *Spirulina* (Figs. 2.51, 2.56(*f*)), are readily available at health-food stores in the developed world, although one wonders how healthy these cyanobacteria really are in regard to the potential for this group of algae to produce cyanotoxins.

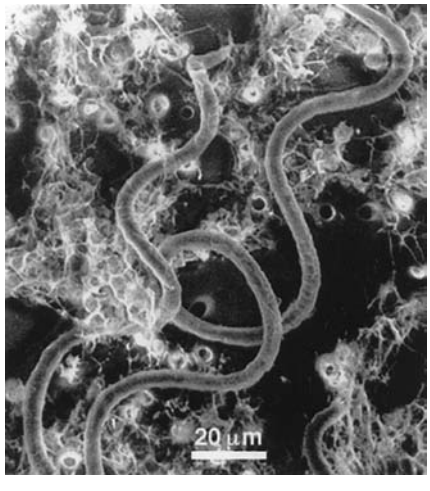


Fig. 2.51 Scanning electron micrograph of *Spirulina platensis*. (From El-Bestaway et al., 1996.)

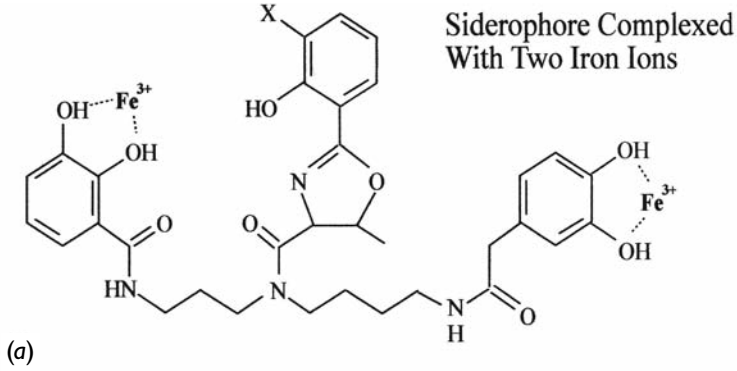
Cyanophages

Cyanophages are viruses that infect and commonly kill cyanobacteria (Suttle and Chan, 1994). Cyanophages can be extremely numerous, concentrations in excess of 100 000 viruses have been observed in surface seawater off the coast of Texas. Normally, however, cyanophages occur at concentrations of 1/10 that of the cyanobacterial host cells. Most cyanobacteria are actually resistant to attack by cyanophages with the cyanophage population being maintained by infection of the relatively rare cyanobacteria that are susceptible to infection. Cyanobacteria in the open ocean are more susceptible to infection than cyanobacteria from inshore waters. High temperature and phosphate limitation increase the probably of cyanobacterial infection by cyanophages (Wilson et al., 1996).

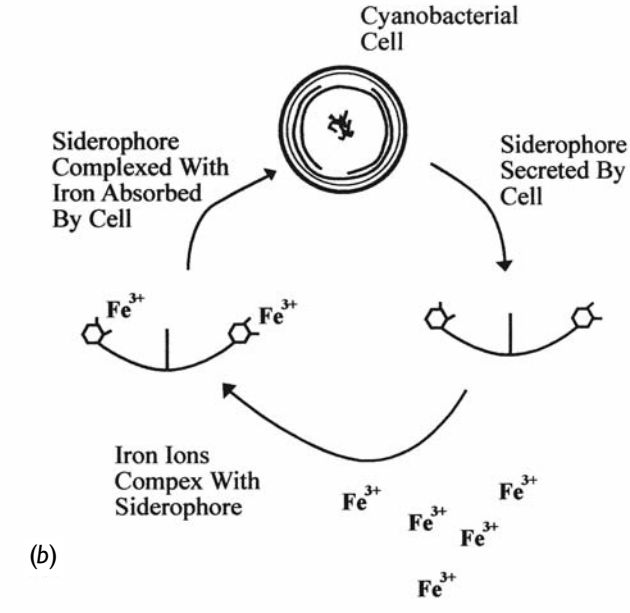
Secretion of antibiotics and siderophores

Some cyanobacteria, such as *Nostoc* (Figs. 2.35, 2.46(*b*), (*c*), (*d*), 2.57(*a*)) secrete antibiotics called **bacteriocins**, which kill related strains of the alga (Flores and Wolk, 1986). A bacteriocin is a proteinaceous antibiotic that is active against prokaryotic strains closely related to the organism that produces the antibiotic. Other cyanobacteria secrete antibiotics that are active against a wide range of cyanobacteria and eukaryotic algae. *Scytonema hofmanni* (Fig. 2.46(*e*)) produces such an antibiotic (Mason et al., 1982; Gleason and Paulson, 1984). This antibiotic, called **cyanobacterin**, is a chlorine-containing λ-lactone (Pignatello et al., 1983). All of these antibiotics probably play an active role in the survival of the producing organism by inhibiting growth of competing organisms.

The obligate requirement for iron, coupled with the low solubility of iron in many aquatic habitats, has led to the evolution of a mechanism for iron acqusition, at the cost of cellular energy and nutritional stores. A number of cyanobacteria release extracellular ferric-specific chelating agents ("**siderophores**") during periods of low iron availability. Siderophores function as extracellular ligands that aid in solubilization and assimilation of Fe^{3+} (Fig. 2.52) (Wilhelm et al., 1996; Barbeau et al., 2003).



(*a*)



(*b*)

Fig. 2.52 (*a*) A siderophore complexed with two ions of iron. (*b*) A cyanobacterial cell secretes a siderophore which complexes with iron ions in the medium. The siderophore complexed iron ions are absorbed by the cell.

Calcium carbonate deposition and fossil record

Many species of cyanobacteria have calcium carbonate in the enveloping mucilage of the cells. In freshwater these algae usually grow in water where carbonate crystallizes out by non-biological physicochemical mechanisms, and the crystals of calcite become trapped in the mucilage of the algae. Normally, only 1% to 2% of the calcium carbonate is actively precipitated by the cells (Pentecost, 1978). There are a large number of different forms of carbonate deposits attributed to the Cyanophyceae (for a review, see Golubić, 1973).

In the marine environment, cyanophycean depositions are the result of trapping and binding of the sediments as well as carbonate precipitation. **Stromatolithic** heads are probably the best known of these forms (Figs. 2.53, 2.55). These heads are firmly gelatinous to almost cartilaginous in texture, predominantly hemispherical, and show fine concentric lamination. In the shallow subtidal waters of south Florida and the Bahamas, they are produced by a single species of *Schizothrix* (Monty, 1967). During the day there is growth of algal filaments, resulting in the algae covering the surface of the stomatolite head. During the night, growth ceases, and sediments accumulate on the surface of the head, forming sediment-rich laminae up to 100 μm thick. In the early part of the day, the algae penetrate through this deposited sediment, and grow a hyaline layer, 200 μm thick, with a low concentration of entrapped sediment. These alternating periods of growth and deposition give a laminated structure to the stromatolite (Reid et al., 2000) (Fig. 2.55). Stromatolites first formed 3500 million years ago although the first stromatolites were formed by non-biological deposition of $CaCO_3$ (Arp et al., 1999) with the first stromatolites formed by cyanobacteria (Fig. 2.54) appearing about 2700 million years ago (Buick, 1992; Dalton, 2002; Brasier et al., 2002).

The production of laminae in stromatolites depends on fluctuations ultimately derived from the physical movements of the earth, sun, and moon, and requires some kind of rhythmicity that causes discontinuity in the accretionary process. The periodicity of laminae is due primarily to the daily photosynthetic cycle of the organisms in the stromatolites. In addition, stromatolites are **heliotropic** and grow toward sunlight (Awramik and Vanyo, 1986). This heliotropism allows the calculation of the extent of a year's deposition in a stromatolite. The yearly cycle of movement of the sun causes the sun to be higher in the sky in the summer and lower in the winter. The heliotropism of the stromatolites causes the stromatolites to grow in a sine waveform over the course of a

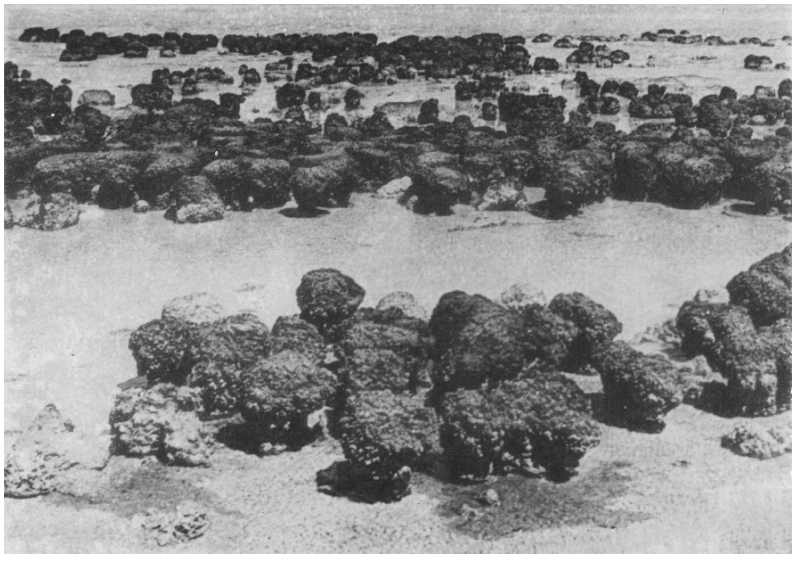


Fig. 2.53 Cyanobacterial stromatolites in the process of formation in Shark Bay, Western Australia. (From Logan, 1961.)

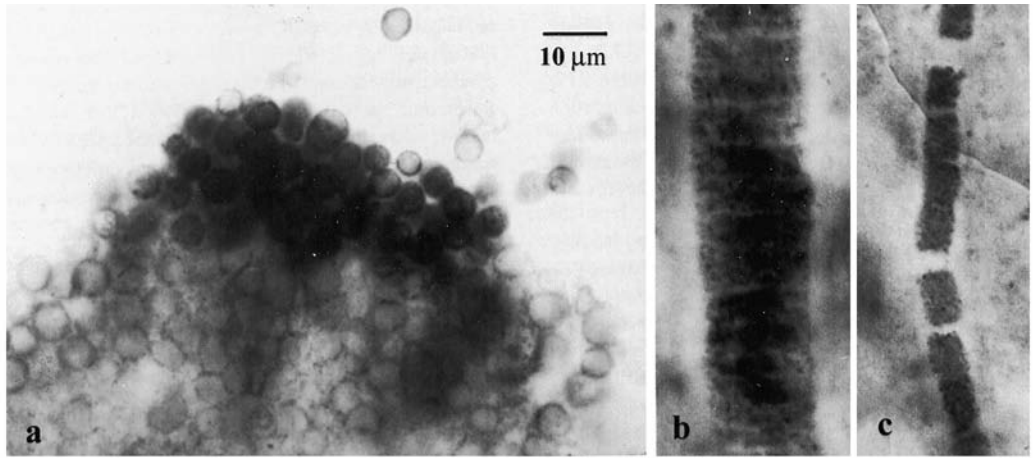


Fig. 2.54 Fossil cyanobacteria preserved in silicified stromatolites of the 1400 million-year-old Gaoyuzhang formation of northern China. (*a*) *Eoentophysalis belcherensis*. (*b*) *Palaeolyngbya barghooriana*. (*c*) *Oscillatoriopsis*. (From Golubic and Seong-Joo, 1999.)

year (Fig. 2.55). Counting the number of laminae in one sine wave has allowed paleontologists to calculate the number of days in a year for a geological period. Such studies have shown that the solar year has varied considerably. For example, approximately 1000 million years ago, the solar year consisted of approximately 435 days (Vanyo and Awramik, 1985).

Up to 2000 million years ago, there were no grazing and boring organisms; thus stromatolites grew uncontested. Without competition, Precambrian stromatolites freely populated enormous areas and most likely grew in water down to a depth of 10 m. The occurrence and size of stromatolites declined dramatically after the evolution of grazing and boring organisms. Today stromatolites grow only in warm waters that are inhospitable to grazers and borers – waters such as the hypersaline waters in Shark Bay, Australia (Fig. 2.53), or in waters with a high tidal current that inhibit borers and grazers, such as in the Bahamas where stromatolites grow to a height of 2 m (Dill et al., 1986).

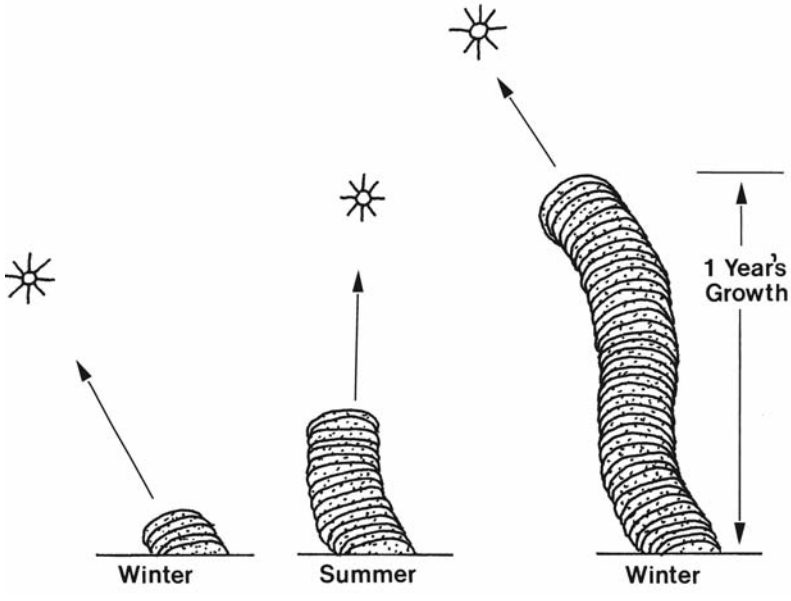


Fig. 2.55 Diagrammatic representation of the growth of a stromatolite over the period of a year. A year's growth is represented by an S-shaped curve.

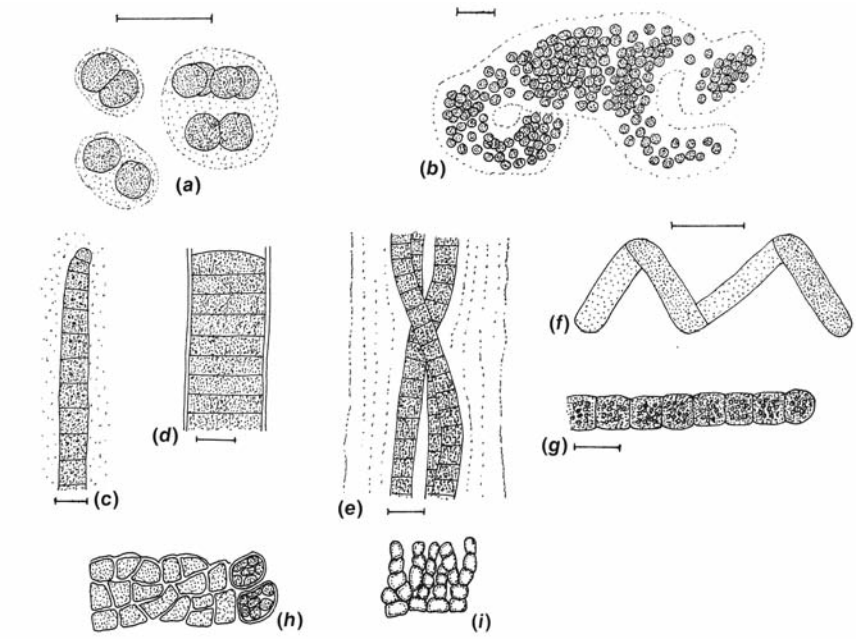


Fig. 2.56 (*a*) *Gloeothece magna.* (*b*) *Microcystis aeruginosa.* (*c*) *Phormidium autumnale.* (*d*) *Lyngbya birgei.* (e) *Hydrocoleus* sp. (*f*) *Spirulina major.* (*g*) *Trichodesmium lacustre.* (*h*,*i*) *Pleurocapsa minor*, surface view showing cells with endospores (*h*) and vertical section of thallus showing erect threads (*i*). Bar = 10 μm.

Classification

Nucleic acid sequencing of cyanobacteria is beginning to elucidate the evolutionary relationships among cyanobacteria (Honda et al., 1999; Nadeau et al., 2001; Turner, 1997). These studies have shown that there is little in common between the morphology of cyanobacteria and their evolutionary relationship. The one exception is the cyanobacteria with heterocysts, which all appear to be closely related. With the classification of cyanobacteria in such a state of flux, I have chosen to simplify the classification by dividing the cyanobacteria into three orders:

Order 1 Chroococcales: single cells or cells loosely bound into gelatinous irregular colonies.

Order 2 Oscillatoriales: filamentous cyanobacteria.

Order 3 Nostocales: filamentous cyanobacteria with heterocysts.

Chroococcales

This order included basically unicellular cyanobacteria which are held together in palmelloid colonies by mucilage. *Gloeothece* (Fig. 2.56(*a*)), *Microcystis* (Figs. 2.48, 2.56(*b*)), *Synechococcus* (Figs. 2.19(*c*), 2.31), and *Synechocystis* (Fig. 2.8) are some of the genera in this order. Although the organisms in this order have a similar morphology, studies involving nucleic acid base composition have shown that the order is actually composed of several distinct and widely separated groups (Honda et al., 1999).

Prochlorococcus marinus (Fig. 2.20) is the dominant photosynthetic organism in tropical and temperate oceans. The cyanobacterium is 0.5 μm in diameter, making it the smallest photosynthetic organism. The cells have chlorophyll *a* and *b*, and lack phycobilin pigments. The complete genome of *Prochlorococcus marinus* has been determined (Dufresne et al., 2003).

Gloeobacter violaceus (Fig. 2.19(*e*)), a cyanobacterium without internal thylakoids, appears to be the most primitive cyanobacterium based on nucleic acid sequencing studies (Honda et al., 1999).

Oscillatoriales

These are filamentous cyanobacteria without heterocysts. Representative cyanobacteria are

Oscillatoria (Figs. 2.17, 2.34(*a*), (*b*), 2.19(*a*), (*b*)), *Trichodesmium* (Figs. 2.31, 2.56(*g*)), *Phormidium* (Figs. 2.13, 2.18(*c*), 2.56(*c*)), *Lyngbya* (Fig. 2.56(*d*)), *Hydrocoleus* (Fig. 2.56(*e*)), and *Spirulina* (Fig. 2.51).

Pleurocapsa (Fig. 2.56(*h*) (*i*)) is composed of an erect and a prostrate system and is therefore **heterotrichous**. *Pleurocapsa* is a widely distributed **lithophyte** (grows on rocks) in the marine and freshwater environment. Initially it consists of a filament creeping over the surface. Later the filament branches and forms a pseudoparenchymatous disc. Development may stop here, or the prostrate basal disc cells may form erect threads (Fig. 2.56(*i*)). Endospores are formed internally by the division of a vegetative cell in three planes.

Nostocales

The cyanobacteria in this order, such as *Nostoc* (Figs. 2.35, 2.46(*b*), (*c*), (*d*), 2.57(*a*)), *Anabaena* (Figs. 2.16, 2.18(*d*)), and *Aulosira* (Fig. 2.46(*a*)), have heterocysts. The most common method of reproduction is by hormogonia. In some genera there is a polarity: heterocysts and/or akinetes are at the base, and a colorless hair is at the apex of the filament. A hair is a region of the trichome where the cells are narrow, elongated, highly vacuolated, and apparently colorless. *Calothrix* (Figs. 2.42(*d*), 2.57(*e*)) is common in the littoral zone of the ocean, where it is attached to rocks. *Rivularia* (Fig. 2.57(*d*)) forms colonies in which the sheaths of one filament are confluent with others. The sheaths are usually heavily encrusted with lime and are very firm. *Rivularia* grows in freshwater submerged on stones and plants. The polarity of the thallus occurs only under conditions of low-nitrogen concentration (Sinclair and Whitton, 1977). When these algae are grown in media containing nitrogenous compounds (e.g., NO_3^-, NH_4) heterocysts are not formed, and the trichomes are not tapered and lack colorless hairs at the apex. These algae then resemble species of genera such as *Oscillatoria* (Figs. 2.17, 2.34(*a*), (*b*), 2.19(*a*), (*b*)). Hairs can also be

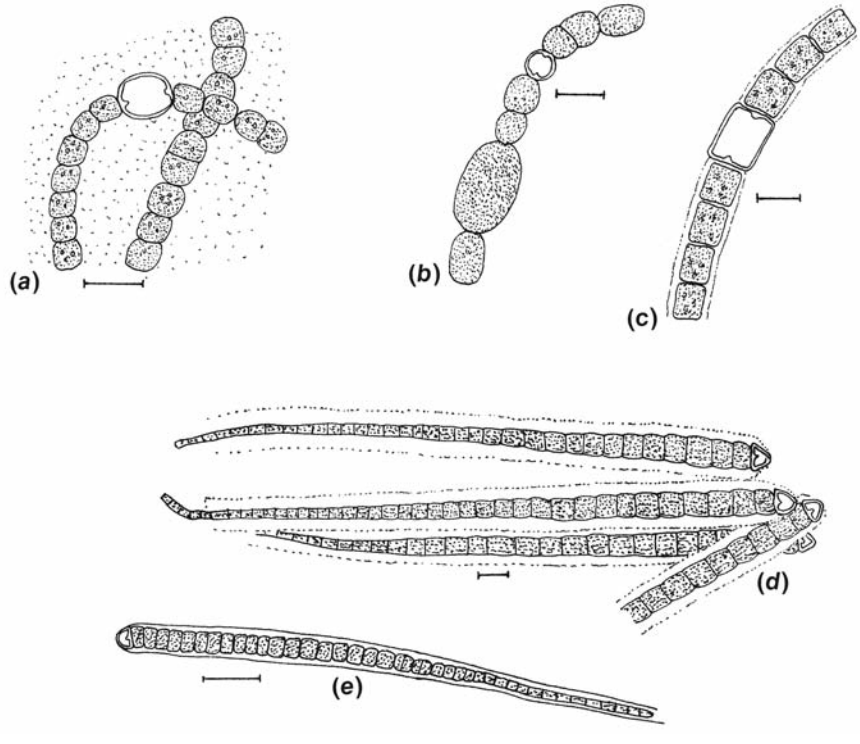


Fig. 2.57 (*a*) *Nostoc linckia.* (*b*) *Anabaena circinalis.* (*c*) *Aulosira implexa.* (*d*) *Rivularia dura.* (e) *Calothrix fusca.* Bar = 10 mm.

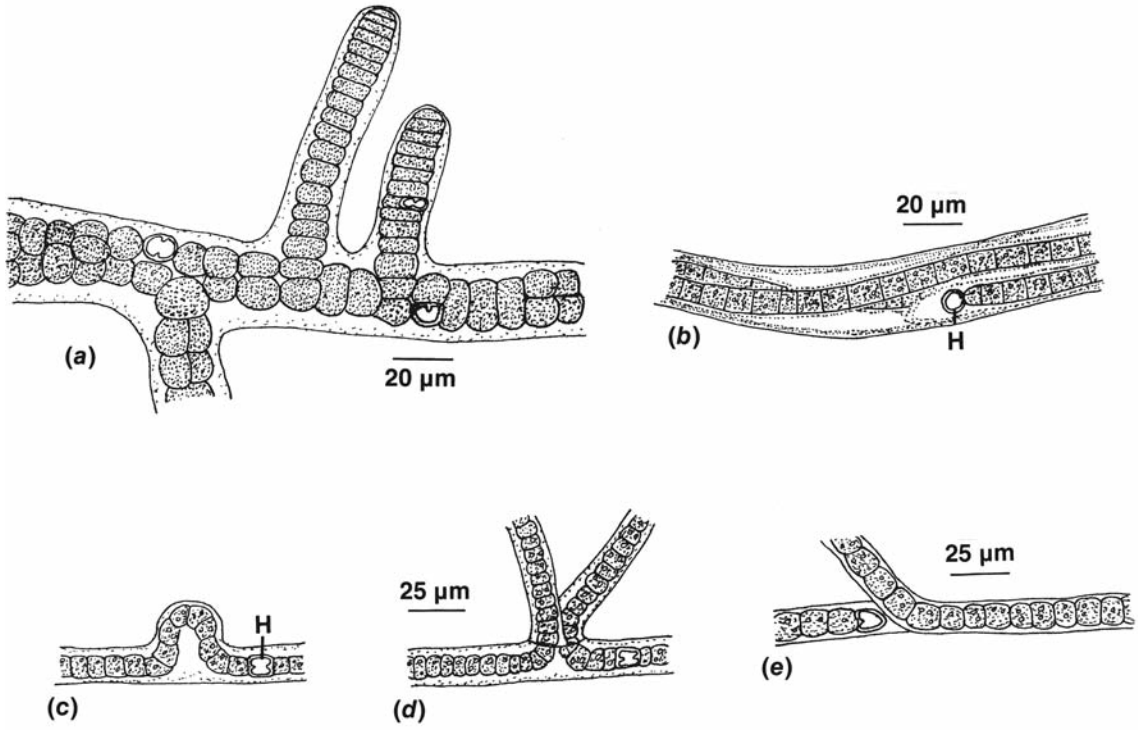


Fig. 2.58 (*a*) *Stigonema turfaceum* showing true branching. (*b*) *Desmonema wrangelii* with a number of trichomes in a sheath. (*c*,*d*) *Scytonema arcangelii* illustrating formation of false branches. (*e*) *Tolypothrix tenuis* with a single false branch. (H) heterocyst. (After Smith, 1950.)

induced to form by growing the algae under conditions of phosphorus deficiency. Addition of phosphorus results in the loss of hairs and the formation of hormogonia (Livingstone and Whitton, 1983).

False branching occurs in some genera in this order. It results when the trichome lodges in the sheath, commonly in the area of a large heterocyst (Fig. 2.58(*c*), (*d*)). Committed cell division in the trichome results in (1) a rupture of the sheath and (2) a break in the trichome that gives the appearance of a branch. The first type of false branching results in only one false branch protruding through the sheath, as in *Tolypothrix* (Fig. 2.58). This type is due to the death of a cell or the formation of a separation disc or necridium (Fig. 2.34) (biconvex in shape because of pressure from adjacent cells, the necridia lyse as they mature). These weak points are normally next to a heterocyst and eventually result in a break of the trichome, with one of the broken ends of the trichome protruding through the sheath as a false branch. The second type of false branching results in the formation of two false branches, as in *Scytonema* (Figs. 2.58(*c*), (*d*), 2.59). Here a loop is formed that protrudes through the sheath. Eventually the loop breaks in the middle as cell division continues, resulting in two false branches. It is probable that the large heterocysts lodging in the sheath cause the immovability of the trichome in the sheath. Experimental evidence that this is so comes from experiments with algae grown in high combined-nitrogen levels, which inhibit both heterocyst formation and false branching.

Stigonema has true branching with a tendency toward multiseriate thalli. The branching axis of *Stigonema* is partly or wholly multiseriate (Figs. 2.58, 2.59). *Stigonema* occurs on wet rocks and reproduces by hormogonia formed on the younger branches. The genus is the most morphologically complex in the cyanobacteria and is often differentiated into upright and prostrate filaments (heterotrichy).

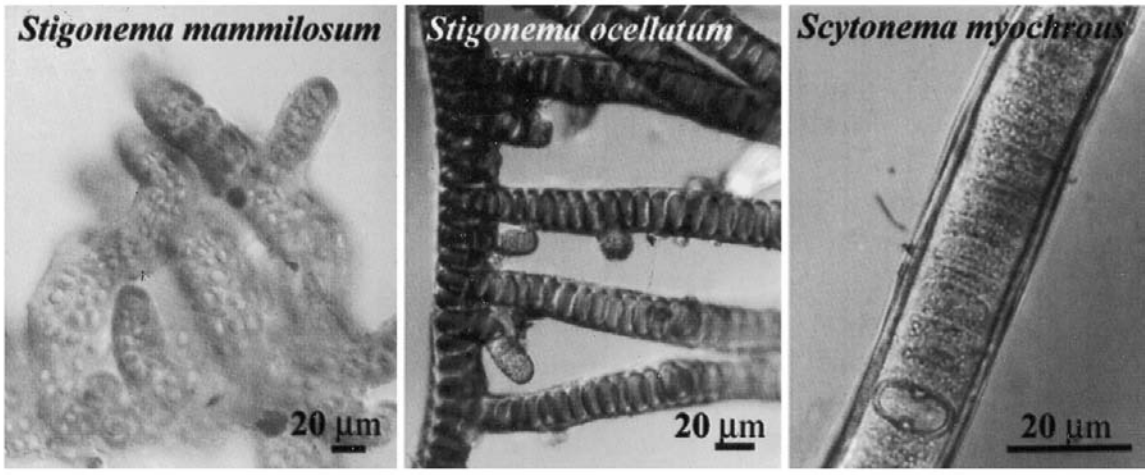


Fig. 2.59 Light micrographs of cyanobacteria in the Nostocales. (From Rascher et al., 2003.)



Fig. 2.60 **Jindong Zhao** Dr. Zhao received his Bachelor's degree in biology from Southwestern Normal University in 1982. He became a Ph.D. student in the Department of Botany, University of Texas at Austin in 1984 and received a Ph.D. degree in Biology in 1989. He spent the next three years as a postdoctoral fellow in Penn State University and the following two years in Applied Biosystems Inc. as a research scientist. Jindong Zhao returned to China and became an associate professor in the College of Life Sciences of Peking University in 1994. He was promoted to full professor in 1998. His laboratory focuses on studies of molecular mechanism of heterocyst differentiation and pattern formation of cyanobacteria.

REFERENCES

Aboulmagd, E., Oppermann-Sanio, F. B., and Steinbuchel, A. (2000). Molecular characterization of the cyanophycin synthetase from *Synechocystis* sp. strain PCC6308. *Arch. Microbiol*. 174:297–306.

Adams, D. G. (2000). Heterocyst development in cyanobacteria. *Curr. Opin. Microbiol*. 3:618–24.

Ahmadjian, V., and Hale, M. E. (1973). *The Lichens*. New York: Academic Press.

Allen, M. M. (1984). Cyanobacterial cell inclusions. *Annu. Rev. Microbiol*. 38:1–25.

Al-Thukair, A. A., and Golubic, S. (1991). New endolithic cyanobacteria from the Arabian Gulf. I. *Hyella immanis* sp. nov. *J. Phycol*. 27:766–80.

Anderson, O. R. (1977). Fine structure of a marine ameba associated with a blue-green alga in the Sargasso Sea. *J. Protozool*. 24:370–6.

Arment, A. R., and Carmichael, W. W. (1996). Evidence that microcystin is a thio template product. *J. Phycol*. 32:591–7.

Arp, G., Reimer, A., and Reitner, J. (1999). Calcification in cyanobacterial biofilms of alkaline salt lakes. *Eur. J. Phycol*. 34:393–403.

Awramik, S. M., and Vanyo, J. P. (1986). Heliotropism in modern stromatolites. *Science* 231:1279–81.

Badger, M. R., Hanson, D., and Price, G. D. (2002). Evolution and diversity of CO_2 concentrating mechanisms in cyanobacteria. *Funct. Plant Biol*. 29:161–73.

Barbeau, K., Rue, E. L., Trick, C. G., Bruland, K. W., and Butler, A. (2003). Photochemical reactivity of siderophores produced by marine heterotrophic bacteria and cyanobacteria based on characteristic Fe(III) binding groups. *Limnol. Oceanogr*. 48:1069–78.

Belay, A., Kato, T., and Ota, Y. (1996). *Spirulina* (*Arthrospira*): potential application as an animal feed supplement. *J. Appl. Phycol*. 8:303–11.

Bell, S. G., and Cobb, G. A. (1994). Cyanobacterial toxins and human health. *Rev. Med. Microbiol*. 5:256–64.

Belnap, J., and Gardner, J. S. (1993). Soil substructure in soils of the Colorado Plateau: the role of the cyanobacterium *Microcoleus vaginatus*. *Great Basin Nat*. 53:40–7.

Bergman, B., and Carpenter, E. J. (1991). Nitrogenase confined to randomly distributed trichomes in the marine cyanobacterium *Trichodesmium thiebautii*. *J. Phycol*. 27:158–65.

Bergman, B., Gallon, J. R., Rai, A. N., and Stal, L. J. (1997). N_2 fixation by non-heterocystous cyanobacteria. *FEMS Microbiol. Rev*. 19:139–85.

Berman-Frank, I., Lundgren, P., Chen, Y-B., et al. (2001). Segregation of nitrogen fixation and oxygenic photosynthesis in the marine cyanobacterium *Trichodesmium*. *Science* 254:1534–7.

Bhattacharjee, S. K. (1977). Unstable protein mediated ultraviolet light resistance in *Anacystis nidulans*. *Nature* 269:82–3.

Bhaya, D. (2004). Light matters: phototaxis and signal transduction in unicellular cyanobacteria. *Mol. Microbiol*. 53:745–54.

Bhaya, D., Watanabe, N., Ogawa, T., and Grossman, A. R. (1999). The role of an alternative sigma factor in motility and pilus formation in the cyanobacterium *Synechocystis* sp. strain PCC6803. *Proc. Natl. Acad. Sci., USA* 96:3188–93.

Bittencourt-Olivera, M., de Olivera, M. C., and Bolch, C. J. S. (2001). Genetic variability of Brazilian strains of the *Microcystis aeruginosa* complex (Cyanobacteria/Cyanophyceae) using phycocyanin intergenic spacer and flanking regions (*cpc*BA). *J. Phycol*. 37:810–18.

Bolch, C. J. S, Orr, P. T., Jones, G. J., and Blackburn, S. J. (1999). Genetic, morphological and toxicological variation among globally distributed strains of *Nodularia* (Cyanobacteria). *J. Phycol*. 35:339–55.

Booker, M. J., and Walsby, A. E. (1981). Bloom formation and stratification by a planktonic blue-green alga in an experimental water column. *Br. Phycol. J*. 16:411–21.

Booth, W. E. (1941). Algae as pioneers in plant succession and their importance in erosion control. *Ecology* 22:38–46.

Brasier, M. D., Green, O. R., Jephcoat, A. P., et al. (2002). Questioning the evidence for Earth's oldest fossils. *Nature* 416:76–81.

Brock, T. D. (1973). Lower pH limit for the existence of blue-green algae: Evolutionary and ecological implications. *Science* 179:480–3.

Buick, R. (1992). The antiquity of oxygenic photosynthesis: evidence from stromatolites in sulphate-deficient archaean lakes. *Science* 255:74.

Caiola, M. G. (1975). A light and electron microscopic study of blue-green algae living in the coralloid roots of *Encephalartos altensteinii* and in culture. *Phycologia* 14:25–33.

Canini, A., Bergman, B., Civitareale, P., Rotilla, G., and Caiola, M. G. (1992). Localization of iron-superoxide dismutase in the cyanobiont of *Azolla filiculoides* Lam. *Protoplasma* 169:1–8.

Carmichael, W. W. (1992). Cyanobacteria secondary metabolites – the cyanotoxins. *J. Appl. Bacteriol*. 72:445–59.

Carmichael, W. W., Drapeau, C., and Anderson, D. M. (2000). Harvesting of *Aphanizomenon flos-aquae* Ralfs ex Born. Flah. Var. *flos-aquae* (Cyanobacteria) from Klamath Lake for human dietary use. *J. Appl. Phycol*. 12:585–95.

Carpenter, E. J., and Price, C. C. (1977). Nitrogen fixation, distribution, and production of *Oscillatoria* (*Trichodesmium*) spp. in the western Sargasso and Caribbean seas. *Limnol. Oceanogr*. 22:60–72.

Carpenter, E. J., Capone, D. C., and Reuter, J. (eds.) (1992). *Marine Pelagic Cyanobacteria*: Trichodesmium *and other Diazotrophs*, Dordecht: Kluwer Academic Publishers.

Castenholz, R. W. (1973). Ecology of blue-green algae in hot-springs. In *The Biology of the Blue-Green Algae*, ed. N. G. Carr and B. A. Whitton, pp. 379–414. Berkeley: Univ. Calif. Press.

Chauvat, F., Corre, B., Herdman, M., and Joset-Espardellier, F. (1982). Energetic and metabolic requirements for the germination of akinetes of the cyanobacterium *Nostoc* PCC7524. *Arch. Microbiol*. 133:44–9.

Chen, H. M., Chien, C-Y., and Huang, T-C. (1996). Regulation and molecular structure of a circadian oscillating protein located in the cell membrane of the prokaryote *Synechococcus* RF-1. *Planta* 199:520–7.

Clark, R. L., and Jensen, T. E. (1969). Ultrastructure of akinete development in a blue-green alga, *Cylindrospermum* sp. *Cytologia* 34:439–48.

Cmiech, H. A., Leedale, G. F., and Reynolds, C. S. (1986). Morphological and ultrastructural variability of planktonic Cyanophyceae in relation to seasonal periodicity. II. *Anabaena solitaria*: Vegetative cells, heterocysts, akinetes. *Br. Phycol. J*. 21:81–92.

Codd, G. A., Bell, S. G., Kaya, K., Ward, C. J., Beattie, K. A., and Metcalf, J. S. (1999). Cyanobacterial toxins, exposure routes and human health. *Eur. J. Phycol*. 34:405–15.

Dalton, R. (2002). Microfossils: squaring up over ancient life. *Nature* 417:782–84.

De Philippis, R., and Vincenzini, M. (1998). Extracellular polysaccharides from cyanobacteria and their possible applications. *FEMS Microbiol. Rev*. 22:151–72.

Desikachary, T. V. (1959). *Cyanophyta*. New Delhi: Indian Council of Agricultural Research.

Dill, R. F., Shinn, E. A., Jones, A. T., Kelly, K., and Steinen, R. P. (1986). Giant subtidal stromatolites forming in normal salinity waters. *Nature* 324:55–9.

Dillon, J. G., and Castenholz, R. W. (1999). Scytonemin, a cyanobacterial sheath pigment, protects against UVC radiation: implications for early photosynthetic life. *J. Phycol*. 35:673–81.

Drouet, F. (1937). The Brazilian Myxophyceae. I. *Am. J. Bot*. 24:598–608.

Drouet, F. (1978). Revision of the Nostocaceae with constricted trichomes. *Beihefte Nova Hedwigia* 57:1–258.

Dufresne, A., Salanoubat, M., Partensky, F., et al. (2003). Genome sequence of the cyanobacterium *Prochlorococcus marinus* SS120, a nearly minimal oxyphototrophic genome. *Proc. Natl. Acad. Sci., USA* 100:10020–5.

El-Bestawy, E., Bellinger, E. G., and Sigee, D. C. (1996). Elemental composition of phytoplankton in a subtropical lake: X-ray microanalytical studies on the dominant algae *Spirulina platensis* (Cyanophyta) and *Cyclotella meneghiniana* (Bacillariophyceae). *Eur. J. Phycol*. 31:157–66.

El-Shehawy, R. M., and Kleiner, D. (2003). Effect of controlled expression of *het*Rgene on heterocyst formation in the filamentous cyanobacterium *Anabaena* sp. PCC 7120. *Physiol. Plantarum* 119:44–8.

Ferguson-Wood, E. J. (1965). *Marine Microbial Ecology*. London: Chapman and Hall.

Ferjani, A., Mustardy, L., Sulpice, R., et al. (2003). Glucoglycerol, a compatible solute, sustains cell division under salt stress. *Plant Physiol*. 131:1628–37.

Ferris, M. J., and Palenik, B. (1998). Niche adaptation in ocean cyanobacteria. *Nature* 396:226–8.

Flores, E., and Wolk, C. P. (1986). Production, by filamentous, nitrogen-fixing cyanobacteria, of a bacteriocin and of other antibiotics that kill related strains. *Arch. Microbiol*. 145:215–19.

Fogg, G. E. (1942). Studies on nitrogen fixation by bluegreen algae. I. Nitrogen fixation by *Anabaena cylindrica* Lemm. *J. Exp. Biol*. 19:78–87.

Fogg, G. E. (1952). The production of extracellular nitrogenous substances by a blue-green alga. *Proc. R. Soc. London* [*B*] 139:372–9.

Fogg, G. E. (1986). Light and ultraphytoplankton. *Nature* 319:96.

Frederick, J. F. (1951). Preliminary studies on the synthesis of polysaccharides in the algae. *Physiol. Plant*. 4:621–6.

Fredriksson, C., and Bergman, B. (1997). Ultrastructural characterization of cells specialized for nitrogen function in a non-heterocystous cyanobacterium, *Trichodesmium* spp. *Protoplasma* 197:76–85.

Fulda, S., Mikkat, S., Schroder, W., and Hagemann, M. (1999). Isolation of salt-induced periplasmic proteins from *Synechocystis* sp. strain PCC 6803. *Arch. Microbiol*. 171:214–7.

Gantt, E., and Conti, S. F. (1969). Ultrastructure of blue-green algae. *J. Bacteriol*. 97:1486–93.

Gao, K., and Ye, C. (2003). Culture of the terrestrial cyanobacterium, *Nostoc flagelliforme* (Cyanophyceae), under aquatic conditions. *J. Phycol*. 39:617–22.

Gates, J. E., Fisher, R. W., Goggin, T. W., and Azrolan, N. I. (1980). Antigenic differences between *Anabaena azollae* fresh from the *Azolla* fern leaf cavity and free-living cyanobacteria. *Arch. Microbiol*. 128:126–9.

Gleason, F. K., and Paulson, J. L. (1984). Site of action of the natural algicide, cyanobacterin, in the blue-green alga, *Synechococcus* sp. *Arch. Microbiol*. 138:273–7.

Glover, H. E., Keller, M. D., and Guillard, R. R. L. (1986). Light quality and oceanic ultraphytoplankters. *Nature* 319:142–3.

Golden, S. S. (2003). Timekeeping in bacteria: the cyanobacterial circadian clock. *Curr. Opin. Microbiol*. 6:535–40.

Golubić, S. (1973). The relationship between blue-green algae and carbonate deposits. In *The Biology of the Blue-Green Algae*, ed. N. G. Carr and B. A. Whitton, pp. 434–72. Berkeley: Univ. Calif. Press.

Golubic, S., and Seong-Joo, L. (1999). Early cyanobacterial fossil record: preservation, palaeoenvironments and identification. *Eur. J. Phycol*. 34:339–48.

Goodwin, T. W. (1974). Carotenoids and biliproteins. In *Algal Physiology and Biochemistry*, ed. W. D. P. Stewart, pp. 176–205. Berkeley: Univ. Calif. Press.

Henson, B. J., Watson, L. E., and Barnum, S. R. (2004). The evolutionary history of nitrogen fixation, as assessed by *nif*D. *J. Molec. Evol*. 58:390–9.

Herdman, M., Janvier, M., Rippka, R., and Stanier, R. Y. (1979). Genome size of cyanobacteria. *J. Gen. Microbiol*. 111:73–85.

Hill, D. J. (1975). The pattern of development of *Anabaena* in the *Azolla–Anabaena* symbiosis. *Planta* 122:179–84.

Hockelmann, C., Moens, T., and Juttner, F. (2004). Odor compounds from cyanobacterial biofilms acting as attractants and repellents for free-living nematodes. *Limnol. Oceanogr.* 49:1809–19.

Hoffman, L. (1999). Marine cyanobacteria in tropical regions: diversity and ecology. *Eur. J. Phycol*. 34:371–9.

Hoiczyk, E. (2000). Gliding motility in cyanobacteria: observations and possible explanations. *Arch. Microbiol*. 174:11–17.

Hoiczyk, E., and Baumeister, W. (1995). Envelope structure of four gliding filamentous cyanobacteria. *J. Bacteriol*. 177:2387–95.

Hoiczyk, E., and Baumeister, W. (1998). The junctional pore complex, a prokaryotic secretion organelle, is the molecular motor underlying gliding motility in cyanobacteria. *Curr. Biol*. 8:1161–8.

Honda, D., Yokota, A., and Sugiyama, J. (1999). Detection of seven major evolutionary lineages in cyanobacteria based on the 16S rRNA gene sequence analysis with new sequences of five marine *Synechococcus* strains. *J. Mol. Evol*. 48:723–30.

Hough, L., Jones, J. K. N., and Wadman, W. H. (1952). An investigation of the polysaccharide components of certain fresh-water algae. *J. Chem. Soc*. 3393–9.

Jang, M.-H., Ha, K., Joo, G.-J., and Takamura, N. (2003). Toxin production of cyanobacteria is increased by exposure to zooplankton. *Freshwater Biol.* 48: 1540–5.

Jarosch, R. (1962). Gliding. In *Physiology and Biochemistry of Algae*, ed. R. A. Lewin, pp. 573–81. New York and London: Academic Press.

Jensen, T. E., and Clark, R. L. (1969). Cell wall and coat of the developing akinete of a *Cylindrospermum* species. *J. Bacteriol*. 97:1494–5.

Jones, J. D., and Jost, M. (1970). Isolation and chemical characterization of gas vacuole membranes from *Microcystis aeruginosa* Kuetz. emend Elenkin. *Arch. Mikrobiol*. 70:43–64.

Kapustka, L. A., and DuBois, J. D. (1987). Dinitrogen fixation by cyanobacteria and associative rhizosphere bacteria in the Arapaho prairie in the sand hills of Nebraska. *Am. J. Bot*. 74:107–13.

Karsten, U. (1996). Growth and organic osmolytes of geographically different isolates of *Microcoleus chthonoplastes* (cyanobacteria) from benthic microbial mats: response to salinity changes. *J. Phycol*. 32:501–6.

Konopka, A., Kromkamp, J., and Mur, L. R. (1987). Regulation of gas vesicle content and buoyancy in light- or phosphate-limited cultures of *Aphanizomenon flos-aquae* (Cyanophyta). *J. Phycol*. 23:70–8.

Kotak, B. G., Lam, A. K-Y., Prepas, E. E., Kenefick, S. L., and Hurdey, S. E. (1995). Variability of the hepatotoxin microcystin-LR in hypertrophic drinking water lakes. *J. Phycol*. 31:248–63.

Kulasooriya, S. A., Lang, N. J., and Fay, P. (1972). The heterocysts of blue-green algae. III. Differentiation and nitrogenase activity. *Proc. R. Soc. Lond.* [*B*] 181:199–209.

Lang, N. J., and Fay, P. (1971). The heterocysts of blue-green algae. II. Details of ultrastructure. *Proc. R. Soc. Lond*. [*B*] 178:193–203.

Lawry, N. H., and Simon, R. D. (1982). The normal and induced occurrence of cyanophycin bodies in several blue-green algae. *J. Phycol*. 18:391–9.

Lesser, M. P., Mazel, C. H., Gorbunov, M. Y., and Falkowski, P. G. (2004). Discovery of symbiotic nitrogen-fixing cyanobacteria in corals. *Science* 305:997–1000.

Li, D-M., and Qi, Y-Z. (1997). *Spirulina* industry in China: present status and future prospects. *J. Appl. Phycol*. 9:25–8.

Li, H., Sherman, D., Bao, S., and Sherman, L. A. (2001a). Pattern of cyanophycin accumulation in nitrogen-fixing and non-nitrogen-fixing cyanobacteria. *Arch. Microbiol*. 176:9–18.

Li, R., Watanabe, M., and Watanabe, M. M. (1997). Akinete formation in planktonic *Anabaena* spp. (Cyanobacterium) by treatment with low temperature. *J. Phycol*. 33:576–84.

Li, R., Carmichael, W. W., Britain, S., et al. (2001b). First report of the cyanotoxins cylindrospermopsin and deoxycylindrospermopsin from *Raphidiopsis curvava* (Cyanobacteria). *J. Phycol*. 37:1121–6.

Little, M. G. (1973). The zonation of marine supralittoral blue-green algae. *Br. Phycol. J.* 8:47–50.

Logan, B. W. (1961). Cryptozoon and associate stromatolites from the Recent, Shark Bay, Western Australia. *J. Geol*. 69:517–33.

Lundgren, P., Soderbach, E., Singer, A., Carpenter, E. J., and Bergman, B. (2001). *Katagnymene*: characterization of a novel marine diazotroph. *J. Phycol*. 37:1052–62.

Mague, T. H., and Holm-Hansen, O. (1975). Nitrogen fixation on a coral reef. *Phycologia* 14:87–92.

Marquardt, J., Morschel, E., Rheil, E., and Westermann, M. (2000). Ultrastructure of *Acaryochloris marina*, an oxyphotobacterium containing chlorophyll *d*. *Arch. Microbiol*. 174:181–8.

Mason, C. P., Edwards, K. R., Carlson, R. E., Pignatello, J., Gleason, F. K., and Woods, J. M. (1982). Isolation of

chlorine-containing antibiotic from the freshwater cyanobacterium *Scytonema hofmanni*. *Science* 215:400–2.

McCausland, M. A., Thompson, P. A., and Blackburn, S. L. (2005). Ecophysiological influence of light and mixing on *Anabaena circinalis* (Nostocales, Cyanobacteria). *Eur. J. Phycol*. 40:9–20.

Meeks, J. C. (1998). Symbiosis between nitrogen-fixing cyanobacteria and plants. *BioScience* 48:266–76.

Meeks, J. C., and Castenholz, R. W. (1971). Growth and photosynthesis in an extreme thermophile, *Synechococcus lividus* (Cyanophyta). *Arch. Mikrobiol*. 78:25–41.

Meeks, J. C., and Elhai, J. (2002). Regulation of cellular differentiation in filamentous cyanobacteria in free-living and plant-associated symbiotic growth states. *Microbiol. Mol. Biol. Rev*. 66:94–121.

Meeks, J. C., Campbell, E. L., Summers, M. L., and Wong, F.C. (2002). Cellular differentiation in the cyanobacterium *Nostoc punctiforme*. *Arch. Microbiol*. 178:395–403.

Miller, S. R., Augustine, S., Olson, T. L., Blankenship, R. E., Selker, J., and Wood, A. M. (2005). Discovery of a free-living chlorophyll *d*-producing cyanobacterium with a hybrid proteobacterial/cyanobacterial small-subunit rRNA gene. *Proc. Natl. Acad. Sci., USA* 102:850–5.

Mitsui, A., Kumazawa, S., Takashi, A., Ikemoto, H., Cao, S., and Arai, T. (1986). Strategy by which nitrogen-fixing unicellular cyanobacteria grow photoautotrophically. *Nature* 323:720–2.

Miyashita, H., Ikemoto, H., Kurano, N., Miyachi, S., and Chihara, M. (2003). *Acaryochloris marina* gen. et sp. nov. (cyanobacteria), an oxygenic photosynthetic prokaryote containing chl *d* as a major pigment. *J. Phycol*. 39:1247–53.

Moffet, J. W., and Brand, L. E. (1996). Production of strong, extracellular Cu chelators by marine cyanobacteria in response to Cu stress. *Limnol. Oceanog*. 41:388–95.

Montejano, G., and Leon-Tejera, H. (2002). Reproduction and baeocyte formation in two species of *Dermocarpella* (Cyanophyceae). *Eur. J. Phycol*. 37:323–7.

Monty, C. L. V. (1967). Distribution and structure of recent stromatolite algal mats, eastern Andros Island, Bahamas. *Ann. Soc. Geol. Belg*. 90:55–99.

Moore, D., McGregor, G. B., and Shaw, G. (2004). Morphological changes during akinete germination in *Cylindrospermopsis raciborskii* (Nostocales, Cyanobacteria). *J. Phycol*. 40:1098–105.

Mori, T., Saveliev, S. V., Xu, Y., et al. (2002). Circadian clock protein KaiC forms ATP-dependent hexameric rings and binds DNA. *Proc. Natl. Acad. Sci., USA* 99:17203–8.

Nadeau, T.-L., and Castenholz, R. W. (2000). Characterization of psychrophilic oscillatorians (cyanobacteria) from Antarctic meltwater ponds. *J. Phycol*. 36:914–23.

Nadeau, T.-L., Milbrandt, E. C., and Castenholz, R. W. (2001). Evolutionary relationships of cultivated Antarctic oscillatorians (cyanobacteria). *J. Phycol*. 37:650–4.

Negri, A. P., Jones, G. J., Blackburn, S. I., Oshima, Y., and Hideyuki, O. (1997). Effect of culture bloom development and of sample storage on paralytic shellfish poisons in the cyanobacterium *Anabaena circinalis*. *J. Phycol*. 33:26–35.

Nobles, D. R., Romanovicz, D. K., and Brown, R. M. (2001). Cellulose in cyanobacteria. Origin of plant cellulose synthase? *Plant Physiol*. 127:529–42.

Oliver, R. L. (1994). Floating and sinking in gas-vacuolate cyanobacteria. *J. Phycol*. 30:161–73.

Oliver, R. L., Thomas, R. H., Reynolds, C. S., and Walsby, A. E. (1985). The sedimentation of buoyant *Microcystis* colonies caused by precipitation with an iron-containing colloid. *Proc. R. Soc. Lond*. [*B*] 223:511–28.

Otero, A., and Vincenzini, M. (2004). *Nostoc* (Cyanophyceae) goes nude: extracellular polysaccharides serve as a sink for reducing power under unbalanced C/N metabolism. *J. Phycol*. 40:74–81.

Padan, E. (1979). Facultative anoxygenic photosynthesis in cyanobacteria. *Annu. Rev. Plant Physiol*. 30:27–40.

Palenik, B., and Haselkorn, R. (1992). Multiple evolutionary origins of prochlorophytes, the chlorophyll *b*-containing prokaryotes. *Nature* 355:265–7.

Pandey, D. C. (1965). A study of the algae from paddy soils of Ballia and Ghazipur districts of Uttar Pradesh, India. I. Cultural and ecological considerations. *Nova Hedwigia* 9:299–334.

Partensky, F., Hess, W. R., and Vaulot, D. (1999). *Prochlorococcus*, a marine photosynthetic prokaryote of global significance. *Microbiol. Mol. Biol. Rev*. 63:106–27.

Pascher, A. (1914). Über Symbiosen von Spaltpilzen und Flagellaten mit Blaualgen. *Ber. Dtsch. Bot. Ges*. 32:339–52.

Pentecost, A. (1978). Blue-green algae and freshwater carbonate deposits. *Proc. R. Soc. Lond.* [*B*] 200:43–61.

Peters, G. A., and Mayne, B. C. (1974). The *Azolla, Anabaena azollae* relationship. I. Initial characterization of the association. *Plant Physiol*. 53:813–19.

Pignatello, J. J., Porwoll, J., Carlson, R. E., Xavier, A., Gleason, F. K., and Wood, J. M. (1983). Structure of the antibiotic cyanobacterin, a chlorine containing

γ-lactone from the freshwater cyanobacterium *Scytonema hofmanni*. *J. Org. Chem*. 48:4035–8.
Postius, C., and Ernst, A. (1999). Mechanisms of dominance: coexistence of picocyanobacterial genotypes in a freshwater ecosystem. *Arch. Microbiol*. 172:69–75.
Potts, M. (1996). The anhydrobiotic cyanobacterial cell. *Physiologia Plantarum* 97:788–94.
Potts, M. (1999). Mechanisms of desiccation tolerance in cyanobacteria. *Eur. J. Phycol*. 34:319–28.
Potts, M., Angeloni, S. V., Ebel, R. E., and Bassam, D. (1992). Myogloblin in a cyanobacterium. *Science* 256:1690–2.
Prescott, G. W. (1962). *Algae of the Western Great Lakes Area*. Dubuque, Iowa: W. C. Brown.
Qiu, B. S., Zhang, A. H., Liu, Z. L., and Gao, K. S. (2004). Studies on the photosynthesis of the terrestrial cyanobacterium *Nostoc flagelliforme* subjected to desiccation and subsequent rehydration. *Phycologia* 43:521–8.
Raikow, D. F., Sarnelle, O., Wilson, A. E., and Hamilton, S. K. (2004). Dominance of the noxious cyanobacterium *Microcystis aeruginosa* on low-nutrient lakes associated with exotic zebra mussels. *Limnol. Oceanog*. 49:482–7.
Rascher, U., Lakatos, M., Budel, B., and Luttge, U. (2003). Photosynthetic capacity of cyanobacteria of a tropical inselberg of the Guiana Highlands. *Eur. J. Phycol*. 38:247–56.
Raymond, J., Siefert, J. L., Staples, C. R., and Blankenship, R.E. (2004). The natural history of nitrogen fixation. *Mol. Biol. Evol*. 21:541–54.
Reid, R. P., Visscher, P. T., Decho, A. W., et al. (2000). The role of microbes in accretion, lamination and early lithification of modern marine stromatolites. *Nature* 406:989–92.
Rinehart, K. L., Namikoshi, M., and Choi, B. W. (1994). Structure and biosynthesis of toxins from blue-green algae (cyanobacteria). *J. Appl. Phycol*. 6:159–76.
Rippka, R., Waterbury, J., and Cohen-Bazire, G. (1974). A cyanobacterium which lacks thylakoids. *Arch. Mikrobiol*. 100:419–36.
Romans, K. M., Carpenter, E. J., and Bergman, B. (1994). Buoyancy regulation in the colonial diazotrophic cyanobacterium *Trichodesmium tenue*, ultrastructure and storage of carbohydrate, polyphosphate, and nitrogen. *J. Phycol*. 30:935–42.
Schutz, K., Happe, T., Troshina, O., et al. (2004). Cyanobacterial H_2 production – a comparative analysis. *Planta* 218:350–9.
Sherman, D. M., Tucker, D., and Sherman, L. A. (2000). Heterocyst development and localization of cyanophycin in N_2-fixing cultures of *Anabaena* sp. PCC 7120 (Cyanobacteria). *J. Phycol*. 36:932–41.
Singh, R. N. (1961). *The Role of Blue-Green Algae in Nitrogen Economy of Indian Agriculture*. New Delhi: Indian Council for Agricultural Research.
Smith, D. C., Muscatine, L., and Lewis, D. (1970). Carbohydrate movement from autotrophs to heterotrophs in parasitic and mutalistic symbiosis. *Biol. Rev.* 44:17–90.
Smith, G. M. (1950). *Freshwater Algae of the United States*. New York: McGraw-Hill.
Smith, G. M. (1955). *Cryptogamic Botany*. Vol. 1. New York: McGraw-Hill.
Spencer, C. N., and King, D. L. (1985). Interactions between light. NH_4^+, and CO_2 in buoyancy regulation of *Anabaena flos-aquae* (Cyanophyceae). *J. Phycol*. 21:194–9.
Spratt, E. R. (1915). The root nodules of the Cycadaceae. *Ann. Bot*. 29:619–26.
Staal, M., Meysman, F. J. R., and Stal, L. J. (2003). Temperature excludes N_2-fixing heterocystous cyanobacteria in the tropical oceans. *Nature* 425:504–7.
Stanier, R. Y. (1973). Autogrophy and heterotrophy in unicellular blue-green algae. In *The Biology of the Blue-Green Algae*, ed. N. G. Carr and B. A. Whitton, pp. 501–18. Berkeley: Univ. Calif. Press.
Stewart, W. D. P., and Pearson, H. W. (1970). Effects of aerobic and anaerobic conditions on growth and metabolism of blue-green algae. *Proc. R. Soc. Lond*. [*B*] 175:293–311.
Storey, W. B. (1968). Somatic reduction in cycads. *Science* 159:648–50.
Sukenik, A., Eshkol, R., Livine, A., and Hadas, O. (2002). Inhibition of growth and photosynthesis of the dinoflagellate *Peridinium gatunense* by *Microcystis* sp. (cyanobacteria): a novel allelopathic mechanism. *Limnol. Ocean*. 47:1656–63.
Suttle, C. A., and Chan, A. M. (1994). Dynamics and distribution of cyanophages and their effect on marine *Synechococcus* spp. *Appl. Env. Microbiol*. 60:3167–74.
Swaminathan, M. S. (1984). Rice. *Sci. Am*. 250(1):80–93.
Tandeau de Marsac, N. (1977). Occurrence and nature of chromatic adaptation in cyanobacteria. *J. Bacteriol*. 130:82–91.
Tang, E. P. Y., Tremblay, R., and Vincent, W. F. (1997). Cyanobacterial dominance of polar freshwater ecosystems: are high-latitude mat-formers adapted to low temperature? *J. Phycol*. 33:171–81.
Terauchi, K., and Ohmori, M. (2004). Blue light stimulates cyanobacterial motility via a cAMP signal transduction system. *Mol. Microbiol*. 52:303–9.

Tischer, I. (1957). Untersuchungen über die granulären Eihschlüsse und das Reduktions-Oxydations-Vermögen der Cyanophyceen. *Arch. Mikrobiol*. 27:400–28.

Turner, S. (1997). Molecular systematics of oxygenic photosynthetic bacteria. *Pl. Syst. Evol.* (*Suppl*). 11:13–52.

Turpin, D. H., Miller, A. G., and Canvin, D. T. (1984). Carboxysome content of *Synechococcus leopoliensis* (Cyanophyta) in response to organic carbon. *J. Phycol*. 20:249–53.

Urback, E., Robertson, D. L., and Chisholm, S. W. (1992). Multiple evolutionary origins of prochlorophytes within the cyanobacterial radiation. *Nature* (*Lond.*) 355:267–70.

Vaishampayan, A., Sinha, R. P., Hader, D.-P., et al. (2001). Cyanobacterial biofertilizers in rice agriculture. *Bot. Rev*. 67:453–516.

van Dok, W., and Hart, B. T. (1995). Akinete differentiation in *Anabaena circinalis* (Cyanophyta). *J. Phycol*. 32:557–65.

Vanyo, J. P., and Awramik, S. M. (1985). Stromatolites and earth–sun–moon dynamics. *Precambrian Res*. 29:121–42.

Wall, D., and Kaiser, D. (1999). Type IV pili and cell motility. *Mol. Microbiol*. 32:1–10.

Walsby, A. E. (1974). The extracellular products of *Anabaena cylindrica* Lemm. I. Isolation of a macromolecular pigment–peptide complex and other components. *Br. Phycol. J.* 9:371–81.

Walsby, A. E. (1978). The properties and buoyancy-providing role of gas vacuoles in *Trichodesmium* Ehrenberg. *Br. Phycol. J*. 13:103–16.

Walsby, A. E. (1994). Gas vesicles. *Microbiol. Rev*. 58:94–144.

Watanabe, A., and Kiyohara, T. (1963). Symbiotic blue-green algae of lichens, liverworts and cycads. In *Studies on Microalgae and Photosynthetic Bacteria*, ed. Japanese Soc. Plant Physiologists, pp. 189–96. Tokyo: University of Tokyo Press.

Watanabe, M. F., Tsuujimura, S., Oishi, S., Niki, T., and Namikoshi, M. (2003). Isolation and identification of homoanatoxin-a from a toxic strain of the cyanobacterium *Raphidiopsis mediterranea* Skuja isolated from Lake Biwa, Japan. *Phycologia* 42:364–9.

Waterbury, J., and Stanier, R. (1977). Two unicellular bacteria which reproduce by budding. *Arch. Microbiol*. 115:249–57.

Watson, S. B. (2003). Cyanobacterial and eukaryotic algal odour compounds: signals or by-products? A review of their biological activity. *Phycologia* 42:332–50.

Weckesser, J., Broll, C., Adhikary, S. P., and Jürgens, U. J. (1987). 2-*O*-methyl-D-xylose containing sheath in the cyanobacterium *Gloeothece* sp. PCC 6501. *Arch. Microbiol*. 147:300–3.

Weller, D., Doemel, W., and Brock, T. D. (1975). Requirement of low oxidation-reduction potential for photosynthesis in a blue-green alga (*Phormidium* sp.). *Arch. Mikrobiol*. 104:7–13.

Whale, G. F., and Walsby, A. E. (1984). Motility of the cyanobacterium *Microcoleus chthonoplastes* in mud. *Br. Phycol. J.* 19:117–23.

Whitton, B. A., and Peat, A. (1969). On *Oscillatoria redekei* Van Goor. *Arch. Mikrobiol*. 68:362–76.

Wildman, R. B., Loescher, J. H., and Winger, C. L. (1975). Development and germination of akinetes of *Aphanizomenon flos-aquae*. *J. Phycol*. 11:96–104.

Wilhelm, S. W., Maxwell, D. P., and Trick, C. G. (1996). Growth, iron requirements, and siderophore production in iron-limited *Synechococcus* PCC 7002. *Limnol. Oceanog*. 41:89–97.

Williams, S. B., Vakonakis, I., Golden, S. G., and LiWang, A. C. (2002). Structure and function from the circadian clock protein KaiA of *Synechococcus elongatus*: a potential clock input mechanism. *Proc. Nat. Acad. Sci., USA* 99:15357–62.

Wilson, W. H., Carr, N. G., and Mann, N. H. (1996). The effect of phosphate status on the kinetics of cyanophage infection in the oceanic cyanobacterium *Synechococcus* sp. WH 7803. *J. Phycol*. 32:506–16.

Winkenbach, F., and Wolk, C. P. (1973). Activities of enzymes of the oxidative and the reductive pentose phosphate pathways in heterocysts of a blue-green alga. *Plant Physiol., Lancaster* 52:480–3.

Zhao, Y., Shi, Y., Zhao, W., et al. (2005). CcbP, a calcium-binding protein from *Anabaena* sp. PCC 7120, provides evidence that calcium ions regulate heterocyst differentiation. *Proc. Natl. Acad. Sci., USA* 16:5744–8.

Part III

Evolution of the chloroplast

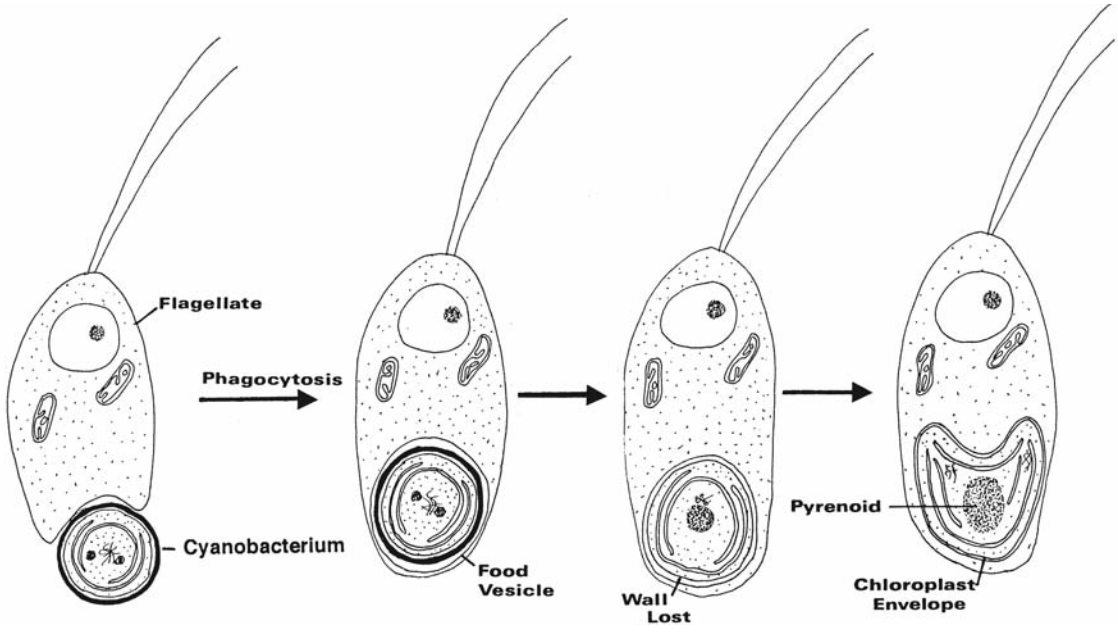


Fig. III.1 Diagrammatic representation of the uptake of a cyanobacterium by a protozoan into a food vesicle. This resulted in the establishment of an endosymbiosis between the cyanobacterium and the protozoan. Through evolution, the endosymbiotic cyanobacterium evolved into a chloroplast surrounded by two membranes of the chloroplast envelope.

The Rhodophyta (red algae) and Chlorophyta (green algae) form a natural group of algae in that they have chloroplasts surrounded by only the two membranes of the chloroplast envelope. The evolutionary event that led to the chloroplast occurred as follows (Fig. III.1). A phagocytotic protozoan took up a cyanobacterium into a food vesicle. Instead of being digested as a source of food, the cyanobacterium lived as an endosymbiont in the protozoan. This event benefited the protozoan because it received some of the photosynthate from the endosymbiotic alga, and it benefited the cyanobacterium because it received a protected stable environment. Through evolution the wall of the endosymbiotic

cyanobacterium was lost. A mutation in the endosymbiont which resulted in a loss of the wall would have been selected for in evolution because it would have facilitated the transfer of compounds between the host and the endosymbiont. The food vesicle membrane of the phagocytotic host became the outer membrane of the chloroplast envelope. The plasma membrane of the cyanobacterium symbiont became the inner membrane of the chloroplast envelope. Rearrangement of the thylakoid membranes and evolution of polyhedral bodies into a pyrenoid completed the transition to a true chloroplast such as occurs in extant green and red algae.

The endosymbiotic origin of chloroplasts was first proposed by the Russian biologist Konstantin Mereschkowsky (1855–1921) (Fig. III.2) with the fundamentals of the idea appearing in his 1905 work, *The Nature and Origins of Chromatophores in the Plant Kingdom* (see Martin and Kowallik, 1999, for English translation). Mereschkowsky worked on the symbiosis between algae and fungi in lichens around the city of Kazan and this led him to his theory on endosymbiosis. He likened plastids to "little green slaves" working for their host cells to produce food from sunshine.

Subsequent cytological and biochemical studies have reinforced Mereschkowsky's theory of an endosymbiotic origin of plastids. Nucleotide sequencing (either directly from rRNA or from DNA encoding rRNAs) has shown the similarity between cyanobacteria and plastids. It has further shown that all plastids evolved from a single endosymbiotic event (McFadden, 2001; Keeling, 2004).



Fig. III.2 **Konstantin Mereschkowsky** Born August 4, 1855 in Warsaw, Poland (then part of Russia). Died by suicide in the Hotel des Familles, Geneva, Switzerland, on January 9, 1921. His father was a high official in the court of the Czar. He was the eldest son, having five brothers and three sisters. He entered the University of St. Petersburg in 1875, where he graduated with the diploma of *Kandidat* (with distinction) in 1880. In 1883 he became a *Privatdocent* at the same university. In 1883 he married Sultanova Olga Petronina by whom he had a son, Boris. From 1881 to 1898 he worked as a pomologist on fruit trees in the Crimea. In 1898 he left his wife and son to a life of poverty and traveled to the United States where he did research on unicellular algae (which he started when he was in the Crimea) at the University of California, Berkeley.

In 1902 he returned to Russia and took the position of curator of the zoology museum at Kazan University. In 1903 he passed his *Magister* with a dissertation "On the Morphology of Diatoms." At that time Mereschkowsky's research was influenced by Andrei Famintsyn, at the University of St. Petersburg, who was trying to cultivate chloroplasts isolated from zooxanthellae. Famintsyn was, however, not interested in having a younger competitor and denigrated Mereschkowsky's research, resulting in bad relations between the two. In 1905 Mereschkowsky published his famous paper in Russian and German "On the Nature and Origin of Chromatophores in the Plant Kingdom." In 1920, in Geneva, he published his most extensive paper on the endosymbiotic origin of chloroplasts "La plant considérée comme un complexe symbiotique."

Mereschkowsky's personal life was a disaster. As a student he had revolutionary ideas. However, by the turn of the century he was a collaborator of the Czar's secret police. He was one of the organizers of the nationalistic, anti-Semitic organization "The Kazan Department of the Union of Russian People." Several of his colleagues were discharged after his denunciations. Mereschkowsky was forced to leave Russia in 1914, not because of his political views, but because of a sex scandal involving pedophilic activities between 1905 and 1914 with 26 young girls. The public scandal was nationwide. He fled to France in February 1918 and finally took refuge in Switzerland. Near the end of his life he lamented that his theory on the symbiotic origin of chloroplast "had made little headway" and that it was "often completely ignored." This was compounded by "finally the war, the revolution." After a particularly odious exchange with R. Chodat, Professor of Botany at the University of Geneva, who prevented Mereschkowsky from speaking, Mereschkowsky commented "One day history will remember me." On Sunday, January 9, 1921, having run out of money, and after paying all his hotel bills, he committed suicide by gassing himself with chloroform. Thus passed away at 65 years of age the most famous evolutionary botanist of the century. For a well written and researched biography of Mereschkowsky see Sapp et al. (2002).

REFERENCES

Keeling, P. J. (2004). Diversity and evolutionary history of plastids and their hosts. *Amer. J. Bot.* 91:1481–93.

Martin, W., and Kowallik, K. V. (1999). Annotated English translation of Mereschkowsky's 1905 paper Uber Natur und Ursprung der Chromatophoren im Pflanzenreiche. *Eur. J. Phycol.* 34:287–95.

McFadden, G. I. (2001). Primary and secondary endosymbiosis and the origin of plastids. *J. Phycol*. 37:951–9.

Mereschkowsky, C. (1905). Uber Natur und Ursprung der Chromatophoren im Pflanzenreiche. *Biol. Zentralbl.* 25:593–604.

Sapp, J., Carrapico, F., and Zolotonosov, M. (2002). Symbiogenesis: the hidden face of Constantin Merezhkowsky. *Hist. Phil. Life Sci*. 24:414–40.

Chapter 3

Glaucophyta

The Glaucophyta include those algae that have endosymbiotic cyanobacteria in the cytoplasm instead of chloroplasts. Because of the nature of their symbiotic association, they are thought to represent intermediates in the evolution of the chloroplast. The endosymbiotic theory of chloroplast evolution, first proposed by Mereschkowsky in 1905, is the one most widely accepted. According to this theory, a cyanobacterium was taken up by a phagocytic organism into a food vesicle. Normally the cyanobacterium would be digested by the flagellate, but by chance a mutation occurred, with the flagellate being unable to digest the cyanobacterium. This was probably a beneficial mutation because the cyanobacterium, by virtue of its lack of feedback inhibition, secreted considerable amounts of metabolites to the host flagellate. The flagellate in turn gave the cyanobacterium a protected environment, and the composite organism was probably able to live in an ecological niche where there were no photosynthetic organisms (i.e., a slightly acid body of water where free-living cyanobacteria do not grow; see Chapter 2). Pascher (1914) coined terms for this association; he called the endosymbiotic cyanobacteria **cyanelles**; the host, a **cyanome**; and the association between the two, a **syncyanosis**. In the original syncyanosis the cyanelle had a wall around it. Because the wall slowed the transfer of compounds from the cyanelle to the host and vice versa, any mutation that resulted in a loss of wall would have been beneficial and selected for in evolution. Most of the cyanelles in the Glaucophyta lack a wall and are surrounded by two membranes – the old food vesicle membrane of the cyanome and the plasma membrane of the cyanelle. As evolution progressed, these two membranes became the chloroplast envelope, the cyanome cytoplasm took over the formation of the storage product and the polyhedral bodies containing ribulose-1,5-bisphosphate carboxylase/oxygenase differentiated into the pyrenoid.

There are a number of similarities between cyanobacteria and chloroplasts that support the endosymbiotic theory: (1) they are about the same size; (2) they evolve oxygen in photosynthesis; (3) they have 70S ribosomes; (4) they contain circular prokaryotic DNA without basic proteins; (5) nucleotide sequencing of rRNA or of DNA encoding rRNAs have shown similarities; (6) they have chlorophyll *a* as the primary photosynthetic pigment.

The pigments of the Glaucophyta are similar to those of the Cyanophyceae: both chlorophyll *a* and the phycobiliproteins are present; however, two of the cyanobacterial carotenoids, myxoxanthophyll and echinenone, are absent (Chapman, 1966).

Although similar to cyanobacteria, the cyanelles should be regarded as organelles rather than endosymbiotic cyanobacteria (Helmchen et al., 1995; McFadden, 2001). Cyanobacteria have over 3000 genes whereas cyanelles have about the same number of genes as plastids (about 200 genes). It is clear the cyanelles (and plastid) genomes have undergone substantial reduction

during endosymbiosis. Many of the missing genes eventually relocated to the nucleus, while other genes were lost – made redundant in the cyanelles' new role as an endosymbiont. For example, cyanobacteria have a respiratory electron-chain whereas plastids do not, the respiratory electron-chain is coded by the nucleus in eukaryotic algae.

The organisms in the Glaucophyta are very old; McFadden (2001) calls them the coelocanths of endosymbiosis. The Glaucophyta probably branched off the evolutionary tree before the divergence of red and green algae from one another (Keeling, 2004).

The fact that in such syncyanoses one is dealing with composite organisms that exhibit features altogether new and no longer characteristic of either partner alone, led Skuja in 1954 to establish the phylum Glaucophyta. It must be appreciated that the organisms in the phylum represent a very old group, and that, when evolving, they were very plastic and undergoing a great deal of change in the attempt to reach the relatively stable level of a cell with a chloroplast. Such a dynamic group was formed consisting of a large number of organisms not well suited to compete with their more highly developed progeny. Such a situation led to the demise of many of the original members of the Glaucophyta, resulting in the existence today of few extant members of the group.

Cyanophora paradoxa is a freshwater flagellate with two cyanelles in the protoplasm, each cyanelle with a central dense body (Fig. 3.1(*a*)). Nitrate reduction, photosynthesis, and respiration in the cyanelles of *Cyanophora paradoxa* are similar to the corresponding processes of chloroplasts and dissimilar to those of cyanobacteria (Floener and Bothe, 1982; Floener et al., 1982). This fact is cited as evidence that the cyanelles of *Cyanophora paradoxa* are close to chloroplasts in evolution. However, the cyanelles of *Cyanophora paradoxa* are primitive in regard to where ribulose-1,5-bisphosphate carboxylase/oxygenase is produced. Ribulose-1,5-bisphosphate carboxylase/oxygenase, the carbon dioxide-fixing enzyme in photosynthesis, consists of 16 subunits, 8 large and 8 small. In higher plants the large subunits are encoded by DNA of the plastids, whereas the small subunits are encoded by nuclear DNA. In *Cyanophora paradoxa*, both sizes of subunits are encoded by cyanelle DNA. This non-cyanobacterial ribulose-1,5-bisphosphate carboxylase/oxygenase in cyanelles is now rationalized as lateral gene transfer or gene substitution from a mitochondrion or plastid (McFadden, 2001). The mechanism of division of cyanelles in *Cyanophora paradoxa* is intermediate between the division of cyanobacteria and that of plastids. Plastids have an inner and outer ring of electron-dense material in the area of the dividing organelle. In division of cyanelles of *Cyanophora paradoxa*, however, there is only an inner ring in the "stroma" inside the plasma membrane ("inner envelope") of the cyanelle. The outer ring, normally outside the outer chloroplast envelope, is missing (Fig. 3.2) (Iino and Hashimoto, 2003).

Glaucocystis is also a freshwater organism, found sparingly in soft-water lakes (lakes low in calcium). It has two groups of cyanelles, one on each side of the nucleus (Fig. 3.1(*b*)). The derivation of *Glaucocystis* from a biflagellate ancestor is evident from the two reduced flagella found inside the cell wall. Both of these organisms have starch formed in the cytoplasm, outside of the cyanelles, indicating that the host has accepted responsibility for the formation of the storage product.

There are other organisms that have endosymbiotic cyanobacteria that are not placed in the Glaucophyta because they represent evolutionary dead ends that did not lead to the evolution of chloroplasts. These organisms have cyanelles that still have a cell wall and are cytologically similar to cyanobacteria, such as the cyanelles of the fungus *Geosiphon* (Schnepf, 1964).

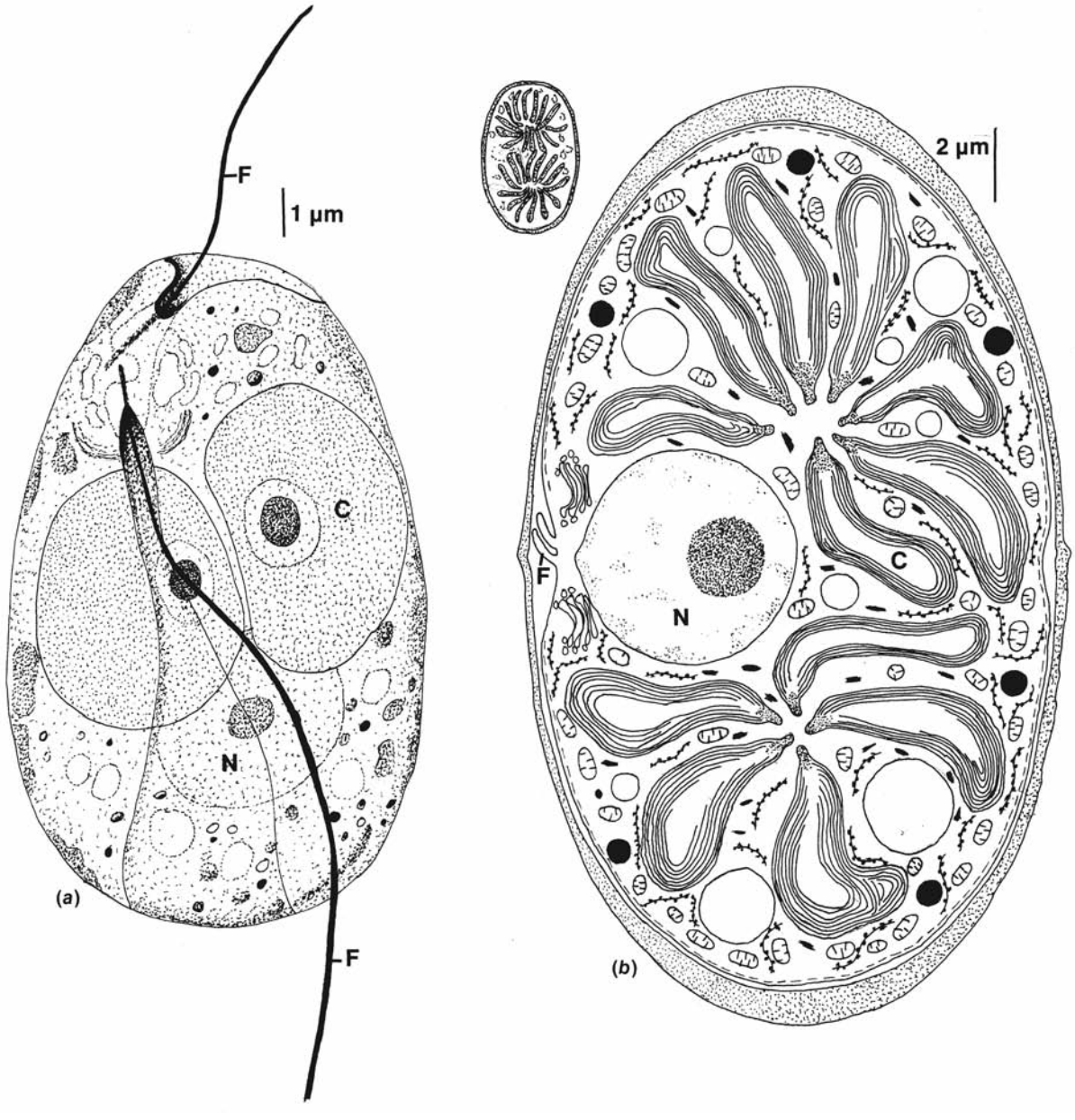


Fig. 3.1 (*a*) *Cyanophora paradoxa* with two cyanelles (C), nucleus (N), and flagella (F). (*b*) Semidiagrammatic drawing of a cell of *Glaucocystis nostochinearum* showing two groups of cyanelles (C), reduced flagella (F), and a nucleus (N). ((*a*) after Mignot et al., 1969; (*b*) after Schnepf et al., 1966.)

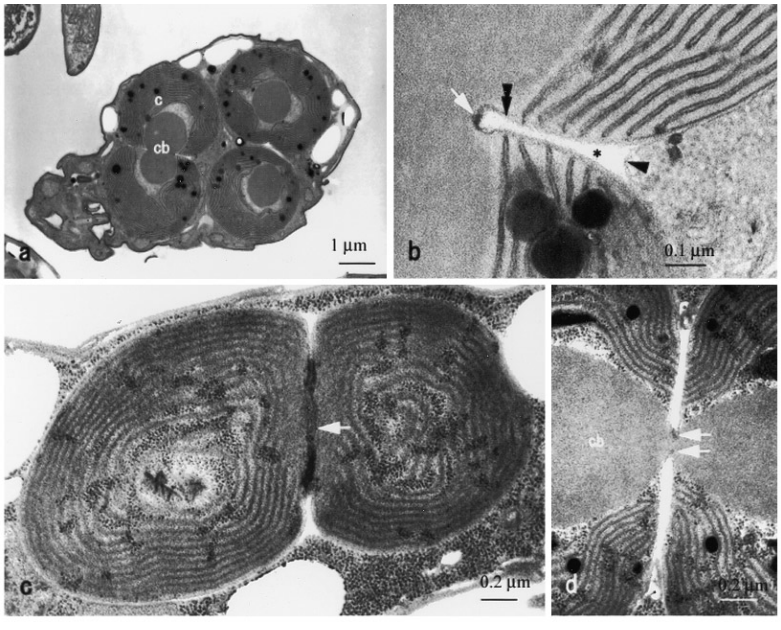


Fig. 3.2 Transmission electron micrographs of sections of dividing cells of *Cyanophora paradoxa*. (*a*) whole cell. (c) Cyanelle; (cb) central body. (*b*) A cross section of a division site with a septum (asterisk) dividing the inner envelope (double arrowhead) and the outer envelope (arrowhead). A cross section of an electron-dense cyanelle ring is seen at the leading edge of the inner envelope (arrow). (*c*) A moderately constricting cyanelle with a cyanelle ring (arrow) observed in a tangential section. (*d*) A deeply constricting division site. At the constricting neck, a pair of cross sections of a cyanelle ring is seen (arrow). (From Iino and Hashimoto, 2003.)

REFERENCES

Chapman, D. J. (1966). Pigments of the symbiotic algae (cyanomes) of *Cyanophora paradoxa* and *Glaucocystis nostochinearum* and two Rhodophyceae, *Porphyridium aeruginosa* and *Asterocytis ramosa*. *Arch. Mikrobiol*. 55:17–25.

Floener, L., and Bothe, H. (1982). Metabolic activities in *Cyanophora paradoxa* and its cyanelles. II. Photosynthesis and respiration. *Planta* 156:78–83.

Floener, L., Danneberg, G., and Bothe, H. (1982). Metabolic activities in *Cyanophora paradoxa* and its cyanelles. I. The enzymes of assimilatory nitrate reduction. *Planta* 156:70–7.

Helmchen, T. A., Bhattacharya, D., and Melkonian, M. (1995). Analysis of ribosomal RNA sequences from glaucocystophyte organelles provide new insights into the evolutionary relationships of plastids. *J. Mol. Evol*. 41:203–10.

Iino, M., and Hashimoto, H. (2003). Intermediate features of cyanelle division of *Cyanophora paradoxa* (Glaucocystophyta) between cyanobacterial and plastid division. *J. Phycol*. 39:561–9.

Keeling, P. J. (2004). Diversity and evolutionary history of plastids and their hosts. *Amer. J. Bot*. 91:1481–93.

McFadden, G. I. (2001). Primary and secondary endosymbiosis and the origin of plastids. *J. Phycol*. 37:951–9.

Mereschkowsky, C. (1905). Ueber Natur und Ursprung den Chromatophoren in Pflanzenreich. *Biol. Zentralbl*. 25:593–604.

Mignot, J. P., Joyon, L., and Pringsheim, E. G. (1969). Quelques particularités structurales de *Cyanophora paradoxa* Korsch., protozoaire flagellé. *J. Protozool*. 16:138–45.

Pascher, A. (1914). Uber Symbiosen von Spaltpilzen und Flagellaten. *Ber. Dtsch. Bot. Ges*. 32:339–52.

Schnepf, E. (1964). Zur Feinstruktur von *Geosiphon pyriforme*. Ein Versuch zur Deutung cytoplasmatischer Membranen und Kompartimente. *Arch. Mikrobiol*. 49:112–31.

Schnepf, E., Koch, W., and Deichgräber, G. (1966). Zur Cytologie und taxonomischen Einordnung von *Glaucocystis*. *Arch. Mikrobiol*. 55:149–74.

Skuja, H. (1954). Glaucophyta. In *Syllabus der Pflanzenfamilien*, by A. Engler, ed. H. Melchoir, and E. Werdermann, Vol. 1, pp. 56–7. Berlin: Borntraeger.

Chapter 4

Rhodophyta

RHODOPHYCEAE

The Rhodophyceae, or **red algae**, comprise the only class in the division Rhodophyta. The Rhodophyceae are probably one of the oldest groups of eukaryotic algae. The red algae are most likely directly descended from a cyanome in the Glaucophyta (see Chapter 3). It is likely that the first red alga evolved into an ecological niche that was unoccupied by cyanobacteria, the only extant photosynthetic alga that evolved oxygen. This ecological niche would have been in waters with a pH less than 5, which, for some unknown reason, cyanobacteria are not able to inhabit (Brock, 1973). Indeed, modern phylogenetic studies utilizing nucleic-acid sequencing have shown that *Cyanidium*, an alga that lives in acidic waters, is probably the oldest extant red alga (Oliveira and Bhattacharya, 2000).

The Rhodophyceae lack flagellated cells, have chlorophyll *a*, phycobiliproteins, floridean starch as a storage product, and thylakoids occurring singly in the chloroplast.

A majority of the seaweeds are red algae, and there are more Rhodophyceae (about 4000 species) than all of the other major seaweed groups combined. Although marine red algae occur at all latitudes, there is a marked shift in their abundance from the equator to colder seas. There are few species in polar and subpolar regions where brown and green algae predominate, but in temperate and tropical regions they far outnumber these groups. The average size of the plants also differs according to geographical region. The larger species of fleshy red algae occur in cool-temperate areas, whereas in tropical seas the Rhodophyceae (except for massive calcareous forms) are mostly small, filamentous plants. The Rhodophyceae also have the ability to live at greater depths in the ocean than do members of the other algal classes. They live at depths as great as 200 m, an ability related to the function of their accessory pigments in photosynthesis. About 200 species of Rhodophyceae are found in freshwater, where they do not reach as great a size as the red seaweeds (Skuja, 1938). The majority of freshwater red algae occur in running waters of small to mid-sized streams (Sheath and Hambrook, 1988). Few red algae occur at currents of less than 30 cm s^{-1}. This fast flow probably favors red algae because loosely attached competitors are washed out and because of a constant replenishment of nutrients and gases.

Cell structure

The major features of a red algal cell (Fig. 4.1) are a chloroplast with one thylakoid per band and no chloroplast E.R., floridean starch grains in the cytoplasm outside the chloroplast, no flagella, pit connections between cells in filamentous genera, and a eukaryotic type of nucleus (Scott et al., 1980).

Cell walls

Cellulose forms the microfibrillar framework in most rhodophycean cell walls, although in the

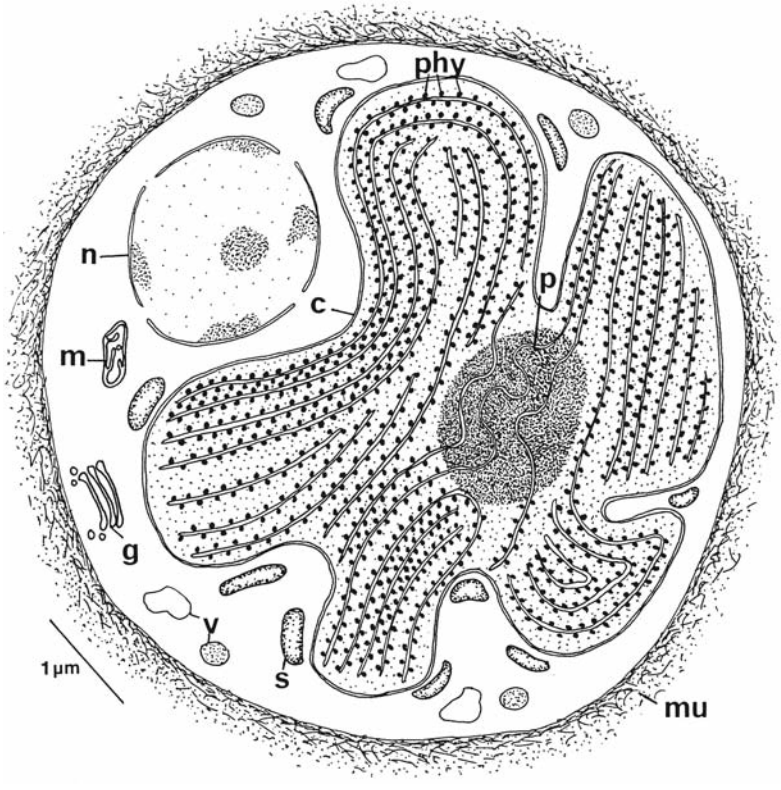


Fig. 4.1 Semidiagrammatic drawing of a cell of *Porphyridium cruentum*. (c) Chloroplast; (g) Golgi; (m) mitochondrion; (mu) mucilage; (n) nucleus; (p) pyrenoid; (phy) phycobilisomes; (s) starch; (v) vesicle. (Adapted from Gantt and Conti, 1965.)

haploid phase of the Bangiales (*Bangia* and *Porphyra*) a β-1,3 linked xylan (polysaccharide composed of xylose residues) performs this function (Frei and Preston, 1964). Unicellular red algae have an amorphous matrix of sulfated polysaccharides without cellulose surrounding the cells (Arad et al., 1993). The amorphous polysaccharides or mucilages occur between the cellulose microfibrils in the rest of the red algae. The two largest groups of amorphous mucilages are the **agars** (Fig. 1.11) and the **carrageenans** (Fig. 4.15). These mucilages may constitute up to 70% of the dry weight of the cell wall. Cuticles, composed mostly of protein, can occur outside the cell wall (Craigie et al., 1992).

Chloroplasts and storage products

Chloroplasts are usually stellate with a central pyrenoid in the morphologically simple Rhodophyceae (Fig. 4.1), whereas in the remainder of the Rhodophyceae they are commonly discoid (Fig. 4.3). In the Rhodophyceae with apical growth, the chloroplasts usually originate from small colorless proplastids with few thylakoids in the apical cell (Lichtlé and Giraud, 1969). Chloroplasts are surrounded by the two membranes of chloroplast envelope with no chloroplast endoplasmic reticulum present (Figs. 4.1, 4.2, 4.3). Thylakoids occur singly inside the chloroplasts. The phycobilin pigments are localized into phycobilisomes on the surface of the thylakoids, a situation similar to that in the cyanobacteria.

Chlorophyll *a* is in the chloroplasts. There have been erroneous reports of chlorophyll *d* occurring in the chloroplast. It has been shown that the chlorophyll *d* in these studies came from the cyanobacterium *Acaryochloris marina*, an epiphyte on red algae (Murakami et al., 2004).

The phycobiliproteins include R-phycocyanin, allophycocyanin, and three forms of phycoerythrin, the phycoerythrins being present in the greatest amount, giving the algae their pinkish color. B-phycoerythrin is present in the more primitive red algae and has been found in *Pophyridium* (Fig. 4.1), *Rhodosorus* (Fig. 4.24 (*a*)), *Rhodochorton* (Fig. 4.31) and *Smithora*. R-phycoerythrin occurs in most higher red algae, and C-phycoerythrin occurs in

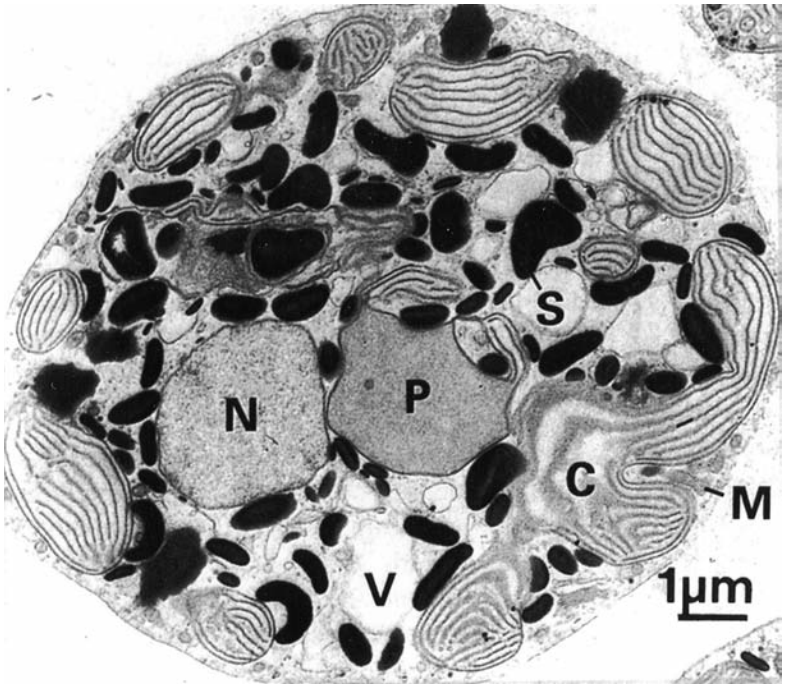


Fig. 4.2 Transmission electron micrograph of a section of a cell of *Rhodella violacea*. (C) Chloroplast; (M) mitochondrion; (N) nucleus; (P) pyrenoid; (S) starch; (V) vacuole. (From Marquardt et al., 1999.)

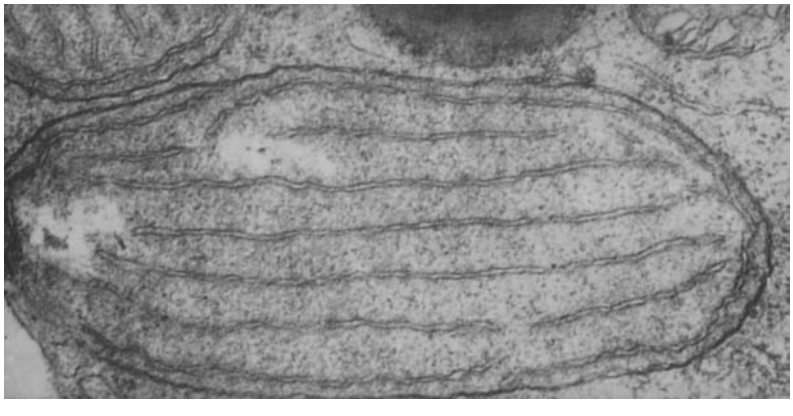


Fig. 4.3 Chloroplast in a carpospore of *Polysiphonia*. (From Tripodi, 1974.)

Porphyridium (Fig. 4.1), *Porphyra* (Fig. 4.27), and *Polysiphonia* (Figs. 4.44, 4.45). The phycobiliproteins are in phycobilisomes on the surface of thylakoids (Fig. 4.1). The phycobilisomes are spherical if both phycoerythrin and phycocyanin are present. The phycobilisomes are discoid if only phycocyanin is present (Gantt, 1969).

Complementary chromatic adaptation occurs in the red algae. Orange and red light stimulate the production of long-wavelength absorbing phycocyanin, while green light stimulates the formation of short-wavelength absorbing phycoerythrin (Sagert and Schubert, 1995). The color will vary.

Floridoside (O-α-D-galactopyranosyl-(1,2)-glycerol) is the major product of photosynthesis in the red algae, although mannitol, sorbitol, digeneaside, and dulcitol also occur (Fig. 4.4) (Barrow et al., 1995; Karsten et al., 2003). The concentration of floridoside increases in red algal cells as the salinity of the medium increases (Reed, 1985). This change in floridoside concentration is thought to compensate, at least in part, for the changes in external osmolarity, thereby preventing water from leaving the algal cells as the salinity increases. The levels of floridoside can be as high as 10% of the tissue dry-weight in some

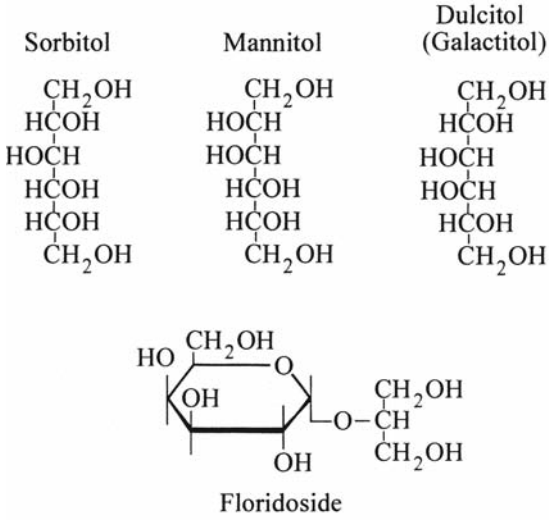


Fig. 4.4 Chemical structure of low molecular polysaccharides that occur in the red algae.

marine red-algal thalli. The first observable product of photosynthesis is phosphoglyceric acid, as is the case in higher plants. Floridoside appears after 30 seconds of illumination and after 2 hours floridoside is the major product of photosynthesis. Floridoside apparently has the same function as sucrose, the common product of photosynthesis in green algae and higher plants.

Floridean starch (Fig. 1.28) is the long-term storage product, occurring as grains in the cytoplasm outside of the chloroplast (Fig. 4.1). Floridean starch is similar to the amylopectin of higher plants, staining red-violet with iodine. In the more primitive Rhodophyceae the starch grains are clustered as a sheath around the pyrenoid of the chloroplast, whereas in the more advanced Rhodophyceae the starch grains are scattered in the cytoplasm (Hara, 1971; Lee, 1974).

Pit connections

Pit connections occur between the cells in all of the orders except the Porphyridiales, and the haploid phase of the Bangiales. It has been pointed out that the term "pit connection" is inappropriate because the structure is neither a "pit" nor a "connection"; however, because the term has been used for so long, it is probably best to retain it. A pit connection consists of a proteinaceous plug core in between two thallus cells (Figs. 4.5, 4.6).

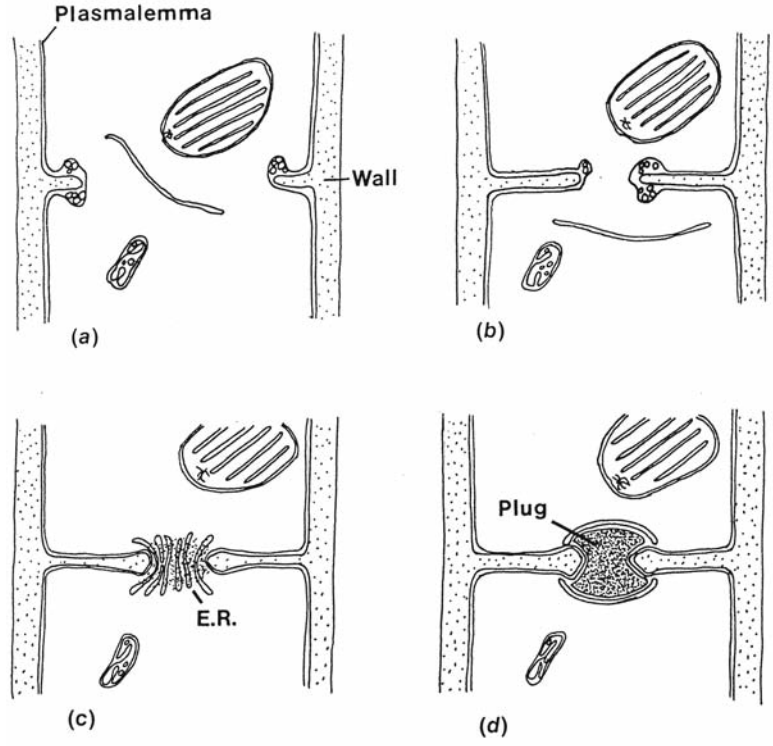


Fig. 4.5 Semidiagrammatic drawing of the formation of a pit connection in a red alga. (*a*) The cross wall begins to furrow inward with the wall precursors found in vesicles derived from the cytoplasm; (*b*) the cross wall septum is complete, leaving an opening (aperture) in the center; (*c*) endoplasmic reticulum lies across the opening in the wall, and electron-dense material condenses in this area; (*d*) the pit connection is formed, consisting of a plug with the plasmalemma continuous from cell to cell. (Adapted from Ramus, 1969, 1971; Lee, 1971.)

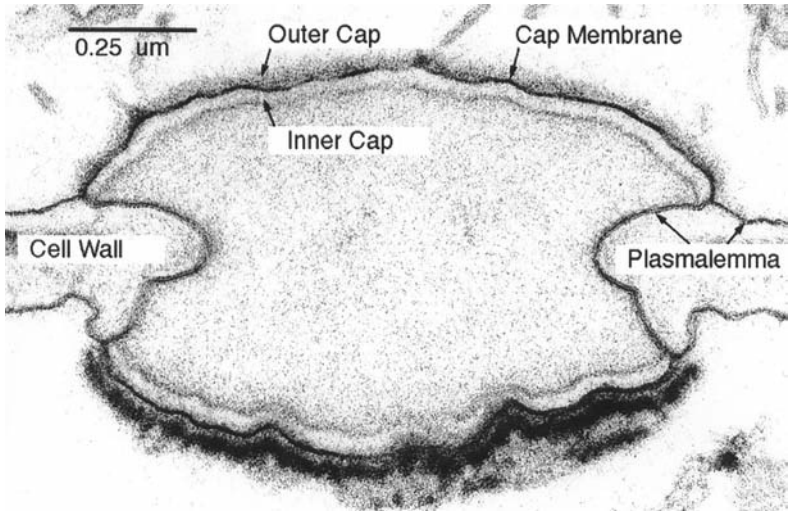


Fig. 4.6 A pit connection between cells of *Palmaria mollis*. The plasma membrane is continuous from cell to cell. The cap membrane is continuous with the plasma membrane. The inner and outer cap layers are on each side of the cap membrane. (From Pueschel, 1987.)

Cap membranes separate the plug core from the adjacent cytoplasm. The cap membrane is continuous with the plasma membrane, which in turn is continuous from one cell to the next. On the inside of the cap membrane can be an inner layer, while on the outside of the cap membrane can be an outer cap layer (Pueschel, 1987). The structure of the pit connection can vary. The more primitive red algae, such as *Rhodochaete* and *Compsopogon*, lack cap membranes and cap layers, with only a plug core present. It has been postulated that this represents the ancestral condition (Pueschel, 1989).

There are two types of pit connections. **Primary pit connections** are formed between two cells during cell division. **Secondary pit connections** result when two cells fuse. Both types of pit connections have the same structure (Kugrens and West, 1973). **Primary pit connections** are formed as follows (Fig. 4.5) (Ramus, 1969): soon after nuclear division, the cross wall grows inward from the lateral wall. When the cross wall is complete, there remains a hole (aperture) in the center through which the protoplasm of the two cells is continuous. A number of parallel vesicles traverse the hole, with electron-dense material condensing around the vesicles. Eventually the vesicles disappear, and the electron-dense material fills the hole. A membrane is formed around this material, producing a plug in the hole. The pit connection has been reported to contain proteins and polysaccharides (Pueschel and Trick, 1991; Ramus, 1971). The pit connection may function as a site of structural strength on the thallus (Kugrens and West, 1973). In some algae the plugs of the pit connections become dislodged from between the cells of a developing gonimoblast, leaving the protoplasm continuous between the cells and allowing the passage of metabolites to the developing reproductive cells (Turner and Evans, 1978).

Calcification

All members of the Corallinales and some of the Nemaliales (*Liagora* (Fig. 4.17 (*a*), (*b*)), *Galaxaura* (Fig. 4.34)) deposit $CaCO_3$ extracelluarly in the cell walls. Anhydrous calcium carbonate occurs in two crystalline forms, **calcite** (rhomboidal) and **aragonite** (orthorhombic) (Fig. 4.7). The two forms differ markedly in specific gravity, hardness, and solubility. The Corallinales deposit $CaCO_3$ primarily as calcite, whereas the calcified members of the Nemaliales deposit $CaCO_3$ primarily as aragonite. In *Liagora* (Fig. 4.17(*a*), (*b*)) (Nemaliales), the aragonite occurs as needle-like crystals in the wall, whereas in the Corallinales, the calcite occurs as massive deposits (Borowitzka et al., 1974). Calcified walls of living cells probably have a mucilaginous component that slows the loss of Ca^{2+} into the medium (Pearse, 1972). If a calcified thallus is killed, the dispersal of the calcified wall is greatly accelerated.

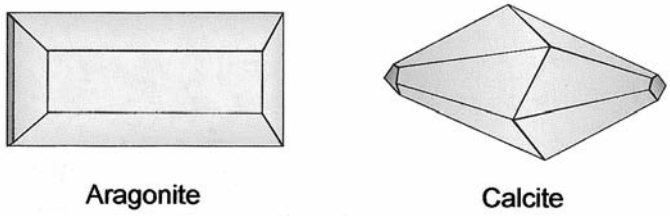


Fig. 4.7 The crystal structure of aragonite and calcite.

Rhodoliths are unattached biogenic (produced from living organisms) nodules composed at least partly of calcified red algae. A rhodolith begins as a central nucleus composed of a pebble or fragment of coral. Non-articulated coralline algae attach to the nucleus and grow. The shape of the rhodolith is determined by its environment, often being generally spherical because of frequent overturning due to water motion. Rhodoliths can reach 30 cm in diameter and be 500–800 years old. Sections of rhodoliths that reveal the banding of the coralline red algae can be used to determine the environment at the time of wall deposition (Halfar et al., 2000).

Skeletons of coralline algae are formed with little biological control, by impregnation of cell walls with magnesium and calcium at a ratio similar to the Mg/Ca in the water. Therefore, the Mg/Ca ratio in the cell walls reflects the Mg/Ca ratio in the water. Analysis of the Mg/Ca ratio in cell walls of fossil coralline red algae since the beginning of the Paleozoic Era have shown that there have been times of "aragonite seas" with relatively high Mg in seawater, resulting in coralline algae with cells walls contain high-Mg calcite and aragonite, and times of "calcite seas" with relatively low-Mg seawater, resulting in coralline algae with low-Mg calcite (Fig. 4.8) (Stanley et al., 2002). The differences in the Mg/Ca ratios in seawater are due to changes in the mid-ocean spreading rates.

The coralline algae thrive in rock pools and on rocky shores exposed to very strong wave action and swift tidal currents. The red algae that have the highest rates of calcification also have the highest rates of photosynthesis and are usually found in waters less than 20 m deep (Goreau, 1963). Calcification of the thallus occurs about two to three times more rapidly in the light than in the dark, although significant calcification does occur in the dark (Okazaki et al., 1970). The above observations have led to the theory that calcification may be linked to photosynthesis (Pearse, 1972). The most quoted theory on calcification is that calcium salts are precipitated from seawater by the alkalinity brought about by the extraction of carbon dioxide during photosynthesis, calcium carbonate being less soluble in alkaline waters than acid. The obvious and often mentioned drawback to this theory is that because all algae carry out photosynthesis, it is difficult to understand why they do not all calcify. Also the continued calcification of corallines in the dark is another argument against this theory.

Seawater is more or less saturated with respect to calcium carbonate, and the addition of either calcium or carbonate will cause the carbonate to precipitate. The concentration of CO_3^{2-} is related through a complex series of equilibria (Digby, 1977a,b):

$$CO_2 + H_2O \rightleftharpoons H_2CO_3 \rightleftharpoons H^+ + HCO_3^- \rightleftharpoons 2H^+ + CO_3^{2-}$$

then

$$CO_3^{2-} + Ca^{2+} \rightleftharpoons CaCO_3 \text{ (ppt.)}$$

The addition of acid will drive the reactions to the left and cause carbonate to dissolve, whereas the addition of base will drive the reactions to the right and form more carbonate. At the pH of seawater (8.4), almost all of the CO_2 in the water is in the form of bicarbonate ion, HCO_3^-. The addition of one equivalent of hydroxyl ions to seawater saturated with respect to calcium carbonate will precipitate one equivalent of calcium carbonate:

$$Ca^{2+} + HCO_3^- + OH^- \rightleftharpoons CaCO_3 \text{ (ppt.)} + H_2O$$

The fact that seawater is nearly saturated with calcium carbonate was demonstrated with seawater from the coast of Maine by Digby (1977a). By raising the pH of this seawater to 9.6, he caused precipitation of carbonates. Calcium carbonate precipitated first, being less soluble, followed by carbonate richer in magnesium.

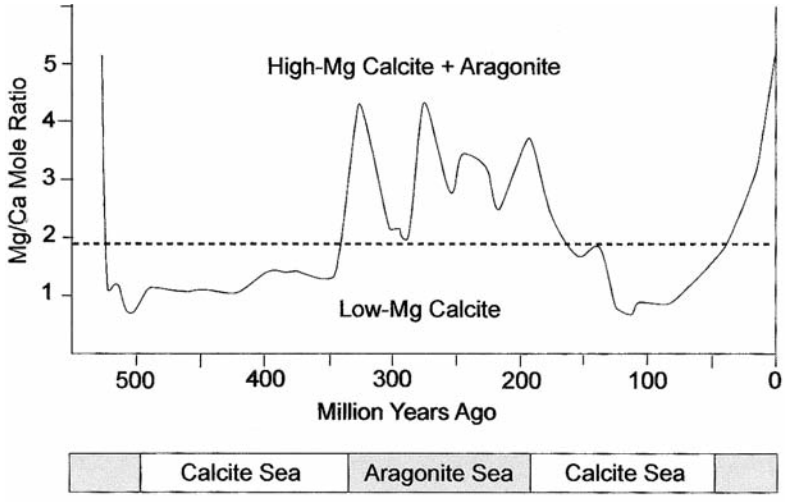


Fig. 4.8 Effects of the Mg/Ca ratio of seawater on the mineralogy of carbonate deposition in coralline red algae. High Mg/Ca ratio in seawater results in the deposition of aragonite and calcite high in Mg, resulting in "aragonite seas." Low Mg/Ca ratio in seawater results in the deposition of calcite low in Mg and "calcite seas." (Modified from Stanley et al., 2002.)

Digby (1977b) proposed a theory of calcification of red algae based on raising the pH of the seawater immediately outside the cells, causing precipitation of carbonates as outlined above. The first process is the normal photosynthetic splitting of water:

$$H_2O \rightarrow \tfrac{1}{2}O_2 + 2H^+ + 2e^-$$

The oxygen then diffuses out of the cell. As mentioned above, in the sea most of the carbon dioxide is in the form of bicarbonate ions; these ions diffuse into the cells and receive the electrons freed initially by photosynthesis. The bicarbonate ions are then converted into carbonate ions and hydrogen according to the following reaction:

$$2HCO_3^- + 2e^- \rightleftharpoons 2H^+ + 2CO_3^{2-}$$

The carbonate ions diffuse out of the cell where they partially dissociate, forming bicarbonate and hydroxyl ions and thereby raising the pH:

$$2CO_3^{2-} + H_2O \rightleftharpoons 2HCO_3^- + 2OH^-$$

When saturation with regard to calcium and carbonate is reached by a rise in pH outside the cells, calcium carbonate precipitates on the walls:

$$2Ca^{2+} + 2CO_3^{2-} = 2CaCO_3 \text{ (ppt.)}$$

Continued precipitation of $CaCO_3$ results in the calcified wall of the Rhodophyceae. Although the above theory explains the mechanism of calcification, it does not explain why calcification is specific to certain red algae.

It has been theorized that calcification of red algal thalli evolved as a protection against grazing by organisms such as limpets, although it has also been pointed out that grazing is beneficial to the coralline algae in that the grazers remove epiphytes from the red algal thallus (Pueschel and Miller, 1996).

Secretory cells

Secretory cells (vesicular cells) occur in some Rhodophyceae (Fig. 4.9(*a*), (*b*)). These cells are colorless at maturity and commonly have a large central vacuole. The secretory cells in *Bonnemaisonia* are prominent and associated with high concentrations of iodine (Fig. 4.9(*a*)). The concentration of iodine can be high enough to produce a blue color in herbarium paper with starch as a filler (the chemical test for starch). Secretory cells are vestigial, lacking the large vacuole with its refractile contents, when these algae are grown in a medium without bromine (Wolk, 1968). Bromine can also occur as granular deposits in mucilage, such as in the thallus medulla of *Thysanocladia densa* (Pallaghy et al., 1983) or in the cuticle of *Polysiphonia nigrescens* (Peders'en et al., 1981).

Other types of secretory cells not associated with the accumulation of halogens occur. The cells are often called secretory cells, even though they are apparently not involved in secretion. In *Antithamnion* (Figs. 4.9(*b*), 4.10(*a*)), these cells

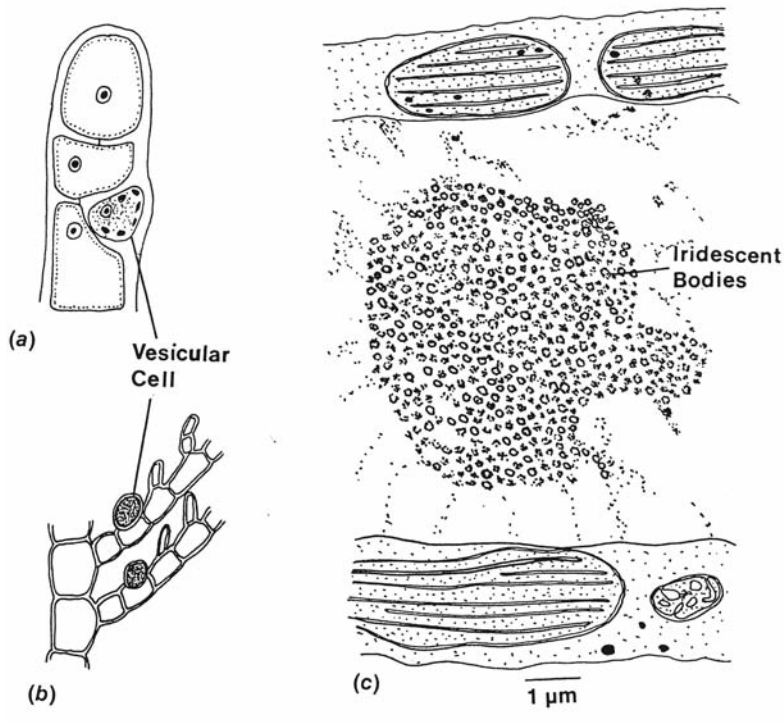


Fig. 4.9 (*a*) Vesicular cell of the *Trailiella* stage of *Bonnemaisonia*. (*b*) Vesicular cells of *Antithamnion plumula*. (*c*) Iridescent bodies in the vacuole of a cell of *Chondria caerulescens*. ((*a*) after Kylin, 1956; (*b*) after Kylin, 1930; (*c*) adapted from Feldmann, 1970a.)

have a large central vacuole containing sulfated acidic polysaccharide (Young and West, 1979). In *Opuntiella californica*, there are "gland cells" with a large vacuole containing a homogeneous proteinaceous material (Young, 1979) (Fig. 4.10(*b*)). These "secretory cells" and "gland cells" may have compounds that act as deterrents to grazing, or they may accumulate special reserves for metabolic use.

Iridescence

The thalli of some Rhodophyceae show a marked blue or green iridescence when observed in reflected light. **Iridescence** is solely a physical interference and is not related to any light-producing phenomena such as phosphorescence or bioluminescence (Gerwick and Lang, 1977). It results from the interference of light waves reflected from the surfaces of very thin multiple laminations separated by equally thin or thinner layers of material with a contrasting refractive index; the layers are uniform and produced by periodic secretion and deposition. Iridescence in the Rhodophyceae has been attributed to different causes by different investigators. Feldmann (1970a,b) found iridescent bodies in *Chondria* (Fig. 4.9(*c*)) and *Gastroclonium*, whereas Gerwick and Lang (1977) attributed the iridescence in *Iridaea* to a multilayer cuticle.

Epiphytes and parasites

Rhodophycean organisms range from autotrophic, independent plants to complete heterotrophic parasites. The spectrum includes non-obligate epiphytes (in the *Acrochaetium–Rhodochorton* complex), obligate epiphytes (*Polysiphonia lanosa* on *Ascophyllum* (Fig. 4.11)), semi parasites that have some photosynthetic pigments (*Choreocolax* (Fig. 4.13), *Gonimophyllum*), and parasites with no coloration (*Harveyella, Holmsella*).

The association between the obligate epiphyte red alga *P. lanosa* and its brown alga host *Ascophyllum* has been well studied. After the spore of *P. lanosa* germinates on the host, the red alga sends down a rhizoid that digests its way into the host tissue by means of enzymatic digestion of the host tissues. The enzymes are discharged from vesicles at the tip of the rhizoid. Once the rhizoid has

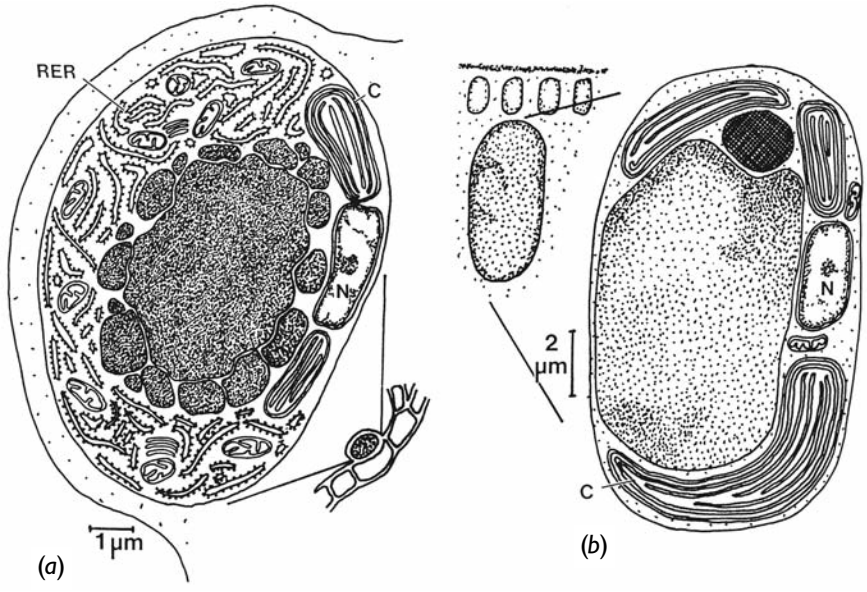


Fig. 4.10 (*a*) Semidiagrammatic drawing of the fine structure of a vesicular cell of *Antithamnion*. The cell has a large central vacuole surrounded by protoplasm containing rough endoplasmic reticulum (RER), mitochondria, chloroplasts (C), and a nucleus (N). (*b*) Semidiagrammatic drawing of the fine structure of a gland cell of *Opuntiella californica*. The cell has a large central vacuole containing chloroplasts (C), a nucleus (N), and mitochondria. ((*a*) after Young and West, 1979; (*b*) after Young, 1979.)

established itself, intrusive cells form the basal parietal cells of the thallus (Fig. 4.11) (Rawlence, 1972). Although *P. lanosa* is an obligate epiphyte, there is no transfer of metabolites from the host to the epiphyte, the epiphyte manufacturing all of its own requirements through photosynthesis (Harlin and Craigie, 1975; Turner and Evans, 1978).

Parasitic red algae can be either adelphoparasites (*adelpho* = brother) or alloparasites (*allo* = other). **Adelphoparasites** are closely related to, or belong to the same family as their hosts and constitute 90% of parasitic red algae (Goff et al., 1996). **Alloparasites** are not closely related to their hosts. The parasitic habit apparently has been adapted more easily when the host is closely related to the parasite (adelphoparasites) than when it is not (alloparasites), partially because it is easier for the parasite to establish secondary pit connections with the host (and therefore transfer nutrients) if the host and parasite are related.

Choreocolax polysiphoniae is an example of a rhodophycean parasite (Fig. 4.12). The alga is a complete parasite and is interesting in that it is parasitic on *Polysiphonia fastigata*, which is itself epiphytic on *Ascophyllum* (Fig. 4.11). Because *Choreocolax* is in the Gigartinales, and *Polysiphonia* is in the Ceramiales, this is a case of alloparasitism. *Choreocolax* consists of a more or less hemispherical white external portion made up of subdichotomously branched filaments enclosed and surrounded by gelatinous matter, and a mass of haustorial cells growing inside the host (Sturch,

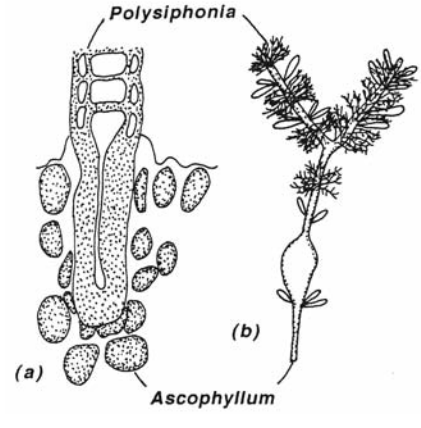


Fig. 4.11 (*a*) The rhizoid of *Polysiphonia lanosa* penetrating tissue of *Ascophyllum nodosum*. (*b*) *Polysiphonia* epiphytic on *Ascophyllum*. ((*a*) after Rawlence, 1972.)

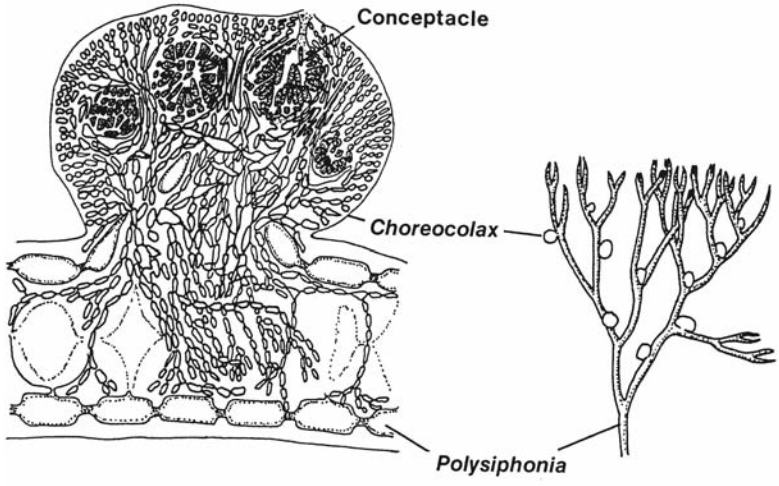


Fig. 4.12 Drawing of a section of *Choreocolax polysiphoniae* on *Polysiphonia*. The parasitic *Choreocolax* has carposporophytes in various stages of development. (After Sturch, 1926.)

1926). When the haustorial cells have reached a certain distance from the original point of infection, they frequently give rise to a second external cushion. Secondary pit connections are established between the haustorial internal filaments of the parasite and the larger cells of the host. Apically dividing filaments of the parasite *Choreocolax* cells produce small conjunctor cells (Fig. 4.13) by the asymmetrical division of a cell. A conjunctor cell contains a highly condensed, small nucleus. The conjunctor cell fuses with an adjacent host *Polysiphonia* cell. The nucleus and cytoplasm of the conjunctor cell are incorporated into the host cell. The pit connection that originally connected the conjunctor cell and the sister *Choreocolax* cell now connects the host *Polysiphonia* cell and the parasite. This is often called a "secondary pit connection," even though it is actually an ordinary pit connection. Up to several hundred *Choreocolax* cells can fuse with a single host cell. The infected host *Polysiphonia* cell enlarges and the vacuole decreases in size with a concomitant increase in cytoplasmic contents (Goff and Coleman, 1984). The chloroplasts become scattered throughout the cytoplasm, instead of lying in the peripheral cytoplasm as they do in the non-infected cells. Although the parasite cells are colorless, they do contain very reduced plastids (Kugrens and West, 1973). In the association between the colorless parasite *Holmsella pachyderma* and the host *Gracilaria verrucosa*, both of which are Rhodophyceae, the main product of photosynthesis, floridoside, is transferred from the host to the parasite where it is accumulated as floridoside, mannitol, and starch (Fig. 4.4) (Evans et al., 1973).

Defense mechanisms of the red algae

Benthic marine red seaweeds are particularly susceptible to being overgrown by epiphytes because

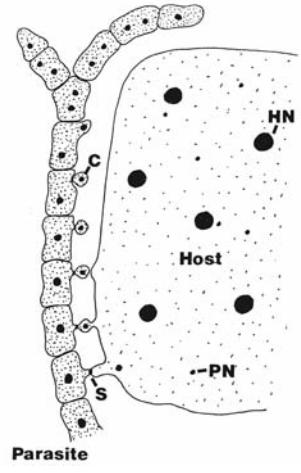


Fig. 4.13 A drawing illustrating the progressive formation of conjunctor cells by a filament of the parasitic red alga *Choreocolax* living on a host *Polysiphonia* cell, leaving the pit connection of the conjunctor cell as a secondary pit connection. (C) Conjunctor cell; (HN) *Polysiphonia* host nucleus; (PN) *Choreocolax* parasite nucleus introduced into the host cell after fusion with the conjunctor cell of the parasite; (S) secondary pit connection. (After Goff and Coleman, 1984.)

they are sessile and are restricted to the photic zone where conditions for fouling organisms are optimal. Epiphytes can significantly harm seaweeds by reducing the light, resulting in decreased photosynthesis and growth, by increasing drag and hence their susceptibility to breakage or being torn from the substrate, and by decreasing the reproductive output of the host.

Some red seaweeds secrete compounds that kill or retard the growth of epiphytes growing on them. *Delisea* secretes halogenated furones (Fig. 4.14) that affect the growth of epiphytes and keep the thallus clean (de Nys et al., 1995).

Gracilaria conferta (Fig. 4.42) has a defense mechanism that limits bacterial infection of the red alga. Invasive bacteria secrete agarases that break down the cell-wall agar of *Gracilaria* into shorter neoagarosehexaose oligosaccharides. *Gracilaria* cells respond to nanomolar concentrations of the oligosaccharides by increasing respiration and producing active oxygen species such as hydrogen peroxide (H_2O_2) and hydroxyl radicals (OH^-) (Potin et al., 1999). The hydrogen peroxide is degraded to water and molecular oxygen:

$$H_2O_2 \rightarrow H_2O + \tfrac{1}{2}O_2$$

Molecular oxygen is toxic and results in the elimination of 90% of the epiphytes within 15 minutes under experimental conditions (Weinberger and Friedlander, 2000). *Gracilaria conferta* has also been shown to release activated oxygen each morning after exposure to light. This short time release of activated oxygen, in addition to the defense related release of hydrogen peroxide, resulted in the selection of epiphytic bacteria that are relatively insensitive to these chemicals. *Corynebacterium-Arthrobacter* 1 bacteria were relatively resistant to hydrogen peroxide whereas *Vibrio 1* and *Flavobacterium 7* bacteria were sensitive (Bouarab et al., 1999; Potin, et al., 1999).

Volatile halocarbons, consisting of brominated, chlorinated or iodinated hydrocarbons, are also produced on exposure of *Gracilaria* cells to the oligosaccharide. These volatile hydrocarbons are electrophilic, attacking a variety of organic compounds and acting as natural **biocides** (pesticides). "White tip" disease of *Gracilaria* is due to the release of these biocides in response to bacterial infection. The bleaching of the tips of the alga is killing some of the algal cells while containing the pathogens at the site of attack (Largo et al., 1995).

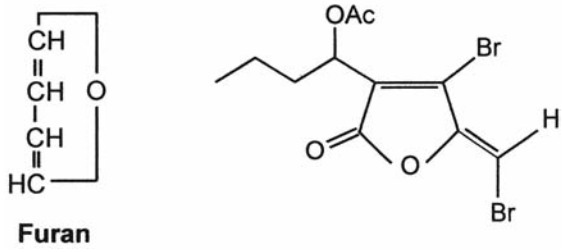


Fig. 4.14 *Left*: The chemical structure of furan, the basic building block of the furanones. *Right*: One of the halogenated furanones released by the red alga *Delisea pulchra*. Halogenated furanones inhibit the growth of epiphytes on this red alga.

Commercial utilization of red algal mucilages

The two most important polysaccharides derived from the Rhodophyceae are agar and carrageenan. **Agar** is defined pharmaceutically as a phycocolloid of red algal origin that is insoluble in cold water but readily soluble in hot water; a 1.5% solution is clear and forms a solid and elastic gel on cooling to 32 to 39 °C, not dissolving again at a temperature below 85 °C. Agar is composed of two polysaccharides, agarose (Fig. 1.11) and agaropectin (Lahaye, 2001).

Agar is obtained commercially from species of *Gelidium* (Figs. 4.40, 4.41) and *Pterocladia* as well as from various other algae, such as *Acanthopeltis*, *Ahnfeltia*, and *Gracilaria* (Fig. 4.42) (Melo, 1998; Mollet et al., 1998). These algae are often loosely referred to as **agarophytes**. Commercial production of agar was a world monopoly of the Japanese for many years, and even in 1939 Japan was still the major producer. Wartime demands in areas deprived of Japanese agar led to the development of agar industries in many of the Allied countries, some of which have continued and prospered while others have declined or disappeared. The agarophytes are collected by diving, dragging, or raking them offshore at low tide. In the traditional processing procedure the

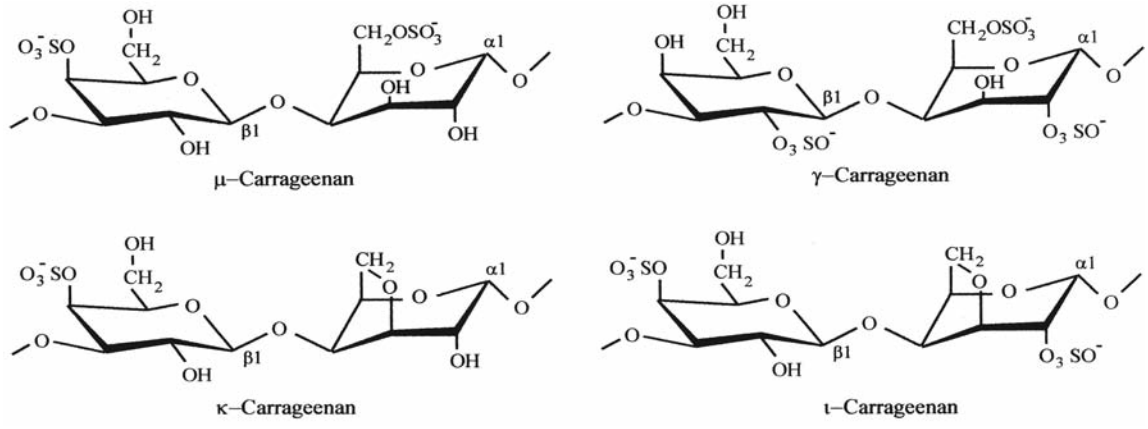


Fig. 4.15 The chemical structures of the different types of carrageenans that occur in the red algae.

plants are then cleaned and bleached in the sun, with several washings in freshwater used to facilitate bleaching. The material is boiled for several hours, and the extract is acidified. This extract is then frozen and thawed. On thawing, water flows from the agar, carrying impurities with it. The agar that remains is dried and marketed as flakes or cakes. The more modern method extracts the agar under pressure in autoclaves. The agar is decolorized and deodorized with activated charcoal, filtered under pressure, and evaporated under reduced pressure. Further purification by freezing is then undertaken.

The greatest use of agar is in association with food preparation and technology, and in the pharmaceutical industry. It is used for gelling and thickening purposes, particularly in the canning of fish and meat, reducing the undesirable effects of the can and providing some protection against shaking of the product in transit. It is also used in the manufacture of processed cheese, mayonnaise, puddings, creams, and jellies. Pharmaceutically agar is used as a laxative, but more frequently it serves as an inert carrier for drug products where slow release of the drug is required, as a stabilizer for emulsions, and as a constituent of cosmetic skin preparations, ointments, and lotions. The use of agar as a stiffening agent for growth media in bacteriology and mycology, which was its main use almost a century ago, is still responsible for a very considerable part of the demand.

Carrageenan (Fig. 4.15) is a phycocolloid similar to agar but with a higher ash content and requiring higher concentrations to form gels. It is composed of varying amounts of the principal components, κ-carrageenan and λ-carrageenans, both negatively charged high-molecular-weight polymers (Chiovitti et al., 1995; Therkelsen, 1993). κ-Carrageenan is distributed throughout the wall while λ-carrageenan is localized to the cuticle (Vreeland et al., 1992). κ-carrageenan precipitates selectively from a cold, dilute solution in the presence of potassium ions. It forms a gel when heated and cooled with potassium ions and is therefore the gelling component. λ-Carrageenan is the non-gelling component and is not precipitated or gelled by potassium. λ-Carrageenan contains galactose-2,6-disulfate, whereas κ-carrageenan contains 3,6-anhydro-D-galactose. It has been shown in *Chondrus crispus* and *Gigartina stellata* that the proportion of κ- and λ-carrageenan in the cell wall varies according to the ploidy of the plant. In the tetrasporophyte the amount of λ-carrageenan present is high as compared with the amount of κ-carrageenan, whereas just the opposite is true in the gametophyte (Chen et al., 1973). Such results may prove valuable in determining the ploidy of Rhodophyceae that have unknown life cycles.

Carrageenan is usually obtained from wild populations of Irish moss, the name for a mixture of *Chondrus crispus* and the various species of *Gigartina*, particularly *G. stellata*. In the Philippines, *Eucheuma*, and in Vietnam and India, *Kappophycus* (Fig. 4.16) are extensively cultivated as a source of carrageenan (Reddy et al., 2003). Commercial extraction is similar to that for agar although





Fig. 4.16 Cultivation of the carrageenan-containing *Kappophycus alvarezii* in an offshore area (*left*) and a shrimp pond (*right*) in Vietnam. (From Ohno et al., 1996.)

carrageenan cannot be purified by freezing. The dried alga is washed with freshwater to reduce the salt content and then boiled with 2 to 4 parts of alga to 100 parts of water. The soluble carrageenan is separated from the insoluble residue in a centrifuge. Following filtration and some evaporation under vacuum, the carrageenan is dried on a rotary drier.

Carrageenans are used extensively for many of the same purposes as agar; however, because of their lower gel strength, carrageenans are used less for stiffening purposes than is agar, although for stabilization of emulsions in paints, cosmetics, and other pharmaceutical preparations carrageenans are preferred to agar. Also, for the stiffening of milk and dairy products, such as ice cream, carrageenans have supplanted agar completely in recent years, and it is in this area that demands for these products are the greatest. One particular use is for instant puddings, sauces, and creams, made possible by the gelling action, which does not require refrigeration.

Carrageenans inhibit human immunodeficiency virus (HIV) replication and reverse transcriptionase *in vitro* (in the test tube) (Bourgougnon et al., 1996). Replication of the HIV virus depends on interaction of a glycoprotein on the HIV virus envelope with a receptor on the target cells in the human body. The sulfated carrageenans prevent attachment of the HIV virus to the target cells. This occurs by the stronger negative R-O-SO_3^- groups on the carrageenan binding to a loop on the HIV molecule. A carrageenan-based vaginal microbicide called Carraguard® has been shown to block HIV and other sexually transmitted diseases *in vitro*. Carraguard has entered clinical trials involving 600 non-pregnant, HIV-negative women in South Africa and Botswana (Spieler, 2002; Smit, 2004).

Reproductive structures

The Rhodophyceae have no flagellated cells or cells with any vestigial structure of flagellation, such as basal bodies. In sexual reproduction, **spermatia** are produced which are carried passively by water currents to the female organ, the **carpogonium** (Figs. 4.17(*a*), 4.18). The fertilized carpogonium produces **gonimoblast filaments** that form **carposporangia** and diploid **carpospores** (Fig. 4.17(*b*)). The carpospores produce the diploid **tetrasporophyte** which subsequently gives rise to haploid **tetraspores**. Advanced red algae form chiefly tetrahedral tetrasporangia (Fig. 4.17(*d*)) with large spores, whereas less advanced groups generally form cruciate or zonate tetrasporangia (Fig. 4.17(*d*), (*e*)) with smaller spores (Ngan and Price, 1979). Tetraspores are generally larger than carpospores. The tetraspores complete the life cycle by germinating to form the gametophyte. Although this is the general life cycle of most Rhodophyceae, there are a number of modifications of it.

The postfertilization events vary from one order to another. The more advanced orders have **auxiliary cells** with which the fertilized

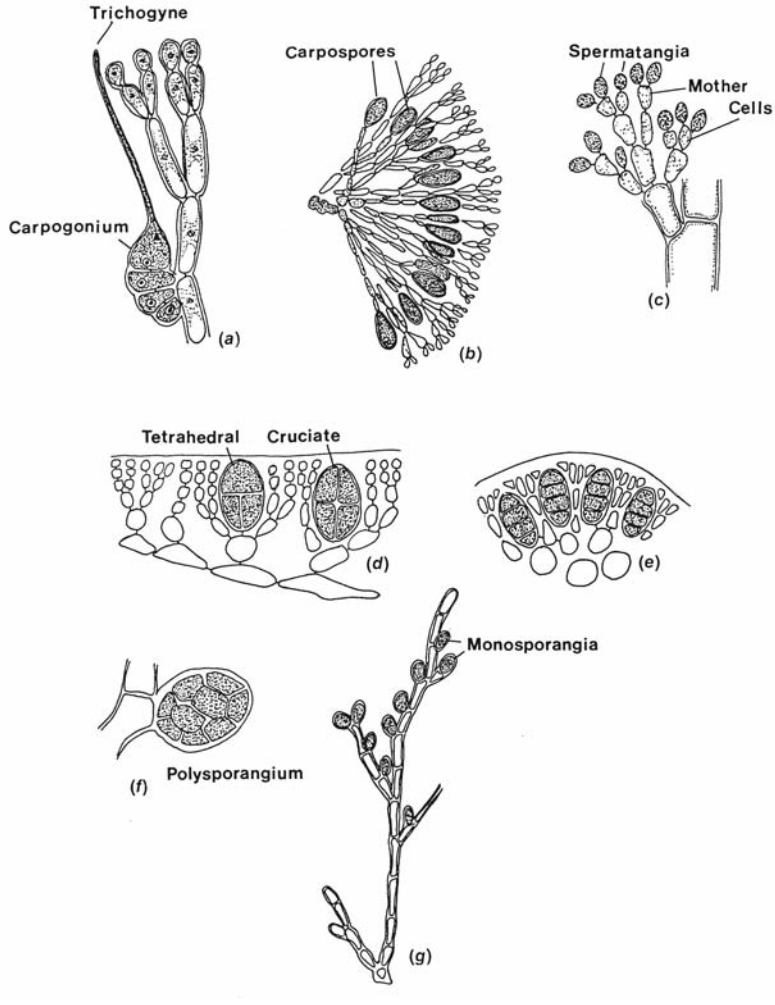


Fig. 4.17 (*a*) A filament of *Liagora viscida* with a carpogonial branch. (*b*) Gonimoblast filaments of *L. viscida* with carpospores. (*c*) A spermatangial branch of *Acrochaetium corymbiferum* with spermatangia and spermatangial mother cells. (*d*) Tetrahedral and cruciate tetrasporangia of *Nemastoma laingii*. (e) Zonate tetrasporangia of *Hypnea musciformis*. (*f*) Polysporangium of *Pleonosporium vancouverianum*. (*g*) Monosporangia of *Kylinia rhipidandra*. ((*a*), (*b*), (*c*), (e) after Kylin, 1930; (*f*) after Kylin, 1924; (*g*) after Kylin, 1928.)

carpogonium fuses to form a multinucleate fusion cell. Papenfuss (1966) recognizes two types of auxiliary cells, nutritive and generative. **Nutritive auxiliary cells** provide nutrients for the developing carposporophyte, whereas **generative auxiliary cells** give rise to **gonimoblast filaments** (Figs. 4.18, 4.33, 4.44). The diploid tissue formed from the fertilized carpogonium forms the gonimoblast filaments. The gonimoblast filaments produce terminal carposporangia, which in turn form the carpospores. The carposporangia enlarge considerably during their maturation because of the development of the chloroplasts and the vesicles containing wall precursors. The pit connection between the carposporangium and the gonimoblast breaks before release of the carpospore. Also during the development of the gonimoblast filaments, the pit connections between the older gonimoblast cells usually dissolve (Kugrens and West, 1972a, 1973, 1974).

Carpogonium

The female organ, or carpogonium, consists of a dilated basal portion and a usually narrow gelatinous elongate tip, the **trichogyne**, which receives the male cells (Figs. 4.6(*a*), 4.10). Usually there are two nuclei in a carpogonium, one in the trichogyne, which degenerates soon after the carpogonium matures, and one in the basal part of the carpogonium, which functions as the female gamate nucleus. In most Rhodophyceae the carpogonium terminates a short, often branched, three- to four-celled lateral called the carpogonial branch. The cell from which the carpogonial

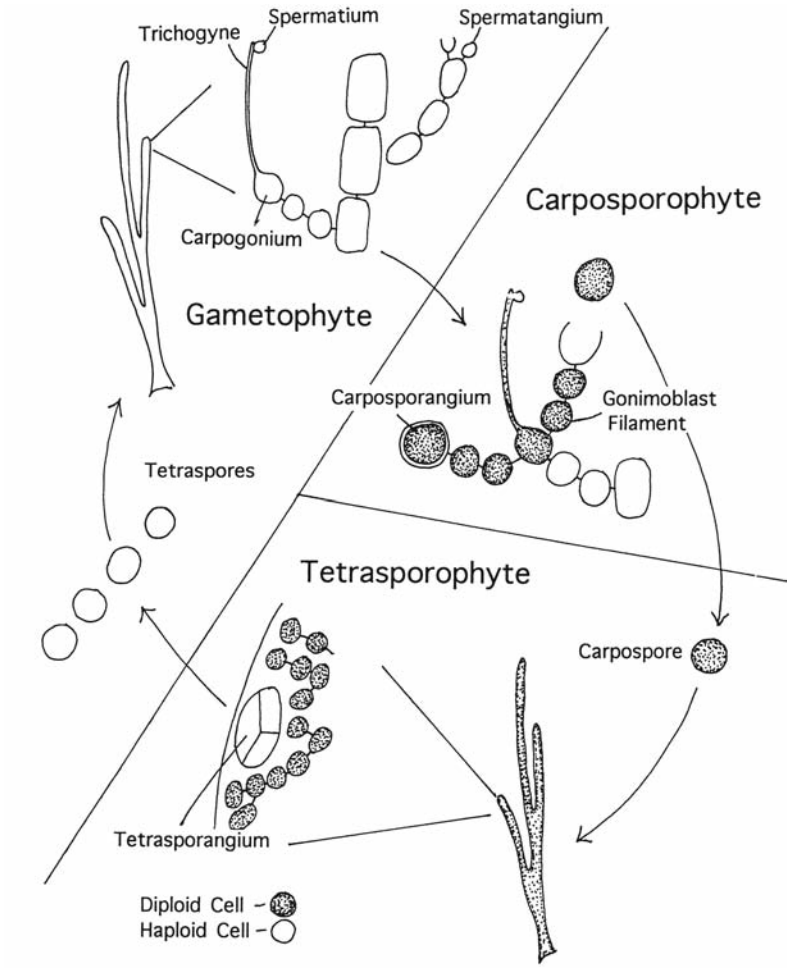


Fig. 4.18 Simplified life cycle of a typical red alga.

branch arises is the **supporting cell**. The carpogonium and carpogonial branch are commonly colorless, although in some Nemaliales this is not true.

Spermatium

The spermatia of the Rhodophyceae are spherical or oblong cells produced in **spermatangia**, a single spermatium being formed in a spermatangium and then released, leaving the empty sporangium (Fig. 4.19). The spermatangia (Fig. 4.22) are formed on spermatangial mother cells (Fig. 4.17(*c*)). The young spermatangia frequently have a pronounced polar orientation, with the nucleus in the apical portion and one or more vacuoles in the basal portion (Scott and Dixon, 1973a). As the spermatangium ages, vacuoles form in the basal area. These vacuoles contain fibrous material (probably mucopolysaccharides) and make up half the volume of the spermatangium. Subsequently the vacuoles fuse to form one large vacuole. The spermatium is released by the gelatinization of the spermatangial wall near the apex and the concurrent release of the fibrous material in the basal vacuole. The fibrous material presumably swells and pushes the spermatium out of the spermatangium (Fig. 4.19). The fibrous material is sticky, and some of it adheres to the spermatium, thereby facilitating attachment to the trichogyne (Fig. 4.22(*c*)). During the development of the spermatium the pit connection with the spermatium mother cell is severed. The mature spermatium is uninucleate, and wall-less, but surrounded by mucilage, and may (Simon-Bichard-Bréaud, 1971; Peyrière, 1971) or may not (Kugrens and West, 1972a; Kugrens, 1974) contain functional chloroplasts.

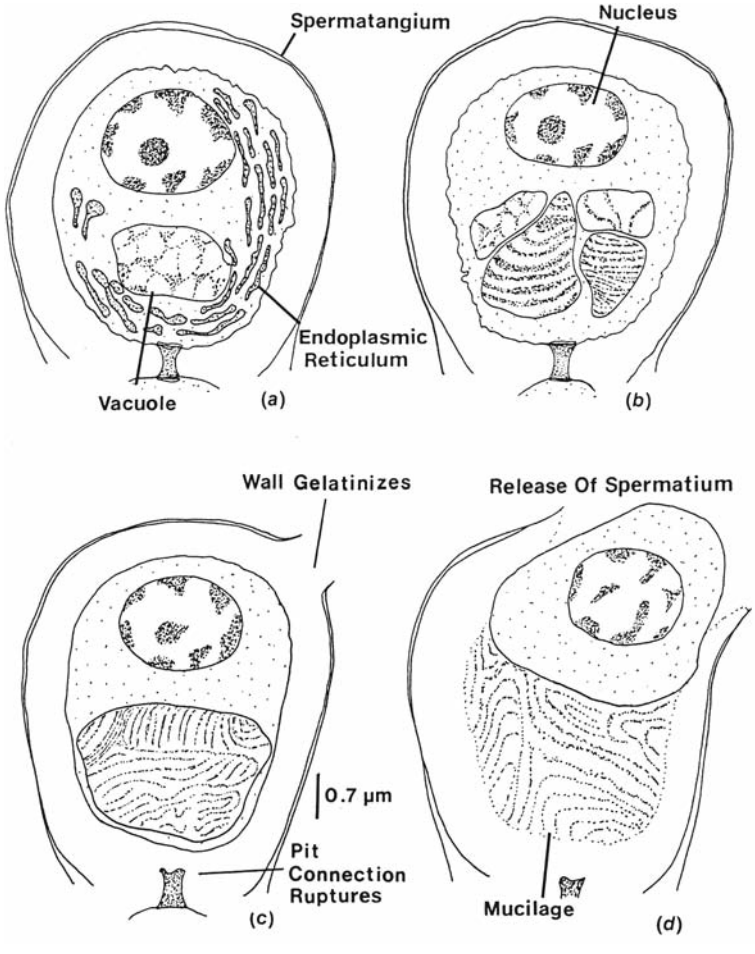


Fig. 4.19 A semidiagrammatic drawing of the formation of the spermatium in the Rhodophyceae. (*a*) Young spermatium. (*b*) Formation of vacuoles containing fibrous material. (*c*) Fusion of vacuoles, breaking of the pit connection, and gelatinization of the wall of the spermatangium. (*d*) Extrusion of mucilage and release of the spermatium. (Adapted from Scott and Dixon, 1973a; Kugrens, 1974.)

Fertilization

The spermatium usually is carried passively by water currents to the trichogyne of the carpogonium, although some spermatia can glide in a manner similar to the gliding in *Porphyridium*. Actin filaments in the spermatium and carpogonium are involved in the subsequent steps (Fig. 4.20) (Kim and Kim, 1999; Pickett-Heaps et al., 2001). The wall of the spermatium and that of the carpogonium dissolve, the male nucleus divides, and the male nuclei move into the carpogonium. Fusion of one male nucleus and the carpogonial nucleus occurs in the basal portion of the carpogonium. Fertilization stimulates the production of polyamine spermine (Fig. 4.21) which steers the carpogonial branch toward the production of carpospores (Sacramento et al., 2004). The trichogyne will usually continue to grow until contact is made with a spermatium. After fertilization has occurred, the trichogyne becomes separated at its base from the rest of the carpogonium by the progressive thickening of the cell wall.

There is a relatively low statistical probability that the non-motile spermatia will be carried to receptive trichogynes of carpogonia. Some species have appendages on the spermatia that extend the reach of the spermatia five- to tenfold resulting in a better chance of attaching to a receptive carpogonium. The appendages are initially contained within vesicles within the spermangia and unfold when the spermatia are released (Fig. 4.22). The appendages increase the surface area of the spermatium more than 30-fold, increasing the likelihood of interaction with a trichogyne of a carpogonium. Moieties of the sugar mannose cover the surface of the appendages. The surface of the trichogyne is covered with the lectin concanavalin A which binds the mannose

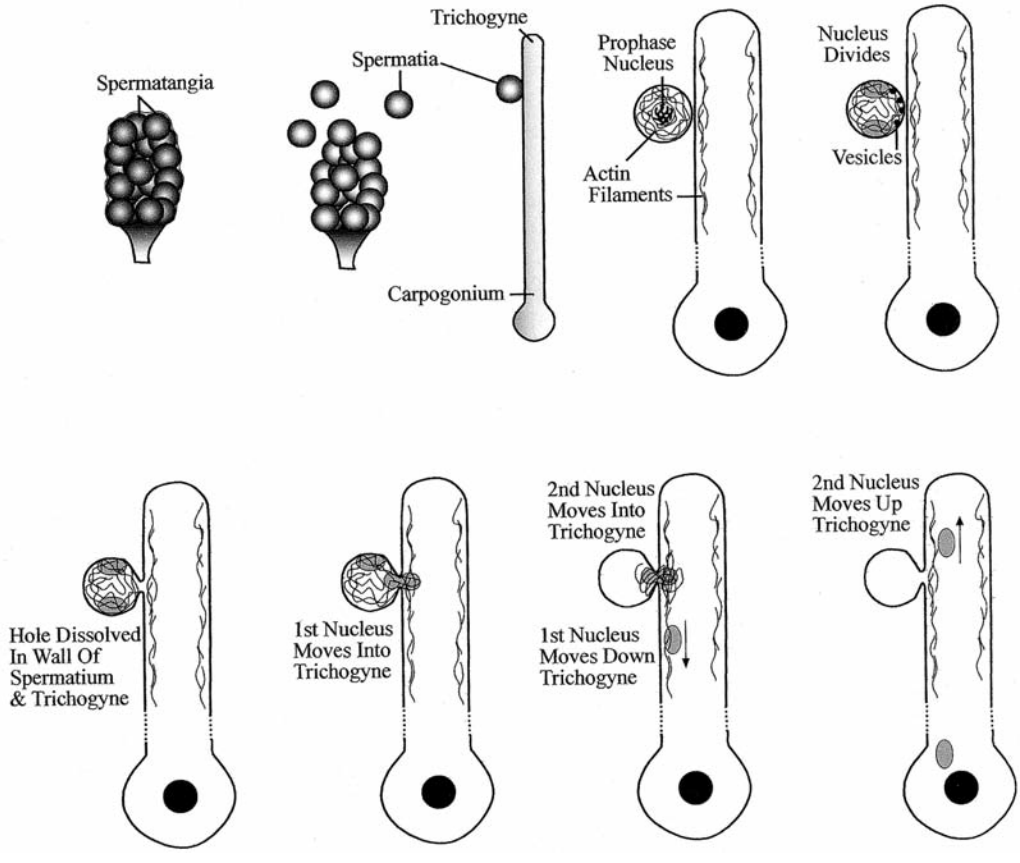


Fig. 4.20 The behavior of the spermatium and its contents during fertilization in a typical red alga. (Modified from Wilson et al., 2003.)

moieties on the spermatangial appendages (Mine et al., 2003).

Meiosporangia and meiospores

Tetrasporangia, polysporangia, and bisporangia formed on diploid plants are generally regarded as being the seat of meiosis although there are exceptions to this. The **tetrasporangia** (Figs. 4.17(*e*), 4.18) form four tetraspores either in a row (zonate), crosswise (cruciate), or most commonly in a tetrad (tetrahedral). In the formation of tetraspores a wall is laid down inside the tetrasporangia by the protoplast, which has prominent dictyosomes (each dictyosome associated with a mitochondrion as is common in the Rhodophyceae; Kugrens and West, 1972b; Scott and Dixon, 1973b). The tetraspores are not joined by pit connections.

Spermine

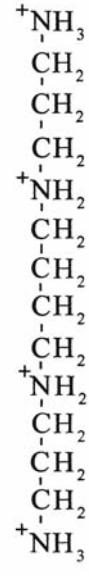


Fig. 4.21 The chemical structure of spermine.

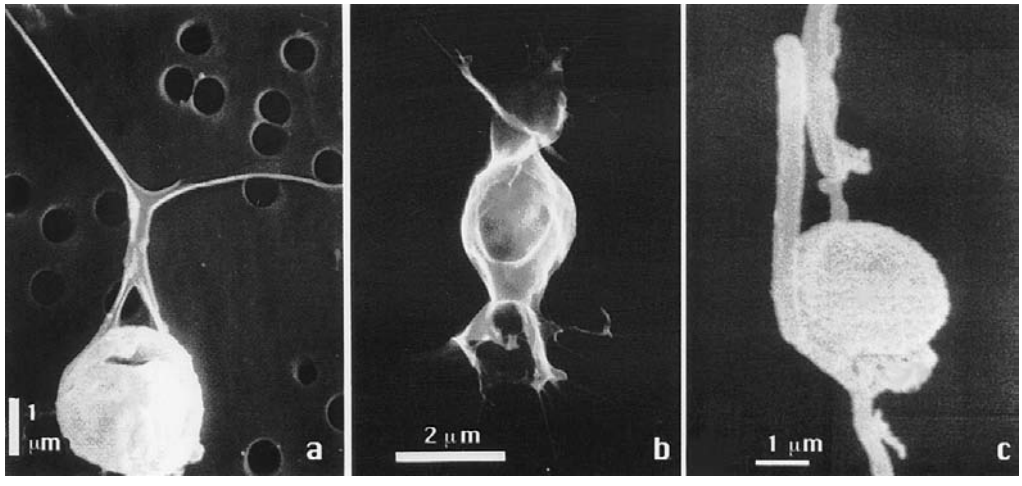


Fig. 4.22 Examples of spermatangial appendages. (*a*) Appendage of *Antithamnion nipponicum*. (*b*) Fimbriate cone-shaped appendages at each end of *Aglaothamnion neglectum*. (*c*) Fibrous strands attached to spermatia of *Tiffaniella snyderae*. ((*a*) from Kim and Fritz, 1993; (*b*) from Magruder, 1984; (*c*) from Fetter and Neushul, 1981.)

In some of the red algae it is possible to control tetrasporogenesis by varying the light period, but there is no general rule that can be applied to the response. In *Rhodochorton purpureum* (West, 1972; Dring and West, 1983) and *Acrochaetium asparagopsis* (Abdel-Rahman, 1982), tetrasporophytes produce tetrasporangia under short-day conditions. According to the physiological clock hypothesis, photoperiodism is controlled by an endogenous free-running **circadian** (approximately 24-hour) oscillation of some biochemical change. Each oscillation involves a regular alternation of two phases (each lasting approximately 12 hours) with a different sensitivity to light. The two phases are a **photophile** (light-loving) phase and a **skotophile** (dark-loving) phase. The initiation of a particular event depends on initiation or inhibition of metabolic changes of short-day or long-day organisms, respectively, by exposure to light at a particular point in the skotophile phase. In the case of *Rhodochorton purpureum* and *Acrochaetium asparagopsis*, light-breaks in the dark (skotophile) phase result in inhibition of tetrasporogenesis, whereas dark-breaks in the light (photophile) phase result in stimulation of tetrasporogenesis. Tetrasporogenesis in these algae is therefore a short-day phenomenon (Abdel-Rahman, 1982).

Polysporangia contain more than four spores, usually in multiples of four (Fig. 4.17(*f*)). Polysporangia probably evolved from tetrasporangia because polysporangia occur predominantly in the most advanced order, the Ceramiales. **Bisporangia** are probably reduced tetrasporangia in which cell division has resulted in two spores after meiosis instead of four.

Asexual spores

Monosporangia (one spore per sporangium) and **parasporangia** (more than one spore per sporangium) produce asexual spores that re-form the parent thallus. Monosporangia can be formed by the release of a vegetative cell from the thallus (*Goniotrichum*, Fig. 4.25(*b*), *Asterocystis*, Fig. 4.25(*a*)), or by the formation of sessile one-celled branches (*Kylinia*, Fig. 4.17(*g*)).

Spore motility

Spores, whether monospores, tetraspores or carpospores, of almost all red algae are capable of motility by gliding. Some spores have smooth, directional and continuous gliding (e.g., *Batrachospermum* at 2.2 μm s^{-1}). In others, movement is non-continuous and unidirectional. Polysaccharide secretion appears to be responsible for the gliding (Pickett-Heaps et al., 2001).

Classification

The Rhodophyta has a single class, the Rhodophyceae. In the past, the Rhodophyceae was divided into two subclasses, the Bangiophycidae and the Florideophycidae. The Bangiophycidae were supposed to lack pit connections, apical growth, and probably sexual reproduction, whereas the Florideophycidae had pit connections, apical growth, and sexual reproduction with a triphasic life cycle. The Bangiophycidae have since been found to have pit connections and apical growth in the *Conchocelis* filamentous stage of the Bangiaceae. Sexual reproduction also occurs in the Bangiaceae. In turn, the Florideophycidae do not necessarily have apical growth (intercalary growth occurs in the Corallinales (Dixon, 1973)), nor do they all have a triphasic life history (e.g., red algae in the Batrachospermales). For the above reasons, the two subclasses have been dropped in this treatment of the Rhodophyceae, as suggested by Gabrielson (Gabrielson, et al., 1985).

The classification of the more advanced orders of the red algae is based on complex characteristics of sexual reproduction. One of the more active fields of phycology in the last couple of decades has been in the application of nucleic-acid sequencing techniques in a delineation of the evolutionary relationships of these algae. While producing a more natural grouping of algae, these excellent studies have produced an even more complex classification system, which is difficult to present to a student taking a first course in phycology, to which this book is directed. In writing the current edition of the book, the author has spent some time trying to decide how to present the classification of the red algae, and has decided that a presentation of all of the more advanced orders would overwhelm the beginning student. As such, the author has selected those red algae that are commonly studied in phycology courses and/or are economically or ecologically important.

Order 1 **Cyanidiales**: unicells that inhabit volcanic areas with pH values ranging from 0.5 to 3.

Order 2 **Porphyridiales**: unicells, or multicellular algae that are held together by mucilage.

Order 3 **Bangiales**: plants having a filamentous phase with pit connections and a macroscopic phase without pit connections.

Order 4 **Acrochaetiales**: algae with a uniseriate filamentous gametophyte and tetrasporophyte (if both are present).

Order 5 **Batrachospermales**: uniaxial (one apical cell per branch); gonimoblast usually develops from the carpogonium or hypogenous cell.

Order 6 **Nemaliales**: multiaxial (more than one apical cell per branch); usually the gonimoblast develops from the carpogonium or the hypogenous cell.

Order 7 **Corallinales**: heavily calcified algae with the reproductive organs in conceptacles.

Order 8 **Gelidiales**: fleshy agarophytes, carpogonial branch consisting of a single cell, the carpogonium, no differentiated auxiliary cells.

Order 9 **Gracilariales**: fleshy agarophytes, two-celled carpogonial branch, no auxiliary cells, or connecting cells.

Order 10 **Ceramiales**: relatively delicate or filamentous forms with an auxiliary cell cut off after fertilization and borne on the supporting cell of a four-celled carpogonial filament.

Sequencing of nucleic acids have shown that the Cyanidiales and Bangiales represent separate natural groupings. The Porphyridiales are a grouping of three separate lines of unicells (Saunders and Hommersand, 2004). The Acrochaetiales, Batrachospermales, Nemaliales, and Corallinales are a natural grouping, as are the Gracilariales, Gelidiales, and Ceramiales (Harper and Saunders, 2001).

Using molecular data, it is estimated that the red algae diverged from other eukaryotes about 1400 million years ago (Yoon et al., 2004). The Cyanidiales diverged from the rest of the red algae soon after that, about 1370 million years ago. The Bangiales diverged from the remaining red algae

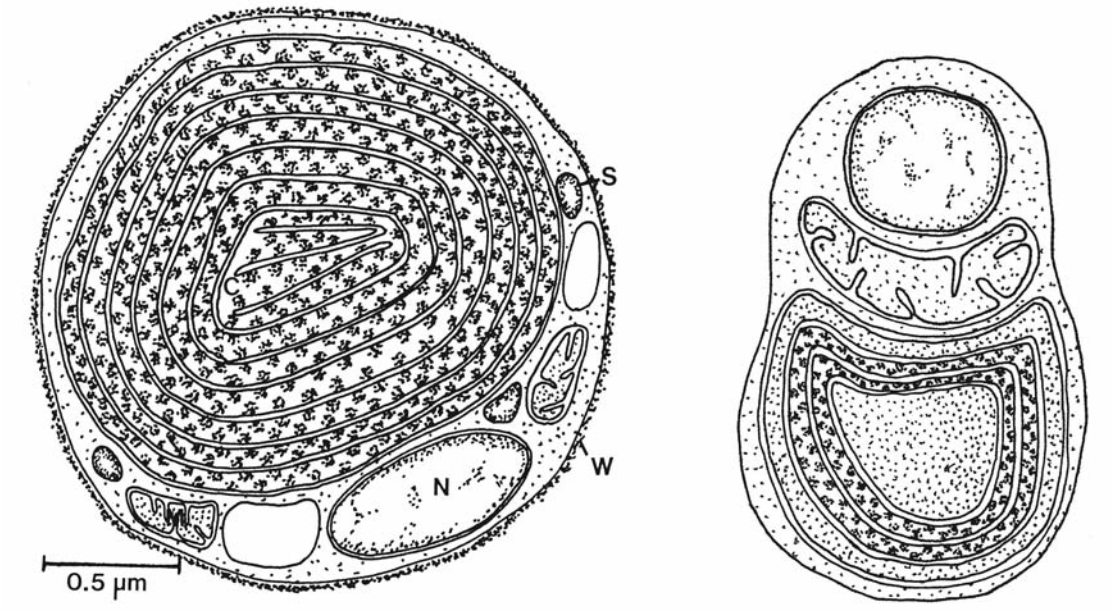


Fig. 4.23 *Left: Cyanidium caldarum. Right: Cyanidioschyzon merolae*. (C) Chloroplast; (M) mitochondrion; (N) nucleus; (S) starch; (W) wall. (*Cyanidium* is after Seckbach and Ikan, 1972.)

about 1000 million years ago. The first fossil convincingly identified as a red alga is a 1200 million-year-old fossil similar to extant *Bangia* (Fig. 4.28) (Butterfield, 2000). Fossil coralline red algae have been recovered from the late Jurassic (160 million years ago) (Wray, 1977).

The relationship between freshwater and marine Rhodophyceae, as well as their evolution, was discussed in an interesting paper by Skuja (1938). He believed that the Rhodophyceae are a very old group (as is borne out by their fossil record) that originated in shallow coastal waters of primitive seas poor in salt. Living in shallow water, these plants had no need of a large quantity of phycoerythrins to absorb the blue-green light present at greater depths of water. Consequently these primitive Rhodophyceae were not pinkish-red but blue-green in color. These plants are represented by the freshwater Rhodophyceae of today, which are predominantly blue-green in color, and found primarily in the more primitive orders such as the Porphyridiales, Bangiales, Acrochaetiales, and Nemaliales. Only later did the Rhodophyceae develop greater quantities of phycoerythrins, and a pinkish-red color, and penetrate into deeper waters where they attained their present state of development.

Cyanidiales

This order contains three unicellular red algae: *Cyanidium caldarum*, *Cyanidioschyzon merolae*, and *Galderia sulphuraria* (Fig. 4.23). These algae inhabit volcanic areas with pH values ranging from 0.5 to 3 and temperatures up to 56°C (Gross et al., 2001).

Cyanidium caldarum and *Cyanidioschyzon merolae* are similar in that each of these unicells contains a single nucleus, mitochondrion, and plastid (Fig. 4.23). They differ in that *Cyanidium* is round, has a cell wall, and forms four endospores while *Cyanidioschyzon* is club shaped, has no cell wall, and divides by binary fission (Ohta et al., 1997). *Cyanidioschyzon* has the smallest genome size (16 520 305 base pairs and 5331 genes) so far recorded in eukaryotes and has had its genome sequence elucidated (Matsuzaki et al., 2004).

Galderia sulphuraria is morphologically similar to *Cyanidium caldarum*. *Galderia sulphuraria*, however, is able to grow heterotrophically while *Cyanidium caldarum* can not.

The algae in the Cyanidiales are probably the most primitive extant algae, evolving into an environment (acidic hot springs) that was an empty ecological niche at the time. The only other photosynthetic algae present at the time

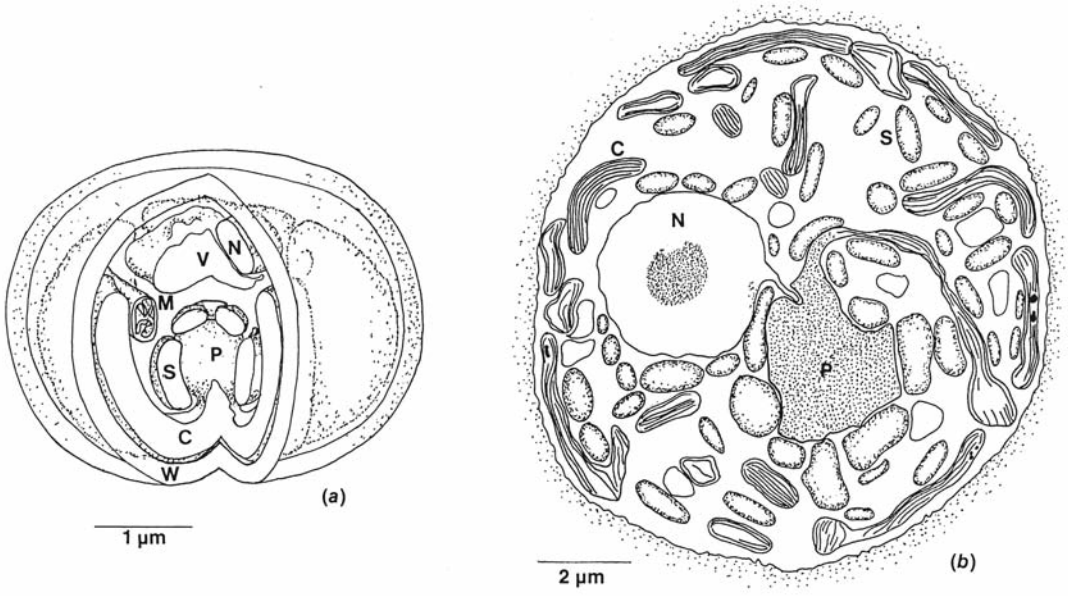


Fig. 4.24 (*a*) A diagrammatic drawing of a cell of *Rhodosorus marinus*. (*b*) A semidiagrammatic drawing of a section through a cell of *Rhodella maculata*. (C) Chloroplast; (M) mitochondrion; (N) nucleus; (P) pyrenoid; (S) starch grain; (V) vacuole; (W) wall. ((*a*) after Giraud, 1962; (*b*) adapted from Evans, 1970.)

were cyanobacteria. Cyanobacteria do not occur in ecological niches below a pH of 5 (Brock, 1973). It, therefore, makes sense that the first eukaryotic alga would have had an evolutionary advantage by evolving in an environment where there were no other photosynthetic algae to compete with.

Porphyridiales

These algae are either unicells or cells embedded in mucilage loosely organized into filaments. There are three evolutionary lines in the order (Oliveira and Bhattacharya, 2000; Karsten et al., 2003).

The unicells in the Porphyridiales are probably derived from monospores, carpospores or tetraspores of more evolutionarily advanced red algae (Ragan et al., 1994; Freshwater et al., 1994). These unicells are differentiated by cytological characteristics. Thus, *Porphyridium* (Fig. 4.1) has a single large stellate chloroplast with a central pyrenoid. *Rhodosorus* (Fig. 4.24(*a*)) has a lobed chloroplast with a basal pyrenoid, and *Rhodella* has a stellate chloroplast with a central pyrenoid, but with a more dissected chloroplast than *Porphyridium* (Figs. 4.2, 4.24(*b*)).

Porphyridium is a common alga on soil and damp walls where it forms several-layered blood-red mucilaginous strata. Even though it is a soil alga, most species grow best in marine liquid media, indicating that it is probably of brackish or marine origin. *Porphyridium* has the ability to glide over a substrate it is in contact with. Overhead illumination results in random movement, whereas unilateral light causes movement toward the light source (Sommerfield and Nichols, 1970). The positively phototactic cells move by the extrusion of mucilage in vesicles in one direction, which results in the formation of a mucilage stalk behind the cells (Lin et al., 1975). *Porphyridium* releases different amounts of polysaccharides, depending on the environmental conditions it is living under (Ramus and Robins, 1975). During the log phase of growth, large Golgi bodies form polysaccharides, which are stored in vesicles under the cell membrane. During the stationary phase of growth in culture, the polysaccharide is secreted outside the cell, giving rise to a capsule. This behavior in culture can be related to the survival of the cells in nature. The rapid log phase of growth is equivalent to a soil environment that is moist with available nutrients. Here the polysaccharides are stored inside the cell, and there is

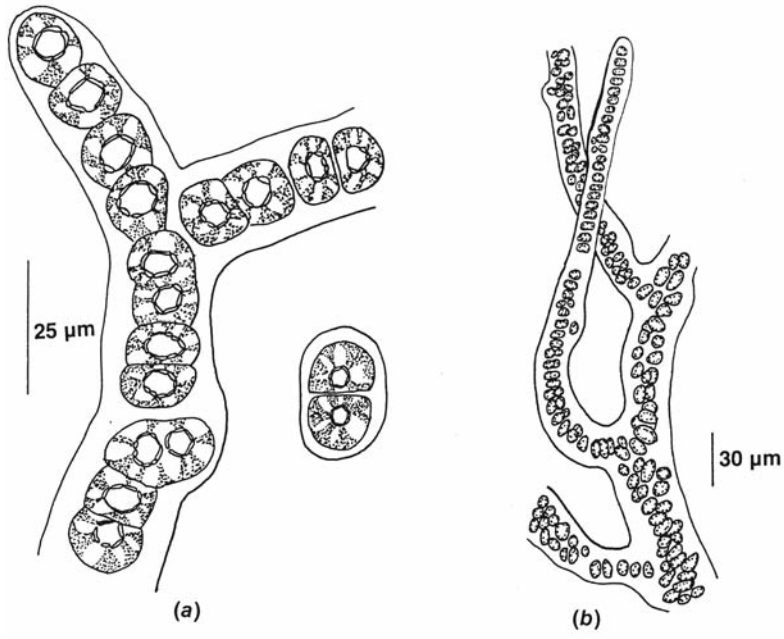


Fig. 4.25 (*a*) *Asterocytis* sp. in the filamentous and bicellular form. (*b*) *Goniotrichum alsidii*. ((*a*) after Belcher and Swale, 1960; (*b*) after Taylor, 1957.)

only a thin mucilage layer around the cell. The stationary phase of growth is equivalent to a soil environment that is drying out with nutrients becoming limiting, thereby causing a cessation of cell growth. Here the polysaccharides are released to the outside of the cell, where they form a capsule that enables the cell to withstand the desiccation that follows.

Also included in this order are algae that have cells joined together in thick mucilaginous filaments. *Goniotrichum* is a common marine epiphyte made up of branched mucilaginous filaments (Fig. 4.25(*b*)). *Goniotrichum* forms monospores simply by the release of a vegetative cell from a filament in photoperiods of over 12 hours of light (Fries, 1963). *Asterocytis* (Fig. 4.25(*a*)) exhibits what is probably an intermediate position in the evolution of a red unicell into a mucilaginous filamentous alga. In normal seawater *Asterocytis* forms branched filaments, whereas in seawater of one-fourth strength the organism forms unicells, which were previously classified in the genus *Chroothece* (Lewin and Robertson, 1971).

Bangiales

The algae in this order show alternation of a haploid thallus stage having no pit connections, with a diploid filamentous *Conchocelis* state that has pit connections (Lee and Fultz, 1970; Kornmann, 1994). The Bangiales is a monophyletic order and is a sister group to the higher red algae (Oliveira and Bhattacharya, 2000).

Porphyra (Figs. 4.26, 4.27) is an intertidal seaweed in the colder waters of the world. The thallus arises from a holdfast and is composed of a sheet of cells one to two layers thick. *Porphyra gardneri* (Fig. 4.27) is a foliose (leafy) monostromatic (single layer of cells) alga found growing epiphytically on several members of brown algae in the Laminariales. In British Columbia, Canada, the host *Laminaria setchellii* has its blade worn back almost to the stipe by November. During December, a new *Laminaria* blade is rapidly produced. The first thalli of *Porphyra gardneri* appear epiphytically on the *Laminaria* at the end of February. **Asexual reproduction** occurs soon after *Porphyra gardneri* appears in February. The margins of the thallus break down and release single-celled **monospores**. After 1 or 2 days, the monospores germinate by sending out long rhizoids that anchor the monospores in the host *Laminaria* tissue. From this, a new leafy thallus appears. Prolific monospore production results in a great increase of *Porphyra gardneri* during the spring months. **Sexual reproduction** begins

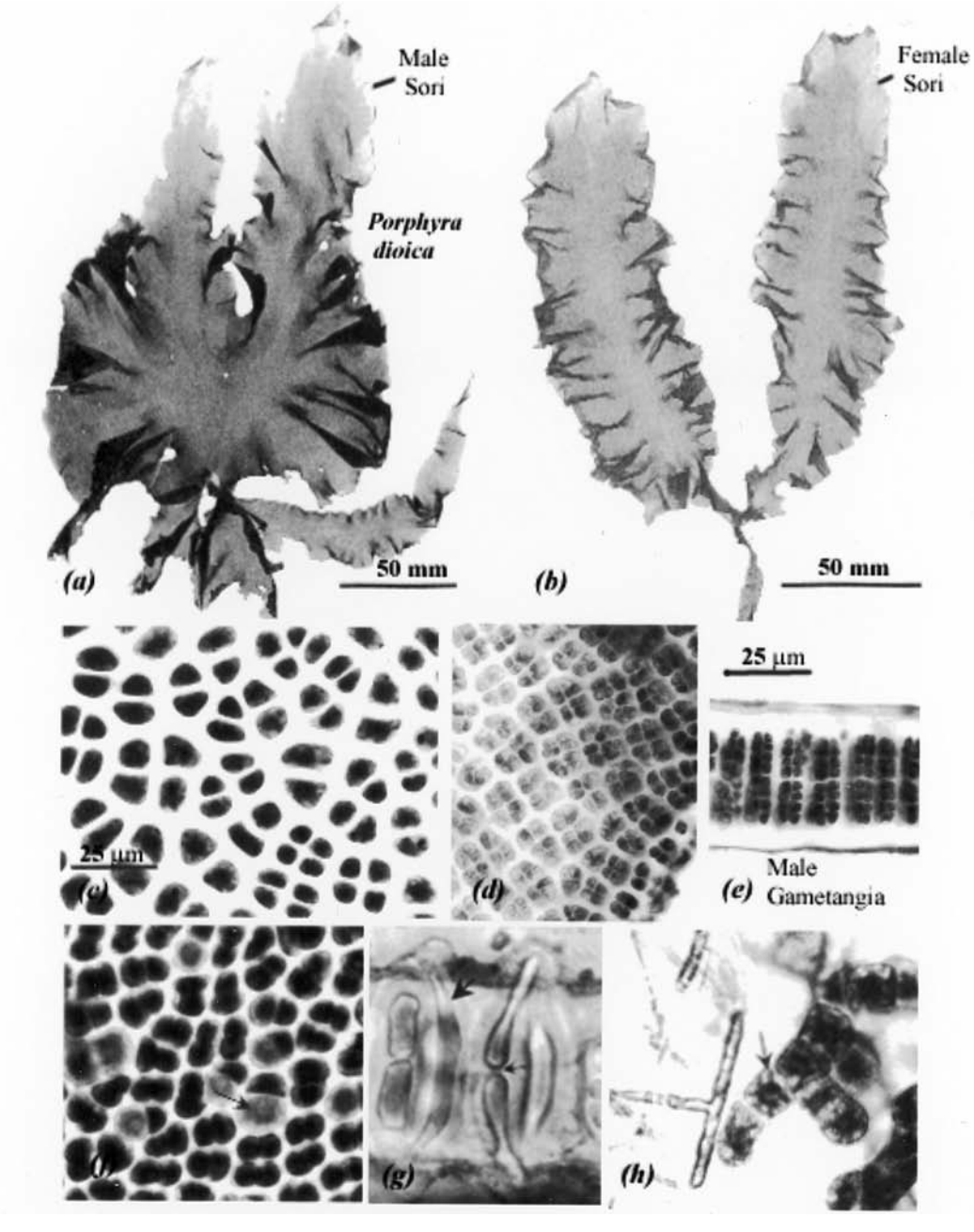


Fig. 4.26 *Porphyra dioica.* (*a*) Male gametophyte with male gametangia in sori. (*b*) Female gametophyte with female gametangia in sori. (*c*) Surface view of vegetative cells in pairs. (*d*) Surface view of male gametangia. (e) Male gametangia in transverse section. (*f*) Gametangial mother cell (arrow) in surface view. (*g*) Carpogonium (large arrow) and first division of fertilized carpogonium (small arrow) in transverse section of thallus. (*h*) *Conchocelis* stage with conchosporangia (arrow). (From Holmes and Brodie, 2004.)

during late April. Spermatium mother cells in the thallus divide to form 64 spermatia. The spermatia contain a degenerate chloroplast with only a few thylakoids. Vesicles containing a fibrous material are discharged by the spermatia just before spermatia liberation. The released spermatia are 3 to 5 µm in diameter, have no starch granules, and are surrounded only by the fibrous

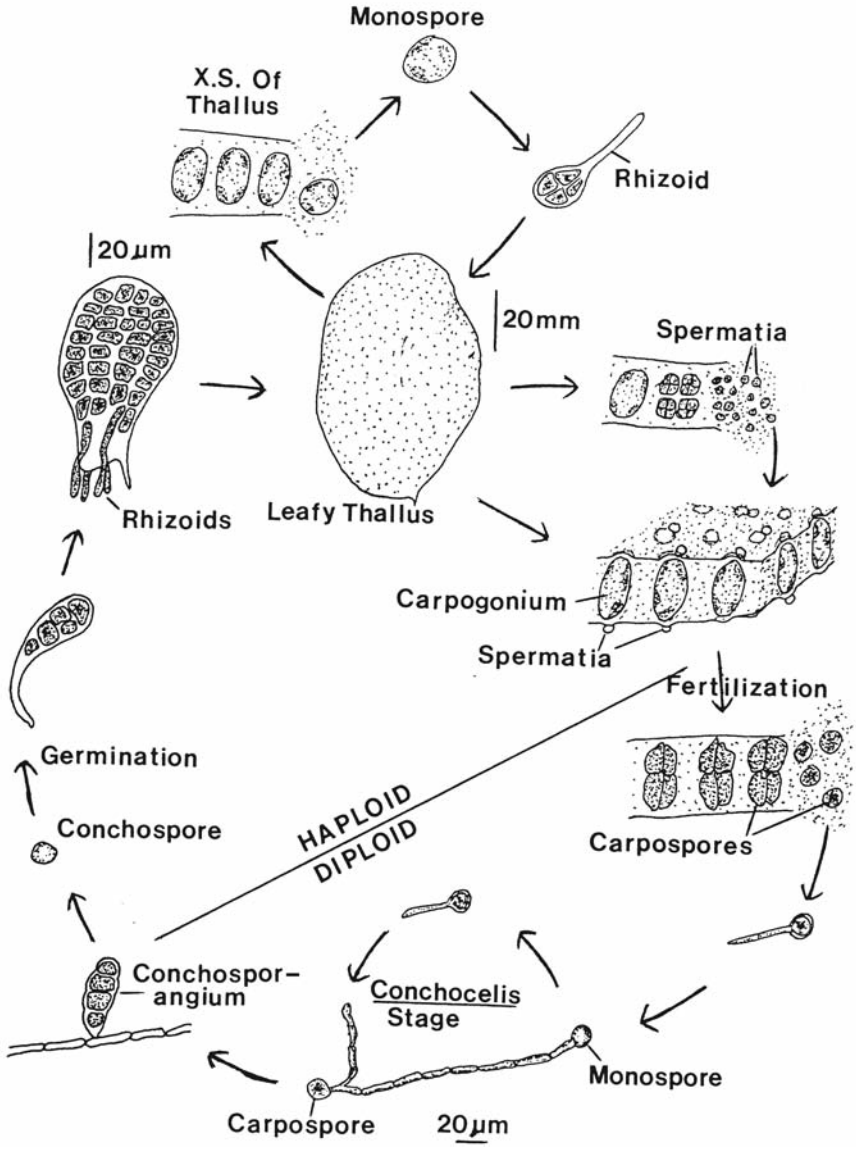


Fig. 4.27 The life cycle of *Porphyra gardneri*. (Adapted from Hawkes, 1978.)

material from the released vesicles. The spermatia are carried to the carpogonia by water currents. Carpogonia (with a chromosome number of 4) differentiate from vegetative cells by the production of a swollen area of the cell wall, the **prototrichogyne**, directly above the carpogonium. In a monostromatic species, such as *Porphyra gardneri*, two prototrichogynes are produced by each carpogonium, one on each surface. In distromatic species, with two sheets of cells in the thallus, a single prototrichogyne is produced per carpogonium. A spermatium attaches to the prototrichogyne, a fertilization canal appears in the prototrichogyne, and the spermatial nucleus moves through the canal to fuse with the carpogonium. By the beginning of May, the fertilized carpogonia have divided to form two to four diploid carpospores (with a chromosome number of 8), 14 to 20 μm in diameter. Maximum carpospore production occurs during the months of June through August. The carpospores germi-

nate in 2 to 3 days to produce the diploid *Conchocelis* stage (Hawkes, 1978). The *Conchocelis* stage is filamentous and commonly lives in shells of dead marine animals. Under long-day conditions, the *Conchocelis* stage differentiates monospores, which re-form the *Conchocelis* stage (Dixon and Richardson, 1970). Under short days the *Conchocelis* stage forms conchosporangia (fertile cell rows), each cell of which produces a conchospore. Conchospores are released from the conchosporangia under low-temperature conditions (about 5 °C) (Chen et al., 1970). The formation of the conchosporangia under short-day conditions is a true photoperiodic response because a light break in the middle of the dark period is inhibitory (Dring, 1967a). A functional phytochrome system is operative, with red light being the most effective in breaking the dark period (Dring, 1967b). This is one of the few demonstrations of a true photoperiodic response in the red algae, and it is unlikely that this phytochrome type of response occurs in sublittoral Rhodophyceae because far-red light penetrates to less than 1 m of seawater and red light no deeper than 10 m (Dixon and Richardson, 1970). On release, the conchospores germinate in a bipolar manner, forming a germling that grows into the thallus phase, completing the life cycle.

Porphyra perforata lives in the intertidal zone, where at low tide the plants are routinely exposed to air drying. As a result of evaporative water loss, the salt concentration of extracellular water can increase up to 10 times above normal levels. During desiccation at low tide, the alga can lose up to 90% of its fresh weight. Such desiccation results in inhibition of photosynthesis. Some of the inhibition of photosynthesis is probably due to a decrease in electron flow between water and photosystem II because of a reduced concentration of water in the cells (Satoh et al., 1983).

Bangia forms upright threads that are at first uniseriate, the cells subsequently undergoing longitudinal division to form a multiseriate filament

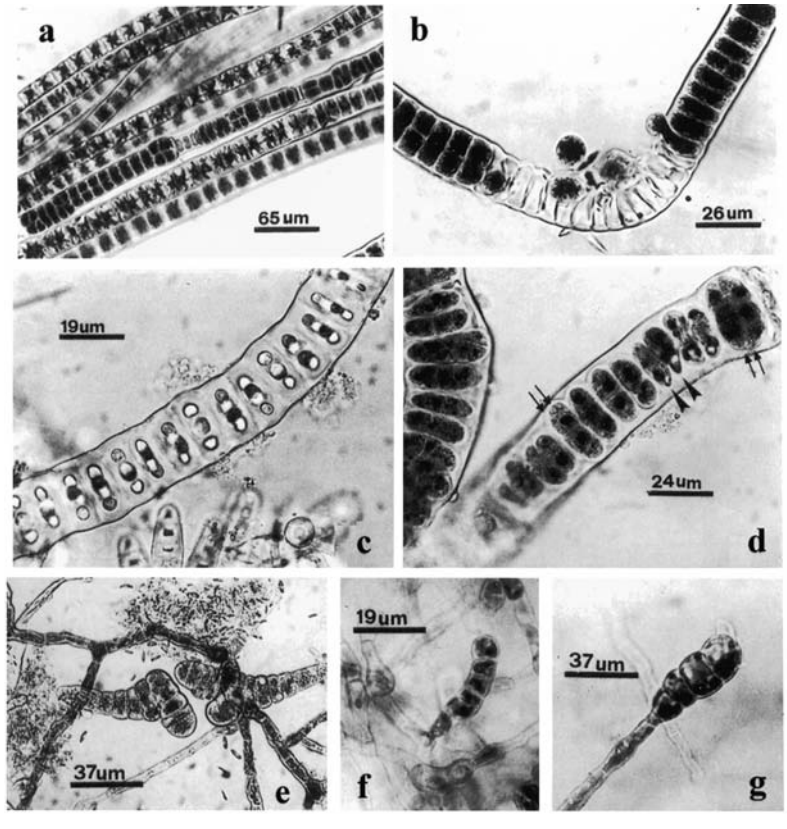


Fig. 4.28 *Bangia atropurpurea.* (*a*) Uniseriate filaments becoming multiseriate by successive division of cells. (*b*) Filament releasing monospores. (*c*) Male gametophytes with spermatia. (*d*) Female gametophytes. Arrowheads show a carpogonium with a single trichogyne. Arrows point to developing zygotes. (e) Conchosporangia. (*f,g*) Monosporangia on sporophytes. (From Gargiulo et al., 2001.)

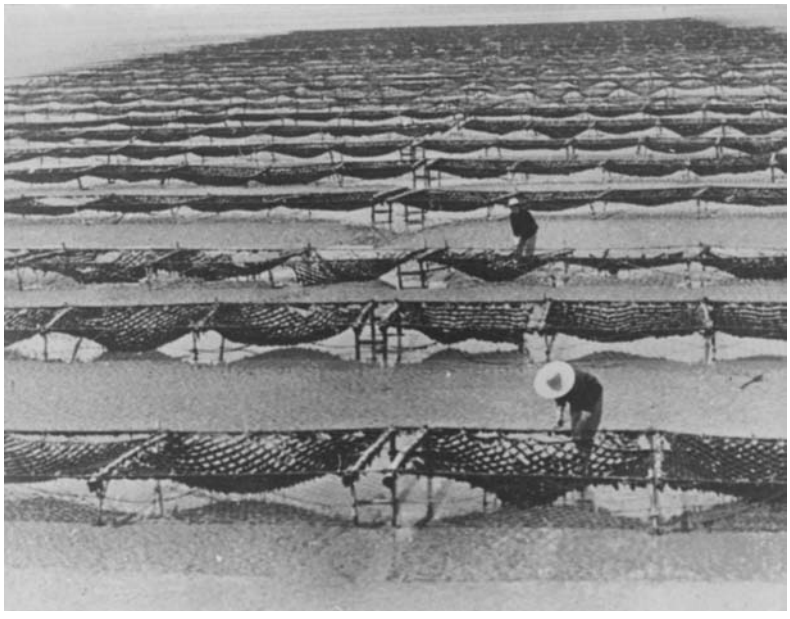


Fig. 4.29 Cultivation nets with *Porphyra* at low tide at Rudang, Jiangsu Province, People's Republic of China. (From Tseng, 1981.)

(Fig. 4.28). *Bangia* occurs in both marine and freshwater environments. *Bangia*-like fossils (*Bangiomorpha pubescens*) have been reported from the 1200 million-year-old Hunting formation on Somerset Island in Canada (Butterfield, 2000). It is possible to adapt freshwater *Bangia fuscopurpurea* to seawater by increasing the salinity by 10% of that of seawater every time the alga sporulates (den Hartog, 1971). If the thallus is moved directly from freshwater to seawater, the plant dies, illustrating that the spores have a better ability to adapt to changed salinity. Such an experiment shows the ease with which some of the smaller red algae can change from one habit to another. *Bangia* has a life cycle similar to that of *Porphyra* (Richardson, 1970; Sommerfeld and Nichols, 1973).

The diploid *Conchocelis* phase of *Porphyra* and *Bangia* differs chemically from the haploid thallus phase (Liu et al., 1996). The *Conchocelis* phase has cellulose in the wall of the cells, whereas in the thallus phase, cellulose is absent and, as the structural polysaccharide, is replaced by a xylan (polysaccharide composed of xylose residues) (Gretz et al., 1980; Mukai et al., 1981). The galactans in the *Conchocelis* phase are also different from those in the thallus phase (Gretz et al., 1983). These chemical differences are in addition to the structural differences, particularly the occurrence of pit connections in the *Conchocelis* phase and their absence in the thallus phase.

The *Conchocelis* phase has been found as the fossil genus *Palaeoconchocelis starmachii* in the Upper Silurian of the Paleozoic (425 million years ago) (Campbell, 1980).

The leafy thallus phase of *Porphyra* is eaten as a vegetable in the Far East and Nova Scotia (Canada). In Japan, *Porphyra* is eaten as a vegetable called *nori*; in Nova Scotia, it is called *laver*. *Porphyra* is cultivated on farms in China (Fig. 4.29) and Japan. In Japan, most of the *Porphyra* comes from *Porphyra* farms in the shallow waters of such places as the Inland Sea and Tokyo Bay, although there is considerable collecting of plants from natural populations. *Porphyra* was first cultivated around 1700 in Tokyo Bay by placing bundles of bamboo or oak bushes (known as hibi) into the mud in early autumn, the usual procedure being to arrange the bundles in regular rows and at such a depth that the twigs were well covered by water at high tide. The modern method is to drive bamboo stakes into the mud in rows and then place netting between the stakes (Mumford and Miura, 1988). The *Conchocelis* stage growing in seashells releases the conchospores, which settle on the brush or nets and germinate to form the foliose *Porphyra* plant. From late November to March, the *Porphyra* plants (sometimes mixed with the green alga *Monostroma*)

are harvested by a person in a narrow boat who picks or scrapes the plants off by hand. The *Porphyra* is brought to the factory, where it is washed and chopped into small fragments. These fragments are stirred in a vat, from which measured amounts of the mixture are dipped by means of a small wooden container and poured over a stiff porous mat. As the liquid drains away, the nori fragments are spread evenly over the mat, which is hung on outdoor bamboo racks to dry. The thin film of dry nori is removed as a sheet from the mat, folded, and packaged for market. The food value of nori or laver lies in its high protein content (25% to 30% of the dry weight), vitamins, and mineral salts, especially iodine. The vitamin C content is about 1½ times that of oranges per unit weight, and it is also rich in vitamin B. Humans digest about 75% of the protein and carbohydrate, and in this respect it is much better than other seaweeds.

Prior to the discovery of the alternate *Conchocelis* phase of *Porphyra* by Drew, the yield of *Porphyra* fluctuated sharply from one year to the next. Up to this time, the number of *Porphyra* plants formed depended on the production of conchospores by the *Conchocelis* phase. These fluctuations in the production of spores have been overcome by the artificial cultivation of the *Conchocelis* phase, usually on shells. The shells containing the *Conchocelis* phase are attached to the nets, or the nets are dipped into baths to which crushed shells have been added. The best settlement of spores occurs in waters of high nitrogen, that is, near sewage outflows. Another way of seeding *Porphyra* is by monospores. Monosporangia have been induced in haploid thalli by three week exposure to allantoin (Fig. 4.30) followed by homogenization of the thalli. The resulting monospores reproduce the haploid thalli of *Porphyra* (Mizuta et al., 2003). Although the production of nori increased until the early 1960s, there has been no increase in production since then, mostly because of increasing pollution of the shallow waters in which *Porphyra* farming is carried out (Dixon, 1973).

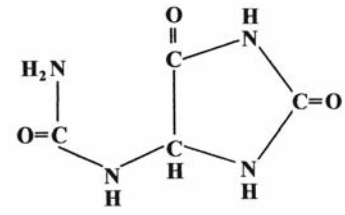


Fig. 4.30 The chemical structure of allantoin, an inducer of monospore formation in *Porphyra*.

Acrochaetiales

Algae with uniseriate filaments are in this order (Chemin, 1937; Feldman, 1953). Papenfuss (1945, 1947) recognizes four major genera in the order: (1) *Rhodochorton*, with each cell containing a few to many small discoid chloroplasts (Fig. 4.31); (2) *Acrochaetium*, with each cell having one parietal or laminate chloroplast (Fig. 4.17(*c*)); (3) *Audouinella*, with each cell having one or more spiral chloroplasts; (4) *Kylinia*, with each cell having one or more stellate chloroplasts (Fig. 4.17(*g*)).

Most of these algae are small epiphytes or endophytes. Some of them may still prove to be the alternate phase of more complex higher Rhodophyceae. *Rhodochorton investiens* can be used as an example of a triphasic life cycle (Fig. 4.31) (Swale and Belcher, 1963). Both the gametophyte and tetrasporophyte produce similar obovoid monospores in monosporangia arising just beneath a cross wall of the filament. The spore is liberated through the apex of the sporangial wall, which remains attached to the filament. After release, the monospores germinate without a resting phase to re-form the parent plant. The gametophyte is monoecious, with a filament ending in a cluster of spermatangia and a carpogonium being borne on the cell under the supporting cell of the spermatangia. The spermatangia occur in groups of four to six, emerging from the enlarged and flattened distal end of a terminal cell. The carpogonia are sessile and appear in the position of branch cells. At the distal end of the carpogonium is a narrow trichogyne. After fertilization, the carpogonium becomes divided by three cross walls into a row of four cells. The first transverse wall develops below the trichogyne, the upper cell then elongating and dividing into three cells. This results in the trichogyne emerging from the second cell of the row. Two-celled gonimoblast

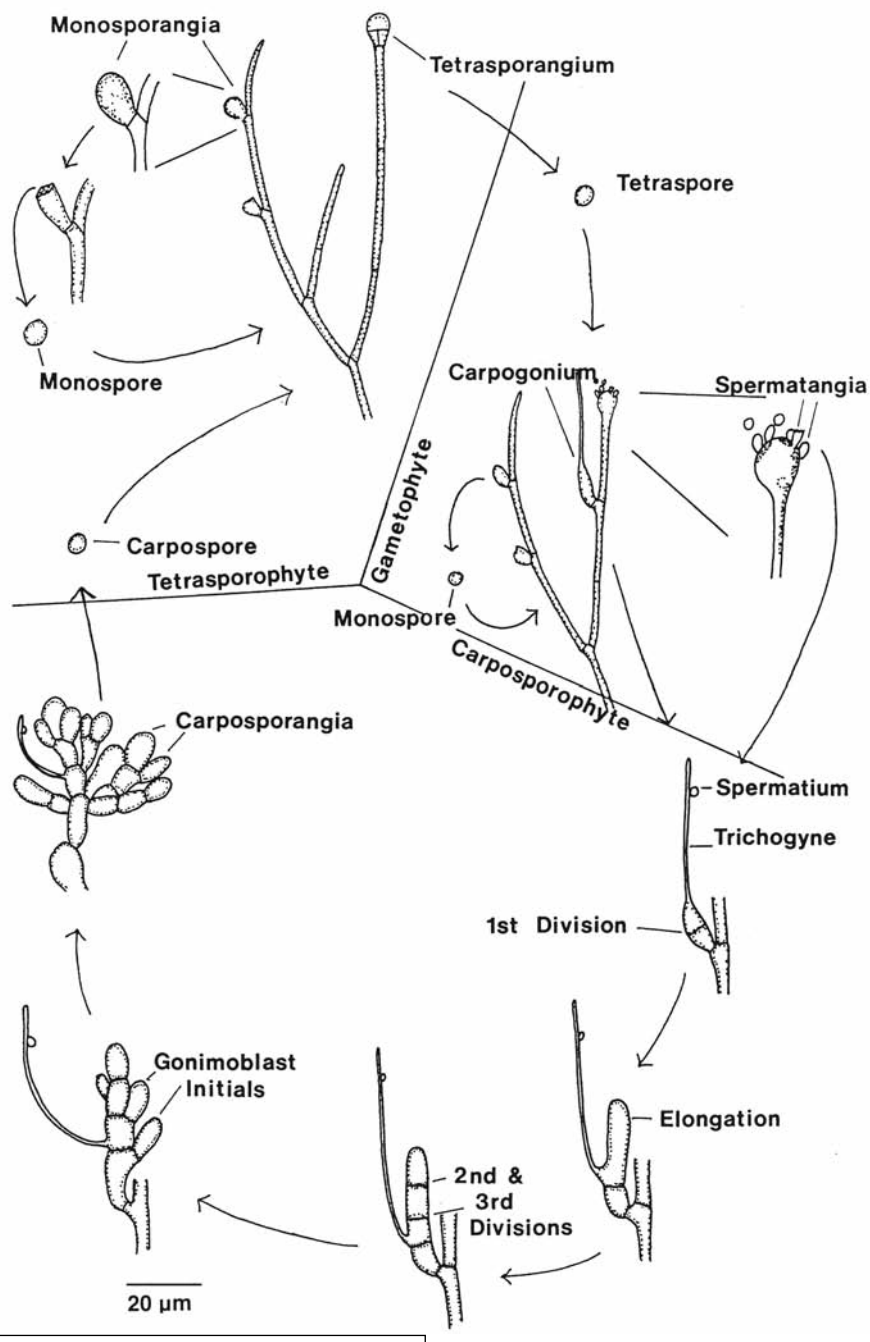


Fig. 4.31 The life cycle of *Rhodochorton investiens*. (Adapted from Swale and Belcher, 1963.)

filaments develop from each cell of the row, each gonimoblast filament producing two to three terminal carpospores. The carpospores germinate to form the tetrasporophyte, with larger cells of deeper color than those of the gametophyte. Tetrasporangia either are sessile or terminate a one-celled branch. The tetraspores germinate to produce the gametophyte, and thus complete the life cycle.

Batrachospermales

This order includes the uniaxial (each filament with a single apical cell) freshwater Rhodophyceae.

The gonimoblasts usually arise from the fertilized carpogonium. No tetraspores are formed, and meiosis probably occurs when the diploid filamentous stage forms the thallus initials.

Batrachospermum (often called the "frog spawn" alga) is a freshwater alga that occurs in well-aerated, slow-moving streams. The gametophyte (Fig. 4.32) appears as delicate violet beads on a string. Each "bead" consists of whorls of branches arising at the cross walls of the elongated cells of the main axis. The gametophytes produce terminal carpogonia on short branches arising from the whorls of branches. Spherical spermatia are formed by small groups of antheridia at the tips of branches. The spermatia are carried to the carpogonium by water currents. After fertilization, the zygote cuts off gonimoblast initials which develop into gonimoblast filaments with terminal carposporangia. The carposporangia release diploid carpospores that germinate into filamentous prothalli. Monospores can be produced by the prothalli. The monospores germinate to re-form the parent plant. The prothalli also form erect filaments that elongate by apical growth. The apical cell of the erect filament cuts off three to five cells mitotically, then undergoes two meiotic divisions. The first meiotic division results in (1) a polar body and (2) a cell that divides again to form a second polar body and the apical cell of the haploid gametophyte. The macroscopic plant is thus composed of basal diploid cells on a haploid plant. The diploid portion of the plant has cells that are larger than those of the haploid portion (Hurdelbrink and Schwantes, 1972; von Stosch and Theil, 1979; Balakrishnan and Chaugle, 1980; Necchi, 2002).

Nemaliales

This order has multiaxial Rhodophyceae (with more than one apical cell), which usually have gonimoblasts developing from the carpogonium or hypogynous cell. There may be auxiliary cells present, but if there are, they are always nutritive auxiliary cells.

Nemalion is a common intertidal alga in north temperate seas. The thallus is a soft gelatinous cylinder reaching a length of 25 cm with a limited number of dichotomous branches (Fig. 4.33), being composed of a number of axial threads or filaments in the center and richly branched laterals around the periphery. The laterals arise from the axial threads and grow out horizontally on all parts of the thallus except for the tip where they radiate out vertically. The laterals are all of about the same length, and their tips intercalate so as to give the thallus an even surface. The central axial cells are colorless, whereas the peripheral laterals usually have a stellate chloroplast with a central pyrenoid.

In *Nemalion*, the plants are homothallic. The carpogonial branch consists of an ordinary lateral of four to seven cells (Fig. 4.33). The elongate trichogyne projects slightly beyond the surface of the thallus. Spermatangial branches are produced from the terminal cells of the laterals, and at the tip of the two- to four-celled spermatangial branch are formed three to four spermatangia. Spermatangia produce spermatia that are released and pass to the trichogyne of the carpogonium where fertilization occurs. After fusion of the two gamete nuclei, the large zygote nucleus and the chloroplast divide into two. The carpogonium then divides transversely into two cells, the upper of which forms the gonimoblasts. The lower cell of the carpogonium gradually fuses with the **hypogynous cells** (those underneath the carpogonium), and eventually the upper carpogonial cell that has produced the gonimoblasts also fuses with these cells. These fusions probably have a nutritive function, providing the developing gonimoblasts and carposporangia with storage products. The gonimoblast threads hang downward, and each cell of the thread forms an upwardly curved two- to three-celled branchlet, the terminal cell of which enlarges to form the carposporangium. The carpospores give rise to a filamentous phase that produces tetraspores under short-day conditions (Cunningham and Guiry, 1989). The tetraspores produce filamentous gametophytes that form the erect axes under long-day conditions.

Galaxaura (Fig. 4.34) is a calcified alga that is widely distributed in the tropics. The calcification occurs as aragonite (Fig. 4.7) in the intercellular spaces of the cortex. *Galaxaura* has a gametophyte and tetrasporophyte that are similar in appearance. Male and female reproductive structures are borne in conceptacles deeply immersed in the medulla of the gametophytes, while tetraspores

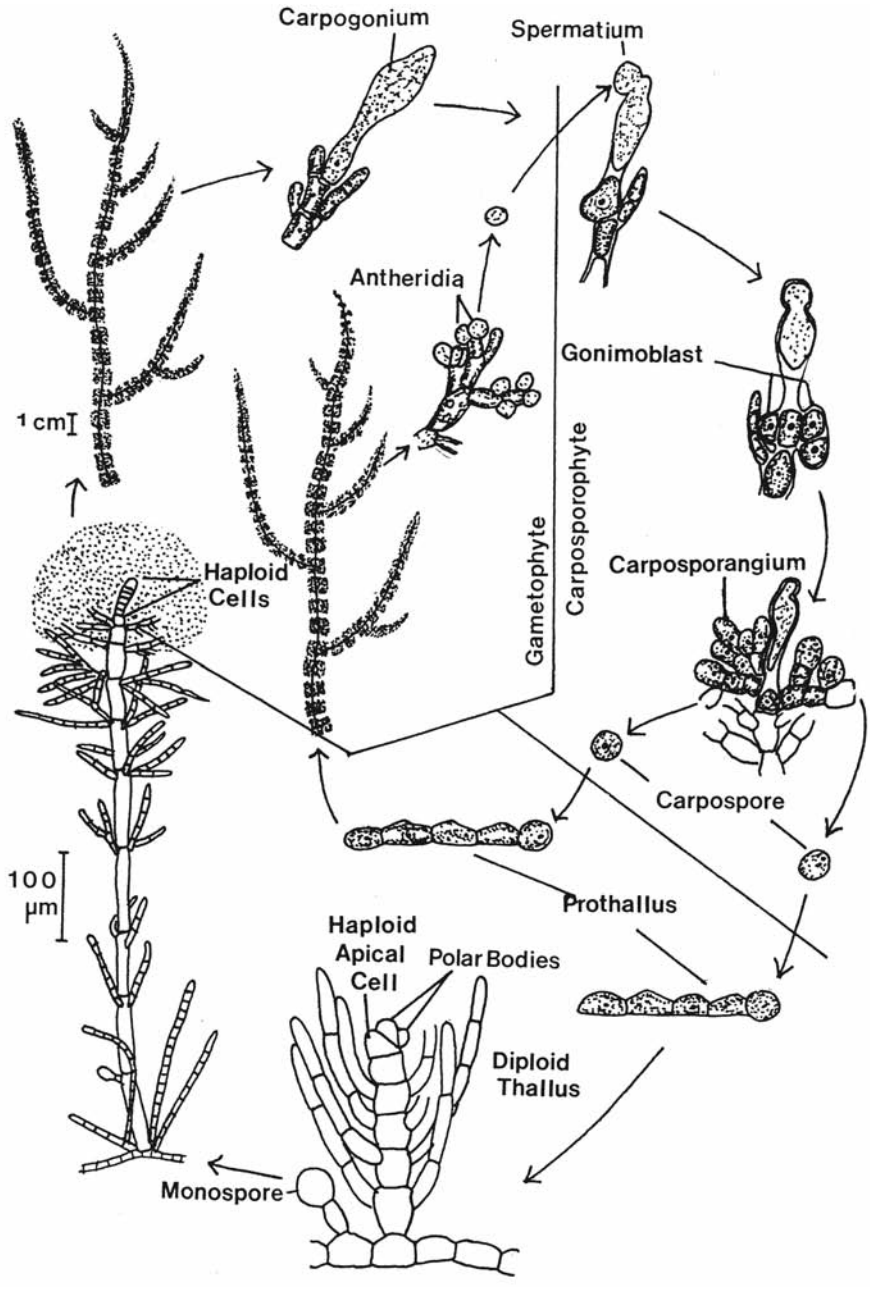


Fig. 4.32 The life cycle of *Batrachospermum* sp. (Adapted from Balakrishnan and Chaugule, 1980; von Stosch and Thiel, 1979.)

occur scattered about the apical end of branches of the tetrasporophyte (Fig. 4.34). *Gymnocodium* and *Permocalculus* are two genera that arose in the Permian of the Paleozoic and became extinct during the Cretaceous of the Mesozoic (Johnson, 1961). The two genera were similar in morphology to *Galaxaura* with weak calcification restricted to an irregular outer zone.

Corallinales

The Corallinales is an order of heavily calcified red algae (Figs. 4.35(*a*), 4.36(*a*), 4.37(*a*)) (Johansen, 1981; Silva and Johansen, 1986). Cytologically, the outer

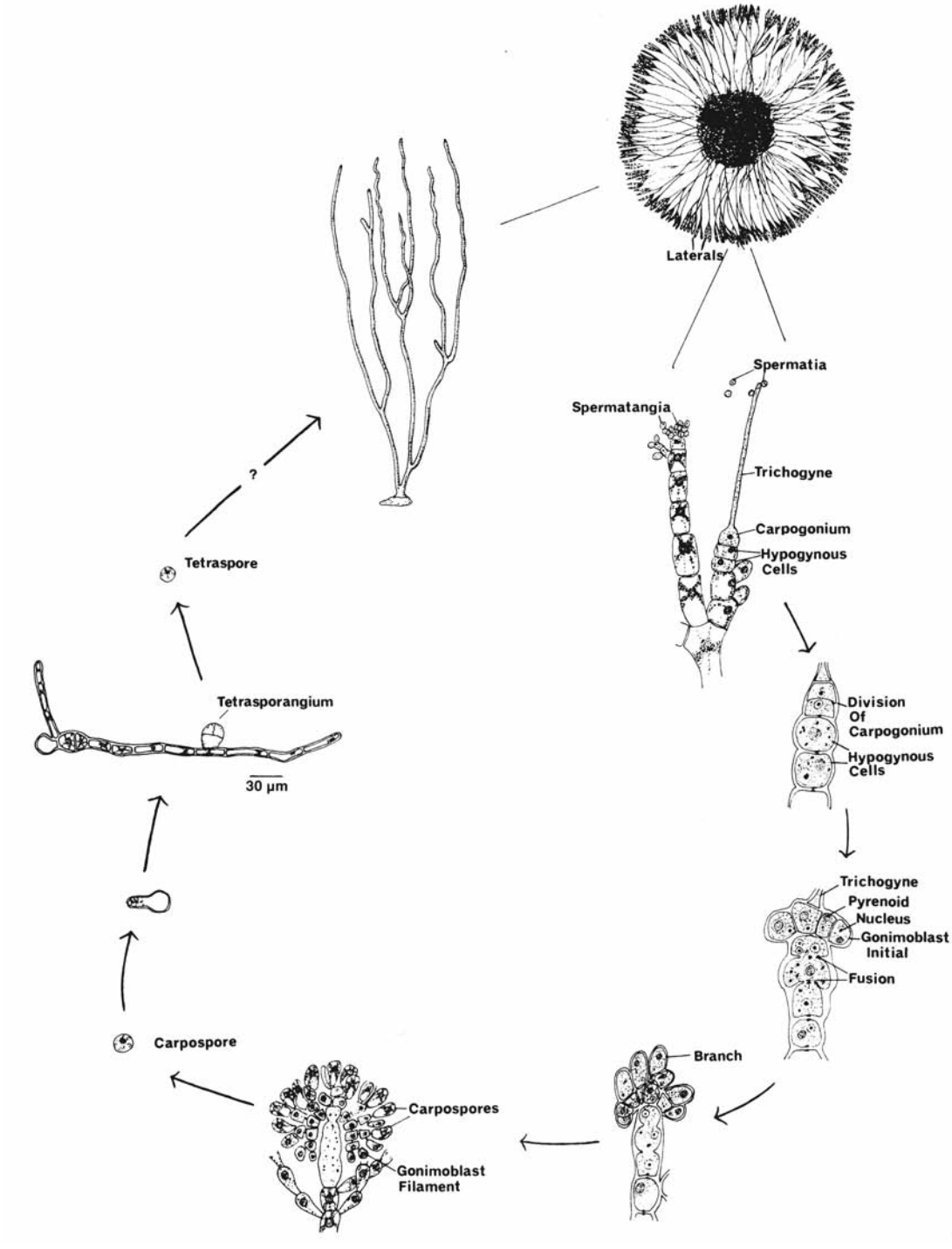


Fig. 4.33 The life cycle of *Nemalion* sp. (Adapted from Oltmanns, 1904; Kylin, 1916; Fries, 1967; Umezaki, 1967.)

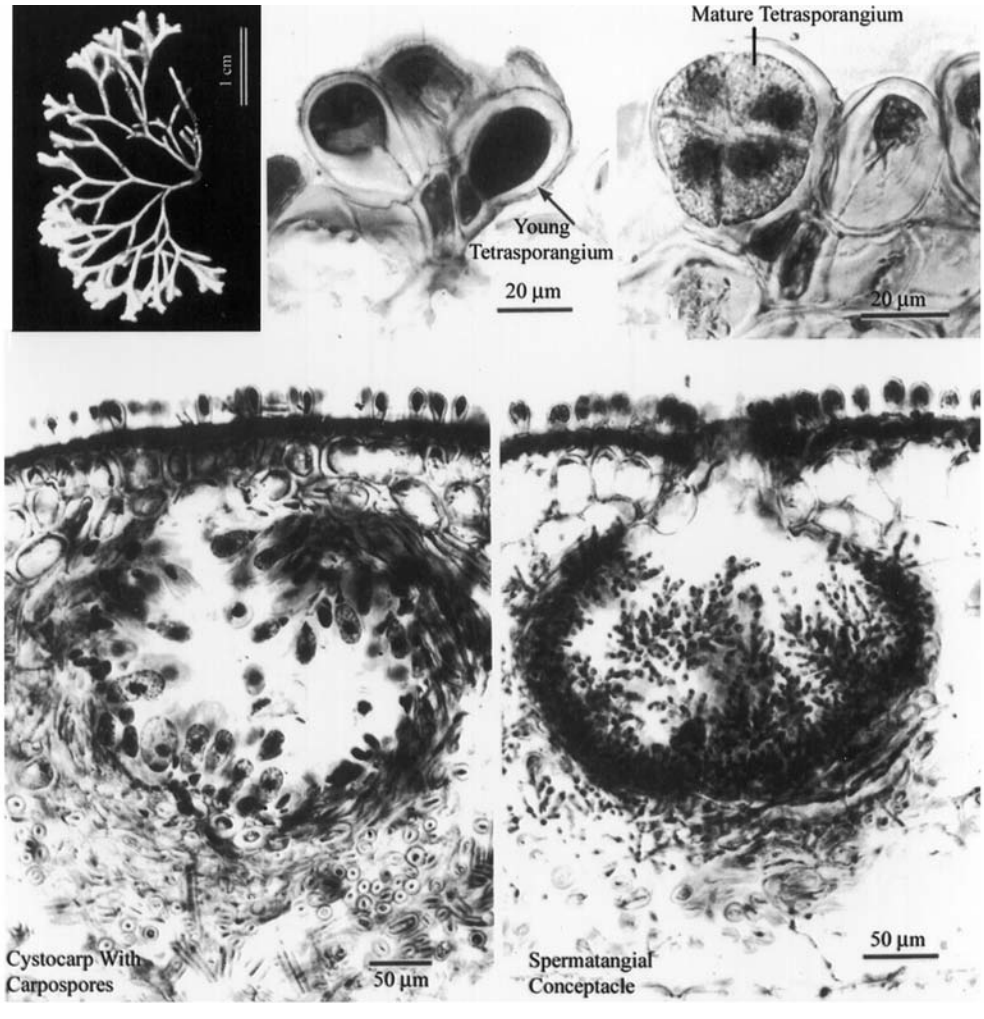


Fig. 4.34 Photographs of vegetative and reproductive structures of *Galaxaura apiculata*. (From Kurihara et al., 2005.)

cap layer of the pit connections is large and dome-shaped (Pueschel and Trick, 1991). The order is characterized by having reproductive organs in **conceptacles** (cavities that open to the thallus surface) opening to the exterior by one or more pores (Figs. 4.35(*d*), 4.37(*b*)). In some genera, the tetrasporic conceptacles differ from sexual conceptacles in having numerous small pores in the roof rather than a single pore. The sexual plants are usually dioecious, with marked differences between male and female conceptacles. Both male and female organs are borne in **nemathecia** (wart-like elevations of the surface containing many reproductive organs), which develop on the floor of the conceptacle. Spermatangia are formed abundantly from short filaments on the conceptacle floor. The female procarp consists of a two-celled carpogonial filament arising from a basal cell that functions as an auxiliary cell (Fig. 4.35(*d*)). The long trichogynes from the many carpogonia project through the conceptacular ostiole. After fertilization, a short ooblast from the carpogonium joins the auxiliary cell. All of the auxiliary cells of the conceptacle then fuse to form a large fusion or placental cell, from the margins of which issue the gonimoblast filaments with their carposporangia (Fig. 4.37(*b*)).

The thallus of the Corallinales is usually divided into two areas, the hypothallus and the perithallus. The **hypothallus** has relatively large cells and forms the basal part of the crustose

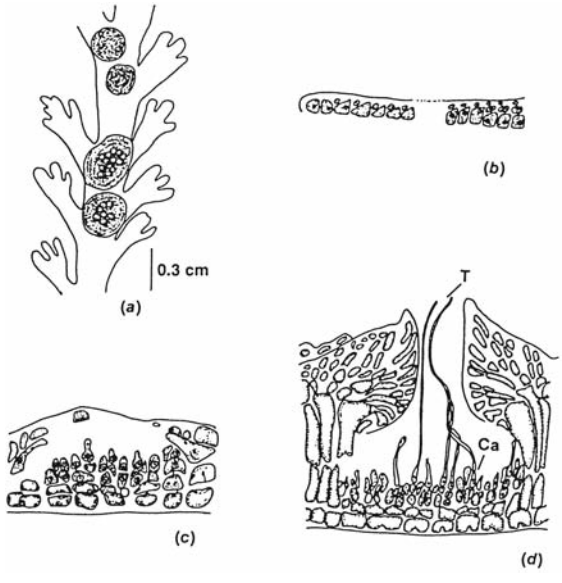


Fig. 4.35 (*a*) *Melobesia marginata* epiphytic on *Laurencia spectabilis*. (*b–d*) *Melobesia lejolisii*: (*b*) section of sterile thallus showing cover cells and (*c*) section of immature fertile thallus. (*d*) *Melobesia limitata*: conceptacle with carpogonia (Ca) and trichogynes (T). ((*a*) after Smith, 1969; (*b*) after Suneson, 1937.)

plants (Figs. 4.36(*b*), 4.37(*b*)) and the central part of the erect branches. Also, in case of injury the scar tissue that develops is hypothallus tissue. The **perithallus** has smaller cells and is located above the hypothallus in crustose forms and outside of the medullar hypothallus in branched forms.

The Corallinaceae of the Corallinales has two subfamilies. The crustose and nodular forms (Figs. 4.35(*a*), 4.36(*a*), 4.37(*a*)) are in the Melobesoideae and the articulated or jointed forms (Fig. 4.38) are in the Corallinoideae (although recent investigations on gene sequences of rRNA have shown that these two subfamilies do not reflect the evolutionary history of the order (Bailey and Chapman, 1998)). In the Melobesoideae, the simplest type of thallus is in *Melobesia*, which has thin pink or red crusts that are widely distributed, especially as epiphytes on other algae and marine plants (Fig. 4.35(*a*)). The thallus consists of one to five layers of prostrate threads compacted to form a disc. A marker feature is the flat cover cells, which also occur in other Corallinales, forming the outer layer of cells (Fig. 4.35(*b*)). *Mesophyllum* and *Lithothamnion* are lithophytes that usually have considerably thicker crusts and sometimes nodules (Figs. 4.36, 4.37).

In the Corallinoideae the plants are multiaxial, having a medulla of elongated cells and a cortex of shorter cells (Fig. 4.38). Calcification normally occurs only in the cell walls of the cortical cells. The plants are composed of a number of calicified segments, each segment joined by a non-calcified joint. The segments consist of calcified cortical and non-calcified medullary

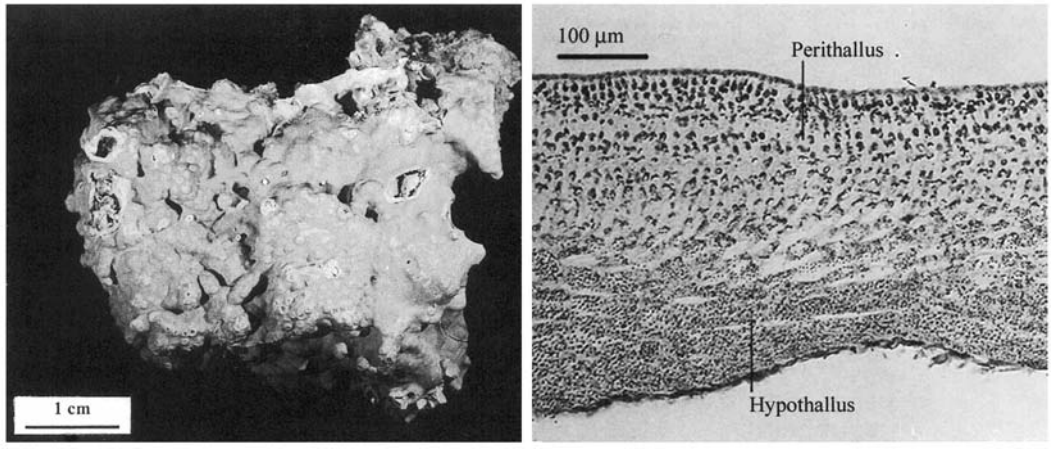


Fig. 4.36 (*Left*) The coralline red alga *Mesophyllum alternans*. (*Right*) Section of the vegetative thallus showing the perithallus and hypothallus. (From Cabioch and Mendoza, 1998.)

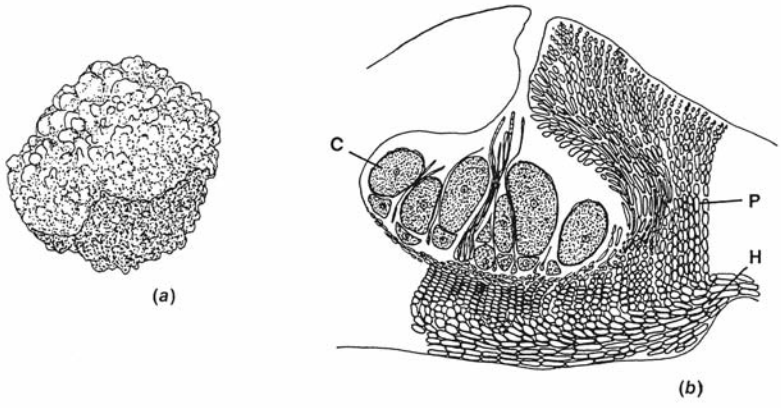


Fig. 4.37 (*a*) *Lithothamnion* sp. (*b*) *L. lenormandi*: drawing of a section of thallus with a hypothallus (H) and perithallus (P). The section includes a mature conceptacle and carposporangia (C). ((*a*) after Oltmanns, 1904; (*b*) after Suneson, 1943.)

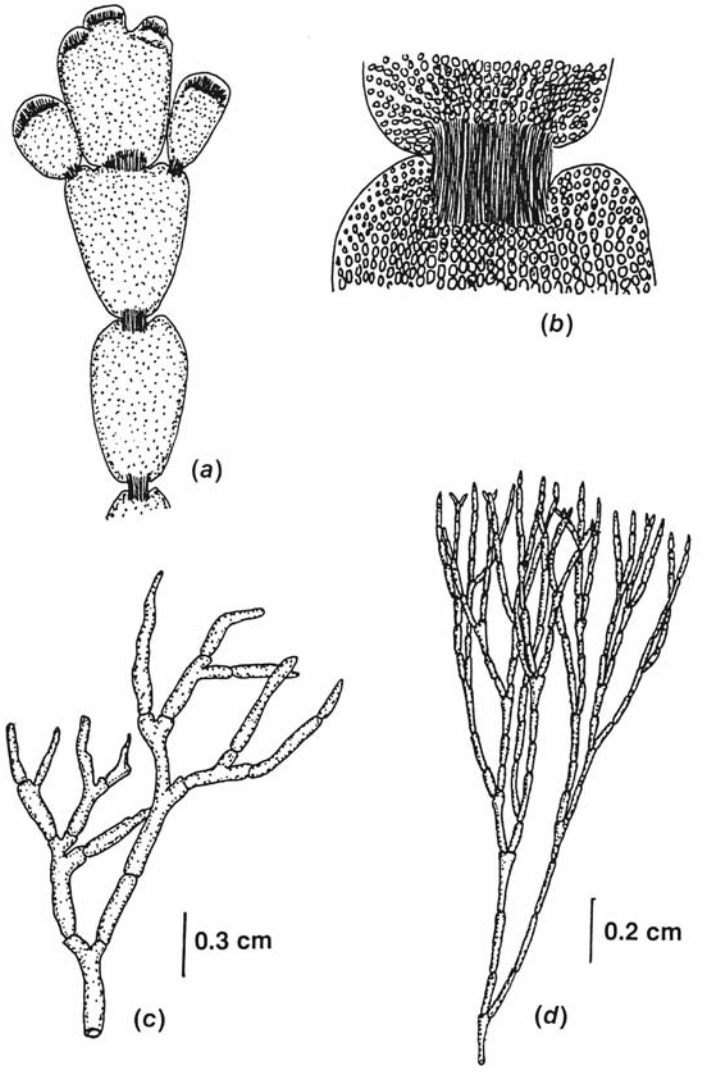


Fig. 4.38 (*a*) *Corallina* sp. (*b*) *Corallina* sp. showing non-calcified joints and calcified segments. (*c*) *Amphiroa rigida* var. *antillana*. (*d*) *Jania rubens*. ((*a*),(*b*) after Oltmanns, 1904; (*c*),(*d*) after Taylor, 1957.)

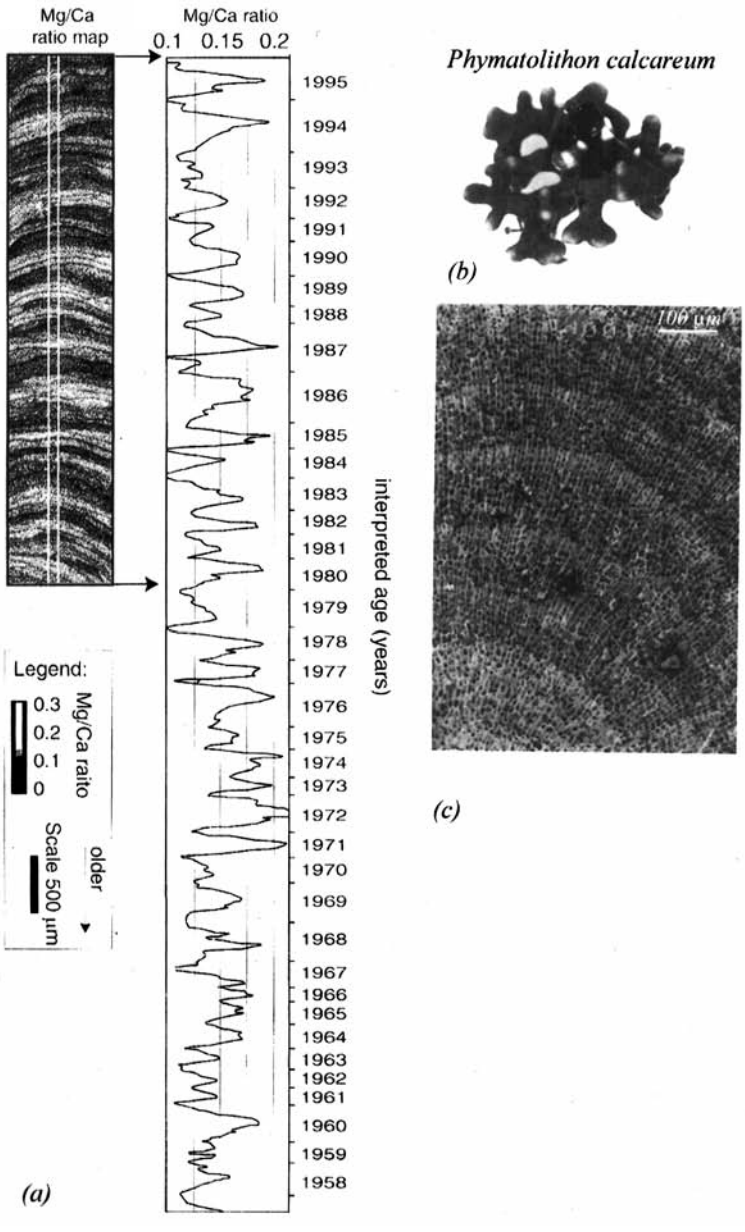


Fig. 4.39 (*a*) *Left*: A micrograph of a section of the thallus of *Lithothamnion glaciale* showing 16 yearly growth bands. *Right*: A 38-year record showing the cycles in the ratio of Mg/Ca cycles. Greater amounts of Mg (e.g., higher Mg/Ca ratios) occur during the summer months. (*b*) Photograph of the coralline red alga *Phymatolithon calcareum*. (*c*) Scanning electron micrograph of a longitudinal section of *Phymatolithon calcareum* showing banding. ((*a*) from Halfar et al., 2000; (*b*),(*c*) from Blake and Maggs, 2003.)

tissue, the arrangement of tissues giving the plants a certain amount of flexibility.

The crustose Corallinaceae occur in the intertidal zone, but only in areas that are not exposed to excessive drying, either on exposed rocks where they are kept moist by spray from breakers or in well-shaded areas. In some places they occur near the high-tide mark but are well covered by other algae. The sublittoral zone is a more favorable area for crustose algal growth, especially on reefs from the low-tide mark to a depth of 25 to 30 m. The depth and agitation of the water have a considerable influence on the growth form of the coralline algae. Crustose types are present at all depths, but the highly ramified or branching forms occur only near the surface, where they are most plentiful down to 30 m. In the crustose forms, the thickest crusts are formed in shallow waters; the crusts become thinner with depth (as a result of thinner hypothalli and smaller cells), probably as a result

of slower growth. The crustose Corallinaceae are among the deepest-growing algae, down to 125 m in clear water. They are also among the longest-living, their life-span ranging from 10 to 50 years (Adey, 1970), probably as a result of their slow growth rate (0.3 to 3 mm $year^{-1}$). The light saturation for photosynthesis for red crustose corallines was found by Adey (1970) to be between 700 and 1000 lux, which is considerably lower than the 4000- to 10 000-lux saturation intensities found for other Rhodophyceae (Kanwisher, 1966; Brown and Richardson, 1968). These light saturation values are probably related to the great depth at which the crustose corallines are able to live.

Maërl is composed of shallow, subtidal deposits of calcareous red algae belonging to the Corallinales. Maërl has been obtained commercially for many years by dredging from the coast of Brittany in France, off Falmouth Harbor in England and Bantry Bay in Ireland. Maërl is placed on acidic soil to increase the pH of the soil for crops (Blunden et al., 1997).

The Corallinaceae form an important part of atolls and reefs (Dawson, 1966; Chisholm, 2003). The reefs are built up by the combined growth of coralline red algae (mostly species of *Porolithon*) and corals. When a reef first breaks the surface, the rigid, branched, brittle corals tend to break and fragment under severe surf action, whereas the massive coralline Rhodophyceae are unaffected by the pounding. In fact, the stronger the pounding, the faster they grow. The coralline reds thus grow into the breaking surf, developing upward and outward to form a rim slightly above sea level. While the corallines are forming the main framework of the reef, 90% of the reef comes to consist of sand and detritus cemented together by the plants and animals. Inside this rim of coralline Rhodophyceae, there is relative calm over the inner part of the reef. Within this inner area, carbonic acid, resulting from the solution of respiratory carbon dioxide produced by the plants and animals living there, tends to dissolve the solid calcareous materials. This dissolution of the inner part of the reef results in a central lagoon that stabilizes itself at a depth of 65 to 100 m.

The reef community is adapted to a low-stress environment characterized by the absence of significant seasonal change. The mean winter temperature of the water where the reefs grow is between 27 and 29 °C, and the difference between the monthly mean temperatures is 3 °C or less. The water is clear (so the penetration of light is at a maximum), agitated, and of normal salinity. Even under these ideal circumstances many reef organisms (e.g., corals) do not grow at depths greater than 20 m.

Non-articulated red algae grow at different rates during the year. This results in bands in the thallus (Fig. 4.39), similar to growth rings in trees. In some cases the banding is annual. Magnesium is present in greater quantities in warmer water, resulting in a higher concentration of magnesium in the portion of the band produced during the summer. The banding in coralline red algae can be an important **paleothermometer** since the algae can be up to 100 years old (Halfar et al., 2000; Blake and Maggs, 2003).

Gelidiales

This is an order of uniaxial marine Rhodophyceae in which the carpogonial branch consists of a single cell, the carpogonium. After fertilization, the carpogonium may fuse with the supporting cell and/or nutritive filaments. The tetrasporophyte and the gametophyte are macroscopic plants, although not necessarily similar. The plants are commonly used in the production of agar, with almost half of the world supply coming from members of this order (Lewis and Hanisak, 1996).

No member of the order has had its life cycle completed in culture, but it is presumed from plants collected in the field that there is a triphasic life cycle of gametophyte, tetrasporophyte, and carposporophyte.

The gametophyte and tetrasporophyte of *Gelidium* have a dome-shaped apical cell that cuts off daughter cells basipetally (Fig. 4.40). The daughter cells divide to form a thallus that soon loses its uniaxial nature in the mature parts. The carpogonia are usually formed on special **ramuli** (branches) with a deep apical notch (Fig. 4.41(*a*)), behind which there is a depression on both surfaces (Figs. 4.40(*b*), 4.41(*a*), (*b*)). The carpogonia are produced in these depressions. The carpogonium is cut off from a cell beneath the surface of the thallus and has a long trichogyne that reaches to the outside of the thallus. The carpogonial branch

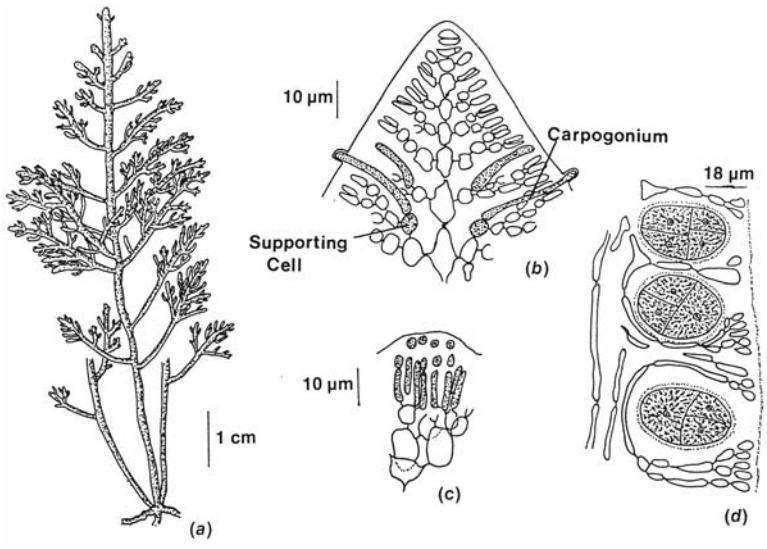


Fig. 4.40 *Gelidium cartilagineum* var. *robustum*. (*a*) Whole plant. (*b*) Section of fertile apex of branch showing apical cell, carpogonia, and supporting cells. (*c*) Section of spermatangial area. (*d*) Section of tetrasporangial area. ((*a*) after Smith, 1969; (*b*),(*c*) after Fan, 1961; (*d*) after Smith, 1938.)

thus consists of a single cell. Nutritive filaments are cut off from the cells at the base of each of the laterals in the fertile area. After fertilization, the carpogonium may fuse with the supporting cell and/or nutritive filaments, with the gonimoblast filaments and carposporangia developing from this fusion cell. Male plants are similar in morphology to female plants, with the spermatangial areas forming irregular patches on the thalli. The cortical cells of a fertile area elongate, fade in color, and become transformed into spermatangial mother cells (Fig. 4.40(*c*)). The colorless spermatangia are formed by transverse division of the mother cell. The tetrasporangial mother cell is a cortical cell that is terminal on a lateral. It divides to produce four tetraspores in either a cruciate or a tetrahedral arrangement (Fig. 4.40(*d*)).

Gracilariales

The Gracilariales are agarophytes that have a female reproductive system with a supporting cell of intercalary origin that bears a two-celled carpogonial branch flanked by two or more sterile branches (Fredericq and Hommersand, 1989).

The plants in the order are fleshy, having a tendency to be flattened or foliose with pseudoparenchymatous tissues that lack filamentous cells in the mature vegetative thallus. The principal genus in the family is *Gracilaria*, a widely distributed northern lithophyte found at low-tide level and below, with about 100 species. The dark-red thallus grows by means of a two-sided apical cell and has tapering branches (Fig. 4.42). There are large isodiametric cells in the medulla, with small cortical cells containing a number of ribbon-shaped chloroplasts. Unicellular hairs arise from enlarged peripheral cells that become multinucleate as they age.

The gametophytic plants are either male or female, and equal numbers of each are produced from tetraspores (Kain and Destombe, 1995). The male plants produce spermatia in antheridial pits over the surface of the thalli. The female plants form supporting cells from the outer layer of the large cells of the medulla (Kylin, 1930), the supporting cells producing the two-celled carpogonial branch and a number of laterals, a cell of which functions as the auxiliary cell. All of the cells of the procarp become multinucleate and develop into nutritive cells except for the carpogonium and the cell beneath it. After fertilization the carpogonium fuses with one of the nutritive cells that is acting as an auxiliary cell. Subsequently, this fusion cell fuses with the other multinucleate nutritive cells. At the same time, the cortical cells above the procarp divide to produce the cystocarp walls, the inner cells of which constitute nutritive cells. Gonimoblast initials are cut off from the fusion cell and develop into an inner sterile area that supports the outer carposporangia. The carposporangia ripen successively from the outside in. In some

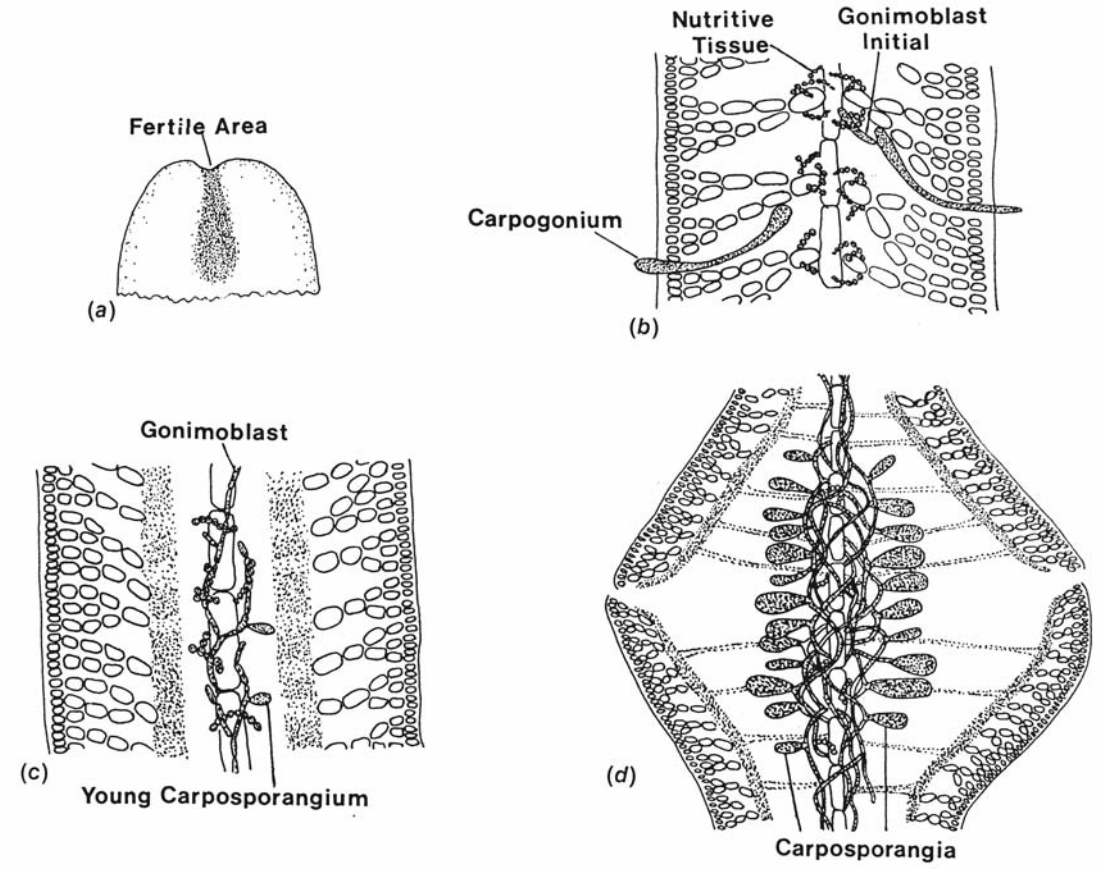


Fig. 4.41 *Gelidium cartilagineum*. (*a*) Apex of fertile thallus. (*b*) Longitudinal section of thallus showing carpogonium. (*c*) Gonimoblast producing young carposporangia. (*d*) Carposporophyte with mature carposporangia. ((*a*) after Kylin, 1928; (*b–d*) after Smith, 1938.)

species, elongate cells radiate from the compact regions of the gonimoblast, penetrating the **pericarp** (cystocarp wall), and become connected with the cells of the pericarp.

The carpospores germinate to produce a parenchymatous disc that forms the tetrasporophyte as an erect protuberance. The tetrasporophyte is morphologically similar to the gametophyte and about the same size as the female gametophyte. Cruciate tetrasporangia are formed terminally on laterals in the cortex and are embedded in the thallus. The tetraspores germinate to form a parenchymatous disc that produces the gametophyte as an erect protuberance (Ogata et al., 1972).

Gracilaria is a major agarophyte, currently providing greater than half of the world's supply of agar. The cultivation of *Gracilaria*, both in the sea and in tanks, has been a principal factor in making this genus a source of agar-containing seaweeds (Lewis and Hanisak, 1996). In Taiwan, *Gracilaria* is farmed in brackish-water ponds as a main food source for the cultivation of the small abalone *Haliotis* (Lee, 1999).

Human consumption of species of the red alga *Gracilaria* has been linked to "**ogonori**" **poisoning** (Noguchi et al., 1994; Smit, 2004). The symptoms are hypotension (abnormally low blood pressure), vomiting, nausea, and death resulting from hypotensive shock. Ogonori poisoning is caused by prostaglandin E_2 (Fig. 4.43). Soaking *Gracilaria* in freshwater results in the production of prostaglandin E_2. This is usually compounded by eating seafood which is rich in prostaglandin E_2.

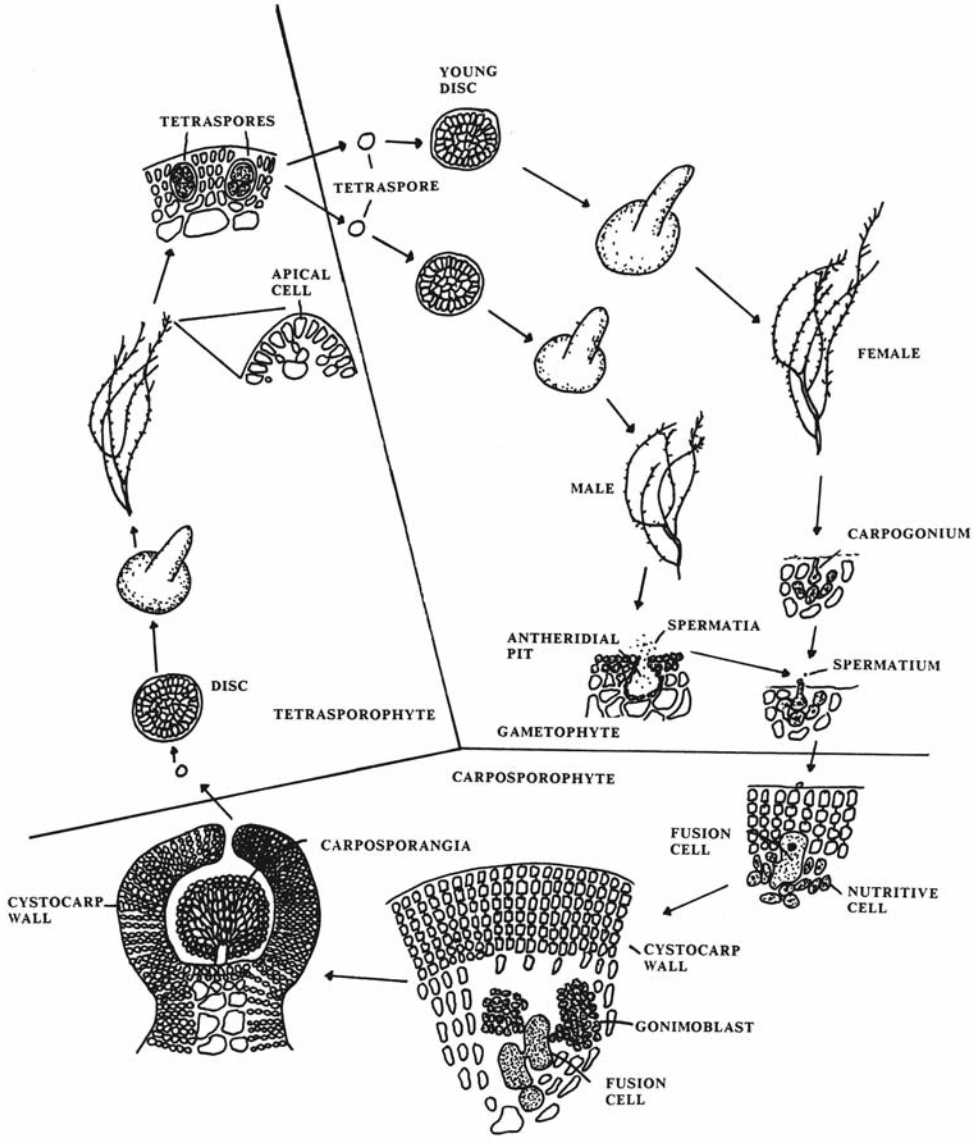


Fig. 4.42 The life cycle of *Gracilaria* spp. (Adapted from Kylin, 1930; Ogata et al., 1972.)

Ceramiales

These plants have the auxiliary cell cut off after fertilization and borne on the supporting cell of the four-celled carpogonial filament. Most of the plants are relatively delicate filamentous or membranous forms.

In *Polysiphonia* the uninucleate, dome-shaped apical cell (Fig. 4.45(*b*)) is polyploid and contains 64 to 128 times the amount of DNA in most of the mature cells in the alga (Goff and Coleman, 1986).

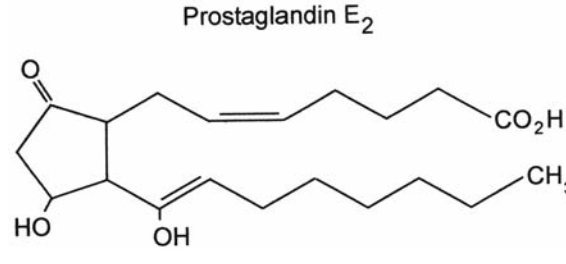


Fig. 4.43 The chemical structure of prostaglandin E_2.

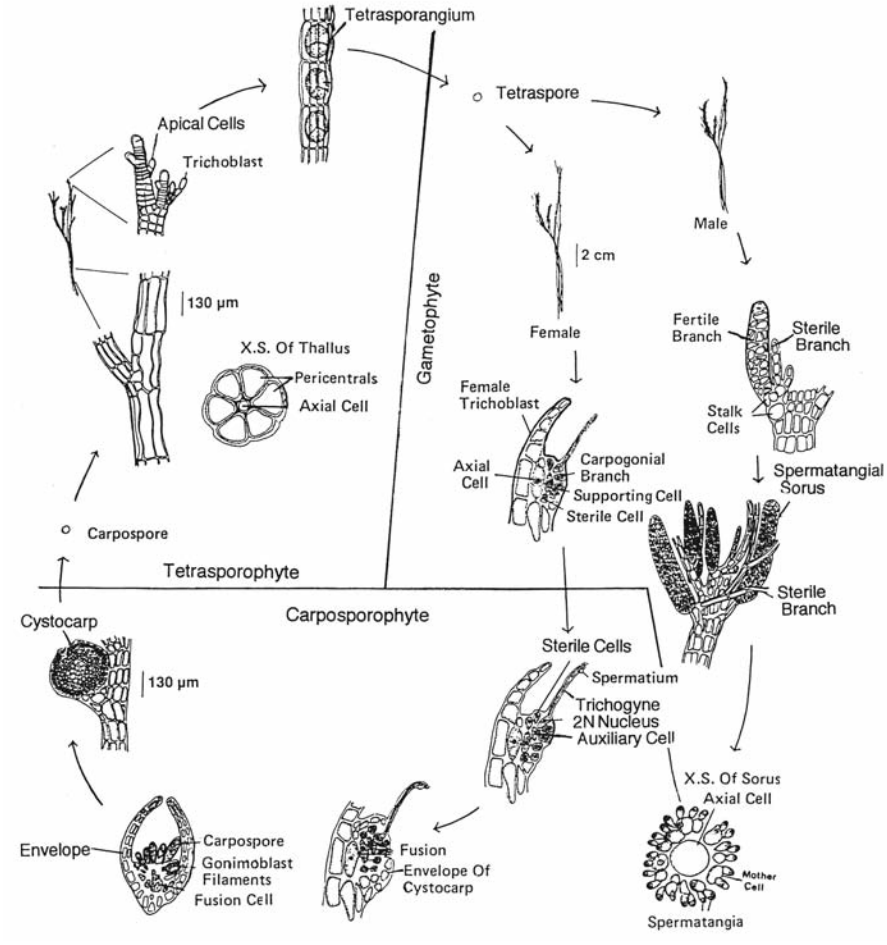


Fig. 4.44 The life cycle of *Polysiphonia* sp. (Adapted from Kylin, 1923; Edwards, 1970a.)

Division of the cells derived from the apical cell is usually not accompanied by DNA replication; therefore, the farther the daughter cell is from the apical cell, the lower the ploidy of the cell, until the ploidy number stabilizes at 1 *n*. The apical cell forms daughter cells that produce lateral branches before dividing longitudinally into central and pericentral cells (Figs. 4.44, 4.45). The pericentrals are the same length as the axial cells. The lateral branches are of two kinds: the ordinary branches and the trichoblasts. The ordinary branches are polysiphonous with unlimited growth, similar to the main axis. The **trichoblasts** are uniseriate, usually colorless, and bear the sex organs (Fig. 4.45(*c*)). The trichoblasts progress through a programmed cell death or **apoptosis** and drop off from the older parts of the thallus (Garbary and Clark, 2001).

Polysiphonia species occur either as lithophytes or as epiphytes on other algae. When the species grows on a solid substrate, some of the polysiphonous axes creep over the substratum to which they are firmly anchored by thick-walled, lobed rhizoids (Fig. 4.45(*d*)). When it grows as an epiphyte on another alga, the rhizoids penetrate that host tissue (Fig. 4.11). The procarps are produced near the base of a trichoblast (Figs. 4.44, 4.45(*g*)). The two basal cells of the trichoblast become polysiphonous, and a procarp develops from a pericentral of the upper of the two basal cells. The pericentral (supporting cell) produces in succession a lateral sterile cell, the four-celled carpogonial branch, and, last, the second sterile cell. The

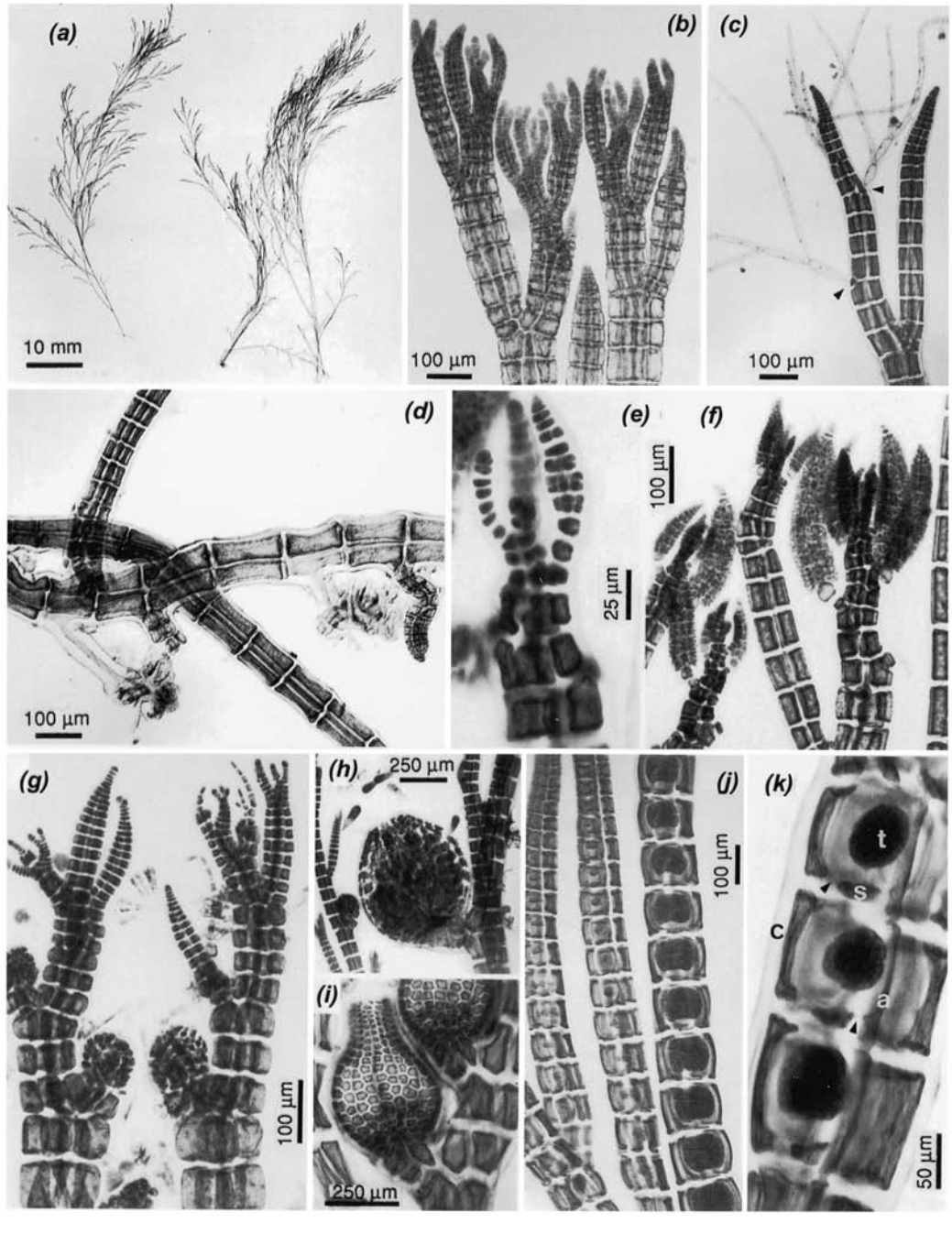


Fig. 4.45 Vegetative and reproductive structures of *Polysiphonia stricta*. (*a*) Habit of thalli from shallow subtidal bedrock. (*b*) Vegetative apices showing large apical cells with oblique branching. (*c*) Trichoblasts, composed of uninucleate cells, attached by small scar cells (arrowheads). (*d*) Prostrate axis attached by unicellular rhizoids in open connection with pericentral cells. (e, *f*) Developing and mature spermatangial branches with sterile tips. (*g*) Tips of female thallus with procarps and early postfertilization cystocarps. (*h*) Mature globose cystocarp, with extruded pyriform carposporangia. (*i*) Mature cystocarp. (*j*) Developing and mature tetrasporangia in long straight rows. (*k*) Tetrasporangia (t), showing pit connections (arrowheads) between tetrasporangial stalk cells (s), central axial cells (a), and cover cells (c). (From Kim et al., 2000.)

sterile cells divide after fertilization and may have a nutritive role. The cells of the carpogonial branch (with the exception of the carpogonium) are commonly binucleate (Kylin, 1923). A large area of endoplasmic reticulum extends from one pit connection to the other pit connection in each cell of the carpogonial branch. This may be how the message of fertilization is transmitted down the carpogonial branch (Broadwater and Scott, 1982).

The male plants of *Polysiphonia* bear spermatangial sori on a trichoblast consisting of a two-celled stalk surmounted by the fertile regions (Figs. 4.44, 4.45(*e*), (*f*)). The upper stalk cell frequently bears a branch. Fertile regions become polysiphonous, and the two pericentrals divide copiously to form a compact layer of mother cells, each of which gives rise to two or three spermatangia (Kylin, 1923). After the spermatium fertilizes the trichogyne, the auxiliary cell is cut off from the supporting cell. The auxiliary cell then fuses with the carpogonium. The male nucleus fuses with the female in the carpogonium (Yamanouchi, 1906), and the diploid nucleus divides once. One of the diploid nuclei passes into the auxiliary cell, which subsequently fuses with the supporting cell. The fusion cell also fuses with the axial cell of the fertile segment. The gonimoblast initials are cut off from the fusion cell and develop into a number of gonimoblast filaments. The terminal cells of these filaments develop into pear-shaped carposporangia. In the meantime, the fusion cell unites with the gonimoblast initial and the fertile cells. The sterile outer envelope of the cystocarp (Fig. 4.45(*b*)) originates from the other pericentrals of the axial cell that gave rise to the fertile pericentral that acted as the supporting cell. The young envelope consists of two lateral valves, composed of fused threads, which enclose the procarp like the shells of an oyster, the trichogyne alone projecting. After fertilization the two valves unite, and the envelope becomes two-layered. The carpospores form a tetrasporophyte, which is similar to the gametophyte, and which forms tetrahedrally arranged tetraspores (Fig. 4.45(*j*), (*k*)) in polysiphonous branches called **stichidia**. The tetraspores then germinate to form the gametophyte (Edwards, 1969).

Polysiphonia denudata completes its life history in 1.5 months in culture; thus the species probably has several life cycles each year (Edwards, 1970a). In some species of *Polysiphonia*, it is possible to influence stages of the life cycle by changing the photoperiod, but there appears to be no regularity among the different species (Edwards, 1970a,b).

In the marine environment, herbivorous damselfish exclude other fish from their territories, and maintain dense stands of filamentous algae. One damselfish, the dusky farmerfish (Fig. 4.46), is unique in that it maintains a monoculture of *Polysiphonia* in coral reefs by selective weeding of other indigestible algae (Hata and Kato, 2003). The farmerfish grazes on the *Polysiphonia* sp. The relationship between the farmerfish and *Polysiphonia* is an example of **mutualism** (a situation where two populations benefit equally).

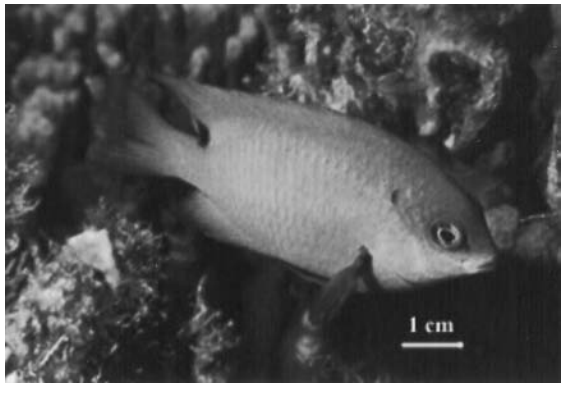


Fig. 4.46 The dusky farmerfish *Stegastes nigricans*, a cultivator of *Polysiphonia* in coral reefs.





Fig. 4.47 *Left*: Heinrichs Leonhards Skuja. *Right*: Harald Kylin. (Photograph of Skuja from Wilen and Wingqvist, 1986; photograph of Kylin from *Die Gattung der Rhodophyceen*, CWK Gleerups Forlag, Lund, Sweden.)

Heinrichs Leonhards Skuja Born September 8, 1892 in Majori, Rigas-Jurmula, Latvia. Died July 19, 1972. During his youth, Dr. Skuja lived close to the Latvian coast and took an early interest in aquatic plants and animals. During World War I, he lived in the Caucasus, where he was engaged in floristic studies on the Apsheron Peninsula. In 1922, he began his academic studies at the faculty of natural sciences at the University of Latvia, passed a *mag. rer. nat.* examination in 1929, and became *dr. rer. nat.* in 1943. In the autumn of 1944, Dr. Skuja arrived in Sweden, where in 1947 he obtained a position as research professor (*laborator*) and in 1958 he was awarded the degree of *doctor honoris causa* by the University of Uppsala. Besides his extensive publications on the algae, Dr. Skuja also published in the areas of general botany, mycology, and lichenology.

Harald Kylin Born Johan Harald Olsson February 5, 1879 near Gothenburg, Sweden. Died 1949. He changed his name to Harald Kylin when he entered the gymnasium (high school) because his father, who was chairman of the parish council, thought Olsson was too common a name. He graduated from Uppsala University in 1901 with a M.Sc. degree and in 1905 with a Licentiate of Philosophy. In 1907 he defended his thesis on algae and became a docent of the University. In 1917 he obtained a chair in botany at the University of Lund and remained there until he retired in 1944. He wrote a large number of publications on the red algae. The last of these was his book *Die Gattung der Rhodophyceen*, which was finished by his wife after his death.



Fig. 4.48 **Gary W. Saunders** (*right* in photograph, with Dr. Gerry Kraft) Born June 30, 1962 in Halifax, Nova Scotia. Dr. Saunders received his B.Sc. in 1985 and his M.Sc. in 1987 from Acadia University. He received his Ph.D. in 1991 from Simon Fraser University. In 1995 he joined the faculty in the Department of Biology at the University of New Brunswick in Canada where he is Professor and Director and Algal Curator of the Connell Memorial Herbarium. Dr. Saunders has been a leader in the field of molecular systematics of the red algae.

REFERENCES

Abdel-Rahman, M. H. (1982). The involvement of an endogenous circadian rhythm in photoperiodic timing in *Acrochaetium asparagopsis* (Rhodophyta, Acrochaetiales). *Br. Phycol. J*. 17:389–400.

Adey, W. H. (1970). The effects of light and temperature on growth rates in boreal-subarctic crustose corallines. *J. Phycol*. 6:269–76.

Arad, S., Dubinsky, O., and Simon, B. (1993). A modified cell wall mutant of the red microalga *Rhodella reticulata* resistant to the herbicide 2,6-dichlorobenzonitrile. *J. Phycol*. 29:309–13.

Bailey, J. C., and Chapman, R. L. (1998). A phylogenetic study of the Corallinales (Rhodophyta) based on nuclear small-subunit rRNA gene sequences. *J. Phycol*. 34:692–705.

Balakrishnan, M. S., and Chaugule, B. (1980). Cytology and life history of *Batrachospermum mahabaleshwarensis. Cryptogamie: Algologie* 1:83–97.

Barrow, K. D., Karsten, U., King, R. J., and West, J. A. (1995). Floridoside in the genus *Laurencia* (Rhodomelaceae: Ceramiales) – a chemosystematic study. *Phycologia* 34:279–83.

Belcher, J. H., and Swale, E. M. F. (1960). Some British freshwater material of *Asterocystis. Br. Phycol. Bull*. 2:33–5.

Blake, C., and Maggs, C. A. (2003). Comparative growth rates and internal banding periodicity of maerl species (Corallinales, Rhodophyta) from northern Europe. *Phycologia* 42:606–12.

Blunden, G., Campbell, S. A., Smith, J. R., Guiry, M. D., Hession, C. C., and Griffin, R. L. (1997). Chemical and physical characteristics of calcified red algal deposits known as maerl. *J. Applied Phycol*. 9:11–17.

Borowitzka, M. A., Larkum, A. W. D., and Nockolds, C. E. (1974). A scanning electron microscope study of the structure and organization of the calcium carbonate deposits of algae. *Phycologia* 13:195–203.

Bouarab, K., Potin, P., Correa, J., and Kloareg, B. (1999). Sulfated oligosaccharides mediate the interaction between a marine red alga and its green algal pathogenic endophyte. *Plant Cell* 11:1635–50.

Bourgougnon, N., Lehaye, M., Quemener, B., Chermann, J-C., Rimbert, M., Cormaci, M., Furnari, G., and Kornprobat, J-M. (1996). Annual variation in composition and *in vitro* anti-HIV-1 activity of the sulfated glucuronogalactan from *Schizymenia dubyi* (Rhodophyta, Gigartinales). *J. Applied Phycol*. 8:1155–61.

Broadwater, S. T., and Scott, J. (1982). Ultrastructure of early development in the female reproductive system of *Polysiphonia harveyi* Bailey (Ceramiales, Rhodophyta). *J. Phycol*. 18:427–41.

Brock, T. D. (1973). Lower pH limit for the existence of blue-green algae: evolutionary and ecological implications. *Science* 179:480–3.

Brown, T. E., and Richardson, F. L. (1968). The effect of growth and environment on the physiology of the algae: Light intensity. *J. Phycol*. 4:38–54.

Butterfield, N. J. (2000). *Bangiomorpha pubescens n*. gen., n. sp.: implications for the evolution of sex, multicellularity, the Mesoproterozoic/ Neoproterozoic radiation of eukaryotes. *Paleobiology* 26:386–404.

Cabioch, J., and Mendoza, M. L. (1998). *Mesophyllum alternans* (Foslie) comb. nov. (Corallinales, Rhodophyta). A mediterraneo-atlantic species, and new considerations on the *Lithothamnion phillippi* Foslie complex. *Phycologia* 37:208–21.

Campbell, S. E. (1980). *Palaeoconchocelis starmachii*, a carbonate boring micro-fossil from the Upper Silurian of Poland (425 million years old): implications for the evolution of the Bangiaceae (Rhodophyta). *Phycologia* 19:25–36.

Chemin, E. (1937). Le développement des spores chez les Rhodophycées. *Rev. Gen. Bot*. 49:205–34, 300–27, 353–74, 424–48, 478–536.

Chen, L. C-M., Edelstein, T., Ogata, E., and McLachlan, J. (1970). The life history of *Porphyra miniata. Can. J. Bot*. 48:385–9.

Chen, L. C-M., McLachlan, J., Neish, A. C., and Shacklock, P. F. (1973). The ratio of kappa- to lamda-carrageenan in nuclear phases of the Rhodophycean alga, *Chondrus crispus* and *Gigartina stellata. J. Mar. Biol. Assoc. UK* 53:11–16.

Chiovitti, A., Liao, M-L., Kraft, G. T., Munro, S. L. A., Craik, D. J., and Bacic, A. (1995). Cell wall polysaccharides from Australian red algae of the family Solieriaceae (Gigartinales, Rhodophyta): iota/kappa/beta-carrageenans from *Melanema dumosum. Phycologia* 34:522–7.

Chisholm, J. R. M. (2003). Primary productivity of reef-building crustose coralline algae. *Limnol. Oceanogr*. 48:1376–87.

Craigie, J. S., Correa, J. A., and Gordon, M. E. (1992). Cuticles from *Chondrus crispus. J. Phycol*. 28:777–86.

Cunningham, E. M., and Guiry, M. D. (1989). A circadian rhythm in the long-day photoperiodic induction of erect axis development in the marine red alga *Nemalion helminthoides. J. Phycol*. 25:705–12.

Dawson, E. Y. (1966). *Marine Botany*. New York: Holt, Rinehart and Winston.

de Nys, R., Steinberg, P. D., Willemsen, P., Dworjanyn, S. A., Gabelish, C. L., and King, R. J. (1995). Broad

spectrum effects of secondary metabolites from the red alga *Delisea pulchra* in antifouling assats. *Biofouling* 8:259–71.

den Hartog, C. (1971). The effect of the salinity tolerance of algae on their distribution, as exemplified by *Bangia*. *Proc. 7th Int. Seaweed Symp*., pp. 274–6.

Digby, P. S. B. (1977a). Growth and calcification in the coralline algae, *Clathromorphum circumscriptum* and *Corallina officinalis*, and the significance of pH in relation to precipitation. *J. Mar. Biol. Assoc. UK* 57:1095–109.

Digby, P. S. B. (1977b). Photosynthesis and respiration in the coralline algae, *Clathromorphum circumscriptum* and *Corallina officinalis* and the metabolic basis of calcification. *J. Mar. Biol. Assoc. UK* 57:1111–24.

Dixon, P. S. (1973). *Biology of the Rhodophyta*, University Reviews in Biology No. 4. Edinburgh: Oliver and Boyd.

Dixon, P. S., and Richardson, W. N. (1970). Growth and reproduction in red algae in relation to light and dark cycles. *Ann. N.Y. Acad. Sci*. 175:764–77.

Dring, M. J. (1967a). Effects of daylength on growth and reproduction of the *Conchocelis*-phase of *Porphyra tenera*. *J. Mar. Biol. Assoc. UK* 47:501–10.

Dring, M. J. (1967b). Phytochrome in red alga, *Porphyra tenera*. *Nature* 215:1411–12.

Dring, M. J., and West, J. A. (1983). Photoperiodic control of tetrasporangium formation in the red alga *Rhodochorton purpureum*. *Planta* 159:143–50.

Edwards, P. (1969). The life history of *Callithamnion byssoides* in culture. *J. Phycol*. 5:266–8.

Edwards, P. (1970a). Field and cultural observations on the growth and reproduction of *Polysiphonia denudata* from Texas, *Br. Phycol. J.* 5:145–53.

Edwards, P. (1970b). Field and cultural studies on the seasonal periodicity of growth and reproduction of selected Texas benthic marine algae. *Contrib. Mar. Sci. Univ. Texas* 14:59–114.

Evans, L. V. (1970). Electron microscopical observations on a new red algal unicell, *Rhodella maculata* gen. nov., sp. nov., *Br. Phycol. J*. 5:1–13.

Evans, L. V., Callow, J. A., and Callow, M. E. (1973). Structural and physiological studies on the parasitic red alga *Holmsella*. *New Phytol*. 72:393–402.

Fan, K-C. (1961). Studies on *Hypneocolax*, with a discussion on the origin of parasitic red algae. *Nova Hedwigia* 3:119–28.

Feldmann, G. (1970a). Sur l'ultrastructure des corps irisants des *Chondria* (Rhodophycées). *C. R. Séances Acad. Sci. Paris* 270:945–50.

Feldmann, G. (1970b). Sur l'ultrastructure de l'appareil irisant du *Gastroclonium clavatum* (Roth.) Ardissonne (Rhodophyceae). *C. R. Séances Acad. Sci. Paris* 270:1244–6.

Feldmann, J. (1953). L'évolution des organes femelles chez les Floridées. *Proc. 1st Int. Seaweed Symp*., pp. 11–12.

Fetter, R., and Neushul, M. (1981). Studies on developing and released spermatia in the red alga, *Tiffaniella snyderae* (Rhodophyta). *J. Phycol*. 17:141–59.

Fredericq, S., and Hommersand, M. H. (1989). Proposal of the Gracilariales ord. nov. (Rhodophyta) based on an analysis of the reproductive development of *Gracilaria verrucosa*. *J. Phycol*. 25:213–19.

Frei, E., and Preston, R. D. (1964). Non-cellulosic structural polysaccharides in algal cell walls. II. Association of xylan and mannan in *Porphyra umbilicalis*. *Proc. R. Soc. Lond.* [*B*] 160:314–27.

Freshwater, D. W., Fredericq, S., Butler, B., Hommersand, M. H., and Chase, M. W. (1994). A gene phylogeny of the red algae (Rhodophyta) based on plastid *rbcL*. *Proc. Natl. Acad. Sci., USA* 91:7281–5.

Fries, L. (1963). On the cultivation of axenic red algae. *Physiol. Plant*. 16:695–708.

Fries, L. (1967). The sporophyte of *Nemalion multifidum* (Weber et J. Ag.). *Sven. Bot. Tidskr*. 61:457–62.

Gabrielson, P. W., Garbary, D. J., and Scagel, R. F. (1985). The nature of the ancestral red alga: Inferences from a cladistic analysis. *BioSystems* 18:335–46.

Gantt, E. (1969). Properties and ultrastructure of phycoerythrin from *Porphyridium cruentum*. *Plant Physiol*. 44:1629–38.

Gantt, E., and Conti, S. F. (1965). The ultrastructure of *Porphyridium cruentum*. *J. Cell Biol*. 26:365–81.

Garbary, D. J., and Clarke, B. (2001). Apoptosis in trichoblast development in *Polysiphonia harveyi* (Rhodophyta). *Phycologia* 40:324–9.

Gargiulo, G. M., Genovese, M., Morabito, M., Culosa, F., and de Mase, E. (2001). Sexual and asexual reproduction in a freshwater population of *Bangia atropurpurea* (Bangiales, Rhodophyta) from eastern Sicily (Italy). *Phycologia* 40:88–96.

Gerwick, W. H., and Lang, N. J. (1977). Structural, chemical and ecological studies on iridescence in *Iridaea* (Rhodophyta). *J. Phycol*. 13:121–7.

Giraud, G. (1962). Les infrastructures de quelques algues et leur physiologie. *J. Microscopie* 1:251–64.

Goff, L. J., and Coleman, A. W. (1984). Transfer of nuclei from a parasite to a host. *Proc. Natl. Acad. Sci. USA* 81:5420–4.

Goff, L. J., and Coleman, A. W. (1986). A novel pattern of apical cell polyploidy, sequential polyploidy reduction and intercellular nuclear transfer in the red alga *Polysiphonia*. *Am. J. Bot*. 73:1109–30.

Goff, L. J., Moon, D. A., Nyvall, P., Stache, B., Mangin, K., and Zuccarello, G. (1996). The evolution of parasitism in the red algae: molecular comparisons of adelphoparasites and their hosts. *J. Phycol*. 32:297–312.

Goreau, T. F. (1963). Calcium carbonate deposition by coralline algae and coral in relation to their roles as reef builders. *Ann. N.Y. Acad. Sci*. 109:127–67.

Gretz, M. R., Aronson, J. M., and Sommerfeld, M. R. (1980). Cellulose in the cell walls of the Bangiophyceae (Rhodophyta). *Science* 207:779–81.

Gretz, M. R., McCandless, E. L., Aronson, J. M., and Sommerfeld, M. R. (1983). The galactan sulfates of the *Conchocelis* phases of *Porphyra leucostricta* and *Bangia atropurpurea* (Rhodophyta). *J. Exp. Bot*. 34:705–11.

Gross, W., Heilmann, I., Lenze, D., and Schnarrenberger, C. (2001). Biogeography of the Cyanidiaceae (Rhodophyta) based on 18S ribosomal RNA sequence data. *Eur. J. Phycol*. 36:275–80.

Halfar, J., Zack, T., Kronz, A., and Zachos, J. C. (2000). Growth and high-resolution paleoenvironmental signals of rhodoliths (coralline red algae): a new biogenic archive. *J. Geophys. Res*. 105:107–22.

Hara, Y. (1971). An electron microscopic study on the chloroplasts of the Rhodophyta. *Proc. 7th Int. Seaweed Symp*., pp. 153–8.

Harlin, M. M., and Craigie, J. S. (1975). The distribution of photosynthate in *Ascophyllum nodosum* as it relates to epiphytic *Polysiphonia lanosa*. *J. Phycol*. 11:109–13.

Harper, J. T., and Saunders, G. W. (2001). Molecular systematics of the Florideophycidae (Rhodophyta) using nuclear large and small subunit rDNA sequence data. *J. Phycol*. 32:1073–82.

Hata, H., and Kato, M. (2003). Demise of monocultural algal farms by exclusion of territorial damselfish. *Mar. Ecol. Progr. Ser*. 263:159–167.

Hawkes, M. W. (1978). Sexual reproduction in *Porphyra gardneri* (Smith et Hollenberg) Hawkes (Bangiales, Rhodophyta). *Phycologia* 17:329–53.

Holmes, M. J., and Brodie, J. (2004). Morphology, seasonal phenology and observations on some aspects of the life history in culture of *Porphyra dioica* (Bangiales, Rhodophyta) from Devon, U.K. *Phycologia* 43:176–88.

Hurdelbrink, L., and Schwantes, H. O. (1972). Sur le cycle de développement de *Batrachospermum*. *Mem. Soc. Bot. Fr*., 269–74.

Johansen, H. W. (1981). *Coralline Algae: A First Synthesis*. Boca Raton, Florida: CRC Press.

Johnson, J. (1961). *Limestone-Building Algae and Algal Limestones*. Colorado School of Mines.

Kain, J. M., and Destombe, C. (1995). A review of the life history, reproduction and phenology of *Gracilaria*. *J. Appl. Phycol*. 7:269–81.

Kanwisher, J. W. (1966). Photosynthesis and respiration in some seaweeds. In *Some Contemporary Studies in Marine Science*, ed. R. Barnes, pp. 407–20. New York: Academic Press.

Karsten, U., West, J. A., Zuccarello, G. C., et al. (2003). Low molecular weight carbohydrates of the Bangiophycidae (Rhodophyta). *J. Phycol*. 39:548–9.

Kim, G. H., and Fritz, L. (1993). Ultrastructure and cytochemistry of early spermatangial development in *Antithamnion nipponicum* (Ceramiaceae, Rhodophyta). *J. Phycol*. 29:797–805.

Kim, G. H., and Kim, S.-H. (1999). The role of F-actin during fertilization in the red alga *Aglaothamnion oosuminse* (Rhodophyta). *J. Phycol*. 35:806–14.

Kim, M.-S., Maggs, C. A., McIvor, L., and Guiry, M. D. (2000). Reappraisal of the type species of *Polysiphonia* (Rhodomelaceae, Rhodophyta). *Eur. J. Phycol*. 35:83–92.

Kornmann, P. (1994). Life histories of monostomatic *Porphyra* species as a basis for taxonomy and classification. *Eur. J. Phycol*. 29:69–71.

Kugrens, P. (1974). Light and electron microscope studies on the development and liberation of *Janczewskia gardneri* Setch. spermatia (Rhodophyta). *Phycologia* 13:295–306.

Kugrens, P., and West, J. A. (1972a). Ultrastructure of spermatial development in the parasitic red alga *Levringiella gardneri* and *Erythrocystis saccata*. *J. Phycol*. 8:331–43.

Kugrens, P., and West, J. A. (1972b). Ultrastructure of tetrasporogenesis in the parasitic red alga *Levringiella gardneri* (Setchell) Kylin. *J. Phycol*. 8:370–83.

Kugrens, P., and West, J. A. (1973). The ultrastructure of an alloparasitic red alga *Choreocolax polysiphoniae*. *Phycologia* 12:175–86.

Kugrens, P., and West, J. A. (1974). The ultrastructure of carposporogenesis in the marine hemiparasitic red alga *Erythrocystis saccata*. *J. Phycol*. 10:139–47.

Kurihara, A., Arai, S., Shimada, S., and Masuda, M. (2005). The conspecificity of *Galaxura apiculata* and *G. hystix* (Nemaliales, Rhodophyta) inferred from

comparative morphology and rbcL and ITS1 sequences. *Eur. J. Phycol*. 40:39–52.
Kylin, H. (1916). Über *Spermothamnion roseolum* (Ag.) Pringsh. und *Trailiella intricata* Batters, *Bot. Not*., 83–92.
Kylin, H. (1923). Studien über die Entwicklungsgeschichte der Florideen. *Sven, Vet. Akad. Handl*. 63, No. 11.
Kylin, H. (1924). Bemerkungen über einige *Ceramium*-Arten. *Bot. Not*., 443–52.
Kylin, H. (1928). Entwicklungsgeschichtliche Florideenstudien. *Lunds Univ. Arsskr. N.F. II* 24, No. 4.
Kylin, H. (1930). Uber die Entwicklungsgeschichtliche der Florideen. *Lunds Univ. Arsskr. N.F. II* 26, No. 6.
Kylin, H. (1956). *Die Gattungen der Rhodophyceen*. Gleerups, Lund.
Lahaye, M. (2001). Developments on gelling algal galatans, their structure and physico-chemistry. *J. Appl. Phycol*. 13:173–84.
Largo, D. B., Fukami, K., Nishijima, T., and Ohno, M. (1995). Notes on thalli whitening called *ice-ice* in red algae, *Eucheuma/Kappaphycus* and *Gracilaria*. *Bull. Mar. Sci. Fish., Kochi Univ*. No. 15: 39–42.
Lee, R. E. (1971). The pit connections of some lower red algae: Ultrastructure and phylogenetic significance. *Br. Phycol. J.* 6:29–38.
Lee, R. E. (1974). Chloroplast structure and starch grain production as phylogenetic indicators in the lower Rhodophyceae. *Br. Phycol. J*. 9:291–5.
Lee, R. E., and Fultz, S. A. (1970). The ultrastructure of the *Conchocelis* stage of the marine red alga *Porphyra leucosticta*. *J. Phycol*. 6:22–8.
Lee, T.-M. (1999). Changes in activities and properties of biosynthetic enzymes in relation to high-temperature-induced proline accumulation in *Gracilaria tenuistipitata* (Gigartinales, Rhodophyta). *Phycologia* 37:433–8.
Lewin, R. A., and Robertson, J. A. (1971). Influence of salinity on the form of *Asterocytis* in pure culture. *J. Phycol*. 7:236–8.
Lewis, R. J., and Hanisak, M. D. (1996). Effects of phosphate and nitrate supply on productivity, agar content and physical properties of agar of *Gracilaria* strain G-16S. *J. Appl. Phycol*. 8:41–9.
Lichtlé, C., and Giraud, G. (1969). Etude ultrastructurale de la zone apicale du thalle du *Polysiphonia elongata* (Harv.) Rhodophyceé, Floridée. Evolution des plastes. *J. Microscopie* 8:867–87.
Lin, H., Sommerfeld, M. R., and Swafford, J. R. (1975). Light and electron microscope observations on motile cells of *Porphyridium purpureum* (Rhodophyta). *J. Phycol*. 11:452–7.
Liu, Y. L., Ross, N., Lanthier, P., and Reith, M. (1996). A gametophyte cell wall protein of the red alga *Porphyra purpurea* (Rhodophyta) contains four apparent polysaccharide-binding domains. *J. Phycol*. 32:995–1003.
Magruder, W. H. (1984). Specialized appendages on spermatia from the red alga *Aglaothamnion neglectum* (Ceramiales, Ceramiaceae) specifically bind with trichogynes. *J. Phycol*. 20:436–40.
Marquardt, J., Schultze, A., Rosenkrau, V., and Wehrmeyer, W. (1999). Ultrastructure and photosynthetic apparatus of *Rhodella violaceae* (Porphyridiales, Rhodophyta) grown under – iron-deficient conditions. *Phycologia* 38:418–27.
Matsuzaki, M., and 41 other authors (2004). Genome sequence of the ultrasmall unicellular red alga *Cyanidioschyzon merolae* 10D. *Nature* 428:653–7.
Melo, R. A. (1998). *Gelidium* commercial exploitation: natural resources and cultivation. *J. Appl. Phycol*. 10:303–14.
Mine, K., Kubouchi, Y., and Okuda, K. (2003). Fine structure of spermatial surface in the red alga *Antithamnion nipponicum* (Rhodophyta). *Phycol. Res*. 51:109–17.
Mizuta, H., Yasui, H., and Saga, N. (2003). A simple method to mass produce monospores in the thallus of *Porphyra yezoensis* Ueda. *J. Appl. Phycol*. 15:345–9.
Mollet, J. C., Rahaoui, A., and Lemoine, Y. (1998). Yields, chemical composition and gel strength of agarocolloids of *Gracilaria gracilis, Gracilariopsis longissima* and newly reported *Gracilaria* cf. *vermiculophylla* from Roscoff (Brittany, France). *J. Appl. Phycol*. 10:59–66.
Mukai, L. S., Craigie, J. S., and Brown, R. G. (1981). Chemical composition and structure of the cell walls of the *Conchocelis* and thallus phases of *Porphyra tenera* (Rhodophyceae). *J. Phycol*. 17:192–8.
Mumford, T. F., and Miura, A. (1988). *Porphyra* as food: cultivation and economics. In *Algae and Human Affairs*, ed. C. A. Lembi and J. P. Waaland, pp. 87–117. Cambridge: Cambridge University Press.
Murakami, A., Miyashita, H., Iseki, M., Adachi, K., and Mimuro, M. (2004). Chlorophyll *d* in an epiphytic cyanobacterium of red algae. *Science* 303:1633.
Necchi, O., and Jimenez, J. C. (2002). Somatic meiosis and development of the juvenile gametophyte in members of the Batrachospermales *sensu lato* (Rhodophyta). *Phycologia* 41:340–7.
Ngan, Y., and Price, I. R. (1979). Systematic significance of spore size in the Florideophycidae (Rhodophyta). *Br. Phycol. J.* 14:285–303.

Noguchi, T., Matsui, T., Miyazawa, K., et al. (1994). Poisoning by the red alga "ogonori" (*Gracilaria verrucosa*) on the Nojima Coast, Yokohama, Kanagawa Prefecture, Japan. *Toxicon* 32:1533–8.

Ogata, E., Matsui, T., and Nakamura, H. (1972). The life cycle of *Gracilaria verrucosa* (Rhodophyceae, Gigartinales) in vitro. *Phycologia* 11:75–80.

Ohno, M., Nang, H. Q., and Hirase, S. (1996). Cultivation and carrageenan yield and quality of *Kappaphycus alvarezii* in the waters of Vietnam. *J. Applied Phycol*. 8:431–7.

Ohta, N., Sato, N., Ueda, K., and Kuroiwa, T. (1997). Analysis of a plastid gene cluster reveals a close relationship between *Cyanidioschyzon* and *Cyanidium*. *J. Plant Res*. 110:235–45.

Okazaki, M., Ikawa, T., Furuya, K., Nisizawa, K., and Miwa, T. (1970). Studies on calcium carbonate deposition of a calcareous red alga *Serraticardia maxima*. *Bot. Mag. Tokyo* 83:193–201.

Oliveira, M. C., and Bhattacharya, D. (2000). Phylogeny of the Bangiophycidae (Rhodophyta) and the secondary endosymbiotic origin of algal plastids. *Amer. J. Bot*. 87:482–92.

Oltmanns, F. (1904). *Morphologie und Biologie der Algen*, Bd. I. Jena.

Pallaghy, C. K., Minchinton, J., Kraft, G. T., and Wetherbee, R. (1983). Presence and distribution of bromine in *Thysanocladia densa* (Solieriaceae, Gigartinales), a marine red alga from the Great Barrier Reef. *J. Phycol*. 19:204–8.

Papenfuss, G. F. (1945). Review of the *Acrochaetium–Rhodochorton* complex of the red algae. *Univ. Calif. Publ. Bot*. 18:299–334.

Papenfuss, G. F. (1947). Further contributions toward an understanding of the *Acrochaetium–Rhodochorton* complex of the red algae. *Univ. Calif. Publ. Bot*. 18:433–47.

Papenfuss, G. F. (1966). A review of the present system of classification of the Florideophycidae. *Phycologia* 5:247–55.

Pearse, V. B. (1972). Radioisotopic study of calcification in the articulated coralline alga *Bossiella orbigniana*. *J. Phycol*. 8:88–97.

Peders'en, M. E. E., Roomans, G. M., and v. Hofsten, A. (1981). Bromine in the cuticle of *Polysiphonia nigrescens:* Localization and content. *J. Phycol*. 17:105–8.

Peyrière, M. (1971). Etude infrastructurale des spermatocystes du *Griffithsia flosculosa* (Rhodophycée). *C. R. Séances Acad. Sci. Paris* 273:2071–4.

Pickett-Heaps, J. D., West, J. A., Wilson, S. M., and McBride, D. L. (2001). Time-lapse videomicroscopy of cell (spore) movement in red algae. *Eur. J. Phycol*. 36:9–22.

Potin, P., Bouarab, K., Kupper, F., and Kloareg, B. (1999). Oligosaccharide recognition signals and defense reactions in marine plant-microbe interactions. *Curr. Opin. Microbiol*. 2:276–83.

Pueschel, C. M. (1987). Absence of cap membrane as a characteristic of pit plugs in some red algal orders. *J. Phycol*. 23:150–6.

Pueschel, C. M. (1989). An expanded survey of the ultrastructure of red algal pit plugs. *J. Phycol*. 25:625–36.

Pueschel, C. M., and Miller, T. J. (1996). Reconsidering prey specializations in an algal-limpet grazing mutualism: Epithallial cell development in *Clathromorphum circumscriptum* (Rhodophyta, Corallinales). *J. Phycol*. 32:28–36.

Pueschel, C. M., and Trick, H. N. (1991). Unusual morphological and cytochemical features of pit plugs in *Clathromorphum circumscriptum* (Rhodophyta; Corallinales). *Br. Phycol. J.* 26:335–42.

Ragan, M. A., Bird, C. J., Rice, E. L., Gutell, R. B., Murphy, C. A., and Singh, R. K. (1994). A molecular phylogeny of the marine red algae (Rhodophyta) based on the nuclear small-subunit rRNA gene. *Proc. Natl. Acad. Sci., USA* 91:7276–80.

Ramus, J. (1969). Pit connection formation in the red alga *Pseudogloiophloea*. *J. Phycol*. 5:57–63.

Ramus, J. (1971). Properties of septal plugs from the red alga *Griffithsia pacifica*. *Phycologia* 10:99–103.

Ramus, J., and Robins, D. M. (1975). The correlation of Golgi activity and polysaccharide secretion in *Porphyridium*. *J. Phycol*. 11:70–4.

Rawlence, D. J. (1972). An ultrastructural study of the relationship between rhizoids of *Polysiphonia lanosa* (L.) Tandy (Rhodophyceae) and the tissue of *Ascophyllum nodosum* (L.) Le Jolis (Phaeophyceae). *Phycologia* 11:279–90.

Reddy, C. R. K., Kumar, G. R. K., Siddhanta, A. K., Tewari, A., and Eswaran, K. (2003). *In vitro* somatic embryogenesis and regeneration of somatic embryos from pigmented callus of *Kappaphycus alvarezii* (Doty) Doty (Rhodophyta, Gigattinales). *J. Phycol*. 39:610–16.

Reed, R. H. (1985). Osmoacclimation in *Bangia atropurpurea* (Rhodophyta, Bangiales): The osmotic role of floridoside. *Br. Phycol. J*. 20:211–18.

Richardson, N. (1970). Studies on the photobiology of *Bangia fuscopurpurea*. *J. Phycol*. 6:215–19.

Sacramento, A. T., Garcia-Jimenez, P., Alcazar, R., Tiburcio, A. F., and Robaina, R. R. (2004). Influence of polyamines on the sporulation of

Grateloupia (Halymeniaceae, Rhodophyta). *J. Phycol*. 40:887–94.

Sagert, S., and Schubert, H. (1995). Acclimation of the photosynthetic apparatus of *Palmaria palmata* (Rhodophyta) to light qualities that preferentially excite photosystem I or photosystem II. *J. Phycol*. 31:547–54.

Satoh, K., Smith, C. M., and Fork, D. C. (1983). Effects of salinity on primary processes of photosynthesis in the red alga *Porphyra perforata*. *Plant Physiol*. 73:643–7.

Saunders, G. W., and Hommersand, M. H. (2004). Assessing red algal supraordinal diversity and taxonomy in the context of contemporary systematic data. *Amer. J. Bot*. 91:1494–507.

Scott, J. L., and Dixon, P. S. (1973a). Ultrastructure of spermatium liberation in the marine red alga *Ptilota densa*. *J. Phycol*. 9:85–91.

Scott, J. L., and Dixon, P. S. (1973b). Ultrastructure of tetrasporogenesis in the marine red alga *Ptilota hypnoides*. *J. Phycol*. 9:29–46.

Scott, J., Bosco, C., Schornstein, K., and Thomas, J. (1980). Ultrastructure of cell division and reproductive differentiation of male plants in the Florideophycidae (Rhodophyta): Cell division in *Polysiphonia*. *J. Phycol*. 16:507–24.

Seckbach, J., and Ikan, R. (1972). Sterols and chloroplast structure of *Cyanidium caldarium*. *Plant Physiol*. 49:457–9.

Sheath, R. G., and Hambrook, J. A. (1988). Mechanical adaptation to flow in freshwater algae. *J. Phycol*. 24:106–11.

Silva, P. C., and Johansen, H. W. (1986). A reappraisal of the order Corallinales (Rhodophyceae). *Br. Phycol. J*. 21:245–54.

Simon-Bichard-Bréaud, J. (1971). Un appareil cinétique dans les gamétocystes mâles d'une Rhodophycée: *Bonnemaisonia hamifera* Hariot. *C. R. Séances Acad. Sci. Paris* 273: 1272–5.

Skuja, H. (1938). Comments on fresh-water Rhodophyceae. *Bot. Rev*. 4:665–76.

Smit, A. J. (2004). Medicinal and pharmaceutical uses of seaweed natural products: a review. *J. Appl. Phycol*. 16:245–62.

Smith, G. M. (1938). *Cryptogamic Botany*, Vol. 1. New York: McGraw-Hill.

Smith, G. M. (1969). *Marine Algae of the Monterey Peninsula, California*. 2nd edn. Stanford, Calif.: Stanford University Press.

Sommerfeld, M. R., and Nichols, H. W. (1970). Comparative studies in the genus *Porphyridium* Naeg. *J. Phycol*. 6:67–78.

Sommerfeld, M. R., and Nichols, H. W. (1973). The life cycle of *Bangia fuscopurpurea* in culture. I. Effects of temperature and photoperiod on the morphology and reproduction of the *Bangia* phase. *J. Phycol*. 9:205–10.

Spieler, R. (2002). Seaweeds compound's anti-HIV efficacy will be tested in southern Africa. *Lancet* 359:1675.

Stanley, S. M., Ries, J. B., and Hardie, L. A. (2002). Low-magnesium calcite produced by coralline algae in seawater of Late Cretaceous composition. *Proc. Natl. Acad. Sci., USA* 99:15323–6.

Sturch, H. H. (1926). *Choreocolax Polysiphoniae* Reinsch. *Ann. Bot*. 40:585–605.

Suneson, S. (1937). Studien über die Entwicklungsgeschichte der Corallinaceen. *Lunds Univ. Arsskr. N.F. II* 33, No. 2:1–132.

Suneson, S. (1943). The structure, life-history and taxonomy of the Swedish Corallinaceae, *Lunds Univ. Arsskr. N.F.* Aud. 2, Bd. 39.

Swale, E. M. F., and Belcher, J. H. (1963). Morphological observations on wild and cultured material of *Rhodochorton investiens* (Lenormand) nov. comb. (*Balbiana investiens* (Lenorm.) Sirodot). *Ann. Bot*. 27:281–90.

Taylor, W. R. (1957). *Marine Algae of the Northeastern Coast of North America*. Ann Arbor: University of Michigan Press.

Therkelsen, G. H. (1993). Carrageenan. In *Industrial Gums: Polysaccharides and Their Derivatives*. 3rd. edn., ed. R. L. Whistler, and J. N. BeMiller, pp. 145–80. San Diego: Academie Press.

Tripodi, G. (1974). Ultrastructural changes during carpospore formation in the red alga *Polysiphonia*. *J. Submicrosc. Cytol*. 6:275–86.

Tseng, C. K. (1981). Commercial cultivation. In *The Biology Of Seaweeds*, ed. C. S. Lobban, and M. J. Wynne. Berkeley and Los Angeles: Univ. Calif. Press.

Turner, C. H. C., and Evans, L. V. (1978). Translocation of photoassimilated ^{14}C in the red alga *Polysiphonia lanosa*. *Br. Phycol. J*. 13:51–5.

Umezaki, I. (1967). The tetrasporophyte of *Nemalion vermiculare* Suringar. *Rev. Algol*. 7:19–24.

von Stosch, H. A., and Theil, G. (1979). A new mode of life history in the freshwater red algal genus *Batrachospermum*. *Am. J. Bot*. 66:105–7.

Vreeland, V., Zablackis, E., and Laetsch, W. M. (1992). Monoclonal antibodies as molecular markers for the intracellular and cell wall distribution of -carrageenan epitopes in *Kappaphycus* (Rhodophyta) during tissue development. *J. Phycol*. 28:328–42.

Weinberger, F., and Friedlander, M. (2000). Response of *Gracilaria conferta* (Rhodophyta) to oligoagars results in defense against agar-degrading epiphytes. *J. Phycol*. 36:1079–86.

West, J. A. (1972). Environmental regulation of reproduction in *Rhodochorton purpureum*. In *Contributions to the Systematics of Benthic Marine Algae of the North Pacific*, ed. I. A. Abbott, and M. Kurogi, pp. 213–30. Kobe: Jpn. Soc. Phycol.

Willen, T., and Wingqvist, E.-M. (1986). Svenska sjoar undersokta av H. Skuja med avseende pa vaxtplankton. *Svensk. Bot. Tidskr*. 80:198–208.

Wilson, S. M., West, J. A., and Pickett-Heaps, J. D. (2003). Time-lapse videomicroscopy of fertilization and the actin cytoskeleton in *Murrayella periclados* (Rhodomelaceae, Rhodophyta). *Phycologia* 42: 638–45.

Wolk, C. P. (1968). Role of bromine in the formation of the refractile inclusions of the vesicle cells of the Bonnemaisoniaceae (Rhodophyta). *Planta* 78:371–8.

Wray, J. L. (1977). *Calcareous Algae*. Amsterdam: Elsevier.

Yamanouchi, S. (1906). The life history of *Polysiphonia violacea. Bot. Gaz*. 42:401–49.

Yoon, H. S., Hackett, J. D., Ciniglia, C., Pinto, G., and Bhattacharya, D. (2004). A molecular timeline for the origin of photosynthetic eukaryotes. *Mol. Biol. Evol*. 21:809–18.

Young, D. N. (1979). Fine structure of the "gland cells" of the red alga, *Opuntiella californica* (Solieriaceae, Gigartinales). *Phycologia* 18:288–95.

Young, D. N., and West, J. A. (1979). Fine structure and histochemistry of vesicle cells of the red alga *Antithamnion defectum* (Ceramiaceae). *J. Phycol*. 15:49–57.

Chapter 5

Chlorophyta

The Chlorophyta, or **green algae**, have chlorophylls *a* and *b*, and form starch with the chloroplast, usually in association with a pyrenoid. The Chlorophyta thus differ from the rest of the eukaryotic algae in forming the storage product in the chloroplast instead of in the cytoplasm. No chloroplast endoplasmic reticulum occurs around the chloroplasts.

The Chlorophyta are primarily freshwater; only about 10% of the algae are marine, whereas 90% are freshwater (Smith, 1955). Some orders are predominantly marine (Caulerpales, Dasycladales, Siphonocladales), whereas others are predominantly freshwater (Ulotrichales, Coleochaetales) or exclusively freshwater (Oedogoniales, Zygnematales). The freshwater species have a cosmopolitan distribution, with few species endemic in a certain area. In the marine environment, the green algae in the warmer tropical and semitropical waters tend to be similar everywhere in the world. This is not true of the Chlorophyta in the colder marine waters; the waters of the Northern and Southern hemispheres have markedly different species. The warmer waters near the equator have acted as a geographical barrier for the evolution of new species and genera.

Cell structure

In the Chlorophyta, microtubular hairs do not occur on the flagella, although fibrillar hairs (*Chlamydomonas*, Fig. 1.7(*b*)) and Golgi-produced scales (*Pyramimonas* (Fig. 5.10), are present in some genera.

Cell walls usually have cellulose as the main structural polysaccharide, although **xylans** or **mannans** often replace cellulose in the Caulerpales (Huizing et al., 1979). The primitive algae in the Prasinophyceae have extracellular scales, or a wall derived from interlacing scales, composed of acidic polysaccharides (Becker et al., 1996). Algae in the Volvocales have walls composed of glycoproteins (Goodenough and Heuser, 1985). Chloroplast pigments are similar to those of higher plants; chlorophyll *a* and *b* are present. The main carotenoid is **lutein**. The siphonaceous genera, as well as the unicells *Tetraselmis* and *Mesostigma*, are the only green algae to have **siphonoxanthin** (Fig. 5.1) and its ester **siphonein** (Yoshi et al., 2003).

Accumulation of carotenoids occurs under conditions of nitrogen deficiency, high irradiance or high salinity. This is particularly true in *Dunaliella* (Figs. 5.62, 5.63) where β-carotene accumulates between thylakoids in the chloroplast, and *Haematococcus* (Fig. 5.63), where **astaxanthin** (Fig. 5.1) accumulates in lipid globules outside the chloroplast (Hagen et al., 2000; Wang et al., 2003). **Hematochrome** is a general term for these carotenoids. Accumulation of hematochromes color the cells orange or red, with hematochrome accumulating up to 8–12% of the cellular contents in *Dunaliella* (Orset and Young, 1999). Animals can not synthesize carotenoids and they acquire the pigments through the food chain from primary producers. Hematochromes are responsible for the coloring in fish, crustaceans and birds (such as the pink in flamingos).

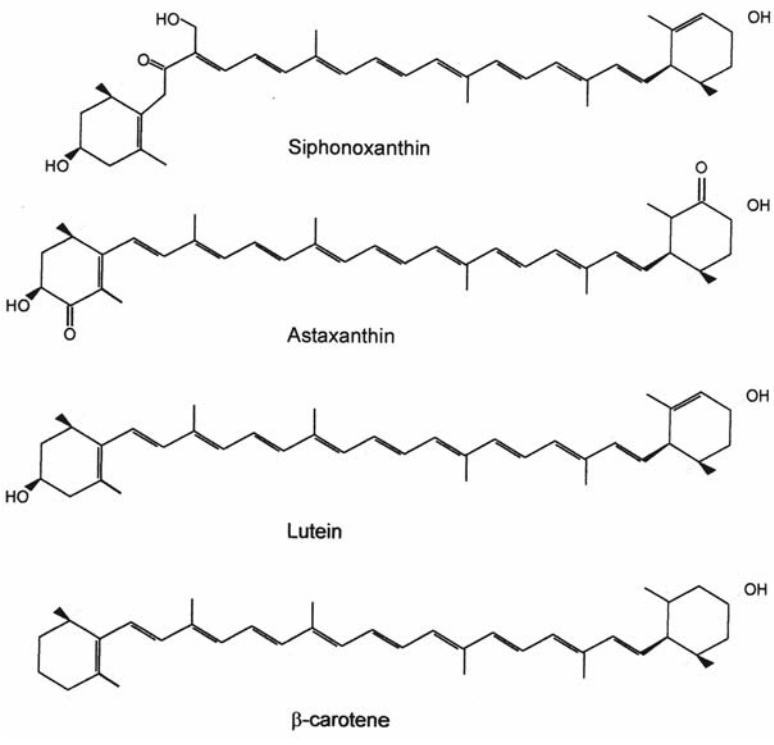


Fig. 5.1 The chemical structures of carotenoids of the Chlorophyta.

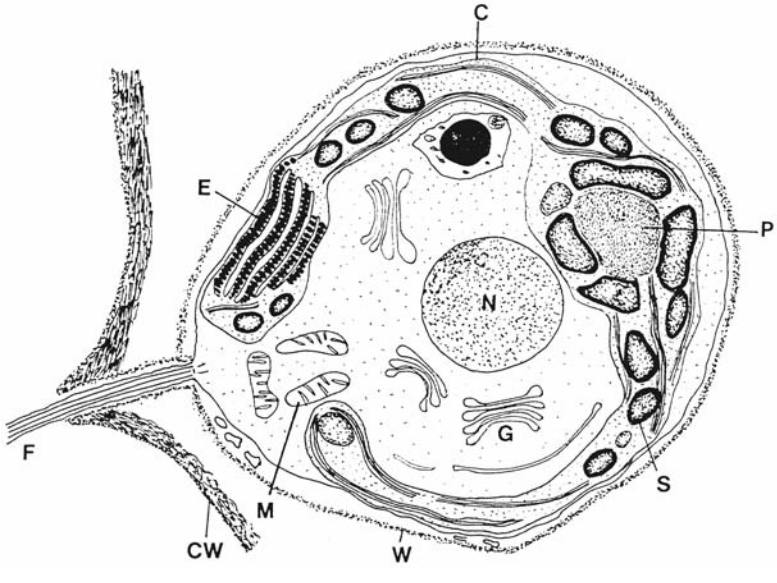


Fig. 5.2 Semidiagrammatic drawing of a cell in a *Volvox* vegetative colony. The colony wall (CW) is distinct from the cell wall (W). (C) Chloroplast; (E) eyespot; (F) flagellum; (G) Golgi; (M) mitochondrion; (N) nucleus; (P) pyrenoid; (S) starch. (Adapted from Pickett-Heaps, 1970.)

Chloroplasts are surrounded only by the double-membrane chloroplast envelope, with no chloroplast endoplasmic reticulum (Fig. 5.2). The thylakoids are grouped into bands of three to five thylakoids without grana. In some of the siphonaceous genera (e.g., *Caulerpa*), amyloplasts containing starch grains and a few thylakoids occur in the chloroplasts.

Starch is formed within the chloroplast, in association with a pyrenoid, if one is present (Fig. 5.2). The starch is similar to that of higher plants and is composed of amylose and amylopectin. The

photosynthetic pathways are similar to those of higher plants, many of these pathways first being worked out in green algae such as *Chlorella*.

Contractile vacuoles are present in vegetative cells of most Volvocales. Usually in biflagellate genera there are two contractile vacuoles at the base of the flagella. When there are two contractile vacuoles, they contract alternately with a rapid contraction and slow distention. The contractile vacuoles may control the water content of the cells where the protoplasm has a higher concentration of solutes than does the medium, leading to a total inflow of water that is compensated by the water pumped out by the contractile vacuoles. The contractile vacuoles may also function in removing wastes from the cells. Contractile vacuoles are sometimes called pulsating vacuoles because of their alternate filling and emptying action.

Phototaxis and eyespots

There are two types of phototactic movement in the Chlorophyta: movement by flagella and movement by the secretion of mucilage.

Most of the flagellated cells that show phototactic movement have an eyespot. In the Chlorophyta, the eyespot or stigma is always in the chloroplast, usually in the anterior portion near the flagella bases (Fig. 5.2). The eyespot consists of one to a number of layers of lipid droplets, usually in the stroma between the chloroplast envelope and the outermost band of thylakoids. The eyespot is usually colored orange-red from the carotenoids in the lipid droplets. The phototactic response varies with light intensity; Strasburger in 1878 (Bendix, 1960) observed that organisms with positive phototaxis at moderate light intensities exhibited negative phototaxis at very high light intensities. He also noted that at a given light intensity, temperature has an effect on phototaxis. *Haematococcus* zoospores (Fig. 5.63) at a given light intensity will be negatively phototactic at 4 °C, positively phototactic at 16–18 °C, and very strongly phototactic at 35 °C. Similar results were obtained with *Ulothrix* (Fig. 5.31) and *Ulva* (Fig. 5.33).

Green algae use a two-instant mechanism for perceiving light (i.e., successive measurements of light are performed by one receptor as the cell changes its position in relation to the light source) (Boscov and Feinleib, 1979). Such a mechanism can operate only if the cell frequently changes its position with respect to the light source. The photoreceptor then compares the light intensity at two different time intervals. The photoreceptor in *Chlamydomonas* is in the plasma membrane above the eyespot (Melkonian and Robenek, 1980b) and consists of a **chromophore** (colored substance) linked to a protein (**opsin** or **apoprotein**) that is embedded in the plasma membrane. The chromophore is **11-*cis*-retinal** (the aldehyde of vitamin A) (Fig. 5.3). Light excitation causes isomerization of 11-*cis*-retinal into all-*trans*, triggering a conformational change that initiates the signaling process. The 11-*cis*-retinal is restored by an enzymatic process. The 11-*cis*-retinal is linked to a protein that varies from alga to alga. In *Chlamydomonas reinhardtii*, the protein is **chlamyopsin**, while in *Volvox carteri* the protein is **volvoxopsin** (Ebnet et al., 1999; Hegemann et al., 2001). Combined, the chromophore 11-*cis*-retinal and the protein produce a rhodopsin, a general class of compounds that absorb light maximally around wavelengths of 500 nm. *Chlamydomonas* has two rhodopsins: ***Chlamydomonas* sensory rhodopsin A** and ***Chlamydomonas* sensory rhodopsin B** (Sineshchekov et al., 2002). *Chlamydomonas* sensory rhodopsin A absorbs light maximally at 510 nm (Fig. 5.3), saturates at high light intensity, and mediates a fast photoreceptor current that is involved in the **photophobic response** (Fig. 5.3). The photophobic response causes the alga to stop and prevents the cell from crossing a light/dark border. *Chlamydomonas* sensory rhodopsin B absorbs light maximally at 470 nm, saturates at low light intensities, and generates a slow photoreceptor current that is involved in phototaxis.

The eyespot acts as an interference filter by reflecting blue and green light back onto the photoreceptor in the plasma membrane (Kriemer and Melkonian, 1990). Different amounts of light are reflected onto the photoreceptor as the alga swims through the medium. This results in changes in membrane potential involving rhodopsin. Entry of calcium into the cell is affected by the membrane potential of the plasma membrane, and, in turn, the concentration of calcium ions in the cytoplasm

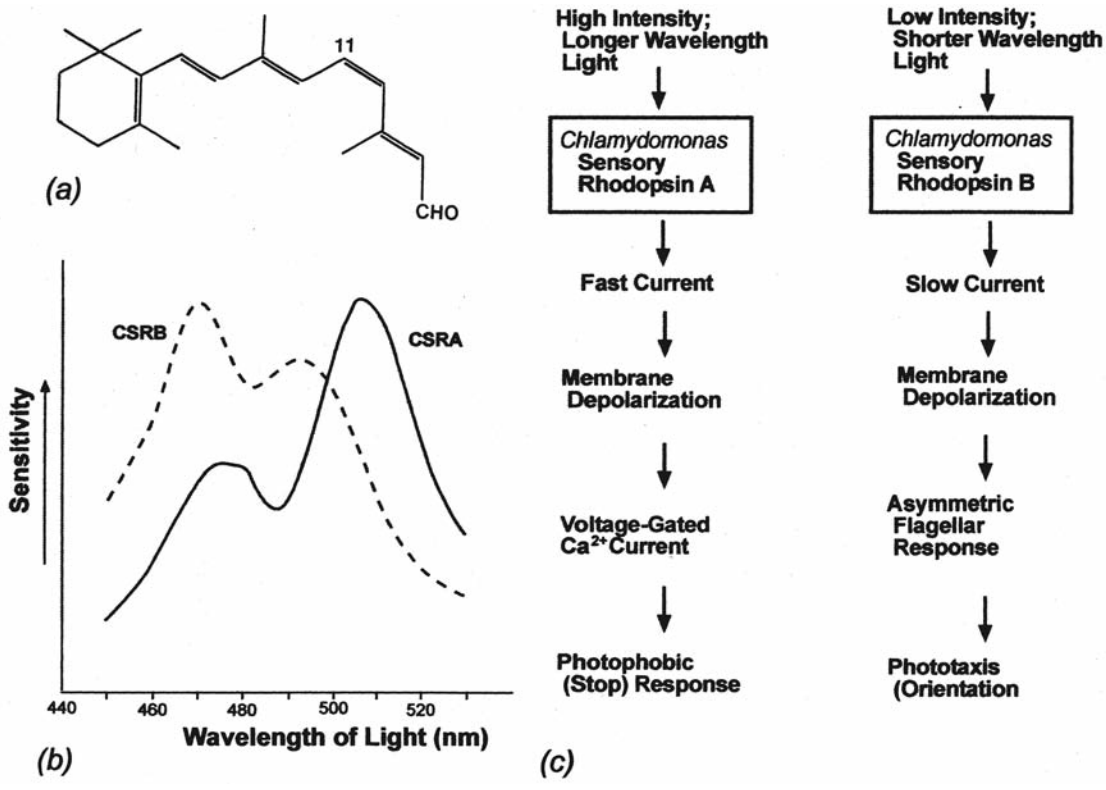


Fig. 5.3 (*a*) The structure of 11-*cis*-retinal, part of the photoreceptor molecule in *Chlamydomonas*. (*b*) Action spectra showing the sensitivity of the photoreceptors *Chlamydomonas* sensory rhodopsin A (CSRA) and *Chlamydomonas* sensory rhodopsin B (CSRB) to different wavelengths of light. (*c*) Scheme of light signal transduction initiated by the two sensory rhodopsin pigments in *Chlamydomonas*. ((*b*),(*c*) adapted from Sineshchekov et al., 2002.)

affects the rate of beating of the flagella. The swimming direction of the cell is affected by the rate of beating, because at one concentration of calcium ions, each flagellum beats differently (Kamiya and Witman, 1984). Therefore, changing the cytoplasmic calcium concentration differentially changes the beat of each flagellum, causing the cell to swim in a different direction. Melkonian and Robenek (1980b), using freeze-fracture replicas, have shown that the plasma membrane and outer membrane of the chloroplast envelope have more particles in the areas of the membranes over the eyespot than in other areas. The portion of the plasma membrane overlying the eyespot of *Chlorosarcinopsis gelatinosa* has 8200 protein particles μm^{-2} in the half of the plasma membrane next to the cytoplasm (Melkonian and Robenek, 1980a). The plasma membrane not over the eyespot has only 2100 particles μm^{-2}. These protein particles in the membranes over the eyespot probably represent a part of the photoreceptor system because they disappear during flagellar retraction and before cell wall secretion, a time when the photoreceptor system would be of no use.

A second type of phototactic movement in the Chlorophyta uses secretion of mucilage. In 1848, Ralfs, in his monograph on desmids, described their movement to the surface of mud brought into the laboratory, and presumed this movement to be due to the stimulus of light. Braun (1851) noticed that young cells of *Penium curtum* quickly aligned their long axis and moved toward the light, accumulating on the lighted side of the vessel they were growing in. The movement in desmids is brought about by the extrusion of slime through cell wall pores in the apical part of the cell (Domozych et al., 1993; Nossag and Kasprik, 1993).

Green algae can also show geotactic responses to gravity. *Chlamydomonas* (Fig. 5.55) exhibits nega-

tive geotaxis by swimming against gravity. Such a feature would be selected for in evolution because when the algal cell (which is heavier than water) is confronted with darkness, it must move up to the surface in order to obtain light for growth and reproduction. In *Chlamydomonas*, negative geotaxis is an energy-dependent response that requires a horizontal swimming path of at least 200 μm because the normal geotactic orientation maneuvers require long gradual turns. The rate of geotaxis is steady but slow relative to the average swimming speed (Bean, 1977).

Asexual reproduction

There are a number of types of asexual reproduction, the simplest being **fragmentation** of colonies into two or more parts, each part becoming a new colony. **Zoosporogenesis** commonly occurs, usually induced by a change in the environment of the alga. In the Chlorophyta, **zoospores** are normally produced in vegetative cells (e.g., *Ulothrix*; Fig. 5.31), and only in a few cases are they formed in specialized sporangia (e.g., *Derbesia*; Fig. 5.42). Zoospores are usually formed in the younger parts of filaments, and the number of zoospores is generally a power of two in uninucleate genera. **Aplanospores** *are non-flagellated and have a wall distinct from the parent cell wall* (e.g., *Trebouxia*; Fig. 5.86(*a*)–(*c*)). Aplanospores are considered to be abortive zoospores and have the ability to form a new plant on germination. **Autospores** are *aplanospores that have the same shape as the parent cell*, and are common in the Chlorellales (e.g., *Chlorella*; Fig. 5.83). Autospores are usually formed in a multiple of two in the parent cell. **Coenobia** *are colonies with a definite number of cells arranged in a specific manner* (e.g., *Volvox*; Fig. 5.69). Genera with colonies arranged in coenobia form daughter colonies with a certain number of cells. In maturation of the daughter coenobia, there is enlargement but no division of vegetative cells in the coenobia.

Sexual reproduction

Sexual reproduction in the Chlorophyceae may be isogamous, anisogamous, or oogamous, with the general line of evolution occurring in the same direction. Usually gametes are specialized cells and not vegetative cells, although in the one-celled Volvocales the latter can occur. If the species is isogamous or anisogamous, the gametes are usually not formed in specialized cells although in the oogamous species, gametes are normally formed in specialized gametangia (e.g., *Coleochaete*, Fig. 5.25). Whereas most Chlorophyta form motile flagellated gametes (zoogametes), in the Zygnematales aplanogametes or amoeboid gametes are formed.

In some of the Chlorophyta, gametogenesis is induced by environmental changes, whereas in others the presence of two sexually different strains is necessary. In the latter, vegetative cells of one sex secrete a substance that initiates sexual differentiation in competent cells of the opposite sex. Such a situation is common in the Volvocales (Starr, 1972; Kirk and Kirk, 1986) and is considered in more detail later. In *Oedogonium* (Fig. 5.95), sex organs form without the complementary strain, but subsequent fertilization is under a complex hormonal control. In other genera, a chemotactic substance is sometimes produced by the egg that attracts the spermatozoids. This does not generally happen in isogamous species. In isogamous species, sexually different gametes meet at random and immediately adhere by means of an **agglutination** reaction. The agglutinative flagellar adhesion between gametes of different sex is designated as the **mating-type reaction**. Initially after mixing, the gametes of opposite sexes adhere by their flagella tips in clusters of up to 25 gametes. Soon the anterior ends of complementary gametes fuse, and the flagella free themselves. The motile zygote then swims for some time before settling and secreting a thick wall.

The mating-type substances (responsible for flagellar agglutination) are localized and function at the flagella tips. It is possible to isolate the mating-type substances that still have the ability to interact with the gametes of the opposite sex. When added to the opposite gamete type, they cause **isoagglutination** (male gametes will clump with each other when a female mating-type substance is added to the culture). The mating-type substances are discussed in more detail for *Chlamydomonas*, which has been most intensively studied.

Table 5.1 | Characteristics of the four classes of green algae

	Micromonado-phyceae	Charophyceae	Ulvophyceae	Chlorophyceae
Position of flagella in cell		Lateral	Anterior	Anterior
Microtubular root		Large band with smaller band	Four, cruciately arranged	Four, cruciately arranged
Rhizoplast	May be present	No	Common	Common
Multilayered structure	May be present	Yes	No	No
Covering on motile cells	Scales	Scales	Scales	Theca
Interzonal spindle	Persistent	Persistent	Persistent	Collapsing
New cross wall formation		Phragmoplast	Cleavage furrow	Phycoplast
Cellulose terminal complex		Rosettes	Linear row	Linear row
Eyespot		None	Common	Common
Glycolate degradation	Glycolate dehydrogenase	Glycolate oxidase	Glycolate dehydrogenase	Glycolate dehydrogenase
Urea degradation		Urease	Urease	Urea amidolyase
Cu/Zn superoxide dismutase		Present	Absent	Absent

Soon after the gametes fuse (**syngamy**), meiosis is known to occur in the thick-walled zygotes of the Volvocales, Ulotrichales, Oedogoniales, Chlorellales, and Zygnematales.

Classification

The four important classes in the Chlorophyta are the Prasinophyceae (Micromonadophyceae), Charophyceae, Ulvophyceae, and the Chlorophyceae (Table 5.1). The classes were originally formulated in the 1970s by Karl Mattox and Kenneth Stewart (Fig. 5.4) working at Miami University of Ohio, and by Jeremy Pickett-Heaps (photograph in Preface) working at the University of Colorado. Their classification scheme was based largely on ultrastructural characteristics. Later investigations utilizing molecular genetics have verified their work.

The Charophyceae are in the line that evolved into land plants (embryophytes). As such, there have been a number of proposals made over the years to include the Charophyceae and land plants into a supergroup (Sluiman, 1985). The latest fashion is the term Viridiplantae for this line of evolution (Cavalier-Smith, 1981). A splinter of this is to include the *Chara* and its relatives with the land plants into the "Steptophyta," casually ignoring the close relationship between *Chara* and the remainder of the lower green algae.

Class 1 **Prasinophyceae**: scaly or naked flagellates with interzonal spindles that are persistent during cytokinesis; primitive green algae, some of which gave rise to the other classes in the Chlorophyta.

Class 2 **Charophyceae**: motile cells asymmetrical; two flagella attached in a lateral position in the cell; flagellar root consisting of a broad band of microtubules and a second smaller microtubular root; multilayered structure (MLS) may be present; no rhizoplast; scales common outside of motile cells; persistent interzonal mitotic spindle in telophase; phragmoplast produces new cross walls after cell division; eyespots usually not present; glycolate broken down by glycolate oxidase; urea broken down by urease; predominantly freshwater; sexual reproduction involves the formation of a dormant zygote; meiosis occurs when the zygote germinates.

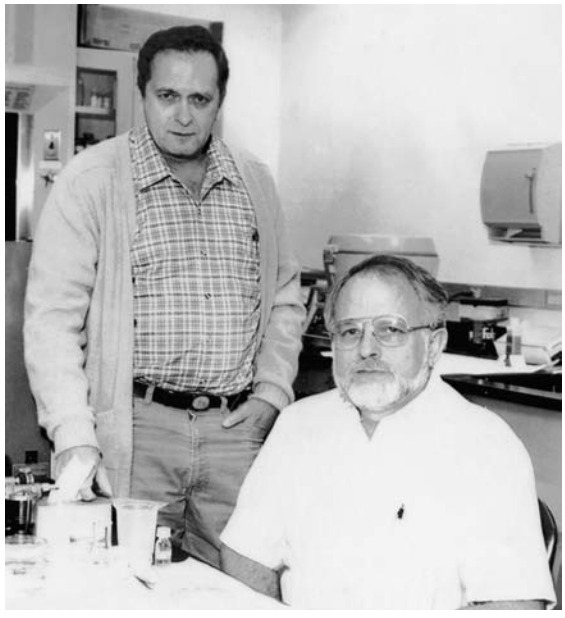


Fig. 5.4 Kenneth Stewart (*left*) and Karl Mattox (*right*).
Kenneth Stewart Born September 4, 1932 in Moberly, Missouri. Dr. Stewart received his B.Sc. from Southern Illinois University at Carbondale, Illinois, in 1954. He served in the Army and worked in non-academic jobs until enrolling at the University of California, Davis, where he received his Ph.D. in 1968. In 1968 he joined the Department of Botany at Miami University, Oxford, Ohio.
Karl Mattox Born August 22, 1936 in Cincinnati, Ohio. He received his B.Sc. (1958) and M.A. (1960) from Miami University, Ohio, and his Ph.D. (1962) from the University of Texas. From 1962 to 1966, he was assistant professor in the Department of Botany at the University of Toronto. In 1966, he moved to the Department of Botany at Miami University.

Class 3 **Ulvophyceae**: flagella attached at anterior end of cell; motile cells have near-radial symmetry externally; flagella roots consist of four cruciately arranged microtubular roots and sometimes a rhizoplast; no multilayered structure (MLS); scales may be present on motile cells; persistent interzonal spindle in telophase; cleavage furrow produces the new cross wall in cell division; eyespots common; glycolate broken down by glycolate dehydrogenase; urea broken down by urease; predominantly marine; no dormant zygotes; alternation of generations common.

Class 4 **Chlorophyceae**: motile cells with radial or near-radial external symmetry; flagella attached at anterior end of cell; flagella roots consist of four cruciately arranged microtubular roots and sometimes a rhizoplast; no multilayered structure (MLS); theca common in motile cells; in telophase, the interzonal spindle collapses; phycoplast produces the new cross wall in cell division; eyespots common; glycolate breakdown by glycolate dehydrogenase; urea broken down by urea amidolyase; predominantly freshwater; zygote undergoes a dormant period; meiosis occurs when the zygote germinates.

Position of flagella in cells

In the **Charophyceae**, the flagella are attached in a lateral position in the cell (Fig. 5.5). In the **Ulvophyceae** and **Chlorophyceae**, the flagella are attached at the anterior end.

Flagellar roots

Flagellar basal bodies are anchored in the protoplast by **microtubular roots** and/or **rhizoplasts** (Fig. 5.5) (Melkonian et al., 1988).

Microtubular roots

Microtubular roots consist of groups of 24-nm diameter microtubules that can have one of two basic configurations: (1) There can be a microtubular root consisting of a *large broad band of microtubules with a smaller second microtubular root* (**Charophyceae**), or (2) there can be *four groups of cruciately arranged microtubular roots* running from the basal bodies (**Ulvophyceae** and **Chlorophyceae**). The cruciately arranged microtubular roots have what is called an X-2-X-2 arrangement. This notation refers to the fact that two of the microtubular roots are usually composed of two microtubules, whereas the two other roots can have different numbers of microtubules in different organisms. Thus *Chlamydomonas moewusii* has a 4-2-4-2 arrangement, whereas motile cells of *Ulothrix* sp. have a 5-2-5-2 arrangement (Moestrup, 1978). One of the roots containing two microtubules is often linked to the outer membrane of

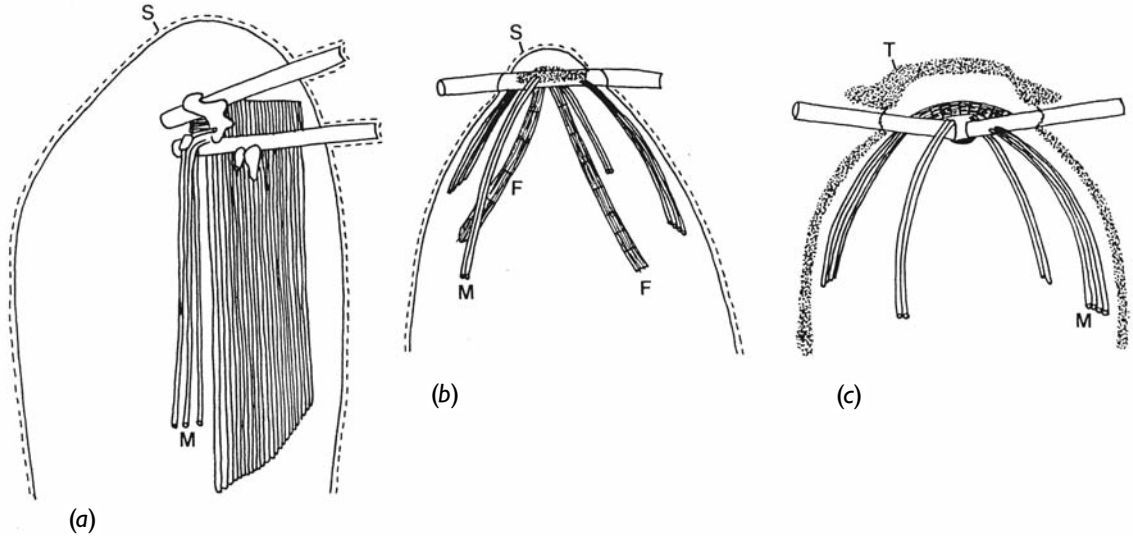


Fig. 5.5 Schematic drawings of the side view of swarmers produced by three of the classes of green algae. (*a*) **Charophyceae**: scaly cell with one large root (the MLS), one smaller root, and flagella extending at an angle from the point of insertion. (*b*) **Ulvophyceae**: four microtubular roots (two of each kind) in a cruciate arrangement, a pair of fibrous roots, and a scaly covering over the cell. (*c*) **Chlorophyceae**: cruciate roots and the cell covered with a theca. (F) Fibrous roots; (M) microtubular root; (S) scales; (T) theca. (After Mattox and Stewart, 1984.)

the chloroplast envelope and is probably involved in phototaxis.

Rhizoplasts (fibrous roots)

A rhizoplast is usually a cylinder containing 5- to 10-nm-diameter filaments interrupted at approximately 80-nm intervals by bands of electron-dense material (in the electron microscope). A rhizoplast runs from the basal bodies posteriorly toward the nucleus. Rhizoplasts are contractile (Salisbury and Floyd, 1978), and the distance between the bands in the rhizoplast varies depending on the state of contraction of the rhizoplast. The size of the filaments in the rhizoplast is similar to that of actin–myosin filaments in animal muscle cells. The method of contraction of the rhizoplast may be similar to that of muscle. Rhizoplasts may be **present** in the **Prasinophyceae**, **Chlorophyceae**, and **Ulvophyceae**, but are **absent** in the **Charophyceae**.

Multilayered structure

A multilayered structure (MLS) (Fig. 5.6) consists of a more or less rectangular body attached to the anterior end of the single broad band of microtubules in the Charophyceae and in the spermatozoids of lower land plants. The MLS lies directly beneath the basal bodies of the flagella. The MLS consists of four layers. The layer closest to the plasma membrane contains the microtubules of the root. Under this are two electron-dense layers. The bottom-most layer is composed of small microtubules. An MLS **may be present** in the **Prasinophyceae** and **Charophyceae**, but is **absent** in the **Chlorophyceae** and **Ulvophyceae**.

Occurrence of scales or a wall on the motile cells

Motile cells covered with scales may occur in the **Prasinophyceae**, **Charophyceae**, and **Ulvophyceae**. The presence of scales on the motile cells is probably the primitive condition. As evolution progressed, the scales became interweaved along their edges so a coherent cell covering was formed, as in the genus *Tetraselmis* (Fig. 5.12) (Domozych et al., 1981; Mattox and Stewart, 1984). The end result of this evolution was the **theca** that covers the motile cells in the **Chlorophyceae**. This theca has a crystalline substructure and is composed of hydroxyproline-rich glycoproteins associated with various polysaccharides (Roberts, 1974;

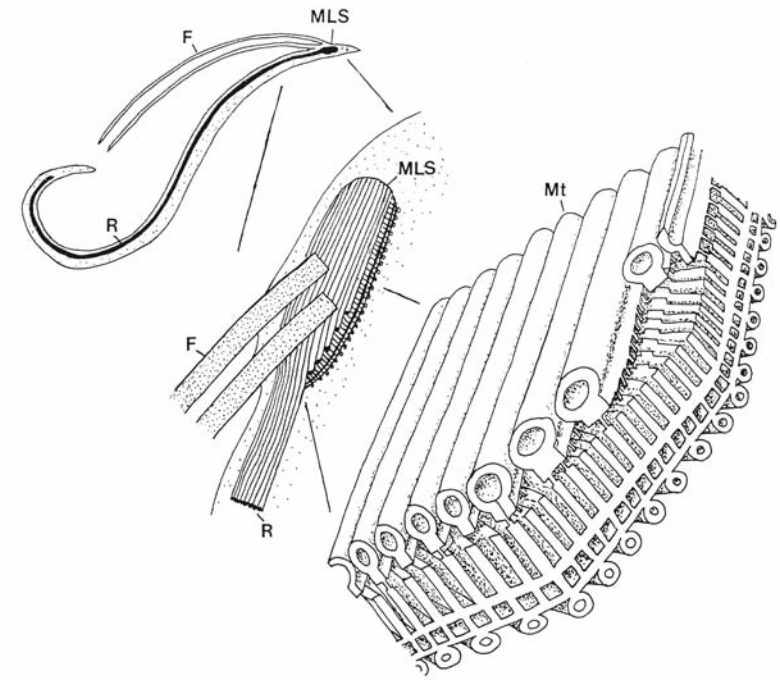


Fig. 5.6 Drawing of a green algal cell containing a multilayered structure. (F) Flagellum; (Mt) microtubule; (MLS) multilayered structure; (R) microtubular root. (Adapted from Carothers and Kreitner, 1967.)

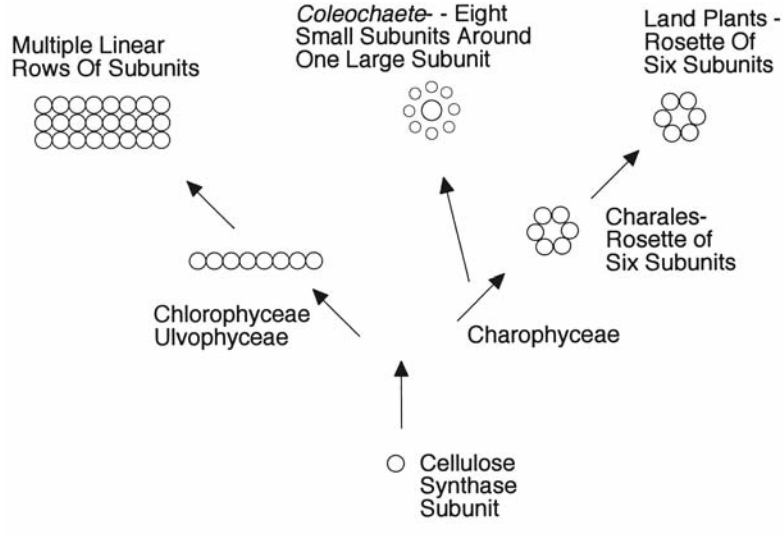


Fig. 5.7 Proteins of cellulose synthetase in the plasma membrane have aggregated into terminal complexes along two phylogenetic lines in the Chlorophyta. Rosettes of cellulose synthetase proteins have evolved in the Charophyceae, while aggregations of linear rows have evolved in the Chlorophyceae and Ulvophyceae. (Adapted from Okuda and Brown, 1992.)

Miller, 1978; Deason, 1983). The theca in motile cells of the Chlorophyceae is thus not to be confused with the cell walls of non-motile stages of the more advanced Chlorophyta, which have **cellulose** as the main skeletal molecule.

Cellulose is produced by the enzyme **cellulose synthetase** that occurs as proteins embedded in the plasma membrane of the cell. Six to ten cellulose synthetase molecules are grouped into a single subunit. The subunits are, in turn, aggregated into **terminal complexes**. In the Chlorophyta, there are two different types of terminal complexes (Fig. 5.7) (Okuda et al., 1994; Tsekos, 1999):

1 In the **Charophyceae**, terminal complexes have subunits aggregated into rosettes.
2 In the **Chlorophyceae** and **Ulvophyceae**, terminal complexes consist of linear rows of subunits.

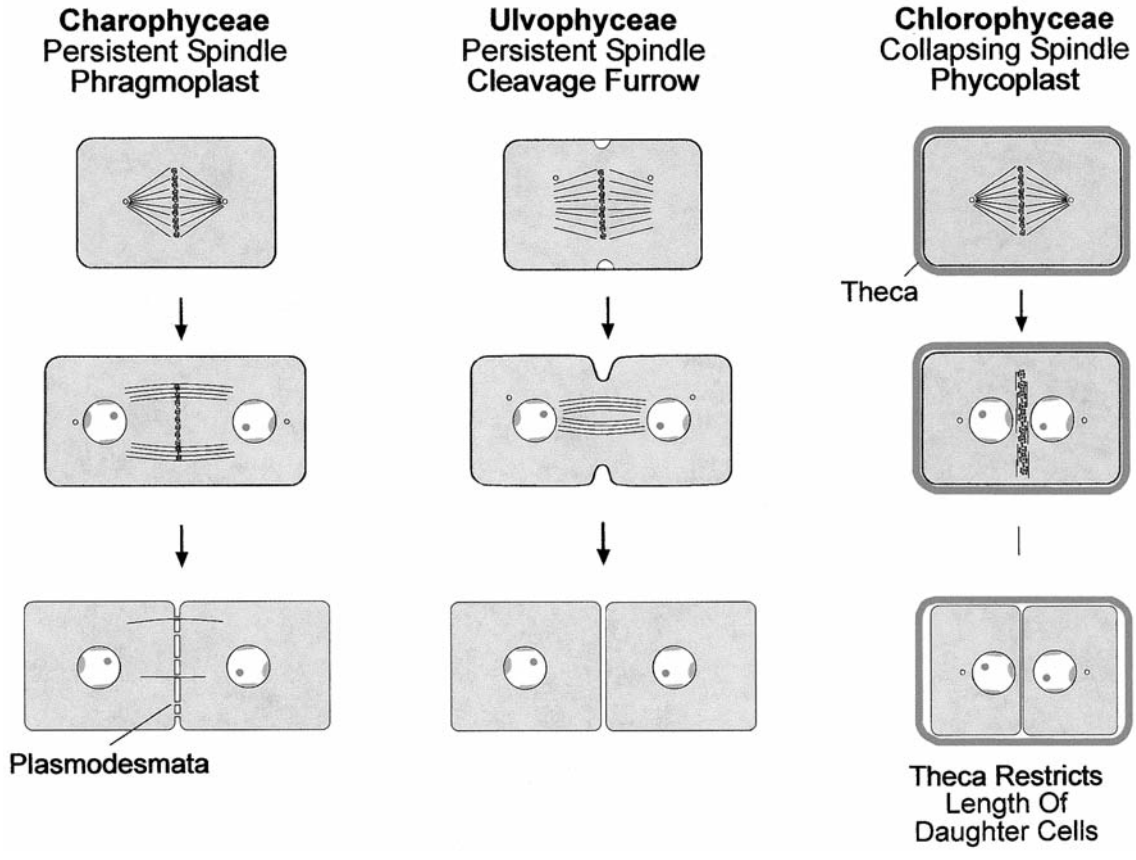


Fig. 5.8 Schematic drawing of the type of cell division in the Charophyceae, Ulvophyceae, and Chlorophyceae.

Cell division

Two types of interzonal spindles occur in telophase cells of the Chlorophyta: the **persistent type** and the **collapsing type**. The new cell wall can be formed between the daughter cells by means of a **phragmoplast**, a **cleavage furrow**, or a **phycoplast**. Three of the classes in the Chlorophyta are characterized by the type of spindle in the class and the way the new cross wall is formed (Fig. 5.8).

Persistent interzonal spindle and phragmoplast (Charophyceae)

In the **Charophyceae**, the **microtubular spindle persists** even after the daughter nuclei have separated in telophase. The daughter nuclei are separated by the length of the persistent spindle while a new cross wall is formed by a **phragmoplast** in the more advanced members. Wall formation by a phragmoplast initially involves the production of vesicles by the dictyosomes. The vesicles contain the components of the new cross walls. The persistent spindle microtubules may function in guiding the vesicles to the area of the new cross wall which will separate the two daughter cells. The vesicles fuse, releasing their contents which form the new cross wall. Plasmodesmata are formed in the cross wall between the daughter cells where the persistent spindle microtubules traverse the cross wall. In some of the primitive Charophyceae, the new cross wall is formed by a phragmoplast in association with an infurrowing of the plasma membrane. In the more advanced Charophyceae (those in the Coleochaetales and Charales), the cross wall is formed only by a phragmoplast.

Persistent interzonal spindle and a cleavage furrow (Ulvophyceae)

In the **Ulvophyceae**, the **interzonal spindle persists** during telophase, holding the daughter

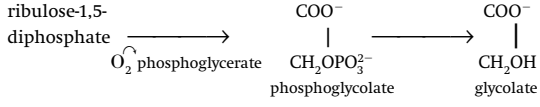
cells apart while the new cross wall is formed by an **infurrowing of the plasma membrane**. As the plasma membrane furrows inward, dictyosome vesicles fuse with the plasma membrane, behind the infurrowing, producing the new cross wall.

Collapsing interzonal spindle and a cleavage furrow (Chlorophyceae)

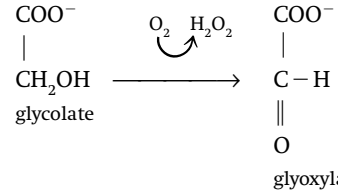
In the **Chlorophyceae**, the **mitotic spindle collapses** after nuclear division. This results in the two daughter nuclei coming close together in telophase because there is no longer a persistent interzonal spindle to hold the nuclei apart. The position of the new cross walls becomes outlined by microtubules of the **phycoplast** that arise perpendicular to the former position of the spindle microtubules. Dictyosome vesicles fuse between the phycoplast microtubules, forming the new cross wall. The Chlorophyceae have motile cells with a cell wall (theca) and thus differ from the Ulvophyceae and Charophyceae. The phycoplast evolved in conjunction with the production of cell walls in these algae (Mattox and Stewart, 1977). During cell division in cells with a persistent spindle (in the Prasinophyceae, Charophyceae, and Ulvophyceae), there is extensive elongation of the cell during anaphase. This cell elongation presents no problem in naked cells or cells covered with scales. However, in the Chlorophyceae the cells are not easily able to elongate in response to the anaphase elongation of the persistent spindle. The reason is that the Chlorophyceae have walls around the motile cells. Therefore, evolution of the phycoplast and collapsing spindle, which does not involve rapid elongation of the daughter cells, presents an evolutionary advantage.

Glycolate degradation

Glycolate, the major substrate of photorespiration, is derived from phosphoglycolate, which is formed by the oxygenation of ribulose-1,5-diphosphate:



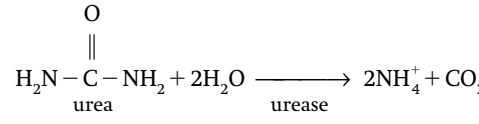
The glycolate is metabolized in microbodies called **peroxisomes**. In the peroxisomes, glycolate is oxidized to glyoxylate. The H_2O_2 produced in the reaction is cleaved by the enzyme **catalase** to H_2O and O_2:



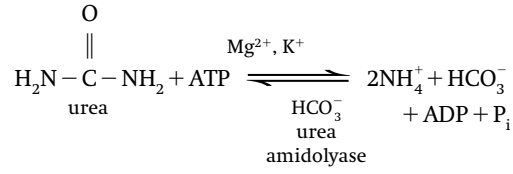
The above oxidation of glycolate can be catalyzed by the enzyme **glycolate dehydrogenase** or the enzyme **glycolate oxidase** (Gruber et al., 1974). In the **Charophyceae**, the reaction is catalyzed by **glycolate oxidase**, whereas in the **Chlorophyceae** and the **Ulvophyceae**, the reaction is catalyzed by **glycolate dehydrogenase** (Suzuki et al., 1991). Glycolate oxidase probably represents the primitive condition since *Cyanophora paradoxa* in the Glaucophyta catalyzes the reaction with this enzyme (Betsche et al., 1992).

Urea degradation

In the **Charophyceae**, **Ulvophyceae**, and **higher plants**, urea is broken down by the enzyme **urease**:



In the **Chlorophyceae**, urea is broken down by the enzyme **urea amidolyase** (Syrett and Al-Houty, 1984):



Superoxide dismutase

Superoxide dismutases (SOD) are a group of enzymes that catalyze the reaction:

$$O_2^- + O_2^- + 2H^+ \rightarrow H_2O_2 + O_2$$

Superoxide dismutases are important because they take highly reactive, potentially damaging

oxygen radicals (O_2^-) and other toxic oxygen species (OH·, singlet oxygen) and convert them to less toxic moieties.

There are three forms of superoxide dismutases, named for the metal in their reaction centers: **iron SOD** (FeSOD), **manganese SOD** (MnSOD), and **copper-zinc SOD** (Cu/Zn SOD). The amino acid sequences and three-dimensional protein structure of FeSOD and MnSOD are very similar, suggesting a close evolutionary relationship, whereas those of Cu/Zn SOD are quite different, indicating very little, if any, evolutionary relationship to the other two (deJesus et al., 1989).

FeSOD and MnSOD occur in all classes of green algae and most land plants. Cu/Zn SOD, however, occurs only in the Charophyceae and land plants, reinforcing the concept that organisms similar to those in the Charophyceae evolved into land plants.

Cu/Zn SOD is the only superoxide dismutase that occurs in the cytosol. MnSOD occurs in the mitochondrion while FeSOD occurs in the chloroplast. DeJesus et al. (1989) argue that green algae evolving to land plants would need superoxide dismutase in the cytosol to counteract oxygen diffusing in from the atmosphere, which would produce damaging radicals in the cytosol. The charophycean lineage of green algae is the only one to have superoxide dismutase in the cytosol and is a major reason for the successful colonization of the land by descendants of the Charophyceae. The other lineages of green algae were unable to make the transition to the land because they had superoxide dismutase restricted to mitochondria, chloroplasts, and peroxisomes and were not able to counteract the production of damaging radicals formed by oxygen diffusing in from the atmosphere.

Prasinophyceae

The Prasinophyceae (Micromonadophyceae) contain primitive green flagellates with scales composed of acidic polysaccharides (Wustman et al., 2004). The class is a catch-all for those algae that "exhibit primitive characteristics for many of the features used to define other classes" (Mattox and Stewart, 1984; Fawley et al., 2000).

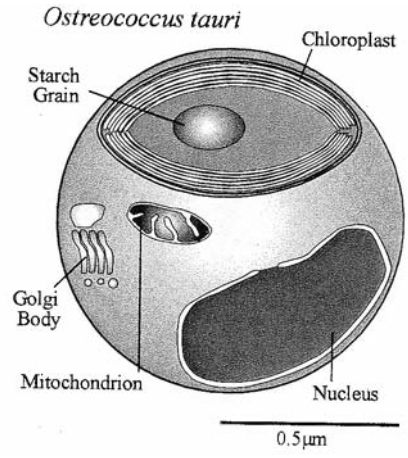


Fig. 5.9 The general organization of *Ostreococcus tauri*.

Ostreococcus tauri (Fig. 5.9) is less than 1 μm in diameter and is the smallest eukaryotic alga known. The alga has a relatively large nucleus, a single chloroplast with a starch granule, a mitochondrion, and a Golgi apparatus. Unlike other algae in the group, there are no scales outside the cell wall (Courties et al., 1998).

Pyramimonas obovata has heart-shaped (cordate) cells, with four flagella arising from an anterior flat-bottomed depression (Fig. 5.10). There are three different layers of scales on the body and two layers on the flagellum (Belcher et al., 1974). The scales are formed in dictyosomes, from which they are transported to the scale reservoir and then to the surface of the cell in vesicles.

Species of *Pyramimonas* have adapted to tidepools by means of a settling rhythm. Cells in tidepools anticipate the incoming tide and move down into the sand where they attach to sand grains by their flagella, before the first waves cover the tide pool. After the tide pool is exposed by the receding tide, the *Pyramimonas* cells move upward into the tide pool. The settling is controlled by an endogenous circadian oscillator and will continue in the laboratory for a few days after the cells are removed from the wild (Griffin and Aken, 1993).

Pterosperma is a genus that is closely related to *Pyramimonas. Pterosperma* produces walled cysts called phycomata (Fig. 5.11) that are similar to microfossils such as *Tasmanites* and *Cymatiosphaera* that have been reported from the Precambrian up to the Holocene (Inouye et al., 1990).

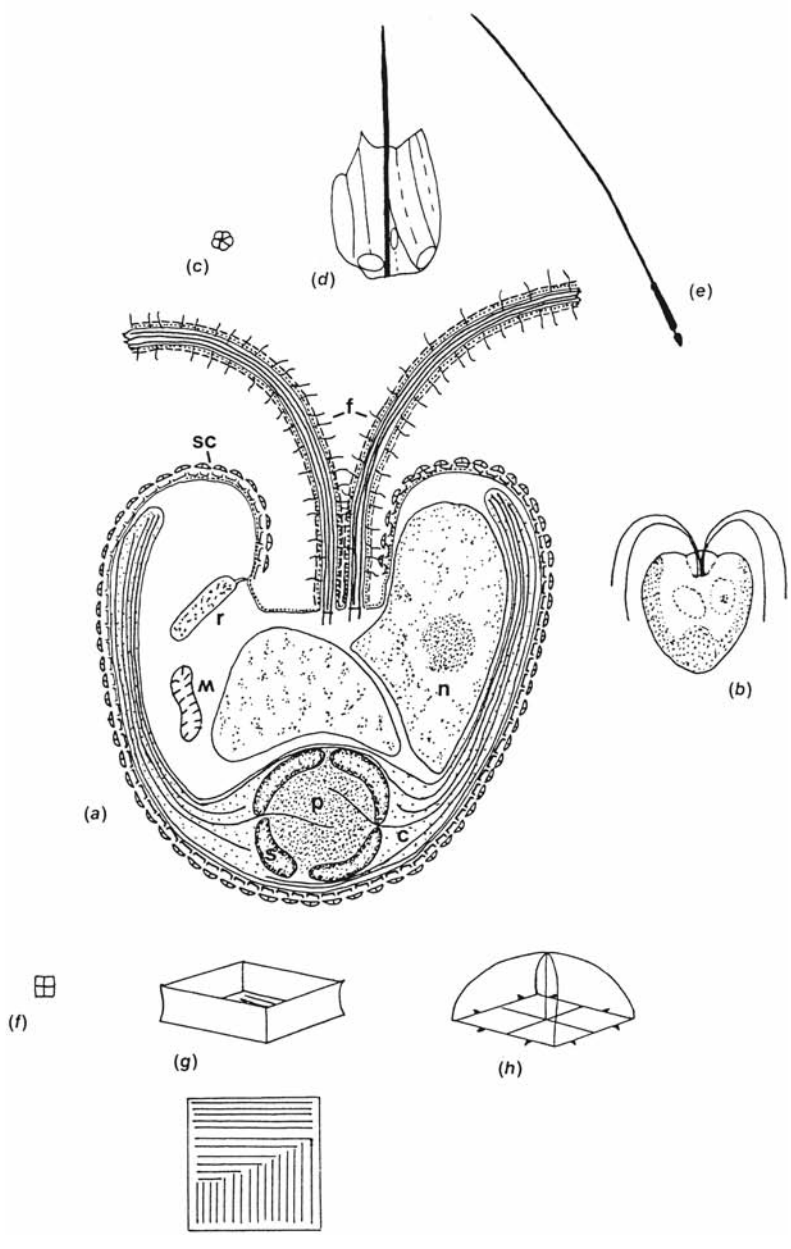


Fig. 5.10 *Pyramimonas obovata.* (*a*) Semidiagrammatic drawing of a cell showing the organelles, two of the four flagella, and the layers of scales on the body and the flagella. (*b*) Whole cell. (*c*) Inner flagella scale. (*d*) Outer flagellar scale. (*e*) Flagellar hair. (*f*) Inner body scale. (*g*) Intermediate body scale, top and side view. (*h*) Outer body scale. (c) Chloroplast; (f) flagellum; (m) mitochondrion; (n) nucleus; (p) pyrenoid; (r) scale reservoir; (s) starch; (sc) scales. (After Belcher et al., 1974.)

Tetraselmis (Fig. 5.12) is commonly found in marine waters. The cells are oval-shaped and surrounded by a theca that is formed by the coalescence of many small stellate scales that are produced in the Golgi apparatus. Four flagella are inserted in an apical pit in the cell. The flagella are covered with hairs and scales, and the flagella emerge from an opening in the theca. There is a cup-shaped chloroplast with a basal pyrenoid. A nucleus occurs in the center of the cell, and Golgi bodies are found anterior to the nucleus.

Tetraselmis produces stellate scales in the Golgi apparatus which fuse extracellularly to yield the theca (Manton and Parke, 1960). The theca is composed of neutral and acidic polysaccharides associated with certain amino acids (Becker et al., 1996), similar to the glycoprotein walls in volvocean flagellates (those green algae in the

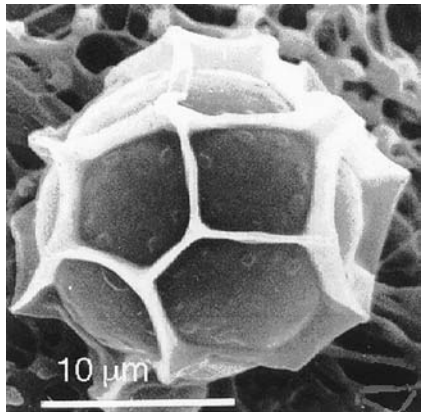


Fig. 5.11 A scanning electron micrograph of a phycoma of *Pterosperma cristatum*. Square, pentagonal or hexagonal compartments are formed by wing-like protrusions of the cell wall. (From Inouye et al., 1990.)

Volvocales) (Roberts, 1974) but unlike the cellulose cell walls in the Charophyceae. The typical volvocean flagellates and eventually the rest of the higher Chlorophyceae probably arose from a flagellate such as *Tetraselmis* or *Mantionella* (Fig. 5.54) (Domozych et al., 1981).

The genus *Tetraselmis* was previously divided into a number of genera including *Tetraselmis*, *Platymonas*, and *Prasinocladus* before it was recognized that all of the cells were similar. All of the organisms are now recognized as the single genus *Tetraselmis* with subgenera (Hori et al., 1982a,b):

Subgenus *Tetraselmis:* spherical pyrenoid into which narrow channels of cytoplasm extend.

Subgenus *Prasinocladia:* pyrenoid not penetrated by cytoplasm but by a single lobe of the nucleus so that the pyrenoid appears cup-shaped in the microscope.

Algae in the subgenus *Prasinocladia* grow as dense yellow-green tufts on rocks or shells in small tide-pools near the high-tide mark (Fig. 5.13) (Chihara, 1963). The plants occur on most temperate coasts. In the mature attached vegetative state, the two to four protoplasts are at the apical area of the wall. Protoplasts are released as zoospores by escaping through a break in the apical area of the wall. The quadriflagellate zoospores swim actively for a while, settle, lose their flagella, and secrete a wall. Germination occurs immediately after settling and first involves the secretion of an outer wall. The protoplast elongates with the deposition of an inner wall, causing a break in the outer wall; and, still surrounded by the elongating inner wall, the protoplast secretes additional wall material and positions itself at the top of the resulting tube. The protoplasts can divide into two cells to form new tubes. Any protoplast is capable of forming flagella and becoming a zoospore.

Convoluta is a small flatworm, several millimeters long (Fig. 5.14(*a*)), that lives on sandy marine shores (Russell and Yonge, 1963). It occurs in large colonies forming green patches on the yellow sand, appearing from beneath the sand immediately after the tide has left it and disappearing just before the tide returns. The green color of the flatworm is due to the presence in the animal of vast numbers of algae. The algae are not present

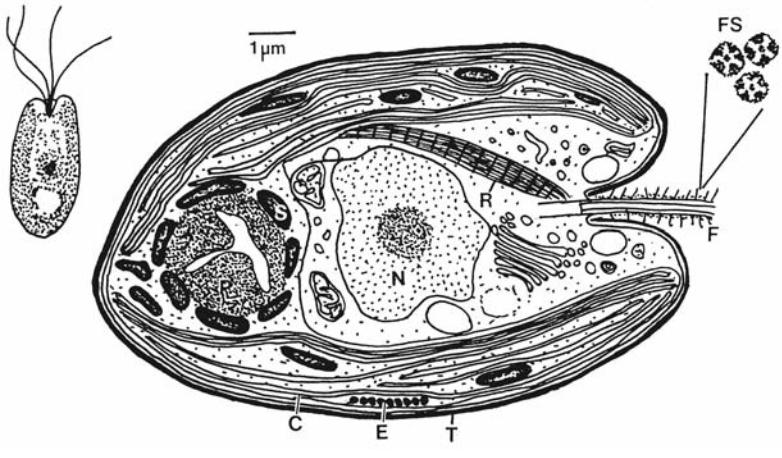


Fig. 5.12 Drawing of a cell of *Tetraselmis*. (C) Chloroplast; (E) eyespot; (F) flagellum; (FS) flagellar scales; (N) nucleus; (P) pyrenoid; (R) rhizoplast (only one of two is shown); (S) starch; (T) theca.

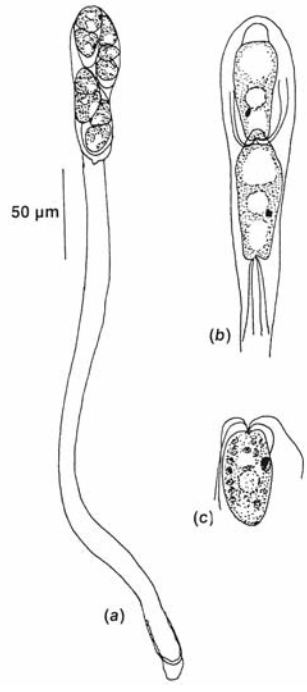


Fig. 5.13 *Tetraselmis* subgenus *Prasinocladia*. (*a*) Vegetative cells on a stalk. (*b*) Zoospores within a stalk. (c) Zoospore. (After Proskauer, 1950.)

in the egg, but there are algae adhering to the egg case that are ingested by the emerging worms. The alga that infects *Convoluta roscoffensis* is *Tetraselmis* (Fig. 5.14(*b*)) (Oschman, 1966). These algae lie in the extracellular spaces between adjacent cells of the animal. The infecting algae undergo morphological alterations within the worms, losing their flagella, theca, and eyespot in that order. The *Tetraselmis* theca does not contain cellulose (Lewin, 1958), a possible explanation for the relative ease with which the worm can dissolve the theca and set up the symbiosis. Upon loss of the theca, the alga assumes an irregularly shaped form, with finger-like processes of the algal cells penetrating between adjacent animal cells. *Convoluta* flatworms may contain algal cells of either the *Tetraselmis* or *Prasinocladia* subgenera, although one animal will usually contain cells of only one subgenus. In the United Kingdom, the flatworms having cells of the *Tetraselmis* subgenus are longer, are more likely to contain gametes, and lay more egg capsules containing more embryos than those containing cells of the *Prasinocladia* subgenus (Douglas, 1985). If the *Convoluta* eggs are not infected by *Tetraselmis*, they fail to develop properly and soon die. In early life, *Convoluta*, like other flatworms, feeds on smaller

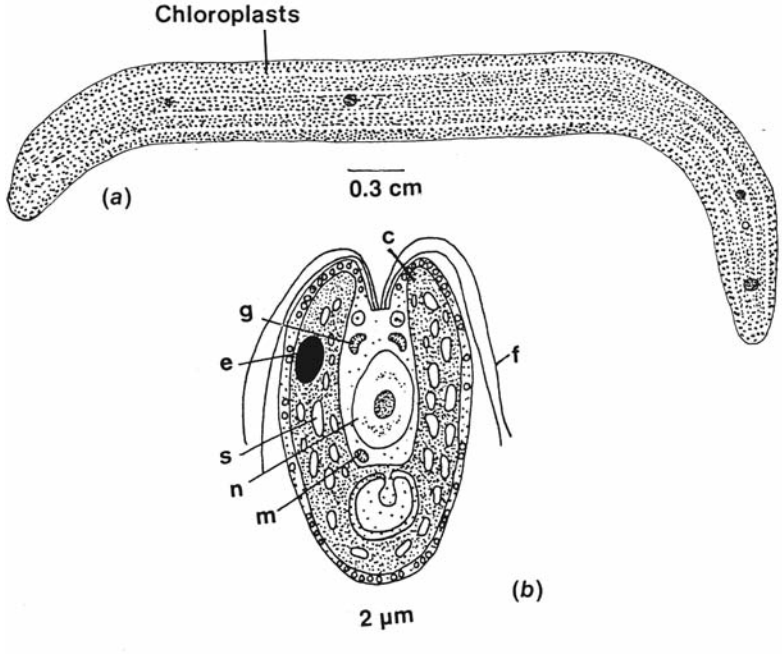


Fig. 5.14 (*a*) *Convoluta roscoffensis* flatworm with symbiotic green algae. (*b*) *Tetraselmis convolutae*, the algal symbiont of *Convoluta*. (c) Chloroplast; (e) eyespot; (f) flagella; (g) Golgi body; (m) mitochondrion; (n) nucleus; (s) starch. ((*a*) after Russell and Yonge, 1963; (*b*) after Parke and Manton, 1967.)

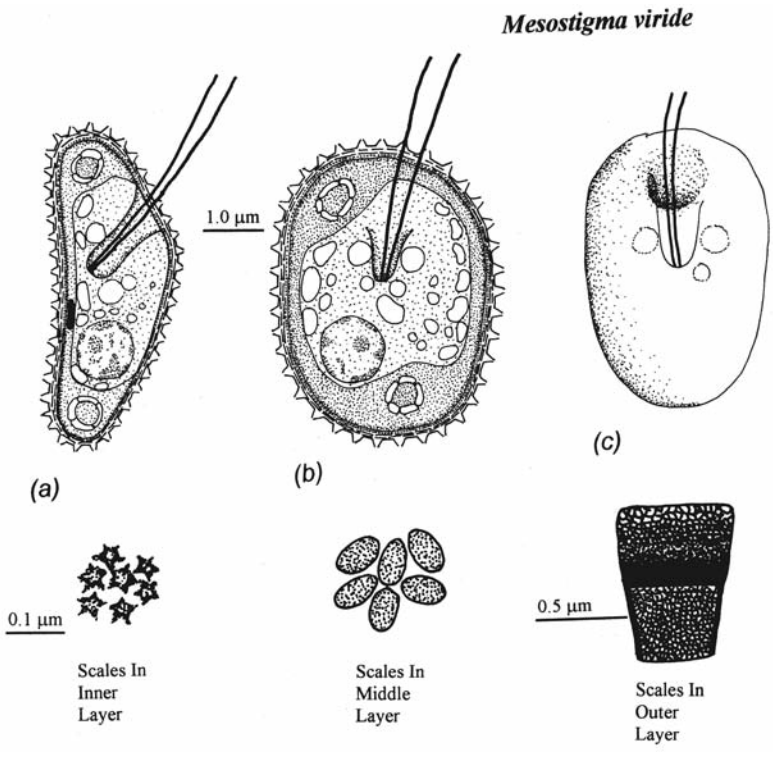


Fig. 5.15 *Mesostigma viride*. Cytology of the cell from the lateral (*a*) and medial (*b*) side. (*c*) Whole cell showing flagellar pit. Scales covering the body are also shown. The inner scales also cover the flagella. (Adapted from Manton and Ettl, 1965; Marin and Melkonian, 1999.)

animals. As the flatworm gets older, it relies on photosynthate from the internal algae, and its digestive organs degenerate so that it is not able to feed like a normal animal. The *Convoluta*, however, needs a more varied diet than just that of algal photosynthate and begins after a time to feed upon the algae – to kill the geese that laid the golden eggs – so that the algae gradually disappear, the flatworm presenting the strange appearance of a green head and a white tail. Finally the flatworm dies of starvation, but not before it has laid a large number of eggs.

Charophyceae

This is the line of algal evolution that led to the development of land plants. The motile cells of the advanced members of the class are similar to the flagellated male gametes of the bryophytes and vascular cryptogams. The *motile cells* of the Charophyceae are *asymmetrical and have two laterally or subapically inserted flagella. The microtubular root system contains a multilayered structure that is associated with a broad microtubular root and a second, smaller, microtubular root. Rhizoplasts are not present. The mitotic spindle is persistent during cytokinesis, and cell division occurs by means of a phragmoplast*. No eyespots occur. Sexual reproduction results in the formation of a dormant zygote. Meiosis occurs when the zygote germinates. Glycolate is broken down by glycolate oxidase, whereas urea is broken down by urease. The algae in the class are predominantly freshwater algae.

The unicellular alga *Mesostigma* is thought to be the closest extant relative to the "ancestral green flagellate" and represents the most primitive alga in the Charophyceae (Marin and Melkonian, 1999; Lemieux et al., 2000). *Mesostigma viride* (Fig. 5.15) is a freshwater biflagellate alga with flagella arising from a depression in the cell (Manton and Ettl, 1965). Each flagella is anchored by two microtubular roots, with one root having an associated multilayered structure (Melkonian, 1989). The single chloroplast contains pyrenoids, an eyespot, and unique pigments (Yoshii et al., 2003). The cell is covered by three layers of scales. An inner layer of five-sided scales, a middle layer of oval-shaped scales, and an outer layer of basket-shaped scales.

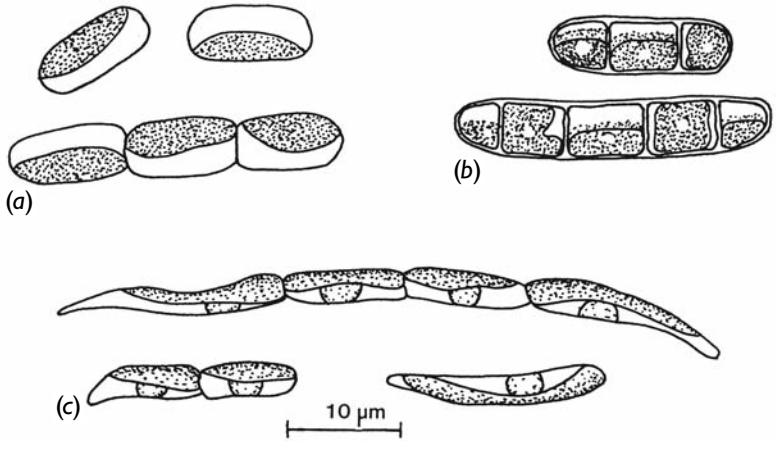


Fig. 5.16 (*a*) *Stichococcus bacillaris*. (*b*) *Klebsormidium sp.* (*c*) *Raphidonema nivale*. ((*c*) after Hoham, 1973.)

Classification

Within the Charophyceae are four important orders:

Order 1 **Klebsormidiales**: unbranched filaments without holdfasts; plasmodesmata absent; zoospores naked and released through a pore in the wall.

Order 2 **Zygnematales**: sexual reproduction by conjugation; unicells or unbranched filaments without holdfasts; plasmodesmata absent in filamentous forms; flagellated cells not produced.

Order 3 **Coleochaetales**: oogamous sexual reproduction; motile cells have a covering of scales, sheathed setae present; unicells, branched filaments or discoid thalli.

Order 4 **Charales**: oogamous sexual reproduction; sterile cells surround antheridia and oogonia; male gametes covered with scales; zoospores not produced; complex plant body with apical growth and differentiation into nodes and internodes; plasmodesmata present.

Klebsormidiales

The algae in this order are terrestrial or freshwater algae with unbranched filaments that do not have holdfasts. Each cell contains a single parietal chloroplast. There are no plasmodesmata between cells. The zoospores are naked and are released through a pore in the wall. Algae definitely placed in this order on the basis of their cytology include *Klebsormidium* (Fig. 5.16(*b*)) (Pickett-Heaps, 1974), *Stichococcus* (Fig. 5.16(*a*)) (Floyd et al., 1972), and *Raphidonema* (Fig. 5.16(*c*)) (Pickett-Heaps, 1976).

Sexual reproduction is isogamous by biflagellate gametes. Reproduction and morphology of the algae in this order are similar to those in species of *Ulothrix*, with which some of the members of the Klebsormidiales were originally classified before their ultrastructural differences became apparent.

Zygnematales

The Zygnematales are a closely related group (McCourt et al., 2000; Gontcharov et al., 2002) of freshwater algae that are unique among the Chlorophyta in having sexual reproduction by isogamous conjugation in which the gametes are non-flagellated. The union of the two gametes can be through a conjugation tube formed by the parent cells, or the gametes can move from their parent cells into the medium and fuse. The zygote or zygospore forms a cell wall and goes through a resting period before germinating meiotically. The life cycle is therefore primarily haploid, with the zygote representing the diploid generation. Zygnematalean algae, particularly *Mougeotia* (Fig. 5.17(*e*)), dominate freshwaters affected by acid precipitation (Graham et al., 1996).

There are basically three types of chloroplasts in the order: (1) spirally twisted bands extending

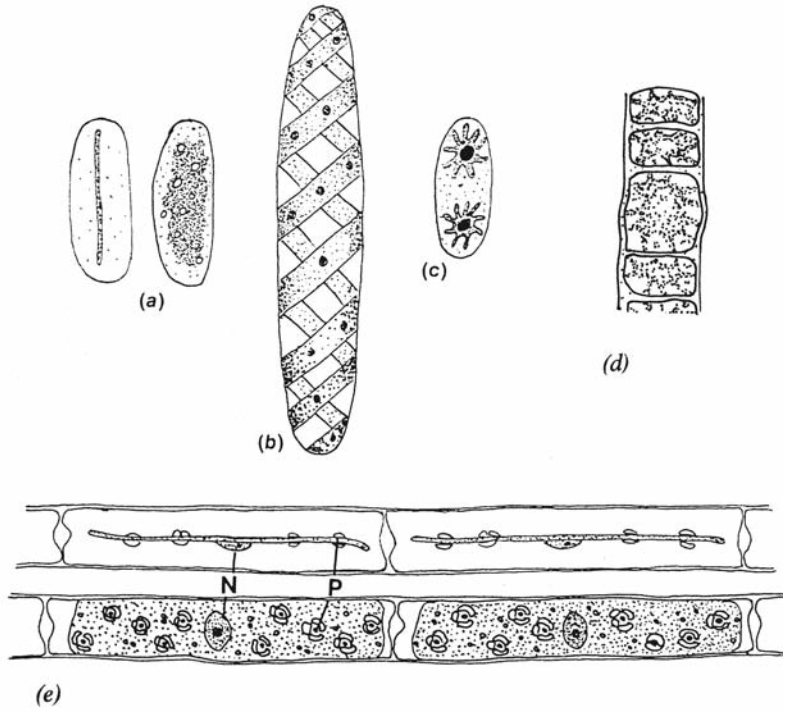


Fig. 5.17 (*a*) *Mesotaenium de greyi*, high- and low-intensity orientations of the chloroplast. (*b*) *Spirotaenia condensata.* (c) *Cylindrocystis brebissonii.* (*d*) *Zygogonium* sp. (e) *Mougeotia scalaris*, above-profile and below-surface views of the chloroplast. (N) Nucleus; (P) pyrenoid.

the length of the cell as in *Spirogyra* (Fig. 5.18) and *Spirotaenia* (Fig. 5.17(*b*)); (2) an axial plate extending the length of the cell as in *Mougeotia* (Fig. 5.17(*e*)) and *Mesotaenium* (Fig. 5.17(*a*)); and (3) two stellate chloroplasts next to each other as in *Cylindrocystis* (Fig. 5.17(c)). In those cells with flat axial chloroplasts, there is a marked chloroplast orientation in response to light intensity. In *Mesotaenium* and *Mougeotia* (Fig. 5.17), the chloroplast presents a surface view to the light under low intensities. When irradiated with high-intensity light, or red light at low intensity, the chloroplast rotates to present an edge view. Actin microfilaments attached to the chloroplasts are directly responsible for movement of the chloroplast (Mineyuki et al., 1995) with a phytochrome system directing actin functioning.

Within the Zygnematales there are three families (some phycologists group the last two families into one family).

Family 1 Zygnemataceae: cylindrical cells united permanently into unbranched filaments; cell wall without pores.

Family 2 Mesotaeniaceae: basically non-filamentous; cell walls without pores; no new semicell formed in cell division.

Family 3 Desmidaceae: basically non-filamentous; cell walls with pores; new semicell formed in cell division.

Zygnemataceae

The cells of the Zygnemataceae are permanently united into unbranched filaments, and the cell walls lack pores. Union of the two aplanogametes is usually by the establishment of a conjugation tube between two cells.

Members of the Zygnemataceae are among the most common filamentous freshwater algae, favoring small stagnant bodies of water, but with a few found attached in the littoral zone of lakes (*Spirogyra adnata*) and in flowing water (Berry and Lembi, 2000). They are especially abundant in the spring months, generally occurring as bright green free-floating masses, with some type of attaching organ present in young stages of several genera. Planktonic species of *Spirogyra* or *Mougeotia* often have twisted or spirally coiled threads. *Zygogonium* (Fig. 5.17(*d*)), which lives next to thermal springs with acidic waters, is responsible for the dense purple mats that occur in the

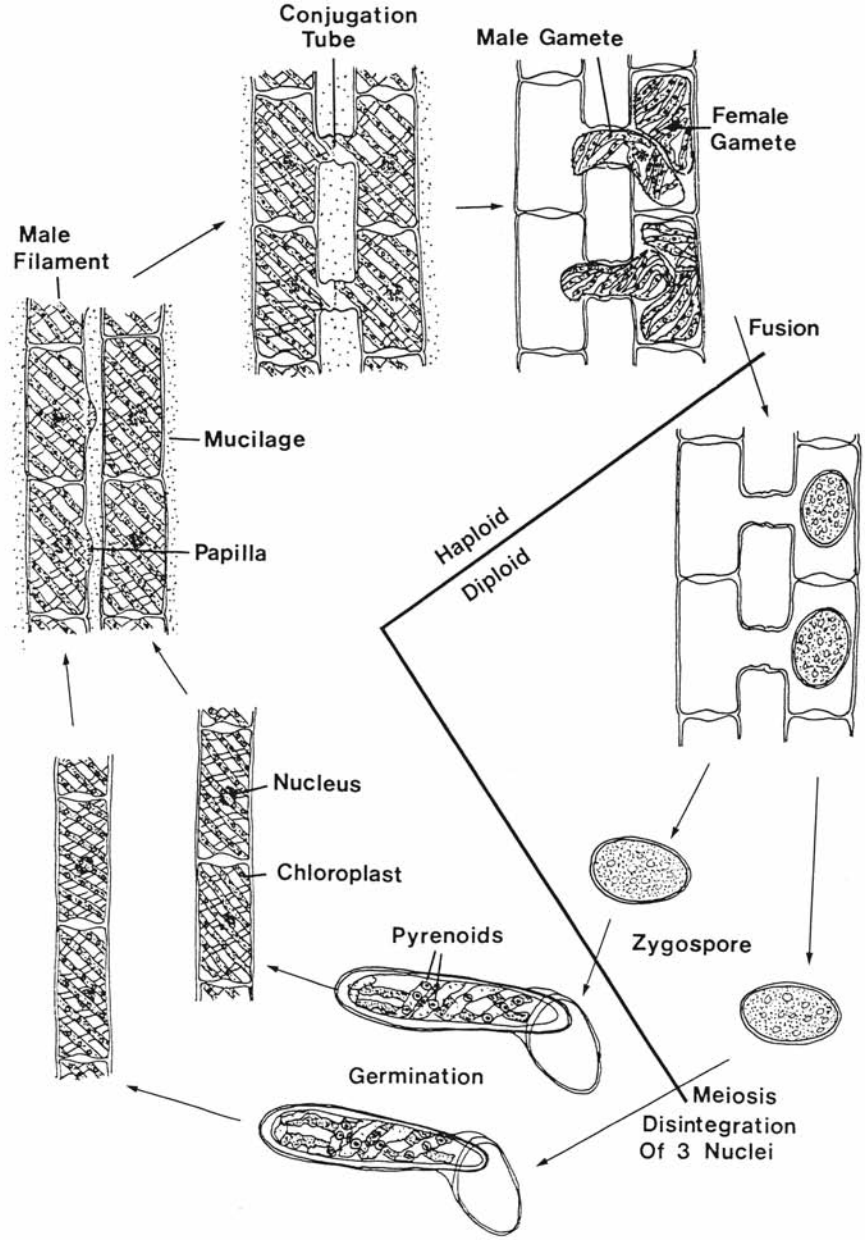


Fig. 5.18 The life cycle of *Spirogyra*.

hot springs of the Yellowstone National Park, where it lives at temperatures of 21 to 30 °C and a pH of 2.4 to 3.1; the optimum temperature for photosynthesis is 25 °C, and the pH optimum is 1 to 5 (Lynn and Brock, 1969).

Spirogyra occurs primarily in the springtime because it tolerates high light intensities in cool water (Graham et al., 1995). *Spirogyra* has ribbon-shaped chloroplasts with a number of pyrenoids along the length of the chloroplast (Fig. 5.18). A nucleus is suspended in the center of the cell. Every cell in the filament except the basal one is capable of cell division. Asexual reproduction occurs by fragmentation of the filaments, whereas sexual reproduction is by conjugation, which is initiated by two filaments coming to lie

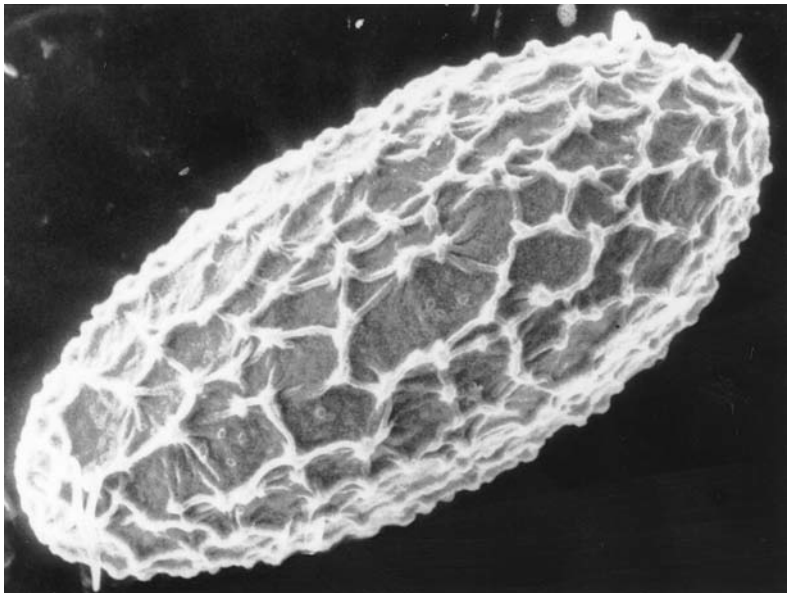


Fig. 5.19 Scanning electron micrograph of a zygote of *Spirogyra acanthopora* showing the sculpturing of the wall. (From Simons et al., 1982.)

next to one another, and being bound together in a layer of mucilage. The cells of one filament put out papillae toward the cells of the opposite filament. Subsequently, papillae arise from opposite and corresponding points on the other filament so that the two papillae are in contact from the beginning of their formation. The two threads are then pushed apart as the papillae elongate. A hole is dissolved at the tips of the papillae so that the conjugation tube is continuous from one cell to the next. The male gamete (the protoplast that moves through the conjugation tube) contracts by the bursting of small contractile vacuoles within the cell membrane, which is followed by a similar contraction of the female gamete as the male gamete moves through the conjugation tube. The male protoplast fuses with the female inside the parent wall of the female. The zygote (zygospore) secretes a three-layered wall around itself. The three layers of the wall from the outside to the inside are the **exospore**, **mesospore**, and **endospore**. The **exospore** is sometimes sculptured (Fig. 5.19) and contains cellulose and/or pectin. The **mesospore** is sometimes colored and contains sporopollenin. The **endospore** is thin and colorless, and contains cellulose and pectin (Simons et al., 1982). Ripening of the zygote is accompanied by the disappearance of chlorophyll and the conversion of the starch into a yellowish oil. During the resting period of the zygote (in nature until the following spring), the nucleus divides meiotically to form four haploid nuclei, three of which disintegrate. The zygote germinates by sending out a tubular growth that ruptures the outer two wall layers while the inner wall extends to accommodate the growth. The outgrowth then undergoes transverse divisions to form the first cells of the filament. The life cycle is thus primarily haploid, with the zygote being the only diploid cell. Conjugation is referred to as "physiologically anisogamous" because of the different behavior of morphologically similar gametes.

The above type of conjugation, which is called **scalariform** conjugation, occurs between two separate filaments. Another type of conjugation is **lateral** conjugation, which occurs between cells of the same filament. Here a conjugation tube is formed between adjacent cells, or in some cases the cross wall between adjacent cells simply dissolves. The members of this family would seem to be excellent tools for the study of fertilization, but this is not so because of the difficulty of inducing sexual reproduction at will.

Spirogyra mats show an unusual phototactic movement toward blue light (optimal at 470 nm), but not red light (Figs. 5.20, 5.21) (Kim et al., 2005). Directing blue light from an angle toward

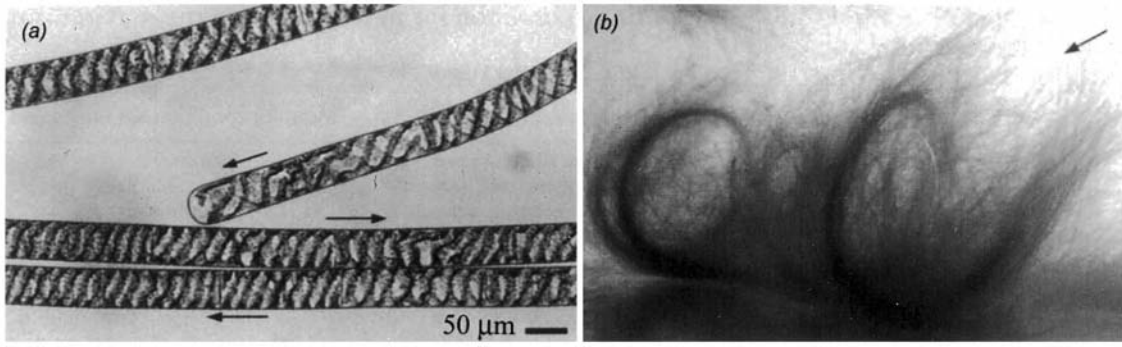


Fig. 5.20 Phototactic movement of *Spirogyra*. (*a*) Gliding movement between filaments. Arrows indicate the direction of filament movement. (*b*) Phototropic curvature of filaments toward light. Arrow shows the direction of light. (From Kim et al., 2005.)

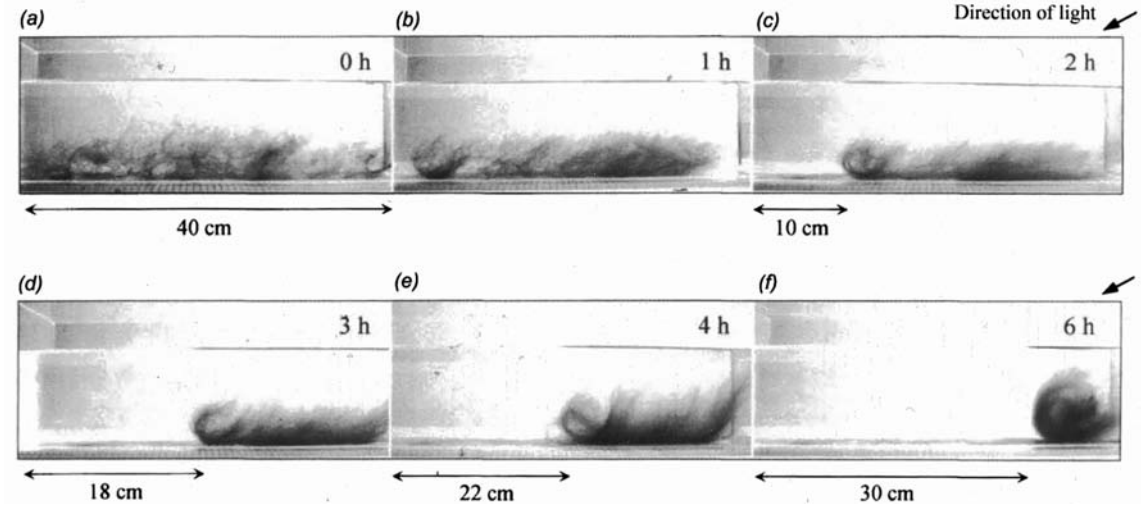


Fig. 5.21 Sequential photographs of *Spirogyra* movement toward the light source. Arrows on the right show the direction of light. (From Kim et al., 2005.)

scattered *Spirogyra* filaments cause the filaments to align toward the light within one hour. The filaments bind with other filaments to form thicker parallel bundles that curve and form an open-loop shape. The bundle of filaments move toward the light source at 10 μm s^{-1} by two different movements, the gliding movement between filaments and curvature of filaments. The bundles of filaments join and form a larger mat when they meet. The coordination of filaments is essential for the phototactic movement. The filaments always form a bundle before they start moving toward light. A single filament repeatedly curls, straightens, and bends, but there is no phototactic movement. Filaments will only glide on other filaments. The exact mechanism involved is not known, but it may be that filaments oriented toward blue light prolong movement and shorten their movement when they are not oriented toward the light.

Mesotaeniaceae

This family has organisms that are basically unicellular, even though in some cases they are joined together to form filaments, and the cells taper to their ends. The walls do not have pores.

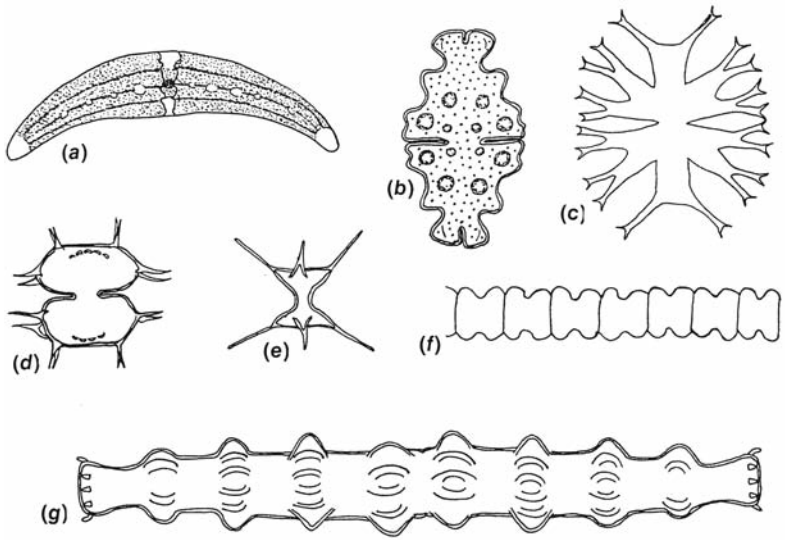


Fig. 5.22 (*a*) *Closterium moniliforme*. (*b*) *Euastrum affine*. (*c*) *Micrasterias radiata*. (*d*) *Xanthidium antilopaeum*. (e) *Staurastrum curvatum*. (*f*) *Spondylosium moniliforme*. (*g*) *Pleurotaenium nodosum*. (After Smith, 1950.)

The Mesotaeniaceae are called the saccoderm desmids; unlike the placoderm desmids of the following family, they do not have a new semicell formed after cell division. The nucleus is central in the cell, and there are three types of chloroplast structure, which are similar to those in the Zygnemataceae. *Mesotaenium* (Fig. 5.17(*a*)), *Cylindrocystis* (Fig. 5.17(*c*)), and *Spirotaenia* (Fig. 5.17(*b*)) are in the family. Sexual reproduction takes place by conjugation and is similar to that in the other two families of the order.

These organisms are indicative of water low in magnesium and calcium and therefore usually unpolluted water. They are common in upland pools and peat bogs; *Mesotaenium* and *Cylindrocystis* are found in wet soil.

Desmidaceae

These are the placoderm desmids. They have two distinct halves or semicells separated by a median constriction, the **sinus**, and joined by a connection zone, the **isthmus**. The cell walls have pores in them (Gerrath, 1969). The cells can be solitary, joined end to end in filamentous colonies. or united in amorphous colonies. Some of these plants have a relatively complex and attractive shape (Fig. 5.22). The taxonomy of many of these desmids is complicated by **polymorphism** (different forms within the same species), which often makes organisms of the same species appear as different species (Sormus and Bicudo, 1974).

Cosmarium botrytis has a central nucleus and two chloroplasts in each semicell, each with a central pyrenoid (Fig. 5.23). At the tip of each semicell are crystals of barium carbonate that move irregularly (Brook, 1989). Mixing cells of opposite strains (mt^+ and mt^-) results in the cells moving about, with each strain indifferent to the other. During this period mt^- cells release a proteinaceous pheromone that causes mt^+ cells to form gametes; likewise mt^- cells are similarly induced to produce gametes by a pheromone (Fukumoto et al., 2003).

After pairing, the cells move around each other and twist about until their broadest faces are in contact, and their longitudinal axes are at right angles. A sphere of mucilage is secreted around the conjugants and also between them, forcing the cells apart. The protoplast escapes from the gametes by the separation of the wall in the region of the isthmus (Starr, 1954). Within 4 to 7 minutes after making contact, the protoplasts fuse, forming an irregularly shaped zygote. The zygote then rounds off and forms a smooth-walled cell. The chromatophores arrange themselves at the periphery of the cytoplasm, and the ornamentation of the wall begins to appear about 1 hour after the fusion of the gametes. Spines develop on the wall, with the tips commonly divided into two or three parts. The zygote germinates meiotically, completing the life cycle.

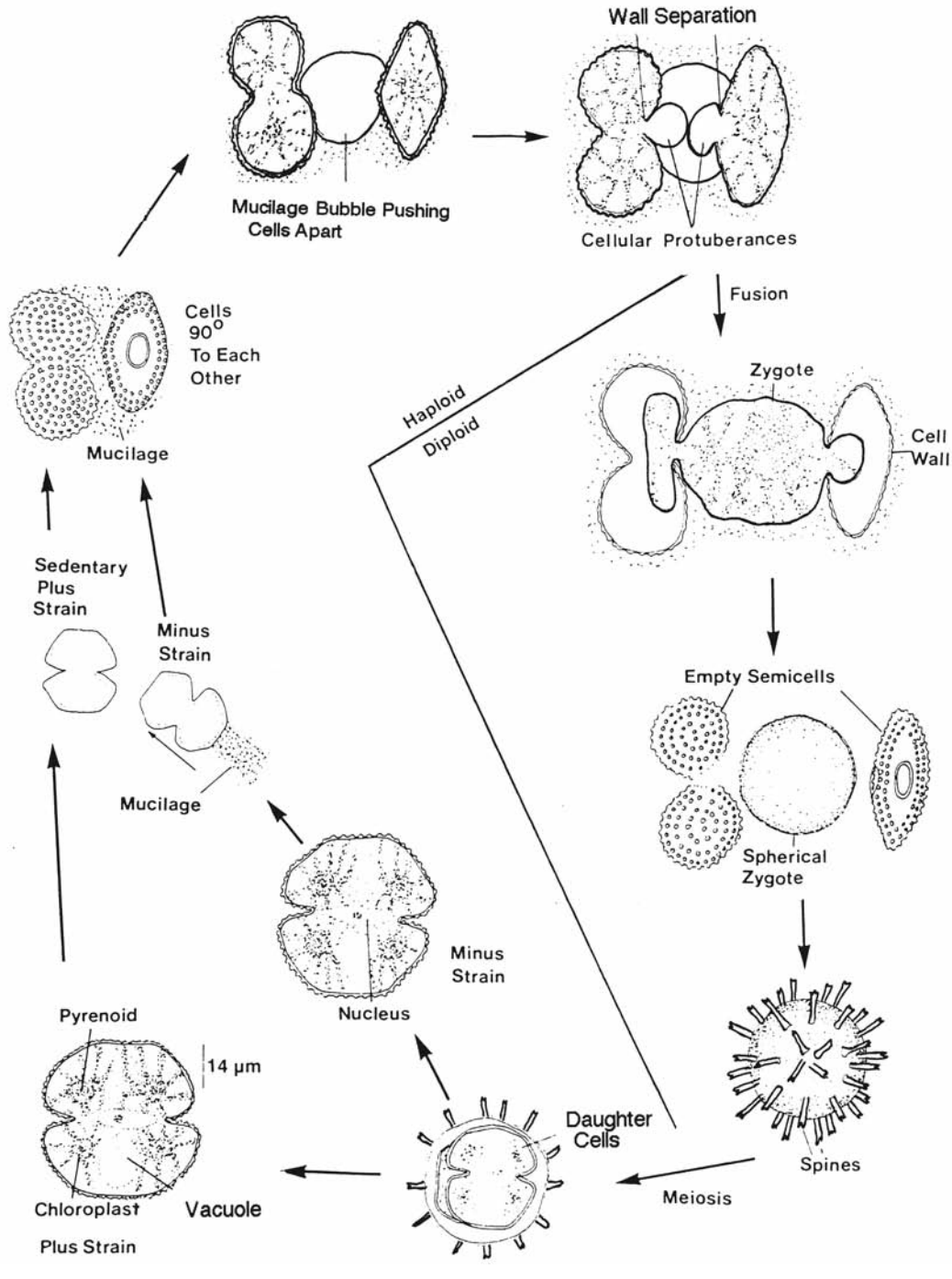


Fig. 5.23 The life cycle of *Cosmarium botrytis*.

The desmids are usually indicators of relatively unpolluted water, low in calcium and magnesium, with a slightly acidic pH. Normally a large number of species are present in such waters, without a single species comprising most of the population.

Coleochaetales

The algae in the Coleochaetales are characterized by the presence of sheathed setae and by oogamous sexual reproduction. Small-subunit ribosomal RNA sequencing (Wilcox et al., 1993; Kranz et al., 1995) has indicated that the green algae in this order evolved into the bryophytes and lycopods. Like the bryophytes and lycopods, the algae in the Coleochaetales have asymmetrical motile cells covered with scales, microtubular roots consisting of a large and small band (Sluiman, 1983), a persistent interzonal spindle, and a phragmoplast at cytokinesis; glycolate is degraded by glycolate oxidase (Tolbert, 1976). In addition some of the species in the Coleochaetales have evolved a protective sheath around the oogonium, which is an advance toward the protected oogonia in the Bryophyta.

Most of *Coleochaete* (Fig. 5.25) occur as epiphytes or endophytes in the shallow littoral zone of freshwater lakes (Ciminio and Delwiche, 2002) and may be observed by microscopic examination of macrophyte leaves or inorganic substrates such as beer cans, soda bottles, or plastic bags discarded by fishermen (Graham, 1984). The thallus is composed of branching filaments, which are free in some species, whereas in others the branches are laterally opposed to form a pseudoparenchymatous disc. All members of the genus have sheathed hairs called **setae** (*Coleochaete* comes from the Greek *koleos* sheath + *chaite* long hair). The base of the setae is covered with a gelatinous material. The setae probably function as an antiherbivore defense, since broken setae exude a substance that repels potential predators (Marchant, 1977).

Zoospores and spermatozoids of *Coleochaete* (Fig. 5.24) are asymmetrical, are covered with scales, and possess multilayered structures and microtubular roots similar to those of lower land plants (Graham and McBride, 1979; Sluiman, 1983). The flagella arise subapically and project to the side of the cell (Fig. 5.24). The flagella are anchored by a microtubular root system composed of a single broad band of microtubules associated with a multilayer structure and a second microtubular root.

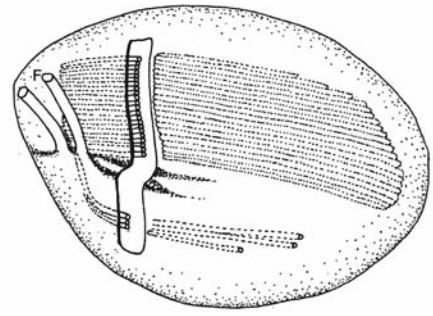


Fig. 5.24 Drawing showing the subapical flagella (F) in a zoospore of *Coleochaete*. The flagella are anchored in the cytoplasm by two microtubular roots. A broad microtubular root is associated with a multilayered structure. There is a small microtubular root composed of three microtubules. (After Sluiman, 1983.)

Asexual reproduction is by biflagellate zoospores which are formed singly in a cell, most frequently in the spring. Initiation of zoosporogenesis is induced primarily by temperature. Northern temperate species undergo zoosporogenesis when brought to 20 °C for a few days (Graham and Krantzfelder, 1986). Day length and irradiance have little effect on zoosporogenesis.

Sexual reproduction in *Coleochaete* is oogamous (Fig. 5.25) and the plants can be homothallic or heterothallic, depending on the species. Antheridia are borne at the tips of the branches, and each antheridium forms a single spermatozoid. Oogonia are modified one-celled branches, and an oogonium is a flask-shaped structure with a long colorless neck, the trichogyne. At maturity the tip of the neck breaks down, with some colorless protoplasm being extruded and the basal protoplast rounding off to form a single egg. The spermatozoid swims into the oogonium and fertilizes the egg. The zygote remains in the oogonium, secretes a thick wall, and greatly increases in size. At the same time there is an upgrowth of branches from the cell below the oogonium and from neighboring cells to form a pseudoparenchymatous layer enclosing the oogonium. The oogonium, with its enclosing sheath layer of cells, becomes reddish and is termed a **spermocarp**; the spermocarps remain dormant over the winter.

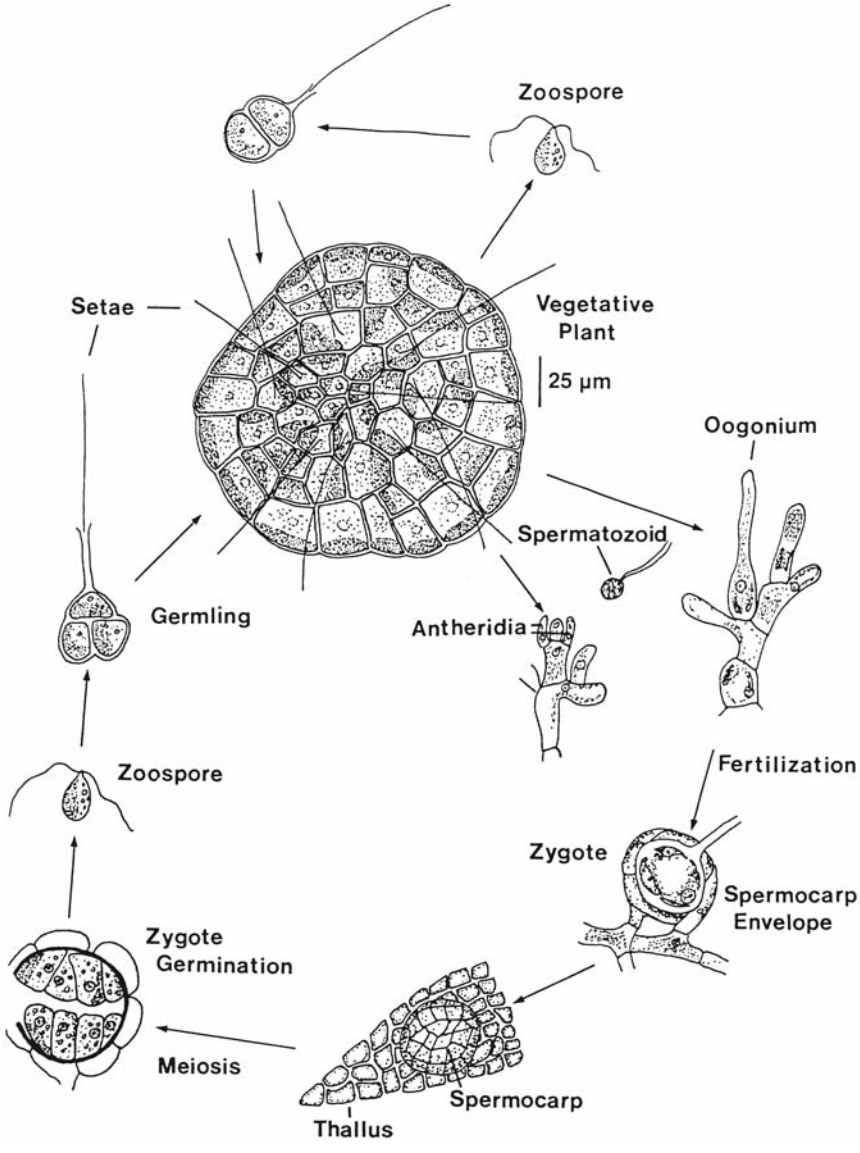


Fig. 5.25 The life cycle of *Coleochaete scutata*. (After Oltmanns, 1898; Smith, 1950.)

The zygote germinates meiotically to form 8 to 32 biflagellate zoospores, which are liberated through a break in the spermocarp and zygote walls, and swim for a short time before settling and developing new thalli.

Charales

The green algae in the Charales have a complex plant body with apical growth and differentiation of the body into **nodes** and **internodes**. Reproduction is oogamous, with sterile cells surrounding the antheridia and oogonia. The male gametes have a cell covering of scales. No zoospores are formed. A phragmoplast develops during cell division, resulting in the formation of a cross wall with plasmodesmata. Land plants (embryophytes) probably evolved from algae similar to those in the Charales (Karol et al., 2001). As such, the Charales are sometimes separated from the rest of the green algae and grouped with embryophytes as **streptophytes** (Lewis and McCourt, 2004).

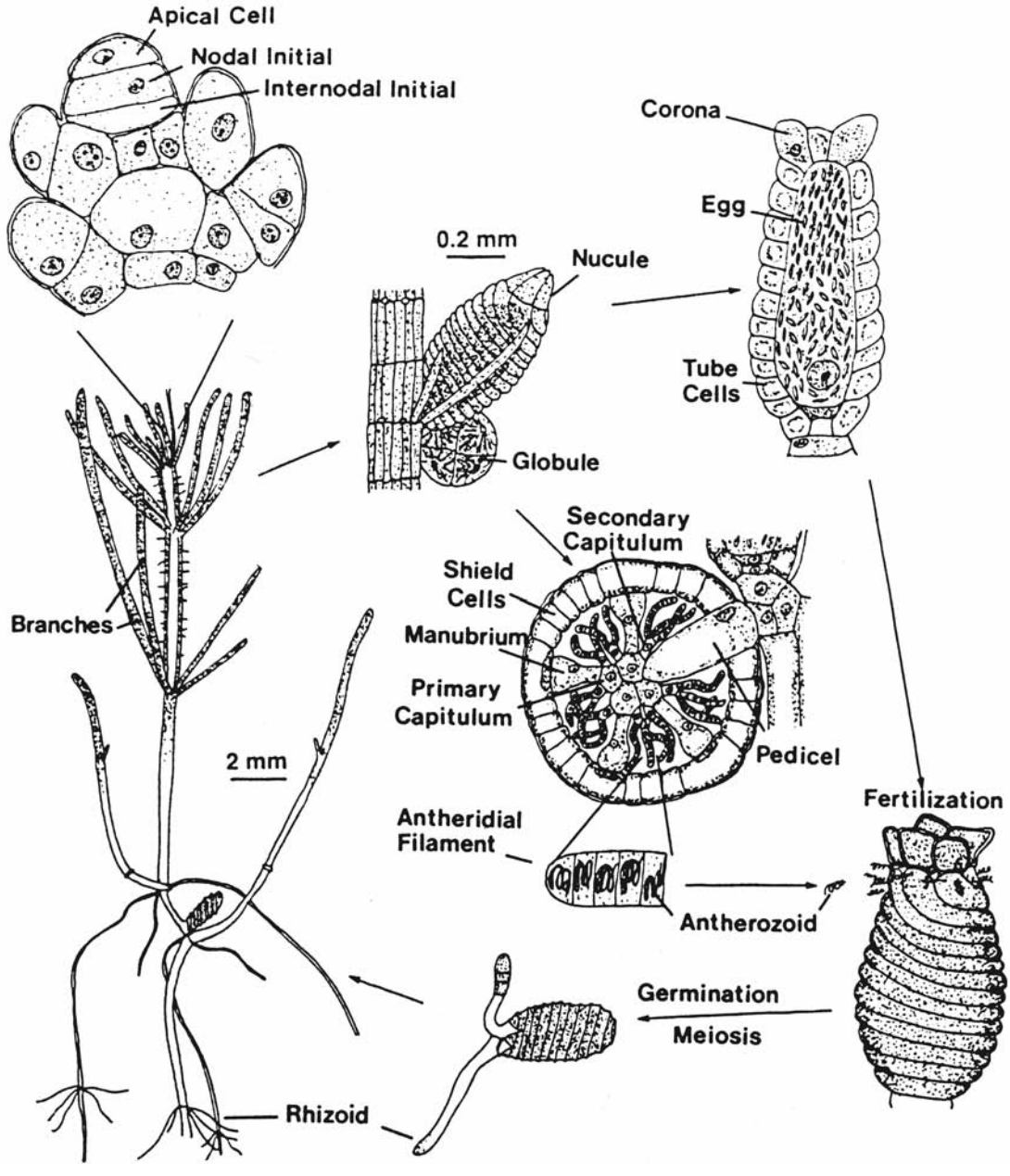


Fig. 5.26 The life cycle of *Chara* sp. (Adapted from Smith, 1955; Scagel et al., 1965.)

The algae in the Charales are primarily freshwater, with only a few species occurring in brackish water. They are most common at the bottom of clear lakes, usually forming extensive growths. Many of the Charales are heavily calcified, with concentrations of plants on the bottom of lakes leading to the formation of **marl** ($CaCO_3$ and $MgCO_3$ deposits) and hence the common name of the Charales, **stoneworts**. Calcification in *Chara* and *Nitella* results from the precipitation of calcium carbonate ($CaCO_3$) in water high in Ca^{2+}. The localized OH^- efflux at certain areas of the internodal cell raises the local CO_3^{2-} ion concentration, leading to $CaCO_3$ supersaturation and precipitation (Lucas, 1979). In *Chara corallina*,

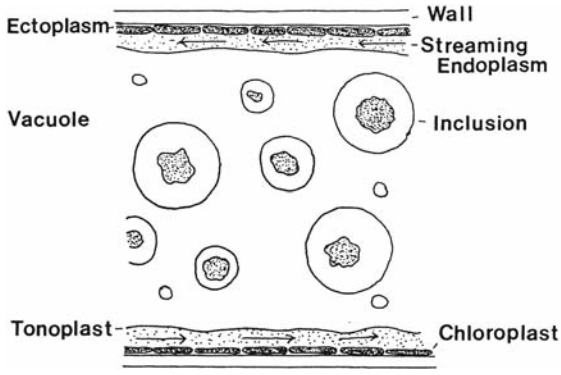


Fig. 5.27 Schematic view of part of an internodal cell of *Nitella*. The chloroplasts are stationary in the ectoderm, whereas the endoderm moves by cytoplasmic streaming. (After Kamitsubo, 1980.)

rectangular crystals of calcite are deposited in bands on the surface of the cell wall of the cylindrical internodal cell. These bands correspond to localized alkaline (pH 9.5 to 10.5) regions on the cells. There is no organic material associated with the crystals, and they are formed entirely outside the cell wall (Borowitza, 1982; Wray, 1977).

The algae in the Charales have an axis divided into nodes and internodes (Fig. 5.26). Each **node** bears a whorl of branches composed of a number of cells that cease to grow after they have reached a certain length. The **internode** consists of a single long cell in *Nitella*. In some genera, such as *Chara*, the internodal cell is ensheathed (corticated) by a layer of vertically elongated cells of a much smaller diameter originating at the nodes (Fig. 5.26). Growth occurs by a dome-shaped apical cell, each derivative of the apical cell dividing transversely into two daughter cells. The upper daughter cell is the nodal initial, and the lower is the internodal initial. The **nodal initial** matures into the cells of the node, and the **internodal initial** matures into the single long cell of the internode (Smith, 1955). The axis is attached to the substratum by uniseriately branched rhizoids. The rhizoids are positively geotropic and grow downward. Near the rhizoid tip are a group of **statoliths** consisting of vacuoles containing crystallites of barium sulfate that may be associated with the response of the rhizoids to gravity (Braun and Richter, 1999).

The uninucleate cells have many small ellipsoidal chloroplasts in longitudinal, spirally twisted, parallel rows. In the center of the cells is a single large vacuole. The large size of the internodal cell and its vacuole has made the cell a favorite tool of physiologists interested in the control of ion uptake in plants. The pH of the cell sap of *Chara* is controlled at about 5 as a result of a dynamic equilibrium between active influx and passive efflux of H^+ across the tonoplast. The H^+ transport system involves two proton (H^+) translocating systems in the tonoplast (Shimmen and MacRobbie, 1987). **Cytoplasmic streaming** is particularly evident in these large internodal cells. The cytoplasm is divided into an inner **endoplasm** next to the vacuole, and an outer **ectoplasm** containing the chloroplasts (Fig. 5.27). Streaming endoplasm follows the orientation of the spirally arranged stationary chloroplasts in the ectoplasm at a rate of 60 $\mu m\ s^{-1}$ at 20 °C. Streaming is due to the interaction of actin microfilaments with cytoplasmic microtubules (Collings et al., 1996).

The Charophyta do not form zoospores, but there are specialized sexual bodies. Asexual reproduction may be effected by (1) star-shaped aggregates of cells developed from the lower nodes, called **amylum stars** because they are filled with starch; (2) **bulbils** developed on rhizoids; and (3) protonema-like outgrowths from a node.

The sexual organs are the **globule** (male) and **nucule** (female) (Fig. 5.28), the terms antheridium and oogonium not being appropriate because the sexual reproductive structures include both a sex organ and a multicellular sheath derived from cells beneath the sex organ (Smith, 1955). Globules and nucules are borne on nodes, usually on the same plant. In *Chara*, the nucule is above the globule.

The globule develops from haploid nodal cells that occur at lateral branches (Kwiatkowska, 2003). Following the first mitotic division of the initial cell, the lower cell develops into a basal cell and does not divide further, while the upper one transforms into the mother cell of the globule (Fig. 5.28). The initial cell of the globule divides three times, longitudinally and transversely, to produce eight cells with their apices joined in the center of the sphere. Successive mitotic divisions produce three cells within each octant yielding a sphere composed of 24 cells. Outer cells become

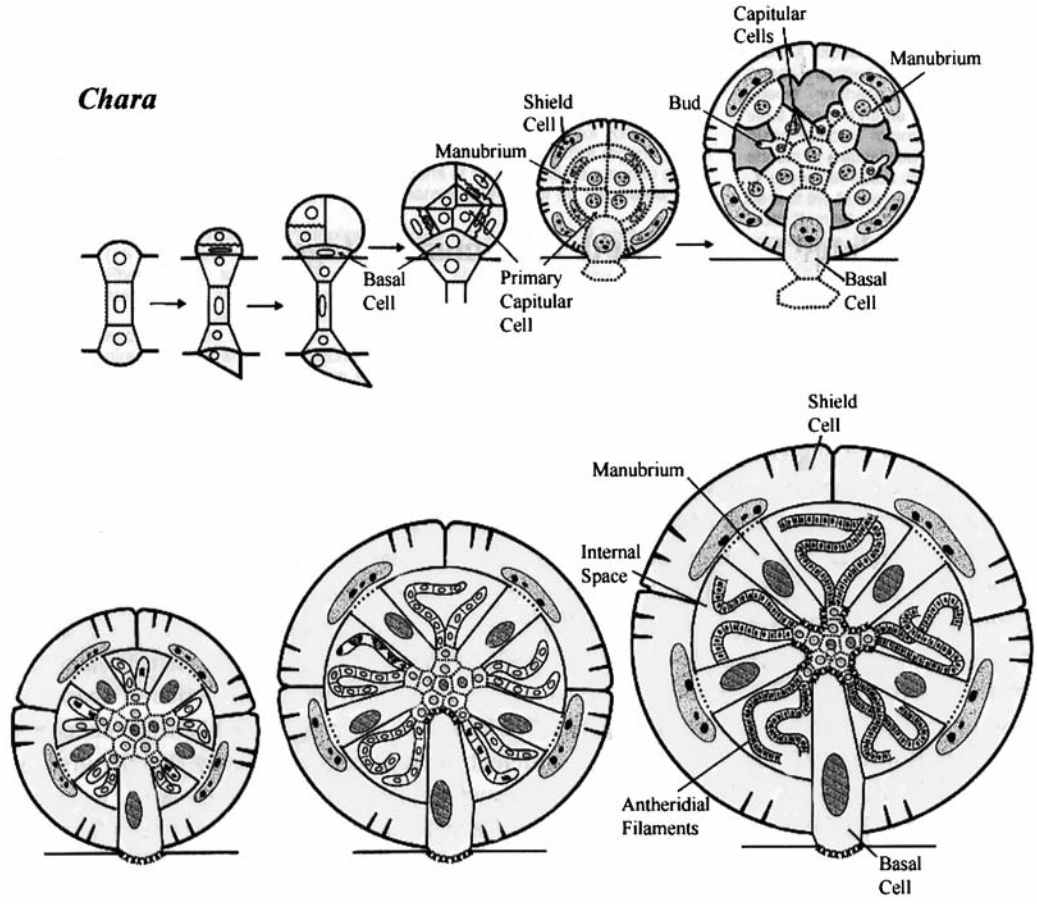


Fig. 5.28 The development of a globule of *Chara*. (From Kwiatkowska, 2003.)

transformed into shield cells that form the colorful cover of the globule due to chromoplasts near the inner wall of the cells. The color changes from pale yellow to orange as the globules mature. The median cells develop into manubria and eight inner cells are transformed into primary capitular cells which give rise to the antheridial filaments. Each cell of an antheridial filament is an antheridium whose protoplast matures into a single antherozoid. The antherozoid is coiled in a compact helix of two and a half turns in the antheridium (Fig. 5.29). When the antherozoids are mature, the shield cells of the globule separate from one another and expose the antheridial filaments. Soon after the antheridial filaments are exposed, and antherozoids emerge backward through a pore in the cell wall.

Liberation of antherozoids generally takes place in the morning, and their swarming may continue until evening (Smith, 1955). The sperm have two somewhat unequal flagella attached subterminally near the anterior end of the cell (Fig. 5.29). There are three different regions within the body of the sperm: (1) the head region, consisting of a microtubular sheath over the mitochondria taking up one-fourth of the body; (2) the middle region, with microtubules covering the nucleus and taking up half of the body; and (3) the tail region, where the microtubules ensheath the plastids. Scales formed by the Golgi are on the outside of the flagella.

The nucule is supported by a pedicel cell, and in the center is the oogonium with its single egg. Five spirally twisted tube cells cover the oogonium except at the tip, where there are five corona cells. When the nucule is mature, the spirally twisted tube cells separate from one another just below

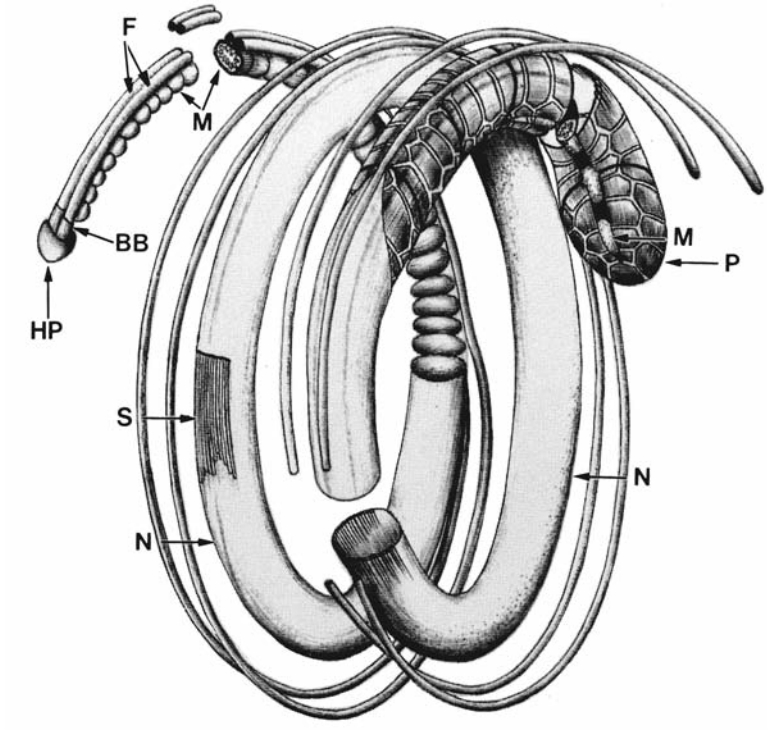


Fig. 5.29 Reconstruction of the mature spermatozoid of *Chara vulgaris*. (BB) Basal bodies; (F) flagella; (HP) head piece; (M) mitochondrion; (N) nucleus; (P) plastid; (S) spline of microtubules. (From Duncan et al., 1997.)

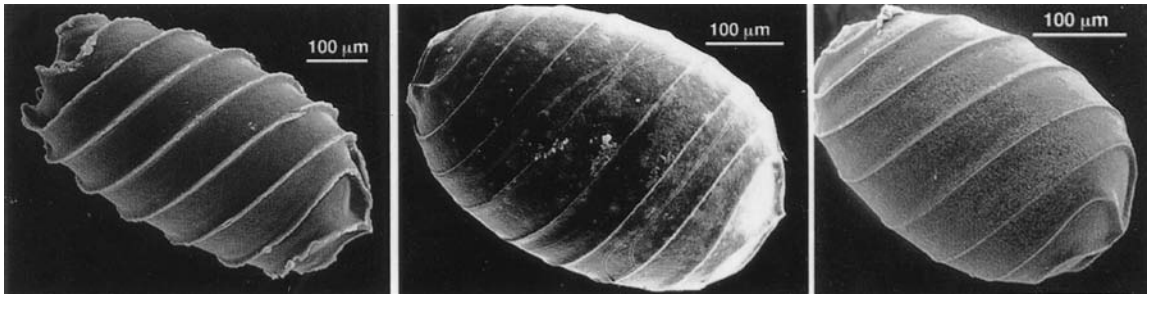


Fig. 5.30 Scanning electron micrographs of zygotes of *Chara muelleri* (*left*) and *Chara fibrosa* (*middle*, *right*). (From Casanova, 1997.)

the corona. Antherozoids swim through these openings to the oogonium, where they penetrate its gelatinized wall. The zygote secretes a thick wall, and the inner wall of the tube cells becomes thickened (Fig. 5.30). Other portions of the walls of the sheath decay, leaving the persisting portions of walls of the tube cells projecting like the threads of a screw. The zygote, with the surrounding remains of the sheath, falls to the bottom of the pool and there germinates after a period of weeks or months (Smith, 1955).

The zygote can be carried considerable distances attached to water fowl (Proctor, 1962). The zygote will not germinate in darkness and needs white or red light (Takatori and Imahori, 1971). Meiosis occurs in the first division of the zygote; thus the thallus is haploid, and the zygote is the only diploid part of the life history.

Because calcification occurs in most genera, the group is well represented as fossils, especially by the female fructification, which when calcified is termed a **gyrogonite**. The earliest fossils of Charales occur in the Uppermost Silurian. All of the extant Charales are placed in the Characeae, which date back to the Upper Carboniferous and which have the enveloping cells of the female

fructification in a left-hand spiral. An extinct family, the Trochiliscaceae, also had a spirally twisted envelope, but it was twisted to the right.

Ulvophyceae

The motile cells of the Ulvophyceae have *apically attached flagella, near-radial symmetry externally, and a cruciate microtubular-root system that is not associated with a multilayered structure*. These characteristics differ from those of the Charophyceae but are similar to those of the Chlorophyceae. The Ulvophyceae, however, differ from the Chlorophyceae in having (1) *a persistent interzonal spindle that does not collapse at telophase, and* (2) *motile cells without a cell wall*.

The algae in the Ulvophyceae are predominantly marine although there are a number of freshwater species. All filamentous marine green algae or larger green seaweeds studied ultrastructurally have been shown to belong to the Ulvophyceae. The life cycle usually involves the alternation of a haploid thallus with a diploid thallus. The wide occurrence of alternation of generations in the Ulvophyceae might be due to the more stable marine environment fostering the evolution of a longer life cycle. Dormant zygotes are not known in the class. A number of genera in the Ulvophyceae produce swarmers with scales (Mattox and Stewart, 1973), indicating that the class had a scaly ancestor.

Classification

The following orders are placed in the Ulvophyceae. Cladistic analysis of nuclear-encoded rRNA sequence data have shown that the Ulotrichales and Ulvales form one group in the class, while the Caulerpales, Siphonocladales, and Dasycladales form a second group (Watanabe et al., 2001).

Order 1 **Ulotrichales**: uninculeate filamentous algae with a parietal chloroplast.
Order 2 **Ulvales**: uninucleate cells with a parietal chloroplast; thallus is a hollow cylinder or a sheet, one or two cells thick.
Order 3 **Cladophorales**: multinucleate filamentous algae with a parietal perforate or reticulate chloroplast.
Order 4 **Dasycladales**: thallus has radial symmetry composed of an erect axis bearing branches; thallus uninucleate but multinucleate just before reproduction; gametes formed in operculate cysts.
Order 5 **Caulerpales**: coenocytic algae lacking cellulose in the walls; siphonoxanthin and siphonein usually present.
Order 6 **Siphonocladales**: algae with segregative cell division; siphonoxanthin present.

Ulotrichales

Uninucleate filamentous green algae with a parietal chloroplast constitute this order.

Ulothrix (Fig. 5.31) is found in quiet or running freshwater and occasionally on wet rocks or soil. The thallus consists of unbranched filaments of indefinite length that are adfixed to the substratum by a special basal cell. All of the cells except the basal one are capable of cell division and forming zoospores or gametes. Species with narrow cells form 1, 2, or 4 quadriflagellate zoospores per cell, whereas those with broad cells form 2, 4, 8, 16, or 32 zoospores per cell. The zoospores have a conspicuous eyespot and are liberated through a pore in the side of the parent wall. Zoospores from species with narrow filaments are the same size, whereas those from broad-celled species form macro- and microzoospores that differ from each other in size, position of the eyespot, and length of the swarming period. Zoospores that are not discharged from the parent may secrete a wall and become thin-walled aplanospores. These later germinate to form a new filament.

Gametes of *Ulothrix* are formed in the same way as zoospores but are biflagellate. The gametes are of the same size, with fusion occurring only between gametes from different filaments; and there is never any parthenogenetic development of unfused gametes. The zygote remains for a while, settles, secretes a thick wall, and undergoes a resting period during which it accumulates a large amount of storage material. The first division of the zygote is meiotic, with the zygote

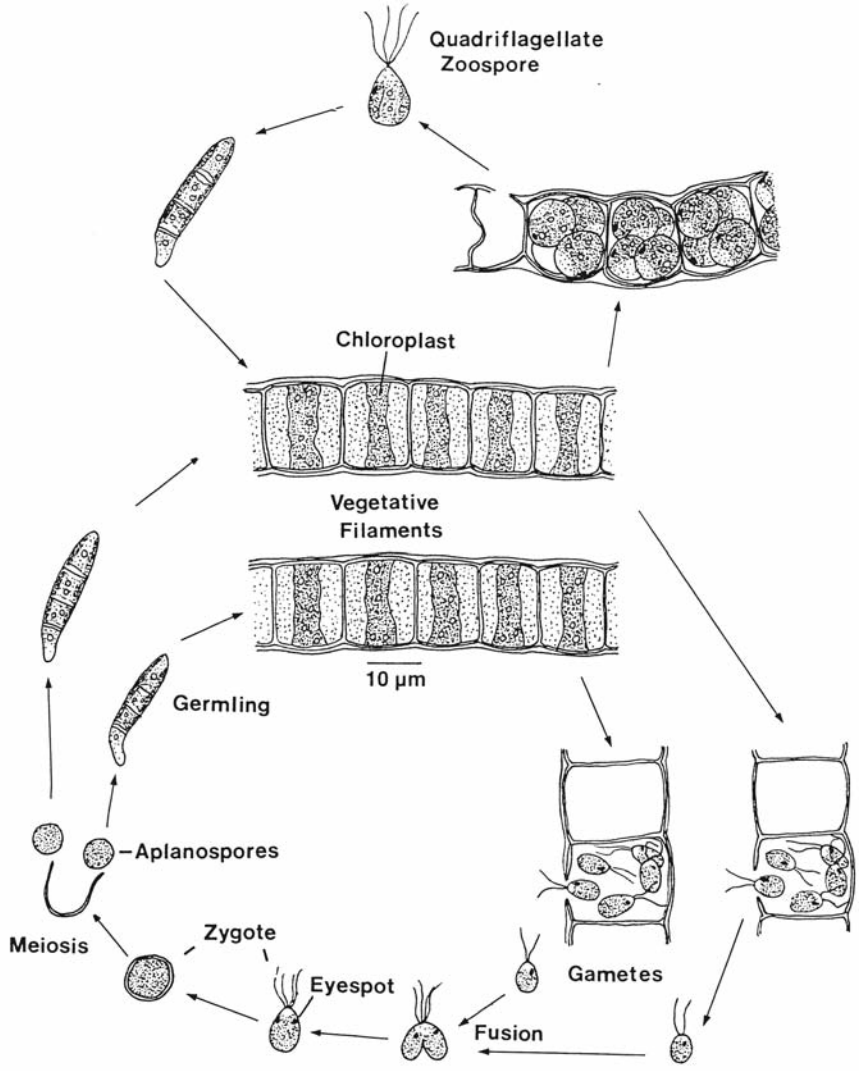


Fig. 5.31 The life cycle of *Ulothrix zonata*. (Adapted from Smith, 1955.)

forming 4 to 16 zoospores or aplanospores (Berger-Perrot et al., 1993).

In many northern lakes in the United States and Canada, *Ulothrix zonata* grows abundantly in early spring in shallow waters along rocky shorelines. *Ulothrix zonata* is dominant until the water temperature reaches 10 °C, when it disappears owing to massive conversion of the thallus to zoospores. At this time, *Cladophora glomerata* becomes the dominant attached alga. In culture, formation of the quadriflagellate zoospores of *Ulothrix zonata* occurs around 20 °C at relatively high light levels (520 μE m^{-2} s^{-1}) and photoperiods of either short-day (8 hours light:16 hours dark) or long-day cycles (16 hours light:8 hours dark). Zoospore formation is minimal at 5 °C, low irradiance (32.5 μE m^{-2} s^{-1}), and neutral day length (12 hours light:12 hours dark) (Graham and Krantzfelder, 1986).

Ulvales

In nature, these plants have a thallus that is either an expanded sheet one (*Monostroma*) or two cells (*Ulva*; Fig. 5.33) thick. *Ulva* can also occur as a hollow cylinder. The genus *Enteromorpha* was previously erected for those *Ulva* in a hollow cylinder. These thalli composed of hollow cylinders are

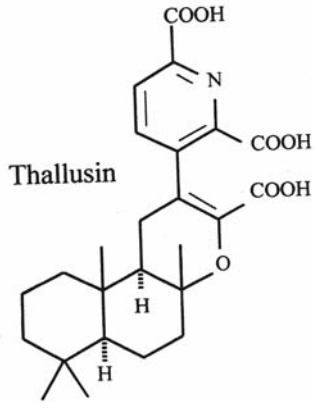


Fig. 5.32 The structure of thallusin, a morphogenetic inducer in *Ulva*. Thallusin is produced by bacteria living on the surface of *Ulva*.

now recognized as species of *Ulva* (Hayden et al., 2003).

The normal morphology of these algae is lost if the plants are grown without bacteria. Under these conditions, *Ulva* develops into a pincushion-like colony, whereas *Monostroma* grows as a group of round cells with rhizoids (Provasoli and Pinter, 1980). Bacteria of the Cytophaga-Flavobacterium-Bacteroides group grow on the surface of the algae and produce a morphogenetic factor called **thallusin** (Fig. 5.32) (Matsuo et al., 2005). The alga absorbs thallusin, resulting in the familiar morphology of the thallus.

Ulva fronds are composed of two layers of cells, with each cell having a large cup-shaped chloroplast toward the exterior of the cell (Fig. 5.33). The holdfast is formed by the cells of the thallus, sending down long slender filaments that coalesce to form the holdfast. The holdfast portion is perennial and proliferates new blades each spring. Cell division may occur anywhere in the thallus, but all divisions are in a plane perpendicular to the thallus surface.

The vegetative state of *Ulva mutabilis* is maintained by the blade cells excreting regulatory factors into the cell walls and into the environment. The production of one of these regulatory factors, a glycoprotein, decreases as the thallus matures. Eventually, the level of this regulatory factor decreases to the point where the regulatory factor is too low to maintain the vegetative state, and gametogenesis begins (Stratmann et al., 1996).

Ulva (Fig. 5.33) has an isomorphic alternation of generations, with the gametophyte forming biflagellate gametes and the sporophyte producing quadriflagellate zoospores. There is a periodic fruiting pattern in the genus, which is controlled by the lunar cycle. Gametes are released a few days before zoospores, with fruiting occurring during a series of neap tides (tide of minimum range occurring at the first and third quarters of the moon) in *U. pertusa* in Japan (Sawada, 1972) and during a series of spring tides (tide of maximum range during the new and full moon) in *U. lobata* on the Pacific Coast of North America (Smith, 1947). *Ulva* (*Enteromorpha*) *intestinalis* also shows a similar fortnightly periodicity at the beginning of a series of spring tides in England, except that here both gametes and zoospores are released at the same time (Fig. 5.34) (Christie and Evans, 1962). Although it is possible to correlate fruiting in the genus with tidal patterns, it is not the tidal movements that induce fruiting and release of swarmers because the plants will exhibit a regular periodicity even when submerged. It is probably the amount of moonlight that the plants receive that gives the initial impetus to fruiting, although this may be timed by the tide as is the case with *Dictyota*.

Reproductive areas form near the margins of *Ulva* fronds (Fig. 5.33), with the fertile portions changing from green to olive-green to brownish green due to the accumulation of γ-carotene (Hiraoka et al., 1998). Gametogenesis and sporogenesis (Melkonian, 1980a,b) are similar and marked by a sharp reduction in photosynthetic capacity (Gulliksen et al., 1982). A cell divides to form 8 to 32 motile cells, with meiosis occurring in the formation of zoospores but not in the formation of gametes. Prior to the development of the motile cells, the mother cell forms a beak-like outgrowth extending to the thallus surface, through which the swarmers escape. The swarmers are released when the thallus is wet by the water of the incoming tide. The positively phototactic biflagellate gametes have a parietal chloroplast with a pyrenoid and eyespot. Haploid fronds are unisexual, so gametes from the same frond will not fuse. Gametes can be the same size, or one can be

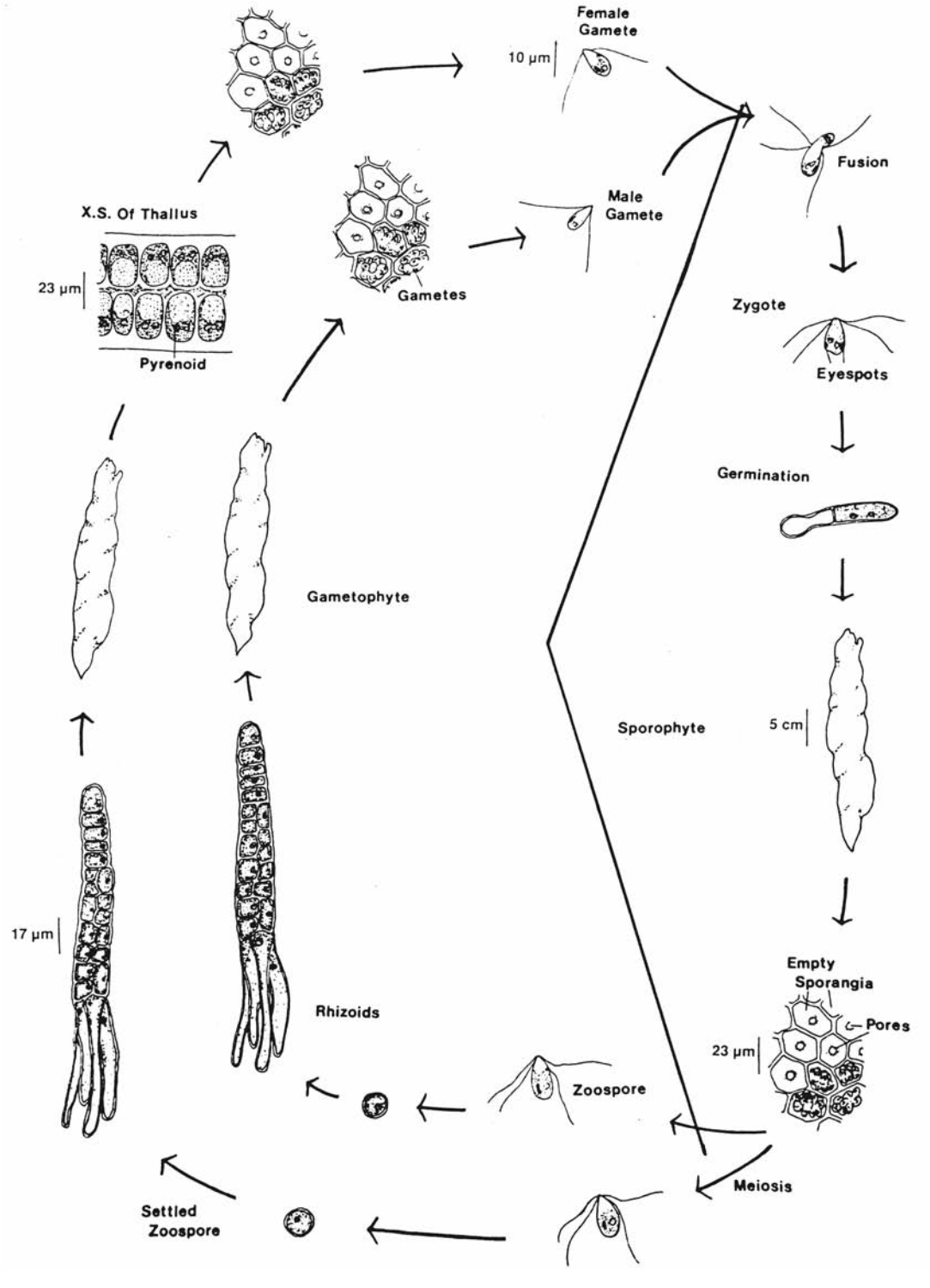


Fig. 5.33 The life cycle of *Ulva arasaki*. (Adapted from Chihara, 1969.)

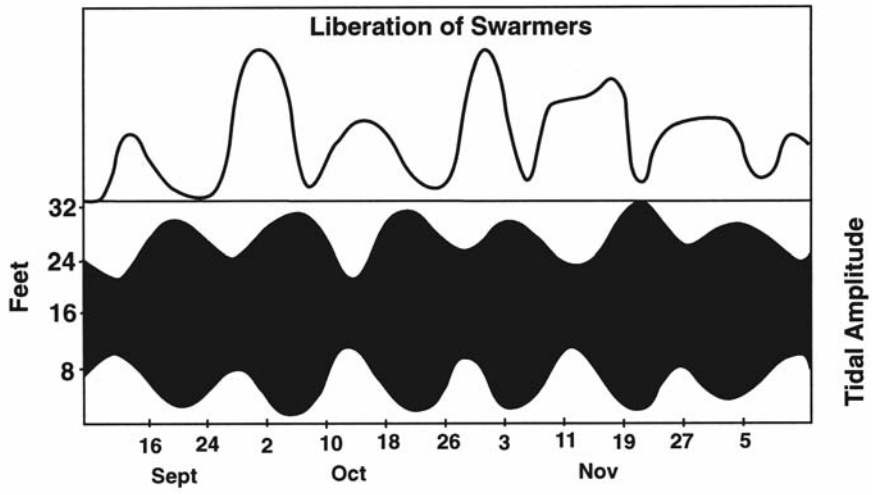


Fig. 5.34 Relationship between liberation of swarmers (gametes and zoospores) by *Ulva* (*Enteromorpha*) *intestinalis* and tidal amplitude. Maximum liberation of swarmers occurs 3 to 5 days before the highest tide of each lunar period. (After Christie and Evans, 1962.)

slightly larger than the other. The mixing of gametes of different strains results in the formation of cell clusters, joined by the tips of their flagella (Miyamura et al., 2003; Miyamura, 2004). Clusters separate almost immediately into mating pairs held together by their flagella (Bråten, 1971). The anterior ends of the gametes fuse within a few seconds, and the flagella separate, with the cells becoming negatively phototactic and swimming away from the light source. Within 3 minutes the cells jackknife and fuse laterally, with the quadriflagellate zygote remaining motile for a couple of minutes. The zygote settles, attaches to the substrate by its anterior flagellated end, and absorbs the flagella into the protoplasm. The zygote secretes a wall as soon as it settles, and nuclear fusion has occurred 30 minutes after the onset of copulation. The chloroplast from the plus gamete disintegrates (Bråten, 1973). In many ways the above process is similar to that in *Chlamydomonas* except that it occurs much more quickly.

Within a few days the zygote germinates, with mitotic division of the nucleus. After the first cell division one cell develops into a rhizoid, whereas the other eventually forms the blade. In some species it is possible to get a parthenogenetic development of gametes into a new plant.

Zoospores of *Ulva* are usually negatively phototactic, whereas gametes are positively phototactic. Upon fusion of gametes, phototaxis is reversed and the partially fused gamete pairs swim away from the light source (Miyamura et al., 2003). The total number of particles in the outer chloroplast envelope membrane over the large eyespot of *Ulva* zoospores is 11 300, whereas over the smaller eyespots of the female and male gametes there are only 5500 and 4900 particles, respectively. The lower number of particles in the gametes may be related to their positive phototaxis, especially because on fusion of the gametes, the total number of particles becomes 10 400, close to that of zoospores, with the fused gametes becoming negatively phototactic (Melkonian, 1980b).

Ulva is normally a marine genus although it can be found in brackish waters, particularly in estuaries. It normally grows on rocks in the middle to low intertidal zone, although the fronds are not situated at the same level throughout the year. During the colder months the plants grow mainly in the middle intertidal zone, covering wide vertical areas. In the warmer months the *Ulva* is lower in the intertidal zone and in a narrower band. Here the fronds are less exposed and subjected to less desiccation, which is more damaging to the plants in the high summer temperatures.

Ulva is an opportunistic alga, capable of rapid colonization and growth when conditions are favorable. This occurs primarily because of a rapid growth rate and the ability to take up and store nutrients available in pulsed supply. Because of

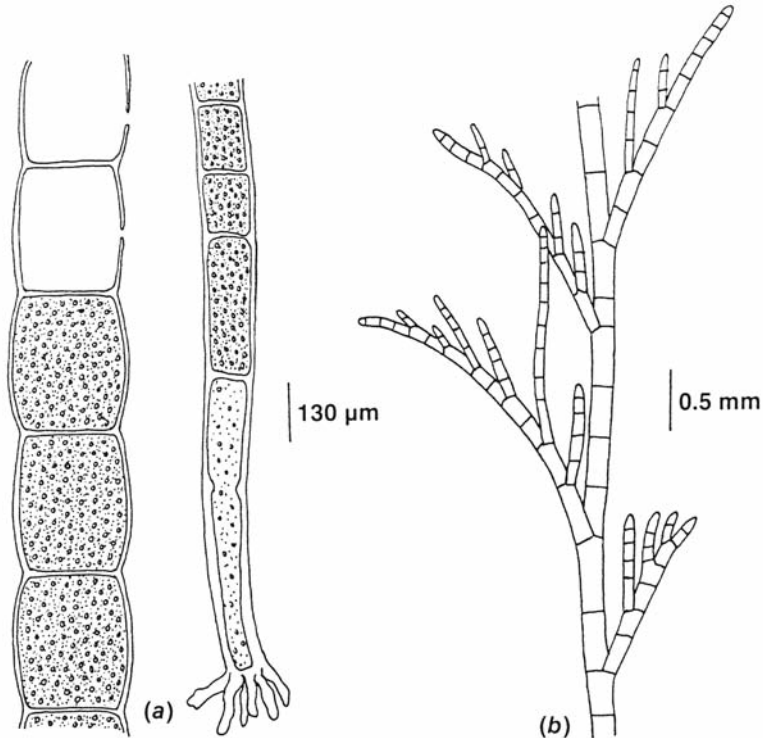


Fig. 5.35 (*a*) *Chaetomorpha aerea*. (*b*) *Cladophora microcladioides*. (After Smith, 1969.)

its ability to quickly respond to enhanced nutrient supply, *Ulva* has proliferated in many areas that have received anthropogenic (related to man) nutrient enrichment. A feature of nuisance growths of *Ulva* in enclosed and semienclosed waters is that *Ulva* comprises a large proportion of drift plants, which may smother other benthic communities or be cast ashore where they decompose, causing considerable aesthetic nuisance (Blomster et al., 2002; Nelson et al., 2003; Kim et al., 2004).

Ulva is commonly known as the sea lettuce or green laver, and has been eaten as a salad or used in soups (Chen, 1998). The chemical composition of dried *U. latuca* is 15% protein, 50% sugar and starch, less than 1% fat, and 11% water, making it usable as roughage in the human digestive system. In World War I, Phillipsen prepared a salad with *U. latuca*, and *Monostroma*, which he flavored with salad cream, vinegar, lemon, pepper, onions, and oil, and which he described as "wonderfully nice, slightly piquant and not inferior to the best garden salad" although one wonders after adding all of his condiments whether he was able to appreciate anything about seaweeds. The eminent French algologist Savaugeau prepared such a salad without condiments and said that "it was leathery and waxy in taste, and in spite of a good digestion I thought I would be ill" (Chapman, 1970).

Cladophorales

The filamentous genera in this order have multinucleate cells, usually with a parietal or reticulate chloroplast. The filaments may be branched or unbranched. The reticulate chloroplast has pyrenoids at the intersections of the reticulum.

Cladophora (Fig. 5.35(*b*)) and *Chaetomorpha* (Figs. 5.35(*a*), 5.36), each with an isomorphic alternation of generations, are common members of this order. *Cladophora*, found in freshwater and marine habitats, may be the most ubiquitous macroalga in freshwaters worldwide (Dodds and Gudder, 1992). This filamentous alga can reach nuisance levels as a result of cultural eutrophication. *Cladophora* is predominantly benthic, and is often found in the region of unidirectional flow or in periodic wave action. In freshwater, it is a mid- to late-succession

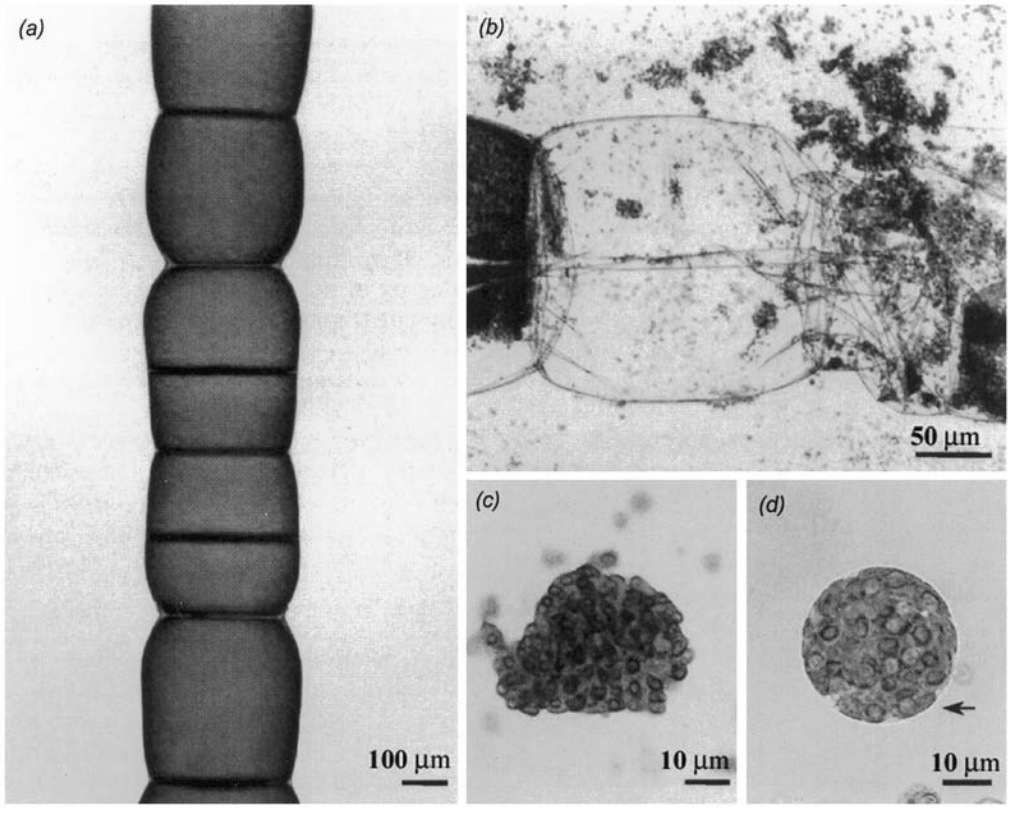


Fig. 5.36 *Chaetomorpha aerea* showing the process by which a new filament is produced from cell contents after disruption of the filament. (*a*) Vegetative filament. (*b*) Protoplasm is expelled from damaged cells and spreads in seawater. (*c*) Extruded cell organelles aggregate in seawater. (*d*) Regenerated protoplast forms an envelope within 10 minutes after wounding. (From Klotchkova et al., 2003.)

species. *Cladophora* is colonized by a wide variety of epiphytes because it offers a substrate that is anchored against flow disturbance.

Dasycladales

The plants in this order are all tropical and subtropical marine plants, most of them calcified. The members of the order are a clearly defined group having the following characteristics: (1) radial symmetry with an erect axis bearing branches; (2) uninucleate vegetative thallus, with a multinucleate condition developing just before reproduction; (3) gametes formed in operculate cysts within specialized gametangia.

The coenocytic algae in the Dasycladales and Caulerpales respond to injury by rapidly forming gel-like wound plugs, thereby preventing loss of cytoplasm. The wound plugs are formed from extruded cytoplasm that forms the plug through interaction of carbohydrates and lectins (Ross et al., 2005). A new cell wall is formed under the gelatinous plug.

The Dasycladales has a paleontological record that extends back to the Precambrian–Cambrian boundary (*ca*. 570 million years ago) (Berger and Kaever, 1992). Of the 175 known fossil genera, only 11 are extant. The Dasycladales are in fact "living fossils." As defined by Stanley (1979), **living fossils** are *organisms that include extant clades that have survived for long intervals of geological time at low numerical diversity and exhibit primitive morphological characteristics that have undergone little evolutionary change*.

There are two families within the order, the first of which is extinct:

Family 1 Receptaculitaceae: laterals produced spirally on erect axis; relatively large plants; all extinct.
Family 2 Dasycladaceae: laterals produced in whorls on erect axis; relatively small plants; extinct and extant.

Receptaculitaceae

The plants in this order existed from the Lower Ordovician to the Permo-Carboniferous Period. They were non-septate marine dasycladaceous algae shaped like a light bulb, with the upper portion consisting of a large number of spiral laterals attached to the main axis. They were calcified, with calcification being heavier around the periphery of the thallus. *Ischadites abbottae* was a Silurian alga that grew in shallow reef water. The thallus was globose, formed by spirally attached laterals with the largest laterals in the mid latitudes (Fig. 5.37). The upper laterals gradually became wider toward the periphery of the plant, then suddenly expanded into heads at the periphery. The main axis and laterals were calcified (Nitecki, 1971).

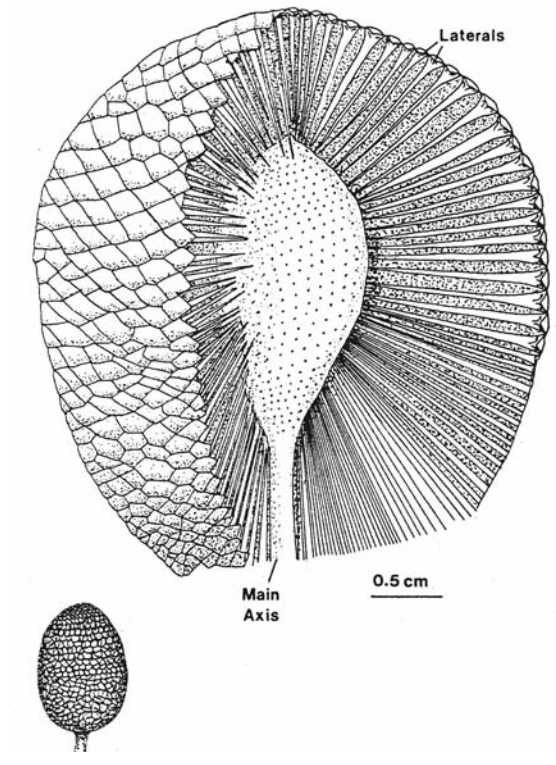


Fig. 5.37 Reconstruction of *Ischadites*, whole plant and cutaway drawing of the upper portion showing main axis, laterals, and lateral scars. (After Nitecki, 1971.)

Dasycladaceae

This family is characterized by a thallus having laterals arranged in whorls on the main axis. There are a number of different algae in the family (Zechman, 2003), with *Acetabularia* (Figs. 5.38, 5.40, 5.41) being the best known (Mandoli, 1998). At maturity *Acetabularia* has a naked axis with a single gametangial disc at the apex. In contrast, the axes of *Dasycladus* (Fig. 5.39(*a*)) and *Neomeris* (Fig. 5.39(*b*)) are enclosed in whorls of laterals that form a fairly solid cortication.

The first fossils of this family appeared about the Middle Silurian, and some of the extant genera are well represented in the fossil record, *Neomeris* going back to the Cretaceous and *Acetabularia* to the Tertiary (Johnson, 1961).

The life cycle of *Acetabularia* (Fig. 5.41) is similar to other plants in the order. *Acetabularia* (mermaid's wineglass) is a warm-water alga found in shallow protected lagoons and on the borders of mangrove swamps, growing on shells, coral fragments, and other algae. The thallus is calcified (Kingsley et al., 2003), with less calcification occurring in warm stagnant water. The young single-celled *Acetabularia* plant has two growing apices, one giving rise to the rhizoidal system that attaches the plants to the substrate, with the other growing apex becoming the erect thallus. As the apex of the axis grows, whorls of sterile hairs are produced just beneath the apex. Each of these whorls is eventually shed, leaving whorls of scars to mark their former attachment positions. During the vegetative growth of the thallus, the nucleus remains in one of the rhizoids.

A mature thallus forms a number of gametangial rays at the apex of the thallus, which can be joined or free from each other, depending on the species. Near the base of each gametangial ray, at the tip of the thallus, is a coronal knob, which commonly bears sterile hairs. The coronal knobs together comprise the corona superior. Some species also have a corona inferior beneath the gametangial rays. Once the gametangial rays have reached full size, the primary nucleus in one of

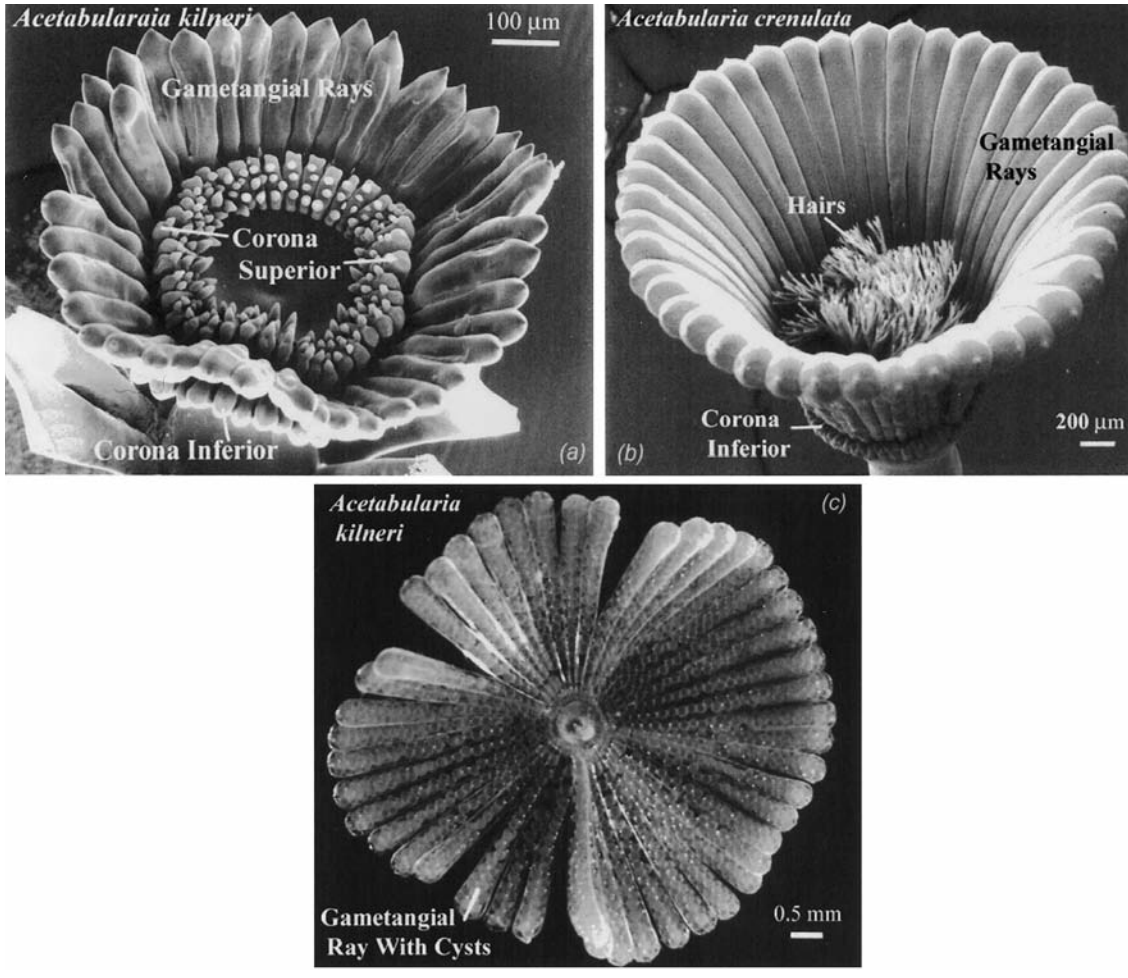


Fig. 5.38 Structure of the thallus of *Acetabularia*. (*a*) and (*b*) are scanning electron micrographs; (*c*) is a light micrograph. (From Berger et al., 2003.)

the rhizoids enlarges to about 20 times its original diameter. This nucleus divides by meiosis (Koop, 1975a) into a large number of small secondary nuclei (Woodcock and Miller, 1973a,b), which are carried by cytoplasmic streaming along microtubules into the gametangial rays (Menzel, 1986). In the rays, each nucleus is held in place, a certain distance from other nuclei, by microtubules (Woodcock, 1971). The cytoplasm contracts around each nucleus, and a wall is formed, producing a resistant resting cyst. The cysts enlarge to many times their original size, a process that is accompanied by a number of nuclear divisions. The gametangial rays fall off, with a plug sealing the supporting part of the thallus (Menzel, 1980). The cysts of *Acetabularia mediterranea* are usually formed in the summer, are strongly calcified, and do not germinate until the following spring, requiring a resting period of 12 to 15 weeks (Koop, 1975b). At germination of the cyst (Cooper and Mandoli, 1999), the protoplasm divides into a thousand or more pyriform biflagellate isogametes. The gametes are released through a lid in the cell wall. Gametes produced by different cysts are morphologically similar, with gametes from a single cyst probably of the same sex. Parthenogenetic development of gametes has been noted. The zygote can germinate soon after fusing of gametes. In *Acetabularia calyculus*, gametes are of two sizes. After fusion to form a zygote, the chloroplasts of the smaller, male gametes are preferentially destroyed,

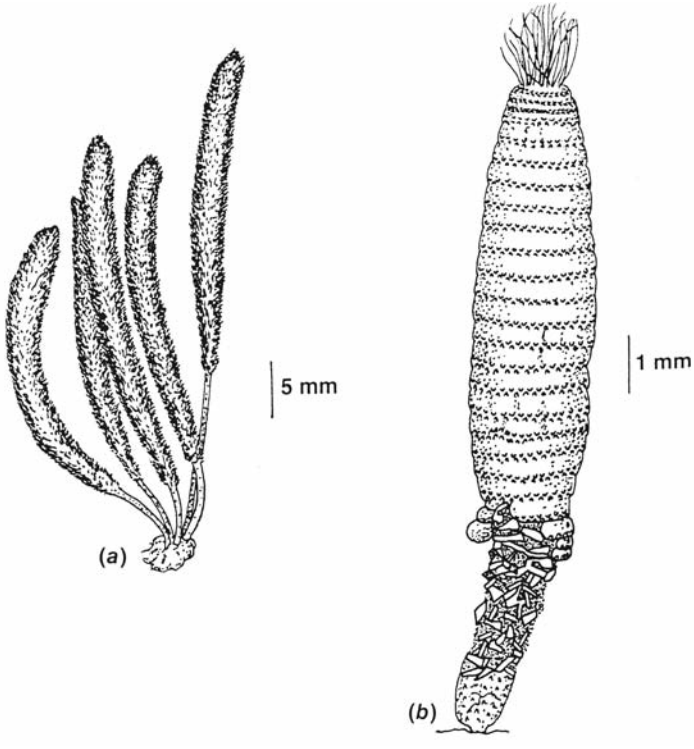


Fig. 5.39 (*a*) *Dasycladus vermicularis*. (*b*) *Neomeris annulata*. (After Taylor, 1960.)

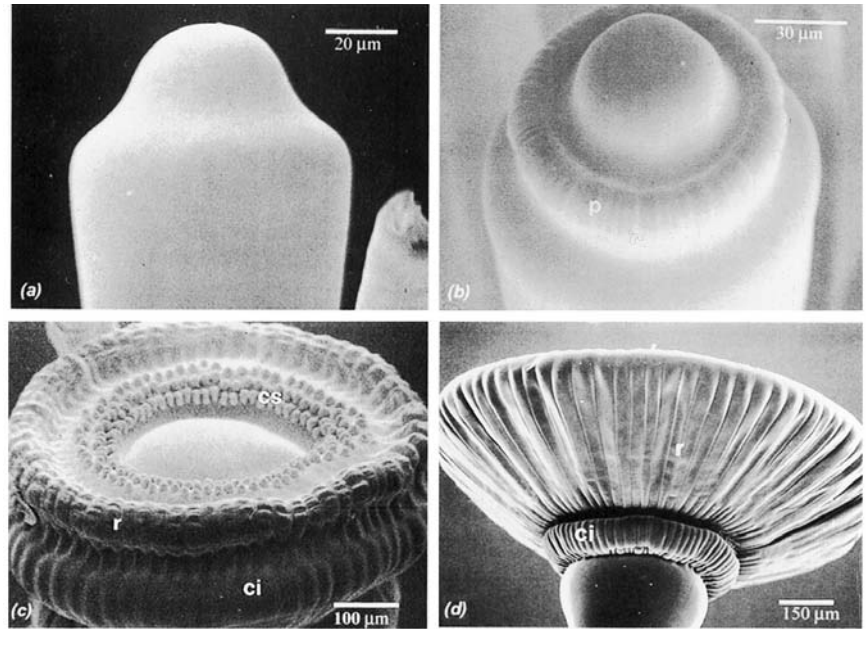


Fig. 5.40 Scanning electron micrographs of cap initiation in *Acetabularia acetabulum*. (ci) Corona inferior; (cs) corona superior; (r) ray cap; (p) primodia. (From Sawitzky et al., 1998.)

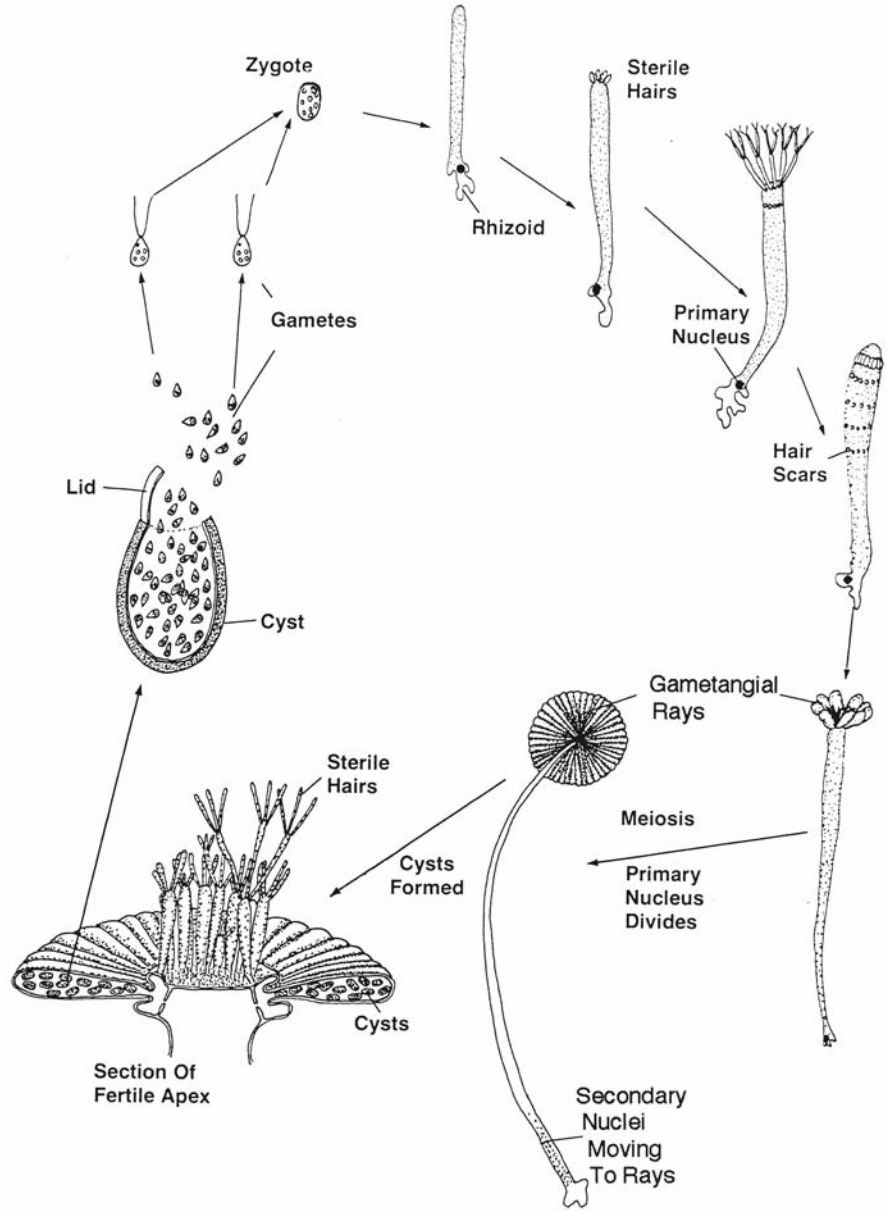


Fig. 5.41 The life cycle of *Acetabularia mediterranea*. (Adapted from Egerod, 1952; Smith, 1955.)

leading to maternal inheritance of chloroplast genes (Kuroiwa, 1985).

Caulerpales

This order contains the **coenocytic** or **siphonaceous** Chlorophyta. The **non-septate thallus** thus resembles a garden hose without any cross walls separating the usually large thallus, except during reproduction. The cells have numerous lens-shaped or fusiform-shaped chloroplasts and, in some cases, amyloplasts. Two carotenoids, **siphonoxanthin** (Fig. 5.1) and **siphonein**, not normally found in the Chlorophyta, occur in this order (with the exception of *Dichotomosiphon*, which has only siphonein; Kleinig, 1969). Cellulose is usually not a wall component and is replaced by a **β-1,3 linked xylan** or a **β-1,4 linked mannan** (Parker, 1970). The

Caulerpales are marine algae and occur as seaweeds in the warmer oceans.

The most important families in the Caulerpales (or Siphonales or Codiales) are as follows:

Family 1 Derbesiaceae: stephanokontic zoospores; no amyloplasts; no oogamous reproduction.
Family 2 Codiaceae: only biflagellate swarmers; thallus basically filamentous; amyloplasts may be present; no oogamous reproduction.
Family 3 Caulerpaceae: only biflagellate swarmers; thallus composed of a stem bearing blades; amyloplasts present; no oogamous reproduction.
Family 4 Dichotomosiphonaceae: oogamous reproduction.

Derbesiaceae

Derbesia (Fig. 5.42) is a filamentous alga found in tropical and temperate waters growing on stones near the low-tide line or on larger algae. The life cycle of *Derbesia* (Feldmann, 1950) involves the alternation of this filamentous sporophyte with a bulbous vesicular gametophyte, the *Halicystis* stage, which was originally described as an independent plant. The *Halicystis* stage is found in deep water, usually epiphytic on a coralline alga. The filamentous *D. tenuissima* sporophyte (Page and Kingsbury, 1968) has an interwoven basal portion that supports erect branched filaments, which are occasionally divided by plug-like septa.

This filamentous sporophyte forms ellipsoidal sporangia as short lateral branches cut off by a septum from the main axis. The sporangia form zoospores meiotically (Neumann, 1969) with a whorl of flagella at one end. The zoospores swim for a while, settle, and germinate to produce a filament that forms the vesicular *Halicystis* gametophyte (Fig. 5.43). The *Halicystis* plants have nuclei arranged in an outer layer under the cell wall, with the chloroplasts in an inner layer next to the large central vacuole. The first visible stage of gamete formation is the migration of protoplasm to the plant apex; this protoplasm becomes separated by a membrane and is now the gametangium. The nuclei in the gametangium undergo synchronous divisions, with the protoplasm cleaving to form the uninucleate gametes.

Plants are heterothallic, producing only one type of gamete. The male plants have olive-green gametangia, whereas those of the female are blackish. Release of the gametes is induced by light, which causes an instantaneous increase in turgor pressure, rupturing the weakened pore area of the wall, and causing a forcible expulsion of the gametes. Following release, the pore is sealed by the gametangial membrane (Wheeler and Page, 1974). Within 12 hours the cell is uniformly green, and it is capable of forming a second gametangium after 24 hours. The biflagellate gametes have one chloroplast in the male and 8 to 12 in the larger female (Roberts et al., 1981). The female gametes are less active than the male. Immediately after mixing, the male gametes surround the female. One of the males begins to fuse with the female, and the whole group of gametes sinks. The zygote germinates to form the filamentous sporophyte. There is a debate as to whether the nuclei from the male and female gametes fuse after plasmogamy of the male and female gametes, or whether karyogamy occurs in the sporangia of the filamentous *Derbesia* phase (Lee et al., 2000; Schnetter and Eckhardt, 2000).

An endogenous rhythm controls gamete formation in the *Halicystis* stage of *D. tenuissima* (Page and Kingsbury, 1968). Gametogenesis has a basic period of 4 to 5 days in the laboratory, but in nature usually occurs in multiples of this figure, and is evidently timed by the tides. The rhythm is unaffected by changes in temperature or light intensity, indicating that it is an endogenous rhythm not directly linked to metabolic processes, such as photosynthesis. After induction of gametogenesis, about 7 hours of dark is necessary for maturation of the gametes, after which light causes their immediate release.

Bryopsis (Fig. 5.44(*d*)) is a common alga in quiet water of tide pools and other sheltered locations. The genus has a main axis that supports lateral upright branches.

The cell walls of the gametophytic phases of *Derbesia tenuissima* and *Bryopsis plumosa* contain large amounts of xylans, whereas the walls of the sporophytes contain large amounts of mannans (Huizing et al., 1979).

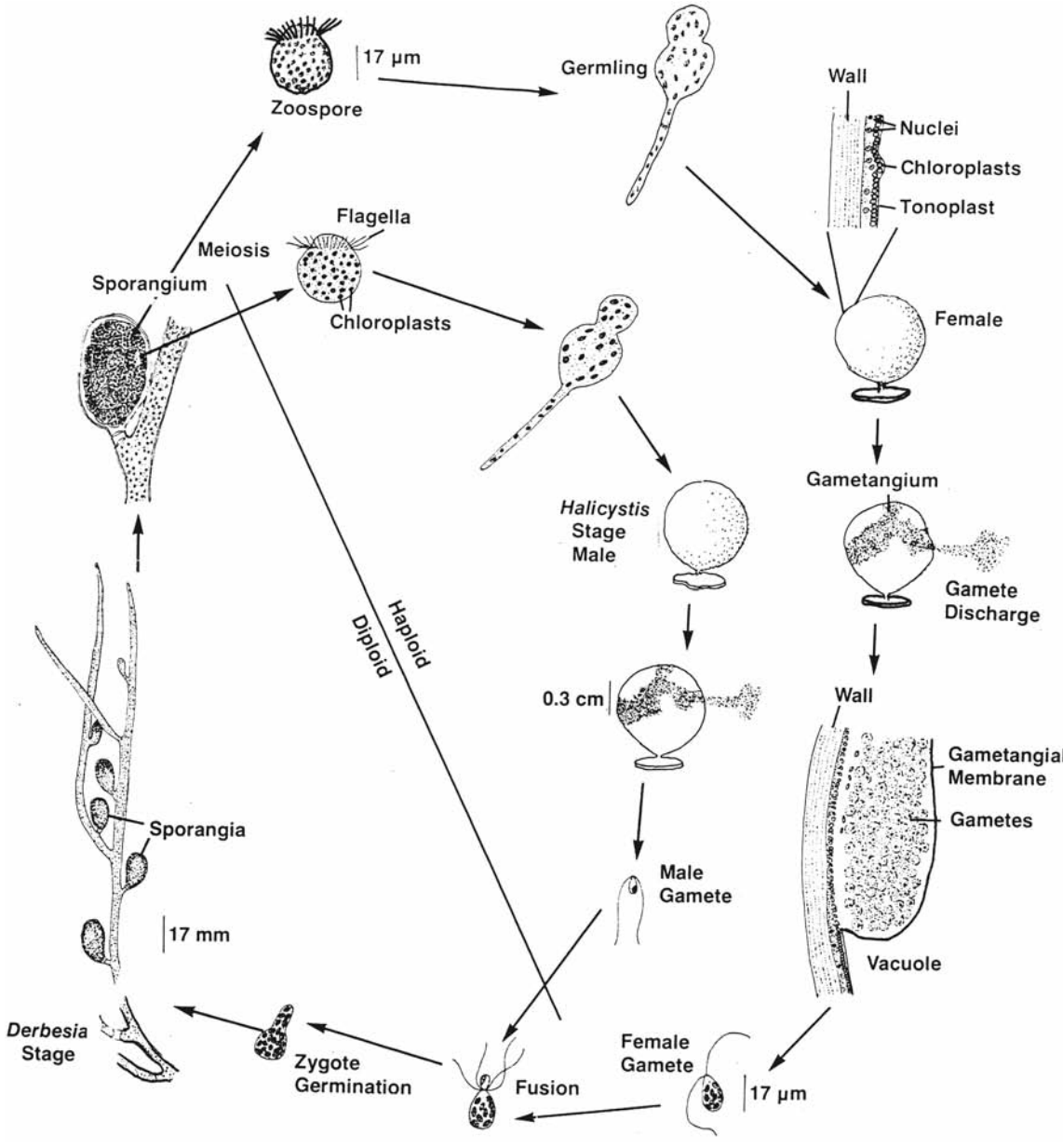


Fig. 5.42 The life cycle of *Derbesia*. (Adapted from Smith, 1955; Zeigler and Kingsbury, 1964.)

Codiaceae

These algae differ from those in the Derbesiaceae in having biflagellate swarmers. The structure of the thallus is basically filamentous. The family can constitute a significant proportion of seaweed populations in tropical waters, including some attractive forms such as "mermaid's fan" (*Udotea*, Fig. 5.44(*f*)) and "Neptune's shaving brush" (*Penicillus*, Fig. 5.44(*e*)).

Codium (Fig. 5.45) occurs from the low-tide mark up to 70 m depth in tropical and temperate marine waters. The genus was originally absent from much of the East Coast of North America. In 1957, *C. fragile* was found along the central Atlantic Coast (Bouck and Morgan, 1957), and it has subsequently spread as far north as Maine. It is probable that the alga was introduced on

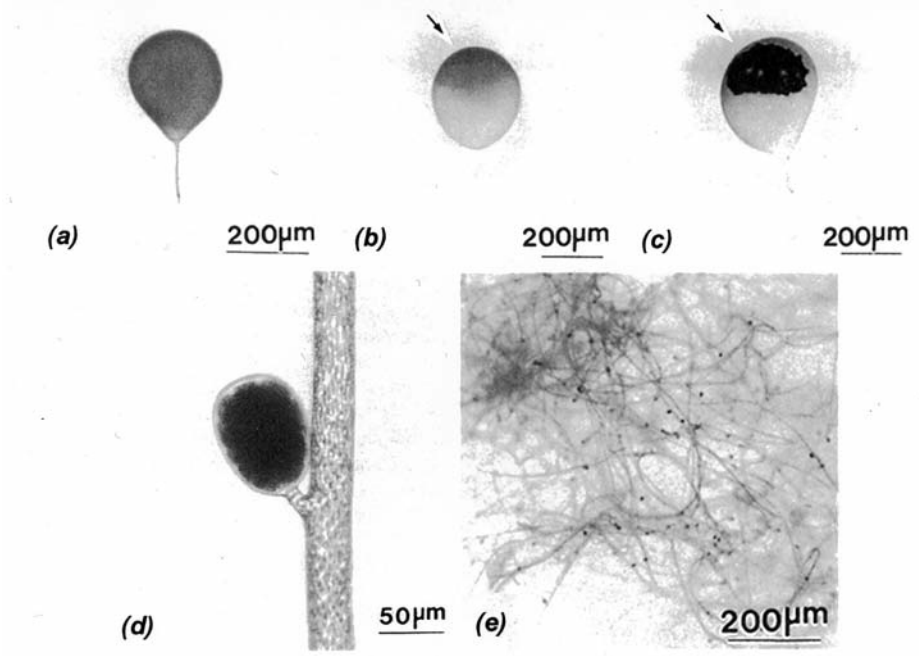


Fig. 5.43 *Derbesia tenuissima*. (*a*) Vegetative *Halicystis* gametophyte. (*b*) Mature male gametophyte (arrow points to gametangium). (*c*) Mature female gametophyte (arrow points to gametangium). (*d*) Sporangium with fully cleaved protoplasm. (e) Mature sporophyte. (From Lee et al., 2000.)

oysters transplanted from Europe. Since its introduction, *Codium* has become a pest in oyster beds, attaching to oysters and causing them to be cast adrift during heavy storms (Fig. 5.46).

The thallus has a crustose prostrate portion that bears several cylindrical dichotomously branched shoots. The shoots have a central medulla composed of interwoven colorless filaments that give rise to inflated branchlets, the **utricles**, which surround the medulla. The utricles have a thick peripheral layer of cytoplasm around a large central vacuole. The discoid chloroplasts are in the outer part of the cytoplasm and the small nuclei in the interior. The colorless filaments of the medulla are divided in places by walls, especially near the base of the utricles. Dark-green female and brown male gametangia are produced from the utricles of the diploid thallus. The gametes are formed meiotically and are released when the lid-like apical portion of a gametangium ruptures, extruding a gelatinous mass with a central canal through which the gametes move. The gametes initially lack flagella and are carried passively. After flagella extrusion, the gametes swim away, with the male gamete fusing with the side of a larger female gamete. The flagella from the male gamete are lost, and the flagella of the female gamete propel the zygote. After settling and flagella retraction, the zygote germinates immediately into a new *Codium* thallus. The gamete thus constitutes the only haploid structure in the life cycle.

Whole plants of *C. fragile* are able to fix nitrogen, owing to an association between the alga and a nitrogen-fixing bacterium (*Azotobacter*) on the surface of the alga (Head and Carpenter, 1975). The alga secretes 0.7 to 1.3 mg glucose per gram of dry weight of the alga per hour, or 16% to 31% of the carbon assimilated to the outside of the thallus. The bacterium uses the secreted glucose and in turn fixes the nitrogen. The nitrogen fixation occurs only under conditions of nitrogen deficiency and is probably an important factor in the growth of *Codium* in shallow bays under oligotrophic conditions.

Codium fragile shows a number of adaptations to its habitat. During winter months when the

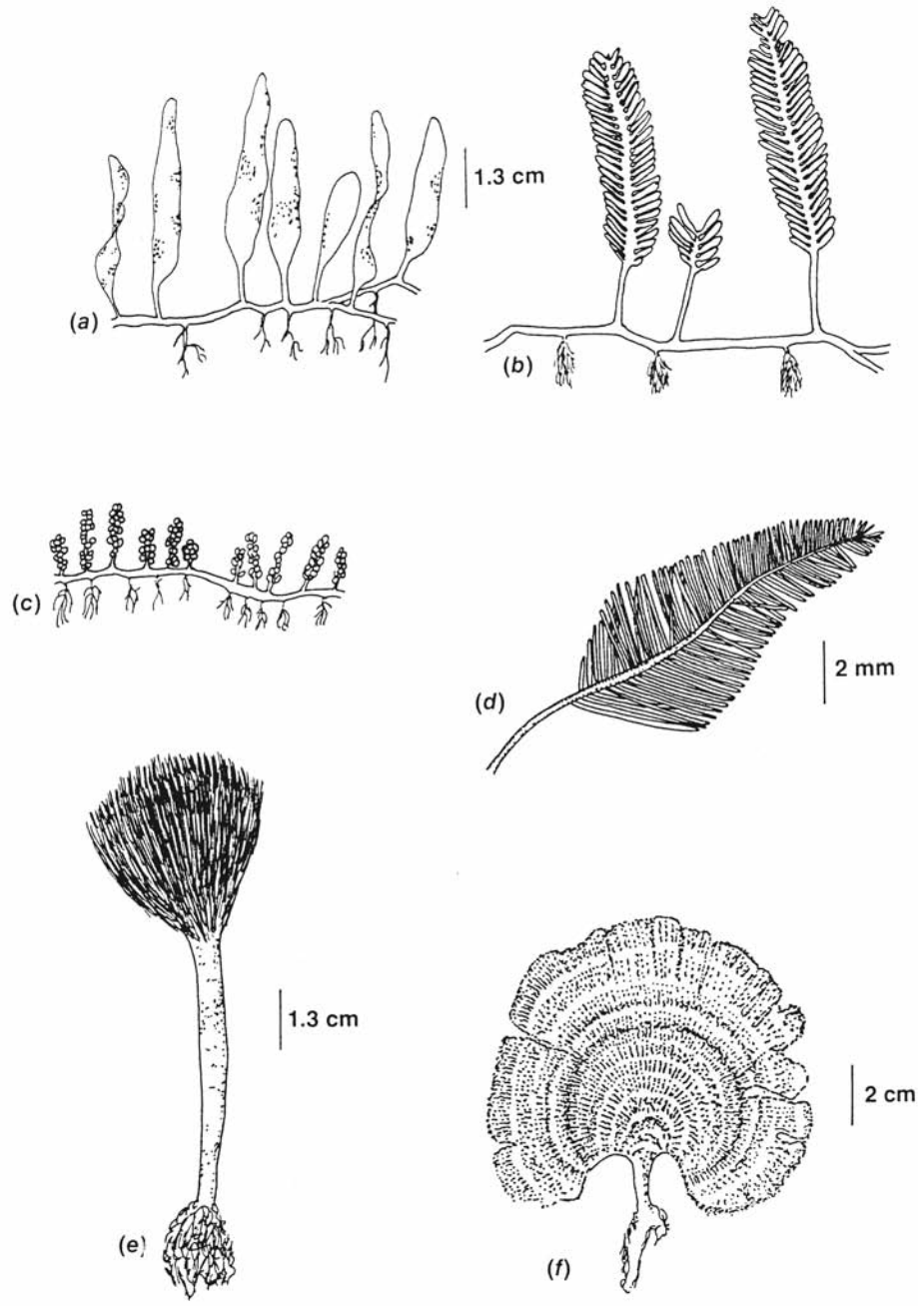


Fig. 5.44 (*a*) *Caulerpa prolifera.* (*b*) *Caulerpa floridana.* (*c*) *Caulerpa microphysa.* (*d*) *Bryopsis plumosa.* (e) *Penicillus capitatus.* (*f*) *Udotea conglutinata.* (After Taylor, 1960.)

availability of dissolved inorganic nitrogen is at its highest in the water, *C. fragile* accumulates reserves of nitrogen which are utilized in times of relative nitrogen deficiency (Hanisak, 1979). The period of maximum carbon fixation, pigment content, and chloroplast size occurs during the early winter when competition from other algae is minimal and variation in tidal amplitude is decreased (Benson et al., 1983). In the summer, the physical environment is more extreme, owing to increased drying in the intertidal zone and

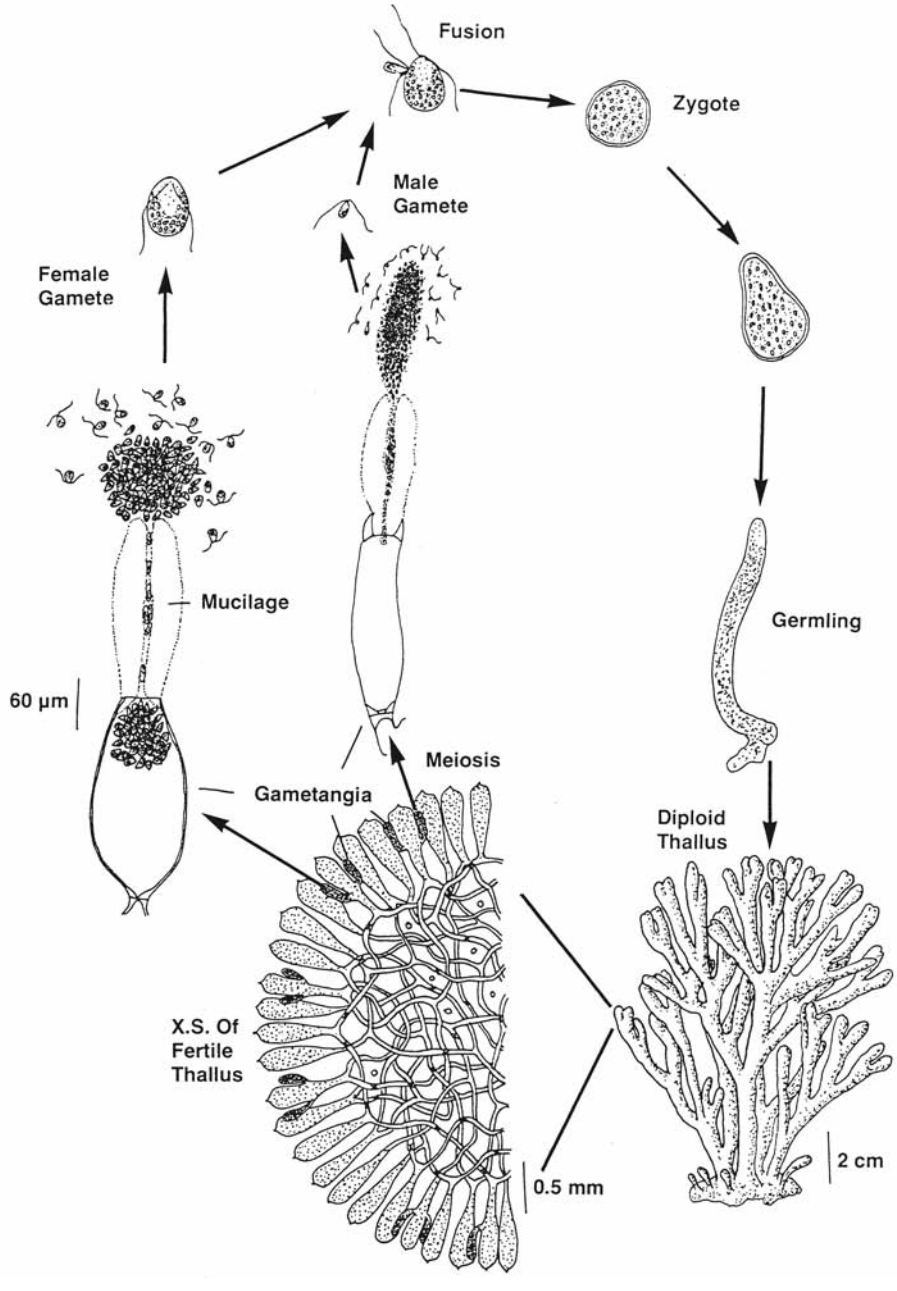


Fig. 5.45 The life cycle of *Codium* sp.

increased competition from other algae. *Codium fragile* effectively retires from much of this competition by undergoing reproduction in the summer. This is accompanied by the development of frond hairs which may increase nutrient uptake.

Symbiotic associations between a number of molluscs and flatworms with chloroplasts of the Codiales are fairly common. Some molluscs (*Elysia*, *Tridachia*, *Placobranchus*) normally feed on siphonaceous Chlorophyceae such as *Codium* and *Caulerpa* by puncturing the cells and sucking out the contents. The chloroplasts are not always digested, and many chloroplasts lodge in the body

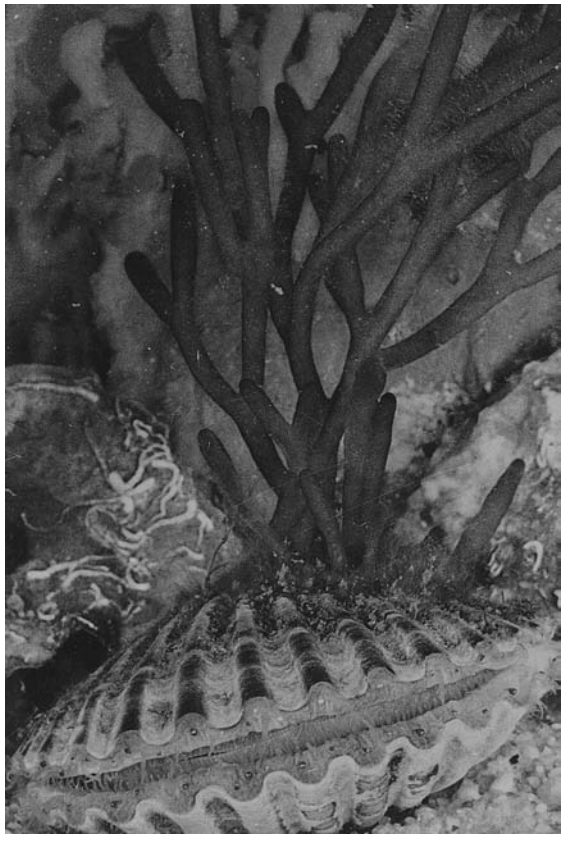


Fig. 5.46 *Codium* sp. on a scallop.

of the animal and actively photosynthesize (Trench et al., 1969, 1973a,b). In *E. viridis*, the chloroplasts can remain functional for at least 3 months when the animals are starved in the light. The rates of photosynthesis of chloroplasts intact in *Codium* and of chloroplasts in *Elysia* are of the same order (Trench et al., 1973b). Chloroplasts isolated from *Codium* release only 2% of their fixed carbon into the medium, mainly as glycolic acid. Isolated chloroplasts in animal homogenate release up to 40% of the fixed carbon, mostly as glucose with some glycolic acid. The animal cells obviously cause the symbiotic chloroplasts to release a large amount of their photosynthate, calculated to be at least 36% of the fixed carbon (Trench et al., 1973b).

The plants of *Halimeda* (Fig. 5.47) consist of calcified segments separated by more or less flexible little calcified nodes. Coenocytic filaments make up the thallus. At the surface of each segment the filaments are inflated to form utricles which are closely appressed to one another in mature plants and form an unbroken surface separating the intercellular spaces from contact with the outside. The cell walls of the utricles are calcified. Occasionally, *Halimeda* plants bear clusters of bead-like reproductive structures on branched stalks arising from the surface of the segments. These form biflagellater swarmers, but it is not known whether they are gametes or zoospores.

Two types of plastids exist in *Halimeda* – amyloplasts and chloroplasts. Both types develop from proplastids (Borowitzka and Larkum, 1974). Actively growing plants of *Halimeda* may add a segment a day, the newly formed segment being noncalcified and white, containing only amyloplasts (Wilbur et al., 1969). At this stage the utricles have not completely closed, leaving intercellular spaces continuous with the outside medium. After the segment is 36 to 48 hours old, the utricles have closed with one another, and aragonite $CaCO_3$ crystals begin to appear on fibrous material outside the walls of the utricles. By the time that calcification has begun, the segment contains well-developed chloroplasts and is green. The older the segment becomes, the fewer amyloplasts and the more chloroplasts there are present.

Incorporation of radioactive ^{45}Ca is stimulated by light, with calcium incorporation into the thallus showing a diurnal rhythm, being greater during the day than during the night (Stark et al., 1969), even under constant illumination. This difference in calcification rates is reflected in the movement of chloroplasts to the periphery of the segments during the day and away from the periphery during the night. The calcification process appears to be a two-step process: first the ions are bound to the wall, with the consequent increase in their concentration, and then the $CaCO_3$ is precipitated. *Halimeda* and *Penicillus* (Fig. 5.44(*e*)) have lower rates of $CaCO_3$ deposition than the calcified red algae (Goreau, 1963).

Halimeda is particularly successful at colonizing bottom habitats where ambient light intensities are from 10 to 20 times less than at the surface. The Halimedas are exceptional among the calcareous Chlorophyta in that they tend to be more heavily calcified in deep than in shallow

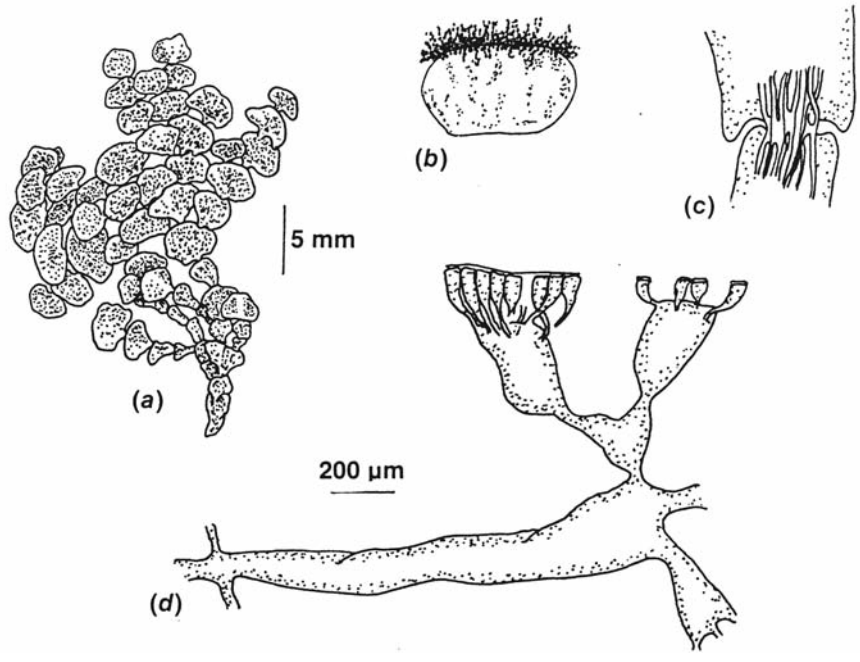


Fig. 5.47 (*a*) *Halimeda tuna.* (*b*) Fertile segment of *Halimeda*. (*c*) Nodal region of *Halimeda opuntia*. (*d*) Central filament of *Halimeda discoidea* with lateral branches forming outer utricles. ((*a*) after Taylor, 1960; (*c*),(*d*) after Egerod, 1952.)

water. Although this difference may be due to a decreased amount of organic matter rather than an increased calcification, the overall effect is opposite to that of other calcareous green algae such as *Penicillus* (Fig. 5.44(*e*)), *Udotea* (Fig. 5.44(*d*)), and *Rhipocephalus*, which are invariably less calcified in deep water. *Halimeda* often performs the major role in calcification in lagoons. Hoskin (1963) examined the sand of Alacran Reef, Mexico, and found that it consisted of 35% *Halimeda*, 29% coral, 8% other coralline algae, 8% mollusks, 6% foraminifera, 1% miscellaneous skeletal grains, 9% fecal pellets, and 4% aggregates by volume.

The family Codiaceae is one of the most important groups of rock-building algae, and, in the course of its long history, has been represented by a large number of genera (Johnson, 1961). In extant (living) plants the calcified genera usually have the outer portion calcified, whereas the inner portion is not. This type of calcification exists in fossil forms, resulting in good preservation in the outer part of the fossil, but with the structural features gradually fading toward the center. A section of *Paleocodium* from the lower Carboniferous (Fig. 5.48(*a*)) shows a structure similar to *Codium* (Fig. 5.46). Restoration of a branch of *Ovulites margaritula* from the Eocene (Fig. 5.48(*b*)) results in a structure similar to *Halimeda*.

Caulerpaceae

The coenocytic plants of this family have two types of plastids – chloroplasts and amyloplasts. *Caulerpa* (Fig. 5.49) is the only genus in the family and is a common inhabitant of intertidal and infratidal tropical and semitropical marine waters. The plants have a creeping green rhizome with root-like colorless rhizoids and frond-like erect shoots. The erect shoots exhibit a considerable variation in morphology, many times resembling the blades of higher plants, after which some of the species are named. The thallus derives support from turgor pressure and from wall ingrowths, the **trabeculae**. The walls have a β-1,3 linked xylan as the main structural component.

Chloroplasts are prominent in the leaves and rhizome but totally lacking in the rhizoids and the extreme apex of the growing rhizome tip

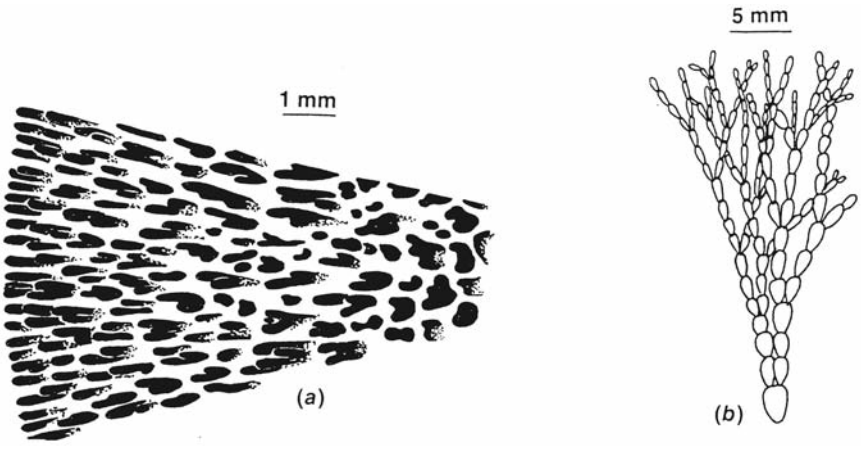


Fig. 5.48 (*a*) Diagrammatic sketch of a section of the thallus of *Paleocodium* from the Lower Carboniferous, showing arrangement of branching filaments. (*b*) Restoration of a branch of *Ovulities margaritula* from the Eocene. ((*a*) after Johnson, 1961; (*b*) after Munier-Chalmas in Johnson, 1961.)

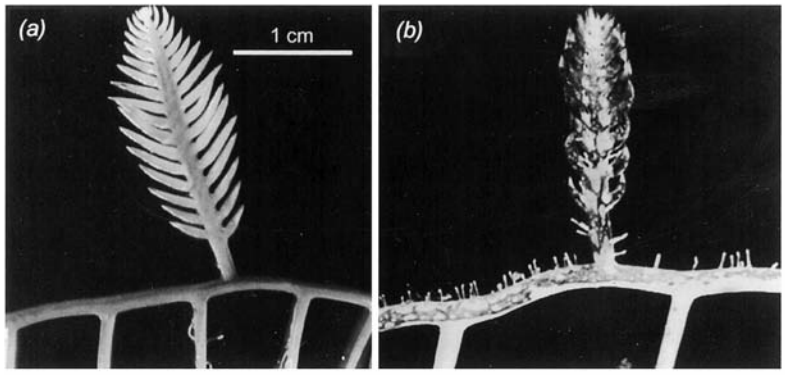


Fig. 5.49 *Caulerpa taxifolia*, non-fertile (*a*) and fertile (*b*) thalli. (From Zuljevic and Antollic, 2000.)

and growing blade. Amyloplast distribution is the reverse of chloroplast distribution, large numbers of amyloplasts being present in the rhizoids and blade tip with few amyloplasts in the rhizome and blades. There is a large central vacuole except at the growing tips.

Mature regions of *Caulerpa* have two systems of protoplasmic streaming: large longitudinal streams in the vacuole and smaller streams oriented 45° to the blade axis in the peripheral cytoplasm. Bundles of microtubules are associated with the cytoplasmic streaming (Sabnis and Jacobs, 1967). The rate of streaming is relatively slow, 3–5 $\mu m\ s^{-1}$, as compared to 60 $\mu m\ s^{-1}$ for *Nitella*.

In sexual reproduction, male and female gametangia are formed on the same frond by migration of the cytoplasm from the rhizomes into the fronds and subsequent cleavage to yield gametes (Fig. 5.49(*b*)) (Goldstein and Morral, 1970). The large female gametes and smaller males are released in a greenish viscous fluid. After a few minutes the gametes agglutinate in groups of up to 50, followed by separation of pairs and the formation of zygotes. The development of *Caulerpa* has not been followed beyond zygote formation.

The development of aquaculture, aquariums and international shipping has led to worldwide exposure of marine environments to

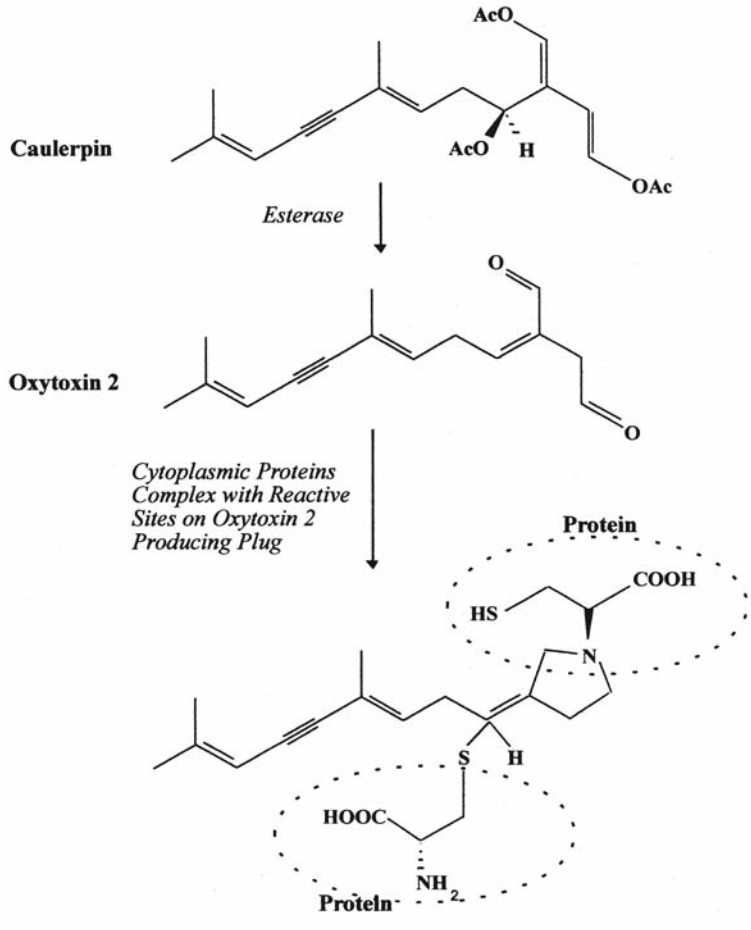


Fig. 5.50 Wounding the coenocytic thallus of *Caulerpa taxifolia* results in conversion of cytoplasmic caulerpin into oxytoxin 2 by an esterase followed by a dehydration. The reactive sites on oxytoxin 2 immediately cross link cytoplasmic proteins, resulting in the formation of a plug that excludes water from the thallus. The whole process is complete within seconds.

non-indigenous species of algae. More than 60 macroalgal species have been introduced into the Mediterranean Sea (Piazzi et al., 2001; Philips and Price, 2002; Verlaque et al., 2003). Species of *Caulerpa* are the more aggressive of these introduced algae, quickly overgrowing native algae by the rapid elongation of its stolons (2 cm d^{-1}). The spread of *Caulerpa* is also due to a unique method of asexual reproduction. No zoospores are formed; instead breakage of the thallus results in new viable plants. On breakage of the coenocytic thallus, the thallus fragments are sealed within seconds by a gelatinous external wound plug that prevents the cytoplasm from coming into contact with seawater (Adolph et al., 2005). The cytoplasm of *Caulerpa* contains caulerpenyne, which on wounding of the thallus is converted by an esterase into **oxytoxin 2** (Fig. 5.50). Oxytoxin 2 is a very reactive 1,4 dialdehyde which cross links cytoplasmic proteins, producing the wound plug.

These *Caulerpa* spp. in the Mediterranean Sea may be Red Sea migrants through the Suez Canal or **Lessepsian species**. The term refers to Ferdinand de Lesseps who designed and led the team that built the Suez Canal. Curiously, there is no similar term for the Panama Canal (which de Lesseps also initially designed). The Panama Canal has a series of higher freshwater lakes which effectively prevent marine species from traveling from one side to the other.

Dichotomosiphonaceae

Dichotomosiphon differs from the rest of the Caulerpales in having oogamous sexual reproduction. The thallus is a dichotomously branched tubular coenocyte bearing colorless rhizoids. Both lens-shaped chloroplasts and amyloplasts are present

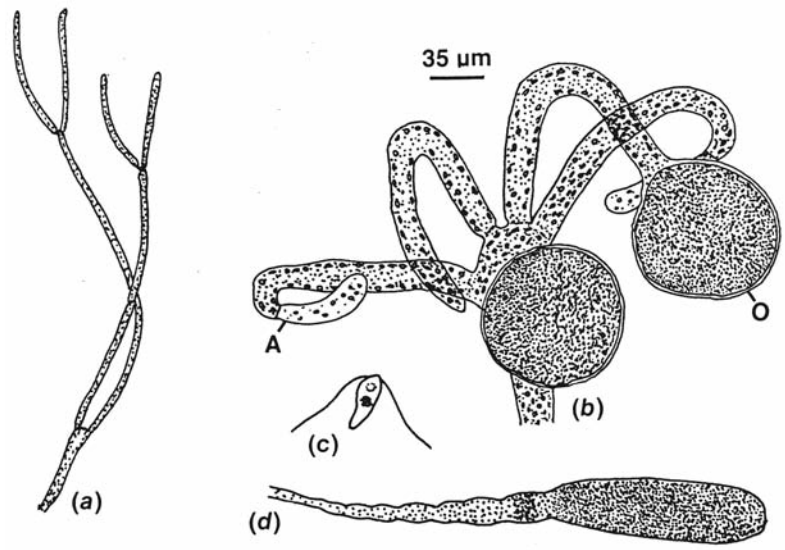


Fig. 5.51 *Dichotomosiphon tuberosus*. (*a*) Vegetative thallus. (*b*) Fertile plants with oogonia (O) and antheridia (A). (*c*) Spermatozoid. (*d*) Portion of thallus with akinetes. ((*b*) after Ernst, 1902; (*c*) after Moestrup and Hoffman, 1975; (*d*) after Smith, 1955.)

in the cytoplasm (Moestrup and Hoffman, 1973). Siphonein is present, but the related pigment siphonoxanthin is absent (Kleinig, 1969). The cell wall has a β-1,3 linked xylan as the main structural wall component (Maeda et al., 1966).

There are two species of *Dichotomosiphon*: the marine *D. pusillus* and the freshwater *D. tuberosus* (Fig. 5.51). The latter grows in lakes with an organic silty bottom, most of the thallus buried, and only the tips of the branches above the silt. In water deeper than 2 m only asexual reproduction occurs, by the formation of akinetes in series at the ends of branches. The akinetes germinate directly to form new thalli (Ernst, 1902). In shallow water, reproduction is sexual, homothallic, and oogamous. Conical antheridia are produced at the tips of branches and separated from the rest of the thallus by a septum. The antheridia burst open explosively at the apex, releasing the biflagellate spermatozoids, which have a single reduced chloroplast but lack an eyespot (Moestrup and Hoffman, 1975). An oogonium is spherical, and just before fertilization develops a small beak-like opening at its apex.

Siphonocladales

These organisms have multicellular thalli, are wholly marine, and are usually tropical. The cells are multinucleate, with reticulate chloroplasts, and divide in a distinct manner known as **segregative cell division**. Most of the organisms have siphonoxanthin (Fig. 5.1) (except *Dictyosphaeria*) in addition to the normal pigments of the Chlorophyta (Kleinig, 1969). Sexual reproduction appears to be isogamous in most cases.

Siphonocladus tropicus initially has an undivided single-celled primary vesicle (Fig. 5.52). In segregative cell division, the continuous protoplast of the primary vesicle breaks into spherical masses of varying size that soon become surrounded by a wall and enlarge to fill the area within the expanding parent vesicle. After each segment has become firmly pressed against adjacent ones, it sends out a lateral protuberance, which constitutes a branch initial. The mature thallus consists of an erect axis with lateral branches (Egerod, 1952).

A young plant of *Valonia* (Fig. 5.52(*h*)) consists of a bladder-like multinucleate primary cell. Small holdfast cells are formed by segregative cell division. A mature cell has a conspicuous central vacuole surrounded by a layer of protoplasm. Any vegetative cell can divide into biflagellate swarmers. Although zygotes have been seen, fusion of gametes has not, but it is presumed that meiosis occurs in the cells immediately before the formation of swarmers.

Valonia is a common tool for investigators interested in the relationship between the vacuole and protoplasm because it is relatively

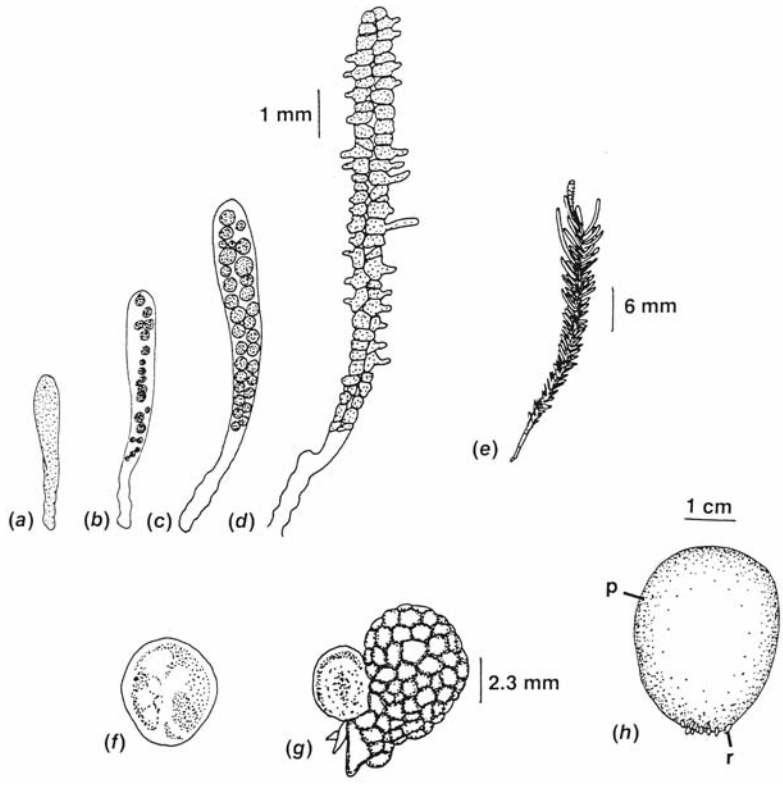


Fig. 5.52 Segregative cell division in *Siphonocladus tropicus*: (*a*) germling; (*b*) cytoplasm in spherical masses; (*c*) expansion of cytoplasmic masses; (*d*) lateral branches forming; (e) mature thallus. *Dictyosphaeria cavernosa:* (*f*) young aseptate vesicle; (*g*) secondary vesicle attached to primary vesicle. (*h*) *Ventricaria ventricosa* (*Valonia ventricosa*). (p) Primary vesicle cell; (r) rhizoidal cell. ((*f*),(*g*) after Egerod, 1952; (*h*) after Taylor, 1960.)

easy to remove the vacuolar contents from the cell. The osmotic values of the vacuolar sap are 1 to 3 atm higher than seawater, with the concentration of potassium in the vacuolar sap being 66 times higher than in seawater (Mimietz et al., 2003).

Damage to the thallus of algae in this order results in the formation of aplanospores through a modified process of segregative cell division. *Ventricaria ventricosa* (*Valonia ventricosa*) lives in coral rubble in tropical reef environments such as the Great Barrier Reef. The alga has a large central vacuole with peripheral protoplasm under the cell wall (Fig. 5.53) (Shepard et al., 2004). The protoplasm has chloroplasts to the outside and nuclei to the inside. These organelles are surrounded by the highly convoluted tonoplast of the central vacuole. The organelles are essentially in islands in the vacuole held together by cytoplasmic strands containing microtubules. The tonoplast is "multifolded" by a factor of nine, giving the protoplasm a spongy appearance. Each nucleus is associated with a certain number of chloroplasts and other organelles, which together can be considered as a fundamental protoplasmic domain. Damage to the thallus results in cytoplasm aggregating around the nuclei to produce aplanospores, with the tonoplast becoming the plasma membrane of the aplanospores.

Chlorophyceae

The distinguishing characteristics of the Chlorophyceae are the **theca outside of the cells** and a **collapsing telophase spindle** that brings the daughter cells close together, followed by **cell division by a phycoplast**. The flagellar root system is cruciate.

Some of the flagellates in the class do not have a theca, but these are assumed to have lost the theca in evolution because the cells have the other characteristics of the class. The Chlorophyceae are predominantly freshwater. The few unicellular, planktonic species that occur in coastal seawater are members of genera that have a much greater number of freshwater species,

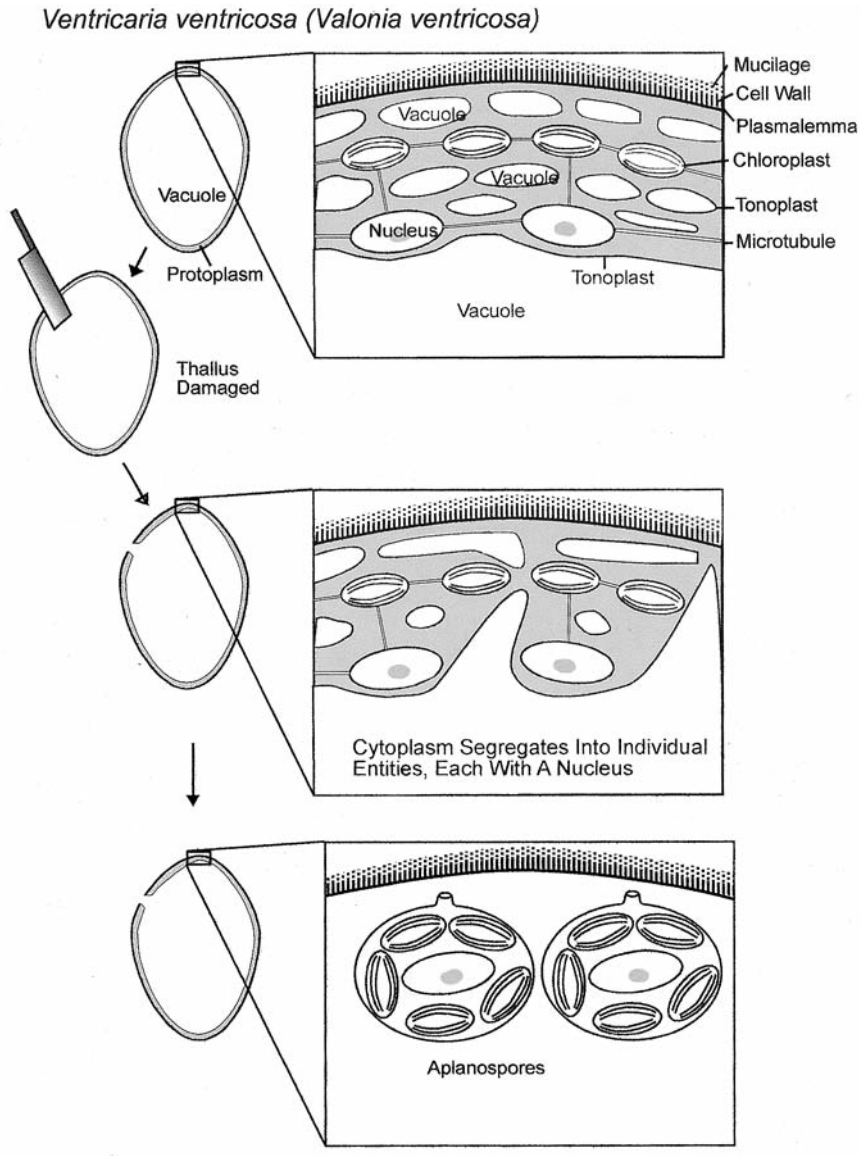


Fig. 5.53 The coenocyte *Ventricaria ventricosa* (*Valonia ventricosa*) has a large central vacuole with a thin layer of protoplasm under the cell wall. The nuclei in the protoplasm, and associated chloroplasts, are held apart by microtubules. The tonoplast is highly convoluted, resulting in the vacuole weaving between the organelles and giving a spongy appearance to the protoplasm. Damage to the thallus results in aggregation of chloroplasts around the nuclei. Aplanospores are formed with the tonoplast of the original cell becoming the plasmalemma of the aplanospores. (Adapted from Shepherd et al., 2004.)

such as *Chlamydomonas*. The Chlorophyceae whose sexual reproduction is known produce a dormant zygote, with meiosis usually occurring when the zygote germinates.

The other characteristics of the Chlorophyceae were described earlier in this chapter and include motile cells with radial or near-radial external symmetry, flagella attached at the anterior end of the cell, the possibility of a rhizoplast, no multilayered structure, eyespots common, glycolate breakdown by glycolate dehydrogenase, and urea breakdown by urea amidolyase.

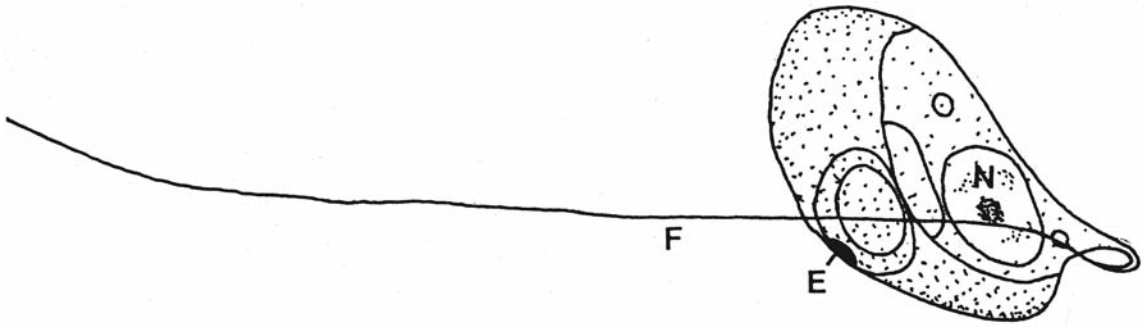


Fig. 5.54 *Mantoniella squamata*. The cell is covered with scales and has a second, very short flagellum (neither of which is shown).

Mantoniella (Fig. 5.54) is a scaly green flagellate with two subapically attached flagella (one of the flagella is very short) (Barlow and Cattolico, 1980). There is one microtubular root composed of four microtubules and a second composed of two microtubules. Duplication of a microtubular root system probably resulted in the cruciate root system of the Chlorophyceae.

Classification

The Chlorophyceae are divided into the following important orders:

Order 1 **Volvocales**: vegetative cells flagellated and motile.
Order 2 **Tetrasporales**: non-filamentous colonies with immobile vegetative cells capable of cell division; pseudocilia may be present.
Order 3 **Prasiolales**: marine, freshwater or terrestrial algae composed of unicells, short filaments or small sheet-like thalli.
Order 4 **Chlorellales**: unicells or non-filamentous colonial algae; vegetative cells non-motile.
Order 5 **Trebouxiales**: green algae involved in a lichen symbiosis.
Order 6 **Sphaeropleales**: unbranched filaments with new walls formed inside the old filament walls, resulting in H-shaped wall pieces.
Order 7 **Chlorosarcinales**: daughter cells retained within parent cell wall; no plasmodesmata present.
Order 8 **Chaetophorales**: branched or unbranched filaments; plasmodesmata present.
Order 9 **Oedogoniales**: uninucleate filamentous freshwater algae with a unique type of cell division; motile spores and gametes with a whorl of flagella at one pole.

Volvocales

In the Volvocales the vegetative cells are flagellated and motile. The algae can be unicellular or multicellular. If they are multicellular, then the number of cells in the vegetative colony is a multiple of two. Almost all of these organisms are freshwater, being abundant in waters high in nitrogenous compounds.

There are two important families in the order:

Family 1 **Chlamydomonadaceae**: unicellular algae.
Family 2 **Volvocaceae**: colonial algae formed into **coenobia**, *colonies with a definite number of cells arranged in a specific manner*.

Chlamydomonadaceae

In this family are all the unicellular Volvocales. All of the genera are uninucleate, and usually the chloroplast is cup-shaped.

Chlamydomonas is a unicellular, biflagellate organism that can be easily grown and manipulated in culture (Harris, 1989, 2001). The uninucleate cells have a cup-shaped, basal chloroplast with a central pyrenoid (Fig. 5.55). There are two

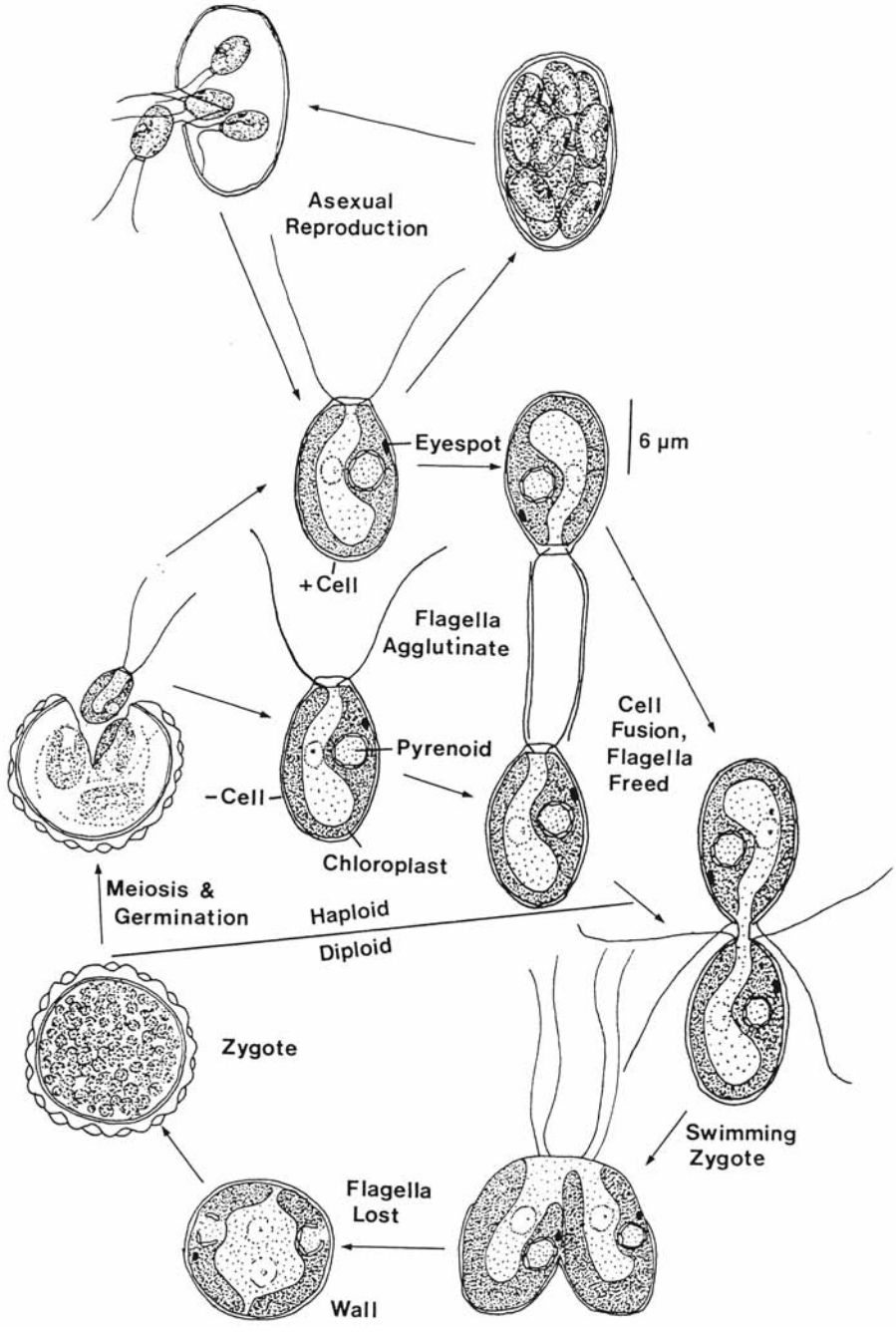


Fig. 5.55 The life cycle of *Chlamydomonas moewusii*. (Adapted from Brown et al., 1968.)

contractile vacuoles at the base of the flagella, and there may, or may not, be an anterior eyespot in the chloroplast. A cell wall usually surrounds the protoplast. When growing on soil, or on agar in the laboratory, *Chlamydomonas* is non-motile and grows in gelatinous colonies. If these colonies are flooded, motile unicells are formed. The cells are widely distributed in freshwaters and in damp soils where they are commonly found in areas with high concentrations of nitrogen, such as farmyard soils.

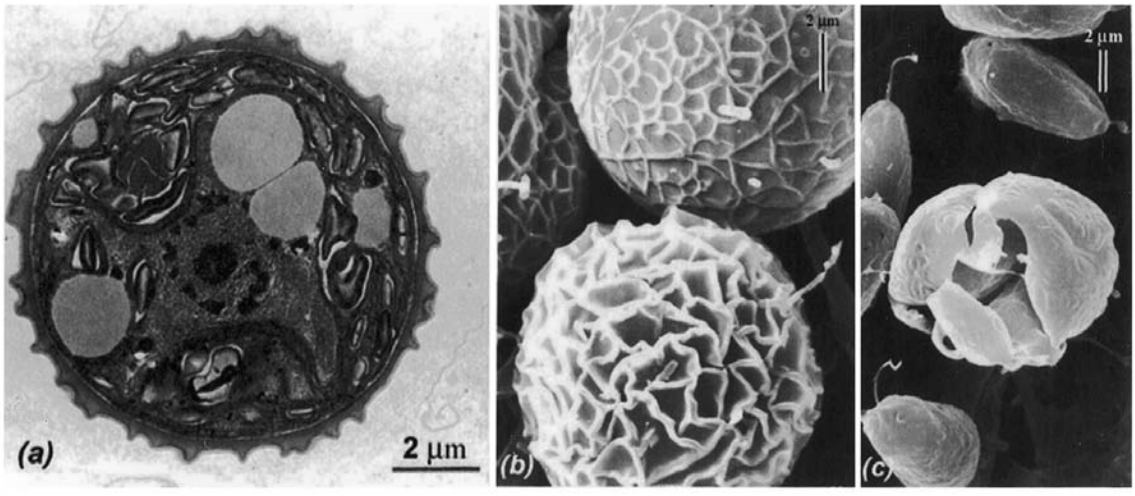


Fig. 5.56 Zygospores of *Chlamydomonas monoica*. (*a*) Transmission electron micrograph of a section of zygospore showing a cytoplasm full of lipid droplets and starch grains. (*b*) Scanning electron micrograph showing a resting zygospore at the bottom of the micrograph. The zygospore swells and the wall becomes less ornamented as the zygospores begin to germinate, as illustrated by the upper zygospore in the micrograph. (*c*) An empty zygospore wall is in the center of the scanning electron micrograph. Notice that after germination, the remaining zygospore wall is smooth. ((*a*) from Van Winkle-Swift and Rickoll, 1997; (*b*),(*c*) from Malmberg and Van Winkle-Swift, 2001.)

Asexual reproduction begins by the *Chlamydomonas* cell coming to rest and usually retracting or discarding the flagella. The protoplast then divides into 2, 4, 8, or 16 daughter protoplasts within the parent wall (Fig. 5.55). These protoplasts develop walls and flagella, and are released on gelatinization of the parent wall, if growing in liquid medium.

Most species of *Chlamydomonas* exhibit isogamous sexual reproduction (Musgrave, 1993). In *C. moewusii* (*C. eugametos*), there is no structural difference between the gametes and the vegetative cells, and gametogenesis involves the production of agglutinins that cover the flagella (Demets et al., 1990). When gametes of a plus strain are mixed with those of a minus strain, the flagella of the opposite strains adhere because of the agglutinins on the flagella. Initially the gametes clump in groups of up to 50 cells with their flagella toward the center and with different numbers of plus and minus gametes in each clump. Eventually pairs of opposite gametes fuse at their anterior ends, the flagella become free, and the pair swims away from the clump. Before fusion of gametes, a hole is dissolved in the wall at the interior end of the gametes, and a fertilization tubule is pushed out through the hole. These tubules fuse at their tips, beginning fusion in the gametes. This connecting tubule shortens, causing the apical portion of the gametes to fuse, followed by jackknifing of the two gametes and lateral fusion. The quadriflagellate zygote swims for a while before settling down and forming the primary zygote wall. The nuclei fuse within 24 hours, and a secondary zygote wall with horns and spines is laid down. As the zygote matures, it may or may not enlarge, depending on the species, but it always accumulates large quantities of oils and starch, which may turn it reddish. Light and carbon dioxide are required for development of the zygote (Lewin, 1957). The wall of the zygospore (zygote) (Fig. 5.56) is multilayered and contains sporopollenin (Malmberg and VanWinkle-Swift, 2001). Zygospore germination occurs in the dark, the inner layer of the zygospore is dissolved away and the sculptured exine splits open to liberate the motile zoospores. The zoospores are formed by meiosis. Usually 4 or 8 zoospores are released, but there can be as many as 16 or 32.

The sequence of events in *Chlamydomonas reinhardtii* is slightly different (Martin and Goodenough, 1975; Huang and Beck, 2003). The

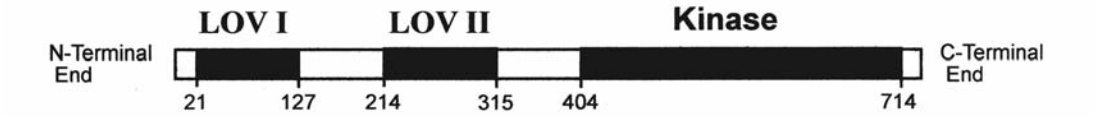


Fig. 5.57 The structure of phototropin. The protein contains two LOV (**L**ight, **O**xygen, **V**oltage) domains that bind flavin mononucleotide (FMN). The kinase is involved in the autophosphorulation of phototropin in the presence of blue light.

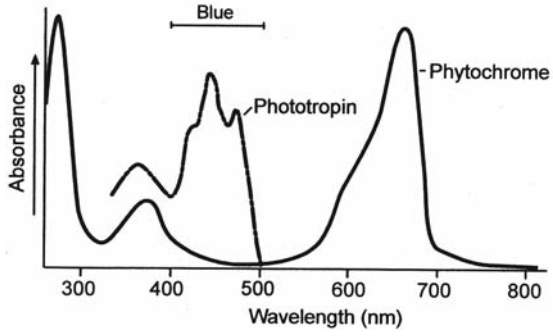


Fig. 5.58 Stylized action spectra typically observed for phototropin-mediated and phytochrome-mediated responses. An action spectrum represents the effectiveness of different wavelengths of light at eliciting the desired response.

formation of mating type "plus" (mt^+) and "minus" (mt^-) pregametes is induced by nitrogen starvation in the dark. The pregametes are mating incompetent and require exposure to blue light in a relatively slow process that results in the formation of gametes. Incubation of the gametes in the dark results in rapid loss of mating competence, probably because of deactivation of flagella proteins involved in sexual agglutination. Exposure to blue light results in rapid reactivation of mating competence. Phosphorulation of the phototropin (Figs. 5.57, 5.58) appears to be the blue-light receptor for activation of pregametes to gametes.

The mating reaction is initiated when mating-type "plus" (mt^+) and minus (mt^-) gametes are mixed together (Snell, 1985). The resulting interactions can be divided into seven stages, all of which are completed within 30 seconds (Fig. 5.59).

1 The cells adhere to one another via *mt*-specific flagellar surface agglutins, which are glycoproteins of extremely high molecular mass. The **agglutins** are rich in hydroxyproline and appear as extended rods bearing globular domains. The agglutins of the minus gametes have a protein that recognizes a particular sugar sequence in the glycoprotein on the flagellum of the plus gamete (possibly a mannose-containing polysaccharide) (Wiese and Hayward, 1972). The agglutins cover the flagellar surface and are continuosly lost and replaced from a large cytoplasmic pool. Agglutination results in activation of a flagellar adenyl cyclase (Fig. 2.9) in each gamete and a ten fold elevation in intracellular cyclic adenosine monophosphate (cAMP) levels (Pasquale and Goodenough, 1987). There is an eightfold increase in the adhesion of the flagellar surfaces by the translocation of inactive agglutin molecules from the plasma membrane of the cell body onto the contiguous flagellar membrane, where the agglutins become active (Pan and Snell, 2000).
2 In a process called "flagellar tip activation", the tips of the flagella acquire amorphous material between the flagellar membrane and the underlying doublet microtubules of the flagellum. The A microtubules in each of the nine outer doublet microtubules extend, causing extension of the flagellar tips.
3 One or more "signals" are transmitted to the cell bodies of the paired cells.
4 As a first response to signaling, cells release an **autolysin** that dissolves the crystalline glycoprotein wall (Imam et al., 1985) surrounding the gametes. The autolysin is an enzyme composed of a single polypeptide with a molecular mass of 62 kilodaltons. Autolysin occurs in an inactive soluble form in vegetative cells. Autolysin is converted to a soluble active form when the cell is transformed into a gamete (Matsuda et al., 1987).

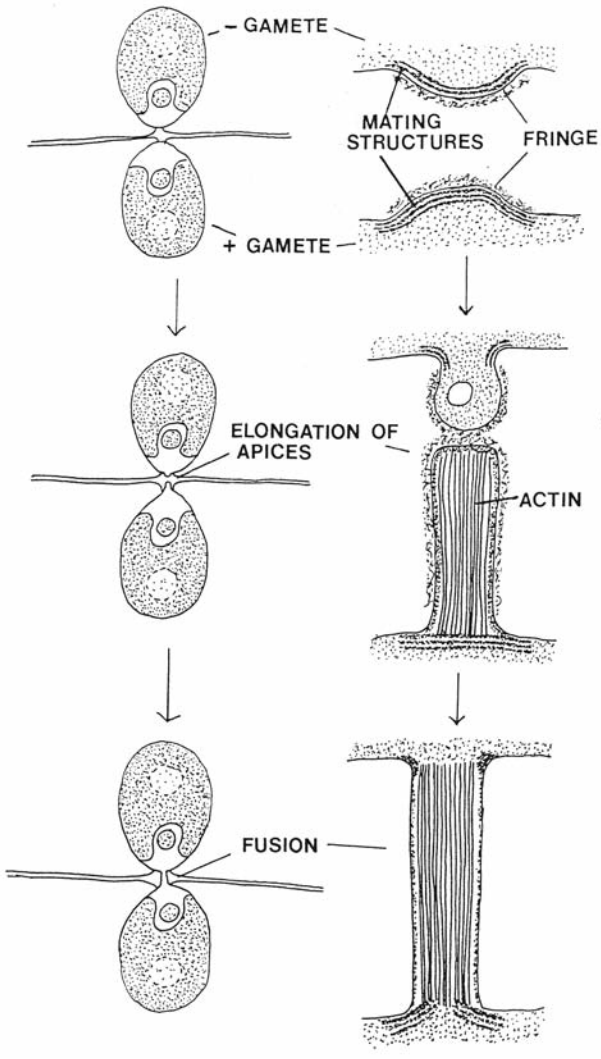


Fig. 5.59 Drawings of fusing cells of *Chlamydomonas reinhardtii* on the left. On the right are enlargements of the apical areas of the fusing cells. (Adapted from Goodenough et al., 1982.)

5 As a second response to signaling, the cells activate their **mating structures**. The plus gamete has a mating structure composed of three electron-dense layers (Fig. 5.59) that lie under the plasma membrane in an apical bud, approximately 1 μm in diameter (Goodenough et al., 1982). The minus gamete has a mating structure composed of two electron-dense plates in a similar apical bud. Covering the plasma membrane of the apical buds of the plus and minus gametes is a **fringe** of fuzzy material that probably contains the recognition apparatus of the plus and minus gametes.

6 The apical bud of the minus gamete elongates slightly into a dome-shaped structure. In the plus gametes, actin microfilaments extend from the mating structure into the bud to form a long, narrow fertilization tubule. Cell fusion occurs when the fringe at the tip of the fertilization tubule of the plus gamete strikes the fringe at the tip of the apical bud of the minus gamete. A narrow cytoplasmic bridge is formed, which opens up to allow full cytoplasmic confluence.

7 The adhering flagella of the resulting quadriflagellate cell lose their agglutinative properties, presumably in response to a

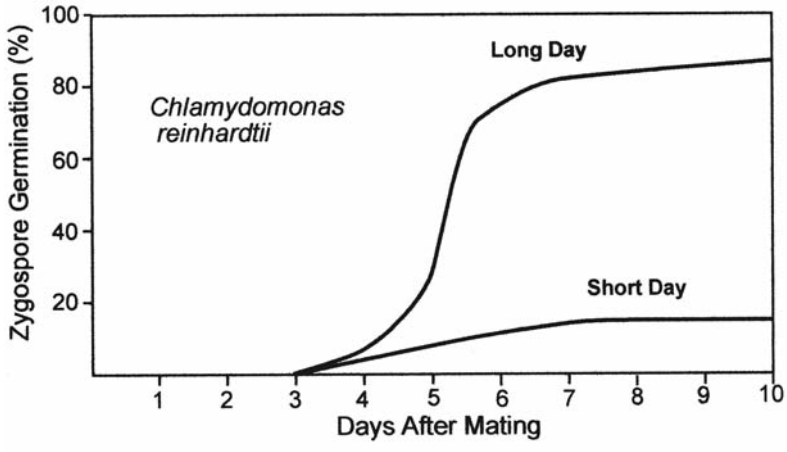


Fig. 5.60 Germination of zygospores of *Chlamydomonas reinhardtii* is stimulated by long days but suppressed in short days. (Modified from Suzuki and Johnson, 2001.)

"signal to disadhere," which is transmitted at the time of cell fusion. The remaining steps leading to the formation of a zygote are similar to those of *Chlamydomonas moewusii.*

Zygospores resist stressful environmental conditions, such as freezing, darkness, desiccation, and starvation. Zygospores undergo meiosis to produce four haploid vegetative cells. Germination of zygospores of *Chlamydomonas reinhardtii* is enhanced under long-day conditions and suppressed under short-day conditions (Fig. 5.60) (Suzuki and Johnson, 2001; Huang and Beck, 2003). The suppression of germination during short days is an adaptive response for overwintering in *Chlamydomonas*. This is an example of **photoperiodic time measurement** in the algae. Photoperiodic time measurement is defined *as the ability of plants or animals to sense the season of the year by measuring the duration of the day and/or night in the natural environment and respond appropriately so as to adapt to seasonal changes in the environment* (Huang and Beck, 2003).

There have been no reports of a chemical attractant (**pheromone**) being secreted by gametes of *Chlamydomonas moewusii* (*C. eugametos*) or *C. reinhardtii*. However, the larger female gamete in *C. allenworthii* secretes the pheromone **lurlene** (Fig. 5.61) which attracts the smaller male gamete (Starr et al., 1995). Sexual reproduction in *C. allenworthii* is triggered by nitrogen starvation, accompanied by fading of cells from green to brownish as the photosynthetic system is degraded. Plastoquinone (the chloroplast electron shuttle between photosystem II and I) in the thylakoid membrane is degraded to the chemically similar lurlene at this time (the name lurlene is taken from **Lurley**, the attractive flaxen-haired Rhenish maiden who lured fishermen to their death) (Jaenicke and Starr, 1996; Mori and Takanashi, 1996). Lurlene at a concentration of 1 pM is sufficient to attract the male gamete to the female. Lurlene ceases to be secreted after the male gamete fuses with the female.

Most species of *Chlamydomonas* are found in small ponds and puddles. An unusual habitat is in the snows of some mountains in western North America (Jones et al., 2001; Hoham et al., 2002). Here *C. nivalis* is responsible for what is known as "red snow." Great numbers of this alga produce the watermelon color associated with these alpine snowfields. The algae grow most abundantly near the surface of old, melting snow in spring and summer, although the resting spores can be found to a depth of more than 60 cm. The algal cells remain until heavy snow covers the surface of the old snow. Upon the arrival of spring, the algal cells migrate upward to the surface of the snow to form another bloom. The algae need melt-water before they will grow, and this need explains their lack of growth in the winter. These snow algae support a unique type of fauna, including various species of protozoans, ciliates, rotifers, nematodes, spiders, and springtails. The last organism in this food chain is the segmented snow worm (*Mesenchytraeus*), which like the algae

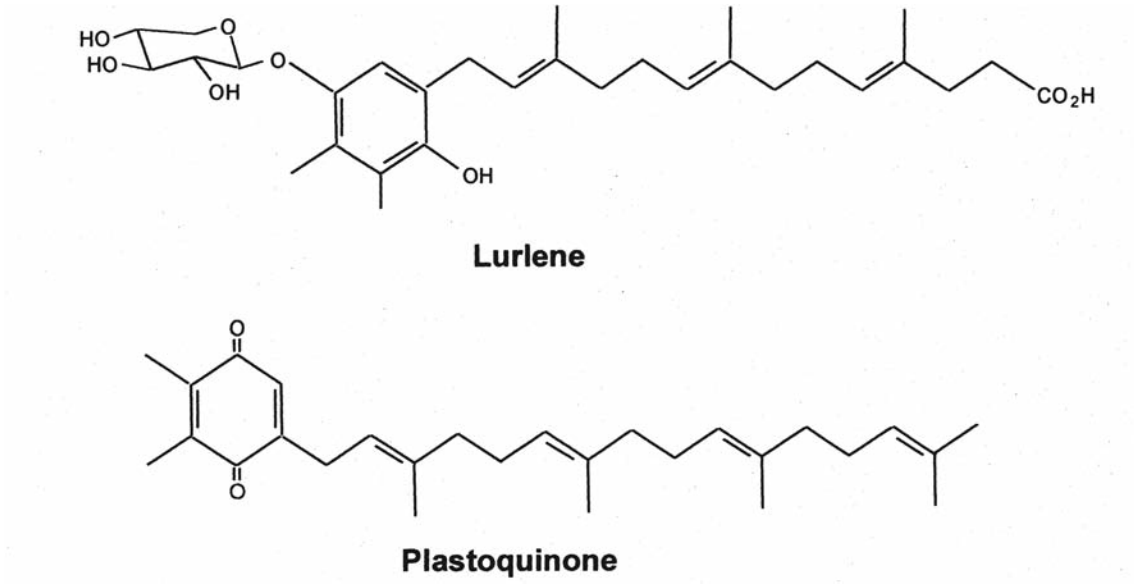


Fig. 5.61 The structure of lurlene and plastoquinone.

is not prevalent during the winter. During an 1891 expedition to the Malaspina Glacier in Alaska, Dr Israel Russel wrote: "In the early morning before the sunlight touched the snow, its surface was literally covered with small slim black worms, about an inch long and having a remarkable snakelike appearance. These creatures were wriggling over the snow in thousands."

Dunaliella (Figs. 5.62, 5.63), a green alga that looks like *Chlamydomonas*, has species that have adapted to life in acid waters and species that have adapted to waters high in salt. *Dunaliella acidophila* is an acid-resistant species that exhibits optimal growth at pH 1.0 (Geib et al., 1996). *Dunaliella salina* (Fig. 5.63) has adapted to waters high in salt, where it is common in places such as the Great Salt Lake of Utah. *D. salina* has two varieties. The first variety has small green halotolerant cells that can grow at NaCl concentrations of 0.5M and above. The second variety has large red halophilic cells that can only grow in saline concentrations above 2M.

Species of *Dunaliella* (Gonzalez et al., 2001) are possibly the most salt-tolerant eukaryotic photosynthetic organisms. *Dunaliella* has two mechanisms that allow it to live in waters of varying salinities (Fisher et al., 1994):

1 *Ion pumps in the plasma membrane* – Plasma membrane proteins are produced when the alga is moved from a low-salinity environment to one of high salinity. These proteins are ion pumps that expel sodium from the protoplasm and control intracellular ion levels.
2 *Production of glycerol* – Lacking a cell wall, *Dunaliella* cells respond to increases or decreases in the external salinity by immediate shrinking or swelling, respectively. Subsequent synthesis or elimination of glycerol results in an intracellular concentration that balances the external salinity and permits the cells to regain their original volume. At the ultrastructural level (Fig. 5.62), an increase in the size of the Golgi body accompanies an increase in cellular glycerol when the cells are placed in a solution of high salinity (Bérubé et al., 1999).

The unicellular *Hematococcus* (Fig. 5.63) accumulates the yellow carotenoid astaxanthin (Fig. 5.1) in the cytoplasm at concentrations up to 5% of the dry weight of the cells. The alga can be added to fish and poultry feed to impart a yellow color to the skin. High concentrations of astaxanthin can be induced by growing the cells under high O_2 concentrations, nitrogen

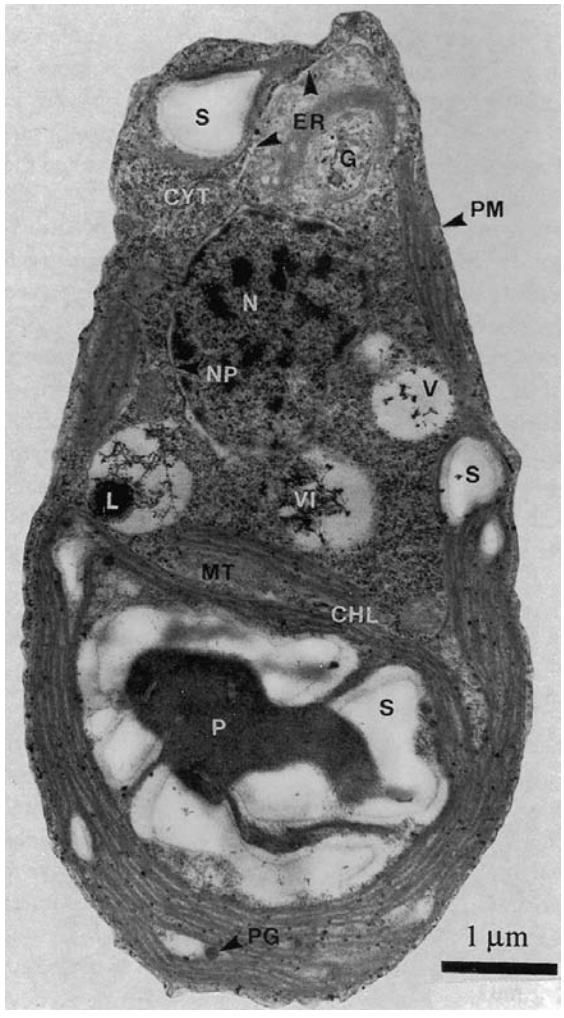


Fig. 5.62 Transmission electron micrograph of a longitudinal section of a cell of *Dunalliela bioculata*. (CHL) Chloroplast; (CYT) cytoplasm; (ER) endoplasmic reticulum; (G) Golgi body; (L) lipid globule; (MT) mitochondrion; (N) nucleus; (NP) nuclear pore; (P) pyrenoid; (PG) plastoglobuli; (PM) plasma membrane; (S) starch; (V) vacuole; (VI) vacuolar inclusion. (From Bérubé et al., 1999.)

limitation or high irradiance (Lee and Ding, 1995; Tan et al., 1995; Ben-Amotz, 1996; Grünewald et al., 1997).

The zoospores of *Phacotus lenticularis* (Fig. 5.64) are surrounded by a lorica containing crystals of calcite (Fig. 4.7). *Phacotus* can occur in high quantities in some lakes (up to 5 million cells per liter) where they have a strong influence on the lake ecosystems (Schlegel et al., 2000).

Volvocaceae

This family includes those colonial Volvocales with a formation of a flat plate (**plakea**) during early development of the colony (Fig. 5.65). The family evolved about 50 million years ago (Nishii, et al., 2003). All of the members of the family undergo a process of inversion after completing embryonic cleavage. The number of cells in a colony is a multiple of two, and each of the cells is surrounded by a gelatinous sheath.

Evolution in the Volvocaceae has resulted in colonies of increasing complexity. The basic cell unit in these organisms (Fig. 5.2) is that of *Chlamydomonas* (Coleman, 1999), the cells joining together to form a colony. The individual cells in the volvocacean colony are held together by an extracellular matrix of hydroxyproline-rich glycoproteins. The extracellular matrix is divided into four zones (Fig. 5.66) (Hallman, 2003): (1) flagellar zone, (2) boundary zone, (3) cellular zone, and (4) deep zone.

Coenobia of most genera exhibit a polarity when swimming, the anterior pole directed forward. The two flagella of each somatic cell beat toward the posterior, and slightly to the right, which causes the colony to revolve to the left as it swims. Hence, the name *Volvox*, which means "fierce roller." Photoreception and flagellar activity permit *Volvox* to swim in the water at rates exceeding 5 meters per hour to collect sunlight during the day near the surface, and essential minerals during the night at the bottom of the lake (Kirk, 1999).

In *Volvox*, the anterior cells change the frequency of the beat of the flagella as the light intensity changes, orienting the colony toward the light source (Fig. 5.67) (Hoops et al., 1999). The beat frequency of the flagella of the posterior cells does not change.

There may be a morphological difference in the size of the cells or eyespots in the posterior versus the anterior ends. The saucer-shaped cells of *Gonium* (Fig. 5.65(*c*)), with 4 to 32 cells, swim with the convex surface forward and have eyespots of a uniform size. In the rest of the Volvocaceae, size differentiation occurs among the eyespots, with larger eyespots in cells in the anterior end. This is so in the spherical coenobium of *Pandorina* with 4 to 32 cells (Fig. 5.65(*d*)),

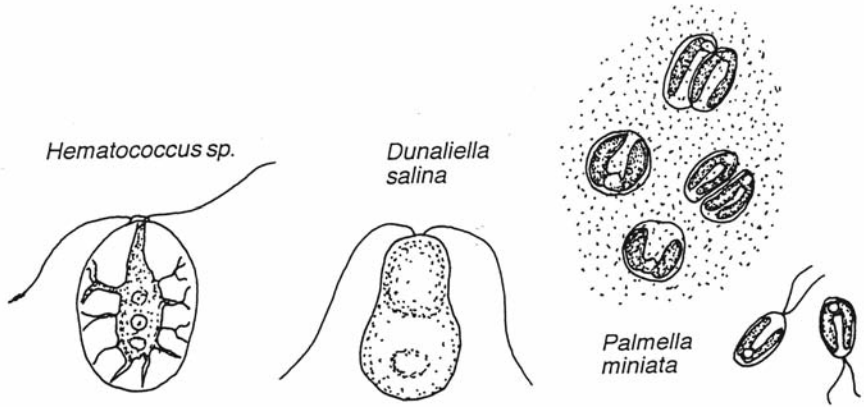


Fig. 5.63 Drawings of motile cells of *Hematococcus* sp. and *Dunaliella salina*, and palmelloid and motile cells of *Palmella miniata*.

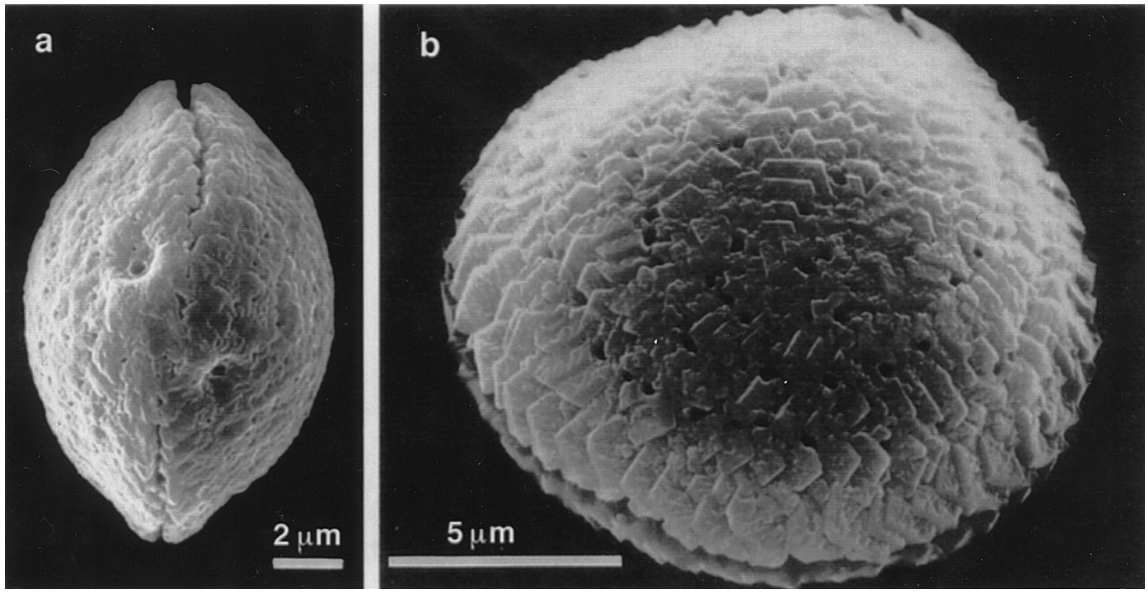


Fig. 5.64 Scanning electron micrographs of zoospores of *Phacotus lenticularis* covered with a lorica composed of crystals of calcite. (From Hepperle and Krienitz, 1996.)

in *Volvulina* (Fig. 5.65(*f*)) with 18 cells in four ranks of four, in *Stephanoon* (Fig. 5.65(*a*)) with 8 to 16 cells in equatorial ranks, in *Eudorina* with a spherical coenobium of 16 to 128 cells, in *Volvox* (Figs. 5.68, 5.69) with spherical colonies of 500 to 10 000 cells, and in *Platydorina* (Fig. 5.65(*b*)) with flattened colonies.

The most highly evolved volvocacean genus is *Volvox*, both in its morphological complexity and in its complex oogamous sexual reproduction. Colonies of *Volvox carteri* are oval to spherical with 2000 to 6000 cells arranged in a single layer (Figs. 5.68, 5.69). Each colony contains a large number of somatic cells and a smaller number of reproductive cells. The protoplast of each somatic cell is typically chlamydomonad and has a single cup-shaped nucleus with a basal

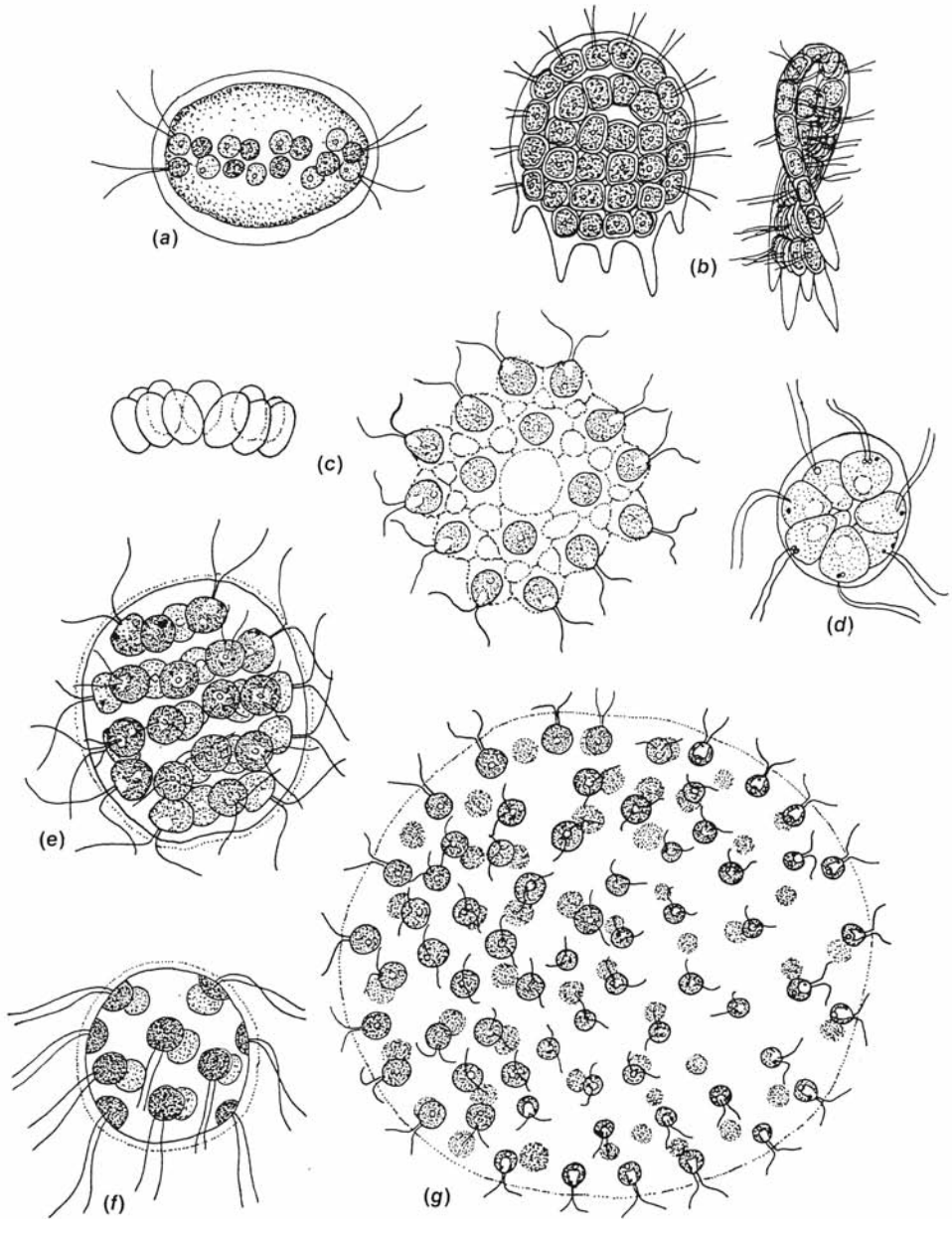


Fig. 5.65 Colonial Volvocales. (*a*) *Stephanoon askenasyi.* (*b*) Front and side views of *Platydorina caudata.* (*c*) Side and front views of *Gonium* sp. (*d*) *Pandorina morum.* (e) *Eudorina unicocca.* (*f*) *Volvulina steinii.* (*g*) *Pleodorina* sp. ((*a*),(*d*) after Huber-Pestalozzi, 1961.)

pyrenoid, an anterior eyespot, a central nucleus, two contractile vacuoles, and two flagella (Fig. 5.2). Daughter colonies are enclosed in vesicles that expand into the interior of the colony.

Vegetative, female, and male colonies of *V. carteri* have similar somatic structure, but each contains a different type of reproductive cell. Vegetative colonies contain cells (gonidia) that give rise to daughter colonies by repeated division; female colonies have eggs, which form zygotes after fertilization; and male colonies contain male initial cells, which divide to form sperm bundles. Female and male colonies develop from gonidia as well as the vegetative colonies.

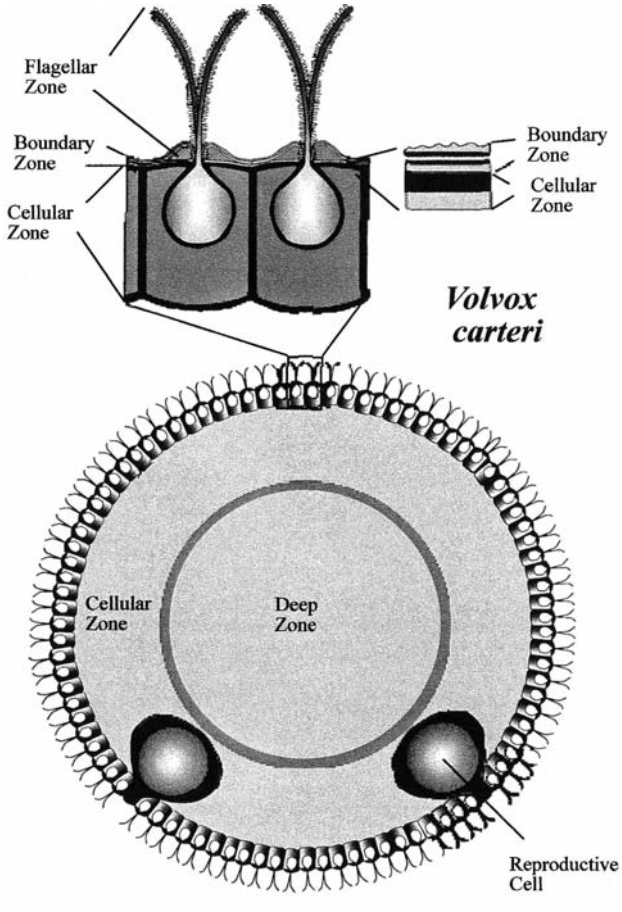


Fig. 5.66 The extracellular matrix comprises more than 95% of a colony of *Volvox carteri* and is divided into four zones: (1) flagellar, (2) boundary, (3) cellular, and (4) deep. (Modified from Hallman, 2003.)

Asexual reproduction occurs in *Volvox* as follows. Each young asexual adult colony of *Volvox carteri* consists of about 2000 small biflagellate somatic cells embedded in the surface and 16 large **gonidia** (asexual reproductive cells) (Fig. 5.69), which are positioned slightly below the surface of a transparent sphere of extracellular matrix. The biflagellate somatic cells are specialized for motility and phototaxis, are incapable of dividing, and are programmed to die at the end of two asexual reproductive cycles. In contrast, the gonidia are non-motile, specialized for growth and reproduction, and potentially immortal. Asexual reproduction in *Volvox carteri* resembles that of classical metazoan models, such as snails, sea urchins, and nematodes. As such, it has been used as a model for embryogenesis research.

Asexual reproduction is completed in 48 hours (Fig. 5.70) and begins with a series of 11–12 rapid cleavage divisions of the gonidium to produce an embryo, with each cell division preceded by a round of DNA replication. The first five divisions are symmetrical, resulting in an embryo with 32 cells of equal size and shape. At the sixth division, 16 cells in the anterior hemisphere divide asymmetrically, producing large-small sister pairs. Each large cell is a gonidial initial destined to produce a gonidium, whereas the smaller sister cells and each of the symmetrically dividing cells of the posterior hemisphere are somatic initials that will differentiate to mature somatic (vegetative) cells. The gonidal initials divide asymmetrically two or three more times, generating an additional somatic cell at each division. Then the gonidial initials withdraw from the division cycle, whereas the somatic initials continue cleaving until they have completed 11 or 12 division cycles altogether. As a consequence of asymmetric divisions, and a different number of divisions completed, gonidial

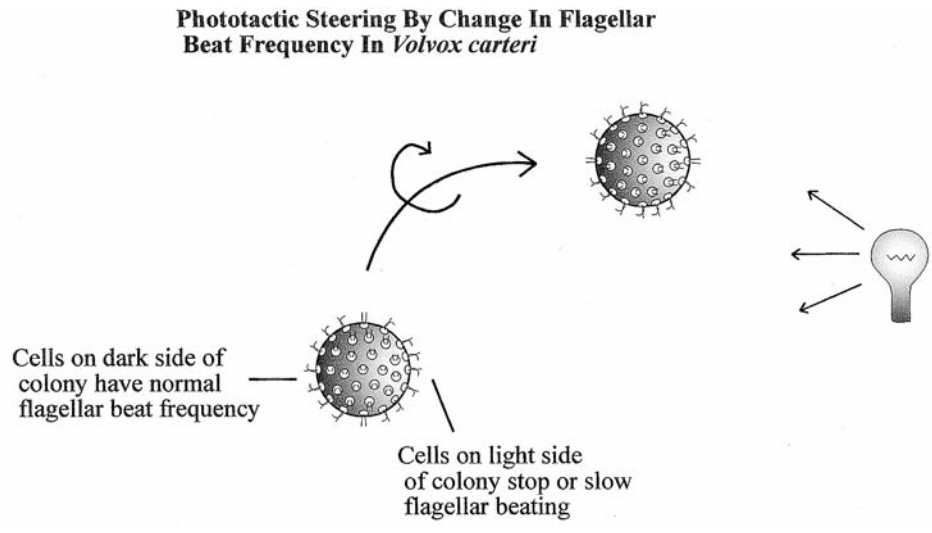


Fig. 5.67 Colonies of *Volvox carteri* swim toward a light source by changing the frequency of the beat of the flagella. (Adapted from Hoops et al., 1999.)

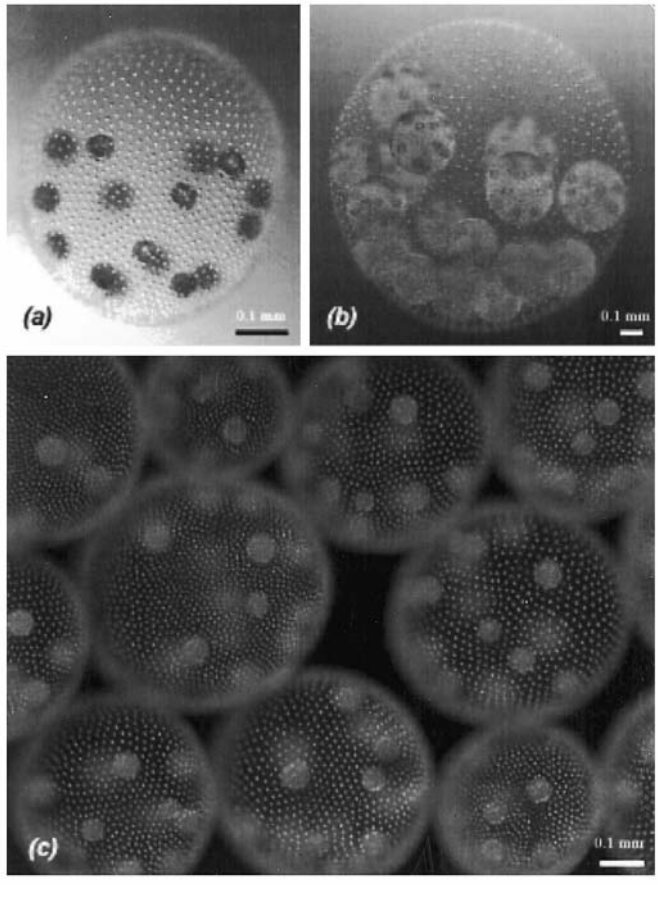


Fig. 5.68 *Volvox carteri.* Asexual individuals. (*a*) Sixteen large asexual reproductive cells are in a colony of ~2000 small biflagellate somatic cells. More than 95% of the volume is composed of extracellular matrix. (*b*) Juvenile colonies within the parent spheroid. Reproductive cells of the next generation are already visible within the juvenile colonies. (*c*) Dark-field image of spheroids with reproductive cells. (From Hallman, 2003.)

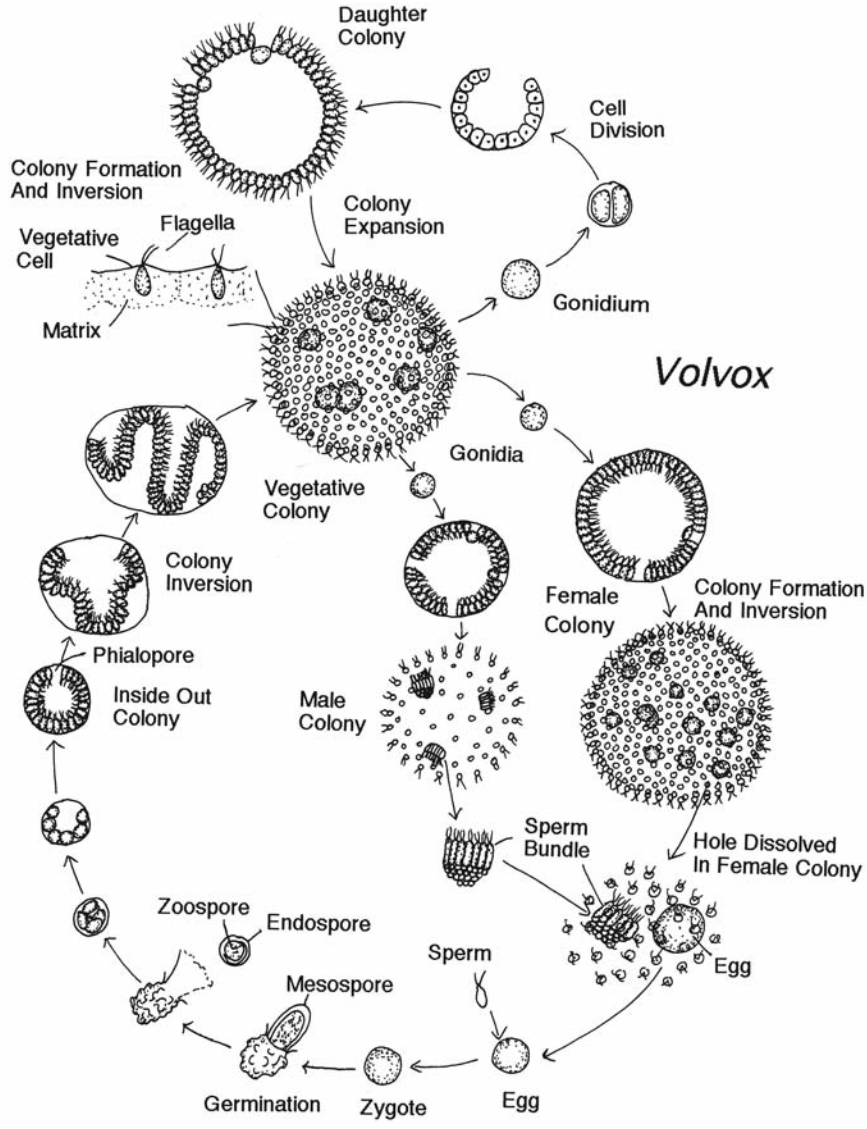


Fig. 5.69 The life history of *Volvox carteri*. (Adapted from Smith, 1944; Kochert, 1968.)

initials are around 30 times the volume of somatic initials at this point. It is the difference in the size of the cells at the end of cleavage, and not a difference in the quality of the cytoplasm, that determines whether the cells will follow the gonidial or somatic pathway of development (Kirk, 1998; Kirk and Nishii, 2001).

There are three categories of genes that control asexual reproduction in *Volvox carteri* (Fig. 5.71) (Kirk, 2001; Schmitt, 2003).

1 *gls* (gonidialess) gene products act in the sixth division in cleaving the embryo to bring about asymmetric division into somatic cells and gonidia. The cleavage plane is determined by the location of the basal body of the flagella. During cell division the flagella are retracted and the basal bodies move under the plasmalemma to the cleavage plane. It is thought the products of the *gls* gene function to position the basal bodies asymmetrically in the cell ensuring that the next cleavage division produces a large and small cell.

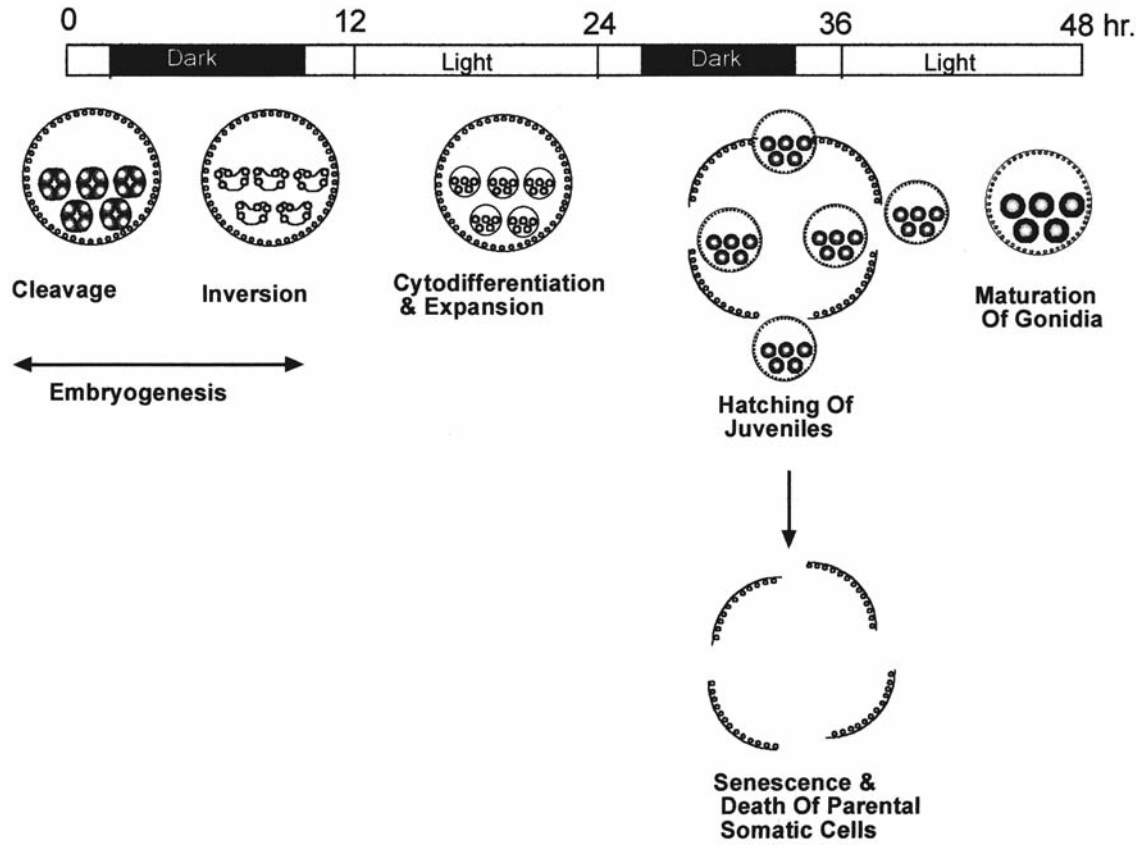


Fig. 5.70 Linear representation of the 48-hour asexual cycle of *Volvox carteri*, as synchronized by a 16:8 hour light:dark regime. (Modified from Stark and Schmitt, 2002.)

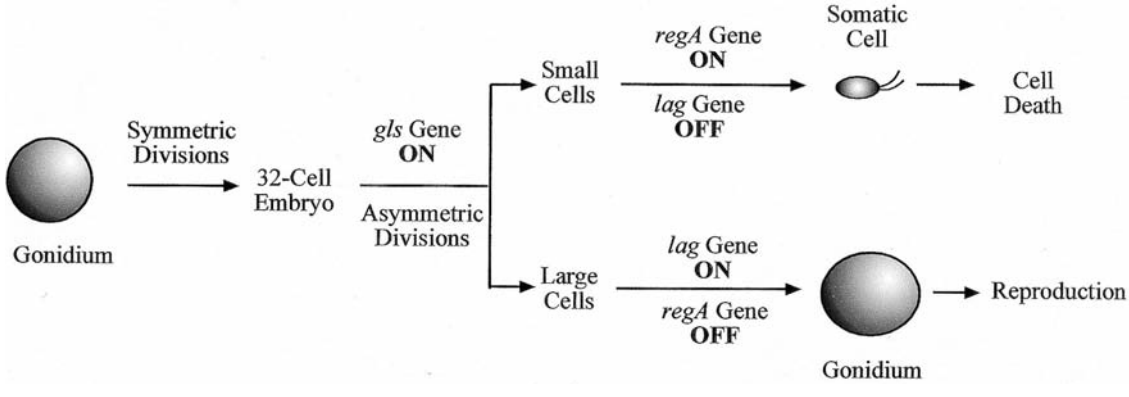


Fig. 5.71 Model of the genetic program controlling the differentiation of somatic and gonidial cell development in *Volvox carteri*.

2 *regA* (**reg**enerator) gene products prevent the development of the small somatic cells into gonidia. The *regA* gene product, RegA, appears early in somatic cell differentiation to direct suppression of reproductive activity (Kirk, 2001; Stark and Schmitt, 2002). RegA is not detectable in embryos or gonidia. The gene *regA* encodes a protein in the nucleus of *V. carteri* cells. The protein arrests the transcription of genes required for chloroplast biogenesis, thereby making it impossible for the photoautotrophic cells to grow enough to reproduce. The minute amounts (0.05%) of the initial gonidial chloroplast that a somatic cell inherits is sufficient to keep it alive and functional until it senesces and dies the fourth day after the first cleavage division.
3 *lag* (**la**te **g**onidia) gene products act in the large pregonidial cells to repress somatic development.

At the end of cleavage, a *V. carteri* embryo contains all of the cells that will be present in an adult, but the embryo is inside out with respect to the adult configuration; the flagellar ends of the somatic cells are all pointing toward the interior and the presumptive gonidia are on the outside. This awkward condition is soon corrected by a morphogenetic rearrangement in which the embryo turns itself right-side out to assume the adult configuration. This process is called "**inversion**", which is unfortunate because "eversion" is a more accurate term. The resemblance of inversion to gastrulation in amphibians has long been noted.

Inversion begins soon after cleavage, when a wave of contraction sweeps over the embryo and a swastika-shaped opening called the **phialopore** appears at the anterior pole of the embryo. Inversion is initiated by cells throughout the colony becoming flask-shaped with thin stalks at their outer ends (Figs. 5.72, 5.73). The cells are connected by a network of cytoplasmic bridges. Incomplete cytokinesis results in each cell linked to its neighbor by a band of about 25 bridges that girdle the equator. Bending of the colony through the phialopore is initiated by the cells moving inward relative to the cytoplasmic bridges. The bridges cannot move because they are part of

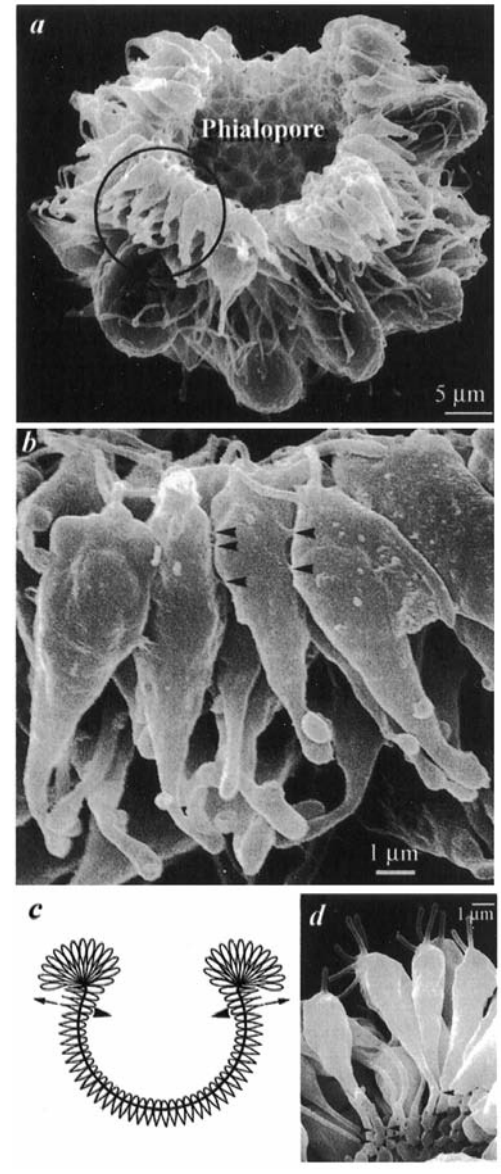


Fig. 5.72 *Volvox carteri*. (*a*) Scanning electron micrograph of a colony beginning to go through the process of inversion. The flask-shaped cells are joined at their base by cytoplasmic bridges. (*b*) Higher magnification of the area circled in (*a*). Arrowheads point to the cytoplasmic bridges. (*c*) Diagram showing how the protoplasm moves towards the base of the cells (arrowheads), elongating the base and moving the cytoplasmic bridges toward the outside of the colony (arrows). The mechanical force generated causes the colony to invert. (d) Scanning electron micrograph of flask-shaped cells in a colony in the latter stages of inversion. The cytoplasmic bridges are now at the apices of the cells (arrowheads). (From Nishii et al., 2003.)

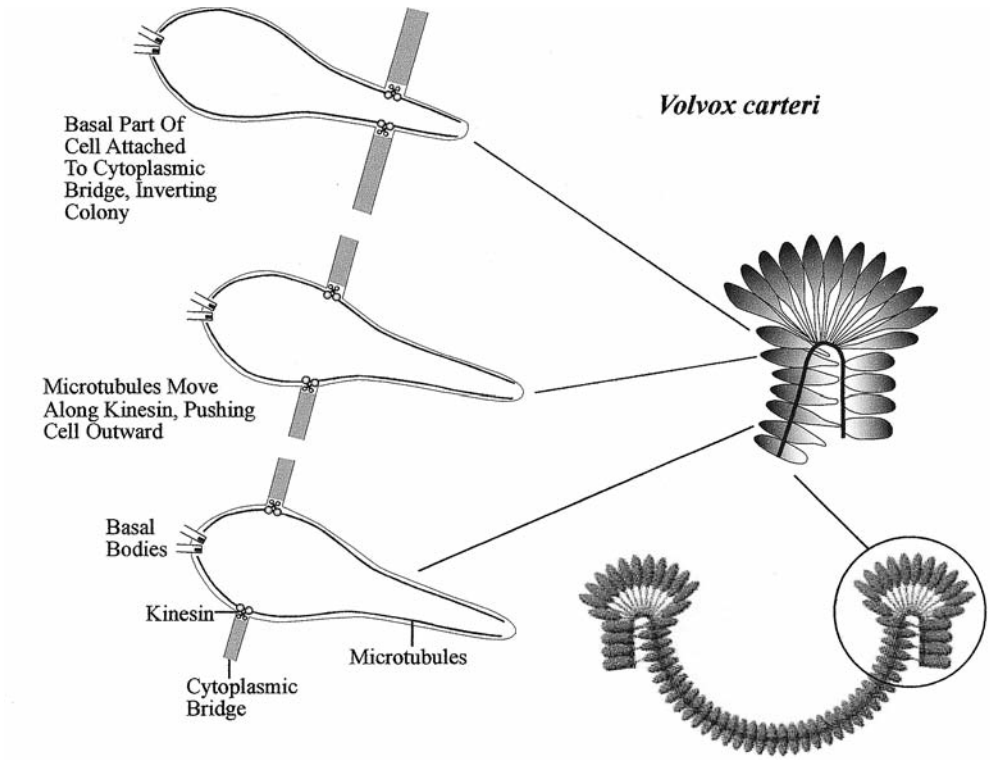


Fig. 5.73 Inversion of a gonidium (embryo) begins when microtubules under the plasmalemma of *Volvox carteri* are drawn apically by kinesin. This brings the whole cell forward, placing forces on the colony, resulting in inversion through the phialopore.

a coherent interconnected network that runs through the entire colony. The inward movement causes the cells to go from being linked to their neighbors at their equator to being linked at their narrow, outermost tips, which in turn forces the cell sheet to bend sharply backward on itself.

Inward movement of the cells relative to the cytoplasmic bridges is caused by the kinesin *invA* interacting with microtubules (Nishii et al., 2003). A **kinesin** is a *mechanochemical protein capable of utilizing chemical energy from ATP hydrolysis to generate mechanical force*. In the presence of ATP, kinesin can bind to and move on microtubules. The *Volvox* cell has a system of peripheral microtubules under the plasmalemma that course in the cytoplasm from the area of the basal bodies to the other side of the cell. The minus (−) end of the microtubules occurs next to the basal bodies while the plus (+) end of the microtubules is at the other end of the cell (Fig. 5.73). Activated kinesin molecules attempt to move toward the plus end of the microtubules. The kinesin, however, is anchored in the cytoplasmic bridge area of the cell so they cannot move. Instead, the kinesin molecules exert a force that causes the microtubules and consequently the entire cell to move upward, resulting in bending of the colony through the phialopore. The bending progresses across the surface of the colony until the colony has turned itself inside out.

At this stage, the cells are held apart by cytoplasmic bridges at their bases. These connections break down in early post-embryogenesis concurrent with the transient production of a hydroxyproline-rich glycoprotein called **ISG** (**inversion-specific glycoprotein**) (Schmitt, 2003). Inversion-specific glycoprotein establishes an extracellular matrix that traps the somatic cells by their flagella (Fig. 5.74), thereby making it impossible for them to change their positioning as their cytoplasmic bridges break down. The inversion-specific glycoprotein also acts as a scaffold for the proper assembly of the rest of the

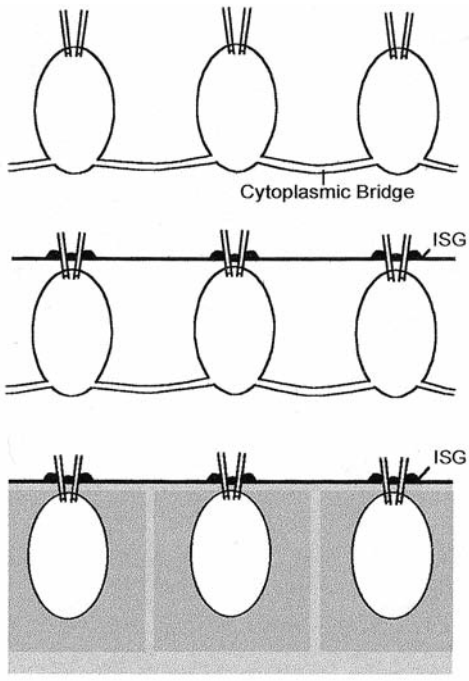


Fig. 5.74 The maintenance of cellular position in *Volvox carteri*.

extracellular matrix (Kirk, 1999; Hallman and Kirk, 2000).

While still contained within the original gonidial wall the daughter colony expands, the gelatinous matrix of the daughter colony forms, and the cells separate from one another. Eyespots develop, and the flagella protrude to their full length. Mature daughter colonies rotate slowly in their vesicles before release through pores in the parent colony matrix over each mature daughter colony (Kochert, 1968). It is possible to synchronize asexual division in *Volvox carteri* with alternating periods of light and dark (Fig. 5.70).

In the formation of female colonies, a gonidium cleaves to form a colony similar to a vegetative colony up to the 16- to 32-cell stage (Fig. 5.69). The next division results in cells larger than the somatic cells, the egg initials, which subsequently develop into eggs. Eggs are flagellated at maturity, but the flagella are not of sufficient length to protrude from the matrix of the colony. The maturation and release of the daughter colony are the same as for the vegetative colony.

Usually in *V. carteri*, male colonies are produced from gonidia that are initially the same size as the vegetative and female colonies, but later do not expand to the same size as these other colonies (Fig. 5.69). These are called dwarf male colonies. Dwarf male colonies are formed from gonidia the same way as the vegetative colonies up to the 32- to 64-cell stage. The next division results in larger cells, the male initials, scattered over the surface of the daughter colony. The dwarf male matures similarly to the vegetative cell except that the male colony does not expand as much. Before release of the dwarf male colony from the parent colony, the male initial divides to form a bowl-shaped mass of 64 to 128 cells that undergoes partial inversion to form a sperm bundle which is convex on one side. Each sperm has two flagella and an eyespot. Release of sperm bundles from the dwarf male colonies occurs through individual escape pores after the dwarf male colonies have been released from the parent colonies.

Strains of *V. carteri* are normally heterothallic (male and female colonies are formed in separate parent colonies). In sexual reproduction, the sperm bundles are released from the male colony and swim in the medium. If the sperm bundles come in contact with vegetative colonies, they swim over the surface of the colony with the flagella in contact with the surface. They soon swim off, however. When the sperm bundle comes in contact with a female colony, the flagella of the sperm bundle and the flagella of the female somatic cells bind, causing the sperm bundle to stick to the female colony (Coggin et al., 1979). A fertilization pore is dissolved in the sheath of the female colony, probably by secretion of a proteolytic enzyme (Hutt and Kochert, 1971). A few somatic cells are usually dissolved out of the female colony and swim off. The sperm bundle breaks down into individual sperm, which move in an amoeboid fashion between the somatic cells of the colony or swim with a corkscrew motion through the watery material in the interior of the colony. The sperm fuse with the eggs, forming zygotes that enlarge, develop an orange coloration, and secrete a thick crenulate wall. The parent female colony persists for some time, but eventually it dissociates and releases the zygotes.

After a resting period, the zygote germinates by splitting the outer zygote wall, with the middle layer of the wall (mesospore) protruding through the fissure in the outer layer. The protoplast has two flagella that beat weakly in the watery interior of the mesospore. After the zoospore is released from the outer zygote wall, the mesospore wall breaks down, leaving the protoplast inside the endospore wall. This protoplast then behaves similarly to a gonidial protoplast and divides to form a young colony of approximately 1000 somatic cells with four gonidia in a single tier.

Sexual type is inherited in a 1:1 ratio, and there is no parthenogenetic development of the eggs.

In *Volvox carteri*, the males make and accumulate a sexual inducer that is a 30-kilodalton glycoprotein (Starr and Jaenicke, 1974). The sexual inducer is released when the sperm are released from the sperm packets. The inducer is effective at 6×10^{-17} M. One sexual male releases enough inducer to convert all the related males and females in a volume of 1000 liters from asexual to sexual reproduction. Under the moderate growth conditions present in a large stable body of water, it is normally only the males that produce the sexual inducer. However, it is possible to force asexual males and females to make the inducer by subjugating the cells to a high temperature for a period of time. One hour at 42.5 °C is a sufficient heat shock to induce the formation of sexuality in *V. carteri* asexual males and females. Without the sexual inducer, the asexual males and females will produce asexual gonidia. In the presence of sexual inducer, the males and females produce sperm packets and eggs, respectively. The heat shock response is an adaptation to life in shallow temporary bodies of water where *Volvox* is often found. In the spring, in such bodies of water there is abundant water and the temperature is relatively low. *Volvox* grows asexually under these conditions. As summer progresses, the temperature in these bodies of water rises, and the organisms begin to dry out. The increase in temperature shocks the *Volvox* into producing the sexual inducer and initiating sexual reproduction. This results in the formation of drought-resistant zygospores, which survive the dry conditions and serve as an overwintering spore. The above-described research by Kirk and Kirk (1986) (Fig. 5.75) has provided an explanation for Powers's (1908) observation that he had great difficulty finding sexual *Volvox* in large bodies of water. Powers further noted that "in the full blaze of Nebraska sunlight, *Volvox* is able to appear, multiply and riot in sexual reproduction in pools of rainwater of scarcely a fortnight duration." It took another 80 years for Kirk and Kirk to discover the heat-shock phenomenon and to explain Powers's observations.

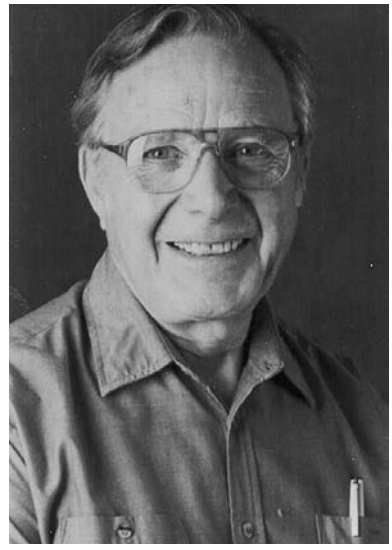


Fig. 5.75 **David Kirk** Born 1934 in Clinton, Massachusetts. He obtained his B.Sc. from Northeastern University in 1956 and his Ph.D. from the University of Wisconsin in 1962. From 1962 to 1969 he was at the University of Chicago, eventually becoming Associate Professor. In 1969 he joined the faculty in the Department of Biology at Washington University in St. Louis where he is a tenured professor. Dr. Kirk has been a leading researcher in the cell biology of *Volvox*.

Tetrasporales

These algae have immobile vegetative cells that are capable of cell division, unlike those in the Chlorellales or Volvocales. The colonies are non-filamentous, and flagellated cells are formed by many genera. Asexual reproduction occurs via the formation of zoospores, aplanospores, or akinetes. Sexual reproduction is isogamous, by

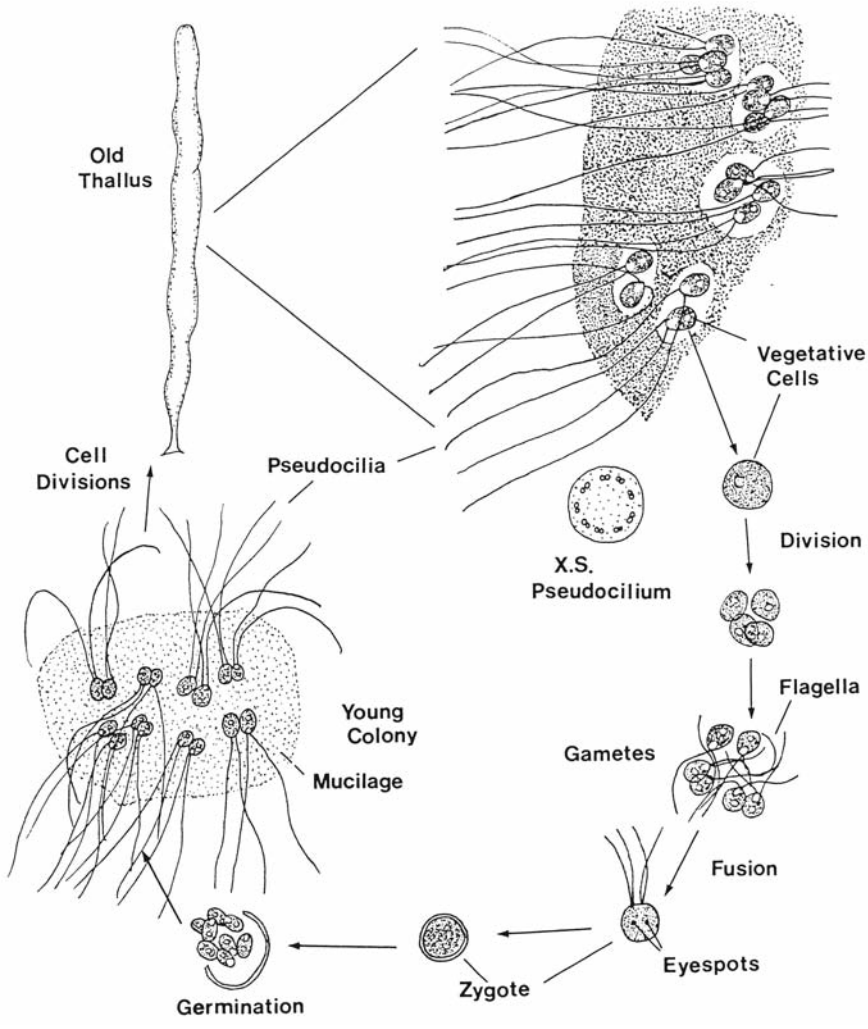


Fig. 5.76 The life cycle of *Tetraspora gelatinosa*. (Adapted from Klyver, 1929.)

fusion of biflagellate gametes. Almost all the organisms are freshwater.

Conventional wisdom has stated that the Tetrasporales evolved from the Volvocales by loss of motility in the vegetative condition. However, data from small subunit ribosomal DNA indicate the line leading to the Tetrasporales is more primitive than the line leading to the Volvocales (Booton et al., 1998).

Two families will be considered here:

Family 1 Tetrasporaceae: cells with pseudocilia.
Family 2 Palmellaceae: cells without pseudocilia.

Tetrasporaceae

The elongated gelatinous thalli of the Tetrasporaceae have vegetative cells in groups of two to four, with each cell having two pseudocilia. **Pseudocilia** are longer than flagella but are evidently related to them because the pseudocilia have a normal basal body but an abnormal $9+0$ configuration of microtubules near the base of the pseudocilia (Lembi and Herndon, 1966; Wujek, 1968). The number of microtubules lessens and becomes more irregular as the end of the pseudocilium is approached.

Colonies of *Tetraspora gelatinosa* (Fig. 5.76) are green, amorphous masses with an outer layer of vegetative cells (Klyver, 1929). They are found in quiet freshwater and can be attached or

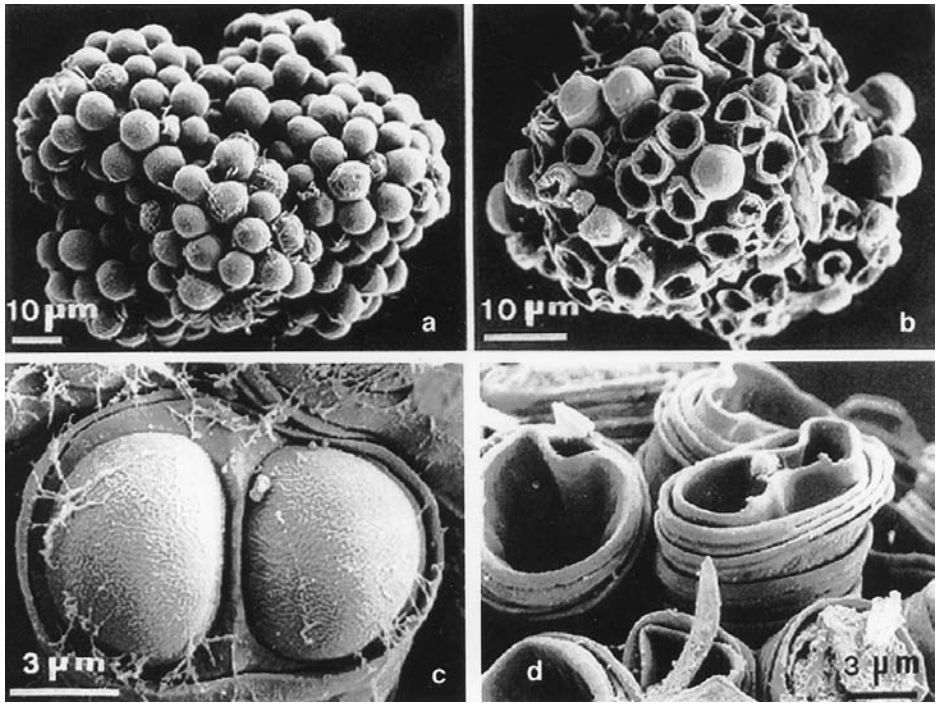


Fig. 5.77 Scanning electron micrographs of *Botryococcus braunii*. (*a*) Colony from the wild. (*b*) Colony showing the cup-shaped mucilaginous bases. (*c*) Two cells in mucilaginous bases. (*d*) Mucilaginous base with no cells. (From Plain et al., 1993.)

free-floating. Each cell has a large cup-shaped chloroplast with a central pyrenoid and two pseudocilia. Growth of the thallus results from vegetative division of the cells. In the formation of isogametes, a vegetative cell divides two to three times, resulting in four or eight pyriform gametes, each with an eyespot and a cup-shaped chloroplast. The biflagellate gametes break free from the colonial mucilage and fuse with each other at their anterior ends. The quadriflagellate zygote swims for a while before settling, retracting its flagella, and forming a cell wall. The zygote germinates, forming four or eight aplanospores without pseudocilia. These aplanospores enlarge, and when they have reached the size of vegetative cells, they divide to form daughter cells that have pseudocilia. The aplanospores and their daughter cells are held together by mucilage, and the aggregation makes up the typical thallus of *Tetraspora*.

Palmellaceae

Members of the Palmellaceae have their cells united in small gelatinous colonies that are generally amorphous but may be of definite shape. *Palmella* (Fig. 5.63) is a freshwater alga composed of cells united by a gelatinous matrix forming colonies of indefinite shape. Asexual division involves the formation of zoospores, and sexual reproduction occurs by formation of isogametes.

Botryococcus braunii (Fig. 5.77) is a free-floating colony of indefinite shape within a hyaline or orange envelope. The colonies are composed of radially arranged cells embedded in a tough mucous envelope. It forms water blooms that have been implicated in the death of fish (Chiang et al., 2004). The cells accumulate a large amount of oil in the autumn, which often obscures the cell contents. This alga has been postulated as the cause of the boghead coals (e.g., torbonite) and the oil shales of the Tertiary Period (Blackburn and Temperley, 1936; Cane, 1977; Wolf et al., 1985). If these deposits are examined under a microscope, it is possible to see plant remains that are similar to extant colonies of *B. braunii*. A hydrocarbon derivative exclusively attributable to *Botryococcus* comprises 1.4% of a Sumatran petroleum

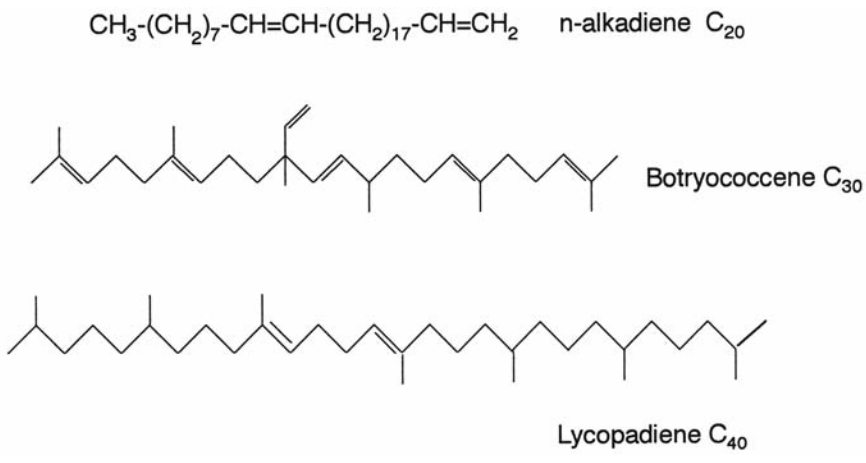


Fig. 5.78 The structure of hydrocarbons isolated from *Botryococcus braunii*. (Modified from Metzger et al., 1990.)

(Moldowan and Seifert, 1980). The cultivation of the alga has been proposed as a renewable source of liquid hydrocarbon fuel (Wake and Hillen, 1980; Yamaguchi, 1997). The resting stage of living *B. braunii* contains up to 70% of its dry weight as alkadienes, botryococcenes or lycopadiene (Fig. 5.78) (Metzger et al., 1990). The hydrocarbons are produced primarily during the exponential and linear growth phases. The dense matrix surrounding the cells is impregnated with the hydrocarbons.

Prasiolales

The Prasiolales and the following two orders, the Chlorellales and the Trebouxiales, are closely related and sometimes placed in a separate class, the Trebouxiophyceae (Sherwood et al., 2000; Lewis and McCourt, 2004).

The members of the order are characterized by a stellate chloroplast with a central pyrenoid. These algae occur in a large variety of habitats, including freshwater, marine, and terrestrial habitats (such as concrete walls, rocks, and tree bark (Rindi and Guiry, 2003)). The principal genus, *Prasiola*, has a unique type of life history, with meiotic divisions in mature sexual thalli resulting in a haploid apex and diploid base.

Prasiola stipitata consists of small, thin, broadly ovate blades appearing as dirty green patches at or above high-tide level, commonly in the spray zone or areas fouled by bird excrement. The cells have a central stellate chloroplast. The diploid thalli can form either diploid spores or haploid gametes (Fig. 5.79), the spore-forming plants growing higher on the shore than the sexual gamete-forming plants (Friedmann, 1959; Friedmann and Manton, 1959).

In the formation of the diploid aplanospore, the vegetative cells in the upper part of the thallus divide, making the upper part of the thallus multilayered. Each cell in this area forms a non-flagellated spore that settles, germinates, and develops into a new diploid plant like the parent (Fig. 5.80).

In the production of gametes, the cells in the upper part of a diploid thallus undergo meiosis, with the subsequent division of the haploid cells resulting in a multilayered upper part of the thallus. The haploid tissue is divided into a patchwork of rectangular darker and lighter areas containing the male and female cells, respectively. The difference in shading is due to the difference in size of the chloroplasts, the larger female cells having the larger chloroplasts. The gametes are liberated after the thalli are wet by the incoming tide. More male gametes are released because of their smaller size and greater production per unit area. The anteriorly biflagellate male gametes swim around the non-motile egg, and one of the male flagella touches the egg. The flagellum fuses with the egg, a step followed by fusion of the bodies of the gametes. The pear-shaped zygote swims vigorously by means of the posteriorly directed remaining male flagellum. At 5 °C, the

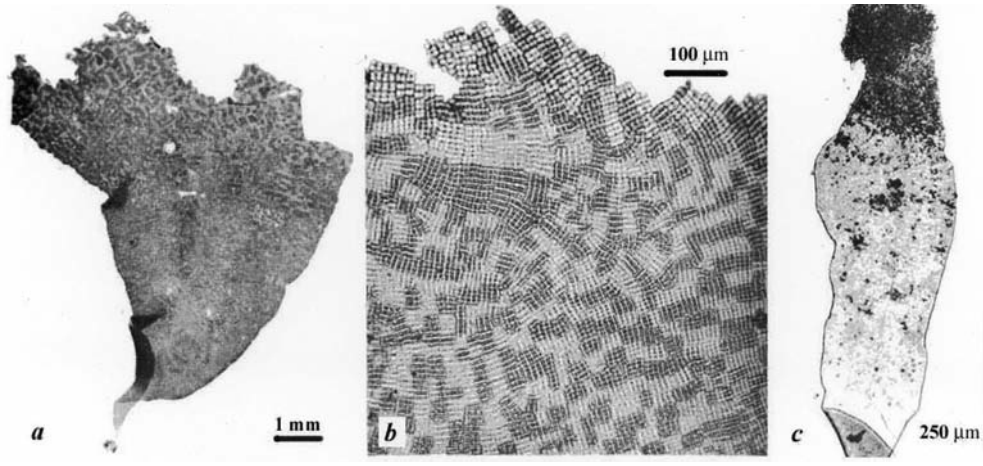


Fig. 5.79 *Prasiola stipitata*. (*a*) Sporophyte producing male and female gametes. (*b*) Apical part of sporophyte thallus with male (dark areas) and female (light areas) gametes. (*c*) Sporophyte producing spores from the apical part of the thallus. (From Friedmann, 1959.)

zygote swims for several hours, retracts the flagellum, sinks, attaches firmly to the substratum, and develops a cell wall. The zygotes germinate into diploid thalli, completing the life cycle (Friedmann, 1959).

Chlorellales

In this order are the algae that have a non-motile vegetative thallus where the thallus comprises only a single cell or a coenobium composed of a definite number of cells arranged in a specific manner. Asexual reproduction occurs by zoospores or aplanospores that are commonly autospores. These autospores are probably no more than daughter cells of the parent thallus. Sexual reproduction can be isogamous, anisogamous, or oogamous. The order is exclusively freshwater.

Chlorococcum (Fig. 5.81) is an alga frequently isolated from beneath the surface of the soil. It sometimes occurs in abundance on damp soil or brickwork. The cells can survive for a long time in the soil. In one study they grew after being in desiccated soil for 59 years (Trainor, 1970). The cells of the same species vary considerably in size, young cells having a thin cell wall and older cells a thick one. The chloroplast in young cells is a massive parietal cup with a single pyrenoid. In older cells the chloroplast becomes diffuse. Asexual reproduction is by zoospores, there never being any vegetative division. The biflagellate zoospores have a cup-shaped chloroplast and an eyespot. Sexual reproduction occurs by the formation of isogametes. Under certain conditions, aplanospores can be produced, which eventually liberate two to four biflagellate gametes. Nearly dormant cells of *Chlorococcum echinozygotum* that have been deprived of nitrogen can be induced to undergo gametogenesis by being placed in fresh medium in darkness without nitrogen (O'Kelley, 1984). If nitrogen is supplied 6 hours after the cells are placed in darkness, zoosporogenesis occurs instead of gametogenesis.

Hydrodictyon reticulatum (Fig. 5.82), or the water net, is a free-floating, relatively rare freshwater alga that forms colonies that are net-like with polygonal or hexagonal meshes. The net is formed by multinucleate elongated cells joined end to end, probably by lectins such as concanavalin A (Hatano and Ueda, 2000). Each cell has a large central vacuole and a reticulate chloroplast with pyrenoids. In asexual reproduction a daughter net is produced inside, and subsequently released from, the parent cell (Pocock, 1960; Marchant and Pickett-Heaps, 1971, 1972a–d). Asexual reproduction begins with the disappearance of pyrenoids, coinciding with the accumulation of starch grains in the fragmenting chloroplasts. Regularly spaced nuclei are surrounded by fragments of chloroplasts. A vesicle forms around and outside of the tonoplast, restricting most of the proto-

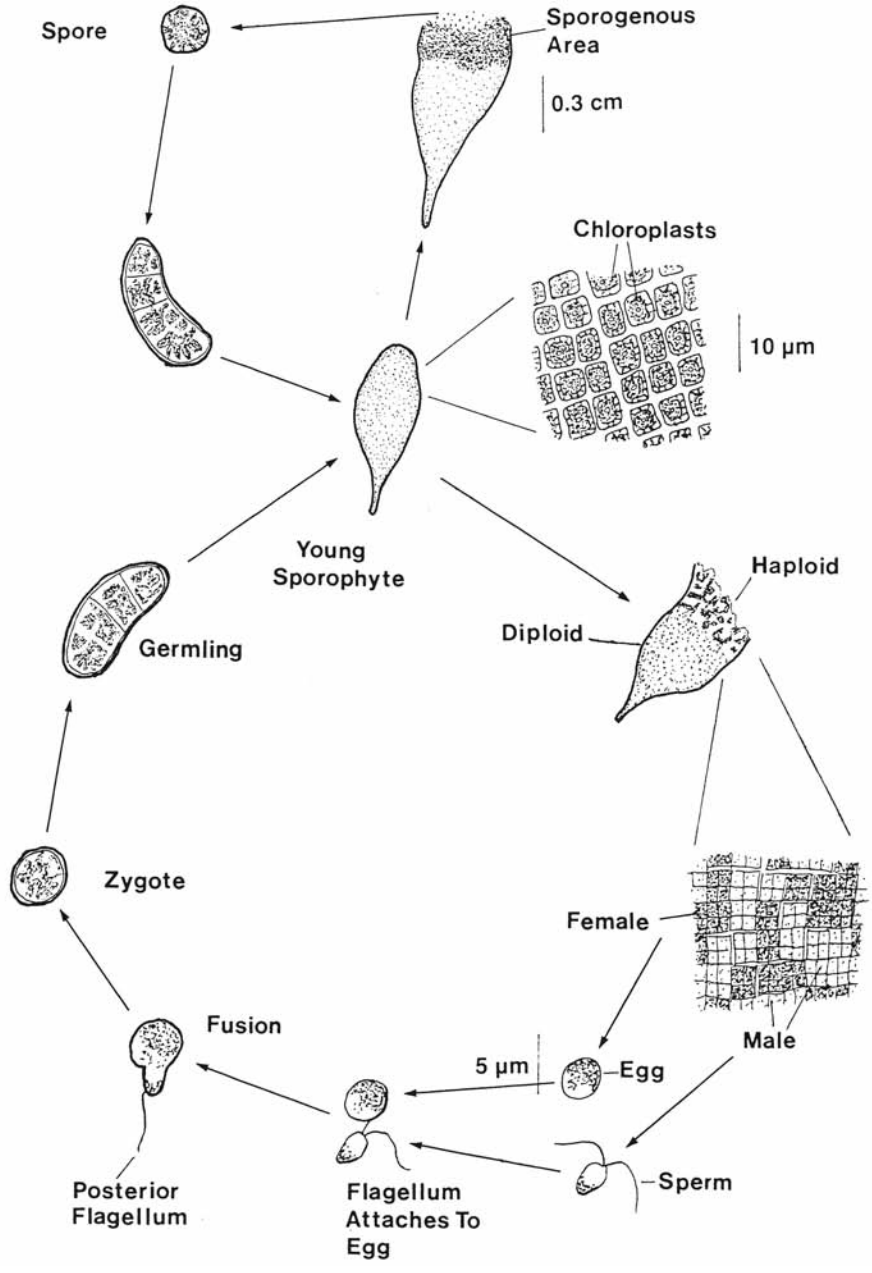


Fig. 5.80 The life cycle of *Prasiola stipitata*. (Adapted from Friedmann, 1959.)

plasm to a small area around the periphery of the cell. The protoplasm divides to produce uninucleate, biflagellate zoospores that actively swim about inside the parent cell. The zoospores stop swimming, become joined in certain areas, and retract their flagella. A daughter net has now been formed within the parent cell, which is released to enlarge to a mature colony.

Chlorella cells are spherical with a cup-shaped chloroplast (Fig. 5.83). The only method of reproduction is by daughter cells that resemble the parent cell. *Chlorella* often forms intracellular symbioses with aquatic invertebrates and protozoa (such as *Paramecium*). In these symbioses, *Chlorella* is held in host vacuoles where the

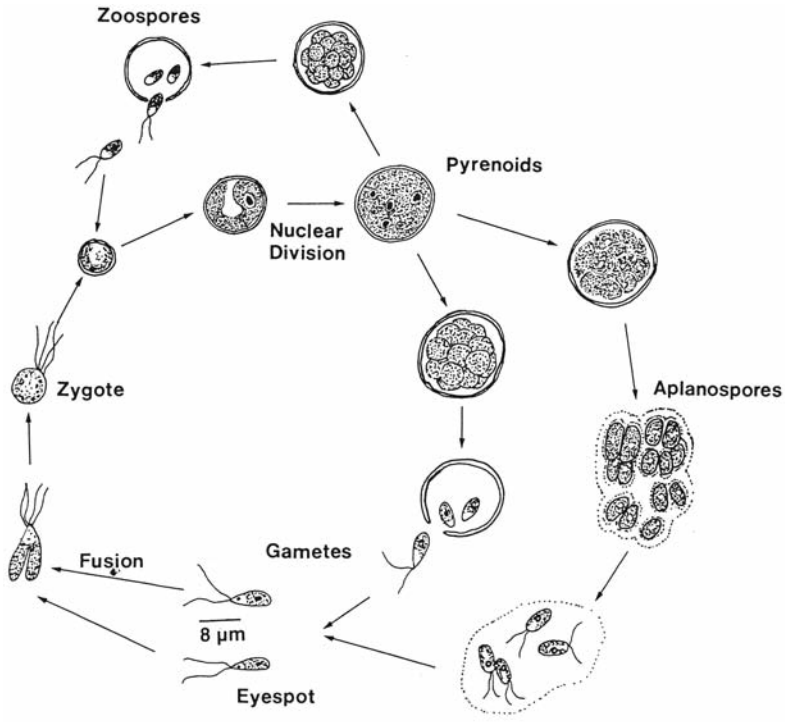


Fig. 5.81 The life cycle of *Chlorococcum humicola*. (Adapted from Bristol, 1919.)

Chlorella synthesizes and releases maltose into the host vacuole. *Chlorella* is held at a low pH in the host vacuoles. Studies on isolated *Chlorella* cells have shown that maximum synthesis and release of maltose occurs at pH 4–5 (Dorling et al., 1997).

Prototheca lacks chlorophyll and resembles a colorless *Chlorella* although the *Prototheca* cells do have starch-containing amyloplasts (Webster et al., 1968). *Prototheca* causes **protothecosis** in animals and humans. This disease is more common than is supposed, but because the small round colorless cells resemble yeasts, the disease, at least in animals, is often incorrectly diagnosed. *Prototheca* cells are fairly common in the soil, where they presumably live by digesting organic matter, and it is from here that most infections occur. In animals most of the reported cases have been severe systemic infections, such as massive invasion of the bloodstream, that have resulted in the death of the animal within a short time (van Kruiningen et al., 1969). Such massive infections have been reported in humans but usually only as secondary invaders after the primary invader has seriously lowered the body's defenses. More common in humans is the subcutaneous type of infection that starts initially as a small lesion and spreads slowly through the lymph glands, covering large areas of the body and preventing the sufferer from performing normal work duties (Fig. 5.84) (Mars et al., 1971).

Scenedesmus is a common alga (Fig. 5.83), often occurring as almost a pure culture in plankton. Cells in the colony occur in multiples of two, with four or eight cells being most common. The species differ mostly in the number and type of spines on the cells and the texture of the wall. The uninucleate cells have a single laminate chloroplast. The morphology of the colony can be varied considerably by varying the medium in which the cells are growing (Egan and Trainor, 1989). In a medium with low phosphorus or low salt concentration, the *Scenedesmus* is induced to grow as unicells, resembling the genera *Chodatella* and *Franceia* (Trainor, 1992) and the same species can also be induced to grow with or without spines. Composed of aggregated proteinaceous tubules, the spines probably aid in the flotation of the colonies (Staehelin and Pickett-Heaps, 1975). *Scenedesmus* occasionally forms zoospores when deprived of nitrogen (Trainor, 1963).

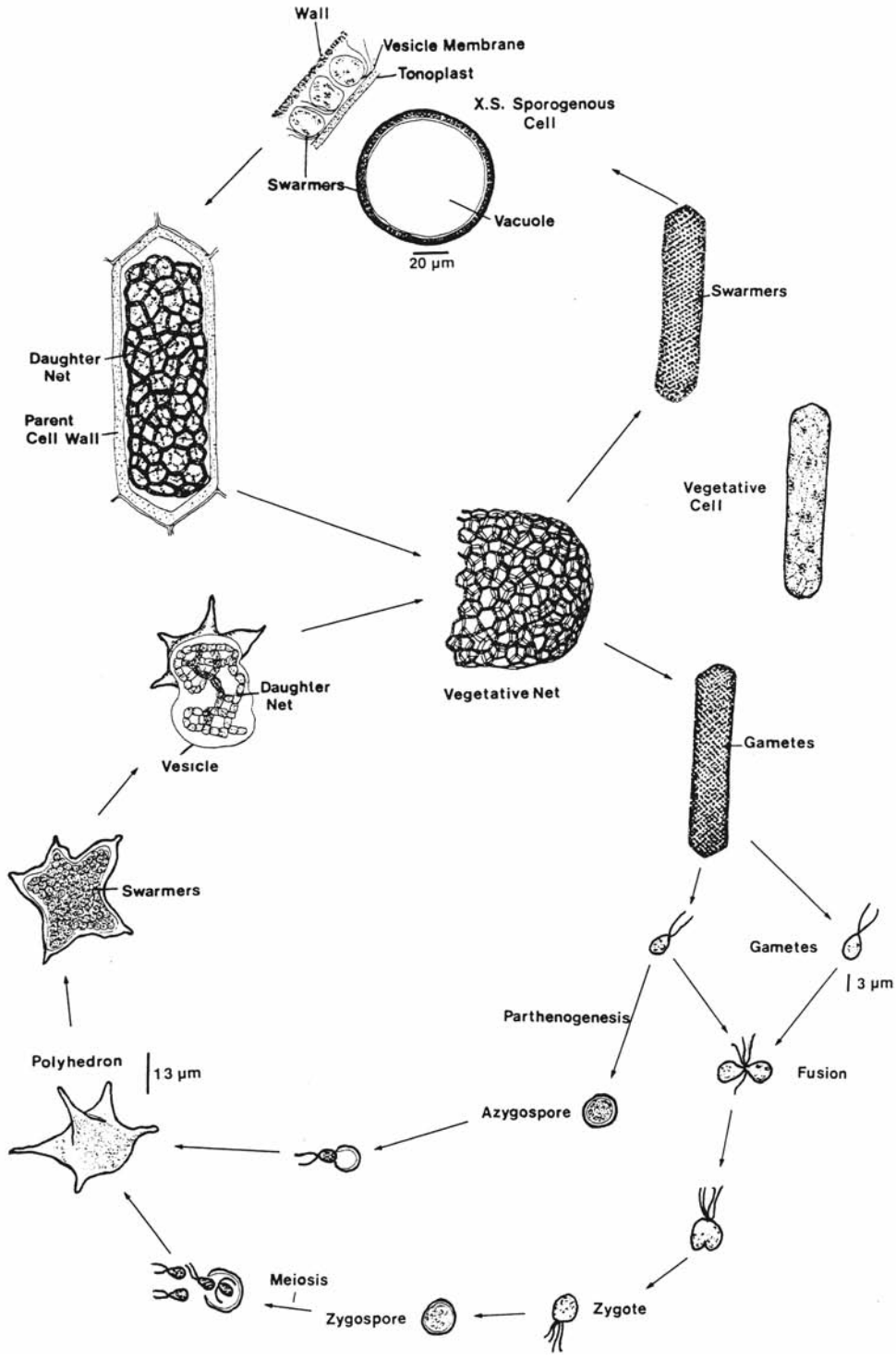


Fig. 5.82 The life cycle of *Hydrodictyon reticulatum*. (Adapted from Pocock, 1960; Marchant and Pickett-Heaps, 1971, 1972a–d.)

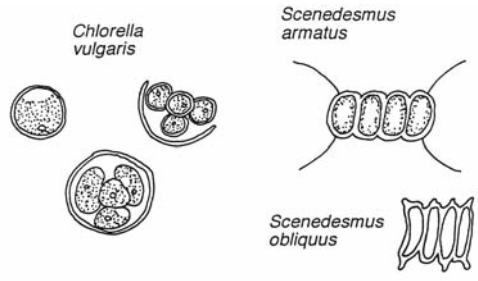


Fig. 5.83 Drawing of *Chlorella vulgaris* (with autospores), *Scenedesmus armatus*, and *S. obliquus*.

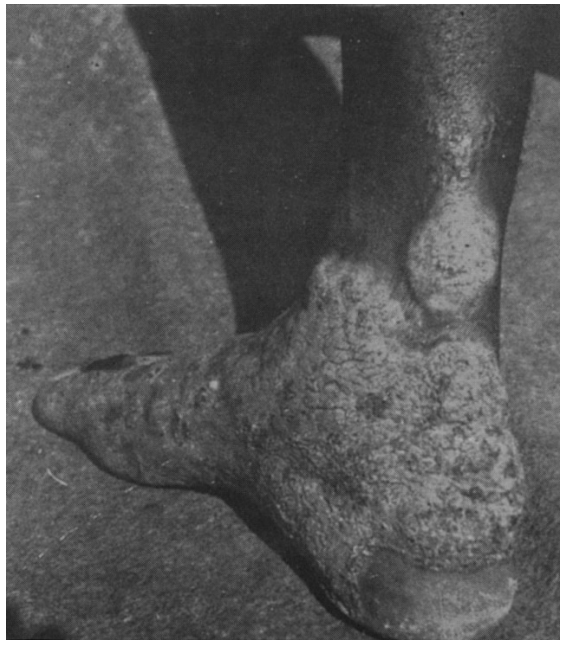


Fig. 5.84 Lesions of protothecosis on the foot and lower leg of a man from Sierra Leone. (From Davies and Wilkinson, 1967.)

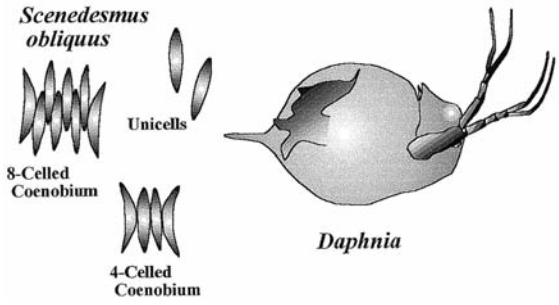


Fig. 5.85 *Scenedesmus obliquus* without grazers occurs primarily as unicells. When grazers such as *Daphnia* are present, *S. obliquus* grows primarily as coenobial colonies.

Many species of *Scenedesmus* grow as unicells in an environment without grazers. In the presence of grazers, such as *Daphnia* (Fig. 5.85), *Scenedesmus* forms multicellular colonies that are not grazed as heavily. **Infochemicals** produced by the grazers induce the formation of coenobia. *Infochemicals are chemicals that, in the natural context, convey information in an interaction between two organisms, evoking a behavioral or physiological response in the receiving organism, which is adaptively favorable to one or both organisms in the interaction.* In the case of *Scenedesmus*, the infochemicals originate from the digestive tract of the grazer. Starved grazers do not produce infochemicals. In the multicellular state, *Scenedesmus* is not grazed as heavily by *Daphnia*. However, the advantages to *Scenedesmus* in the unicellular state include smaller sinking velocity and advantageous surface to volume ratio in terms of nutrient uptake and light harvesting (Lurling, 1998, 1999).

Unicellular green algae, such as *Chlorella*, have been extensively investigated as possible new sources of food for an increasing world population (Yamaguchi, 1997). *Chlorella* produces little cellulose or other carbohydrate wall material; thus more of the cell is digestible in *Chlorella* than in an alga with a large amount of cellulose. Exponentially growing *Chlorella* cells contain about 50% protein, 5% chlorophyll, and a large number of vitamins. Much greater quantities of biomass can be obtained per unit area with algae than with higher plants. When the growth of algae is linked to the purification of sewage in oxidation ponds, yields of 112 000 kg hectare^{-1} year^{-1} of dried algae can be obtained. At the same time, the algae are taking up elements such as nitrogen and phosphorus, and reducing the biological oxygen demand (an indication of the organic material in the water) by 85% (McGarry and Tongkasame, 1971). The algae obtained make a very good stock feed, and attempts have been made to utilize it as human food, although the algae in the human digestive tract lead to undesirable intestinal floras that often result in gas in the intestine. A second line of investigation in this

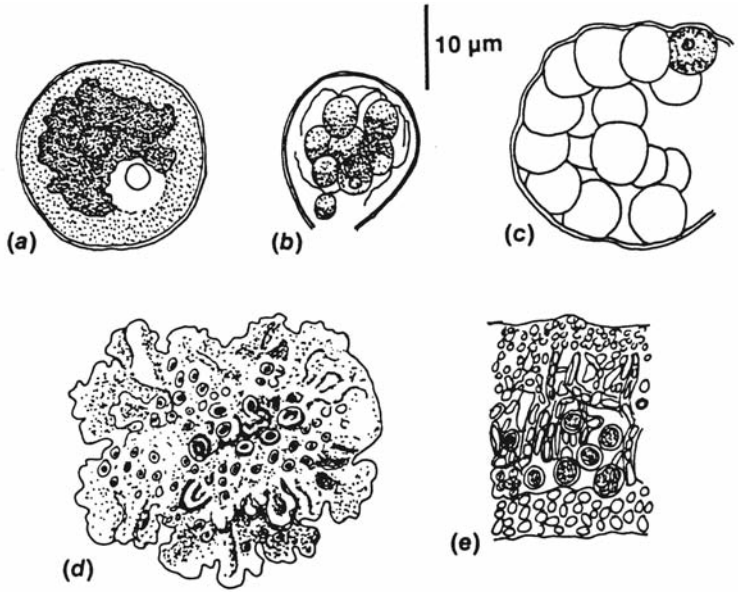


Fig. 5.86 *Trebouxia* sp.: (*a*) vegetative cell; (*b*) zoospores being released; (*c*) aplanospores being released. The *Trebouxia*-containing lichen *Xanthoria parietina*; (*d*) whole thallus; (e) section of thallus showing spherical *Trebouxia* cells. ((*a*)–(*c*) after Ahmadjian, 1960; (*d*),(e) after Fünfstück, 1907.)

area has been to provide food and oxygen for space and submarine travel. In such a setup, carbon dioxide from human respiration is taken up for use in photosynthesis, with the oxygen produced being respired by humans. A man uses about 600 liters of oxygen daily, and a gas exchange unit that would produce this amount of oxygen would also produce almost enough biomass to provide sufficient food for one man as well (Fogg, 1971).

Trebouxiales

This order represents the "lichen algae group" (Lewis and McCourt, 2004). Note that not all lichenized algae are in this group: other **phycobionts** (algal partner in a lichen symbiosis, the fungus is the **mycobiont**) include cyanobacteria, *Trentepholia* (Ulvophyceae), and *Heterococcus* (Xanthophyceae).

Trebouxia (Figs. 5.86, 5.87) is the most common green alga as a phycobiont in a lichen symbiosis. The genus also is found as a free-living alga, and, when free-living, it is usually twice the size of the alga in the lichen symbiosis (see Ahmadjian, 1993, for a review). *Trebouxia* has a massive chloroplast with a single pyrenoid. When it is growing in the lichen association, reproduction is normally by autospores, although under wet conditions zoospores may be formed. When the alga is grown in liquid culture, zoospores are formed. Sexual reproduction is isogamous or anisogamous by the fusion of biflagellate gametes. Lichenized *Trebouxia* produces primarily sugar alcohols (80% ribitol) from photosynthetic processes, whereas free-living *Trebouxia* forms much smaller amounts of sugar alcohols (15% ribitol) and greater quantities of other carbohydrates (Green, 1970). Richardson (1973) has summarized the differences between algae growing as phycobionts (algae in the lichen association) and the free-living ones: the free-living algae (1) synthesize less sugar or sugar alcohol, (2) form more polysaccharides, (3) develop cell sheaths not seen in phycobionts, and (4) release less photosynthate into the surrounding medium. *Trebouxia* is able to grow saprophytically in the dark in the absence of light (Ahmadjian, 1960).

Lichen mycobionts are able to discriminate between suitable and unsuitable algal partners. The mycobiont *Xanthoria parietina* secretes a protein that will bind only to the cell walls of species of *Trebouxia* and *Pseudotrebouxia*, algal genera that normally make up this lichen symbiosis (Bubrick and Galun, 1980). The cell walls of these algae are characterized by high levels of acidic polysaccharide and a protein coat on the cell wall surface. Members of other algal families do not bind the lichen protein. In the lichen *Cladonia cristatella*, compatible phycobionts have fungal haustoria in most of the phycobiont cells. Fungal haustoria are usually used by the fungus to transfer nutrients

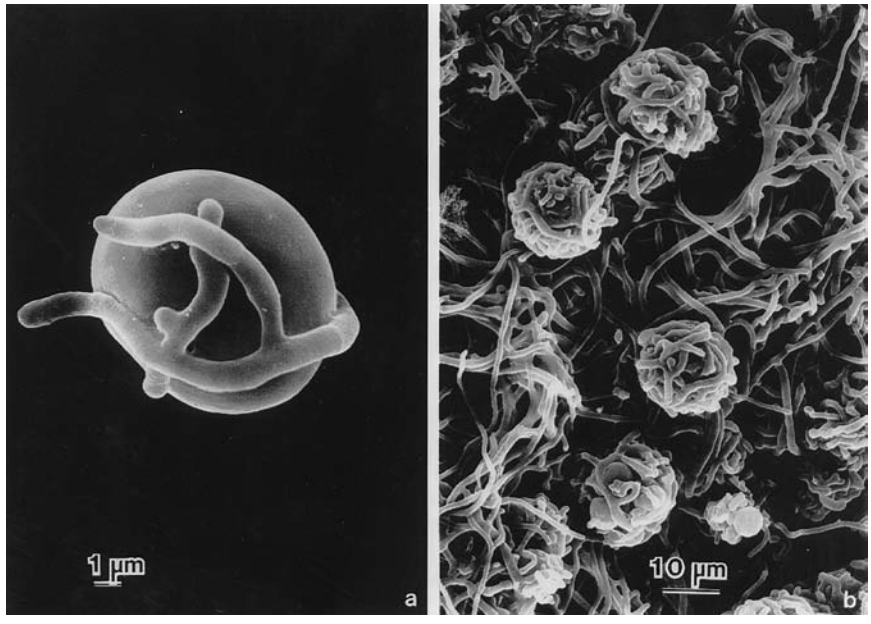


Fig. 5.87 The beginning of a lichen. (*a*) Scanning electron micrograph of the envelopment of a cell of the phycobiont *Trebouxia erici* by the hyphae of the mycobiont *Cladonia cristatella*. (*b*) The mycobiont has completely enveloped the cells of the phycobiont, and the hyphae have formed the thallus of the lichen. (From Ahmadjian and Jacobs, 1981.)

from a host to the fungus when the host is a parasitized organism. However, in lichens, transfer of metabolites to the fungus is minimal (Collins and Farrar, 1978; Hessler and Peveling, 1978). This is probably a case of controlled parasitism (Ahmadjian and Jacobs, 1981).

Sphaeropleales

These filamentous Chlorophyceae have a mature lateral wall that consists of segments, rather than having a continuous structure. In *Microspora*, there are H-shaped wall segments that arise from two separate phases of wall secretion (Fig. 5.88) (Pickett-Heaps, 1973). During interphase, cell expansion is accommodated by the interlocking H-segments moving apart. At the same time, a new cylindrical wall is secreted inside these segments. Then during cytokinesis, the newly formed cross wall turns this cylinder into the typical wall segment. A similar wall occurs in the Oedogoniales, but the algae in the Sphaeropleales lack the unusual structure of the Oedogoniales. The wall structure in the Sphaeropleales is similar to that in the Xanthophyceae, and it is probable that the filaments in both algal groups evolved from a unicellular alga, although independently of each other. The Sphaeropleales probably evolved from an alga in the Chlorellales (Cáceres et al., 1997).

Algae in the Sphaeropleales (Figs. 5.88, 5.89) typically occur in shallow freshwater habitats that are inundated only periodically. The ephemeral vegetative stage (often lasting a few weeks or less) occurs during short intervals of flooding, whereas the thick-walled, resistant zygotes persist in the soil through long dry periods, thereby enabling long-term survival of these algae. The zygotes are ornamented and sometimes have **cirri** (Fig. 5.90), curled appendages composed of organic material, on their surface (Hoffman and Buchheim, 1989).

Sphaeroplea has multinucleate cells arranged end to end in unbranched filaments (Buchheim et al., 2001) (Fig. 5.89). The alga is freshwater, occurring on periodically wet ground, completing its life cycle within 4 to 5 weeks. Within a cell the cytoplasm is restricted to a number of transverse bands, each band separated by a vacuole. Each cytoplasmic band has several nuclei and a band-shaped chloroplast with several pyrenoids, or numerous discoid chloroplasts. There is also a

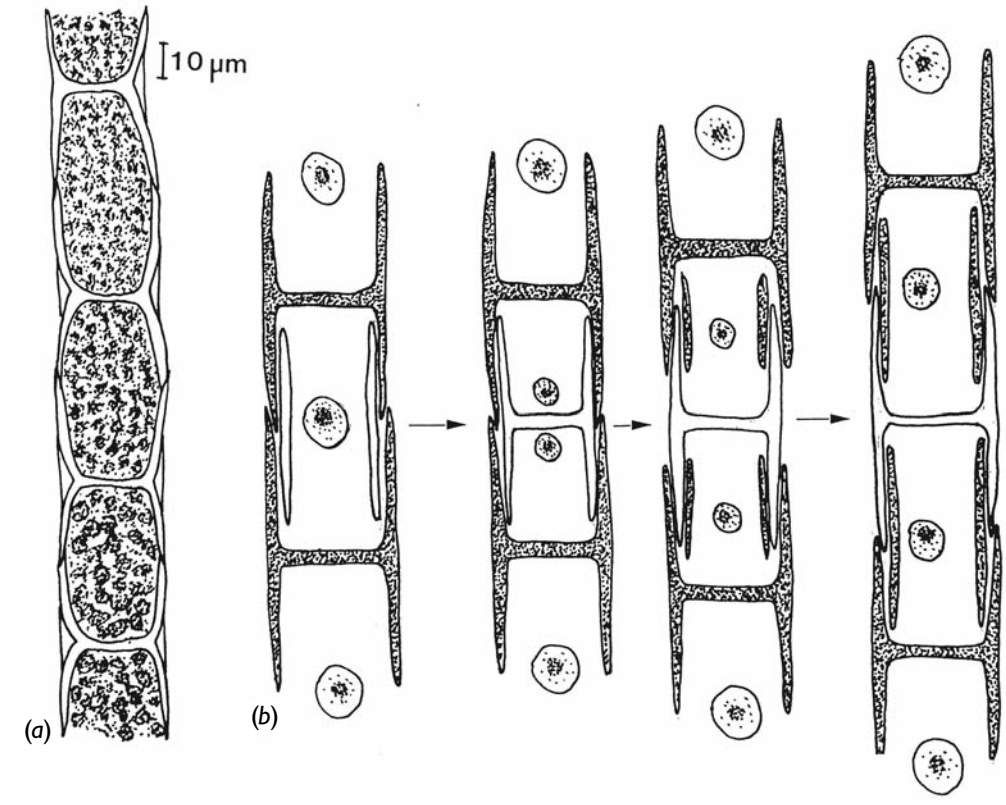


Fig. 5.88 *Microspora crassior*. (*a*) Filament. (*b*) Diagrammatic representation of wall deposition. Initially the interphase cell is enclosed by two H-shaped segments and a central cylinder. At cytokinesis, a cross wall is deposited in the middle of the cylinder. During cell expansion, the two H-shaped segments move apart while a new cylinder is secreted inside the H-shaped segments. ((*b*) after Pickett-Heaps, 1973.)

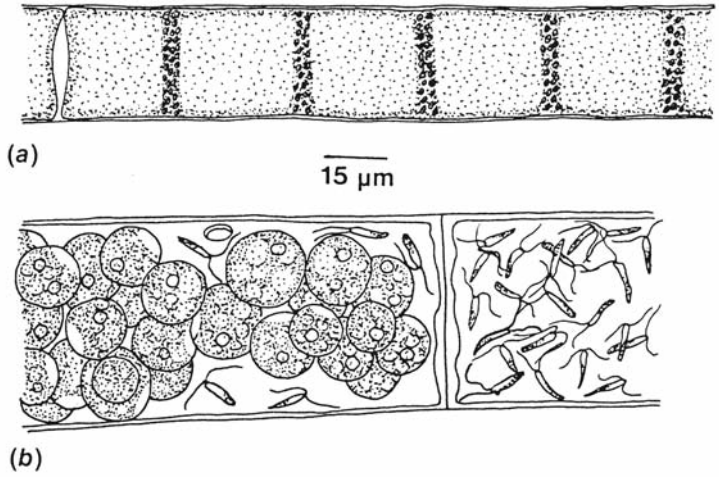


Fig. 5.89 *Sphaeroplea annulina*. (*a*) Part of a vegetative cell. (*b*) Portion of an oogonium in which the eggs are being fertilized, and a portion of an adjoining antheridium. (After Smith, 1955.)



Fig. 5.90 Scanning electron micrograph of a zygote of *Sphaeoplea fragilis* showing the sculptured exterior and a long curved cirrus. (From Hoffman and Buchheim, 1989.)

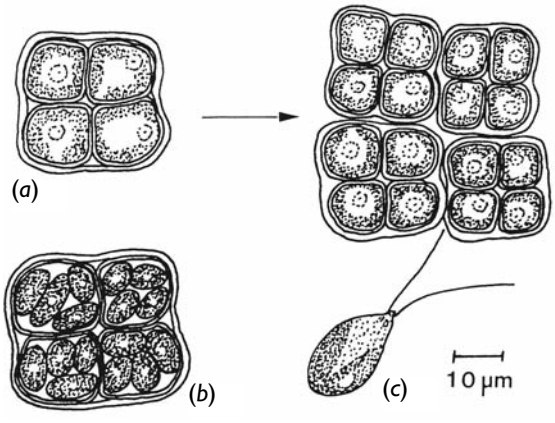


Fig. 5.91 *Chlorosarcina* sp. (*a*) Packet of cells dividing by desmoschisis to produce daughter colonies, each enclosed within the cell wall of the parent cell. (*b*) Colony-forming zoospores. (*c*) Zoospore.

thin layer of cytoplasm without chloroplasts between the vacuoles and the side walls. Asexual reproduction occurs by fragmentation of the filaments. Sexual reproduction is usually oogamous, with eggs and spermatozoids formed in alternate cells of the same filament or in different filaments. The spindle-shaped biflagellate spermatozoids escape through pores in the side walls of the antheridial cell and swim to the oogonial cells. The eggs, when first formed, are multinucleate, with all the nuclei but one disintegrating. The oogonial cells have pores in their walls through which the spermatozoids enter, swim about the eggs, and eventually fuse with them. Zygotes form a thick ornamented cell with a reddish protoplast, and are released by the decay of the oogonial cell. Zygotes germinate by forming four biflagellate ovoid zoospores, which settle and germinate into a new filament.

Chlorosarcinales

The algae in this order have a type of cell division (**desmoschisis**) that results in the formation of a number of cells, each with its own cell wall, within the cell wall of the parent cell. The genera in the Chlorosarcinales lack the plasmodesmata and complexity found in the Chaetophorales and Oedogoniales.

Chlorosarcina occurs free-living in the soil, or it can occur as an endophyte within the epidermis of aquatic vascular plants. Each cell contains a parietal chloroplast and has a cell wall that separates the cell from the other cells inside the old parental cell wall (Fig. 5.91). During **desmoschisis**, the protoplasm of a cell divides at successively perpendicular planes to build up cuboidal packets of cells. Cell walls are formed around the newly divided protoplast, next to the parent cell wall which remains intact. Eventually the colonies fragment to distribute the alga. Asexual reproduction can occur by the formation of four to eight biflagellate zoospores per cell,

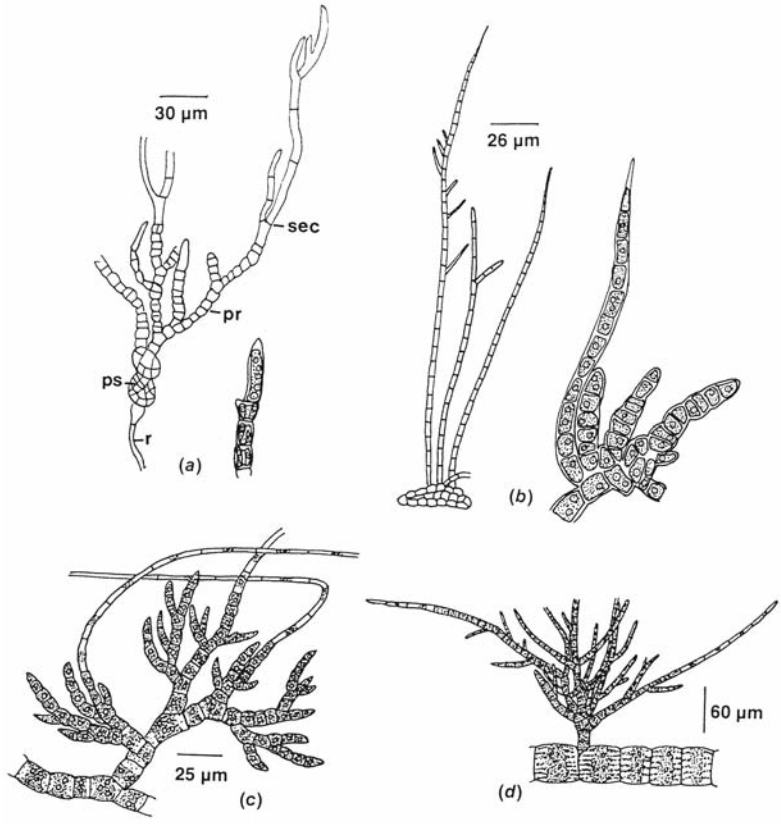


Fig. 5.92 (*a*) *Fritschiella tuberosa* showing prostrate system (ps), protonema (pr), projecting secondary branches (sec), and a rhizoid (r). Also shown is the tip of a branch. (*b*) *Stigeoclonium farctum*, old and young plants with erect and prostrate portions. (*c*) *Chaetophora incrassata*. (*d*) *Draparnaldia glomerata*. ((*a*) after Iyengar, 1932; (*b*) after Butcher, 1932; (*c*),(*d*) after Smith, 1920.)

which are released by softening in one area of the cell wall.

Chaetophorales

The Chaetophorales, along with the Oedogoniales, mark the most complex organization attained within the Chlorophyceae. The Chaetophorales have plasmodesmata, a characteristic of true multicellularity. In many ways, the level of organization in the Chaetophorales parallels that attained by the Coleochaetales in the Charophyceae.

The Chaetophorales have branched filaments with uninucleate cells that contain a single parietal chloroplast. Many of the plants exhibit **heterotrichy**; that is, there are *two different types of filaments, one constituting the prostrate system and the other the erect system*. In the past, these organisms were postulated to be the precursors of higher plants because they show the differentiation of filaments into different systems. An evolutionary progression from *Stigeoclonium* (Fig. 5.92(*b*)) to *Chaetophora* (Fig. 5.92(*c*)) to *Draparnaldia* (Fig. 5.92(*d*)) to *Fritschiella* (Fig. 5.92(*a*)) illustrates increasing differentiation toward what one would expect a primitive land plant to look like. As stated earlier, however, the above algae divide by a phycoplast and are therefore not in a direct line to higher plants.

Stigeoclonium (Fig. 5.92(*b*)) is a common freshwater alga found attached in flowing water. It has a very wide tolerance to organic pollution and can be indicative of heavily polluted water (McLean, 1974; McLean and Benson-Evans, 1974) although it will also grow in unpolluted water. The thallus is differentiated into prostrate and erect portions, with the terminal parts of the branches usually drawn out into colorless hairs. Vegetative reproduction can take place by fragmentation, although the erect portion does not grow well after detachment from the prostrate portion. Quadriflagellate zoospores are frequently formed when a thallus is brought into the laboratory, with most of the cells in the smaller

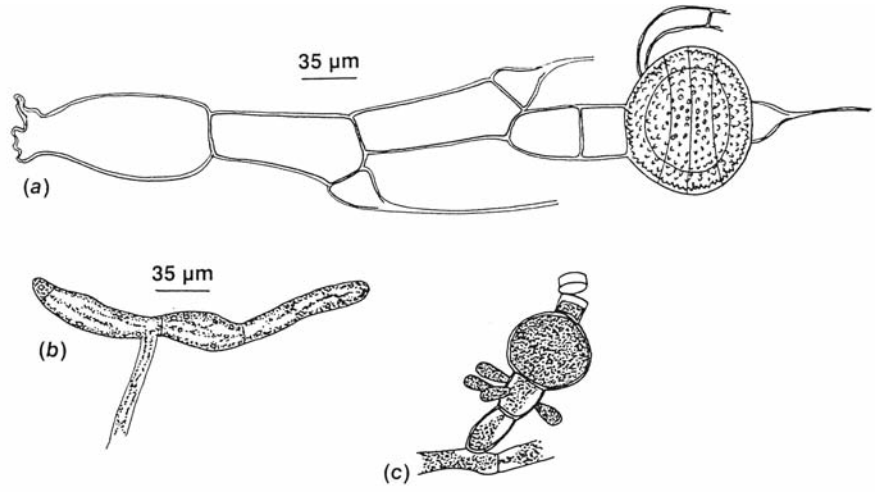


Fig. 5.93 (*a*) *Bulbochaete gigantea*, filament with zygote. (*b*),(*c*) *Oedocladium hazenii*, germling with rhizoid (*b*) and portion of a filament with empty androsporangia, immature dwarf males, and an unfertilized egg (*c*). (After Smith, 1950.)

branches sporulating a day after being brought in. A cell forms a single zoospore. After settling on its anterior end, the zoospore develops into a new filament. In sexual reproduction, gametes are produced in cells of erect filaments after a cruciate, presumably meiotic, process of division (Simons and van Beem, 1987). The gametes can be biflagellate or quadriflagellate. Fusion of gametes produces a zygote which germinates into a juvenile plant in which the original zygote remains visible as an embryonic cell.

Oedogoniales

The filamentous, freshwater, uninucleate algae in this order are characterized by a unique type of cell division and the production of motile reproductive cells with a whorl of flagella at one pole (stephanokonts). Sexual reproduction is oogamous, and asexual reproduction can be by zoospores or akinetes.

The Oedogoniales and its single family, the Oedogoniaceae, have only three genera – *Oedogonium* (Fig. 5.94), *Oedocladium* (Fig. 5.93(*b*), (*c*)), and *Bulbochaete* (Fig. 5.93(*a*)). *Oedogonium* is unbranched, whereas *Oedocladium* and *Bulbochaete* are branched. *Bulbochaete* has long colorless hairs (Fig. 5.93(*a*)); *Oedocladium* lacks hairs (Fig. 5.93(*b*), (*c*)). These algae are usually present in permanent bodies of water such as ponds or lakes. If they are growing in moving water, they are seldom in the fruiting condition. Normally fruiting takes places in the summertime. The plants may be epiphytic on aquatic plants and other algae, or they may be free-floating.

Chloroplasts in this order are reticulate, extending from one end of the cell to the other. The many pyrenoids are at the intersections of the reticulum. Plasmodesmata are present between cells, and the ones in *Bulbochaete* are similar to those of higher plants (Fraser and Gunning, 1969).

Cell division involves the breaking of the parent wall and the formation of apical caps. In *Oedogonium*, cell division (Fig. 5.94) is initiated by the formation of a ring under the wall in the upper part of the cell (Hill and Machlis, 1968). The ring enlarges by the coalescence of material produced in the cytoplasm. While the ring is being produced, the nucleus migrates to the center of the cell and divides mitotically. During late telophase, the new cross wall begins to form by means of a phycoplast. The daughter cells elongate, causing a split in the parent wall near the apical ring. This rent in the cell wall is covered by the material in the apical ring, which expands as the cells elongate. Each daughter cell eventually elongates to about the same length as the mother cell, elongation being completed within 15 minutes. The material of the ring becomes the cuticle, and a new cell wall is laid down under it. During the elongation of the daughter cells, the new transverse wall has moved up to the base of the

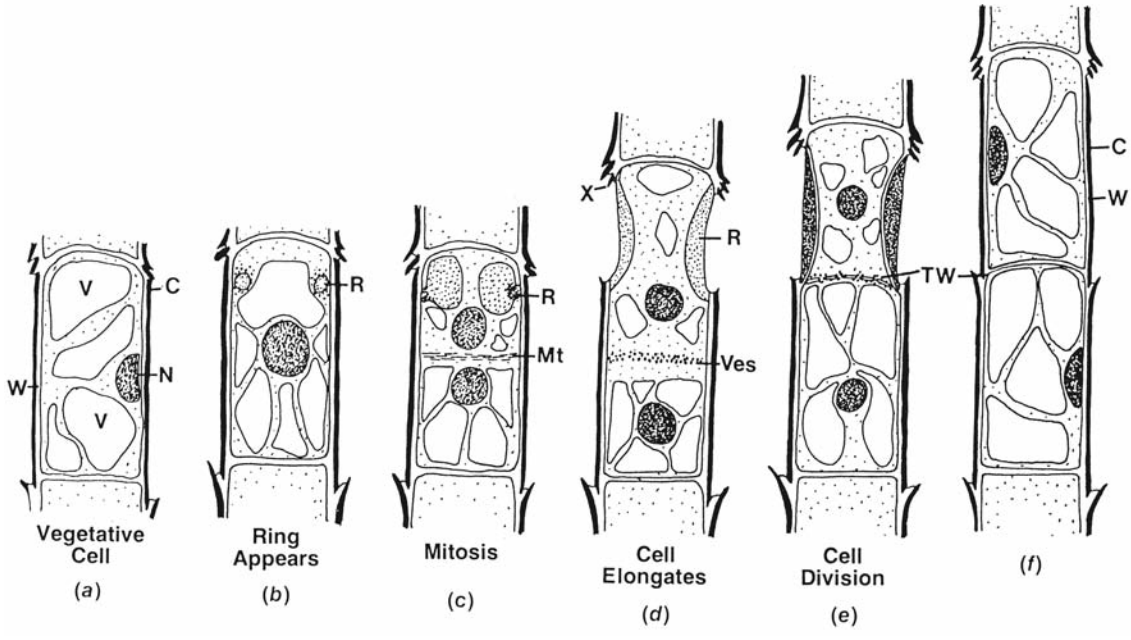


Fig. 5.94 Cell division in *Oedogonium*. (C) cuticle; (Mt) microtubules; (N) nucleus; (R) ring; (TW) transverse wall; (V) vacuole; (Ves) vesicles; (W) wall; (X) cap. (After Hill and Machlis, 1968.)

newly formed secondary wall and fused with it. Because cell division is intercalary in *Oedogonium*, division of every cell in the filament and repeated division of the daughter cells result in alternate cells with and without caps of old cell walls. This theoretical condition usually does not occur in nature. Repeated division of the distal daughter cell commonly results in filaments in which a cell with an apical cap is successively followed by several cells without caps.

Asexual reproduction (Fig. 5.95) is by means of zoospores in all three genera. Zoospores are formed singly within a cell and usually only in those cells with apical caps. The earliest sign of zoosporogenesis is the appearance of a small electron-dense mass in an invagination of the nuclear envelope (Pickett-Heaps, 1971). From this the centrioles appear and multiply rapidly, forming two adjacent rows near the nucleus. The nucleus, with its two rows of centrioles, moves to the lateral wall. The two rows of centrioles move apart in the center to form a circle of centrioles under the plasmalemma. The centrioles extrude the flagella and the flagella roots. The Golgi secrete a fibrillar hyaline layer around the zoospore, which makes up the vesicle in which the zoospore is initially encased. The Golgi also secrete mucilage to the base of the zoospore, which probably aids in extrusion of the zoospore. The lateral wall of the parent cell splits at the apical cap, and the zoospore in a vesicle emerges through the aperture. The vesicle has two layers with a ring (Retallack and Butler, 1970); it opens in the area of the ring, releasing the zoospore. The zoospore has about 30 flagella linked together by a striated root at the apical end (Hoffman and Manton, 1962); it swims for about an hour, settles, retracts its flagella, and develops a holdfast that attaches to the substrata. This then develops into a new filament. Aplanospores can also be formed, and resemble oogonia.

Sexual reproduction is oogamous and, depending on the behavior of the male filaments, either macrandrous if the male filament forms the sperm directly, or nannandrous if the sperm are produced in a special dwarf male filament. In many species of *Oedogonium*, it is relatively easy to induce sexual reproduction by placing old filaments in fresh media and saturating the atmosphere with carbon dioxide. Nitrogen limitation has also been reported to induce the formation of oogonia (Singh and Chaudhary, 1990).

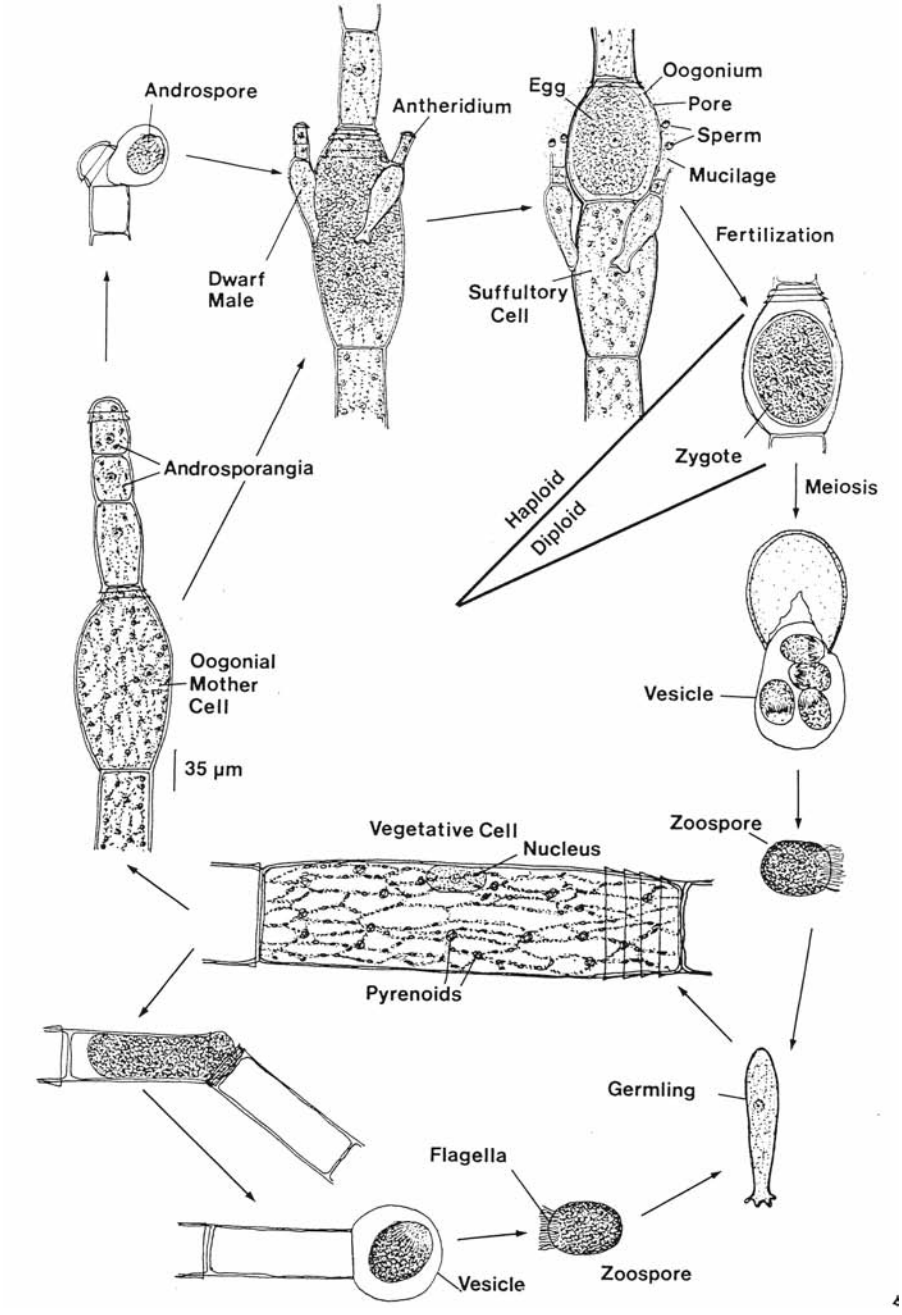


Fig. 5.95 The life cycle of a nannandrous species of *Oedogonium*. (Adapted from Smith, 1955.)

Oogonia have a similar developmental pattern in macrandrous (Fig. 5.96) and nannandrous species (Fig. 5.95) (Leonardi et al., 1998). The intercalary or terminal oogonial mother cells divide transversely, with one cell becoming the oogonium and the other either a suffultory (supporting) cell or a second oogonial mother cell. If one cell becomes another oogonial mother cell, then the oogonia are produced in series. The oogonia initially are wider than the vegetative cells and have a number of apical caps at their upper end from previous cell divisions. As the oogonium

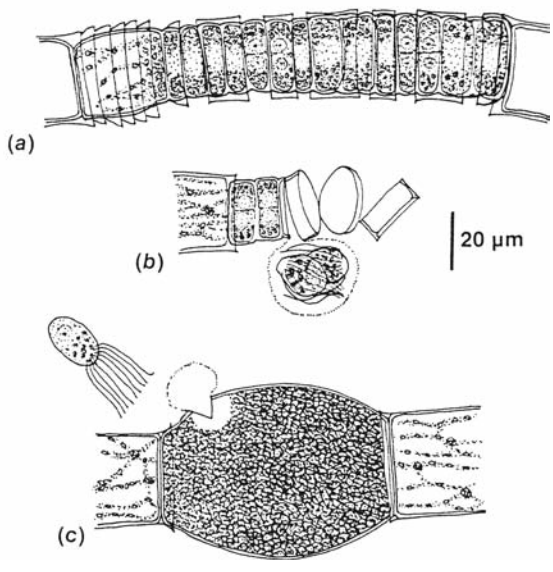


Fig. 5.96 Gametogenesis in the macrandrous *Oedogonium crassum*. (*a*) Antheridia. (*b*) Liberation of sperm. (*c*) Oogonium with a single egg attracting a spermatozoid. (After Smith, 1955.)

matures, it swells and becomes globose, forming a small pore or crack in the oogonial wall. The protoplast develops into an egg. Just prior to fertilization the central nucleus moves to just under the fertilization pore, and gelatinous material is extruded through the pore.

Macrandrous species form terminal or intercalary antheridia by an unequal division of an antheridial mother cell (Fig. 5.96). In this division, the upper cell is much shorter than the lower. The lower cell then divides repeatedly to produce a series of 2 to 40 antheridia. Each antheridium forms two sperm, which are liberated in a vesicle by transverse splitting of the wall. The sperm then escape from the vesicle. The sperm are similar in structure to the zoospores but smaller and more elongated with a crown of about 30 flagella (Hoffman and Manton, 1963), and are yellowish-green because of their reduced plastids. In a macrandrous species such as *Oedogonium cardiacum* (Hoffman, 1960), the sperm are attracted to the oogonium by a chemotactic substance secreted by the oogonium.

In nannandrous species (Leonardi et al., 1998), male filaments form **androsporangia** in a manner similar to the formation of antheridia by macrandrous species, except only one **androspore** is produced per sporangium. The androspore can develop in one of three ways depending on the environment (Hill et al., 1989).

1 In an environment with low nitrate or ammonium concentration, the androspore produces a cyst that will eventually produce another androspore. The cycle will continue until the nitrate or ammonium concentration in the environment increases.
2 If there is a large amount of nitrate or ammonium in the water, the androspore will produce a vegetative male thallus that is indistinguishable from the parent. This is similar to the situation in nature when a rainstorm washes nutrients into a nutrient-depleted environment.
3 If the environment contains the female pheromone "circein," the androspore is attracted to the female oogonium that is secreting the pheromone. The androspore attaches to the oogonial mother cell and causes the oogonial mother cell to divide into the oogonium and a lower **suffultory cell** to which the androspore is now attached. The production of the substance that attracted the androspore now ceases. If the attachment of the androspores to the oogonial mother cell is prevented by coating the oogonial mother cell with agar, then the oogonial mother cell continues to attract androspores, but the divison of the oogonial mother cell does not occur. Female differentiation beyond the oogonial mother cell stage must be triggered by direct contact of the attached androspore. The main advantage of a nannandrous system is that differentiation of the male is a prerequisite for differentiation of the female, thus ensuring the presence of a male for the receptive female.

The attached androspore on the suffultory cell next elongates and develops into a two-celled dwarf male filament. The growth of the dwarf male is toward the oogonium under the influence of a chemotactic substance secreted by the oogonium. The apical cell of the male filament is an

antheridium, which forms two sperm. The oogonium secretes a thick gelatinous sheath that includes the tip of the dwarf male. The sperm are released and trapped in this gel. After about 1 hour of random movement in the gel, the sperm aggregate at a certain spot on the upper third of the oogonium. The sperm extend their anterior end so that this end is flexible (Hoffman, 1973). A protoplasmic papilla suddenly appears through the wall of the oogonium, and all the spermatozoids in the vicinity attach to this papilla by their anterior ends. Within a second the papilla is withdrawn through the pore in the wall, taking with it a single sperm. The remaining sperm hover about the pore for about 5 minutes before they disperse in the gel. Four hormone-controlled steps are thus involved in fertilization: (1) the chemotaxis of the androspores; (2) the directed growth of the dwarf males; (3) the triggering of the division of the oogonial mother cell; and (4) the chemotaxis of the sperm to the prospective opening of the oogonium (Rawitscher-Kunkel and Machlis, 1962).

Nannandrous species are thought to have evolved from macrandrous ones by parthenogenetic germination of sperm to form dwarf male filaments.

The zygote is separated from the oogonial wall by a space, and after fertilization a wall is soon formed around the zygote. As the zygote matures, there is an accumulation of a reddish oil in the protoplasm. Eventually the zygote is liberated by decay of the oogonial wall. It undergoes a rest period during which its nucleus divides by meiosis to form four haploid nuclei. Shortly before germination, the protoplast becomes green and forms four daughter protoplasts, each of which becomes a zoospore. The zoospores are released and develop into filaments in the same manner as in asexual reproduction. The life cycle is thus mostly haploid, the zygote being the only diploid structure.

REFERENCES

Adolph, S., Jung, V., Rattke, J., and Pohnert, G. (2005). Wound closure in the invasive green alga *Caulerpa taxifolia* by enzymatic activation of a protein crosslinker. *Angew. Chem. Int. Ed*. 44:2–4.

Ahmadjian, V. (1960). Some new and interesting species of *Trebouxia*, a genus of lichenized algae. *Am. J. Bot*. 47:677–83.

Ahmadjian, V. (1993). *The Lichen Symbiosis*. New York: John Wiley.

Ahmadjian, V., and Jacobs, J. B. (1981). Relationship between fungus and alga in the lichen *Cladonia cristatella* Tuck. *Nature* 289:169–72.

Barlow, S. B., and Cattolico, R. A. (1980). Fine structure of the scale-covered green flagellate *Mantoniella squamata* (Manton et Parke) Desikachary. *Br. Phycol. J*. 15:321–33.

Bean, B. (1977). Geotactic behaviour of *Chlamydomonas. J. Protozool*. 24:394–401.

Becker, B., Perasso, L., Kammer, A., Salzburg, M., and Melkonian, M. (1996). Scale-associated glycoproteins of *Scherffelia dubia* (Chlorophyta) form high-molecular-weight complexes between the scale layers and the flagellar membrane. *Planta* 199:503–10.

Belcher, J. H., Pennick, N. C., and Clarke, K. J. (1974). On the identity of *Asteromonas propulsum* Butcher. *Br. Phycol. J*. 9:101–6.

Ben-Amotz, A. (1996). Effect of low temperature on the stereoisomer composition of β-carotene in the halotolerant alga *Dunaliella bardawil. J. Phycol*. 32:272–5.

Bendix, S. W. (1960). Phototaxis. *Bot. Rev*. 26:145–208.

Benson, E. E., Rutter, J. C., and Cobb, A. H. (1983). Seasonal variation in frond morphology and chloroplast physiology of the intertidal alga *Codium fragile* (Suringar) Hariot. *New Phytol*. 95:569–80.

Berger, S., and Kaever, M. J. (1992). *Dascladales: An Illustrated Monograph of a Fascinating Algal Order*. Stuttgart: Thieme.

Berger, S., Fetweiss, U., Gleissberg, S., et al. (2003). 18S rDNA phylogeny and evolution of cap development in Polyphysaceae (formerly Acetabulariaceae; Dasycladales, Chlorophyta). *Phycologia* 42:506–61.

Berger-Perrot, Y., Thomas, J-Cl., and L'Hardy-Halos, M-Th. (1993). Gametangia, gametes, fertilization and zygote development in *Ulothrix flacca* var. *roscoffensis* (Chlorophyta). *Phycologia* 32:356–66.

Berry, H. A., and Lembi, C. A. (2000). Effects of temperature and irradiance on the seasonal variation of a *Spirogyra* (Chlorophyta) population in a Midwestern lake (U.S.A.). *J. Phycol*. 36:842–51.

Bérubé, K. A., Dodge, J. D., and Ford, T. W. (1999). Effects of chronic salt stress on the ultrastructure of *Dunaliella bioculata* (Chlorophyta, Volvocales): mechanisms of response and recovery. *Eur. J. Phycol*. 34:117–23.

Betsche, T., Schaller, D., and Melkonian, M. (1992). Identification and characterization of glycolate oxidase and related enzymes from the endocyanotic algae *Cyanophora paradoxa* and from pea leaves. *Plant Physiol*. 98:887–93.

Blackburn, K., and Temperley, B. N. (1936). *Botryococcus* and the algal coals. *Proc. R. Soc. Edinburgh* 58:841–6.

Blomster, J., Back, S., Fewer, D. P., et al. (2002). Novel morphology in *Enteromorpha* (Ulvophyceae) forming green tides. *Amer. J. Bot*. 89:1756–63.

Booton, G. C., Floyd, G. L., and Fuerst, P. A. (1998). Polyphyly of tetrasporalean green algae inferred from nuclear small-subunit ribosomal DNA. *J. Phycol*. 39:306–11.

Borowitzka, M. A. (1982). Morphological and cytological aspects of algal calcification. *Int. Rev. Cytol*. 74:127–62.

Borowitzka, M.A., and Larkum, A. W. D. (1974). Chloroplast development in the caulerpalean alga *Halimeda*. *Protoplasma* 81:131–44.

Boscov, J. S., and Feinleib, M. E. (1979). Phototactic response of *Chlamydomonas* to flashes of light. II. Response of individual cells. *Photochem. Photobiol*. 30:499–505.

Bouck, G. B., and Morgan, E. (1957). The occurrence of *Codium* in Long Island waters. *Bull. Torrey Bot. Club* 84:384–7.

Bråten, T. (1971). The ultrastructure of fertilization and zygote formation in the green alga. *Ulva mutabilis* Føyn. *J. Cell Sci*. 9:621–35.

Bråten, T. (1973). Autoradiographic evidence for the rapid disintegration of one chloroplast in the zygote of the green alga *Ulva mutabilis*. *J. Cell Sci*. 12:385–9.

Braun, A. (1851). *Betrachtungen über die Erscheinung der Verjungung in der Natur*., Leipzig.

Braun, M., and Richter, P. (1999). Relocalization of the calcium gradient and a dihydropyridine receptor is involved in upward bending by bulging *Chara* protonema, but not in downward bending by bowing of *Chara* rhizoids. *Planta* 209:414–23.

Bristol, B. M. (1919). On a Malay form of *Chlorococcum humicola* (Naeg.) Rabenh. *J. Linn. Soc. Bot*. 44:473–82.

Brook, A. J. (1989). Barium sulphate crystals and desmids. *Brit Phycol. J.* 24:299–300.

Brown, R. M., Johnson, C., and Bold, H. C. (1968). Electron and phase-contrast microscopy of sexual reproduction in *Chlamydomonas moewusii*. *J. Phycol*. 4:100–20.

Bubrick, P., and Galun, M. (1980). Proteins from the lichen *Xanthoria parietina* which bind to phycobiont cell walls. Correlation between binding patterns and cell wall cytochemistry. *Protoplasma* 104:167–73.

Buchheim, M. A., Michalopulos, E. A., and Buchheim, J. A. (2001). Phylogeny of the Chlorophyceae with special reference to the Sphaeropleales: a study of 18S and 26S rDNA data. *J. Phycol*. 37:819–35.

Butcher, R. N. (1932). Notes on new and little-known algae from the beds of rivers. *New Phytol*. 31:289–309.

Cáceres, E. J., Hoffman, L. R., and Leonardi, P. I. (1997). Fine structure of the male and female gametes of *Atractomorpha porcata* (Sphaeropleaceae, Chlorophyta) with emphasis on the development and absolute configuration of the flagellar apparatus. *J. Phycol*. 33:948–59.

Cane, R. F. (1977). Coorgongite, balkashite and related substances – An annotated bibliography. *Trans. R. Soc. S. Aust*. 101:153–64.

Carothers, Z. B., and Kreitner, G. L. (1967). Studies of spermatogenesis in the Hepaticae. I. Ultrastructure of the *Vierergruppe* in *Marchantia*. *J. Cell Biol*. 33:43–51.

Casanova, M. T. (1997). Oospore variation in three species of *Chara* (Charales, Chlorophyta). *Phycologia* 36:274–80.

Cavalier-Smith, T. (1981). Eukaryote kingdoms: seven or nine? *BioSystems* 14:461–81.

Chapman, V. J. (1970). *Seaweeds and Their Uses*, 2nd edn. London: Methuen.

Chen, Y.-C. (1998). Development of protoplasts from holdfasts and vegetative thalli of *Monostroma latissimum* (Chlorophyta, Monostromataceae) for algal seed stock. *J. Phycol*. 34:1075–81.

Chiang, I.-Z., Huang, W.-Y., and Wu, J.-T. (2004). Allelochemicals of *Botryococcus braunii* (Chlorophyceae). *J. Phycol*. 40:474–80.

Chihara, M. (1963). The life history of *Prasinocladus ascus* as found in Japan, with special reference to the systematic position of the genus. *Phycologia* 3:19–28.

Chihara, M. (1969). *Ulva arasakii*, a new species of green algae: its life history and taxonomy. *Bull. Nat. Sci. Mus. (Japan)* 12:849–62.

Christie, A. O., and Evans, L. V. (1962). Periodicity in the liberation of gametes and zoospores of *Enteromorpha intestinalis* Link. *Nature* 193:193–4.

Cimino, M. T., and Delwiche. C. F. (2002). Molecular and morphological data identify a cryptic species complex in endophytic members of the genus *Coleochaete* Breb. (Charophyta: Coleochaetaceae). *J. Phycol*. 38:1213–21.

Coggin, S. J., Hutt, W., and Kochert, G. (1979). Sperm bundle–female somatic cell interaction in the fertilization process of *Volvox carteri* f. *weismannia* (Chlorophyta). *J. Phycol*. 15:247–51.

Coleman, A. W. (1999). Phylogenetic analysis of "Volvocaceae" for comparative genetic studies. *Proc. Natl. Acad. Sci., U.S.A.* 96:13892–7.

Collings, D. A., Wasteneys, G. B., and Williamson, R. E. (1996). Actin microtubule interactions in the alga *Nitella*: analysis of the mechanism by which microtubule depolymerization potentiates cytochalasin's effects in streaming. *Protoplasma* 191:178–90.

Collins, C. R., and Farrar, J. F. (1978). Structural resistances to mass transfer in the lichen *Xanthoria parietina*. *New Phytol*. 81:71–83.

Cooper, J. J., and Mandoli, D. F. (1999). Physiological factors that aid differentiation of zygotes and early juveniles of *Acetabularia acetabulum* (Chlorophyta). *J. Phycol*. 35:143–51.

Courties, C., Perasso, R., Chretiennot-Dinet, M.-J., Govy, M., Guillou, L., and Troussellier, M. (1998). Phylogenetic analysis and genome size of *Ostreococcus tauri* (Chlorophyta, Prasinophyceae). *J. Phycol*. 34:844–9.

Daugbjerg, N., Moestrup, Ø., and Arctander, P. (1995). Phylogeny of genera of Prasinophyceae and Pedinophyceae (Chlorophyta) deduced from molecular analysis of the *rbs* gene. *Phycological Research* 43:203–13.

Davies, R. R., and Wilkinson, J. L. (1967). Human protothecosis: Supplementary studies. *Ann. Trop. Med. Parasitol*. 61:112–15.

Deason, T. R. (1983). Cell wall structure and composition as taxonomic characters in the coccoid Chlorophyceae. *J. Phycol*. 19:248–51.

deJesus, M. D., Tabatabai, F., and Chapman, D. J. (1989). Taxonomic distribution of copper–zinc superoxide dismutase in green algae and its phylogenetic importance. *J. Phycol*. 25:767–72.

Demets, R., Tomson, A. M., Stegwee, D., and van de Ende, H. (1990). Cell–cell coordination in conjugating *Chlamydomonas* gametes. *Protoplasma* 158:188–99.

Dodds, W. K., and Gudder, D. A. (1992). The ecology of *Cladophora*. *J. Phycol*. 28:415–27.

Domozych, C. R., Plante, K., Blair, P., Paliules, L., and Domozych, D. S. (1993). Mucilage processing and secretion in the green alga *Closterium*. I. Cytology and biochemistry. *J. Phycol*. 29:650–9.

Domozych, D. S., Stewart, K. D., and Mattox, K. R. (1981). Development of the cell wall in *Tetraselmis:* Role of the Golgi apparatus and extracellular wall assembly. *J. Cell Sci*. 52:351–71.

Dorling, M., McAuley, P. J., and Hodge, H. (1997). Effect of pH on growth and carbon metabolism of maltose-releasing *Chlorella* (Chlorophyta). *Eur. J. Phycol*. 32:19–24.

Douglas, A. E. (1985). Growth and reproduction of *Convoluta roscoffensis* containing different naturally occurring algal symbionts. *J. Mar. Biol. Assoc. UK* 65:871–9.

Duncan, T. M., Renzaglia, K. S., and Garbary, D. J. (1997). Ultrastructure and phylogeny of the spermatozoid of *Chara vulgaris* (Charophyceae). *Pl. Syst. Evol*. 204:125–40.

Ebnet, E., Fischer, M., Deininger, W., and Hegemann, P. (1999). Volvoxrhodopsin, a light-regulated sensory photoreceptor of the spheroidal alga *Volvox carteri*. *Plant Cell* 11:1473–84.

Egan, P. F., and Trainor, F. R. (1989). The role of unicells in the polymorphic *Scenedesmus armatus* (Chlorophyceae). *J. Phycol*. 25:65–70.

Egerod, L. E. (1952). An analysis of the siphonaceous Chlorophycophyta. *Univ. Calif. Publ. Bot*. 25:325–454.

Ernst, A. (1902). *Dichotomosiphon tuberosus* (A. Br.) Ernst, eine neue oogame Süsswasser-Siphonee. *Beih. Bot. Zentralbl*. 13:115–48.

Fawley, M. W., Yun, Y., and Qin, M. (2000). Phylogenetic analyses of 18S rDNA sequences reveal a new coccoid lineage of the Prasinophyceae (Chlorophyta). *J. Phycol*. 36:387–93.

Feldmann, J. (1950). Sur l'existence d'une alternance de générations entre *l'Halicystis parvula* Schmitz et le *Derbesia tenuissima* (De Not.) Crn. *C. R. Séances Acad. Sci. Paris* 230:322–33.

Fisher, M., Pick, U., and Zamir, A. (1994). A salt-induced 60-kilodalton plasma membrane protein plays a potential role in extreme halotolerence of the alga *Dunaliella*. *Plant Physiol*. 106:1359–65.

Floyd, G. L., Stewart, K. D., and Mattox, K. R. (1972). Cellular organization, mitosis and cytokinesis in the ulotrichalean alga, *Klebsormidium*. *J. Phycol*. 8:176–84.

Fogg, G. E. (1971). Recycling through algae. *Proc. R. Soc. Lond*. [B] 179:201–7.

Fraser, T. W., and Gunning, B. E. S. (1969). The ultrastructure of plasmodesmata in the filamentous green alga *Bulbochaete hiloensis* (Nordst.) Tiffany. *Planta* 88:244–54.

Friedmann, I. (1959). Structure, life history and sex determination of *Prasiola stipitata* Suhr. *Ann. Bot. N. S.* 23:571–94.

Friedmann, I., and Manton, I. (1959). Gametes, fertilization and zygote development in *P. stipitata*. *Nova Hedwigia* 1:333–44.

Fukumoto, R., Fuji, T., and Sekimoto, H. (2003). Cloning and characterization of a cDNA encoding a sexual cell division-inducing pheromone from a unicellular green alga *Closterium ehrenbergii* (Chlorophyta). *J. Phycol*. 39:931–6.

Fünfstück, M. (1907). Lichenes. In *Die Naturlichen Pflanzenfamilien*, ed. A. Engler, and K. Prantl. Leipzig: Engelmann.

Geib, K., Golldack, D., and Gimmler, H. (1996). Is there a requirement for an external carbonic anhydrase in the extremely acid-resistant green alga *Dunaliella acidophila*? *Eur. J. Phycol*. 31:273–84.

Goldstein, M., and Morral, S. (1970). Gametogenesis and fertilization in *Caulerpa*. *Ann. NY Acad. Sci*. 175:660–72.

Gontcharov, A. A., Marin, B., and Melkonian, M. (2002). Molecular phylogeny of conjugating green algae (Zygnemophyceae, Streptophyta) inferred from SSU rDNA sequence comparisons. *J. Mol. Evol.* 56:89–104.

Gonzalez, M. A., Coleman, A. W., Gomez, P. J., and Montoya, R. (2001). Phylogenetic relationship among various strains of *Dunaliella* (Chlorophyceae) based on nuclear ITS rDNA sequences. *J. Phycol*. 37:604–11.

Goodenough, U. W., and Heuser, J. E. (1985). The *Chlamydomonas* cell wall and its constituent glycoproteins analyzed by the quick-freeze, deep-etch technique. *J. Cell Biol*. 101:1550–68.

Goodenough, U. W., Detmers, P. A., and Hwang, C. (1982). Activation for cell fusion in *Chlamydomonas*: Analysis of wild-type gametes and nonfusing mutants. *J. Cell Biol*. 92:378–86.

Goreau, T. F. (1963). Calcium carbonate deposition by coralline algae and corals in relation to their roles as reef-builders. *Ann. NY Acad. Sci*. 109:127–67.

Graham, J. M., Arancibia-Avile, P., and Graham, L. E. (1996). Physiological ecology of a species of the filamentous green alga *Mougeotia* under acid conditions: light and temperature effects on photosynthesis and respiration. *Limnol. Oceanogr*. 41:253–62.

Graham, J. M., Lembi, C. A., Adrian, H. L., and Spencer, D. F. (1995). Physiological responses to temperature and irradiance in *Spirogyra* (Zygnematales, Charophyceae). *J. Phycol*. 31:334–40.

Graham, L. E. (1984). *Coleochaete* and the origin of land plants. *Am. J. Bot*. 71:603–8.

Graham, L. E., and McBride, G. E. (1979). The occurrence and phylogenetic significance of a multilayered structure in *Coleochaete* spermatozoids. *Am. J. Bot*. 66:887–94.

Graham, L. E., and Kranzfelder, J. A. (1986). Irradiance, daylength and temperature effects on zoosporogenesis in *Coleochaete scutata* (Charophyceae). *J. Phycol*. 22:35–9.

Green, T. G. A. (1970). The biology of lichen symbionts, DPhil. thesis, Oxford.

Griffin, N. J., and Aken, M. E. (1993). Rhythmic settling behavior in *Pyramimonas parkae* (Prasinophyceae). *J. Phycol*. 29:9–15.

Gruber, P. J., Frederick, S. E., and Tolbert, N. E. (1974). Enzymes related to lactate metabolism in green algae and lower land plants. *Plant Physiol*. 53:167–70.

Grünewald, K., Hagen, C., and Braune, W. (1997). Secondary carotenoid accumulation in flagellates of the green alga *Haematococcus lacustris*. *Eur. J. Phycol*. 32:387–92.

Gulliksen, O. M., Hushovd, O. T., Texmon, I., and Nordby, Ø. (1982). Changes in respiration, photosynthesis and protein composition during induced synchronous formation of gametes and zoospores in *Ulva mutabilis* Føyn. *Planta* 156:33–40.

Hagen, C., Grünewald, K., Schmidt, S., and Müller, J. (2000). Accumulation of secondary carotenoid in flagellates of *Haematococcus pluvialis* (Chlorophyta) is accompanied by an increase in per unit chlorophyll productivity of photosynthesis. *Eur. J. Phycol*. 35:75–82.

Hallman, A. (2003). Extracellular matrix and sex-inducing pheromone in *Volvox*. *Int. Rev. Cytol.* 227:131–82.

Hallman, A., and Kirk, D. L. (2000). The developmentally regulated ECM glycoprotein ISG plays an essential role in organizing the ECM and orienting cells of *Volvox*. *J. Cell Sci*. 113:4605–17.

Hanisak, M. D. (1979). Nitrogen limitation of *Codium fragile* ssp. *tomentosoides* as determined by tissue analysis. *Mar. Biol*. 50:333–7.

Harris, E. H. (1989). *The* Chlamydomonas *Sourcebook: A Comprehensive Guide To Biology And Laboratory Use*. San Diego: Academic Press.

Harris, E. H. (2001). *Chlamydomonas* as a model organism. *Annu. Rev. Plant Physiol. Mol. Biol.* 52:363–506.

Hatano, K., and Ueda, J. (2000). Effects of concanavalin A on net formation of zoospores in *Hydrodictyon reticulatum* (Chlorococcales, Chlorophyceae). *Phycol. Res.* 48:155–60.

Hayden, H. S., Blomster, J., Maggs, C. A., Silva, P. C., Stanhope, M. J., and Waaland, J. R. (2003). Linnaeus was right all along: *Ulva* and *Enteromorpha* are not distinct genera. *Eur. J. Phycol*. 38:277–94.

Head, W. D., and Carpenter, E. J. (1975). Nitrogen fixation associated with the marine macroalga *Codium fragile*. *Limnol. Oceanogr*. 20:815–23.

Hegemann, P., Fuhrmann, M., and Kateriya, A. (2001). Algal sensory photoreceptors. *J. Phycol*. 37:668–76.

Hepperle, D., and Krienitz, L. (1996). The extracellular calcification of zoospores of *Phacotus lenticularis*

(Chlorophyta, Chlamydomonadales). *Eur. J. Phycol*. 31:11–21.

Hessler, R., and Peveling, E. (1978). Die Lokalisation von ^{14}C-Assimilaten von Flechtenthalli von *Cladonia incrassata* Floerke und *Hypogymnia physodes* (L.) Ach. *Z. Pflanzenphysiol*. 86:287–302.

Hill, G. J. C., and Machlis, L. (1968). An ultrastructural study of vegetative cell division in *Oedogonium borisianum*. *J. Phycol*. 4:261–71.

Hill, G. J. C., Cunningham, M. R., Byrne, M. M., Ferry, T. P., and Halvorsen, J. S. (1989). Chemical control of androspore morphogenesis in *Oedogonium donnelli* (Chlorophyta, Oedogoniales). *J. Phycol*. 25:368–76.

Hiraoka, M., Obata, S., and Ohno, M. (1998). Pigment content of the reproductive cells of *Ulva pertusa* (Ulvales, Ulvophyceae): evidence of anisogamy. *Phycologia* 37:222–6.

Hodick, D. (1994). Negative gravitropism in *Chara* protonemata: a model integrating the opposite gravitropic responses of protonemata and rhizoids. *Planta* 195:43–9.

Hoffman, L. (1960). Chemotaxis of *Oedogonium* sperms. *Southwest. Nat*. 5:111–16.

Hoffman, L. (1973). Fertilization in *Oedogonium*. I. Plasmogamy. *J. Phycol*. 9:62–84.

Hoffman, L., and Manton, I. (1962). Observations on the fine structure of the zoospore of *Oedogonium cardiacum* with special reference to the flagellar apparatus. *J. Exp. Bot*. 13:443–9.

Hoffman, L., and Manton, I. (1963). Observations on the fine structure of *Oedogonium* II. The spermatozoid of *O. cardiacum*. *Am. J. Bot*. 50:455–63.

Hoffman, L. R., and Buchheim, M. A. (1989). Zygote appendages (cirri), a new structural feature in the Sphaeropleaceae (Chlorophyceae). *J. Phycol*. 25:149–59.

Hoham, R. W. (1973). Pleiomorphism in the snow alga *Raphidonema nivale* Lagerh. (Chlorophyta), and a revision of the genus *Rhaphidonema* Lagerh. *Syesis* 6:255–63.

Hoham, R. W., Bonome, T. A., Martin, C. W., and Leebens-Mack, J. H. (2002). A combined 18S and *rbc*L phylogenetic analysis of *Chloromonas* and *Chlamydomonas* (Chlorophyceae, Volvocales) emphasizing snow and other cold-temperature habitats. *J. Phycol*. 38:1051–64.

Hoops, H. J., Brighton, M. C., Stickles, S. M., and Clement, P.R. (1999). A test of two possible mechanisms for phototactic steering in *Volvox carteri* (Chlorophyceae). *J. Phycol*. 35:539–47.

Hori, T., Norris, R. E., and Chihara, M. (1982a). Studies on the ultrastructure and taxonomy of the genus *Tetraselmis* (Prasinophyceae). I. Subgenus *Tetraselmis*. *Bot. Mag. (Tokyo)* 95:49–61.

Hori, T., Norris, R. E., and Chihara, M. (1982b). Studies on the ultrastructure and taxonomy of the genus *Tetraselmis* (Prasinophyceae). II. Subgenus *Prasinocladia*. *Bot. Mag. (Tokyo)* 96:385–92.

Hoskin, C. M. (1963). Recent carbonate sedimentation on Alacran Reef, Yucatan, Mexico. *Nat. Acad. Sci. Nat. Res. Council Publ.* 1089.

Huang, K., and Beck, C. F. (2003). Phototropin is the blue-light receptor that controls multiple steps in the sexual life cycle of the green alga *Chlamydomonas reinhardtii*. *Proc. Natl. Acad. Sci., USA* 100:6269–74.

Huber-Pestalozzi, G. (1961). Volvocales. In *Die Binnengewässer*, Vol. 16, Part 5. Stuttgart, Germany: E. Schweizerbart'sche Verlagsbuchhandlung.

Huizing, H. J., Rietema, H., and Sietsma, J. H. (1979). Cell wall constituents of several siphonaceous green algae in relation to morphology and taxonomy. *Br. Phycol. J.* 14:25–32.

Hutt, W., and Kochert, G. (1971). Effects of some protein and nucleic acid synthesis inhibitors on fertilization in *Volvox carteri*. *J. Phycol*. 7:316–20.

Imam, S. H., Buchanan, M. J., Shin, H. C., and Snell, W. J. (1985). The *Chlamydomonas* cell wall: Characterization of the wall framework. *J. Cell Biol*. 101:1599–607.

Inouye, I., Hori, T., and Chihara, M. (1990). Absolute configuration analysis of the flagellar apparatus of *Pterosperma cristatum* (Prasinophyceae) and consideration of its phylogenetic position. *J. Phycol*. 26:329–44.

Iyengar, M. O. P. (1932). *Fritschiella*, a new terrestrial member of the Chaetophoraceae. *New Phytol*. 31:329–35.

Jaenicke, L., and Starr, R. C. (1996). The lurlenes, a new class of plastoquinone-related pheromones from *Chlamydomonas allensworthii* (Chlorophyceae). *Eur. J. Biochem*. 241:581–5.

Johnson, H. J. (1961). *Limestone-Building Algae and Algal Limestones*. Boulder, Colo: Johnson Publ.

Jones, H. G., Pomeroy, J. W., Walker, D. A., and Hoham, R. W. (2001). *Snow Ecology*. Cambridge: Cambridge University Press.

Kamitsubo, E. (1980). Cytoplasmic streaming in characean cells: role of subcortical fibrils. *Can J. Bot*. 58:760–5.

Kamiya, R., and Witman, G. B. (1984). Submicromolecular levels of calcium control the

balance of beating between the two flagella in demembranated models of *Chlamydomonas. J. Cell Biol*. 98:97–107.

Karol, K. G., McCourt, R. M., Cimino, M. T., and Delwiche, C. F. (2001). The closest living relatives of land plants. *Science* 294:2351–3.

Kim, G. H., Yoon, M., and Klotchkova, T. A. (2005). A moving mat: phototaxis in the filamentous green alga *Spirogyra* (Chlorophyta, Zygnemataceae). *J. Phycol*. 41:232–7.

Kim, K. Y., Choi, T. S. W., Kim, J. H., Han, T., Shin, H. W., and Garbary, D. J. (2004). Physiological ecology and seasonality of *Ulva pertusa* on a temperate rocky shore. *Phycologia* 43:483–92.

Kim, Y-S., Oyaizu, H., Matsumoto, S., Watanabe, M-M., and Nozaki, H. (1994). Chloroplast small-subunit ribosomal RNA gene sequence from *Chlamydomonas parkae* (Chlorophyta): Molecular phylogeny of a green alga with a peculiar pigment composition. *Eur. J. Phycol*. 29:213–17.

Kingsley, R. J., Van Gilder, R., LeGeros, R. Z., and Watabe, N. (2003). Multimineral calcareous deposits in the marine alga *Acetabularia acetabulum* (Chlorophyta, Dasycladaceae). *J. Phycol*. 39:937–47.

Kirk, D. L., and Kirk, M. M. (1986). Heat shock elicits production of sexual inducer in *Volvox. Science* 231:51–4.

Kirk, D. L. (1998). Volvox: *Molecular-Genetic Origins of Multicellularity and Cellular Differentiation*. Cambridge: Cambridge University Press.

Kirk, D. L. (1999). Evolution of multicellularity in the volvocine algae. *Curr. Opin. Plant Biol*. 2:496–501.

Kirk, D.L. (2001). Germ-soma differentiation in *Volvox. Dev. Biol*. 238:213–23.

Kirk, D. L., and Nishii, I. (2001). *Volvox carteri* as a model for studying the genetic and cytological control or morphogenesis. *Dev. Growth Differ*. 43:621–31.

Kleinig, H. (1969). Carotenoids of siphonous green algae: A chemotaxonomical study. *J. Phycol*. 5:281–4.

Klotchkova, T. A., Chah, O., West, J. A., and Kim, G. H. (2003). Cytochemical and ultrastructural studies on protoplast formation from disintegrated cells of the marine alga *Chaetomorpha aerea* (Chlorophyta). *Eur. J. Phycol*. 38:205–16.

Klyver, F. D. (1929). Notes on the life history of *Tetraspora gelatinosa* (Vauch.) Desv. *Arch. Protistenk*. 66:290–6.

Kochert, G. (1968). Differentiation of reproductive cells in *Volvox carteri. J. Protozool*. 15:438–52.

Koop, H-U. (1975a). Über den Ort der Meiose bei *Acetabularia mediterranea. Protoplasma* 85:109–14.

Koop. H-U. (1975b). Germination of cysts of *Acetabularia mediterranea. Protoplasma* 84:137–46.

Kranz, H. D., Mikš, D., Siegler, M-L., Capesius, I., Sensen, C. W., and Huss, V. A. R. (1995). The origin of land plants: Phylogenetic relationships among charophytes, bryophytes, and vascular plants inferred from complete small-subunit ribosomal RNA gene sequences. *J. Mol. Evol*. 41:74–84.

Kriemer, G., and Melkonian, M. (1990). Reflection confocal laser scanning microscopy of eyespots in flagellated green algae. *Eur. J. Cell Biol*. 53:101–11.

Kuroiwa, T. (1985). Mechanisms of maternal inheritance of chloroplast DNA: An active digestion hypothesis. *Microbiol. Sci*. 2:267–70.

Kwiatkowska, M. (2003). Plasmodesmal changes are related to different developmental stages of antheridia of *Chara* species. *Protoplasma* 222:1–11.

Lee, S.-H., Motomura, T., and Ichimura, T. (2000). Nuclear phase alternation in the life cycle of *Derbesia* (Chlorophyta). *Phycologia* 39:441–7.

Lee, Y-K., and Ding, S-Y. (1995). Effects of dissolved oxygen partial pressure on the accumulation of astaxanthin in chemostat cultures of *Haematococcus lacustris* (Chlorophyta). *J. Phycol*. 31:922–4.

Lembi, C. A., and Herndon, W. R. (1966). Fine structure of the pseudocilia of *Tetraspora. Can. J. Bot*. 44:710–12.

Lemieux, C., Otis, C., and Turmel, M. (2000). Ancestral chloroplast genome in *Mesostigma viride* reveals an early branch of green plant evolution. *Nature* 403:649–52.

Leonardi, P. I., Caceres, E. J., and Velez, C. G. (1998). Fine structure of dwarf males in *Oedogonium pluviale* (Chlorophyceae). *J. Phycol*. 34:250–6.

Lewin, R. A. (1957). The zygote of *Chlamydomonas moewusii. Can. J. Bot*. 35:795–807.

Lewin, R. A. (1958). The cell walls of *Platymonas. J. Gen. Microbiol*. 19:87–90.

Lewis, L. A., and McCourt, R. M. (2004). Green algae and the origin of land plants. *Amer. J. Bot*. 91:1535–56.

Lucas, W. C. (1979). Alkaline band formation in *Chara corallina. Plant Physiol*. 63:248–54.

Lurling, M. (1998). Effect of grazing-associated infochemicals as growth and morphological development in *Scenedesmus acutus* (Chlorophyceae). *J. Phycol*. 34:578–86.

Lurling, M. (1999). Grazer-induced coenobial formation in clonal cultures of *Scenedesmus*

obliquus (Chlorococcales, Chlorophyceae). *J. Phycol*. 35:19–23.

Lynn, R., and Brock, T. D. (1969). Notes on the ecology of a species of *Zygogonium* (Kütz) in Yellowstone National Park. *J. Phycol*. 5:181–5.

McCourt, R. M. (2000). Phylogeny of the conjugating green algae (Zygnemophyceae) based on *rbc*L sequences. *J. Phycol*. 36:747–58.

McCourt, R. M., Karol, K. G., Kaplan, S., and Hoshaw, R. W. (1995). Using *rbc*L sequences to test hypotheses of chloroplast and thallus evolution in conjugating green algae (Zygnematales, Charophyceae). *J. Phycol*. 31:989–95.

McGarry, M. G., and Tongkasame, C. (1971). Water reclamation and algae harvesting. *Water Pollut. Control Fed. J*. 43:824–35.

McLean, R. O. (1974). The tolerance of *Stigeoclonium tenue* Kütz. to heavy metals in South Wales. *Br. Phycol. J*. 9:91–5.

McLean, R. O., and Benson-Evans, K. (1974). The distribution of *Stigeoclonium tenue* Kütz. in South Wales in relation to its use as an indicator of organic pollution. *Br. Phycol. J*. 9:83–9.

Maeda, M., Kuroda, K., Iriki, Y., Chihara, M., Nisizawa, K., and Miwa, T. (1966). Chemical nature of major cell wall constituents of *Vaucheria* and *Dichotomosiphon* with special reference to their phylogenetic positions. *Bot. Mag. Tokyo* 79:634–43.

Malmberg, A. E., and VanWinkle-Swift, K. P. (2001). Zygospore germination in *Chlamydomonas monoica* (Chlorophyta): timing and pattern of secondary zygospore wall degradation in relation to cytoplasmic events. *J. Phycol*. 37:86–94.

Mandoli, D. F. (1998). Whatever happened to *Acetabularia*? Bringing a once classic model system into the age of molecular genetics. *Int. Rev. Cytol*. 182:1–68.

Manton, I., and Ettl, H. (1965). Observations on the fine structure of *Mesostigma viride* Lauterborn. *J. Linn. Soc. (Bot.)* 59:175–84.

Manton, I., and Parke, M. (1960). Further observations on green flagellates with special reference to possible relatives of *Chromulina pusilla* Butcher. *J. Mar. Biol. Assoc*. 39:275–98.

Marchant, H. J. (1977). Ultrastructure, development and cytoplasmic rotation of seta-bearing cells of *Coleochaete scutata*. *J. Phycol*. 13:28–36.

Marchant, H. J., and Pickett-Heaps, J. D. (1971). Ultrastructure and differentiation of *Hydrodictyon reticulatum*. II. Formation of zoids within the coenobium. *Aust. J. Biol. Sci*. 24:471–86.

Marchant, H. J., and Pickett-Heaps, J. D. (1972a). Ultrastructure and differentiation of *Hydrodictyon reticulatum*. III. Formation of the vegetative daughter net. *Aust. J. Biol. Sci*. 25:265–78.

Marchant, H. J., and Pickett-Heaps, J. D. (1972b). Ultrastructure and differentiation of *Hydrodictyon reticulatum*. IV. Conjugation of gametes and the development of zoospores and azygospores. *Aust. J. Biol. Sci*. 25:279–91.

Marchant, H. J., and Pickett-Heaps, J. D. (1972c). Ultrastructure and differentiation of *Hydrodictyon reticulatum*. V. Development of polyhedra. *Aust. J. Biol. Sci*. 25:1187–97.

Marchant, H. J., and Pickett-Heaps, J. D. (1972d). Ultrastructure and differentiation of *Hydrodictyon reticulatum*. VI. Formation of the germ net. *Aust. J. Biol. Sci*. 25:1199–213.

Marin, B., and Melkonian, M. (1999). Mesostigmatophyceae, a new class of streptophyte green algae revealed by SSU rRNA sequence comparisons. *Protist* 150:399–417.

Mars, P. W., Rabson, A. R., Rippey, J. J., and Ajello, L. (1971). Cutaneous protothecosis. *Br. J. Dermatol.* 85, *Suppl*. 7:76–84.

Martin, N. C., and Goodenough, U. W. (1975). Gametic differentiation in *Chlamydomonas reinhardtii*. I. Production of gametes and their fine structure. *J. Cell Biol*. 67:587–605.

Matsuda, Y., Saito, T., Yamaguchi, T., Koseki, M., and Hayashi, K. (1987). Topography of cell wall lytic enzyme in *Chlamydomonas reinhardtii:* Form and location of the stored enzyme in vegetative cell and gamete. *J. Cell Biol*. 104:321–9.

Matsuo, Y., Imagawa, H., Nishizawa, M., and Shizuri, Y. (2005). Isolation of an algal inducer from a marine bacterium. *Science* 307:1598.

Mattox, K. R., and Stewart, K. D. (1973). Observations on the zoospores of *Pseudodendoclonium basiliense* and *Trichosarcina polymorpha* (Chlorophyceae). *Can. J. Bot*. 51:1425–30.

Mattox, K. R., and Stewart, K. D. (1977). Cell division in the scaly green flagellate *Heteromastix angulata* and its bearing on the origin of the Chlorophyceae. *Am. J. Bot*. 64:931–45.

Mattox, K. R., and Stewart, K. D. (1984). Classification of the green algae; A concept based on comparative cytology. In *Systematics of the Green Algae* ed. D. E. G. Irvine, and D. M. John, pp. 29–72. London and Orlando: Academic Press.

Melkonian, M. (1980a). Flagellar roots, mating structure and gametic fusion in the green alga *Ulva lactuca* (Ulvales). *J. Cell Sci*. 46:149–69.

Melkonian, M. (1980b). Flagellar apparatus, mating structure and gametic fusion in *Ulva lactuca* (Ulvales, Chlorophyceae). *Br. Phycol. J.* 15:197.

Melkonian, M. (1989). Flagellar apparatus ultrastructure in *Mesostigma viride* (Prasinophyceae). *Plant Syst. Evol*. 164:93–122.

Melkonian, M., and Robenek, H. (1980a). Eyespot membranes in newly released zoospores of the green alga *Chlorosarcinopsis gelatinosa* (Chlorosarcinales) and their fate during zoospores settlement. *Protoplasma* 104:129–40.

Melkonian, M., and Robenek, H. (1980b). Eyespot membranes of *Chlamydomonas reinhardtii:* A freeze-fracture study. *J. Ultrastruct. Res*. 72:90–102.

Melkonian, M., Schulze, D., McFadden, G. I., and Robenek, H.. (1988). A polyclonal antibody (anti-centrin) distinguishes between the two types of fibrous flagellar roots in green algae. *Protoplasma* 144:56–61.

Menzel, D. (1980). Plug formation and peroxidase accumulation in two orders of siphonous green algae (Caulerpales and Dasycladales) in relation to fertilization and injury. *Phycologia* 19:37–48.

Menzel, D. (1986). Visualization of cytoskeletal changes through the life cycle in *Acetabularia. Protoplasma* 134:30–42.

Metzger, P., Allard, B., Casadevall, E., Berkaloff, C., and Couté, A. (1990). Structure and chemistry of a new chemical race of *Botryococcus braunii* (Chlorophyceae) that produces lycopadiene, a tetraterpenoid hydrocarbon. *J. Phycol*. 26:258–66.

Miller, D. H. (1978). Cell wall chemistry and ultrastructure of *Chlorococcum oleofaciens* (Chlorophyceae). *J. Phycol*. 14:189–94.

Mimietz, S., Heidecker, M., Krohne, G., Wegner, L.-H., and Zimmerman, U. (2003). Impact of hypoosmotic challenges on spongy architecture of the cytoplasm of the giant marine alga *Valonia utricularis. Protoplasma* 222:117–28.

Mineyuki, Y., Kataoka, H., Masuda, Y., and Nagai, R. (1995). Dynamic changes in the actin cytoskeleton during the high-fluence rate response of the *Mougeotia* chloroplast. *Protoplasma* 185:222–29.

Miyamura, S. (2004). Visualization of the rapid fertilization process of the marine green alga, *Ulva arasaki* Chihara (Ulvophyceae, Chlorophyta) using high-speed video microscopy. *Cytologia* 69:197–201.

Miyamura, S., Hori, T., and Nagumo, T. (2003). Eyespot behavior during the fertilization of gametes in *Ulva arasaki* Chihara (Ulvophyceae, Chlorophyta). *Phycol. Res*. 51:143–6.

Moestrup, Ø. (1978). On the phylogenetic validity of the flagellar apparatus in green algae and other chlorophyll *a* and *b* containing plants. *BioSystems* 10:117–44.

Moestrup, Ø., and Hoffman, L. R. (1973). Ultrastructure of the green alga *Dichotomosiphon tuberosus* with special reference to the occurrence of striated tubules in the chloroplast. *J. Phycol*. 9:430–7.

Moestrup, Ø., and Hoffman, L. R. (1975). A study of the spermatozoids of *Dichotomosiphon tuberosus* (Chlorophyceae). *J. Phycol*. 11:225–35.

Moldowan, J. M., and Seifert, W. K. (1980). First discovery of botrycoccane in petroleum. *J.S.C. Chem. Comm*., 912–14.

Mori, K., and Takanashi, S. (1996). Synthesis of lurlene, the sex pheromone of the green flagellate *Chlamydomonas allwensworthii. Tetrahedron Lett*. 37:1821–4.

Musgrave, A. (1993). Mating in *Chlamydomonas. Prog. Phycol. Res*. 9:193–237.

Nelson, T. A., Lee, D. J., and Smith, B. C. (2003). Are "green tides" harmful algal blooms? Toxic properties of water soluble extracts from two bloom-forming macroalgae, *Ulva fenestrata* and *Ulvaria obscura* (Ulvophyceae). *J. Phycol*. 39:874–9.

Neumann, K. (1969). Protonema mit Riesenkern bei der siphonalen Grünalge *Bryopsis hypnoides* und weitere cytologische Befunde. *Helgol. Wiss. Meeresunters*. 19:45–57.

Nishii, I., Ogihara, S., and Kirk, D. L. (2003). A kinesin, *invA*, plays an essential role in *Volvox* morphogenesis. *Cell* 113:743–53.

Nitecki, M. H. (1971). *Ischadites abbottae*, a new North American Silurian species (Dasycladales). *Phycologia* 10:263–75.

Nossag, J., and Kasprik, W. (1993). The movement of *Micrasterias thomasiana* (Desmidaceae, Zygnematophyceae) in directed blue light. *Phycologia* 32:332–7.

O'Kelley, J. C. (1984). Nitrogen and gamete production in *Chlorococcum echinozygotum. J. Phycol*. 20:220–5.

Okuda, K., and Brown, R. M. (1992). A new putative cellulose-synthesizing complex of *Coleochaete scutata*. *Protoplasma* 168:51–63.

Okuda, K., Tsekos, I., and Brown, R. M. (1994). Cellulose microfibril assembly in *Erythrocladia subintegra* Rosenv.: An ideal system for understanding the relationship between synthesizing complexes (TCs) and microfibril crystallization. *Protoplasma* 180:49–58.

Oltmanns, F. (1898). Die Entwickelung der Sexualorgane bei *Coleochaete pulvinata. Flora* 85:1–14.

Orset, S., and Young, A. J. (1999). Low-temperature-induced synthesis of α-carotene in the microalga *Dunaliella salina* (Chlorophyta). *J. Phycol*. 35:320–7.

Oschman, L. J. (1966). Development of the symbiosis of *Convoluta roscoffensis* Graff and *Platymonas* sp. *J. Phycol*. 2:105–11.

Page, J. Z., and Kingsbury, J. M. (1968). Culture studies on the marine green alga *Halicystis parvula – Derbesia tenuissima*. II. Synchrony and periodicity in gamete formation and release. *Am. J. Bot*. 55:1–11.

Pan, J., and Snell, W. J. (2000). Signal transduction during fertilization in the unicellular green alga, *Chlamydomonas. Curr. Opin. Microbiol*. 3:596–602.

Parke, M., and Manton, I. (1967). The specific identity of the algal symbiont in *Convoluta roscoffensis. J. Mar. Biol. Assoc. UK* 47:445–64.

Parker, B. C. (1970). Significance of cell wall chemistry to phylogeny in the algae. *Ann. NY Acad. Sci*. 175:417–28.

Pasquale, S. M., and Goodenough, U. W. (1987). Cyclic AMP functions as a primary sexual signal in gametes of *Chlamydomonas reinhardtii. J. Cell Biol*. 105:2279–92.

Philips, J. A., and Price, I. R. (2002). How different is Mediterranean *Caulerpa taxifolia* (Caulerpales: Chlorophyta) to other populations of the species? *Mar. Ecol. Progr. Ser*. 238:61–71.

Piazzi, L., Ceccherelli, G., and Cinelli, F. (2001). Threat to macroalgal diversity: effect of the introduced green alga *Caulerpa racemosa* in the Mediterranean. Mar. Ecol. Progr. Ser. 210:149–59.

Pickett-Heaps, J. D. (1970). Some ultrastructural features of *Volvox* with particular reference to the phenomenon of inversion. *Planta* 90:174–90.

Pickett-Heaps, J. D. (1971). Reproduction by zoospores in *Oedogonium*. I. Zoosporogenesis. *Protoplasma* 72:275–314.

Pickett-Heaps, J. D. (1973). Cell division and wall structure in *Microspora. New Phytol*. 72:347–55.

Pickett-Heaps, J. D. (1974). Cell division in *Stichococcus. Br. Phycol. J.* 9:63–73.

Pickett-Heaps, J. D. (1976). Cell division in *Raphidonema longiseta. Arch. Protiskenkd*. 118:209–14.

Plain, N., Largeau, C., Derenne, S., and Couté, A. (1993). Variabilité morphologique de *Botryococcus braunii* (Chlorococcales, Chlorophyta) corrélations avec les conditions de croissance et la teneur en lipides. *Phycologia* 32:259–65.

Pocock, M. A. (1960). *Hydrodictyon:* A comparative biological study. *J. S. Afr. Bot*. 26:167–319.

Powers, J. H. (1908). Further studies in *Volvox*, with description of three new species. *Trans. Am. Microsc. Soc*. 28:141–75.

Proctor, V. W. (1962). Viability of *Chara* oospores taken from migrating water birds. *Ecology* 43:528–9.

Proskauer, J. (1950). On *Prasinocladus. Am. J. Bot*. 37:59–66.

Provasoli, L, and Pinter, I. J. (1980). Bacteria induced polymorphism in an axenic laboratory strain of *Ulva lactuca* (Chlorophyceae). *J. Phycol*. 16:196–201.

Rawitscher-Kunkel, E., and Machlis, L. (1962). The hormonal integration of sexual reproduction in *Oedogonium. Am. J. Bot.* 49:177–83.

Retallack, B., and Butler, R. D. (1970). The development and structure of the zoospore vesicle in *Bulbochaete hiloensis. Arch. Mikrobiol*. 72:223–37.

Richardson, D. H. S. (1973). Photosynthesis and carbohydrate movement. In *The Lichens*, ed. V. Ahmadjian, and M. E. Hale, pp. 249–88. New York and London: Academic Press.

Rindi, F., and Guiry, M. D. (2003). Composition and distribution of subaerial algal assemblages in Galway City, Western Ireland. *Cryptogamie Algologie* 24:245–67.

Roberts, K. (1974). Crystalline glycoprotein cell walls of algae: Their structure, composition and assembly. *Philos. Trans. R. Soc. Lond*. [*B*], 268:129–46.

Roberts, K. R., Sluiman, H. J., Stewart, K. D., and Mattox, K. R. (1981). Comparative cytology and taxonomy of the Ulvaphyceae. III. The flagellar apparatuses of the anisogametes of *Derbesia tenuissima* (Chlorophyta). *J. Phycol*. 17:330–40.

Ross, C., Vreeland, V., Waite, J. H., and Jacobs, R. S. (2005). Rapid assembly of a wound plug: stage one of a two-stage wound repair mechanism in the giant unicellular chlorophyte *Dasycladus vermicularis* (Chlorophyceae). *J. Phycol*. 41:46–54.

Russell, F. S., and Yonge, C. M. (1963). *The Seas*. 2nd edn. London and New York: Frederick Warne and Co.

Sabnis, D. D., and Jacobs, W. P. (1967). Cytoplasmic streaming and microtubules in the coenocytic marine alga, *Caulerpa prolifera. J. Cell Sci.* 2:465–72.

Salisbury, J. L., and Floyd, G. L. (1978). Calcium-induced contraction of the rhizoplast of a quadriflagellate green alga. *Science* 202:975–6.

Sawada, T. (1972). Periodic fruiting of *Ulva pertusa* at three localities in Japan. *Proc. 7th Int. Seaweed Symp*., pp. 229–30. Tokyo: University of Tokyo Press.

Sawitzky, H., Gleissberg, S., and Berger, S. (1998). Phylogenetic implictions of patterns of cap development in selected species of *Acetabularia*/*Polyphysa* (Dasycladaceae, Chlorophyta). *Phycologia* 37:478–85.

Scagel, R. F., Bandoni, R. J., Rouse, G. E., Scofield, W. B., Stein, J. R., and Taylor, T. M. C. (1965). *An Evolutionary Survey of the Plant Kingdom*. Belmont, CA: Wadsworth.

Schlegel, I., Krienitz, L., and Hepperle, D. (2000). Variability of calcification of *Phacotus lenticularis* (Chlorophyta, Chlamydomonadales) in nature and culture. *Phycologia* 39:318–22.

Schmitt, R. (2003). Differentiation of germinal and somatic cells in *Volvox carteri. Curr. Opin. Microbiol*. 6:608–13.

Schnetter, R., and Eckhardt, R. (2000). Does karyogamy follow plasmogamy in the life cycle of *Derbesia tenuissima* (Chlorophyta). *Phycologia* 39:355–7.

Shepherd, V. A., Beilby, M. J., and Bisson, M. A. (2004). When is a cell not a cell? A theory relating coenocytic structure to the unusual electrophysiology of *Ventricaria ventricosa (Valonia ventricosa). Protoplasma* 223:79–91.

Sherwood, A. R., Garbary, D. J., and Sheath, R. G. (2000). Assessing the phylogenetic position of the Prasiolales (Chlorophyta) using *rbc*L and 18S rRNA gene sequence data. *Phycologia* 39:139–46.

Shimmen, T., and MacRobbie, E. A. C. (1987). Demonstration of two proton translocating systems in tonoplast of permeabilized *Nitella* cell. *Protoplasma* 136:205–7.

Simons, J., and van Beem, A. P. (1987). Observations on asexual and sexual reproduction in *Stigeoclonium helveticum* Vischer (Chlorophyta) with implications for the life history. *Phycologia* 26:356–62.

Simons, J., van Beem, A. P., and de Vries, P. J. R. (1982). Structure and chemical composition of the spore wall in *Spirogyra* (Zygnemataceae, Chlorophyceae). *Acta Bot. Neerl*. 31:359–70.

Singh, H. V., and Chaudhary, B. R. (1990). Nutrient effects on the formation of oogonia in *Oedogonium hatei* (Chlorophyta). *Phycologia* 29:332–7.

Sluiman, H. J. (1983). The flagellar apparatus of the zoospore of the filamentous green alga *Coleochaete pulvinata:* Absolute configuration and phylogenetic significance. *Protoplasma* 115:160–75.

Sluiman, H. J. (1985). A cladistic evaluation of the lower and higher green plants (Viridiplantae). *Plant Syst. Evol*. 149:217–32.

Sineshchekov, O. A., Jung, K.-H., and Spudich, J. L. (2002). Two rhodopsins mediate phototaxis to low- and high-intensity light in *Chlamydomonas reinhardtii. Proc. Natl. Acad. Sci., USA* 99:8689–94.

Smith, G. M. (1920). *Phytoplankton of the Inland Lakes of Wisconsin*, Part I. State of Wisconsin Publ.

Smith, G. M. (1944). A comparative study of the species of *Volvox. Trans. Am. Microsc. Soc*. 63:265–310.

Smith, G. M. (1947). On the reproduction of some Pacific Coast species of *Ulva. Am. J. Bot*. 34:80–7.

Smith, G. M. (1950). *The Freshwater Algae of the United States*. New York: McGraw-Hill.

Smith, G. M. (1955). *Cryptogamic Botany*, Vol. 1, 2nd edn. New York: McGraw-Hill.

Smith, G. M. (1969). *Marine Algae of the Monterey Peninsula*. Stanford, Calif: Stanford University Press.

Snell, W. J. (1985). Cell–cell interactions in *Chlamydomonas. Annu. Rev. Plant Physiol*. 36:287–315.

Sormus, L., and Bicudo, C. E. M. (1974). Polymorphism in the desmid *Micrasterias pinnatifida* and its taxonomical implications. *J. Phycol*. 10:274–9.

Staehelin, L. A., and Pickett-Heaps, J. D. (1975). The ultrastructure of *Scenedesmus* (Chlorophyceae) I. Species with the "reticulate" or "warty" type of ornamental layer. *J. Phycol*. 11:163–85.

Stanley, S. M. (1979). *Macroevolution*. San Francisco: W. H. Freeman.

Stark, K., and Schmitt, R. (2002). Genetic control of germ-soma differentiation in *Volvox carteri. Protist* 153:99–107.

Stark, L. M., Almodovar, L., and Krauss, R. W. (1969). Factors affecting the rate of calcification in *Halimeda opuntia* (L.) Lamouroux and *Halimeda discoidea* Decaisne. *J. Phycol*. 5:305–12.

Starr, R. C. (1954). Heterothallism in *Cosmarium botrytis* var. *subtumidum. Am. J. Bot*. 41:601–7.

Starr, R. C. (1972). A working model for the control of differentiation during development of the embryo of *Volvox carteri* f. *nagariensis. Soc. Bot. Fr. Memoires*, pp. 175–82.

Starr, R. C., and Jaenicke, L. (1974). Purification and characterization of the hormone initiating sexual morphogenesis in *Volvox carteri* f. *nagariensis Iyengar. Proc. Natl. Acad. Sci. USA* 71:1050–4.

Starr, R. C., Marner, F. J., and Jaenicke, L. (1995). Chemoattraction of male gametes by a pheromone produced by female gametes of *Chlamydomonas. Proc. Natl. Acad. Sci., USA*. 92:641–5.

Steinkötter, J., Bhattacharya, D., Semmelroth, I., Bibeau, C., and Melkonian, M. (1994). Prasinophytes form independent lineages within the Chlorophyta: Evidence from ribosomal RNA sequence comparisons. *J. Phycol*. 30:340–5.

Stratmann, J., Paputsoglu, G., and Oertel, W. (1996). Differentiation of *Ulva mutabilis* (Chlorophyta) gametangia and gamete release are controlled by extracellular inhibitors. *J. Phycol*. 32:1009–21.

Suzuki, L., and Johnson, C. H. (2001). Algae know the time of day: circadian and photoperiodic programs. *J. Phycol*. 37:933–42.

Suzuki, K., Iwamoto, K., Yokoyama, S., and Ikawa, T. (1991). Glycolate-oxidizing enzymes in algae. *J. Phycol*. 27:492–8.

Syrett, P. J., and Al-Houty, F. A. A. (1984). The phylogenetic significance of the occurrence of urease/urea amidolyase and glycollate oxidase/glycollate dehydrogenase in green algae. *Br. Phycol. J.* 19:11–21.

Takatori, S., and Imahori, K. (1971). Light reactions in the control of oospore germination of *Chara delicatula. Phycologia* 10:221–8.

Tan, S., Cunningham, F. X., Youmana, M., Grabowski, B., Sun, Z., and Gantt, E. (1995). Cytochrome loss in astaxanthin-accumulating red cells of *Hematococcus pluvialis* (Chlorophyceae): Comparison of photosynthetic activity, photosynthetic enzymes, and thylakoid membrane polypeptides in red and green cells. *J. Phycol*. 31:897–905.

Taylor, W. R. (1960). *Marine Algae of the Eastern Tropical and Subtropical Coasts of the Americas*. Ann Arbor: University of Michigan Press.

Tolbert, N. E. (1976). Glycollate oxidase and glycollate dehydrogenase in marine algae and plants. *Aust. J. Plant Physiol*. 3:129–32.

Trainor, F. R. (1963). Zoospores on *Scenedesmus obliquus. Science* 142:1673–4.

Trainor, F. R. (1970). Survival of algae in a dessicated soil. *Phycologia* 9:111–13.

Trainor, F. R. (1992). Cyclomorphosis in *Scenedesmus armatus* (Chlorophyta): an ordered sequence of ecomorph development. *J. Phycol*. 28:552–8.

Trench, R. K., Greene, R. W., and Bystrom, B. G. (1969). Chloroplasts as functional organelles in animal tissues. *J. Cell Biol*. 42:404–17.

Trench, R. K., Boyle, J. E., and Smith, D. C. (1973a). The association between chloroplasts of *Codium fragile* and the mollusc *Elysia viridis*. I. Characteristics of isolated *Codium* chloroplasts. *Proc. R. Soc. Lond.* [*B*] 184:51–61.

Trench, R. K., Boyle, J. E., and Smith, D. C. (1973b). The association between chloroplasts of *Codium fragile* and the mollusc *Elysia viridis*. II. Chloroplast ultrastructure and photosynthetic carbon fixation in *E. viridis. Proc. R. Soc. Lond*. [*B*] 184:63–81.

Tsekos, I. (1999). The sites of cellulose synthesis in algae: diversity and evolution of cellulase-synthesizing enzyme complexes. *J. Phycol*. 35:635–55.

Van Kruiningen, H. J., Garner, F. M., and Schiefer, B. (1969). Protothecosis in a dog. *Pathol. Vet*. 6:348–54.

vanWinkle-Swift, K. P., and Rickoll, W. L. (1997). The zygospore wall of *Chlamydomonas monoica* (Chlorophyceae): morphogenesis and evidence for the presence of sporopollenin. *J. Phycol*. 33:655–65.

Verlaque, M., Durand, C., Huisman, J. M., Boudouresque, C.-F., and LeParco, Y. (2003). On the identity and origin of the Mediterranean invasive *Caulerpa racemosa* (Caulerpales, Chlorophyta). *Eur. J. Phycol*. 38:325–39.

Wake, L. V., and Hillen, L. W. (1980). Study of a "bloom" of the oil-rich alga *Botryococcus braunii* in the Darwin River Reservation. *Biotech. Bioeng*. 22:1637–56.

Wang, B., Zarka, A., Trebst, A., and Boussiba, S. (2003). Astaxanthin accumulation in *Haematococcus pluvialis* (Chlorophyceae) as an active photoprotective process under high irradiance. *J. Phycol*. 39:1116–24.

Watanabe, S., Kuroda, N., and Maiwa, F. (2001). Phylogenetic status of *Helicodictyon planctonicum and Desmochloris halophila* gen. et comb. nov. and the definition of the class Ulvophyceae (Chlorophyta). *Phycologia* 40:421–34.

Webster, D. A., Hackett, D. P., and Park, R. B. (1968). The respiratory chain of colorless algae. III. Electron microscopy. *J. Ultrastruct. Res*. 21:514–23.

Wheeler, A. E., and Page, J. Z. (1974). The ultrastructure of *Derbesia tenuissima* (de Notaris) Crouan. I. Organization of the gametophyte protoplast, gametangium, and gametangial pore. *J. Phycol*. 10:336–52.

Wiese, L., and Hayward, P. C. (1972). On sexual agglutination and mating-type substances in isogamous dioecious chlamydomonads. III. The sensitivity of sex cell contact to various enzymes. *Am. J. Bot*. 59:530–6.

Wilbur, K. M., Colinvaux, L. H., and Watabe, N. (1969). Electron microscope study of calcification in the alga *Halimeda* (order Siphonales). *Phycologia* 8:27–35.

Wilcox, L. W., Fuerst, P. A., and Floyd, G. L. (1993). Phylogenetic relationships of four charophycean green algae inferred from complete nuclear-encoded small subunit rRNA gene sequences. *Amer. J. Bot*. 80:1028–33.

Wolf, F. R., Nonomura, A. M., and Bassham, J. A. (1985). Growth and branched hydrocarbon production in a strain of *Botryococcus braunii* (Chlorophyta). *J. Phycol*. 21:388–96.

Woodcock, C. L. F. (1971). The anchoring of nuclei by cytoplasmic microtubules in *Acetabularia. J. Cell Sci.* 8:611–21.

Woodcock, C. L. F., and Miller, G. J. (1973a). Ultrastructural features of the life cycle of *Acetabularia mediterranea*. I. Gametogenesis. *Protoplasma* 77:313–29.

Woodcock, C. L. F., and Miller, G. J. (1973b). Ultrastructural features of the life cycle of *Acetabularia mediterranea*. II. Events associated with the division of the primary nucleus and the formation of cysts. *Protoplasma* 77:331–41.

Wray, J. L. (1977). *Calcareous Algae*. Amsterdam: Elsevier.

Wujek, D. E. (1968). Some observations on the fine structure of three genera in the Tetrasporaceae. *Ohio J. Sci*. 68:187–91.

Wustman, B. A., Melkonian, M., and Becker, B. (2004). A study of cell wall and flagella formation during cell division in the scaly green alga, *Scherffelia dubia* (Chlorophyta). *J. Phycol*. 46:895–910.

Yamaguchi, K. (1997). Recent advances in microalgal bioscience in Japan, with special reference to utilization of biomass and metabolites: a review. *J. Appl. Phycol*. 8:487–502.

Yoshii, Y., Takaichi, S., Maoka, T., and Inouye, I. (2003). Photosynthetic pigment composition in the primitive green alga *Mesostigma viride* (Prasinophyceae): phylogenetic and evolutionary implications. *J. Phycol*. 39:570–6.

Zechman, F. W. (2003). Phylogeny of the Dasycladales (Chlorophyta, Ulvophyceae) based on analyses of Rubisco large subunit (*rbc*L) gene sequences. *J. Phycol*. 39:819–27.

Zeigler, J. R., and Kingsbury, J. M. (1964). Cultural studies on the marine green alga *Halicystis parvula–Derbesia tenuissima*. I. Normal and abnormal sexual and asexual reproduction. *Phycologia* 4:105–16.

Zuljevic, A., and Antollic, B. (2000). Synchronous release of male gametes of *Caulerpa taxifolia* (Caulerpales, Chlorophyta) in the Mediterranean Sea. *Phycologia* 39:257–9.

Part IV

Evolution of one membrane of chloroplast endoplasmic reticulum

The Euglenophyta (euglenoids), Apicomplexa, and Dinophyta (dinoflagellates) are a natural grouping in that they are the only algal groups to have one membrane of chloroplast endoplasmic reticulum. Chloroplast endoplasmic reticulum evolved when a chloroplast from a eukaryotic alga was taken into a food vesicle by a phagocytotic euglenoid, apicomplexan or dinoflagellate (Fig. IV.1) (Lee, 1977; Gibbs, 1978). Normally the cell would have digested the chloroplast as a source of food. However, in this case the chloroplast remained in the cytoplasm of the host as an endosymbiont. The host benefited from the association by receiving photosynthate from the endosymbiotic chloroplast. The endosymbiotic chloroplast benefited from the high concentration of carbon dioxide in the acidic environment of the host vesicle. Eventually the food vesicle membrane of the host became the single membrane of chloroplast endoplasmic reticulum surrounding the chloroplast. It is probable that the plastid of the euglenoids evolved by the capture of a green-algal chloroplast. The plastids of the dinoflagellates and apicomplexans probably are derived from an endosymbiotic red-algal chloroplast.

It appears that algae with chloroplast endoplasmic reticulum were selected for in evolution because of their ability to outcompete other algae in environments which are low in dissolved CO_2. Before explaining the mechanism by which these algae are able to outcompete, it is necessary to understand the equilibria governing the distribution of carbon species in water.

Carbon occurs in water as dissolved inorganic carbon (DIC) which is composed of HCO_3^-, CO_3^{-2} and CO_2.

$$H_2O + CO_2 \rightleftharpoons H_2CO_3 \rightleftharpoons H^+ + HCO_3^- \rightleftharpoons 2H^+ + CO_3^-$$

Seawater in equilibrium with the atmosphere at pH 8.2 and 25 °C contains about 2200 μm of dissolved inorganic carbon. At this pH, 10 μm

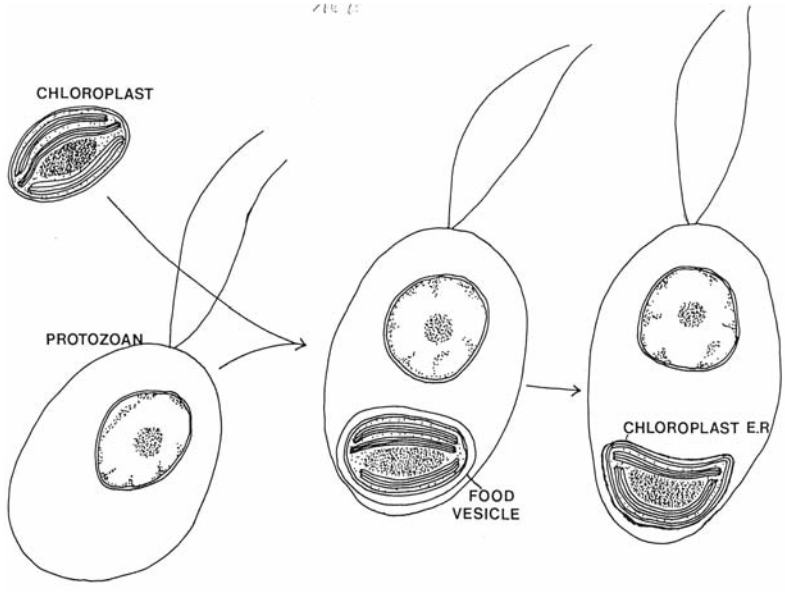


Fig. IV.1 Drawing illustrating the protable sequence of evolutionary events that led to a chloroplast being surrounded by a single membrane of chloroplast endoplasmic reticulum. Initially a chloroplast was taken up by a phagocytotic protozoan into a food vesicle, with the food vesicle membrane eventually evolving into the single membrane of chloroplast endoplasmic reticulum surrounding the chloroplast

occurs as CO_2, 200 μm occurs as CO_3^{-2} with the remainder occurring as HCO_3^-. As the pH is lowered, more of the dissolved inorganic carbon occurs as CO_2. At pH 1 virtually all the dissolved inorganic carbon occurs as CO_2, with HCO_3^- completely absent.

Carbon dioxide is the form of carbon that is fixed by the carboxylating enzyme in photosynthesis, ribulose 1,5-bisphosphate carboxylase/oxygenase (Rubisco) (Falkowski and Raven, 1998). Many microalgae have developed a CO_2 concentrating mechanism (CCM) that concentrates CO_2 inside cells to a level several times higher than the CO_2 in the external medium (Fridlyand, 1997; Sukenik et al., 1997). The CO_2 concentrating mechanisms pumps bicarbonate (HCO_3^-) outside the cell through the plasma membrane and chloroplast membrane into the chloroplast. Once inside the chloroplast, the dissolved inorganic carbon stays mostly as HCO_3^- because the stroma is alkaline. A significant amount of the HCO_3^- passes into the lumen of the thylakoids, where in illuminated chloroplasts, the pH is about 5 (Fridlyand, 1997). The enzyme carbonic anhydrase is attached to the thylakoid membranes (Raven, 1997). In the lumen of the thylakoids, carbonic anhydrase converts the HCO_3^- to CO_2 at a rate hundreds of times faster than the non-enzymatic conversion.

$$HCO_3^- + H^+ \rightarrow CO_2 + H_2O$$

The result is a CO_2 concentration that is ten times higher than HCO_3^- in the lumen of the thylakoids (Raven, 1997).

Efflux of the CO_2 from the thylakoid lumen to the chloroplast stroma suppresses Rubisco oxygenase activity and stimulates carboxylase activity in the stroma (or pyrenoid if one is present). Through carboxylation by Rubisco, the CO_2 enters into the carbon reduction cycle. Thus the

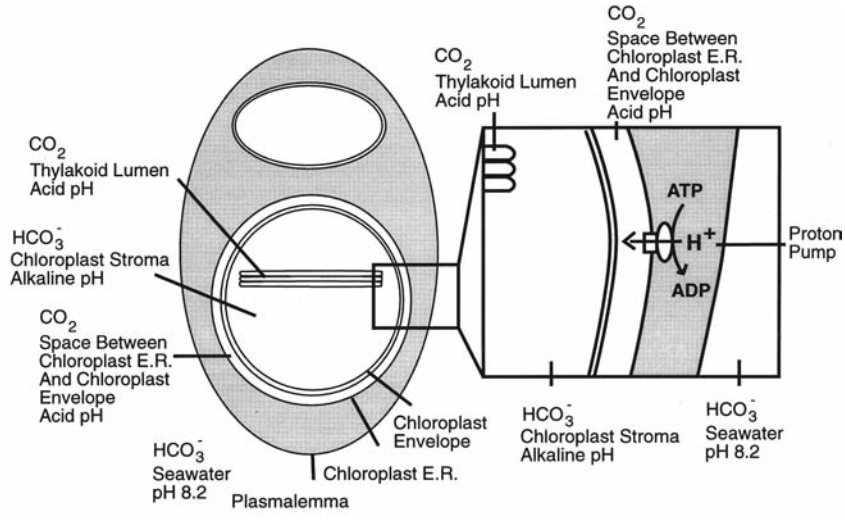


Fig. IV.2 Diagrammatic representation of the compartments present in an alga with one membrane of chloroplast endoplasmic reticulum. The pH and predominant form of dissolved inorganic carbon are indicated for each compartment.

evolutionary goal of the carbon concentrating mechanism is to increase the concentration of CO_2 at the location of Rubisco.

Once generated by carbonic anhydrase, the CO_2 rapidly diffuses away from the thylakoid lumen and out of the chloroplast, reducing the effectiveness of the carbon concentrating mechanism. Algae with chloroplast E.R. have limited the egress of CO_2 by the following mechanism (Fig. IV.2). The volume between the chloroplast envelope and chloroplast endoplasmic reticulum most likely has an acid pH since the membrane of chloroplast E.R. next to the chloroplast envelope was the vacuolar membrane in the original endosymbiosis leading to the establishment of chloroplast E.R. (Lee, 1977; Gibbs, 1978). An acidic pH in the volume between the chloroplast envelope and the adjacent membrane of chloroplast E.R. is therefore probable since the pH of digestive vacuoles of phagocytic protozoa is usually acidic when tested for acid phosphatase (optimal pH 5). An acid pH in the volume between the chloroplast envelope and chloroplast E.R. would contain a relatively high concentration of CO_2, and a relatively low concentration of HCO_3^-, because of the effect of pH on the balance between the two entities. The chloroplast membranes are relatively permeable to CO_2 so the CO_2 in this space would freely move into the chloroplast stroma. A relatively high concentration of CO_2 would, therefore, be maintained in the chloroplast with CO_2 entering both from the acidic thylakoid lumen and the acidic space between the chloroplast E.R. and chloroplast envelope. This would provide algae with chloroplast E.R. with an abundant supply of CO_2 for photosynthesis, particularly in the

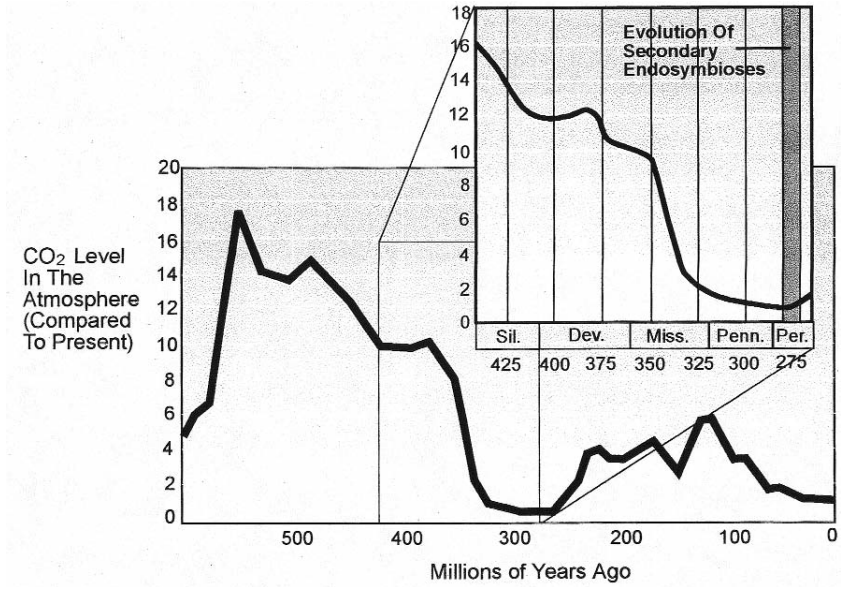


Fig. IV.3 The amount of CO_2 in the atmosphere over the past 600 Ma. The time of evolution of secondary endosymbioses around 275 Ma is shown in the insert.

marine environment where at pH 8.2, the dissolved CO_2 concentration is particularly low. In such an environment, algae with chloroplast endoplasmic reticulum had a competitive advantage and were selected for in evolution.

On the basis of a molecular clock, Medlin et al. (1997) postulated that the original secondary endosymbiosis occurred between 260 and 285 million years ago (Ma). Atmospheric CO_2 levels were at record lows at this time (Fig. IV.3), levels not reached again until Recent times. Such an environment favored algae that were better able to photosynthesize in a low CO_2 environment, e.g., those algae with chloroplast endoplasmic reticulum. Thus, the radiation of algae with chloroplast endoplasmic reticulum occurred at a time when the more efficient CO_2 mechanism of these algae enabled them to outcompete other algae without chloroplast endoplasmic reticulum.

REFERENCES

Falkowski, P. G., and Raven, J. (1997). *Aquatic Photosynthesis*. Oxford: Blackwell Science.

Fridlyand, L. E. (1997). Models of CO_2 concentrating mechanisms in microalgae taking into account cell and chloroplast structure. *BioSystems* 44:41–57.

Gibbs, S. P. (1978). The chloroplasts of *Euglena* may have evolved from symbiotic green algae. *Canadian J. Bot.* 56:2883–9.

Lee, R. E. (1977). Evolution of algal flagellates with chloroplast endoplasmic reticulum from the ciliates. *South African J. of Sci.* 73:179–82.

Medlin, L. K., Kooistra, W. H. C. F., Gersonde, R., Sims, P. A., and Wellbrock, U. (1997). Is the origin of the diatoms related to the end-Permian mass extinction? *Nova Hedwigia* 65:1–11.

Raven, J. (1997). CO_2 concentrating mechanisms: a direct role for thylakoid lumen acidification? *Plant Cell Env*. 20:147–54.

Sukenik, A., Tchernov, D., Kaplan, A., Huertas, E. Lubian, L. M., and Livne, A. (1997). Uptake, efflux, and photosynthetic utilization of inorganic carbon by the marine eustigmatophyte *Nannochloropsis* sp. *J. Phycol*. 33:969–74.

Chapter 6

Euglenophyta

EUGLENOPHYCEAE

Euglenoid flagellates occur in most freshwater habitats: puddles, ditches, ponds, streams, lakes, and rivers, particularly waters contaminated by animal pollution or decaying organic matter (Buetow, 1968). Usually larger bodies of purer water, such as rivers, lakes, and reservoirs, have sparser populations of less common euglenoids as planktonic organisms. Marine euglenoids are more common than supposed, with *Eutreptia*, *Eutreptiella* (Figs. 6.11, 6.14(*c*)), and *Klebsiella* occurring exclusively in marine or brackish water, and many other genera having one or a few marine species. These occur in the open sea, in tidal zones among seaweeds, and as sand inhabitants on beaches. Brackish species of *Euglena* (Figs. 6.1, 6.2, 6.3, 6.7, 6.14(*c*)) often color estuarine mud flats green when light intensity is low, the green color disappearing in full sunlight as the euglenoids creep away from the surface. There are also several parasitic euglenoid flagellates, mostly species of *Khawkinea*, *Euglenamorpha*, and *Hegneria*.

Euglenoids are characterized by chlorophylls *a* and *b*, one membrane of chloroplast endoplasmic reticulum, a mesokaryotic nucleus, flagella with fibrillar hairs in one row, no sexual reproduction, and paramylon or chrysolaminarin as the storage product in the cytoplasm.

Euglenoid cells have two basal bodies and one or two emergent flagella (Fig. 6.2). The flagella are similar to those of trypanosomes in having a **paraxonemal rod** (**paraxial rod**) that runs the length of the flagellum inside the flagellar membrane (Ngô and Bouck, 1998; Bastin and Gul, 1999; Talke and Preisfeld, 2002). The paraflagellar rod is composed of two major proteins forming an elongated alpha-helical stalk that parallels the axoneme. The one emergent flagellum in *Euglena*

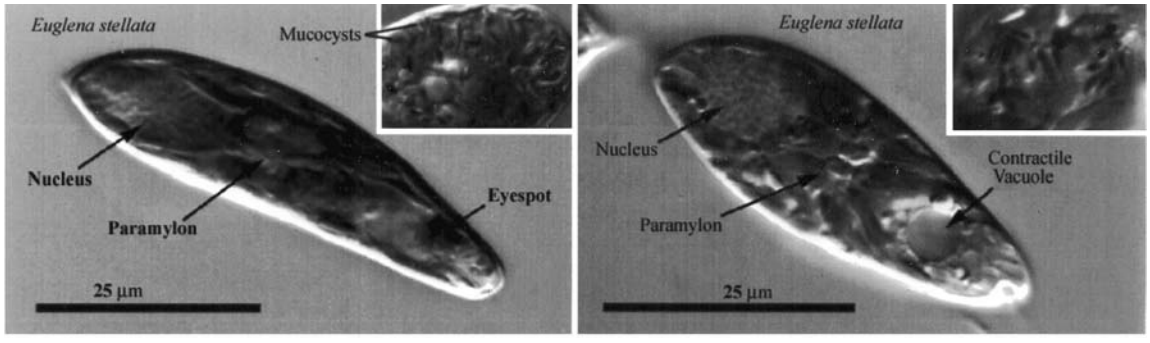


Fig. 6.1 Light micrographs of *Euglena stellata.* (From Shin and Triemer, 2004.)

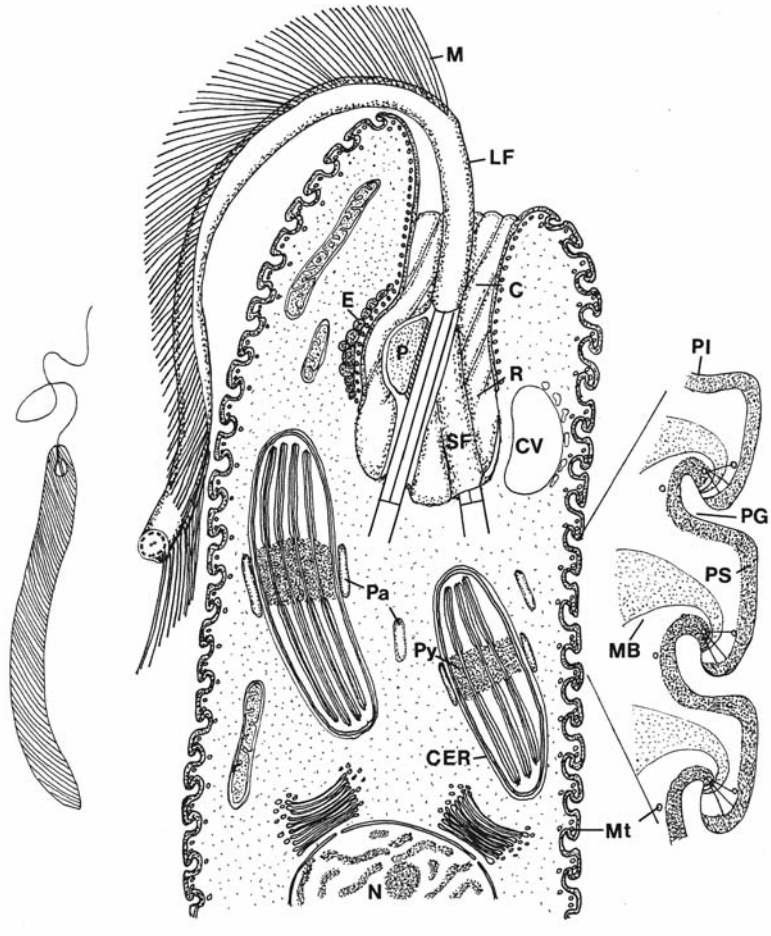


Fig. 6.2 A semidiagrammatic drawing of the fine structure of the anterior part of a *Euglena* cell. (C) Canal; (CER) chloroplast endoplasmic reticulum; (CV) contractile vacuole; (E) eyespot; (LF) long flagellum; (M) mastigonemes; (MB) muciferous body; (Mt) microtubules; (N) nucleus; (P) paraflagellar swelling; (Pa) paramylon; (PG) pellicle groove; (Pl) plasmalemma; (PS) pellicle strip; (Py) pyrenoid; (R) reservoir; (SF) short flagellum. (Adapted from Mignot, 1966; Jahn and Bovee, 1968.)

has helically arranged fibrillar hairs (no microtubules) attached along the length of the flagellar membrane. The fibrillar hairs are of two lengths: there is a single helical row of long (3 μm) hairs and two helical rows of short (1.5 μm) hairs in *Euglena* (Bouck et al., 1978). Other genera have flagella similar to *Euglena* (Hilenski and Walne, 1985). There are two basic types of flagellar movement in the class. The first group (including the Eutreptiales and Euglenales) has the flagellum continually motile from base to apex, resulting in cell gyration with the anterior end of the cell tracing a wide circle. The swimming rate of *Euglena gracilis* (Figs. 6.7, 6.14(*a*)) depends on the temperature: at 10 °C it is 15 μm s^{-1} while at 30 °C it is 84 μm s^{-1} (Lee, 1954). The second group (including *Peranema* (Fig. 6.13), *Entosiphon*, and *Sphenomonas*) has the flagellum held out straight in front of the cell with just the tip motile, resulting in smooth swimming or gliding locomotion in contact with the substratum or air–water interface at rates up to 30 μm s^{-1} (Saito et al., 2003).

Euglenoid cells are surrounded by a pellicle that has four main components: the plasma membrane, repeating proteinaceous units called strips, subtending microtubules, and tubular cisternae of endoplasmic reticulum (Figs. 6.2, 6.3, 6.4, 6.5) (Leander and Farmer, 2000, 2001a). The strips are arranged in parallel, are characteristic of the species, and are composed primarily of the proteinaceous articulins. Below each strip is a set of parallel microtubules, where each microtubule occupies a discrete position relative to the strip. The cisterna of endoplasmic reticulum is also intimately associated with each strip and appears to function as a reservoir for calcium.

Each strip of the pellicle has a thick side and a thinner flange side (Figs. 6.5, 6.6). In the

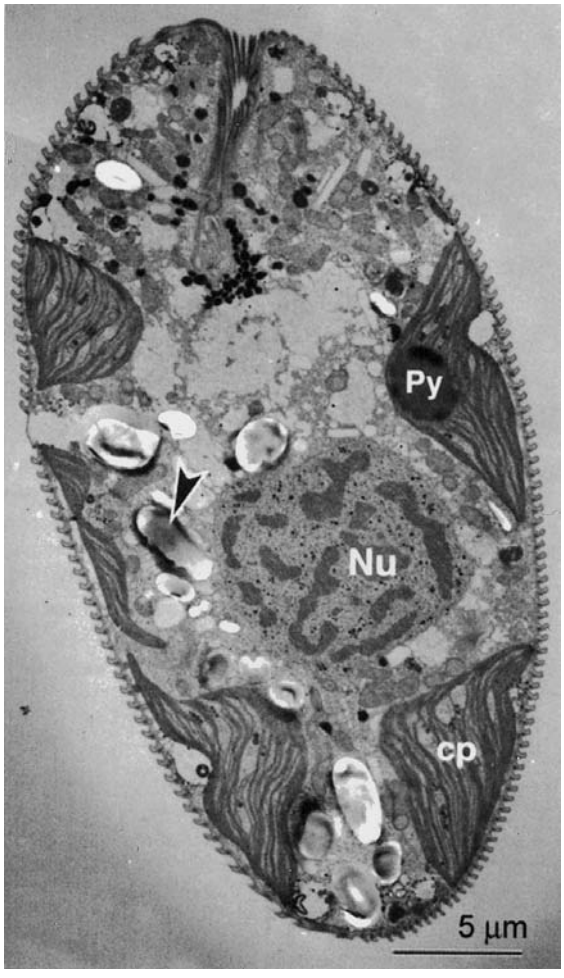


Fig. 6.3 *Euglena rustica*. Transmission electron micrograph of a mid sagittal section of a cell. (Arrow) Paramylon granule; (cp) chloroplast; (Py) pyrenoid; (Nu) nucleus. (From Brown et al., 2002.)

construction of the pellicle, the thick end of one strip fits under the thin flange end of the second strip. This structure gives the pellicle an alternating pattern of ridges and grooves. In *Euglena gracilis* (Figs. 6.5, 6.7, 6.14(*a*)) there are about 40 of the S-shaped strips overlapping at their lateral margins, under the plasma membrane. The region of strip overlap is occupied by a set of microtubule-associated bridges and microtubule-independent bridges.

Muciferous bodies occur under the pellicle strips and contain a water-soluble mucopolysaccharide. The muciferous bodies open to the outside through pores between the strips of the pellicle. The muciferous bodies function in the formation of the stalk in *Colacium*, lorica formation in *Trachelomonas*, cyst formation and lubrication during euglenoid movement (Leander and Farmer, 2000).

Some euglenoids have a flexible pellicle that allows the cells to undergo a flowing movement known as **euglenoid movement** (Fig. 6.7). This type of movement occurs only when the cells are not swimming and results from sideways movement of the pellicle strips. The movement may be induced by the binding of Ca^{2+} from the endoplasmic reticulum directly under the strips of the pellicle (Murata et al., 2000).

Euglena gracilis changes its shape two times per day when grown under the synchronizing effect of a daily light–dark cycle. At the beginning of the light period, when photosynthetic capacity is low (as measured by the ability of the cells to evolve oxygen), the population of cells is largely **spherical**. The **mean cell length** of the population **increases to a maximum** in the middle of the light period when photosynthetic capacity is greatest, and then decreases for the remainder of the 24-hour period. The population becomes **spherical** by the end of the 24-hour period when the cycle reinitiates. These changes are also observed under dim light conditions and are therefore controlled by a biological clock and represent a circadian rhythm in cell shape (Lonergan, 1983).

The locomotory flagellum or flagella emerge from an anterior invagination of the cell, which consists of a narrow tubular portion, the **canal**, and a spherical or pyriform chamber, the **reservoir** (Figs. 6.2, 6.8). The canal is a rigid structure, whereas the reservoir easily changes shape and is regularly distorted by the discharge of the contractile vacuole. The rigidity of the canal is maintained by microtubules that form a flat helix around the canal, in much the same position as hoops on a barrel. The pellicle lines the canal but not the reservoir, the reservoir being the only part of the cell covered solely by the plasmalemma. A cylindrical pocket arises as an infolding of the plasma membrane of the reservoir in *Euglena*, *Colacium*, and *Peranema* and is probably common in the euglenoids (Willey and Wibel, 1985a; Surek

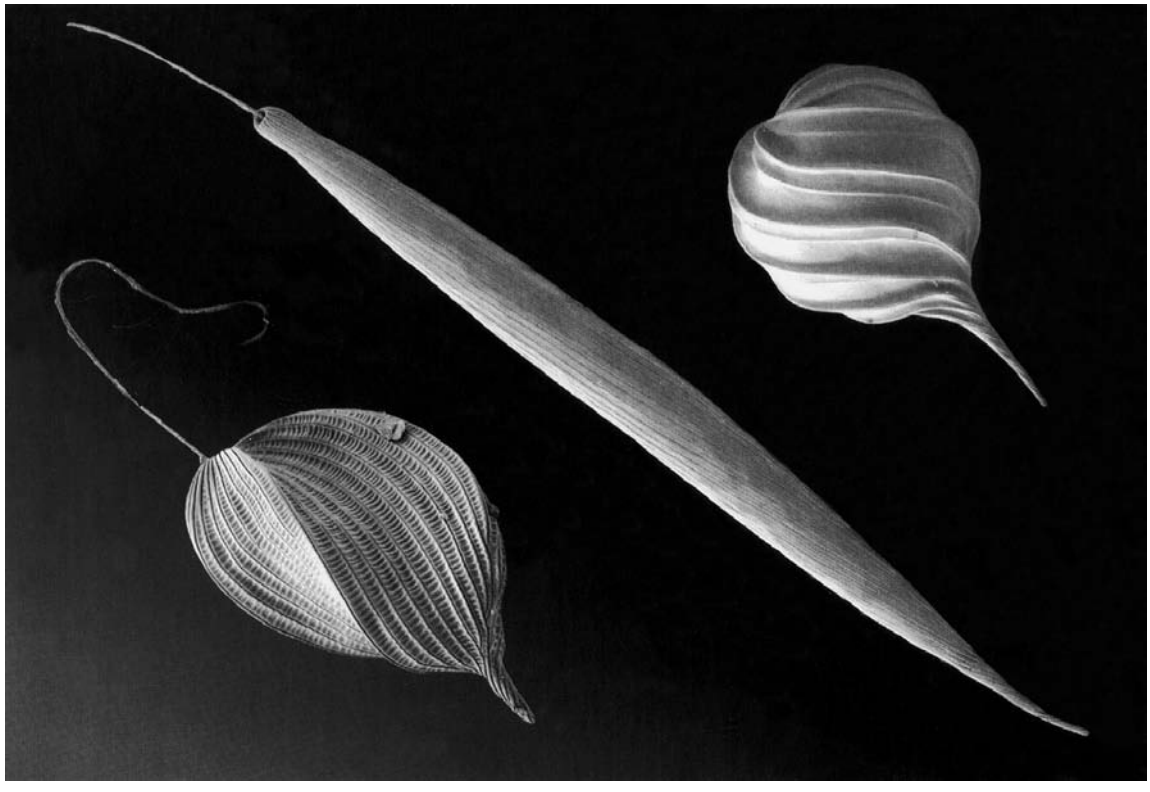


Fig. 6.4 Scanning electron micrographs of euglenoids showing the helical pellicle of *Phacus triqueter* (*lower left*), *Euglena acus* (*middle*), and *Lepocincilis ovata* (*upper right*). (From Leander and Farmer, 2001b.)

and Melkonian, 1986). The reservoir pocket is similar to the cytosome found in protozoa assigned to the Kinetoplastida (Willey and Wibel, 1985b). In the Kinetoplastida (bodonids and trypanosomatids), the cytosome is associated with the uptake of food organisms by phagotrophy, and the reservoir pocket has a similar function in the phagotrophic euglenoids (e.g., *Peranema*; Fig. 6.13) where the pocket is called a **cytosome**.

The contractile vacuole (Figs. 6.1, 6.2, 6.13, 6.14), in the anterior part of the cell next to the reservoir, has an osmoregulatory function, expelling excessive water taken into the cell. The contractile vacuole fills and empties at regular intervals of 15 to 60 seconds. It empties into the reservoir, from which the water is carried out through the canal (Leedale, 1967).

Mitochondria are of typical algal type. Colorless euglenoids always have more mitochondria than do equivalent-sized green ones. When green cells are decolorized by heat or streptomycin, they have a sevenfold increase in mitochondrial volume, reflecting a change from autotrophic to heterotrophic nutrition. The formation of two mitochondrial enzymes, fumarase and succinate dehydrogenase, necessary for dark respiration of substrates, is repressed by light (Davis and Merrett, 1974).

Nucleus and nuclear division

The euglenoid nucleus is of the mesokaryotic type, having chromosomes that are permanently condensed during the mitotic cycle, a nucleolus (endosome) that does not disperse during nuclear division, no microtubules from chromosomes to pole spindles, and a nuclear envelope that is intact during nuclear division (Fig. 6.9). The chromosome number is usually high, and polyploidy probably occurs in some genera (Gravilã, 1996).

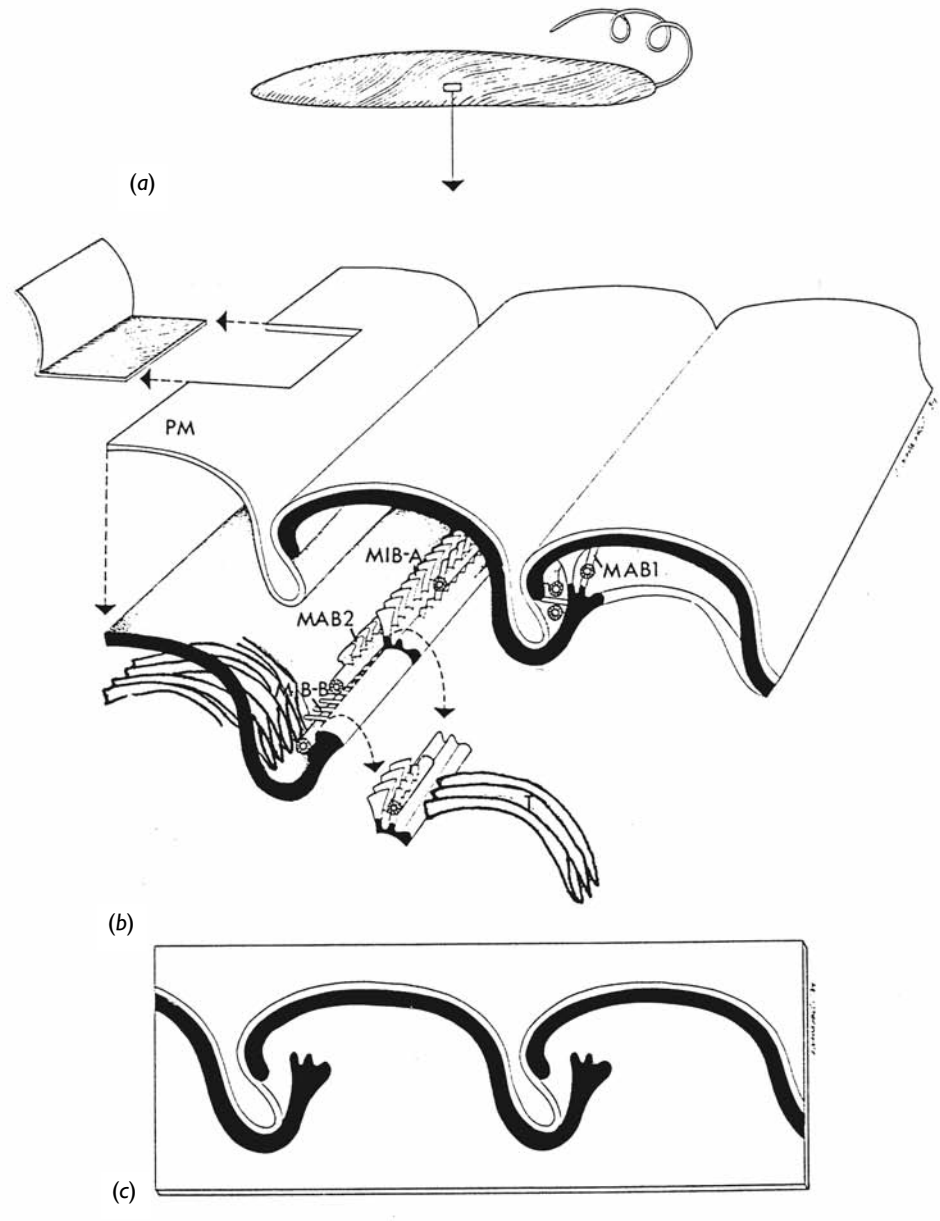


Fig. 6.5 *Euglena gracilis*. Diagrams of a whole swimming cell (*a*) and transverse sections of the cell surface (*b*) and (*c*), illustrating details of the articulating S-shaped strips of the membrane skeleton and the infrastructure associated with strip overlap. The position of the skeleton and bridges seems well suited to mediate the sliding of adjacent strips that is presumed to occur during shape changes. (MAB1, MAB2) Microtubule-associated bridges between the pellicle strips; (MIB-A, MIB-B) microtubule-independent bridges between the pellicle strips; (PM) plasma membrane; (T) transverse fiber. (From Dubreuil and Bouck, 1985.)

Mitosis in euglenoids (Leedale, 1970; Chaly et al., 1977) begins during early prophase with the nucleus migrating from the center of the cell to an anterior position. Microtubules appear in the nucleus, but they do not attach to the chromosomes. At metaphase, bundles of microtubules are among the chromosomes, and the nucleolus has started to elongate along the division axis. In anaphase, the intact nuclear envelope elongates along the division axis, the nucleolus divides, and

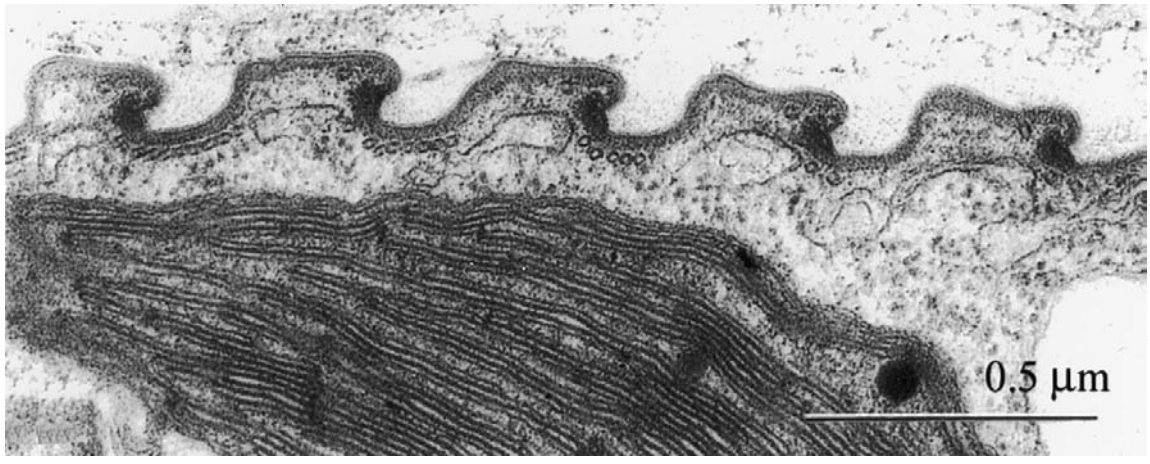


Fig. 6.6 Transmission electron micrograph of a section of the pellicle area of *Euglena terricola*. (From Leander and Farmer, 2001a.)

the daughter chromosomes disperse into the two daughter nuclei.

Eyespot, paraflagellar swelling, and phototaxis

The **eyespot** (**stigma**) is a collection of orange-red lipid droplets, independent of the chloroplast (Figs. 6.1, 6.2, 6.14). The eyespot is in the anterior part of the cell, curving to ensheath the neck of the reservoir on the dorsal side. In most euglenoids the eyespot consists of a compact group of 20 to 50 droplets, although in *Eutreptia* and *Khawkinea* it may consist of just one or two large droplets. The eyespot has been reported to contain α-carotene and seven xanthophylls (Sperling Pagni et al., 1981), mainly β-carotene (Batra and Tollin, 1964), or a β-carotene derivative, echineone (Krinsky and Goldsmith, 1960). The independence of the eyespot is emphasized by the existence of colorless species with an eyespot but no plastids. One flagellum of all green euglenoids bears a lateral swelling near the transition zone from canal to reservoir; in *Euglena* (Figs. 6.2, 6.14(*a*)), the swelling is on the longer flagellum. The swelling is composed of a crystalline body next to the axoneme and inside the flagellar membrane.

All euglenoid species with an eyespot and flagellar swelling exhibit phototaxis, usually swimming away from bright light (negative phototaxis) and away from darkness toward subdued light (positive photoaxis) to accumulate in a region of low light intensity. Upon sudden changes in its environment, the cell responds with a transient sideways turn by swinging out its one emergent flagellum. At low light intensities (less than 1.4 W m^{-2}), the alga swims toward the light source, whereas at higher light intensities, it moves away from the light source. According to the shading hypothesis (Häder, 1987), positive phototaxis is brought about by repetitive step-down photophobic responses. During forward locomotion, the cells rotate helically with a frequency of 1 to 2 hertz (cycles per second). In lateral light, each time the stigma (eyespot) intercepts the light beam impinging on the paraflagellar body, the flagellum swings out temporarily and turns the front end of the cell toward the light source by a fraction until the cell is aligned in the light direction.

Euglena bleached of its chlorophyll but retaining its eyespot and photoreceptor (paraflagellar swelling) is still positively phototactic, eliminating chlorophyll and chloroplasts in the phototaxis directly. A *Euglena* bleached of all pigments but retaining its photoreceptor is negatively phototactic; this rules out the possibility that the carotenoids of the eyespot are directly stimulatory in phototaxis. A *Euglena* lacking a photoreceptor and all pigments, like *Astasia* (Fig. 6.14(*b*)), is no

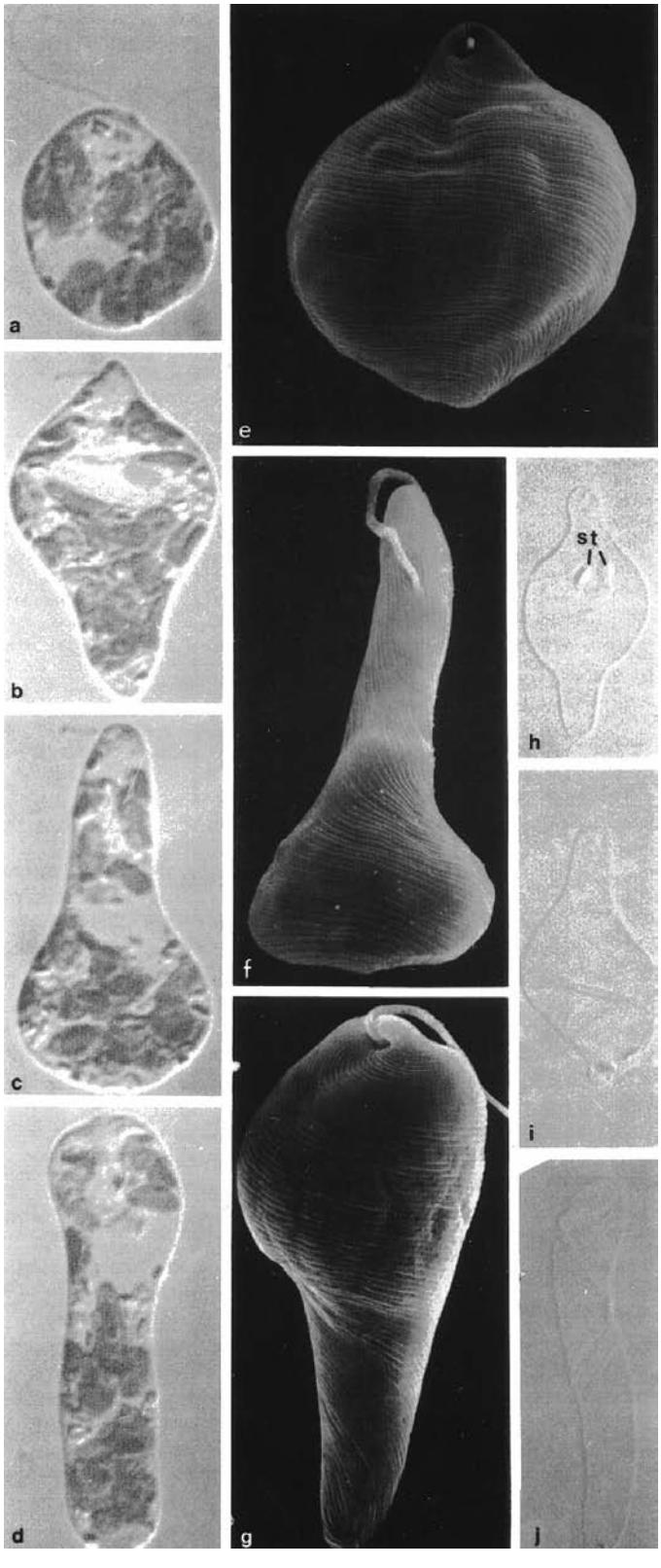


Fig. 6.7 *Euglena gracilis*. (*a*)–(*d*). Sequence of shape changes photographed at 5-second intervals of a cell undergoing euglenoid movements. The nearly spherical cell in (*a*) initiates a forward wave of dilation in (*b*), which reaches the anterior of the cell, and then recovers by an inward flow of cytoplasm to initiate a new wave at (*c*). The new wave progresses forward, and the cell recovers in (*d*). Scanning electron microscope micrographs in (e)–(*g*) illustrate the positions of surface ridges and grooves during selected stages of deformation. Nearly horizontal strips in (e) reorient to longitudinal in cells, initiating (*f*) or completing (*g*) the cycle. In (*h*)–(*j*), cell ghosts are shown with the changes in cell shape. (From Dubreuil and Bouck, 1985.)

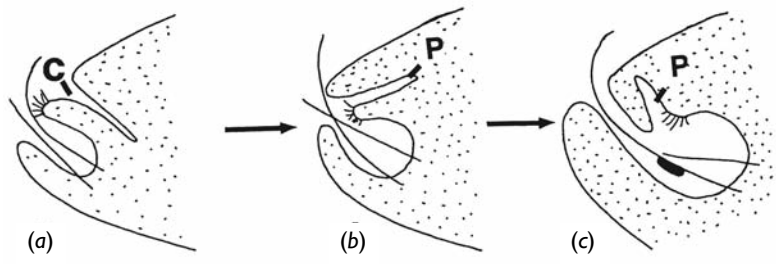


Fig. 6.8 Semidiagrammatic drawings of the anterior portion of *Bodo* (Kinetoplastida) (*a*), *Peranema* (Euglenophyceae) (*b*), and *Colacium* (Euglenophyceae) (*c*), illustrating probable evolution of the euglenoids. (C) Cytosome; (P) pocket. (After Willey and Wibel, 1985b.)

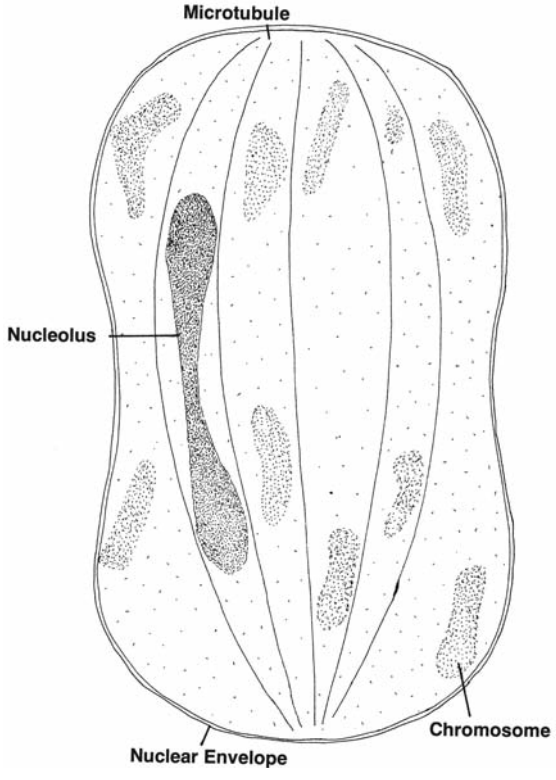


Fig. 6.9 A semidiagrammatic drawing of an anaphase nucleus of *Euglena* with nuclear envelope intact, the nucleolus pinching in two, and the chromosomes not attached to spindle microtubules.

longer phototactic (Jahn and Bovee, 1968). The flagellar swelling is therefore the photoreceptor or light-sensitive organelle. It has a sensitive maximum at 410 nm, explaining the phototactic peak at that wavelength. Positive phototaxis occurs only if the eyespot, with its absorptive range of 400 to 630 nm, periodically shades the photoreceptor.

There is a circadian rhythm in phototaxis in *Euglena*, with phototaxis operative during the light period and not operative during the dark period. Even if light is introduced during the normal dark period, the *Euglena* cell does not respond phototactically. The phototactic response in the direction of the light source plainly involves the photoreceptor, but why this is incapable of reacting during dark periods when the light is reintroduced is not known. Continuous darkness does not eliminate the rhythm unless continued for so long a period that complete bleaching results, and the cells become photonegative. It is possible that the non-operative nature of photaxis during this time is related to mitotic division occurring during this period. Leedale (1959) found that green euglenoids have almost perfectly circadianly synchronized mitotic cycles, mitosis occurring at the beginning of the dark period, requiring one hour of dark to trigger the division. During mitotic division, *Euglena* normally rounds up and loses its flagellum; but even if the flagellum is not shed, the cells are still unable to swim ably during this period. Because phototactic insensitivity coincides with the generation time of *Euglena* during dark hours, it perhaps is of no surprise that motility loss, generation time, and absence of phototaxis should coincide as they do (Jahn and Bovee, 1968).

A phototactic circadian rhythm also exists in the movement of mud flat *Euglena*. The mouth of the River Avon in Bristol, England, is an estuary with very large tidal differences in water level. The mud flats which are exposed at low tide become green in spots owing to an accumulation of *Euglena obtusa* on the surface of the mud (Bracher, 1937; Palmer and Round, 1965). Before the incoming tide floods the mud flats, the *Euglena* cells move back down into the mud, a pattern of behavior that avoids the washing away of the *Euglena* by the tide. *Euglena proxima* exhibits a similar movement and it has been shown that the

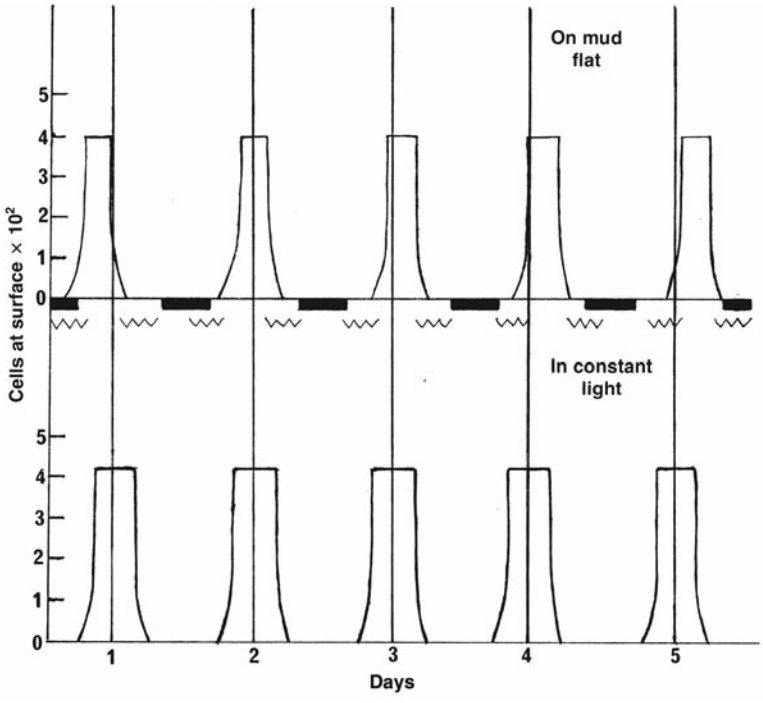


Fig. 6.10 The vertical migration rhythm in *Euglena obtusa* on a mud flat (top curve), and in constant light in the laboratory (bottom curve). The dark bars on the upper abscissa represent night, whereas the wavy lines indicate when the tide covered the mud flats. (After Palmer and Round, 1965.)

cells absorb a significant amount of nutrients in the mud during this part of the migration cycle (Kingston, 2002). *Euglena* cells accumulate at the surface of the mud only when the low tides occur during daylight, no cells being found on the surface during low tides (Fig. 6.10). The above observation indicate that phototaxis is the main mechanism involved, with the *Euglena* cells swimming toward the light during the day to reach the surface of the mud. If the *Euglena* cells are brought into the laboratory and placed in constant light (980 lux), the cells display a circadian rhythm in their vertical migration. The phase of this circadian rhythm is determined by the last dark period in nature, be it night or a dark period resulting from the covering of the mud flat by murky water at high tide. Thus the rhythm is actually circadian, entrained by the tidally caused light–dark cycle, rather than truly tidal.

Muciferous bodies and extracellular structures

Muciferous bodies (mucocysts), containing water-soluble polysaccharides, occur in helical rows under the pellicle in all species of euglenoid flagellates (Fig. 6.2). The muciferous bodies open to the outside of the cell through pores that course between the strips of the pellicle. Euglenoid cells are permanently coated with a thin slime layer from the muciferous bodies (Rosowski, 1977). It sometimes accumulates at the posterior end of the cell as a trailer of slime, and some species have the habit of sticking to a substratum by their posterior ends. Species with large muciferous bodies eject the contents on irritation and produce a copious slime layer around the cell (Hilenski and Walne, 1983). In *Euglena gracilis* (Figs. 6.7, 6.14(*a*)) the slime is composed of glycoproteins and polysaccharides (Cogburn and Schiff, 1984). The envelopes and stalks of *Colacium* (Figs. 6.15, 6.16) are formed of carbohydrate extruded by mucocysts in the anterior portion of the cell (Willey, 1984). The cylindrical stalks are composed of an inner and outer core of mildly acidic carbohydrate. The stalk is continuous with the canal and anterior part of the cell (Willey et al., 1977). The envelopes of such species as *Trachelomonas* (Figs. 6.12, 6.14(*d*)) are built up by inorganic deposition on a foundation of mucilaginous threads.

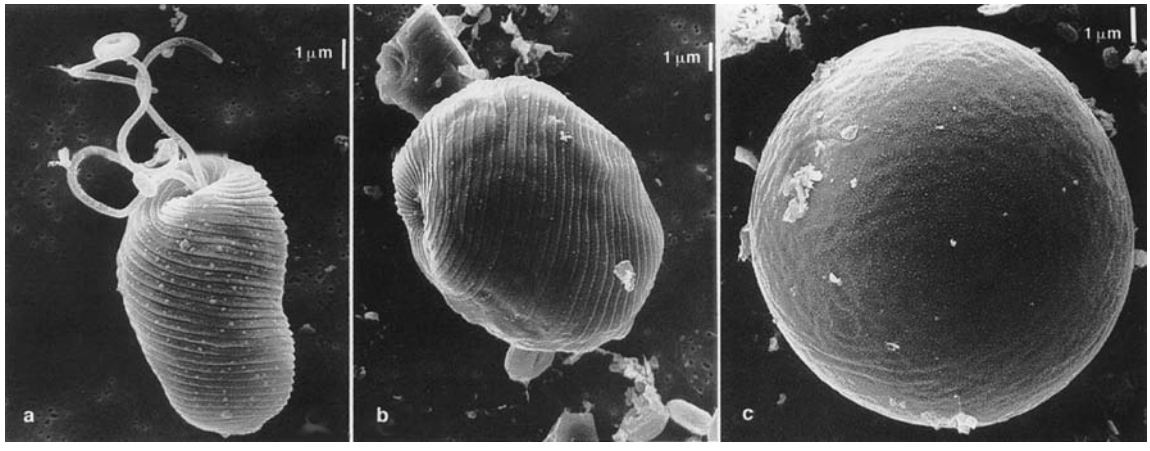


Fig. 6.11 Scanning electron micrographs of the encystment of *Eutreptiella gymnastica*. The vegetative cell (*a*) loses its flagella, forms a large number of paramylon grains, and begins to round up (*b*). The cell swells and produces a mucilaginous covering (*c*). (From Olli, 1996.)

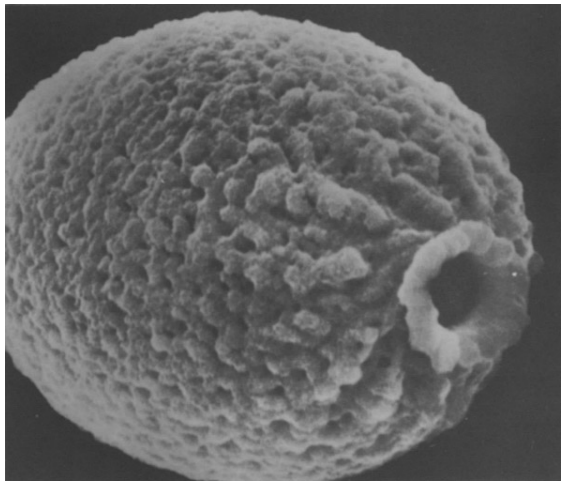


Fig. 6.12 Scanning electron micrograph of the mineralized envelope of *Trachelomonas lefevrei*. (From Dunlap et al., 1983.)

Cysts are formed by euglenoids as a means of surviving unfavorable periods. The cell rounds off and secretes a thick sheath of mucilage (Fig. 6.11) that survives for months until the cell emerges by cracking the cyst. In conditions of partial desiccation or excessive light, the slime sheath sometimes acts as a temporary cyst, cells emerging from the sheath as soon as conditions improve. In certain genera (*Euglena* and *Eutreptia*), cell division within the slime layer leads to the formation of a palmelloid colony, which may form extensive sheets of cells covering many square feet of mud surface (Leedale, 1967).

Trachelomonas is a large genus of free-swimming green euglenoids, characterized by encasement of the cell in a patterned mineralized envelope with a rimmed apical pore through which the flagellum emerges (Figs. 6.12, 6.14(*d*)). Most of the species are defined by the form and ornamentation of the envelopes, characteristics that can be changed by varying conditions of growth, especially iron and manganese supply. This has resulted in some described species being growth forms of other species (Pringsheim, 1953). The process of envelope formation involves mineralization of an initial fibrillar envelope which is probably derived as a secretion of the mucilaginous bodies (Pringsheim, 1953; Leedale, 1975). It begins with longitudinal division of the parent protoplast, the two daughter cells rotating within the envelope, and one or both squeezing out through the pore. Each naked daughter cell then secretes a new envelope externally, at first delicate and colorless but already the size and shape of the old one. Under good growth conditions, the envelope slowly becomes thicker and ornamented, first yellow, then brown. Under conditions of manganese deficiency, the envelope usually remains thin and unornamented. Envelope substructure is species specific, with a given species producing one of two general types of substructure: (1) weft or fibrillar deposits composed primarily of **manganese**, or (2) fine

granules composed primarily of **iron** (Dodge, 1975; Leedale, 1975; Walne, 1980; West and Walne, 1980; West et al., 1980).

Pellicular ornamentation occurs in a number of euglenoids, particularly in species of *Phacus* (Figs. 6.4, 6.14(*e*)) and in the *Euglena spirogyra* complex. The process is related to envelope formation in *Trachelomonas* (Figs. 6.12, 6.14(*d*)) and stalk formation in *Colacium* (Figs. 6.15, 6.16).

Chloroplasts and storage products

Euglenoid chloroplasts arose from a secondary endosymbiosis. The chloroplasts originated from the chloroplasts of a scaly flagellate in the green algal class Prasinophyceae (Marin, 2004). The euglenoid chloroplasts are surrounded by two membranes of the chloroplast envelope plus one membrane of chloroplast endoplasmic reticulum; the latter membrane is not continuous with the nuclear membrane (Figs. 6.2, 6.3, 6.14). The chloroplasts are usually discoid or plate-like with a central pyrenoid. The thylakoids are grouped into bands of three, with two thylakoid bands traversing the pyrenoid.

A shield of paramylon grains surrounds the pyrenoid, but outside the chloroplast, in phototropically grown cells (Figs. 6.2, 6.3, 6.14). Paramylon granules are distributed throughout the cytoplasm in heterotrophically grown cells in the dark (Bäumer et al., 2001). Gottlieb isolated the granules in 1850, and showed that they were composed of a carbohydrate that although isomeric with starch (amylon), was not stained with iodine. For this reason, they were termed **paramylon granules**. They have since been shown to be composed of a β-1,3 linked glucan (Barsanti et al., 2001). The paramylon granule is a membrane-bounded crystal composed of two types of segments – rectangular solids and wedges (Kiss et al., 1987). The liquid storage product, chrysolaminarin, can be an alternative storage product in some Euglenophyceae such as *Eutreptiella gymnastica* (Fig. 6.11) and *Sphenomonas laevis* where it can occur with solid paramylon grains in the same cell (Leedale, 1967; Throndsen, 1969). Whereas the paramylon usually occurs as a shield of grains, the chrysolaminarin occurs in vacuoles primarily in the anterior part of the cell (Throndsen, 1973).

Nutrition

The Euglenophyceae have a number of modes of nutrition, depending on the species involved. No euglenoid has yet been demonstrated to be fully **photoautotrophic** – capable of living on a medium devoid of all organic compounds (including vitamins), with carbon dioxide as a carbon source, nitrates or ammonium salts as a nitrogen source, and light as an energy source. All green euglenoid flagellates so far studied are **photoauxotrophic** – capable of growing in a medium devoid of organic nutrients, with carbon dioxide, ammonium salts, and light, but needing at least one vitamin. *Euglena gracilis* has an absolute requirement for vitamin B_{12} (Hutner and Provasoli, 1955), it having been calculated that between 4900 and 22 000 molecules of vitamin B_{12} are necessary for cell division (Carell, 1969). Vitamin B_{12}-starved cells increase in cell volume, sometimes to 10 times the size of control organisms, the cells in the final stage of vitamin B_{12} starvation often being polylobed, polynucleate, and containing more than the normal number of chloroplasts per cell (Bertaux and Valencia, 1971, 1973; Carell, 1969). During vitamin B_{12} starvation, total cellular RNA and protein increase 400% to 500% compared with controls (Carell et al., 1970). The chloroplast number per cell increases during this period, although the ratio of chloroplast protein to total cellular protein remains constant, evidence for the independence of chloroplast division from nuclear division (Bré and Lefort-Tran, 1974). Although the protein increase is 400% to 500% during vitamin B_{12} starvation, the total DNA increases only about 180%, suggesting that a particular step in DNA replication may be preferentially affected by the vitamin (Bré et al., 1975).

As *Euglena* cells age, they become immobile and spherical, with a tendency to form enlarged "giant" cells and to accumulate orange to black pigment bodies. Aging also results in the formation of larger numbers of lysosomes and microbodies with an increase in the degradation of organelles (Gomez et al., 1974). The older cells

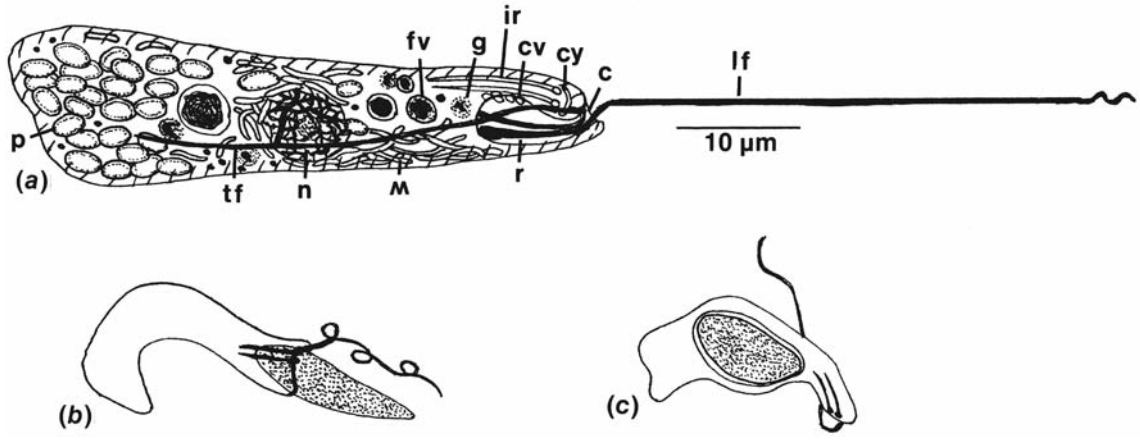


Fig. 6.13 *Peranema trichophorum*. (*a*) General cell structure. (*b*),(*c*) Two stages in the ingestion of a cell of *Euglena* (stippled cell). (c) Canal; (cv) contractile vacuoles; (cy) rim of cytosome; (fv) food vesicle; (g) Golgi; (ir) ingestion rods; (lf) leading flagellum; (m) mitochondrion; (n) nucleus; (p) paramylon; (tf) trailing flagellum. (After Leedale, 1967.)

undergo a shift from carbohydrate to fat oxidation, as evidenced by an increase in malate synthetase, the enzyme involved in the glycolate bypass, important in the oxidation of fats.

The euglenoids belong to the osmotrophic acetate flagellates, having the ability to grow photosynthetically in the light or heterotrophically in the dark. In either state, the fixed carbon is used as a source of energy or as building blocks for cell constituents. The substrates that can be used for heterotrophic growth vary from one species to another, with the permeability of the substrate into the cell probably being the most important factor. As a rule, the most readily utilized substrates are acetic and butryic acids and the corresponding alcohols (e.g., ethanol). The two most commonly used substrates are acetate and ethanol.

Classification

Studies on rRNA of euglenoids support a monophyletic origin of the Euglenophyceae with the kinetoplastids as a sister clade (Preisfeld et al., 2000; Nudelman et al., 2003). The phagotrophic euglenoids (e.g., *Peranema*; Fig. 6.13) evolved before the phototrophic and osmotrophic species. The phototrophic species evolved from a single secondary endosymbiotic event involving a chloroplast from a green alga in the Prasinophyceae (Marin, 2004). Osmotrophic genera such as *Astasia* (Fig. 6.14(*b*)) contain chloroplast genetic material indicating they evolved from photosynthetic euglenoids (Sekiguchi et al., 2002).

Three orders of euglenoids are presented here. Investigations utilizing nucleic acid sequencing have shown the organisms in the Euglenales to have evolved most recently (Marin, 2004).

Order 1 Heteronematales: two emergent flagella, the longer flagellum directed anteriorly and the shorter one directed posteriorly during swimming; special ingestion organelle present.

Order 2 Eutreptiales: two emergent flagella, one directed anteriorly and the other laterally or posteriorly during swimming; no special ingestion organelle.

Order 3 Euglenales: two flagella, only one of which emerges from the canal; no special ingestion organelle.

Heteronematales

Here the colorless cells have a special ingestion organelle (Triemer, 1997), and are phagocytic, taking up food particles whole and digesting them in food vesicles. *Peranema trichophorum* is a euglenoid that ingests other cells and detritus (Leedale, 1967) (Fig. 6.13). The ingestion apparatus consists

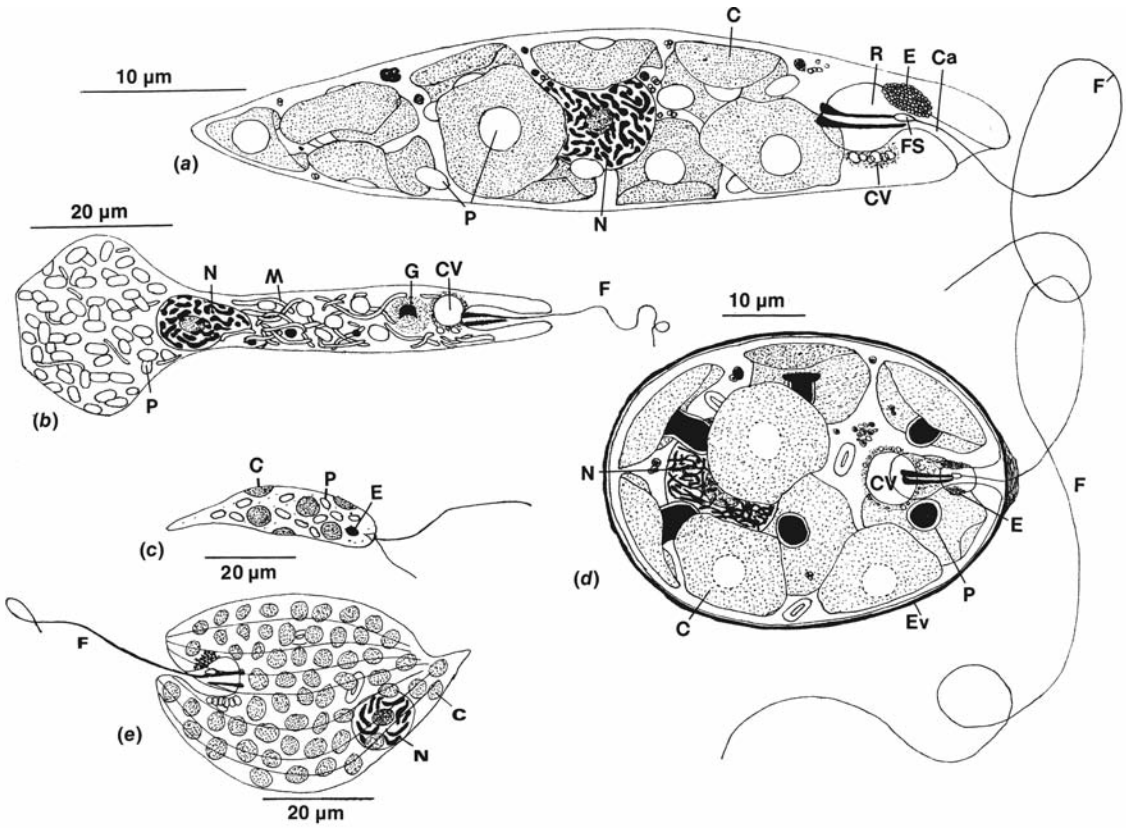


Fig. 6.14 (*a*) *Euglena gracilis*. (*b*) *Astasia klebsii*. (*c*) *Eutreptiella marina*. (*d*) *Trachelomonas grandis*. (e) *Phacus triqueter*. (C) Chloroplast; (Ca) canal; (CV) contractile vacuole; (E) eyespot; (Ev) envelope; (F) emergent flagellum; (FS) flagellar swelling; (M) mitochondrion; (N) nucleus; (P) paramylon grains or paramylon sheath around chloroplast; (R) reservoir. (After Leedale, 1967.)

of two parallel tapering rods, the hooked anterior ends of which are attached to the stiffened rim of the **cytosome**. The latter is a permanent "mouth" situated in a subapical position independent of the canal opening. There is no permanent "gullet," and food vacuoles are formed at the cytosome only when feeding takes place. *Peranema* normally ingests food particles and living organisms by engulfing them whole into food vacuoles. The ingestion rods are protruded and attached to the surface of the prey, which is then pulled through the cytosome in connection with a wave of euglenoid movement from the *Peranema* cell. With a large prey, such as *Euglena*, the rods are detached, moved, and attached again farther along the prey, so that more of it can be pulled into the predator. By repeated pullings, the whole *Euglena* is engulfed, the process taking up to 15 minutes. A second form of attack, reserved for larger algal cells, consists of cutting and sucking rather than engulfing. Several *Peranema* cells converge on their prey, with their ingestion rods protruded and used to rasp a way through the prey's wall or periplast. *Euglena spirogyra* pellicle is cut through in about 10 minutes, with the cell contents sucked out into a temporary food canal below the cytosome. If the prey is large enough, the predators finally enter the cell and engulf what remains of the prey. The food vacuoles decrease in size as digestion proceeds, the indigestible remains being finally ejected through a "defecation area" of constant position at the posterior end of the cell. It is possible to show that chemotaxis is important in directing *Peranema* to its prey by bursting open living algal cells in a suspension of *Peranema*, the peranemas streaming in from all directions for the meal.

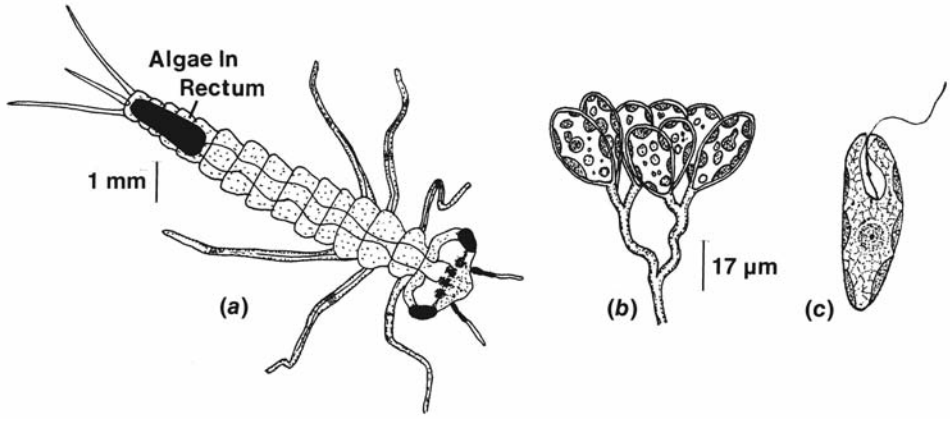


Fig. 6.15 (*a*) Larva of the damselfly *Ischnura verticalis* with a plug of *Colacium libellee* in the rectum. (*b*), (*c*) Colony and single swimming cell of *Colacium vesiculosum*. ((*a*) adapted from Rosowski and Willey, 1975; (*b*), (*c*) after Stein and Johnson in Huber-Pestalozzi, 1955.)

Eutreptiales

The organisms in the Eutreptiales have two emergent flagella and no special ingestion organelles. *Eutreptia* and *Eutreptiella* (Figs. 6.11, 6.14(*c*)) are estuarine or marine genera, while *Distigma* is characteristic of acid freshwaters.

Euglenales

In this primarily freshwater order, the flagellum without the paraflagellar swelling has been reduced so that it does not emerge from the canal. Common genera in the order are the green photosynthetic *Euglena* (Figs. 6.1, 6.2, 6.3, 6.7, 6.14(*a*)), *Trachelomonas* (Figs. 6.12, 6.14(*d*)), and *Phacus* (Figs. 6.4, 6.14(*d*)), as well as the colorless osmotrophic *Astasia* (Fig. 6.14(*b*)).

Colacium libellee is a member of this order that establishes itself in the rectum of damselfly nymphs during the winter in colder lakes (Figs.

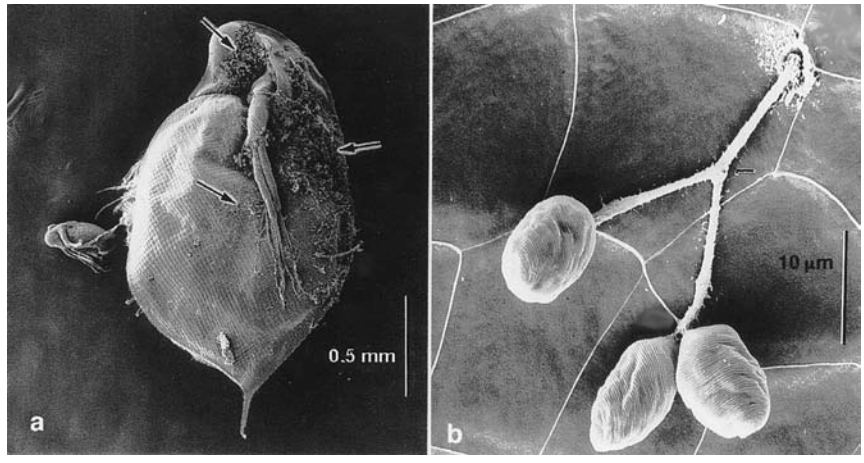


Fig. 6.16 Scanning electron micrographs of the euglenoid *Colacium vesiculosum* on the freshwater arthropod *Daphnia pulex*. (*a*) Arrows point to large concentrations of *Colacium* on *Daphnia.* (*b*) A colony of *Colacium* attached by mucilage stalks to *Daphnia*. (From Al-Dhaheri and Willey, 1996.)

6.15, 6.16). During the warm summer months the damselfly nymphs and *C. libellee* live separately. With the onset of winter, the *Colacium* cells attach to the cuticle of the rectum of the damselfly larvae, forming a conspicuous green plug that colors the terminal four segments of the abdomen dark green. In the rectum, the *Colacium* is in a palmelloid state, lacking a flagellar swelling and eyespot. As the peripheral waters of the lake freeze, the damselfly nymphs move to deeper water. Here the damselfly nymphs form a protected, motile, translucent microhabitat for the *Colacium*; the damselfly nymphs probably also provide a source of nutrients for the *Colacium* cells, which helps the alga to survive the unfavorable winter conditions. In spring, the damselfly nymphs swim to warmer water, at which time the *Colacium* cells swim out of the rectum to establish a free-living existence in the summer. If algal-free damselfly nymphs are placed in water with *C. libellae*, the alga will establish itself within 36 hours in the damselfly nymph rectum. Other species are not able to infect the nymphs (Willey et al., 1970, 1973; Willey, 1972; Rosowski and Willey, 1975).

REFERENCES

Al-Dhaheri, R. S., and Willey, P. L. (1996). Colonization and reproduction of the epibiotic flagellate *Colacium vesiculosum* (Euglenophyceae) in *Daphnia pulex*. *J. Phycol*. 32:770–4.

Barsanti, L., Vismara, R., Passarelli, V., and Gualtieri, P. (2001). Paramylon (β-1,3- glucan) content in wild type and WZSL mutant of *Euglena gracilis*. Effects of growth conditions. *J. Appl. Phycol*. 13:59–65.

Bastin, P., and Gull, K. (1999). Assembly and function of complex flagellar structures illustrated by the paraflagellar rod of trypanosomes. *Protist* 150:113–23.

Batra, P. P., and Tollin, G. (1964). Phototaxis in *Euglena*. I. Isolation of the eyespot granules and identification of the eye-spot pigments. *Biochem. Biophys. Acta* 79:371–8.

Bäumer, D., Preisfeld, A., and Ruppel, H.G. (2001). Isolation and characterization of paramylon synthase from *Euglena gracilis* (Euglenophyceae). *J. Phycol*. 37:38–46.

Bertaux, O., and Valencia, R. (1971). Effects de la carence B_{12} sur les cellules synchrones de *Euglena gracilis:* Blocage de la division cellulaire, polyploidie et gigantisme. *J. Physiol. (London)* 63:167A.

Bertaux, O., and Valencia, R. (1973). Blocage de la division cellulaire et malformations induites par carence B_{12} chez les cellules synchrones de *Euglena gracilis Z. C. R. Séances Acad. Sci. Paris* 276:753–6.

Bouck, G. B., Rogalski, A., and Valaitis, A. (1978). Surface organization and composition of *Euglena*. II. Flagellar mastigonemes. *J. Cell Biol*. 77:805–26.

Bracher, R. (1937). The light relations of *Euglena limosa* Gard. Part I. The influence of intensity and quality of light on phototaxy. *J. Linn. Soc. Bot*. 51:23–42.

Bré, M. H., and Lefort-Tran, M. (1974). Influence de l'avitaminose B_{12} sur les chloroplastes de l'*Euglena gracilis* Z. en milieu lactate. *C. R. Séances Acad. Sci. Paris* 278:1349–52.

Bré, M. H., Diamond, J., and Jacques, R. (1975). Factors mediating the vitamin B_{12} requirement of *Euglena*. *J. Protozool*. 22:432–4.

Brown, P. J. P., Leander, B. S., and Farmer, M. A. (2002). Redescription of *Euglena rustica* (Euglenophyceae), a rare euglenophyte from the intertidal zone. *Phycologia* 41:445–52.

Carell, E. F. (1969). Studies on chloroplast development and replication in *Euglena*. I. Vitamin B_{12} and chloroplast replication. *J. Cell Biol*. 41:431–40.

Carell, E. F., Johnston, P. L., and Christopher, A. R. (1970). Vitamin B_{12} and the macromolecular composition of *Euglena*. *J. Cell Biol*. 47:525–30.

Chaly, N., Lord, A., and Lafontaine, J. G. (1977). A light- and electron-microscope study of nuclear structure throughout the cell cycle in the euglenoid *Astasia longa* (Jahn). *J. Cell Sci*. 27:23–45.

Cogburn, J. N., and Schiff, J. A. (1984). Purification and properties of the mucus of *Euglena gracilis* (Euglenophyceae). *J. Phycol*. 20:533–44.

Davis, B., and Merrett, M. J. (1974). The effect of light on the synthesis of mitochondrial enzymes in division-synchronized *Euglena* cultures. *Plant Physiol*. 53:575–80.

Dodge, J. D. (1975). The fine structure of *Trachelmonas* (Euglenophyceae). *Arch. Protistenk*. 117:65–77.

Dubreuil, R. R., and Bouck, G. B. (1985). The membrane skeleton of a unicellular organism consists of bridged, articulating strips. *J. Cell Biol*. 101:1884–96.

Dunlap, J. R., Walne, P. L., and Bentley, J. (1983). Microarchitecture and elemental spatial segregation of envelopes of *Trachelomonas lefevrei* (Euglenophyceae). *Protoplasma* 117:97–106.

Gomez, M. P., Harris, J. B., and Walne, P. L. (1974). Studies of *Euglena gracilis* in aging cultures. I. Light microscopy and cytochemistry. *Br. Phycol. J.* 9:163–74.

Gottleib, J. (1850). Ueber eine neue, mit Starkmehl isomere Substanz. *Ann. Chem. Pharm*. 75:51–61.

Gravilă , L. (1996). Light and electron microscope studies of euglenoid nuclei. In *Cytology, Genetics and Molecular Biology of Algae*, ed. B. R. Chaudhary, and S. B. Agrawal, pp. 193–213. Amsterdam, The Netherlands: SPB Academic Pub.

Häder, D-P. (1987). Polarotaxis, gravitaxis and vertical phototaxis in the green flagellate, *Euglena gracilis. Arch. Microbiol*. 147:179–83.

Hilenski, L. L., and Walne, P. L. (1983). Ultrastructure of mucocysts in *Peranema trichophorum* (Euglenophyceae). *J. Protozool*. 30:491–6.

Hilenski, L. L., and Walne, P. L. (1985). Ultrastructure of the flagella of the colorless phagotroph *Peranema trichophorum* (Euglenophyceae). I. Flagellar mastigonemes. *J. Phycol*. 21:114–25.

Huber-Pestalozzi, G. (1955). Euglenophycean. *Das Phytoplankton des Susswassers*, Vol. 16, Part 4. Stuttgart: E. Schweizerbart'sche Verlagsbuchhandlung.

Hutner, S. H., and Provasoli, L. (1955). Comparative biochemistry of flagellates. In *Biochemistry and Physiology of Protozoa*, ed. S. H. Hutner, and A. Lwoff, Vol. 2, pp. 1–40. New York and London: Academic Press.

Jahn, T. L., and Bovee, E. C. (1968). Locomotive and motile response in *Euglena*. In *The Biology of Euglena*, ed. D. E. Búetow, I:45–108. New York and London: Academic Press.

Kingston, M. B. (2002). Effect of subsurface nutrient supplies on the vertical migration of *Euglena proxima* (Euglenophyta). *J. Phycol*. 38:872–80.

Kiss, J. Z., Vasconcelos, A. C., and Triemer, R. E. (1987). Structure of the euglenoid storage carbohydrate, paramylon. *Am. J. Bot*. 74:877–82.

Krinsky, N. I., and Goldsmith, T. H. (1960). The carotenoids of the flagellated alga, *Euglena gracilis. Arch. Biochem. Biophys*. 91:271–9.

Leander, B. S., and Farmer, M. A. (2000). Comparative morphology of the euglenoid pellicle. I. Patterns of strips and pores. *J. Eukary. Microbiol*. 47:469–79.

Leander, B. S., and Farmer, M. A. (2001a). Comparative morphology of the euglenoid pellicle. II. Diversity of strip substructure. *J. Eukary. Microbiol.* 48:202–17.

Leander, B. S., and Farmer, M. A. (2001b). Evolution of *Phacus* (Euglenophyceae) as inferred from pellicle morphology and SSU rDNA. *J. Phycol*. 37:143–59.

Leedale, G. F. (1959). Periodicity of mitosis and cell division in the Euglenineae. *Biol. Bull*. 116:162–74.

Leedale, G. F. (1967). *Euglenoid Flagellates*. Englewood Cliffs, NJ: Prentice Hall.

Leedale, G. F. (1970). Phylogenetic aspects of nuclear cytology in the algae. *Ann. NY Acad. Sci*. 175(2):429–53.

Leedale, G. F. (1975). Envelope formation and structure in the euglenoid genus *Trachelomonas. Br. Phycol. J.* 10:17–41.

Lonergan, T. A. (1983). Regulation of cell shape in *Euglena gracilis*. I. Involvement of the biological clock, respiration, photosynthesis, and cytoskeleton. *Plant Physiol*. 71:719–30.

Marin, B. (2004). Origin and fate of chloroplasts in the Euglenoida. *Protist* 155:13–14.

Mignot, J-P. (1966). Structure et ultrastructure de quelques Euglénomonadines. *Protistologica* 2:51–117.

Murata, K., Okamoto, M., and Suzaki, T. (2000). Morphological change of cell-membrane-integrated crystal structure induced by cell shape change in *Euglena gracilis*. *Protoplasma* 214:73–9.

Ngô, H. M., and Bouck, G. B. (1998). Heterogeneity and a coiled coil predication of trypanosomatid-like flagellar rod proteins in *Euglena*. *J. Eukary. Microbiol*. 45:323–33.

Nudelman, A. A., Rossa, M. S., Conforti, V., and Triemer, R. E. (2003). Phylogeny of Euglenophyceae based on small subunit rDNA sequences: taxonomic implications. *J. Phycol*. 39:226–35.

Olli, K. (1996). Resting cyst formation of *Eutreptiella gymnastica* (Euglenophyceae) in the northern coastal Baltic Sea. *J. Phycol.* 32:535–42.

Palmer, J. D., and Round, F. E. (1965). Persistent, vertical-migration rhythms in the benthic microflora. I. The effect of light and temperature on the rhythmic behaviour of *Euglena obtusa. J. Mar. Biol. Assoc. UK* 45:567–82.

Preisfeld, A., Berger, S., Busse, I., Liller, S., and Ruppel, H. G. (2000). Phylogenetic analyses of various euglenoid taxa (Euglenozoa) based on 18S rDNA sequence data. *J. Phycol*. 36:220–6.

Pringsheim, E. G. (1953). Observations on some species of *Trachelomonas* grown in culture. *New Phytol*. 52:93–113, 238–66.

Rosowski, J. R., and Willey, R. L. (1975). *Colacium libellae* sp. nov. (Euglenophyceae), a photosynthetic inhabitant of the larval damselfly rectum. *J. Phycol*. 11:310–15.

Saito, A., Suetomo, Y., Arikawa, M., et al. (2003) Gliding movement in *Peranema trichophorum* is powered by flagellar surface motility. *Cell Motil. Cytoskel*. 55:244–53.

Sekiguchi, H., Moriya, M., Nakayama, T., and Inouye, I. (2002). Vestigial chloroplasts in heterotrophic stramenopiles *Pteridomonas danica* and *Ciliophrys infusionum* (Dictyochophyceae). *Protist* 153:157–67.

Shin, W., and Triemer, R. E. (2004). Phylogenetic analysis on the genus *Euglena* (Euglenophyceae) with particular reference to the species *Euglena viridis*. *J. Phycol*. 40:759–71.

Sperling Pagni, P. G., Walne, P. L., and Pagni, R. M. (1981). On the occurrence of α-carotene in isolated stigmata of *Euglena gracilis* var. *bacillaris*. *Phycologia* 20:431–4.

Surek, B., and Melkonian, M. (1986). A cryptic cytosome is present in *Euglena*. *Protoplasma* 133:39–49.

Talke, S., and Preisfield, A. (2002). Molecular evolution of euglenozoan paraxonemal rod genes *par1* and *par2* coincides with phylogenetic reconstruction based on small subunit rDNA data. *J. Phycol*. 38:995–1003.

Throndsen, J. (1969). Flagellates of Norwegian coastal waters. *Nytt Mag. Bot.* 16:161–216.

Throndsen, J. (1973). Fine structure of *Eutreptiella gymnastica* (Euglenophyceae). *Norw. J. Bot*. 20:271–80.

Walne, P. L. (1980). Euglenoid flagellates. In *Phytoflagellates*, ed. E. Cox, pp. 165–212. North Holland: Elsevier.

West, L. K., and Walne, P. L. (1980). *Trachelomonas hispada* var. *coronata* (Euglenophyceae). II. Envelope substructure. *J. Phycol*. 16:498–506.

West, L. K., Walne, P. L., and Bentley, J. (1980). *Trachelomonas hispida* var. *coronata* (Euglenophyceae). III. Envelope elemental composition and mineralization. *J. Phycol*. 16:582–91.

Willey, R. L. (1972). The damselfly (*Odonata*) hindgut as a host for the euglenoid *Colacium*. *Trans. Am. Microsc. Soc*. 91:585–93.

Willey, R. L. (1984). Fine structure of the mucocysts of *Colacium calvum* (Euglenophyceae). *J. Phycol*. 20:426–30.

Willey, R. L., and Wibel, R. G. (1985a). The reservoir cytoskeleton and a possible cytosomal homologue in *Colacium* (Euglenophyceae). *J. Phycol*. 21:570–7.

Willey, R. L., and Wibel, R. G. (1985b). A cytosome/cytopharynx in green euglenoid flagellates (Euglenales) and its phylogenetic implications. *BioSystems* 18:369–76.

Willey, R. L., Bowen, W. R., and Durban, E. M. (1970). Symbiosis between *Euglena* and damselfly nymphs is seasonal. *Science* 170:80–1.

Willey, R. L., Durban, E. M., and Bowen, W. R. (1973). Ultrastructural observations of a *Colacium* palmella: The reservoir, eyespot, and flagella. *J. Phycol*. 9:211–15.

Chapter 7

Dinophyta

DINOPHYCEAE

These organisms are important members of the plankton in both fresh and marine waters, although a much greater variety of forms is found in marine members. Generally the Dinophyceae are less important in the colder polar waters than in warmer waters. The highly elaborate Dinophysales (Fig. 7.56(*d*), (*e*)) are essentially a tropical group.

A typical motile dinoflagellate (Figs. 7.1, 7.2) consists of an **epicone** and **hypocone** divided by the transverse **girdle** or **cingulum**. The epicone and hypocone are normally divided into a number of **thecal plates**, the exact number and arrangement of which are characteristic of the particular genus (Figs. 7.1, 7.3, 7.21(*b*), 7.25(*b*)). There is a **longitudinal sulcus** running perpendicular to the girdle. The longitudinal and transverse flagella emerge through the thecal plates in the area where the girdle and sulcus meet. The longitudinal flagellum projects out from the cell, whereas the transverse flagellum is wave-like and is closely appressed to the girdle. The cells can be photosynthetic or colorless and heterotrophic. Photosynthetic organisms have chloroplasts surrounded by one membrane of chloroplast E.R., which is not continuous with the outer

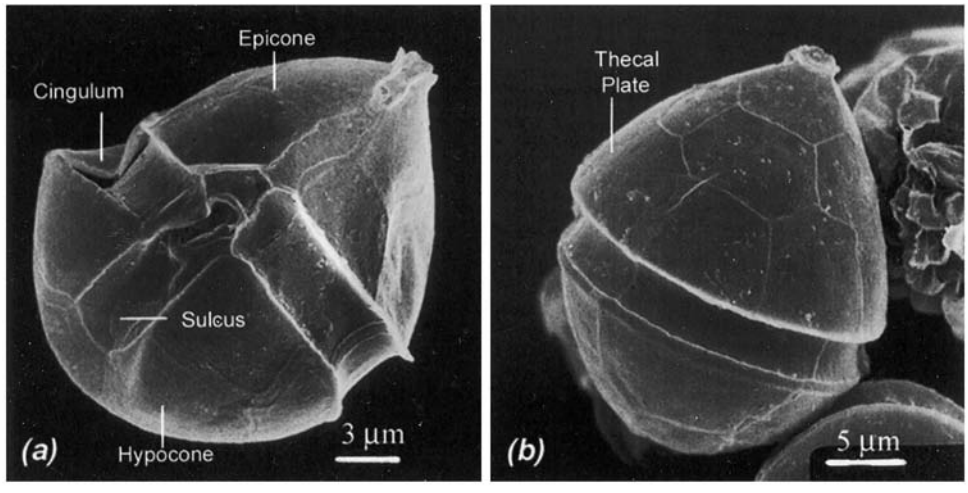


Fig. 7.1 *Scrippsiella trochoidea*.Scanning electron micrographs showing the thecal plates in ventral (*a*) and dorsal (*b*) view. (From Janofske, 2000.)

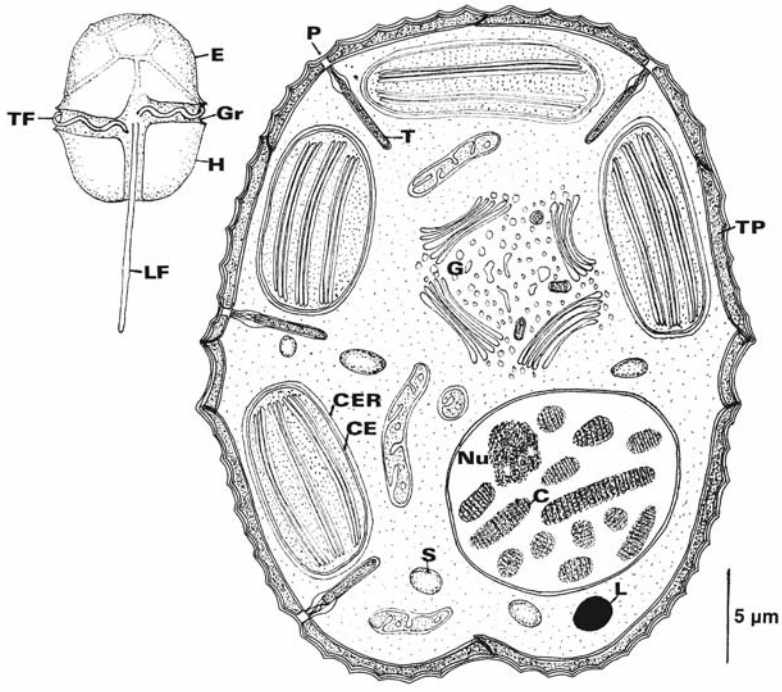


Fig. 7.2 Light and electron microscopical drawings of *Peridinium* sp., a dinoflagellate showing many of the features of the class. (C) Chromosome; (CE) chloroplast envelope; (CER) chloroplast endoplasmic reticulum; (E) epicone; (G) Golgi apparatus; (Gr) girdle; (H) hypocone; (L) lipid globule; (LF) longitudinal flagellum; (Nu) nucleolus; (P) trichocyst pore; (S) starch; (T) trichocyst; (TF) transverse flagellum; (TP) thecal plate.

membrane of the nuclear envelope. Chlorophylls *a* and c_2 are present in the chloroplasts, with **peridinin** and **neoperidinin** being the main carotenoids. About half of the Dinophyceae that have been examined by electron microscopy have pyrenoids in the chloroplasts (Dodge and Crawford, 1970). The storage product is **starch**, similar to the starch of higher plants (Vogel and Meeuse, 1968), which is found in the cytoplasm. An eyespot may be present. The nucleus has permanently condensed chromosomes and is called a **dinokaryotic** or **mesokaryotic** nucleus.

Cell structure

Theca

The thecal structure of motile Dinophyceae consists of an outer plasmalemma beneath which lies a single layer of flattened vesicles (Figs. 7.2, 7.3(*c*), 7.5) (Dodge and Crawford, 1970; Sekida et al., 2004). These vesicles, which normally contain cellulosic plates, give the theca its characteristic structure. The actual form and arrangement of the thecal plates varies from none in the phagotrophic *Oxyrrhis marina*, to very thick plates with flanges at the edges in *Ceratium* (Figs. 7.12, 7.57) and *Peridinium* spp. (Figs. 7.2, 7.11).

Amphiesma is the term used to specify the outermost layers of the dinoflagellate cell (Schütt, 1895) and includes all of the thecal plates with their lists (ribs), the peripheral vesicles, and the attendant microtubules. All types of amphiesma have the plasma membranes (continuous with the flagellar membrane) on the outside. The most complex type of amphiesma (Fig. 7.5(*a*)) consists of a single-membrane-bounded vesicle under the plasma membrane. Inside this vesicle are a number of cellulosic thecal plates subtended by a proteinaceous pellicle (Morrill and Loeblich, 1983a). A less complex amphiesma consists of a number of vesicles under the plasma membrane, each vesicle containing a thecal plate (Fig. 7.5(*b*), (*c*)). The least complex amphiesma has a number of vesicles without plates under the plasma membrane (Fig. 7.5(*d*)). Numerous pores generally occur within the amphiesma with a trichocyst beneath each pore (Fig. 7.4).

Outside of the plasma membrane of *Amphidinium carteri* (Fig. 7.16) there is a **glycocalyx** composed of acidic polysaccharides. The glycocalyx probably is formed by the discharge of

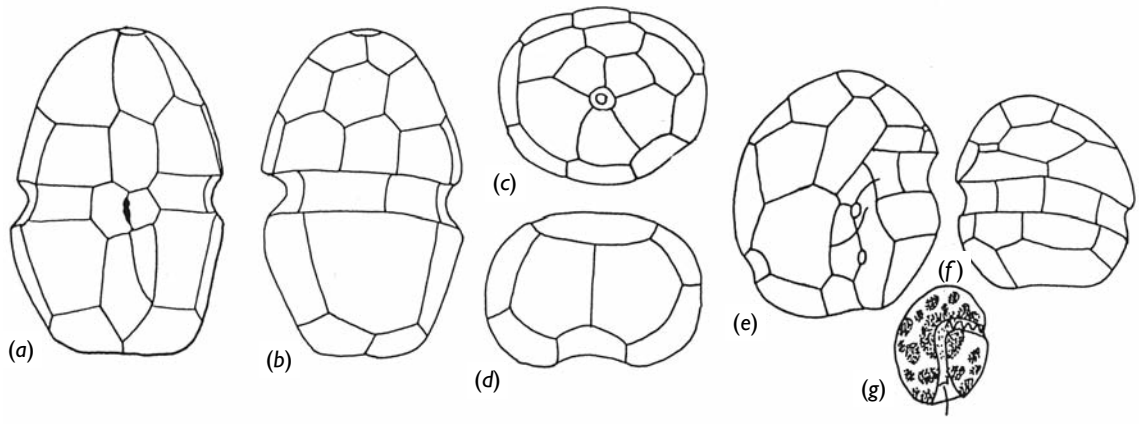


Fig. 7.3 (*a*)–(*d*) *Cachonina niei* showing the arrangement of thecal plates: (*a*) ventral, (*b*) dorsal, (*c*) apical, and (*d*) posterior views. (e)–(*g*) *Cryptothecodinium cohnii*: (e) ventral and (*f*) dorsal views, (*g*) living cell. ((*a*)–(*d*) after Loeblich, 1968; (e)–(*g*) after Chatton, 1952.)

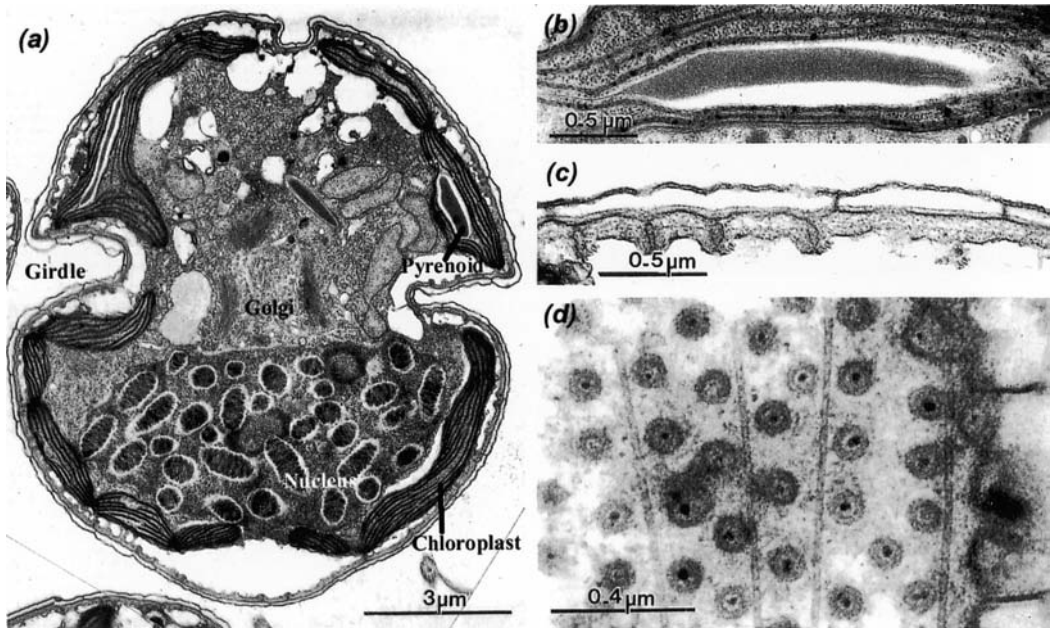


Fig. 7.4 Transmission electron micrographs of sections of cells of *Karlodinium veneficum*. (*a*) Cell. (*b*) Detail of pyrenoid in chloroplast. (*c*) Transverse section of amphiesma showing amphiesmal vesicles. (*d*) Tangential section of cell showing plugs in amphiesma. (From Daugbjerg et al., 2000.)

cytoplasmic mucocysts to the outside of the cell. Such a glycocalyx probably exists in most Dinophyceae (Klut et al., 1985).

In many dinoflagellates, cell division usually involves sharing of the mother cell thecal plates between the daughter cells, with the daughter cells producing the new thecal plates that they lack. However, in certain peridinoid genera the

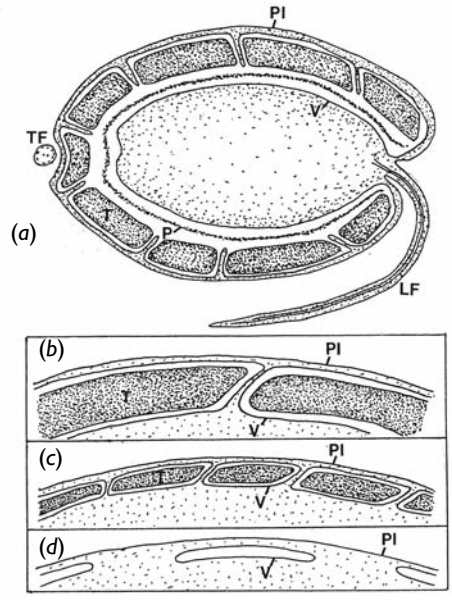


Fig. 7.5 Representative drawings of different types of amphiesmal arrangements in the Dinophyceae. (*a*) Cross section of a dinoflagellate with the most complex type of amphiesma. The outer plasma membrane (PI) is continuous with the flagellar membrane. The cellulosic thecal plate (T) and a proteinaceous pellicle (P) are enclosed in a large vesicle (V). (*b*)–(*d*) Less complicated types of amphiesma occurring in other Dinophyceae. (LF) Longitudinal flagellum; (TF) transverse flagellum. (After Morrill and Loeblich, 1983a.)

theca is completely shed (**ecdysis**) at cell division, followed by the formation of a thickened pellicle around the cell to form an **ecdysal cyst** (Bricheux et al., 1992; Höhfeld and Melkonian, 1992). New thecal vesicles are produced under the pellicle with the cell escaping from the cyst (Figs. 7.6, 7.7). Ecdysis in *Gambierdiscus toxicus* is induced by a glycerol compound (Fig. 7.8) that is released by the green alga *Bryopsis* sp. (Sakamoto et al., 2000). The dinoflagellate occupies the thallisphere of this green alga.

Scales

Although relatively rare, scales occur outside the plasma membrane in some Dinophyceae (Figs. 7.9, 7.10) (Sekida et al., 2003). In *Heterocapsa*, the scales are formed in Golgi vesicles that migrate to the area of the basal bodies, where the scales are released outside the cell (Morrill and Loeblich, 1983b).

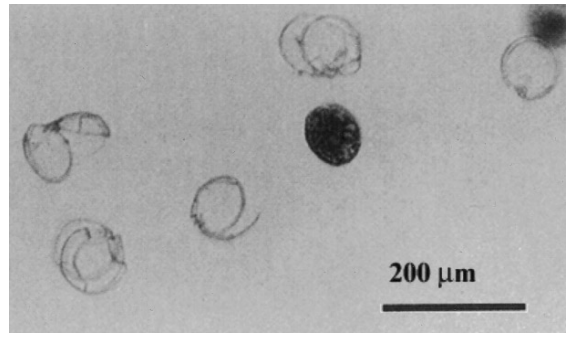


Fig. 7.6 Ecdysis in *Gambierdiscus toxicus*. (From Sakamoto et al., 2000.)

Flagella

Generally, dinoflagellates have a transverse flagellum that fits into the transverse girdle and a longitudinal flagellum that projects out from the longitudinal sulcus (Figs. 7.2, 7.11, 7.13) (Roberts and Roberts, 1991). The two flagella are inserted into the cell in the area of the intersection of the girdle and sulcus. The longitudinal flagellum usually has a wide basal portion and a thinner apical portion. In the basal portion the flagellar sheath surrounds packing material plus the axoneme, whereas at the apical portion the flagellar sheath surrounds only the axoneme. Fibrillar hairs 0.5 μm long and 10 nm wide may cover the entire flagellum (Leadbeater and Dodge, 1967a). Mechanical stimulus of cells of *Ceratium tripos* (Fig. 7.12) causes the longitudinal flagellum to be retracted and folded so that the flagellum lies along the sulcus (Maruyama, 1982). The longitudinal flagellum contains an R-fiber running along the length of the flagellum. Retraction of the flagellum occurs when the R-fiber contracts to one third of its length. Influx of Ca^{2+} into the longitudinal flagellum causes retraction of the R-fiber (Maruyama, 1985).

The transverse flagellum is about two to three times as long as the longitudinal flagellum and has a helical shape (Figs. 7.12, 7.13, 7.14). The transverse flagellum consists of (1) an axoneme whose form approximates a helix, (2) a striated strand that runs parallel to the longitudinal axis of the axoneme but outside the loops of the coil, and (3) a flagellar sheath that encloses both axoneme and striated strand (Berdach, 1977). The striated strand

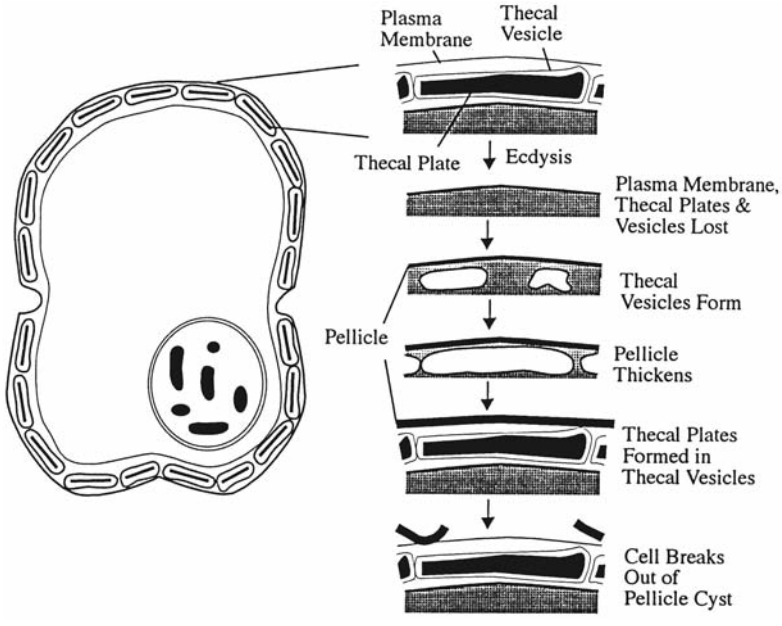
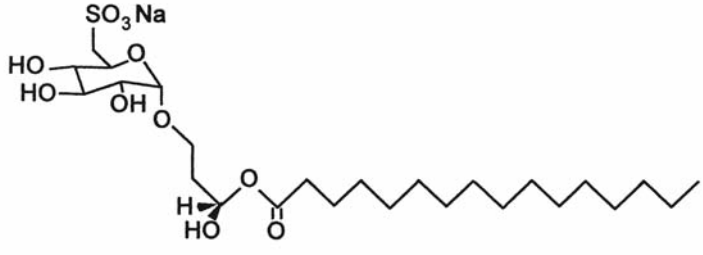


Fig. 7.7 Ecdysis and the formation of new thecal vesicles in *Glenodinium foliaceum*. Ecdysis results in the loss of the plasma membrane, thecal plates, and vesicles. A pellicle forms from a layer that existed under the thecal vesicles. New thecal vesicles and plates are formed under the thickening pellicle. When the amphiesma is mature, the wall breaks out of the pellicle cyst. (Drawn from transmission electron micrographs in Bricheux et al., 1992.)



1-*O*-palmitoyl-3-*O*-(6'-sulfo-a-D-quinovopyranosyl)-*sn*-glycerol (PSQG)

Fig. 7.8 The compound released by the green alga *Bryopsis* that induces ecdysis in the dinoflagellate *Gambierdiscus toxicus*.

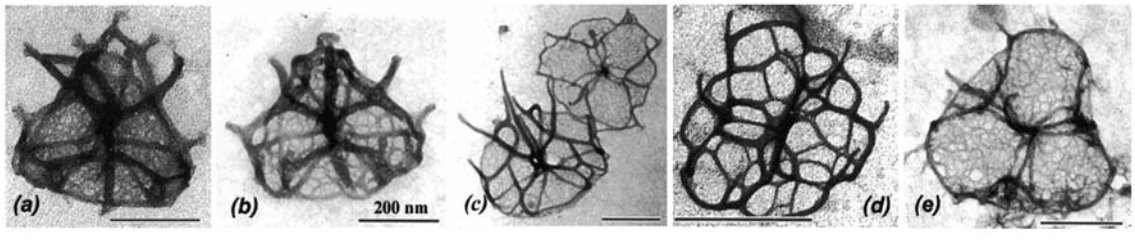


Fig. 7.9 Transmission electron micrographs of scales of different species of *Heterocapsa*. (*a*) *H. triquetra.* (*b*) *H. arctica.* (*c*) *H. circularisquama.* (*d*) *H. horiguchi.* (e) *H. ildefina*. (From Iwataki et al., 2004.)

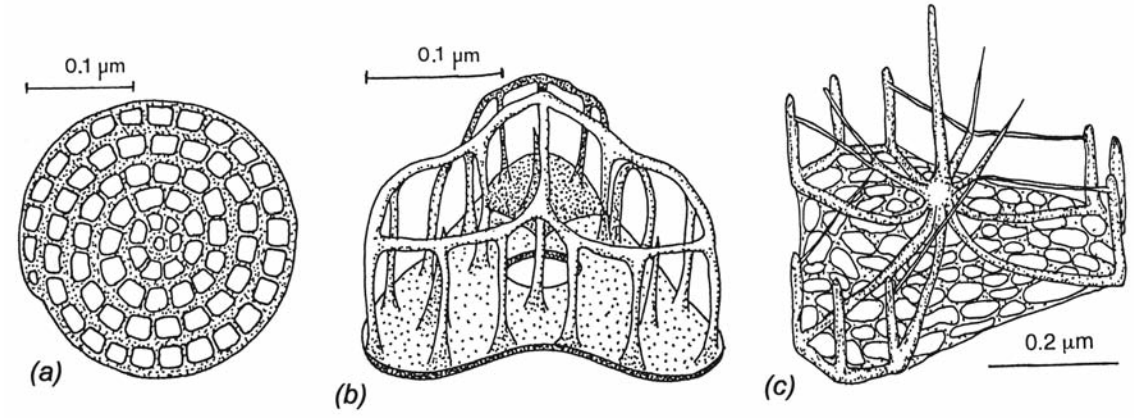


Fig. 7.10 Dinoflagellate scales. (*a*) *Oxyrrhis marina.* (*b*) *Heterocapsa niei.* (*c*) *Katodinium rotundatum.* ((*a*) after Clarke and Pennick, 1976; (*b*) after Morrill and Loeblich, 1983b; (*c*) after Hansen, 1989.)

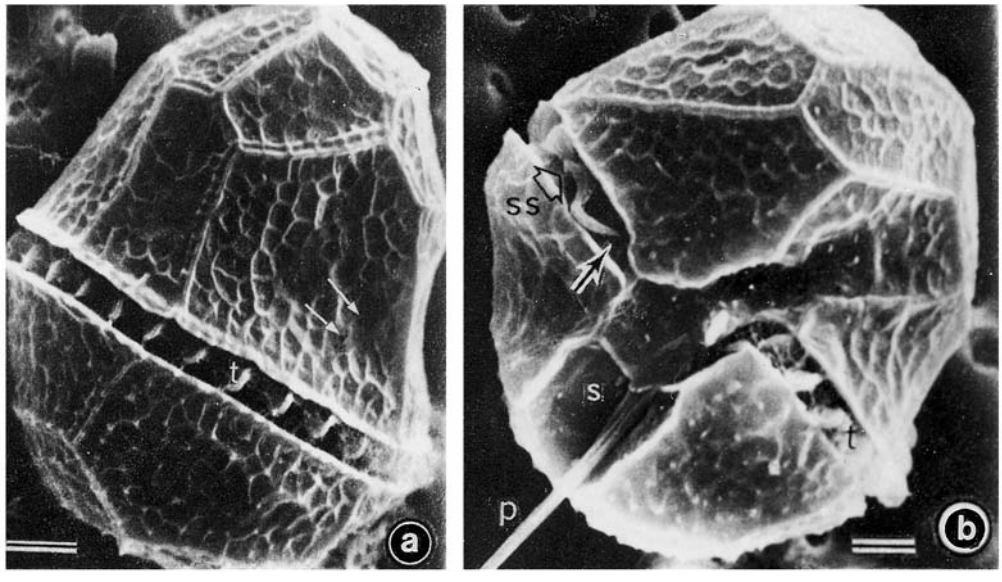


Fig. 7.11 Dorsal and ventral views of cells of *Peridinium cinctum* in the scanning electron microscope. (p) Posterior (longitudinal) flagellum; (s) longitudinal sulcus; (ss) striated strand; (t) transverse flagellum. Bar = 5μm. (From Berdach, 1977.)

contains **centrin**, a Ca^{2+}-modulated contractile protein (Höhfeld et al., 1988). Contraction of the striated strand leads to supercoiling of the axoneme. On one side of the axoneme, a unilateral row of fibrillar hairs, 2 to 4 μm long and 10 nm wide, is attached to the flagellar sheath. The final micrometer of the flagellum lacks the striated strand and hairs, with the axoneme tightly covered by the flagellar sheath. The axoneme is a left-handed screw; waves propagated from the attached end toward the free end create a downward thrust at the outermost edges of the coil. The flagellum causes a direct forward movement while at the same time causing the cell to rotate. The flagellar beat always proceeds

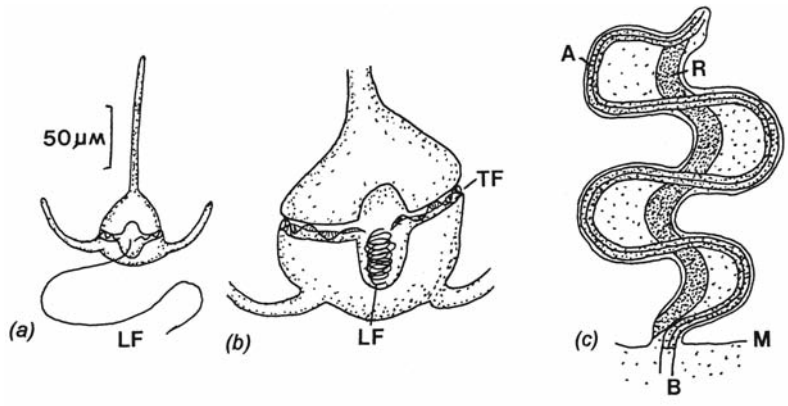


Fig. 7.12 *Ceratium tripos*. (*a*) Vegetative cell with a relaxed longitudinal flagellum (LF) at full length. (*b*) A cell with the longitudinal flagellum (LF) fully contracted and folded in the sulcus. (TF) transverse flagellum. (*c*) Schematic drawing of a retracted flagellum showing the contracted R-fiber (R) and the axoneme (A). (B) Basal body; (M) plasma membrane. (Adapted from Maruyama, 1982.)

counterclockwise when seen from the cell apex (**leiotropic** direction). The cell always rotates in the direction of the flagellar beat (in the leiotropic direction), with the fluid propelled in the opposite direction (in the **dexiotropic** direction) (Fig. 7.15) (Gaines and Taylor, 1985; Fenchel, 2001). The longitudinal flagellum swings in a narrow orbit acting as a rudder.

The dinoflagellates are the fastest swimmers among the algae although they are slower than *Mesodinium*, the photosynthetic symbiosis between a ciliate and a cryptophyte (see Chapter 9, Cryptophyta, Symbiotic associations). Dinoflagellates swim from 200 to 500 $\mu m\ s^{-1}$ (Raven and Richardson, 1984). The cells of *Lingulodinium polyedrum* (Fig. 7.40) swim at a linear rate of 250 $\mu m\ s^{-1}$ at 20 °C whereas cells of *Gyrodinium* swim at a mean linear rate of velocity of 319 $\mu m\ s^{-1}$ at 20 °C. Marine dinoflagellates frequently move into deeper, nutrient-rich waters at night and better illuminated waters near the surface during the day. The **diel** (over a 24-hour period) migrations of dinoflagellates are 5 to 10 m in relatively quiet waters. A dinoflagellate swimming at 500 $\mu m\ s^{-1}$ would take about 6 hours of the 24-hour period for 5 m of upward migration around dawn, and a further 6 hours for downward migration around dusk (Raven and Richardson, 1984).

Pusule

A **pusule** is a sac-like structure that opens by means of a pore into the flagellar canal and probably has an osmoregulatory function similar to that of a contractile vacuole. The pusule of

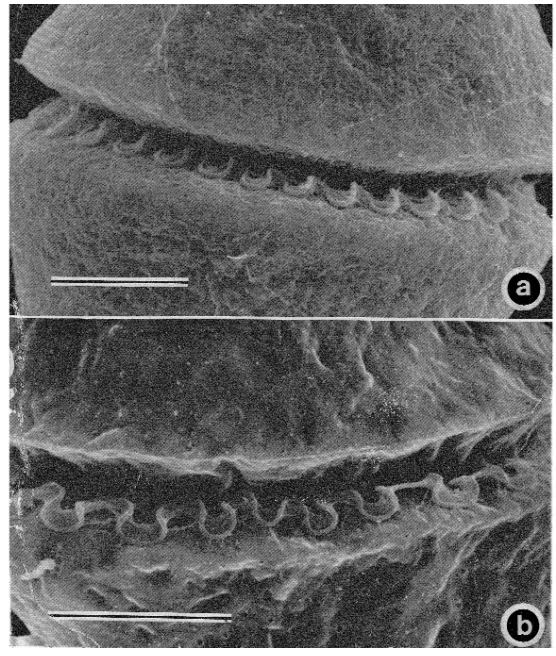


Fig. 7.13 Scanning electron micrograph showing the form of the transverse flagellum in *Akashiwo sanguinea* (= *Gymnodinium sanguineum*) (*a*) and *Gyrodinium uncatenum* (*b*). Bar = 10 μm. (From Gaines and Taylor, 1985.)

Amphidinium carteri is representative of those dinoflagellates that have a pusule (Fig. 7.16) (Dodge and Crawford, 1968). In this organism there are two pusules, one associated with each flagellar canal. The pusule consists of about 40 vesicles which open by small pores into the flagellar canal. Whereas the flagellar canal is lined by a single membrane continuous with the plasma

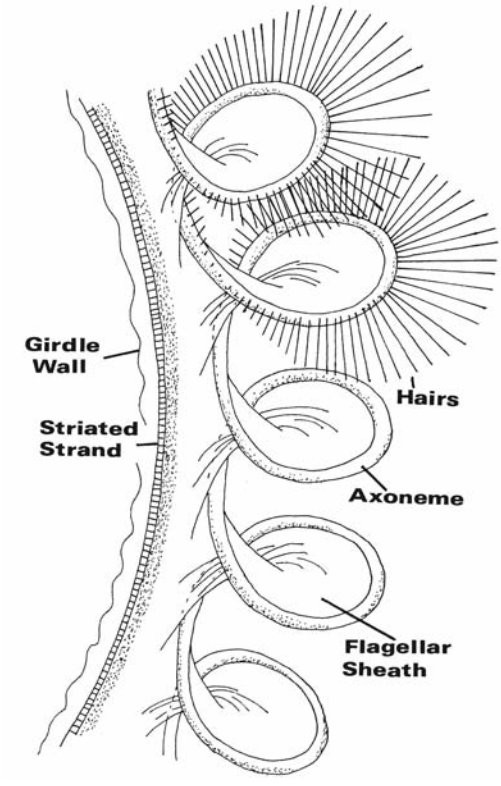


Fig. 7.14 Diagram of part of the transverse flagellum of *Peridinium cinctum*. Only a portion of the fibrillar hairs have been drawn in. (After Berdach, 1977.)

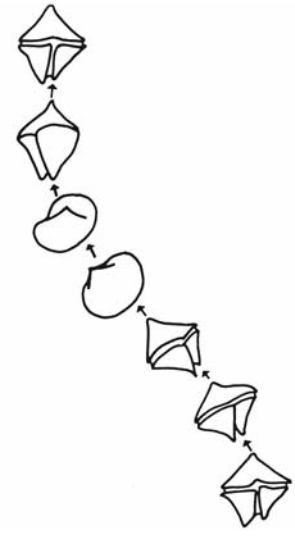


Fig. 7.15 Tracings from successive video frames of *Protoperidinium conicum* swimming, showing the leiotropic rotation of the cell. Time between intervals is 1/5 second. (From Gaines and Taylor, 1985.)

membrane, the pusule vesicles are lined by a double membrane.

Chloroplasts and pigments

The plastids of most photosynthetic dinoflagellates originated from a secondary endosymbiosis with a red alga. These plastids are surrounded by three membranes (two membranes of chloroplast envelope and one membrane of chloroplast endoplasmic reticulum) (Fig. 7.2) and contain chlorophyll *a* and *c*, and peridinin (Fig. 7.17) as the major photosynthetic pigments (Ishida and Green, 2002).

There are a small number of dinoflagllates that have plastids derived from a tertiary endosymbiosis (Fig. 7.18). **Tertiary endosymbiosis** begins with the loss of the plastid (originally derived from a secondary endosymbiosis) from a dinoflagellate followed by endosymbiosis of an alga from the Prymnesiophyceae (a haptophyte alga). All of the protoplasm of the endosymbiont was lost, except for the chloroplast surrounded by one membrane of chloroplast endoplasmic reticulum, which became the permanent chloroplast of the dinoflagellate. Instead of peridinin, these algae have 19′-hexanoyloxy-fucoxanthin (Fig. 7.17) and/or 19′butanoyloxy-fucoxanthin, pigments characteristic of the Prymnesiophyceae. *Karenia brevis* (Fig. 7.19(*a*)), *Karenia mikimotoi* (Fig. 7.19(*b*)), and *Karlodinium veneficum* (Fig. 7.34) are dinoflagellates that are derived from tertiary endosymbioses (Ishida and Green, 2002; Takishita et al., 2005; Yoon et al., 2002).

A number of dinoflagellates contain short-term plastids stolen from their food source (**kleptoplastids**) and it is sometimes difficult to distinguish between these plastids and permanent plastids (Keeling, 2004). Dinoflagellates have transferred most of the plastid genome to the nucleus of the cell, making them the only eukaryotes that encode the majority of the plastid genes in the nucleus (Hackett et al., 2004). Having the genes for plastid-targeted proteins may actually be an advantage since it provides the cell with the freedom to replace the original plastid with a new one (Green,

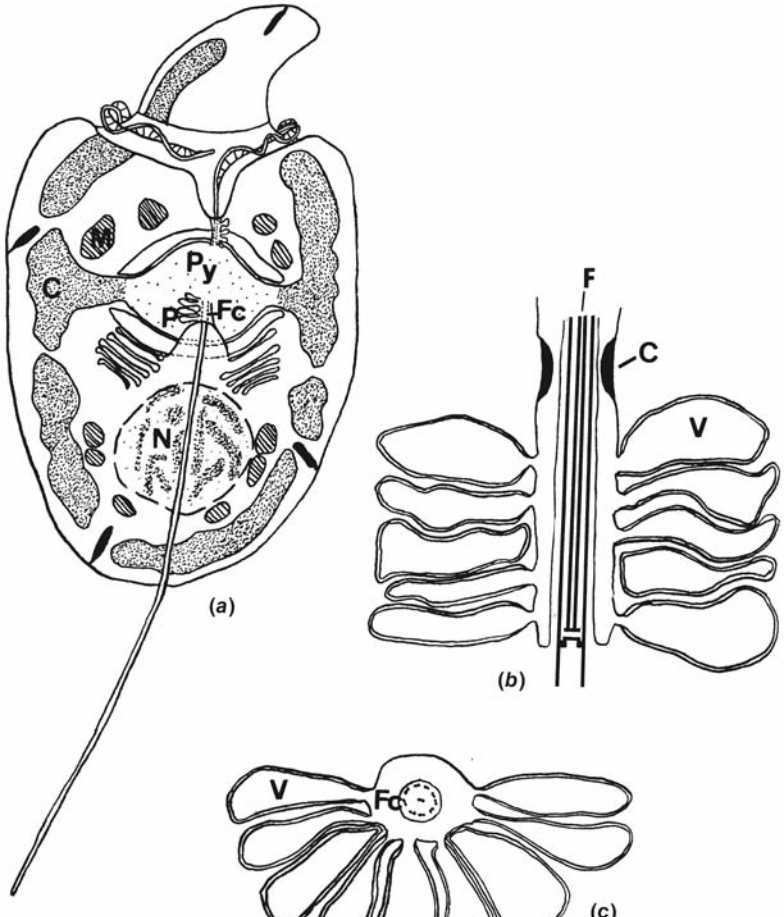


Fig. 7.16 (*a*) Drawing of *Amphidinium carteri*. The small epicone is separated from the hypocone by the encircling girdle, which contains the transverse flagellum. The peripheral chloroplast (C) is shown only at the sides of the cell so the positions of the nucleus (N), mitochondria (M), pyrenoid (Py), and the pusule (P) associated with the flagellar canals can be seen. (*b*) Longitudinal section through a pusule showing the flagellar pore constriction (C), the pusule vesicles (V), and the flagellum (F). (*c*) Transverse section of a pusule showing the flagellum within the flagellar canal (Fc) and the pusule vesicles (V) opening into the canal. (From Dodge and Crawford, 1968.)

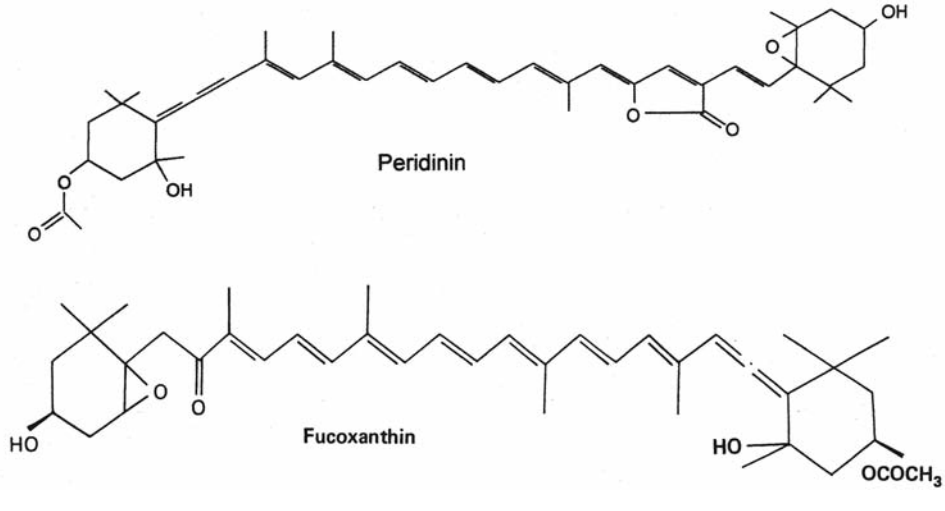


Fig. 7.17 The chemical structure of peridinin and 19′-hexanoyloxy-fucoxanthin. Peridinin has three rings instead of the two found in other light-harvesting carotenoids.

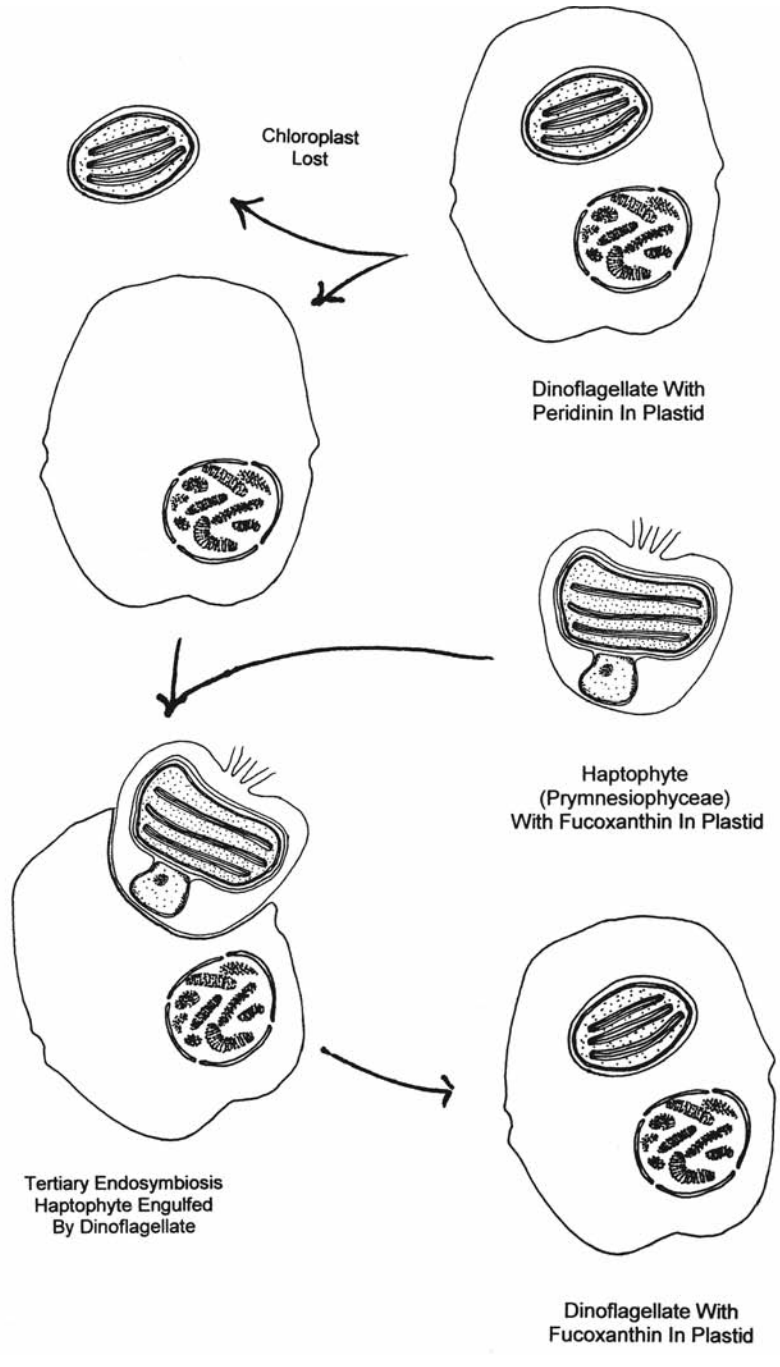


Fig. 7.18 The sequence of events leading to plastids evolved from a tertiary endosymbiosis.

2004). The plastid genome of peridinin-containing dinoflagellates is reduced and broken up into mini-circles that encode only 16 proteins.

Most of the chlorophyll *a* and peridinin occur together in a water-soluble protein complex called peridinin–chlorophyll *a*–protein (PCP). Within the chromophore the peridinin and chlorophyll *a* are in a 4:1 ratio (Prézelin and Haxo, 1976). PCP is similar to the phycobiliproteins in cyanobacteria

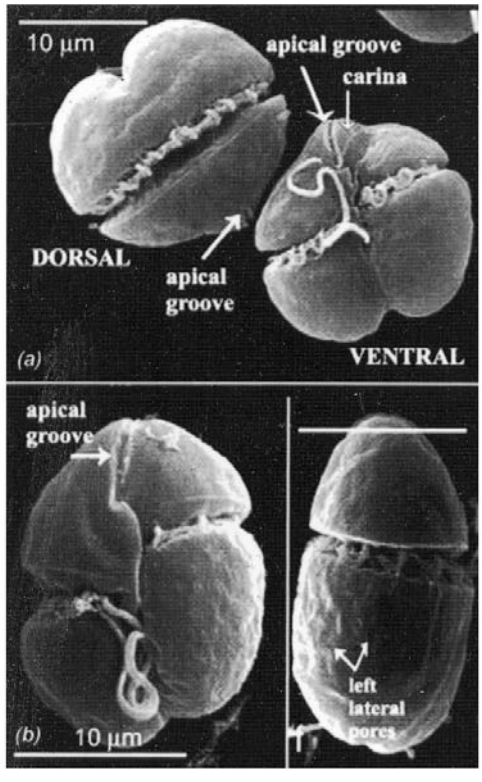


Fig. 7.19 Scanning electron micrographs of (*a*) *Karenia* (*Gymnodinium*) *brevis* and (*b*) *Karenia* (*Gymnodinium*) *mikimoto*. (From Haywood et al., 2004.)

and red algae in that it is on the surface of thylakoids, is water-soluble, and acts as a light-harvesting pigment. If *Glenodinium* (Fig. 7.22) is cultured under decreasing light intensity (to 1/12 of the original light intensity) the amount of PCP increases about seven fold, whereas the amount of chlorophyll *a* and peridinin not associated with PCP increases only 1.5 times. Little change occurs in chlorophyll *c* (Prézelin, 1976). This is a type of chromatic adaptation; as the cells receive less light (i.e., grow in deeper water), they produce more PCP, with the peridinin capturing light and passing it to chlorophyll *a*.

Phototaxis and eyespots

The action spectra for phototaxis is the same in all dinoflagellates that have been studied, with maximum phototaxis obtained at a wavelength of 450 nm (Fig. 7.20) (Horiguchi et al., 1999). An eyespot is not necessary for a phototactic response, indicating that the phototactic machinery was carried in the host organisms in the endosymbiosis leading to photosynthetic dinoflagellates (e.g., the phototactic receptor is not in the eyespot but is probably associated with the plasma membrane).

Less than 5% of the Dinophyceae contain eyespots, and those that do are mostly freshwater species; yet the eyespots are among the most complex in the algae.

The simplest type of eyespot consists of a collection of lipid globules in the cytoplasm not surrounded by a membrane (e.g., *Woloszynskia coronata*) (Dodge, 1971) (Fig. 7.21). A second type of eyespot consists of a row of lipid globules in a plastid-like structure at the cell periphery (e.g., *Peridinium westii, W. tenuissima*) (Messer and Ben-Shaul, 1969; Crawford et al., 1970).

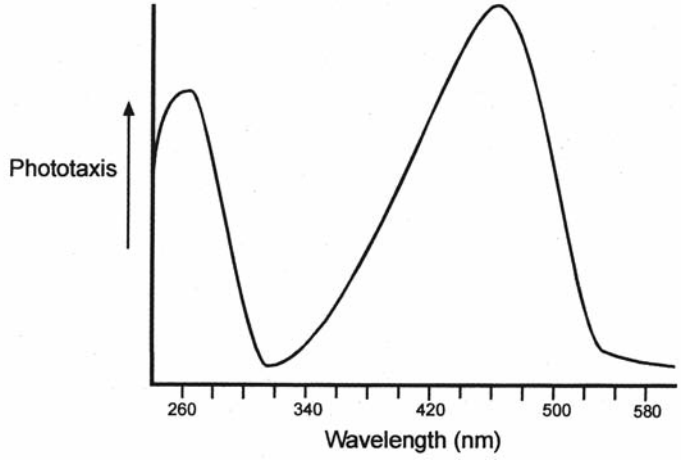


Fig. 7.20 The effect of different wavelengths of light on phototaxis in dinoflagellates. Maximum photosynthesis occurs at a wavelength around 450 nm. (Adapted from Horiguchi et al., 1999.)

The eyespot of *Glenodinium foliaceum* (Dodge and Crawford, 1969) is immediately under the anterior portion of the sulcus and is about 6 μm long and 3 μm wide (Fig. 7.22). It is more or less rectangular in outline with a hook-shaped projection at the anterior end. This flattened sac-like structure contains two rows of large lipid globules separated by a granular space. Surrounding the eyespot is a triple-membrane envelope identical in appearance to that surrounding the chloroplasts. Adjacent to the eyespot is a non-membrane-bounded lamellar body consisting of a stack of flattened vesicles arranged more or less parallel to one another. The lamellar body is about 2 μm long and 0.75 μm wide, and contains up to 50 vesicles. The vesicles are connected at their edges, and also at the ends of the stack, with rough endoplasmic reticulum.

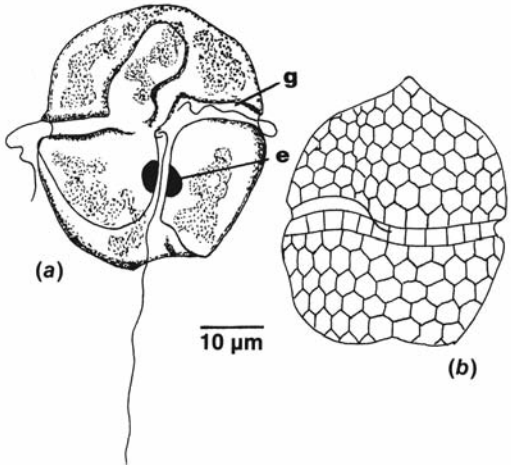


Fig. 7.21 *Woloszynskia tenuissima*. (*a*) Ventral view showing the two flagella, the girdle (g), and the eyespot (e). (*b*) Side view showing the thecal plates, which were not drawn in (*a*). (After Crawford et al., 1970.)

The most complex type of eyespot is found in the Warnowiaceae of the Peridiniales. The eyespot in *Nematodinium armatum* (Moronin and Francis, 1967) and that in *Erythropsis cornuta* (Gruet, 1965) have been studied at the fine-structural level and found to be essentially similar in construction (Figs. 7.23, 7.24). In *N. armatum*, the eyespot is located toward the rear of the cell alongside the girdle, and consists of a **lens** mounted in front of a **pigment cup**, oriented so that the axis through the center of the lens and pigment cup is nearly perpendicular to the longitudinal axis of the cell body. The lens lies just below the plasmalemma. The pigment cup is made up of three main parts. Most of its wall consists of

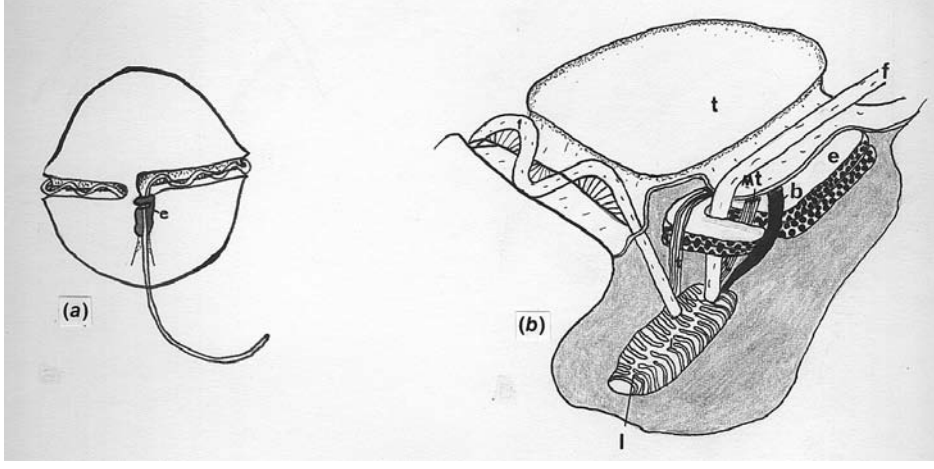


Fig. 7.22 (*a*) A ventral view of a cell of *Glenodinium foliaceum* showing the location of the eyespot (e). (*b*) Three-dimensional diagram of the eyespot area. The two flagella arise just above the lamellar body (l). The eyespot (e) lies beneath the sulcus. (mt) Microtubular roots; (b) banded root; (t) thecal plate. (After Dodge and Crawford, 1969.)

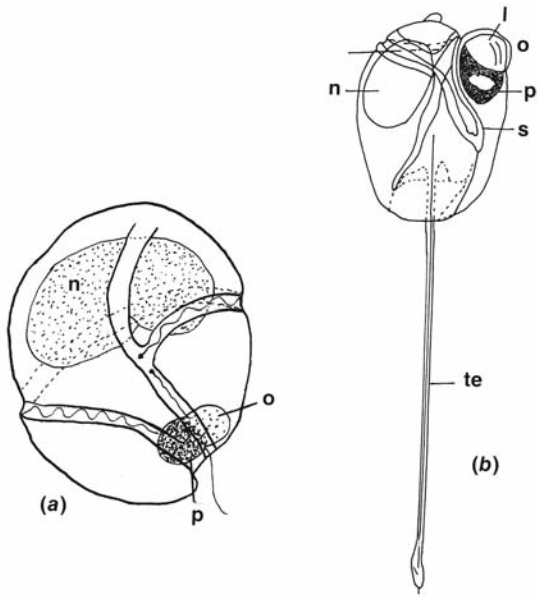


Fig. 7.23 (*a*) *Nematodinium armatum.* (*b*) *Erythropsis cornuta.* (l) Lens; (n) nucleus; (o) ocellus (eyespot); (p) pigment cup; (s) longitudinal sulcus; (te) tentacle.

a single layer of large oblong pigment granules 0.3 μm in diameter. Toward the lip of the cup, the pigment granules are smaller and loosely arranged in several layers. Within the base of the cup is a dense layer of fibrils 33 nm in diameter, parallel to the axis of the eyespot; this layer is covered by a mat of transverse fibrils and has been named the **retinoid** because of its supposed light-receptive function. Above the retinoid is a canal that opens into a furrow of the transverse flagellum; the outermost membrane on the cell surface is continuous with the membrane of the canal. The lens unit is a complex structure completely surrounded by mitochondria. Inside the mitochondria is a granular layer separated by a membrane from the lens. The central core of the lens consists of membrane-bounded domed or concentric layers of dense material; the major bulk of the lens surrounds this core and consists of several large, nearly empty lobes. Between the core and the lobes is a network of vesicles of intermediate size.

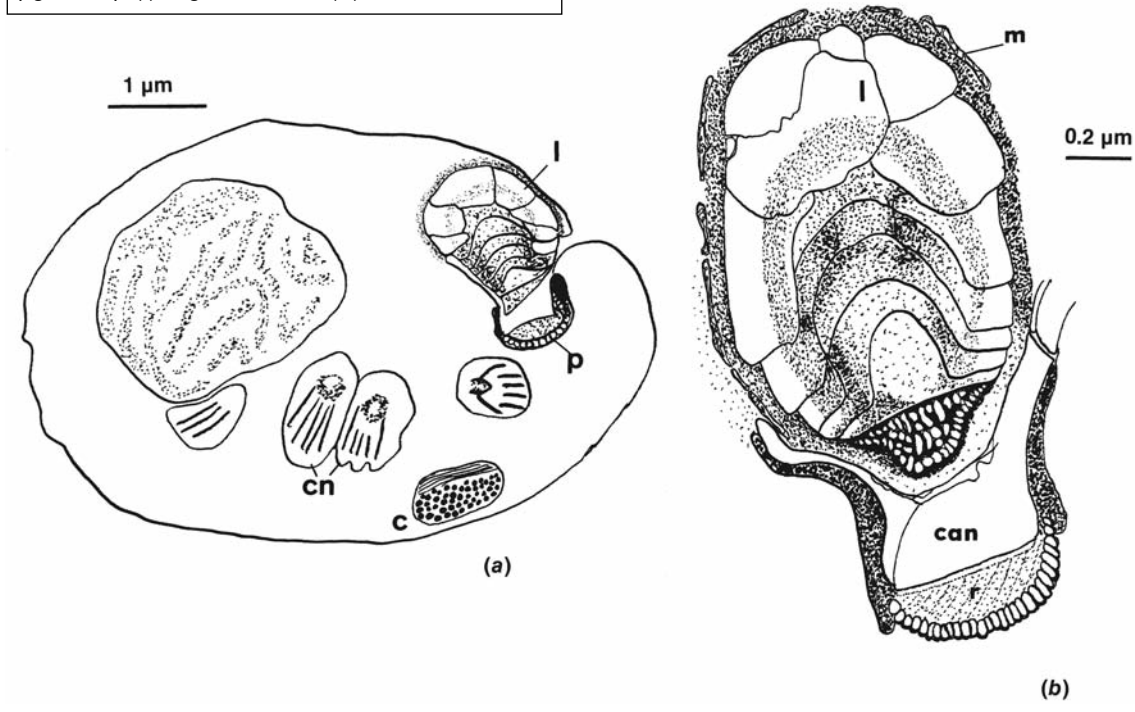


Fig. 7.24 (*a*) A cell of *Nematodinium armatum*, showing the lens (l), pigment cup (p), cnidocysts (cn), and a chloroplast (c). (*b*) A complete eyespot (ocellus) with retinoid (r), canal leading to outside (can), and mitochondria (m) surrounding the lens (l). (After Moronin and Francis, 1967.)

Nucleus

The first dinoflagellates to evolve had nuclei similar to other algae with a closed mitosis and histones associated with the nucleic acids (Taylor, 1999). *Oxyrrhis* (Fig. 7.56(*a*)) is representative of such a dinoflagellate having microtubules formed inside the nuclear membrane during mitosis (Triemer, 1982; Gao and Li, 1986). Histones were gradually lost as dinoflagellate evolution proceeded and a type of mitosis evolved with the mitotic spindle outside the nuclear membrane.

The nuclei of the more advanced dinoflagellates are striking cytologically in that they have their chromatin condensed into 2.5 nm fibrils in the interphase nuclei (Figs. 7.2, 7.4). The organization of the chromatin is different from either prokarytoic or eukaryotic cells and has been referred to as **mesokaryotic** or **dinokaryotic** (Rizzo, 1991).

Unicellular eukaryotic organisms usually have between 0.046 and 3 picograms (pg) of DNA per nucleus. Dinoflagellates, however, have much more DNA in their nuclei, with values ranging from 3.8 pg per nucleus in *Cryptothecodinium cohnii* (Fig. 7.3(*e*)–(*g*)) to 200 pg per nucleus in *Lingulodinium polyedrum* (Fig. 7.40(*b*)) corresponding to about 200 000 Mb (in comparison, hexploid *Triticum* wheat is 16 000 Mb and the haploid human genome is 3 180 Mb) (Sigee, 1984). This implies that a large amount of the DNA is genetically inactive (structural DNA) in dinoflagellates.

Nuclear division in the more advanced dinoflagellates has the nuclear envelope remaining intact during division, the nucleolus persisting and dividing by pinching in two, and the chromosomes attached to the nuclear envelope (Barlow and Triemer, 1988).

Mitosis in *Syndinium* (Fig. 7.25(*a*)) can be used as an example of the more advanced type in the dinoflagellates. The onset of division is usually marked by the duplication of the flagellar bases from two to four. Throughout this stage the nucleus enlarges, and many Y- and V-shaped chromosomes are found. The nucleus becomes invaginated, resulting in the formation of 1 to 15 channels traversing the dividing nucleus (Fig. 7.26). The channels contain tunnels of cytoplasm passing through the nucleus outside of the nuclear membrane. There are bundles of microtubules in these channels, which are not connected to the intact nuclear envelope. The chromosomes are probably attached to the nuclear membrane or a specialized kinetochore in the nuclear membrane. At metaphase there is no formation of a metaphase plate as is common with eukaryotes, and the chromosomes are still scattered. The nucleolus persists throughout the whole nuclear cycle and divides by constricting in the middle. In anaphase the cell and nucleus expand laterally, and the chromosomes move to opposite ends of the nucleus. With continued lateral expansion, the central isthmus eventually severs, and the two daughter nuclei become independent (Leadbeater and Dodge, 1967b; Kubai and Ris, 1969; Ris and Kubai, 1974).

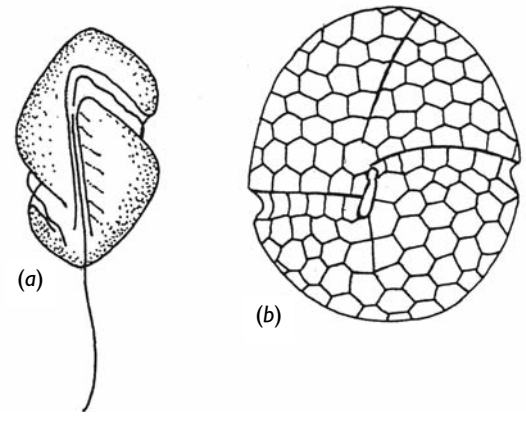


Fig. 7.25 (*a*) *Syndinium turbo.* (*b*) *Gymnodinium neglectum.* ((*a*) after Chatton, 1952; (*b*) after Schiller, 1933.)

Projectiles

The Dinophyceae have a number of different projectiles, which are fired out of the cell when it is irritated, resulting in a sudden movement of the cell in the opposite direction from the discharge.

A **trichocyst** has a membrane-bounded, rod-shaped crystalline core (Bouck and Sweeney, 1966) (Fig. 7.27). Along the anterior one-third of the core are short, fine, tubular elements that project slightly downward. At the extreme outer end of the core, a group of 20 to 22 fibers extend from the outer part of the core to the enclosing membrane, and still finer fibrils then connect

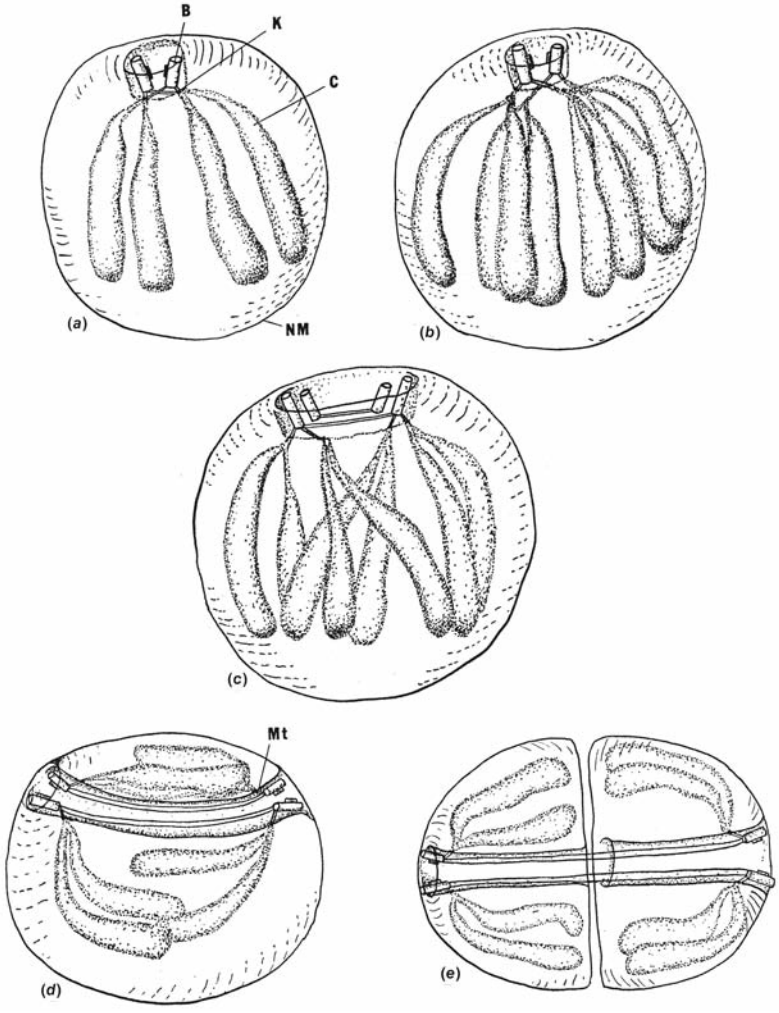


Fig. 7.26 Diagrammatic representation of nuclear division in *Syndinium* sp. (*a*) Interphase. (*b*) Early division; kinetochores and chromosomes have duplicated. (*c*) Early stage of chromosome segregation. Central spindle between separating basal bodies of flagella. (*d*) Late stage of chromosome separation. Central spindle in cytoplasmic channel through nucleus. (e) Division of nucleus. (B) Basal body of flagellum; (K) kinetochore; (C) chromosome; (Mt) microtubules; (NM) nuclear membrane. (After Ris and Kubai, 1974.)

the larger fibrils to the apical portion of the trichocyst membrane. Just within the enclosing membrane are fine, thread-like, opaque hoops. The outer part of the trichocyst membrane is attached to the plasma membrane between the thecal vesicles or to the thecal vesicles beneath round, thin areas of thecal plates that form trichocyst pores. Trichocysts originate in areas rich in Golgi bodies and are probably derived from them initially as spherical vesicles that eventually become spindle-shaped and develop into the trichocysts. On irritation a "charged" trichocyst is converted to a "discharged" trichocyst in a few milliseconds, possibly by the rapid uptake of water. The discharged trichocysts are straight, tapering rods many times longer than the charged trichocyst (up to 200 μm long in *Prorocentrum*) (Figs. 7.30(*c*), 7.55, 7.56(*c*)). The discharged trichocyst has transverse banding, with a major period of 50 to 80 nm. Although most dinoflagellates have trichocysts, ultrastructural investigations have shown that some do not (i.e., *Gymnodinium neglectum* (Fig. 7.25(*b*)), *Aureodinium pigmentosum, Woloszynskia tylota*, and the symbiotic *Symbiodinium microadriaticum*). The actual benefit of trichocysts to the cell (if any) is still obscure. They could be a mechanism for quick escape as the cells move sharply in the opposite direction of discharge, or they could be able to directly "spear" a naked intruder.

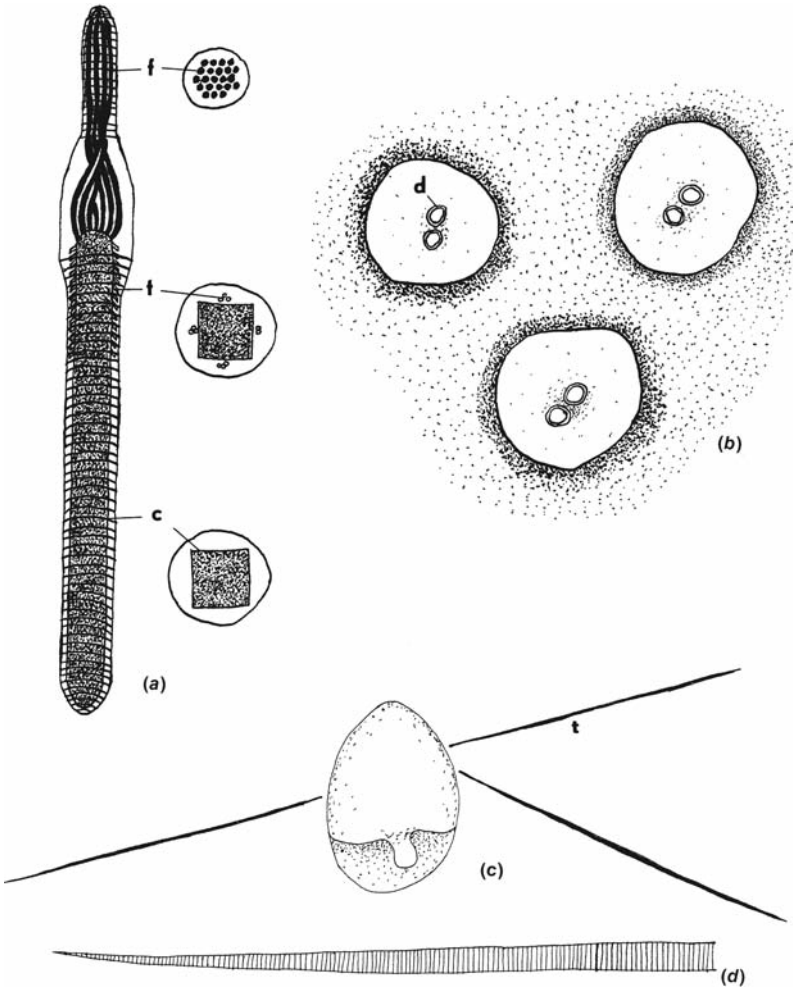


Fig. 7.27 (*a*) Diagram of a longitudinal section and cross sections of a charged trichocyst of *Lingulodinium polyedrum*. The single membrane limiting the trichocyst is lined on its inner surface with fine hoops or spirals. Within the membrane is a crystalline core (c) composed of long rods or plates. Along the upper one-third of the core, short tubules (t) protrude downward and outward. At the anterior portion of the core, a series of fibers (f) attach to the core to still finer fibrils, which eventually reach to the anterior portion of the enclosing membrane. (*b*) Drawing of a segment of a wall plate of *Lingulodinium polyedrum*. Pore-like thin areas in the plate contain two or three slightly ridged discs (d) through which the trichocyst is discharged. (*c*) Cell of *Oxyrrhis* with discharged trichocysts. (*d*) Drawing of the tip of a discharged trichocyst showing striations. ((*a*),(*b*) after Bouck and Sweeney, 1966.)

Accumulation body

This is a large vesicle containing the remains of digested organelles (Figs. 7.36(*c*), 7.53(*b*)). It is probably similar to the Corps de Maupas of the Cryptophyceae and the digestive vesicles of other flagellates (Zhou and Fritz, 1994). An accumulation body is particularly common in symbiotic Dinophyceae.

Resting spores or cysts or hypnospores and fossil Dinophyceae

The **resting spore** or **cyst** of most dinoflagellates is morphologically distinct from the parent cell. They are 30 to 70 μm in diameter with smooth or spinose bodies (Figs. 7.28, 7.36). The newly formed cysts of *Scrippsiella trochoidea* have ten times more carbohydrate and 1.5% the respiratory rate of vegetative cells (Brooks and Andersen, 1990).

The cell walls of the cysts are highly resistant to decay and contain **dinosporin**, a chemical similar to sporopollenin in the pollen of higher plants (Kokinos et al., 1998). The cysts are extremely resistant and are preserved in ancient sediments where they are of value in paleoecological studies. Fossilized cysts are called **hystrichosphaerids** (**hystrichospores**) and are included in fossilized cyst-like structures of unicellular algae called **acritrachs**. These fossilized dinoflagellates first appeared in the Triassic and reached a peak in the Jurassic and Cretaceous, followed by a decrease in the Tertiary (MacRae et al., 1996).

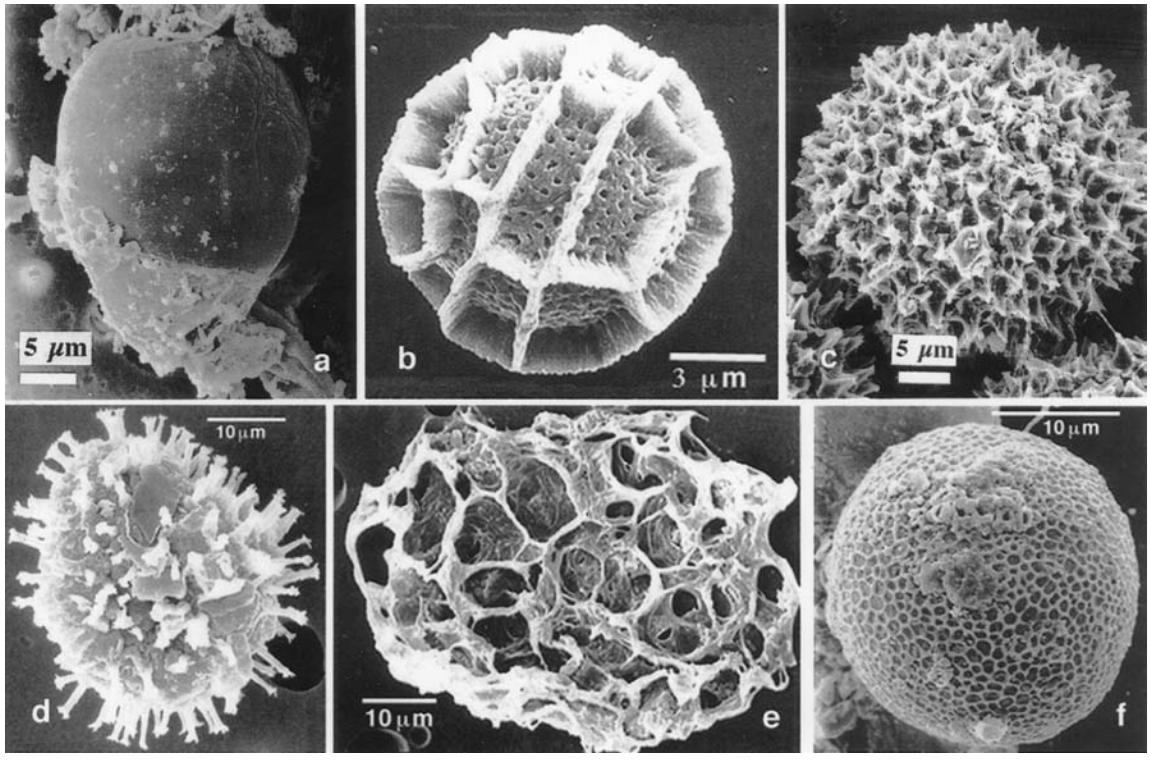


Fig. 7.28 Dinoflagellate cysts. (*a*) *Alexandrium catenella.* (*b*) *Calciodinellum operosum.* (*c*) *Scrippsiella trophoidea.* (*d*) *Gonyaulax grindleyi.* (e) *Polykrikos schwartzii.* (*f*) *Gymnodinium catenatum.* ((*d*)–(*f*) from Ellegaard et al., 1994; (*b*) from Montresor et al., 1997; (*a*),(*c*) from Meksumpun et al., 1994.)

Hystrichosphaerids were discovered independently by paleontologists and classified under a separate taxonomic scheme consisting of only fossil species. Many extant resting spores are identical to hystrichosphaerids of the Tertiary and Quarternary, with the result that there are two names for the same structure.

The process of encystment or resting spore formation is regulated by a complex interaction of day length, temperature, and nutrient concentration (Kremp, 2001; Sgrosso et al., 2001). Melatonin levels increase by several orders of magnitude during encystment and may function in preventing oxidation of the lipids in the cyst (Balzer and Hardeland, 1996). In the freshwater dinoflagellate *Woloszynskia tylota*, encystment involves the following changes (Bibby and Dodge, 1972): (1) replacement of the theca by a thin amorphous outer wall, which gradually thickens by the deposition of material on its inner face; (2) the appearance of a layer of closely packed lipid droplets at the cytoplasmic margin of the mature cyst; (3) the reduction in size or disappearance of cytoplasmic structures such as chloroplasts, Golgi bodies, and pusules; and (4) the enlargement of a central orange-brown body and cytoplasmic vacuoles containing crystals. Cysts are recognizable because they lack chromatophores and have a microgranular brown cytoplasm and a red eyespot (if the organism normally has an eyespot). Calcification of cysts in some genera occurs by the deposition of calcium carbonate crystals in the narrow space between the cell wall and the plasma membrane (Montresor et al., 1997). The cysts of *Ceratium hirundinella* contain an outer silicon layer (Chapman et al., 1982).

A small number of dinoflagellates produce siliceous skeletons, with the protoplasm wrapped around the skeleton. The best known species is the heterotrophic non-armored *Actiniscus pentasterias* (Fig. 7.29) (Hansen, 1993).

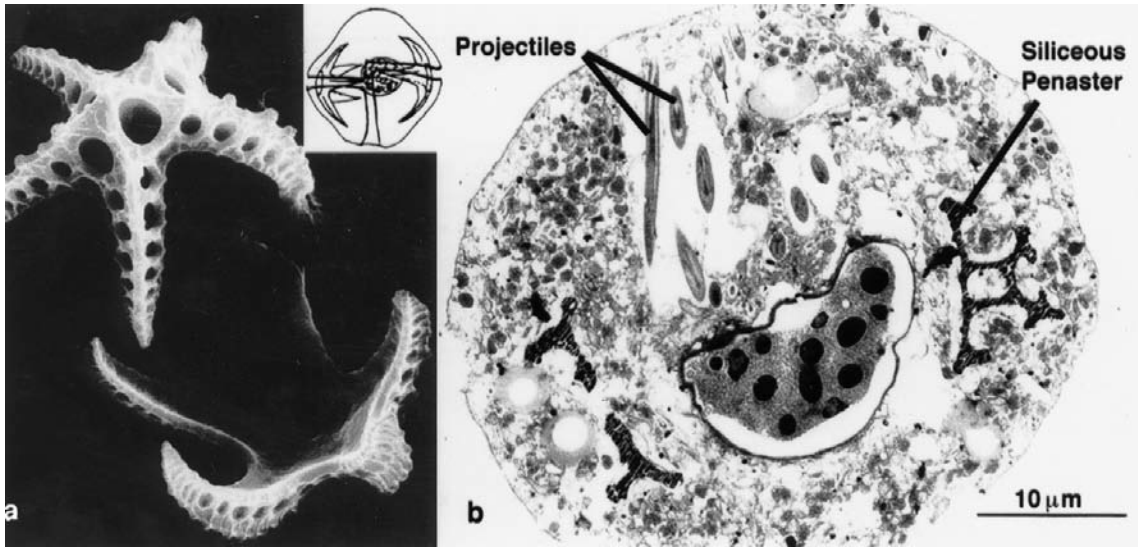


Fig. 7.29 *Actiniscus pentasterias*. (*a*) Scanning electron micrograph of the siliceous internal skeleton (two pentasters). (*b*) Transmission electron micrograph showing two pentasters surrounding the nucleus. (From Hansen, 1993; Preisig, 1994.)

Toxins

Some Dinophyceae have the ability to produce very potent toxins which cause the death of fish and shellfish during **red tides** when there are dinoflagellate blooms that color the water red. The dinoflagellates become lodged in the gills of the shellfish, and when shellfish are eaten by humans or animals, poisoning results.

Historically, red tides and paralytic shellfish poisoning have been mentioned many times (Shilo, 1967). One of the plagues that struck Egypt was described in the Bible: "all the waters that were in the river were turned to blood. And the fish that was in the river died; and the river stank, and the Egyptians could not drink the water of the river . . ." (Exodus 7:17). This description is strongly reminiscent of the poisonous red tides. Darwin, in his description of discolored water in 1832 during his voyage on the *Beagle*, graphically described blooms of algae that were dinoflagellates.

Death and illness caused by consumption of poisonous mussels and clams were reported by Captain Cook and Captain George Vancouver during their expeditions to the coast of the Pacific Northwest. An old custom among Indian tribes along the coast of Alaska was to station sentries to watch for the marine luminescence occurring during hot weather, which they understood to be associated with Kal-Ko-O, their name for mussel poisoning.

All of the dinoflagellates that have been convincingly demonstrated to produce toxins contain chloroplasts, indicating that the ability to produce toxins may have been derived from endosymbiotic cyanobacteria.

1 **Diarrhetic shellfish poisoning**. This occurs primarily in temperate regions and is caused by species of the planktonic dinoflagellates *Exuviaella*, *Dinophysis* (Fig. 7.30(*a*), (*b*)), and *Prorocentrum* (Figs. 7.30(*c*), 7.55, 7.56(*c*)). Diarrhetic shellfish poisoning is caused by the polyether carboxylic acids okadaic acid, macrolide toxins, and yessotoxin (Figs. 7.31, 23.3, 23.4). The toxins are powerful inhibitors of serine- and threonine-protein phosphatases PP1 and PP2A and induce severe gastroenteritis (Zhou and Fritz, 1994; Morton and Tindall, 1995; Suzuki et al., 1997).

The polyether carboxylic acid okadaic acid is initially formed inside the dinoflagellate cell as dinophysistoxin-4 (Fig. 7.31). This weakly sulfated derivative of okadaic acid is not toxic to the dinoflagellate cell. Dinophysistoxin-4 is

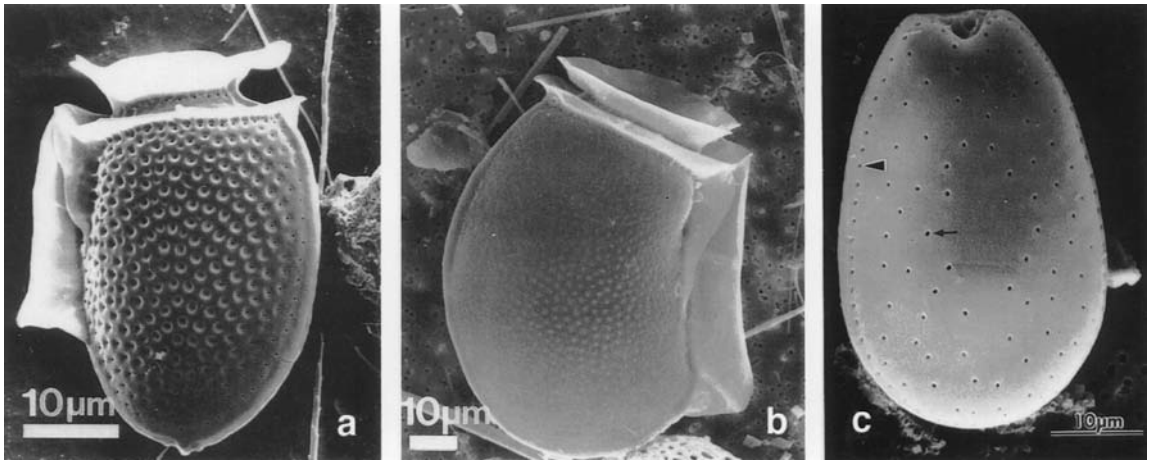


Fig. 7.30 Scanning electron micrographs of dinoflagellates that cause diarrhetic shellfish poisoning. (*a*) *Dinophysis acuminata.* (*b*) *Dinophysis fortii.* (*c*) *Prorocentrum lima* with the arrows pointing to pores in the theca. (From Hallegraeff, 1993.)

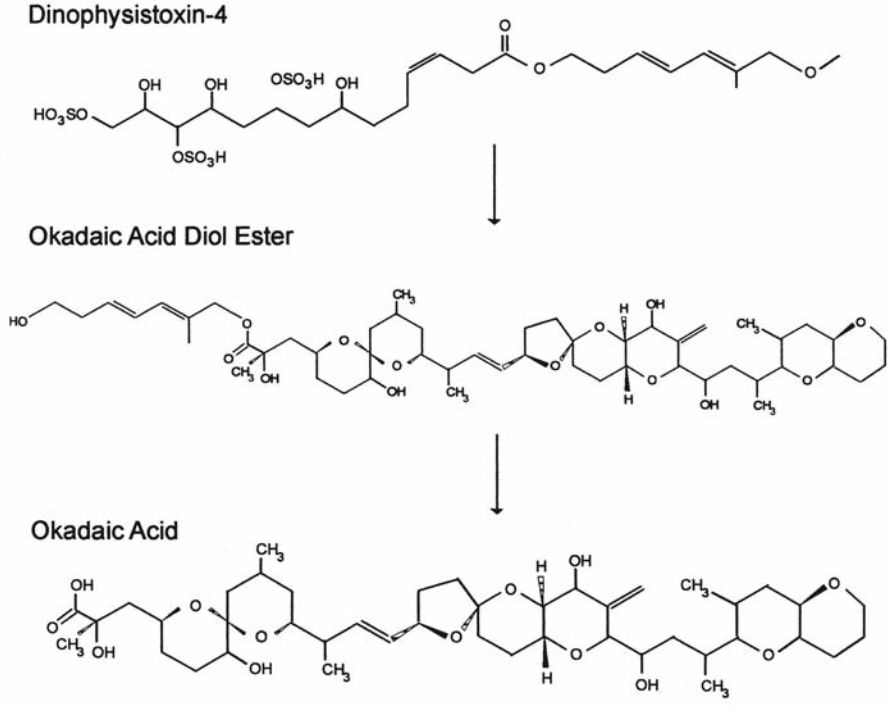


Fig. 7.31 Dinophysistoxin-4 is produced in the dinoflagellate cell and released to the environment, where it is hydrolyzed to okadaic acid diol ester. Okadaic acid diol ester is lipid soluble and passes through the cell membrane of the shellfish where it is hydrolyzed to toxic okadaic acid.

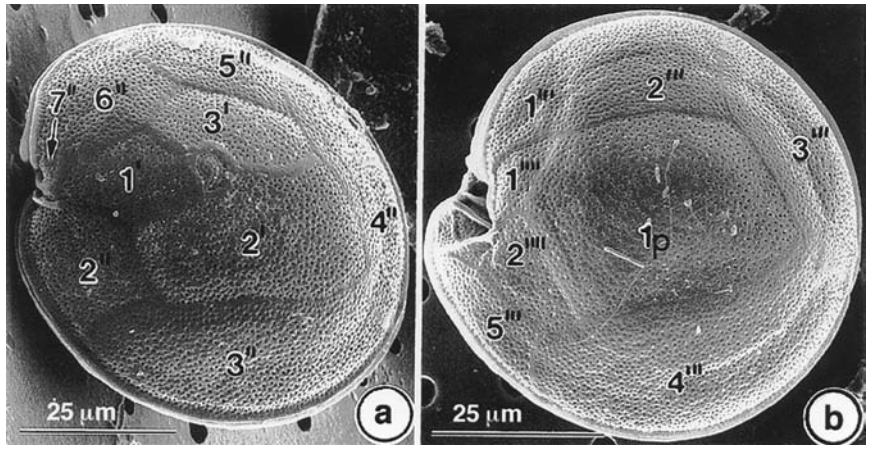


Fig. 7.32 Scanning electron micrographs of *Gambierdiscus toxicus*, the causative organism of ciguatera fish poisoning. (*a*) Epithecal view. (*b*) Hypothecal view. The numbers refer to arrangements of the plates. (From Faust, 1995.)

either excreted by the dinoflagellate cell, or is released on death of the cell. Dinophysistoxin-4 is hydrolyzed in the medium to okadaic acid diol ester, which is lipid soluble and can pass through cell membranes. Thus, okadaic acid diol ester can be taken up by cells which further hydrolyze the compound to okadaic acid. Research has shown that okadaic acid with a free acid moiety is the toxic form of the compound (Hu et al., 1999; Windust et al., 2000).

2 **Ciguatera fish poisoning.** This occurs primarily in tropical regions with the common causative agent being *Gambierdiscus* (Figs. 7.6, 7.32) which is common circumtropically between 32° N and 32° S. The dinoflagellate contains gambieric acids, ciguatoxins, and maitotoxins (Fig. 7.33), putative Ca^{2+} channel activators that result in breakdown of the cell membrane (Igarashi et al., 1999). *Gambierdiscus* is epyphytic on macroalgae that are eaten by herbivorous fish and shellfish, which, in turn, are eaten by humans. In French Polynesia alone, approximately 1000 cases of ciguatera fish poisoning are reported every year (Chinain et al., 1997). The term ciguatera is derived from the Spanish term "cigua" for the turban shell, which was commonly eaten before the illness developed. The typical course of ciguatera fish poisoning is diarrhea for two days, followed by general weakness for one to two days. Occasionally the condition is fatal (Withers, 1982).

3 **Paralytic shellfish poisoning.** This is caused by species of *Alexandrium* (*A. catanella*, *A. acatenella*, *A. excavatum* (Fig. 7.35), *A. tamarensis*), *Pyrodinium bahamense* (Fig. 7.34), and *Gymnodinium catenatum* (Fig. 7.34). These dinoflagellates produce a group of toxins that are derivatives of saxitoxin (Fig. 23.2). Saxitoxins are potent neurotoxins acting upon voltage-gated Na^+-channels, preventing influx of Na^+, thereby preventing the generation of an action potential (Cembella, 2003).

Alexandrium excavatum is a toxic red-tide dinoflagellate (Fig. 7.35). The vegetative cells divide to produce motile gametes that subsequently fuse. In the early stages of gamete fusion, when superficial contact is apparent, fusing pairs swim poorly and settle in the water. The motile quadriflagellate planozygotes swim for a few days before losing their flagella and thecal plates, and encyst to form resting cysts (hypnospores) (Figs. 7.28(*a*), 7.36) that can survive for 5 to 15 years. The hypnospores contain storage products and have a thick, three-layer wall (Kennaway and Lewis, 2004). Cyst germination is controlled by a biological clock with a 12 month maturation period (Perez, et al., 1998). Each hypnospore undergoes meiosis with two cell divisions to produce haploid vegetative cells, completing the life cycle (Destombe and Cembella, 1990; Nagai et al., 2003).

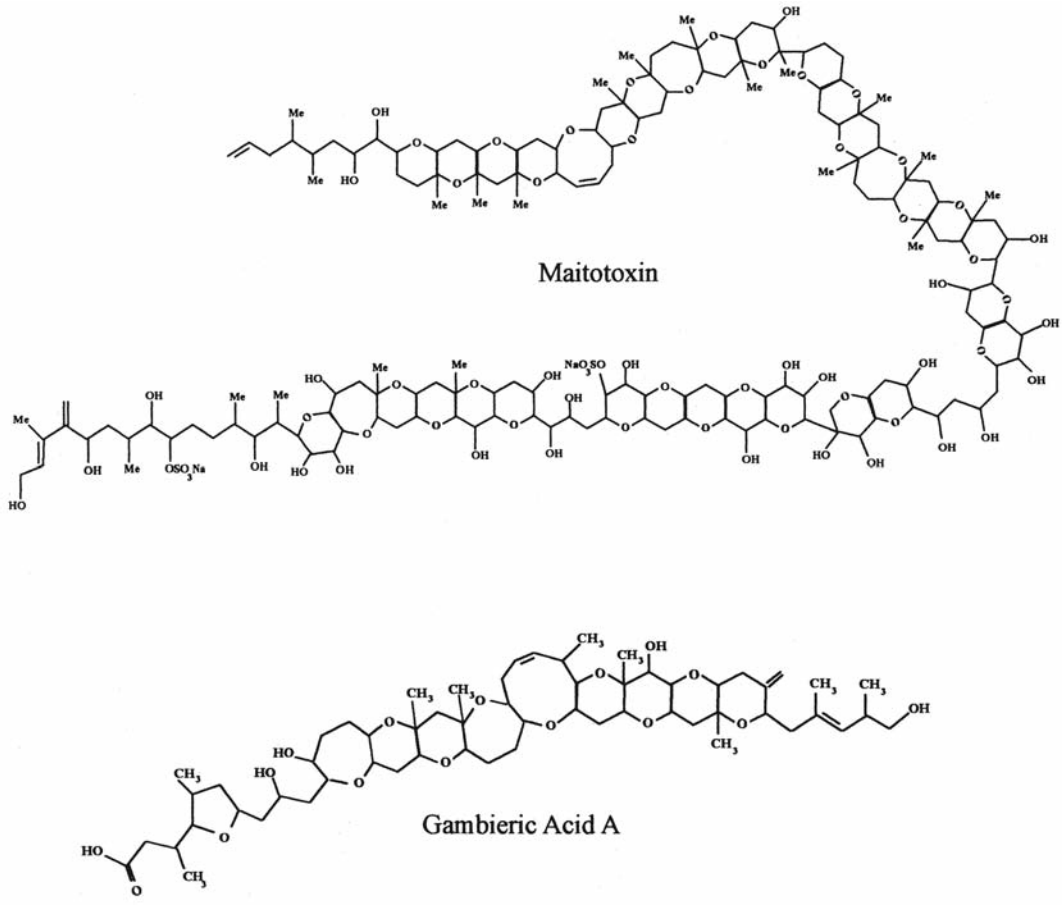


Fig. 7.33 The chemical structure of maitotoxin and gambieric acid.

The amount of toxin in cells of *Alexandrium* is relatively low when nutrients are in ready supply (John and Flynn, 2002). The toxin concentration is highest under conditions of phosphorus deficiency, possibly because free amino acids (precursors of toxins) accumulate under conditions of phosphorus deficiency.

Cells of dinoflagellates that produce toxins are avoided by grazing copepods, indicating that the extra energy put into toxin production is more than offset by the decreased grazing of the dinoflagellate cells (Guisande et al., 2002).

A number of factors have been suggested as the cause of red tides:

1 **High surface-water temperatures**: Dinoflagellates favor warm water, and are generally more abundant near the surface. This does not necessarily mean that they occur only in warm seas, because the surface of the sea in normally cool areas may be warmed up during periods of hot, calm weather.
2 **Wind**: A strong, offshore wind aids upwelling, whereas a gentle onshore wind concentrates the bloom near the coast. On the other hand, heavy weather and strong winds disperse the bloom. Storms also result in the death of dinoflagellates and can prevent the development of red tides (Juhl and Latz, 2002; Sullivan and Swift, 2003).
3 **Light intensity**: There is usually a period of bright, sunny, calm weather before outbreaks.
4 **Nutrients**: Red tides usually occur after an upwelling has stopped, but the nutrients brought to the surface do not, themselves, appear to be the direct cause of these blooms (Grindley and Nel, 1970). It is thought that

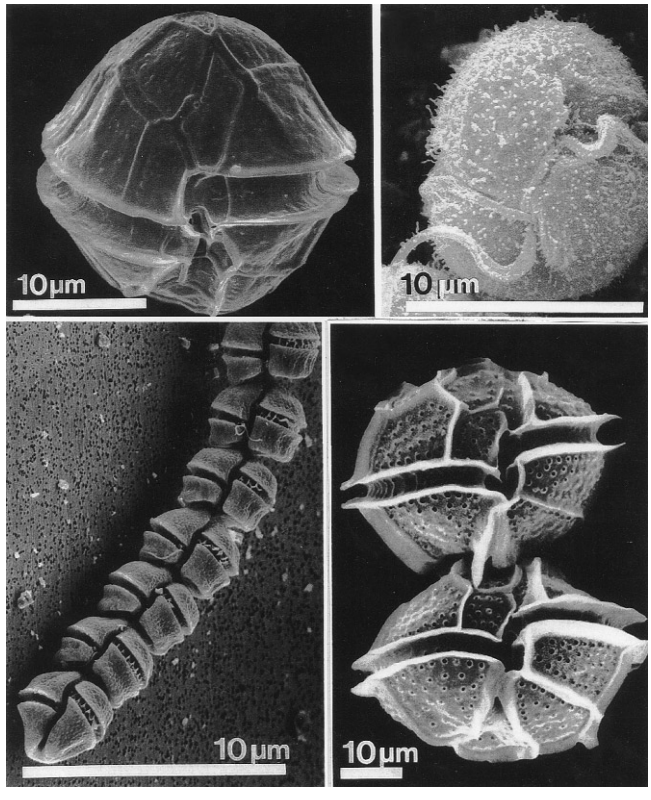


Fig. 7.34 Scanning electron micrographs of poisonous dinoflagellates. *Alexandrium minutum* (*upper left*), *Karlodinium veneficum* (= *Gymnodinium galatheanum*) (*upper right*), *Gymnodinium catenatus* (*bottom left*), *Pyrodinium bahamense* var. *compressum* (*bottom right*). *Karlodinium micrum* has killed cage-reared fish, while the others cause paralytic shellfish poisoning. (From Hallegraeff, 1993.)

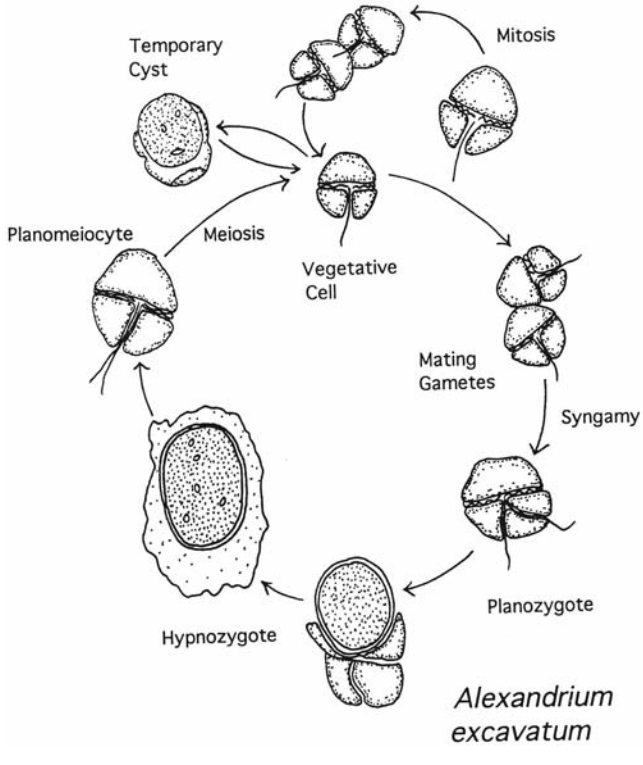


Fig. 7.35 The life cycle of *Alexandrium excavatum*. (Adapted from Destombe and Cembella, 1990.)

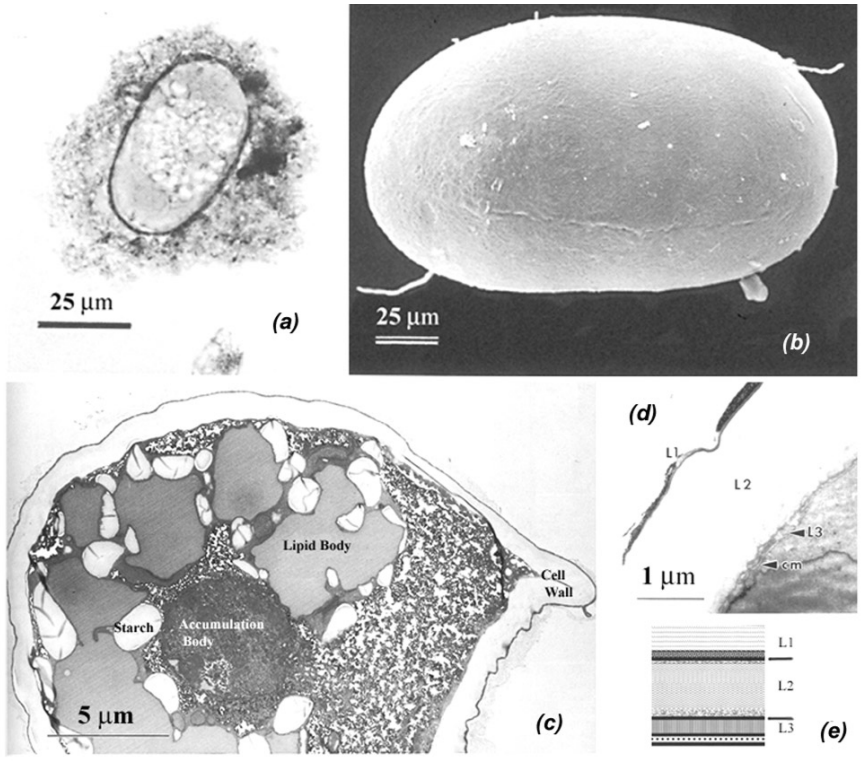


Fig. 7.36 Hypnospores (resting spores) of *Alexandrium*. (*a*) Light micrograph of a hypnospore surrounded by mucus. (*b*) Scanning electron micrograph showing the smooth surface of a hypnospore. (*c*) Transmission electron micrograph showing the large amount of storage products in a hypnospore. (*d*) Transmission electron micrograph of the layers of the cell wall. (e) Illustration of the layers of the cell wall. (cm) Cell membrane. (From Kennaway and Lewis, 2004.)

preceding blooms of diatoms may impoverish the water and reduce one or more of the inorganic nutrients to a level favorable for the growth of dinoflagellates (but too low for the diatoms), and also allow the production of organic nutrients such as vitamin B_{12}, which are important for their growth.

Dinoflagellates and oil and coal deposits

Blooms of dinoflagellates have most likely been responsible for some of the oil deposits of the world, including the North Sea oil deposit (Downie, 1956; Gallois, 1976). The best studied oil deposits are the oil shales of the Kimmeridge Clay deposits in England, which vary from less than 100 m in thickness to over 500 m and are composed of a number of different layers: clays and black and brown shales intermixed with occasional thin limestones. The limestones are composed primarily of coccolithophorids, whereas the shales contain yellow-brown organic matter called **kerogen**. Kerogen contains a large amount of amorphous organic matter, from which it is impossible to determine its biological origin. In addition to the amorphous organic matter, there are found large numbers of dinoflagellates and their hystrichospores, as well as some coccoliths. The best known Kimmeridge Clay deposit is the Kimmeridge Coal, a highly bituminous shale, about 80 cm thick. The Kimmeridge Coal has long been used as a solid fuel, and in the latter half of the last century much interest was taken in it as a source of oil. However, the high sulfur content and the relative thinness of the "coal" bed prevented the economic exploitation of the oil.

The Kimmeridge Clay oil shales were formed from algal blooms in seas that were to some

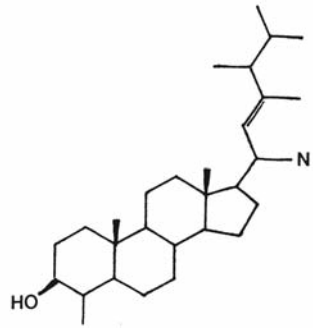


Fig. 7.37 The structure of dinosterol, the major sterol in dinoflagellates.

degree land-locked, with salinity a little beneath the average salinity of the open ocean. These seas were rich in land-derived nutrients, allowing the water to support blooms of toxic dinoflagellates. These blooms deoxygenated and poisoned the water, providing the temporary anaerobic bottom conditions required for the preservation of organic matter. It is interesting that one of the bivalves commonly poisoned by toxic dinoflagellate blooms today is *Lucinoma borealis*, and the bivalve that forms the most extensive plasters in the Kimmeridge Clay oil shales is the related *Lucina miniscula*.

Petroleum deposits and ancient sediments contain 4α-methylsteroidal hydrocarbons, which probably originated from 4α-methylsterols in dinoflagellates (Robinson et al., 1984). The dinoflagellates differ from other classes of algae with respect to the dominance of 4α-methylsterols among their sterol components and the uniqueness of certain of these 4α-methylsterol structures (Leblond and Chapman, 2002; Giner et al., 2003). The principal sterol of several marine dinoflagellates, and organisms with dinoflagellate symbionts, is **dinosterol** (Fig. 7.37).

Bioluminescence

About, about, in reel and rout
The death-fires danced at night
The water, like a witch's oils
Burnt green, and blue, and white

Samuel Taylor Coleridge
The Rime of the Ancient Mariner

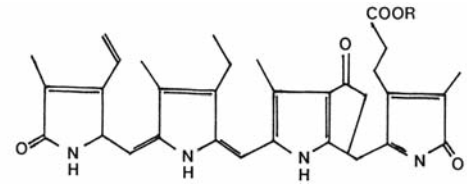


Fig. 7.38 A possible partial structure of dinoflagellate luciferin. (After Dunlap and Hastings, 1981; Hastings, 1986.)

Mariners from early times have marveled at the displays of bioluminescence that accompany large populations of dinoflagellates. The burning seas were at first thought to be of supernatural origin, omens of the pleasure or displeasure of the gods. As science began to usurp the explanation of natural phenomena from religion, the light emitted from friction between salt molecules or from phosphorus burning in water was invoked; the term **phosphorescence** still survives today from the explanation. By 1800, living cells were suspected, but the last experiments were not settled in favor of a biological origin until 1830 (Sweeney, 1979).

There are two types of light emission in living organisms: (1) **bioluminescence** (**chemiluminescence**), in which *energy from an exergonic chemical reaction is transformed into light energy;* and (2) **photoluminescence**, which is dependent on the *prior absorption of light* (Hastings, 1986). Many marine, but no freshwater dinoflagellates are capable of bioluminescence. The Dinophyceae are the main contributors to marine bioluminescence, emitting a bluish-green (maximum wavelength at 474 nm) flash of light of 0.1-second duration when the cells are stimulated. The luminescent wake of a moving ship or the phosphorescence of tropical bays is usually caused primarily by Dinophyceae.

The compound responsible for bioluminescence is **luciferin** (Fig. 7.38), which is oxidized with the aid of the enzyme **luciferase**, resulting in the emissions of light. Luciferin and luciferase are terms for a general class of compounds, and not of a specific chemical structure. Bioluminescence occurs in many organisms in many different phyla, ranging from bacteria to dinoflagellates to jellyfish and brittle stars to worms, fireflies, molluscs, and fish (Hastings, 1986). In bacteria, luciferin is a reduced flavin; in insects it is a (benzo)thiazole nucleus; and in dinoflagellates it is a tetrapyrrole.

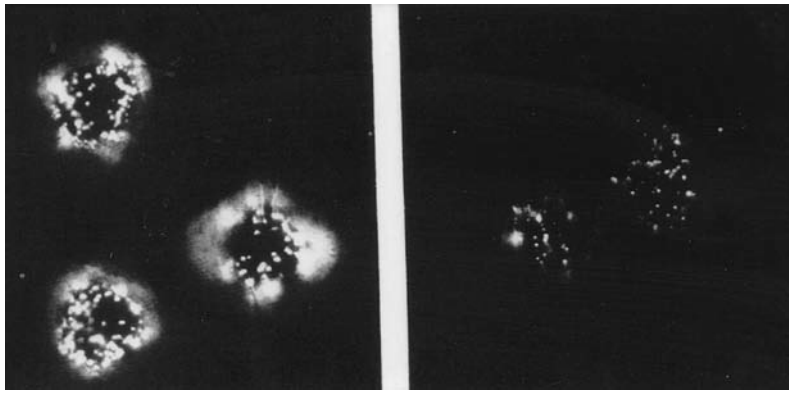


Fig. 7.39 The white spots in these photographs of *Lingulodinium* cells indicate fluorescence and thus localization of luciferin, the substrate that reacts with the enzyme luciferase and oxygen to produce light. The intensity of the luciferin fluorescence is greater in the night phase (*left*) of the circadian cycle of bioluminescence than in the day phase (*right*). The amount of luciferase shows a similar oscillation during the daily cycle. (From Johnson et al., 1985.)

Likewise, luciferase has different structures, although all luciferases share the feature of being **oxygenases** (enzymes that add oxygen to compounds). The necessity for oxygen in bioluminescence was actually discovered by Boyle in 1667, who showed with his air (vacuum) pump that:

> a piece of shining (bioluminescent) wood . . . gave a vivid light . . . which was manifestly lessened . . . [at] about the seventh suck, losing its light more and more as the air was still further pumped out. . . . Wherefore we let in outward air and had the pleasure to see the seemingly extinguished light revive so fast and perfectly, that it looked to us almost like a little flash of lightening. (Cited in Harvey, 1952, p. 142).

In the basic reaction of bioluminescence (Hastings, 1983), a luciferin is oxidized by a luciferase, resulting in an electronically excited product $(P)^*$ which emits a photon ($h\nu$) on decomposition:

$$\text{luciferin} + O_2 \xrightarrow{\text{luciferase}} (P)^* \rightarrow P + h\nu$$

Luciferin in the dinoflagellates has been reported to be a linear tetrapyrrole (Fig. 7.38). Associated with dinoflagellate luciferin is a **luciferin-binding protein (LBP)** which sequesters luciferin at alkaline pH and releases it under acidic conditions (Sulzman et al., 1978). It has been postulated that the flash of bioluminescent light may occur simply by a lowering of the pH from 8.0 to 6.5. Agitation of cells depolarizes the vacuolar membrane, allowing a flux of protons (H^+) and acidification of the peripheral cytoplasm (Johnson et al., 1985). Lowering the pH causes two pH-dependent reactions to occur: (1) release of luciferin from its binding protein at acidic pH, and (2) activation of luciferase followed by emission of a photon of blue-green light.

Luciferin, luciferase, and luciferase-binding protein occur in particles called **scintillons** (**flashing units**) that are approximately 0.5 to 1.5 μm in diameter (Sweeney, 1980). Scintillations occur in cytoplasmic invaginations in the vacuolar membrane. Flashes of blue-green light are produced when an action potential proceeds along the vacuolar membrane, causing an outflow of protons from the acidic contents of the vacuole. The resulting drop in the pH in the scintillon causes flashes of light (Nicolas et al., 1991).

In *Lingulodinium polyedrum* (Figs. 7.39, 7.40), most bioluminescence occurs during the night phase of a circadian rhythm (Fig. 7.41) (Fritz et al., 1991). This is due to a ten fold increase in luciferase and luciferin-binding protein during the night phase. Daytime photoinhibition of bioluminescence is considered a mechanism to conserve the energy of cells when ambient light levels are high enough to render the bioluminescent flash ineffective (Buskey and Swift, 1983). The position of bioluminescence in *Pyrocystis fusiformis* (Fig. 7.40(*a*)) varies over 24 hours (Sweeney, 1980; Seo and Fritz, 2000). During the day, bioluminescence emanates from a spherical mass of tightly packed vesicles near the nucleus, whereas at night bioluminescence occurs in the peripheral cytoplasm. There is a reverse movement of chloroplasts, with the organelles in the cell periphery during the day and the chloroplasts concentrating around the nucleus at night.

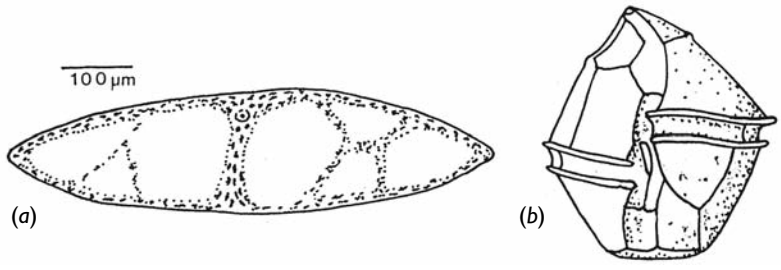


Fig. 7.40 (*a*) *Pyrocystis fusiformis*. (*b*) *Lingulodinium polyedrum* (*5 Gonyaulax polyedra*).

Dinoflagellates can emit light in three modes: (1) they can flash when stimulated mechanically, chemically, or electrically; (2) they can flash spontaneously; and (3) late at night they can glow dimly (Sweeney, 1979). The maximum amount of light emitted in a flash differs widely among species, with larger species emitting more light per flash than smaller ones. In a population of dinoflagellates, the cells emit an average of one flash per cell per day (Hastings and Krasnow, 1981). It is not clear whether each cell flashes once and only once during this period, or whether some cells are responsible for a larger share of the flashes whereas others do not emit at all. The nutritional status of a cell influences the brightness of the flash. *Noctiluca* with green algal symbionts (Fig. 7.54) shows an increase in the photons emitted per flash as the intensity of the illumination of the dinoflagellate, and therefore photosynthesis, increases. Different isolates of the same species in genera such as *Dissodinium* and *Pyrocystis* (Figs. 7.40(*a*), 7.49(*c*), (*d*)) can be bioluminescent or not (Swift et al., 1973; Schmidt et al., 1978).

Pyrocystis (Figs. 7.40(*a*), 7.49(*c*), (*d*)), one of the most strongly phosphorescent dinoflagellates, is the chief source of diffused phosphorescence in the sea in equatorial regions (Swift et al., 1973). Species of *Pyrocystis* produce at least 1000 times more bioluminescence per cell than members of the genus *Lingulodinium* (Figs. 7.39, 7.40) and about 100 times as much light per cell as *Ceratium fusus, Peridinium pentagonium*, and *Pyrodinium bahamense*.

There are two theories concerning the adaptive value of bioluminescence to dinoflagellates, both of which relate to nighttime grazing of the dinoflagellates:

1 "Burglar alarm" hypothesis. This hypothesis argues that dinoflagellates render themselves dangerous as prey to invertebrate grazers because they generate a signal identifying the location of invertebrate food to individuals two levels up the food chain from the dinoflagellates (Abrahams and Townsend, 1993). Bioluminescence generated by dinoflagellates serves to attract predators of the grazers of the dinoflagellates.
2 "Startle" hypothesis. In this hypothesis, mechanical stimulation of a bioluminescent dinoflagellate by a grazer produces a flash of light that startles an invertebrate grazer, such as a copepod, and causes the copepod to swim away with its feeding appendage retracted (Buskey and Swift, 1983).

Whichever theory is correct, experiments have shown that copepods consume only half as many dinoflagellates at night, indicating that the bioluminescence is serving as a deterrent to grazing (Buskey et al., 1983).

Rhythms

Many Dinophyceae exhibit rhythmic processes, with the best known of the rhythms in the algae being those in the dinoflagellate *Lingulodinium polyedrum* (Figs. 7.39, 7.40) (Sweeney, 1969). It produces light via bioluminescence by forming its own dinoflagellate-specific luciferin and luciferase. The cells emit a flash of light when the seawater in which they are swimming is given a sharp shake or stirred vigorously. When the luminescence is measured while the culture is being stirred, the amount of light that the cells emit is not always the same and depends upon their recent history. If they have been growing in natural illumination or on a light–dark cycle, the amount of light emitted will be markedly

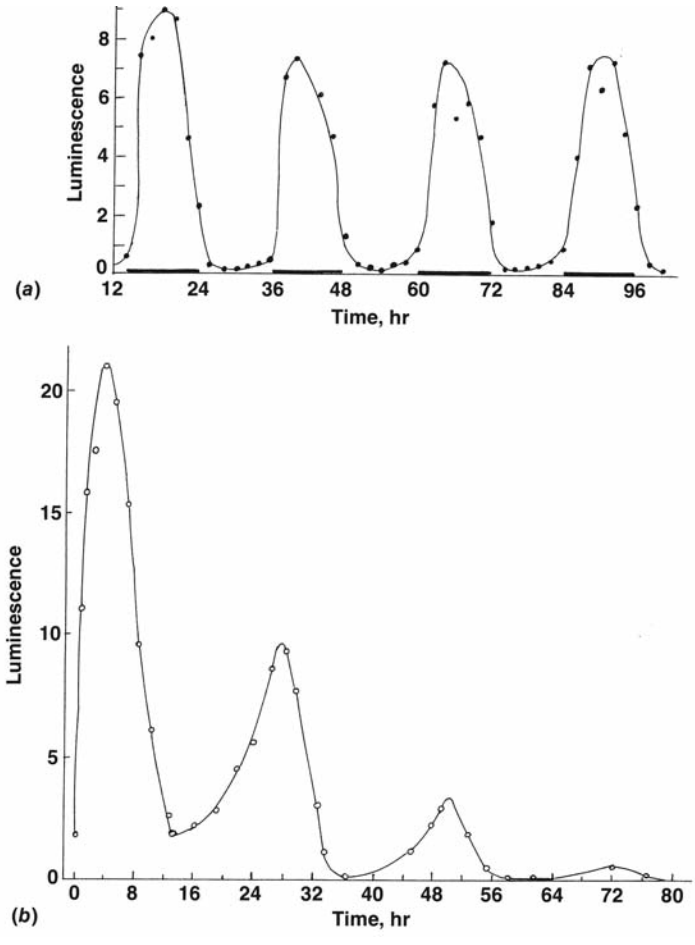


Fig. 7.41 The rhythm of stimulated luminescence in *Lingulodinium polyedrum* measured in (*a*) a light–dark cycle of 12:12 and (*b*) in complete dark. (After Sweeney, 1969.)

dependent on the time of day when measurements are made. If luminescence is elicited during the day, the amount of light will be low, and very hard stirring will be required to bring about any luminescence at all. But if the cells are stimulated at night, a great deal more light will result, and the most delicate shake will produce a flash. When the amount of luminescence is plotted as a function of the time of day, a graph such as that in Fig. 7.41(*a*), will result. The greatest luminescence will be produced in the middle of the dark period, whereas toward morning, flashes will gradually become smaller and a greater stimulus will be required. The rhythm is circadian (which means literally about (*circa*) a day (*diem*)), as shown by the persistence of changes in brightness of luminescence when the cells are kept in the dark (Fig. 7.41(*b*)). In continuous darkness, the cycle continues for as long as 4 days, but the amplitude becomes successively smaller. If the cells are kept in continuous light, the reduction in amplitude is no longer evident. Cycles continue for at least 3 weeks in continuous light of appropriate intensity (Fig. 7.42).

When photosynthesis in *Lingulodinium polyedrum* is measured, either as oxygen production or carbon dioxide fixation, it is also found to be rhythmic (Fig. 7.45). The rhythm is circadian and continues under conditions of continuous light. The maximum rate of photosynthesis occurs, as one would expect, in the middle of the day. The rhythm in photosynthesis is due to changes in photosystem II (Samuelsson et al., 1983) (Fig. 7.43).

A third rhythm with a circadian period in *Lingulodinium polyedrum* is that of cell division (Fig. 7.45); all cell division occurring during 30 minutes when cultures are in a light–dark cycle. When the light–dark cycle is 12:12, then this

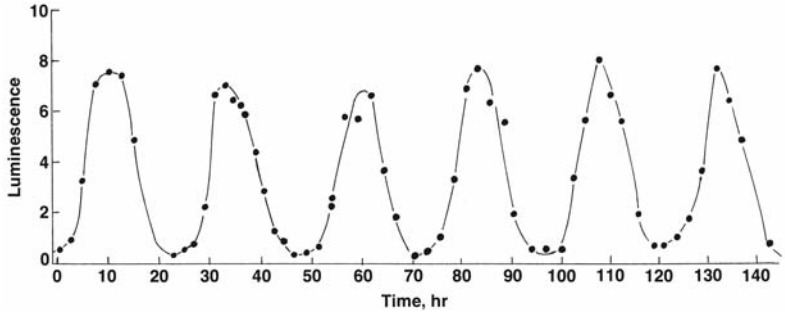


Fig. 7.42 The rhythm of stimulated luminescence in *Lingulodinium polyedrum* measured in continuous light (1000 lux). (After Sweeney, 1969.)

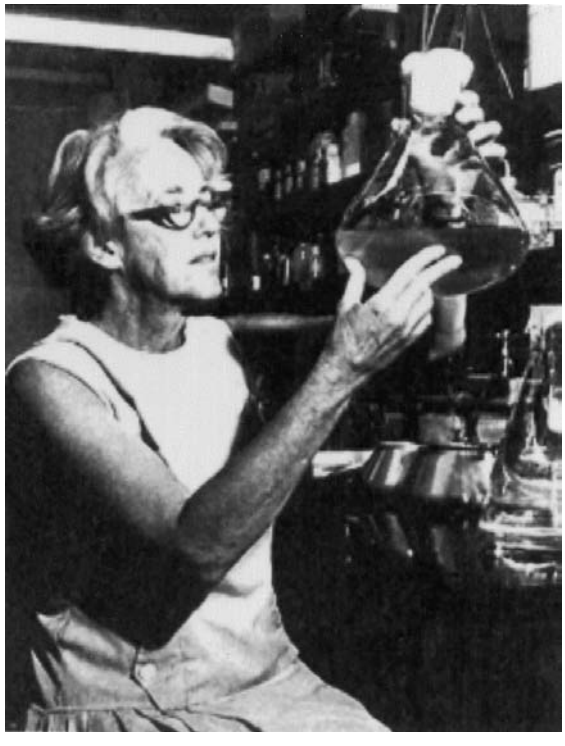


Fig. 7.43 **Beatrice M. Sweeney** Dr. Sweeney's investigations established the rhythmic phenomena of dinoflagellates. Born August 11, 1914, in Boston, Massachusetts. Died June 30, 1989 in Woods Hole, Massachusetts. She received her A.B. from Smith College (1936) and her Ph.D. from Radcliffe College (1942). She worked as a laboratory and research assistant at the Mayo Clinic (1942–43) and Scripps Institution of Oceanography (1947–55). From 1961 to 1967, she was a biologist and lecturer at Yale University. In 1967 she moved to the Department of Biological Sciences at the University of California, Santa Barbara. She published two editions of her book *Rhythmic Phenomena in Plants*. (Photo from Garbary and Wynne, 1996.)

30 minutes spans "dawn." An investigation of other light–dark cycles, such as 7:7, shows that the dark–light transition is not the determining factor because division takes place about 12 hours after the beginning of the dark period, even though this time is considerably after the beginning of the next light period. In continuous light of low intensity where other rhythms of *Lingulodinium polyedrum* persist, very little cell division takes place, and the average generation time may be as long as 6 days. However, those cells that are ready to divide do so only at the expected time in each 24 hours.

A fourth type of rhythm involves the vertical migration of dinoflagellate cells in the water column (Eppley et al., 1968; Horiguchi and Pienaar, 1988; Lombard and Capon, 1971; Roenneberg and Deng, 1997). Before dawn, the cells rise to the surface, where they form dense clouds (aggregations), and before night fall, they again sink to lower depths (Fig. 7.44). In the marine environment, this vertical migration exposes the cells to several gradients: (1) Nutrients are more concentrated at lower depths (accumulating at the bottom of the ocean or at thermoclines) while surface waters are often practically devoid of nutrients. (2) Temperatures at the surface exceed those in deeper waters. (3) Variations in light intensities. (4) In shallow waters, differences in washout by the tidal waters.

In *Lingulodinium polyedrum*, there exists a control over luminescence, photosynthesis, and cell division, so that each process reaches a maximum and then declines in an orderly fashion during each 24 hours (Fig. 7.45). A single process, a biological clock, may control all of these processes. It appears that the part of the cell that may be the controlling agent is the plasma membrane

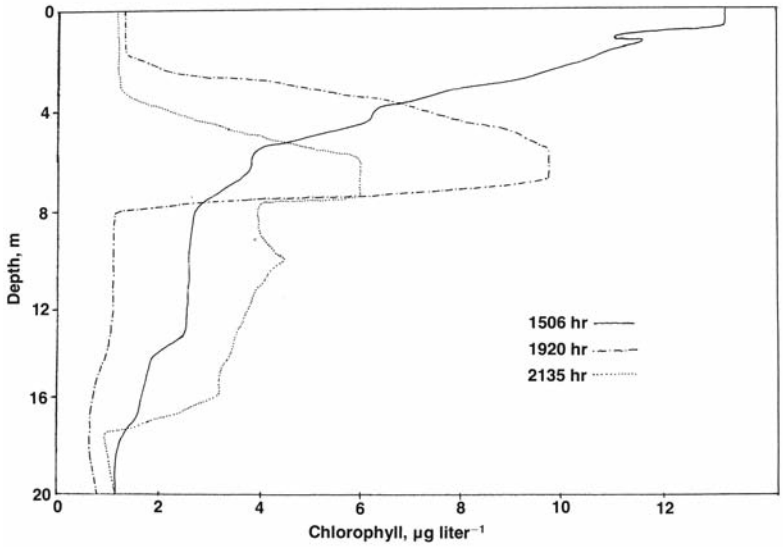


Fig. 7.44 Profiles of chlorophyll *a* during *a* bloom of dinoflagellates showing the vertical migration of dinoflagellates at different times of the day. (After Eppley et al., 1968.)

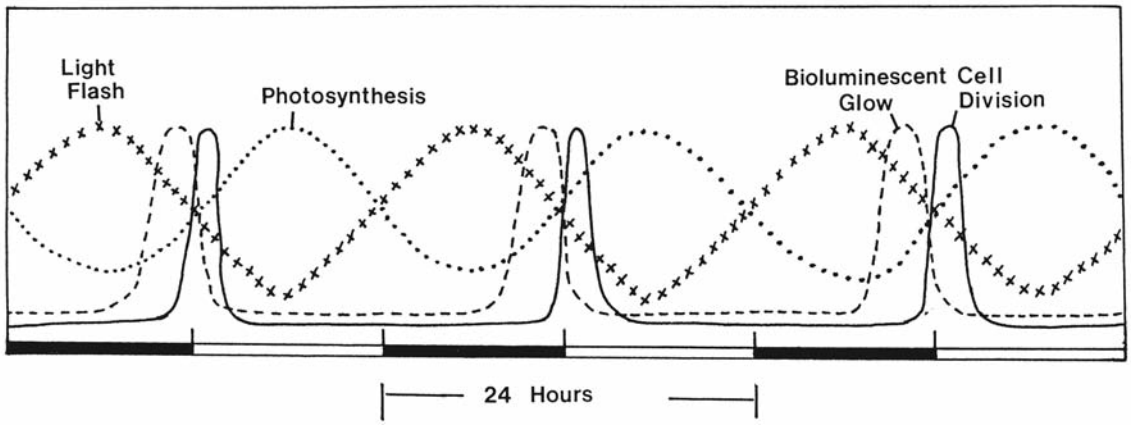


Fig. 7.45 Circadian rhythmicity has been identified in at least four distinct biological processes of the unicellular *Lingulodinium polyedrum*. Although the four rhythms peak at different times of the 24-hour day, as represented here diagrammatically, they are all synchronized with the circadian clock. Perturbations that reset the clock will phase-shift all four rhythms simultaneously, suggesting that all of these overt rhythms are driven by a single pacemaker. (After Johnson and Hastings, 1986.)

because there is a rhythmic reorganization of the plasma membrane over a 24-hour period in synchronized cells (Adamich et al., 1976).

Although the phases at which the rhythms peak in *Lingulodinium polyedrum* are different, it is generally believed that they are all controlled by a single pacemaker (Johnson and Hastings, 1986). The rhythmic processes seem to have no feedback mechanism and thus appear to be driven systems. For example, photosynthesis can be completely inhibited with a specific herbicide, but the bioluminescence rhythm continues and its phase is not altered. Such observations on *Lingulodinium polyedrum* suggest models of circadian organization like those in Fig. 7.46. The central pacemaker is phased to the solar light cycle by means of a photoreceptor and an entraining pathway, and it controls the expression of the different rhythms, such as cell division, bioluminescence, and photosynthesis.

Two different systems time the circadian rhythm in dinoflagellates, a red-light sensitive

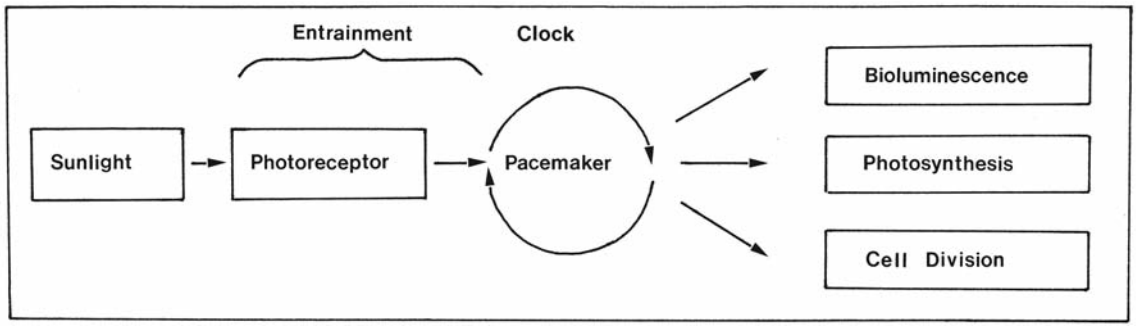


Fig. 7.46 Diagram showing how a single endogenous clock within a *Lingulodinium polyedrum* cell can control a multiplicity of observed rhythms. (After Johnson and Hastings, 1986.)

system that delays the timing, and a blue-light sensitive system that advances the timing to dawn (Roenneberg and Deng, 1997). These light systems probably stimulate or depress the production of melatonin in the cells. An increase in the concentration of melatonin appears to mark the end of the light phase. There is a circadian rhythm in the production of melatonin, with a rapid increase in melatonin concentration at the end of the light phase and a subsequent decline during the dark phase, reaching a minimal value in the light phase. The concentration of melatonin in dinoflagellate cells is similar to that in the mammalian pineal gland (Balzer and Hardeland, 1996). Melatonin may represent a common basis for photoperiodism in organisms as distant as dinoflagellates and vertebrates, a fact that suggests an ancient mechanism for mediating information about darkness within the circadian cycle (Pöggeler et al., 1991).

Heterotrophic dinoflagellates

An estimated half of the more than 2000 living dinoflagellate species lack chloroplasts and are exclusively heterotrophic (Hansen and Calado, 1999; Jacobsen, 1999). In addition, many dinoflagellates that contain chloroplasts are capable of **mixotrophy** where a portion of their nutrients is obtained heterotrophically, particularly when nutrient conditions are low in the environment (Smalley et al., 2003).

The different modes of heterotrophy are: (1) **phagotrophy** through the direct engulfment of prey; (2) **pallium feeding** where the prey is engulfed by a cytoplasmic veil – the palium – with digestion of the food taking place outside of the dinoflagellate cell; (3) **peduncle feeding (myzocytosis)** involving the uptake of intracellular material of the prey through a cytoplasmic extension – the peduncle – leaving the plasma membrane and extracellular material of the prey behind; and (4) **osmotrophy** or the uptake of dissolved substances (Höhfeld and Melkonian, 1998).

Direct engulfment of prey

The large cells of *Noctiluca* have a 300-μm-long food-gathering **tentacle** that is covered with a slimy exudate (Fig. 7.47) (Sweeney, 1978; Nawata and Sibaoka, 1983). Two wing-like extensions of the cells form an **oral pouch** at the base of the tentacle. At the bottom of the oral pouch is a **cytosome** that opens like a slit during ingestion of food organisms. Collision of other organisms in the medium with the mucus-covered tentacle tip results in attachment of the other organisms to the tentacle. Continued collisions result in the formation of a clump of cells adhering to the tentacle. The tentacle is primarily in an extended configuration during this time. The tentacle now bends so that the tentacle tip moves to the bottom of the oral pouch. The cytoplasm streams vigorously toward the cytosome and then aggregates around the cytosome (Nawata and Sibaoka, 1987). The cytosome opens, the tentacle tip is inserted into it, the food organisms are swept into the cytosome, and the tentacle tip is retracted. The cytosome opening closes, and the food organisms are engulfed in a food vesicle in

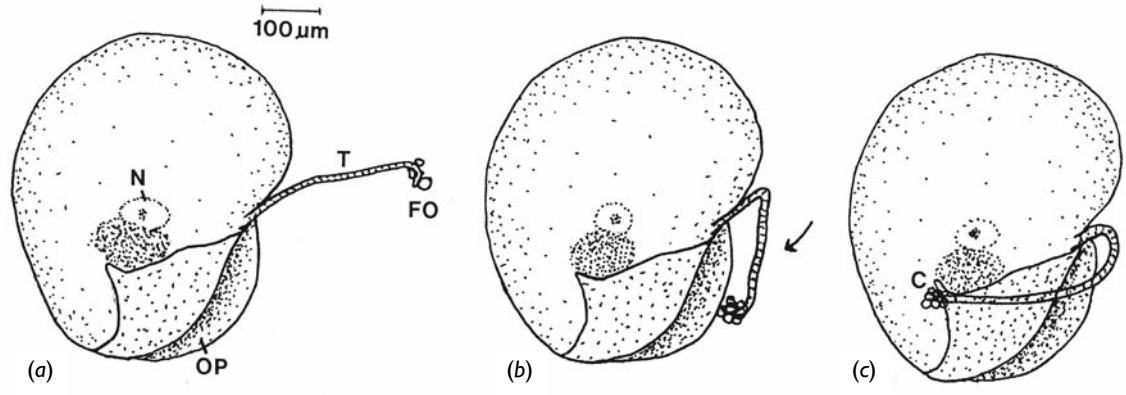


Fig. 7.47 Drawing of the ingestion of food organisms (other algae, bacteria) by *Noctiluca*. (*a*) The tentacle (T) is in an extended configuration. Any food organisms (FO) that collide with the mucus-covered tentacle tip, stick to the tentacle. (N) Nucleus; (OP) oral pouch. (*b*) The tentacle bends back toward the oral pouch. (*c*) The cytosome (C) at the base of the oral pouch opens, the tentacle tip is inserted into the cytosome, and the food organisms are swept into a food vacuole. (After Nawata and Sibaoka, 1983.)

the cytoplasm. The food organisms are digested in the food vesicle. In the cell under the microscope, long strands of mucus containing food organisms can be seen spirally coiled in the food vacuoles.

Polykrikos kofoides feeds by initially spearing its prey with a nematocyst (Figs. 7.48, 7.49(*a*), (*b*)). The prey organism is pulled into the posterior sulcus, with the prey eventually being completely engulfed into a food vacuole.

Pallium feeding

This occurs only in thecate species and utilizes a feeding veil, the **pallium**, which emerges from the flagellar pore and encloses the prey. The prey protoplasm is digested by enzymes released into the pallium, and the digestion products are transported into the feeding cell. *Protoperidinium* (Fig. 7.50) and *Diplopsalis* (Naustvoll, 1998) feed in this manner. These dinoflagellates swim in a straight line until they encounter a prey organism. The dinoflagellate then changes swimming behavior by slowing down and swimming in tight circles around the prey for less than one minute. A thin filament of cytoplasm (about 1 μm in diameter) emerges from the sulcal pore and attaches to the prey (Fig. 7.50). A pseudopod is extended along the filament while the filament is retracted, pulling the prey closer to the dinoflagellate. The pseudopod advances at 2 to 6 μm s^{-1} until it reaches the prey. The pseudopod conforms to projections,

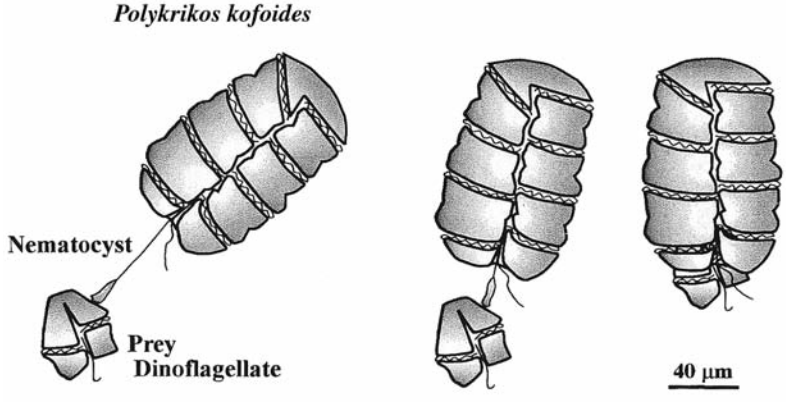


Fig. 7.48 *Polykrikos kofoides* captures prey by firing a nematocyst into the prey and bringing the tethered prey into the posterior portion of the cell. The prey is engulfed and digested by the dinoflagellate. (Modified from Matsuoka et al., 2000.)

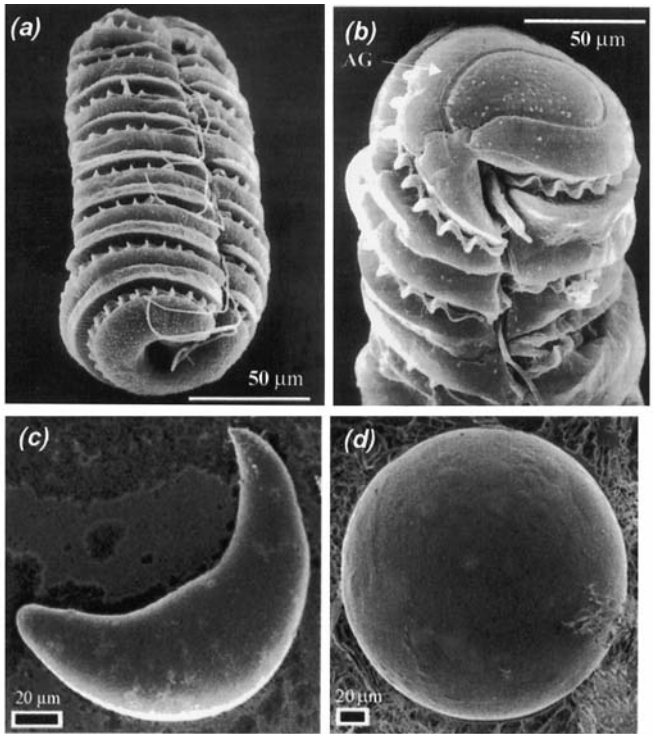


Fig. 7.49 (*a*),(*b*) Scanning electron micrographs of 8-cell pseudocolonies of *Polykrikos schwartzii*. Ventral view (*a*) and apical view (*b*) showing the apical groove. (*c*),(*d*) Scanning electron micrographs of *Pyrocystis lunula* (*c*) and *Pyrocystis noctiluca* (*d*). *Pyrocystis* is unusual among dinoflagellates in existing primarily in the non-motile vegetative state. *Pyrocystis* is a major source of bioluminescence in the ocean. ((*a*),(*b*) from Nagai et al., 2002; (*c*),(*d*) from Seo and Fritz, 2002.)

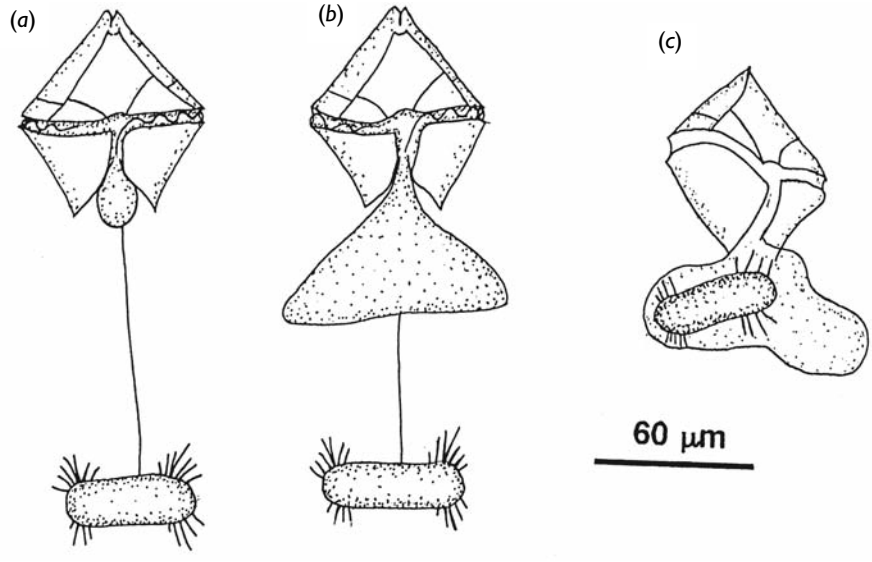


Fig. 7.50 The heterotrophic dinoflagellate *Protoperidinium conicum* feeding on the diatom *Corethron hystria*. Initially the dinoflagellate attaches to the prey by a long thin filament (*a*). Next a pseudopod extends along the filament (*b*) and engulfs the prey (*c*), which is digested. (After Jacobsen and Anderson, 1986.)

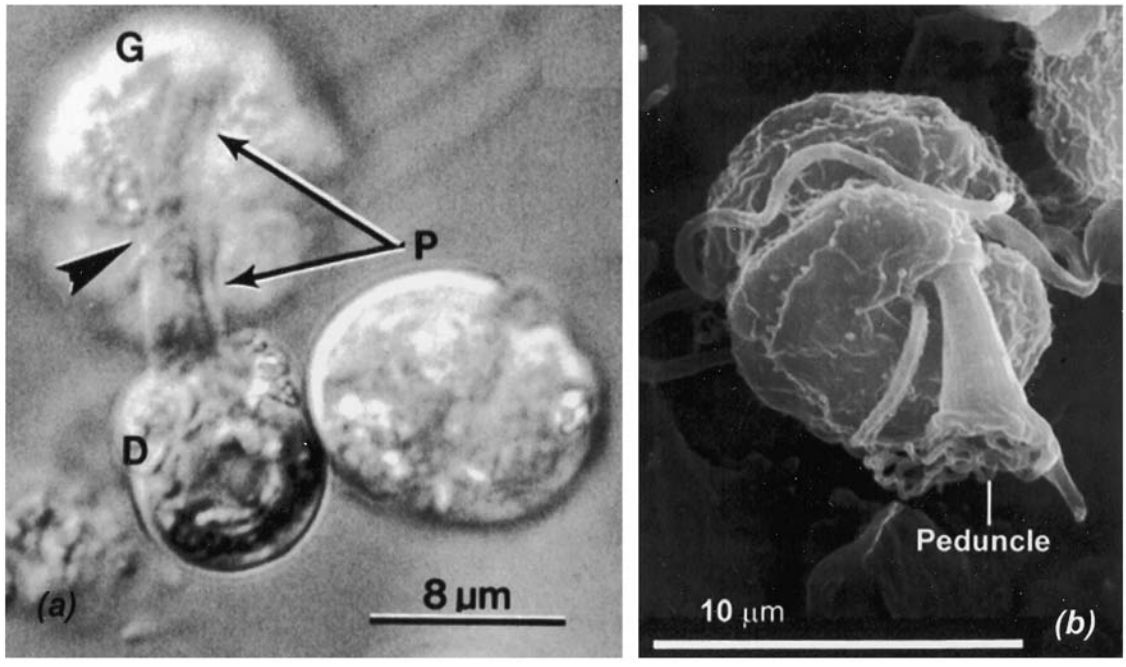


Fig. 7.51 (*a*) Light micrograph of the dinoflagellate *Gymnodinium fungiforme* (G) ingesting the protoplasm of *Dunaliella salina* (D). The peduncle (P) of *G. fungiforme* has attached to *D. salina* with the protoplasm of *D. salina* passing through the enlarged and extended peduncle into the dinoflagellate. (*b*) Scanning electron micrograph of a zoospore of *Pfiesteria piscicida* showing the peduncle. ((*a*) from Spero, 1982; (*b*) from Lewitus et al., 1999.)

such as spines, and can engulf an organism many times larger than the dinoflagellate. The prey is digested in the pseudopod, with the pseudopod showing active cytoplasmic streaming at a velocity of about 5 μm s^{-1}. A diatom is digested by the dinoflagellate in about 30 minutes, at which time the pseudopod is rapidly retracted (at a rate of 10 μm s^{-1}) into the dinoflagellate.

Peduncle feeding

Gymnodinium fungiforme contains an extensible **peduncle** (Lee, 1977), a projection of cytoplasm full of microtubules, in the epicone just above the intersection of the sulcus and cingulum (Figs. 7.51(*a*), 7.52) (Spero and Moree, 1981). The peduncle can extend from 8 to 12 μm to attach to, and make a hole into, the prey (Spero, 1982). The cytoplasm of the prey moves through the peduncle to the dinoflagellate cytoplasm. After feeding is complete, the microtubules of the peduncle, and the peduncle itself, retract back into the dinoflagellate cytoplasm. Feeding is characterized by the aggregation of numbers of the dinoflagellate on the prey organism. A small green alga, such as *Dunaliella*, has five to ten dinoflagellates attached by their peduncles, whereas a ciliate may have 400 to 500 dinoflagellates attached to it. The peduncle of *G. fungiforme* apparently cannot penetrate a cell wall, so the dinoflagellate feeds only on prey that lacks a cell wall, or on injured higher organisms. The marine ciliate *Condylostoma magnum* is not fed on by *G. fungiforme* until it is injured (in the laboratory by piercing it with a micropipette). Within 15 seconds, more than 100 dinoflagellates will congregate around the wound. When a ciliate is taken from a dying culture and placed in a *G. fungiforme* culture, the dinoflagellate cells congregate around the posterior end of the ciliate. Initially small strands of ciliate cytoplasm are pulled off by groups of one to five dinoflagellates. As the ciliate begins to leak cytoplasm through these small wounds, large aggregations of phagotrophic dinoflagellates are formed. Approximately 20 to 30 minutes later, the cilate is completely digested. The attacking cells are small (9 μm long and 6 μm wide), clear cells

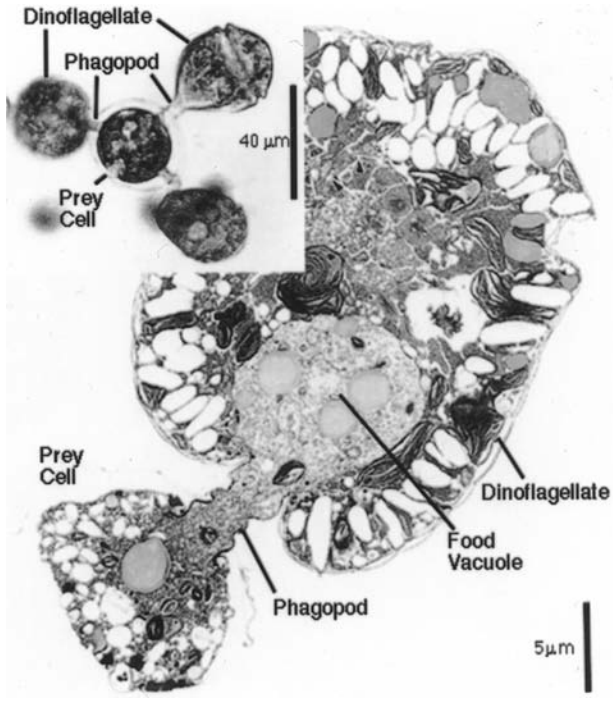


Fig. 7.52 *Amphidinium cryophilum* attached to a prey organism by a peduncle. The inset shows a light micrograph of three cells of *A. cryophilum* attached to a prey cell. (From Wilcox and Wedemeyer, 1991.)

that swell to 20 times their original size with food vacuoles after ingesting a victim. These large cells barely move or are motionless. *Gymnodinium fungiforme* is attracted to a variety of amino acids and other organic compounds (Spero, 1985). Glycine, taurine, and serine attract the dinoflagellate at threshold detection levels of 10^{-8} M, followed by dextrose at 10^{-7} and alanine, proline, and threonine at 10^{-6} M. Glycine, taurine, and alanine are three of the most abundant free amino acids found in invertebrates and protozoa, which are the major food organisms of *G. fungiforme*.

Pfiesteria piscicida is a heterotrophic dinoflagellate that is responsible for many of the fish kills along the Atlantic coast of the Southeastern United States (Burkholder and Glasgow, 1997). *P. piscicida* belongs to the "ambush–predator" group of dinoflagellates which chemically detect their prey and then swarm in a direct attack on the prey. The zoospores have a peduncle that is thin and tapered when the dinoflagellate is not feeding. In the presence of fish, the dinoflagellate zoospores feed on the fish by phagocytizing fish tissue through the peduncle. The peduncle is swollen with haustoria-like penetrating extensions when feeding on the fish (Fig. 7.51(*b*)).

Symbiotic dinoflagellates

Symbiotic dinoflagellates (**zooxanthellae**) occur in almost all species of tropical and reef-building corals, jellyfish, and sea anemones (Cnidaria). The dinoflagellates are coccoid spheres in the symbiotic state and have been assigned to the genus *Symbiodinium*. Studies on nucleic acid makeup have revealed the dinoflagellates to be a diverse group, although the dinoflagellate inhabiting one type of Cnidaria remains a constant (Baillie et al., 2000; Rodriguez-Lanetty et al., 2004).

Symbiodinium cells change into typical gymnodinoid form when placed in culture. Cultured and symbiotic *Symbiodinium* differ physiologically. The symbiotic cells grow ten times slower than cultured cells. The host exerts strong control over the translocation of metabolites from the dinoflagellate endosymbiont, resulting in 98% of the carbon fixed by the endosymbiont being released to the host. In contrast, cultured cells release only 10% of their photosynthetically fixed carbon (Trench, 1993). The host animal cells secrete the amino acid taurine which causes the

dinoflagellate to release photosynthate outside the cell for absorption by the animal cells (Wang and Douglas, 1997).

Corals with symbiotic dinoflagellates do not incorporate calcium into their skeletons as fast as corals without symbiotic dinoflagellates. During the daytime, corals with and without symbiotic dinoflagellates calcify at the same rate. Calcification occurs three times faster during the day than at night (Gattuso et al., 2001).

In the symbiosis between the marine anemones and marine dinoflagellates, the dry weight ratio of host to alga is about 300:1 (Taylor, 1969). When the anemone is subjected to poor growing conditions, it responds by excreting some of the dinoflagellate cells, which the anemone obviously has difficulty in maintaining. Even under normal growing conditions the algal population divides too rapidly, and the anemone reacts by pruning the population down to a level it can support. In this situation the older dinoflagellate cells in the outer regions of the host (crown and tentacles) respond by thickening the outer secreted layer around the cell wall and subsequently forming cysts. As the thickness of the cyst's outer layer increases, the cells begin to show signs of degeneration. The host then seems to become sensitive to the degenerate condition of the cysts and reacts by removing them from these outer regions and transporting them to the mesenteries as intracellular inclusions of its undifferentiated amoeboid cells. They are stored in the mesenteries in varying states of decomposition until they are finally excreted by the host.

In the flatworm *Amphiscolops langerhansi*, D. L. Taylor (1971) has found that the cells of the dinoflagellate *Amphidinium klebsii* occur exclusively between the cells of the peripheral parenchyma of the host and appear as a conspicuous layer below the composite muscle (Fig. 7.53). Each cell of *Amphidinium* has a specific and uniform orientation within the host. The anterior of the cell is directed toward the central parenchyma, and the posterior with the large nucleus is directed toward the epithelium. By rearing the flatworm from eggs, it is possible to obtain individuals without the dinoflagellate symbiont. When these flatworms are grown in culture with a number of different types of dinoflagellates, only species of *Amphidinium* are able to infect the host. When contact is made, the animal seizes and ingests the alga. Once inside the flatworm, the alga is not retained in the central digestive paranchyma but passes freely between the animal cells to the peripheral parenchyma, where it comes to lie intercellularly below the composite muscle. The alga remains unchanged within the host and still has its typical two flagella. In nature the association between the flatworm and the dinoflagellate is probably essential for the survival of the animal. It is not known whether the dinoflagellate receives any benefit.

In addition to Dinophyceae living symbiotically inside other organisms, there are other organisms that live inside dinoflagellate cells. *Noctiluca scintillans* is a heterotrophic omnivorous feeder that ingests zooplankton, mesozooplankton, and their eggs (Fig. 7.47) (Hansen et al., 2004). However, in the tropical to subtropical areas of Southeast Asia, a green form of *N. scintillans* is found. The cells have 6 000 to 12 000 green flagellates actively swimming in the fluid within the large vacuoles (Fig. 7.54), especially around the periphery of the vacuole. The green flagellate resembles the green alga *Pedinomonas* in being bright green, 2×5 μm in size, with no eyespot, and having a single posterior flagellum. Whether the dinoflagellate gains any advantage from the association is not known.

Classification

There is a single class in the Dinophyta, the Dinophyceae. Four orders are considered here. Molecular studies have shown that the Prorocentrales, Peridiniales, and Gymnodiniales represent three clear lines of evolution (Zardoya et al., 1995). The Dinophysiales are probably related to the Prorocentrales since they are both divided vertically into two halves.

Order 1 Prorocentrales: cell wall divided vertically into two halves; no girdle; two flagella borne at cell apex.

Order 2 Dinophysiales: cell wall divided vertically into two halves, cells with elaborate extensions of the theca.

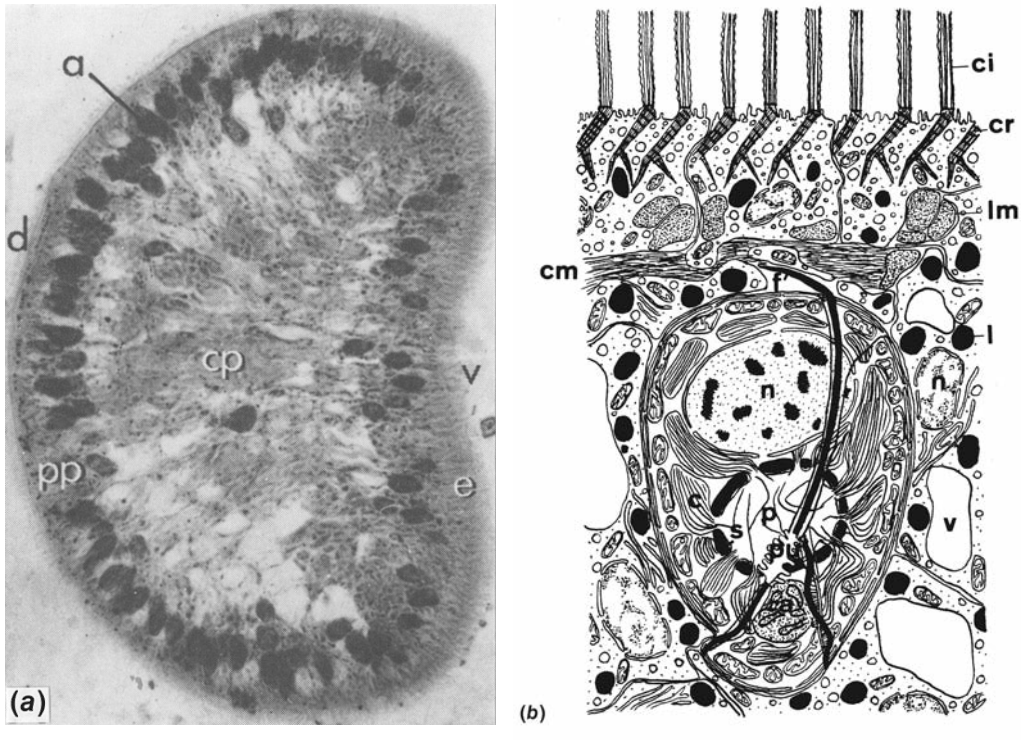


Fig. 7.53 (*a*) Cross section of the flatworm *Amphiscolops langerhansii* showing the dinoflagellate *Amphidinium klebsii* (a) in the peripheral parenchyma (pp). (cp) Central parenchyma; (d) dorsal surface; (e) epithelium; (v) ventral surface. ×90. (*b*) Diagrammatic reconstruction of the above association. (a) Accumulation body; (c) chloroplast; (ci) cilia; (cm) circular muscle; (cr) ciliary root; (f) flagellum; (l) lipid; (lm) longitudinal muscle; (n) nucleus; (p) pyrenoid; (pu) pusule; (s) starch; (v) vacuole. (After D. Taylor, 1971.)

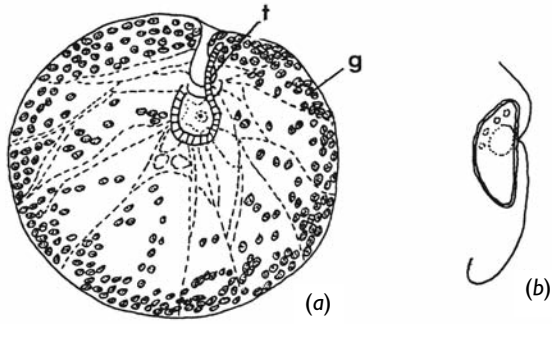


Fig. 7.54 *Noctiluca* containing green algae in its vacuoles. (*a*) Whole cell. (g) Green algae; (t) tentacle. (*b*) Green symbiont. (After Sweeney, 1971.)

Order 3 Peridiniales: motile cells with an epicone and hypocone separated by a girdle, relatively thick theca.

Order 4 Gymnodiniales: motile cells with an epicone and hypocone separated by a girdle; theca thin or reduced to empty vesicles.

Prorocentrales

These cells have the cell wall divided vertically into two halves, no girdle, and two apically inserted flagella, *Prorocentrum* (Figs. 7.55, 7.56(*b*), (*c*)) can be used as an example of the order. The cell is divided vertically into two halves, each half containing a relatively thick thecal plate, the suture joining them running from the anterior to the posterior end. The cell is flattened parallel to the suture so the two halves are like two watch glasses. The two flagella emerge apically through a pore, and there is a single tooth containing cytoplasm. Usually there are two brownish-yellow chloroplasts, apposed to the two valves. Asexual reproduction takes place by longitudinal division, the daughter cells retaining one valve of the parent and forming a new second valve.

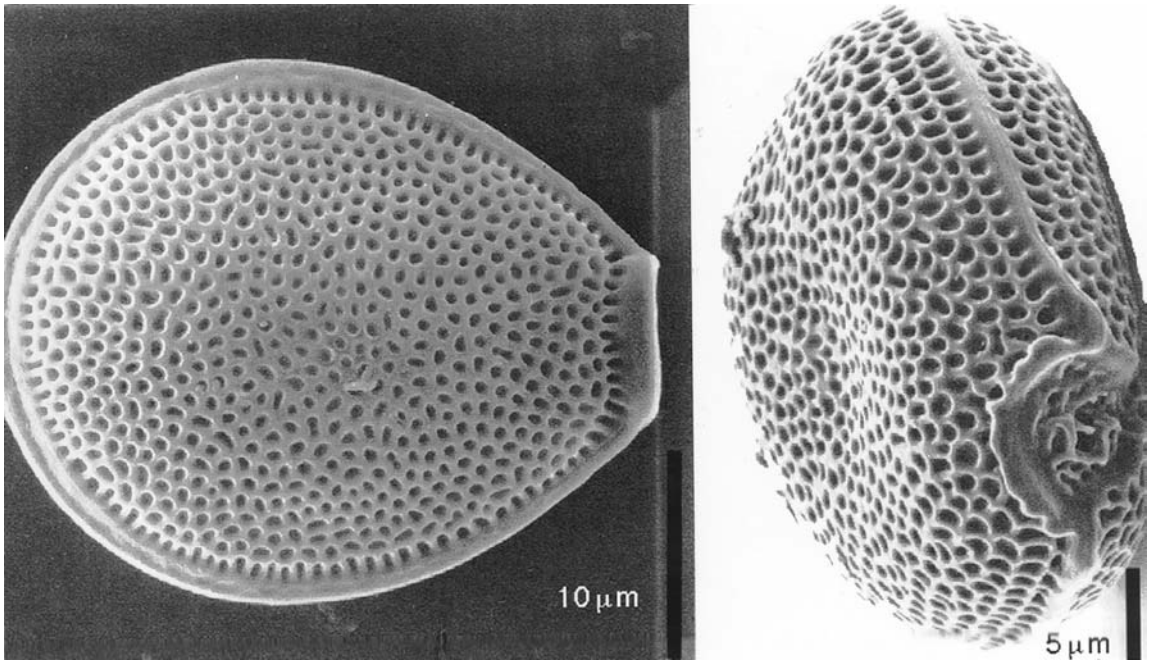


Fig. 7.55 Scanning electron micrographs of *Prorocentrum hoffmanianum*. (From Faust, 1990.)

Dinophysiales

This order consists of morphologically complex organisms that are mainly in tropical seas, with the cells having adaptations to the floating habit such as elaborate wings (**lists**). One of the more complex organisms in this order is *Ornithocercus* (Fig. 7.56(*d*), (*e*)). The cell is divided vertically into two halves by an anterior posterior suture. The cells have a girdle and sulcus, with the side having the sulcus being the ventral side and the opposite side being the dorsal side. The respective flagella lie in the girdle and transverse sulcus. The epicone is usually much smaller than the hypocone, and the edges of the thecal plates next to the girdle and sulcus are expanded into the lists. In asexual reproduction the cell is cleaved vertically, with the two halves separating and the missing half being formed by the protoplasm. The oldest fossil of this group is *Nannoceratopsis* from the Lower Jurassic (Loeblich, 1974, 1976).

Peridiniales

The dinoflagellates in this order have relatively thick thecal plates, in contrast to the next order, the Gymnodiniales, which has no, or thin, thecal plates. The algae in this order have the classic dinoflagellate structure (Figs. 7.1, 7.2) with an epicone and hypocone and two furrows, the transverse girdle and the longitudinal sulcus.

The widely distributed genus *Ceratium* (Figs. 7.12, 7.57, 7.58) is markedly asymmetric, with one apical horn and two to three long antapical horns filled with cytoplasm. The girdle is nearly horizontal and divides the body into two approximately equal, but dissimilar halves. In the middle of the ventral surface is a large rhombic hyaline area, which is probably similar to a sulcus. Like other Dinophyceae and Prymnesiophyceae, *Ceratium* is more common in warmer water than in colder polar waters. There are fewer than ten species common in the colder waters of the North Atlantic, whereas more than 20 species are common in the warmer more southerly waters (Graham and Bronikovsky, 1944). *Ceratium* is one of the members of the phytoplankton that has **shade forms** which show an increase in frequency from the surface to 100 m depth. These shade forms are found only in the relatively sterile warm oceanic waters where the upper layers are usually depleted of nitrogen and phosphorus. The shade forms of *Ceratium* have a survival value in that

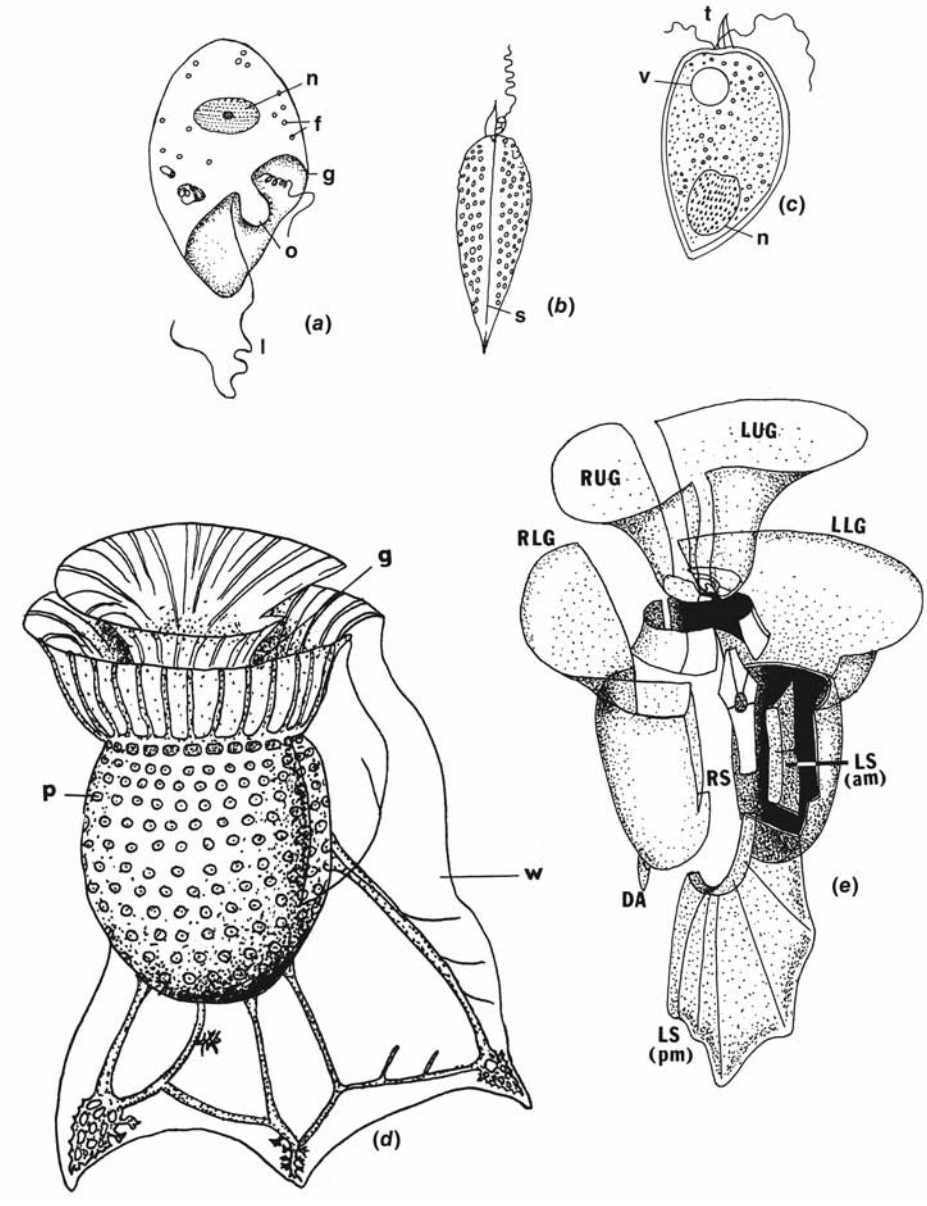


Fig. 7.56 (*a*) *Oxyrrhis marina*. (f) Fat globule; (g) girdle; (l) longitudinal flagellum; (n) nucleus; (o) tentacle. (*b*),(*c*) *Prorocentrum micans*, side (*b*) and front (*c*) views. (n) Nucleus; (s) suture; (v) vacuole. (*d*),(e) *Ornithoceros magnificus*, a right-hand view (*d*) and an "exploded" view (e) of the theca. (DA) Dorsal accessory moiety of the left sulcal list; (LLG) left lower girdle list; (LS(am)) anterior moiety of the left sulcal list; (LS(pm)) posterior moiety of the left sulcal list; (LUG) left upper girdle list; (RS) right sulcal list; (RLG and RUG) right lower and upper girdle list; (g) girdle; (p) pore; (w) wing. ((*d*),(e) after F. Taylor, 1971.)

they are able to take advantage of the higher levels of nitrogen and phosphorus deeper in the water and still are able to receive enough light to keep their photosynthetic rate above their respiratory rate. These shade forms adapt themselves to absorb the maximum amount of light by increasing the surface area of the cell by expansion of the cell body and/or horns and packing these extensions with chloroplasts. Long-horned forms are found among surface forms also, but the shade

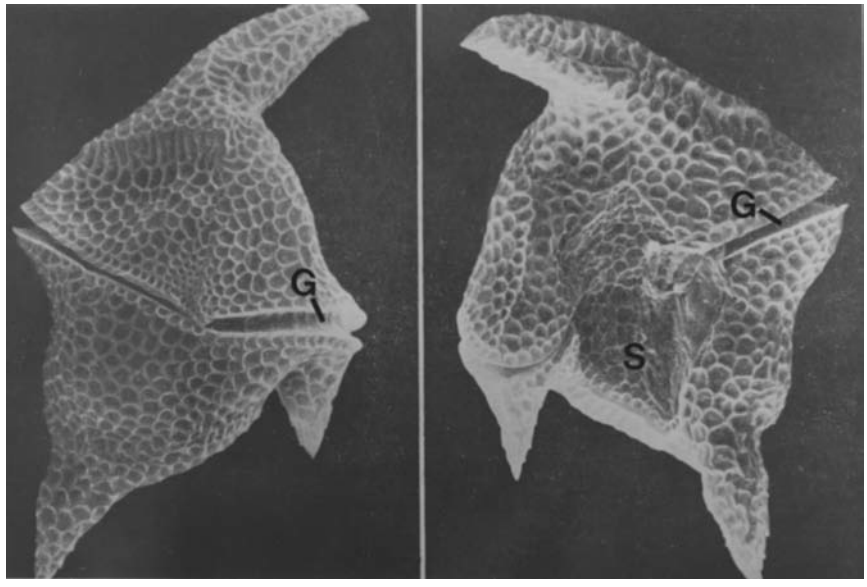


Fig. 7.57 Scanning electron micrographs of both sides of a vegetative cell of *Ceratium cornutum*. (G) Girdle; (S) sulcus. (From Happach-Kasan, 1982.)

forms always have their horns crowded with chloroplasts.

Ceratium horridum has a life cycle that is more or less similar to the known life cycle of other Dinophyceae. Von Stosch (1972) (Fig. 7.60) has shown that the vegetative cells of *C. horridum* are haploid. The male gametes are smaller than the female gametes; thus fusion in this organism is anisogamous (Fig. 7.58). The male gamete attaches by its ventral side to the ventral side of the female gamete. The cell wall of the male then breaks up into its individual plates, which are taken up into the female cytoplasm. The naked male gamete fuses with the female gamete to produce a zygote. The zygote remains motile (planozygote) through all of the following steps. The planozygote grows for several days, ending up as a large cell with unusually long horns and a thick cell wall. Finally, the nucleus enlarges, and nuclear cycloses (movement) begins. At its highest speed the chromosomal mass circulates once every 30 seconds. After some hours the motion slows down and stops, and approximately 12 hours later meiosis commences. The first meiotic division halves the chromosome number and gives rise to one flagellate with normally sized antapical, and abnormally long apical horns and a second flagellate with normally sized apical, and abnormally long antapical horns. After 2 to 3 days the second meiotic division takes place to yield haploid vegetative cells.

Gymnodiniales

The dinoflagellates in this order are similar to those in the previous order, the Peridiniales, except that they have thin or no thecal plates.

The life cycle of *Gymnodinium pseudopalustre* is a representative of the order. Vegetative multiplication results in daughter cells that remain attached to each other for at least 12 hours (Fig. 7.59). Gametes are formed when an actively growing culture at 21 °C is subjected to a short-day treatment (10 hours light) at 15 °C (von Stosch, 1973). Gamete differentiation occurs by divisions that give rise to cells lower in mass and poorer in plastids and pigments than the vegetative cells. Apart from their smaller size and lighter color, the gametes are not obviously different from vegetative cells. They are incapable of living for long as vegetative cells and die if fusion does not occur. The gametes are homothallic; thus gametes from a single strain will fuse.

Initially, small groups of two to ten gametes swarm around each other in a weaving motion. A copulation pair occurs between two gametes, with the pair swimming rapidly while turning slowly on a common axis. Copulation is isogamous although

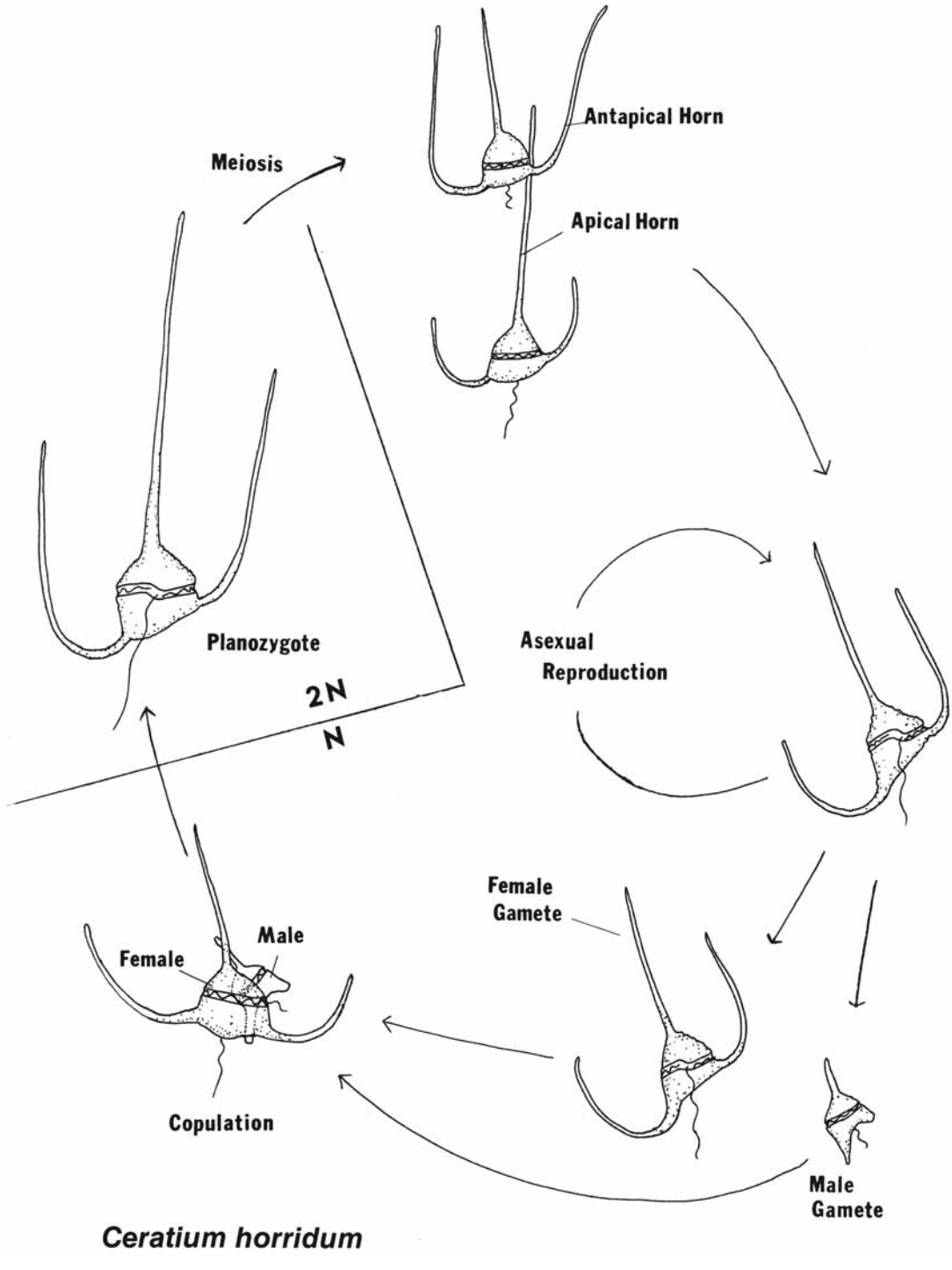


Fig. 7.58 The life cycle of *Ceratium horridum*. (Adapted from von Stosch, 1972.)

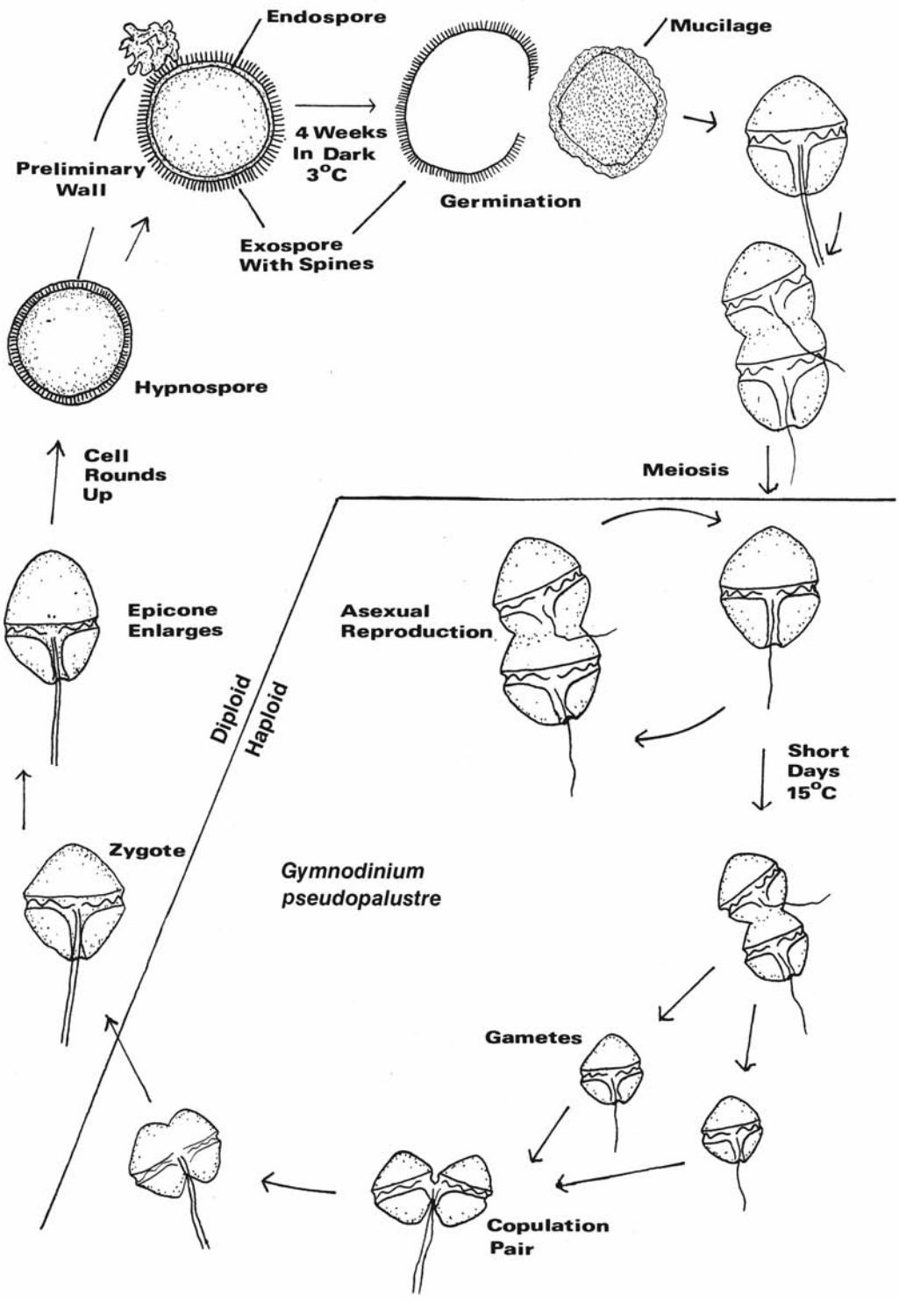


Fig. 7.59 The life cycle of *Gymnodinium pseudopalustre*. (Adapted from von Stosch, 1973.)

there can be a slight difference in the size of the gametes. The cells are joined together by a hyaline globular bridge slightly below the intersection of the transverse and posterior grooves. After 30 minutes the fusion of protoplasts has begun, with the bridge between the two cells enlarging. At the end of fusion a cell similar to a vegetative cell is attained. The flagella and nuclei of each gamete are still distinct. The zygote grows, at first having the shape of a vegetative cell, and later the epicone elongates. One of the transverse flagella is lost during this development, but both of the posterior flagella persist. The non-motile zygote suddenly rounds off and secretes a preliminary wall. This wall is subsequently inflated, giving rise to a hyaline area between the wall and the protoplast surface. An ornamentation of small separated granules now appears on the protoplast wall, which grow out radially to become spines while the hyaline area increases in width. The preliminary wall then bursts and crumples away to one side of the spore. The preliminary wall is necessary for formation of the hypnospore. The duration of the preliminary wall is only about 9 minutes.

During the next 48 hours the hypnospore matures, with the plastids bleaching and becoming inconspicuous, masses of red oil appearing, the starch becoming indistinct, and the two nuclei now fusing. A thick cellulosic endospore is also secreted under the exospore with its spines. The hypnospores germinate after treatment for 4 weeks in the dark at 3 °C before being returned to light and higher temperature. After the cellulosic endospore has been digested away, approaching release of the swarmer is indicated by a slight contraction of the protoplast so that the transverse groove of the prospective flagellate becomes visible. The space between the spore wall and the surface of the swarmer is filled with mucilage. Eventually the wall bursts, and the swarmer escapes, enveloped in mucilage. The swarmer frees itself from the mucilage and swims away. The swarmer is rather plump and of oval shape at first, and, apart from red oil globules, nearly colorless; but later it acquires brown pigment, and its form becomes similar to that of the vegetative cell. Two "skiing track" posterior flagella have reappeared. The swarmer then goes through two meiotic divisions, resulting in four haploid flagellates.

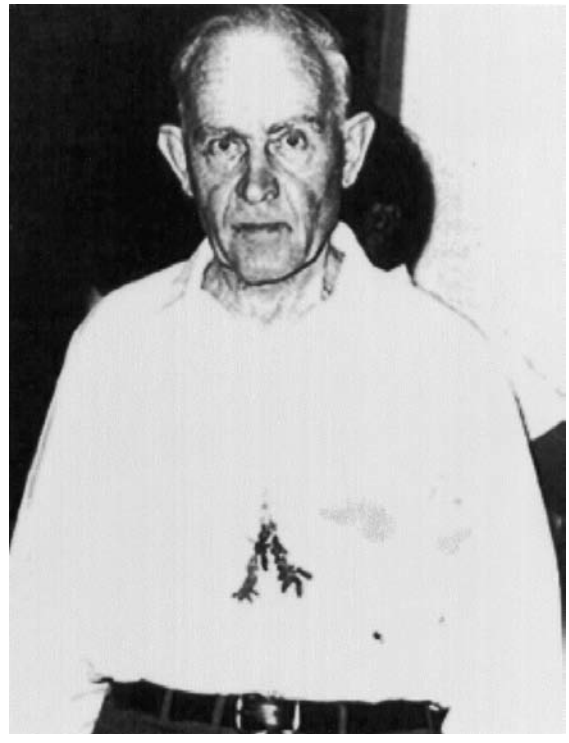


Fig. 7.60 **Hans Adolf von Stosch**, 1908–1987. Dr. von Stosch was born in Berlin and studied at the Universities of Kiel, Gottingen, and Munich. Before World War II he worked at the University of Konigsberg/ Ostppreussen. He became a soldier in 1939, was taken prisoner in Tunisia in 1943, and was released in England in 1947. He obtained a position at the Technical University in Darmstadt, where he began his studies on algae in earnest. In 1955, he moved to the University of Marburg where he stayed until his retirement in 1976. His work on the life histories of dinoflagellates is some of the best work done on the group. (Photo from Garbary and Wynne, 1996.)

REFERENCES

Abrahams, M. V., and Townsend, L. D. (1993). Bioluminescence in dinoflagellates: a test of the burglar alarm hypothesis. *Ecology* 74:258–60.

Adamich, M., Laris, P. C., and Sweeney, B. M. (1976). In vivo evidence for a circadian rhythm in membranes of *Gonyaulax*. *Nature* 261:583–5.

Baillie, B. K., Belda-Baillie, C. A., and Maruyama, T. (2000). Conspecificity and indo-pacific distribution of *Symbiodinium* genotypes (Dinophyceae) from giant clams. *J. Phycol*. 36:1153–61.

Balzer, I., and Hardeland, R. (1996). Melatonin in algae and higher plants – possible new roles as a phytochrome and antioxidant. *Bot. Acta* 109:180–3.

Barlow, S. B., and Triemer, R. E. (1988). The mitotic apparatus of the dinoflagellate *Amphidinium carterae. Protoplasma* 145:16–26.

Berdach, J. T. (1977). In situ preservation of the transverse flagellum of *Peridinium cinctum* (Dinophyceae) for scanning electron microscopy. *J. Phycol*. 13:243–51.

Bibby, B. T., and Dodge, J. D. (1972). The encystment of a freshwater dinoflagellate: A light and electron-microscopical study. *Br. Phycol. J.* 7:85–100.

Bouck, G. B., and Sweeney, B. M. (1966). The fine structure and ontogeny of trichocysts in marine dinoflagellates. *Protoplasma* 61:205–23.

Bricheux, G., Mahoney, D. G., and Gibbs, S. P. (1992). Development of the pellicle and thecal plates following ecdysis in the dinoflagellate *Glenodinium foliaceaum. Protoplasma* 168:159–71.

Brooks, B. J., and Anderson, D. M. (1990). Biochemical composition and metabolic activity of *Scrippsiella trochoidea* (Dinophyceae) resting cysts. *J. Phycol*. 26:289–98.

Burkholder, J. M., and Glasgow, H. B. (1997). Trophic controls on stage transformation of a toxic ambush-predator dinoflagellate. *J. Euk. Microbiol*. 44:200–5.

Buskey, E. J., and Swift, E. (1983). Behavioral responses of *Acartia hudsonica* to simulated dinoflagellate bioluminescence. *J. Exp. Mar. Biol. Ecol*. 77:43–58.

Cembella, A. D. (2003). Chemical ecology of eukaryotic microalgae in marine ecosystems. *Phycologia* 42:420–47.

Chapman, D. V., Dodge, J. D., and Heaney, S. J. (1982). Cyst formation in the freshwater dinoflagellate *Ceratium hirundinella. J. Phycol*. 18:121–9.

Chatton, E. (1952). Classe des dinoflagelles ou peridiniens. In *Traité de Zoologie*, ed. P-P. Grassé, pp. 304–406. Paris: Masson.

Chinain, M., Germain, M., Sako, Y., Pauillac, S., and Legrand, A-M. (1997). Intraspecific variation in the dinoflagellate *Gambierdiscus toxicus* (Dinophyceae). I. Isoenzyme analysis. *J. Phycol*. 33:36–43.

Clarke, K. J., and Pennick, N. C. (1976). The occurrence of body scales in *Oxyrrhis marina* Dujardin. *Br. Phycol. J.* 11:345–8.

Crawford, R. M., Dodge, J. D., and Happey, C. M. (1970). The dinoflagellate genus *Woloszynskia*. I. Fine structure and ecology of *W. tenuissima* from Abbot's Pool, Somerset. *Nova Hedwigia* 19:825–40.

Daugbjerg, N., Hansen, G., Larsen, J., and Moestrup, O. (2000). Phylogeny of some major genera of dinoflagellates based on ultrastructure and partial LSU rDNA sequence data, including the erection of three new genera of unarmoured dinoflagellates. *Phycologia* 39:302–17.

Destombe, C., and Cembella, A. (1990). Mating-type determination, gamete recognition and reproductive success in *Alexandrium excavatum* (Gonyaulacales, Dinophyta), a toxic red-tide dinoflagellate. *Phycologia* 29:315–25.

Dodge, J. D. (1971). Fine structure of the Pyrrophyta. *Bot. Rev*. 37:481–508.

Dodge, J. D., and Crawford, R. M. (1968). Fine structure of the dinoflagellate *Amphidinium carteri* Hulbert. *Protistologica* 4:231–42.

Dodge, J. D., and Crawford, R. M. (1969). Observations of the fine structure of the eyespot and associated structures in the dinoflagellate *Glenodinium foliaceum. J. Cell Sci*. 5:479–93.

Dodge, J. D., and Crawford, R. M. (1970). A survey of thecal fine structure in the Dinophyceae. *J. Linn. Soc. Bot*. 63:53–67.

Downie, C. (1956). Microplankton from the Kimmeridge Clay. *Q. J. Geol. Soc. Lond*. 112:413–34.

Dunlap, J. C., and Hastings, J. W. (1981). Biochemistry of dinoflagellate bioluminescence: Purification and characterization of dinoflagellate luciferin from *Pyrocystis lunula. Biochemistry* 20:983–9.

Ellegaard, M., Christensen, N. F., and Moestrup, O. (1994). Dinoflagellate cysts from recent Danish marine sediments. *Eur. J. Phycol.* 29:183–94.

Eppley, R. W., Holm-Hansen, O., and Strickland, J. D. H. (1968). Some observations on the vertical migration of dinoflagellates. *J. Phycol*. 4:333–40.

Faust, M. A. (1990). Morphological details of six benthic species of *Prorocentrum* (Pyrrophyta) from a mangrove island, Twin Cays, Belize, including two new species. *J. Phycol*. 26:548–58.

Faust, M. A. (1995). Observation of sand-dwelling toxic dinoflagellates (Dinophyceae) from widely differing sites, including two new species. *J. Phycol*. 31:996–1003.

Fenchel, T. (2001). How dinoflagellates swim. *Protist* 152:329–38.

Fritz, L., Milos, P., Morse, D., and Hastings, J. W. (1991). *In situ* hybridization of luciferase-binding protein anti-sense RNA to thin sections of the bioluminescent dinoflagellate *Gonyaulax polyedra. J. Phycol*. 27:436–41.

Gaines, G., and Taylor, F. J. R. (1984). Extracellular digestion in marine dinoflagellates. *J. Plank. Res*. 6:1057–61.

Gaines, G., and Taylor, F. J. R. (1985). Form and function of the dinoflagellate transverse flagellum. *J. Protozool*. 32:290–6.

Gallois, R. W. (1976). Coccolith blooms in the Kimmeridge Clay and origin of the North Sea oil. *Nature* 259:473–5.

Garbary, D. J., and Wynne, M. J. (1996). *Prominent Phycologists of the 20th Century*. Hantsport, Nova Scotia: Lancelot Press.

Gattuso, J.-P., Reynaud-Vaganay, S., Furla, P., Romaine-Lioud, S., and Jaubert, J. (2000). Calcification does not stimulate photosynthesis in the zooxanthellate scleractinian coral *Stylophora pistillata*. *Limnol. Oceanogr*. 45:246–50.

Gao, X-P., and Li, J-Y. (1986). Nuclear division in the marine dinoflagellate *Oxyrrhis marina*. *J. Cell Sci* . 85:161–75.

Giner, J.-L., Faraldos, J. A., and Boyer, G. L. (2003). Novel sterols of the toxic dinoflagellate *Karenia brevis* (Dinophyceae): a defensive function for unusual marine sterols. *J. Phycol*. 39:315–19.

Graham, H. W., and Bronikovsky, N. (1944). The genus *Ceratium* in the Pacific and North Atlantic oceans. *Carnegie Inst. Washington Publ.* 565:1–209.

Green, B. R. (2004). The chloroplast genome of dinoflagellates: a reduced instruction set? *Protist* 155:23–31.

Grindley, J. R., and Nel, E. A. (1970). Red water and mussel poisoning at Elands Bay, December 1966. *Fish Bull., S. Afr*. 6:36–55.

Grindley, J. R., and Sapeika, N. (1969). The cause of mussel poisoning in South Africa. *S. Afr. Med. J.* 43:275–9.

Gruet, C. (1965). Structure fine de l'ocelle d'*Erythropsis pavillardi* Hetwig, Péridinien Warnowiidae Lindemann. *C. R. Séances Acad. Sci., Paris* 261:1904–7.

Guisande, C., Frangopulos, M., Carolenuto, Y., Maneiro, I., Riveiro, I., and Vergara, A.R. (2002). Fate of paralytic shellfish poisoning toxins ingested by the copepod *Acartia clausi*. *Mar. Ecol. Progr. Ser*. 240:105–15.

Hackett, J. D., Anderson, D. M., Erdner, D. L., and Bhattacharya, D. (2004). Dinoflagellates: a remarkable evolutionary experiment. *Amer. J. Bot*. 91:1523–34.

Hallegraeff, G. M. (1993). A review of harmful algal blooms and their apparent global increase. *Phycologia* 32:79–99.

Hansen, G. (1989). Ultrastructure and morphogenesis of scales in *Katodinium rotundatum* (Lohmann) Loeblich (Dinophyceae). *Phycologia* 28:385–94.

Hansen, G. (1993). Light and electron microscopical observation of the dinoflagellate *Actiniscus pentasterias* (Dinophyceae). *J. Phycol*. 29:486–99.

Hansen, P. J., and Calado, A. J. (1999). Phagotrophic mechanisms and prey selection in free-living dinoflagellates. *J. Eukary. Microbiol*. 46:382–9.

Hansen, P. J., Miranda, L., and Azanza, R. (2004). Green *Noctiluca scintillans*: a dinoflagellate with its own greenhouse. *Mar. Ecol. Progr. Ser*. 275:79–87.

Happach-Kasan, C. (1982). Beobachtungen zum Bau der Theka von *Ceratium cornutum*, (Ehrenb,) Clap. et Lachm. (Dinophyta). *Arch. Protistenk*. 125:181–207.

Harvey, E. N. (1952). *Bioluminescence*. New York: Academic Press.

Hastings, J. W. (1983). Biological diversity, chemical mechanisms, and the evolutionary origins of bioluminescent systems. *J. Mol. Evol*. 19:309–21.

Hastings, J. W. (1986). Bioluminescence in bacteria and dinoflagellates. In *Light Emission in Plants and Bacteria*, pp. 363–98. New York: Academic Press.

Hastings, J. W., and Krasnow, R. (1981). Temporal regulation in the individual *Gonyaulax* cell. In *International Cell Biology 1980–1981*, Proc. 2nd Int. Cong. on Cell Biology, pp. 815–823. Berlin: Springer-Verlag.

Haywood, A. J., Steidinger, K. A., Truby, E. W., et al. (2004). Comparative morphology and molecular phylogenetic analysis of three new species of the genus *Karenia* (Dinophyceae) from New Zealand. *J. Phycol*. 40:165–79.

Höhfeld, I., and Melkonian, M. (1992). Amphiesmal ultrastructure of dinoflagellates, A reevaluation of pellicle formation. *J. Phycol*. 28:82–9.

Höhfeld, I., and Melkonian, M. (1998). Lifting the curtain? The microtubular cytoskeleton of *Oxyrrhis marina* (Dinophyceae) and its rearrangement during phagocytosis. *Protist* 149:75–88.

Höhfeld, I., Otten, J., and Melkonian, M. (1988). Contractile eukaryotic flagella: Centrin is involved. *Protoplasma* 147:16–24.

Horiguchi, T., and Pienaar, R. N. (1988). Ultrastructure of a new sand-dwelling dinoflagellate *Scrippsiella arenicola* sp. nov. *J. Phycol*. 24:426–38.

Horiguchi, T., Kawai, H., Kubota, M., Takahasdi, T., and Watanabe, M. (1999). Phototactic responses of four marine dinoflagellates with different types of eyespot and chloroplast. *Phycol. Res*. 47:101–7.

Hu, T., Burton, I., Curtis, J. M., et al. (1999). Oxidative transformation of a naturally occurring okadaic acid diol ester by the diatom *Thalassiosira weisflogii*. *Tetrahedron Lett*. 40:3981–4.

Igarashi, T., Aritake, S., and Yasumoto, T. (1999). Mechanisms underlying the hemolytic and ichthyotoxic activities of maitotoxin. *Nat. Toxins* 7:71–9.

Ishida, K., and Green, B. R. (2002). Second- and third-hand chloroplasts in dinoflagellates: phylogeny of oxygen-evolving enhancer 1 (PsbO) protein reveals replacement of a nuclear-encoded plastid gene by that of a haptophye tertiary endosymbiosis. *Proc. Natl. Acad. Sci., USA* 99:9294–9.

Iwataki, M., Hansen, G., Sawaguchii, T., Hiroishi, S., and Fukuyo, Y. (2004). Investigations of body scales in twelve *Heterocapsa* species (Peridiniales, Dinophyceae), including a new species *H. pseudotriquetra* sp. nov. *Phycologia* 43:394–403.

Jacobsen, D. M. (1999). A brief history of dinoflagellate feeding research. *J. Eukary. Microbiol*. 46:376–81.

Jacobsen, D. M., and Anderson, D. M. (1986). Thecate heterotrophic dinoflagellates: Feeding behavior and mechanisms. *J. Phycol*. 22:249–58.

Janofske, B. (2000). *Scrippsiela trochoidea* and *Scrippsiela regalis*, nov. comb. (Peridiniales, Dinophyceae): a comparison. *J. Phycol*. 36:178–89.

John, E. H., and Flynn, K. J. (2002). Modelling changes in paralytic shellfish toxin content of dinoflagellates in response to nitrogen and phosphorus supply. *Mar. Ecol. Progr. Ser*. 225:147–60.

Johnson, C. H., and Hastings, J. W. (1986). The elusive mechanism of the circadian clock. *Am. Sci*. 74:29–36.

Johnson, C. H., Inoué, S., Flint, A., and Hastings, J. W. (1985). Compartmentalization of algal bioluminescence: Autofluoresence of bioluminescent particles in the dinoflagellate *Gonyaulax* as studied with image-intensified video microscopy and flow cytometry. *J. Cell Biol*. 100:1435–46.

Juhl, A. R., and Latz, M. J. (2002). Mechanisms of fluid shear-induced inhibition of population growth in a red-tide dinoflagellate. *J. Phycol*. 38:683–94.

Keeling, P. J. (2004). Diversity and evolutionary history of plastids and their hosts. *Amer. J. Bot*. 91:1481–93.

Kennaway, G. M., and Lewis, J. M. (2004). An ultrastructural study of hypnospores of *Alexandrium* species (Dinophyceae). *Phycologia* 43:353–63.

Klut, M. E., Bisalputra, T., and Antia, N. J. (1985). Some cytochemical studies on the cell surface of *Amphidinium carteri* (Dinophyceae). *Protoplasma* 129:93–9.

Kokinos, J. P., Eglinton, T. I., Goni, M., Boon, J. J., Martoglio, P. A., and Anderson, D. A. (1998). Characterization of a highly resistant biomacromolecular material in the cell wall of a marine dinoflagellate resting cyst. *Org. Geochem*. 28:265–88.

Kremp, A. (2001). Effects of cyst resuspension on germination and seeding of two bloom-forming dinoflagellates in the Baltic Sea. *Mar. Ecol. Progr. Ser*. 216:57–66.

Kubai, D. F., and Ris, H. (1969). Division in the dinoflagellate *Gyrodinium cohnii* (Schiller). A new type of nuclear reproduction. *J. Cell Biol*. 40:508–28.

Leadbeater, B. S. C., and Dodge, J. D. (1967a). Fine structure of the dinoflagellate transverse flagellum. *Nature* 213:421–2.

Leadbeater. B. S. C., and Dodge, J. D. (1967b). An electron microscope study of nuclear and cell division in a dinoflagellate. *Arch. Mikrobiol*. 57:239–54.

Leblond, J. D., and Chapman, P. J. (2002). A survey of the sterol composition of the marine dinoflagellates *Karenia brevis, Karenia mikimoto*, and *Karlodinium micrum*: distribution of sterols within other members of the class Dinophyceae. *J. Phycol*. 38:670–82.

Lee, R. E. (1977). Saprophytic and phagocytic isolates of the colorless heterotrophic dinoflagellate *Gyrodinium lebouriae* Herdman *J. Mar. Biol. Assoc. UK* 57:303–15.

Lewitus, A. J., Glasgow, H. B., and Burkholder, J. M. (1999). Kleptoplastidy in the toxic dinoflagellate *Pfiesteia piscicida* (Dinophyceae). *J. Phycol*. 35:305–12.

Loeblich, A. R. (1968). A new marine dinoflagellate genus, *Cachonia*, in axenic culture from the Salton Sea, California with remarks on the genus *Peridinium. Proc. Biol. Soc. Wash*. 81:91–6.

Loeblich, A. R. (1974). Protistan phylogeny as indicated by the fossil record. *Taxon* 23:277–90.

Loeblich, A. R. (1976). Dinoflagellate evolution: Speculation and evidence. *J. Protozol*. 23:13–28.

Lombard, E. H., and Capon, B. (1971). Observations on the tide pool behaviour of *Peridinium gregarium. J. Phycol*. 7:188–94.

MacRae, R. A., Fensome, R. A., and Williams, G. L. (1996). Fossil dinoflagellate diversity, originations, and extinctions and their significance. *Can. J. Bot*. 74:1687–94.

Maruyama, T. (1982). Fine structure of the longitudinal flagellum in *Ceratium tripos*, a marine dinoflagellate. *J. Cell Sci*. 58:109–23.

Maruyama, T. (1985). Ionic control of the longitudinal flagellum in *Ceratium tripos* (Dinoflagellida). *J. Protozool*. 3:106–10.

Matsuoka, K., Cho, H.-J., and Jacobsen, D. M. (2000). Observations of the feeding behavior and growth rates of the heterotrophic dinoflagellate *Polykrikos kofoidii* (Polykrikaceae, Dinophyceae). *Phycologia* 39:82–6.

Meksumpun, S., Montani, S., and Uematsu, M. (1994). Elemental composition of cell walls of three marine phytoflagellates, *Chattonella antiqua* (Raphidophyceae), *Alexandrium catenella* and *Scrippsiella trochoidea* (Dinophyceae). *Phycologia* 33:275–80.

Messer, G., and Ben-Shaul, Y. (1969). Fine structure of *Peridinium westii* Lemm., a freshwater dinoflagellate. *J. Protozool*. 16:272–80.

Montresor, M., Janofske, D., and Willems, H. (1997). The cyst-theca relationship in *Calciodinellum operosum* emend. (Peridinales, Dinophyceae) and a new approach for the study of calcareous cysts. *J. Phycol*. 33:122–31.

Moronin, L., and Francis, D. (1967). The fine structure of *Nematodinium armatum*, a naked dinoflagellate. *J. Microscopie* 6:759–72.

Morrill, L. C., and Loeblich, A. R. (1983a). Ultrastructure of the dinoflagellate amphisema. *Int. Rev. Cytol*. 82:151–80.

Morrill, L. C., and Loeblich, A. R. (1983b). Formation and release of body scales in the dinoflagellate genus *Heterocapsa*. *J. Mar. Biol. Assoc. UK* 63:905–13.

Morton, S. L., and Tindall, D. R. (1995). Morphological and biochemical variability of the toxic dinoflagellate *Prorocentrum lima* isolated from three locations at Heron Island, Australia. *J. Phycol*. 31:914–21.

Nagai, S., Matsuyama, Y., Takayama, H., and Kotani, Y. (2002). Morphology of *Polykrikos kofoidii* and *P. schwartzii* (Dinophyceae, Polykrikaceae) cysts obtained in culture. *Phycologia* 41:319–27.

Nagai, S., Itakura, S., Matsuyama, Y., and Kotani, Y. (2003). Encystment under laboratory conditions of the toxic dinoflagellate *Alexandrium tamiyavanichii* (Dinophyceae) isolated from Seto Island Sea, Japan. *Phycologia* 42:646–53.

Naustvoll, L.-J. (1998). Growth and grazing by the thecate heterotrophic dinoflagellate *Diplopsalis lenticula* (Diplopsalidaceae, Dinophyceae). *Phycologia* 37:1–9.

Nawata, T., and Sibaoka, T. (1983). Experimental induction of feeding behavior in *Noctiluca miliaris*. *Protoplasma* 115:34–42.

Nawata, T., and Sibaoka, T. (1987). Local ion currents controlling the localized cytoplasmic movement associated with feeding initiation of *Noctiluca*. *Protoplasma* 137:125–33.

Nicolas, M. T., Morse, D., Bassot, J-M. and Hastings, J. W. (1991). Colocalization of luciferin binding protein and luciferase to the scintillons of *Gonyaulax polyedra* revealed by double immunolabeling after fast-freeze fixation. *Protoplasma* 160:159–66.

Perez, C. C., Roy, S., Levasseur, M., and Andersen, D. M. (1998). Control of germination of *Alexandrium tamarensis* (Dinophyceae) cysts from the lower St. Lawrence estuary (Canada). *J. Phycol*. 34:242–9.

Pöggeler, B., Balzer, I., Hardeland, R., and Lerchl, A. (1991). Pineal hormone melatonin oscillates also in the dinoflagellate *Gonyaulax polyedra*. *Naturwissenschaften* 78:268–9.

Preisig, H. R. (1994). Siliceous structures and silicification in flagellated protists. *Protoplasma* 181:1–28.

Prézilin, B. B. (1976). The role of peridinin-chlorophyll *a*-proteins in the photosynthetic light adaptation of the marine dinoflagellate, *Glenodinium* sp. *Planta* 130:225–33.

Prézilin, B. B., and Haxo, F. T. (1976). Purification and characterization of peridinin-chlorophyll α-proteins from the marine dinoflagellates *Glenodinium* sp. and *Gonyaulax polyedra*. *Planta* 128:133–41.

Raven, J. A., and Richardson, K. (1984). Dinophyte flagella: A cost–benefit analysis. *New Phytol*. 98:259–76.

Ris, H., and Kubai, D. F. (1974). An unusual mitotic mechanism in the parasitic protozoan *Syndinium* sp. *J. Cell Biol*. 60:702–20.

Rizzo, P. J. (1991). The enigma of the dinoflagellate chromosome. *J. Protozool*. 38:246–52.

Roberts, K. R., and Roberts, J. E. (1991). The flagellar apparatus and cytoskeleton of the dinoflagellate. *Protoplasma* 164:105–22.

Robinson, N., Eglinton, G., Brassell, S. C., and Cranwell, P. A. (1984). Dinoflagellate origin for sedimentary 4α-methylsteroids and 5α(*H*)-stanols. *Nature* 308:439–42.

Rodriguez-Lanetty, M., Krupp, D. A., and Weis, V. M. (2004). Distinct ITS types of *Symbiodinium* in Clade C correlate with cnidarian/dinoflagellate specificity during onset of symbiosis. *Mar. Ecol. Progr. Ser*. 275:97–102.

Roenneberg, T., and Deng, T-S. (1997). Photobiology of the *Gonyaulax* circadian system. I. Different phase response curves for red and blue light. *Planta* 202:494–501.

Sakamoto, B., Hokama, Y., Horgen, F. D., Scheuer, P. J., Kan, Y., and Nagai, H. (2000). Isolation of a sulfoquinovosyl monoacylglycerol from *Bryopsis* sp. (Chlorophyta): identification of a factor causing a possible species specific ecdysis response in *Gamierdiscus toxicus* (Dinophyceae). *J. Phycol*. 36:924–31.

Samuelsson, G., Sweeney, B. M., Matlock, H. A., and Prézilin, B. B. (1983). Changes in photosystem II account for the circadian rhythm in photosynthesis in *Gonyaulax polyedra*. *Plant Physiol*. 73:329–31.

Schiller, J. (1933). Dinoflagellatae. In *Dr L. Rabenhorst's Kryptogamen-Flora*, Vol. 10. pp. 1–617. Leutershausen: Strauss and Cramer.

Schmidt, R. J., Gooch, V. D., Loeblich, A. R., and Hastings, J. W. (1978). Comparative study of luminescent and nonluminescent strains of *Gonyaulax excavata* (Pyrrhophyta). *J. Phycol*. 14:5–9.

Schütt, F. (1895). Die Peridineen der Plankton-Expedition. *Ergeb. Plankton Exped. Humboldt-Stiftung.* 4; M.a. A:1–170.

Sekida, S., Horiguchi, T., and Okuda, K. (2004). Development of thecal plates and pellicle in the dinoflagellate *Scrippsiella hexapraecingula* (Peridiniales, Dinophyceae) elucidated by changes in stainability of the associated membranes. *Eur. J. Phycol*. 39:105–14.

Seo, K. S., and Fritz, L. (2000). Cell ultrastructural changes correlate with circadian rhythms in *Pyrocystis lunula* (Pyrrophyta). *J. Phycol*. 36:351–8.

Sgrosso, S., Esposito, F., and Montresor, M. (2001). Temperature and daylength regulate encystment in calcareous cyst-forming dinoflagellates. *Mar. Ecol. Progr. Ser*. 211:77–87.

Shilo, M. (1967). Information and mode of action of algal toxins. *Bacteriol. Rev.* 31:180–93.

Sigee, D. C. (1984). Structural DNA and genetically active DNA in dinoflagellate chromosomes. *BioSystems* 16:302–10.

Smalley, G. W., Coats, D. W., and Stoecker, D. K. (2003). Feeding in the mixotrophic dinoflagellate *Ceratium furca* is influenced by intracellular nutrient concentrations. *Mar. Biol. Progr. Ser*. 262:137–51.

Spero, H. J. (1982). Phagotrophy in *Gymnodinium fungiforme* (Pyrrophyta): The peduncle as an organelle of ingestion. *J. Phycol*. 18:356–60.

Spero, H. J. (1985). Chemosensory capabilities in the phagotrophic dinoflagellate *Gymnodinium fungiforme. J. Phycol*. 21:181–4.

Spero, H. J., and Moree, M. D. (1981). Phagotrophic feeding and its importance to the life cycle of the holozoic dinoflagellate, *Gymnodinium fungiforme. J. Phycol*. 17:43–57.

Sullivan, J. M., and Swift, E. (2003). Effects of small-scale turbulence on net growth rate and size of ten species of marine dinoflagellates. *J. Phycol*. 39:83–94.

Sulzman, F. N., Krieger, N. R., Gooch, V. D., and Hastings, J. W. (1978). A circadian rhythm of the luciferin binding protein from *Gonyaulax polyedra. J. Comp. Physiol*. 128:251–7.

Suzuki, L., and Johnson, C. H. (2001). Algae know the time of day: circadian and photoperiodic programs. *J. Phycol*. 37:933–42.

Suzuki, T., Mitsuya, T., Imai, M., and Yamasaki, M. (1997). DSP toxin contents in *Dinophysis fortii* and scallops collected at Mutsu Bay, Japan. *J. Applied Phycol*. 8:509–15.

Sweeney, B. M. (1969). *Rhythmic Phenomena in Plants*. London and New York: Academic Press.

Sweeney, B. M. (1971). Laboratory studies of a green *Noctiluca* from New Guinea. *J. Phycol*. 7:53–8.

Sweeney, B. M. (1978). Ultrastructure of *Noctiluca miliaris* (Pyrrophyta) with green flagellate symbionts. *J. Phycol*. 14:116–20.

Sweeney, B. M. (1979). The bioluminescence of dinoflagellates. In *Biochemistry and Physiology of Protozoa*, ed. M. Levandowsky, and S. H. Hutner, Vol. 1, pp. 287–306. New York: Academic Press.

Sweeney, B. M. (1980). Intracellular source of bioluminescence. *Int. Rev. Cytol*. 68:173–95.

Swift, E., Biggley, W. H., and Seliger, H. H. (1973). Species of oceanic dinoflagellates in the genera *Dissodinium* and *Pyrocystis*: Interclonal and intraspecific comparisons of color and photon yield of bioluminescence. *J. Phycol*. 9:420–6.

Takishita, K., Ishida, K.-I., Ishikura, M., and Maruyama. T. (2005). Phylogeny of the *psbC* gene, coding a photosystem II component CP 43, suggests separate origins for the peridinin- and fucoxanthin derivative-containing plastids of dinoflagellates. *Phycologia* 44:26–34.

Taylor, D. L. (1969). On the regulation and maintenance of algal numbers in zooxanthellae-coelenterate symbiosis, with a note on the nutritional relationship in *Anemonia sulcata. J. Mar. Biol. Assoc. UK* 49:1057–65.

Taylor, D. L. (1971). On the symbiosis between *Amphidinium klebsii* (Dinophyceae) and *Amphiscolops langerhansi* (Turbellaria: Acoela). *J. Mar. Biol. Assoc. UK* 51:301–13.

Taylor, F. J. R. (1971). Scanning electron microscopy of thecae of the dinoflagellate genus *Ornithocercus. J. Phycol*. 7:249–58.

Taylor, F. J. R. (1999). Morphology (tabulation) and molecular evidence for dinoflagellate phylogeny reinforce each other. *J. Phycol*. 35:1–3.

Trench, R. K. (1993). Microlgal–invertebrate symbioses: a review. *Endocytobios Cell Res*. 9:135–75.

Triemer, R. E. (1982). A unique mitotic variation in the marine dinoflagellate *Oxyrrhis marina* (Pyrrophyta). *J. Phycol*. 18:399–411.

Vogel, K., and Meeuse, B. J. D. (1968). Characterization of the reserve granules from the dinoflagellate *Thecadinium inclination* Balech. *J. Phycol*. 4:317–18.

von Stosch, H. A. (1972). La signification cytologique de la "cyclose nucléaire" dans le cycle de vie des Dinoflagellés. *Soc. Bot. Fr., Memoires*, pp. 201–12.

von Stosch, H. A. (1973). Observations on vegetative reproduction and sexual life cycles of two freshwater dinoflagellates, *Gymnodinium pseudopalustre* Schiller and *Woloszynskia apiculata* sp. nov. *Br. Phycol. J*. 8:105–34.

Wang, J-T., and Douglas, A. E. (1997). Nutrients signals and photosynthate release by symbiotic algae. *Plant Physiol*. 114:631–6.

Wilcox, L. W., and Wedemeyer, G. J. (1991). Phagotrophy in the freshwater photosynthetic dinoflagellate *Amphidinium cryophilum. J. Phycol*. 27:600–9.

Windust, A. J., Hu, T., Wright, J. L. C., Quilliam, M. A., and McLachlan, J. L. (2000). Oxidative metabolism by *Thalassiosira weisflogii* (Bacillariophyceae) of a diol-ester of okadaic acid, the diarrhetic shellfish poisoning. *J. Phycol*. 36:342–50.

Withers, N. (1982). Ciguatera fish poisoning. *Annu. Rev. Med.* 33:97–111.

Yoon, H. S., Hackett, J. D., and Bhattacharya, D. (2002). A single origin of the peridinin- and fucoxanthin-containing plastids in dinoflagellates through tertiary endosymbiosis. *Proc. Natl. Acad. Sci., USA* 99:11724–9.

Zardoya, R., Costas, E., Lopez-Rodas, V., Garrido-Pertierra, A., and Bautista, J. M. (1995). Revised dinoflagellate phylogeny inferred from molecular analysis of large-subunit ribosomal RNA sequences. *J. Mol. Evol*. 41:637–45.

Zhou, J., and Fritz, L. (1994). Okadaic acid localizes to chloroplasts in the DSP-toxin-producing dinoflagellates *Prorocentrum lima* and *Prorocentrum maculosum. Phycologia* 33:455–61.

Chapter 8

Apicomplexa

Algae are organisms that have plastids, or organisms that are derived from cells whose ancestors possessed plastids. Until 1994, it was thought that the apicomplexa did not have plastids (and consequently were not covered in phycology textbooks). Then it was shown that a known organelle in many apicomplexa was actually a reduced colorless plastid called an apicoplast (Fig. 8.1) (Wilson, 1993; Wilson et al., 1994). Molecular studies have shown that the apicoplast and dinoflagellate plastids originated from red algae by a single endosymbiotic event that occurred relatively early in eukaryotic evolution (Fast et al., 2001).

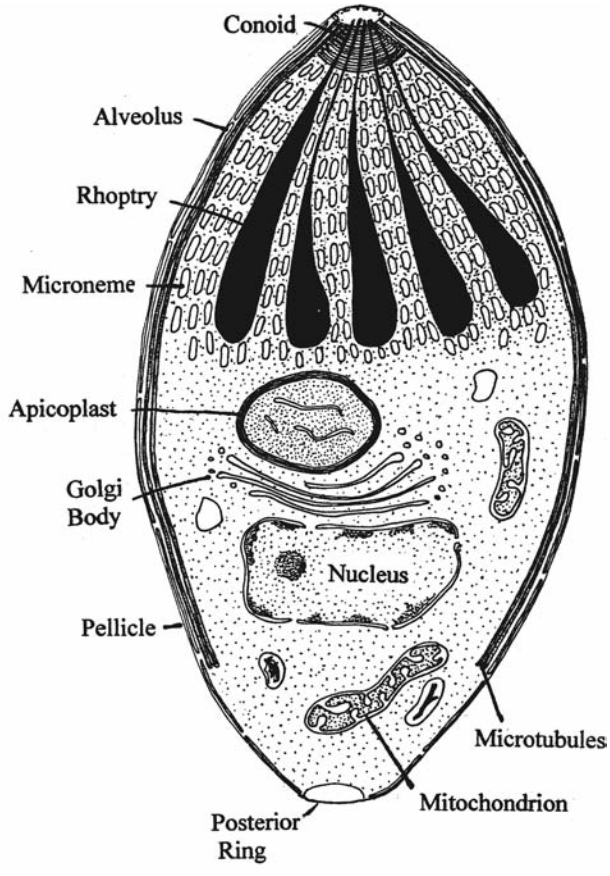


Fig. 8.1 Drawing of the basic cytology of an apicomplexan cell.

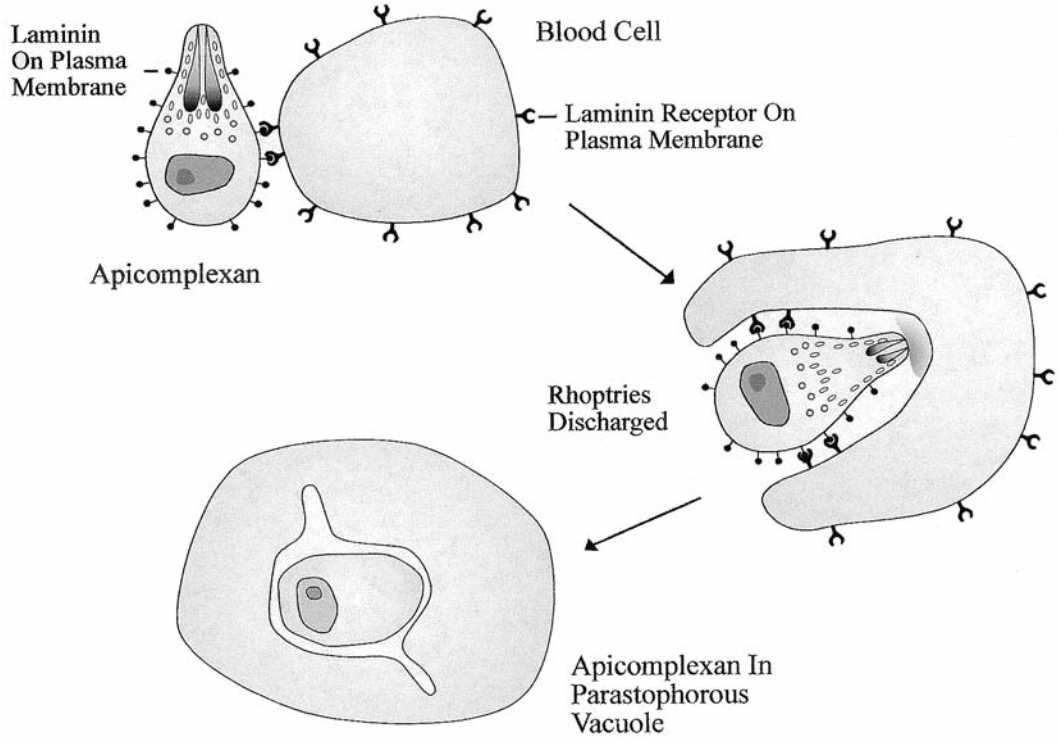


Fig. 8.2 General scheme by which an apicomplexan infects a blood cell. The apicomplexan has a characteristic laminin polysaccharide on the surface of the plasma membrane that binds with laminin receptors on the blood cell. This forms a tight junction between the apicomplexan and blood cell. The apicomplexan discharges its rhoptries. The blood cell phagocytoses the apicomplex into a parasitophorous vacuole. (Modified from Sam-Yellowe, 1996.)

The discovery of the apicoplast generated considerable interest since most apicomplexans are unicellular endoparasites that cause some of the most significant tropical diseases (Foth and McFadden, 2003). Malaria in humans is produced by the apicomplexan *Plasmodium*. About 300 million people are infected with malaria, leading to one million deaths annually (Ralph et al., 2004). Apicomplexans cause other serious diseases in livestock and humans, such as cryptosporidiosis, babesiosis (Texas cattle fever), theileriosis (East Coast fever), and toxoplasmosis. The realization that these endoparasites were once algae raised hopes that the apicoplast might be a drug target for two reasons. The first is that the apicoplast is essential for the survival of *Plasmodium* and *Toxoplasma*. The second is that drugs effective against prokaryotic organisms might be effective against the apicoplast since all plastids originally evolved from endosymbiotic prokaryotic cyanobacteria. Apicomplexans are absolutely dependent on the apicoplast, which has led to speculation that this curious organelle is a potential "Achilles heel" of parasites, such as *Plasmodium*.

The typical apicomplexan vegetative cell (merozoite) (Fig. 8.1) has an **apicoplast** surrounded by four membranes. The inner two membranes are the inner and outer plastid membranes while the outer membranes are derived from the vacuolar membrane and the plasma membrane of the endosymbiotic red alga.

The **apical complex** consists of a **polar ring** and a **conoid** formed of spirally coiled microtubules (Fig. 8.1). The apicomplexan has laminin polysaccharide on its surface while the host cell has a laminin receptor (Fig. 8.2). The apicomplexan parasite attaches to the host cell with the conoid protruding to produce a **stylet** that forms a tight junction between the apicomplexan parasite and host cell. The apicomplexan cell is taken

up into the host cell in the **parasitophorous vacuole**. The contents of the **rhoptries** and **micronemes** are emptied into the space between the apicomplexan plasma membrane and the parasitophorous vacuole membrane.

Apicomplexans have a layer of flattened membranous sacs or **alveoli** (Fig. 8.1) beneath the plasma membrane that comprise the subpellicular membrane complex, similar to that found in the dinoflagellates.

Katablepharis (Fig. 8.3) is a heterotrophic unicellular flagellate that lacks a plastid. *Katablepharis* cells have ejectisomes and was classified with the Cryptophyceae. However, ultrastructural studies (Lee and Kugrens, 1991; Lee et al., 1991) revealed the presence of an anterior conoid apparatus involved in phagocytosis of prey. The conoid apparatus is very similar to those of the apicomplexans and it is likely that *Katablepharis* should be classified as an apicomplexan.

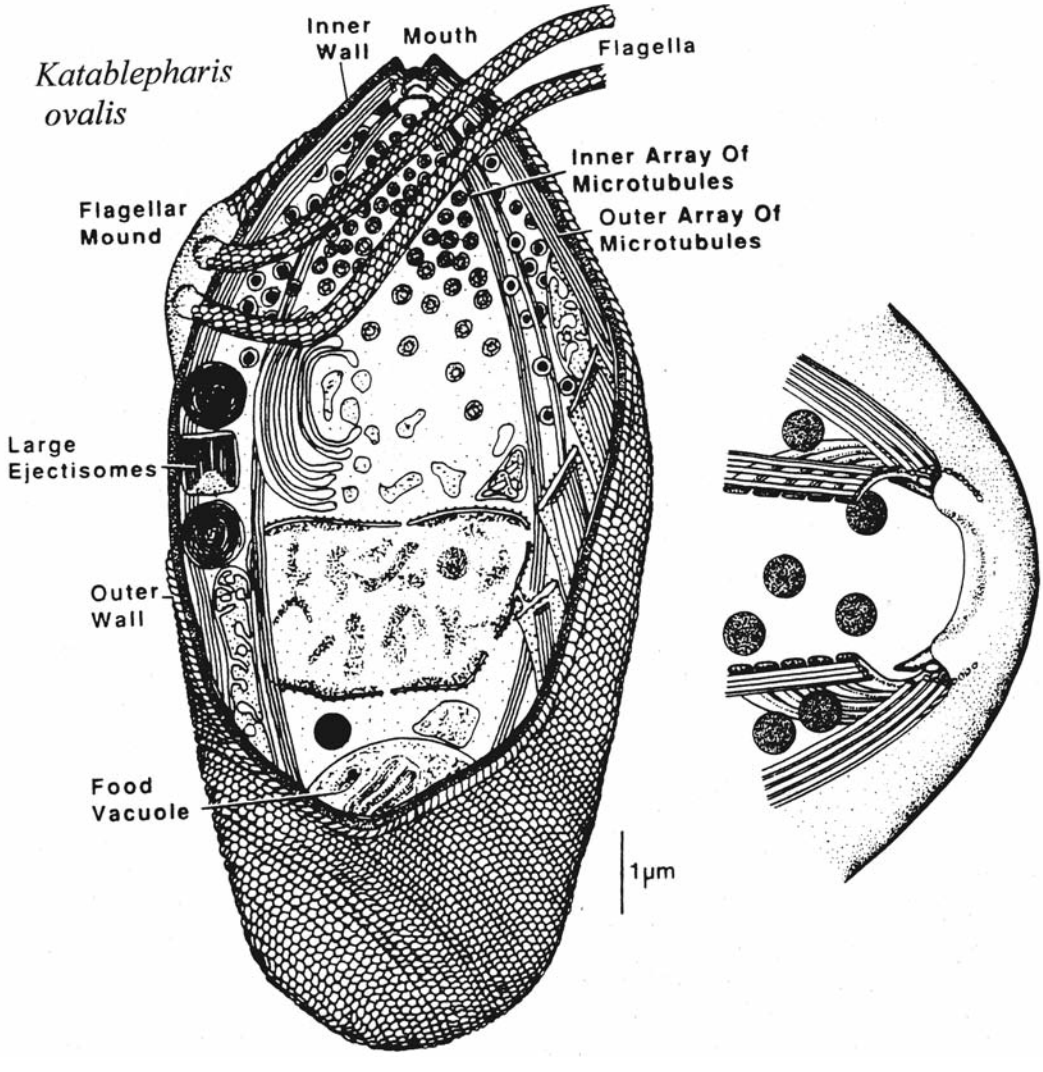


Fig. 8.3 Drawings of *Katablepharis ovalis*. *Left*: whole cell. *Right*: anterior part of cell. (From Lee and Kugrens, 1991; Lee et al., 1991.)

REFERENCES

Fast, N. M., Kissinger, J. C., Roos, D. S., and Keeling, P. J. (2001). Nuclear-encoded, plastid-targeted genes suggest a single common origin for apicomplexan and dinoflagellate plastids. *Mol. Biol. Evol.* 18:418–26.

Foth, B. J., and McFadden, G. I. (2003). The apicoplast: a plastid in *Plasmodium falciparum* and other apicomplexan parasites. *Int. Rev. Cytol.* 224:57–110.

Lee, R. E., and Kugrens, P. (1991). *Katablepharis ovalis,* a colorless flagellate with interesting cytological characteristics. *J. Phycol.* 27:505–15.

Lee, R. E., Kugrens, P., and Mylnikov, A. P. (1991). Feeding apparatus of the colorless flagellate *Katablepharis* (Cryptophyceae). *J. Phycol.* 27:725–33.

Ralph, S. A., van Dooren, G. G., Waller, R. F., et al. (2004). Metabolic maps and functions of the *Plasmodium falciparum* apicoplast. *Nat. Rev./Microbio.* 2:203–16.

Sam-Yellowe, T. Y. (1996). Rhoptry organelles of the Apicomplexa: their role in host cell invasion and intracellular survival. *Parasitol. Today* 12:308–16.

Wilson, R. J. (1993). Plastids better red than dead. *Nature* 366:638.

Wilson, R. J., Williamson, D. H., and Preiser, P. (1994). Malaria and other apicomplexans: the "plant" connection. *Infect. Agents Dis.* 3:29–37.

Part V

Evolution of two membranes of chloroplast endoplasmic reticulum and the Chlorarachniophyta

Algae with two membranes of chloroplast endoplasmic reticulum (chloroplast E.R.) have the inner membrane of chloroplast E.R. surrounding the chloroplast envelope. The outer membrane of chloroplast E.R. is continuous with the outer membrane of the nuclear envelope and has ribosomes on the outer surface (Fig. V.1).

The algae with two membranes of chloroplast E.R. evolved by a secondary endosymbiosis (Fig. V.1) (Lee, 1977) when a phagocytic protozoan took up a eukaryotic photosynthetic alga into a food vesicle. Instead of being phagocytosed by the protozoan, the photosynthetic alga became established as an endosymbiont within the food vesicle of the protozoan. The endosymbiotic photosynthetic alga benefited from the acidic environment in the food vesicle that kept much of the inorganic carbon in the form of carbon dioxide, the form needed by ribulose bisphosphate/carboxylase for carbon fixation (see Part IV for further explanation). The host benefited by receiving some of the photosynthate from the endosymbiotic alga. The food vesicle membrane eventually fused with the endoplasmic reticulum of the host protozoan, resulting in ribosomes on the outer surface of this membrane, which became the outer membrane of the chloroplast E.R. Through evolution, ATP production and other functions of the endosymbiont's mitochondrion were taken over by the mitochondria of the protozoan host, and the mitochondria of the endosymbiont were lost. The host nucleus also took over some of the genetic control of the endosymbiont, with a reduction in the size and function of the nucleus of the endosymbiont. The resulting cytology is characteristic of the extant algae in the Chlorarachniophyta and Cryptophyta, which have a nucleomorph representing the degraded endosymbiotic nucleus, as well as storage product produced in what remains of the endosymbiont cytoplasm.

The type of chloroplast E.R. that exists in the Heterokontophyta and the Prymnesiophyta resulted from further reduction. The nucleomorph

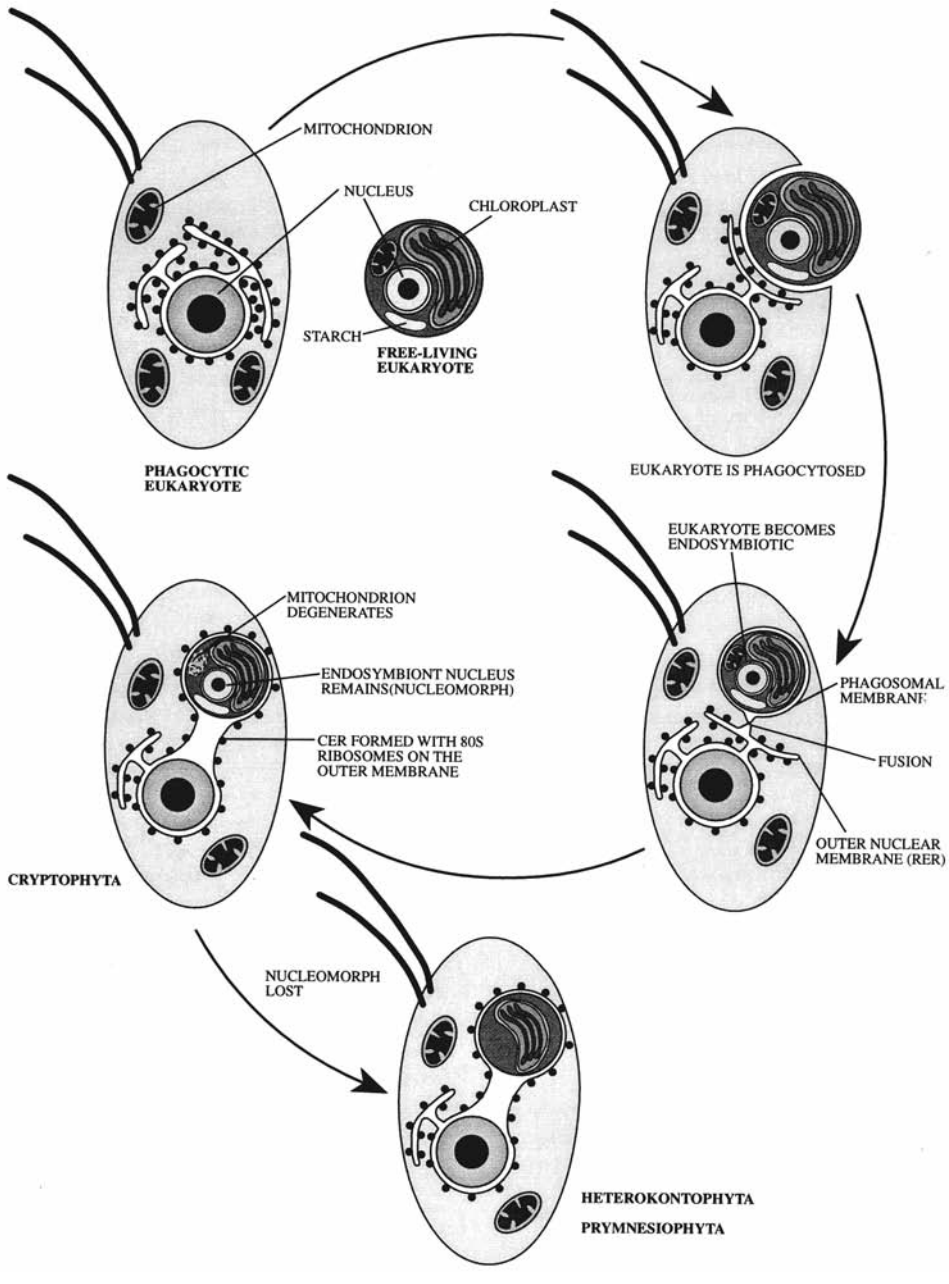


Fig. V.1 The sequence of events that led to the evolution of algae with two membranes of chloroplast endoplasmic reticulum. (Drawing by Brec Clay.)

was completely lost and storage product formation was taken over by the host. The resulting cell had two membranes of chloroplast envelope surrounding the chloroplast. Outside of this was the inner membrane of chloroplast E.R. that was the remains of the plasma membrane of the endosymbiont. Outside of this was the outer membrane of

chloroplast E.R. which was the remains of the food vesicle membrane of the host.

Although the above evolutionary scheme is discussed in one sequence, it is probable that two membranes of chloroplast E.R. evolved at least three times, with one line leading to the Chlorarachniophyta, a second to the Cryptophyta, and the third (or more) leading to the Heterokontophyta and Prymnesiophyta.

The algae with two membranes of chloroplast E.R. are:

Chlorarachniophyta: chloroplast derived from a green alga, chlorophyll *a* and *b* present, nucleomorph between inner and outer membrane of chloroplast E.R.

Cryptophyta: Chlorophyll *a* and *c*, phycobiliproteins, nucleomorph between inner and outer membranes of chloroplast E.R., starch in grains between inner membrane of chloroplast E.R. and chloroplast envelope, periplast inside plasma membrane, tripartite hairs on flagella.

Heterokontophyta: tripartite hairs on anterior tinsel flagellum, posterior whiplash flagellum, chlorophyll *a* and *c*, fucoxanthin, storage product usually chrysolaminarin in vesicles in cytoplasm.

Prymnesiophyta (haptophytes): two whiplash flagella, haptonema present, chlorophyll *a* and *c*, fucoxanthin, scales common outside cell, storage product usually chrysolaminarin in vesicles in cytoplasm.

Chlorarachniophyta

These algae (Fig. V.2) represent an intermediate stage in the evolution of two membranes of chloroplast endoplasmic reticulum. This group has a small number of green amoebae that have ingested green algal cells in the past, with the green algal cells evolving into endosymbionts within the amoeba host (Fig. V.3) (Hibberd and Norris, 1984). A **nucleomorph** or reduced nucleus occurs in the green algal symbiont. The reduced nature of the nucleomorph implies that some of the functions originally coded by the DNA of the endosymbiont nucleus have been taken over by the nucleus of the host amoeba. The chloroplast (e.g., endosymbiont chloroplast) contains chlorophyll *a* and *b* and is surrounded by four membranes. The innermost two membranes are those of the chloroplast envelope of the endosymbiont. The next membrane is the plasma membrane of the endosymbiont and the outer membrane represents the food-vacuole membrane of the amoeba host. Thus, the algae in the Chlorarachniophyta represent an intermediate stage in the evolution of the chloroplasts of some of the algae in the Heterokontophyta.

Chlorarachnion reptans is a marine amoeba that forms large plasmodia with the individual cells linked by a network of reticulopodia (Geitler, 1930; Hibberd and Norris, 1984). The cells are naked and contain a number of lobed chloroplasts, each with a central pyrenoid (Fig. V.3). Four

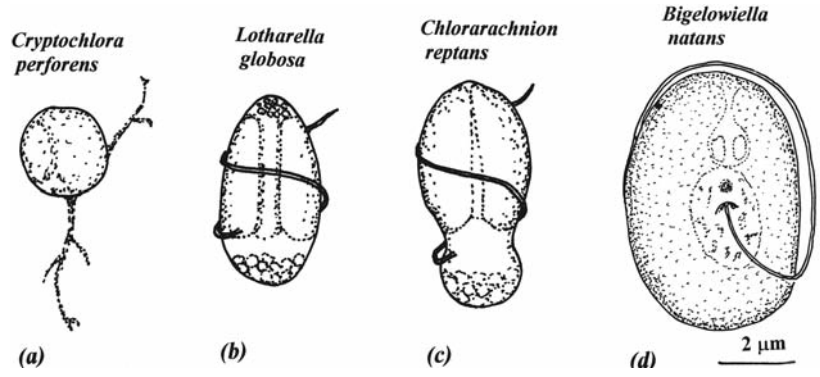


Fig. V.2 Examples of algae in the Chlorarachniophyta. ((*a*) adapted from Calderon-Saenz and Schnettner, 1989; (*b*) adapted from Ishida et al., 1996; (*c*) adapted from Hibberd and Norris, 1984; (*d*) adapted from Moestrup and Sengco, 2001.)

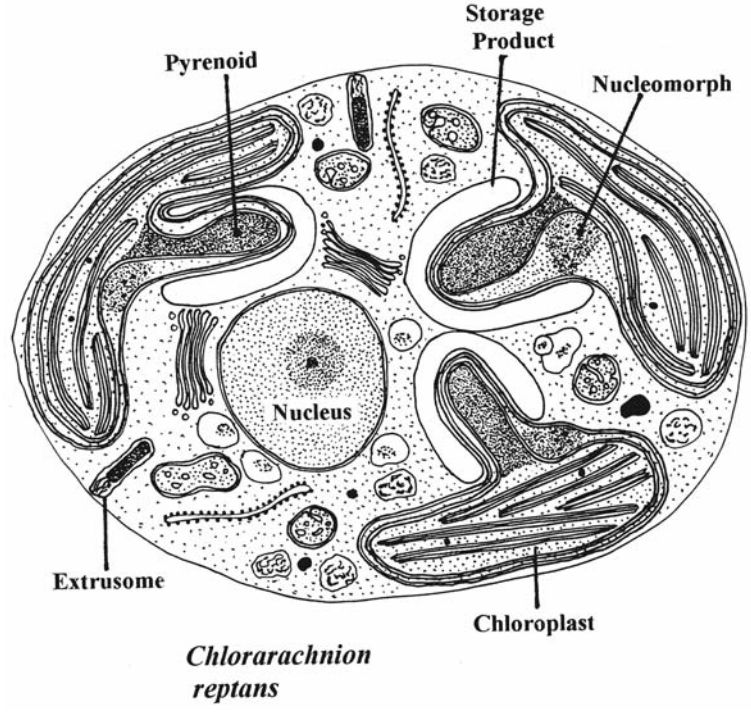


Fig. V.3 Semidiagrammatic drawing of the cell structure of *Chlorarachnion reptans*. (Adapted from Hibberd and Norris, 1984.)

membranes surround the chloroplast, which has a pyrenoid and nucleomorph. A vesicle containing the storage product caps the pyrenoid. *Chlorarachnion* means "green spider" for the web-like network of reticulopodia (pseudopodia) in which are embedded the green amoeboid cells.

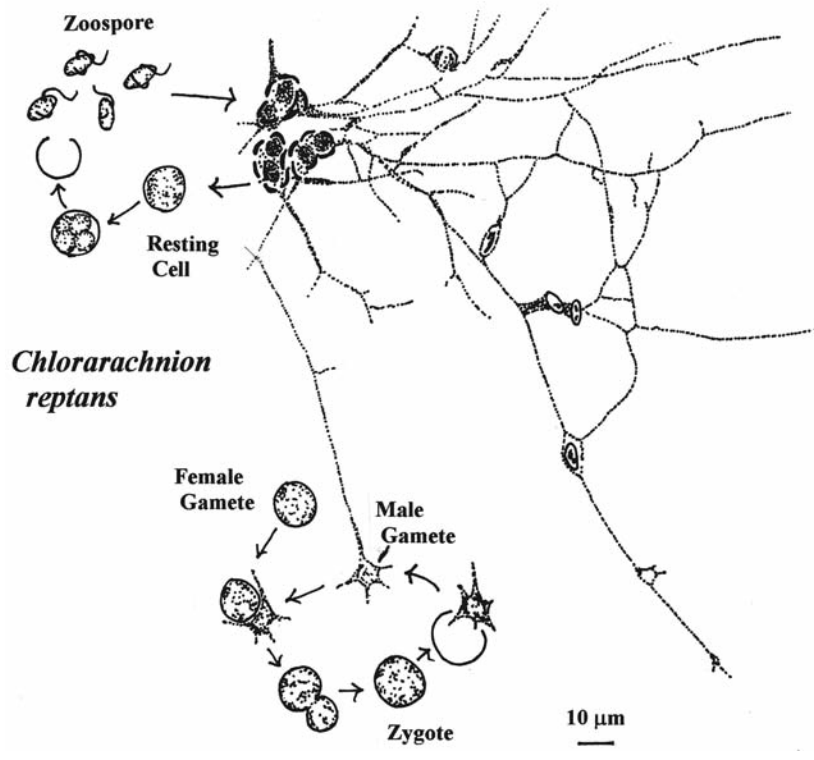


Fig. V.4 *Chlorarachnion reptans.* (Adapted from Hibberd and Norris, 1984; Grell, 1990.)

The cells move over the reticulopodia and ingest other algal cells and bacteria as a food source.

Under nutrient deprivation, the star-shaped vegetative cells become resting cells by retracting their reticulopodia, rounding up and secreting a thin cell wall (Grell, 1990). The resting cells apparently rely principally on photosynthate from the chloroplasts as a food source. The resting cells germinate to star-shaped vegetative cells under favorable conditions. Zoosporogenesis occurs by a resting cell dividing twice to produce four zoospores, each with a single flagellum wrapped around the cell body (Fig. V.1(*c*) and V.4). The zoospores settle to produce the star-shaped vegetative cells. Sexual reproduction occurs when a non-motile female gamete is approached by a motile, star-shaped, male gamete. The gametes fuse producing a zygote that germinates into a star-shaped vegetative cell (Grell, 1990).

REFERENCES

Calderon-Saenz, E., and Schnetter, R. (1989). Morphology, biology, and systematics of *Cryptochlora perforans* (Chloroarachniophyta), a phagotrophic marine alga. *Pl. Syst. Evol.* 163:165–76.

Geitler, L. (1930). Ein grunes Filarplaasmodium und andere neue Protisten. *Arch. Protistenkd.* 69:615–36.

Grell, K. G. (1990). Some light microscope observations on *Chlorarachnion reptans* Geitler. *Arch. Protistenkd.* 138:271–90.

Hibberd, D. J., and Norris, R. E. (1984). Cytology and ultrastructure of *Chlorarachnion reptans* (Chloroarachniophyta division nova, Chloroarachniophyceae classis nova). *J. Phycol.* 20:310–30.

Ishida, K., Nakayama, T., and Hara, Y. (1996). Taxonomic studies on the Chlorarchniophyta. II. Generic delimitation of the chlorarachniophytes and description of *Gymnochlora syellata* gen. et sp. nov. and *Lotharella* gen. nov. *Phycol. Res.* 44:37–45.

Lee, R. E. (1977). Evolution of algal flagellates with chloroplast endoplasmic reticulum from the ciliates. *South African J. Sci.* 73:179–82.

Moestrup, Ø., and Sengco, M. (2001). Ultrastructural studies on *Bigelowiella natans*, gen. et sp. nov., a chlorarachniophyte flagellate. *J. Phycol.* 37:624–6.

Chapter 9

Cryptophyta

CRYPTOPHYCEAE

This group is composed primarily of flagellates that occur in both marine and freshwater environments. The cells contain chlorophylls *a* and c_2 and phycobiliproteins that occur inside the thylakoids of the chloroplast. The cell body is asymmetric with a clearly defined dorsi-ventral/right-left sides (Figs. 9.1, 9.9, 9.10). The asymmetric cell shape results in a peculiar swaying motion during swimming. Most cryptophytes have a single lobed chloroplast with a central pyrenoid.

Cell structure

There are two apically or laterally attached flagella at the base of a depression. Each flagellum is approximately the same length as the body of the cell (Figs. 9.1, 9.8, 9.9, 9.10). Depending on the species, there are one or two rows of microtubular hairs attached to the flagellum. In *Cryptomonas* sp., the hairs on one flagellum are 2.5 μm long and in two rows whereas the hairs on the other flagellum are only 1 μm long and arranged in a single row (Heath et al., 1970; Kugrens et al., 1987). Small, 150-nm-diameter organic scales (Fig. 9.2) are common on the flagellar surface and sometimes on the cell body (Lee and Kugrens, 1986).

The outer portion of the cell, or **periplast** (Gantt, 1971), is composed of the plasma membrane and a plate, or series of plates, directly under the plasma membrane (Figs. 9.1, 9.10) (Kugrens and Lee, 1987). The number and shape of these plates are used to characterize genera taking into consideration that the haploid and diploid phases of a single genus can have different plates (Hoef-Emden and Melkonian, 2003). New periplast plates are added in an area adjacent to the vestibulum (Brett and Wetherbee, 1996). Sulfated fucose-rich polysaccharides can be excreted outside of the cell (Giroldo and Vieira, 2002).

The chloroplast most likely evolved from a symbiosis between an organism similar to the phagocytic cryptomonad *Goniomonas* and a red alga (Kugrens and Lee, 1991; Liaud et al., 1997; McFadden et al., 1994). The chloroplast is surrounded by two membranes of chloroplast endoplasmic reticulum and the two membranes of the chloroplast envelope (Fig. 9.1). Between the outer membrane and the inner membrane of the chloroplast endoplasmic reticulum are starch grains and a nucleomorph (Figs. 9.1, 9.4). The nucleomorph contains three minute paired-chromosomes with 531 genes (humans have at least 31 000 genes) that encode 30 proteins targeted into the chloroplast (Douglas et al., 2001; Cavalier-Smith, 2002). The nucleomorph is probably the remnant of the nucleus of the endosymbiont in the event that led to chloroplast E.R. The nucleomorph is surrounded by an envelope that has pores similar to those in a nuclear envelope. The nucleomorph exhibits a rudimentary type of division utilizing microtubules (Morrall and Greenwood, 1982). The nucleomorph divides in preprophase of the main nucleus following basal body replication, but before division of the chloroplast and the chloroplast endoplasmic reticulum (McKerracher

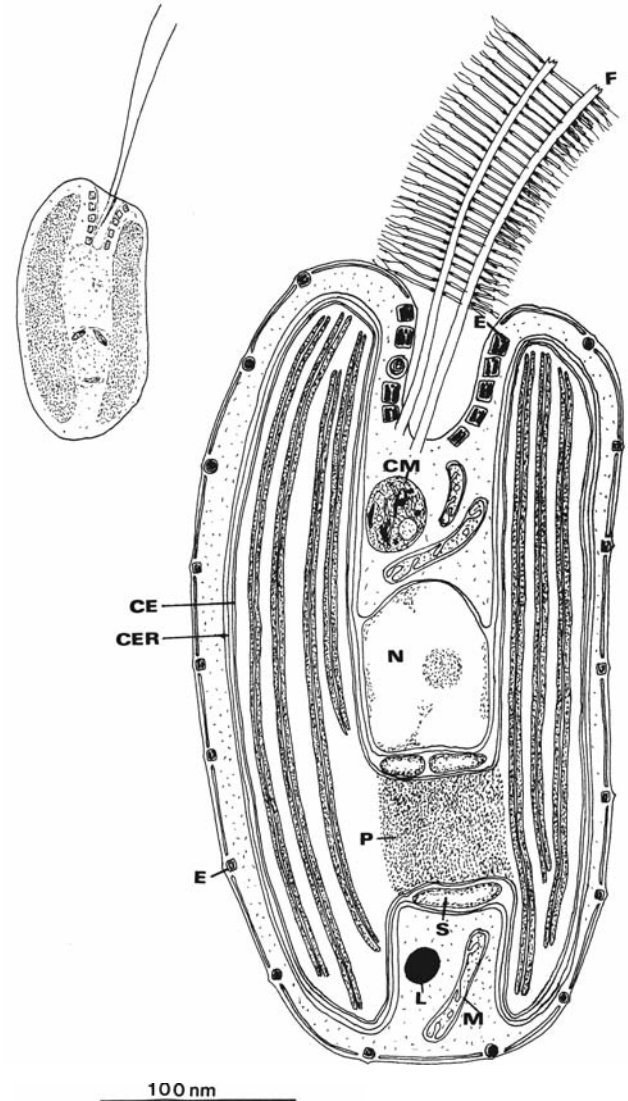


Fig. 9.1 Drawing of a cell of the Cryptophyceae as seen in the light and electron microscope. (CE) Chloroplast envelope; (CER) chloroplast endoplasmic reticulum; (CM) Corps de Maupas; (D) dorsal; (E) ejectisome; (L) lipid; (M) mitochondrion; (N) nucleus; (NM) nucleomorph; (P) pyrenoid; (PP) periplast plate; (S) starch; (V) ventral.

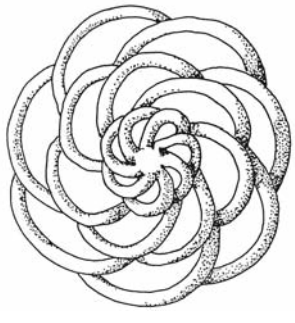


Fig. 9.2 Drawing of the most common type of flagellar scale found in freshwater cryptophytes. (From Lee and Kugrens, 1986.)

and Gibbs, 1982). The only cryptophyte that is known to lack a nucleomorph is *Goniomonas* (Figs. 9.8, 9.9(*c*)), a colorless cryptophyte that lacks a plastid. A second colorless cryptophyte, *Chilomonas* (Fig. 9.9(*b*)), is a reduced form of a photosynthetic cryptophyte and contains a leucoplast and a nucleomorph (McKerracher and Gibbs, 1982).

In the chloroplast, the thylakoids are grouped in pairs (Fig. 9.3), and there are no connections between adjacent thylakoids. The Cryptophyta is the only group to have this arrangement of thylakoids. Chlorophylls *a* and c_2 are present. The major carotenoid present is α-carotene, and the major xanthophyll, diatoxanthin. There are three spectral types of phycoerythrin and three spectral

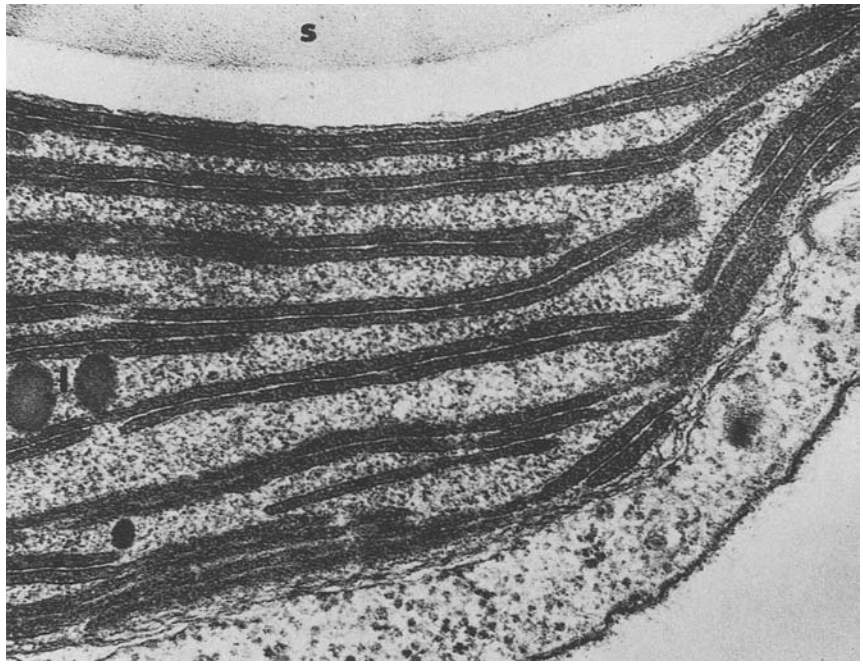


Fig. 9.3 Transmission electron micrograph of part of a chloroplast of *Chroomonas mesostigmatica*. The thylakoids are grouped in pairs. The dense contents of the thylakoids represent the phycobilisomes. Also present are lipid droplets (l) and a large starch grain (s). × 50 000. (From Dodge, 1969.)

types of phycocyanin, all of which are different from the phycobiliproteins found in the cyanobacteria and red algae (Hill and Rowan, 1989). The phycobiliproteins are in the intrathylakoid space (inside the thylakoids (Fig. 9.3) (Gantt et al., 1971; Spear-Bernstein and Miller, 1984), and are not on the stromal side of the thylakoids in phycobilisomes as occurs in the cyanobacteria and red algae. Each photosynthetic cryptophyte has only one species of phycobiliprotein – either a phycoerythrin or a phycocyanin – but never both. No allophycocyanin is present (Gantt, 1979). Allophycocyanin acts as a bridge in the transfer of light energy from phycoerythrin and phycocyanin to chlorophyll *a* of the reaction center in red algae and cyanobacteria. The presence of allophycocyanin may not be necessary in the cryptophytes because the greater absorption range of cryptophycean phycobiliproteins in conjunction with chlorophyll *c* overlaps the chlorophyll *a* absorption spectrum. There is a variation in the amount of pigments under different light-intensity conditions. Cells of *Cryptomonas* grown under low light-intensity conditions (10 μE m^{-2} s^{-1}) contain twice as much of chlorophylls *a* and c_2, and six times as much phycoerythrin per cell, as those grown under high light-intensity conditions (260 μE m^{-2} s^{-1}) (Thinh, 1983). Under low light-intensity conditions there is a higher concentration of phycoerythrin and the thylakoids are thicker.

The reserve product (similar in appearance to starch grains) is appressed to the pyrenoid area outside of the chloroplast envelope but inside the chloroplast E.R. The cryptophytes are the only algae that form their storage product in this area. The starch is an α-1,4-glucan composed of about 30% amylose and amylopectin. Cryptophycean starch is similar to potato starch and starch found in the green algae and dinoflagellates (Antia et al., 1979).

Some of the Cryptophyceae have eyespots. The eyespots that have been reported consist of lipid granules inside the chloroplast envelope. In *Chroomonas mesostigmatica*, the red eyespot is in the center of the cell (Fig. 9.4) and is an extension of the chloroplast beyond the pyrenoid (Dodge, 1969). In *Cryptomonas rostella*, the eyespot is

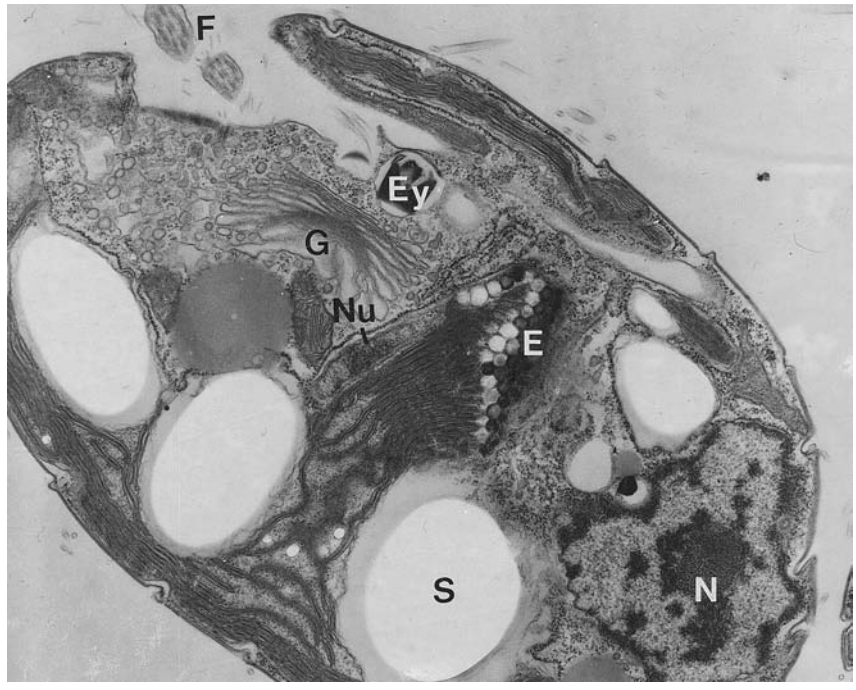


Fig. 9.4 Transmission electron micrograph of a cell of *Chroomonas mesostigmatica* showing the eyespot (E) present in the chloroplast. (Ey) Ejectisome; (F) flagellum; (G) Golgi; (N) nucleus; (Nu) nucleomorph; (S) starch. (Micrograph provided by Paul Kugrens.)

beneath the chloroplast membrane near the depression. Some of the Cryptophyceae exhibit positive phototaxis, with maximum sensitivity of the colorless *Chilomonas* being in the blue at 366 nm (Halldal, 1958).

The Cryptophyceae have projectiles called **ejectisomes**, which are of different structure from the trichocysts of the Dinophyceae and which are probably closely related to the R-bodies of the kappa particles of the ciliates (Hovasse et al., 1967; Kugrens et al., 1994). Within a cell there are usually large ejectisomes near the anterior depression and smaller ejectisomes around the cell periphery (Figs. 9.1, 9.4, 9.8). Both sizes of ejectisomes have the same structure; they are made up of two unequal-sized bodies enclosed within a single membrane (Fig. 9.5). Each of these bodies is a long tape curled up on a very tight spiral. The tape is tapered, with the greatest width being on the outside of the ejectisome. The smaller body is joined to the first and sits at an angle within the V-shaped portion of the larger body. The two bodies actually constitute one long tape with two spirals. The bodies are always arranged so that the smaller body is near the surface. The ejectisomes discharge when the organism is irritated (Fig. 9.5), the discharged ejectisome being a long tubular structure with a short portion at an angle to the long portion. The discharged small ejectisome from the cell periphery is 4 μm long, whereas that of a larger ejectisome from under the anterior depression is about 20 μm long. The discharge of the ejectisome results in a movement of the organism in the opposite direction. The discharge of the ejectisome could function as an escape mechanism, or it could be a direct defense mechanism causing damage to an offending organism. Ejectisomes originate in vesicles in the area of Golgi bodies.

The **Corps de Maupas** is a large vesicular structure in the anterior portion of the cell (Fig. 9.1). Its main function is probably that of disposing of unwanted protoplasmic structures by digestion (Lucas, 1970a,b).

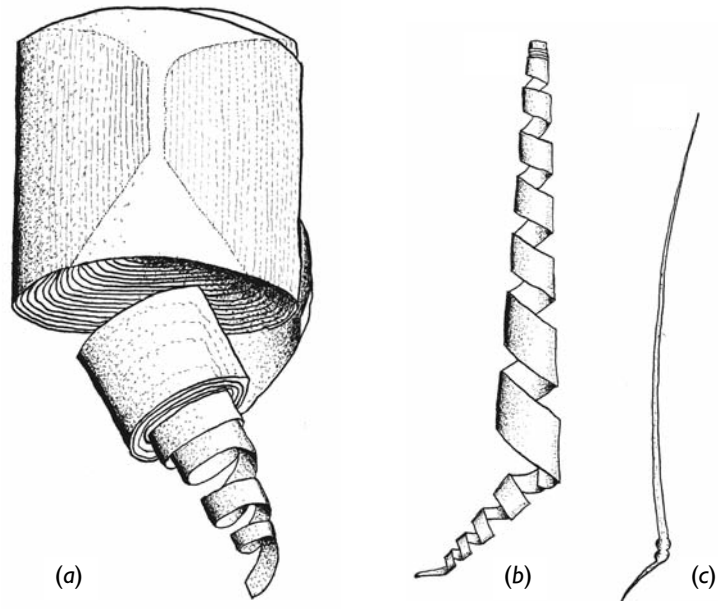


Fig. 9.5 (*a*) General organization of an ejectisome showing the two subparts. (*b*) A model of an ejectisome being fired outside of the cell. (*c*) A drawing of a discharged ejectisome. (After Hovasse et al., 1967.)

Ecology

In comparison with other algal groups, the Cryptophyta appear to be especially light sensitive, often forming the deepest living populations in clear oligotrophic lakes (Nauwerk, 1968). In higher mountain and north temperate lakes, cryptomonads and other flagellates are present in the water column throughout the winter. Because of the low light intensity under snow and ice cover, these algae concentrate in surface waters to receive sufficient light from net photosynthesis (Wright, 1964; Pechlauer, 1971). Survival at these extremely low light levels depends not only on a highly efficient photosynthetic system, but also on slow rates of cell respiration at low water temperatures and reduced winter zooplankton grazing. In spring, with the disappearance of snow and resulting sudden increase in light in Arctic and mountain lakes, cryptomonads suffer considerable light stress, such that the biomass maximum moves to deeper waters (Kalff and Welch, 1974).

Cryptophytes will often undergo diel vertical migrations with an amplitude less than 5 meters. In small humic forest lakes, species of *Cryptomonas* are positively phototactic in the morning, moving into the phosphorus-depleted upper layer. Later in the day the cells move away from the uppermost water layer, avoiding high levels of irradiance, and move into the phosphorus-rich hypolimnion (Knapp et al., 2003). A further advantage of this cycle is the reduction of grazing pressure by zooplankton (for which cryptophytes are a preferred food) (Loret et al., 2000) which often migrate in the reverse direction.

Cryptophyte algae are mixotrophic, capable of phototropy and phagotrophy. Phagocytotic ingestion of bacteria is thought primarily to provide a source of phosphorus and nitrogen in nutrient-limiting conditions (Urabe et al., 2000). These algae are also chemotactic, swimming in a straight line until they reach a nutrient patch, at which time the cells stop and tumble in the volume of high-nutrient concentration (Lee et al., 1999).

Cryptophytes are the dominant algae in the freshwater lakes of Antarctica. The best studied lakes are those in the McMurdo Dry Valleys (Fig. 9.6) (Roberts and Laybourne-Parry, 1999; McKnight et al., 2000). The McMurdo Dry Valleys are the largest ice-free areas in Antarctica (about 4000 km^2) and constitute a polar desert with temperatures ranging from -45 °C to 5 °C. These valleys remain ice free because the Trans-Antarctic Mountains not only block the flow of the ice sheet, but also block the flow of moisture, the valleys

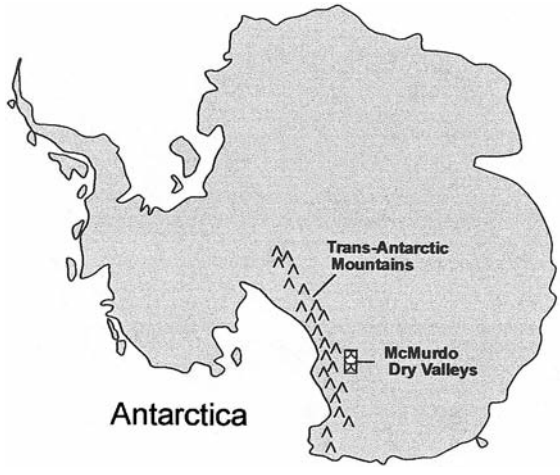


Fig. 9.6 The location of the McMurdo Dry Valleys in Antarctica.

receive only about 10 cm of snow a year. The lakes are fed by glacial melt streams that flow for 6–10 weeks during the brief austral (southern) summer. The lakes are perennially covered by debris-containing ice caps up to 5 m thick that reduce light penetration. In addition, the sun does not arise above the horizon for a number of months during the austral winter. These lakes are highly stratified because of a lack of forces that could generate turnover of the water column (e.g., wind, water temperature changes). Cryptophytes dominate the lower stratified levels where they live heterotrophically during winter months, taking up about one bacterium per hour by phagocytosis (Roberts and Laybourn-Parry, 1999). During the summer months, the cryptophytes are mixotrophic (combining heterotrophy and autotrophy by photosynthesis). A key to the survival of cryptophytes in this environment is maintaining the population in the vegetative state, rather than entering a resting state. The cryptophyte population can respond quickly when "good" conditions return in the short Antarctic summer.

Symbiotic associations

Mesodinium rubrum is a marine planktonic holotrich ciliate of extremely wide geographical distribution that colors the water in which it is growing red. It has been recorded from neritic locations such as bays and fjords; away from the coast it is usually associated with regions of upwelling and in such conditions the blooms have been recorded as extending over areas as large as 100 square miles. The color of the ciliate (Fig. 9.7) is due to numerous reddish-brown chloroplasts, which belong to a single cryptophycean alga that lives symbiotically inside the ciliate (Gustafson et al., 2000). The cryptophyte is surrounded by a single membrane, and has a nucleus and the normal cytology and pigments of the Cryptophyceae. The endosymbiotic cryptophyte is able to fix ^{14}C in the light, evolve oxygen in photosynthesis, and assimilate ^{32}P, indicating that it is a functioning autotroph. The association is probably similar to that of symbiotes in other classes, with the endosymbiont providing the host with photosynthate and the host providing the endosymbiont with a protected environment. Blooms of *Mesodinium rubrum* are a regular feature of upwelling ecosystems. The organism has three characteristics that enable it to compete effectively with other autotrophic plankton (Smith and Barber, 1979). (1) It is motile, swimming at rates of 2.0 to 7.2 m h^{-1}, an order of magnitude greater than the maximum swimming speeds attained by dinoflagellates. (2) It has strong phototropisms, being positively phototactic in an increasing light regime in the morning and negatively phototactic in decreasing light and in nutrient-depleted waters. (3) It has extremely high photosynthetic rates (1000 to 2000 mg C m^{-3} h^{-1}), equaling the highest ever observed for oceanic plankton. Conventional dinoflagellate or diatom blooms typically have only 60 to 70 mg C m^{-3} h^{-1}.

Classification

There are three recognizable groups within the Cryptophyceae (Marin et al., 1998; Deane et al., 2002):

Order 1 Goniomonadales: colorless cells with no plastids.

Order 2 Cryptomonadales: cells usually reddish in color with chloroplasts containing the phycobiliprotein Cr-phycoerythrin.

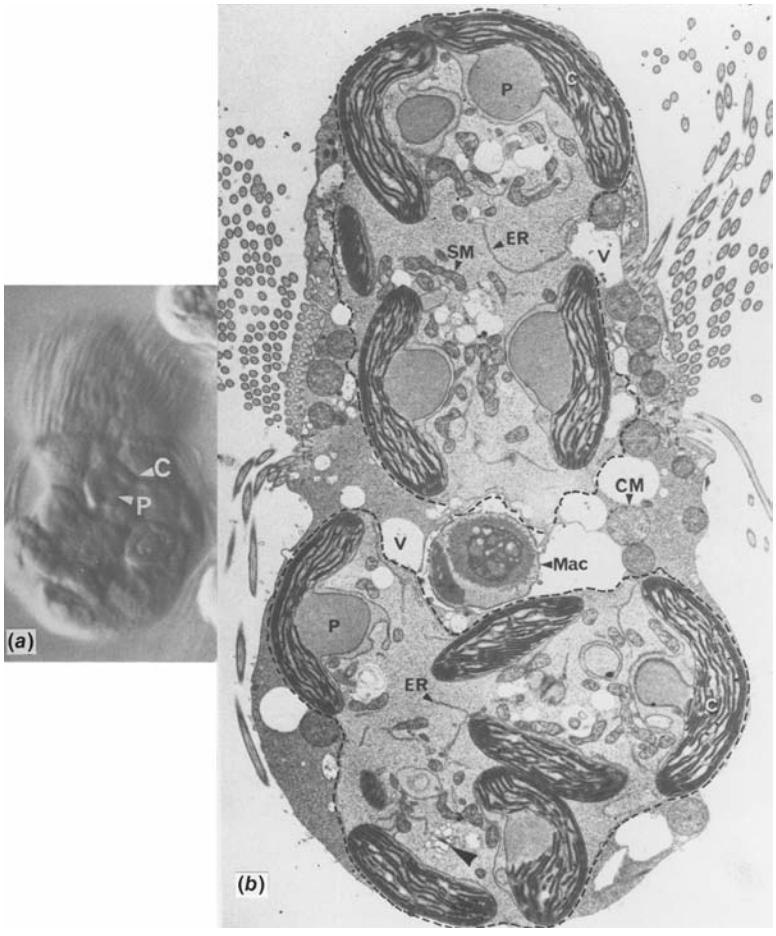


Fig. 9.7 *Mesodinium rubrum* with its cryptomonad symbiont. (*a*) Light micrograph of the ciliate showing the chloroplast (C) and pyrenoid (P) of the cryptomonad endosymbiont. (*b*) Transmssion electron micrograph. The dotted lines indicate the boundary between the cytoplasm of the ciliate and the cryptomonad symbiont; the difference in density of the two cells is particularly clear. The symbiont nucleus, one of the macronuclei, and the micronucleus of the ciliate are out of the plane of the section. (CM) Ciliate mitochondrion; (ER) endoplasmic reticulum; (Mac) macronucleus; (P) pyrenoid; (SM) symbiont mitochondrion; (V) vacuole. The large arrowhead indicates a possible region of Golgi activity. × 4500. (From Hibberd, 1977.)

Order 3 Chroomonadales: the remainder of the cryptophyte algae, often blue-green in color due to chloroplasts containing the phycobiliprotein Cr-phycocyanin.

Goniomonadales

Goniomonas (Figs. 9.8, 9.9(*c*)), a colorless alga with freshwater and marine species, is the sole alga in the order. *Goniomonas* is colorless and does not contain a plastid. Food organisms are taken up by an anterior tubular invagination, the infundibulum, and digested in food vacuoles in the cytoplasm. Storage granules occur inside an extension of the outer membrane of the nuclear envelope. Large ejectisomes occur under the anterior plasma membrane and small ejectisomes occur between the periplast plates.

Cryptomonadales

Cryptomonas (Figs. 9.9(*a*), 9.10, 9.11) and *Chilomonas* (Fig. 9.9(*b*)) are the only two genera in the order. *Cryptomonas* spp. are reddish in color due to the presence of the phycobiliprotein Cr-phycoerythrin in a bilobed chloroplast joined in the center by a pyrenoid. *Chilomonas* is a reduced form of *Cryptomonas* (Hoef-Emden and Melkonian, 2003) containing a leucoplast without photosynthetic pigments.

Cryptomonas has an asymmetric shape, which can be attributed, in part, to a subapical depression called the **vestibulum** which may extend internally to form a **gullet** or progress along the ventral surface into a **furrow** (Fig. 9.10(*b*)) (Kugrens and Lee, 1991). Large ejectosomes occur in rows under the furrow. Sexual reproduction occurs in *Cryptomonas* (Fig. 9.11) (Kugrens and Lee, 1988).

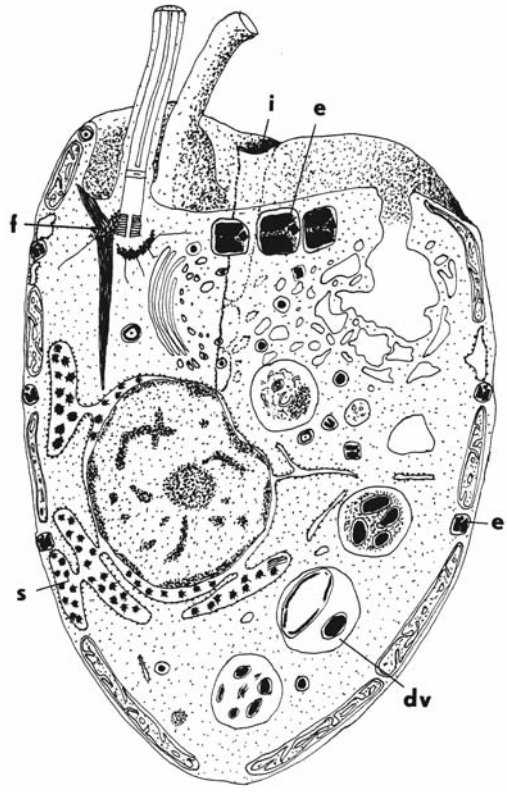


Fig. 9.8 Reconstruction of a cell of *Goniomonas truncata*. (f) Flagellar roots; (s) storage granules; (e) ejectisome; (dv) digestive vacuole; (i) infundibulum. (After Mignot, 1965.)

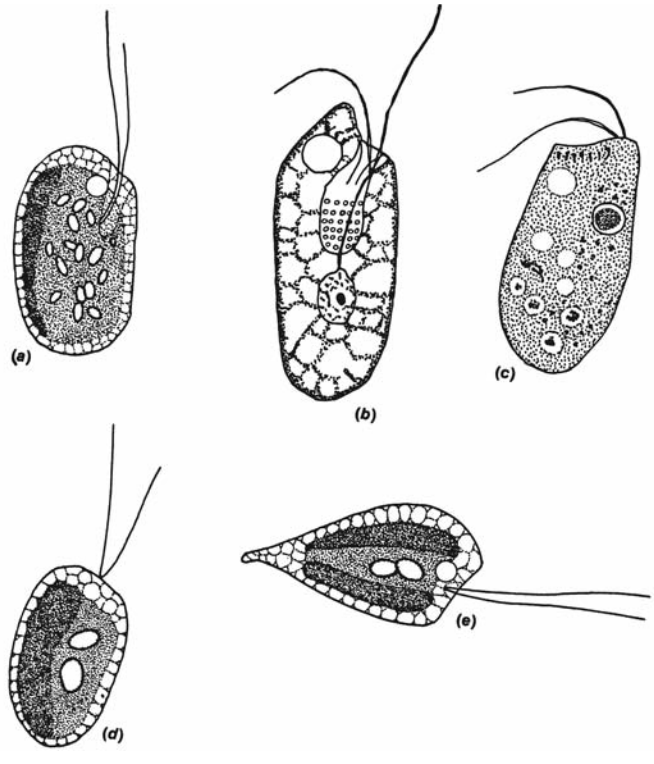


Fig. 9.9 (*a*) *Cryptomonas erosa.* (*b*) *Chilomonas paramecium.* (*c*) *Goniomonas truncata.* (*d*) *Rhodomonas lacustris.* (*e*) *Chroomonas nordstedtii.*

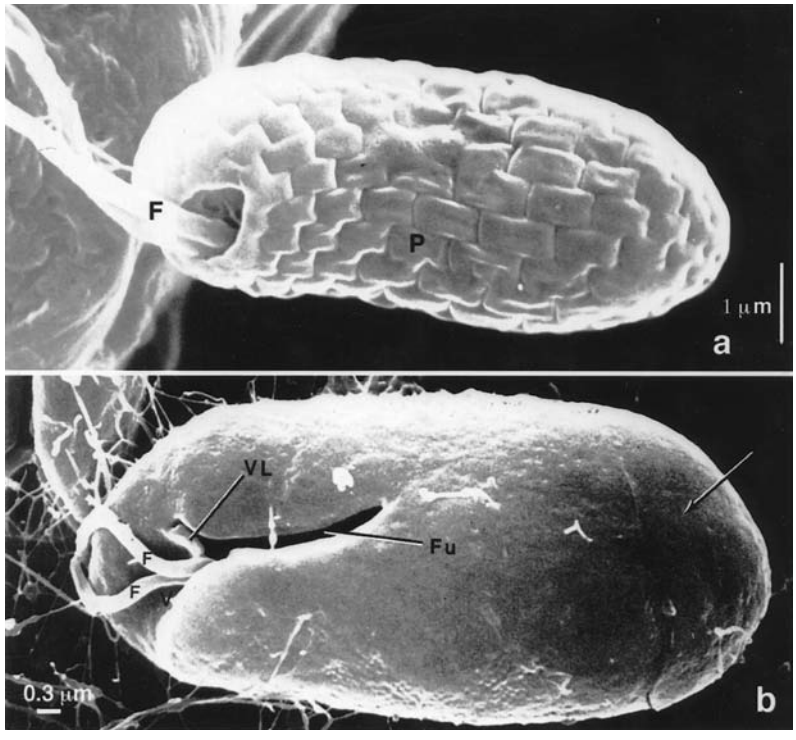


Fig. 9.10 Scanning electron micrographs of *Chroomonas oblonga* (*a*) and *Cryptomonas sp.* (*b*). *Chroomonas oblonga* has multiple periplast plates (P) under the plasma membrane, no furrow is present, and the flagella (F) arise from an anterior vestibular depression. *Cryptomonas* sp. has a smooth surface that is produced by a single periplast plate under the plasma membrane. The furrow (Fu) is an extension of the anterior vestibulum. A vestibular ligule (VL) overlaps the vestibulum. (From Kugrens et al., 1986.)

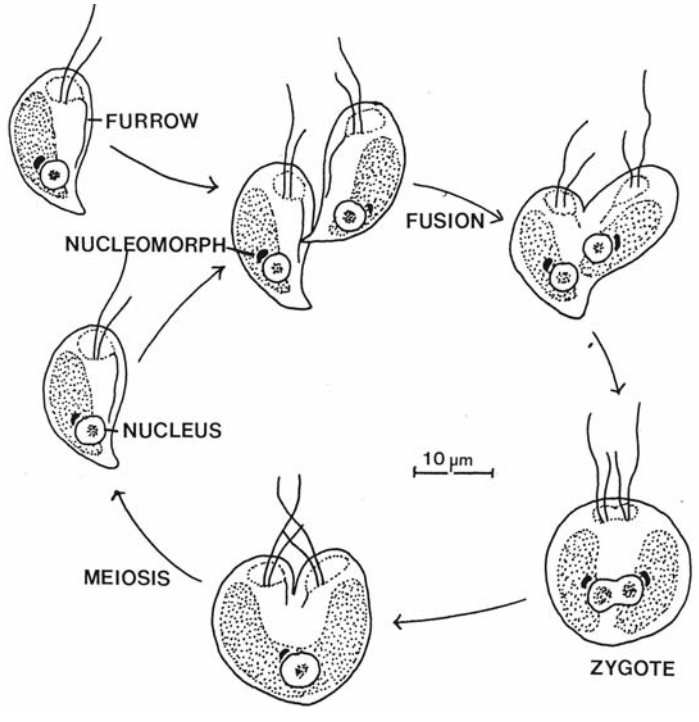


Fig. 9.11 The life cycle of *Cryptomonas* sp. (Adapted from Kugrens and Lee, 1988.)

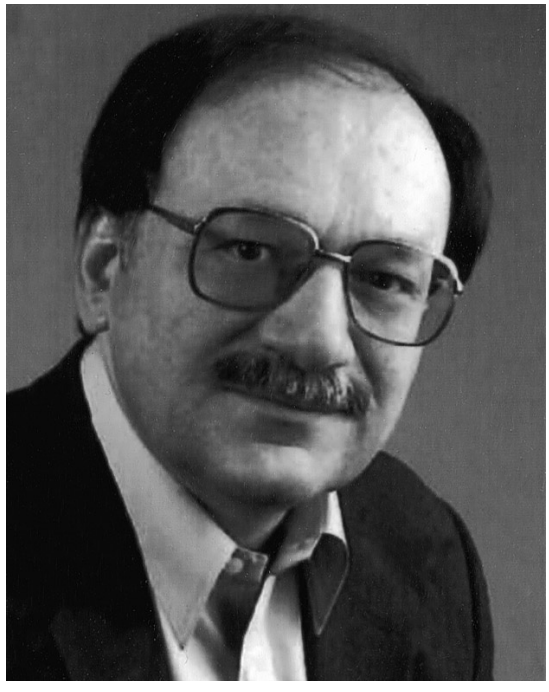


Fig. 9.12 **Michael Melkonian** Born October 4, 1948. Dr. Melkonian received a Diploma in Biology (1974) from the University of Hamburg. From 1978 to 1983, he was Wissenschaftlicher Assistent at the Botanisches Institut, University of Münster, and in 1983 Habilitation (Venia Legendi) in Botany and Privatdozent at the Botanisches Institut. From 1986 to 1988 he was a Heisenberg Fellow, German Research Foundation (DFG), at Münster. In 1988 he moved to the Institute of Botany at the University of Cologne where he is a full professor.

Chroomonadales

The remaining cyptophyte algae are placed in this order. Many, though not all, of these algae are blue-green in color due to the presence of the phycobiliproteins Cr-phycocyanin in the chloroplasts. *Chroomonas* (Fig. 9.9(*e*)) has an anterior vestibulum in the chloroplast. *Chroomonas* (Figs. 9.9(*e*), 9.10(*a*)) has an anterior vestibulum through which the two flagella emerge.

REFERENCES

Antia, N. J., Cheng, J. Y., Foyle, R. A. J., and Percival, E. (1979). Marine cryptomonad starch from autolysis of glycerol-grown *Chroomonas salina*. *J. Phycol*. 15:57–62.

Brett, S. J., and Wetherbee, R. (1996). Periplast development in Cryptophyceae. II. Development of the inner periplast component in *Rhinomonas pauea*, *Proteomonas sulcata* [haplomorph], *Rhodomonas baltica*, and *Cryptomonas ovata*. *Protoplasma* 192:40–8.

Cavalier-Smith, T. (2002). Nucleomorphs: enslaved algal nuclei. *Curr. Opin. Microbiol.* 5:612–9.

Deane, J. A., Strachan, I. M., Saunders, G. W., Hill, D. R. A., and McFadden, G. I. (2002). Cryptomonad evolution: nuclear 18S rDNA phylogeny versus cell morphology and pigmentation. *J. Phycol*. 38:1236–44.

Dodge, J. D. (1969). The ultrastructure of *Chroomonas mesostigmatica* Butcher (Cryptophyceae). *Arch. Mikrobiol*. 69:266–80.

Douglas, S., Zauner, S., Fraunholz, M., et al. (2001). The highly reduced genome of an enslaved algal nucleus. *Nature* 410:1091–6.

Gantt, E. (1971). Micromorphology of the periplast of *Chroomonas* sp. (Cryptophyceae). *J. Phycol*. 7:177–84.

Gantt, E. (1979). Phycobiliproteins of Cryptophyceae. In *Biochemistry of Protozoa*, ed. N. Levandowsky, and S. A. Hutner, pp. 121–37. New York: Academic Press.

Gantt, E., Edwards, M. R., and Provasoli, L. (1971). Chloroplast structure of the Cryptophyceae. Evidence for phycobiliproteins within the intrathylakoidal spaces. *J. Cell Biol*. 48:280–90.

Giroldo, D., and Vieira, A. A. H. (2002). An extracellular surface fucose-rich polysaccharide produced by a tropical strain of *Cryptomonas obovata* (Cryptophyceae). *J. Appl. Phycol.* 14:185–91.

Gustafson, D. E., Stoecker, D. K., Johnson, M. D., van Heukelem, W. F., and Sneider, K. (2000). Cryptophyte algae are robbed of their organelles by the marine ciliate *Mesodinium rubrum*. *Nature* 405:1049–52.

Halldal, P. (1958). Action spectra of phototaxis and related problems in Volvocales: *Ulva*-gametes and Dinophyceae. *Physiol. Plant*. 11:118–53.

Heath, I. B., Greenwood, A. D., and Griffiths, H. B. (1970). The origin of flimmer in *Saprolegnia*, *Dictyuchus*, *Synura* and *Cryptomonas*. *J. Cell Sci*. 7:445–61.

Hibberd, D. J. (1977). Observations on the ultrastructure of the cryptomonad endosymbiont of the red water ciliate *Mesodinium rubrum*. *J. Mar. Biol. Assoc. UK* 57:45–61.

Hill, D. R. A., and Rowan, K. S. (1989). The biliproteins of the Cryptophyceae. *Phycologia* 28:455–3.

Hoef-Emden, K., and Melkonian, M. (2003). Revision of the genus *Cryptomonas* (Cryptophyceae): a combination of molecular phylogeny and morphology provides insights into a long-hidden dimorphism. *Protist* 154:371–409.

Hovasse, R., Mignot, J. P., and Joyon, L. (1967). Nouvelles observations sur les trichocystes des Cryptomonadines et les "R bodies" des particules kappa de *Paramecium aurelia* Killer. *Prostistologica* 3:241–55.

Kalff, J., and Welch, H. E. (1974). Phytoplankton production in Char Lake, a natural polar lake, Cornwallis Is., Northwest Territories. *J. Fish. Res. Board Can*. 31:621–36.

Knapp, C. W., deNoyelles, F., Graham, D. W., and Bergin, S. (2003). Physical and chemical conditions surrounding the diurnal vertical migration of *Cryptomonas* spp. (Cryptophyceae) in a seasonally stratified midwestern reservoir (USA). *J. Phycol*. 39:855–61.

Kugrens, P., and Lee, R. E. (1987). An ultrastructural survey of cryptomonad periplasts using quick-freezing freeze-fracture techniques. *J. Phycol*. 23:365–76.

Kugrens, P., and Lee, R. E. (1988). Ultrastructure of fertilization in a cryptomonad. *J. Phycol*. 24:385–93.

Kugrens, P., and Lee, R. E. (1991). Organization of cryptomonads. In *The Biology of Free-living Heterotrophic Flagellates*, ed. P. J. Patterson, and J. Larsen, pp. 219–33. Oxford: Clarendon Press.

Kugrens, P., Lee, R. E., and Kugrens, P. (1986). The occurrence and structure of flagellar scales in some freshwater cryptophytes. *J. Phycol*. 22:549–52.

Kugrens, P., Lee, R. E., and Andersen, R. A. (1987). Ultrastructural variations in cryptomonad flagella. *J. Phycol*. 23:511–18.

Kugrens, P., Lee, R. E., and Corliss, J. O. (1994). Ultrstructure, biogenesis, and functions of extrusive organelles in selected non-ciliate protists. *Protoplasma* 181:164–90.

Lee, E. S., Lewitus, A. J., and Zimmer, R. K. (1999). Chemoreception in a marine cryptophyte: behavioral plasticity in response to amino acids and nitrate. *Limnol. Oceanogr*. 44:1571–4.

Lee, R. E., and Corliss, J. O. (1994). Ultrastructure, biogenesis, and functions of extrusive organelles in selected non-ciliate protists. *Protoplasma* 181:164–90.

Lee, R. E., and Kugrens, P. (1986). The occurrence and structure of flagellar scales in some freshwater cryptophytes. *J. Phycol*. 22:549–52.

Liaud, M-F., Brandt, U., Scherzinger, M., and Cerff, R. (1997). Evolutionary origin of cryptomonad microalgae. Two novel chloroplast/cytosol-specific GAPDH genes as potential markers of ancestral endosymbiont and host cell components. *J. Mol. Evol*. 44 (Suppl. 1): 528–37.

Loret, P., Pastoureaud, A., Bacher, C., and Delesalle, B. (2000). Phytoplankton composition and selective feeding of the pearl oyster *Pinctada margaitifera* in the Takapoto lagoon (Tuamotu Archipelago, French Polynesia): *in situ* study using optical microscopy and HPLC pigment analysis. *Mar. Ecol. Progr. Ser.* 199:55–67.

Lucas, I. A. N. (1970a). Observations on the fine structure of the Cryptophyceae. I. The genus *Cryptomonas. J. Phycol*. 6:30–8.

Lucas, I. A. N. (1970b). Observations on the ultrastructure of representatives of the genera *Hemiselmis* and *Chroomonas* (Cryptophyceae) *Br. Phycol. J.* 5:29–37.

McFadden, G. I., Gilson, P. R., and Hill, D. R. A. (1994). *Goniomonas*: rRNA sequences indicate that this phagotrophic flagellate is a close relative of the host component of cryptomonads. *Eur. J. Phycol*. 29:29–32.

McKerracher, L., and Gibbs, S. P. (1982). Cell of nucleomorph division in the alga *Cryptomonas. Can. J. Bot*. 60:2440–52.

McKnight, D. M., Howes, B. L., Taylor, C. D., and Goehringer, D. D. (2000). Phytoplankton dynamics in a stably stratified Antarctic lake during winter conditions. *J. Phycol*. 36:852–61.

Maier, U-G., Hofmann, C. J. B., Eschbach, S., Wolters, J., and Igloi, G. (1991). Demonstration of nucleomorph-encoded small subunit ribosomal RNA in cryptomonads. *Mol. Gen. Genet*. 230:155–60.

Marin, B., Klingberg, M., and Melkonian, N. (1998). Phylogenetic relationships among the Cryptophyta: analyses of nuclear-encoded SSU rRNA sequences support the monophyly of extant plastid-containing lineages. *Protist* 149:265–76.

Mignot, J. P. (1965). Etrude ultrastructurale de *Cyathomonas truncata* From. (Flagellé Cryptomonadine). *J. Microscopie* 4:239–52.

Morrall, S., and Greenwood, A. D. (1982). Ultrastructure of nucleomorph division in species of Cryptophyceae and its evolutionary implications. *J. Cell Sci.* 54:311–28.

Nauwerk, A. (1968). Das Phytoplankton des Latnjajaure 1954–55. *Schweiz. Z. Hydrol*. 30:188–216.

Pechlauer, R. (1971). Factors that control the production rate and biomass of phytoplankton in high-mountain lakes. *Mitt. Int. Ver. Theor. Angew. Limnol*. 19:124–5.

Roberts, E. C., and Laybourn-Parry, J. (1999). Mixotrophic cryptophytes and their predators in the Dry Valley lakes of Antarctica. *Freshwater Biol*. 41:737–46.

Smith, W. O., and Barber, R. T. (1979). A carbon budget for the autotrophic ciliate *Mesodinium rubrum. J. Phycol*. 15:27–33.

Spear-Bernstein, L., and Miller, K. R. (1984). Unique localization of the phycobiliprotein light-harvesting pigment in the Cryptophyceae. *J. Phycol*. 25:412–19.

Thinh, L-V. (1983). Effect of irradiance on the physiology and ultrastructure of the marine cryptomonad, *Cryptomonas* strain Lis (Cryptophyceae). *Phycologia* 22:7–11.

Urabe, J., Gurung, T. B., Yoshida, T., et al. (2000). Diel changes in phagotrophy by *Cryptomonas* in Lake Biwa. *Limnol. Oceanogr.* 45:1558–63.

Wright, R. T. (1964). Dynamics of a phytoplankton community in an ice-covered lake. *Limnol. Oceanogr*. 9:163–78.

Chapter 10

Heterokontophyta

The algae in the Heterokontophyta usually have cells with an anterior tinsel and posterior whiplash flagellum (Fig. 10.1). The plastids contain chlorophylls *a* and *c* along with fucoxanthin. The storage product is usually chrysolaminarin in cytoplasmic vesicles.

The following classes are commonly recognized (Andersen, 2004):

Chrysophyceae (golden-brown algae) (Chapter 10)
Synurophyceae (Chapter 11)
Eustigmatophyceae (Chapter 12)
Pinguiophyceae (Chapter 13)
Dictyochophyceae (silicoflagellates) (Chapter 14)
Pelagophyceae (Chapter 15)
Bolidophyceae (Chapter 16)
Bacillariophyceae (diatoms) (Chapter 17)
Raphidophyceae (chloromonads) (Chapter 18)
Xanthophyceae (yellow-green algae) (Chapter 19)
Phaeothamniophyceae (Chapter 20)
Phaeophyceae (brown algae) (Chapter 21)

CHRYSOPHYCEAE

The Chrysophyceae are distinguished chemically by having chlorophylls *a*, c_1, and c_2 (Andersen and Mulkey, 1983) and structurally by two flagella inserted into the cell perpendicular to each other, one photoreceptor on the short flagellum that is usually shaded by an eyespot in the anterior portion of the chloroplast, contractile vacuoles in the anterior portion of the cell, chloroplast endoplasmic reticulum, and radially or biradially symmetrical silica scales (if they are present). The storage product is chrysolaminarin. Many members of the class produce statospores enclosed in a silicified wall with a terminal pore.

Most of the species in the Chrysophyceae are freshwater and occur in soft waters (low in calcium). Many of the freshwater species are in the plankton of lakes where they are present in abundance. The coccoid and filamentous genera are found mostly in cold springs and brooks, where they occur as gelatinous or crustous growths on stones and woodwork. Most of the Chrysophyceae are sensitive to changes in the environment and survive the unfavorable periods as statospores.

Cell structure

Flagella and eyespot

Many of the Chrysophyceae have a tinsel flagellum that is inserted at the anterior end of the cell parallel to the cell axis (Fig. 10.1) and a whiplash flagellum that is inserted approximately perpendicular to the tinsel flagellum. The whiplash flagellum is often reduced to a short stub. The hairs on the tinsel flagellum are usually tripartite microtubular hairs (Hill and Outka, 1974), although tripartite and fibrillar hairs have been reported in *Ochromonas* (Bouck, 1971) (Fig. 10.2). Flagellar scales have been seen in a couple of genera (Andersen, 1982). The posterior whiplash flagellum is usually the shorter flagellum and has a swelling at its base on the side toward the cell

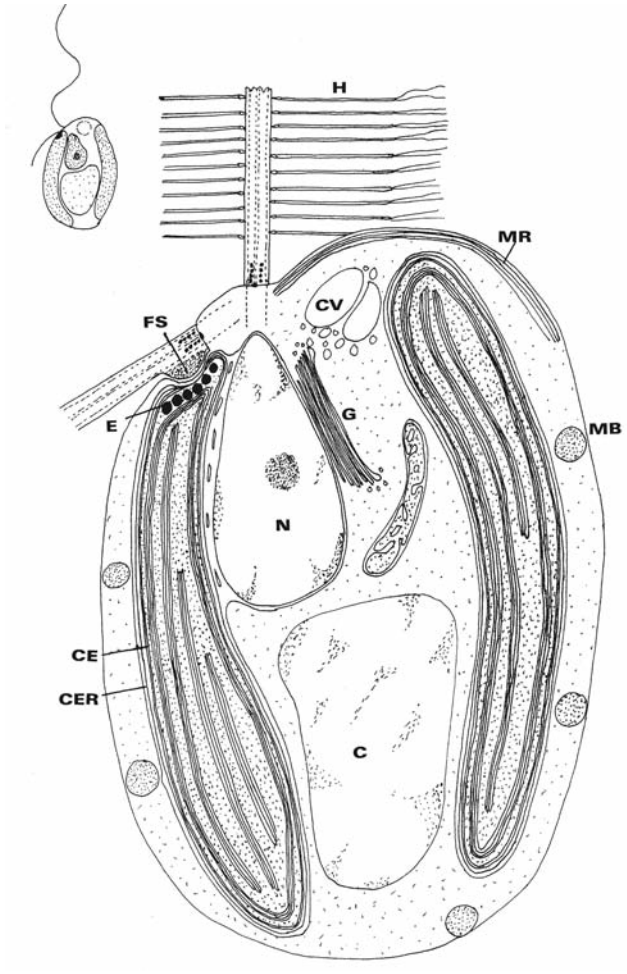


Fig. 10.1 Semidiagrammatic drawing of a light and electron microscopical view of the basic organization of a cell of the Chrysophyceae. (C) Chrysolaminarin vesicle; (CE) chloroplast envelope; (CER) chloroplast endoplasmic reticulum; (CV) contractile vacuole; (E) eyespot; (FS) flagellar swelling; (G) Golgi body; (H) hair of the anterior flagellum; (MB) muciferous body; (MR) microtubular root of flagellum; (N) nucleus. (Adapted from Hibberd, 1976.)

(Fig. 10.1). This flagellar swelling contains an electron-dense area referred to as the photoreceptor. The flagellar swelling contains **retinal**, the chromophore of rhodopsin-like proteins, suggesting that a rhodopsin-like protein is the photoreceptor in the Chrysophyceae (Walne et al., 1995). The flagellar swelling fits into a depression of the cell immediately beneath which, inside the chloroplast, is the eyespot. The eyespot consists of lipid globules inside the anterior portion of the chloroplast, between the chloroplast envelope and the first band of thylakoids.

In *Ochromonas*, the long tinsel flagellum beats in one plane and pulls the cell forward, whereas the shorter flagellum is flexed over the anterior eyespot and appears to play little role. During forward movement the cell rotates because of the shape of the body.

Internal organelles

The chloroplasts are parietal and usually only a few in number, often only one or two. Chlorophylls *a*, c_1, and c_2 are present, with the main carotenoid being fucoxanthin. The chloroplasts are surrounded by two membranes of chloroplast E.R., the outer membrane of which is usually continuous with the outer membrane of the nuclear envelope (Fig. 10.1). The thylakoids are usually grouped three to a band.

The chloroplast of *Ochromonas danica* will form a small proplastid if the cells are grown in the dark (Gibbs, 1962). The proplastid contains a single thylakoid, a few small vesicles, and a large number of dense granules. The chlorophyll *a* content of the proplastid is about 1.2% of the mature chloroplast. On exposure of the proplastid to light, vesicles appear that fuse to form the thylakoids. After 2 days

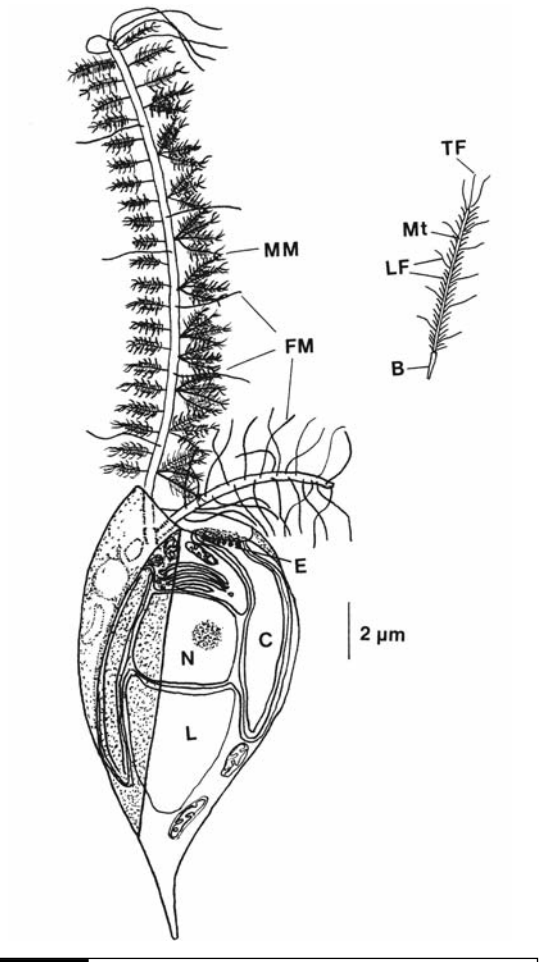


Fig. 10.2 *Ochromonas danica*. (B) Basal attachment region; (C) chloroplast; (E) eyespot; (FM) fibrillar hair; (L) leucosin; (LF) lateral filament; (MM) microtubular hair; (Mt) microtubule; (N) nucleus; (TF) terminal filament. (After Bouck, 1971.)

in the light, the chloroplasts have reached their mature form, although it takes 8 days for them to acquire their full complement of chlorophyll.

Pyrenoids are common in chloroplasts of the Chrysophyceae. They consist of a granular area that is different in appearance from the stroma. Few, if any, thylakoids traverse the pyrenoid area.

The storage product is **chrysolaminarin** (**leucosin**), a β-1,3 linked glucan, supposedly found in a posterior vesicle (Fig. 10.1). The actual function of the so-called chrysolaminarin vesicle may be more complex than supposed with the discovery of microorganisms in the chrysolaminarin vesicle of *Ochromonas* (Daley et al., 1973; Dubowsky, 1974). The chrysolaminarin vesicle is much larger in organisms grown in the dark on a synthetic medium than in cells grown in the light. The opposite would be expected if the vesicle stored chrysolaminarin, the accumulation product of photosynthesis in the light. It may be that the structure may also function as a digestive vesicle, breaking down material taken up by the cell into building blocks for metabolism and growth.

The single nucleus is pear-shaped (pyriform), with its narrow anterior end extended in the direction of the basal bodies (Fig. 10.1). There is a single, large Golgi body which lies against the nucleus in the anterior part of the cell, often in a concavity in the nuclear envelope. Contractile vacuoles are common, usually occurring in the anterior part of the cell next to the Golgi apparatus. There is often a complex system of vesicles associated with the contractile vacuoles similar to the pusule system in the Dinophyceae. Lipid bodies can also be found in the protoplasm. In young cells there are usually few lipid bodies; however, as the cell ages, the lipid bodies become larger and more numerous until they fill the protoplasm.

Two different types of projectiles occur in the Chrysophyceae, muciferous bodies and discobolocysts, the former like the muciferous bodies in the Prymnesiophyceae, Raphidophyceae, and Dinophyceae. The muciferous bodies (Fig. 10.1) contain granular material and are bonded by a single membrane. On discharge the contents of the vesicle often form a fibrous network outside the cell. The **discobolocysts** are similar to the muciferous bodies and have been described in the most detail by Hibberd (1970), in *Ochromonas tuberculatus* (Fig. 10.3). The discobolocysts are in the outer layer of cytoplasm and consist of a single membrane-bounded vesicle with a hollow disc in the outward-facing part of the vesicles. The discharge of the discobolocyst is explosive, taking place by the expansion of the projectile into a thin thread 6 to 11 µm long, the disc being at the tip of the mucilage. As the discharge occurs, the cell jerks violently under the recoil to a distance of 5 µm. After the discharge of either muciferous bodies or discobolocysts, the protoplast recovers without any deleterious effects. Both of the projectiles originate in the area of the Golgi apparatus.

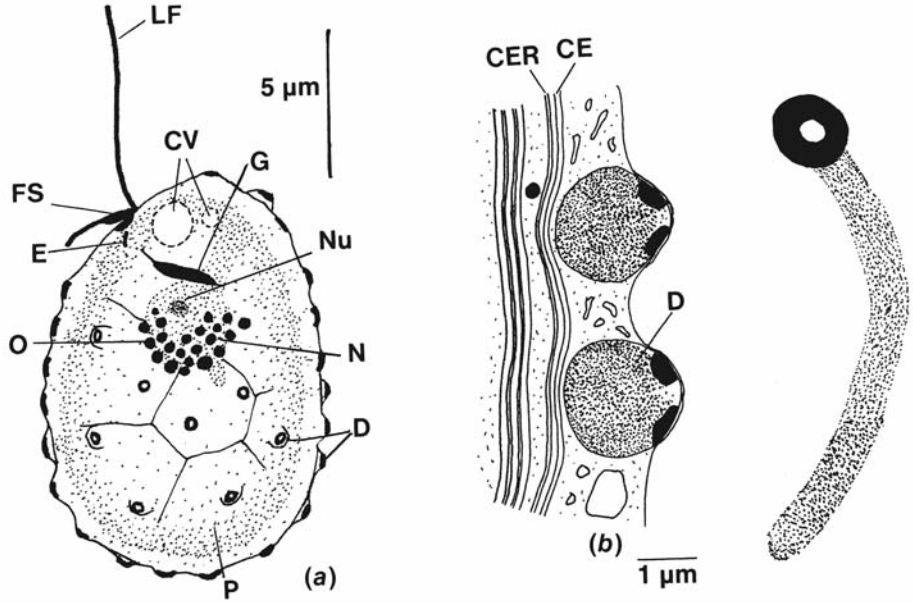


Fig. 10.3 (*a*) *Ochromonas tuberculatus*. (*b*) Charged and discharged discobolocysts. (CE) Chloroplast envelope; (CER) chloroplast endoplasmic reticulum; (CV) contractile vacuole; (D) discobolocyst; (E) eyespot; (FS) flagellar swelling; (G) Golgi body; (LF) long flagellum; (N) nucleus; (Nu) nucleolus; (O) oil; (P) plastid. (After Hibberd, 1970.)

Extracellular deposits

Cell walls composed of cellulose (Herth and Zugenmaier, 1979), loricas, and silicified scales and walls, occur in some of the Chrysophyceae (Preisig, 1994). Silica scales, such as those in *Paraphysomonas* (Fig. 10.4), are radially or biradially symmetrical. The scales are arranged loosely outside the plasma membrane without any clearly defined pattern. Like the Bacillariophyceae and Synurophyceae, the scales of the Chrysophyceae are formed inside a silica deposition vesicle that is derived from endoplasmic reticulum (Schnepf and Deichgraber, 1969). This arrangement differs from that of the calcified scales of the Prymnesiophyceae and the Chlorophyta, which are formed by the Golgi apparatus. Scale formation is also similar to frustule formation in the diatoms in that the addition of germanium (a competitive inhibitor of silicon utilization) to the growth medium results in inhibition of growth (Lee, 1978). Organic scales without mineralization also occur in the Chrysophyceae. In *Chromulina placentula*, there is a single layer of organic scales covering the posterior portion of the cell, the scales being very similar to those found in the Prymnesiophyceae (Throndsen, 1971).

In one of the orders (Parmales), silicified walls occur which are composed of five or eight parts (Figs. 10.14, 10.15) (Booth and Marchant, 1987). Loricas, such as those in *Pseudokephyrion pseudospirale* and *Kephyrion rubri claustri*, can also be mineralized. Manganese can occur in loricas as needle-like structures, whereas iron occurs as granular deposits (Dunlap et al., 1987).

Some of the species have a **lorica** (an envelope around the protoplast, but not generally attached to the protoplast as a wall is). In *Dinobryon* (Fig. 10.11), the lorica is composed of an interwoven system of microfibrils (Kristiansen, 1969). The formation of the lorica begins when a small funnel-shaped piece arises from the cell. The protoplast then rotates on its axis following a spiral course and secreting the remainder of the lorica. When the lorica is complete, the protoplast withdraws to its base. Several strains of *Ochromonas malhamensis* and *O. sociabilis* produce a delicate lorica consisting of a 10- to 20-µm hollow stalk and a cup-shaped envelope that encloses a long protoplasmic filament and the basal half of the cell, respectively. The lorica of *O. malhamensis* is composed of the polysaccharide chitin (Herth et al., 1977). The lorica can be mineralized as is the case with

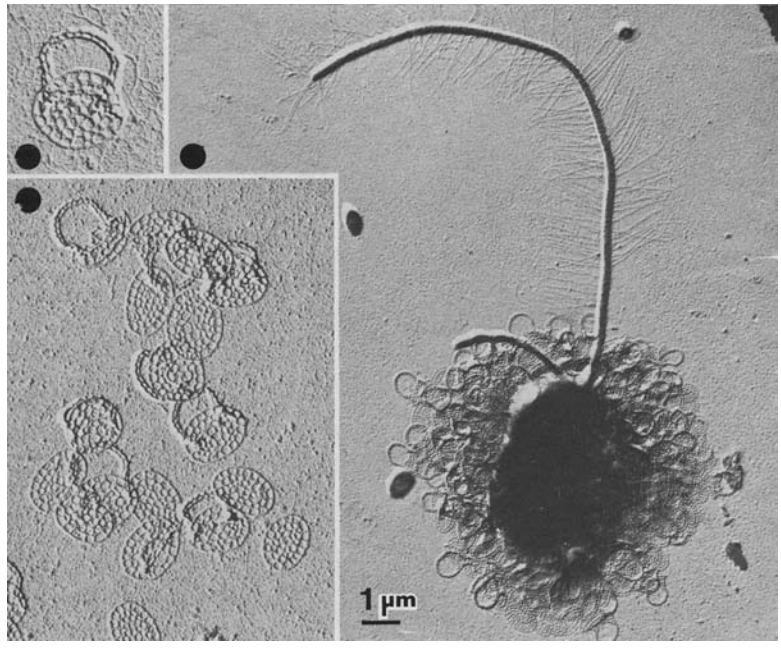


Fig. 10.4 Transmission electron micrographs of *Paraphysomonas sigillifera* showing a whole cell with a long tinsel flagellum and a short whiplash flagellum. Also included are higher-magnification micrographs of the scales. (From Thomsen et al., 1981.)

Chrysococcus rufescens (Fig. 10.5). This alga has a basically mucilaginous lorica surrounding the cell (Belcher, 1969). In young cells the lorica is very transparent, probably consisting just of mucilage. At a later stage, dark needle-shaped crystals appear, which are primarily oriented parallel to the cell surface. The crystals ultimately unite to form a felty mass outside the cell.

Anthophysa vegetans (Fig. 10.10(*b*), (*c*)) is a freshwater colonial alga that produces a mineralized stalk that can contain salts of calcium, iron, or manganese. The minerals in the environment determine color and the mineral composition of the stalk (Lee and Kugrens, 1989).

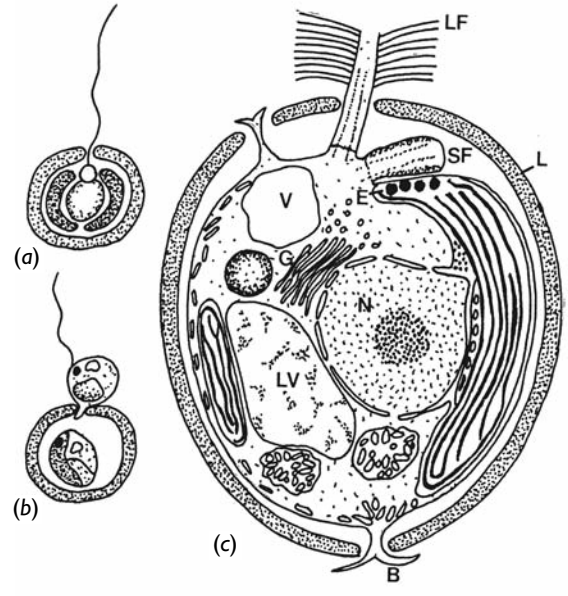


Fig. 10.5 *Chrysococcus rufescens*. (*a*) Whole cell. (*b*) Cell undergoing reproduction. (*c*) Ultrastructure of vegetative cell. (B) Branched cytoplasmic process; (E) eyespot; (G) Golgi; (L) lorica; (LV) leucosin vesicle; (LF) long flagellum; (N) nucleus; (SF) short flagellum; (V) contractile vacuole. ((*c*) after Belcher, 1969.)

Statospores

The formation of a **cyst** or **statospore** or **resting spore** is one character by which a member of the Chrysophyceae or Synurophyceae may be unequivocally recognized. **Statospores** are mostly

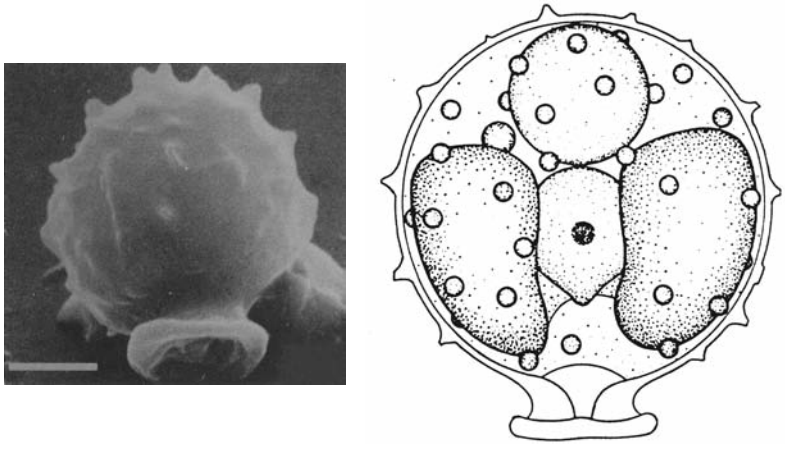


Fig. 10.6 Statospore of *Ochromonas sphaerocystis*. Bar = 5 μm. (From Andersen, 1982.)

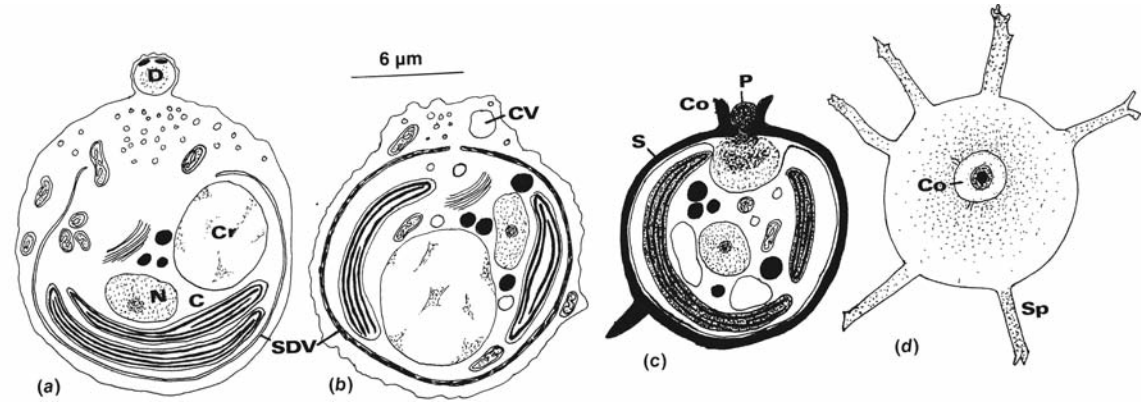


Fig. 10.7 Formation of a statospore or cyst in *Ochromonas tuberculata*. (*a*)–(*c*) The formation of the statospore. (*d*) A mature statospore as seen from the collar end. (C) Chloroplast; (Co) collar of statospore; (Cr) chrysolaminarin vesicle; (CV) contractile vacuole; (D) discobolocyst; (N) nucleus; (P) plug in pore of statospore; (S) statospore wall; (SDV) silica deposition vesicle; (Sp) spine. (Adapted from Hibberd, 1977.)

spherical, ellipsoidal, or ovate in shape, and the outer surface may be smooth or variously ornamented with warts, spines, or arms (Figs. 10.6, 10.7). Wall ornamentation is species specific. The statospore has a pore with a collar that is closed by a plug. A vegetative cell forms a statospore internally. In the formation of a statospore the cells become non-motile, any projectiles are discharged, and there is considerable contractile vacuole activity (Sheath et al., 1975; Hibberd, 1977). A nearly spherical vesicle called the silica deposition vesicle is formed in the cytoplasm, and silica is deposited inside the vesicle (Fig. 10.7) (Preisig, 1994). A complete sphere of silica is formed, interrupted only by the developing pore and collar. The nucleus, chloroplast, flagellar basal bodies, mitochondria, Golgi body, chrysolaminarin vesicle, and ribosomes are segregated to the inside of the silica deposition vesicle, whereas outside there are mitochondria, ribosomes, contractile vacuoles, and small vesicles. After the spines, pore, and collar have been formed in the silica deposition vesicle, a plug is formed by the cytoplasm in the pore area. With the formation of the unsilicified plug, contact is lost between the protoplasm inside the statospore and that outside, with the inner membrane of the silica deposition vesicle becoming the new plasmalemma. When a statospore germinates, there is a dissolution of the plug or separation of it from the spore wall. The protoplast then moves out of the statospore by amoeboid motion, forming flagella as it moves out.

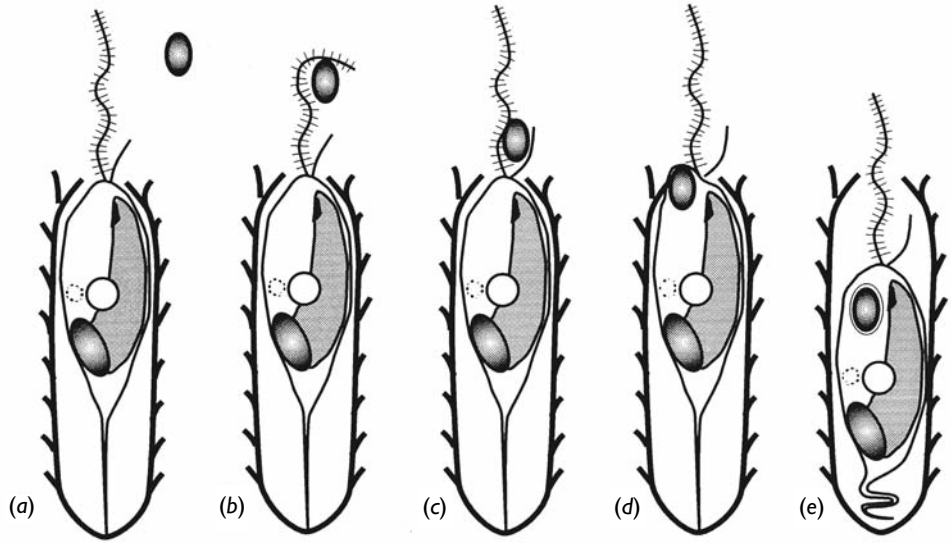


Fig. 10.8 Phagotrophy in *Epipyxia pulchra*. The cell has a posterior stalk by which it is attached to a lorica. (*a*) The long tinsel flagellum beats in such a way that water and suspended particles are drawn to the cell. (*b*) A particle is seized by the long tinsel flagellum. (*c*) The particle is maneuvered between the two flagella. (*d*) A feeding cap from the cell envelopes the particle. (*e*) The particle is enclosed within a food vacuole within the cytoplasm. The stalk has pulled the cell into the lorica. (Modified from Wetherbee and Andersen, 1992.)

Nutrition

Nutrition in the Chrysophyceae can be either phototrophic, phagotrophic, or mixotrophic (photosynthetic organism capable of taking up particles and molecules from the medium) (Zhang and Watanabe, 2001). *Dinobryon* (Fig. 10.11) is a mixotrophic chrysophyte that can have half of the carbon in the cells derived from ingestion of microorganisms (Caron et al., 1993). *Dinobryon* has the ability to compete with crustaceans, rotifers, and ciliates in capturing microorganisms. Under low-light conditions, *Dinobryon* can ingest an average of three bacterial cells every five minutes (Bird and Kalff, 1986). Chrysophytes have the ability to ingest prey up to 30 times larger than themselves. The ability to take up microorganisms appears to be about the same for pigmented and non-pigmented chrysophytes (Zhang et al., 1996).

Like other mixotrophic chrysophytes, *Epipyxis pulchra* phagocytizes food particles that are both living (bacteria, small algae, or even cells of its own kind) and non-living (detritus, fecal material) (Wetherbee and Andersen, 1992). During prey gathering, the long flagellum, which is adorned with stiff hairs, beats rapidly to direct a strong current towards the cell while the short, smooth flagellum moves very little. When a potential food particle is drawn by current to contact the flagellar surface, the long flagellum stops beating and positions itself, in concert with the short flagellum, to seize the prey between the two flagella (Fig. 10.8). Both flagella briefly rotate the prey before selecting or rejecting it. If selected as food, the prey is held in place until a complex collecting cup emanates out and engulfs the prey. The cup plus the prey, now a food vacuole, is then retracted back into the cell proper.

Isofloridoside, a product of photosynthesis in *Ochromonas malhamensis*, is used to adapt the cells to changes in the dissolved substances (osmotic pressure) of the medium. As the osmotic pressure of the medium increases, *O. malhamensis* responds by increasing the concentration of isofloridoside inside the cell, preventing water loss to the medium (Kauss, 1967).

Ecology

Fauré-Fremiet (1950) has shown that *Chromulina psammobia* moves up to the surface of mud flats at

low tide, and as the tide comes in, the flagellate moves down in the mud so as not to be washed away. The basis for the migration is a reversal in the phototactic response, the cells being positively phototactic at low tide and negatively phototactic at high tide. The presence of mud is not necessary for the changes in phototaxis, which will continue for 6 to 7 days in the laboratory, more or less synchronized with the tide. After this the phototaxis changes gradually until the cells are always positively phototactic.

Dinobryon (Fig. 10.11) is a freshwater alga that is almost never found in waters with a high concentration of phosphorus. This observation led some investigators to conclude that high concentrations of phosphorus are inhibitory to growth of the alga. More detailed work (Lehman, 1976) showed this not to be true, that *Dinobryon* in culture grows well at high concentrations of phosphorus. What happens in nature is that other algae grow faster and outcompete *Dinobryon* at higher concentrations of phosphorus; only when **vernal** (spring) **blooms** of diatoms or other phytoplankton have reduced phosphorus to a level that inhibits their own growth will *Dinobryon* compete effectively. This demonstrates a basic rule among algae (Eppley et al., 1969; Fuhs et al., 1972), which is *algae that have efficient uptake of nutrients (are able to utilize low levels of a nutrient) usually have lower maximum intrinsic growth rates than algae that are less efficient in taking up nutrients*. These differences represent two variations of an adaptive scheme for nutrient utilization. Some species exploit a resource-laden environment rapidly, whereas others display measured efficiency in utilizing an energy source. Energy trade-offs among competing intracellular processes might preclude organisms from excelling at both simultaneously.

Dinobryon uses phosphate not only as inorganic phosphate but also as organically bound phosphate in moderate-sized molecules (glycerophosphate, uridylic acid, adenylic acid) (Lehman, 1976). It can also use nitrogen either from inorganic sources or from organic molecules (urea, glycine, uridylic acid, adenylic acid). Its capacity to utilize these organic sources and its phagocytosis of whole particles imply that *Dinobryon* is suited to occupy the water column when death and decline of previous bloom-forming organisms release products of cell breakdown to solution. It is also at these times, when ambient levels of dissolved inorganic nutrients have become somewhat depleted, that the potentials of the cells for effective uptake of nutrients show their advantage.

Although high concentrations of phosphorus do not inhibit the growth of *Dinobryon*, high concentrations of potassium do (Lehman, 1976). The concentrations necessary for inhibition are commonly found in many lakes. As an example, in one Swedish lake, *D. sertularia* appears in June a few weeks after the ice breaks, with the alga persisting in the cool water until early autumn (Willén, 1961). Its period of abundance matches exactly with a summertime decrease in potassium caused partly by the precipitation of potassium by clay colloids and partly by the uptake by littoral vegetation (Ahl, 1966). The disappearance of *Dinobryon* corresponds to increased concentration of potassium as the element is released from dying vegetation.

Chrysophytes are notorious for their production of fishy or rancid smells, reflecting release of unsaturated aldehydes derived from the high cell content of polyunsaturated acids. *Uroglena* (Fig. 10.10(*a*)) and *Dinobryon* (Fig. 10.11) produce unsaturated fatty-acid derivatives (Fig. 10.9) that contribute to these smells (Watson and Satchwill, 2003). These chemicals are classified as **algal volatile organic compounds** (AVOCs).

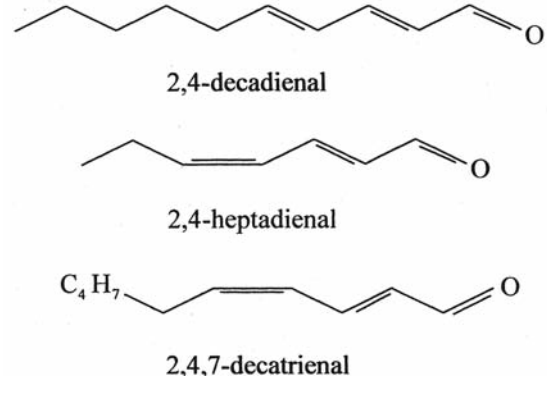


Fig. 10.9 Three unsaturated fatty-acid derivatives produced by chrysophytes that result in rancid or fishy odors.

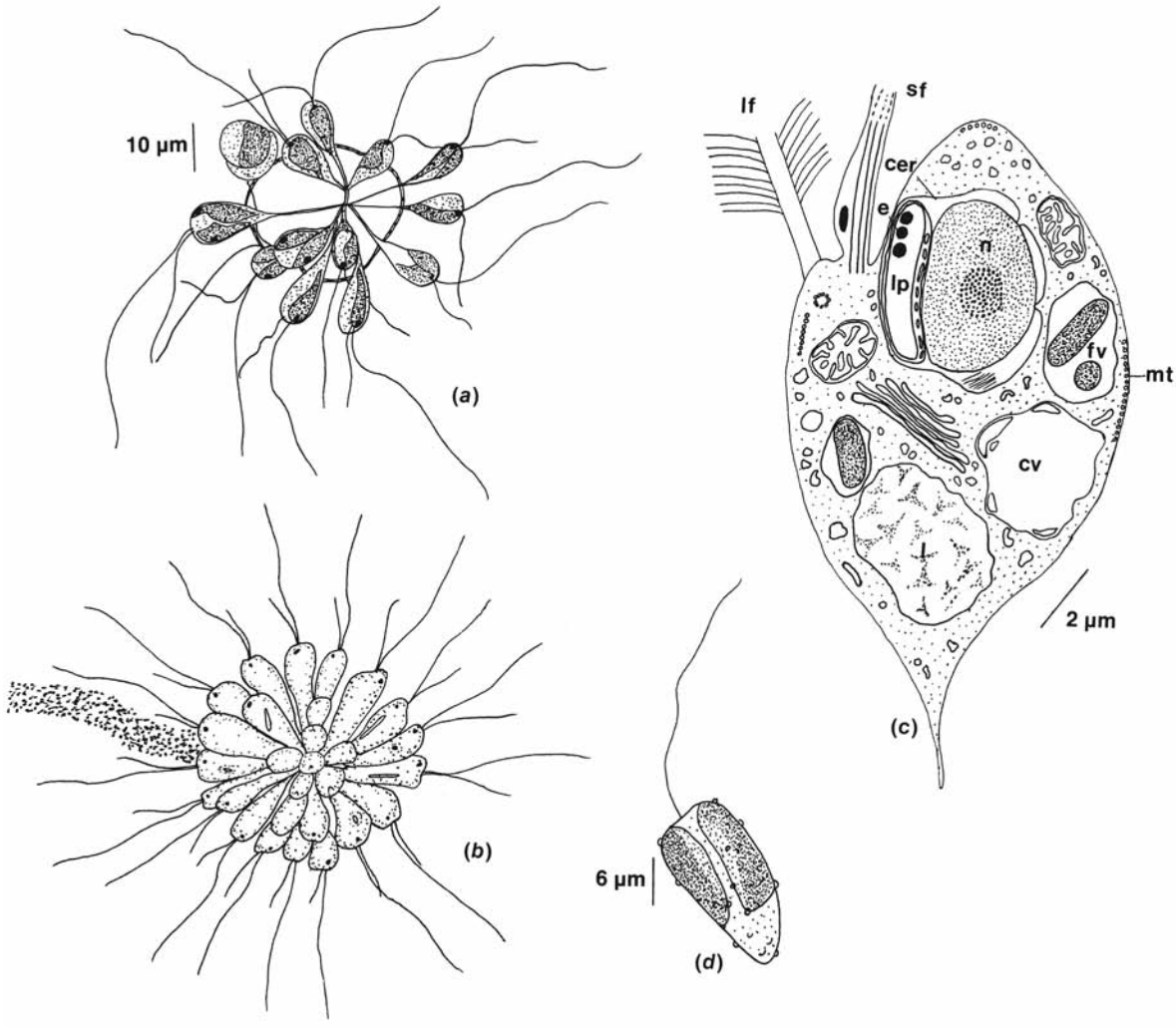


Fig. 10.10 (*a*) *Uroglena conradii.* (*b*), (*c*) *Anthophysa vegetans.* (*d*) *Chromulina conica.* (cer) Chloroplast endoplasmic reticulum; (cv) contractile vacuole; (e) eyespot; (fv) food vacuole; (l) leucosin; (lf) long flagellum; (lp) leucoplast; (mt) microtubules; (n) nucleus; (sf) short flagellum. ((*a*), (*d*) after Schiller, 1929; (*b*) after Pringsheim, 1946; (*c*) after Belcher and Swale, 1972.)

Classification

Three of the orders of the Chrysophyceae (Preisig, 1995) will be considered here:

Order 1 Chromulinales: cells with the flagella inserted into the anterior portion of the cell.

Order 2 Parmales: cells with siliceous walls composed of five or eight plates.

Order 3 Chrysomeridales: motile naked cells with laterally inserted flagella and an eyespot, motile cells similar to those in the brown algae.

Chromulinales

All of the organisms in this order have a unicell with two apically inserted flagella somewhere in their life history. One of the flagella is tinsel with mastigonemes and directed forward, while the second flagellum is whiplash (lacking mastigonemes) and is inserted at approximately 90° to the tinsel flagellum (e.g., *Ochromonas*,

Figs. 10.2, 10.3). In some of the genera (e.g., *Chromulina*, Fig. 10.10(*d*)) the whiplash flagellum is reduced to a stub. There are usually two parietal chloroplasts, a central nucleus, and a large posterior chrysolaminarin vesicle.

Within the order there is a progression from the unicellular to the colonial form (Fig. 10.10) as exemplified by *Uroglena* (Fig. 10.10(*a*)) and *Anthophysa* (Fig. 10.10(*b*), (*c*)). Some of the genera, such as *Dinobryon* (Fig. 10.11), have cells surrounded by a lorica. In *Chrysococcus* (Fig. 10.5), the cell is surrounded by a lorica that has pores in it.

In the Chromulinales there is a frequent tendency toward loss of photosynthetic activity and adaptation to various forms of phagotrophy and chemo-organotrophy. Associated with this is a diminution of the chloroplast as in *Anthophysa* (Fig. 10.10(*b*), (*c*)), which has a leucoplast with a pigmented eyespot. The end of this reduction is represented by *Paraphysomonas* (Fig. 10.4), which has no trace of an eyespot or plastid. Along with the reduction in the chloroplast have arisen adaptations for feeding, such as in *Anthophysa*, which beats its long flagellum, creating a water current toward the cells, which brings with it bacteria from as far away as 200 μm. The bacteria strike the anterior end of the cells and are ingested at the point where they touch. The bacteria sink into the cytoplasm, which closes behind them, and are completely in the cell within 2 to 3 seconds of contact (Belcher and Swale, 1972).

In *Dinobryon cylindricum*, sexual reproduction is heterothallic and dioeceous, and morphologically and physiologically anisogamous (Fig. 10.11) (Sandgren, 1981). Cells of the second or third tier of the colony (the basal cell being the oldest) are the best potential gamete-producing cells. Gametes are produced mainly in exponentially growing populations. Female cells release a chemical **erogen** that causes male cells to divide once. One of the male cells remains in the lorica, whereas the other swims away as a naked male gamete, instead of attaching to the lorica mouth and building a new lorica as a vegetative cell would. The non-loricate male gamete (which is structurally similar to an *Ochromonas* cell) swims to the female cell in its lorica, the flagella become oriented parallel to each other, and fusion occurs at the anterior end of each cell. Plasmogamy results in a quadriflagellate planozygote that fills the lorica. Nuclear fusion does not occur. After 30 minutes, the flagella have been lost and the zygote creeps to the lorica mouth by amoeboid movement. A thin cellulose encystment vesicle is formed as a lorica extension, the zygote rounds up, and a binucleate statospore (Fig. 10.12) is formed. In *D. divergens*, most statospores settle to the lake bottom and germinate early the next year (Sheath el al., 1975). Statospore germination occurs by the formation of a cellulosic vesicle at the statospore pore, followed by a presumably meiotic cleavage into four daughter cells that migrate into the vesicle. The *Ochromonas*-like swarmers escape to form new vegetative cells.

Asexually produced statospores of *Dinobryon cylindricum* may occur in exponential or stationary-phase populations, depending upon the clones involved (Sandgren, 1980, 1981). Asexual statospores (cysts) are formed at a much lower frequency (0.05% or less) than sexual statospores unless the population is placed in a nitrogen-depleted environment where asexual encystment can reach 4%. The continual production of a low number of the resistant statospores by a *Dinobryon* population acts as a hedge against a rapid unfavorable change in environmental conditions that would kill the vegetative cells.

The first event in statospore formation is vegetative cell enlargement so that the cell begins to bulge out of the lorica. The Golgi form vesicles that fuse to form a continuous silica deposition vesicle in the peripheral cytoplasm. The silica deposition vesicle has a pore that eventually will be the statospore pore. Precipitation of silica proceeds in the silica deposition vesicle to form the silicified statospore wall. The portion of the cytoplasm that is exterior to the wall retracts through the pore in the cyst wall into the statospore interior. The small amount of cytoplasm outside the wall forms the collar around the pore. A plug is formed in the cyst wall, sealing the statospore protoplasm. The mature statospore has two nuclei, two plastids, and a rich supply of energy reserves in the form of oil and chrysolaminarin.

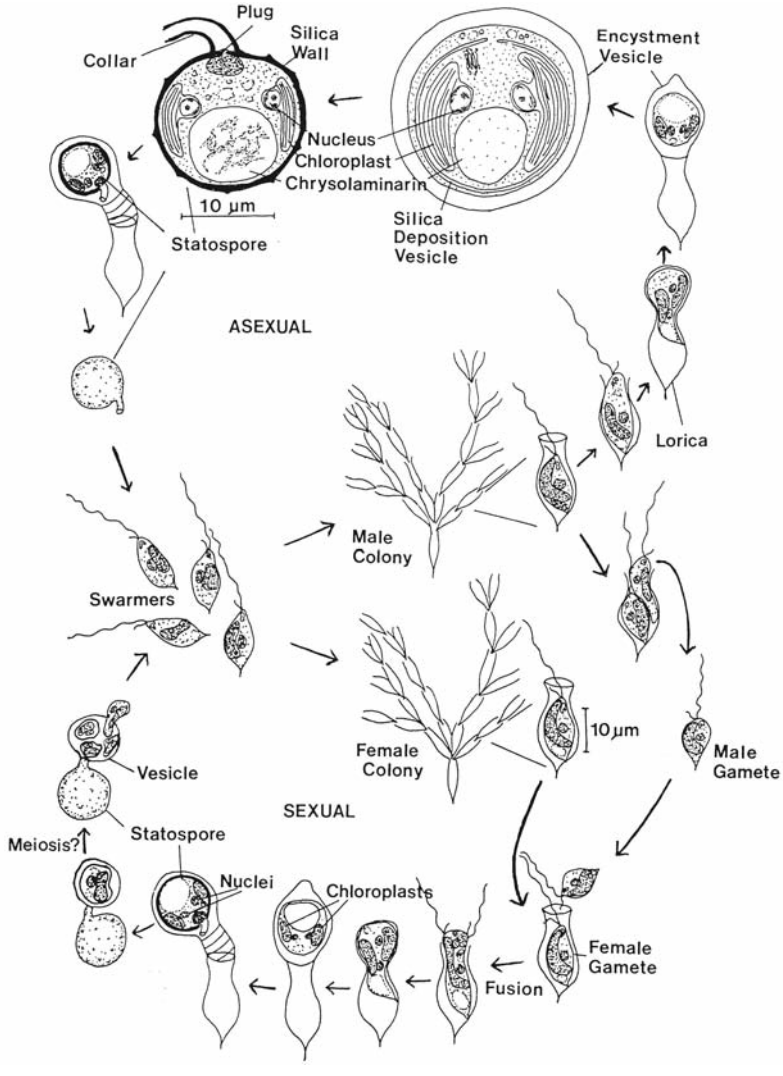


Fig. 10.11 The life cycle of *Dinobryon*. (Adapted from Sheath et al., 1975; Sandgren, 1980, 1981.)



Fig. 10.12 Scanning electron micrograph of a cyst of *Dinobryon cylindricum*. Bar = 5 µm. (From Sandgren, 1983.)

Chrysophaera (Fig. 10.13) is an example of a colonial alga in the order. This organism has a dominant spherical non-motile stage with cells adhering to each other and the substrate in irregular clusters. The smallest individuals are unicellular, but individuals with up to 256 cells within a common mucilaginous envelope are not uncommon. All the cells within the envelope have a long tinsel flagellum and a short stub of the second flagellum (Belcher, 1974). When a colony is placed in distilled water, it begins to swell within

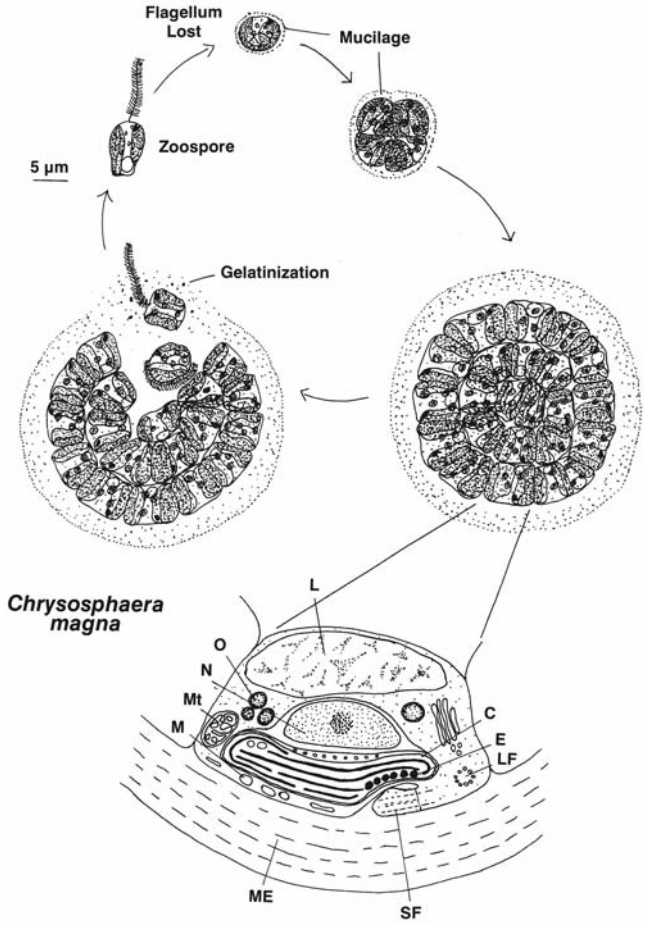


Fig. 10.13 The life cycle of *Chrysosphaera magna*. (C) Chloroplast; (E) eyespot; (L) leucosin vesicle; (LF) basal body of long flagellum; (M) muciferous body; (Mt) mitochondria; (ME) mucilaginous envelope; (N) nucleus; (O) oil; (SF) short flagellum. (After Belcher, 1974.)

15 minutes, and the mucilage gelatinizes on one side. The zoospores are released a few minutes later and swim for about 2 minutes before they shed their flagella, settle down, form a mucilaginous envelope, and become identical in appearance to the youngest coccoid stages.

Parmales

The Parmales consist of small cells, generally 2 to 5 μm in diameter, each with a chloroplast (Marchant and McEldowney, 1986) and a silicified cell wall composed of five to eight plates (Figs. 10.14, 10.15). In the Pentalaminaceae there are five wall plates whereas in the Octolaminaceae there are eight wall plates (Booth and Marchant, 1987). Members of the Parmales occur at concentrations of 10^5 cells per liter in polar and subpolar marine waters, making them one of the more abundant groups in these waters.

Four different shapes of plates occur around the cells (Figs. 10.14, 10.15) (Booth and Marchant, 1987). A **shield plate** or **round plate** is a circular plate with or without a central knob or process. A **triradiate plate** has three arms equally spaced, each arm fitting between two shield plates. A **ventral plate** is a round plate of greater diameter than that of shield plates; it is found in *Triparma* on the opposite side of the sphere from the triradiate plate. **Girdle plates** are three oblong plates in *Triparma*, juxtaposed end to end to form a ring around the ventral plate between it and the other four plates. Ornamentation of various types (papillae, wings, spines, keels) occurs on the plates.

Chrysomeridales

These algae have zoospores with the flagella more or less laterally inserted into the cell body. There

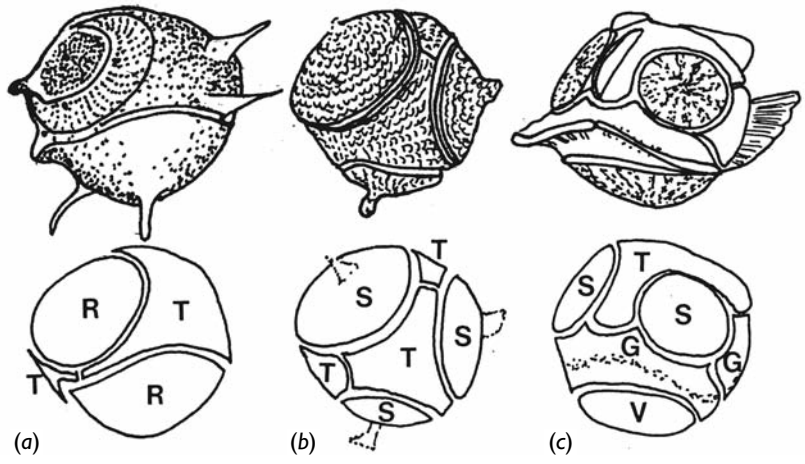


Fig. 10.14 Three genera in the Parmales. (*a*) *Pentalamina*. (*b*) *Tetraparma*. (*c*) *Triparma*. (G) Girdle plate; (R) round plate; (S) shield plate; (T) triradiate plate; (V) ventral plate. (After Booth and Marchant, 1987.)

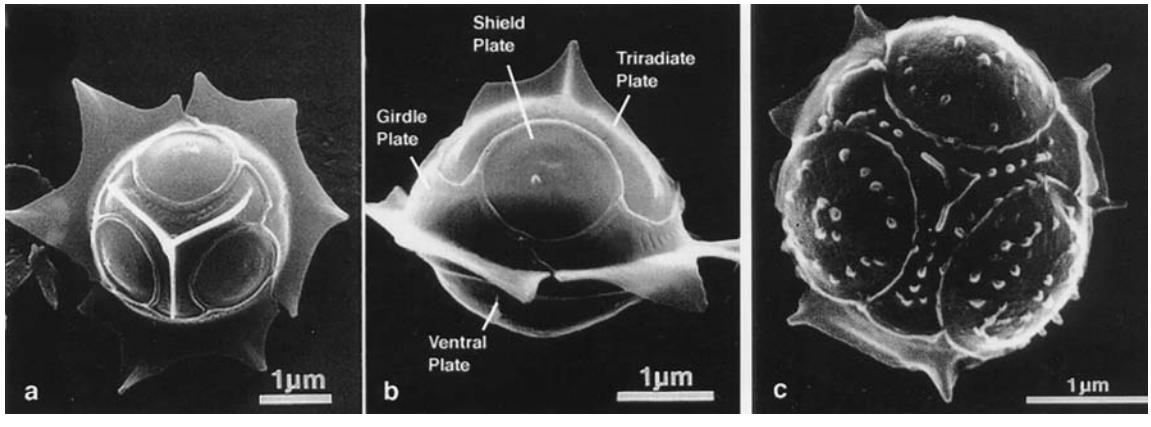


Fig. 10.15 (*a*), (*b*) *Triparma laevis*. (*c*) *Triparma strigata*. (From Kosman et al., 1993.)

is an eyespot in the chloroplast and the accessory pigment violaxanthin is present. The similarities in the zoospores of the algae in this order have led to the speculation that the Phaeophyceae (brown algae) probably evolved from an alga similar to *Giraudyopsis* in this order (Fig. 10.16) (O'Kelly, 1989; Saunders et al., 1997). The algae in the Chrysomeridales, however, lack the unilocular and plurilocular sporangia, as well as the plasmodesmata and alginates characteristic of the Phaeophyceae.



Fig. 10.16 *Giraudyopsis stelliger*. (After Dangeard, 1966.)



Fig. 10.17 **Adolph Pascher** Born May 31, 1881 in Tusset, Bohmerwalde, Province of Krummau, Austria-Hungary. Died by his own hand May 1945. Dr. Pascher was brought up in the Bohmerwalde, a snowy mountainous area, where he attended small schools until he went to the University of Prague. Here he was able to use his first microscope, a tool he was to use for the rest of his life. He graduated from the University of Prague in 1909. From 1909 to 1912, at a time when he suffered from a chronic illness, he studied pharmaceutical botany. From 1912 to 1927, he worked as a lecturer at different universities including the German Technical University in Prague. During this time he performed phycological research at a hydrobiological station in Hirschberg, Germany, and at another hydrobiological station that he founded in Upper Bohemia in Czechoslovakia. In 1927, he became director of the Botanical Institute and Gardens at the University of Prague. In the early 1930s, Dr. Pascher became involved in the Nazi Brown Shirt movement, which resulted in a hiatus of his numerous publications from 1933 to 1938. In 1939, he started publishing again while remaining active in the Nazi administration. With the fall of the Third Reich, he shot himself in May 1945. Dr. Pascher could be considered as the most prominent phycologist of his time. As stated by Prescott (1951) "His work exerted a greater influence than that of any other phycologist in clarifying modern concepts of algal taxonomy and phylogeny . . . it was his erudite interpretation of facts, nevertheless, which placed the studies of Pascher in a corner stone position."

REFERENCES

Ahl, T. (1966). Chemical conditions in Ösbysjön, Djursholm. 2. The major constituents. *Oikos* 17:175–6.

Andersen, R. A. (1982). A light and electron microscopical investigation of *Ochromonas sphaerocystis* Matvienko (Chrysophyceae): The statospore, vegetative cell and its peripheral vesicles. *Phycologia* 21:390–8.

Andersen, R. A. (2004). Biology and systematic of heterokont and haptophyte algae. *Amer. J. Bot.* 91:1508–22.

Anderson, R. A., and Mulkey, T. J. (1983). The occurrence of chlorophylls c_1 and c_2 in the Chrysophyceae. *J. Phycol.* 19:289–94.

Belcher, J. H. (1969). A morphological study of the phytoflagellate *Chrysococcus rufescens* Klebs in culture. *Br. Phycol. J.* 4:105–17.

Belcher, J. H. (1974). *Chrysophaera magna* sp. nov., a new coccoid member of the Chrysophyceae. *Br. Phycol. J.* 9:139–44.

Belcher, J. H., and Swale, E. M. F. (1972). The morphology and fine structure of the colourless colonial flagellate *Anthophysa vegetans* (O. F. Müller) Stein. *Br. Phycol. J.* 7:335–46.

Bird, D. F., and Kalff, J. (1986). Bacterial grazing by planktonic lake algae. *Science* 231:493–4.

Booth, B. C., and Marchant, H. J. (1987). Parmales, a new order of marine chrysophytes, with descriptions of three new genera and seven new species. *J. Phycol.* 23:245–60.

Bouck, G. B. (1971). The structure, origin, isolation, and composition of the tubular mastigonemes of the *Ochromonas* flagellum. *J. Cell Biol.* 50:362–84.

Caron, D. A., Sanders, R. W., Lim, E-L., Marrasé, C., Amaral, L. A., Whitney, S., Aoki, R. B., and Porter, K. G. (1993). Light-dependent phagotrophy in the freshwater mixotrophic chrysophyte *Dinobryon cylindricum*. *Microbial Ecol.* 25:93–111.

Daley, R. J., Morris, G. P., and Brown, S. R. (1973). Phagotrophic ingestion of a blue-green alga by *Ochromonas*. *J. Protozool.* 20:58–61.

Dangeard, P. (1966). Sur le nouveau genre *Giraudyopsis* P.D. *Le Botantiste* 49:99–108.

Dubowsky, N. (1974). Selectivity of ingestion and digestion in the chrysomonad flagellate *Ochromonas malhamensis*. *J. Protozool.* 21:295–8.

Dunlap, J. R., Walne, P. L., and Preisig, H. R. (1987). Manganese mineralization in chrysophycean loricas. *Phycologia* 26:394–6.

Eppley, R. W., Rogers, J. N., and McCarthy, J. J. (1969). Half-saturation constants for uptake of nitrate and

ammonium by marine phytoplankton. *Limnol. Oceanogr*. 14:912–20.
Fauré-Fremiet, E. (1950). Rythme de marée d'une *Chromulina psammophile. Bull. Biol. Fr. Belg*. 84:207–14.
Fuhs, G. W., Demmerle, S. D., Canelli, E., and Chen, M. (1972). Characterization of phosphorus-limited algae (with reflections on the limiting nutrient concept). *Am. Soc. Limnol. Oceanogr. Spec. Symp*. 1:113–32.
Gibbs, S. P. (1962). Nuclear envelope–chloroplast relationships in algae. *J. Cell Biol*. 14:433–44.
Herth, W., and Zugenmaier, P. (1979). The lorica of *Dinobryon. J. Ultrastruct. Res*. 69:262–72.
Herth, W., Kuppel, A., and Schnepf, E. (1977). Chitinous fibrils in the lorica of the flagellate chrysophyte *Poteriochromonas stipitata* (Syn. *Ochromonas malhamensis*). *J. Cell Biol*. 73:311–21.
Hibberd, D. J. (1970). Observations on the cytology and ultrastructure of *Ochromonas tuberculatus* sp. nov. (Chrysophyceae), with special reference to the discobolocysts. *Br. Phycol. J*. 5:119–43.
Hibberd, D. J. (1976). The ultrastructure and taxonomy of the Chrysophyceae and Prymnesiophyceae (Haptophyceae): A survey with some new observations on the ultrastructure of the Chrysophyceae. *Bot. J. Linn. Soc*. 72:55–80.
Hibberd, D. J. (1977). Ultrastructure of cyst formation in *Ochromonas tuberculata* (Chrysophyceae). *J. Phycol*. 13:309–20.
Hill, F. G., and Outka, D. E. (1974). The structure and origin of mastigonemes in *Ochromonas minute* and *Monas* sp. *J. Protozool*. 21:299–312.
Kauss, H. (1967). Metabolism of isofluoridoside (*O*-α-D-galactopyranosyl-[1 → 1]-glycerol) and osmotic balance in the freshwater alga *Ochromonas. Nature* 214:1129–30.
Kosman, C. A., Thomsen, H. A., and Ostergaarad, J. B. (1993). Parmales (Chrysophyceae) from Mexican, Californian, Baltic, Arctic and Antarctic waters with a description of a new subspecies and several new forms. *Phycologia* 32:116–28.
Kristiansen, J. (1969). Lorica structure in *Chrysolykos* (Chrysophyceae). *Bot. Tidsskr*. 64:162–8.
Lee, R. E. (1978). Formation of scales in *Paraphysomonas vestita* and the inhibition of growth by germanium dioxide. *J. Protozool*. 25:163–6.
Lee, R. E., and Kugrens, P. (1989). Biomineralization in *Anthophysa vegetans* (Chrysophyceae). *J. Phycol*. 25:591–6.
Lehman, J. T. (1976). Ecological and nutritional studies on *Dinobryon* Ehrenb: Seasonal periodicity and the phosphate toxicity problem. *Limnol. Oceanogr*. 21:646–64.
Marchant, H. J., and McEldowney, A. (1986). Nanoplankton siliceous cysts from Antarctica are algae. *Mar. Biol. (Berl.)* 92:53–7.
O'Kelly, C. J. (1989). The evolutionary origin of the brown algae: information from the studies of motile cell ultrastructure. In *The Chrysophyte Algae: Problems and Perspectives*, ed. J. C. Green, B. S. C. Leadbeater, and W. L. Diver, pp. 255–78. Oxford: Clarendon Press.
Preisig, H. R. (1994). Siliceous structures and silicification in flagellated protists, *Protoplasma* 181:29–42.
Preisig, H. R. (1995). A modern concept of chrysophyte classification. In *Chrysophyte Algae*, ed. C. D. Sandgren, J. R. Smol, and J. Kristiansen, pp. 46–74. Cambridge: Cambridge University Press.
Prescott, G. W. (1951). History of phycology. In *Manual of Phycology*, ed. G. M. Smith, pp. 1–12. New York: The Ronal Press Co.
Pringsheim, E. G. (1946). On iron flagellates. *Philos. Trans. R. Soc.* [*B*] 232:311–42.
Sandgren, C. D. (1980). An ultrastructural investigation of resting cyst formation in *Dinobryon cylindricum* Imhof (Chrysophyceae, Chrysophycophyta). *Protistologica* 16:259–76.
Sandgren, C. D. (1981). Characteristics of sexual and asexual resting cyst (statospore) formation in *Dinobryon cylindricum* Imhof (Chrysophyta). *J. Phycol*. 17:199–210.
Sandgren, C. D. (1983). Morphological variability in populations of chrysophycean resting cysts. I. Genetic (interclonal) and encystment temperature effects on morphology. *J. Phycol*. 19:64–70.
Saunders, G. W., Potter, D., and Andersen, R. A. (1997). Phylogenetic affinities of the Sarcinochrysidales and Chrysomeridales (Heterokonta) based on analyses of molecular and combined data. *J. Phycol*. 33:310–18.
Schiller, J. (1929). Neue Chryso- and Cryptomonaden aus Altwässern der Donau bei Wien. *Arch. Protistenk*. 66:436–58.
Schnepf, E., and Deichgraber, G. (1969). Uber die Feinstruktur von *Synura petersenii* unter besonderer Berücksuchtigung der Morphogenesis ihrer Kieselschuppen. *Protoplasma* 68:85–106.
Sheath, R. G., Hellebust, J. A., and Sawa, T. (1975). The statospore of *Dinobryon divergens* Imhoff: Formation and germination in a subarctic lake. *J. Phycol*. 11:131–8.
Thomsen, H. A., Zimmerman, B., Moestrup. Ø., and Kristiansen, J. (1981). Some new freshwater species of *Paraphysomonas* (Chrysophyceae). *Nord. J. Bot.* 1:559–81.

Throndsen, J. (1971). *Apedinella* gen. nov. and the fine structure of *A. spinifera* (Throndsen) comb. nov. *Norw. J. Bot*. 18:47–64.

Walne, P. L., Passarelli, V., Lenzi, P., Barsanti, L., and Gualtieri, P. (1995). Isolation of the flagellar swelling and identification of retinal in the phototactic flagellate, *Ochromonas danica* (Chrysophyceae). *J. Euk. Microbiol*. 42:7–11.

Watson, S. B., and Satchwill, T. (2003). Chrysophyte odour production: resource-mediated changes at the cell and population levels. *Phycologia* 42:393–405.

Wetherbee, R., and Andersen, R. A. (1992). Flagella of a chrysophycean alga play an active role in prey capture and selection. Direction observations on *Epipyxis pulchra* using image enhanced video microscopy. *Protoplasma* 166:1–7.

Willén, T. (1961). The phytoplankton of Ösbysjön Djursholm. 1. Seasonal and vertical distribution of the species. *Oikos* 12:36–79.

Zhang, X., and Watanabe, M. M. (2001). Grazing and growth of the mixotrophic chrysomonad *Poterioochromonas malhamensis* (Chrysophyceae) feeding on algae. *J. Phycol*. 37:738–43.

Zhang, X., Watanabe, M. M., and Inouye, I. (1996). Light and electron microscopy of grazing by *Poterioochromonas malhamensis* (Chrysophyceae) on a range of phytoplankton taxa. *J. Phycol*. 32:37–46.

Chapter 11

Heterokontophyta

SYNUROPHYCEAE

The Synurophyceae are closely related to the Chrysophyceae (Ariztia et al., 1991). The Synurophyceae differ, however, from the Chrysophyceae in the following: the Synurophyceae have chlorophylls *a* and c_1 (Andersen and Mulkey, 1983), the flagella are inserted into the cell approximately parallel to one another (Fig. 11.1), there is a photoreceptor near the base of each flagellum, there is no eyespot, and the contractile vacuole is in the posterior portion of the cell (Lavau et al., 1997; Andersen et al., 1999). Chloroplast endoplasmic reticulum is present in a few species, but absent in most. The cells usually are covered by bilaterally symmetrical scales.

In the Synurophyceae, scales composed of silica commonly occur outside the cell (Figs. 11.1, 11.2). The scales are bilaterally symmetrical and are formed in a silica deposition vesicle. The membrane of the silica deposition vesicle (the **silicalemma**) controls the shape of the scale along with proteins and glycoproteins that adhere the developing scale to the silicalemma (Schultz et al., 2001). The presence of germanium in the medium results in inhibition of scale formation (Klaveness and Guillard, 1975). The scales are carried in the scale vesicle to the plasma membrane where the plasma membrane and the scale vesicle fuse, releasing the scales outside the cell (Beech et al., 1990). The scales are held next to the cell in an organic envelope (Ludwig et al., 1996), which is either hyaline or yellow-brown, the latter appearance being due to the impregnation of iron salts. The scales of the Synurophyceae are commonly composed of a number of parts, such as the dome, shield, and bristle of *Mallomonas* (Lavau and Wetherbee, 1994) (Fig. 11.2). The scales of the Synurophyceae are overlapped precisely so that the anterior end of one scale overlaps the right margin of the scale to its left (Leadbeater, 1990).

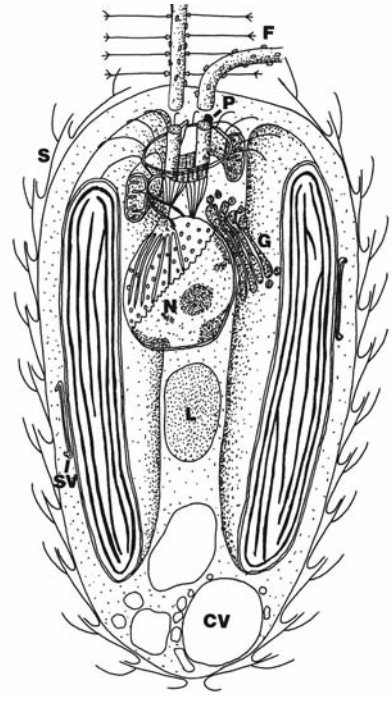


Fig. 11.1 Semidiagrammatic drawing of the cytology of *Synura*, showing the characteristic cytology of the Synurophyceae. (CV) Contractile vacuole; (F) flagella; (G) Golgi; (L) chrysolaminarin vesicle; (N) nucleus; (P) photoreceptor; (S) scale; (SV) scale vesicle. (Adapted from Andersen, 1985.)

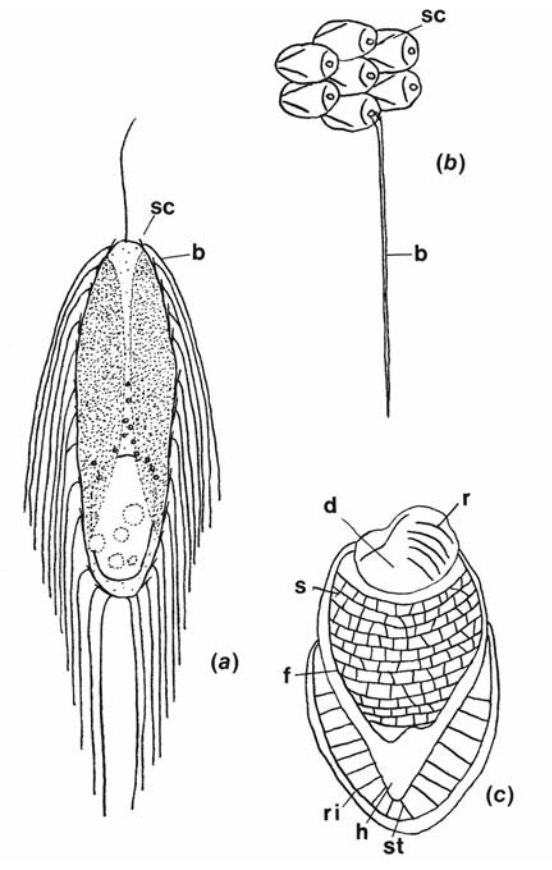


Fig. 11.2 *Mallomonas zellensis*. (*a*) Whole cell. (*b*) Scales. (*c*) A scale with the bristle removed. (b) Bristle; (d) dome; (f) flange; (h) hood; (r) ribs; (ri) rim; (s) shield; (sc) scale; (st) strut. (After Fott, 1962.)

The scales are cemented together to form a scale case by the organic envelope (Fig. 11.4). This precise arrangement of scales differs from the loosely arranged scales of the Chrysophyceae.

Tessellaria volvocina (Fig. 11.3) is a colonial member of the class that has a large number of cells encased within a multilayer covering of siliceous scales. The individual cells of *T. volvocina* do not have a covering of scales (Tyler et al., 1989; Pipes and Leedale, 1992).

Analysis of lake sediments often reveals the presence of the silicified scales of the Synurophyceae as well as the silicified frustules of diatoms (Smol et al., 1984; Dixit et al., 1999). Analysis of the species that produced these silicified deposits can often result in a history of environmental conditions in the lake. Diatoms usually do not grow in waters below a pH of 5.8 to 6, whereas several members of the Synurophyceae thrive in acidic lakes (Saxby-Rouen et al., 1997). As environmental concerns over the acidification of lakes by acid rains increase, these species will probably be more widely used as indicators of lake acidification.

Unlike the Chrysophyceae, the Synurophyceae are not phagocytotic, probably because the fixed scale-case is solidly formed and bacteria and food particles cannot easily reach the cell membrane. The cysts (statospores or stromatocysts) of the Synurophyceae are usually more elaborate than those of the Chrysophyceae.

Classification

The Synurophyceae share affinities with the Bacillariophyceae, Chrysophyceae, and Phaeophyceae (Lavau et al., 1997; Andersen et al., 1999). Because of their silicified outer covering, they have been called "flagellated diatoms"; yet they have many of the characteristics of the Chrysophyceae such as statospores.

There is a single class, the Synurales. All of the organisms are flagellates. Siphonaceous forms do not exist, as true filaments cannot be formed by organisms with a silica scale-case, and coccoid forms would be similar to diatoms. The diatoms *Corethron*, *Rhizosolenia*, and *Attheya* are similar in appearance to coccoid Synurophyceae (Andersen, 1987).

Synura (Fig. 11.4) is a widely distributed colonial member of the class. The life cycle of *Synura petersenii* (Figs. 11.5(*a*), 11.6) has been described by Sandgren and Flanagin (1986). Vegetative colonies of *S. petersenii* normally consist of a number of biflagellate cells joined at their posterior end. The cells are covered with silicified scales (Leadbeater, 1990). Each cell has two parietal chloroplasts, a central nucleus, and a large posterior chrysolamarin vacuole. Sexual reproduction in *S. petersenii* is isogamous and heterothallic. Gametes appear when two compatible clones are mixed. No special culture conditions are required to induce sexual behavior. Actively growing cell populations are continually

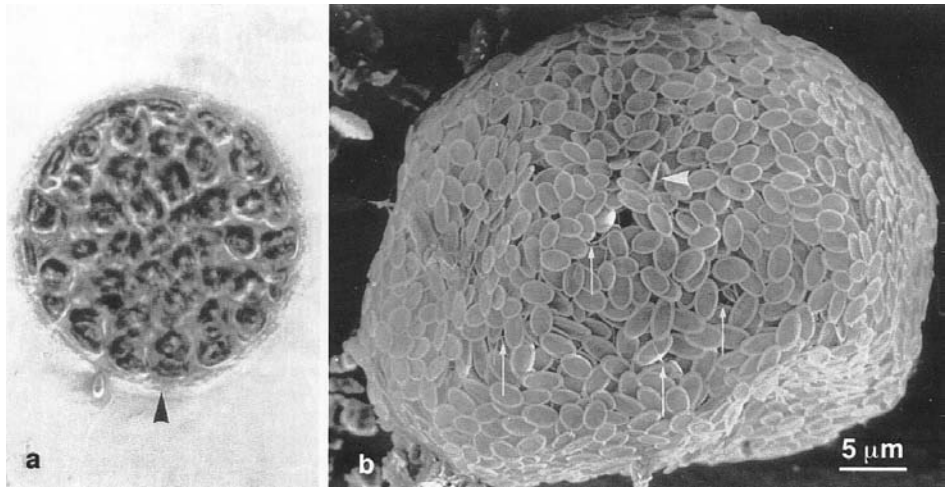


Fig. 11.3 *Tessellaria volvocina*. (*a*) Light micrograph. Arrowhead points to a scale case. (*b*) Scanning electron micrograph showing overlapping of plate scales and rare spine scales (arrowhead). (From Tyler et al., 1989.)

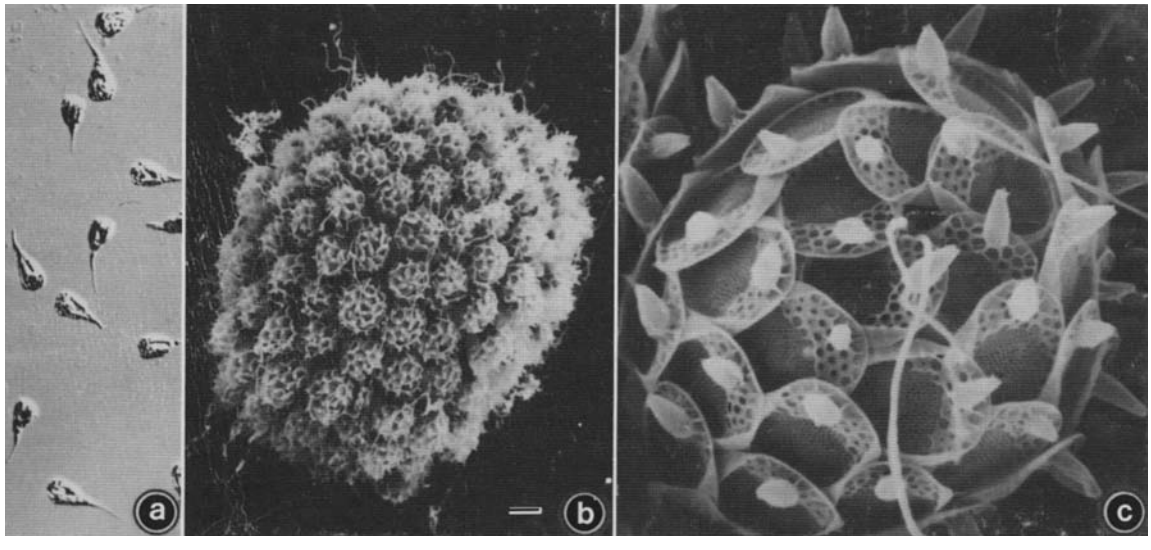


Fig. 11.4 *Synura uvella*. (*a*) Light micrograph. (*b*) Scanning electron micrograph of a colony of cells. (*c*) Scanning electron micrograph of a single cell showing the two flagella emerging from an apical pore in the scale case. Bar = 10 μm. (From Andersen, 1985.)

receptive to mating when mixed with a sufficient number of cells from a compatible clone. Male gametes are solitary biflagellate cells that appear similar to vegetative cells. The solitary male gametes are probably released from the colonies of the male clone. The female gametes occur in colonies or as solitary cells, and are also similar in appearance to vegetative cells. Male and female gametes initially contact each other anteriorly; this is followed by lateral fusion. The silica scale layers mingle so that the resulting fusion cell maintains a complete scale layer. The biflagellate planozygote undergoes minor shape changes

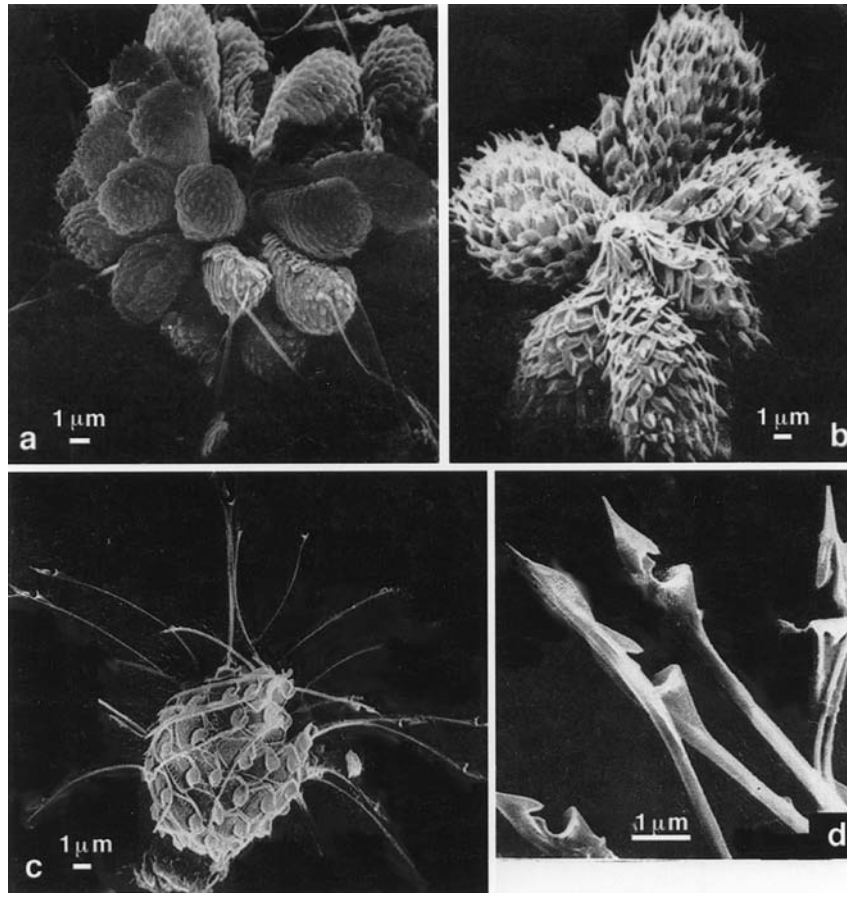


Fig. 11.5 Scanning electron micrographs. (*a*) *Synura petersenii*, whole colony. (*b*) *S. echinulata*. (*c*) *Mallomonas acaroides*, whole cell. (*d*) *M. acaroides*, distal end of helmet bristles. Bar = 1 μm. (From Dürrschmidt, 1984.)

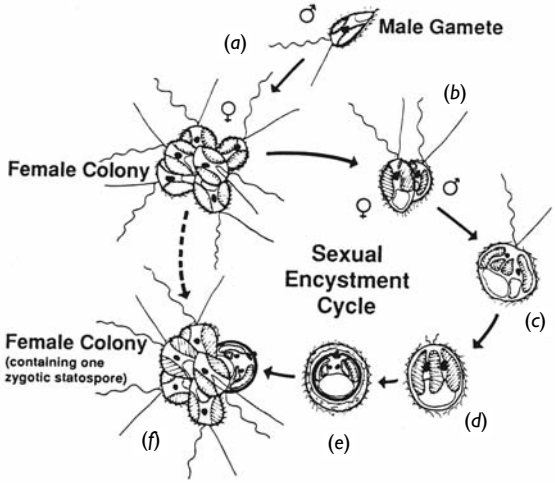


Fig. 11.6 Process of sexual copulation and zygotic encystment in *Synura petersenii*. (*a*) Initial contact of a solitary male gamete with a female gamete within a colony. (*b*) An early stage in plasmogamy characterized by the lateral fusion of cells, each with active flagellar pairs. (*c*) A biflagellate planozygote stage with the fusion cell containing four plastids, two nuclei, and two chrysolaminarin vesicles. Note that the planozygote is completely covered with scales. (*d*) An early stage in zygotic encystment during which the remaining flagella are lost and significant rearrangement of cytoplasmic organelles occurs to establish a symmetrical orientation. Fusion of chrysolaminarin vesicles occurs, and the nuclei become associated with the inner margins of the plastids. (e) A mature zygotic statospore as it ultimately appears taking the place of the female gamete in the colony. (*f*) Germination of statospore. (From Sandgren and Flanagin, 1986.)

and either oscillates in place or swims sluggishly for at least 4 to 8 hours. During this time, the four chloroplasts assume a symmetrical orientation around the flagellar bases as is typical of vegetative *Synura* cells, and the two large chrysolaminarin vesicles fuse to occupy the cell posterior. The flagella are lost, and the zygote becomes spherical as cyst wall deposition begins. After 6 to 8 hours, a morphologically mature zygote statospore is produced. Mature zygospores are observed as solitary objects if the female gametes are solitary. If the female gametes are in a colony, then the zygospores take the place of the female gametes in the female colonies. Female colonies can have as many as eight statospores, apparently as the result of numerous cells serving as female gametes. The cyst is an unornamented sphere, 13 to 16 μm in diameter, and has a single, small recessed pore that lacks a surrounding collar. Presumably, statospores germinate meiotically to produce haploid cells. The number of statospores produced is in the range of 1% to 20% of the vegetative cell density. In addition, some statospores are produced asexually and can be seen in the clones before they are mixed.

REFERENCES

Andersen, R. A. (1985). The flagellar apparatus of the golden alga *Synura uvella:* Four absolute orientations. *Protoplasma* 128:94–106.

Andersen, R. A. (1987). Synurophyceae classis nov., a new class of algae. *Am. J. Bot*. 74:337–53.

Andersen, R. A., and Mulkey, T. J. (1983). The occurrence of chlorophylls c_1 and c_2 in the Chrysophyceae. *J. Phycol*. 19:289–94.

Andersen, R. A., van de Peer, Y., Potter, D., Sexton, J. P., Kawachi, M., and LaJeunesse, T. (1999). Phylogenetic analysis of the SSU rRNA from members of the Chrysophyceae. *Protist* 150:71–84.

Beech, P. L., Wetherbee, R., and Pickett-Heaps, J. D. (1990). Secretion and development of bristles in *Mallomonas splendens* (Synurophyceae). *J. Phycol*. 26:112–22.

Dixit, S. S., Dixit, A. S., and Smol, J. P. (1999). Lake sediment chrysophyte scales from the northeastern U.S.A. and their relationship to environmental variables. *J. Phycol* . 35:903–18.

Dürrschmidt, M. (1984). Studies on scale-bearing Chrysophyceae from the Giessen area, Federal Republic of Germany. *Nord. J. Bot*. 4:123–43.

Fott, B. (1962). Taxonomy of *Mallomonas* based on electron micrographs of scales. *Preslia* 34:69–84.

Klaveness, D., and Guillard, R. R. L. (1975). The requirement for silicon in *Synura petersenii* (Chrysophyceae). *J. Phycol*. 11:349–55.

Lavau, S., and Wetherbee, R. (1994). Structure and development of the scale case of *Mallomonas adamas* (Synurophyceae). *Protoplasma* 181:259–68.

Lavau, S., Saunders, G. W., and Wetherbee, R. (1997). A phylogenetic analysis of the Synurophyceae using molecular data and scale case morphology. *J. Phycol*. 33:135–51.

Leadbeater, B. S. C. (1990). Ultrastructure and assembly of the scale case in *Synura* (Synurophyceae Andersen). *Br. Phycol. J*. 25:117–32.

Ludwig, M., Lind, J. L., Miller, E. A., and Wetherbee, R. (1996). High molecular mass glycoprotein associated with the siliceous cell scales and bristles of *Mallomonas splendens* (Synurophyceae) may be involved in cell surface development and maintenance. *Planta* 199:219–28.

Pipes, L. D., and Leedale, G. F. (1992). Scale formation in *Tessellaria volvocina* (Synurophyceae). *Br. Phycol. J*. 27:11–19.

Sandgren, C. D., and Flanagin, J. (1986). Heterothallic sexuality and density dependent encystment in the chrysophycean alga *Synura petersenii* Korsch. *J. Phycol.* 22:206–16.

Saxby-Rouen, K. J., Leadbeater, B. S. C., and Reynolds, C. S. (1997). The growth response of *Synura petersenii* (Synurophyceae) to photon flux density, temperature, and pH. *Phycologia* 36:233–43.

Schultz, T. F., Egerton-Warburton, L., Crawford, S. A., and Wetherbee, R. (2001). Identification of a 41kDa protein embedded in the biosilica of scales and bristles isolated from *Mallomonas splendens* (Synurophyceae, Ochrophyta). *Protist* 152:315–27.

Smol, J. P., Charles, D. F., and Whitehead, D. R. (1984). Mallomonadacean microfossils provide evidence of recent lake acidification. *Nature* 307:628–30.

Tyler, P. A., Pipes, L. D., Croome, R. L., and Leedale, G. F. (1989). *Tessellaria volvocina* rediscovered. *Br. Phycol. J*. 24:329–37.

Chapter 12

Heterokontophyta

EUSTIGMATOPHYCEAE

Eustimatophytes are yellow-green unicells that occur in freshwater, brackish water, and seawater as well as in the soil. The cells are similar to those in the Xanthophyceae, but differ in having an eyespot outside the chloroplast (Fig. 12.1) (the eyespot in the Xanthophyceae is in the chloroplast) (Hibberd and Leedale, 1970). Other characteristics of the class include a basal swelling of the tinsel flagellum adjacent to the eyespot, only chlorophyll *a*, chloroplasts without girdle lamellae and no peripheral ring of DNA, and chloroplast endoplasmic reticulum not connected to the nuclear envelope (Schnepf et al., 1996).

The eyespot (Figs. 12.1, 12.2) is a large orange-red body at the anterior of the motile cell and

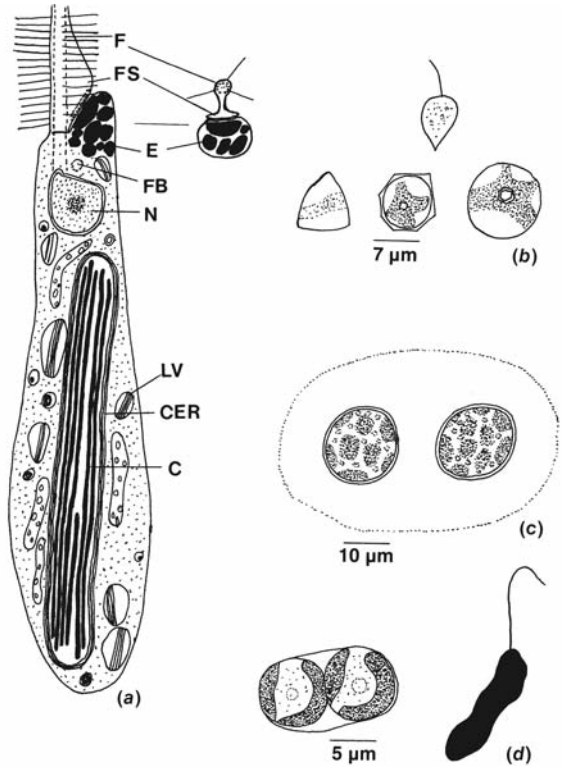


Fig. 12.1 (*a*) Diagrammatic representation of the basic morphology of a zoospore of the Eustigmatophyceae. (C) Chloroplast; (CER) chloroplast endoplasmic reticulum; (E) eyespot; (F) long flagellum; (FB) basal body of short flagellum; (FS) flagellar swelling; (LV) lamellate vesicles; (N) nucleus. (*b*) *Polyhedriella helvetica*, zoospore and vegetative cells. (*c*) *Chlorobotrys regularis*. (*d*) *Pleurochloris magna*, vegetative cell and zoospore. ((*a*) after Hibberd and Leedale, 1972; (*b*) after Fritsch and John, 1942; (*c*) after Smith, 1950; (*d*) after Boye Petersen, 1932.)

is completely independent of the chloroplast. It consists of an irregular group of droplets with no membrane around the whole complex of droplets. The flagellar sheath is extended to form a T-shaped flagellar swelling at the base of the tinsel flagellum (Figs. 12.1, 12.2). This swelling is always closely appressed to the plasmalemma in the region of the eyespot. In turn, in the eyespot there is a large droplet closely applied to the plasmalemma in the area of the flagellar swelling.

The chloroplasts of the Eustigmatophyceae have chlorophyll *a* and *β*-carotene, with the two major xanthophylls being violaxanthin and vaucheriaxanthin (Whittle and Casselton, 1969; Antia and Cheng, 1982), the only difference in pigments compared to the Xanthophyceae being the presence of violaxanthin and the absence of antheraxanthin. Violaxanthin is the major light-harvesting pigment in the Eustigmatophyceae (Owens et al., 1987).

The Eustigmatophyceae is a monophyletic group (Andersen et al., 1998). Most of the species produce zoospores with only a single emergent flagellum (*Pleurochloris magna*, Fig. 12.1(*d*); *Polyedriella helvetica*, Fig. 12.1(*b*), Hibberd and Leedale, 1972), but there is a second basal body present, indicating that the cells had a biflagellate ancestor. The emergent flagellum is tinsel with microtubular hairs, and the flagellum is inserted subapically. Two of the algae in the class, *Ellipsoidion acuminatum* and *Pseudocharaciopsis texensis* (Fig. 12.2) (Lee and Bold, 1973), have zoospores with a long forward tinsel flagellum and a short posteriorly directed smooth

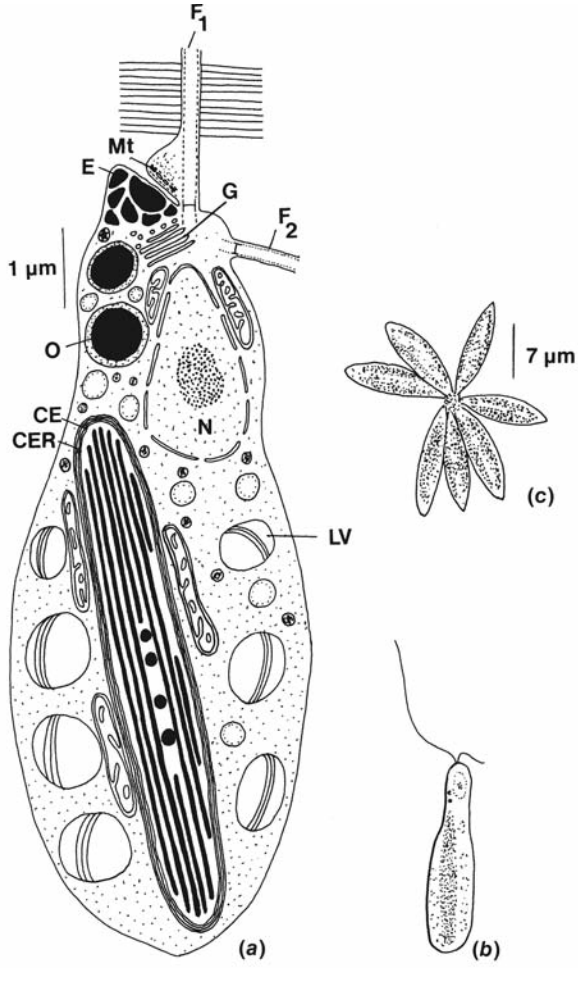


Fig. 12.2 *Pseudocharaciopsis texensis*: (*a*), (*b*) zoospores; (*c*) vegetative cells. (CE) Chloroplast envelope; (CER) chloroplast endoplasmic reticulum; (E) eyespot; (F_1) long flagellum; (F_2) short flagellum; (G) Golgi; (LV) lamellate vacuoles; (Mt) microtubules; (N) nucleus; (O) oil body. (After Lee and Bold, 1973.)

flagellum. One of the organisms, *Chlorobotrys regularis* (Fig. 12.1(*c*)), does not form zoospores (Hibberd, 1974).

REFERENCES

Andersen, R. A., Brett, R. W., Potter, D., and Sexton, J. P. (1998). Phylogeny of the Eustigmatophyceae based upon 18S rDNA, with emphasis on *Nannochloropsis*. *Protist* 149:61–74.

Antia, N. J., and Cheng, J. Y. (1982). The keto-carotenoids of two marine coccoid members of the Eustigmatophyceae. *Br. Phycol. J*. 17:39–50.

Boye Petersen, J. (1932). Einge neue Erdalgen. *Arch. Protistenk*. 76:395–408.

Fritsch, F. E., and John, R. P. (1942). An ecological and taxonomic study of the algae of British soils. II. Consideration of the species observed. I. Chlorophyceae. *Ann. Bot. N.S.* 6:371–95.

Hibberd, D. J. (1974). Observations on the cytology and ultrastructure of *Chlorobotrys regularis* (West) Bohlin with special reference to its taxonomic position in the Eustigmatophyceae. *Br. Phycol. J*. 9:37–46.

Hibberd, D. J., and Leedale, G. F. (1970). Eustigmatophyceae – a new algal class with unique organization of the motile cell. *Nature* 225:758–60.

Hibberd, D. J., and Leedale, G. F. (1972). Observations on the cytology and ultrastructure of the new algal class Eustigmatophyceae. *Ann. Bot. N.S.* 36:49–71.

Lee, K. W., and Bold, H. C. (1973). *Pseudocharaciopsis texensis* gen. et sp. nov., a new member of the Eustigmatophyceae. *Br. Phycol. J*. 8:31–7.

Owens, T. G., Gallagher, J. C., and Alberte, R. S. (1987). Photosynthetic light-harvesting function of violaxanthin in *Nannochloropsis* spp. (Eustigmatophyceae). *J. Phycol*. 23:79–85.

Schnepf, E., Niemann, A., and Wilhelm, C. (1996). *Pseudostaurastrum limneticum*, a Eustigmatophycean alga with astigmatic zoospores: morphogenesis, fine structure, pigment composition and taxonomy. *Arch. Protistenk*. 146:237–49.

Smith, G. M. (1950). *The Freshwater Algae of the United States*, 2nd edn. New York and London: McGraw-Hill.

Whittle, S. J., and Casselton, P. J. (1969). The chloroplast pigments of some green and yellow-green algae. *Br. Phycol. J*. 4:55–64.

Chapter 13

Heterokontophyta

PINGUIOPHYCEAE

The Pinguiophyceae is a class of marine planktonic algae that were previously classed as "chrysophytes." Analysis of nuclear-encoded 18S rRNA and chloroplast-encoded *rbc*L gene sequences uncovered the close relationship of the organisms in this class (Kawachi et al., 2002). The class is characterized by unusually high concentrations of polyunsaturated acids, especially 20:5 (n-3) (EPA-eicosapentaenoic acid) in the cells (Kawachi et al., 1996) (Fig. 13.1). These fatty acids are the basis for choosing the latin noun "Pingue" (meaning fat, grease) as the root of the class name. The high percentage of unsaturated fatty acids, and the lack of a cell wall, make these algae desirable as a source of unsaturated fatty acids and of animal feed.

$CH_3CH_2(CH{=}CHCH_2)_5(CH_2)_2COOH$

Eicosapentaenoic Acid

Fig. 13.1 The structure of eicosapentaenoic acid, a polyunsaturated fatty acid found in high concentrations in algae in the Pinguiophyceae.

The cells (Figs. 13.2, 13.3) (Honda and Inouye,

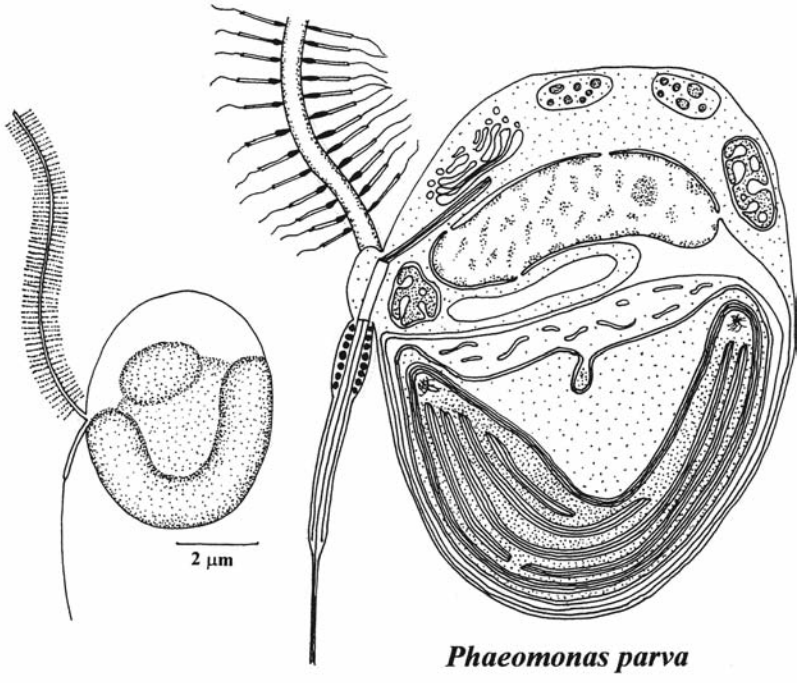


Fig. 13.2 Ultrastructural characteristics of an alga in the Pinguiophyceae.

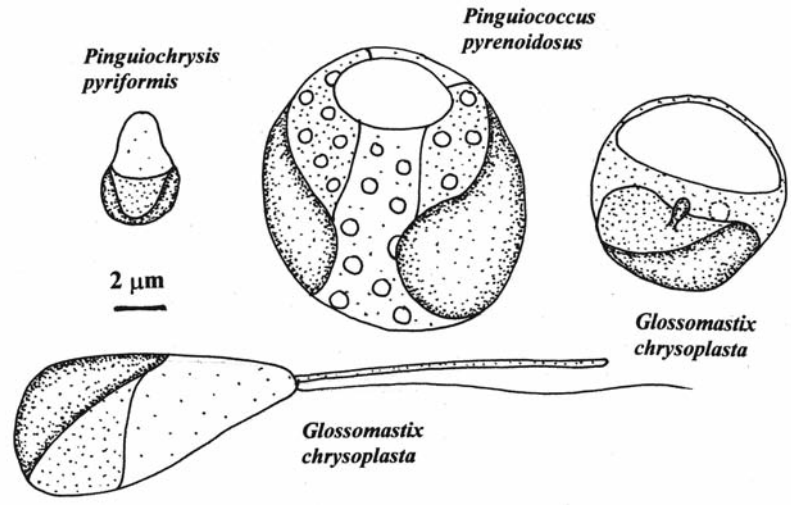


Fig. 13.3 Algae classified in the Pinguiophyceae.

2002) are derived from a typical heterokont ancestor with an anterior tinsel flagellum with tripartite hairs and a posterior smooth whiplash flagellum (although many of the genera have lost one or both flagella through evolution). The chloroplasts have two membranes of chloroplast endoplasmic reticulum, the outer membrane continuous with the nuclear envelope. A girdle band of thylakoids occurs under the chloroplast envelope. Pyrenoids occur in the chloroplast and the mitochondria have tubular cristae. Chlorophyll *a* and chlorophyll *c*-related pigments as well as fucoxanthin, violaxanthin, zeaxanthin, and β-carotene are present.

REFERENCES

Honda, D., and Inouye, I. (2002). Ultrastructure and taxonomy of a marine photosynthetic stramenopile *Phaeomonas parva* gen. et sp. nov. (Pinguiophyceae) with emphasis on the flagellar apparatus architecture. *Phycol. Res*. 50:75–89.

Kawachi, M., Kato, M., Ikemoto, H., and Miiyachi, S. (1996). Fatty acid composition of a new marine picoplankton species of the Chromophyta. *J. Appl. Phycol*. 8:397–401.

Kawachi, M., Inouye, I., Honda, D., et al. (2002). The Pinguiophyceae *classis nova*, a new class of photosynthetic stramenopiles whose members produce large amounts of omega-3 fatty acids. *Phycol. Res*. 50:31–47.

Chapter 14

Heterokontophyta

DICTYOCHOPHYCEAE

These golden-brown algae are characterized by tentacles or rhizopodia on basically amoeboid vegetative cells (Moestrup, 1995; Preisig, 1995). Amoeboid cells are relatively rare among the algae, being mostly restricted to the Dictyochophyceae and the Xanthophyceae (Hibberd and Chretiennot-Dinet, 1979). The algae in the Dictyochophyceae have been previously classified in the Chrysophyceae, although molecular evidence shows them to be most closely related to the Pelagophyceae (Cavalier-Smith et al., 1995) or Eustigmatophyceae (Daugbjerg and Andersen, 1997).

Classification

The Dictyochophyceae can be divided into three orders (Preisig, 1995):

Order 1 Rhizochromulinales: marine and freshwater unicells with tentacles.
Order 2 Pedinellales: unicells with a long anterior flagellum and a second flagellum reduced to a basal body, usually three to six chloroplasts (if chloroplasts are present), marine and freshwater.
Order 3 Dictyocales: marine unicells with an external silicified skeleton.

Rhizochromulinales

This order contains the more primitive organisms in the order (O'Kelly and Wujek, 1995). *Rhizochromulina* (Fig. 14.1(*a*), (*b*)) has amoeboid non-flagellated vegetative cells with many fine beaded-filipodia and a single golden-brown chloroplast (Hibberd and Chretiennot-Dinet, 1979). The fusiform zoospore has a single tinsel flagellum with a second basal body in the protoplasm (Fig. 14.1(*b*)). *Chrysoamoeba* (Fig. 14.1(*d*)) lives as a solitary amoeba for the greater part of its life cycle, transforming into swimming cells with a single long flagellum only for short periods. In *Phaeaster* (Fig. 14.1(*c*)), the anterior portion of the cell is drawn out into rhizopodia.

Pedinellales

The pedinellids are unique in containing genera that are phototrophic (*Apedinella* (Fig. 14.2(*c*)), *Pseudopedinella*), mixotrophic (able to photosynthesize and take up organic compounds) (*Pedinella*) (Figs. 14.2(*a*), (*b*), 14.3, 14.4), and phagotrophic (*Pteridomonas*, *Ciliophrys*). The phagotrophic genera have vestigial chloroplasts and evolved from genera with chloroplasts (Sekiguchi et al., 2002). The organisms in this order have three interconnected microtubules (triads) that course from the nuclear envelope through tentacles (if they are present) to the plasma membrane (Fig. 14.2(*a*)) (Daugbjerg, 1996). A long apical flagellum is extended into a lateral wing by a paraxonemal rod (Figs. 14.2, 14.3(*b*)). The apical flagellum is inserted in a pit and there is a second flagellum that is reduced to a basal body. The basal bodies are at a slight angle to each other. The cells are radially symmetrical with a large central nucleus and a posterior Golgi apparatus. There are usually three to six chloroplasts present

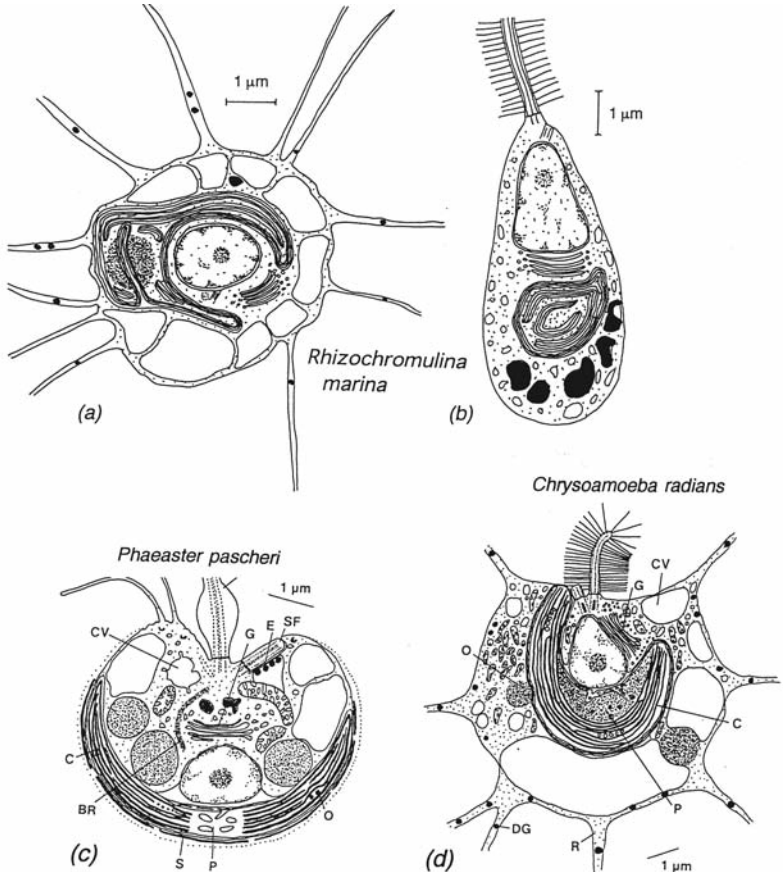


Fig. 14.1 (*a*), (*b*) *Rhizochromulina marina*. Vegetative cell (*a*) and zoospore (*b*). (*c*) *Phaeaster pascheri*. (*d*) *Chrysoamoeba radians*. (BR) Basal root; (C) chloroplast; (CV) contractile vacuole; (DG) dense granule; (E) eyespot; (G) Golgi body; (LF) long flagellum; (O) oil; (P) pyrenoid; (R) rhizopodium; (S) scale; (SF) short flagellum. ((*a*), (*b*) Redrawn from Hibberd and Chretiennot-Dinet, 1979; (*c*) redrawn from Belcher and Swale, 1971; (*d*) redrawn from Hibberd, 1971.)

if the organism is phototrophic (whereas in the Chrysophyceae there are usually only one or two chloroplasts). Some genera, such as *Pedinella* (Fig. 14.4(*d*), (*e*)) and *Apedinella* (Fig. 14.2(*c*)), have scales attached to the plasma membrane by microligaments (Koutoulis et al., 1988).

A posterior trailing stalk, associated with a system of vacuoles, can be present. *Pedinella* (Figs. 14.2(*a*), 14.4) cells rotate while swimming, trailing the stalk behind. The stalk appears to be sticky, and swimming cells will often adhere to a substrate by means of the stalk. *Pedinella* can undergo phagotrophy and ingest other small cells. Bacteria are passed down the flagellum and adhere to the plasma membrane, just outside the row of tentacles. Secretions of the muciferous bodies in this region provide an adhesive that sticks the cells to the plasmalemma. Usually within a minute, the bacteria become enveloped in a sheet of cytoplasm that is extruded from the cell.

Dictyocales

The Dictyocales or silicoflagellates are a group of cosmopolitan marine flagellates, presently represented by only one extant genus *Dictyocha*, although an abundance of taxa have been described from fossil siliceous skeletons (Henriksen et al., 1993).

Silicoflagellate cells have one emergent flagellum and a skeleton of hollow siliceous rods outside of the protoplasm. The skeleton can be a simple ring, an ellipse, or a triangle, but it is often much more complete. In *Dictyocha fibula* (Fig. 14.5), the skeleton is composed of a series of peripheral polygons surrounding a central hexagon. The nucleus is in the center of the protoplasm with a number of cytoplasmic processes extending from the central mass. The chloroplasts are usually in the cytoplasmic processes (van Valkenburg, 1971a, b). Most species have chloroplasts that are derived from secondary endosymbioses, although

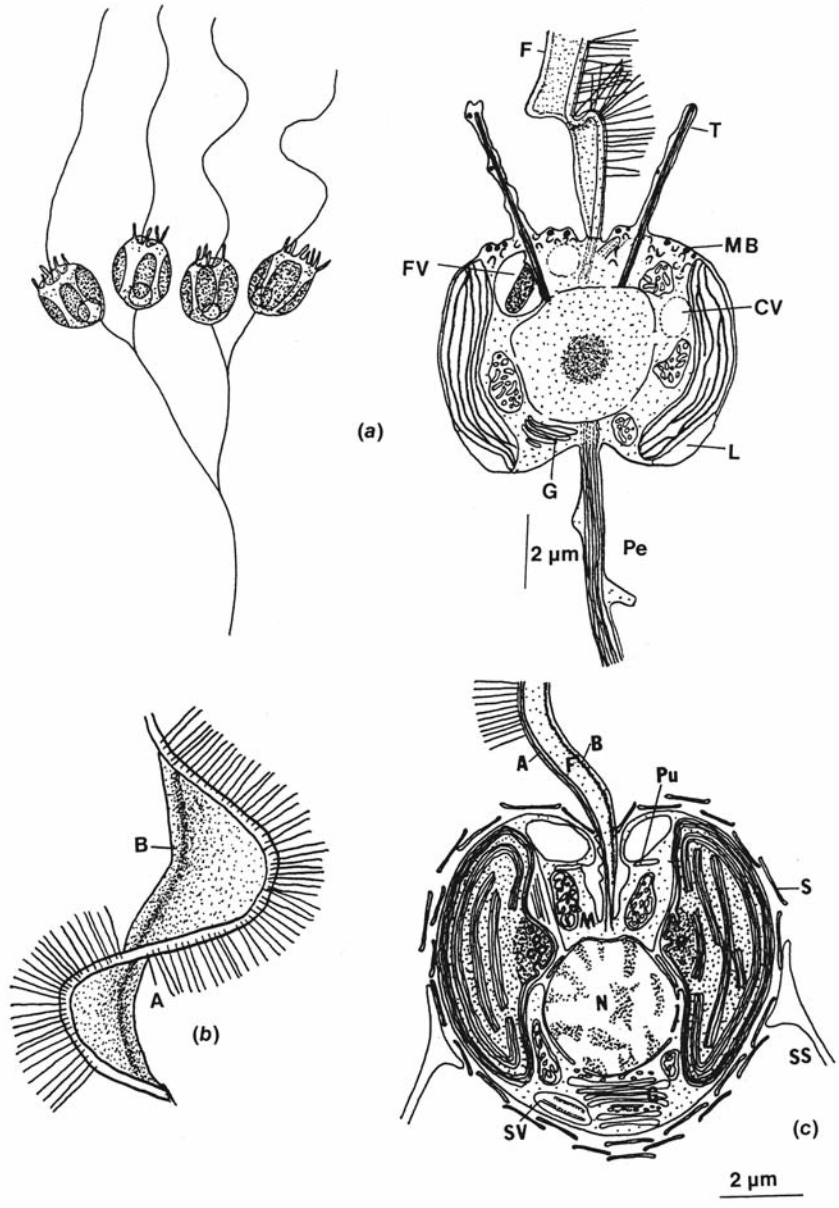


Fig. 14.2 (*a*) *Pedinella hexacostata* in the light and electron microscope. (*b*) Structure of the winged flagellum of *P. hexacostata*. (*c*) *Apedinella spinifera*. (A) Axoneme of flagellum; (B) paraxonemal rod of flagellum; (CV) contractile vacuole; (F) flagellum with hairs; (FV) food vacuole; (G) Golgi body; (L) leucosin; (M) mitochondrion; (MB) muciferous body; (N) nucleus; (Pe) peduncle; (Pu) pusule; (S) scale; (SS) spined scale; (SV) scale vesicle; (T) tentacle. ((*a*), (*b*) after Swale, 1969; (*c*) after Throndsen, 1971.)

there has been a report of chloroplasts derived from haptophytes through tertiary endosymbioses (Daugbjerg and Henriksen, 2001).

In *Dictyocha speculum*, the skeleton-bearing cells multiply vegetatively by mitotic division (Fig. 14.6) (Hendriksen et al., 1993). Cells connected by bridges develop and give rise to large spherical cells without skeletons that become multinucleate. Uninucleate swarmers with a single flagellum develop in the large spherical cells. The swarmers are released and grow into large multinucleate

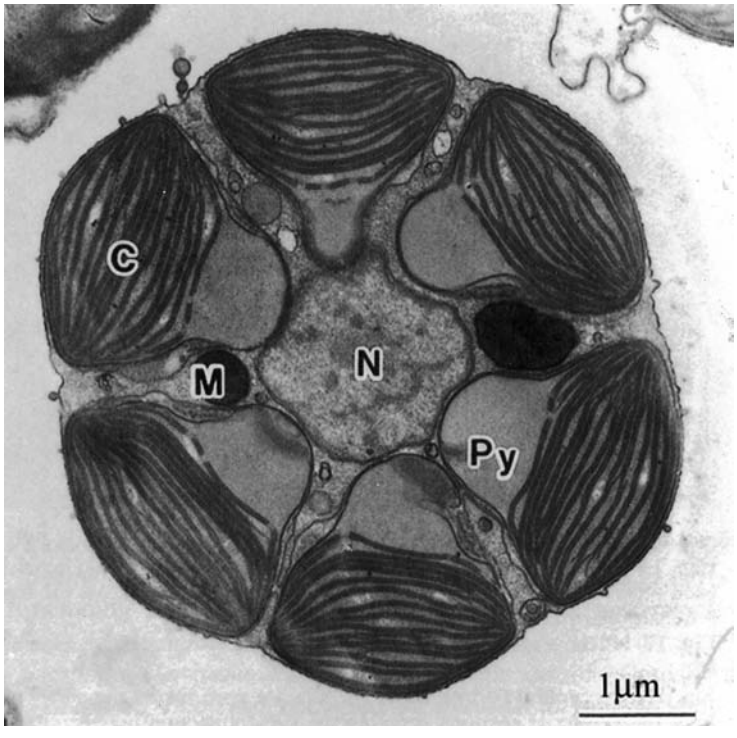


Fig. 14.3 *Pedinella squamata.* Transmission electron micrograph. (C) Chloroplast; (M) mitochondrion; (N) nucleus; (Py) pyrenoid. (From Sekiguchi et al., 2003.)

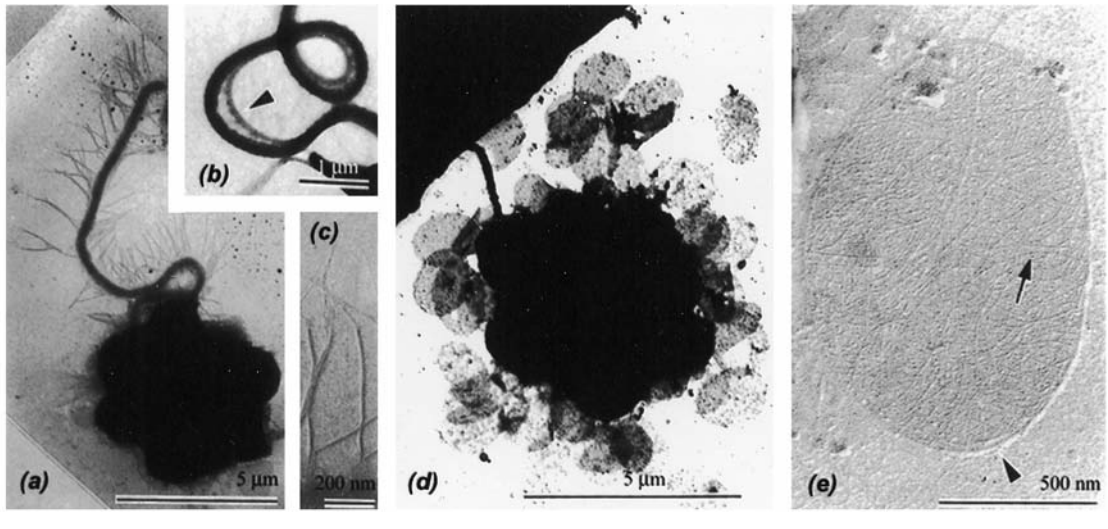


Fig. 14.4 *Pedinella squamata.* Transmission electron micrographs. (*a*) Whole mount of a cell showing the flagellum and mastigonemes. (*b*) Higher magnification of a flagellum showing a paraxonemal rod (arrowhead). (*c*) Higher magnification of mastigonemes with no lateral filaments on the shafts. (*d*) Plate scales scattered about a whole mount of a cell. (*e*) A single plate scale with fibers (arrow) and the marginal rim (arrowhead). (From Sekiguchi et al., 2003.)

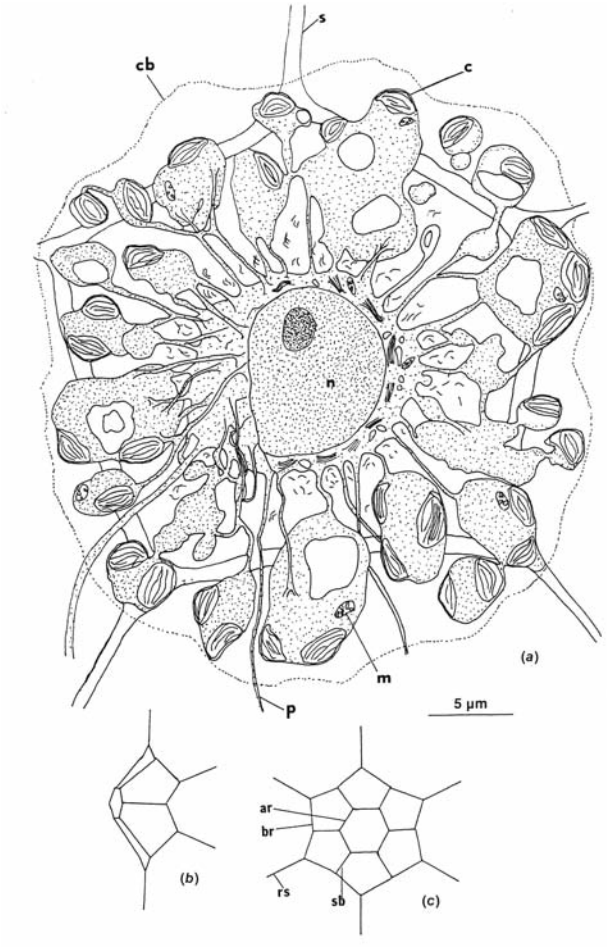


Fig. 14.5 (*a*) A drawing of the fine structure of *Dictyocha fibula*. (*b*), (*c*) Side and front views of the skeleton of *Dictyocha*. (ar) Apical ring; (br) basal ring; (c) chloroplast; (cb) cell boundary; (m) mitochondrion; (n) nucleus; (p) pseudopodium; (rs) radial spine; (s) silica skeleton; (sb) supporting bar. (After van Valkenburg, 1971a,b.)

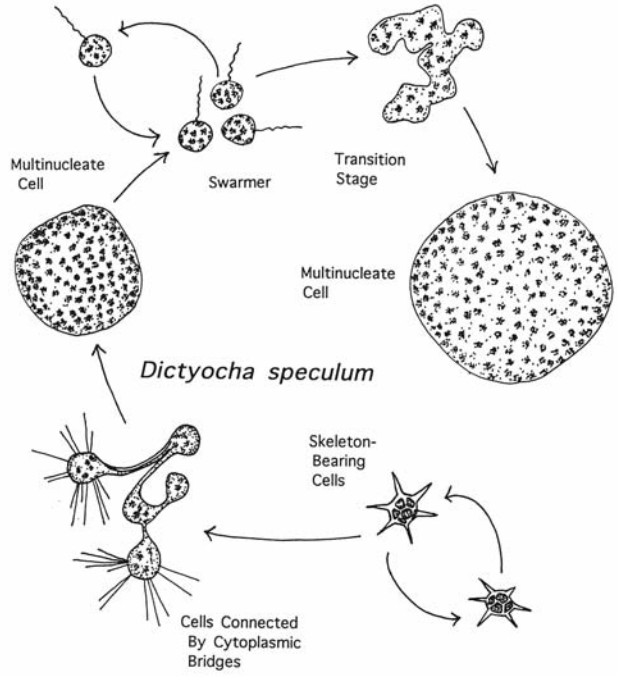


Fig. 14.6 Growth stages of the silicoflagellate *Dictyocha speculum*. (Adapted from Henriksen et al., 1993.)

cells, which are probably a form of resting cell. All of the cells are of the same ploidy level and sexual reproduction is not known.

The silicoflagellates originated in the Cretaceous, with the earlier forms having a simpler skeleton than those existing today. Fossils of silicoflagellates are common in calcareous chalks along with members of the Prymnesiophyceae. Silicoflagellates constitute a prominent part of the phytoplankton in the colder seas of today.

REFERENCES

Belcher, J. H., and Swale, E. M. F. (1971). The microanatomy of *Phaeaster pascheri* Scherffel (Chrysophyceae). *Br. Phycol. J.* 6:157–69.

Cavalier-Smith, T., Chao, E. E., and Allsopp, T. E. P. (1995). Ribosomal RNA evidence for chloroplast loss within Heterokonta: pedinellid relationships and a revised classification of ochristan algae. *Arch. Protistenkd*. 145:209–20.

Daugbjerg, N. (1996). *Mesopedinella arctica* gen. et sp. nov. (Pedinelles, Dictyochophyceae). I. Fine structure of a new marine phytoflagellate from Arctic Canada. *Phycologia* 35:435–45.

Daugbjerg, N., and Andersen, R. A. (1997). A molecular phylogeny of heterokont algae based on analyses of chloroplast-encoded *rbc*L sequence data. *J. Phycol*. 33:1031–41.

Daugbjerg, N., and Henriksen, P. (2001). Pigment composition and *rbc*L sequence data from the silicoflagellate *Dictyocha speculum*: a heterokont alga with pigments similar to some haptophytes. *J. Phycol*. 37:1110–20.

Henriksen, P., Knipschildt, F., Moestrup, Ø., and Thomsen, H. A. (1993). Autecology, life history and toxicology of the silicoflagellate *Dictyocha speculum* (Silicoflagellata, Dictyochophyceae). *Phycologia* 32:29–39.

Hibberd, D. J. (1971). Observations on the cytology and ultrastructure of *Chrysoamoeba radians* Klebs (Chrysophyceae). *Br. Phycol. J.* 6:207–23.

Hibberd, D. J., and Chretiennot-Dinet, M.-J. (1979). The ultrastructure and taxonomy of *Rhizochromulina marina* gen. et sp. nov., an amoeboid marine chrysophyte. *J. Mar. Biol. Assn., UK* 59:179–93.

Koutoulis, A., McFadden, G. I., and Wetherbee, R. (1988). Spine-scale reorientation in *Apedinella radians* (Pedinelles, Chrysophyceae): the microarchitecture and immunocytochemistry of the associated cytoskeleton. *Protoplasma* 147:25–41.

Moestrup, Ø. (1995). Current status of chrysophyte 'splinter groups': synurophytes, pedinellids, silicoflagellates. In *Chrysophyte Algae*, ed. C. D. Sandgren, J. R. Smol, and J. Kristiansen, pp. 75–91. Cambridge: Cambridge University Press.

Preisig, H. R. (1995). A modern concept of chrysophyte classification. In *Chrysophyte Algae*, ed. C. D. Sandgren, J. R. Smol, and J. Kristiansen, pp. 46–74. Cambridge: Cambridge University Press.

Sekiguchi, H., Moriya, M., Nakayama, T., and Inouye, I. (2002). Vestigial chloroplasts in heterotrophic stramenopiles *Pteridomonas danica* and *Ciliophrys infusionum* (Dictyochophyceae). *Protist* 153:157–67.

Sekiguchi, H., Kawachi, M., Nakayama, T., and Inouye, I. (2003). A taxonomic re-evaluation of the Pedinellales (Dictyophyceae) based on morphological, behavioural and molecular data. *Phycologia* 42:165–82.

Swale, E. M. F. (1969). A study of the nanoplankton flagellate *Pedinella hexacostata* Vysotshiĭ by light and electron microscopy. *Br. Phycol. J*. 4:65–86.

Throndsen, J. (1971). *Apedinella* gen. nov. and the fine structure of *A. spinifera* (Throndsen) comb. nov. *Norw. J. Bot*. 18:47–64.

van Valkenburg, S. D. (1971a). Observations on the fine structure of *Dictyocha fibula* Ehrenberg. I. The skeleton. *J. Phycol*. 7:113–18.

van Valkenburg (1971b). Observations on the fine structure of *Dictyocha fibula* Ehrenberg. II. The protoplast. *J. Phycol*. 7:118–32.

Chapter 15

Heterokontophyta

PELAGOPHYCEAE

The Pelagophyceae are a group of basically unicellular algae that are cytologically similar to the Chrysophyceae, in which they were previously classified (Andersen et al., 1993). The cells are very small (3–5 μm) members of the ultraplankton and appear as small spheres with indistinct protoplasm under the light microscope. Recent studies on the sequences of small-subunit RNA nucleotides in these algae have shown them to be closely related to each other and distinct from other members of the Heterokontophyta (Saunders et al., 1997). While these algae have been shown to be distinct from other members of the Heterokontophyta based on molecular data, they do not have cytological or morphological characters which are very different from other members of the phylum.

Pelagomonas calceolata is a very small (1.5 μm × 3 μm) ultraplanktonic marine alga with a single tinsel flagellum and basal body, and a single chloroplast and mitochondrion (Fig. 15.1(*c*)) (Andersen et al., 1993). Another member of the marine ultraplankton is *Pelagococcus subviridis*, a green-gold spherical non-motile cell (2.5–3.0 μm) with a single chloroplast, mitochondrion, and nucleus (Fig. 15.1(*a*)) (Vesk and Jeffery, 1987).

Members of the class are economically important because some of the algae produce "brown tides." *Aureoumbra lagunensis* (Fig. 15.1(*b*)) is the causative agent of brown tides in Texas (DeYoe et al., 1997), while *Aureococcus anophagefferens* forms brown tides along the coasts of New Jersey, New York, and Rhode Island. The numbers of cells in brown tides can be so large that they can exclude light from the benthic eelgrass (*Zostera marine*), resulting in elimination of the eelgrass. The larvae of the bay scallop feed off eelgrass and the bay scallop industry was virtually wiped out for a number of years after a brown tide in the waters off the northeast United States (Nicholls, 1995).

Aureoumbra lagunensis (Fig. 15.1(*b*)) is able to grow at its maximum rate at salinities as high as 70 PSU (**practical salinity units**; seawater is about 35 PSU). Few algae are able to survive these hypersaline conditions. In addition, the surface of the cells are covered with a slime layer that reduces predation (Liu and Buskey, 2000). A combination of these advantages enables *A. lagunensis* to outcompete other algae.

Aureococcus anophagefferens (Fig. 15.2) is a psychrophilic alga that is able to grow at low temperatures and survive extended periods of darkness. This explains its ability to form algal blooms (Popels and Hutchins, 2002). Dense cell populations of 100 000 cells ml^{-1} were recorded before the ice formed in Great Bay, Long Island, New York. Two months later, after the ice had melted the cell populations were still as high as 60 000 cells ml^{-1}, concentrations that still were at bloom levels (Gobler et al., 2002). It has been shown that filter feeders grow at a reduced rate when cells of *Aureococcus* are present (Greenfield et al., 2004).

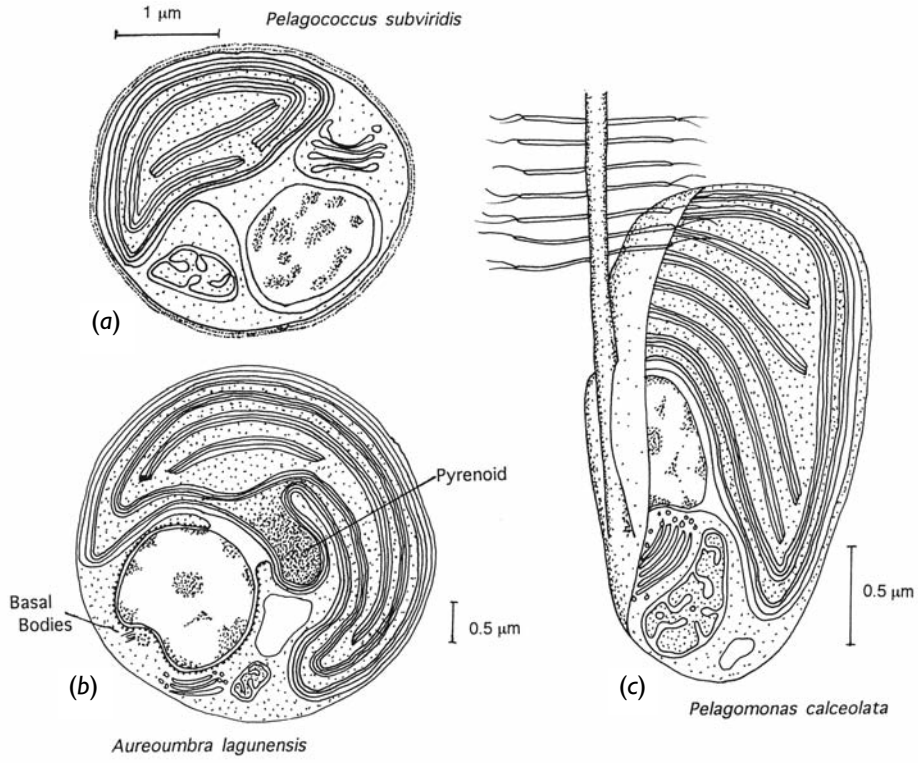


Fig. 15.1 (*a*) *Pelagococcus subviridis* showing the single chloroplast, nucleus, and mitochondrion. (*b*) *Aureoumbra lagunensis* with the characteristic stalked pyrenoid and two basal bodies near the nucleus. (*c*) *Pelagomonas calceolata* showing the single flagellum fitting into a groove in the cell. ((*a*) adapted from Vesk and Jeffery, 1987; (*b*) adapted from DeYoe et al., 1997; (c) adapted from Andersen et al., 1993.)

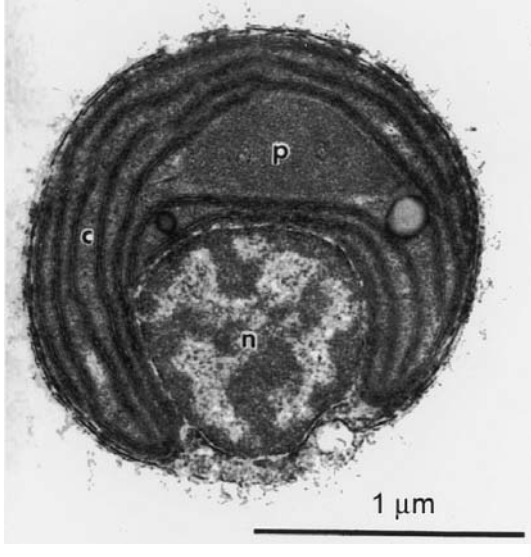


Fig. 15.2 Transmission electron micrograph of a section of a cell of *Aureococcus anophagefferens*. (c) Chloroplast; (n) nucleus; (p) pyrenoid. (From Sieburth et al., 1988.)

REFERENCES

Andersen, R. A., Saunders, G. W., Paskind, M. P., and Sexton, J. P. (1993). Ultrastructure and 18S rRNA gene sequence for *Pelagomonas calceolata* gen. et sp. nov. and the description of a new algal class, the Pelagophyceae classis nov. *J. Phycol*. 29:701–15.

DeYoe, H. R., Stockwell, D. A., Bidigare, R. R., Latasa, M., Johson, P. W., Hargraves, P. E., and Suttle, C. A. (1997). Description and characterization of the algal species *Aureoumbra lagunensis* gen. at sp. nov. and referral of *Aureoumbra* and *Aureococcus* to the Pelagophyceae. *J. Phycol*. 33:1042–8.

Gobler, C. J., Renaghan, M. J., and Buck, N. J. (2002). Impacts of nutrients and grazing mortality on the abundance of *Aureococcus anophagefferens* during a New York brown tide bloom. *Limnol. Oceanogr*. 47:129–41.

Greenfield, D. I., Lonsdale, D. J., Cerrato, R. M., and Lopez, G. R. (2004). Effects of background

concentrations of *Aureococcus anophagefferens* (brown tide) on growth and feeding in the bivalve *Mercenaria mercenaria*. *Mar. Biol. Progr. Ser*. 274:171–81.

Liu, H., and Buskey, E. J. (2000). The exopolymer secretions (EPS) layer surrounding *Aureoumbra lagunensis* cells affects growth, grazing, and behavior of protozoa. *Limnol. Oceanogr*. 45:1187–91.

Nicholls, K. H. (1995). Chrysophyte blooms in the plankton and neuston of marine and freshwater systems. In *Chrysophyte Algae, Ecology, Phylogeny and Development*, ed. C. D. Sandgren, J. P. Smol, and J. Kristiansen, pp. 181–213. Cambridge: Cambridge University Press.

Popels, L. C., and Hutchins, D. A. (2002). Factors affecting dark survival of the brown tide alga *Aureococcus anophagefferens* (Pelagophyceae). *J. Phycol*. 38:738–44.

Saunders, G. W., Potter, D., and Andersen, R. A. (1997). Phylogenetic affinities of the Sarcinochrysidales and Chrysomeridales (Heterokonta) based on analysis of molecular and combined data. *J. Phycol*. 33:310–18.

Sieburth, J. M., Johnson, P. W., and Hargraves, P. E. (1988). Ultrastructure and ecology of *Aureococcus anophagefferens* gen. et sp. nov. (Chrysophyceae): the dominant picoplankter during a bloom in Narragansett Bay, Rhode Island, summer 1985. *J. Phycol*. 24:416–25.

Vesk, M., and Jeffrey, S. W. (1987). Ultrastructure and pigments of two strains of the picoplanktonic alga *Pelagococcus subviridis* (Chrysophyceae). *J. Phycol*. 23:322–36.

Chapter 16

Heterokontophyta

BOLIDOPHYCEAE

This is a small order of flagellated marine picophytoplankton that is related to the diatoms (Bacillariophyceae) (Guillou et al., 1999). The cells contain chlorophylls *a*, c_1, c_2, c_3, β-carotene, diatoxanthin, and fucoxanthin, as do the diatoms, It is probable that the diatoms originated from a motile ancestor similar to those in this class (although there is no report of silicification in the Bolidophyceae).

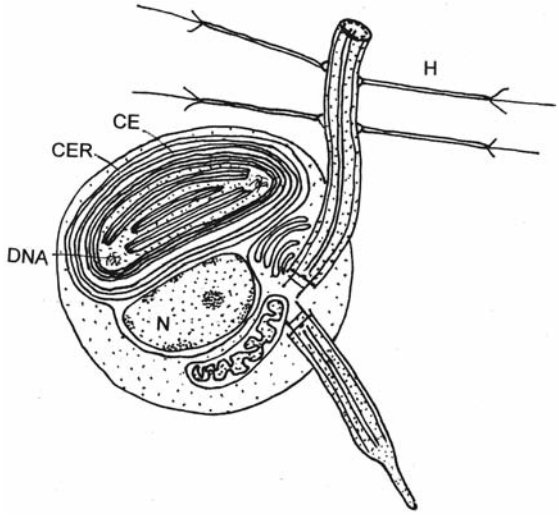


Fig. 16.1 Semidiagrammatic drawing of the cytology of *Bolidomonas*. (CE) Chloroplast envelope; (CER) chloroplast endoplasmic reticulum; (H) tripartite flagellar hair; (N) nucleus. (Adapted from Guillou et al., 1999.)

Bolidomonas is a unicell with a long tinsel flagella bearing tripartite tubular hairs and a shorter smooth flagellum (Fig. 16.1). The cell is only 1.2 μm in diameter and has a simple internal organization. There is one plastid, mitochondrion, and Golgi apparatus. There are two membranes of chloroplast endoplasmic reticulum, with the outer membrane continuous with the outer membrane of the nuclear envelope. The DNA is contained within a ring-shaped genophore and there is no eyespot.

REFERENCE

Guillou, L., Chretiennot-Dinet, M.-J., Medlin, L. K., Claustre, H., Loiseaux-de Goer, S., and Vaulot, D. (1999). *Bolidomonas*: a new genus with two species belonging to a new algal class, the Bolidophyceae (Heterokonta). *J. Phycol*. 35:368–81.

Chapter 17

Heterokontophyta

BACILLARIOPHYCEAE

The Bacillariophyceae or the diatoms probably evolved from a scaly member of the Chrysophyceae (similar to the organisms in the Parmales) or Bolidophyceae (Guillou et al., 1999). The diatoms are unicellular, sometimes colonial algae found in almost every aquatic habitat as free-living photosynthetic autotrophs, colorless heterotrophs, or photosynthetic symbiotes (Schmaljohann and Röttger, 1978). They may occur as plankton or periphyton, with most brownish-green films on substrates such as rocks or aquatic plants being composed of attached diatoms. The cells are surrounded by a rigid two-part box-like cell wall composed of silica, called the **frustule**. The chloroplasts contain chlorophylls *a*, c_1, and c_2 with the major carotenoid being the golden-brown fucoxanthin, which gives the cells their characteristic color.

In discussing diatoms and silica, there is often confusion over terminology in regard to silicon. **Silicon** is the element. **Silica** is a short convenient designation for **silicon dioxide** (SiO_2) in all of its crystalline, amorphous, and hydrated or hydroxylated forms. **Silicate** is any of the ionized forms of monosilicic acid [$Si(OH)_4$] (Iler, 1979).

Cell structure

The two-part frustule surrounds protoplasm that has a more or less central nucleus suspended in a system of protoplasmic threads. The chloroplasts occupy most of the cell (Figs. 17.17, 17.46) usually as two parietal plastids although sometimes as numerous discoid plastids. The storage product, chrysolaminarin, occurs in vesicles in the protoplasm.

Cell wall

The characteristic feature of the Bacillariophyceae is their ability to secrete an external wall composed of silica, the frustule. It is constructed of two almost equal halves, the smaller fitting into the larger like a Petri dish (Figs. 17.1, 17.9, 17.10, 17.41). The outer of the two half-walls is the **epitheca** and the inner the **hypotheca**. Each theca is composed of two parts, the **valve**, a more or less flattened plate, and the **connecting band**, attached to the edge of the valve. The two connecting bands, one attached to each valve, are called the **girdle** (von Stosch, 1975). Sometimes the connecting bands themselves are called **girdle bands** (Fig. 17.41). Occasionally there are one or more additional bands between the valve and the girdle, which are called **intercalary bands**. When an appreciable part of the edge of the valve is bent inward, this portion is called the **mantle** or **valve-jacket**. The girdle bands, often furnished with minute teeth, hold the valves together by their edges. The value margin thus butts onto the end of the girdle band and is usually connected to it by a pectinaceous film. If this film is destroyed, the valve and girdle bands separate.

The siliceous material of the frustule is laid down in certain regular patterns that leave the wall ornamented. According to Hendey (1964), the ornamentation of diatoms can be divided into four basic types: (1) **centric** and radial, where the

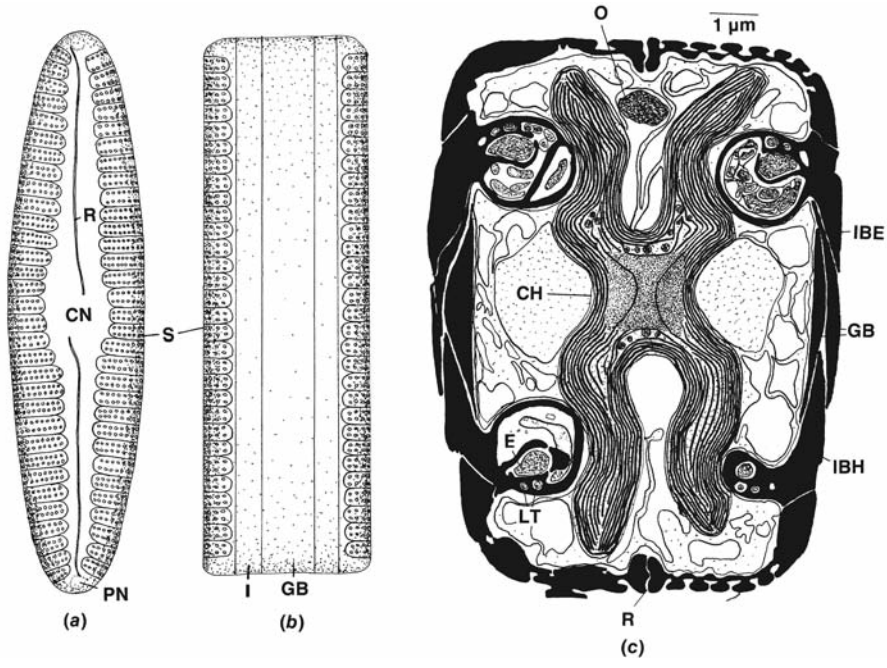


Fig. 17.1 Light microscopical drawing of valve (*a*) and girdle (*b*) views of the diatom *Mastogloia*. (*c*) Drawing of a transverse section of *M. grevillei* in the transmission electron microscope. (Ch) Chloroplast; (CN) central nodule; (E) elongate chamber of a septum; (GB) girdle band; (I) intercalary band; (IBE) intercalary band of the epitheca; (IBH) intercalary band of the hypotheca; (LT) locule tubule; (O) oil; (R) raphe; (S) stria. ((*c*) adapted from Stoermer et al., 1965.)

structure is arranged according to a central point, for example, *Coscinodiscus* (Fig. 17.2(*a*)); (2) **trellisoid**, where the structure is arranged uniformly over the surface without reference to a point or line, for example, *Eunotia* (Fig. 17.2(*b*)); (3) **gonoid**, where the structure is dominated by angles, for example, *Triceratium* (Fig. 17.2(*c*)); (4) **pennate**,

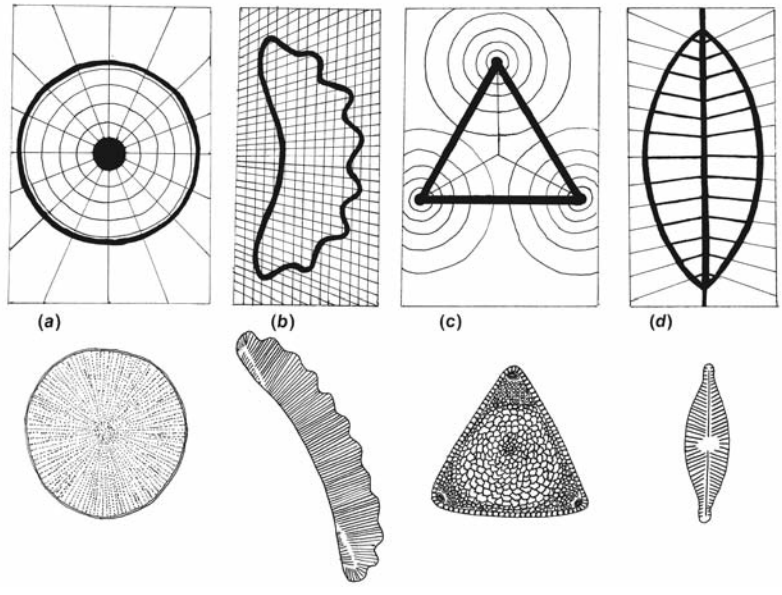


Fig. 17.2 The basic patterns of ornamentation in the Bacillariophyceae. (*a*) Centric and radial (example *Coscinodiscus*). (*b*) Trellisoid, with structure arranged margin to margin (example *Eunotia*). (*c*) Gonoid, with structure supported by angles (example *Triceratium*). (*d*) Pennate, symmetrical about an apical line (example *Navicula*). (After Hendey, 1964.)

where the structure is symmetrically arranged upon either side of a central line – for example, *Navicula* (Fig. 17.2(*d*)).

Some pennate diatoms have a raphe system composed of the **raphe** (a longitudinal slot in the theca), divided into two parts by the **central nodule** (Figs. 17.3, 17.4, 17.5). Each half of the raphe terminates in a swelling of the wall called the **polar nodule**. The ornamentation in the pennate diatoms is **bilaterally symmetrical** around the raphe. In those pennate diatom valves that do not have a raphe system, there is instead an unornamented area running down the center of the valve, which is called the **pseudoraphe** (Fig. 17.3). The raphe is not a simple cleft in the wall but is instead an S-shaped slit that is wider at the outer and inner tissue, and thinner in the middle partition region (Fig. 17.5).

Besides the raphe, there are basically two types of wall perforations within the Bacillariophyceae: the simple **pore** or hole, and the more complex **loculus** or **areola** (Figs. 17.6, 17.12) (Hendey, 1964; Ross and Sims, 1972). The pore consists of a simple hole within a usually homogeneous silicified wall

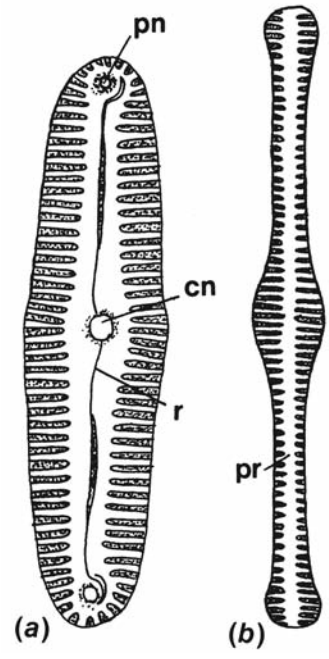


Fig. 17.3 (*a*) A cell with a raphe system (*Pinnularia viridis*). (cn) Central nodule; (pn) polar nodule; (r) raphe. (*b*) A cell with a pseudoraphe (pr) (*Tabellaria fenestrata*).

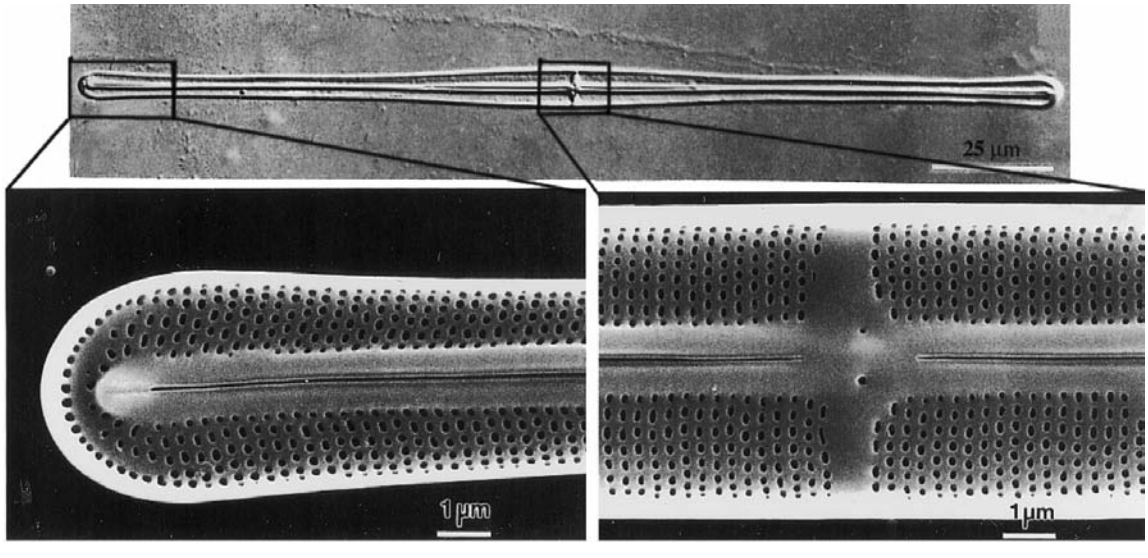


Fig. 17.4 *Climaconeis colemaniae*. Light and scanning electron micrographs of the frustule. The valve contains linear striae, each with 6–8 poroid aerolae. The valve contains a raphe opening. Two pores occur in the area of the central nodule. (From Prasad et al., 2000.)

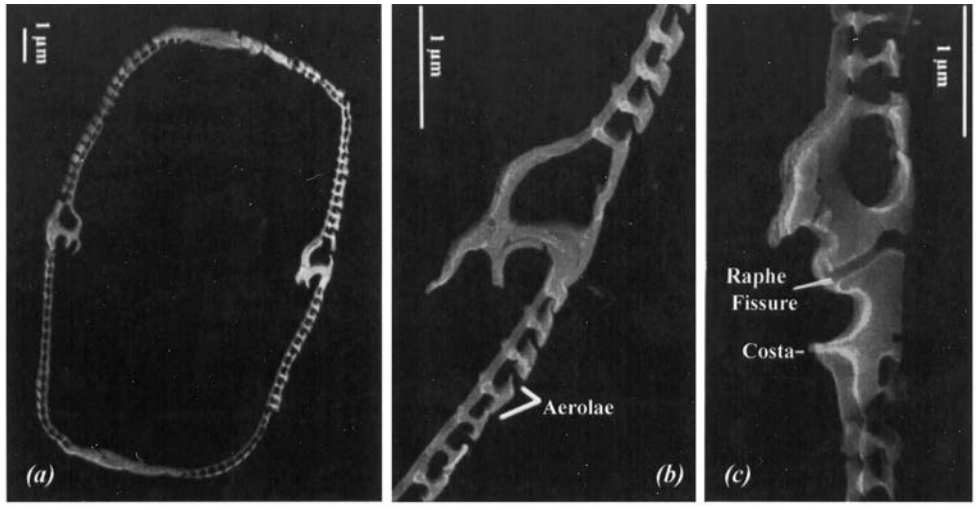


Fig. 17.5 Scanning electron micrographs of sections of the frustule of *Haslea nipkowii*. (From Poulin et al., 2004.)

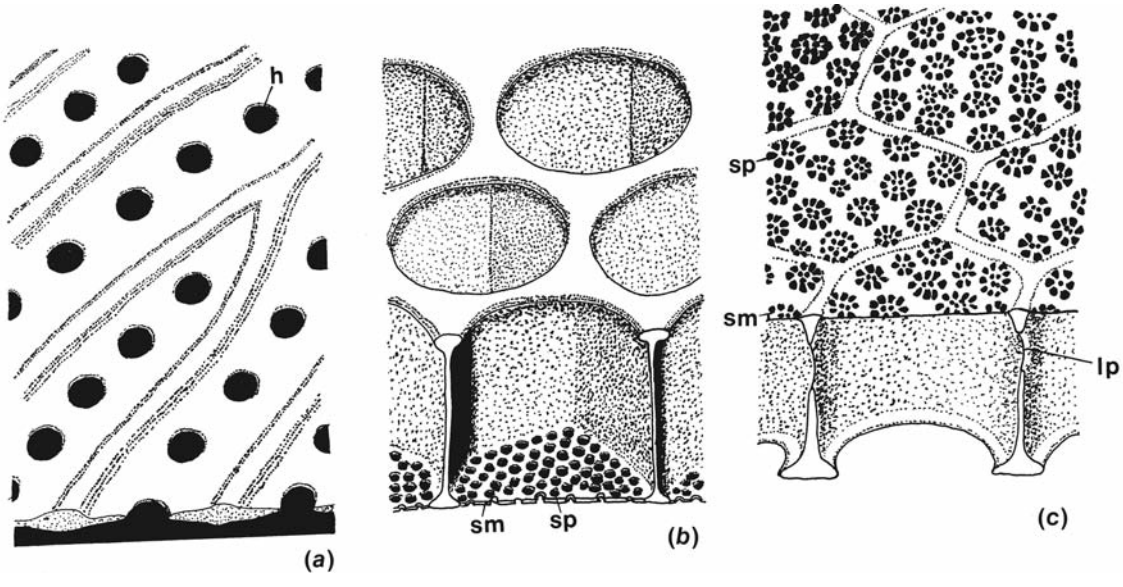


Fig. 17.6 The types of openings in frustule walls. (*a*) Hole or pore (*Chaetoceros didymos* var. *anglica*). (*b*) Loculus opening outward (*Coscinodiscus linatus*). (*c*) Loculus opening inward (*Thalassiosira wailesii*). (h) Hole; (lp) lateral pore or pass pore; (sm) sieve membrane; (sp) sieve pore. (After Hendey, 1971.)

that is frequently strengthened by **ribs** and **costae** (Figs. 17.5, 17.27). If the pore is occluded by a plate, then it is called a **poroid**. The loculus consists of a usually hexagonal chamber in the wall that is separated from other loculi by vertical spacers, which often have pores in them to allow for communication between loculi (Fig. 17.6(*b*), (*c*)). At one end of the loculus is a **sieve membrane** (**pore membrane**, **velum**, **cribrum**) (Figs. 17.6, 17.7). The sieve membrane can be on the outside (an inward-opening loculus) or on the inside (an outward-opening loculus) (Fig. 17.6(*b*), (*c*)). The structure of the valve wall with loculi thus resembles a honeycomb. Pores or loculi (**punctae**) in a single row are referred to as **stria** (plural **striae**) (Figs. 17.1, 17.4).

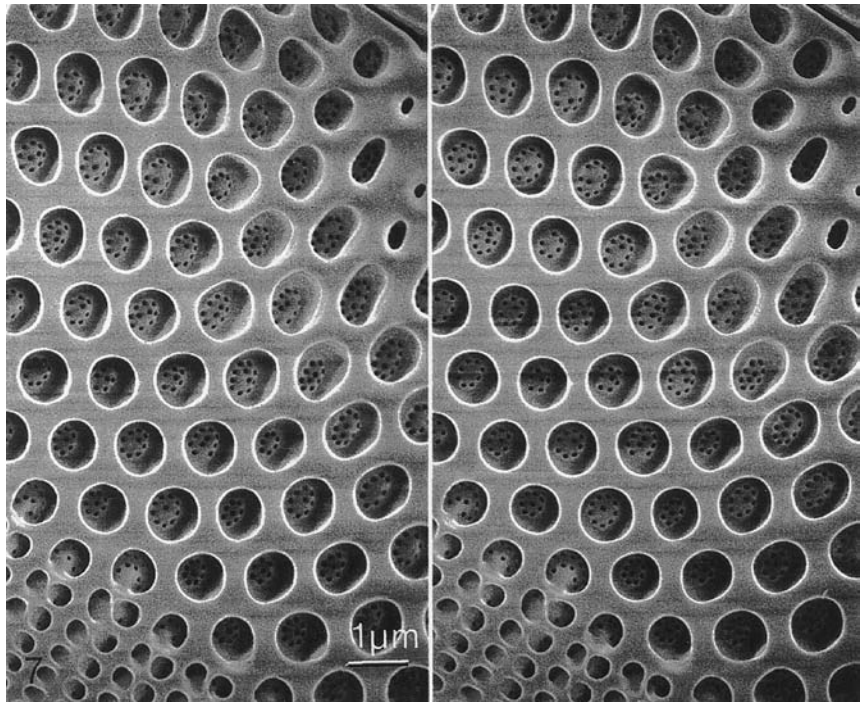


Fig. 17.7 Stereopair illustrating details of the external areolar pattern and structure in *Mastogloia angulata*. If a stereo viewer is not available, bring the photograph about 6 inches (15 cm) from your eyes and cross your eyes to view in three dimensions the loculi, each with a sieve membrane at the bottom of the loculi. (From Navarro, 1993.)

The girdle bands in some diatoms have the same sculpturing as the valve, but in many others sculpturing on the girdle and valve is different. In some cases, the girdle bands have no sculpturing.

Special pores (mucilage or slime pores) (Fig. 17.18) through which mucilage is secreted are known in many diatoms. In the pennate diatoms, these pores usually occur singly near one or both poles of the valve and generally occupy thickenings in the walls.

The valve surface can have extensions, called **processes**, whose main function appears to be to maintain contact between contiguous cells and to assist colony formation. These processes are given different names: **Cornutate** processes are horn-like; **strutted** processes are ones that have been reduced to a boss at the apex of a valve (Figs. 17.8, 17.38(*c*), (*d*)); **spinulae** are very small processes; **awns** or **setae** are hollow and elongated (Figs. 17.32, 17.44).

The frustule is composed of **quartzite** or hydrated amorphous silica that may also have small amounts of aluminum, magnesium, iron, and titanium mixed with it (Mehta et al., 1961; Lewin, 1962). Diatom frustules from marine plankton contain 96.5% SiO_2 and 1.5% Al_2O_3 or Fe_2O_3 (Rogall, 1939). The inorganic component of the frustule is enveloped by an organic component or "skin" (Reimann et al., 1965), the latter composed of amino acids and sugars (Coombs and Volcani, 1968; Hecky et al., 1973) with the amino acid hydroxyproline and collagen present (Nakajima and Volcani, 1969).

Cell division and the formation of the new wall

The normal asexual method of reproduction is by division of one cell into two, the valves of the parent cell becoming the epithecas of the daughter cells with each daughter cell producing a new hypotheca (Figs. 17.9, 17.10). As a result of cell division, one of the daughter cells is of the same size as the parent cell, and the other is smaller. As the size of the cell decreases, so does the relative width to height and the morphology of the cell; in other words, the smaller cells are

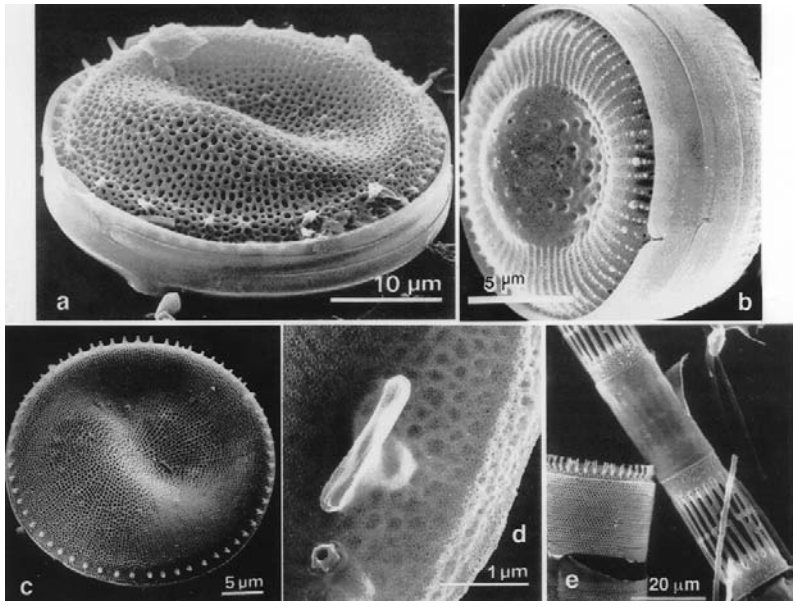


Fig. 17.8 Scanning electron micrographs of centric diatoms. (*a*) *Thalassiosira lacustris*. Undulated hypovalve with strutted processes and part of epitheca showing distal pattern of band openings. (*b*) *Cyclotella striata*. A frustule showing the epitheca, intercalary, and girdle bands. (*c*), (*d*) *Thalassiosira gessneri*. Valve showing undulation, aerolation, and subcentral and marginal rings of strutted processes (*c*). Higher magnification of labiate and strutted processes (*d*). (*e*) *Skeletonema costatum* showing the marginal ring of strutted processes used in chain formation. ((*a*), (*c*), (*d*) from Hasle and Lange, 1989; (*b*) from Prasad et al., 1990; (*e*) from Medlin et al., 1993.)

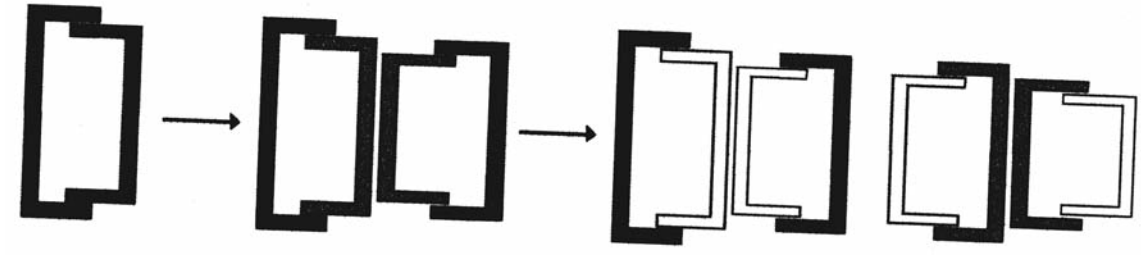


Fig. 17.9 Diagrammatic representation of a diatom cell in girdle view showing the reduction in size through two divisions. (After Hendey, 1964.)

not geometrically proportional to the larger ones from which they arise.

Uptake of silica is confined to a period of the cell cycle following cytokinesis and prior to the separation of the two daughter cells (Sullivan, 1977). Cellular energy for silicification and transport comes from aerobic respiration without any direct involvement of photosynthetic energy (Martin-Jezequel et al., 2000).

Diatoms have an absolute requirement for silicon if cell division is to take place. In water, solid silica dissociates to produce undissociated silicic acid $Si(OH)_4$:

$$SiO_2\,(\text{solid}) + 2\,H_2O \rightleftharpoons Si(OH)_4$$

By increasing the concentration in solution with a pH less than 9, or decreasing the pH of a saturated solution, silicic acid will autopolymerize to form amorphous silica. Amorphous silica is the form of silicon in diatom cell walls. Although silicon is the second most abundant element in the Earth's crust, its availability is limited by its solubility in water. The growth of marine diatoms can so deplete surface waters of silicon that their further growth is prevented (Hildebrand, 2004).

The $Si(OH)_4$ in marine waters is about 6 ppm. In the global ocean, about 97% of the dissolved Si is present as $Si(OH)_4$, with the pH of seawater buffered at about 8.0 by the CO_2-carbonate system (Del Amo and Brzezinski, 1999). However, in freshwater lakes where pH values reach up to 10, $Si(OH)_4$ is only about 23% of the total dissolved silicon, most of the rest being present as ionized

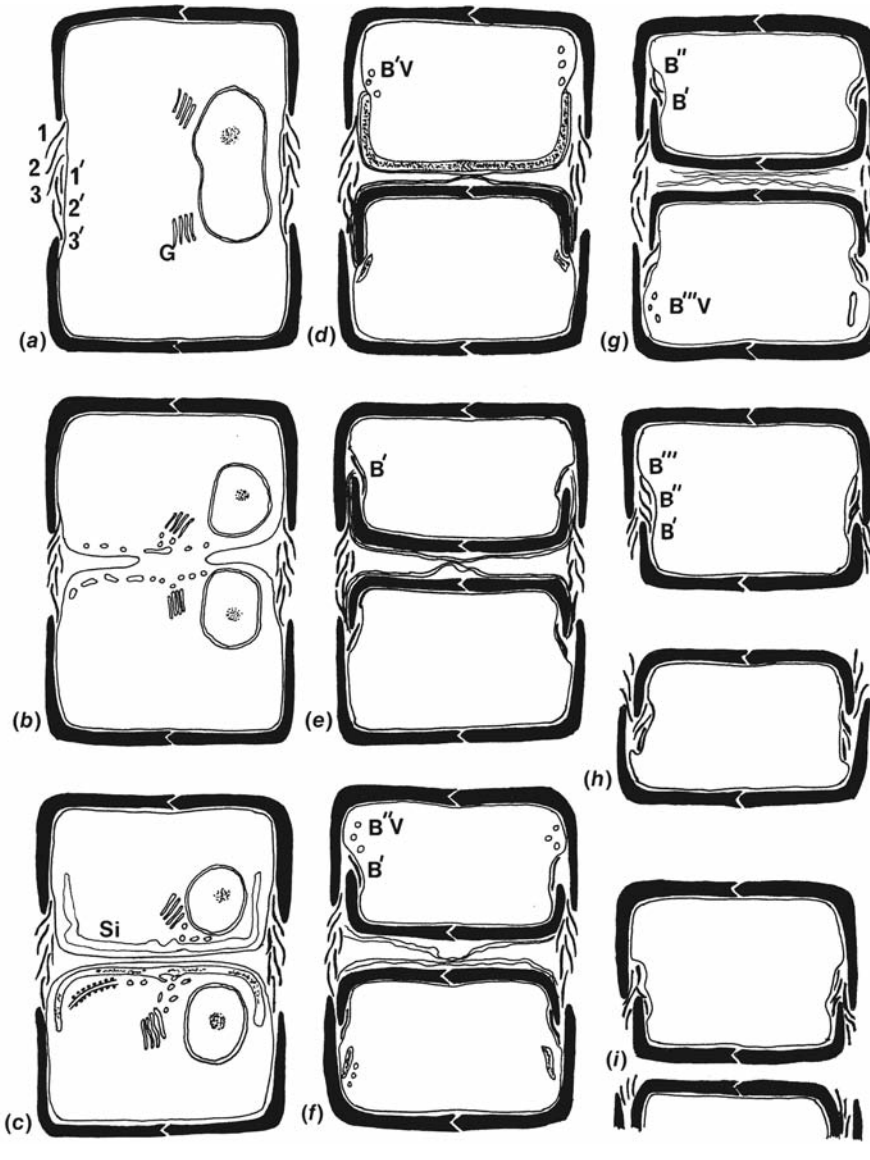


Fig. 17.10 Diagrammatic representation of the stages of frustule formation, including girdle band formation, in *Gomphonema parvulum*. (*a*) The nucleus divides, and the cell elongates. (*b*) There is invagination of the plasma membrane. (*c*) Formation of the silicalemma occurs by the fusion of Golgi-derived vesicles. (*d*) Silica is deposited within the silicalemma to form the valves; vesicles accumulate in the area of the first girdle band. (e) The first girdle band is formed within a vesicle and secreted to the outside. The internal membrane of the silicalemma becomes the new plasmalemma, and the old plasmalemma and the outer membrane of the silicalemma are lost. (*f*)–(*i*) The second and third girdle bands are formed. (After Dawson, 1973.)

silicic acid $SiO(OH)_3^-$ according to the following formula:

$$Si(OH)_4 + H_2O \rightleftharpoons SiO(OH)_3^- + H^-$$

Silica is taken up into the diatom cell as $Si(OH)_4$ by a protein as an active silicon transporter requiring metabolic energy (Hildebrand et al., 2004; Wetherbee et al., 2004). Silicic acid transport is coupled to sodium in marine diatoms and sodium and perhaps potassium in freshwater diatoms. The transport in marine species has the characteristics of a sodium/silicic acid symporter

with a $Si(OH)_4$:Na^+ ratio of 1:1. At least five types of silicic acid transporter (*SIT*) genes have been isolated. Germanium (germanic acid) and silicic acid are competitive inhibitors of each other but germanium can not be incorporated into the diatom cell wall.

Prior to cell division, the cell elongates, pushing the epitheca away from the hypotheca, and the nucleus divides. After the protoplasm has divided (Fig. 17.10) into two by the invagination of the plasmalemma, the Golgi bodies produce translucent vesicles which collect beneath the plasmalemma. These vesicles fuse to form the **silicalemma** or membrane of the **silica deposition vesicle** (Li et al., 1989). The vesicle gradually expands and assumes the shape of a new valve (Schmid and Volcani, 1983). Two silica deposition vesicles are formed per cell with silica deposited in each to form two new hypovalves (Brzezinski and Conley, 1994). The silicon is probably packaged by Golgi into vesicles that are transported to the silica deposition vesicle by microfilaments in the cytoplasm. At the silica deposition vesicle, the small, silica-laden vesicles fuse with the silicalemma, adding membrane material to the silicalemma, and releasing silica to the interior of the silica deposition vesicle (Fig. 17.10). The silica deposition vesicle determines the ultimate form of the silicified frustule (Fig. 17.15). Silica is deposited as amorphous silica in the form of spheres 30–50 nm in diameter (Figs. 17.11, 17.12) (Crawford et al., 2001).

The silica deposition vesicles are acidic, the low pH facilitating fast nucleation and aggregation of silica particles (Vrieling et al., 1999). The acidic environment also protects the newly formed valves from dissolution before coverage by an organic casing prior to secretion.

The silica deposition vesicles contain peptides called **silaffins** (Fig. 17.13) that cause the precipitation of silicic acid into silica nanospheres (Figs. 17.12, 17.14) (Kroger et al., 1999, 2000; Kroger and Sumper, 2004). Different diatom species have different silaffins that, in turn, have different polyamine chains (Fig. 17.13) attached to the silaffins. Different silaffins produce different sized silica nanospheres and it may be that the specific silaffin controls the frustule ornamentation, a characteristic of the individual diatom species.

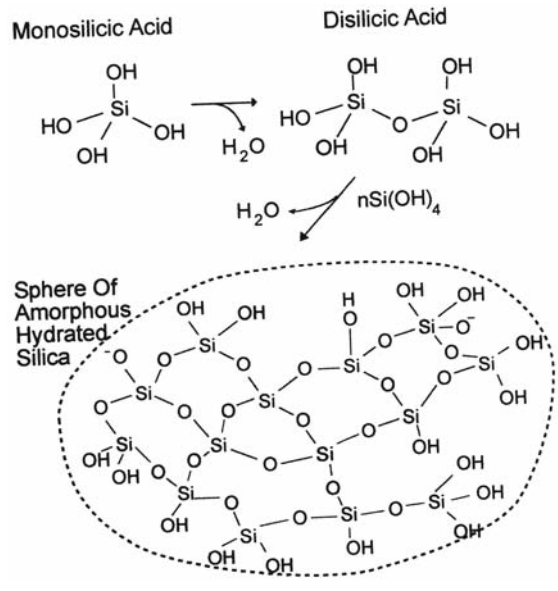


Fig. 17.11 The formation of a sphere of hydrated amorphous silica from molecules of monosilicic acid.

The discovery of silaffins has generated considerable commercial interest since silica-based materials such as resins, molecular sieves, and catalysts are widely used in industry. The production of the manufactured silica-based materials currently requires extremes of temperature, pressure, and pH. In contrast, biosilicification with silaffins proceeds at ambient temperatures and pressures.

A class of glycoproteins, called **frustulins**, is also associated with the silica deposition vesicle. The frustulins are associated with deposition of the organic casing around the silicified frustule (Perry and Keeling-Tucker, 2000).

When the deposition of silica is complete, the inner membrane of the silicalemma becomes the plasmalemma of the daughter cell, and original plasmalemma and the external membrane of the silicalemma are lost (Fig. 17.10). After the epitheca and the hypotheca are formed, Golgi vesicles now collect and fuse to form the silicalemma of the girdle band. The girdle band is deposited outside the cell in the area between the hypovalve and epivalve when silica deposition is complete. If there are further girdle bands, they are formed in the same manner (Dawson, 1973).

Although amorphous silica is slowly soluble at the pH of natural waters, the silica frustule of

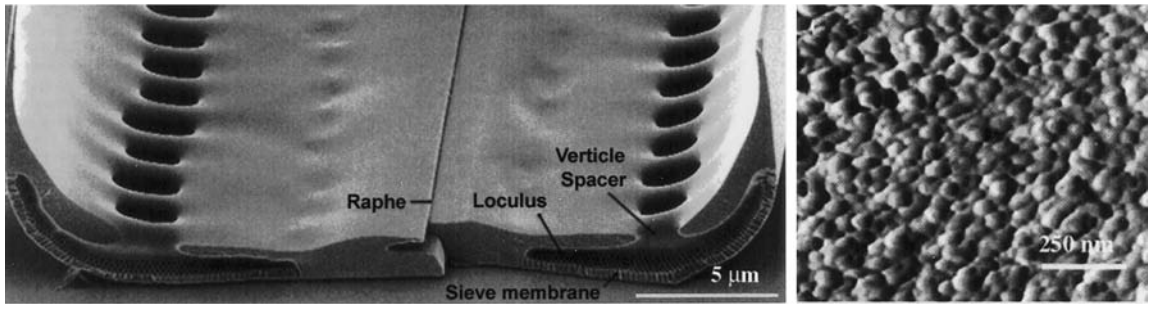
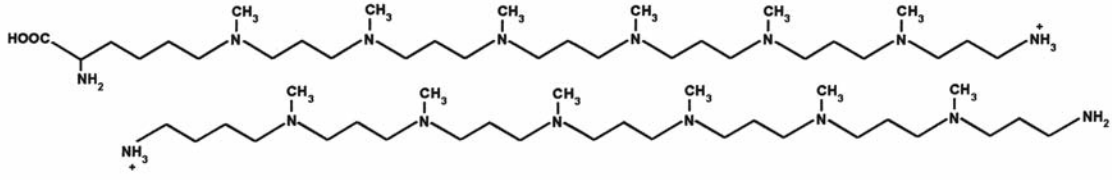


Fig. 17.12 *Pinnularia viridis*. *Left*: Scanning electron micrograph of a cross section of a cleaned valve. *Right*: Atomic force micrograph of the surface of a cleaved area of a valve showing the 40–45 nm silica spheres that compose the valve. (From Crawford et al., 2001.)



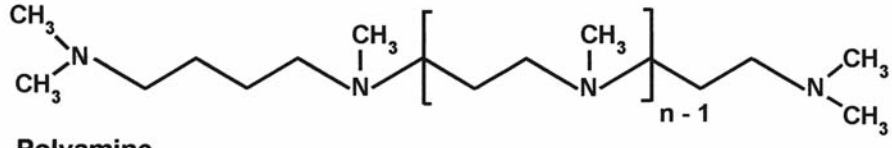


Fig. 17.13 Schematic structure of silaffin and the polyamine side chains of silaffin, two molecules that control the precipitation of silica spheres in diatoms. (Adapted from Kroger et al., 1999.)

living diatoms appears to be protected by the layer of organic material that surrounded the frustule. After death, the silica usually dissolves (Bidle and Azam, 1999). In certain environments, however, the walls of planktonic diatoms may settle and accumulate on the bottom faster than they dissolve, thereby forming **diatomaceous ooze**.

Extracellular mucilage, biolfouling, and gliding

Diatoms produce five types of mucilaginous aggregation: (1) tubes, (2) pads, (3) stalks, (4) fibrils, and (5) adhering films (Figs. 17.16, 17.17, 17.18) (Hoagland et al., 1993). Stalks, pads, and tubes are more common in freshwater diatoms than in marine diatoms (Staats et al., 1999).

A substantial part of the carbon fixed by benthic diatoms is secreted as extracellular mucilages (de Brouwer and Stal, 2002). The biofilms produced by the diatoms play an important part in stabilizing mud flats where the diatoms grow. In the open ocean, the mucilage produced by planktonic diatoms is the triggering mechanism in the formation of "marine snow", which is sticky gelatinous aggregations of bacteria and algae (up to 100 mm in diameter) that create serious problems for fisheries (Alcoverro et al., 2000). The wind drives the marine snow onto the beaches,

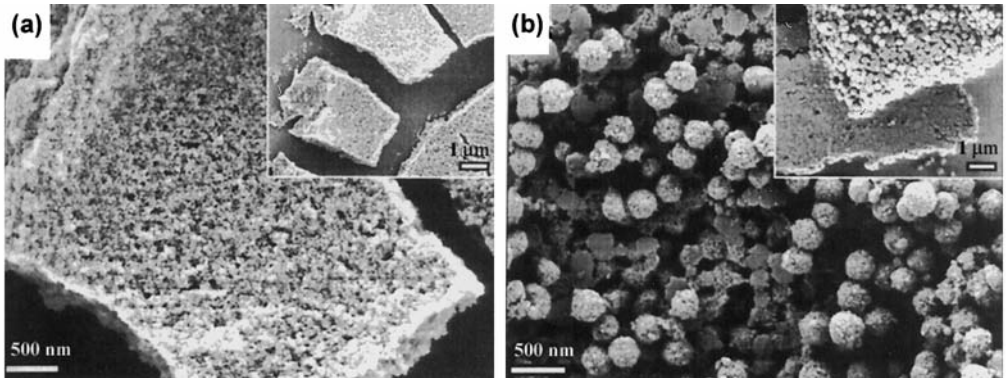


Fig. 17.14 Scanning electron micrographs of silica spheres precipitated out of solution using two different silaffins and polyamines. The silica spheres in (*a*) are much smaller than the silica spheres in (*b*). The size of the silica spheres is controlled by the type of silaffin and/or polyamine in the silica deposition vesicle of the diatom. (From Kroger et al., 2000.)

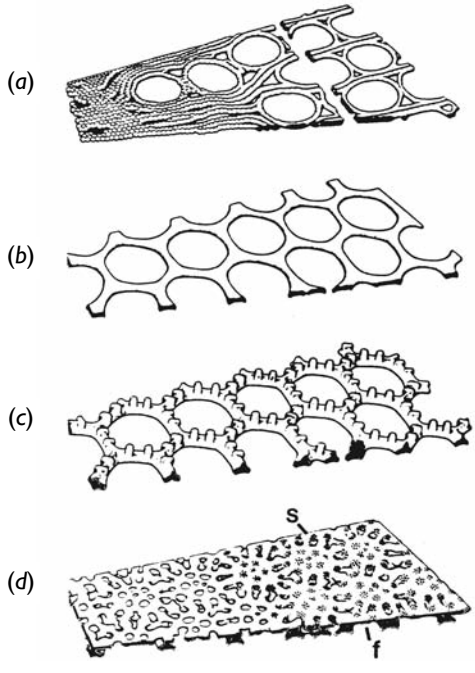


Fig. 17.15 Drawings of the formation of the frustule of the centric diatom *Coscinodiscus wailesii*. Initially silica is deposited in the part of the frustule that will be next to the plasma membrane in the mature frustule (*a*) and (*b*). Subsequently the exterior portion of the frustule is deposited in (*c*) and (*d*). The mature frustule has a sieve membrane (s) on the exterior and a foramen (f) on the interior of the loculus. (From Schmid and Volcani, 1983.)

reducing the recreational suitability of the beaches. Extracellular mucilage production by diatoms is stimulated when phosphorus is limited, leading to marine snow blooms. Bacteria growing in the aggregates produce gas bubbles that give the marine snow positive buoyancy. The organisms in the aggregates benefit from reduced predation by grazers.

Diatoms are ubiquitous fouling microorganisms, attaching to submerged structures by secreting insoluble mucilages. *Achnanthes longipes* is a common marine fouling diatom that is highly resistant to toxic antifouling coatings (Johnson et al., 1995). It produces a stalk that elevates it above the toxic coatings on ship bottoms (Fig. 17.17). Fouling of ship bottoms increases the frictional drag, leading to excess fuel consumption. Cleaning ship hulls coasts millions of dollars each year, leading to an additional loss of revenue (Chiovitti et al., 2003).

Motility

Some diatoms are able to glide over the surface of a substrate, leaving a mucilaginous trail in their wake. **Gliding** *is restricted to those pennate diatoms with a raphe* (Figs. 17.3, 17.4, 17.5) *and those centric diatoms with labiate processes* (Figs. 17.19, 17.20, 17.32). The gliding movement is characterized by large fluctuations in the velocity of movement, with great changes in speed occurring within tenths of seconds (Edgar, 1979). In pennate diatoms, the path of the diatom seems to be essentially dependent on the shape of the raphe.

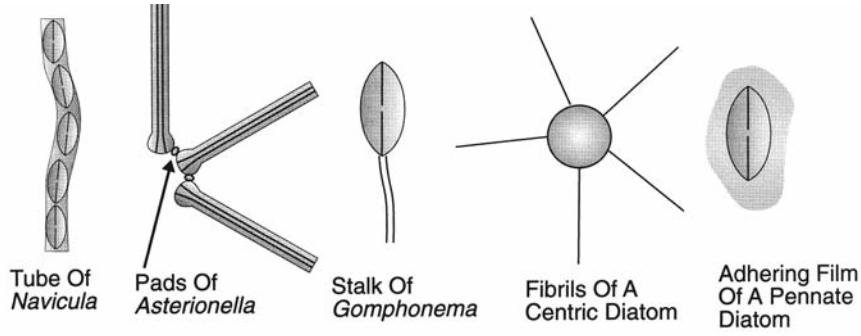


Fig. 17.16 Forms of extracellular mucilage in diatoms. (Modified from Hoagland et al., 1993.)

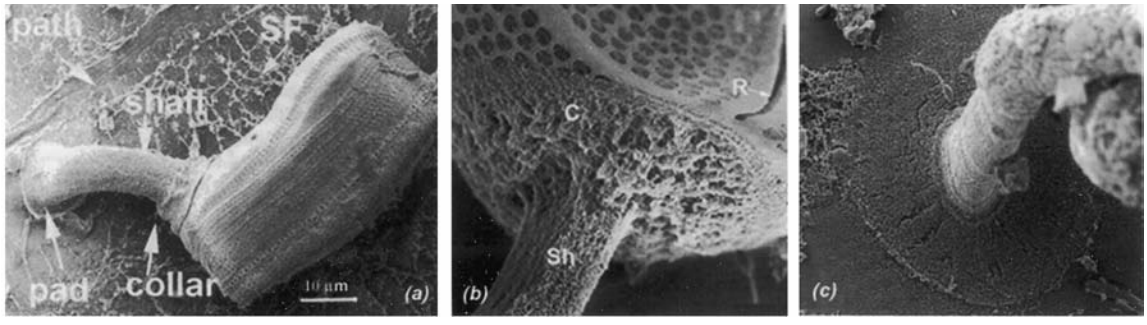


Fig. 17.17 Scanning electron micrographs of *Achnanthes longipes*. (*a*) Whole cell showing the pad, shaft, and collar of the mucilaginous stalk. Also shown is a path of mucilage left by the gliding diatom and surface film (SF) of mucilage left on the substratum. (*b*) The attachment of the collar (C) of the stalk (Sh) on the cell. (R) Raphe. (*c*) The attachment of the pad to the substratum. (From Wang et al., 2000.)

Nultsch (1956) distinguished at least three types: (1) the *Navicula* type, with a straight movement; (2) the *Amphora* type, in which the path is usually curved; and (3) the *Nitzschia* type, which always exhibits curved pathways with two different radii. The observed rates of gliding in diatoms vary from 2 to 14 $\mu m\ s^{-1}$ at room temperature (Cohn and Weitzell, 1996). *Nitzschia palea* is able to penetrate into 2% agar and to move within the medium. The less solid the substrate is, the slower the movement of the diatom; the rate of movement of *Nitzschia putrida* was found to be 2.7 $\mu m\ s^{-1}$ on glass but only 0.8 $\mu m\ s^{-1}$ on agar (Wagner, 1934). Many of the diatoms exhibit backward and forward movements in which the direction may alternate at intervals of a minute. According to von Denffer (1949), the motility of *N. palea* is dependent on light. In liquid cultures the cells tend to agglutinate into spherical clumps, loosely held together by mucilage. When they are transferred to a glass slide, the cells move away from one another. These movements do not take place in darkness.

Diatoms can glide only when the valve containing a raphe is in contact with the surface. If the diatom cell settles with the girdle contacting the substrate, the diatom secretes a mucilaginous tether from the portion of the raphe near the central nodule (Fig.17.18). The tether attaches to the substratum and the cell pulls itself onto a valve containing a raphe using the tether. Sometimes tethers are produced from raphes on opposite sides of the cell. This results in the cell being tethered on both sides of the cell. Withdrawal of the tethers causes the cell to rock back and forth until one of the tethers breaks and the cell rights itself on the substratum. The mucilage that comprises the tether is different from the mucilage involved in gliding (Higgins et al., 2003).

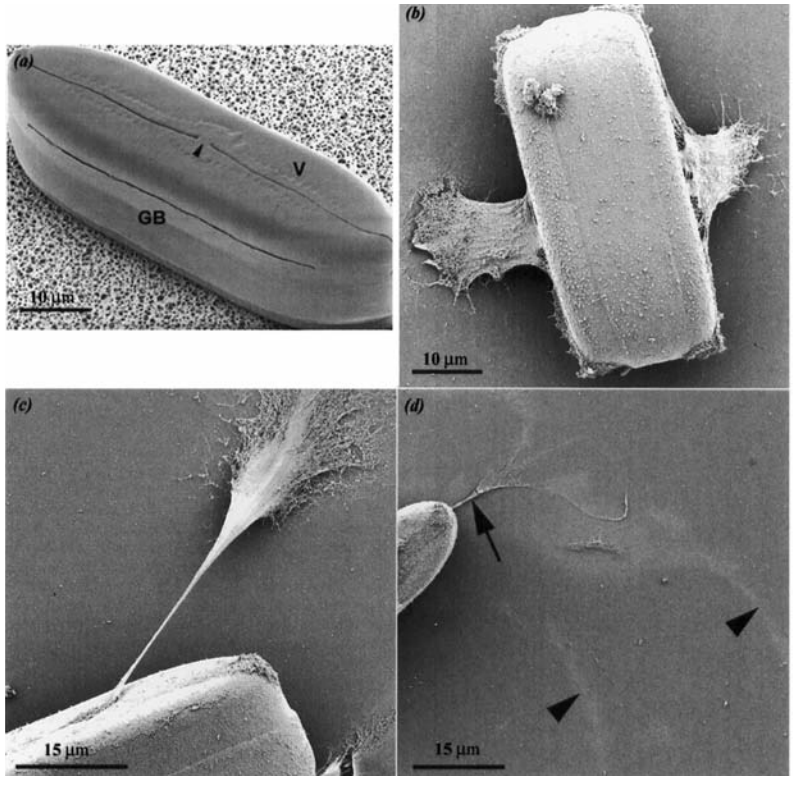


Fig. 17.18 Scanning electron micrographs of *Pinnularia viridis*. (*a*) Cell showing raphe (longitudinal slit) in the middle of the valve (V). The girdle bands (GB) are located around the periphery of the cell. Arrowhead points to the central nodule. (*b*) A cell that has settled on the girdle bands. Tether mucilage is secreted from the raphes of each valve. The tether mucilage is attached to the substrate. (*c*) Tether mucilage extending from the raphe in the central nodule area to the substrate. (*d*) Tether mucilage connected to fine curved threads (arrowheads). (From Higgins et al., 2003.)

Those pennate diatoms that glide have bundles of actin microfilaments running parallel to the raphe (Pickett-Heaps et al., 1979a,b). The microfilament bundles may serve to orient crystalloid bodies containing mucilaginous material in the cytoplasm immediately below the raphe. On an appropriate stimulus, the mucilaginous material is released into the raphe system from the area of the central or terminal pore (Fig. 17.4) (Drum and Hopkins, 1966). The mucilaginous material then streams in the raphe in one direction until it strikes an object to which it adheres. If the object is fixed, then the streaming in the raphe forces the diatom to move in the opposite direction. Nearly all motile diatoms must adhere to the substratum in the area of their raphe in order for movement to occur.

Some of the benthic centric diatoms with labiate processes (Figs. 17.19, 17.20, 17.32) are capable of gliding when attached to a substrate. The labiate processes have a pore in the center, and the mucilage is secreted through the pore. In *Actinocyclus subtilis* (Fig. 17.20), secretion of the mucilage through the labiate process causes the diatom to move forward while rotating at the same time (Medlin et al., 1986).

Diatoms that are attached to a substrate and are motile on the substrate have the advantages of (1) being held in position in moving water; (2) avoiding burial by moving up and over sediments; (3) moving to colonize vacant areas; and (4) moving to areas with more light and/or nutrients (Medlin et al., 1986).

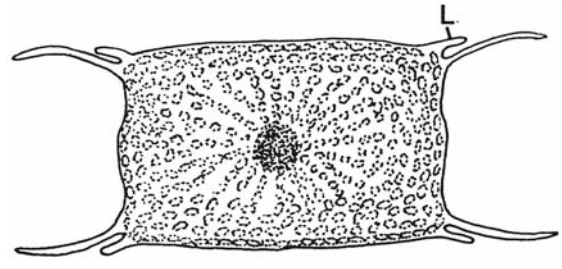


Fig. 17.19 Drawing of a side view of *Odontella sinensis* showing the location of the labiate processes (L). (After Pickett-Heaps et al., 1986.)

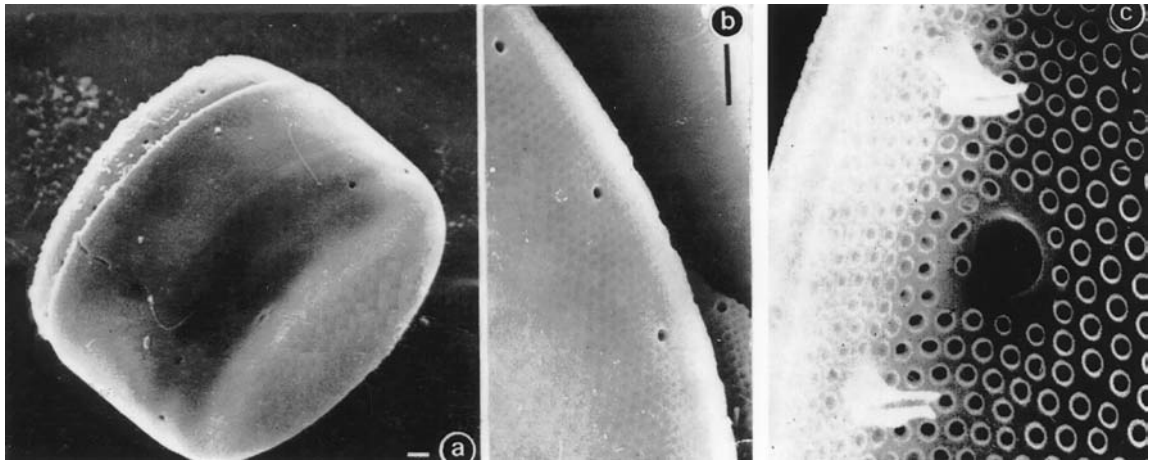


Fig. 17.20 Scanning electron micrographs of *Actinocyclus subtilis*. (*a*) Whole cell. (*b*) Detail of the labiate processes, showing how they open to the outside by a simple hole. (*c*) Internal view of an acid-cleaned valve showing structure of two labiate processes. Internally, each labiate process consists of a short tube that projects from the valve mantle to a slit-like opening. Bar = 1 μm. (From Andersen et al., 1986.)

Plastids and storage products

The chloroplasts are surrounded by two membranes of the chloroplast envelope, outside of which are the two membranes of the chloroplast E.R., the outer membrane being continuous with the outer membrane of the nuclear envelope. The thylakoids within the chloroplast are grouped three to a band, and in most chloroplasts there is a more or less central pyrenoid (Fig. 17.1). The pyrenoid is usually crossed by widely spaced bands of thylakoids, which in some cases are reduced from the normal three thylakoids per band to two. The chloroplasts contain chlorophylls *a*, c_1, and c_2, with an *a*:*c* ratio of 4:1 in *Phaeodactylum tricornutum* (Mann and Myers, 1968). Fucoxanthin is the principal carotenoid, giving the cells their golden-brown color. Fucoxanthin is an efficient carotenoid in the transfer of energy to chlorophyll *a* and is part of photosystem II of photosynthesis.

There are also colorless or **apochlorotic** diatoms that live on decaying marine vegetation and the mucilages of large seaweeds (Lewin and Lewin, 1967). With the light microscope these diatoms have no apparent plastids, although when examined at the fine-structural level they can be seen to have proplastids with little if any internal membrane system. The proplastids have no detectable chlorophylls or carotenoids (Lauritis et al., 1968).

The storage product in the Bacillariophyceae is chrysolaminarin, which is located in vesicles in the cell (Granum and Myklestad, 2001). Chrysolaminarin differs from the laminarin found in the Phaeophyceae (Fig. 1.28) by lacking a terminal mannitol residue at the reducing end of the polysaccharide (Chiovitti et al., 2004).

Diatoms contain unique 4α-methyl sterols, such as 4-desmethylsterol and cholesterol (Fig. 17.21), that are useful as diatom markers in the water column and in organic sediments (Mansour et al., 1999).

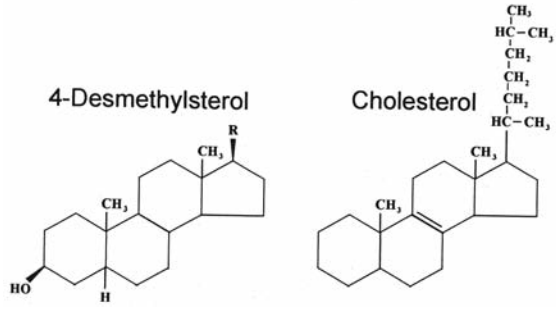


Fig. 17.21 Two 4α-methyl sterols that occur in diatoms.

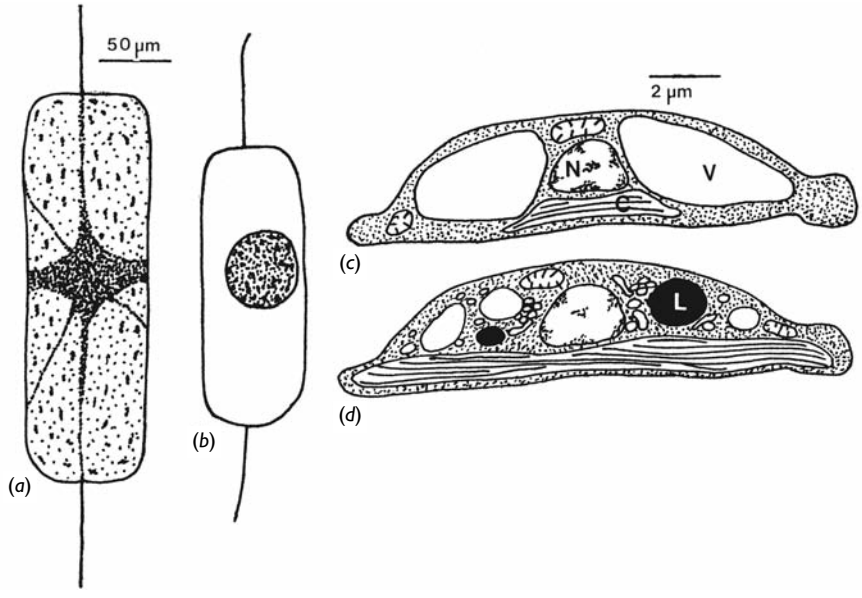


Fig. 17.22 (*a*), (*b*) *Ditylum brightwelli*. (*a*) Vegetative cell. (*b*) Resting spore. (*c*), (*d*) *Amphora coffaeformis*. Drawings of the ultrastructure of a vegetative cell (*c*) and a resting cell (*d*). (C) Chloroplast; (L) lipid; (N) nucleus; (V) vacuole. ((*a*), (*b*) after Gross, 1940; (*c*), (*d*) after Anderson, 1975.)

Resting spores and resting cells

Some diatom cells form thick, ornamented walls at different times in their life cycle and become **resting spores** (Fig. 17.22) (McQuoid and Hobson, 1996). If such cells are planktonic, they fall to the bottom where, presumably, they await more favorable conditions. In *Ditylum brightwelli* (Gross, 1940), the resting spore is formed by the protoplasm shrinking and the plasmalemma drawing away from the cell wall (Fig. 17.22(*a*), (*b*)). The resting spore then formed has a much smaller volume than the original cell, the main decrease being due to the loss of vacuoles and their contents. In germination, the resting spore produces a number of fine protoplasmic strands, which radiate in all directions. Chloroplasts are gradually released from the central mass and move along the processes while the whole protoplast expands. After 2 days, the protoplast has assumed a spherical shape, resembling an auxospore. This protoplast elongates and becomes cylindrical, with a valve appearing at one end within 24 hours and a second valve appearing at the other end after 48 hours. The new cells are much wider than the parent cells. As noted above, the normal method of reproduction, by binary fission, results in a decreased size in the daughter cells. In some species a certain size is reached when sexually or asexually produced auxospores may reestablish the maximum cell size (Nagai et al., 1995). It is, however, known that auxospore formation is generally infrequent, probably taking place once in two or more years in some species. Resting spore formation is therefore a much more frequent method of reestablishment of cell size (Fig. 17.44).

Resting spores are formed after the diatom cells have been subjected to a stress shock. In the ocean, light, temperature, and salinity are relatively stable, with sudden changes rarely occurring, even though there are seasonal changes. In the marine environment, it is usually stress shocks from nutrient depletion that trigger resting spore formation (Davis et al., 1980). Because of the exponential nature of phytoplankton growth, the limiting nutrient is reduced from a considerable level to near zero during the last doubling of the phytoplankton at the end of a bloom (in 1 day or less for many diatoms). Thus a sudden nutrient shock is a typical feature at the end of a diatom bloom.

Marine centric diatoms commonly form morphologically different resting spores, whereas

there are only a few pennate diatoms that do. *Eunotia soleirolii* is one of the few freshwater pennate diatoms that form resting spores (von Stosch and Fecher, 1979). In the freshwater environment, diatoms are subjected to more environmental shocks than in the marine environment. *Eunotia soleirolii* will form resting spores when subjected to (1) high temperatures (24 °C); (2) high or low pH; or (3) iron, silica, phosphate, or nitrate deficiencies. In many other diatoms, resting spores germinate when placed in fresh medium. However, the resting spores of *E. soleirolii* require dormancy to be broken by a dark period at −2 °C to 15 °C for a minimum of 4 to 5 weeks. Thus *E. soleirolii* thrives in colder seasons in northern Europe and is induced to form resting spores by rising temperatures and perhaps concomitant nutrient deficiencies. The resting spores are viable for up to 3 years, but would normally last the summer before dormancy would be broken by the cold temperature of autumn, resulting in germination of the resting spores.

Resting cells have the same morphology as vegetative cells and do not form a protective layer, thereby differing from resting spores. Growing vegetative cells of *Amphora coffaeformis* require 4 weeks in the dark to form resting cells (Anderson, 1975). Formation of resting cells initially involves autophagic activity, with the breakdown of existing structures. Large vacuoles decrease in size, and many small ones develop; the mitochondria become fewer; and large lipid bodies are formed (Fig. 17.22). The resting cells contain as much chlorophyll as the vegetative cells, and the whole cell appears to be a parsimonious assemblage of organelles prepared to resume metabolism and growth upon return to favorable conditions. During the summer, diatom cells sink into deep water below the euphotic zone, where they form resting cells and become dormant. Such cells remain viable for at least 2 months in such an environment (Anderson, 1976). Their respiratory rate is 20% that of normal cells, and their photosynthetic capability is very low. Vertical mixing brings these cells and nutrient-rich water to the surface, and within 2 days the cells become active and begin to reproduce. Viable resting cells of diatoms have been collected at 6150-m water depth in the North Atlantic.

Auxospores

Auxospore formation is a second mechanism (in addition to resting spores) for reestablishing the original size of the cell. The auxospores are formed by the fusion of two gametes. In the centric and gonoid diatoms, the male gamete is motile (Fig. 17.45), whereas the female gamete (egg) is nonmotile (Figs. 17.42, 17.44). In the pennate and trellisoid diatoms, both gametes are non-flagellated (Figs. 17.29, 17.46) (Chepurnov et al., 2004).

Depending on the species, auxospores develop in one of three different ways (Fig. 17.23) (von Stosch, 1982; Medlin and Kaczmarska, 2004).

1 *Isodiametric auxospores*. Centric diatoms such as *Melosira* (Figs. 17.35, 17.40, 17.41, 17.42, 17.43), *Coscinodiscus* (Figs. 17.2(*a*), 17.6(*b*), 17.15, 17.38(*a*), (*b*)), and *Stephanopyxis* (Figs. 17.33(*a*), 17.38(*c*), (*d*)) produce this type of auxospore. The globular auxospore more or less maintains its shape during development. The auxospore usually is attached to the parent valves during maturation. The auxospore has a wall with embedded scales (Fig. 17.24), inside of which are produced the roughly dome-shaped valves of the mature vegetative cells.
2 *Properizonial auxospores*. Centric diatoms such as *Chaetoceros* (Figs. 17.6(*a*), 17.32, 17.44, 17.45) produce non-isodiametric (non-spherical) mature auxospores. The immature globular auxospore splits and bands are produced from an asymmetrical auxospore. The bands are collectively called the properizonium. In *Chaetoceros*, a fan-like assortment of bands is formed on the dorsal surface of the auxospore while the ventral surface is composed of a primary envelope containing scales. The mature auxospore produces a flattened frustule similar in shape to the vegetative cell.
3 *Perizonial auxospores*. Pennate diatoms such as *Navicula* (Figs. 17.2(*d*), 17.16, 17.25, 17.26(*a*), 17.33(*b*), 17.35) and *Pseudo-nitzschia* (Figs. 17.27, 17.29) form this type of non-isodiametric mature auxospore (Sato et al., 2004). The immature globular auxospore has scales embedded in a primary wall. The primary auxosore wall splits and separates into two

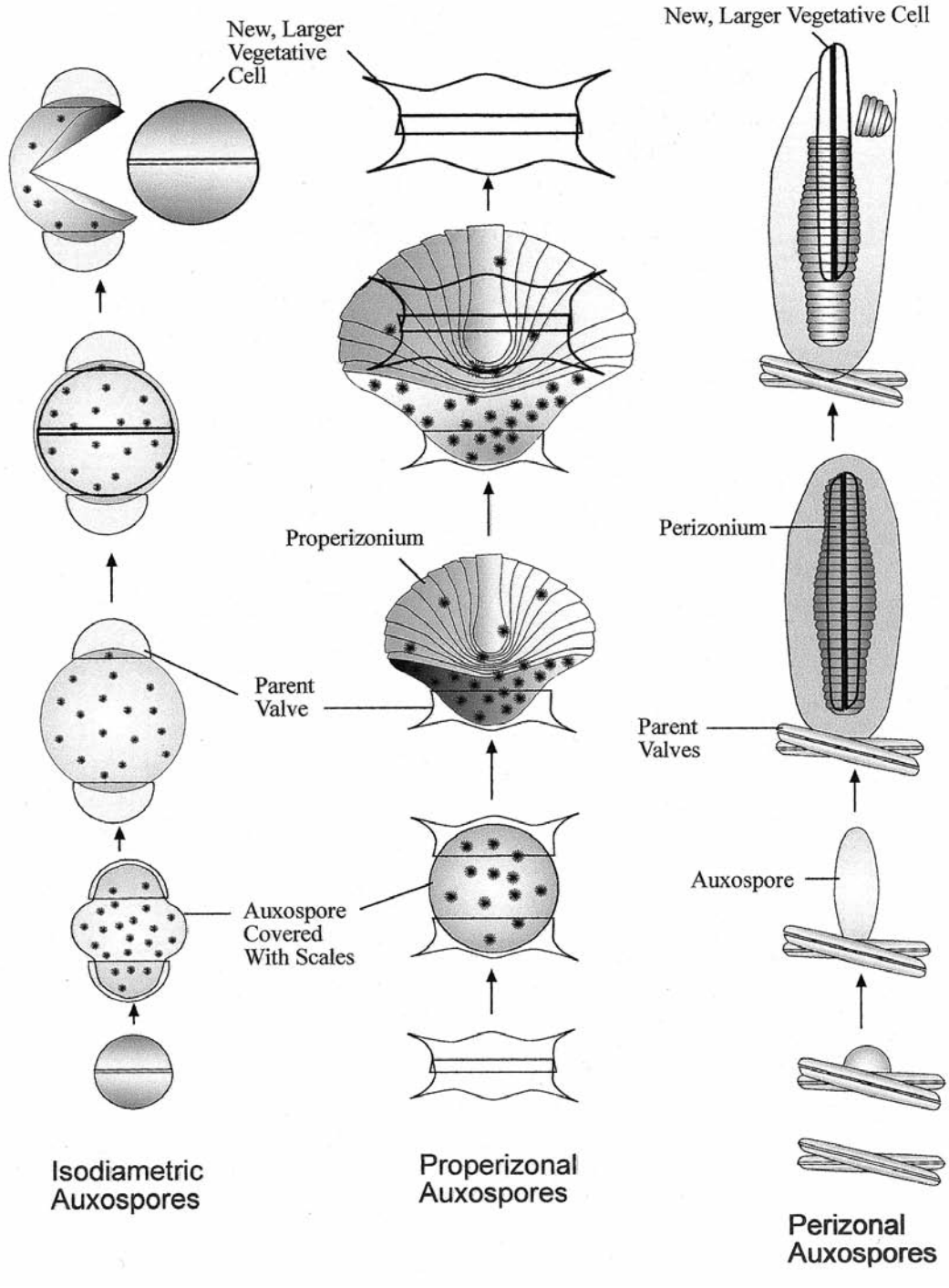


Fig. 17.23 Diagrammatic summary of the three types of sexual auxospores in diatoms.

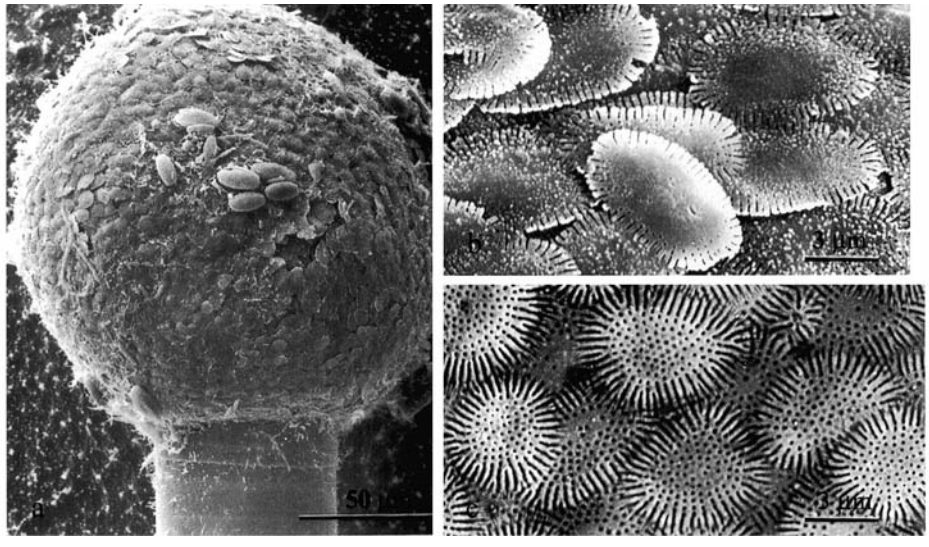


Fig. 17.24 *Ellerbeckia arenaria.* Scanning electron micrographs of auxospores. (*Left*) Scale-covered auxospore perched in the epitheca. (*Top right*) External view of scales. (*Bottom right*) Internal view of scales. (From Schmid and Crawford, 2001.)

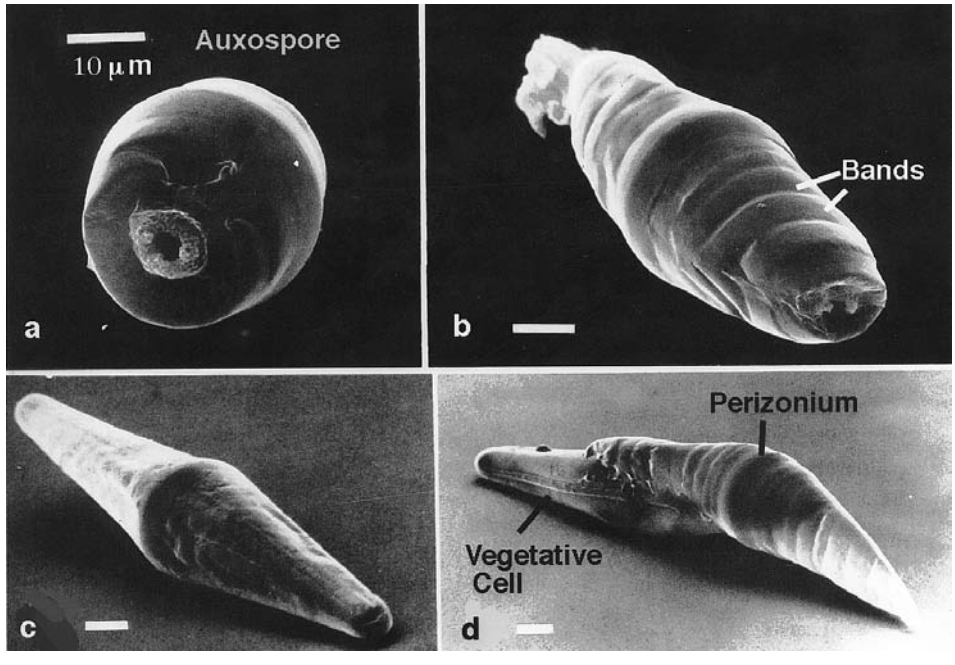


Fig 17.25 Scanning electron micrographs of sexual stages of *Navicula cuspidata.* (*a*) Immature auxospore. (*b*) Auxospore midway through elongation. The underlying perizonal bands are evident. (*c*) Mature auxospore showing biconical shape of the perizonium. (*d*) Vegetative cell emerging from the perizonium. (From Cohn et al., 1989.)

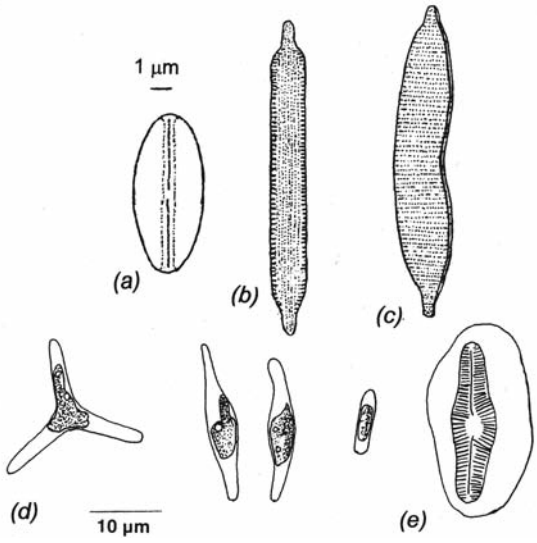


Fig. 17.26 (*a*) *Navicula pelliculosa.* (*b*) *Nitzschia palea.* (*c*) *Hantzschia amphioxys.* (*d*), (e) *Phaeodactylum tricornutum.* (*d*) Three forms, triradiate, fusiform, and oval. The alga is pleomorphic, ovate cells form on agar or solutions low in calcium while fusiform and triradiate cells occur in liquid medium. (e) An oval cell embedding in mucilage with a single valve. (After Wilson, 1946.)

equal halves. The auxospore produces bands that mold the cell into the tubular perizonium. The new pennate frustule is formed within the perizonium of the mature auxospore.

Sexual reproduction in diatoms can occur only after two general conditions have been met (Edlund and Stoermer, 1997). First, cells must reach a minimum size range, typically 30–40% of their maximum size. Second, there must be the presence of correct environmental conditions. These include combinations of temperature, light, nutrients, trace metals, organic growth factors, and osmolarity (Potapova and Snoeijs, 1997). Contrary to most other algal groups, sexuality is primarily a means of size restoration, and is not normally a factor in dormancy or dispersal (Edlund and Stoermer, 1997).

Rhythmic phenomena

It is possible to synchronize the division of diatom cells in a culture in a couple of different ways. Lewin (1966) has shown that removal of silicon from cultures of *Navicula pelliculosa* (Fig. 17.26(*a*)) stops growth of the cells at a stage prior to cytokinesis. When silica is added to the culture, all of the cells then divide synchronously. Another way of obtaining synchronized cell divisions is by keeping the diatoms in the dark for a long period followed by exposure to light. In *Nitzschia palea* (Fig. 17.26(*b*)) the shortest time that can be obtained between cell divisions is 16 hours (von Denffer, 1949). If the cells are grown on an 8 hour light : 8 hour dark cycle, synchronously dividing cells are obtained. If the cycle is shortened to 6 hours light:6 hours dark, then cell division occurs every second dark period because there is insufficient time for the diatom to prepare itself for the next division.

Fauré-Fremiet (1951) was the first to observe that the diatom *Hantzschia amphioxys* (Fig. 17.26(*c*)) accumulates on mud flats in certain areas during low tides, causing brown spots on the mud. The cells can glide rapidly at a rate of half their length in a second and can reverse their phototactic response. During low tide the cells are positively phototactic, so that they come to the surface of the mud, and at high tide they are negatively phototactic, so that they descend into the mud. At high tide they also exude a mucilaginous material, which causes them to stick to one another and to sand grains. This rhythmic phenomenon prevents the cells from being washed away by the tide.

Physiology

For growth of *Navicula pelliculosa* (Fig. 17.26(*a*)), silicon cannot be replaced by any of the elements similar to it in physical and chemical properties or in atomic radius, such as Ge, C, Sn, Pb, As, P, B, Al, Mg, or Fe (Lewin, 1962). Lewin (1966) has shown that with a mixture of algae and other organisms, concentrations of germanium dioxide (GeO_2) above 1.5 mg liter^{-1} will specifically suppress the growth of diatoms. In cultures of many types of algae, diatom contaminants frequently grow so fast that they obscure the growth of the algae the investigator is working with. The finding that GeO_2 specifically inhibits diatom growth was a welcome one for phycologists working on algal cultures. In experiments with 14 pure cultures of diatoms, 1 mg liter^{-1} of GeO_2 reduced the growth rate significantly; 10 mg liter^{-1} was even more inhibitory to growth and in a few cases killed the cells. *Phaeodactylum tricornutum* (Fig. 17.46(*d*)), a diatom with little or no silicified wall, was the least sensitive to GeO_2 of the diatoms tested. By increasing the amount of SiO_2 in solution, it is possible to reverse the inhibitory effect of GeO_2 on growth. The results indicate that GeO_2 is a specific inhibitor of silicate utilization because concentrations of GeO_2 as high as 400 mg liter^{-1} have no effect on respiration. The minimum inhibitory concentrations of GeO_2 depends to a certain extent on the pH and concentration of the nutrient medium. Such inhibitory concentrations are rarely, if ever, reached in natural waters, the highest concentration reported being that of a mineral spring in Niigata Prefecture, Japan, which contained only 0.03 mg liter^{-1} of Ge, with normal concentrations in seawater being about 5×10^{-5} mg liter^{-1}.

In addition to responding adversely to germanium in solution, diatoms are sensitive to copper. Erickson (1972) has shown that *Thalassiosira pseudonana* has its growth inhibited at concentrations of copper as low as 5 μg liter^{-1}. The presence of detritus affects the toxicity to a certain extent. Concentrations of 0.25 ppm copper as $CuSO_4 \cdot 5H_2O$ are normally used to control algal blooms without affecting fish in freshwater lakes. Copper toxicity and silicon metabolism are linked in several marine diatoms. *Skeletonema costatum* (Fig. 17.8(*e*), 17.31(*a*)) and *Thalassiosira pseudonana* exhibit slower growth in the presence of copper. Inhibition of growth by copper is alleviated by increasing the silicic acid concentration in the media (Morel et al., 1978; Rueter et al., 1981). It is probable that copper interferes with the silicic acid transport site across the plasma membrane and slows uptake of silicic acid (Rueter et al., 1981; Rueter, 1983).

The effects of heavy metals on diatoms can be divided into three groups (Thomas et al., 1980): (1) Cu, Zi, and Ge affect the biochemical pathway of silicon metabolism; (2) Hg, Cd, and Pb interfere with cell division and cause morphologically distorted cells to be produced; and (3) Cr, Ni, Se, and Sb have no effects up to a concentration of 1 μM, well above the concentrations that show effects with other toxic metals.

Some normally photosynthetic diatoms are able to grow under heterotrophic conditions (Kroger, 2001). In two studies (Lewin, 1953; Lewin and Lewin, 1960), a number of cultures of photosynthetic diatoms were found that would grow heterotrophically, usually only with glucose as a carbon source. One of these diatoms, *Cyclotella cryptica* (Hellebust, 1971), can grow in the dark in an organic medium with glucose (but not lactate or tryptone) as the sole carbon source. When the organism is growing in the light, it does not have the mechanism for the utilization of glucose in the medium. It requires about 24 hours in the dark in a glucose medium before it is able to use the glucose as a carbon source. This lag period indicates that the lack of light induces an uptake and/or assimilation system for the glucose. White (1974) suggested that such facultative heterotrophy enables these diatoms to settle into bottom deposits, live heterotrophically for long periods, then rise and begin photosynthesis again. Although the above diatoms still have functional chloroplasts, there are some apochlorotic diatoms lacking functional chloroplasts (Lewin and Lewin, 1967). The latter, which are species of *Nitzschia* (Fig. 17.26(*b*)), are able to grow with lactate or succinate as the sole organic carbon source.

Amnesic shellfish poisoning occurs when shellfish filter diatoms from the genera *Nitzschia* (Figs. 17.26(*b*), 17.35), *Pseudo-nitzschia* (Figs. 17.27,

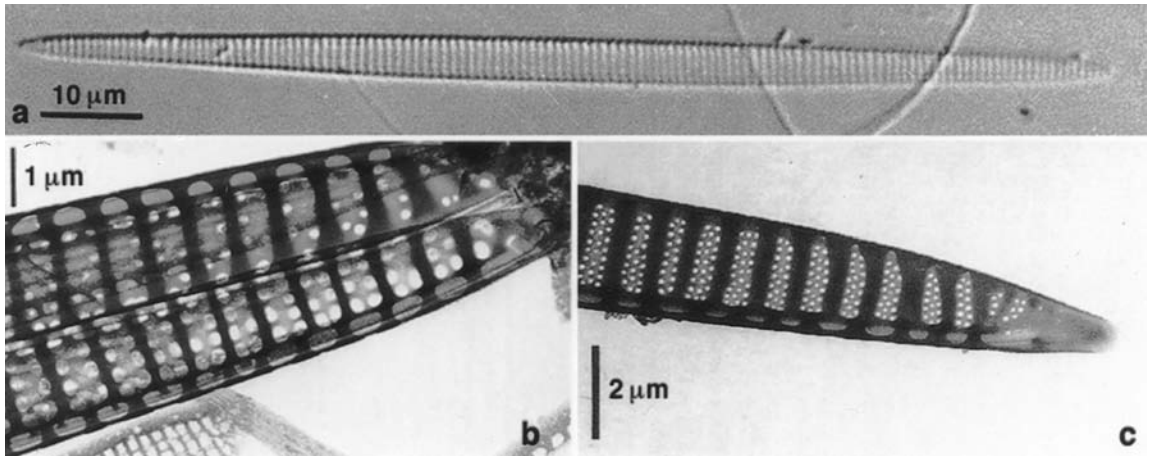


Fig. 17.27 *Pseudo-nitzschia*, a diatom responsible for amnesic shellfish poisoning. (*a*) Light micrograph of one valve. (*b*), (*c*) Transmission electron micrographs of the ends of cleaned valves showing the ribs and poroids. (From Hasle, 1995.)

17.29), and *Amphora* (Figs. 17.22(*c*), (*d*)), 17.35) from marine waters (Bates, 2000; Lundholm and Moestrup, 2000). Subsequent ingestion of the shellfish by man and birds results in memory loss (amnesia), abdominal cramps, vomiting, disorientation, and even death. Amnesic shellfish poisoning was first recognized in 1987 in Prince Edward Island, Canada, where it caused 3 deaths and 105 other affected individuals after blue mussels were eaten (Subba Rao et al., 1988). The diatom produces domoic acid, a derivative of the neuroexcitatory amino acid L-glutamic acid (Fig. 17.28). Domoic acid is especially prevalent in moribund cells of the diatom and can be induced by depriving the cells of nutrients, particularly silicate and phosphate (Pan et al., 1996).

Sexual reproduction in *Pseudo-nitzschia multiseries* is on an internal clock controlled by the size of the cells (Davidovich and Bates, 1998). A maximum cell size is attained after sexual reproduction by auxospore germination producing vegetative cells with a length of 120–170 μm (Fig. 17.29). Sexual reproduction is induced in nature about three years later after successive cell divisions have decreased the cell size by 30–40%. Mating in *P. multiseries* begins when cells of different strains contact each other, valve to valve in parallel. Gametogenesis occurs by cells dividing meiotically to form morphologically similar nonflagellated gametes. The valves of the parent frustules separate and gametes from one cell (male) travel by amoeboid movement to the passive gametes in the other cell (female). Within a couple of minutes, the gametes fuse to form a spherical zygote that expands to produce auxospores still attached to one of the parent valves. The fully expanded auxospore still has unfused

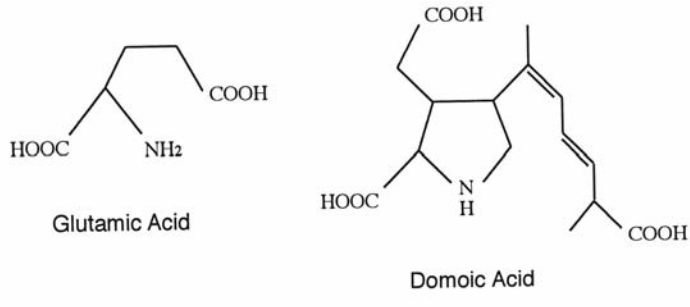


Fig. 17.28 The structure of domoic acid, the causative chemical of amnesic shellfish poisoning, and its analog, L-glutamic acid.

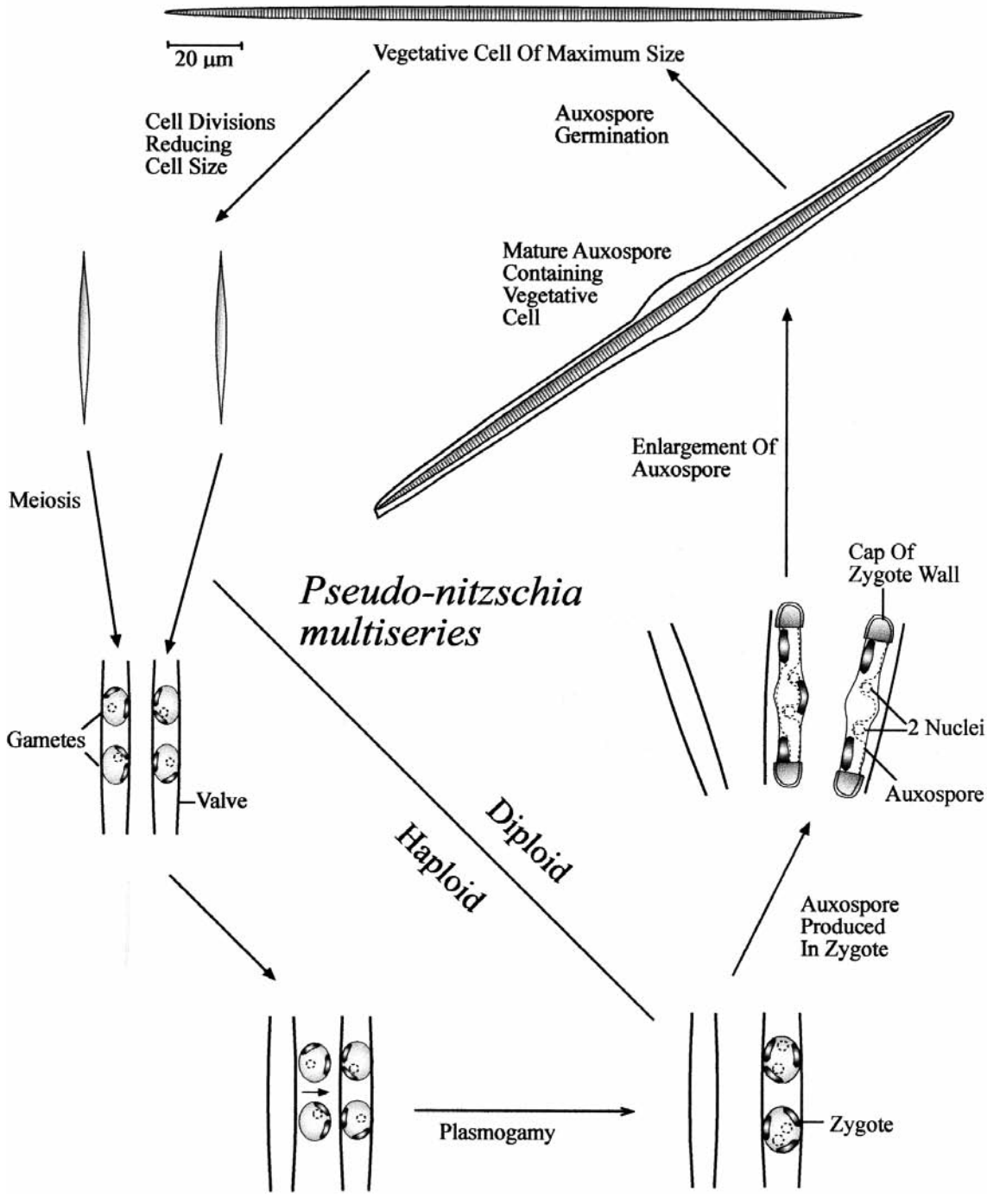


Fig. 17.29 The life cycle of the toxic diatom *Pseudo-nitzschia multiseries*. (Modified from Davidovich and Bates, 1998.)

nuclei and chloroplasts from the gametes. Most of the auxospore volume is occupied by a single vacuole. The auxospores germinate to produce vegetative cells of maximal cell size. Physiologically sexual reproduction is isogamous because the cells of one clone are passive (female) remaining within the parent frustule, while the cells of the other clone are active (male), moving to the passive gametes of the other clone.

Chemical defense against predation

Diatoms are preferred food for invertebrates such as copepods. Some diatoms (e.g., *Phaeodactylum tricornutum*, *Skeletonema pseudocostatum*) have evolved a mechanism to reduce predation by releasing chemicals that reduces the fecundity of the next generations of invertebrates. Diatoms cells contain large quantities of highly unsaturated fatty acids such as eicosanoic acid (Fig. 17.30(*a*)) in vesicles in the cytoplasm. Death of cells during feeding by invertebrates results in the release of the unsaturated fatty acids into the seawater. Upon release, phospholipases convert the unsaturated fatty acids eicosatetraenoic acid and eicosapentaenoic acid into the unsaturated short-chain aldehydes 2,4-decadienal and 2,4,7-decatrienal (Fig. 17.30(*b*)) (Miralto et al., 1999; Pohnert, 2002; Pohnert and Boland, 2002; Pohnert et al., 2002). These short-chain fatty-acid aldehydes are toxic to developmental stages of a range of invertebrates including copepods, sea urchins, polychaetes, and ascidians (although similar saturated fatty acids with a terminal aldehyde group, such as tridecanal (Fig. 17.30(*b*)), are not toxic to copepod eggs) (Caldwell et al., 2004). They appear to work by affecting cell membrane characteristics and microtubule and microfilament stability (Casotti et al., 2005). Future generations of grazers are sabotaged, encouraging the survivability of diatom populations.

Eicosanoic acid in the diatom cell is not toxic to the diatom cell; the chemical is only toxic after the unsaturated fatty acid is released into the environment and converted into an aldehyde. Thus, the diatom cells are able to invest their metabolic energy into the formation of unsaturated fatty acids utilized in normal cell activities. When the cells are damaged, the unsaturated fatty acids are released and converted into toxic compounds that reduce the numbers of the next generation of grazers (Pohnert, 2002). Interestingly, the released aldehydes also are toxic to diatoms (Casotti et al., 2005). However, the diatoms cells are being destroyed by the grazing and are already out of the gene pool.

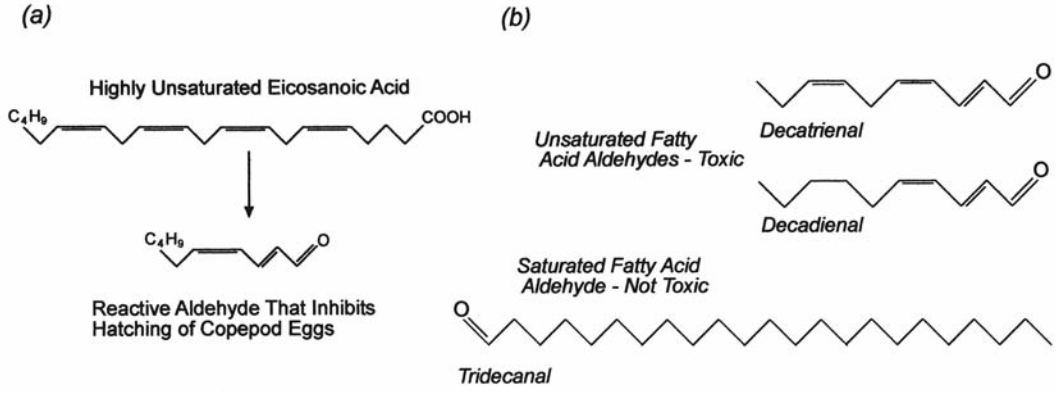


Fig. 17.30 (*a*) The reaction by which a non-toxic highly unsaturated fatty acid is converted by a phospholipase into a reactive unsaturated fatty-acid aldehyde that is toxic to invertebrates. The reaction is initiated by wounding of the diatom cell. (*b*) Two unsaturated fatty-acid aldehydes, decatrienal and decadienal, that are toxic to invertebrates and a saturated fatty-acid aldehyde, tridecanal, that is not toxic.

Ecology

Diatoms comprise the main component of the open-water marine flora and a significant part of the freshwater flora. Attached diatoms can be characterized by the brown scums found on various kinds of substrata, as well as the fluffy brown growths caused by abundant epiphytic diatoms. The pennate diatoms are represented in about equal numbers in the freshwater and marine habitats, whereas the centric and gonoid diatoms are present predominantly in the marine environment. Generally speaking, in the marine environment the colder the water is, the greater the diatom population. The populations of diatoms in the open oceans usually have a large number of species with the total number of organisms being low, in contrast to the diatoms living close to the shore, where the total number of diatoms is very high, but the number of different species within the population is low. This situation is actually fairly typical of oligotrophic, unenriched waters (the open ocean) versus eutrophic, enriched waters (the coastal waters receiving enrichment from the land).

Marine environment

The maintenance of oceanic diatoms in the water column involves some adaptation of the cells to make them buoyant. The silicified wall of diatoms has a density of about 2.600, comprising up to 50% of the dry weight of the cell (see Smayda, 1970, for a review). The density of seawater varies from 1.021 to 1.028; therefore, planktonic diatoms must have cellular components that are lighter than seawater to achieve neutral or positive buoyancy. The density of the cytoplasm in marine organisms is slightly heavier than seawater, varying from 1.030 to 1.100. This leaves only the vacuole as a likely source of positive buoyancy in diatoms. In fact, most planktonic diatoms have a large vacuole whose contents, while being isotonic, are lighter than seawater. For example, the vacuolar sap of the planktonic diatom *Ditylum brightwelli* (Figs. 17.22(*a*), (*b*), 17.31(*b*), (*c*)) has a density of 1.0202, less than that of seawater. The vacuole of these diatoms contains lighter ions than the surrounding seawater: the concentration of Na^+ is great relative to K^+ (the latter element is heavier by about 40%), there is a relatively high concentration of light NH_4^+ ions, and divalent relatively heavy ions, especially SO_4^{2-}, are excluded. This ionic mechanism of buoyancy is probably important in planktonic diatoms as long as they are above a certain size (20 μm diameter in *Ditylum*), below which the size of the vacuole is too small to provide the necessary lift to the cell. The ionic mechanism of buoyancy cannot be applied to the flotation of freshwater phytoplankton because of the low quantity of salts in the water. In freshwater, most colonial diatoms are encased in a gelatinous sac of low density which aids the flotation of the organisms. Settling in the water column is slowed by increasing the surface area relative to the volume, thereby increasing the drag of the cell in the water. In diatoms this can be accomplished by setae (*Chaetoceros*, Figs. 17.6(*a*), 17.32, 17.44, 17.45) or by cells shaped as discs (*Coscinodiscus*, Figs. 17.2(*a*), 17.6(*b*), 17.15, 17.38(*a*), (*b*)), ribbons (*Fragilaria*, Fig. 17.31(*d*), (*e*)), or elongate forms (*Rhizosolenia*, Fig. 17.33(*c*)). The aggregation of diatom cells into chains increases the settling rate of the cells because it decreases the surface area. Increasing the size of diatom cells results in an increase in the ascension rate. The largest diatom cells can ascend up to 8 meters per hour (Moore and Villareal, 1996).

Planktonic diatoms can vary in density during the day, moving up and down in the water column. This causes a constant flow of water over the surface of the diatom, enabling a better absorption of nutrients. *Ditylum brightwelli* (Figs. 17.22(*a*), (*b*), 17.31(*b*), (*c*)) is a diatom with a variation in sedimentation rates, the greatest rate of settling occurring during the latter half of the light period and the least settling occurring at the end of the dark period (Fisher and Harrison, 1996). The insignificance of fat deposits in buoying up cells can be seen here, where the cells contain the maximum amount of fat during the period of maximum settling (Andersen and Sweeney, 1977). Sedimentation of diatoms in the ocean continues in many cases until an increased density of the water, due to either a thermocline or greater water depth, causes them to remain steady in the water column. In the central north Pacific Ocean, there is a widespread deep (110- to 130-m depth) chlorophyll layer containing pigments of living algae, not detritus. This chlorophyll maximum

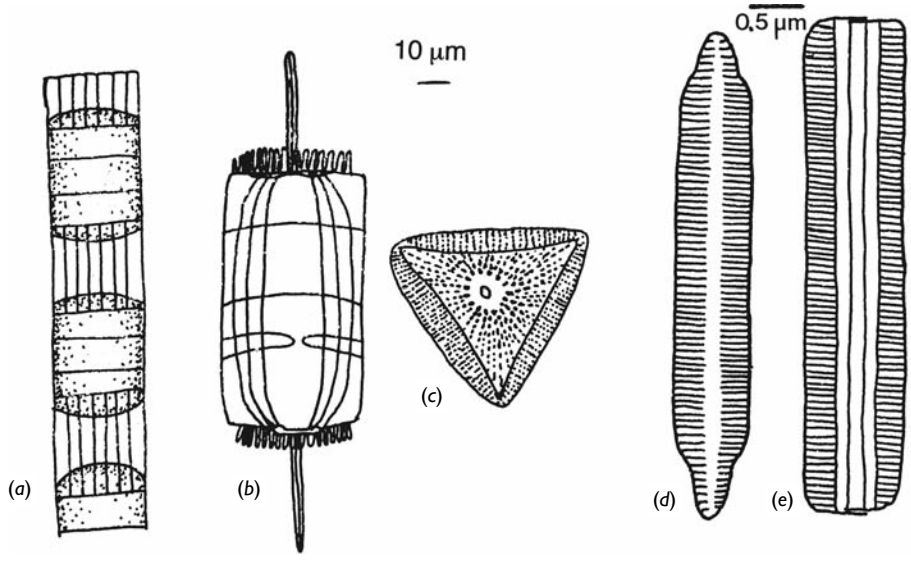


Fig. 17.31 (*a*) *Skeletonema costatum.* (*b*), (*c*) *Ditylum brightwelli.* (*b*) Girdle view. (*c*) Valve view. (*d*), (e) *Fragilaria virescens*, valve and girdle view.

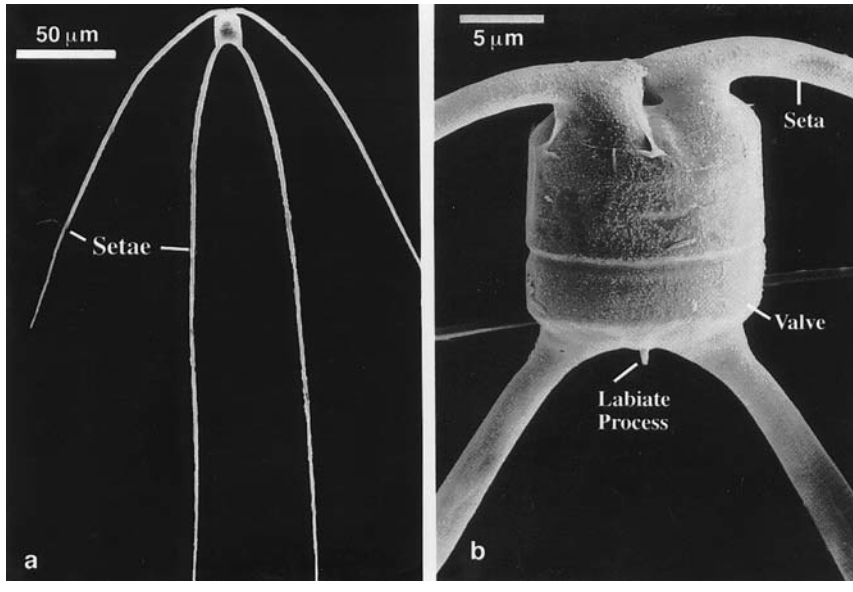


Fig. 17.32 Scanning electron micrograph of *Chaetoceros peruvianus* showing the setae and a labiate process. (From Pickett-Heaps et al., 1994.)

contains growing organisms and is not an accumulation of moribund cells (Venrick et al., 1973; Jeffrey, 1976). Diatoms make up a good proportion of these cells and are able to grow there by virtue of an adaptation of the cells to the decreased light (Jeffrey and Vesk, 1977). The light that penetrates down to this depth is composed principally of low-intensity blue-green light with a maximum at about 480 nm. It has been shown with the marine diatom *Stephanopyxis turris* (Figs. 17.33(*a*), 17.38(*c*), (*d*)) that blue-green light increases the

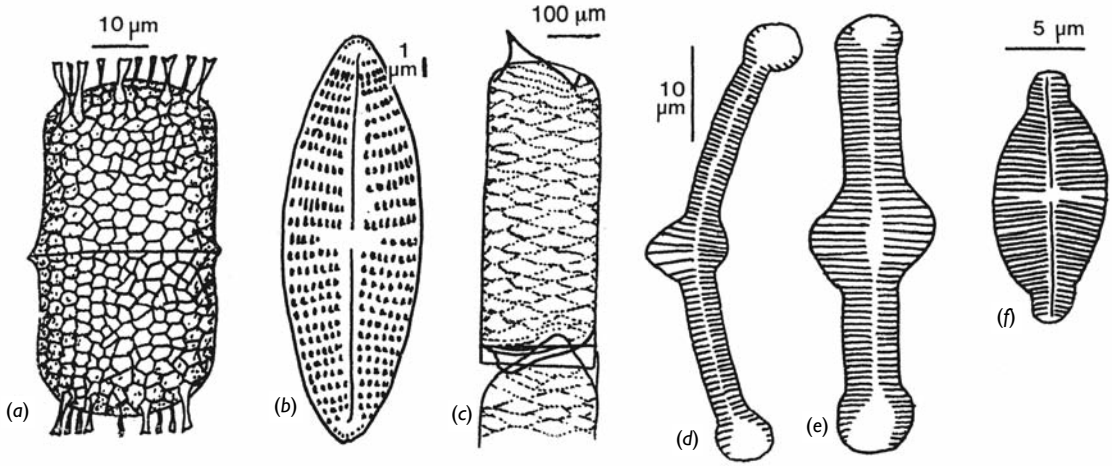


Fig. 17.33 (*a*) *Stephanopyxis turris.* (*b*) *Navicula glaciei.* (*c*) *Rhizosolenia castracanei.* (*d*) *Tabellaria fenestrata.* (e) *Tabellaria flocculosa.* (*f*) *Achnanthes exigua.*

amount of chlorophyll up to 100% when compared to white light, with an appropriate increase in chloroplasts but with no change in the chlorophyll:carotenoid ratio. At the same time, blue-green light enhances the photosynthetic fixation of carbon dioxide. Thus the diatoms living at great water depth receiving only blue-green light "switch on" a mechanism for more efficient photon capture of light and increased fixation of carbon dioxide. They are therefore able to remain viable and grow at a water depth that has a low amount of light.

Symbioses between nitrogen-fixing (diazotrophic) bacteria and cyanobacteria, and the diatom genera *Rhizosolenia* and *Hemiaulus* are common in warm oligotrophic seas (Villareal, 1989). *Rhizosolenia castracanei* (Fig. 17.33(*c*)) and *R. imbricata* var. *shrubsolei* form free-floating diatom mats in oligotrophic central oceanic regions, such as the Sargasso Sea and the North Pacific Gyre (where *Rhizosolenia* mats make up 98% of all living diatom silicon (Shipe et al., 1999)). In these areas the fixation of nitrogen by the endosymbionts contribute a significant amount of nitrogen to the ecosystem (Martinez et al., 1983). The *Rhizosolenia* cells migrate vertically in the column at a rate of several meters per hour and can be found to a depth of 150 meters (Richardson et al., 1996; Villareal and Carpenter, 1994). Cells that are deprived of nitrogen are negatively buoyant and sink below the euphotic zone into waters that are relatively high in nutrients. After taking up nutrients, the cells become positively buoyant and move up into the euphotic zone and resume photosynthesis.

Freshwater environment

Many planktonic diatoms have regular annual fluctuations in growth that can be attributed to environmental conditions. *Asterionella formosa* is one of these diatoms (Fig. 17.16), a common freshwater planktonic diatom that forms large spring growths and smaller autumn ones (Fig. 17.34) (Lund, 1949, 1950). During the winter months, light and temperature limit the growth of the diatoms; lower temperature affects respiration more than photosynthesis so that the compensation point is lowered, and the possibility that photosynthesis will exceed respiration is increased. With the beginning of spring and consequent increase in temperature and light, there is a rapid growth of cells until the middle of spring, when another factor becomes limiting – this time the concentration of dissolved silica in the water; the growth of diatoms then results in much of the dissolved silica being incorporated into the siliceous frustules. Once the concentration of dissolved silica reaches 0.5 mg liter^{-1}, most diatoms cease growth. Because the silica is now limiting, the number of diatoms falls off rapidly and increase only to a lesser degree in the fall when more

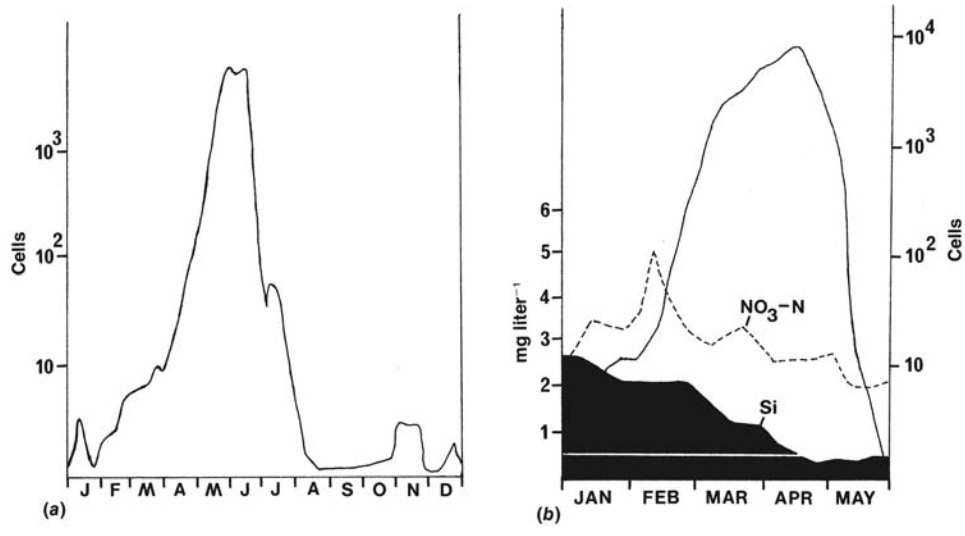


Fig. 17.34 (*a*) Seasonal distribution of live cells of *Asterionella* in Lake Windermere, England, plotted on a logarithmic scale in the 0- to 5-m water column. The horizontal axis represents the months of 1947. (*b*) Numbers of *Asterionella formosa* (solid line) and the concentrations of dissolved silica and nitrate-nitrogen in mg liter^{-1} in the 0- to 5-m water column in Esthwaite Water, England. The white line represents the 0.5 mg liter^{-1} concentration of silica necessary for growth of diatoms. ((*a*) after Lund, 1949; (*b*) after Lund, 1950.)

dissolved silica is available from the breakdown of the frustules of the spring population and the inflow of water containing silica from streams. There are other factors, such as grazing by invertebrates and fungal parasitism, that also check the growth of *Asterionella*, but they are only of secondary significance.

Enrichment of streams by run off from agricultural land, or input from industry, results in the diatom community being dominated by the "agricultural guild" (Fig. 17.35) (Richardson et al., 1996). The appearance of these diatom species in water samples is an indication of the deterioration of water quality.

The diatoms also make up a large part of the periphyton or the attached algae in freshwaters. These attached diatoms in streams have two opposing factors acting on their growth (Reisen and Spencer, 1970): (1) any increase in current retards the attachment of the diatoms to the substrate, and (2) the increase in current results in an increase in the growth of the diatoms. This leads to the observation that the diatoms growing in fast-flowing streams usually have a higher total standing crop in the long term than those in slow-flowing streams, although initially the fast-flowing water results in a lower number of diatoms being attached to the substrate. The diatoms in the fast-flowing water are, however, able to grow much faster and soon grow so rapidly that they overcome the disadvantage caused by low initial attachment numbers.

Attached diatoms in standing waters have good growth in spring, as do the planktonic diatoms, but do not show as marked a decrease in growth when the concentration of silica in water reaches 0.5 mg liter^{-1} or less. This can be seen by the growth of the diatom *Tabellaria flocculosa* (Fig. 17.33(*e*), (*f*)) on stems of the reeds *Phragmites communis* and *Schoenoplectus lacustris* (Fig. 17.36) (Knudson, 1957). In the May–June period, when the dissolved silica in the water is usually less than 0.5 mg liter^{-1}, there is a decrease in the number of diatoms, but not as great as that of planktonic diatoms, probably because of leaching of silica from the stems of the host plants. A second difference between planktonic and epiphytic diatom seasonal growth is that in the epiphytic diatoms, maximum growth normally occurs in the winter, possibly owing to the secretion by the host of some organic products that are used by epiphytic diatoms.

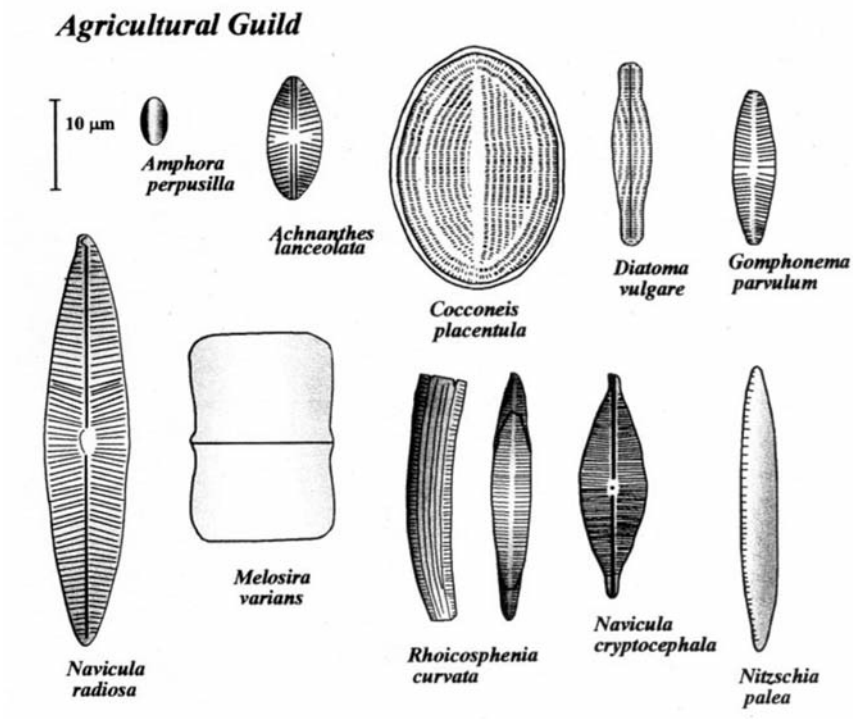


Fig. 17.35 Diatoms that are characteristic of eutrophic freshwaters. The diatoms make up the "agricultural guild", named for waters that are polluted by runoff from agricultural land that have been fertilized with nitrogen, phosphorus, and potash.

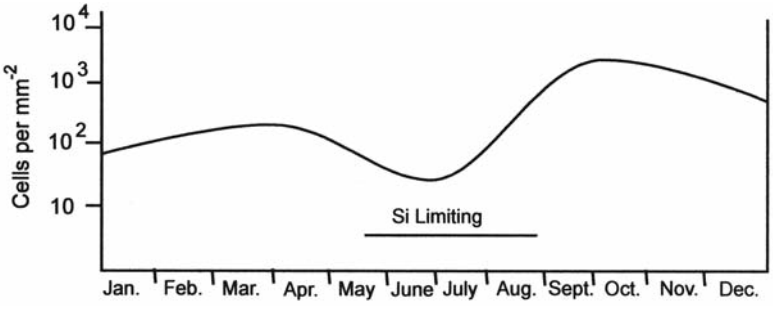


Fig. 17.36 Seasonal fluctuations of epiphytic *Tabellaria flocculosa* on *Phragmites communis* and *Schoenoplectus lacustris* stems. The straight line represents the period when dissolved silica is less then 0.5 mg liter^{-1}. (After Knudson, 1957.)

In freshwater habitats, diatoms often comprise the dominant algal flora in thermal waters between 30 and 40 °C. Fairchild and Sheriden (1974) showed that *Achnanthes exigua* (Fig. 17.33(*f*)) isolated from a hot spring showed optimum photosynthesis at 42 °C, with maximum and minimum temperatures for growth at 44 and 10 °C, respectively – characteristics of a thermophilic organism. This particular diatom is usually associated with an algal mat covered by a shallow layer of water in these hot springs.

Fossil diatoms

The fossil record of diatoms begins in the Jurassic Period (185 million years ago) with diatoms becoming more common in the mid-Cretaceous

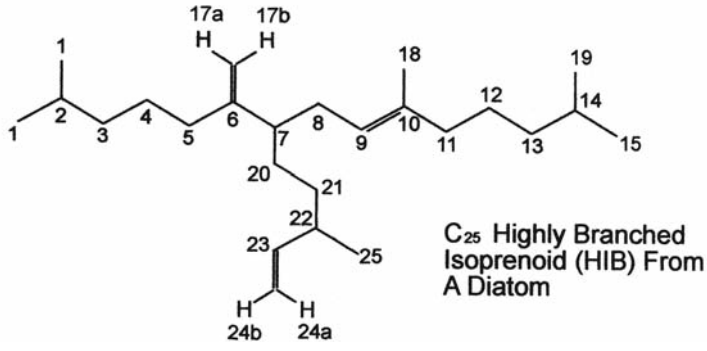


Fig. 17.37 Chemical structure of a highly branched alkene characteristic of diatoms.

(Medlin et al., 1997). The fossil record indicates that centric diatoms evolved before pinnate diatoms (Round et al., 1990). Another way of dating diatoms is by molecular fossils. Some diatom genera (*Rhizosolenia*, Fig. 17.33(*c*); *Haslea*, *Navicula*, Figs. 17.2(*d*), 17.16, 17.26(*a*), 17.33(*b*), 17.35; and *Pleurosigma*) contain unique isoprenoids called highly branched isoprenoid (HBI) alkenes that have a T-branch formed by attachment of a C_{10} isoprenoid unit to a C_{15} isoprenoid unit (Fig. 17.37) (Damste et al., 2004). The occurrence of these alkenes in sediments beginning 90 million years ago parallels the widespread explosion of diatoms in the marine environment at this time.

After death of diatom cells, the frustule usually dissolves after bacteria degrade the organic casing around the frustule (Bidle and Azam, 1999). However, under certain circumstances, the frustules remain intact and accumulate at the bottom of the water (Fig. 17.38). Where conditions are exceptionally favorable and long continued, such accumulations may reach considerable thickness. Deposits of fossil diatoms, known as diatomaceous earth or *kieselguhr*, are found in various parts of the world. None of these deposits originated earlier than the Cretaceous; some diatomaceous earths originated in freshwaters, others in the ocean. However, known deposits of marine species are found inland and above the ocean as a result of geological changes. The best-known and most extensive deposits of marine species are those at Lompoc, California, where the beds are several kilometers in extent and 200 m in thickness (Fig. 17.39). Most of the commercially available diatomaceous earth comes from California, where the deposits are worked as open quarries. In quarrying, the overburden of soil is removed, and the diatomaceous earth is mined. Diatomaceous earth is also obtained from lakes in Florida by dredging with a suction pump and carrying the material through sluiceways to settling tanks. The material from some deposits can be used directly; that from other deposits must be incinerated to remove organic substances.

The industrial uses of diatomaceous earth are varied. One of the first uses was as a mild abrasive in toothpaste and metal polishes. Diatomaceous earth was also used as an absorbent for liquid nitroglycerin to make dynamite that could be transported with comparative safety. The inert medium used in the present-day manufacture of dynamite is wood meal. Probably the most extensive industrial use of diatomaceous earth is in the filtration of liquids, especially those of sugar refineries. Another major use is in the insulation of boilers, blast furnaces, and other places where a high temperature is maintained.

Analysis of sediments containing remains of diatoms can provide information on past environmental conditions of lakes (Reavic et al., 1998; Clavero et al., 2000). This technique has been applied to late glacial and postglacial diatom deposits in the English Lake District (Round, 1957, 1961). During the end of the last glacial period, there were few diatoms present, with the sediments being mostly of inorganic origin, indicating that the lakes initially were very oligotrophic and lacked planktonic diatoms. This period was followed by diatoms characteristic of melt waters under semi-arctic conditions (*Melosira arenaria*, Fig. 17.40(*a*). *Cyclotella antique*, Fig. 17.40(*b*); *Gyrosigma*, Fig. 17.40(*d*); *Cymatopleura*, Fig. 17.40(*e*);

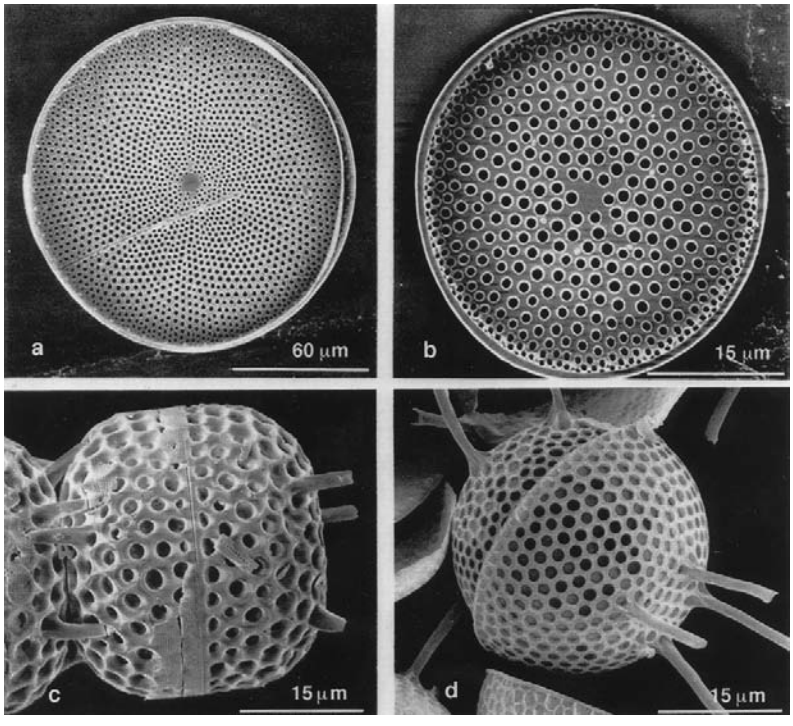


Fig. 17.38 Scanning electron micrographs of fossil diatoms compared with frustules of living diatoms from the same genera. (*a*) *Coscinodiscus radiatus* from Cretaceous sediments. (*b*) *Coscinodiscus radiatus* from recent plankton. (*c*) *Stephanopyxis turris* from Cretaceous sediments. (*d*) *Stephanopyxis broschi* from recent plankton. (From Medlin et al., 1993.)

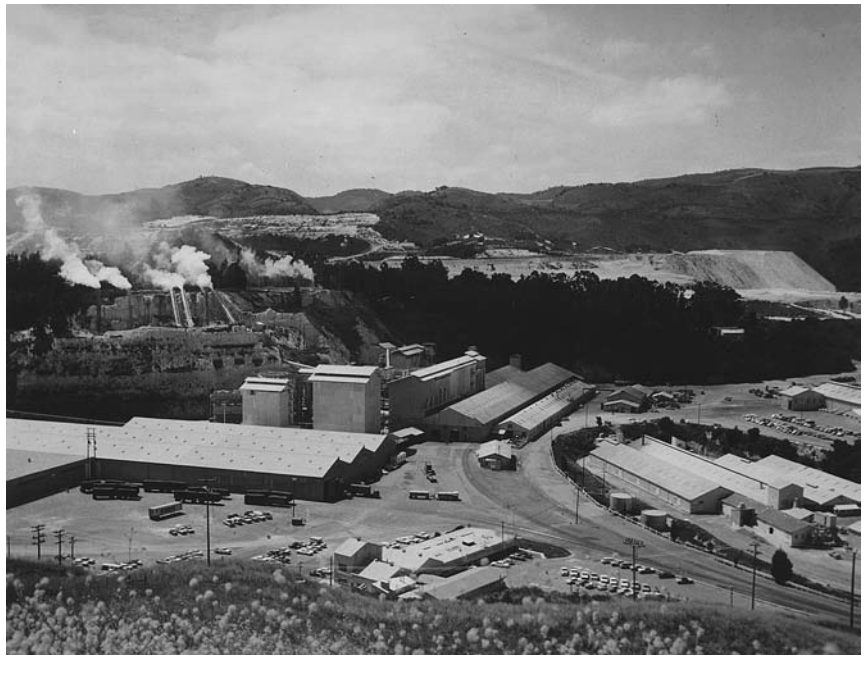


Fig. 17.39 Diatomaceous earth mine at Lompoc, California, with deposits of diatomaceous earth in the background. (Courtesy of Johns-Manville Corporation.)

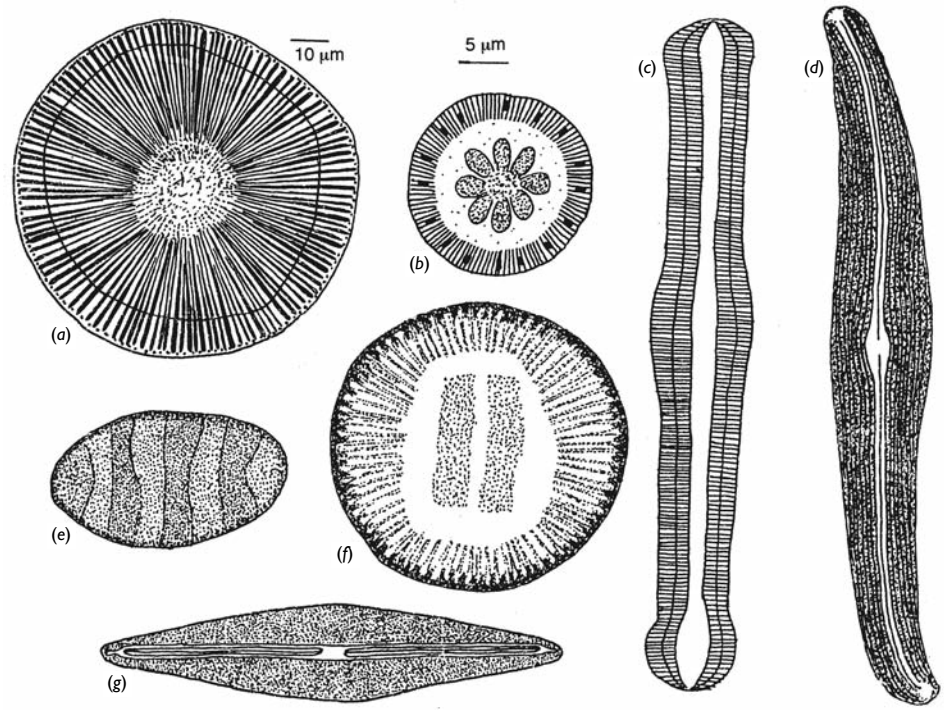


Fig. 17.40 (*a*) *Melosira arenaria.* (*b*) *Cyclotella antique.* (*c*) *Rhopalodia gibba.* (*d*) *Gyrosigma attenuatum.* (e) *Cymatopleura elliptica.* (*f*) *Campylodiscus clypeus.* (*g*) *Frustulia rhomboides.*

Campylodiscus, Fig. 17.40(*f*)) indicating leaching of base-rich components from surrounding rocks into the lakes. The next area of sediments showed a decrease in alkaline-water species and an increase in acid-water species (*Eunotia*, Fig. 17.2(*b*); *Anomoeoneis*; *Frustulia*, Fig. 17.40(*g*); *Tabellaria*, Figs. 17.3(*b*), 17.33(*d*), (*e*)), a trend that has continued up to recent times. This trend is related to a decrease in bases being leached from the rocks because no new rock surfaces have been exposed, and to a decline in the stands of birch/pine on the land. At the top of the sediments are remains of *Asterionella formosa*, indicating a recent change of waters to less acidic, more eutrophic conditions, a state related to man's activities. *A. formosa* is a diatom that grows readily in eutrophic waters and shows changes in colony morphology, depending on nutrients in the water. Under optimum growth conditions, the colonies average eight cells, whereas under phosphate limitation the number of cells per colony drops to two, and under silicate limitation the number of cells per colony increases to 20. Under both P and Si limitations, there is a decrease in growth rate (Tilman et al., 1976).

Classification

The diatoms probably originated about 200 million years ago in the late Permian (Medlin et al., 1997) from a scaly member of the Chrysophyceae or Bolidophyceae (Guillou et al., 1999). Two scales evolved into valves, while other scales formed the girdle bands. The first diatom had a centric organization with two dome-shaped valves and many scale-like bands (Round et al., 1990). The first recognizable fossils are centric diatoms from the early Cretaceous with pennate diatoms being recorded from the late Cretaceous. The first pennate diatom fossils were araphid (no raphe) with raphid diatoms appearing in the middle Eocene.

The Bacillariophyceae can be divided into two orders as follows:

Order 1 Biddulphiales: radial or gonoid ornamentation; many chloroplasts; no raphe; resting spores formed; motile spermatozoids with a single tinsel

flagellum; oogamous sexual reproduction.

Order 2 Bacillariales: pennate or trellisoid ornamentation; one or two chloroplasts; raphes possibly present with gliding; no flagellated spermatozoids; sexual reproduction by conjugation.

Biddulphiales

The Biddulphiales or Centrales is primarily a marine planktonic group having cells with gonoid or centric ornamentation (Fig. 17.2). *Melosira*, a common golden-brown diatom found in marine and freshwater environments, consists of cylindrical cells with a greater length than breadth (Figs. 17.35, 17.40, 17.41, 17.42). There are a number of girdle bands which form incomplete rings around the cell without their ends meeting. Both the valve and the girdle bands are ornamented with small spines. The diatom is usually filamentous, with the cells joined end to end by their valves so that to the inexperienced eye it resembles a filamentous chrysophycean alga with the cells always in girdle view. Gametogenesis is initiated after the cells have undergone a number of mitotic cell divisions that have reduced the size of the frustule below a certain critical limit. Von Stosch (1951) has elucidated the following events in the life cycle of *Melosira varians* (Fig. 17.42). In the male cells, gametogenesis starts with the nucleus undergoing two meiotic divisions to produce four haploid nuclei. A plasma membrane is formed around each nucleus and a small amount of parent cell protoplasm. The remaining protoplasm of the mother cell now lacks a nucleus and begins to degenerate. A single flagellum is produced by each male gamete, the epitheca separates from the hypotheca, and the male gametes are released into the medium. In the female cells, while the nucleus is undergoing the first meiotic division, one of the girdle bands separates from the edge of the valve, leaving an area of protoplasm open to the medium. The male gamete swims to the area of the female cell where the girdle band has separated from the valve edge. During telophase of the first meiotic division of the female cell, the cytoplasm of the male gamete fuses with that of the female cell. One of the nuclei of the first meiotic division in the female cell degenerates while the other nucleus undergoes a second meiotic division. From the second meiotic division, one of the female nuclei again degenerates, and the other becomes the egg nucleus. The male nucleus fuses with the egg nucleus to form the zygote or auxospore nucleus. The resulting auxospore (Fig. 17.43) then swells, pushing apart the hypotheca and epitheca until the auxospore is attached to both or one theca by a small protuberance only. The auxospore has an outer organic wall and an inner wall made of siliceous scales (Crawford, 1974). A new cell wall of maximum dimensions is now produced within

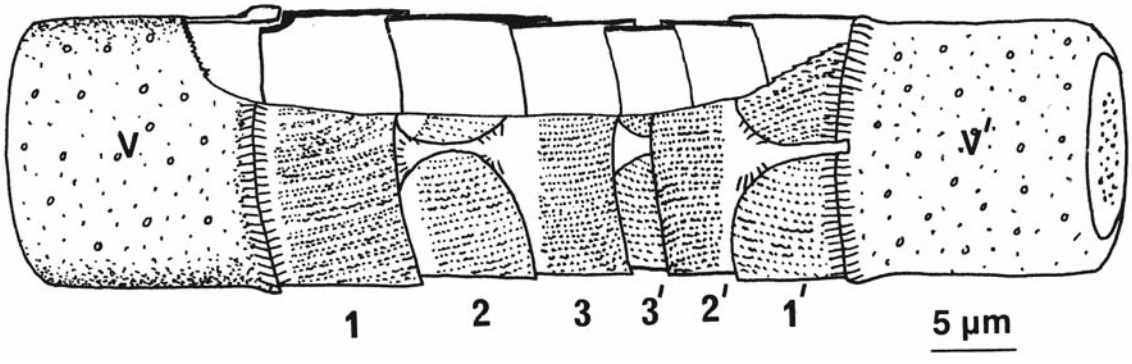


Fig. 17.41 Semidiagrammatic representation of a cell of *Melosira varians* composed of two valves, V and V′, two girdle band series: 1, 2, 3, and, underlapping these, the younger series 1′, 2′, 3′. (After Crawford, 1971.)

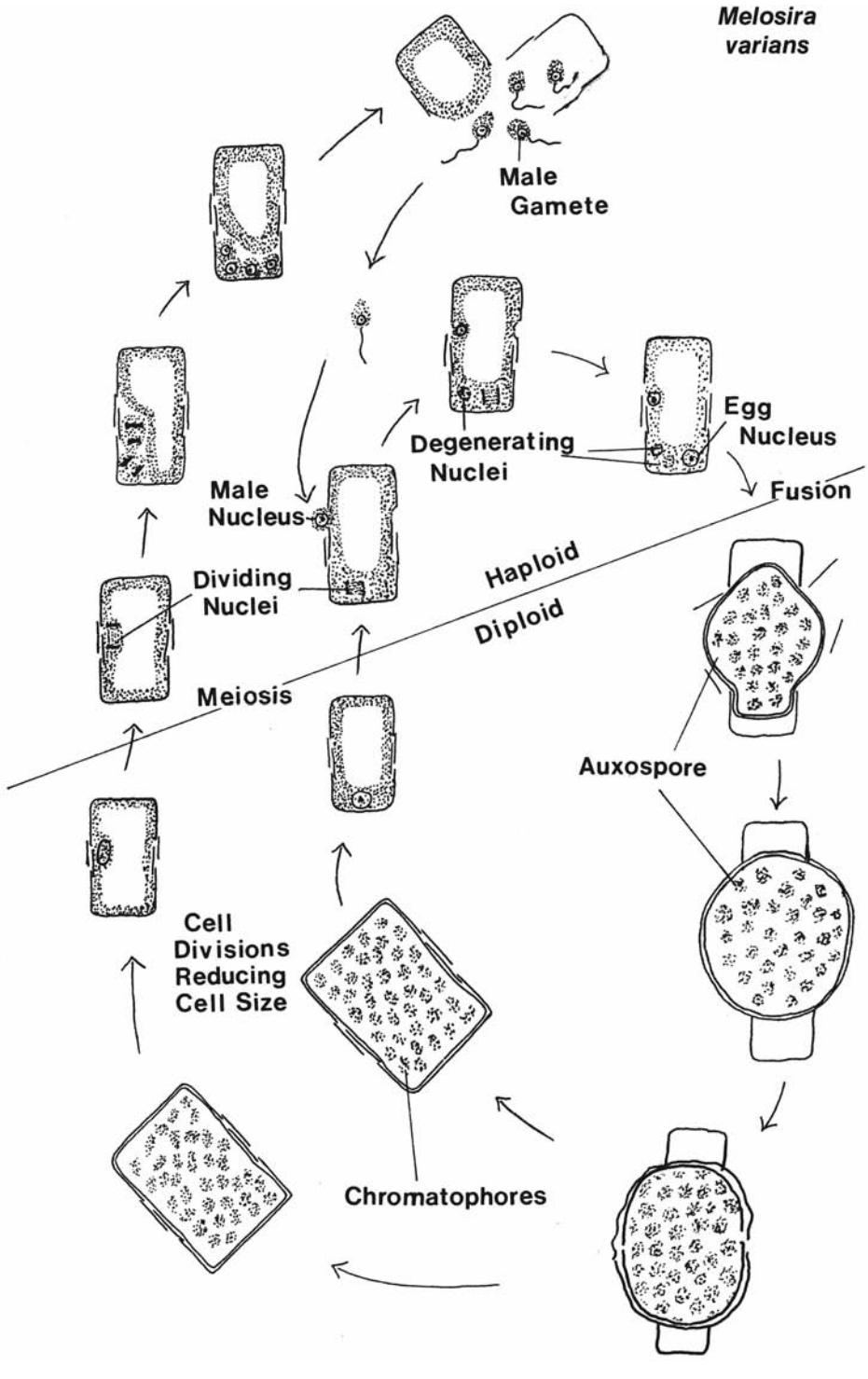


Fig. 17.42 The life cycle of *Melosira varians*. (Adapted from von Stosch, 1951.)

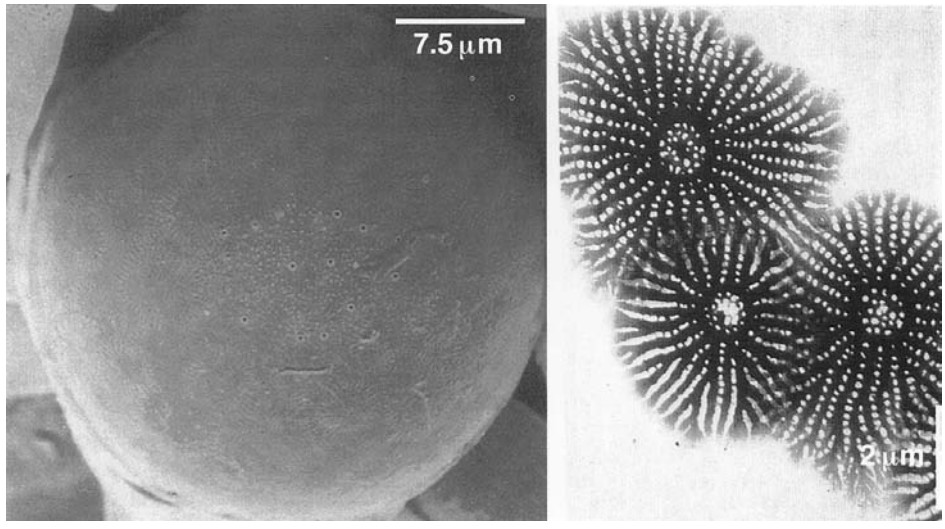


Fig. 17.43 Electron micrographs of an auxospore of *Melosira nummuloides* (*left*) showing the scales covering the auxospore (*right*). (From Medlin et al., 1993.)

the auxospore. This cell divides to give rise to a new filament.

Melosira is capable of producing dormant cells in freshwater environments. The dormant cells have the protoplasm condensed to a dark-brown protoplasmic mass in one part of the frustule (Sicko-Goad et al., 1986). The dormant cells settle into the sediment, where they are capable of surviving for up to 20 years. Normally, however, the dormant cells are swept up by normal recirculation of lake waters during lake overturns (Lund, 1959). Within 24 hours of being swept out of the sediments, the dormant cells of *Melosira* differentiate into vegetative cells.

Chaetoceros (Figs. 17.6(*a*), 17.32, 17.44, 17.45) has more than 160 species, the largest number of any planktonic diatom. The genus is widespread in warm and cold waters. The life cycle of *Chaetoceros diadema* has been elucidated by Hargraves (1972) (Fig. 17.44). *Chaetoceros diadema* is a colonial marine diatom, with cells united by their long setae to form filaments. The different phases of the life cycle are characterized by different sizes and shapes of cells. Gametogenesis is initiated at temperatures between 2 and 5 °C (French and Hargraves, 1985). The cells that produce the male gametes are about 1.5 to 2 times as wide as high. These cells divide to produce 32 male gametes, presumably by meiosis, which are released as uniflagellate swarmers. The cells that produce the female gametes are about twice as high as wide. The exact nuclear events that lead to the production of the egg are not known, but the male gamete (Fig. 17.45) swims to the girdle area of the female cell, casts off its flagellum, and fuses with the female gamete inside the frustule. The cell contents of the auxospore-forming cell are then extruded through the girdle region into a thin hyaline envelope. This cell then produces the auxospore, which, in turn, produces new cells with frustules of maximum size. These large daughter cells remain attached to the auxospore parent wall through two divisions of the daughter cells. The hyaline envelope of the auxospore is sloughed off after the first division. Any of the vegetative cells have the ability to produce resting spores after nitrogen depletion of the culture medium at temperatures that allow vegetative growth (French and Hargraves, 1985). The resting spores germinate to produce cells larger than the original cells. The resting spores occur within the parent cell as heavily siliceous bodies, having usually convex, often dissimilar, upper and lower surfaces bearing spines.

Bacillariales

The Bacillariales or Pennales order contains cells that occur both in freshwater and in marine

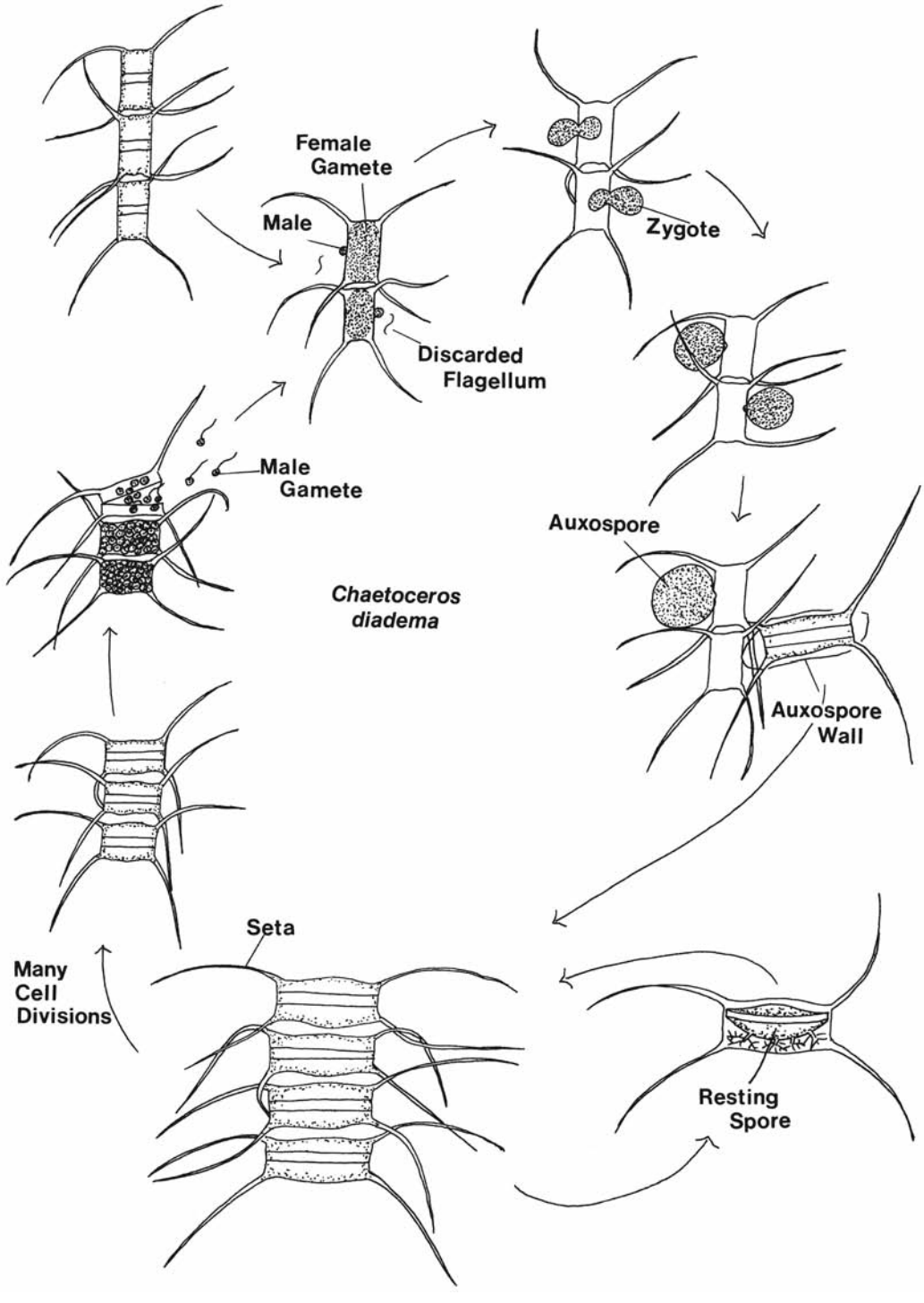


Fig. 17.44 The life cycle of *Chaetoceros diadema*. (Adapted from Hargraves, 1972.)

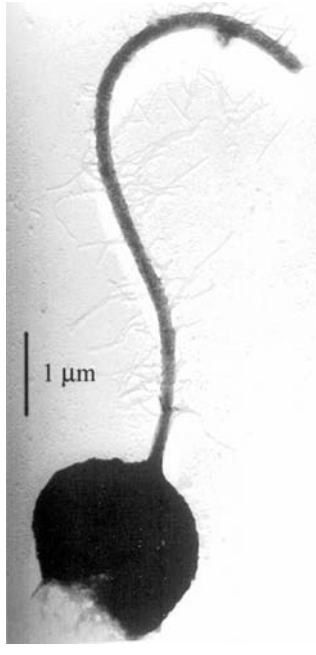
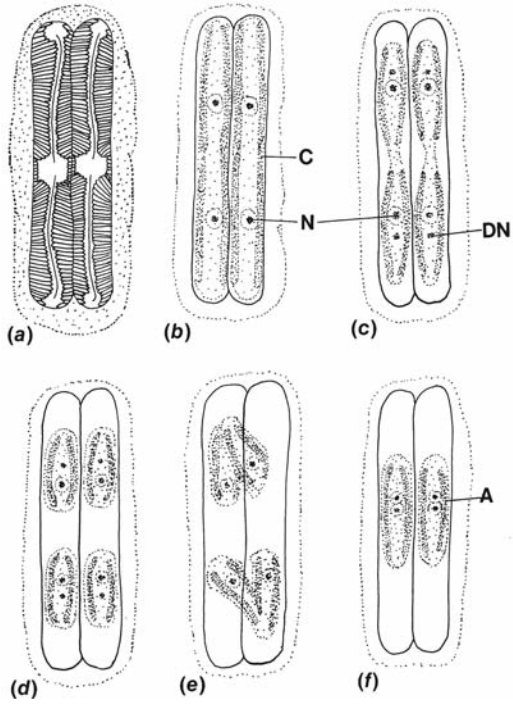


Fig. 17.45 *Chaetoceros laciniosus*. A transmission electron micrograph of a shadowed preparation of a whole mount of a spermatozoid showing the single tinsel flagellum. (From Jensen et al., 2003.)

environments. These cells have either pennate or trellisoid ornamentation (Fig. 17.2). The life cycle of these organisms involves fusion of two gametes by conjugation and common genera such as *Nitzschia* (Figs. 17.26(*b*), 17.35), *Pseudo-nitzschia* (Figs. 17.27, 17.29), *Navicula* (Figs. 17.2(*d*), 17.16, 17.25, 17.26(*a*), 17.33(*b*), 17.35), *Amphora* (Figs. 17.22(*c*), (*d*), 17.35), *Cymbella*, and *Pinnularia* (Figs. 17.3(*a*), 17.12, 17.18, 17.46) have essentially the same life cycle. In *Pinnularia*, the cells have rounded poles with more or less parallel sides (Fig. 17.46). Auxospore formation is a sexual process initiated after cell divisions have reduced the cell to a certain critical size. Two cells come together and invest themselves in a mucous envelope (Hendey, 1964). The nucleus in each cell undergoes two meiotic divisions followed by cytokinesis into two cells. Two gametes are thus formed per mother cell, each protoplast receiving one functional and one degenerating nucleus. One gamete from each mother cell moves to the contiguous mother cell to fuse with the passive gamete. In this manner, one zygote (auxospore) is formed within each mother cell. These auxospores become greatly enlarged, and eventually new siliceous frustules



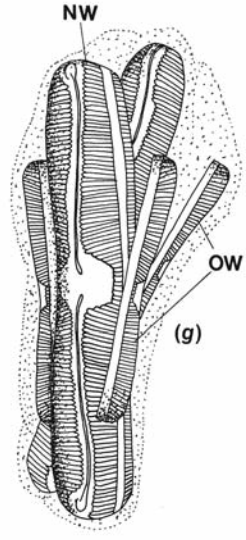


Fig. 17.46 Auxospore formation in *Pinnularia*. (*a*) Two cells lie next to each other. (*b*)–(*d*) Meiosis occurs in each mother cell, resulting in two gametes per mother cell, each with one functional nucleus (N) and one degenerate nucleus (DN). (e) One gamete from each mother cell passes to the other mother cell. (*f*) There is one auxospore (A) per mother cell frustule. (*g*) Each auxospore has produced a new large daughter cell (NW), with the old cell walls (OW) of the mother cells still embedded in the mucilage. (C) Chloroplast. (After Hendey, 1964.)

of maximum size are produced within each auxospore. The four discarded valves of the mother cells are often seen attached to the newly formed frustules.

The life cycle of *Pseudo-nitzschia* (Fig. 17.29) is similar to *Pinnularia*.

REFERENCES

Alcoverro, T., Conte, E., and Mazzella, L. (2000). Production of mucilage by the Adriatic epipelic diatom *Cylindrotheca closterium* (Bacillariophyceae) under nutrient limitation. *J. Phycol*. 36:1087–95.

Andersen, L. W. J., and Sweeney, B. M. (1977). Diel changes in sedimentary characteristics of *Ditylum brightwelli*: Changes in cellular lipid and effects of respiratory inhibitors and ion transport modifiers. *Limnol. Oceanogr*. 22:539–52.

Andersen, R. A., Medlin, L. K., and Crawford, R. M. (1986). An investigation of the cell wall components of *Actinocyclus subtilis* (Bacillariophyceae). *J. Phycol*. 22:466–79.

Anderson, O. R. (1975). The ultrastructure and cytochemistry of resting cell formation in *Amphora coffaeformis* (Bacillariophyceae). *J. Phycol*. 11:272–81.

Anderson, O. R. (1976). Respiration and photosynthesis during resting cell formation in *Amphora coffaeformis* (Ag.) Kütz. *Limnol. Oceanogr*. 21:452–6.

Bates, S. S. (2000). Domoic-acid-producing diatoms: another genus added. *J. Phycol*. 36:978–85.

Beattie, A., Hirst, E. L., and Percival, E. (1961). Studies on the metabolism of the Chrysophyceae. Comparative structural investigations on leucosin (chrysolaminarin) separated from diatoms and laminarin from brown algae. *Biochem. J*. 79:531–6.

Bidle, K. D., and Azam, F. (1999). Accelerated dissolution of diatom silica by marine bacterial assemblages. *Nature* 397:508–12.

Branton, D., Cohen, C. M., and Tyler, T. (1981). Interaction of cytoskeletal proteins on the human erythrocyte membrane. *Cell* 24:24–32.

Brzezinski, M. A., and Conley, D. J. (1994). Silicon deposition during the cell cycle of *Thalassiosira weissflogii* (Bacillariophyceae) determined using dual rhodamine 123 and propidium iodide staining. *J. Phycol*. 30:45–55.

Caldwell, G. S., Bentley, M. G., and Olive, P. J. W. (2004). First evidence of sperm motility inhibition by the diatom aldehyde 2E,4E-decadienal. *Mar. Ecol. Progr. Ser*. 273:97–108.

Casotti, R., Mazza, S., Brunet, C., Vantrepotte, V., Ianora, A., and Miralto, A. (2005). Growth inhibition and toxicity of the diatom aldehyde 2-*trans*,4-*trans*-decadienal on *Thalassiosira weissflogii*. *J. Phycol*. 41:7–20.

Chepurnov, V. A., Mann, D. G., Sabbe, K., and Vyverman, W. (2004). Experimental studies on sexual reproduction in diatoms. *Int. Rev. Cytol*. 237:91–154.

Chiovitti, A., Bacic, A., Burke, J., and Wetherbee, R. (2003). Heterogenous xylose-rich glycans are associated with extracellular glycoproteins in the biofouling diatom *Craspedostauros australis* (Bacllariophyceae). *Eur. J. Phycol*. 38:351–60.

Chiovitti, A., Molino, P., Crawford, S. A., Teng, R., Spurck, T., and Wetherbee, R. (2004). The glucans extracted with warm water from diatoms are mainly derived from intracellular chrysolaminarin and not extracellular polysaccharides. *Eur. J. Phycol*. 39:117–28.

Clavero, E., Hernandez-Marine, M., Grimalt, J. O., and Garcia-Pichel, F. (2000). Salinity tolerance of diatoms from thalassic hypersaline environments. *J. Phycol*. 36:1021–34.

Cohn, S. A., and Weitzell, R. E. (1996). Ecological consideration of diatom cell motility. I. Characterization of motility and adhesion in four diatom species. *J. Phycol*. 32:918–39.

Cohn, S. A., Spurck, T. P., and Pickett-Heaps, J. D. (1989). Perizonium and initial valve formation in the diatom *Navicula cuspidata* (Bacillariophyceae). *J. Phycol*. 25:15–26.

Cooksey, K. E., and Cooksey, B. (1974). Calcium deficiency can induce the transition from oval to fusiform cells in cultures of *Phaeodactylum tricornutum* Bohlin. *J. Phycol*. 10:89–90.

Coombs, J., and Volcani, B. E. (1968). Studies on the biochemistry and fine structure of silica shell formation in diatoms. Chemical changes in the wall of *Navicula pelliculosa* during its formation. *Planta* 82:280–92.

Crawford, R. M. (1971). The fine structure of the frustule of *Melosira varians* C. A. Agardh, *Br. Phycol. J*. 6:175–86.

Crawford, R. M. (1974). The auxospore wall of the marine diatom *Melosira nummuloides* (Dillw.) C. Ag. and related species. *Br. Phycol. J*. 9:9–20.

Crawford, S. A., Higgins, M. J., Mulvaney, P., and Wetherbee, R. (2001). Nanostructure of the diatom frustule as revealed by atomic force and scanning electron microscopy. *J. Phycol*. 37:543–54.

Damste, J. S. S., Muyzer, G., Abbas, B., et al. (2004). The rise of rhizosolenid diatoms. *Science* 304:584–7.

Davidovich, N. A. and Bates, S. S. (1998). Sexual reproduction in the pennate diatoms *Pseudo-nitzschia multi-*

series and *P. pseudodelicatissima* (Bacillariophyceae). *J. Phycol*. 34:126–37.

Davis, C. O., Hollibaugh, J. T., Seibert, D. L. R., Thomas, W. H., and Harrison, P. J. (1980). Formation of resting spores by *Leptocylindrus danicus* (Bacillariophyceae) in a controlled experimental ecosystem. *J. Phycol*. 16:296–302.

Dawson, P. A. (1973). Observations on the structure of some forms of *Gomphonema parvulum* Kütz. III. Frustule formation. *J. Phycol*. 9:353–64.

de Brouwer, J. F. C., and Stal, L. J. (2002). Daily fluctuation of exopolymers in cultures of the benthic diatoms *Cylindrotheca closterium* amd *Nitzschia* sp. (Bacillariophyceae). *J. Phycol*. 38:464–72.

Del Amo, Y., and Brzezinski, M. A. (1999). The chemical form of dissolved Si taken up by marine diatoms. *J. Phycol*. 35:1162–70.

Drum, R. W., and Hopkins, J. T. (1966). Diatom locomotion: An explanation. *Protoplasma* 62:1–33.

Edgar, L. A. (1979). Diatom locomotion: Computer assisted analysis of cine film. *Br. Phycol. J*. 14:83–101.

Edlund, M. B., and Stoermer, E. F. (1997). Ecological, evolutionary, and systematic significance of diatom life histories. *J. Phycol*. 33:897–918.

Erickson, S. J. (1972). Toxicity of copper to *Thalassiosira pseudonana* in unenriched inshore seawater. *J. Phycol*. 8:318–23.

Fairchild, E., and Sheriden, R. P. (1974). A physiological investigation of the hot spring diatom *Achnanthes exigua*. Grün. *J. Phycol*. 10:1–4.

Fauré-Fremiet, E. (1951). The tidal rhythm of the diatom *Hantzschia amphioxys. Biol. Bull*. 100:173–7.

Fisher, A. E., and Harrison, P. J. (1996). Does carbohydrate content effect the sinking rate of marine diatoms. *J. Phycol*. 32:360–5.

French, F. W., and Hargraves, P. E. (1985). Spore formation in the life cycles of the diatoms *Chaetoceros diadema* and *Leptocylindrus danicus. J. Phycol*. 21:477–83.

Granum, E., and Myklestad, S. M. (2001). Mobilization of β-1,3-glucan and biosynthesis of amino acids induced by NH_4^+ addition to N-limited cells of the marine diatom *Skeletonema costatum* (Bacillariophyceae). *J. Phycol*. 37:772–82.

Gross, F. (1940). The development of isolated resting spores into auxospores in *Ditylum brightwelli* (West). *J. Mar. Biol. Assoc. UK* 24:375–80.

Guillou, L., Chretiennot-Dinet, M.-J., Medlin, L. K., Claustre, H., Loiseaux-de Goer, S., and Vaulot, D. (1999). *Bolidomonas*: a new genus with two species belonging to a new algal class, the Bolidophyceae (Heterokonta). *J. Phycol*. 35:368–81.

Hargraves, P. E. (1972). Studies on marine planktonic diatoms. I. *Chaetoceros diadema* (Ehr.) Gran.: Life cycle, structural morphology, and regional distribution. *Phycologia* 11:247–57.

Hasle, G. R. (1995). *Pseudo-nitzschia punges* and *P. multiseries* (Bacillariophyceae): nomenclature history, morphology and distribution. *J. Phycol*. 31:428–35.

Hasle, G. R., and Lange, C. B. (1989). Freshwater and brackish water *Thalassiosira* (Bacillariophyceae): taxa with tangentially undulated valves. *Phycologia* 28:120–35.

Hecky, R. F., Mopper, K., Kilham, P., and Degens, E. T. (1973). The amino acid and sugar composition of diatom cell walls. *Mar. Biol*. 19:323–31.

Hellebust, J. A. (1971). Glucose uptake by *Cyclotella cryptica:* Dark induction and light inactivation of transport system. *J. Phycol*. 7:345–49.

Hendey, N. I. (1964). An introductory account of the smaller algae of British coastal waters. Part V. Bacillariophyceae (diatoms). *Fish. Invest. Ser. IV*. H.M.S.O., London.

Hendey, N. I. (1971). Electron microscope studies and the classification of diatoms. In *The Micropaleontology of Oceans*, ed. B. M. Funnell, and W. R. Riedel, pp. 625–31. Cambridge: Cambridge University Press.

Higgins, M. J., Molino, P., Mulvaney, P., and Wetherbee, R. (2003). The structure and nanomechanical properties of the adhesive mucilage that mediates diatom-substratum adhesion and motility. *J. Phycol*. 39:1181–93.

Hildebrand, M. (2004). Silicic acid transport and its control during cell wall silicification in diatoms. In *Biomineralization*: *Progress in Biology, Molecular Biology and Application*, ed. E. Baeuerlein, pp. 158–76. Weinheim: Wiley-VCH.

Hoagland, K. D., Rosowski, J. R., Gretz, M. R., and Romer, S. C. (1993). Diatom extracellular polymeric substances: Function, fine structure, chemistry, and physiology. *J. Phycol*. 29:537–66.

Iler, R. K. (1979). *The Chemistry of Silica*. New York: John Wiley.

Jeffrey, S. W. (1976). A report of green algal pigments in the central north Pacific Ocean. *Mar. Biol*. 37:33–7.

Jeffrey, S. W., and Vesk, M. (1977). Effect of blue-green light on photosynthetic pigments and chloroplast structure in the marine diatom *Stephanopyxis turris. J. Phycol*. 13:271–9.

Jensen, K. G., Moestrup, Ø., and Schmid, A.-M. (2003). Ultrastructure of the male gametes from two centric diatoms, *Chaetoceros laciniosus* and *Coscinodiscus wailesii* (Bacillariophyceae). *Phycologia* 42:98–105.

Johnson, L. M., Hoagland, K. D., and Gretz, M. R. (1995). Effects of bromide and iodide on stalk secretion in the biofouling diatom *Achnanthes longipes* (Bacillariophyceae). *J. Phycol*. 31:401–12.

Knudson, B. M. (1957). Ecology of the epiphytic diatom *Tabellaria flocculosa* (Roth) Kütz. var. *flocculosa* in three English lakes. *J. Ecol*. 45:93–112.

Kroger, N. (2001). The sweetness of diatom molecular engineering. *J. Phycol*. 37:657–8.

Kroger, N., and Sumper, M. (2004). The molceular basis of diatom biosilica formation. In *Biomineralization: Progress in Biology, Molecular Biology and Application*, ed. E. Baeuerlein, pp. 137–58. Weinheim: Wiley-VCH.

Kroger, N., Deutzmann, R. and Sumper, M. (1999). Polycationic peptides from diatom biosilica that direct silica nanosphere formation. *Science* 286:1129–32.

Kroger, N., Deutzmann, R. and Sumper, M. (2000). Species-specific polyamines from diatoms control silica morphology. *Proc. Natl. Acad. Sci., USA* 97:14133–8.

Lauritis, J. A., Coombs, J., and Volcani, B. E. (1968). Studies on the biochemistry and fine structure of silica shell formation in diatoms. IV. Fine structure of the apochlorotic diatom *Nitzschia alba* Lewin and Lewin. *Arch. Mikrobiol*. 62:1–16.

Lewin, J. C. (1953). Heterotrophy in diatoms. *J. Gen. Microbiol*. 9:305–13.

Lewin, J. C. (1962). Silicification. In *Physiology and Biochemistry of the Algae*, ed. R. A. Lewin, pp. 445–55. New York: Academic Press.

Lewin, J. C. (1966). Silicon metabolism in diatoms. V. Germanium dioxide, a specific inhibitor of diatom growth. *Phycologia* 6:1–12.

Lewin, J. C., and Lewin, R. A. (1960). Auxotrophy and heterotrophy in marine littoral diatoms. *Can. J. Microbiol*. 6:127–34.

Lewin, J. C., and Lewin, R. A. (1967). Culture and nutrition of some apochlorotic diatoms of the genus *Nitzschia*. *J. Gen. Microbiol*. 46:361–7.

Li, C-W., Chu, S., and Lee, M. (1989). Characterizing the silica deposition vesicle of diatoms. *Protoplasma* 151:156–63.

Lund, J. W. G. (1949). Studies on *Asterionella*. I. The origin and nature of the cells producing seasonal maxima. *J. Ecol*. 37:389–419.

Lund, J. W. G. (1950). Studies on *Asterionella formosa* Hass. II. Nutrient depletion and the spring maximum *J. Ecol*. 38:1–14, 15–35.

Lund, J. W. G. (1959). Buoyancy in relation to the ecology of freshwater phytoplankton, *Br. Phycol. Bull*. 7:17.

Lundholm, N., and Moestrup, O. (2000). Morphology of the marine diatom *Nitzschia navis-varingica*, sp. nov. (Bacillariophyceae), another producer of the neurotoxin domoic acid. *J. Phycol*. 36:1162–74.

McQuoid, M. R., and Hobson, L. A. (1996). Diatom resting stages. *J. Phycol*. 32:889–902.

Mann, J. E., and Myers, J. (1968). On pigments, growth and photosynthesis of *Phaeodactylum tricornutum. J. Phycol*. 4:349–55.

Mansour, M. P., Volkman, J. K., Jackson, A. E., and Blackburn, S.I. (1999). The fatty acid and sterol composition of five marine dinoflagellates. *J. Phycol*. 35:710–29.

Martinez, L. A., Silver, M. W., King, J. M., and Alldredge, A. L. (1983). Nitrogen fixation by floating diatom mats: A source of new nitrogen to oligotrophic ocean waters. *Science* 221:152–4.

Martin-Jezequel, V., Hildebrand, M., and Brzezinski, M. A. (2000). Silicon metabolism in diatoms: implications for growth. *J. Phycol*. 36:821–40.

Medlin, L. K., and Kaczmarka, I. (2004). Evolution of the diatoms: V. Morphological and cytological support for the major clades and a taxonomic revision. *Phycologia* 43:245–70.

Medlin, L. K., Crawford, R. M., and Andersen, R. A. (1986). Histochemical and ultrastructural evidence for the function of the labiate process in the movement of centric diatoms. *Br. Phycol. J*. 21:297–301.

Medlin, L. K., Williams, D. M., and Sims, P. A. (1993). The evolution of the diatoms (Bacillariophyta). I. Origin of the group and assessment of the monophyly of its major divisions. *Eur. J. Phycol*. 28:261–75.

Medlin, L. K., Kooistra, W. H. C. F., Gersonde, R., Sims, P. A., and Wellbrock, U. (1997). Is the origin of diatoms related to the end-Permian mass extinction? *Nova Hedwigia* 65:1–11.

Mehta, S. C., Venkataraman, G. S., and Das, S. C. (1961). The fine structure and the cell wall nature of *Diatoma hiemale* var. *mesodan* (Her.) Grun. *Rev. Algol., N.S.* 6:49–52.

Miralto, A., Barone, G., Romano, G. et al. (1999). The insidious effect of diatoms on copepod reproduction. *Nature* 402:173–6.

Moore, J. K., and Villareal, T. A. (1996). Size-ascent rate relationships in positively buoyant marine diatoms. *Limnol. Oceanog*. 41:1514–20.

Morel, N. M. L., Rueter, J. G., and Morel, F. M. M. (1978). Copper toxicity to *Skeletonema costatum. J. Phycol*. 14:43–8.

Nagai, S., Hori, Y., Manabe, T., and Imai, I. (1995). Restoration of cell size by vegetative cell enlargement

in *Coscinodiscus wailesii* (Bacillariophyceae). *Phycologia* 34:533–55.

Nakajima, T., and Volcani, B. E. (1969). 3,4-Dihydroxyproline: a new amino acid from diatom cell walls. *Science* 164:1400–1.

Navarro, J. N. (1993). Three-dimensional imaging of diatom ultrastructure with high resolution low-voltage SEM. *Phycologia* 32:151–6.

Nultsch, W. (1956). Studien über die Phototaxis der Diatomeen. *Arch. Protistenk.* 101:1–68.

Pan, Y., Subba Rao, D. V., and Mann, K. H. (1996). Changes in domoic acid production and cellular chemical composition of the toxigenic diatom *Pseudo-nitzschia multiseries* under phosphate limitation. *J. Phycol.* 32:371–81.

Perry, C. C., and Keeling-Tucker, T. (2000). Biosilicification: the role of the organic matrix in structure control. *J. Biol. Inorg. Chem.* 5:537–50.

Pickett-Heaps, J. D., Tippit, D. H., and Andreozzi, J. A. (1979a). Cell division in the pennate diatom *Pinnularia*. III. The valve and associated organelles. *Biol. Cellulaire* 35:195–8.

Pickett-Heaps, J. D., Tippit, D. H., and Andreozzi, J. A. (1979b). Cell division in the pennate diatom *Pinnularia*. IV. Valve morphogenesis. *Biol. Cellulaire* 35:199–206.

Pickett-Heaps, J. D., Hill, D. R. A., and Wetherbee, R. (1986). Cellular movement in the centric diatom *Odontella sinensis*. *J. Phycol.* 22:334–9.

Pickett-Heaps, J. D., Carpenter, J., and Koutoulis, A. (1994). Valve and seta (spine) morphogenesis in the centric diatom *Chaetoceros peruvianus* Brightwell. *Protoplasma* 181:269–82.

Pohnert, G. (2002). Phospholipase A_2 activity triggers the wound-activated chemical defense in the diatom *Thalassiosira rotula*. *Plant Physiol.* 129:103–11.

Pohnert, G., and Boland, W. (2002). The oxylipin chemistry of attraction and defense in brown algae and diatoms. *Nat. Prod. Rep.* 19:108–22.

Pohnert, G., Lumineau, O., Cueff, A., et al. (2002). Are volatile unsaturated aldehydes from diatoms the main line of chemical defence against copepods? *Mar. Ecol. Progr. Ser.* 245:33–45.

Potapova, M., and Snoeijs, P. (1997). The natural life cycle in the wild populations of *Diatoma moniliformis* (Bacillariophyceae) and its disruption in an aberrant environment. *J. Phycol.* 33:924–37.

Poulin, M., Masse, G., Belt, S. T., Delavault, P., Rousseau, J.-M., and Rowland, S. J. (2004). Morphological, biochemical and molecular evidence for the transfer of *Gyrosigma nipkowii* Meister to the genus *Halsea* (Bacillariophyta). *Eur. J. Phycol.* 39:181–95.

Prasad, A. K. S. K., Nienow, J. A., and Livingstone, R. J. (1990). The genus *Cyclotella* (Bacillariophyta) in Choctawhatchee Bay Florida, with special reference to *C. striata* and *C. choctawhatcheeana* sp. nov. *Phycologia* 29:418–36.

Prasad, A. K. S. K., Riddle, K. A., and Nienow, J. A. (2000). Marine diatom genus *Climaconeis* (Berkeleyaceae, Bacillariophyta): two new species, *Climaconeis koenigii*, and *C. colemaniae*, from Florida Bay, U.S.A. *Phycologia* 39:199–211.

Reavic, E. D., Smol, J.-P., Carignan, R., and Lorrain, S. (1998). Diatom paleolimnology of two fluvial lakes in the St. Lawrence River. A reconstruction of environmental changes during the last century. *J. Phycol.* 34:446–56.

Reimann, B. E. F., Lewin, J. C., and Volcani, B. E. (1965). Studies on the biochemistry and fine structure of silica shell formation in diatoms. I. The structure of the cell wall of *Cylindrotheca fusiformis* Reimann and Lewin. *J. Cell Biol.* 24:39–55.

Reisen, W. K., and Spencer, D. J. (1970). Succession and current demand relationships of diatoms on artifical substrates in Prater's Creek, South Carolina, *J. Phycol.* 6:117–21.

Richardson, J. L., Mody, N. S., and Stacey, M. E. (1996). Diatoms and water quality in Lancaster County (PA) streams: a 45-year perspective. *Pennsylvania Acad. Sci.* 70:30–9.

Rogall, E. (1939). Über den Feinbau der Lieselmembran der Diatomeen. *Planta* 29:279–91.

Ross, R., and Sims, P. A. (1972). The fine structure of the frustule in centric diatoms: A suggested terminology. *Br. Phycol. J.* 7:139–63.

Round, F. E. (1957). The late-glacial and post-glacial diatom succession in the Kentmere valley deposit. I. Introduction, methods and flora. *New Phytol.* 56:98–126.

Round, F. E. (1961). The diatoms of a core from Esthwaite water. *New Phytol.* 60:43–59.

Round, F. E., Crawford, R. M., and Mann, D. G. (1990). *The Diatoms*. Cambridge: Cambridge University Press. 747 pp.

Rueter, J. G. (1983). Effect of copper on growth, silicic acid uptake and soluble pools of silicic acid in the marine diatom, *Thalassiosira weisflogii* (Bacillariophyceae). *J. Phycol.* 19:101–4.

Rueter, J. G., Chisholm, S. W., and Morel, F. M. M. (1981). Effects of copper toxicity on silicic acid uptake and growth in *Thalassiosira pseudonana*. *J. Phycol.* 17:270–8.

Sato, S., Nagumo, T., and Tanaka, J. (2004). Auxospore formation and the morphology of the initial cell of

marine araphid diaton *Gephyria media* (Bacillariophyceae). *J. Phycol*. 40:684–91.

Schmaljohann, R., and Röttger, R. (1978). The ultrastructure and taxonomic identity of the symbiotic algae of *Heterostegina depressa* (Foraminifera: Nummulitidae). *J. Mar. Biol. Assoc. UK* 58:227–37.

Schmid, A.-M. M., and Crawford, R. M. (2001). *Ellerbeckia arenaria* (Bacillariophyceae): formation of auxospores and initial cells. *Eur. J. Phycol*. 36:307–20.

Schmid, A.-M. M., and Volcani, B. E. (1983). Wall morphogenesis in *Coscinodiscus wailesii* Gran and Angst. I. Valve morphology and development of its architecture. *J. Phycol*. 19:387–402.

Shipe, R. F., Brzezinski, M. A., Pilskaln, C., and Villareal, T. A. (1999). *Rhizosolenia* mats: an overlooked source of silica production in the open sea. *Limnol. Oceanogr*. 44:1282–92.

Sicko-Goad, L., Stoermer, E. F., and Fahnensteil, G. (1986). Rejuvenation of *Melosira granulata* (Bacillariophyceae) resting cells from anoxic sediments of Douglas Lake, Michigan. I. Light microscopy and ^{14}C uptake. *J. Phycol*. 22:22–8.

Smayda, T. J. (1970). The suspension and sinking of phytoplankton in the sea. *Oceanogr. Mar. Biol. Annu. Rev.* 8:353–414.

Staats, N., de Winder, B., Stal, L. J., and Mur, L. R. (1999). Isolation and characterization of extracellular polysaccharides from the epipelic diatoms *Cylindrotheca closterium* and *Navicula salinarum. Eur. J. Phycol*. 34:161–9.

Stoermer, E. F., Pankratz, H. S., and Drum, R. W. (1965). The fine structure of *Mastogloia grevillei* Wm. Smith, *Protoplasma* 59:1–13.

Subba Rao, D. V., Quilliam, M. A., and Pocklinton, R. (1988). Domoic acid – a neurotoxic amino acid produced by the marine diatom *Nitzschia pungens* in culture. *Can. J. Fish. Aquat. Sci*. 45:2076–9.

Sullivan, C. W. (1977). Diatom mineralization of silicic acid. II. Regulation of $Si(OH)_4$ transport rates during the cell cycle of *Navicula pelliculosa. J. Phycol*. 13:86–91.

Thomas, W. H., Hollibaugh, J. T., and Seibert, D. L. R. (1980). Effects of heavy metals on the morphology of some marine phytoplankton. *Phycologia* 19:202–9.

Tilman, D., Kilham, S. S., and Kilham, P. (1976). Morphometric changes in *Asterionella formosa* colonies: phosphate and silicate limitation. *Limnol. Oceanogr*. 21:883–6.

Venrich, E. L., McGowan, J. A., and Mantyla, A. W. (1973). Deep maxima of photosynthetic chlorophyll in the Pacific Ocean. *Fish. Bull*. 71:41–52.

Villareal, T. A. (1989). Division cycles in the nitrogen-fixing *Rhizosolenia* (Bacillariophyceae)–*Richelia* (Nostocaceae) symbiosis. *Br. Phycol. J.* 24:357–65.

Villareal, T. A., and Carpenter, E. J. (1994). Chemical composition and photosynthetic characteristics of *Ethmodiscus rex* (Bacillariophyceae): evidence for vertical migration. *J. Phycol*. 30:1–8.

von Denffer, D. (1949). Die planktonische Massenkultur pennatur Grunddiatomeen. *Arch. Mikrobiol*. 14:159–202.

von Stosch, H. A. (1951). Entwicklungsgeschichtliche Untersuchungen an zentrischen Diatomeen. I. Die Auxosporenbildung von *Melosira varians. Arch. Mikrobiol*. 16:101–35.

von Stosch, H. A. (1975). An amended terminology of the diatom girdle. *Nova Hedwigia, Beih*. 53:1–28.

von Stosch, H. A. (1982). On auxospore envelopes in diatoms. *Bacillaria* 5:127–48.

von Stosch, H. A., and Fecher, K. (1979). "Internal thecae" of *Eunotia soleirolii* (Bacillariophyceae): Development, structure and function as resting spores. *J. Phycol*. 15:233–43.

Vrieling, E. G., Gieskes, W. W. C., and Beelen, T. P. M. (1999). Silicon deposition in diatoms: control by the pH inside the silicon deposition vesicle. *J. Phycol*. 35:548–59.

Wagner, J. (1934). Beuträge zur Kenntnis der *Nitzschia putrida* Benecke, insbesonders ihrer Bewegung. *Arch. Protistenk*. 82:86–113.

Wang, Y., Chen, Y., Lain, C., and Gretz, M. R. (2000). Extracellular matrix assembly in diatoms (Bacillariophyceae). IV. Ultrastructure of *Achnanthes longipes* and *Cymbella cistula* as revealed by high-pressure freezing/freeze substitution and cryo-field emission scanning electron microscopy. *J. Phycol*. 36:367–78.

Wetherbee, R., Crawford, S., and Mulvaney, P. (2004). The nanostructure and development of diatom biosilica. In *Biomineralization Progress Biology, Molecular Biology and Application*, ed. E. Baeuerlein, pp. 177–93. Weinheim: Wiley-VCH.

White, A. W. (1974). Growth of two facultatively heterotrophic marine centric diatoms. *J. Phycol*. 10:292–300.

Wilson, D. P. (1946). The triradiate and other forms of *Nitzschia closterium* (Ehrenberg) Wm. Smith, forma *minutissima* of Allen and Nelson. *J. Mar. Biol. Assn., U.K.* 26:235–70.

Chapter 18

Heterokontophyta

RAPHIDOPHYCEAE

The Raphidophyceae, or chloromonads, have chlorophylls *a* and *c*, and two membranes of chloroplast endoplasmic reticulum. The anterior flagellum is commonly tinsel, whereas the posterior flagellum is naked (Figs. 18.1, 18.2, 18.3). The freshwater species of the Raphidophyceae are green, whereas the marine forms are yellowish and contain the carotenoid fucoxanthin (Vesk and Moestrup, 1987). The closest relatives of the Raphidophyceae are the Eustigmatophyceae and the Chrysophyceae (Cavalier-Smith and Chao, 1996).

Marine species are euryhaline and eurythermic (tolerant of a wide salinity and temperature range) and occur in temperate and subtropical waters worldwide. Marine genera are *Chattonella* (Fig. 18.3), *Fibrocapsa* (Fig. 18.1(*b*)), and *Heterosigma* (Fig. 18.1(*a*)). Many of the marine species produce neurotoxic compounds that are similar to brevetoxin (Fig.18.2).

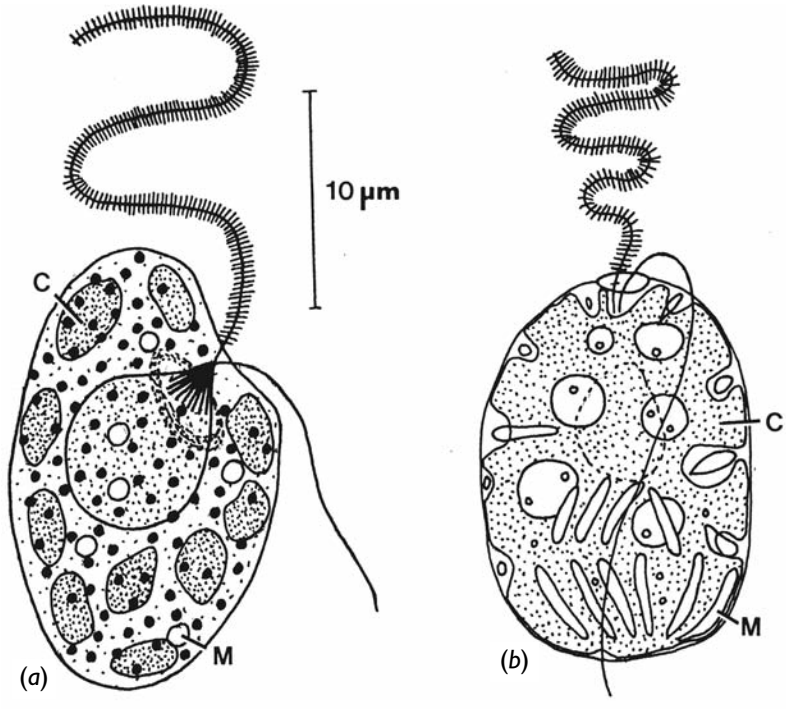


Fig. 18.1 (*a*) *Heterosigma carterae*. (*b*) *Fibrocapsa japonica*. (C) Chloroplast; (M) mucocyst. ((*a*) after Leadbeater, 1969; (*b*) after Hara and Chihara, 1985.)

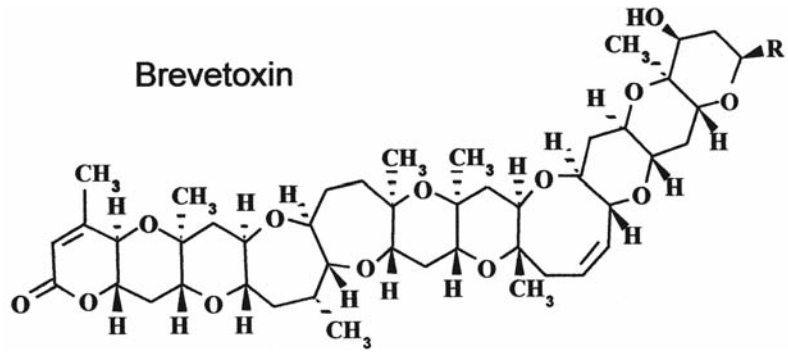


Fig. 18.2 The chemical structure of brevetoxin.

Uptake of the toxin by fish results in depolarization of nerves supplying the heart. This reduces the heart rate, thereby lowering blood pressure, which in turn affects the transfer of oxygen to the gill lamellae, creating hypoxic conditions that lead to fish mortality (Tyrrell et al., 2001).

Toxic red-tide blooms of the marine *Chattonella antiqua* and *Heterosigma carterae* (Taylor, 1992) have occurred in the Seto Inland Sea in Japan (Watanabe et al., 1988). These red tides occurred in the summer when a salinity and temperature stratification occurred at a depth of 5–10 meters. There was little mixing of waters above and below the stratified layer resulting in the upper layer being deficient in nutrients while the bottom layer was anaerobic. *Heterosigma carterae* flourishes under these conditions because it has a daily vertical migration of 10 to 15 meters and this allows the alga to move between the stratified layers. This migration enables *H. carterae* to use the nutrients in the lower layers, and light and oxygen in the upper layer, resulting in the red-tide blooms of the organism. The migration is correlated with the production and degradation of cytoplasmic fat particles (Wada et al., 1987). *Heterosigma carterae* has a wide salinity tolerance in culture (3 to 50%) and loses its motility at temperatures below 10 °C. At 5 to 10 °C, the alga forms non-motile masses capable of surviving in continuous darkness for up to 15 weeks (Han et al., 2002). This is a far longer dark period than the motile cells can tolerate and still live. In Narragansett Bay, Rhode Island, blooms of *H. carterae* occur during a period of low nitrogen concentration, but at a time when phosphate levels are near a yearly maximum (Tomas, 1979).

Chattonella antiqua is a marine raphidophyte that produces blooms in coastal Japan. In 1972, a bloom killed 500 million dollars worth of caged yellow-tail fish in the Seto Inland Sea (Okaichi, 1989). *C. antiqua* has the highest toxicity during the early to mid-logarithmic phase. After reaching the stationary phase, the toxicity decreases markedly (Khan et al., 1996). The life cycle of *Chattonella antiqua* involves a vegetative propagation phase and a non-motile dormant phase (Fig. 18.3) (Yamaguchi and Imai, 1994). The vegetative diploid cells grow by binary fission under normal growth conditions. Small haploid cells are produced when the nutrients are depleted in the medium. These haploid cells change into cysts under low-light conditions and spend several months dormant in bottom sediments. The period of dormancy usually lasts from the end of summer to the following spring and is enforced by low temperatures (Imai and Itoh, 1987). Swarmers germinate from the cysts and somehow become diploid, although how diploidization occurs is not known. The resulting diploid vegetative cells complete the life history.

In freshwater, Raphidophyceae are associated with mud bottoms or ponds with abundant macrophytes. *Vacuolaria* contains chlorophylls *a* and *c* as well as the carotenoid *β*-carotene and the xanthophylls lutein epoxide and antheraxanthin (Chapman and Haxo, 1966; Guillard and Lorenzen, 1972). The numerous chloroplasts have three thylakoids per band, and there are two membranes of chloroplast E.R. around the chloroplasts (Koch and Schnepf, 1967; Mignot, 1967). *Vacuolaria* (Fig. 18.4(*a*)) can be free-swimming or in a palmelloid state. In the palmelloid condition,

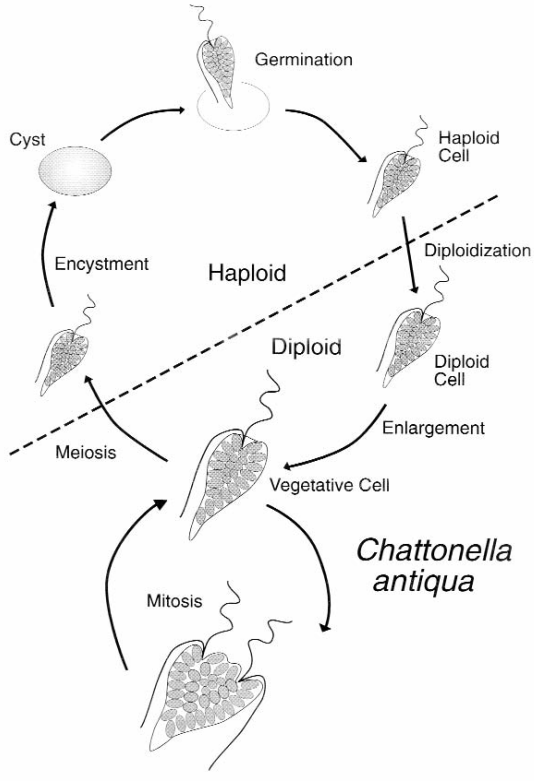


Fig. 18.3 The life cycle of *Chattonella antiqua*. (Adapted from Yamaguchi and Imai, 1994.)

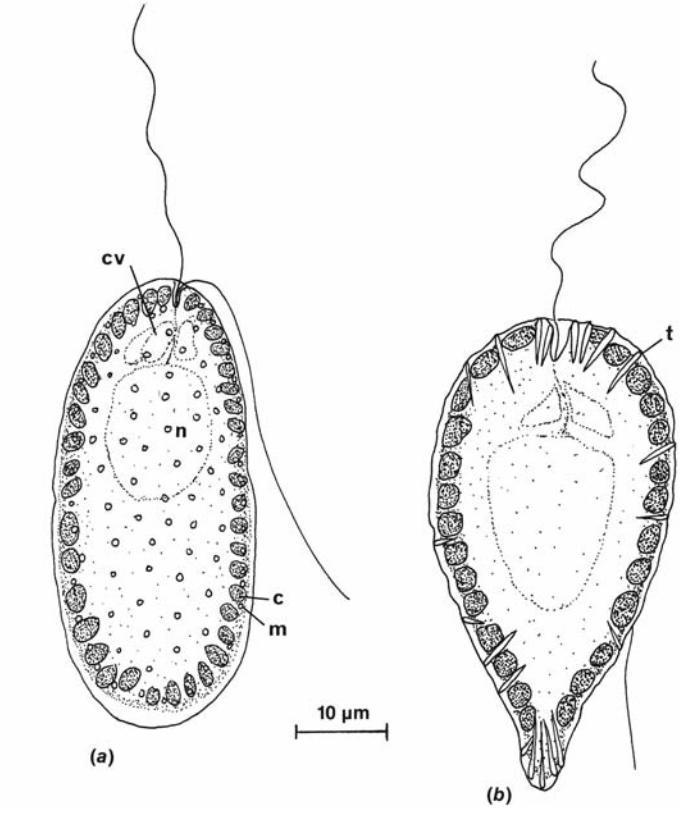


Fig. 18.4 (*a*) *Vacuolaria virescens*, showing chloroplasts (c), mucilaginous bodies (m), flagella, contractile vacuoles (cv), and the nucleus (n); (*b*) *Gonyostomum semen* with chloroplasts, trichocysts (t), contractile vacuoles, and the nucleus. (After Mignot, 1967.)

the cells are more or less spherical, 35 to 50 μm in diameter, yellow-green with each cell surrounded by a thick gelatinous matrix. In the free-swimming state, the organisms vary considerably in shape from broadly ovate to elongate. The flagella emerge from a simple notch slightly to one side of the anterior ventral region. The anteriorly directed flagellum has microtubular hairs, whereas the posteriorly directed flagellum is whiplash. There is no stigma, but the organism is positively phototactic. *Vacuolaria* divides only in the palmelloid state. Mitosis is typically eukaryotic, with the nuclear membrane remaining intact (Heywood and Godward, 1972). No sexual reproduction has been reported in *Vacuolaria*. Occasionally the cells form cysts with the resistant sheaths surrounding the cells (Spencer, 1971).

Vacuolaria has muciferous bodies (mucocysts) in the peripheral cytoplasm (Fig. 18.4(*a*)), which are similar in structure to those in the Prymnesiophyceae and Chrysophyceae. The genus *Gonyostomum* (Fig. 18.4(*b*)) has trichocysts similar to those in the Dinophyceae (Mignot, 1967).

REFERENCES

Cavalier-Smith, T., and Chao, E. E. (1996). 18S rRNA sequence of *Heterosigma carterae* (Raphidophyceae), and the phylogeny of heterokont algae (Ochrophyta). *Phycologia* 35:500–10.

Chapman, D. J., and Haxo, F. T. (1966). Chloroplast pigments of the Chloromonadophyceae. *J. Phycol*. 2:89–91.

Guillard, R. R. L., and Lorenzen, C. J. (1972). Yellow-green algae with chlorophyllide *c*. *J. Phycol*. 8:10–14.

Han, M.-S., Kim, Y.-P. and Cattolico, R. A. (2002). *Heterosigma akashiwo* (Raphidophyceae) resting cell formation in batch culture: strain identity versus physiological response. *J. Phycol.* 38:304–17.

Hara, Y., and Chihara, M. (1985). Ultrastructure and taxonomy of *Fibrocapsa japonica* (Class Raphidophyceae). *Arch. Protistenk*. 130:133–41.

Heywood, P., and Godward, M. B. E. (1972). Centromeric organization in the chloromonadophycean alga *Vacuolaria virescens. Chromosoma* 39:333–9.

Imai, I., and Itoh, K. (1987). Annual life cycle of *Chattonella* spp., causative flagellates of noxious red tides in the Inland Sea of Japan. *Marine Biology* 94:287–92.

Khan, S., Arakawa, O., and Onoue, Y. (1996). A toxicological study of the marine phytoflagellate, *Chattonella antiqua* (Raphidophyceae). *Phycologia* 35:239–44.

Koch, W., and Schnepf, E. (1967). Einige elektronenmikroskopische Beobachtungen an *Vacuolaria virescens Ciénk. Arch. Mikrobiol*. 57:196–8.

Leadbeater, B. S. C. (1969). A fine structural study of *Olisthodiscus luteus* Carter. *Br. Phycol. J.* 4:3–17.

Mignot, J. -P. (1967). Structure et ultrastructure de quelques Chloromonadines. *Protistologia* 3:5–24.

Okaichi, T. (1989). Red tide problems in the Seto Inland Sea, Japan. In *Red Tides: Biology, Environmental Science and Toxicology*, ed. T. Okaichi, D. M. Anderson, and T. Nemoto, pp. 137–42. New York: Elsevier Science Publishing.

Spencer, L. B. (1971). A study of *Vacuolaria virescens* Cienkowski. *J. Phycol*. 7:274–9.

Taylor, F. J. R. (1992). The taxonomy of harmful marine phytoplankton. *G. Bot. Ital*. 126:209–19.

Tomas, C. R. (1979). *Olisthodiscus luteus* (Chrysophyceae). III. Uptake and utilization of nitrogen and phosphorus. *J. Phycol*. 15:5–12.

Tyrrell, J. V., Bergquist, P. R., Bergquist, P. L., and Scholin, C. A. (2001). Detection and enumeration of *Heterosigma akashiwo* and *Fibrocapsa japonica* (Raphidophyceae) using rRNA-targeted oligonucleotide probes. *Phycologia* 40:457–67.

Vesk, M., and Moestrup, Ø. (1987). The flagellar root system in *Heterosigma akashiwo* (Raphidophyceae). *Protoplasma* 137:15–28.

Wada, M., Hara, Y., Kato, M., Yamada, M., and Fujii, T. (1987). Diurnal appearance, fine structure and chemical composition of fatty particles in *Heterosigma akashiwo* (Raphidophyceae). *Protoplasma* 137:134–9.

Watanabe, M., Kohata, K., and Kunugi, M. (1988). Phosphate accumulation and metabolism by *Heterosigma akashiwo* (Raphidophyceae) during diel vertical migration in a stratified microsm. *J. Phycol*. 24:22–8.

Yamaguchi, M., and Imai, I. (1994). A microfluorometric analysis of nuclear DNA at different stages in the life history of *Chattonella antiqua* and *Chattonella marina* (Raphidophyceae). *Phycologia* 33:163–70.

Chapter 19

Heterokontophyta

XANTHOPHYCEAE

The Xanthophyceae contain primarily freshwater and terrestrial algae with a few marine representatives. The class is characterized by motile cells with a forwardly directed tinsel flagellum and a posteriorly directed whiplash flagellum (Figs. 19.1, 19.5(*c*)). The chloroplasts contain chlorophylls *a* and *c* (Sullivan et al., 1990), lack fucoxanthin, and are colored yellowish-green. The eyespot in motile cells is always in the chloroplast (Figs. 19.1, 19.5(*c*)), and the chloroplasts are surrounded by two membranes of chloroplast endoplasmic reticulum. The outer membrane of the chloroplast E.R. is usually continuous with the outer membrane of the nucleus. In most non-motile cells the wall is composed of two overlapping halves (Figs. 19.2 (*d*), (*e*), (*f*), 19.3, 19.4). Molecular data have shown the Xanthophyceae is most closely related to the Phaeophyceae (Ariztia et al., 1991; Potter et al., 1997). Although the class is commonly called the Xanthophyceae, the proper name is the Tribophyceae since there is no genus in the class that can lend its name to Xanthophyceae (Hibberd, 1981).

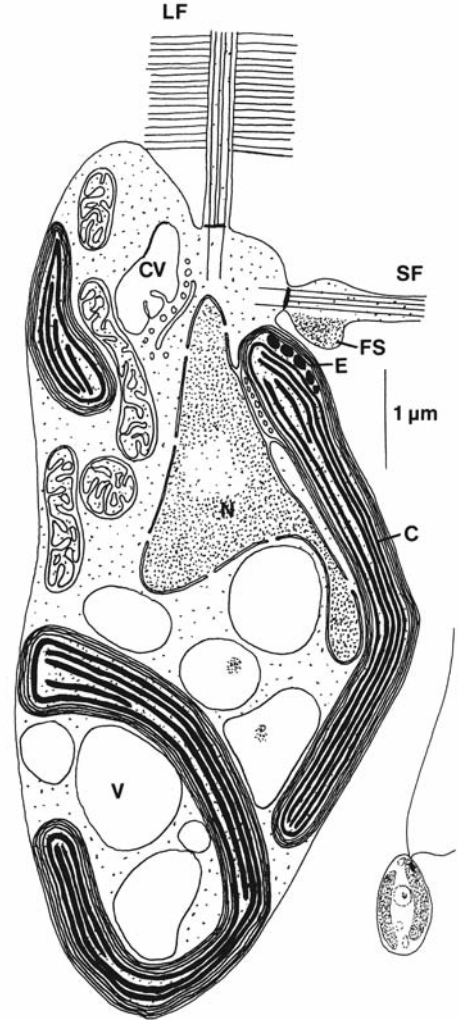


Fig. 19.1 Light and electron microscopical drawing of a zoospore of a typical member of the Xanthophyceae, *Mischococcus sphaerocephalus*. (C) Chloroplast; (CV) contractile vacuole; (E) eyespot; (FS) flagellar swelling; (LF) long flagellum with hairs; (N) nucleus; (SF) short flagellum; (V) vacuole. (Adapted from Hibberd and Leedale, 1971.)

Cell structure

Cell wall

The cell walls of two Xanthophyceae, *Tribonema* (Figs. 19.2, 19.3) (Cleare and Percival, 1973) and *Vaucheria* (Figs. 19.7, 19.8), are composed of cellulose (Parker et al., 1963). In *Vaucheria* cellulose comprises 90% of the wall, with the remaining

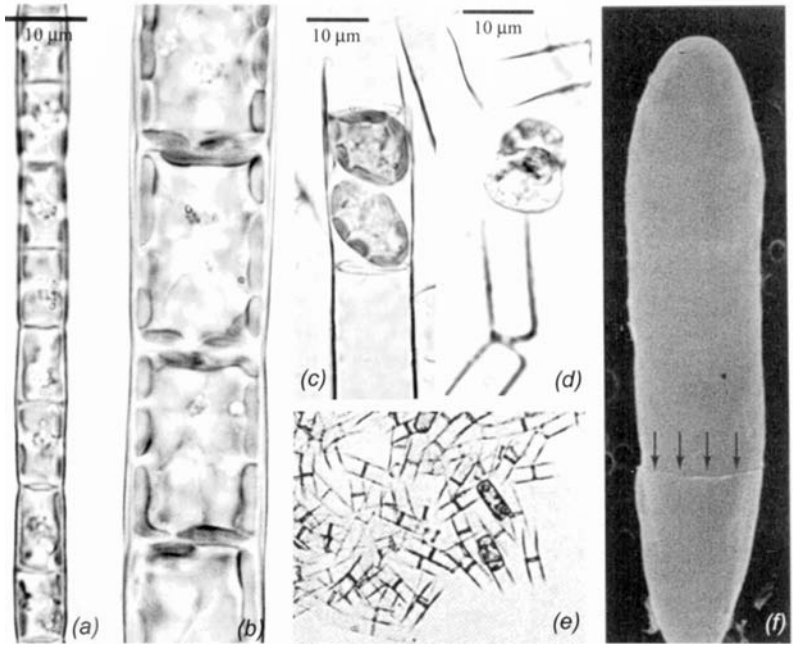


Fig. 19.2 Light microscopy of filaments of *Tribonema regulare* (*a*) and *Tribonema utriculosum* (*b*). (*c*) *Tribonema viride*, zoosporangium containing two zoospores. (*d*) Liberated zoospores of *Tribonema regulare*. (e) H-shaped cell walls of *Tribonema regulare* remaining after liberation of zoospores. (*f*) Scanning electron micrograph of a two-celled filament of *Tribonema viridae* showing the margin of an overlapping H-piece (arrows). (From Lokhorst and Star, 2003.)

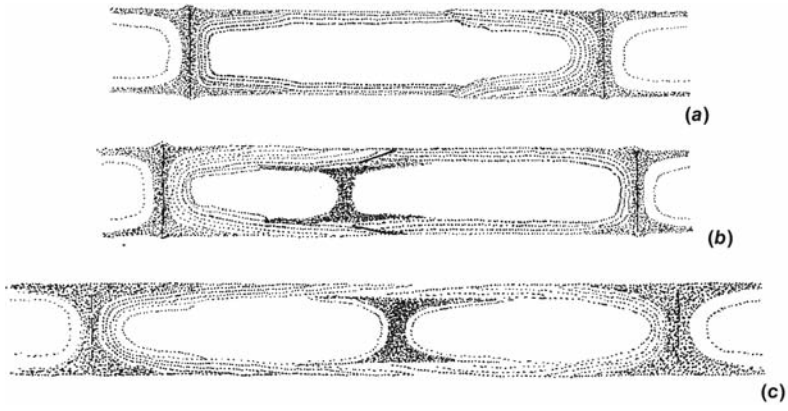


Fig. 19.3 Wall structure of *Tribonema bombycinum*, after treatment with potassium hydroxide. (*a*) Two H-pieces articulated to enclose a single protoplast. (*b*), (*c*) Recently divided cell showing the intercalation of a new H-piece. (After Smith, 1938.)

portion being amorphous polysaccharides composed primarily of glucose and uronic acids.

Many of the algae in the class have walls composed of two overlapping halves that fit together as do the two parts of the bacteriologist's Petri dish (Figs. 19.2(*d*), (*e*), (*f*), 19.3, 19.4). The two-part nature of the wall cannot be delineated with the light microscope unless the cells have been treated with certain reagents such as concentrated potassium hydroxide. A typical example is the wall of *Ophiocytium majus* (one study places *Ophiocytium* in the closely related Eustigmatophyceae based on the sequence of mitochondrial cytochrome oxidase (Ehara et al., 1997)), which is tubular in shape (Fig. 19.4). The wall is composed of two parts, a cap of constant size fitted over a tubular basal portion. As the cell grows and increases in length, the tubular basal portion elongates, but the cap remains the same size. The rims of both the cap and the tube are finely tapered and overlap for some distance so that the bipartite condition is not normally apparent in living cells. A layer of intercalary material, presumably functioning as a cementing substance, separates the cap from the tubular part of the wall. Filamentous genera, such as

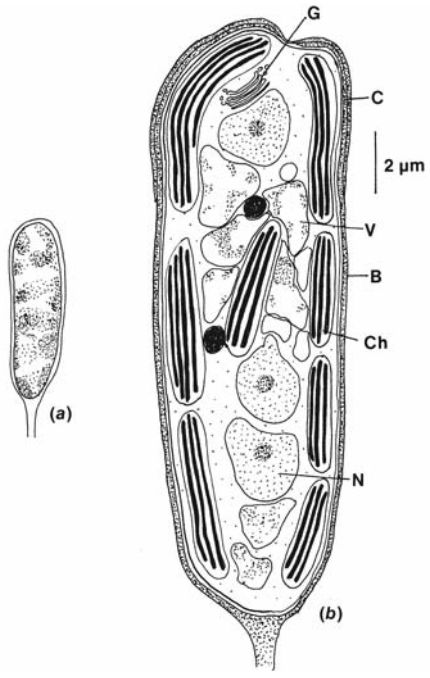


Fig. 19.4 *Ophiocytium majus*. (*a*) Vegetative cell. (*b*) Semidiagrammatic drawing of the fine structure of a vegetative cell. (B) Basal tubular portion of wall; (C) cap of wall; (Ch) chloroplast; (G) Golgi; (N) nucleus; (V) vesicle. (Adapted from Hibberd and Leedale, 1971.)

Tribonema (Figs. 19.2, 19.3), have a wall composed of H-shaped pieces. These alternately overlap each other so that each protoplast is enclosed by halves of two successive H-pieces (Lokhorst and Star, 1988).

Chloroplasts and food reserves

Two membranes of chloroplast E.R. surround the chloroplasts, the outer membrane of chloroplast E.R. being continuous with the outer membrane of the nuclear envelope (Fig. 19.1) (Hibberd and Leedale, 1971). The thylakoids are grouped into bands of three and in many genera there is a pyrenoid in the chloroplast (Fig. 19.5) (Marchant, 1972). The eyespot consists of globules beneath the chloroplast envelope at the anterior end of the chloroplast (Figs. 19.1, 19.5). Where the short flagellum passes over the eyespot, the flagellar sheath is dilated into the flagellar swelling, which is closely applied to the plasmalemma in the area of the eyespot.

Chlorophylls *a* and *c* are present in the chloroplasts (Sullivan et al., 1990), with the major carotenoids being diadinoxanthin, heteroxanthin and vaucheriaxanthin ester.

Mannitol and glucose accumulate during photosynthesis in the plastids (Cleare and Percival, 1973). The principal storage product is probably a β-1,3 linked glucan similar to paramylon, although lipids have been suggested as also being important.

Asexual reproduction

Xanthophycean organisms multiply asexually by fragmentation, zoospores, and aplanospores. In addition, they have the ability to form specialized resting spores. Fragmentation is limited to the tetrasporine and filamentous colonies, and is due to the breaking of the colony into parts.

Zoospores are formed by a majority of the genera. The zoospores are biflagellate, with the forward tinsel flagellum usually being four to six times longer than the shorter whiplash flagellum (Figs. 19.1, 19.5). The zoospores are naked and usually pyriform (pear-shaped). Zoospore production has been studied at the fine-structural level in *Pseudobumilleriopsis pyrenoidosa* by Deason (1971) (Fig. 19.5). This alga has rod-shaped cells with several nuclei and laminate chloroplasts. Vegetative cells prior to zoosporogenesis have the nuclei and vacuoles in the center of the cell, whereas the chloroplasts are flattened against the plasmalemma. The first indication of cleavage in zoosporogenesis is the appearance of vacuoles between the ends of adjacent chloroplasts. The chloroplasts move away from the plasmalemma, and each becomes associated with a nucleus. The vacuoles then coalesce and separate the nucleus–chloroplast pairs, each of which becomes a zoospore. Basal bodies are present near the nuclei of the vegetative cells; the basal bodies migrate to one end of the chloroplast as cleavage begins and produce flagella early in zoosporogenesis. One to 16 zoospores are produced, which are released by dissolution and/or separation of the sporangial walls where they overlap. In the zoospore, the chloroplast is massive and has a pyrenoid. The nucleus is elongate, and there are two or more contractile vacuoles present.

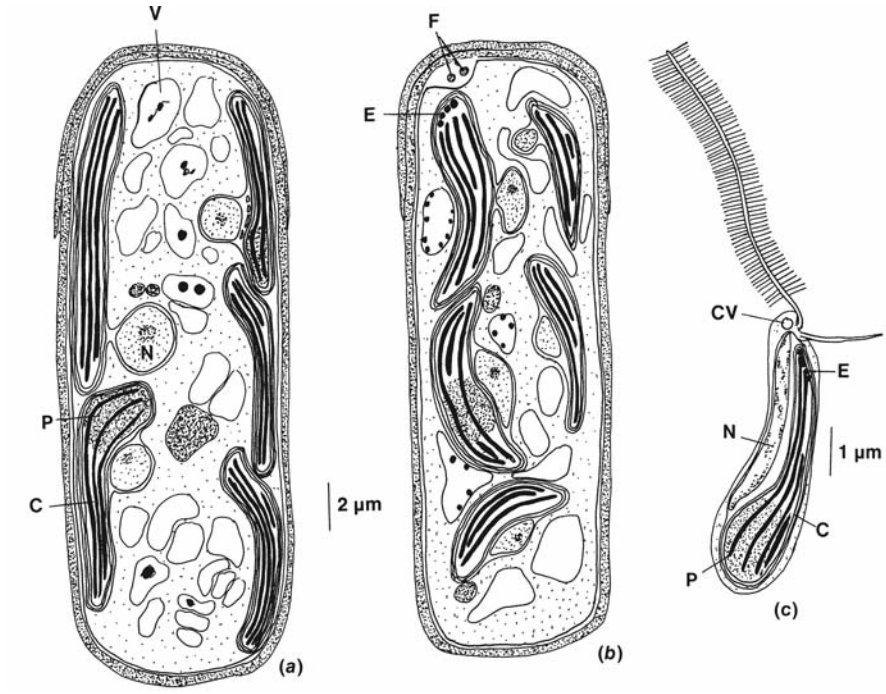


Fig. 19.5 *Pseudobumilleriopsis pyrenoidosa.* (*a*) Vegetative cell. (*b*) Cell undergoing zoosporogenesis. (*c*) Zoospore. (C) Chloroplast; (CV) contractile vacuole; (E) eyespot; (F) flagella; (N) nucleus; (P) pyrenoid; (V) vacuole. (Adapted from Deason, 1971.)

Instead of producing zoospores, the entire protoplast may produce a single aplanospore or divide into a number of parts, each of which becomes an aplanospore. In some cases, environmental conditions determine whether the alga reproduces by zoospores or aplanospores. Submerged thalli of *Botrydium* produce zoospores; those living on damp soil produce aplanospores (Rostafiński and Woronin, 1877) (Fig. 19.6). An aplanospore liberated from a parent cell can grow directly into a new plant, or it may give rise to zoospores, which develop into new plants.

Some flagellates and rhizopodial cells produce cysts or statospores endogenously, similar to those in the Chrysophyceae. In their formation, there is an internal delimitation of a spherical protoplast that is separated from the peripheral portion of the mother cell's protoplast by a membrane. The endogenously differentiated protoplast then secretes a wall with two overlapping halves. Vegetative cells can also change directly into spore-like resting stages, with much thicker walls and more abundant food reserves than the vegetative cells. These spore-like cells, in which the spore wall is not distinct from the parent wall, are called akinetes and are usually found in filamentous genera.

Sexual reproduction

There are few reliable reports of sexual reproduction in the Xanthophyceae. Sexual reproduction has only been established in three genera: *Botrydium* (Fig. 19.6), *Tribonema* (Fig. 19.2), and *Vaucheria* (Fig. 19.8). In the first two genera, both gametes are flagellated, whereas in *Vaucheria* reproduction is oogamous.

Four orders will be considered here:

Order 1 Mischococcales: small coccoid cells.
Order 2 Tribonematales: filamentous organisms, not coenocytic.
Order 3 Botrydiales: globose multinucleate thallus with colorless rhizoids.
Order 4 Vaucheriales: filamentous coenocyte.

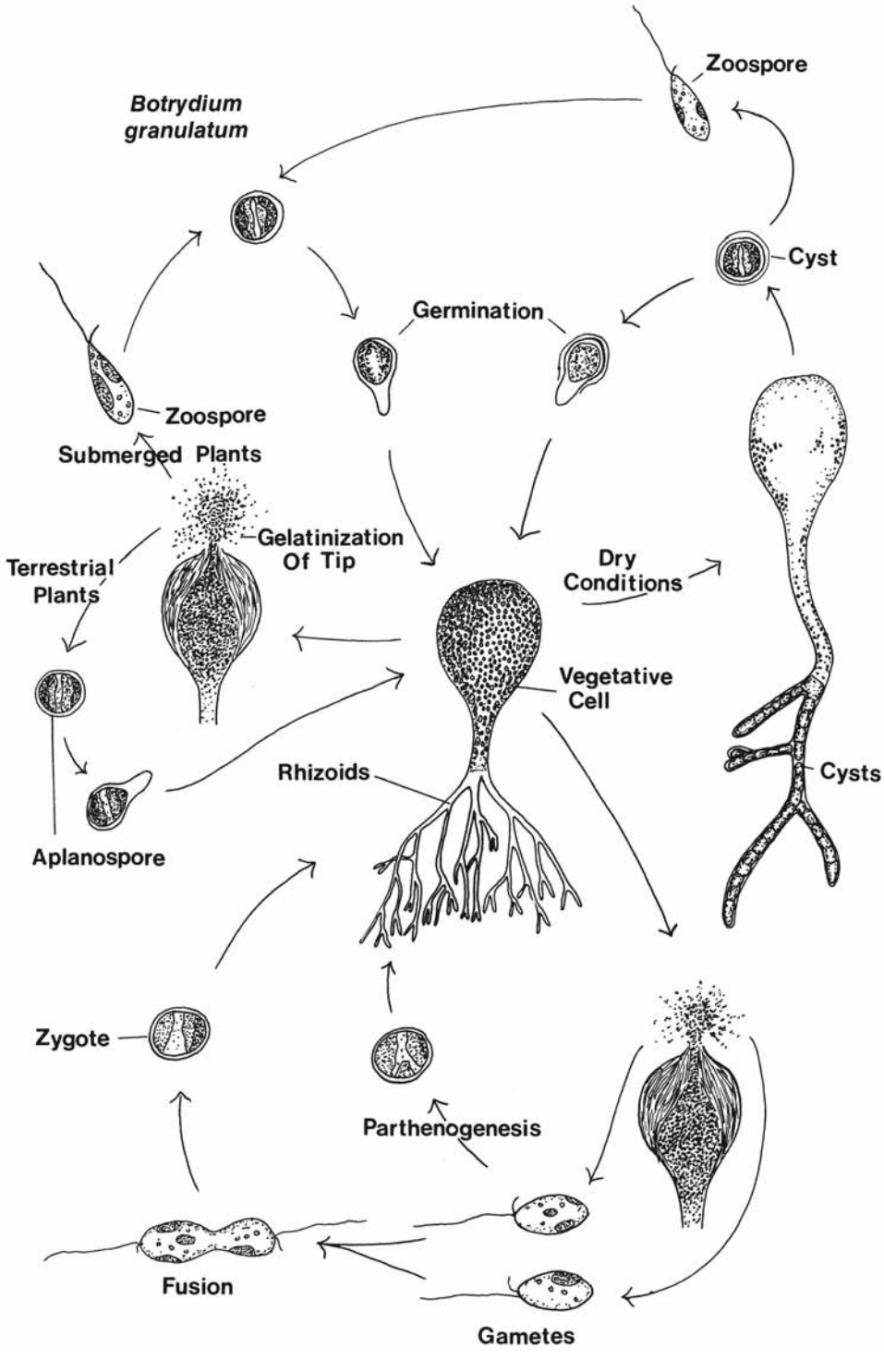


Fig. 19.6 The life cycle of *Botrydium granulatum*. (Adapted from Rostafiński and Woronin, 1877; Kolkwitz, 1926; Rosenberg, 1930.)

Mischococcales

This order is characterized by small coccoid cells and contains about two-thirds xanthophyte algae (Bailey and Andersen, 1998). *Mischococcus* (Fig. 19.1) and *Pseudobumilleriopsis* (Fig. 19.5) are examples of algae in this order.

Tribonematales

The algae in this order have cylindrical cells uniseriately united end to end in branched or unbranched filaments. *Tribonema* is composed of barrel-shaped cells that are two to five times longer than they are wide (Figs. 19.2, 19.3). The wall is composed of two H-shaped pieces overlapping in the middle of the cell. The protoplast is uninucleate and contains a number of discoid chloroplasts. Asexual reproduction is by fragmentation of the filaments, by zoospores, or by aplanospores. Aplanospores are produced more frequently than zoospores and are released by the pulling apart of the two portions of the cell wall. Akinetes can also be formed by the filaments (Smith, 1950). Sexual reproduction is isogamous, one of a uniting pair of gametes coming to rest and withdrawing its flagella just before the other swims up to it and unites with it (Scherffel, 1901).

Botrydiales

Botrydium is a unicellular multinucleate alga consisting of a usually globose aerial portion with chloroplasts and a colorless rhizoidal portion that penetrates the soil (Fig. 19.6). The shape of the aerial part is influenced by environmental conditions. It is usually elongate when growing in shaded habitats and spherical when growing in brightly illuminated places (Moore and Carter, 1926). The aerial portion has a relatively tough wall within which is a delicate layer of cytoplasm containing many nuclei and chloroplasts. The branched rhizoidal system has no chloroplasts but does have many nuclei. The cells are incapable of vegetative division, and the only method by which new plants may be formed is by production of zoospores or aplanospores. According to Rakován and Fridvalsky (1970), the formation of either aplanospores or zoospores begins at night, and the cells must be illuminated 8 to 9 hours after the beginning of the process for flagella to develop. If there is no illumination, aplanospores develop. In the formation of these spores, three to five chloroplasts become associated with a nucleus in the mother cell, and cleavage occurs with each zoospore containing the above organelles. If the spore is an aplanospore, then a wall is secreted; if it is a zoospore, no wall is formed. Motile gametes are apparently formed in a similar manner (Iyengar, 1925; Miller, 1927), and sexual reproduction can be isogamous or anisogamous, with the cells being either homothallic or heterothallic. The gametes become apposed by their anterior ends when uniting in pairs to form a zygote. Gametes that have not fused develop parthenogenetically into thalli. A germinating zygote develops directly into a new vegetative thallus.

Botrydium also produces cysts or resting spores during periods of dry conditions (Miller, 1927). In *B. granulatum*, the protoplast migrates into the rhizoids where division occurs to produce a large number of thick-walled cysts. These cysts can either germinate directly to form a new thallus or give rise to zoospores.

Vaucheriales

There is only one genus, *Vaucheria* (Figs. 19.7, 19.8), in this order. *Vaucheria* diverged early in evolution from other members of the order (Bailey and Andersen, 1998). *Vaucheria* has a relatively thin cell wall within which the cytoplasm is restricted to the periphery of the coenocyte, with the center being occupied by a large central vacuole (Fig. 19.7). In the cytoplasm, the numerous elliptical chloroplasts with pyrenoids are to the outside, whereas the nuclei are toward the center. Growth of the filaments is restricted to the apex which has a large number of vesicles, mitochondria, and dictyosomes. Chloroplasts, nuclei, and the large central vacuole are not found at the growing tip (Ott and Brown, 1974a). The large central vacuole contains lipids, degenerated chloroplasts, and crystals and extends the entire length of the filament except for the area immediately behind the growing tip. Cytoplasmic streaming takes place in the area of the large central vacuole and directly involves the nuclei, mitochondria, and their associated dictysomes. The cytoplasmic streaming involves two separate systems, the first based on microtubules that move the nuclei, and the

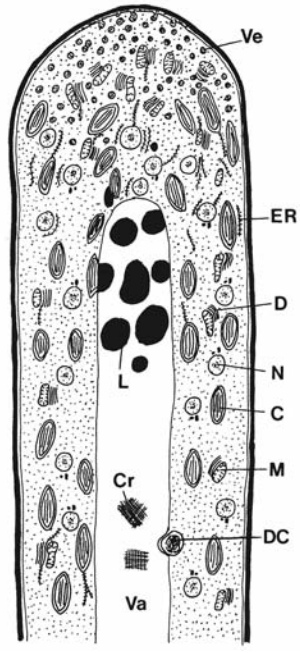


Fig. 19.7 Schematic representation of the tip of a vegetative filament of *Vaucheria dillwynii*. (C) Chloroplast; (Cr) crystal; (D) dictyosome; (DC) degenerate chloroplast; (ER) endoplasmic reticulum; (L) lipid body; (M) mitochondrion; (N) nucleus; (Va) vacuole; (Ve) vesicle. (After Ott and Brown, 1974a.)

second based on microfilaments that move the mitochondria and their associated dictyosomes. The chloroplasts do not migrate in patterns of definite streaming but have a more or less random movement, not associated with either microtubules or microfilaments.

Although *Vaucheria* can develop transverse septa that block off injured portions of the coenocyte, there is little reproduction by accidental breaking of filaments. Asexual reproduction of aquatic individuals is usually by means of multiflagellate, multinucleate zoospores (Birckner, 1912) (Fig. 19.8), which are produced singly in club-shaped sporangia at the swollen ends of filaments. In their production large numbers of chloroplasts and nuclei stream into the tip of the filament, the central vacuole decreases in size, and the tips appear dark green. A band of colorless protoplasm now appears at the base of the developing sporangium, which breaks in the middle to form two protoplasts. The two protoplasts approach each other, and a septum is formed. Within the sporangium, vesicles are produced (Ott and Brown, 1974b), around which nuclei become oriented with a pair of basal bodies between each nucleus and the vesicle membrane. Flagella are produced through the vesicle membrane, and the vesicles migrate to the plasmalemma. The nuclei with their flagella pairs thus come to lie in the peripheral area of the cell. The wall at the apex of the sporangium gelatinizes, forming a narrow aperture; the zoospore pushes its way through the aperture and swims in the medium. The nuclei in the sporangium are separated from each other by a number of vacuoles, and one flagellum of each pair is slightly longer than the other (Greenwood et al., 1957). There is no eyespot or pyrenoid in the zoospore (Greenwood, 1959). The zoospores are sluggish in their movements, swimming for only about 15 minutes. On coming to rest, the flagella are withdrawn, and a thin wall is secreted. Germination follows almost immediately by the protrusion of one or two tubular outgrowths, one of which attaches itself to the substratum by means of a colorless lobed holdfast. Instead of producing zoospores, terrestrial individuals may have the entire contents of the sporangium develop into an aplanospore. Zoospores can be obtained if vegetative filaments kept moist for some days are soaked in water, or transferred from a nutritive solution into distilled water, or removed from running water to still water (Klebs, 1896; Starr, 1964).

Sexual reproduction is oogamous and usually homothallic with meiosis occurring before the production of gametes (Al-Kubaisi and Schwantes, 1981). The life cycle is therefore diplontic with the diploid phase predominant. Sex organs are common on filaments growing in damp soil or in quiet water, but are infrequent if they are growing in flowing water. The antheridia and oogonia are borne adjacent to each other and on a common lateral branch or on adjacent lateral branches. The sex organs are cut off by a septum. The oogonium has a single egg and is filled with oil and chloroplasts. The mature oogonium produces a beak, the tip of which gelatinizes, forming an aperture. A portion of colorless cytoplasm of the egg projects through the aperture, and the egg contracts.

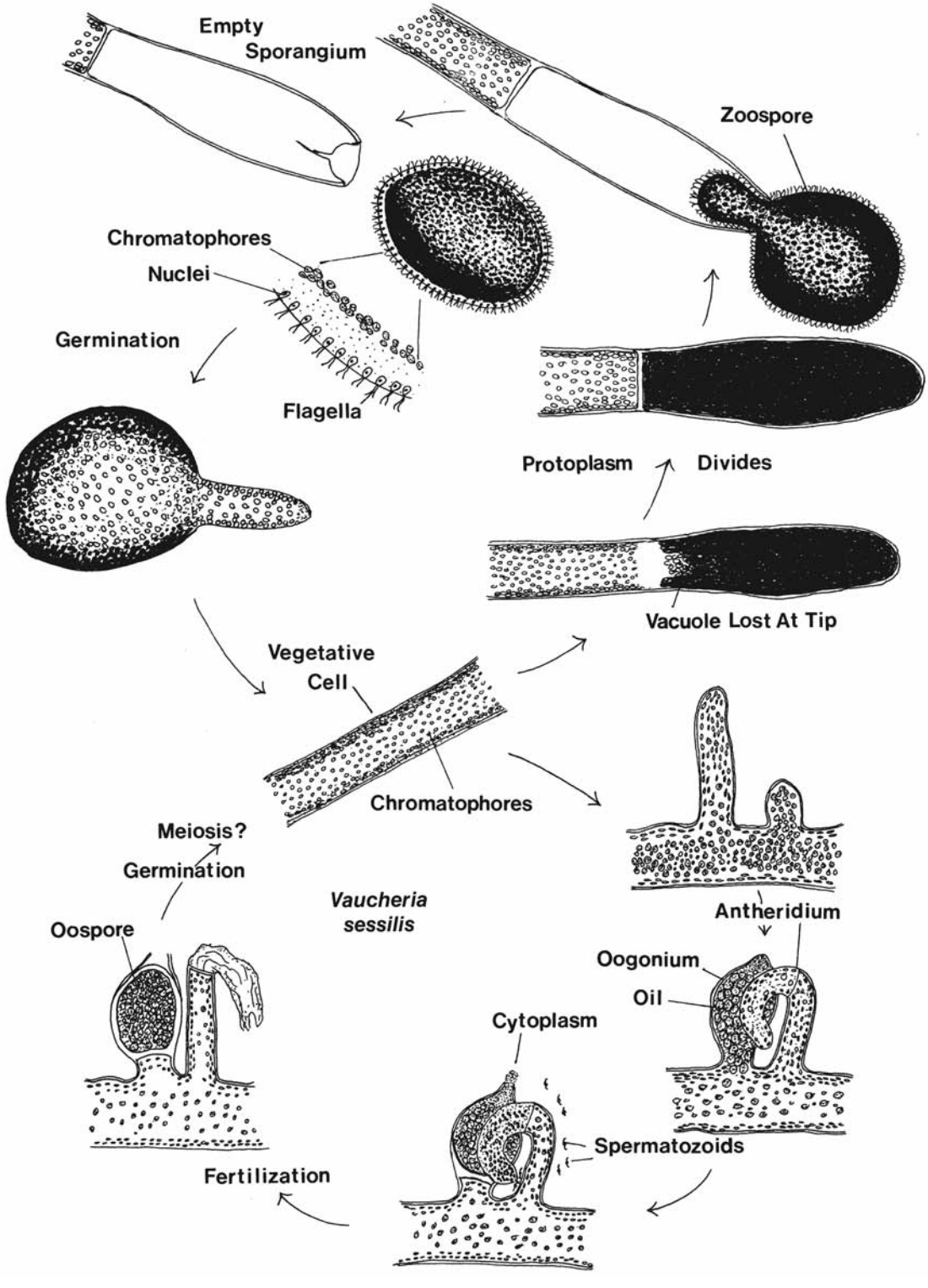


Fig. 19.8 The life cycle of *Vaucheria sessilis*.

The antheridia usually develop as strongly curved cylindrical tubes that become cut off by a septum, usually fairly high up in the tube. The mature antheridium has the spermatozoids produced in a specific area between the central and peripheral cytoplasm (Moestrup, 1970). The central and peripheral cytoplasm contain those parts of the cytoplasm that are not included in the spermatozoids: the chloroplasts, vacuoles, and many mitochondria (Ott and Brown, 1978). An aperture appears in the antheridium, and the spermatozoids are released. The spermatozoids are cylindrical posteriorly but have a flattened proboscis in the anterior portion (Fig. 19.9). There is a forward-projecting tinsel flagellum with two lateral rows of hairs, and a slightly longer trailing smooth flagellum. The nucleus is elongated and worm-like, as are the three or four mitochondria. There is neither a chloroplast nor an eyespot, but there is a Golgi body near the basal bodies of the flagella. The proboscis consists of eight or nine microtubules running beneath the plasmalemma with vesicles in between the microtubules.

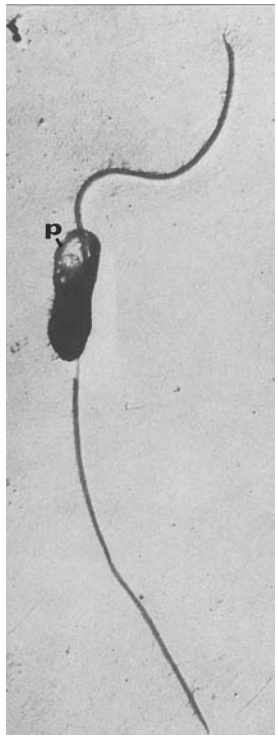


Fig. 19.9 Shadowcast whole mount of a sperm of *Vaucheria synandra*. A proboscis (p) is present on the anterior part of the cell. (From Moestrup, 1970.)

Fertilization is accomplished by the spermatozoids fusing with the egg protoplasm through the aperture in the oogonium. The zygote secretes a wall, and the oil droplets fuse to form a small number of central droplets. The oospore is colored by the oil and the degeneration products of chlorophyll. It remains in the oogonium until it is liberated by the decay of the oogonial wall. The oospore then remains dormant for a few months before germinating, probably by meiosis, into a new filament.

Vaucheria is one of the algae that exhibit chloroplast orientation movements in the light. In the dark, the chloroplasts are uniformly distributed in the peripheral cytoplasm (Fig. 19.10); in low-intensity light, they are oriented to the top and bottom of the coenocyte to trap the maximum light; in high light intensities, they are along the sides of the filament, thereby receiving less light (Fischer-Arnold, 1963; for a review, see Haupt and Schönbohm, 1970). The action spectrum for chloroplast movement in *Vaucheria* is similar to that of higher plants and closely resembles that of the action spectrum of flavins, from which it has been concluded that flavins located in the plasma membrane act as the photoreceptive pigments (Blatt, 1983). That the photoreceptor is not the chloroplast can be demonstrated with a microbeam of light. Irradiation with a microbeam results in chloroplast movement, whether or not the chloroplasts receive light. In addition to being able to perceive light, the cell also has the ability to determine the direction of the light. The theoretical basis for this perception is derived from a lens effect by the cell on the light that it receives (Fig. 19.10(*c*)). The cell acts as a collecting lens, focusing light to the rear of the cell. This results in the light bypassing some parts of the cell along the flanks, thus establishing a front-to-rear gradient. The movement of the chloroplasts relies on energy from two metabolic processes, respiration and photosynthesis. Inhibitors of respiration and photosynthesis abolish the chloroplast movement, whereas inhibitors of photosynthesis just slow down the chloroplast movement. If ATP is added along with photosynthetic inhibitors, chloroplast movement is normal.

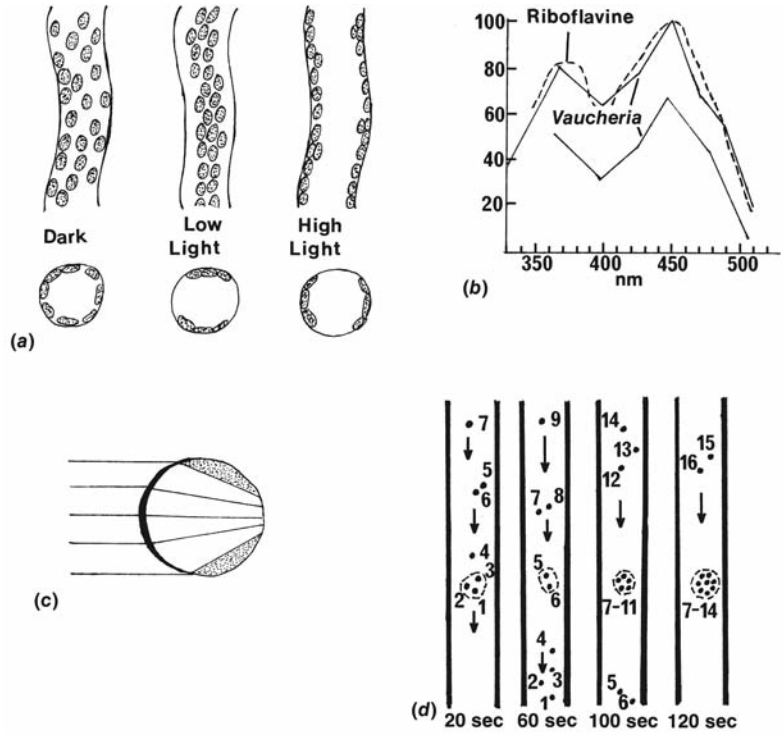


Fig. 19.10 (*a*) Position of chloroplasts of *Vaucheria* in the dark, and in low and high light intensities. (*b*) Action spectrum of chloroplast orientation movement in *Vaucheria* under low light (lower curve) and high light (upper curve) intensities. Vertical axis is relative quantum efficiency. (*c*) Diagrammatic representation of the lens effect of light passing through a *Vaucheria* coenocyte. (*d*) Movements of single chloroplasts in *Vaucheria* under low light intensity. A beam of light (dashed area) causes accumulation of chloroplasts in the illuminated area. (After Haupt and Schönbohm, 1970.)

There are two possible mechanisms to explain chloroplast movement. In the first or "active movement" the chloroplast moves relative to the rest of the protoplasm, whereas in the second or "passive movement" the protoplasm moves, carrying with it the chloroplast and other organelles. In *Vaucheria*, passive movement occurs. If chloroplast movement is followed at high or low intensity, it can be seen that not only chloroplasts, but also other organelles and inclusions are rearranged by light. Furthermore, if only a small area of the filament is irradiated with a spot of light, a strong accumulation of cytoplasm plus inclusions can be observed at this place (Fig. 19.10(*d*)). The organelles are actually trapped in a portion of the cytoplasm as they stream through the cell. Illumination of an area of *Vaucheria* results in the formation of an actin fiber network that acts as a trapping mechanism (Blatt, 1983).

REFERENCES

Al-Kubaisi, K. H., and Schwantes, H. O. (1981). Cytophotometrische Untersichungen zum Generationswechel autotropher und heterotrophen siphonaler Organismen (*Vaucheria sessilis* und *Saprolegnia ferax*). *Nova Hedwigia* 34:301–16.

Ariztia, E. V., Andersen, R. A., and Sogin, M. L. (1991). A new phylogeny for chromophyte algae using 16S-like rRNA sequences from *Mallomonas papillosa* (Synurophyceae) and *Tribonema aequales* (Xanthophyceae). *J. Phycol*. 27:428–36.

Bailey, J. C., and Andersen, R. A. (1998). Phylogenetic relationships among nine species of the Xanthophyceae inferred from *rbc*L and 18S rRNA gene sequences. *Phycologia* 37:458–66.

Birckner, V. (1912). Die Beobachtung von Zoosporenbildung bei *Vaucheria aversa* Hass. *Flora* 104:167–71.

Blatt, M. R. (1983). The action spectrum for chloroplast movements and evidence for blue-light–photoreceptor cycling in the *Vaucheria*. *Planta* 159:267–76.

Cleare, M., and Percival, E. (1973). Carbohydrates of the freshwater alga *Tribonema aequale*. II. Preliminary photosynthetic studies with ^{14}C. *Br. Phycol. J.* 8:181–4.

Deason, T. R. (1971). The fine structure of sporogenesis in the Xanthophycean alga *Pseudobumilleriopsis pyrenoidosa*. *J. Phycol*. 7:101–7.

Ehara, M., Hayashi-Ishimura, Y., Inagaki, Y., and Ohama, T. (1997). Use of a deviant mitochondrial genetic code in yellow-green algae as a landmark for segregating members within the phylum. *J. Mol. Evol.* 45:119–24.

Fischer-Arnold, G. (1963). Untersuchungen über die Chloroplastenbewegung bei *Vaucheria sessilis*. *Protoplasma* 56:495–506.

Greenwood, A. D. (1959). Observations on the structure of the zoospores of *Vaucheria*. II. *J. Exp. Bot.* 10:55–68.

Greenwood, A. D., Manton, I., and Clarke, B. (1957). Observations on the structure of the zoospores of *Vaucheria*. *J. Exp. Bot.* 8:71–86.

Haupt, W., and Schönbohm, E. (1970). Light-oriented chloroplast movements. In *Photobiology of Microorganisms*; ed. P. Halldal, pp. 283–307. London: Wiley-Interscience.

Hibberd, D. J. (1981). Notes on the taxonomy and nomenclature of the algal classes Eustigmatophyceae and Tribophyceae (synonym Xanthophyceae). *Bot. J. Linn. Soc.* 82:93–119.

Hibberd, D. J., and Leedale, G. F. (1971). Cytology and ultrastructure of the Xanthophyceae. II. The zoospore and vegetative cell of coccoid forms, with special reference to *Ophiocytium majus* Naegeli. *Br. Phycol. J.* 6:1–23.

Iyengar, M. O. P. (1925). Note on two species of *Botrydium* from India. *J. Indian Bot. Soc.* 4:193–201.

Klebs, G. (1896). *Die Bedingungen de Fortpflanzung bei einigen Algen und Pilzen*. Jena.

Kolkwitz, R. (1926). Zur Ökologie und Systematic von *Botrydium granulatum* (L) Grev. *Ber. Dtsch. Bot. Ges.* 44:533–40.

Lokhorst, G. M., and Star, W. (1988). Mitosis and cytokinesis in *Tribonema regulare* (Tribophyceae, Chrysophyta). *Protoplasma* 145:7–15.

Lokhorst, G. M., and Star, W. (2003). The flagellar apparatus in *Tribonema* (Xanthophyceae) reinvestigated. *Phycologia* 42:31–43.

Marchant, H. J. (1972). Pyrenoids of *Vaucheria woroniniana*. Heering. *Br. Phycol. J.* 7:81–4.

Miller, V. (1927). Untersuchungen über die Gattung *Botrydium* Wallroth. II. Spezieller Teil. *Ber Dtsch. Bot. Ges.* 45:161–70.

Moestrup, Ø. (1970). On the fine structure of the spermatozoids of *Vaucheria sescuplicaria* and on later stages in spermatogenesis. *J. Mar. Biol. Assoc. UK* 50:513–23.

Moore, G. T., and Carter, N. (1926). Further studies on the subterranean algal flora of the Missouri Botanical Garden. *Ann. Mo. Bot. Gard.* 13:101–40.

Ott, D. W., and Brown, R. M., Jr. (1974a). Developmental cytology of the genus *Vaucheria*. I. Organization of the vegetative filament. *Br. Phycol. J.* 9:111–26.

Ott, D. W., and Brown, R. M., Jr. (1974b). Developmental cytology of the genus *Vaucheria*. II. Sporogenesis in *V. fontinalis* (L) Christensen. *Br. Phycol. J.* 9:333–51.

Ott, D. W., and Brown, R. M. (1978). Developmental cytology of the genus *Vaucheria*. IV. Spermatogenesis. *Br. Phycol. J.* 13:69–85.

Parker, B. C., Preston, R. D., and Fogg, G. E. (1963). Studies of the structure and chemical composition of the cell walls of Vaucheriaceae and Saprolegniaceae. *Proc. R. Soc. Lond.* [*B*] 158:435–45.

Potter, D., Saunders, G. W., and Andersen, R. A. (1997). Phylogenetic relationships of the Raphidophyceae and Xanthophyceae as inferred from nucleotide sequences of the 18S ribosomal RNA gene. *Am. J. Bot.* 84:966–72.

Rakován, J. N., and Fridvalsky, L. (1970). Electron microscope studies on the gonidiogenesis of *Botrydium granulatum* (L) Grev. (Xanthophyceae). *Ann. Univ. Sci. Budap. Sect. Biol.* 12:209–12.

Rosenberg, M. (1930). Die geschlechtliche Fortpflanzung von *Botrydium granulatum* Grev. *Oesterr. Bot. Z.* 79:289–96.

Rostafiński, J., and Woronin, M. (1877). Ueber *Botrydium granulatum*. *Bot. Zig.* 35:649–71.

Scherffel, A. (1901). Kleiner Beitrag zur Phylogenie einiger Gruppen neiderer Organismen. *Bot. Ztg.* 59:143–58.

Smith, G. M. (1938). *Cryptogamic Botany*, Vol. 1. *Algae and Fungi*. New York and London: McGraw-Hill.

Smith, G. M. (1950). *The Fresh-Water Algae of the United States*, 2nd edn. New York and London: McGraw Hill.

Starr, R. C. (1964). The culture collection of algae at Indiana University. *Am. J. Bot.* 51:1013–44.

Sullivan, C. M., Entwisle, T. J., and Rowan, K. S. (1990). The identification of chlorophyll *c* in the Tribophyceae (= Xanthophyceae) using spectrophotofluorometry. *Phycologia* 29:285–91.

Chapter 20

Heterokontophyta

PHAEOTHAMNIOPHYCEAE

Recent nucleotide sequencing has uncovered an evolutionary line of golden-brown algae not related to other golden-brown algae (Bailey et al., 1998). These algae have been placed in the class Phaeothamniophyceae, a class that is most closely related to the Xanthophyceae and Phaeophyceae. The cytology of these three classes is similar (Fig. 20.1). The cells have two membranes of chloroplast endoplasmic reticulum with the outer membrane of chloroplast E.R. continuous with the outer membrane of the nuclear envelope. The chloroplasts have a ring-shaped genophore and girdle lamellae. The flagella are inserted

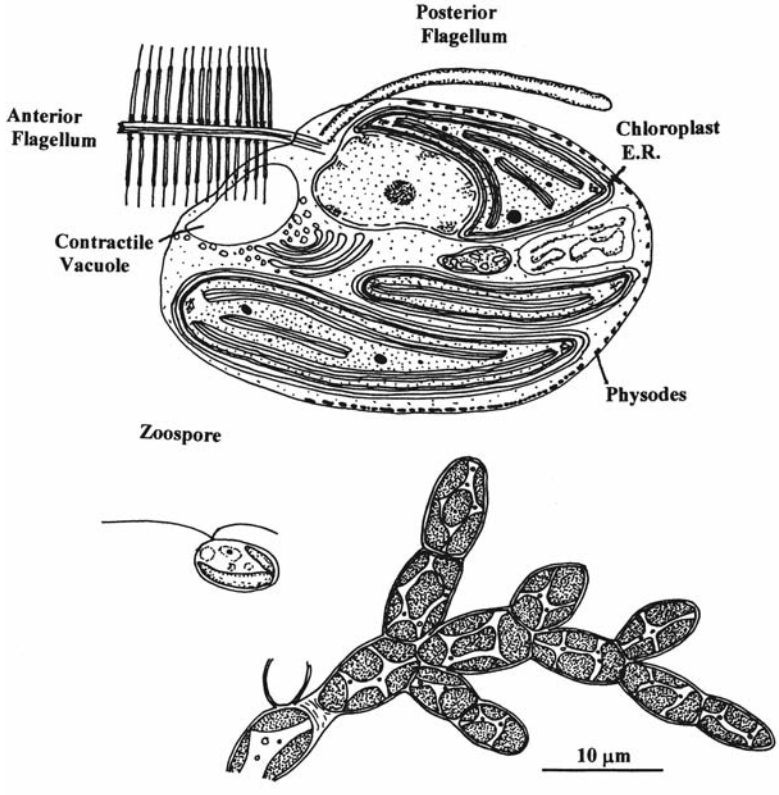


Fig. 20.1 A filament and zoospore of *Phaeothamnion polychrysis*. Also included is the fine structure of a zoospore.

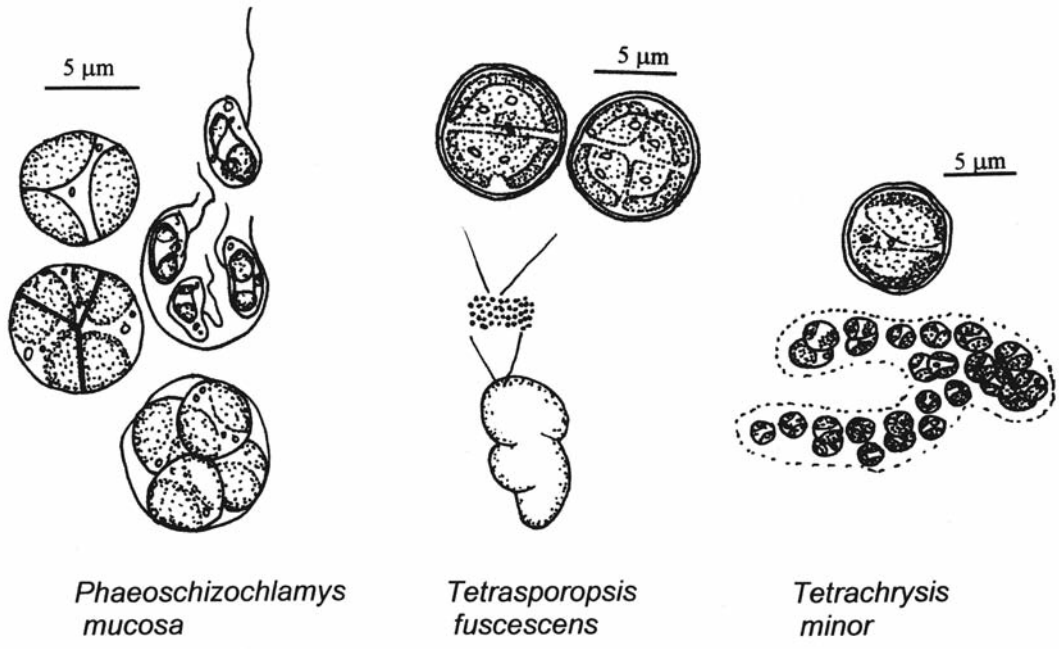


Fig. 20.2 Some algae classified in the Phaeothamniophyceae.

laterally into the motile cells. The anterior tinsel flagellum has tripartite hairs that lack lateral filaments. The posterior flagellum lacks hairs. New daughter cells are formed by **eleutheroschisis** (parent cell wall is completely cast off and new daughter cell walls are formed). Vesicles under the plasma membrane appear similar to the **physodes** that occur in the Phaeophyceae. The Phaeothamniophyceae is the only class of algae where fucoxanthin and heteroxanthin occur together. Endogenous siliceous cysts (statospores) are not produced by these algae.

Phaeothamnion is a filamentous brown alga that produces zoospores that settle to produce new filaments (Fig. 20.1) (Andersen et al., 1998). *Tetrachrysis* occurs in environments such as peat ponds and has cells embedded in a common mucilage (Dop et al., 1980) (Fig. 20.2). *Tetrasporopsis* is a colonial freshwater alga that consists of a brown, gelatinous, bladdery sac (Entwisle and Andersen, 1990) (Fig. 20.2). *Phaeoschizochlamys* occurs among detritus or suspended between other freshwater algae. The cells occur in mucilage of different shapes up to 0.5 mm in diameter (Fig. 20.2). The cells divide to form four autospores containing two chloroplasts.

REFERENCES

Andersen, R. A., Potter, D., Bidigare, R. R., Latasa, M., Rowar, K., and O'Kelly, C. J. (1998). Characterization and phylogenetic position of the enigmatic golden alga *Phaeothamnion confervicola:* ultrastructure, pigment composition and partial SSU rDNA sequence. *J. Phycol.* 34:286–98.

Bailey, J. C., Bidigare, R. R., Christensen, S. J., and Andersen, R. A. (1998). Phaeothamniophyceae classis nova: a new lineage of chromophytes based upon photosynthetic pigments, *rbc*L sequence analysis and ultrastructure. *Protist* 149:245–63.

Dop, A. J., Kosterman, Y., and van Oers, F. (1980). Coccoid and palmelloid benthic Chrysophyceae from the Netherlands. *Acta Bot. Neerl.* 29:87–102.

Entwisle, T. J., and Andersen, R. A. (1990). A re-examination of *Tetrasporopsis* (Chrysophyceae) and a description of *Dermatochrysis* gen. nov. (Chrysophyceae): a monostromatic algae lacking cells walls. *Phycologia* 29:263–74.

Chapter 21

Heterokontophyta

PHAEOPHYCEAE

The Phaeophyceae, or brown algae, derive their characteristic color from the large amounts of the carotenoid fucoxanthin in their chloroplasts as well as from any phaeophycean tannins that might be present. The chloroplasts also have chlorophylls *a*, c_1, and c_2. There are two membranes of chloroplast E.R., which are usually continuous with the outer membrane of the nuclear envelope. The storage product is laminarin. There are no unicellular or colonial organisms in the order, and the algae are basically filamentous, pseudoparenchymatous, or parenchymatous. They are found almost exclusively in the marine habitat, there being only four genera containing freshwater species, that is, *Heribaudiella*, *Pleurocladia*, *Bodanella*, and *Sphacelaria* (Fig. 21.1) (Schloesser and Blum, 1980). A number of marine forms penetrate into brackish water, where

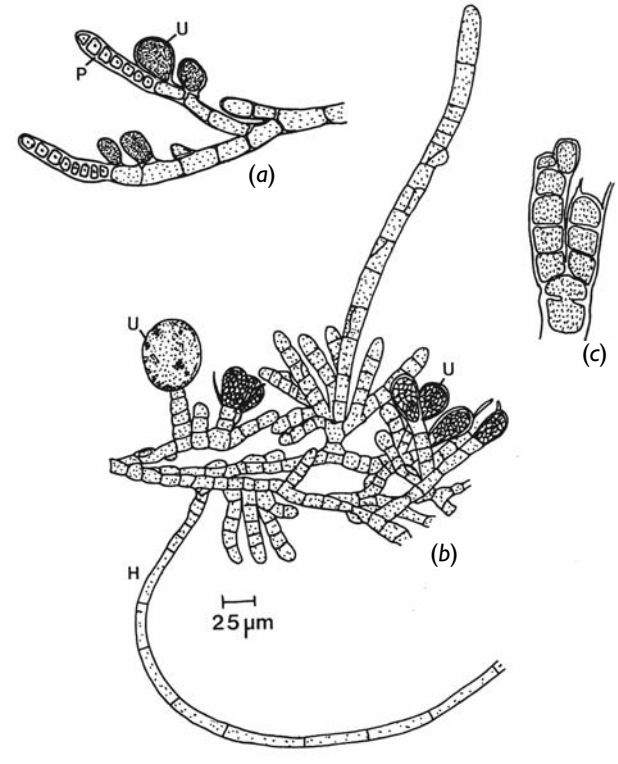


Fig. 21.1 Some freshwater brown algae. (*a*) *Pleurocladia lacustris*. (*b*) *Sphacelaria lacustris*. (*c*) *Heribaudiella fluviatilis*. (H) Hair; (P) pleurilocular sporangia; (U) unilocular sporangia. ((*b*) after Schloesser and Blum, 1980.)

they often form an important part of the salt marsh flora. These brackish water plants have almost totally lost the ability to reproduce sexually, and propagate by vegetative means only. Most of the Phaeophyceae grow in the intertidal belt and the upper littoral region. They dominate these regions in colder waters, particularly in the Northern Hemisphere, where the number of phaeophycean species is less than that of the Rhodophyceae, but the number of phaeophycean plants is much greater. In the tropics, the only place where large numbers of Phaeophyceae are found is the Sargasso Sea of the Atlantic.

The Phaeophyceae probably evolved from an organism in the Phaeothamniophyceae, which have motile cells similar to those in the Phaeophyceae, but lack the characteristic unilocular and plurilocular sporangia of the Phaeophyceae (Bailey et al., 1998).

Cell structure

The cell structure (Figs. 21.2, 21.3) is in many ways similar to that of the Chrysophyceae, Prymnesiophyceae, Bacillariophyceae, and Xanthophyceae, which are closely related to the Phaeophyceae. The main difference lies in the large amounts of extracellular polysaccharides surrounding the protoplast.

Cell walls

Phaeophycean cell walls are generally composed of at least two layers, with **cellulose** making up the main structural skeleton (Kloareg and Quatrano, 1988). The amorphous component of the cell wall is made up of **alginic acid** and **fucoidin**, whereas the mucilage and cuticle are composed primarily of alginic acid (Evans and Holligan, 1972a; Vreeland, 1972). Alginic acid is basically made up of β-1,4 linked mannuronic acid units that have a variable amount of guluronic acid units attached through C-1 and C-4 linkages (Fig. 1.7). Fucoidin is composed primarily of α-1,2 linked sulfated-fucose units, with a lesser amount of α-1,4 linked sulfated-fucose units (Fig. 1.7). The relative quantities of alginic acid and fucoidin vary between species, different parts of the plant, and different environments.

Calcification of the wall occurs only in some

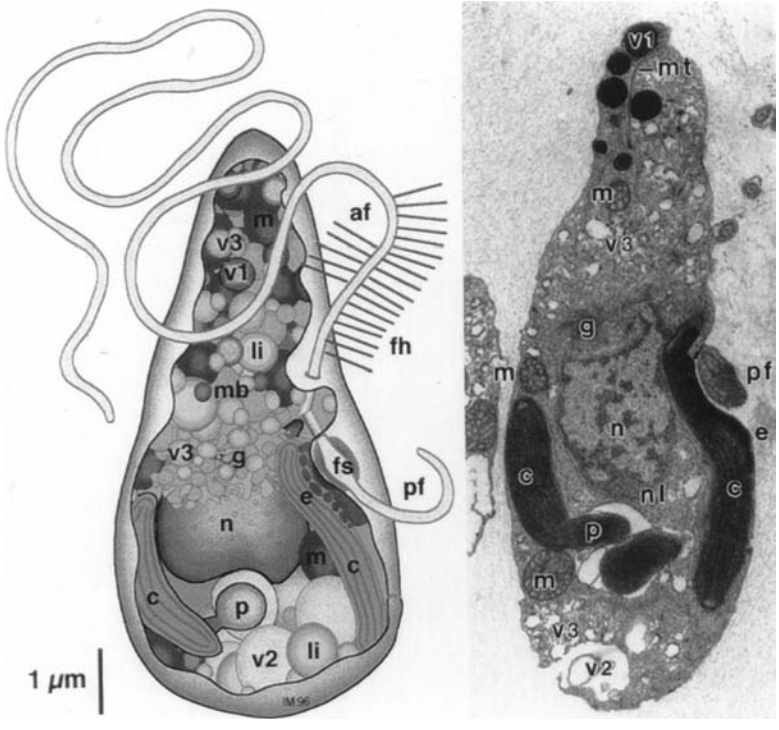


Fig. 21.2 *Left*: Diagrammatic representation of a male gamete of *Ectocarpus siliculosus* showing the distribution of cellular organelles. *Right*: Transmission electron micrograph of a thin section of a male gamete of *E. siliculosus*. (af) Anterior flagellum; (c) chloroplast; (e) eyespot; (fh) flagellar hairs (present along entire length, for clarity only shown on part of the flagellum); (fs) proximal swelling of the posterior flagellum; (g) Golgi apparatus; (li) lipid body; (m) mitochondrion; (mb) microbody; (mt) microtubules; (n) nucleus; (p) pyrenoid; (pf) posterior flagellum; (v1) physode; (v2) storage granule; (v3) vesicles with cell wall or adhesive material. (From Maier, 1997a.)

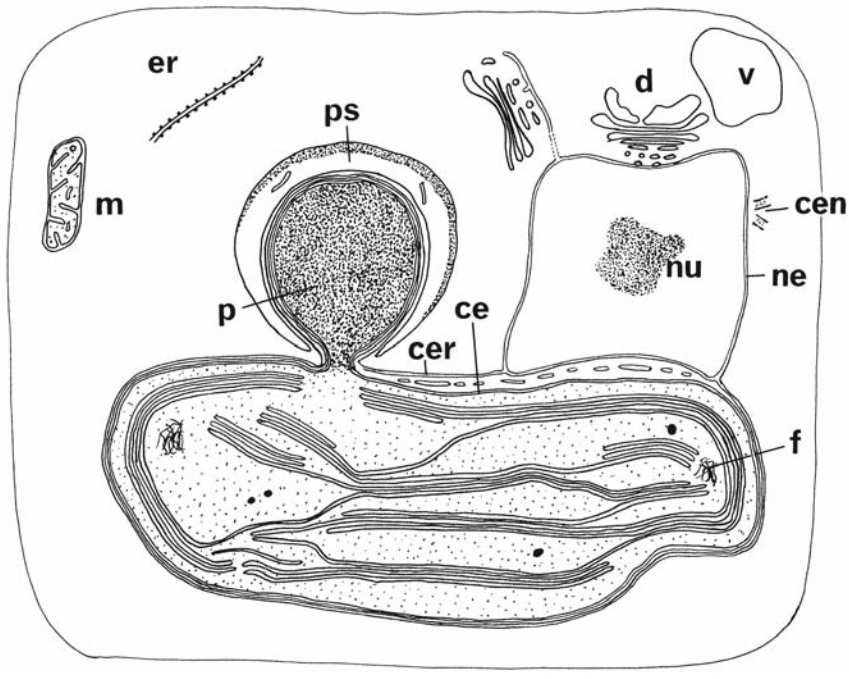


Fig. 21.3 Diagram of a hypothetical brown algal cell. (ce) Chloroplast envelope; (cen) centrioles; (cer) chloroplast endoplasmic reticulum; (d) dictyosome; (er) endoplasmic reticulum; (f) DNA fibrils; (m) mitochondrion; (ne) nuclear envelope; (nu) nucleolus; (p) pyrenoid; (ps) pyrenoid sac; (v) vacuole. (From Bouck, 1965.)

species of *Padina* where calcium carbonate is deposited as needle-shaped crystals of aragonite in concentric bands on the surface of the fan-like thallus (Borowitzka et al., 1974).

The parenchymatous Phaeophyceae have plasmodesmata or pores between most of the cells. These pores are bounded by the plasmalemma, and protoplasm is continuous from one cell to the next through them. In the Laminariales, Fucales, and Dictyotales, the pores are grouped in primary pit areas, whereas in the more primitive parenchymatous Phaeophyceae the plasmodesmata are scattered in the cell wall (Bisalputra, 1966; Bourne and Cole, 1968; Cole, 1970).

Flagella and eyespot

Generally the motile cells of the Phaeophyceae (always zoospores or gametes, as there are no motile vegetative cells) have a long anterior tinsel flagellum with tripartite hairs and a shorter posteriorly directed whiplash flagellum (Fig. 21.2) (Bouck, 1969; Loiseaux and West, 1970). The Fucales (Fig. 21.44) are an exception to this, with the posterior flagellum of the spermatozoid being longer than the anterior flagellum. The posterior flagellum usually has a swelling near the base, and this swelling fits into a depression of the cell immediately above the eyespot. The eyespot consists of 40 to 80 lipid globules arranged in a single layer between the outermost band of the thylakoids and the chloroplast envelope. The **eyespot** (**stigma**) acts as a concave mirror focusing light onto the flagellar swelling, which is the photoreceptor site for phototaxis in brown-algal flagellate cells (Kawai et al., 1996). Light at 420 and 460 nm is most effective in phototaxis in the brown algae, and is probably detected by a flavin-like substance in the flagellar swelling of the posterior flagellum (Kawai et al., 1991).

Chloroplasts and photosynthesis

The chloroplasts of the Phaeophyceae have three thylakoids per band and are surrounded by the chloroplast envelope and two membranes of chloroplast E.R. (Figs. 21.3, 21.4). The outer membrane of the chloroplast E.R. is generally continu-

ous with the outer membrane of the nuclear envelope in the Ectocarpales but appears to be discontinuous in the Dictyotales, Laminariales, and Fucales. Membrane-bounded tubules are common in the area between the chloroplast E.R. and chloroplast envelope where the latter two are not closely appressed (Bouck, 1965; Evans, 1968). Microfibrils of DNA occur in the plastids, and in *Sphacelaria* sp. there is a ring-shaped genophore inside the outermost band of thylakoids (Bisalputra and Burton, 1969). The DNA microfibrils are both linear and circular and are attached to the thylakoid membranes. The plastids contain chlorophylls *a*, c_1, and c_2, with the major carotenoid being fucoxanthin.

All the phaeophycean orders have representatives with pyrenoids (Figs. 21.3, 21.4) (Chi, 1971), but their presence, even in one species, can vary according to the stage of the plant. If the species is one that has pyrenoids only in some stages, then a pyrenoid is usually present in the eggs and/or sporelings but absent in the macroscopic phase, spermatozoids, and/or zoospores (Bourne and Cole, 1968; Evans, 1968; Bisalputra et al., 1971). A pyrenoid in the Phaeophyceae is usually a stalk-like structure set off from the main body of the chloroplast and containing a granular substance not traversed by thylakoids. Surrounding the pyrenoid but outside the chloroplast E.R. is a membrane-bounded sac that presumably contains the reserve product. The long-term storage product is **laminarin** (Fig. 1.7), a β-1,3 linked glucan. The sugar alcohol, D-**mannitol** (Fig. 1.7) is, however, the accumulation product (up to 25% of the dry weight of some *Laminaria* species in the autumn) of photosynthesis.

In a number of brown algae, the mannitol concentration in the cell increases or decreases as the salinity of the surrounding medium increases or decreases (Reed et al., 1985). This osmoregulatory mechanism prevents the cells from bursting in hypotonic media or shrinking in hypertonic media. The increase in mannitol concentration occurs in the dark as well as in the light, showing that photosynthesis is not involved in the process.

The brown algae are unique among the algae in having uptake of inorganic carbon, and therefore photosynthetic carbon fixation, stimulated by blue light (Forster and Dring, 1994). Most of the Phaeophyceae live in the littoral zone where they receive a generous amount of light. Photosynthesis is usually limited by the supply of inorganic carbon in this environment. The Phaeophyceae have evolved a mechanism to increase the amount of inorganic carbon uptake, but only when the cells are illuminated by blue light, thereby conserving the energy required for the process when the cells are in the dark. The only brown algae that do not have this mechanism are the fucoids, which appear to have evolved a separated carbon-concentrating mechanism.

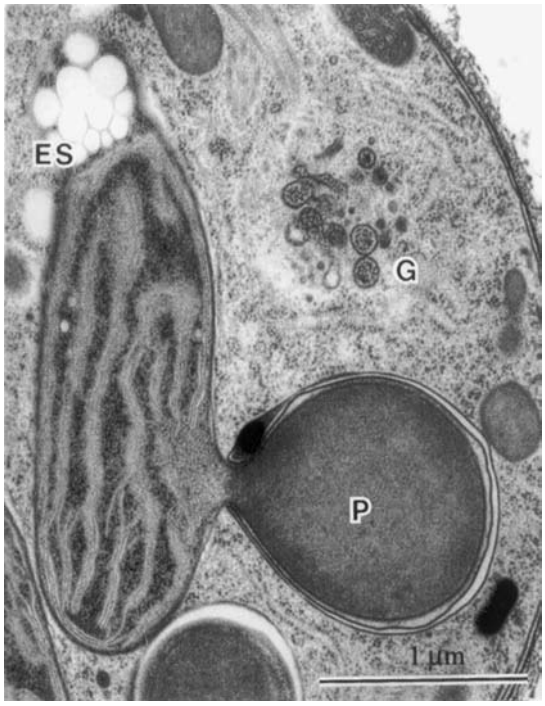


Fig. 21.4 A transmission electron micrograph of a portion of a cell of *Scytosiphon lomentaria*. (ES) Eyespot; (g) Golgi; (P) pyrenoid. (From Nagasato and Motomura, 2002.)

Phlorotannins and physodes

Phlorotannins (**phaeophycean tannins**) are stored in physodes (Fig. 21.5) in the cytoplasm of many brown algae. Phlorotannins are formed by Golgi in the perinuclear area of the cell by polymerization of phloroglucinol (1,3,5-tri-hydroxybenzene) (Fig. 21.6) through the acetate-malonate pathway (Schoenwaelder and Clayton, 2000; Pavia

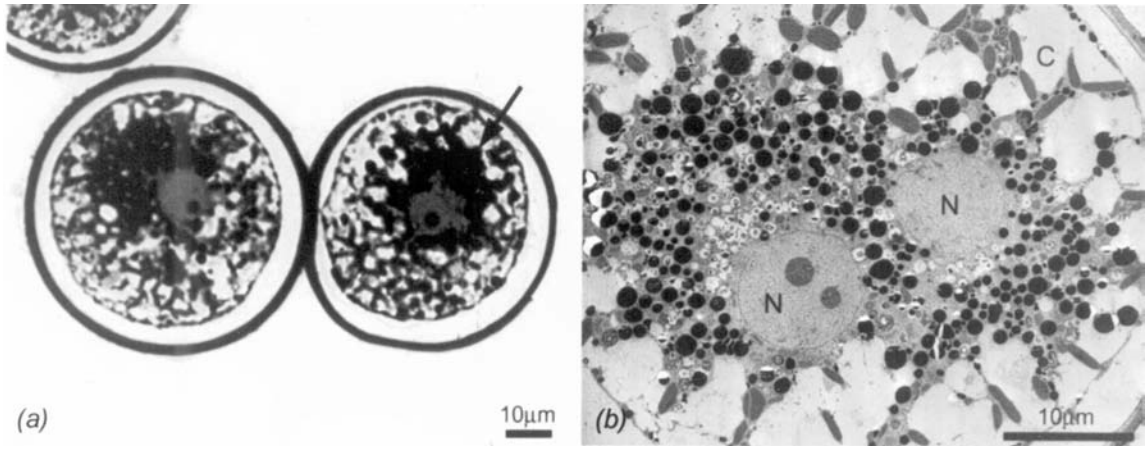


Fig. 21.5 Physodes in zygotes of *Hormosira banksii*. (*a*) Bright-field microscopy of sectioned zygotes showing accumulation of physodes around the nucleus (arrow). (*b*) Transmission electron micrograph showing physodes around the nucleus. (From Schoenwaelder and Clayton, 2000.)

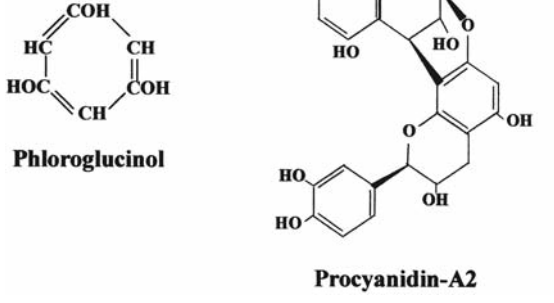


Fig. 21.6 Chemical structure of phloroglucinal, the basic building block of polyphenols and the chemical structure of the polyphenol procyanidin.

et al., 2003). The phlorotannins in the physodes appear as a colorless, highly refractive acidic fluid that stains red with vanillin and hydrochloric acid. The tannins are non-glycosidic (do not contain sugars), bind proteins, have strong reducing action, and are astringent to the taste. They are readily oxidized in air, resulting in the formation of a black pigment, **phycophaein**, giving dried brown algae their characteristic black color.

The phlorotannin content of brown algae varies from 1% to 15% of dry mass. Phlorotannins occur at high levels in brown algae of the temperate and tropical Atlantic, whereas levels are low (less than 2% of dry mass) in the tropical Pacific and Indo-Pacific (Targett and Arnold, 1998). In temperate areas, the fucoids (Fucales) have high concentrations of phlorotannins whereas kelps (Laminariales) have low concentrations of phlorotannins. The same species of brown alga will have a higher phlorotannin content when deprived of nitrogen (Van Alstyne and Pelletreau, 2000).

Phlorotannins have been postulated to function in (1) deterring grazing by herbivores, (2) absorbing ultraviolet radiation, and (3) serving as a component of cell walls (Henry and Van Alstyne, 2004). The effect of phlorotannins as a chemical defense against herbivores has been best studied. Phlorotannins deter feeding by inhibiting the glycosidases of gastropods (Shibata et al., 2002). Phlorotannins of high molecular weight inhibit herbivory more than phlorotannins of low molecular weight (Target and Arnold, 1998; Kubanek et al., 2004). There is variation among herbivores in the effectiveness of phlorotannins against grazing. Herbivores with digestive systems containing surfactants (wetting agents) or high pH are able to tolerate phlorotannins better. Phlorotannins are not normally secreted outside the cell (Shibata et al., 2002). It is necessary for the cells to be damaged before the phlorotannins are released.

Phlorotannins are always present in brown algae and thus are a "constitutive" chemical defense. Stimulation of phlorotannin synthesis by

grazing would be "inducible" chemical defense, which does not occur in most brown algae (Luder and Clayton, 2004). Synthesis of phlorotannins may be induced by the growth regulator jasmonic acid as it is in higher plants (Arnold et al., 2001).

Eggs of the Phaeophyceae contain phenolic vesicles just under the plasma membrane that are discharged outside the cells by exocytosis after fertilization. It has been postulated that the discharge of these phenolic vesicles has a toxic effect on spermatozoids and acts as a polyspermy block before the primary wall is secreted (Clayton and Ashburner, 1994). These peripheral phenolic vesicles are distinguishable from physodes, which also contain phenolic compounds, but which are significantly larger and tend to be localized around the egg nucleus.

Life history

The unilocular sporangium (Fig. 21.7(*b*))is generally considered to be the site of meiosis, the haploid zoospores that are released forming the gametophyte generation. The gametophyte then produces the gametes, which fuse to form the zygote (Bell, 1997). Although meiotic divisions have been considered the rule in the unilocular sporangium, a disturbingly large number of investigations have not found this to be the case. In these investigations there is a "direct" type of life history, with no meiosis or fusion occurring. More research is needed in this area to clarify the situation. In the phaeophycean life cycle, a **plethysmothallus** is a filamentous stage (or one composed of compacted filaments) that can multiply itself by spores (usually zoospores from plurilocular sporangia) (Papenfuss, 1951).

The thallus of many Phaeophyceae is relatively large and complex with a number of different types of growth that include: (1) **diffuse**, with most of the cells of the plant capable of cell division (*Ectocarpus*, Fig. 21.17 and *Petalonia*, Fig. 21.20); (2) **apical**, with a single cell at the apex giving rise to the cells beneath (*Dictyota*, Fig. 21.11 and *Sphacelaria*, Fig. 21.13); (3) **trichothallic**, where a cell divides to form a hair above and a thallus below (*Cutleria*, Fig. 21.14 and *Dermarestia*, Fig. 21.15); (4) **promeristem**, with a non-dividing apical cell controlling a large number of smaller meristematic, dividing promeristematic cells beneath it (*Fucus*, Fig. 21.41); (5) **intercalary**, with

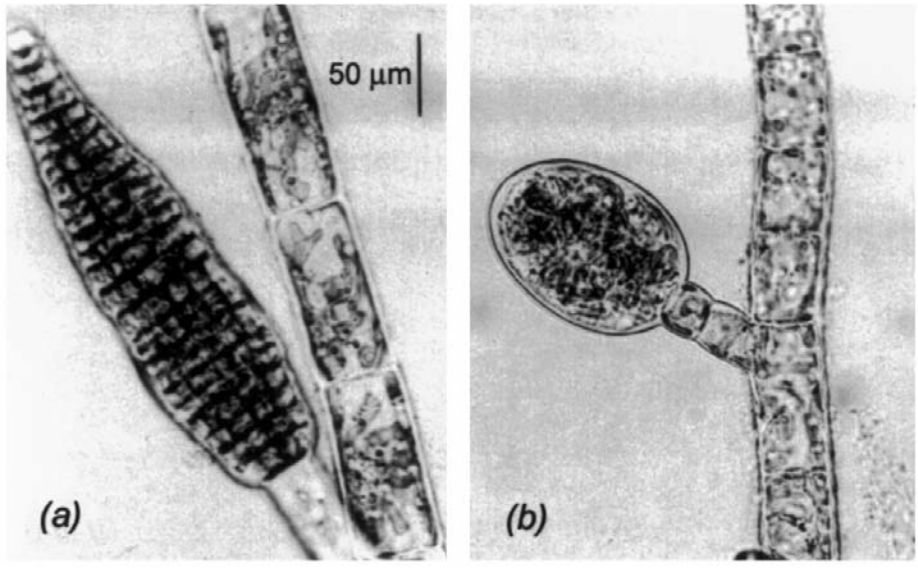


Fig. 21.7 *Ectocarpus fasciculatus*, plurilocular (*a*) and unilocular (*b*) sporangia. (From Dixon et al., 2000.)

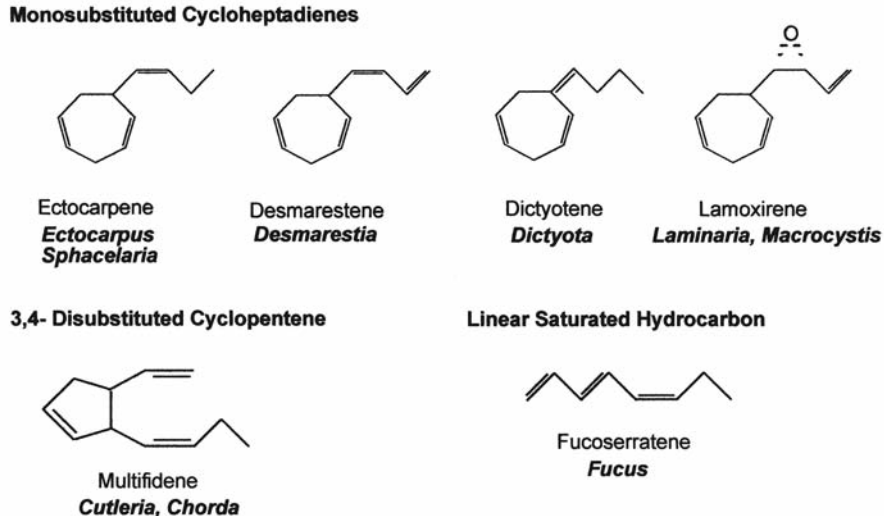


Fig. 21.8 The chemical structure of some brown algal pheromones with the names of the algae that secrete the pheromones. (Modified from Pohnert and Boland, 2002.)

a zone of meristematic cells forming tissue above and below the meristem (*Laminaria*, Figs. 21.24, 21.23); (6) **meristoderm**, with a layer of usually peripheral cells dividing periclinally (parallel to the surface of the thallus) to form a tissue below the meristoderm (usually cortex) and occasionally anticlinally (perpendicular to the surface of the thallus) to add more cells to the meristoderm (*Fucus*, Fig. 21.41).

Investigations on the sexual hormones of the brown algae in the 1970s and 1980s by Müller (Fig. 21.9) and his associates represent a major advancement in the knowledge of the brown algae (Müller, 1982; Maier and Müller, 1986). A **sexual hormone** (**sirenine**, **pheromone**) is a diffusible substance that coordinates cellular activities during sexual reproduction. Two types of biological effects mediated by sexual hormones occur in the brown algae: (1) the explosive discharge of spermatozoids from antheridia, and (2) the attraction of male gametes by female gametes or eggs. All sexual hormones in the brown algae are unsaturated hydrocarbons (have at least one double or triple bond) (Fig. 21.8) (Müller et al., 1982). With the exception of the *Fucus* sperm attractant, all of the sexual hormones in the brown algae are C_8 to C_{11} olefins (unsaturated open-chain hydrocarbons containing at least one double bond), most of them incorporating a five- or seven-membered ring structure. All of the attractions in the brown algae identified so far are highly volatile and hydrophobic. Very small amounts of the pheromones are released, only 0.6 fmol per cell per hour from *Ectocarpus siliculosus* gametes. However, the non-polar nature of the pheromones contrasts strongly with the highly polar nature of water, making the pheromones easily recognizable to the responding cells. Perception of the pheromone starts with the simple partition from water of the non-polar pheromone into the lipid plasma membrane of the gamete that contains the macromolecular receptors (Pohnert and Boland, 2002). The substances have a very strong tendency to leave the aqueous solution and escape into the air. This characteristic helps to avoid the buildup of chronic concentrations which would decrease the efficiency of the gradients around the female cells. The attractants probably do not function more than 0.5 mm away from the female cells, and thus attraction is clearly a short-distance phenomenon (Müller, 1982). The sexual hormones include **ectocarpene** from *Ectocarpus* (Müller et al., 1971), **desmarestene** from *Demarestia aculeata* (Müller et al., 1982), **lamoxirene** from *Laminaria* (Müller et al., 1985a,b), **multifidene** from *Cutleria multifida* (Jaenicke et al., 1974), **dictyopterene C′** from *Dictyota dichotoma* (Müller et al., 1981), and

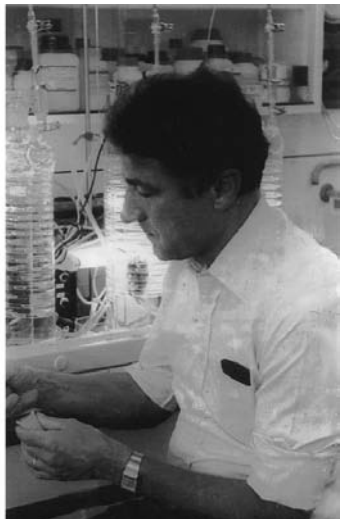


Fig. 21.9 Dieter G. Muller Born January 24, 1935, in Stuttgart, Germany. From 1956 to 1961, Dr. Muller studied at the Universitat Tubingen; from 1961 to 1963, he was a Postdoctoral Fellow at the University of Pennsylvania; from 1964 to 1973, he was Wissenschaftlicher Mitarbeiter at the Max-Planck-Institut fur Zuchtungsforschung at Koln-Vogelsang. In 1973, he received his Habilation at the University of Koln; and since 1973, he has been professor in the Fakultat für Biologie at the Universitat Konstanz. In 1964, Dr. Muller received strong support from Professor J. Straub, director of the Max-Planck-Institut, Koln, to work out in detail the life cycle of *Ectocarpus siliculosus*. After evidence for a sexual hormone was discovered, a cooperation scheme was established with the Institut für Biochemie at the University of Koln. These two events led to the characterization of the sexual hormones of the brown algae.

fucoserratene from *Fucus serratus* and *F. vesiculosus* (Müller and Jaenicke, 1973) (Fig. 21.9).

Classification

The Phaeophyceae are an ancient lineage, originating between 150 (Medlin et al., 1997) and 200 million years ago (Lim et al., 1986). The Xanthophyceae and Phaeothamniophyceae are the closest known sister taxa to the Phaeophyceae. The first true brown alga was probably similar to the extant *Choristocarpus tenellus* (Fig. 21.10) with creeping filaments, apical growth, and an isomorphic life history (de Reviers and Rousseau, 1999; Draisma et al., 2001).

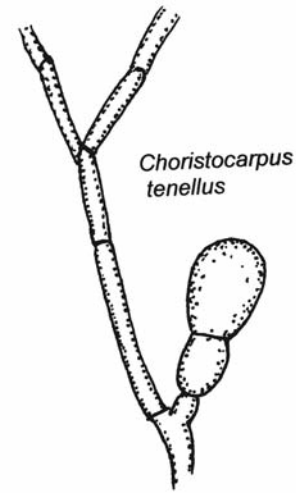


Fig. 21.10 *Choristocarpus tenellus* showing the uniseriate filament and a propagule with an apical cell.

Within the Phaeophyceae, the Fucales are a sister group to the remainder of the algae in the class. The early divergence of the Fucales is consistent with the presence of a proboscis in the spermatozoids of *Vaucheria* and *Fucus* (de Reviers and Rousseau, 1999). Fossils similar to *Cutleria* occur in 25 million-year-old Miocene deposits while fossils similar to algae in the Laminariales and Fucales occur in 16–20 million year old Miocene deposits.

The orders considered here are presented in an evolutionary sequence with the Dictyotales and Sphacelariales being the most ancient and the Ectocarpales and the Laminariales the most recent (de Reviers and Rousseau, 1999; Draisma et al., 2001).

Order 1 **Dictyotales**: growth by an apical cell; meiosis occurring in the production of four to eight non-motile spores; oogamous sexual reproduction.

Order 2 **Sphacelariales**: growth by an apical cell; daughter cells divided longitudinally to give a polysiphonous structure; isogamous sexual reproduction.

Order 3 **Cutleriales**: trichothallic growth forming a fan-like thallus in at least one generation; anisogamous sexual reproduction.

Order 4 **Desmarestiales**: trichothallic growth forming axial cells; oogamous sexual reproduction.

Order 5 **Ectocarpales**: thallus consisting of filaments or filaments compacted together; reproduction isogamous or anisogamous.

Order 6 **Laminariales**: diploid thallus parenchymatous resulting from an intercalary meristem between the stipe and blade; reproduction oogamous.

Order 7 **Fucales**: growth primarily by a promeristem; gametophyte reduced to egg and sperm; oogamous sexual reproduction.

Dictyotales

This order has organisms that grow by means of an apical cell or by a marginal row of apical cells. There is an isomorphic alternation of erect, flattened, parenchymatous thalli. A distinctive character of this order is the modification of the unilocular sporangia to produce four to eight large aplanospores. Sexual reproduction is oogamous. The Dictyotales are common in warmer waters throughout the world.

Dictyota dichotoma has a single apical cell that forms the flattened annual thallus (Fig. 21.11). The mature thallus consists of three layers: a middle layer composed of large cells with few or no chloroplasts, surrounded on both sides by a layer of small cells densely packed with chloroplasts. Gametophytes form sex organs in projecting sori. Gametogenesis can be artificially induced by exposure of the gametophytes to blue light (Kumke, 1973). An oogonium develops from a surface cell that divides into a stalk cell and the oogonium proper. Each oogonium produces a single egg, which is liberated through the gelatinized apex of the wall. There are usually 25 to 50 oogonia in a sorus with sterile oogonia at the margin. The deep-brown color of the female sori contrasts with the white glistening spots that comprise the male sori. The male sori can be recognized early in their development by the disintegration of the chloroplasts in the cells. Like the oogonia, the antheridia develop from surface cells. These cells enlarge and divide horizontally into a stalk cell and a primary spermatogenous cell. This cell divides and redivides in vertical and horizontal planes into between 650 and 1500 compartments (Williams, 1904). The content of each locule becomes a pear-shaped sperm with a single, laterally inserted, tinsel flagellum and an anterior eyespot (Phillips and Clayton, 1993). Although there is only one emergent flagellum, a second basal body is present (Manton, 1959), indicating a derivation from a biflagellate ancestor. The mature sperms are set free by dissolution of the walls of the antheridium. The male sorus is surrounded by elongated sterile cells that are regarded as undeveloped antheridia. The egg secretes the pheromone **dictyotene** (Fig. 21.8) (Pohnert and Boland, 2002) that attracts the sperm. The sperm fertilizes the egg to produce the zygote that germinates into the sporophyte; unfertilized eggs can germinate parthenogenetically but seldom develop normally and soon abort. The sporophytes produce haploid aplanospores (tetraspores) on the surface of the thallus. The tetrasporangia occur singly or in small groups. The naked tetraspores are released by gelatinization of the apex of the sporangium, and soon after liberation the large motionless spores secrete a cellulose wall and develop into the gametophytes.

In *D. dichotoma*, the gametes are released at regular intervals. This was first noticed by Williams (1905) in Great Britain, where the gametes are released fortnightly. Müller (1962) showed that moonlight is the synchronizing factor for the release. When he grew the alga in natural light, gametes were released every 14 to 15 days. If the alga was grown under artificial conditions with a 14 hours light:10 hours dark cycle, then few gametes were released, and there was no synchronony. If the artificially lighted cultures had the lights left on all night, then 10 days later a burst of gametes was released. The lights being left on all night simulated moonlight.

Species of *Dictyota* produce terpenoids, such as pachydictyol and (6R)-6-hydroxydichotoma-3, 14-diene-1,17,dial (Fig. 21.12), that inhibit grazing of *Dictyota* by herbivorous fish, amphipods, and sea urchins (Schmitt et al., 1998; Pereira et al., 2000).

The only calcified genus in the Phaeophyceae, *Padina*, is in the Dictyotales.

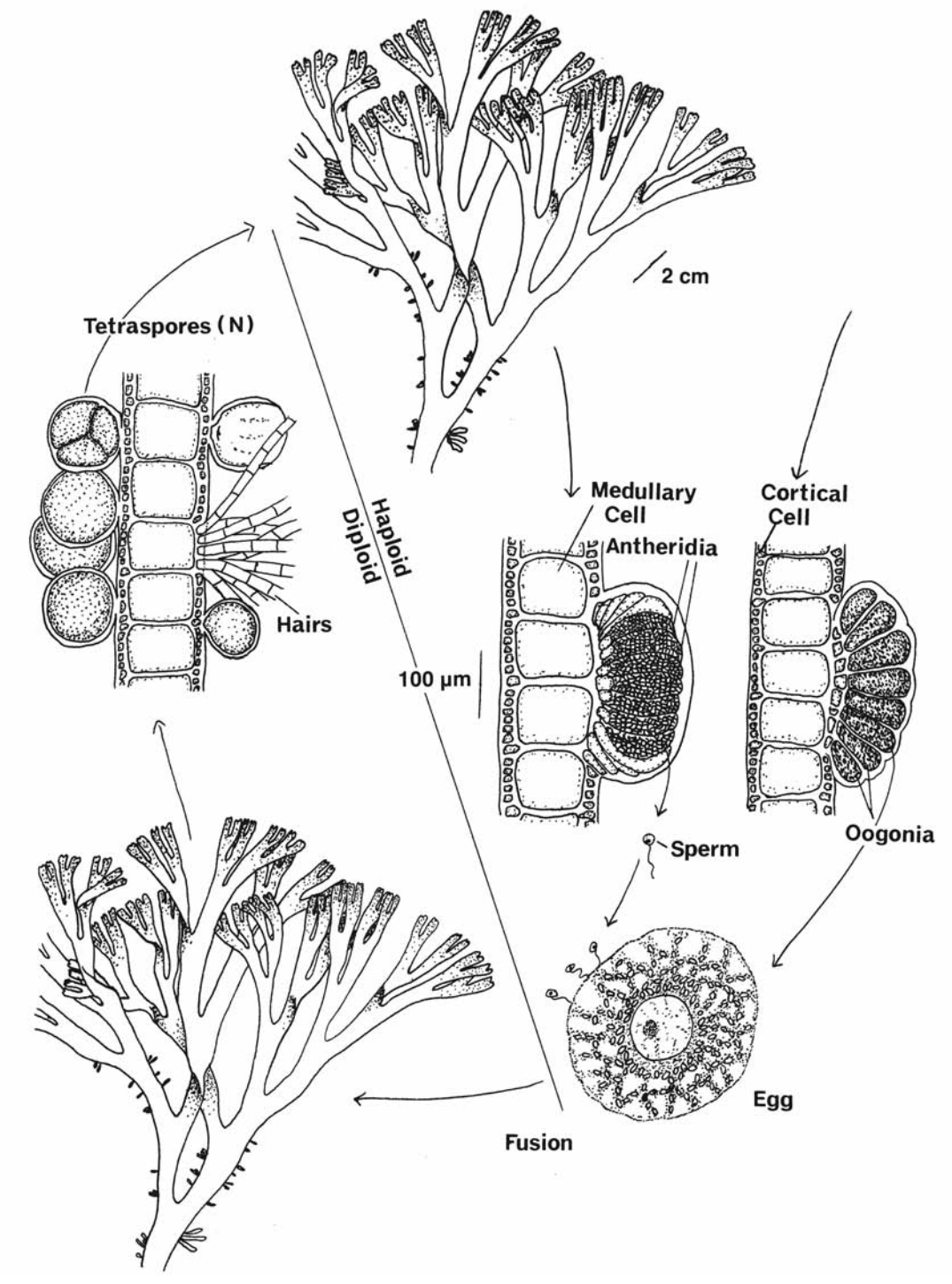


Fig. 21.11 The life cycle of *Dictyota dichotoma*. (Adapted from Thuret and Bornet, 1878; Williams, 1898; Taylor, 1960.)

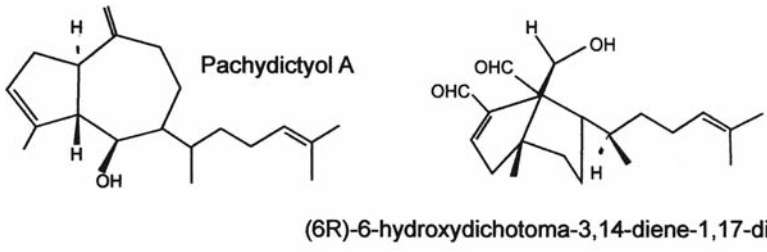


Fig. 21.12 The chemical structure of two secondary metabolites secreted by *Dictyota* spp. that act as antifoulants.

Sphacelariales

This order is characterized by an apical meristematic cell that divides transversely to produce the daughter cells. The algae produce distinctive vegetative propagules. Another less precise characteristic is blackening of the cell walls when treated with bleaching liquid (Draisma et al., 2002).

Sphacelaria (Fig. 21.13) grows attached to rocks or other algae and has one or more freely branched shoots arising from a discoid holdfast. The apical cell undergoes transverse divisions, with subsequent longitudinal septation of the daughter cells to produce a polysiphonous structure. Although the maturing axes and branches undergo septation into smaller and smaller cells, they do not enlarge; thus the diameter of the filament is essentially the same from the base to the apex. Older axes, though, may become corticated by downward-growing filaments. The erect axes are usually abundantly branched, usually in a regular, distichous manner.

Asexual reproduction is by means of **propagula** (Fig. 21.13), which are specialized branchlets of distinctive form that are produced throughout the vegetative parts of the plants. They are formed much more frequently than sporangia or gametangia. Each propagule has an apical cell and usually two to three protuberances. After falling from the parent plant and contacting a suitable substrate, the propagule develops into a new plant. Propagula are formed only at temperatures above 12 °C and under daylight conditions longer than 12 hours (Colijn and van den Hoek, 1971).

In *S. bipinnata*, the sporophyte forms both unilocular and plurilocular sporangia terminally on branches (Fig. 21.13). The plurilocular sporangia produce zoospores that re-form the parent sporophyte. Meiosis occurs in the production of zoospores in the unilocular sporangia (Clint, 1927). Over 200 zoospores are released through an apical pore in the unilocular sporangium (Papenfuss, 1934). The zoospores germinate to presumably form gametophytes that are similar to the sporophytes. The gametophytes produce plurilocular gametangia of one type, which release isogamous gametes. **Ectocarpene** (Fig. 21.8) is used as a pheromone in gamete attraction (Pohnert and Boland, 2002). The fusion of gametes takes place while they are motile and produces a quadriflagellate zygote that may continue moving for several hours. The life cycle of another species, *S. furcigera*, involves anisogamy and unisexual gametophytes, which are somewhat smaller than the sporophytes (van den Hoek and Flinterman, 1968). The life cycle is controlled by temperature and photoperiod.

Cutleriales

This order contains only two genera, *Cutleria* and *Zanardinia*. The genera show an alternation of generations that is heteromorphic in *Cutleria* and isomorphic in *Zanardinia*. The thallus is flattened, blade-like, or disc-like, with entirely or partially trichothallic growth. The sporophytes produce only unilocular sporangia, whereas the gametophytes are heterothallic and markedly anisogamous.

Cutleria is a warm-water plant of the Northern Hemisphere that may be closely related to *Saccorhiza* in the Laminariales (Rousseau et al., 1997). The gametophyte is an erect, flattened blade with numerous dichotomies (Fig. 21.14). Growth is trichothallic at the base of many erect uniseriate hairs at the upper margin of the blade. The cells that are cut off below the hairs contribute to the thallus. The innermost of these cells gradually enlarge to form the medulla, whereas

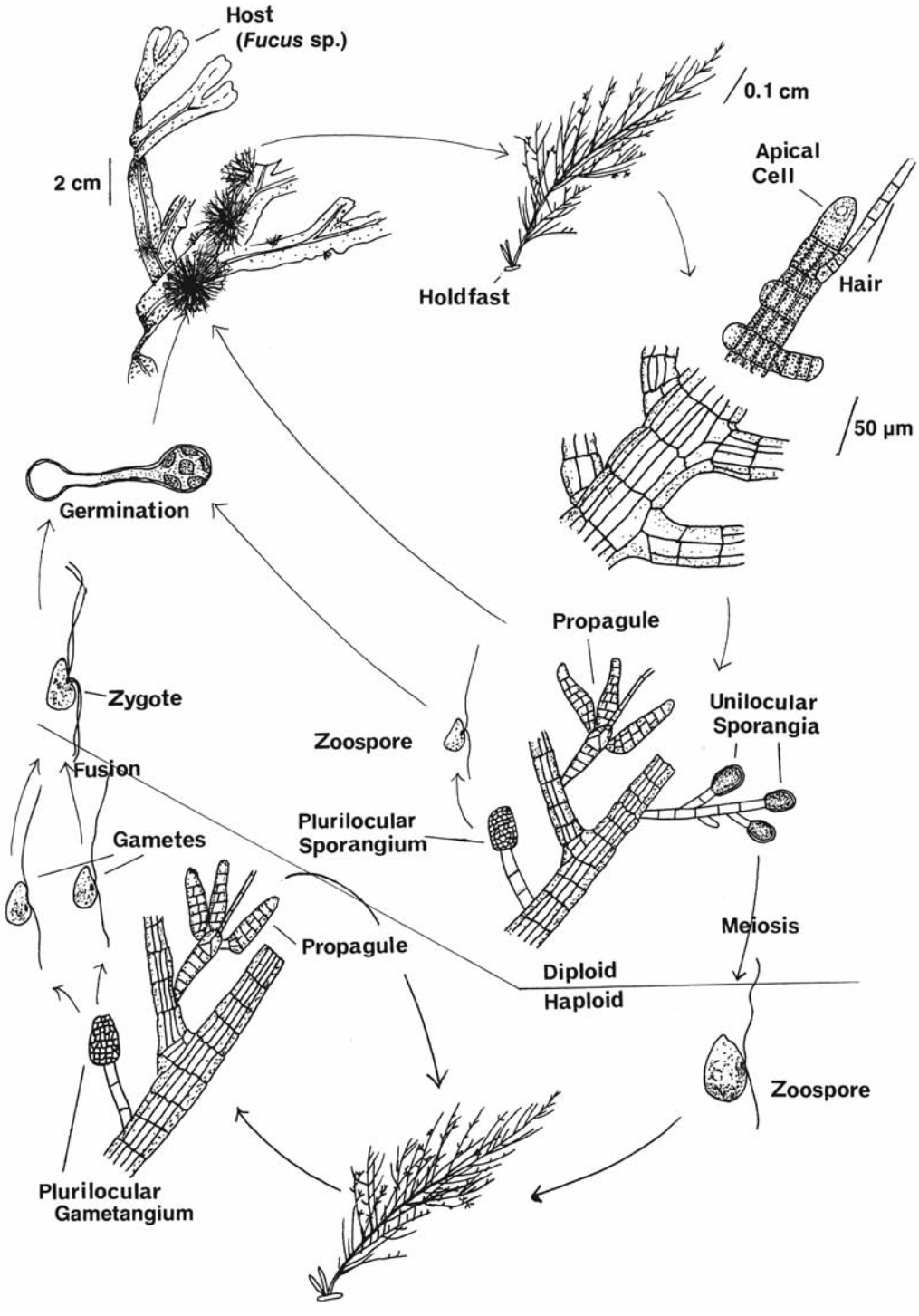


Fig. 21.13 The life cycle of *Sphacelaria* (*S. cirrhosa* and *S. bipinnata*). (Adapted from Savaugeau, 1900–14; Papenfuss, 1934; Taylor, 1957.)

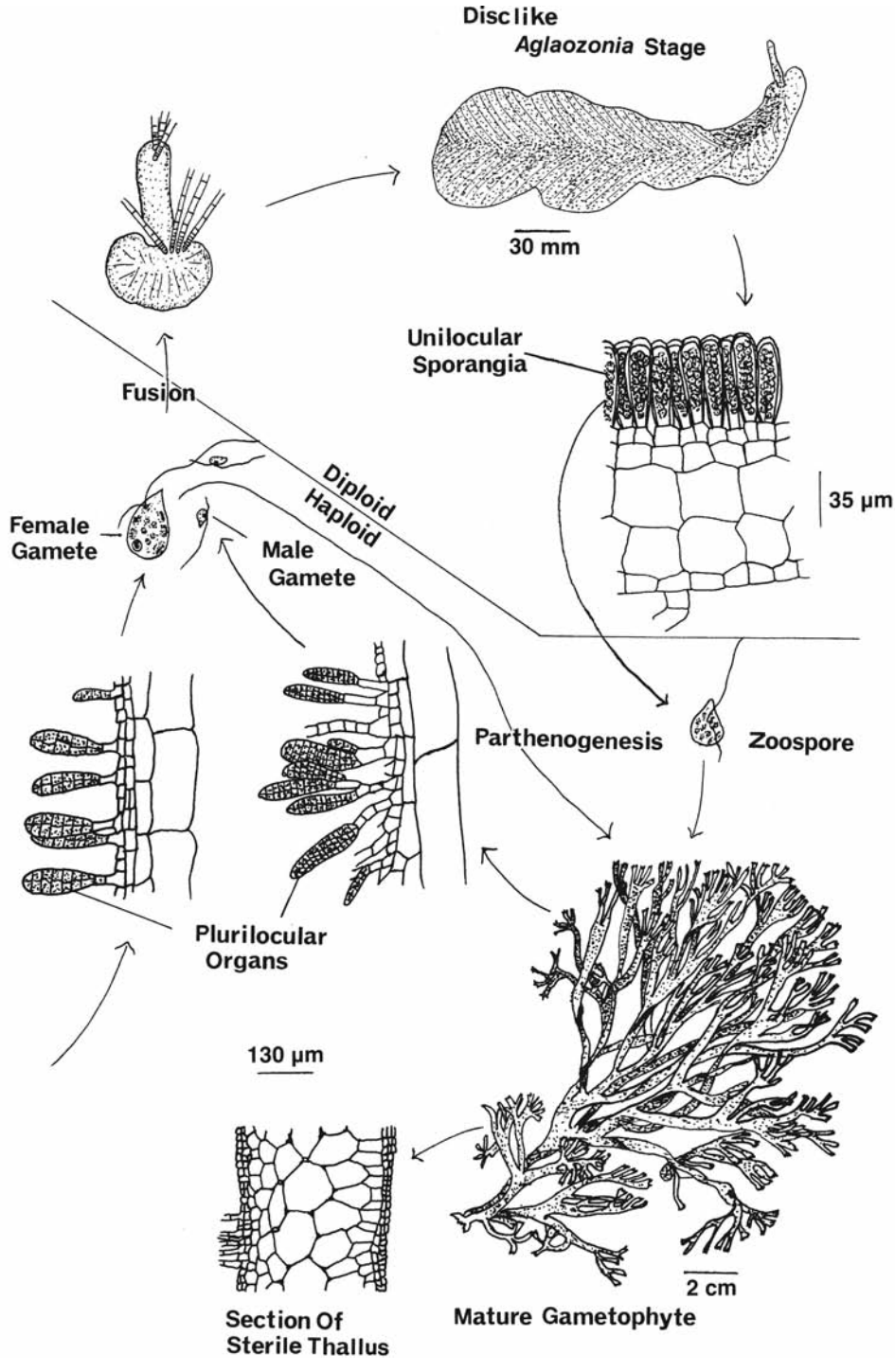


Fig. 21.14 The life cycle of *Cutleria multifida*. (Adapted from Kuckuck, 1899; Savaugeau, 1899.)

the outer ones undergo divisions to form the cortex. The gametophytes are heterothallic, with the sex organs developing in clusters on the surface of the thallus. A superficial epidermal cell may develop directly into a male gametangium, or it may develop into a branched hair that bears several gametangia. The male gametangium consists of a stalk cell on which there are 20 or more tiers of cells, each tier composed of eight cells. The protoplast of each cell forms a biflagellate male gamete, which escapes through a pore in the gametangial wall to the outside. Female gametangia develop similarly to the male, but with a smaller number of larger cells. Female gametangia are four to seven tiers high, with only four cells in each tier. Free-swimming male gametes are pyriform, with a single reddish chloroplast at the place of flagella insertion. Free-swimming female gametes are also pyriform, but are much larger and have a dozen or so chloroplasts. The female gametes release a highly volatile, low-molecular-weight compound, **multifidene** (Fig. 21.8) (Pohnert and Boland, 2002) that attracts the male gametes (Müller, 1974). When the gametes fuse, the male gametes are actively swimming while the female are sluggish or immobile. Fusion of the two nuclei follows within a few hours, and the zygote begins to develop into the sporophyte within a day. Unfertilized female gametes develop parthenogenetically into gametophytes.

The zygote germinates to produce the sporophyte, which was first described as a separate genus, *Aglaozonia*. At first, growth is trichothallic and vertically upward into a columnar structure. Upward growth ceases when the plant is about 10 days old, and all further growth is laterally outward from the base of the column. Repeated cell division at the base of the column forms a flat, disc-like tissue that expands laterally as a result of division and redivision of the marginal cells. The sporophyte is homologous to a minute erect thallus subtended by an enlarged fertile holdfast. The disc-like portion of the thallus is several cells thick, and the outer cells are differentiated into an epidermis-like layer. The holdfast is attached to the substratum by numerous multicellular rhizoids growing from the ventral epidermal cells. The unilocular sporangia are formed in sori on the dorsal surface of the sporpohyte. A single epidermal cell divides into one to six stalk cells and a single terminal unilocular sporangium. In the unilocular sporangium 8, 16, or 32 large, pyriform, haploid zoospores are formed, each with several chloroplasts. The zoospores escape through a large apical pore in the sporangial wall, swarm for 10 to 90 minutes, then settle down, round up, and secrete a wall. The zoospores then divide to form the gametophyte.

Although germlings from zygotes and from zoospores of the *Aglaozonia* sporophytes have not been grown to maturity in culture, they have been grown to a sufficiently advanced stage to show that the two stages are alternate generations of each other. In Europe, the sporophyte is perennial and fruits in winter or spring, whereas the gametophyte is a spring annual that disappears during the summer.

Fossils of a plant similar in structure to *Cutleria*, called *Limnophycus paradoxa*, have been described from the Miocene (25 million years old) deposits in Germany.

Desmarestiales

In this order there is an alternation of a large macroscopic sporophyte with a small filamentous gametophyte (Fig. 21.15). The gametophyte forms oogonia and sperm, with the result that reproduction is oogamous. Growth of the sporophyte is trichothallic, and the main axis is corticated by downward-growing cells. In this treatment, the organisms sometimes considered in the Sporochnales are placed in the Desmarestiales, as suggested by Russell and Fletcher (1975).

Sporophytes of *Desmarestia* may reach a length of 2 to 3 m and occur primarily in the sublittoral region in colder waters of both the Northern and the Southern Hemisphere. The plants (Figs. 21.15, 21.16) have trichothallic growth from an intercalary meristem composed of flattened cells that cut off cells to the terminal hair above, and cells to the thallus below. The cells of the terminal hair continually wear away, and each of these cells usually bears one or two unbranched laterals. The cells produced below the meristem cut off two opposite laterals in one plane, which lengthen by means of a basal meristem. Cortication of the thallus begins by the basal cells of the lateral cutting off a number of cells that gradually form a

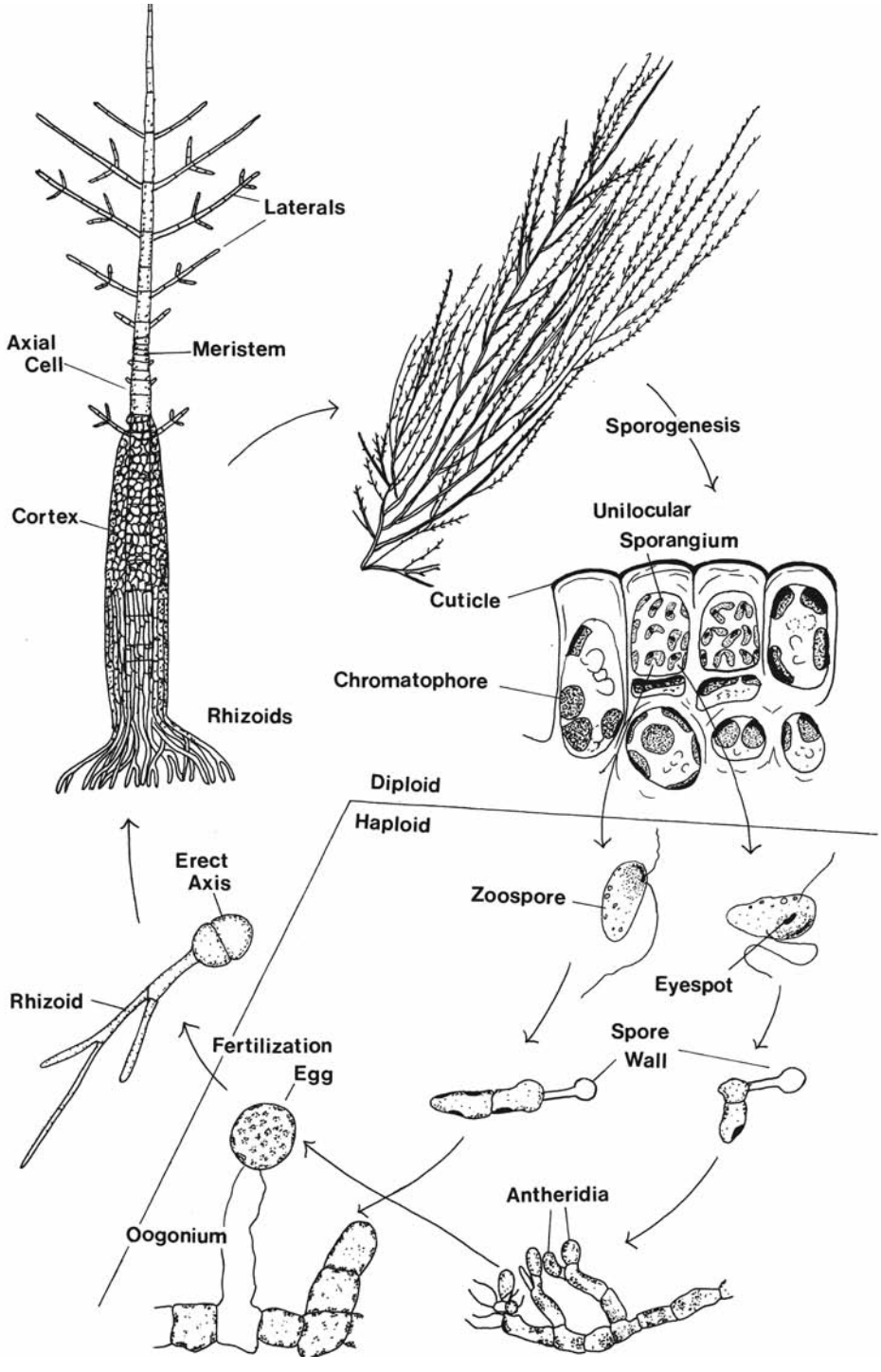


Fig. 21.15 The life cycle of *Desmarestia*. (Adapted from Schreiber, 1932; Chapman and Burrows, 1971.)

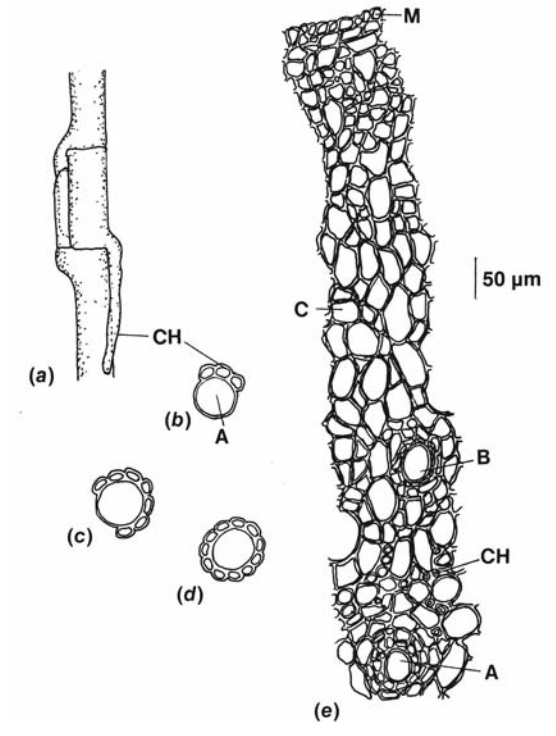


Fig. 21.16 *Desmarestia*. (*a*)–(*d*) Cortication of an axial cell (A) by corticating hyphae (CH). (e) Partial section of a mature thallus. (B,C) Laterals; (M) meristoderm.

complete one-layered envelope around the elongating axial cell that produced the lateral. The cells of this one-layered envelope soon undergo periclinal division, with the outer layer that is produced behaving as a meristem. This meristem then produces the cells of the cortex to the inside, with the result that the axial cells and laterals are progressively buried. In addition to this primary growth, the cells of the inner cortex are capable of secondary growth, enlarging to form hyphae that push their way downward between the cells of the cortex. Trumpet hyphal cells occur in the medulla. These cells have perforate end walls with callose and probably function in conduction of nutrients as do the sieve filaments in the Laminariales (Moe and Silva, 1981).

D. aculeata (Fig. 21.15) produces unilocular sporangia on the sporophytes in the winter by the tangential division of a surface cell of the cortex. Meiosis apparently occurs in the production of a few biflagellate zoospores formed in each small unilocular sporangium. The zoospores have an eyespot and a single chloroplast. Released zoospores settle, lose their flagella, and round up within 24 hours. The cell contents move out into a germ tube immediately after settling. The sporelings produce female and male gametophytes in roughly similar numbers, the male gametophytes having small cells and being less densely pigmented than the female gametophytes. Gametophytes grow vegetatively only in red light, with differentiation of oogonia and antheridia occurring under blue or white light (Müller and Lüthe, 1981). About 11 days to 3 weeks after germination of spores, conical antheridia and lateral oogonia appear on the gametophytes. The tubular oogonia dehisce apically to liberate the egg, which usually adheres to the gelatinized aperture. A single spermatozoid is released from each antheridium through a narrow apical aperture. The freshly released eggs secrete three volatile chemicals that cause the antheridia to burst and attract free spermatozoids to the eggs. The three sexual hormones are **desmarestene**, **ectocarpene**, and **viridene** (Fig. 21.8). Desmarestene is the most potent of the three sexual hormones (Müller et al., 1982). Sporophyte development begins with the production of a tube from one side of the zygote and a lightly pigmented rhizoid from the opposite pole. The initial tube goes on to produce an oppositely branched uniseriate filament, which forms a trichothallic meristem below most of the lateral branches. Cortication of the thallus begins, as has already been described, to produce a mature sporophyte and complete the life cycle. Gametophytes of *Desmarestia* (Andersen, 1982) and the Laminariales have several features in common, including clusters of unicellular antheridia, vertically elongated intercalary oogonia, attachment of the extruded egg to the oogonial apex, and growth of the young sporophyte upon the oogonial apex.

Some of the species of *Desmarestia* accumulate large amounts of malic acid, lowering the pH of the vacuolar sap to as low as 2. In collecting seaweeds, the species of *Desmarestia* should be kept separate because some of their cells will rupture, releasing acid and killing the other seaweeds.

In the Antarctic waters, members of the Desmarestiales provide the bulk of the biomass of benthic seaweeds. They are perennial, covering

large areas of water to depths of about 40 m. The largest and most abundant species (*D. anceps* and *D. menziesii*) form thickets, but not the protective canopy characteristic of many kelps. The Antarctic possesses the only cold-water flora without Laminariales, although in sub-Antarctic waters there are vast stands of kelps (*Macrocystis* and *Lessonia*) (Moe and Silva, 1977).

The Desmarestiales and the Laminariales have a number of similar development characteristics (Tan and Druehl, 1996) that include (1) vegetative development of the gametophyte in red light; (2) requirement of white or blue light for development of antheridia and oogonia; (3) existence of spermatozoid-releasing and -attracting factors secreted by eggs; (4) unusually long and flexible hind flagella; (5) lack of eyespots in spermatozoids; and (6) formation of sexual organs by the gametophyte, representing an exhaustive and almost lethal effort for the gametophytes.

Ectocarpales

These algae consist of filaments or of filaments compacted together. In the order it is possible to see the gradual morphological evolution from a filamentous structure to **pseudoparenchymatous** (**haplostichous**) complex structures of compacted filaments (from the Ectocarpaceae to the Ralfsiaceae, and Splachnidiaceae). Along another line, the filamentous thallus has evolved by the division of the filament into true **parenchymatous** (**polystichous**) thalli (from the Ectocarpaceae to the Scytosiphonaceae). Most of the algae in the order are **heterotrichous**, with the thallus consisting of two different parts: (1) the prostrate creeping disc that functions as a holdfast, and (2) the erect filamentous, bulbous, or foliose stage. In some of the algae, both systems are evident (*Scytosiphon*, Fig. 21.19), whereas in others the erect stage is reduced to filaments of a few cells and the thallus is crustose (*Ralfsia*, Fig. 21.18), and in yet others the erect stage is predominant with the prostrate system reduced to a small holdfast (*Petalonia*, Fig. 21.20). Even within the same alga, there can be a stage that consists of only a thin crust, whereas the alternate stage has a well-developed erect stage.

Nucleic-acid sequencing studies have shown a strong relationship between the Ectocarpales, Desmarestiales and Laminariales (Draisma et al., 2001).

Four of the families in the Ectocarpales will be considered here.

Family 1 Ectocarpaceae: plants with free-filamentous construction with no adherence of filaments to each other.
Family 2 Ralfsiaceae: algae with a basal layer supporting erect filaments that are compacted together to form a tissue.
Family 3 Scytosiphonaceae: parenchymatous thalli with mostly diffuse growth.
Family 4 Splachnidiaceae: plants with trichothallic growth and unilocular sporangia formed in conceptacles.

Ectocarpaceae

These organisms have free-filamentous construction with no adherence of the filaments to each other. *Ectocarpus* is the prevalent genus, and is composed of freely branched, uniseriate filaments differentiated into prostrate and erect systems. The prostrate parts are rhizoid-like and often penetrate the substrate. Growth can be diffuse or more or less clearly trichothallic, with intercalary cell divisions confined to certain areas of the filaments. Some workers divide up the family into different genera on the basis of cytology and morphology, whereas others consider that the family contains the single genus *Ectocarpus* (Russell and Garbary, 1978).

The life cycle of *E. siliculosus* (Fig. 21.17) can be taken as representative of the family (Papenfuss, 1935). The haploid and diploid phases are both filamentous, but the diploid filaments have longer cells than the haploid filaments. The diploid plants produce unilocular and plurilocular sporangia either on the same plant or on separate plants. These sporangia discharge their zoospores between 0600 and 1200 hours. The mother cell of a unilocular sporangium can be distinguished from a branch initial by the spherical shape and large nucleus of the mother cell. The cell is initially vacuolate, but the physodes and vacuoles are soon extruded from the cell and become lodged in the wall (Loiseaux, 1973). The chloroplasts and nuclei of the unilocular sporangium divide in regular sequence, with the

chloroplasts next to the wall and the nuclei in the center of the cell (Knight, 1929). The nuclei divide meiotically. A chloroplast then becomes associated with a nucleus, and a zoospore is delimited around it. A small perforation occurs at the apex of the unilocular sporangium, and up to 32 haploid zoospores ooze out of the sporangium in a gelatinous matrix. The perforation is small, and zoospores are relatively large, being twice the size of gametes and zoospores from plurilocular sporangia. The zoospores initially swim in a straight pattern, then display circling movements as they explore appropriate surfaces for settling (Iken et al., 2001). The zoospores prefer to settle on a hydrophobic surface, preferably one with a microbial film. The zoospores germinate within 2 to 3 hours to produce haploid filaments.

The plurilocular organs (Fig. 21.17) are modified lateral branches that are divided into as many as 660 cubical cells, each containing a motile cell. The plurilocular sporangia on the diploid filaments produce zoospores that remain motile for 3 to 5 hours, settle, and within 2 to 5 hours germinate to produce diploid filaments like the parent. The germ tube of the sporeling arises from the narrow, anterior flagellated end of the zoospore, which is always oriented toward the light. The plurilocular organs on the haploid filaments are smaller than those on the diploid filaments, and produce either zoospores or gametes. The motile gametes are all of the same size but differ physiologically. The female gametes settle down about 5 minutes after liberation and secrete a sexual hormone called **ectocarpene** [all-*cis*-1-(cycloheptadien-2′,5′-yl)-1-butene] (Fig. 21.8) (Müller et al., 1971). Male gametes (Fig. 21.17) (Maier, 1997a,b) move very rapidly (269 μm per second) in a straight line in open seawater when no female gametes are around (Müller, 1978). The motile male gametes (which can remain motile for up to 8 hours) swim in circular paths on encountering ectocarpene, the diameter of the circular path decreasing in response to increasing ectocarpene concentration (Müller, 1982). As soon as the female gamete is reached, a firm contact is established between the apical part of the front flagellum of the male gamete and the plasma membrane of the female gamete. The posterior

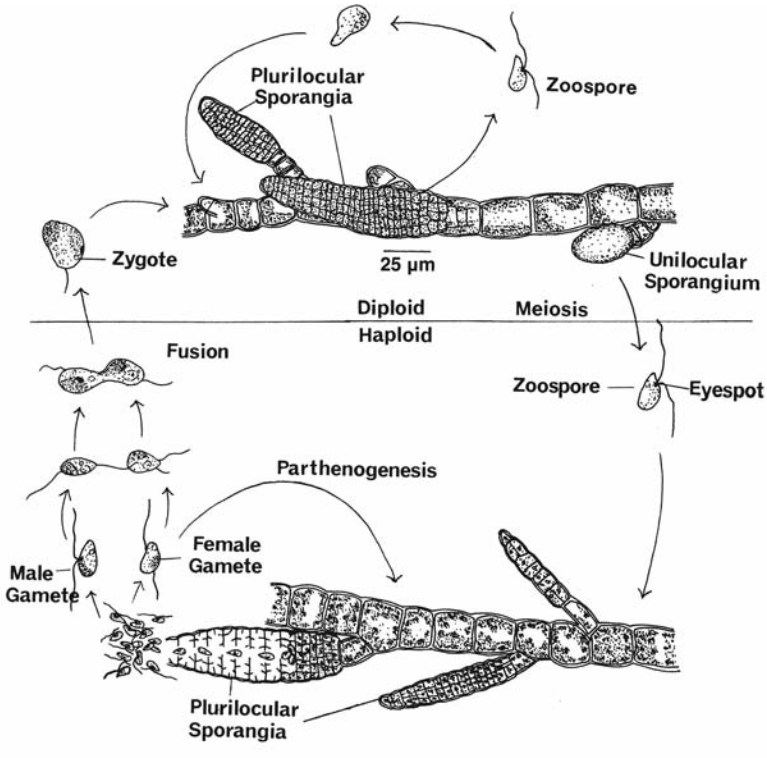


Fig. 21.17 The life cycle of *Ectocarpus siliculosis*.

ends of the two gametes fuse to form the zygote. The process of fusion takes about 20 seconds, and after fusion the zygote loses its attraction for male gametes as indicated by the dispersion of the male gametes near the zygote. The zygotes take 2 to 3 days to germinate, and the sporelings develop more slowly than those from diploid zoospores. Some of the unfused gametes have the ability to germinate parthenogenetically to give rise to haploid filaments again. This germination is slow, requiring 36 to 48 hours. Clonal populations of *E. siliculosus* from different parts of the world are interfertile, indicating that there has been little genetic isolation of the species (Müller, 1979). Ectocarpene isolated from *E. siliculosus* attracts male gametes of two other species of *Ectocarpus*, indicating that ectocarpene can be artificially synthesized and is effective in attracting male gametes.

Ectocarpus has a fairly wide tolerance to changes in temperatures and salinity. Several studies (Boalch, 1961; Edwards, 1969) have shown that *E. siliculosus* will grow and produce sporangia at temperatures between 10 and 29 °C. Müller (1962) found that at 13 °C this species produces unilocular sporangia, at 19 °C plurilocular sporangia, and at 16 °C both types of sporangia. It has the ability to grow in salinities from 0.5 to 1.5 times that of seawater at 20 °C, and 0.25 to 1.75 times that of seawater at 15 °C. The alga is an obligate photoautotroph and will not grow on any supplied carbon source in the dark. Although it will not grow in the dark, it has the ability to survive up to 150 days of darkness and still remain viable.

Ralfsiaceae

These algae have a basal layer of branched, radiating, laterally coalesced filaments attached to the substratum by the cell wall or by rhizoids. From this basal layer, chloroplast-bearing filaments arise that are compacted together to give a firm tissue. *Ralfsia* (Fig. 21.18) probably has an isomorphic alternation of generations. The brown crust-like diploid plants produce unilocular sporangia at the base of loosely associated multicellular paraphyses. Zoospores are most likely produced by meiosis in the unilocular sporangium, and the zoospores give rise to haploid crusts. These gametophytes form plurilocular sporangia that are terminal on erect filaments and probably produce motile cells that can act as gametes or zoospores (Kylin, 1934; Edelstein et al., 1968; Hollenberg, 1969).

Some of the algae that have been placed in this family are the alternate phase of the life cycle of other higher algae and as such have been removed from the family.

Scytosiphonaceae

The Scytosiphonaceae, Dictyosiphonaceae, and Punctariaceae are sometimes grouped together in a separate order, the Dictyosiphonales. The members of these three families all have parenchymatous thalli resulting from diffuse or apical growth, and both gametes are motile. These algae, though, have many structural similarities to the more complex members of the Ectocarpales such as the Splachnidiaceae, and will be considered as members of the Ectocarpales, as suggested by Russell and Fletcher (1975).

In the Scytosiphonaceae, growth is diffuse although in some older plants growth can be suprabasal. The macroscopic phase of the plant produces plurilocular sporangia, but not unilocular sporangia. *Scytosiphon lomentaria* (Fig. 21.19) is a common intertidal rock-pool alga. It has a narrow, cylindrical thallus up to 50 cm long, gradually tapering from apex to base. The thallus has occasional constrictions, and the plants grow in tufts with smaller individuals showing no or few constrictions. *Petalonia* (Fig. 21.20) has flat leafy fronds consisting of larger medullary cells covered with smaller cortical cells. In the North Atlantic, *Petalonia fascia* and *Scytosiphon lomentaria* occur in the same area. This area is limited on the north by the 0 °C summer isotherm and on the south by the 17 °C winter isotherm (Fig. 17.9) (van den Hoek, 1982).

The life cycle of *Petalonia* (Fig. 21.20) and *Scytosiphon* (Fig. 21.19) has precipitated some controversy. Workers are more or less divided into the North American School (Wynne, 1969; Edelstein et al., 1970; Loiseaux, 1970; Kapraun and Boone, 1987), who claim that meiosis and fusion of gametes do not occur, and the Japanese and Australian school (Nakamura, 1965, 1972; Tatewaki, 1966; Clayton, 1980), who believe that meiosis occurs in the unilocular sporangia and

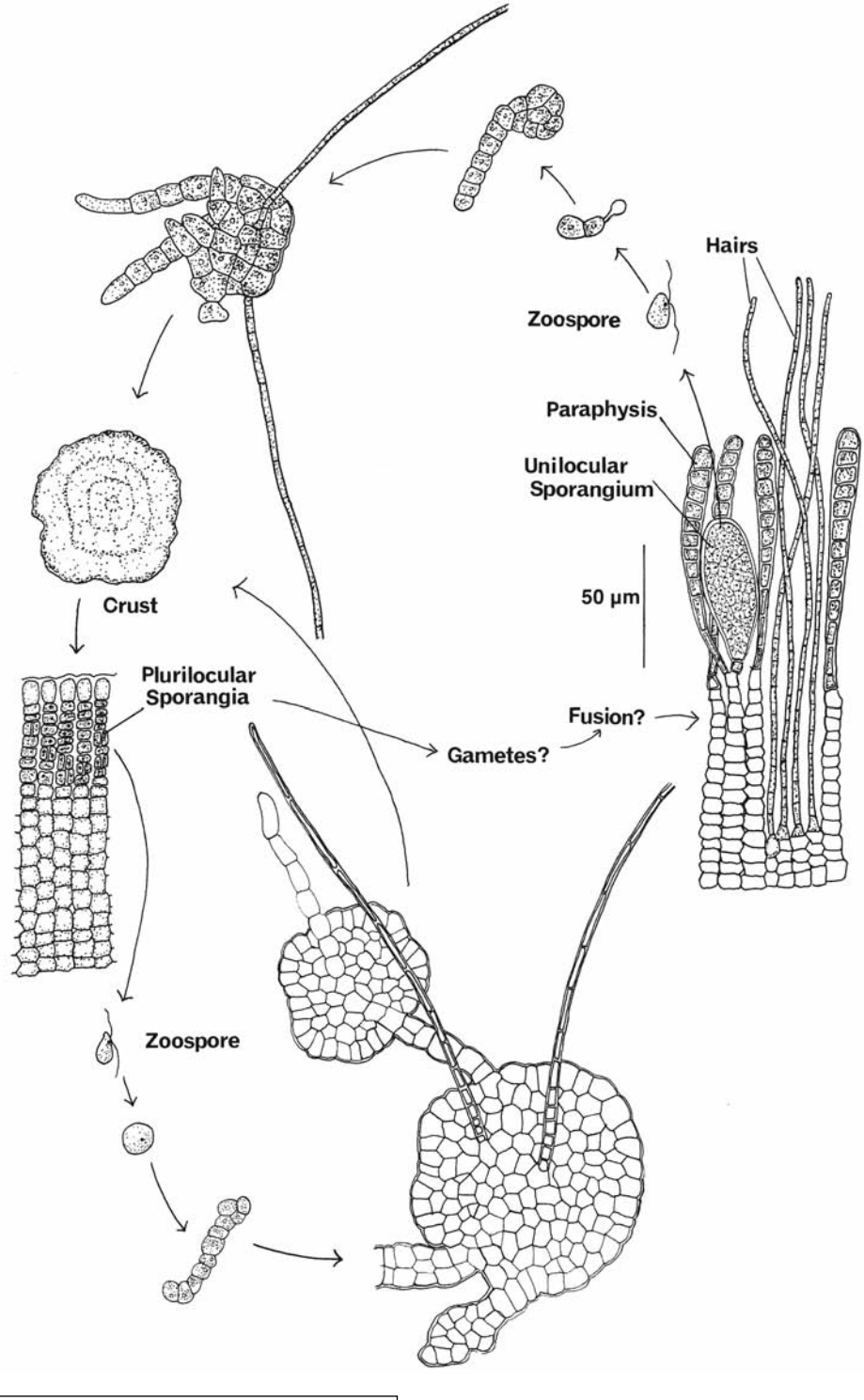


Fig. 21.18 The life cycle of *Ralfsia confusa*. (Adapted from Hollenberg, 1969.)

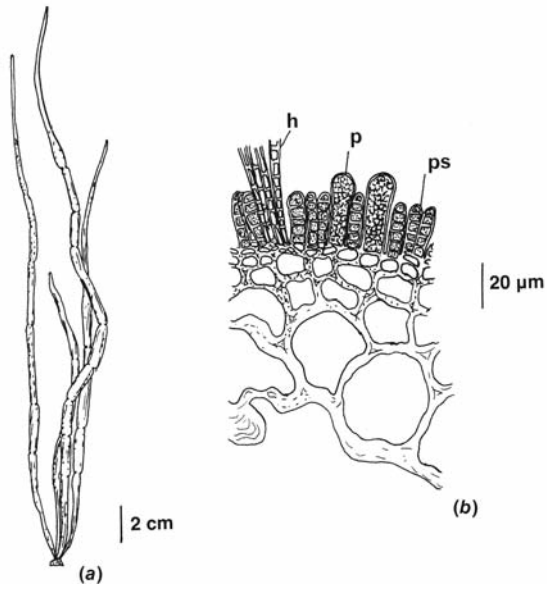


Fig. 21.19 *Scytosiphon lomentaria*. (*a*) Whole plant. (*b*) Portion of a section of the hollow plant showing hairs (h), paraphyses (p), and plurilocular sporangia (ps). (After Taylor, 1957.)

that the motile cells from the plurilocular sporangia function as gametes. The difference in results may be due to different local strains of the same alga. Both groups agree, however, that there are two different morphological phases, a macroscopic phase that produces plurilocular organs and a crustose phase that forms unilocular sporangia.

According to Wynne (1969), *P. fascia* (Fig. 21.20) has the following life cycle. The foliose thalli are annual and usually have erect lanceolate blades on a small discoid holdfast. The blades produce plurilocular sporangia that release negatively phototactic zoospores, with a period of motility lasting up to 24 hours. These zoospores settle and form filamentous germlings with the protoplast not being evacuated from the spore cell. The filaments branch, with the branches spreading laterally to form discs, with each cell having a single parietal plastid and a large pyrenoid. These discs can develop along two different lines, depending on the environmental conditions. Under short days and low temperature, the discs produce erect, uniseriate processes, the blade initials; these then become parenchymatous by subsequent longitudinal divisions, yielding the upright flattened blade. The surface cell of the blade undergoes numerous anti- and periclinal divisions to form dense lateral files that are the plurilocular organs. The sori cover most of the thallus except for the holdfast and the margin of the blades. The zoospores of the plurilocular organs settle and germinate to form new discs like the original ones. Under long days and high temperature, the discs develop into polystromatic crusts that resemble species of *Ralfsia*. After 4 weeks in culture these crusts reach maturity and are composed of a basal layer of cuboidal cells seldom exceeding six to ten cells in thickness and a layer of paraphyses supported by the basal layer. The paraphyses consist of four to six cells with a conspicuous cuticle covering the paraphyses. This cuticle is evidently secreted by the terminal cells of the paraphyses. A unilocular sporangium is formed by the basal cell of a paraphysis undergoing an unequal division to produce a cell that protrudes from one side. This cell enlarges laterally and upward, a basal cell is laid down, and a unilocular sporangium is formed. The sporangium cleaves up into 128, 256, or more zoospores, which are released by dissolution of the apex of the sporangium. The zoospores free themselves from the enveloping mucilage, swim away, exhibiting negative phototaxis, and, after several hours, settle down. The germlings give rise to the original discs again. Therefore, in the above life cycle the motile cells produced by both the unilocular and plurilocular organs behave similarly, germinating to form discs.

From the above discussion it can be seen that the morphology of the plant is dependent on environmental conditions. In addition, Lüning and Dring (1973) have shown that the type of light will affect the morphology of *Petalonia* and *Scytosiphon*. Among other effects, in red light the prostrate system consists of sparsely branched, uniseriate filaments, whereas under blue or white light it consists of profusely branched filaments. Hsiao (1969, 1970) showed that there are certain minimal concentrations of iodine in the water necessary for the different forms of *P. fascia*. In order to have the formation of the crust-like *Ralfsia* stage, 4.0×10^{-5} M KI was necessary, and, for the formation of blades, 4.0×10^{-6} M KI. Filamentous stages

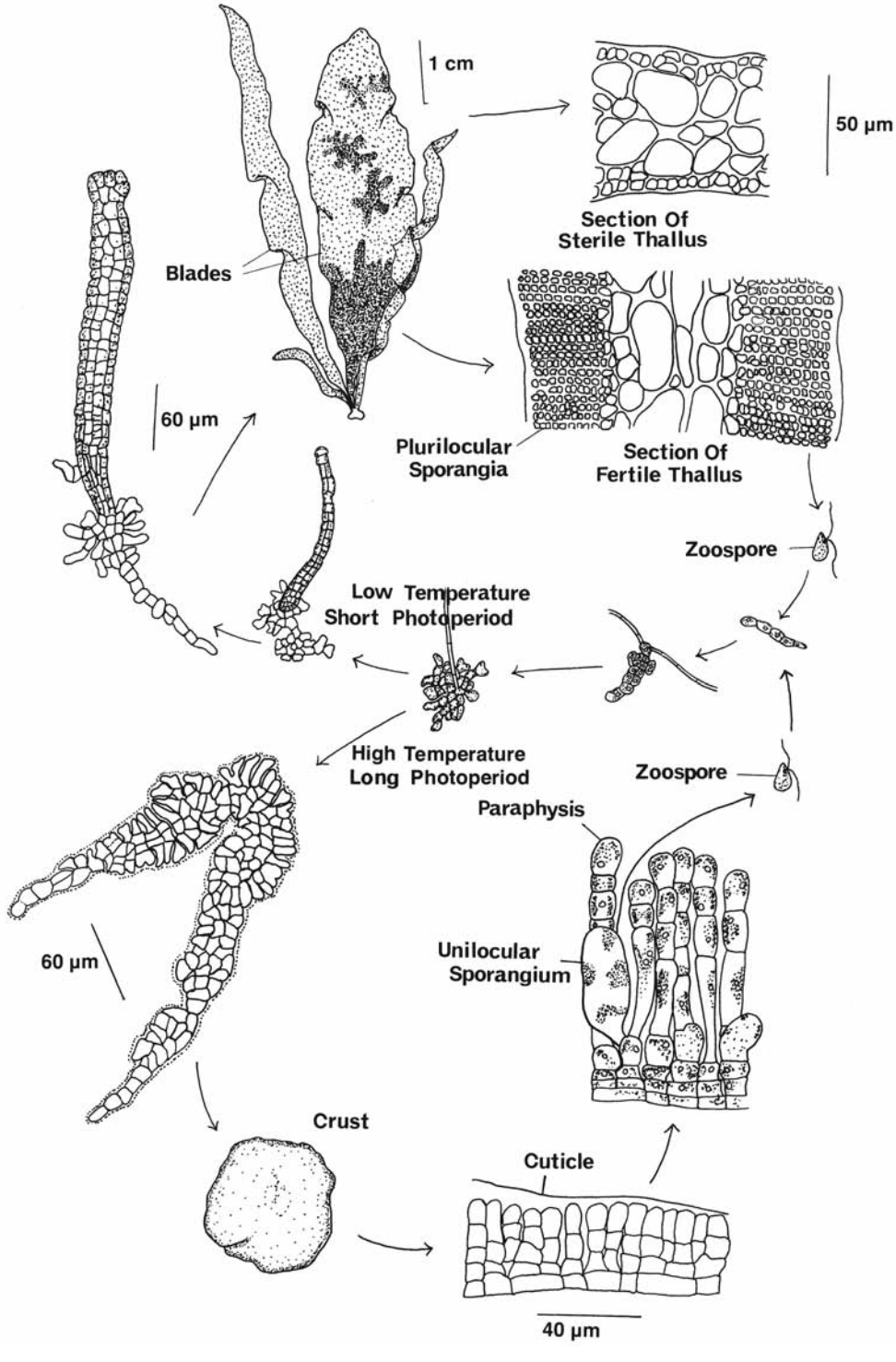


Fig. 21.20 The life cycle of *Petalonia fascia*. (After Smith, 1969; Wynne, 1969.)

of the alga will grow in an iodine-free medium. He also found that the crusts and blades grow at moderate temperatures, whereas the filamentous stages grow at the more extreme temperatures.

Splachnidiaceae

This family contains one genus, *Splachnidium*, a perennial alga of the Southern Hemisphere. The plant consists of a gelatinous, monopodially branched, hollow thallus attached by a basal disc (Fig. 21.21). The alga is interesting, because along with *Notheia* (Nizamuddin and Womersely, 1960; Gibson and Clayton, 1987) and *Acroseira*, it has a number of morphological and reproductive similarities with the Fucales. Nucleic-acid sequencing, however, has shown that these algae are not closely related to the Fucales and represent convergent evolution (de Reviers and Rousseau, 1999). Like members of the Fucales, *Splachnidium* forms its reproductive bodies in conceptacles, the thallus is divided into a medulla with hyphae and a cortex, and there is a type of trichothallic growth (found in young fucalian sporophytes). The conceptacles originate in the immediate origin of the apex by localized cell division, leading to overarching of certain parts of the surface. Hairs are produced from the inner surface of the conceptacles and project through the ostiole, a situation similar to that in the Fucales. The large unilocular sporangia containing the zoospores arise successively from cells of the inner lining. The zoospores germinate to form filamentous thalli that produce plurilocular sporangia containing gametes. After fusion, the large macroscopic phase is formed again (Price and Ducker, 1966).

Laminariales

The members of this order are parenchymatous with growth from an intercalary meristem between the stipe and blade. The plants have an alternation of a large sporophyte with a microscopic gametophyte. Sexual reproduction is oogamous. With the exception of *Chorda* (Fig. 21.35) and *Saccorhiza* (Fig. 21.29), the Laminariales lack an eyespot and an associated flagellar swelling in the motile cells (Henry and Cole, 1982; Henry, 1987).

The Laminariales are very large plants that are usually distributed in the colder waters of the world. Many of the genera have sporophytes that

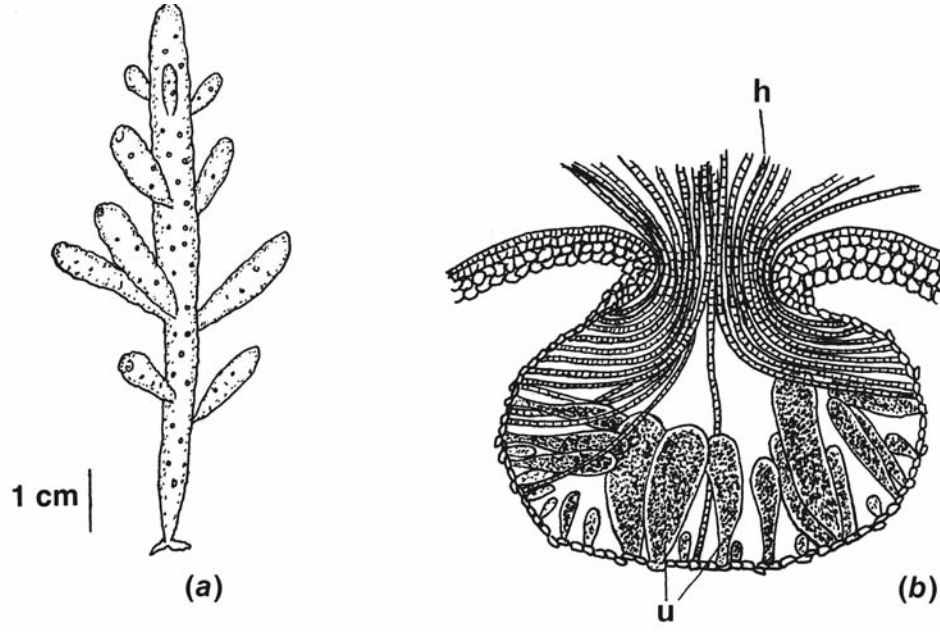


Fig. 21.21 *Splachnidium*. (*a*) Whole plant. (*b*) Section of a conceptacle with hairs (h) and unilocular sporangia (u).

are able to grow vegetatively in warmer waters, but their microscopic gametophytes fail to produce gametes above 10 to 15 °C, thereby preventing the distribution of plants in waters warmer than this (Sjøtun and Schoschina, 2002). The first fossils of Laminariales are dated 16 million years ago and it appears that the order originated about this time in the North Pacific during a strong polar cooling trend (Estes and Steinberg, 1988; Saunders and Dreuhl, 1992).

Morphology and anatomy

With the exception of the genus *Chorda* (Fig. 21.35), the sporophytes are differentiated into a holdfast, stipe, and blade (Figs. 21.27, 21.29). An intercalary meristem between the stipe and blade adds tissue to both. The blade length often remains about the same because the increase in length at the base often equals the loss by abrasion at the apex. The blades of most genera last for one year, but in many cases the stipe and the base of the blade are perennial. Examples of recorded life spans for kelps are 13 years for *Pterygophora californica* (Fig. 21.22), 11 to 18 years for *Laminaria hyperborea* (Fig. 21.30(*d*)), and 4 to 8 years for *Macrocystis pyrifera* (Fig. 21.32) (Lobban, 1978). The most frequent cause of death appears to be the tearing of the alga from the rocks by storms. The blades usually stop growing in late summer and begin to disintegrate in the autumn after the plant has discharged its zoospores. The sporophytes are very durable and will withstand a great deal of stress without breaking. When members of the order are washed up on the beach, the plant is usually intact, with the haptera firmly attached to a stone that has come loose from the bottom. The haptera accomplish their firm attachment to the substratum by the growth of rhizoidal cells from the outer meristoderm cells (Tovey and Moss, 1978). These rhizoidal cells fill every microscopic crevice of the substratum until an exact profile of the substratum is built up. Mucilage is also secreted by the cells. The haptera grow downward, not in response to gravity but because they are negatively phototropic, growing away from light (Buggeln, 1974).

There are three different tissues in the sporophyte: the central medulla, the cortex, and the

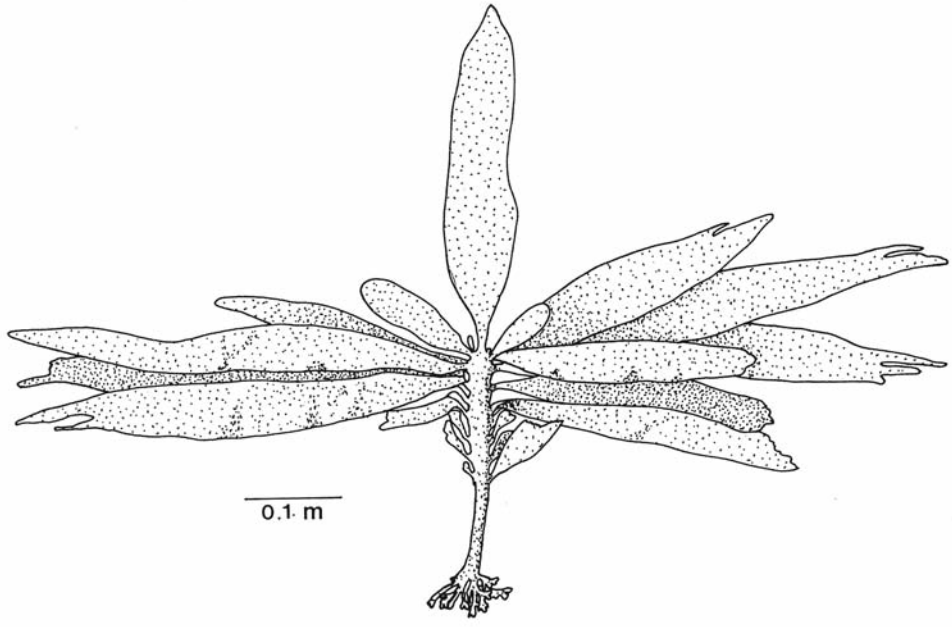


Fig. 21.22 A small plant of *Pterygophora californica*. (After Smith, 1969.)

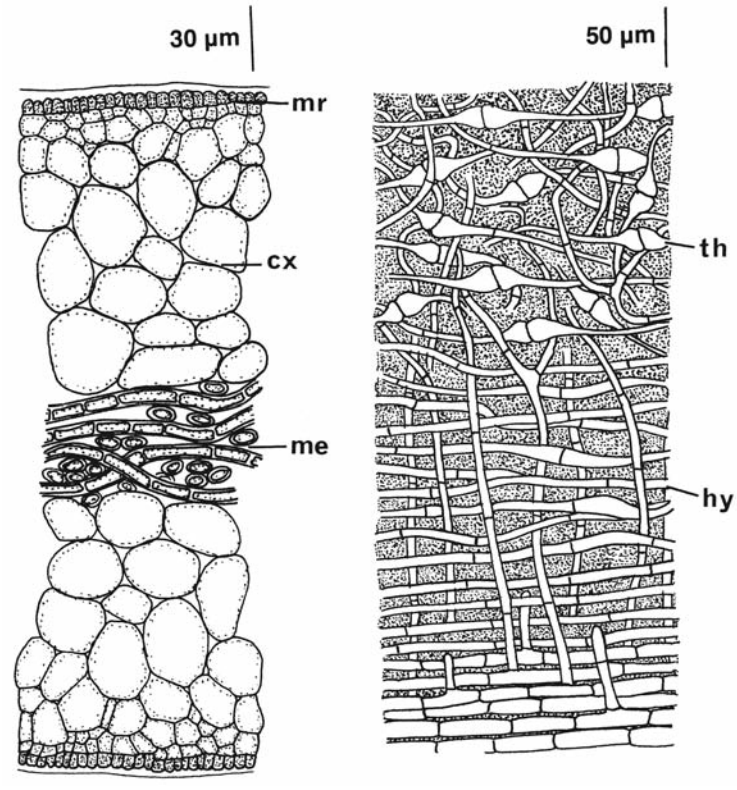


Fig. 21.23 Sections of lamina (*left*) and the central portion of a stipe (*right*) of a member of the Laminariales. (cx) Cortex; (hy) hyphae; (me) medulla; (mr) meristoderm; (th) trumpet hyphae.

epidermis (Figs. 21.23, 21.25). The haptera lacks a medulla, but all three tissues are present in the stipe and blade. The stipe and blade have the same anatomy, the only difference being the cylindrical to elliptical shape of the stipe and the flattened shape of the blade. At the thallus surface are the photosynthetic, meristematic cells of the meristoderm, which add to the girth of the organ (Fig. 21.23). The meristoderm is composed of small cells that cut off daughter cells to the inside, which in turn form the cells of the outer cortex. The meristoderm is usually covered with a layer of mucilage. The meristoderm in the blade is active throughout the life of the blade, dividing primarily periclinically. In the stipe of some genera (e.g., *Laminaria*), the meristematic activity is transferred to a cortical layer at a depth of four to eight cells beneath the surface, with the result that the tissue to the outside is shed as the stipe increases in width.

Inside the meristoderm are the larger cells of the inner and outer cortex followed by the tangled elongate cells that make up the medulla. The outer cortex differentiates cells to the inner cortex, whereas the inner cortex differentiates cells to the medulla. The cells of the inner cortex and medulla often form cross connections between adjacent cells (Fig. 21.24(*c*)). In their formation, two adjacent parent cells cut off small cells that elongate toward each other. When they meet, the end walls dissolve, and the cells are continuous. Another type of cells are the **hyphae**, which originate as outgrowths of cells of the cortex and develop into slender, often branched cells of considerable length that grow into the mucilage of the medulla. The medullary cells are in longitudinal rows; and, because they do not have the ability to divide after they are formed, they are drawn out into long cells by the elongation of the thallus from expansion of cells and the meristematic activity of the meristoderm. These medullary elements are often called **trumpet hyphae** because as they are drawn out, the centers become constricted whereas the septal

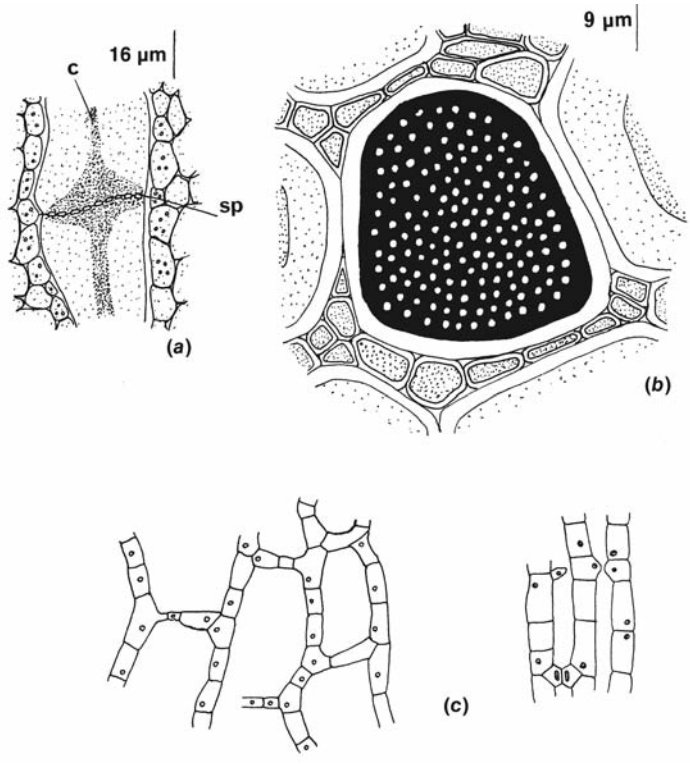


Fig. 21.24 (*a*), (*b*) Sections of a sieve cell from the medulla of an organism in the Laminariales. The sieve plate (sp) has pores with associated callose (c). (*c*) Cells of the inner cortex and medulla with cross connections. ((*a*), (*b*) after Scagel, 1971.)

areas maintain their original diameter (Figs. 21.23, 21.24(*a*), (*b*), 21.25). Another name for trumpet hyphae is **sieve cells** because there are sieve plates with pores separating the cells. The pores of the sieve plates appear to have evolved from plasmodesmata, which are common in other Phaeophyceae.

Within the Laminariales there is an evolutionary development of sieve cells (Sideman and Scheirer, 1977). In *Laminaria*, the sieve plates have pores ranging from 0.06 to 0.09 µm in diameter; no **callose** associated with the pores; and nuclei, vacuoles, and mitochondria in the sieve cells. As evolution proceeded through *Alaria* (Fig. 21.39) and *Nereocystis* (Fig. 21.38) to *Macrocystis* (Fig. 21.32), the pores in the sieve plates became larger, callose became associated with the pores, and the cells lost organelles. *Macrocystis* has sieve cells with 2.4- to 6.0-µm pores, callose associated with the pores, and only mitochondria in the cells. The sieve cells of *Macrocystis* differ from sieve elements of the angiosperms in that there are no companion cells present, and there is no large central vacuole. The presence of large numbers of mitochondria in sieve cells of *Macrocystis* probably reflects the lack of a companion cell, with the mitochondria producing the energy necessary for cell processes. In the Laminariales, there is active transport of the products of photosynthesis through the sieve cells, mostly as mannitol (Parker, 1965). The rate at which the mannitol moves depends on the type of sieve cell present (Lüning et al., 1972). In the well-developed sieve cells of *Macrocystis*, the organic products move as fast as 65 to 78 cm hour^{-1}, both toward the base for storage in the basal region and toward the apex to provide the rapidly growing apex with substrates (Sargent and Lantrip, 1952; Parker, 1963, 1965). In *Laminaria* and *Saccorhiza*, with their less developed sieve walls, the rate of transport is about five times slower than in *Macrocystis* (Cabello-Pasini and Alberte, 2001).

In the stipes and blades of some of the Laminariales, there is an interconnected system of mucilage canals in the cortex (Grenville et al., 1982) (Figs. 21.25, 21.26). In *Laminaria saccharina* and *L. hyperborea*, these mucilage canals are lined

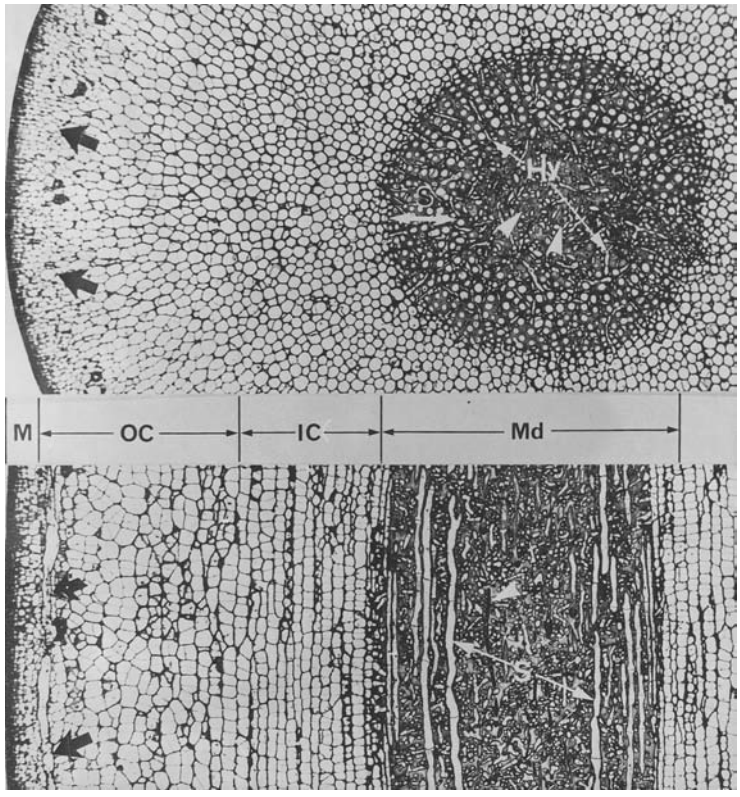


Fig. 21.25 Cross (*upper*) and nearly radial longitudinal (*lower*) sections through a stipe of *Macrocystis integrifolia*, showing the anatomy of a member of the Laminariales. The mucilage ducts (black arrows) are arranged in a ring at the fringe of the outer cortex (OC). Note the sieve elements in radial rows (S) in the outer region of the medulla and the obliterated sieve elements (white arrowheads) in the center of the medulla. Hyphal cells (Hy) anastomose through the medulla. (IC) Inner cortex; (M) meristoderm; (Md) medulla; (OC) outer cortex. (From Shih et al., 1983.)

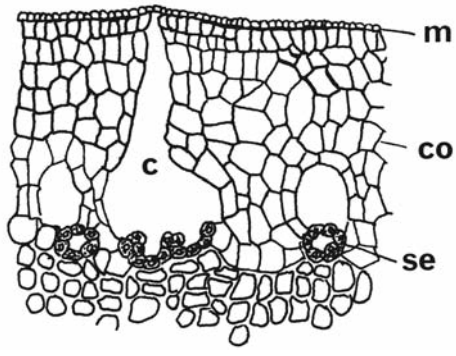


Fig. 21.26 *Laminaria cloustoni*, transverse section of a stipe showing mucilage canals (c) and secretory cells (se). (m) Meristoderm; (co) cortex. (After Guignard, 1892.)

by secretory cells which are linked by plasmodesmata (Evans et al., 1973). The secretory cells produce and secrete fucoidin into the canal, from which it goes to the outside of the thallus. These are the only cells that secrete fucoidin in the thallus, and, like secretory cells in other organisms, they have numerous large Golgi bodies surrounding the nucleus.

Life cycle

The life cycle of a member of the Laminariales involves the alternation of a large sporophyte with a microscopic gametophyte (Figs. 21.27, 21.29).

The intercalary meristem between the stipe and the blade secretes chemicals that travel distally to inhibit the formation of reproductive sori on the sporophyte (Lüning et al., 2000). The production of the inhibitory chemicals is greatest during the rapid growth in the first part of the year. Activity of the intercalary meristem and growth slows as the season progresses resulting in decreased production of the chemical inhibitors. The level of inhibitory substances decreases to a point where the formation of sori occurs on the sporophyte in the second part of the growing season. The sori contain unilocular sporangia intermingled with paraphyses. First, a superficial cell widens to form a basal cell and a paraphysis. The basal cell widens, and paraphysis elongates. The upper end of the

paraphysis becomes swollen and mucilaginous, forming a covering over the basal cells. The basal cell now produces a unilocular sporangium next to the paraphysis. Thirty-two (*Laminaria*) to 128 (*Saccorhiza*) haploid zoospores are formed in the unilocular sporangium (Motomura et al., 1997), and the zoospores are released through the thickened apex of the sporangium. The zoospores have a single chloroplast (in *Chorda*, they have a number of chloroplasts) and may or may not have an eyespot (Evans, 1966). The zoospores are positively chemotactic towards nutrients (Amsler and Neushel, 1989) and can be transported for several kilometers (Reed et al., 1988) during the 48 hours that they swim about. After settling, the zoospores produce the gametophytes. The gametophytes in most of the Laminariales are dioecious, with separate male and female plants. However, *Chorda* (Fig. 21.35) is monoecious, and there are conflicting reports as to whether the gametophytes of *Saccorhiza* (Fig. 21.29) are monoecious or dioecious (Norton, 1972; Henry, 1987). In *Laminaria* (Fig. 21.27), Evans (1965) showed that there is probably an X/Y sex-determining mechanism, with segregation taking place at the meiotic division in the unilocular sporangium. The zoospores contain glycoproteins in small vesicles in the peripheral cytoplasm that are released when the zoospores settle (Oliveira et al., 1980). These glycoproteins adhere the cells to the substratum. The settled zoospore secretes a thin wall around itself, with a slender germ tube emerging; the protoplasm of the zoospore moves out of the original spore and into a swelling at the tip of the germ tube; a wall is formed between the swelling and the original spore; the cell in the swelling now divides to form the gametophyte. It is only at this stage that the female gametophyte looks different from the male. The male gametophyte has smaller cells and is more branched than the female. The male gametophytes produce small colorless antheridia (Fig. 21.28). In the female gametophyte, elongated oogonia are formed that produce a single egg. Under long-day conditions (16 hours light : 8 hours dark), eggs are released during the dark cycle, mostly during the first 30 minutes of darkness (Lüning, 1981). The release is apparently controlled by a circadian rhythm. After the female cell has emerged, the thick plastic edges of the wall contract and form a platform on which the egg remains for some time. The sexual hormone **lamoxirene** is secreted by the eggs as they are released in at least 21 species in the families Laminariaceae, Alariaceae, and Lessoniaceae (Lüning and Müller, 1978; Müller et al., 1979, 1985). Spermatozoids are ejected from the antheridia within a few seconds of exposure to lamoxirene. The spermatozoids are attracted to the eggs where fertilization takes place (Motomura, 1991). The chemical formula of lamoxirene is 1-(1′,2′-*cis*-epoxibut-3′-enyl)-cyclohepta-2,5-diene; it has a molecular weight of 162 and the empirical formula $C_{11}H_{14}O$ (Fig. 21.8) (Marner et al., 1984). The sexual hormones ectocarpene and desmarestene (Fig. 21.8) are also present, but they do not have hormonal activity in *Laminaria* or *Macrocystis*. In the Laminariales, the zygote germinates to form a flat proembryo that subsequently develops into the mature sporophyte.

Environmental conditions, particularly light and temperature, usually control the life cycle in the Laminariales. Sporophytes will normally not grow at temperatures above 18 to 20 °C (Cheng, 1969; Nakahara and Nakamura, 1973), and sori will not be produced at these temperatures. If a mature sorus of *Laminaria* is placed in water at 20 °C, the sporangia cease to discharge zoospores and disintegrate. The gametophytes are also subject to environmental control. Gametophytes will grow for varying periods of time before forming gametangia. In some cases oogonia are produced by the settled zoospore, whereas at other times the gametophyte grows indefinitely without forming gametes. Lüning and Dring (1972, 1975) showed that if gametophytes are grown in red light at 15 °C, they will grow indefinitely without ever becoming fertile. If these gametophytes are subjected to 6 to 12 hours of blue light, they will produce gametes. Also the gametophytes will not produce gametes if the temperature is above 10 to 12 °C (Sundene, 1963; Vadas, 1972; Nakahara and Nakamura, 1973); or if the water has less than 5 μg liter^{-1} of NO_3-N (Hsiao and Druehl, 1973). The gametophytes have the ability to withstand long periods of darkness and then resume growth when light again becomes available (Kain, 1966). Thus in nature the size of the gametophyte and the time of gametogenesis are probably controlled by environmental conditions.

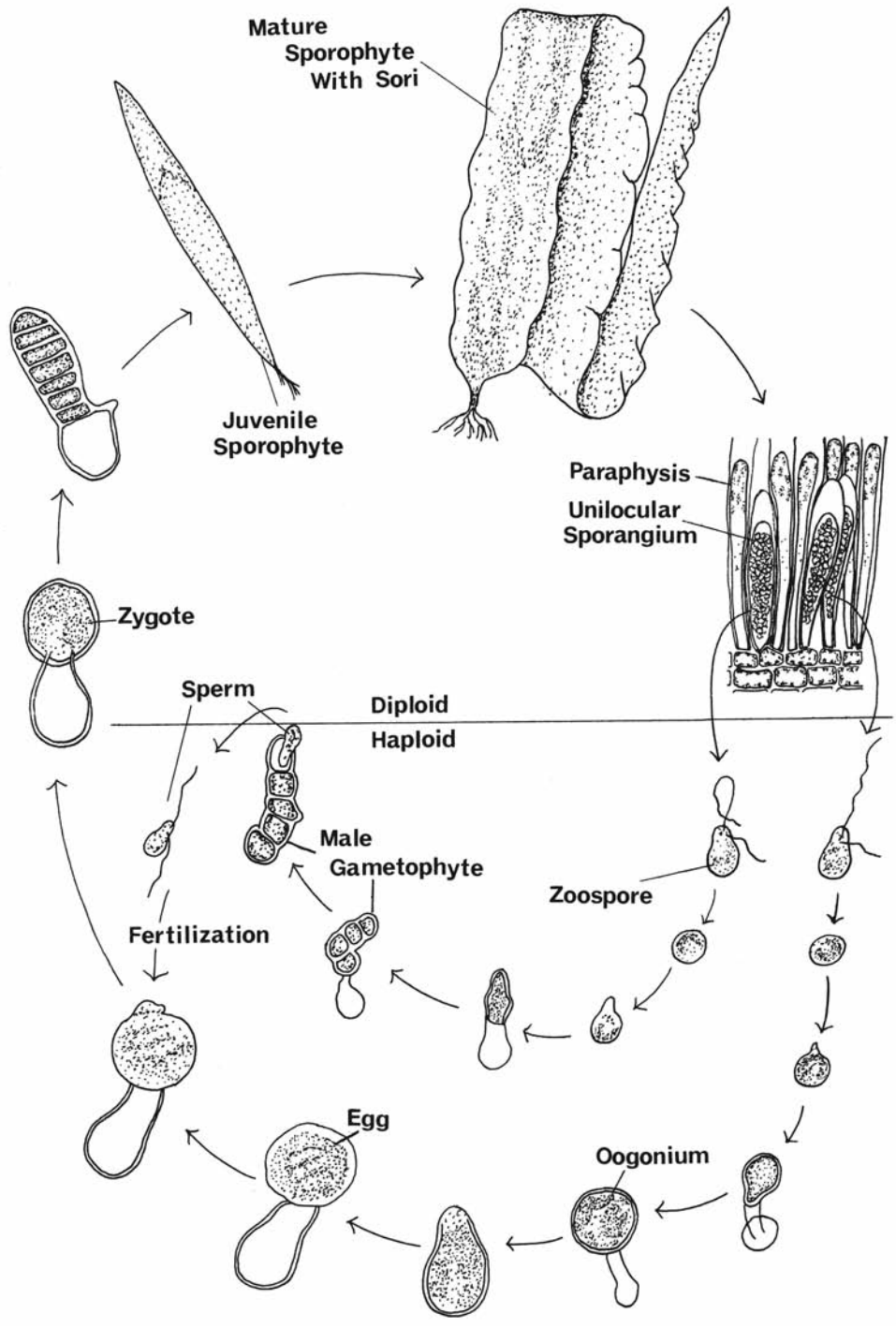


Fig. 21.27 The life cycle of *Laminaria japonica*. (After Cheng, 1969.)

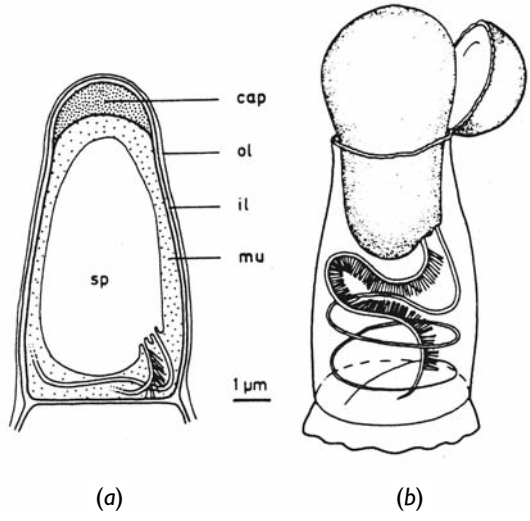


Fig. 21.28 The antheridium of *Laminaria digitata*. (*a*) Mature antheridium. (il) Inner layer of cell wall; (ol) outer layer of cell wall; (mu) mucilage; (sp) spermatozoid. The cap is pushed away and the spermatozoid is forced out of the antheridium. (From Maier, 1982.)

Ecology

Laminaria plants from northern waters are generally much larger with longer stipes and have a greater blade area than those from more southerly waters, a phenomenon that is probably due to their being older plants rather than their having greater growth rates (Larkum, 1972).

Laminaria hyperborea (Fig. 21.30(*d*)) and *L. digitata* (Fig. 21.30(*c*)) form dense underwater forests in the eastern cold temperate northern Atlantic. Similarly, *Laminaria solidungula* produces dense growths in the Alaskan Beaufort Sea. These kelps exhibit a seasonal growth pattern with a phase of fast growth prevailing from early winter to early summer, and a summer and autumn phase with a reduced or complete cessation of growth. These growth patterns are an ecological strategy, whereby storage of photosynthate during the well-lit summer and autumn enables the algae to start growth by remobilization and translocation of stored carbohydrates early in the dark winter when nutrient supply is optimal due to plankton remineralization. This **circannual** (approximately annual) **rhythm** is under endogenous photoperiodic control (Henley and Dunton, 1997; Schaffelke and Lüning, 1994).

Another factor affecting the morphology of the sporophyte is the environment in which the plant is growing. *Saccorhiza polyschides* sporophytes growing in weak current produce curved blades that are heart-shaped (cordate) at their base (Fig. 21.31). These blades lack subdivisions (digits) and are so fragile that they tear under their own weight when removed from the water. In contrast, plants growing in strong current develop very long, flat, tough blades, narrowly triangular (cuneate) at the base and divided into as many as 30 digits. In habitats without current but exposed to wave action, the sporophytes produce short, flat, extremely tough blades with only three to ten digits. Anatomically, the greater toughness of blades is the result of a larger number of cortical cells increasing the thickness of the thallus (Norton and Burrows, 1969). Somewhat similar results with *Laminaria digitata* (Fig. 12.30(*c*)) (Sundene, 1962(*a*)) and *Alaria esculeata* (Fig. 21.39) (Sundene, 1962(*b*)) have been reported.

Many species of *Laminaria*, such as *L. hyperborea* (Fig. 12.30(*d*)), produce very thick stands or forests of sporophytes beneath the low-tide mark. As the depth increases, the plants become sparser, forming an open "park" (Larkum, 1972). *Macrocystis* and *Laminaria* have primary production rates that rank among the highest in the world, reaching an annual net production in the range of 1000 to 2000 g m^{-1} of carbon (Mann and Chapman, 1975). The forests of the giant kelp *Macrocystis pyrifera* (Fig. 21.32) form continuous beds up to 8 km long and 1 km wide along the Pacific Coast of North and South America (Gaines and Roughgarden, 1987). The extent of these forests and the density of plants vary greatly in space and time because of storms (Dayton et al., 1984), herbivores, and predators (Duggins, 1980), and also major current features such as El Niño. The decline in canopy area due to large winter storms of the 1982–83 El Niño was particularly dramatic (Dayton and Tegner, 1984).

These stands of *Macrocystis* and *Laminaria* are often depopulated by storms which dislodge the plants and cast them on the beach. A small mollusc, *Patina pellucida*, frequently browses the holdfast system, thereby weakening the attachment of the plants to the substratum and making

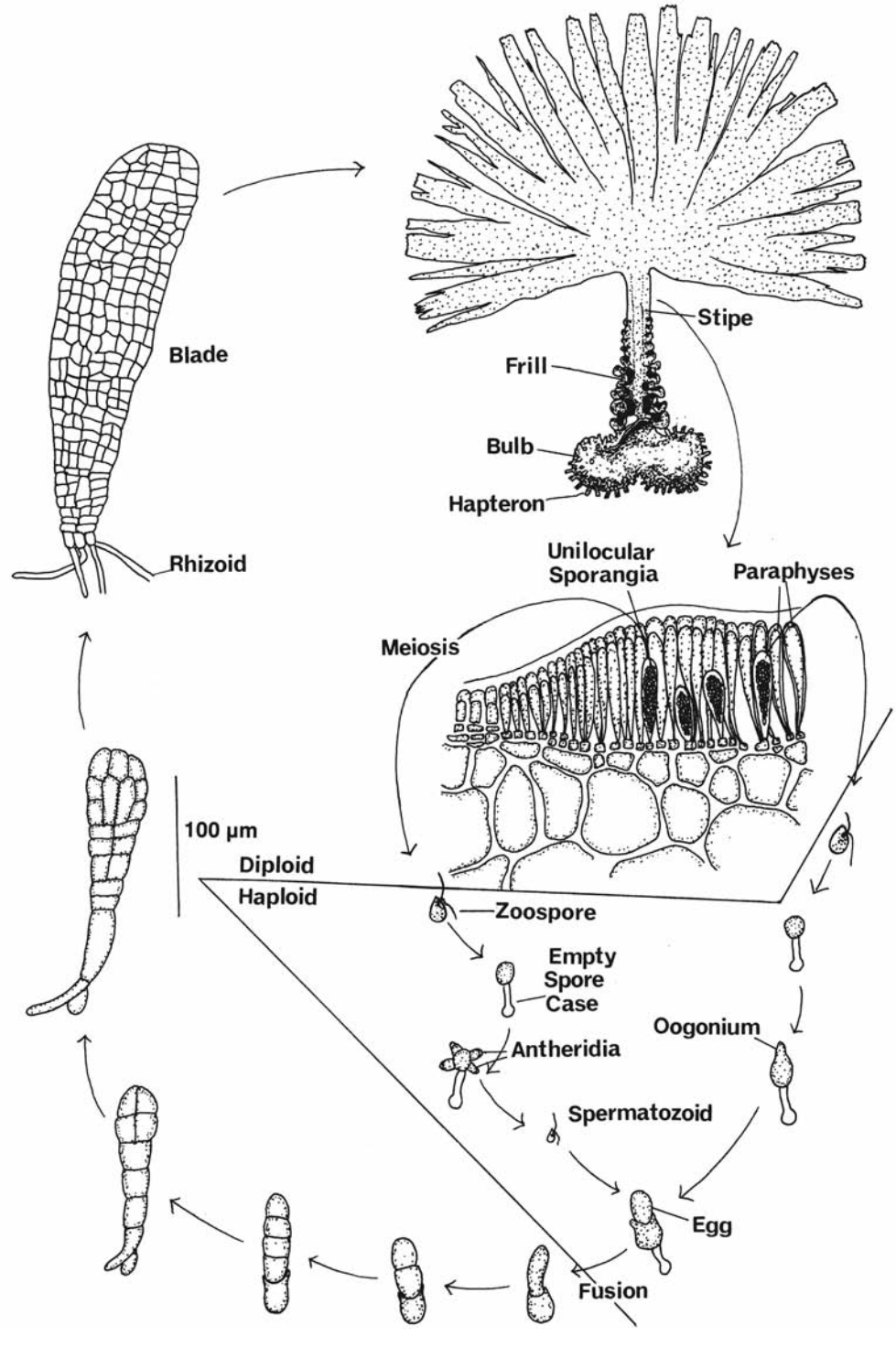


Fig. 21.29 The life cycle of *Saccorhiza* sp. (Adapted from Norton and Burrows, 1969.)

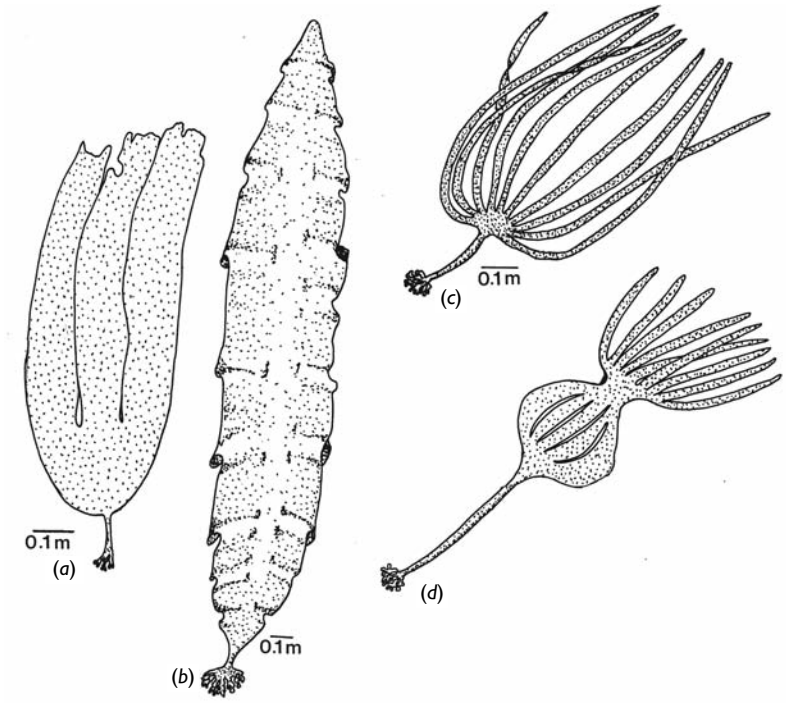


Fig. 21.30 Morphology of some species of *Laminaria*. (*a*) *L. groenlandica*. (*b*) *L. saccharina*. (*c*) *L. digitata*. (*d*) *L. hyperborea*. ((*a*) after Scagel, 1971.)

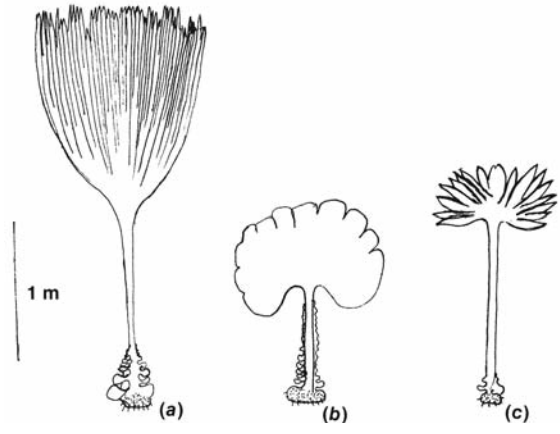


Fig. 21.31 *Saccorhiza polyschides* sporophytes from (*a*) strong current, (*b*) weak current, and (*c*) area with wave action. (After Norton and Burrows, 1969.)

them more susceptible to storm damage. Sea urchins, such as *Paracentrotus lividus* will also eat members of the Laminariales, and one study (Norton, 1978) showed that in their appetites they exhibit a preference for *Saccorhiza polyschides* (Fig. 21.31) to *Laminaria saccharina* (Fig. 21.30(*b*)). In the last two centuries there has been a marked decrease in the shallow-water kelp forests in the North Pacific, due to the near extinction of sea otter. Prior to this, the sea otters ate large quantities of sea urchins that ate the kelp. With their normal predators gone, the sea urchins were free to devastate the kelp forests (Estes and Steinberg, 1988).

The species of Laminariales present in a particular area is determined by the environment of the area. Around Vancouver Island, British Columbia, Druehl (1967) noticed that there were three prevalent forms of *Laminaria: L. saccharina* (Fig. 12.30(*b*)) and a long- and short-stipe form of *L. groenlandica* (Fig. 12.30(*a*)). The two forms of *L. groenlandica* occurred in surf: the long-stipe form in heavy surf, and the short-stipe form in moderate surf. *Laminaria saccharina* was found only in areas that had no surf. In the United Kingdom, Boney (1966) found that *Laminaria hyperborea* (Fig. 12.30(*b*)) dominates in regions of moderate or severe wave action, whereas *L. saccharina* is in sheltered areas.

Even in the long term, populations of *Laminaria* can vary. Walker (1956) reported that a *Laminaria* population off the coast of Scotland varied in density over a 10-year period, and that

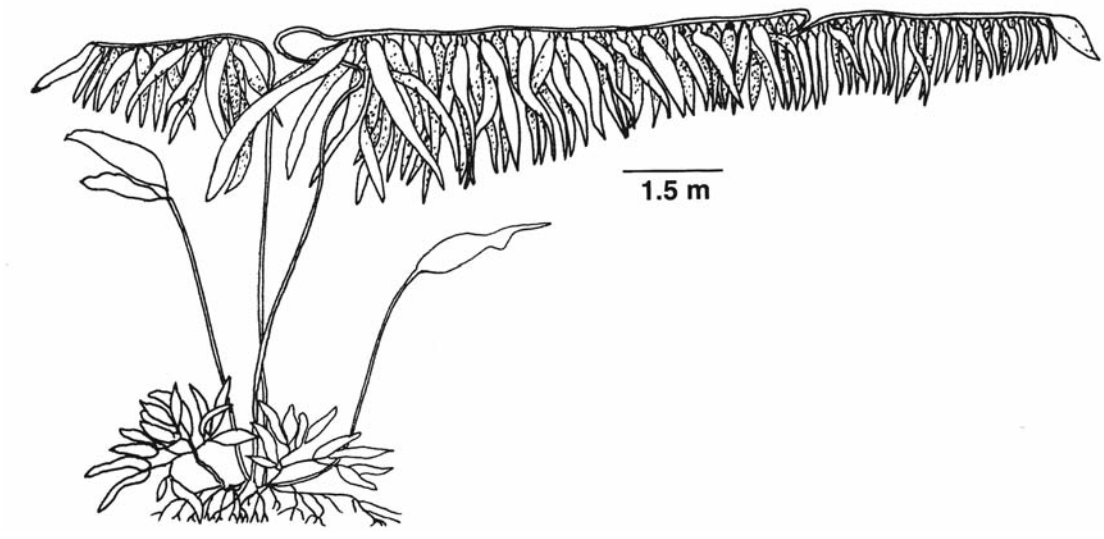


Fig. 21.32 *Macrocystis pyrifera.*

this variation showed a strong correlation with sunspot activity and weather changes.

Concentric rings of dense tissue at the base of the stipe can be used to indicate the age of perennial laminarian algae such as *Laminaria* and *Ecklonia*. Dark rings are produced by cortical meristem during slow growth in autumn and winter, and pale rings are produced in winter and spring (Novaczek, 1981; Klinger and DeWeede, 1988).

Invasion of *Laminaria* thalli by bacteria (such as *Pseudoalteromonas bacteriolytica*) results in degradation of the extracellular polysaccharides of the alga, producing breakdown products such as oligoguluronates. These oligoguluronates initiate a defense mechanism by the *Laminaria*. First there is an increase in respiration of the *Laminaria* cells, followed by the production of hydrogen peroxide (H_2O_2). The concentration of hydrogen peroxide is high enough to kill the invading bacterial cells (Potin et al., 1999).

Metabolism and composition

The proportion of laminarin and mannitol (Fig. 1.7) as dry matter increases steeply during the active photosynthetic period from April to September. On the other hand, the proportion of alginic acid and cellulose in the dry matter decreases during this period. The opposite occurs from October to April, with the relative amounts of alginic acid and cellulose increasing. These variations are much greater in the frond, which has a high growth rate, than in the stipe, where the growth is slower.

Black (1954a) showed that in a mature frond of *L. saccharina* (Fig. 21.30(*b*)), where the part near the tip was 7 months old, there was a marked variation in composition along the length. Near the stipe (i.e., the actively growing region and, therefore, the youngest) there was, on a fresh-weight basis, about 3% mannitol and little or no alginic acid or laminarin. About a third of the way along the frond mannitol was at a maximum of about 6%, with laminarin 2% and alginic acid 2.5%, whereas two-thirds of the way up the frond the mannitol content was only 2%, with laminarin at 6% and alginic acid 4%. Variations in the composition of whole fronds can, therefore, be due largely to changes in proportions of old and new tissues.

According to Percival and McDowell (1967), seasonal variations in the Laminariaceae are consistent with the following observations:

1 Mannitol is the first product of photosynthesis to accumulate in appreciable quantities and is the main carbohydrate in tissues that are increasing by active cell division.
2 During photosynthesis in tissues that are largely growing by cell enlargement, there is

an increase in the proportion of dry solids, made up of mannitol and salts of alginic acid and laminarin. Protein and cellulose are also being synthesized during this period (Pueschel and Karb, 2001). Formation of mannitol and laminarin continues after the other constituents have built up to a constant level in each unit of tissue, thereby increasing the dry solids content and reducing the proportion of alginate, cellulose, and protein on a dry-weight basis. Thus, in late summer, mannitol and laminarin are at high levels and alginic acid, cellulose, and protein are at a minimum on this basis.

3 Laminarin may be formed from mannitol, and during active growth mannitol can be formed faster than its rate of conversion into laminarin so that both substances increase in amount. When growth slows down or stops owing to lack of nutrients, shortage of light, or low temperatures, laminarin increases with loss of mannitol. In late summer, there may be a temporary reduction in mannitol content owing to depletion of phosphate in the water, whereas the laminarin content does not drop until later.

4 During spore formation and periods when respiration is greater than photosynthesis, both laminarin and mannitol are used up. As there is little change in the amounts of other constituents, the proportion of alginate, cellulose, and protein, calculated on a dry-weight basis, increases.

Economic uses

Over 4 million tons of kelps are harvested annually, mainly from mariculture in Asia (China, Japan, Korea) or from natural populations in Europe and North and South America. Overall, the algae in the Laminariales are the largest marine crop in terms of annual landings (Asensi et al., 2001).

The first use of kelps was for kelp ash (Kupper et al., 1998). The brown seaweeds were collected and dried on the shore, and the dried seaweeds were burned in a kiln with the product after burning being a hard cake. The cake constituted the kelp ash. The first use of kelp ash began sometime in the seventeenth century when French peasants used it for glazing pottery and making low-quality glass. This use lasted for about 200 years until the discovery of Barilla soda, made from certain coastal salt-rich plants. This substance produced a better-quality glass, and kelp ash ceased to be used for glass. In 1811, it was discovered that kelp ash contained large amounts of iodine. Using the best seaweeds properly burned, the kelp contained 1.4% to 1.8% iodine, or about 15 kg per ton. At that time iodine was in demand as a cure for goiter, an enlargement of the thyroid gland caused by lack of iodine (even today much of the table salt consumed is iodized, although not from kelp ash). In 1846, there were 20 manufacturers of iodine in Glasgow alone. Subsequently the discovery of mineral deposits of iodine, particularly in Chile, caused a decline in the kelp ash industry.

The current industrial use of kelps is for the alginate that they contain, which has a variety of uses. Algin was first discovered by Stanford in the early 1880s, although it was not obtained in a purified state until 1896 by Krefting. Algin comprises about 10% of the dry weight of the kelps (Smith, 1955), and is mostly the salt of alginic acid. The main area of algin production is the West Coast of the United States, where large stands of *Macrocystis* grow (Fig. 21.32), with the upper portion of the thallus growing on or near the surface of the water. Because of the large numbers of *Macrocystis* and the way they grow, it is possible to harvest the alga by a motor-driven barge equipped with scythe-like blades 3 feet below the surface of the water. The five-person crew of a barge can harvest 300 tons of kelp a day. The development of algin industries in other parts of the world has been hindered by the high cost of harvesting kelps by hand. One of the uses of algin is in the making of ice cream; practically all manufacturers of ice cream add algin before freezing their product. This prevents the water in the ice cream from forming coarse ice crystals, and thus results in a smoother product (Smith, 1955). About half of the consumption of algin is in the making of ice cream and other dairy products. Also, the water-retaining properties of algin are utilized in a variety of ways in the baking industry, including the addition of algin to frostings to prevent undue drying. The colloidal nature of algin makes it useful as a suspending and emulsifying agent. In the rubber

industry, it is used as a creaming and stabilizing agent in the processing of natural and synthetic rubber latex. When added to paints, alginates keep the pigments in suspension and make a product that can be brushed on a surface without showing brush marks. Alginates are also used as suspending agents in a wide variety of pharmaceutical products.

The first medicinal use of brown algae in the literature occurred in Li Shih-Chen's sixteenth-century herbal *Pen Ts'ao Kang Mu* ("Outlines of Chinese Materia Medica"), where brown algae were listed as a cure for goiter by virtue of the iodine they contained. In Europe, goiter was treated by giving kelp pills or kelp ash, which medicinally was known as *Aethiops vegetabilis*. Short pieces of *Laminaria* stipe were used in surgery for opening fistulae (natural openings), because of the swelling properties of the stipe. Brown algae have been recommended as cures for a number of medicinal purposes without any real benefit being derived. For example, the Indians of Sitka, Alaska, used stipes of the bull kelp (*Nereocystis*) as a cure for headaches. The afflicted individual would place the thin end of the stipe in one ear and the bulb or pneumatocyst on a hot stone. Steam would then be generated in the bulb and pass through the hollow stipe and subsequently into the ear of the individual, supposedly clearing up the headache.

Brown seaweeds have also been used as green manure for the soil and as food for animals and humans. The large brown seaweeds are fed to cattle, horses, and sheep in many northern countries, either as a whole food source during the winter or more commonly as a supplement to other foods. Seaweeds are used as a food source by humans, especially in Japan and China. "Kombu" is a food made from members of the Laminariales in Japan. The algae are collected from July to October, are spread out on beaches to dry, and the stipe and hapteron are cut off. The blade is left until a gloss appears on it; then it is sent to the factory. At the factory a number of different forms of kombu are made, one of the most common being green (*ao*) kombu. This is prepared by boiling the alga, dying it green, pressing it, and then shredding it. The shavings are laid out on mats, dried, and packaged. This green kombu can be boiled with meat, fish, and soups, or it can be used as a vegetable. In mainland China, *Laminaria*, known as "haidai" (sea belt), has been widely used as a food and medicine for over 1500 years. When properly prepared, especially if cooked with pork and soybean sauce, it is an inexpensive dish. It is especially popular during the season when green vegetables are not readily available. Every kilogram of dried kelp can produce 262 kcal of energy plus a number of important vitamins and minerals (Cheng, 1969; Tseng, 1981).

Naturally occurring populations of Laminariales usually serve as a source of algae. The only exception to this is in mainland China where in 1946, following the evacuation of the Japanese, the culture of kelps on rafts was initiated (Fig. 21.33). The first step in the growing of kelps is the placing of short bamboo splint ladders in the sea, hanging from rafts in late autumn. Zoospores settle on the splints and form gametophytes and gametes, with the zygotes germinating to form young sporophytes. By January, the young sporophytes are removed from the splints and transferred to ropes that make up the rafts. The most popular type of raft is the single-line bamboo tube raft (Fig. 21.33). A typical raft is constructed by tying bamboo end to end in a single line to a rope 60 m long. This floating raft is anchored at each end by a rope, which is driven into the sea bottom. On each raft are hung earthenware jars containing ammonium nitrate, which seeps through the jars, thereby fertilizing the surrounding water. Young sporophytes averaging 10 cm in length are attached to the ropes by inserting the basal end of the stipe through the strands of the rope. The lines are then hung in the water attached to the bamboo tubes. With proper care, sporophytes may reach 3 m or more in length within 4 to 5 months, and are then harvested (Cheng, 1969) (Fig. 21.34).

Classification

The Laminariales are divided into four families:

Family 1	Chordaceae: sporophyte hollow, whip-like, and not differentiated into a stipe and blade.
Family 2	Laminariaceae: transition zone with intercalary meristem not subdivided

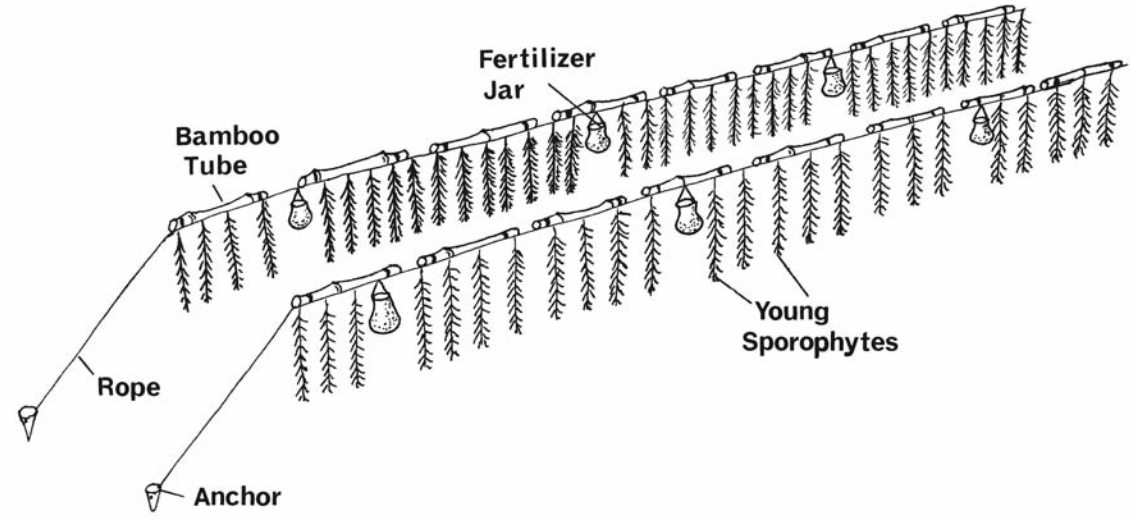


Fig. 21.33 Single-line bamboo rafts used for kelp cultivation in mainland China. The porous earthenware jars are filled with fertilizer that seeps out into the ocean. (After Cheng, 1969.)



Fig. 21.34 Harvesting *Laminaria* grown on rafts in mainland China. (From Cheng, 1969.)

so that there is a simple primary stipe; sori not on special organs.

Family 3 Lessoniaceae: transition zone with intercalary meristem subdivided so that there are a number of secondary stipes in addition to the primary stipe.

Family 4 Alariaceae: sori borne on special sporophylls.

CHORDACEAE

This family has a single genus, *Chorda* (Fig. 21.35) which is not closely related to the rest of the algae in the order (Draisma et al., 2001). The plant is an annual, hollow, whip-like alga that grows in the sublittoral regions of the Northern Hemisphere. The cylindrical sporophyte is long (up to 2.6 m) but seldom wider than 1 cm. The genus differs from other Laminariales in two characteristics: the sporophyte has a meristematic zone beneath the apex, and the young sporophyte has one or more apical hairs. In both of these characteristics, the genus resembles some members of the Dictyosiphonaceae of the Ectocarpales, such as *Dictyosiphon*. *Chorda* has characteristics that might be considered intermediate between the Ectocarpales and the Laminariales.

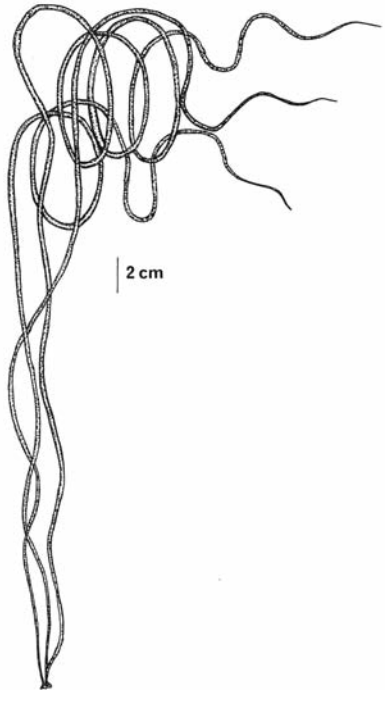


Fig. 21.35 *Chorda filum.*

Chorda has a life cycle similar to *Laminaria* (Fig. 21.27) except that the gametophyte is monoecious (oogonia and antheridia on the same thallus) (Maier, 1984). Freshly released eggs give off a sexual hormone that causes explosive discharge of spermatozoids from the antheridia and subsequent chemotaxis toward the egg (Maier et al., 1984; Müller et al., 1985).

LAMINARIACEAE

In this family the sporophyte is divided into a holdfast, stipe, and blade. The blade is produced whole by the intercalary meristem even though it may later fragment into a number of digits. *Laminaria* (Fig. 21.27) has already been discussed. *Saccorhiza bulbosa* (Fig. 21.29) is an annual found on the Atlantic shores of Europe and North Africa. The mature sporophyte has a divided (digitate) blade, sometimes exceeding 2 m in length, borne at the end of a flattened stipe. The stipe is spirally twisted in its lower portion, and below the twist there is a large inverted bell-shaped outgrowth that covers the holdfast and the basal part of the stipe. The bell develops in the young plant from the intercalary basal meristem, and the stipe subsequently develops undulating wings. The blades have cryptostomata with hairs.

LESSONIACEAE

Although any splitting of the blade in the Laminariaceae does not extend down into the basal intercalary meristem, in the Lessoniaceae it does. This means that the secondary blades produced have their own secondary stipes.

Lessonia nigrescens, a species from the Southern Hemisphere, has entire young blades that soon develop a median split, resulting in a blade with two segments, each with its own secondary stipe (Fig. 21.36). The blades continue to split until the mature, much-divided sporophyte is formed. *Postelsia palmaeformis* (sea palm) has a short thick primary stipe that supports the secondary blades and stipes (Fig. 21.37). The plants occur on the Pacific Coast of North America in habitats exposed to the full violence of the waves.

The largest of the algae in the family are *Nereocystis* (Fig. 21.38), *Pelagophycus*, and *Macrocystis*

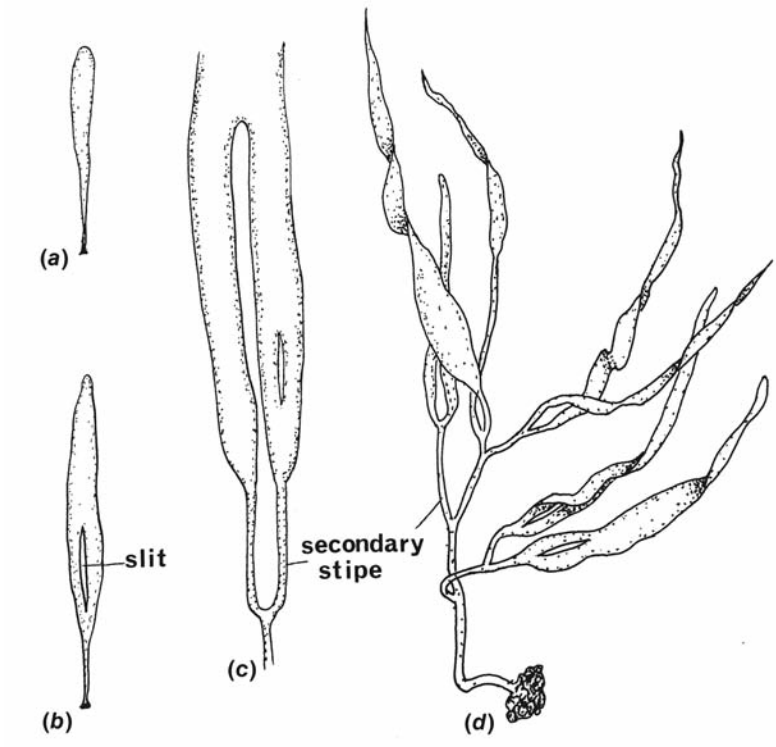


Fig. 21.36 *Lessonia nigrescens.* (*a*)–(*c*) Successive stages in the splitting of the blade to produce secondary stipes and secondary blades. (*d*) Mature plant.

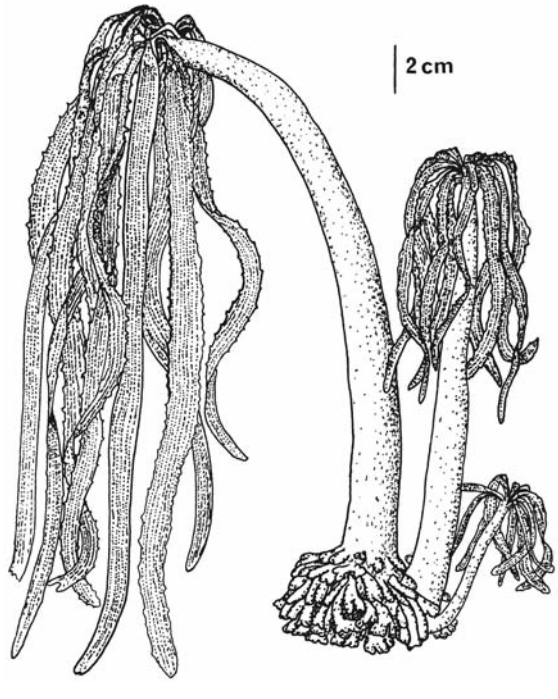


Fig. 21.37 *Postelsia palmaeformis.*

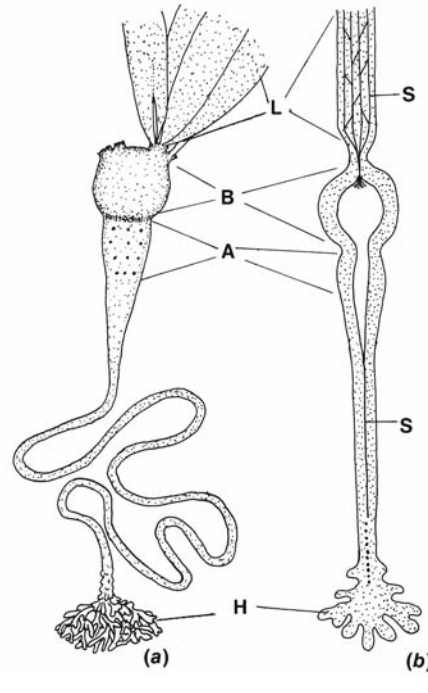


Fig. 21.38 Sporophyte of *Nereocystis.* (*a*) Whole plant. (*b*) Semidiagrammatic longitudinal section. (A) Apophysis of stipe; (B) gas-filled bulb of stipe; (H) holdfast; (L) lamina; (S) sieve filaments. (After Nicholson, 1970.)

(Fig. 21.32). *Nereocystis luetkeana* (bull kelp) has a tough whip-like stipe up to 25 m long that terminates in a large air bladder (Fig. 21.38). This air bladder supports secondary stipes and blades that hang down from the surface of the sea. The remarkable aspect of this large seaweed is that it is an annual plant that can grow as much as 6 cm a day. *Julescraneia grandicornis* is a fossil alga from Miocene diatomite of California that resembles *Nereocystis* (Parker and Dawson, 1966). *Macrocystis* (Fig. 21.32) may grow up to 50 m in length and has a life of 5 years, although the individual secondary blades have a life of only 6 months. As in *Lessonia* there is successive splitting of the primary blade, but in *Macrocystis* the growth of one of the two segments is arrested. This leads to a long curtain type of thallus. Each of the segments has an air bladder at the base of the secondary stipe, allowing the secondary blade to hang down from the surface of the water.

ALARIACEAE

The sporophytes in this family have the sori formed on special sporophylls. *Alaria* (Fig. 21.39) has a lamina with a wavy margin and a midrib. The short stipe produces thick tongue-shaped sporophylls in the summer, which, after maturation of the sori, are shed during autumn and winter, leaving scars on the stipe. During the winter the blade wears down to the basal meristematic zone, and a new blade is produced the following season.

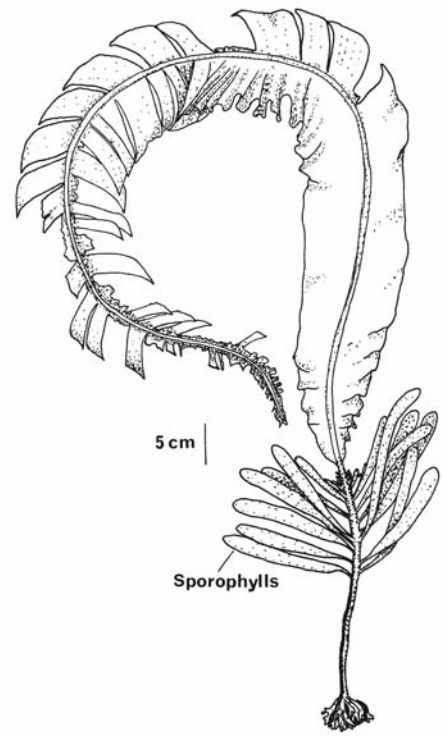


Fig. 21.39 *Alaria esculenta*. The old distal part of the blade is partly eroded away, and the sporophylls are fully developed. (After Taylor, 1957.)

Fucales

The organisms in this order are parenchymatous with growth from an apical cell. The haploid generation is reduced to the egg and sperm, with the remainder of the life cycle being diploid. The gametes are borne in special cavities, the **conceptacles**, and gametic union is always oogamous. Conceptacles may be scattered over the surface of the thallus, but more frequently they are limited to the inflated tips of special branches, the **receptacles**. The Fucales are worldwide in distribution, but those of the Arctic and north temperate seas differ considerably from those of the Antarctic and south temperate waters, *Fucus* (Fig. 21.40) is a common genus in northern waters, whereas in tropical and subtropical waters *Sargassum* (Fig. 21.51) is present. In Australian waters, *Cystophora* is a predominant member of the flora, with the large *Durvillea* being common in sub-Antarctic waters.

Gene sequencing has revealed that the Fucales diverged early from the remainder of the Phaeophyceae (Draisma et al., 2001).

Morphology and anatomy

The genus *Fucus* will be used as the representative genus in this order (Fig. 21.40). The thallus is much branched and is supported by a short narrow stalk that is attached to a discoid holdfast. The branching is dichotomous, with each flattened segment having a prominent central midrib surrounded on both sides by a narrower wing. The wings usually bear scattered **cryptoblasts**, which are basically sterile conceptacles with large numbers of hairs, that facilitate the uptake of nutrients from the seawater (Hurd et al., 1993). At certain times of the year, the tips of the branches

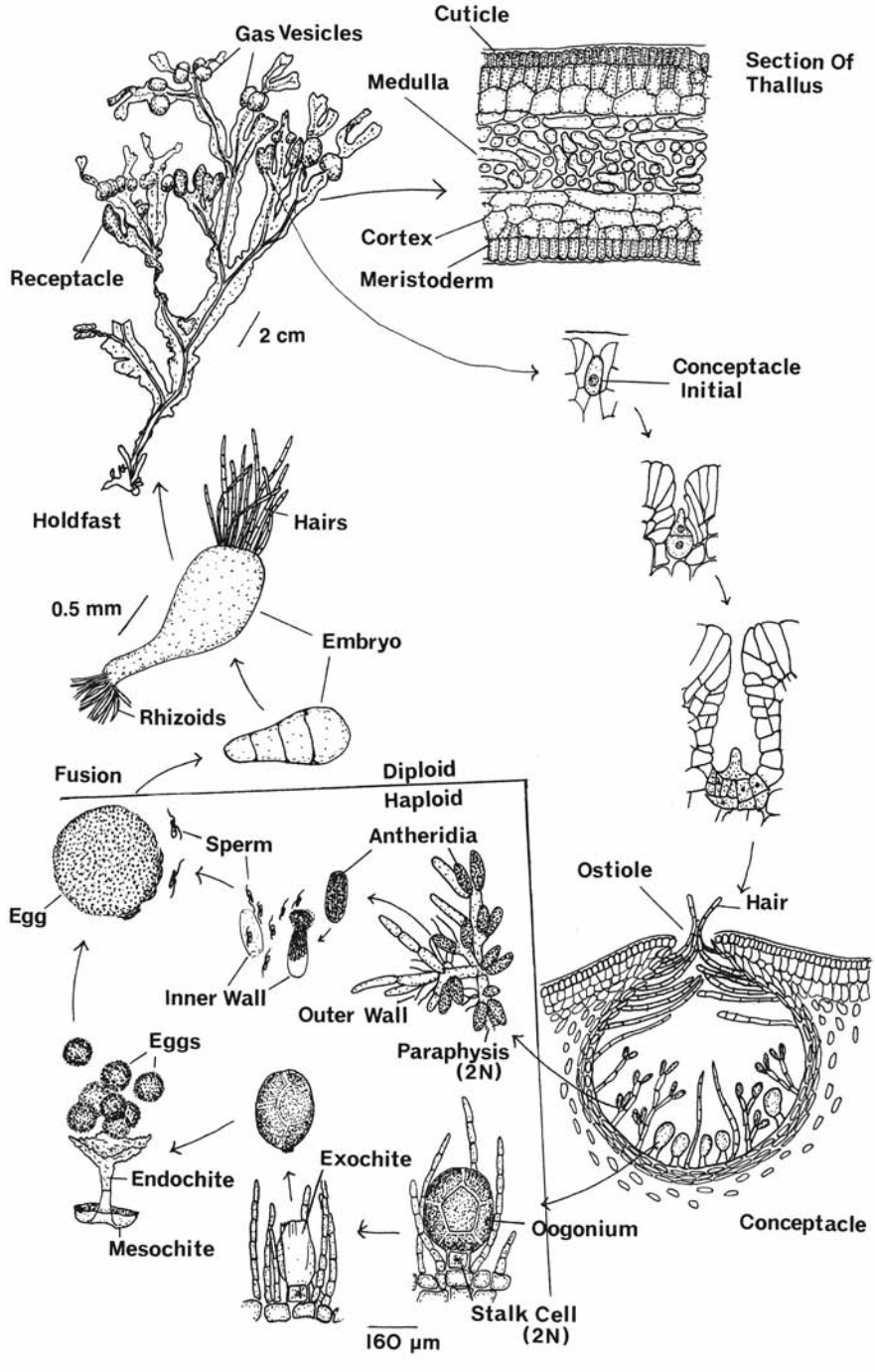


Fig. 21.40 The life cycle of *Fucus* sp. (*F. vesiculosus* and *F. serratus*). (Adapted from Thuret, 1854; Oltmanns, 1889; Nienburg, 1931; Taylor, 1957.)

are swollen into receptacles that contain the fertile conceptacles. The inflation of the receptacles is due to the production of a large amount of mucilage.

Each branch has an apical cell at its apex (Fig. 21.41). The apical cell divides several times a year, resulting in the formation of a dichotomy or fork, with one arm of the fork being longer than the other. The apical cell in mature Fucaceae is a four-sided pyramid with a flattened base. In the other families and in young Fucaceae, the apical cell is a three-sided pyramid. According to Moss (1967), the apical cell itself does not divide (except in the formation of forks), and instead stimulates the cells around it to divide. Thus a meristematic zone extends beneath and around the sides of the apical cell and is called the **promeristem**. The cells of the **promeristem**, similar to meristematic cells in other organisms, are very small. At the sides of the promeristem the cells enlarge and divide only transversely, yielding the flattened wings. Mucilage is deposited between the derivatives of the promeristem, causing the files of cells to separate, remaining in contact only where there are pits. The apical cell shows apical dominance, inhibiting the development of laterals beneath it (Moss, 1965, 1970). If the apical cell is destroyed, then the underlying lateral will develop into a new apical cell.

The second meristem in the apical area of the thallus is the **meristoderm** or outer row of cells derived from the promeristem. This is a closely packed layer of brick-shaped cells that divides anticlinally at first and then periclinally to produce new tissues to the inside.

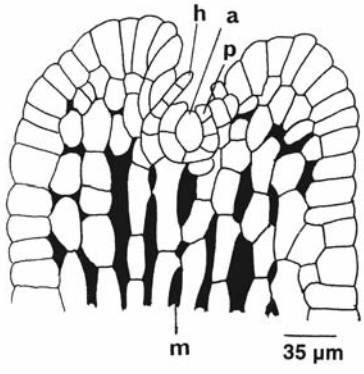


Fig. 21.41 Upper portion of a mature juvenile thallus of *Fucus*, showing the apical depression, apical cell (a), remnants of terminal hairs (h), the promeristem (p), and the medulla (m). (After Oltmanns, 1889.)

The anatomy of the Fucales is similar to that of the Laminariales, with a mucilaginous cuticle covering the epidermal layer of cells (Figs. 21.41, 21.42). Inside this is the cortex with the medulla in the center. Hyphae are produced by the inner cortical cells, but there are no trumpet hyphae present. There is an orientation of organelles within the epidermal cells. They have an outer layer of alginic acid vesicles with a basal nucleus and chloroplasts (Fulcher and McCully, 1969; Rawlence, 1973). The cap of alginic acid vesicles may shield the chloroplasts and nucleus from intense illumination, especially at low tide when the plants are usually exposed. The organelles of the cortical cells are arranged just the reverse of the epidermal cells, having an outer layer of chloroplasts. The chloroplasts of the medullary and hyphal cells are much reduced.

Like the Laminariales, the Fucales are able to translocate organic materials (Floc'h and Penot, 1972). Mannitol (Fig. 1.7) is the form of photosynthate translocated. The growing apex acts as a sink, with the mannitol translocated to the growing apex from the blades of the alga (Diouris, 1989). Structurally, the Fucales have a system of conducting elements very similar to the Laminariales. In the Fucales, the sieve elements run from the apical meristem to the base of the plant. The medullary elements have sieve plates (1 μm thick) at their ends. The pores in the sieve plates enable a continuous system of cytoplasm for the translocation of materials both longitudinally and transversely through the cross connections. The pores in the sieve plates are 0.1 μm^2 or less, which makes them smaller than the pores reported in the Laminariales (*Alaria* has pores ranging in size from 0.1 to 0.3 μm^2) (Moss, 1983).

Gas vesicles (air bladders) (Fig. 21.40) originate not far from the apex as a result of growth of the surface layers of cells accompanied by an increase in the thickness of the cortex. This leads to the rupture of the medulla, the remnants of which are commonly around the edge of the hollow. The air bladders are apparently filled with gases similar to those in the atmosphere.



Fig. 21.42 *Fucus virsoides.* Transverse section of a mature thallus. A mucilaginous cuticle covers the outer epidermal layer in the cortex with the medulla in the center. (From Mariani et al., 1985.)

Life cycle

Fucus will again be used as an example of a typical member of the Fucales (Fig. 21.40). The gametes are borne in conceptacles (Fig. 21.43) that are similar to the cryptoblasts except that the colorless hairs are restricted to a small area near the aperture. The wall of the conceptacle is lined with flat cells that bear branched paraphyses with few chloroplasts. The conceptacles originate from an initial that is a superficial cell of the thallus. The initial divides into an outer tongue cell and an inner basal cell. The tongue cell either degenerates or does not contribute to the development of the conceptacle. The basal cell then divides to form the floor of the conceptacle. At the same time, the cells surrounding the original initial grow and divide so that the derivatives of the initial cell become open to the outside. The mature conceptacle consequently has cells lining the floor derived from the conceptular initial and cells lining the walls derived from the cells surrounding the original initial.

The gametes are released into the seawater during daytime and at times when there is little water motion, reducing the amount of gamete dilution, and ensuring high rates of fertilization (usually about 95%) (Pearson and Brawley, 1998; Ladah et al., 2003). Tide-pool populations of fucoids release their gametes during low tide when the tide pools are isolated and calm. Intertidal populations release their gametes at slack high tide when the water is calmest.

The plants are either monoecious or dioecious, and in the monoecious forms the antheridia and oogonia can be in the same or different conceptacles. The antheridia are usually formed on paraphyses. Antheridial parent cells are distinguished by dense cytoplasm with few vacuoles, a large central vacuole, and chloroplasts with only a few thylakoids (Berkaloff and Rousseau, 1979). Following meiosis, which occurs during the first two divisions of the primary nucleus, the nuclei undergo four mitoses. Mature antheridia (Fig. 21.43(*c*), (*d*)) thus contain 64 nuclei, each of which becomes incorporated into a spermatozoid. Cells in the receptacle release potassium and chloride ions into the mucilage of the conceptacle. This results in swelling of the mucilage that carries the antheridia (or oogonia in the female conceptacle) out of the conceptacle into the seawater (Speransky et al., 2001). The wall of the antheridium is composed of two layers. At liberation, the outer wall ruptures, releasing the inner wall containing the spermatozoids and mucilage. This packet passes out of the conceptacle and into the sea, where the inner wall gelatinizes at one or both ends, releasing the spermatozoids.

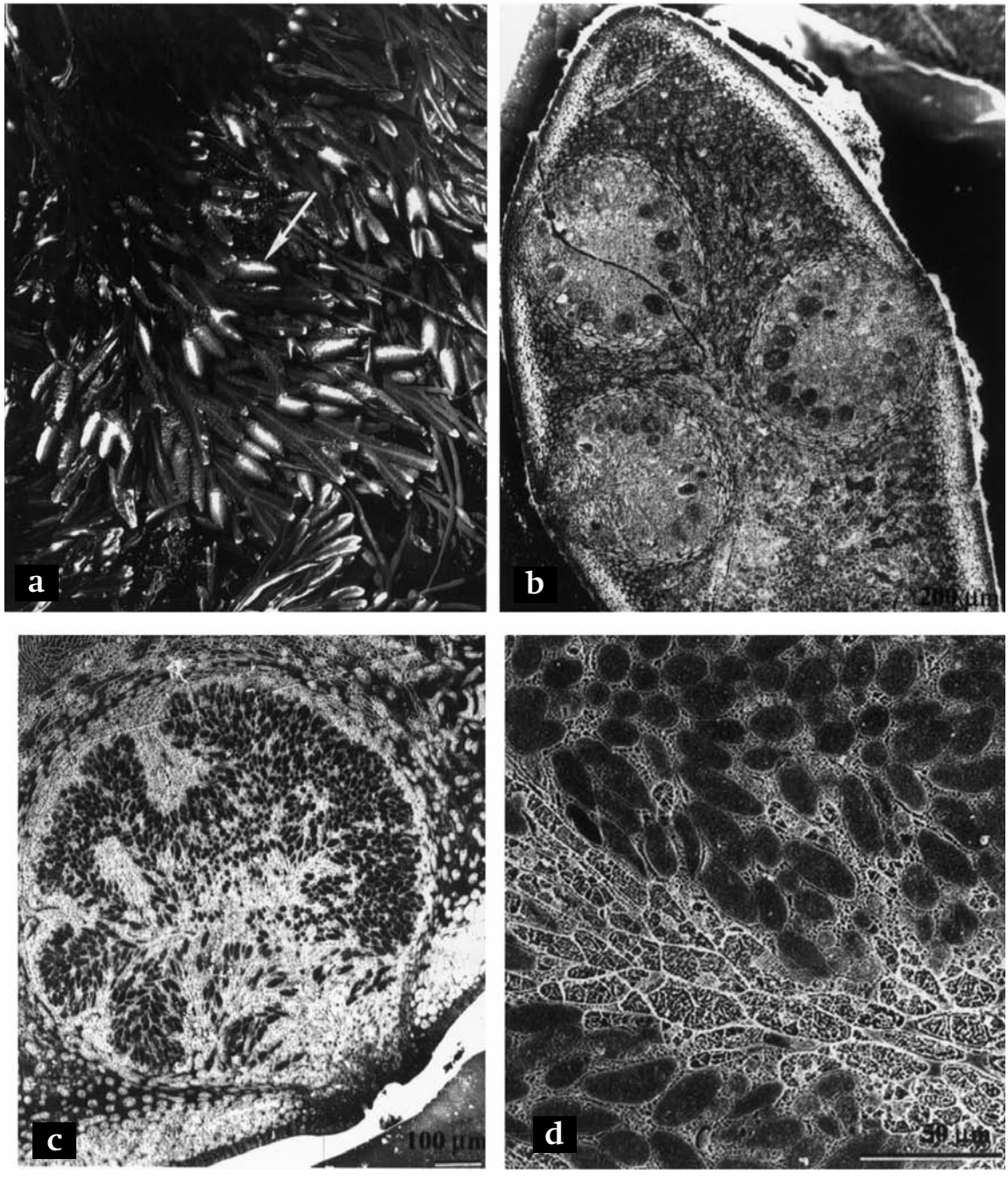


Fig. 21.43 *Fucus vesiculosus*. (*a*) Whole plant showing receptacle (arrow). (*b*) Cross section of a female receptacle showing three conceptacles. (*c*) Cross section of a male conceptacle. (*d*) Branched antheridial filaments bearing antheridia. (*b*), (*c*), (*d*) are scanning electron micrographs of frozen tissue. (From Speransky et al., 1999.)

The spermatozoids are spherical at first and then uncoil to give the elongated biflagellate form (Fig. 21.44). There is an eyespot consisting of a single layer of pigment globules inside a reduced chloroplast. The basal portion of the posterior flagellum is closely applied to the plasmalemma in the area of the eyespot. The anterior portion of the cell contains 13 microtubules that make up the **proboscis**, a structure that may function in the detection of the female sex attractant. The proboscis microtubules pass from the area of the basal bodies, extending themselves in one plane in front of the spermatozoid, and then pass beneath the plasmalemma to the posterior portion of the cell (Manton and Clarke, 1950, 1951, 1956).

The oogonia are usually borne on a stalk cell that is embedded in the wall of the conceptacle (Figs. 21.40, 21.43 (*b*)). The oogonial cell undergoes three nuclear divisions, yielding eight haploid nuclei. The cytoplasm then cleaves into eight eggs. The wall of the oogonium is composed of three layers, the thin outer layer or **exochite**, the thick middle layer or **mesochite**, and the thin inner layer or **endochite**. When the oogonium is mature, the exochite ruptures, releasing the packet of eggs, still surrounded by the other two wall layers, into the sea. In the sea, the mesochite ruptures apically, slips backward, and exposes the eggs within the endochite. The endochite rapidly dissolves, releasing the eggs.

The sperm are attracted to the eggs by a species-non-specific pheromone, **fucoserraten** (Fig. 21.8), released by the eggs (Müller and Jaenicke, 1973). The species-specific recognition between eggs and sperm is based on specific oligosaccharides on the eggs and sperm. The oligosaccharide side chains of the egg-surface glycoproteins contain fucosyl, mannosyl, and/or glucosyl residues (Wright et al., 1995a). The surface of

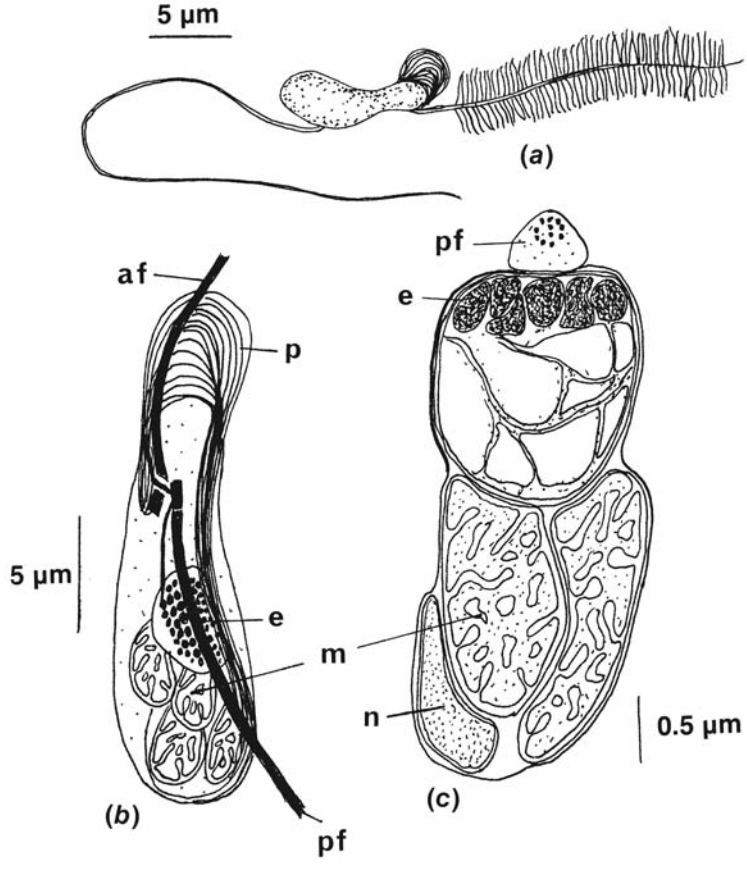


Fig. 21.44 Spermatozoid of *Fucus*. (*a*) Whole spermatozoid. (*b*) Semidiagrammatic drawing showing the anterior flagellum (af), eyespot (e), mitochondria (m), proboscis (p), and the posterior flagellum (pf). (*c*) Section through a spermatozoid illustrating the close appression of the posterior flagellum (pf) to the eyespot area (e) of the reduced chloroplast. (n) Nucleus. (After Manton and Clarke, 1956.)

the egg is not homogeneous, but instead is organized into different domains, each containing different glycoproteins (Stafford et al., 1992). Likewise, the sperm contain glycoproteins organized into domains on the anterior flagellum plasma membrane, the mastigonemes of the anterior flagellum, and the sperm body (Jones et al., 1988). On reaching the egg surface, sperm exhibit a characteristic behavior involving movement over the plasma membrane of the egg and a probing or "searching" of the egg membrane with the anterior flagellum (Brawley, 1991). The glycoproteins on the sperm eventually bind to the complementary glycoproteins on the egg. This results in two "blocks" to further sperm penetration (Wright et al., 1995b):

1 A "fast block" within seconds (Fig. 21.45) caused by depolarization of the plasma membrane due to Na^+ and Ca^{2+} influx. Excess sperm detach from the egg following depolarization.
2 A "slow block" results from the formation of a cell wall around the zygote (Fig. 21.46) by the release of cellulose, phenolics, sulfated fucans, vanadate peroxidase, and alginates from cortical vesicles to form the adhesive **glycocalyx** (Vreeland et al., 1998; Schoenwaelder and Clayton, 1999).

The male nucleus migrates to the female nucleus along associated microtubules. As it migrates, the nuclear envelope of the male nucleus breaks up. The egg nucleus becomes convoluted along the surface nearest the advancing male nucleus. Immediately prior to nuclear fusion, many egg mitochondria accumulate in the vicinity of the male nucleus (Brawley et al., 1976).

The spherical zygote germinates by forming a primary rhizoid from one side, while the rest of the zygote gives rise to the embryo. There are a number of stages in the determination of which part of the zygote will develop into the rhizoid and which will develop into the embryo (Fig. 21.47) (Belanger and Quatrano, 2000; Bisgrove and Kropf, 2004):

1 **Apolar** – In the early stages of development, the fucoid zygotes are apolar and appear to have no inherent order. However, staining of the cells shows the accumulation of F-actin under the plasma membrane in the area of the zygote where the sperm entered.
2 **Axis induction** – A potential polar axis is generated within the zygote. The axis is determined by a number of environmental stimuli, including the direction of incident light, the position of neighboring zygotes, water currents, chemical or ionic gradients, and electrical fields. If none of these stimuli occurs, the axis will be where the sperm originally entered the zygote. During axis induction, the polarity is labile and can be re-oriented by the subsequent exposure to a stimulus in a different direction. F-actin microfilaments are produced *de novo* in the area where the rhizoid will develop (e.g., the shaded area of the zygote in light is responsible for axis induction).
3 **Axis fixation** – The F-actin microfilaments guide Golgi vesicles to the plasma membrane where the vesicles release components of a cell wall that is different in composition from the glycocalyx. At this point the axis is fixed and is no longer susceptible to re-orientation by the environment.

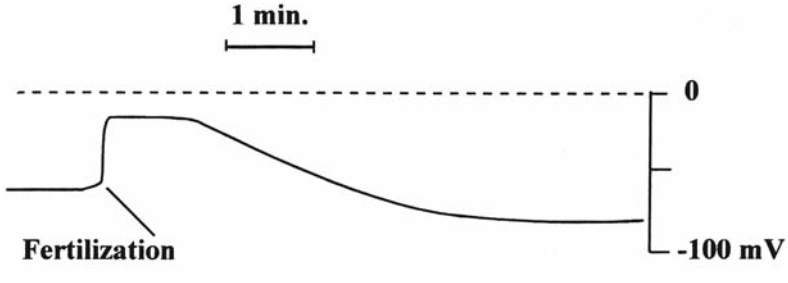


Fig. 21.45 The fast block after fertilization of a *Fucus* egg by a sperm. The potential of the plasma membrane of the egg drops as Na^+ flows into the zygote after fertilization.

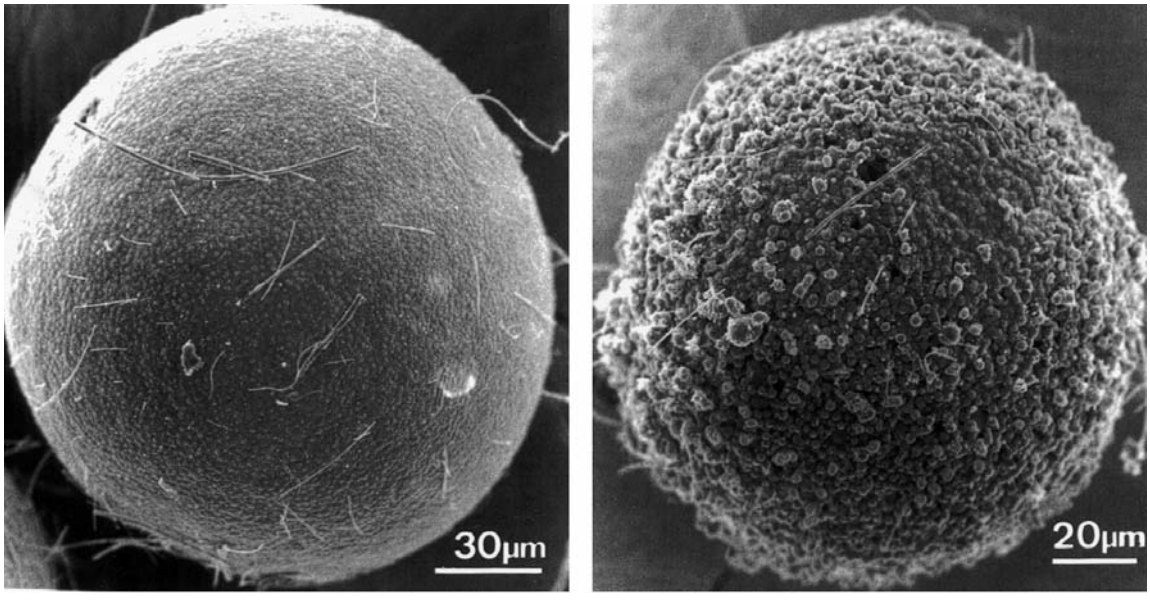


Fig. 21.46 Scanning electron micrographs of the egg (*left*) and zygote (*right*) of the fucoid *Acrocarpia paniculata*. After fertilization, the zygote extrudes droplets of material that produce the glycocalyx. (From Schoenwaelder and Clayton, 1998.)

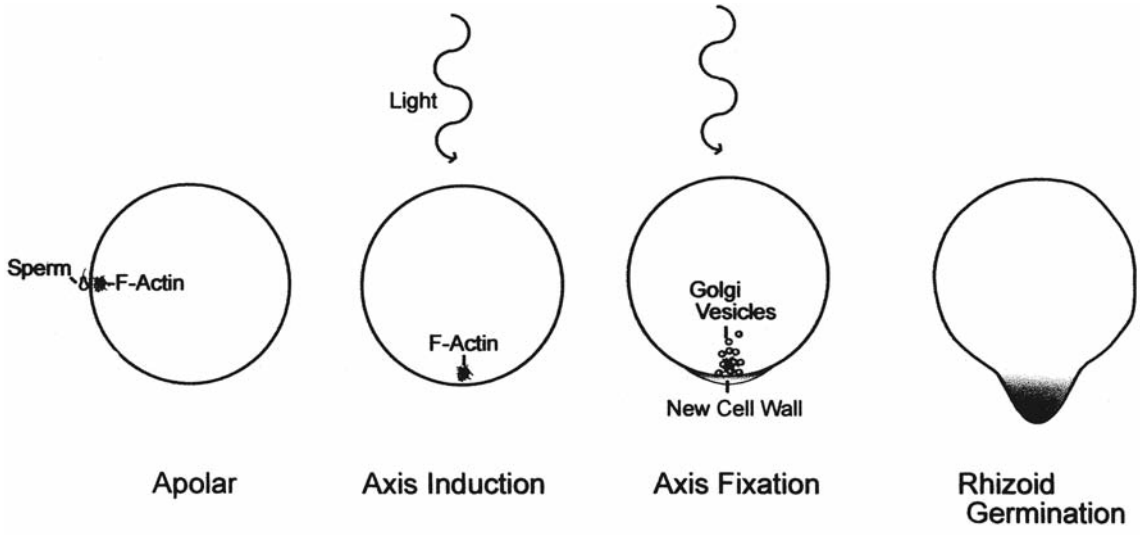


Fig. 21.47 Diagram showing the key events in establishing a polar axis and site of rhizoid germination in a *Fucus* embryo.

4 **Rhizoid germination** – The spherical symmetry of the zygote is broken by the emergence of a polar bulge representing the emergence of the rhizoid. The direction of the rhizoid germination defines the direction of the polar axis. Unequal cytokinesis follows, perpendicular to the direction of rhizoid germination, yielding an embryo consisting of two freshly differentiated cells, a large rounded thallus cell, which is the precursor of the frond and receives most of the chloroplasts, and a smaller rhizoid cell, which generates the stipe and holdfast.

The embryo divides to form a minute cylindrical plant with at least one apical cell with trichothallic growth, producing a hair above (which may function in the uptake of nutrients (Steen, 2003)) and the thallus below. Eventually the apical cell ceases production of the hair and becomes the three-sided apical cell, which later becomes four-sided. It is only after the initiation of the apical cell that the thallus begins to assume its mature flattened shape.

The Fucales show a periodicity in the formation of receptacles and conceptacles. In *Fucus* and *Ascophyllum* (Fig. 21.49) in the North Atlantic, receptacle initiation is a short-day phenomenon, with receptacles being initiated in a 8:16 and 12:12 light–dark photoperiod and inhibited under a 16:8 and continuous light photoperiod (Bird and McLachlan, 1976; Terry and Moss, 1980). White light in the dark period inhibits the short-day response. In the field, conceptacle development commences during September and October, and continues during the following spring until gametes are mature and are liberated during April and May. Following gamete discharge, the conceptacle-bearing receptacles and the rest of the lateral shoot are shed. *Halidrys* (Fig. 21.50) (Moss and Sheader, 1973) has a different periodicity, with vegetative growth in the spring and summer followed by initiation of the conceptacles. The gametes are then shed during the winter. Even though this is the darkest period of the year, the gametes are able to germinate and secure themselves to a substrate with their rhizoids. These germlings are then able to sustain themselves during the periods of little light and subsequently grow normally as soon as there is sufficient daylight. Many of the Fucales show a temperature tolerance similar to that of the Laminariales, with 20 °C being the highest temperature at which eggs of *Halidrys* will germinate.

Ecology

Both the geographical distribution and the location on the shore of a member of the Fucales depend on the ability of the fertilized egg to settle and germinate under the environmental conditions present (Chapman, 1995). Embryos of *Pelvetia fastigata* (Fig. 21.48) will almost all survive if they settle under adult *Pelvetia* thalli. Those that settle on exposed rock will almost all die. Within red-algal tufts, most of the younger embryos survive, with survival declining with the increasing age of the settling embryos (Brawley and Johnson, 1991). Sedimentation on top of the embryos reduces embryo survival, particularly if hydrogen sulfide is present (Chapman and Fletcher, 2002; Bergstrom et al., 2003). In addition, the newly attached zygotes also fall prey to browsing molluscs – in particular, the limpets and *Littorina* species or periwinkles. The mollusc pressure on fucoid development is one

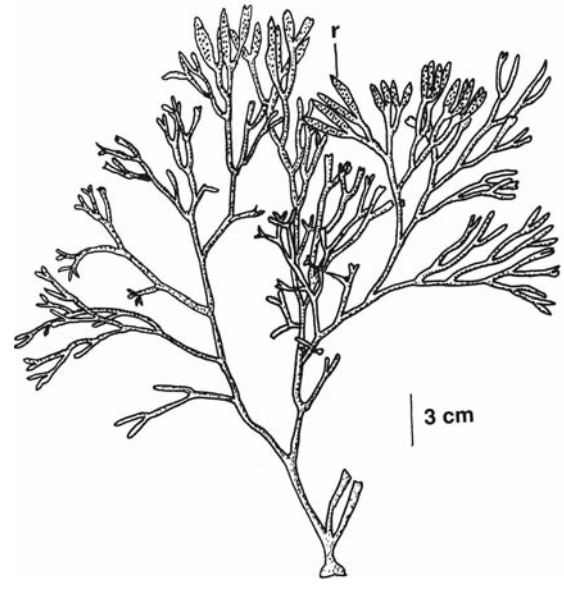


Fig. 21.48 *Pelvetia fastigata*. (r) Receptacle. (After Smith, 1969.)

of the key factors in determining the number of plants present.

Lodge (1948) carried out an experiment on the Isle of Man to determine the rate of recolonization of a shore with primarily fucoid algae. A strip of shore 5 m wide was cleared of all macroscopic biological life. In the first spring after the clearance, green algae (*Enteromorpha*, *Urospora*, and *Chaetomorpha*) covered the shore, along with diatoms. *Fucus* germlings then developed beneath the green algae, starting first at the high-tide mark and then establishing themselves toward the low-water mark. The main *Fucus* species during the first year was *F. vesiculosis*, whereas during the second year *F. serratus* became prominent. After the fucoids became established, the green algae gradually disappeared, and a sparse undergrowth of red algae appeared (*Dumontia*, *Laurencia*). After two years the *Fucus* plants dominated the shore, covering a more diverse undergrowth. By this time the limpets had started to recolonize the shore, slowing down colonization by algae. Seven years after the beginning of the experiment, the shore had returned to its original condition.

The littoral Fucales are adapted to the difficult conditions in which they live, being able to withstand freezing temperatures and summer temperatures up to 34 to 36 °C (Malm and Kautsky, 2003). The zonation of the different fucoid species is due partly to their ability to photosynthesize better when exposed to air (Madsen and Maberly, 1990) and partly to withstand desiccation during both germination and growth. The plants that live higher up in the littoral zone have thicker walls, more fucoidin, and a higher water content, and reach their dry weight on evaporation later than those lower in the littoral zone. The proportion of polysaccharides also reflects the fucoid position in the littoral zone. *Fucus spiralis* and *Pelvetia canaliculata*, which grow highest in the littoral zone, contain the highest amount of fucoidin, 18% to 24% of the dry weight. *Fucus serratus*, which grows near the low-tide mark, has much less fucoidin, about 13% on a dry-weight basis (Black, 1954b).

Generally the life-span of most shore fucoids is about 2 to 3 years (Boney, 1966). The only exception to this being *Ascophyllum* (Fig. 21.49), which has an average age from 12 to 15 years. The average age of the *Ascophyllum* plants will vary according to their position in the littoral zone. On the Welsh coast, plants from the top of the littoral zone were found to be 4 to 5 years old, whereas those from the bottom of the zone were 5 to 15 years old (David, 1943). Although being long-lived, *Ascophyllum* produces a paucity of sporelings and it takes a couple of decades for recolonization of a denuded area. This has resulted in severely depleted populations in areas where the alga is commercially exploited (Bacon and Vadas, 1991).

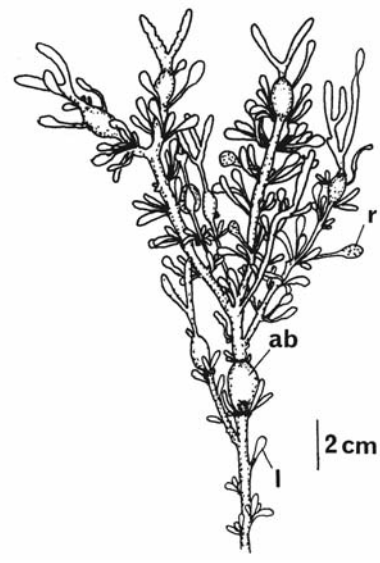


Fig. 21.49 *Ascophyllum nodosum*. Small portion of the distal end of a plant in late summer condition. (ab) Air bladder; (l) lateral; (r) receptacle. (After Taylor, 1957.)

Morphology of fucoid plants will vary with environment. Moss and Sheader (1973) showed that in *Halidrys siliquosa* (Fig. 21.50) the germlings at 10 °C in total darkness produced long rhizoids and a short thallus. If the same plants were grown at a high light intensity (5936 lux), the thalli were long and unbranched, whereas the rhizoids remained short but were pigmented. If the thalli were grown at 20 °C under high light intensity, branched thalli were obtained. Vesiculation will also vary with the environment. *Fucus vesiculosus* growing in areas subjected to very severe wave action will lack vesicles, whereas those growing in calmer areas have gas

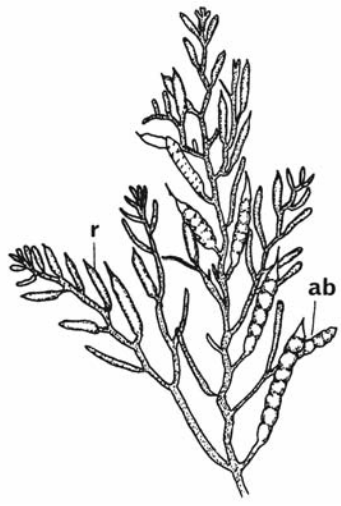


Fig. 21.50 *Halidrys siliquosa*. (ab) Air bladder; (r) receptacle.

vesicles. A minimum branch length seems necessary before vesicle formation can begin, and vesiculation is postponed to the following year if growth has not attained this minimum length (Boney, 1966).

Although the members of the order are normally lithophytes, they are also widely represented by unattached growth-forms lacking holdfasts and propagating mostly vegetatively. These free-living forms arise by vegetative growth of detached branches of the normal attached form that have been transported to a sheltered habitat, or by the development of zygotes in a quiet environment into unattached plants. These unattached plants are referred to as **ecads**, a term for a plant whose morphology has been altered by growth in an unusual environment. Most of these ecads are found in sheltered habitats such as bays and salt marshes.

Fucoids are basically salt-water algae. Attempts to colonize habitats of lower salinity fail, probably because the "fast block" after fertilization (see section on reproduction of *Fucus*) relies on depolarization of the egg membrane by Na^+ (e.g., NaCl) flowing in from seawater (Serrão et al., 1999). Low salinity causes loss of the fast block and more than one sperm fertilizing the egg. This commonly results in lost embryos because polyspermy is almost always lethal.

In discussing salt marsh ecads, Boney (1966) states that the fucoids show the following characteristics: (1) vegetative propagation as the main means of propagation; (2) absence of a holdfast; (3) dwarf habit; (4) spiral twisting of the thallus; and (5) profuse branching. Many of the salt marsh forms grow embedded (but not attached by holdfasts) in a muddy substratum, and some are entwined around the stem bases of the dominant angiosperms. The protection afforded by the canopy of angiosperms enables the fucoids to survive at high levels in the marshes.

Ascophyllum nodosum ecad *mackaii* is an unattached form common in Scotland (Gibb, 1957; Moss, 1971). Normally if a plant of *Ascophyllum* becomes detached from rocks in the intertidal zone, it is cast up by the waves and soon disintegrates. In the unusually calm waters at the head of some Scottish lochs, the detached thalli are gently covered and uncovered as the tide advances and recedes, but they never dry out and disintegrate. The external forms of the attached plant and of the ecad are in complete contrast. The attached plant is flattened in one plane and generally dichotomizes once a year in the spring after differentiation of an air bladder. During the summer a series of lateral nodes are developed, from which receptacles are produced as laterals the following year. This yearly cycle of differentiation is completely lacking in the marsh form of the ecad. Here there are no air bladders and no regular dichotomy to mark off one year's growth from another. Instead, apical branching is frequent and in all planes, giving rise to the characteristic cushion form of the ecad. Also there are no lateral nodes and thus no lateral meristems to give rise to lateral branches. Instead, receptacles are sometimes differentiated behind the apices of any branch, apparently at random.

The form of the ecad is caused by the destruction of the apical meristem and the lateral nodes of the ecad. The branches are eventually regenerated from wound-healing tissue to give rise to the reduced ecad form. Growth of the ecad is slow, and large tufts on the shore may have taken several years to grow. The ecad often still has a prominent apical cell, but there is little meristematic activity when compared to the

attached plant. This results in a thallus with little cortex.

The receptacles of the ecad are small when compared to those of the attached plant. The eggs are also small and of variable size. The number of germlings produced from the ecad eggs is low. The time of gamete discharge in the ecad approximates that of nearby attached plants.

The Sargasso Sea is in a gyre in the Atlantic Ocean between 20° and 35° north latitude and is made up of huge masses of floating *Sargassum* (gulfweed) (Fig. 21.51). The immense tracts of *Sargassum* are formed by continuous vegetative reproduction of the plants in the area. Holdfasts are never found. Occasionally, conceptacles can be seen, but they are always functionless, and the maintenance of the population is entirely by vegetative means.

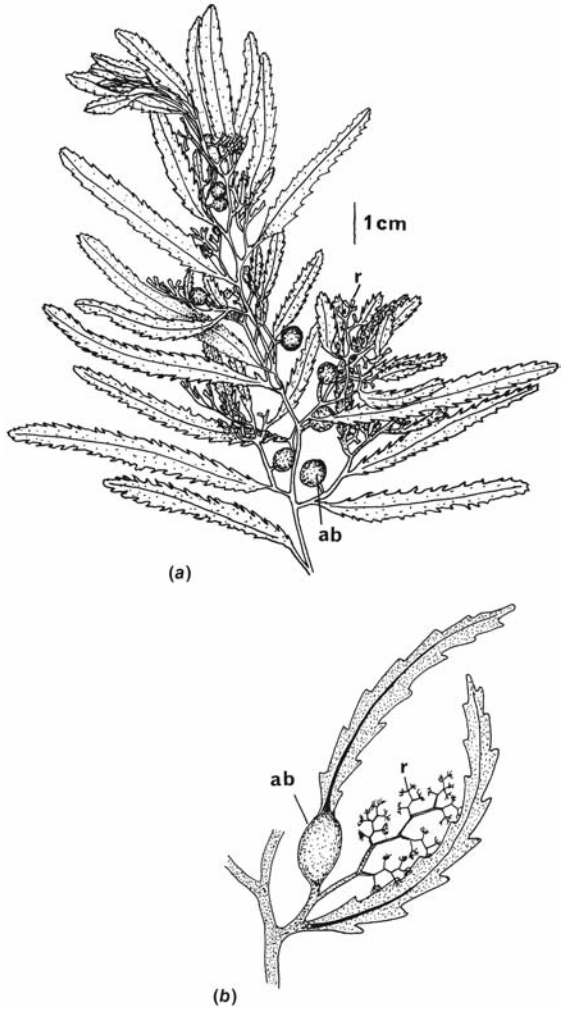


Fig. 21.51 *Sargassum filipendula*. (*a*) Part of a main branch. (*b*) *S. longifolium*. (ab) Air bladder; (r) receptacle. ((*a*) after Taylor, 1960.)

REFERENCES

Amsler, C. D., and Neushel, M. (1989). Chemotactic effects of nutrients on spores of the kelps *Macrocystis pyrifera* and *Pterygophora californica*. *Mar. Biol*. (Berlin) 102:557–64.

Andersen, R. J. (1982). The life history of *Desmarestia firma* (C. Ag.) Skottsb. (Phaeophyceae, Desmarestiales). *Phycologia* 21:316–22.

Arnold, T. M., Targett, N. M., Tanner, C. E., Hatch, W. L., and Ferrari, K. E. (2001). Evidence for methyl jasmonate-induced phlorotannin production in *Fucus vesiculosus* (Phaeophyceae). *J. Phycol.* 37:1026–9.

Asensi, A., Gall, E. A., Marie, D., Billot, C., Dion, P., and Kloareg, B. (2001). Clonal propagation of *Laminaria digitata* (Phaeophyceae) sporophytes through a diploid cell-filament suspension. *J. Phycol.* 37:411–17.

Bacon, L. E., and Vadas, R. L. (1991). A model for gamete release in *Ascophyllum nodosum* (Phaeophyta). *J. Phycol*. 27:166–73.

Bailey, J. C., Bidigare, R. R., Christensen, S. J., and Andersen, R. A. (1998). Phaeothamniophyceae classis nova: a new lineage of chromophytes based upon photosynthetic pigments, *rbc*L sequence analysis and ultrastructure. *Protist* 149:245–63.

Belanger, K. D., and Quatrano, R. S. (2000). Polarity: the role of localized secretion. *Curr. Opin. Plant Biol*. 3:67–72.

Bell, G. (1997). The evolution of the life cycle of brown seaweeds. *Biol. J. Linnean Soc*. 60:21–38.

Bergstrom, L., Berger, R., and Kautsky, L. (2003). Negative effects of nutrient enrichment on the establishment of *Fucus vesiculosus* in the Baltic Sea. *Eur. J. Phycol.* 38:41–6.

Berkaloff, C., and Rousseau, B. (1979). Ultrastructure of male gametogenesis in *Fucus serratus* (Phaeophyceae). *J. Phycol*. 15:163–73.

Bird, N. L., and McLachlan, J. (1976). Control of formation of receptacles in *Fucus distichus* L., subsp. *distichus* (Phaeophyceae, Fucales). *Phycologia* 15:79–84.

Bisalputra, T. (1966). Electron microscopic study of protoplasmic continuity in certain brown algae. *Can.J. Bot*. 44:89–93.

Bisalputra, T., and Burton, H. (1969). The ultrastructure of the chloroplast of a brown alga *Sphacelaria* sp. II. Association between the chloroplast DNA and the photosynthetic lamellae. *J. Ultrastruct. Res*. 29:224–35.

Bisalputra, T., Shields, M., and Markam, J. W. (1971). *In situ* observations of the fine structure of *Laminaria* gametophytes and embryos in culture. I. Methods and the ultrastructure of the zygote. *J. Microscopie* 10:83–98.

Bisgrove, S. R., and Kropf, D. L. (2004). Cytokinesis in brown algae: studies of asymmetric division in fucoid zygotes. *Protoplasma* 223:163–73.

Black, W. A. P. (1954a). Concentration gradients and their significance in *Laminaria saccharina* (L.) Lamour. *J. Mar. Biol. Assoc. UK* 33:49–60.

Black, W. A. P. (1954b). The seasonal variation in the combined L-fucose content of the common British Laminariaceae and Fucaceae. *J. Sci. Food Agric*. 5:445–54.

Boalch, G. T. (1961). Studies on *Ectocarpus* in culture. *J. Mar. Biol. Assoc. UK* 41:287–304.

Boney, A. D. (1966). *A Biology of Marine Algae*. London: Hutchinson.

Borowitzka, M. A., Larkum, A. W. D., and Nockolds, C. E. (1974). A scanning electron microscope study of the structure and organisation of the calcium carbonate deposits of algae. *Phycologia* 13:195–203.

Bouck, G. B. (1965). Fine structure and organelle associations in brown algae. *J. Cell Biol*. 26:523–37.

Bouck, G. B. (1969). Extracellular microtubules. The origin, structure and attachment of flagellar hairs in *Fucus* and *Ascophyllum* antherozoids. *J. Cell Biol*. 40:446–60.

Bourne, V. L., and Cole, K. (1968). Some observations on the fine structure of the marine brown alga *Phaeostrophion irregulare*. *Can. J. Bot*. 46:1369–75.

Brawley, S. H. (1991). The fast block against polyspermy in fucoid algae is an electrical block. *Dev. Biol*. 144:94–106.

Brawley, S. H., and Johnson, L. E. (1991). Survival of fucoid embryos in the intertidal zone depends upon developmental stage and microhabitat. *J. Phycol*. 27:179–86.

Brawley, S. H., Wetherbee, R., and Quatrano, R. S. (1976). Fine structural studies of the gametes and embryo of *Fucus vesiculosus* L. (Phaeophyta). *J. Cell Sci*. 20:233–54.

Buggeln, R. G. (1974). Negative phototropism of the haptera of *Alaria esculenta* (Laminariales). *J. Phycol*. 10:80–2.

Cabello-Pasini, A., and Alberte, R. S. (2001). Expression of carboxylating enzymes in *Laminaria setchellii* (Phaeophyceae). *Phycologia* 40:351–8.

Chapman, A. R. O. (1995). Functional ecology of fucoid algae: twenty-three years of progress. *Phycologia* 34:1–32.

Chapman, A. R. O., and Burrows, E. M. (1971). Field and culture studies of *Desmarestia aculeata* (L.) Lamour. *Phycologia* 10:63–76.

Chapman, A. S., and Fletcher, R. L. (2002). Differential effects of sediments on survival and growth of *Fucus serratus* embryos (Fucales, Phaeophyceae). *J. Phycol.* 38:894–903.

Cheng, T-H. (1969). Production of kelp. A major source of China's exploitation of the sea. *Econ. Bot*. 23:215–36.

Chi, E. Y. (1971). Brown algal pyrenoids. *Protoplasma* 72:101–4.

Clayton, M. N. (1980). Sexual reproduction – A rare occurrence in the life history of the complanate form of *Scytosiphon* (Scytosiphonaceae, Phaeophyta) from southern Australia. *Br. J. Phycol*.15:105–18.

Clayton, M. N., and Ashburner, C. M. (1994). Secretion of phenolic bodies following fertilization in *Durvillaea potatorum* (Durvillaeales, Phaeophyta). *Eur. J. Phycol*. 29:1–9.

Clint, H. B. (1927). The life history and cytology of *Sphacelaria bipinnata Sauv. Publ. Hartley Bot. Lab. Liverpool* 3:1–19.

Cole, K. (1970). Ultrastructural characteristics in some species in the order Scytosiphonales. *Phycologia* 9:275–83.

Colijn, F., and van den Hoek, C. (1971). The life history of *Sphacelaria furcigera* Kütz. (Phaeophyceae). II. The influence of daylength and temperature on sexual and vegetative reproduction. *Nova Hedwigia* 21:899–922.

David, H. M. (1943). Studies in the autecology of *Ascophyllum nodosum* Le Jol. *J. Ecol*. 31:178–98.

Dayton, P. K., and Tegner, M. J. (1984). Catastrophic storms, El Niño, and patch stability in a southern California kelp community. *Science* 224:283–5.

Dayton, P. K., Currie, V., Gerrodette, T., Keller, B. D., Rosenthal, G., and Ven Tresca, D. (1984). Patch dynamics and stability of some California kelp communities. *Ecol. Monogr*. 54:253–89.

de Reviers, B., and Rousseau, F. (1999). Towards a new classification of the brown algae. In *Progress*

in Phycological Research, ed. F. E. Round and D. J. Chapman, Vol. 13, pp. 107–201. Bristol: Biopress Ltd.

Diouris, M. (1989). Long-distance transport of ^{14}C-labelled assimilate in the Fucales: nature of translocated substances in *Fucus serratus*. *Phycologia* 28:504–11.

Dixon, N. M., Leadbeater, B. S. C., and Wood, K. R. (2000). Frequency of viral infection in a field population of *Ectocarpus fasciculatus* (Ectocarpales, Phaeophyceae). *Phycologia* 39:528–63.

Draisma, S. G. A., Prud'homme van Reine, W. F., Stam, W. T., and Olsen, J. L. (2001). A reassessment of phylogenetic relationships within the Phaeophyceae based on Rubisco large subunit and ribosomal DNA sequences. *J. Phycol.* 37:586–603.

Draisma, S. G. A., Olsen, J. L., Stam, W. T., and Prud'homme van Reine, W. F. (2002). Phylogenetic relationships within the Sphacelariales (Phaeophyceae): *rbc*L, RUBISCO spacer and morphology. *Eur. J. Phycol.* 37:385–401.

Druehl, L. D. (1967). Distribution of two species of *Laminaria* as related to some environmental factors. *J. Phycol*. 3:103–8.

Duggins, D. O. (1980). Kelp beds and sea otters: An experimental approach. *Ecology* 61:447–53.

Edelstein, T., Chen, L., and McLachlan, J. (1968). Sporangia of *Ralfsia fungiformis* (Gunn.) Setchell and Gardner. *J. Phycol*. 4:157–60.

Edelstein, T., Chen, L. C-M., and McLachlan, J. (1970). The life cycle of *Ralfsia clavata* and *R. borneti. Can. J. Bot*. 48:527–31.

Edwards, P. (1969). Field and cultural studies on the seasonal periodicity of growth and reproduction of selected Texas benthic marine algae. *Contrib. Mar. Sci. Univ. Texas* 14:59–114.

Estes, J. A., and Steinberg, P. D. (1988). Predation, herbivory, and kelp evolution. *Paleobiology* 14:19–36.

Evans, L. V. (1965). Cytological studies in the Laminariales. *Ann. Bot*. 29:541–62.

Evans, L. V. (1966). Distribution of pyrenoids from some brown algae. *J. Cell Sci*. 1:449–54.

Evans, L. V. (1968). Chloroplast morphology and fine structure in British fucoids. *New Phytol*. 67:173–8.

Evans, L. V., and Holligan, M. S. (1972). Correlated light and electron microscope studies on brown algae. I. Localization of alginic acid and sulphated polysaccharides in *Dictyota*. *New Phytol*. 71:1161–72.

Evans, L. V., Simpson, M., and Callow, M. E. (1973). Sulphated polysaccharide synthesis in brown algae. *Planta* 110:237–52.

Floc'h, J. Y., and Penot, M. (1972). Transport du ^{32}P et du ^{86}Rb chez quelques algues brunes: Orientation des migrations et voies de conduction. *Physiologie Végétale* 10:677–86.

Forster, R. M., and Dring, M. J. (1994). Influence of blue light on the photosynthetic capacity of marine plants from different taxonomic, ecological and morphological groups. *Eur. J. Phycol*. 29:21–7.

Fulcher, R. G., and McCully, M. E. (1969). Histological studies on the genus *Fucus*. IV. Regeneration and adventure embryony. *Can. J. Bot*. 47:1643–9.

Gaines, S. D., and Roughgarden, J. (1987). Fish in offshore kelp forests affect recruitment to intertidal populations. *Science* 235:479–81.

Gibb, D. C. (1957). The free-living forms of *Ascophyllum nodosum* (L.) Le Jol. *J. Ecol*. 45:49–83.

Gibson, G., and Clayton, M. N. (1987). Sexual reproduction, early development and branching in *Notheia anomala* (Phaeophyta) and its classification in the Fucales. *Phycologia* 26:363–73.

Grenville, D. J., Peterson, R. L., Barrales, H. L., and Gerrath, J. F. (1982). Structure and development of the secretory cells and duct system in *Macrocystis pyrifera* (L.) C. A. Agardh. *J. Phycol*. 18:232–40.

Guignard, L. (1892). Observations sur l'appareil mucifere des Laminariacées. *Ann. Sci. Nat. Bot. VII* 15:1–46.

Henley, W. J., and Dunton, K. H. (1997). Effects of nitrogen supply and continuous darkness on growth and photosynthesis of the arctic kelp *Laminaria solidungula*. *Limnol. Oceanog*. 42:209–16.

Henry, B. E., and Van Alstyne, K. L. (2004). Effects of UV radiation on growth and phorotannins in *Fucus gardneri* (Phaeophyceae) juveniles and embryos. *J. Phycol.* 40:527–33.

Henry, E. C. (1987). Primitive reproductive characters and a photoperiodic response in *Saccorhiza dermatodea* (Laminariales, Phaeophyceae). *Br. Phycol. J.* 22:23–31.

Henry, E. C., and Cole, K. M. (1982). Ultrastructure of swarmers in the Laminariales (Phaeophyceae). I. Zoospores. *J. Phycol*. 18:550–69.

Hollenberg, G. J. (1969). An account of the Ralfsiaceae (Phaeophyta) of California. *J. Phycol*. 5:290–301.

Hsiao, S. I. C. (1969). Life history and iodine nutrition of the marine brown alga, *Petalonia fascia* (O. F. Müll.) Kuntze. *Can. J. Bot*. 47:1611–16.

Hsiao, S. I. C. (1970). Light and temperature effects on the growth, morphology, and reproduction of *Petalonia fascia*. *Can. J. Bot*. 48:1359–61.

Hsiao, S. I. C., and Druehl, L. D. (1973). Environmental control of gametogenesis in *Laminaria saccharina*. IV. In situ development of gametophytes and young sporophytes. *J. Phycol*. 9:160–4.

Hurd, C. L., Galvin, R. S., Norton, T. A., and Dring, M. J. (1993). Production of hylaine hairs by intertidal species of *Fucus* (Fucales) and their role in phosphate uptake. *J. Phycol*. 29:160–5.

Iken, K., Amsler, C. D., Greer, S. P., and McClintock, J. B. (2001). Qualitative and quantitative studies of the swimming behaviour of *Hincksia irregularis* (Phaeophyceae) spores: ecological implications and parameters for quantitative swimming assays. *Phycologia* 40:359–66.

Jaenicke, L., Müller, D. G., and Moore, R. E. (1974). Multifidene and aucantene, C_{11} hydrocarbons in the male attracting essential oil from the gynogametes of *Cutleria multifida* (Smith) Grev. (Phaeophyta). *J. Am. Chem. Soc.* 96:3324–5.

Jones, J. L., Callow, J. A., and Green, J. R. (1988). Monoclonal antibodies to sperm antigens of the brown alga *Fucus serratus* exhibit region-, gamete-, species- and genus-preferential binding. *Planta* 176:298–306.

Kain, J. M. (1966). The role of light in the ecology of *Laminaria hyperborea. Br. Ecol. Soc. Symp*. 6:319–34.

Kapraun, D. F., and Boone, P. W. (1987). Karyological studies of three species of Scytosiphonaceae (Phaeophyta) from coastal North Carolina. *J. Phycol.* 23:318–22.

Kawai, H., Kubota, M., Kondo, T., and Watanabe, M. (1991). Action spectra for phototaxis in zoospores of the brown alga *Pseudochorda gracilis. Protoplasma* 161:17–22.

Kawai, H., Nakamura, S., Mimuro, M., Furuya, M., and Watanabe, M. (1996). Microspectrofluorometry of the autofluorescent flagellum in phototactic algal zoids. *Protoplasma* 191:172–7.

Klinger, T., and DeWeede, R. E. (1988). Stipe rings, age and size in populations of *Laminaria setchelli* Silva (Laminariales, Phaeophyta) in British Columbia. *Phycologia* 27:234–40.

Kloareg, D., and Quatrano, R. S. (1988). Structure of the cell walls of marine algae and ecophysiological functions of the matrix polysaccharides. *Oceanogr. Mar. Biol. Rev*. 26:234–40.

Knight, M. (1929). Studies in the Ectocarpaceae. II. The life-history and cytology of *Ectocarpus siliculosus* Dillw. *Trans. R. Soc. Edinburgh* 56:307–32.

Kubanek, J., Lester, S. E., Fenical, W., and Hay, M. E. (2004). Ambiguous role of phlorotannins as chemical defenses in the brown alga *Fucus vesiculosus. Mar. Ecol. Progr. Ser.* 277:79–93.

Kuckuck, P. (1899). Über den generationwechsel von *Cutleria multifida* (Engl. Bot.) Grev. *Wiss. Meeresunters. Helgoland N.F.* 3:95–116.

Kumke, J. (1973). Beiträge zur Periodizität der Oogon-Entleerung bei *Dictyota dichotoma* (Phaeophyta). *Z. Pfl. Physiol*. 70:191–210.

Kupper, F. C., Schweigert, N., Gall, E. A., Legendre, J.-M., Vilter, H., and Kloareg, B. (1998). Iodine uptake in Laminariales involves extracellular, haloperoxidase-mediated oxidation of iodide. *Planta* 207:163–71.

Kylin, H. (1934). Zur Kenntnis der Entwicklungsgeschichte einiger Phaeophyceen. *Lunds Univ. Årsskr. N.F. Avd.* 30:1–19.

Ladah, L., Bermudez, R., Pearson, G., and Serrao, E. (2003). Fertilization success and recruitment of dioecious and hermaphroditic fucoid seaweeds with contrasting distributions near their southern limit. *Mar. Ecol. Progr. Ser.* 262:173–83.

Larkum, A. W. D. (1972). Frond structure and growth in *Laminaria hyperborea. J. Mar. Biol. Assoc. UK* 52:405–18.

Lim, B.-L., Kawai, H., Hori, H., and Osawa, S. (1986). Molecular evolution of 5S ribosomal RNA from red and brown algae. *Japanese J. Genet.* 61:169–76.

Lobban, C. S. (1978). The growth and death of the *Macrocystis* sporophyte (Phaeophyceae, Laminariales). *Phycologia* 17:196–212.

Lodge, S. M. (1948). Algal growth in the absence of *Patella* on an experimental strip of seashore. *Proc. Trans. Liverpool Biol. Soc*. 61:78–83.

Loiseaux, S. (1970). *Streblonema anomalum* S. et G. and *Compsonema sporangiiferum* S. et G. stages in the life history of a minute *Scytosiphon. Phycologia* 9:185–91.

Loiseaux, S. (1973). Ultrastructure of zoidogenesis in unilocular zoidocysts of several brown algae. *J. Phycol*. 9:277–89.

Loiseaux, S., and West, J. A. (1970). Brown algal mastigonemes: Comparative ultrastructure. *Trans. Am. Microsc. Soc*. 89:524–32.

Luder, U. H., and Clayton, M. N. (2004). Induction of phlorotannins in the brown macroalga *Ecklonia radiata* (Laminariales, Phaeophyta) in response to simulated herbivory – the first microscopic study. *Planta* 218:928–37.

Lüning, K. (1981). Egg release in gametophytes of *Laminaria saccharina*: Induction by darkness and inhibition by blue light and U.V. *Br. Phycol. J.* 16:379–93.

Lüning, K., and Dring, M. J. (1972). Reproduction induced by blue light in female gametophytes of *Laminaria saccharina*. *Planta* 104:252–6.

Lüning, K., and Dring, M. J. (1973). The influence of light quality on the development of the brown algae *Petalonia* and *Scytosiphon*. *Br. Phycol. J*. 8:333–8.

Lüning, K., and Dring, M. J. (1975). Reproduction, growth and photosynthesis of gametophytes of *Laminaria saccharina* grown in blue and red light. *Mar. Biol.* 29:195–200.

Lüning, K., and Müller, D. G. (1978). Chemical interaction in sexual reproduction of several Laminariales (Phaeophyceae): Release and attraction of spermatozoids. *Z. Pflanzenphysiol*. 89:333–41.

Lüning, K., Schmitz, K., and Willenbrink, J. (1972). Translocation of ^{14}C-labelled assimilates in two *Laminaria* species. *Proc. VII Int. Seaweed Symp*. 420–5.

Lüning, K., Wagner, A., and Buchholz, C. (2000). Evidence for inhibitors of sporangium formation in *Laminaria digitata* (Phaeophyceae) during the season of rapid growth. *J. Phycol.* 36:1129–34.

Madsen, T. V., and Maberly, S. C. (1990). A comparison of air and water as environments for photosynthesis by the intertidal alga *Fucus spiralis* (Phaeophyta). *J. Phycol*. 26:24–30.

Maier, I. (1982). New aspects of pheromone-triggered spermatozoid release in *Laminaria digitata* (Phaeophyta). *Protoplasma* 113:137–43.

Maier, I. (1984). Culture studies of *Chorda tomentosa* (Phaeophyta, Laminariales). *Br. Phycol. J.* 19:95–106.

Maier, I. (1997a). The fine structure of the male gamete of *Ectocarpus siliculosus* (Ectocarpales, Phaeophyceae). I. General structure of the cell. *Eur. J. Phycol*. 32:241–53.

Maier, I. (1997b). The fine structure of the male gamete of *Ectocarpus siliculosus* (Ectocarpales, Phaeophyceae). II. The flagellar apparatus. *Eur. J. Phycol*. 32:255–66.

Maier, I., and Müller, D. G. (1986). Sexual pheromones in algae. *Biol. Bull*. 170:145–75.

Maier, L., Müller, D. G., Gassmann, G., Boland, W., Marner, F-J., and Jaenicke, L. (1984). Pheromone-triggered gamete release in *Chorda tomentosa*. *Naturwissenschaften* 71:48–9.

Malm, T., and Kautsky, L. (2003). Differences in life-history characteristics are consistent with the vertical distribution pattern of *Fucus serratus* and *Fucus vesiculosus* (Fucales, Phaeophyceae) in the central Baltic Sea. *J. Phycol.* 39:880–7.

Mann, K. H., and Chapman, A. R. O. (1975). Primary production of marine macrophytes. In *Photosynthesis and Productivity in Different Environments*, ed. J. P. Cooper, *Int. Biol. Prog*. 3:307–33. Cambridge: Cambridge University Press.

Manton, I. (1959). Observations on the internal structure of the spermatozoid of *Dictyota*. *J. Exp. Bot*. 10:448–61.

Manton, I., and Clarke, B. (1950). Electron microscope observations of the spermatozoid of *Fucus*. *Nature* 166:973–4.

Manton, I., and Clarke, B. (1951). Electron microscope observations on the zoospores of *Pylaiella* and *Laminaria*. *J. Exp. Bot*. 23:242–6.

Manton, I., and Clarke, B. (1956). Observations with the electron microscope on the internal structure of the spermatozoid of *Fucus*. *J. Exp. Bot*. 7:416–32.

Mariani, P., Tolomio, C., and Braghetta, P. (1985). An ultrastructural approach to the adaptive role of the cell wall in the intertidal alga *Fucus virsoides*. *Protoplasma* 128:208–17.

Marner, F-J., Müller, B., and Jaenicke, L. (1984). Lamoxirene, the *Laminaria*-pheromone: Structural proof of the spermatozoid releasing and attracting factor of Laminariales. *Z. Naturforsch*. 39c:689–91.

Medlin, L. K., Kooistra, W. H. C. F., Potter, D., Saunders, G. W., and Andersen, R. A. (1997). Phylogenetic relationships of the "golden algae" (haptophytes, heterokont chromophytes) and their plastids. In *Origins of Algae and Their Plastids*, ed. D. Bhattacharya, pp. 187–219. Vienna: Springer-Verlag.

Moe, R. L., and Silva, P. C. (1977). Antarctic marine flora: Uniquely devoid of kelps. *Science* 196:1206–8.

Moe, R. L., and Silva, P. C. (1981). Morphology and taxonomy of *Himantothallus* (including *Phaeoglossum* and *Phyllogigas*), an Antarctic member of the Desmarestiales (Phaeophyceae). *J. Phycol*. 17:15–29.

Moss, B. (1965). Apical dominance in *Fucus vesiculosus*. *New Phytol*. 64:387–92.

Moss, B., (1967). The apical meristem of *Fucus*. *New Phytol*. 66:67–74.

Moss, B. (1970). Meristems and growth control in *Ascophyllum nodosum* (L.) Le Jol. *New Phytol*. 69:253–60.

Moss, B. (1971). Meristems and morphogenesis in *Ascophyllum nodosum* ecad *mackii* (Cotton). *Br. Phycol. J*. 6:187–93.

Moss, B. (1983). Sieve elements in the Fucales. *New Phytol*. 93:433–7.

Moss, B., and Sheader, A. (1973). The effect of light and temperature upon the germination and growth of *Halidrys siliquosa* (L.) Lygnb. (Phaeophyceae, Fucales). *Phycologia* 12:63–8.

Motomura, T. (1991). Immunofluorescence microscopy of fertilization and parthenogenesis in *Laminaria angusta* (Phaeophyta). *J. Phycol*. 27:248–57.

Motomura, T., Ichimura, T., and Melkonian, M. (1997). Coordinative nuclear and chloroplast division in unilocular sporangia of *Laminaria angustata* (Laminariales, Phaeophyceae). *J. Phycol*. 33:266–71.

Müller, D. (1962). Über jahres und lunarperiodische Erscheinungen bei einigen Braunalgen. *Bot. Mar*. 4:140–55.

Müller, D. (1974). Sexual reproduction and isolation of a sex attractant in *Cutleria multifida* (Smith) Grev. (Phaeophyta). *Biochem Physiol. Pflanz*. 165:212–15.

Müller, D. (1978). Locomotive responses of male gametes to the species specific sex attractant in *Ectocarpus siliculosus* (Phaeophyta). *Arch. Protistenk*. 120:371–77.

Müller, D. (1979). Genetic affinity of *Ectocarpus siliculosus* (Dillw.) Lyngb. from the Mediterranean, North Atlantic and Australia. *Phycologia* 18:312–18.

Müller, D. (1982). Sexuality and sex attraction. In *The Biology of Seaweeds* eds. C. S. Lobban, and M. J. Wynne, pp. 661–74. Los Angeles and Berkeley: Univ. Calif. Press.

Müller, D., and Jaenicke, L. (1973). Fucoserraten, the female sex attractant of *Fucus serratus* L. (Phaeophyta). *FEBS Lett*. 30:137–9.

Müller, D., and Lüthe, N. M. (1981). Hormonal interaction in sexual reproduction of *Desmarestia aculeata* (Phaeophyceae). *Br. Phycol. J.* 16:351–6.

Müller, D., Jaenicke, L., Donike, M., and Akintobi, T. (1971). Sex attractant in a brown alga: Chemical structure. *Science* 171:815–17.

Müller, D., Gassmann, G., and Lüning, K. (1979). Isolation of a spermatozoid-releasing and -attracting substance from female gametophytes of *Laminaria digitata*. *Nature* 279:430–1.

Müller, D., Gassmann, G., Boland, W., Marner, F., and Jaenicke, L. (1981). *Dictyota dichotoma* (Phaeophyceae): Identification of sperm attractant. *Science* 212:1040–1.

Müller, D., Peters, A., Gassmann, G., Boland, W., Marner, F-J., and Jaenicke, L. (1982). Identification of a sexual hormone and related substances in the marine alga *Desmarestia*. *Naturwissenschaften* 69:290–1.

Müller, D., Maier, I., and Gassmann, G. (1985). Survey on sexual pheromone specificity in Laminariales (Phaeophyceae). *Phycologia* 24:475–84.

Nagasato, C., and Motomura, T. (2002). New pyrenoid formation in the brown alga, *Scytosiphon lomentaria* (Scytosiphonales, Phaeophyceae). *J. Phycol.* 38:800–6.

Nakahara, H., and Nakamura,Y. (1973). Parthenogenesis, apogamy and apospory in *Alaria crassifolia* (Laminariales). *Mar. Biol*. 18:327–32.

Nakamura, Y. (1965). Development of zoospores in *Ralfsia*-like thallus, with special reference to the life cycle of the Scytosiphonales. *Bot. Mag. Tokyo* 78:109–10.

Nakamura, Y. (1972). A proposal on the classification of the Phaeophyta. In *Contributions to the Systematics of Benthic Marine Algae of the North Pacific*, ed. I. A. Abbott, and M. Kurogi, pp. 147–56. New York: Academic Press.

Nicholson, N. L. (1970). Field studies on the giant kelp *Nereocystis*. *J. Phycol*. 6:177–82.

Nienberg, W. (1931). Die Entwicklung der Keimlinge von *Fucus vesiculosus* und ihre Bedeutung für die Phylogenie der Phaeophyceen. *Wiss. Meeresunters. Abt. Kiel N.F.* 21:49–63.

Nizamuddin, M., and Womersley, H. B. S. (1960). Structure and systematic position of the Australian brown alga, *Notheia anomala*. *Nature* 187:673–4.

Norton, T. A. (1972). The development of *Saccorhiza dermatodea* (Phaeophyceae, Laminariales) in culture. *Phycologia* 11:81–6.

Norton, T. A. (1978). The factors influencing the distribution of *Saccorhiza polyschides* in the region of Lough Ine. *J. Mar. Biol. Assoc. UK* 58:527–36.

Norton, T. A., and Burrows, E. M. (1969). Studies on marine algae of the British Isles. 7. *Saccorhiza polyschides* (Lightf.) Batt. *Br. Phycol. J*. 4:19–53.

Novaczek, I. (1981). Stipe growth rings in *Ecklonia radiata* (C. Ag.) J. Ag. (Laminariales). *Br. Phycol. J*. 16:363–71.

Oliveira, L., Walker, D. C., and Bisalputra, T. (1980). Ultrastructural, cytochemical and enzymatic studies on the adhesive "plaques" of the brown alga, *Laminaria saccharina* (L.) Lamour. and *Nereocystis leutkeana* (Nert.) Post. et Rupr. *Protoplasma* 104:1–15.

Oltmanns, F. (1889). Beitrage zur Kenntniss der Fucaceen. *Bibl. Bot*. 3(14):1–100.

Papenfuss, G. F. (1934). Alternation of generations in *Sphacelaria bipinnata* Sauv. *Bot. Not*. 437–44.

Papenfuss, G. F. (1935). Alternation of generations in *Ectocarpus siliculosus*. *Bot. Gaz*. 96:421–46.

Papenfuss, G. F. (1951). Phaeophyta. In *Manual of Phycology*, ed. G. M. Smith, pp. 119–38. Waltham, MA: Chronica Botanica.

Parker, B. C. (1963). Translocation in the giant kelp *Macrocystis*. *Science* 140:891–2.

Parker, B. C. (1965). Translocation in the giant kelp *Macrocystis*. I. Rates, direction, quantity of C^{14}-labelled products and fluorescein. *J. Phycol*. 1:41–6.

Parker, B. C., and Dawson, E. Y. (1966). Non-calcareous marine algae from California Miocene deposits. *Nova Hedwigia* 10:273–95.

Pavia, H., Toth, G. B., Lindgren, A., and Aberg, P. (2003). Intraspecific variation in the phlorotannin content of the brown alga *Ascophyllum nodosum. Phycologia* 42:378–83.

Pearson, G. A., and Brawley, S. H. (1998). A model for signal transduction during gamete release in the fucoid alga *Pelvetia compressa*. *Plant Physiol.* 118:305–13.

Percival, E., and McDowell, R. H. (1967). *Chemistry and Enzymology of Marine Algal Polysaccharides*. London: Academic Press.

Pereira, R. C., Cavalcanti, D. N., and Teixeira, V. L. (2000). Effects of secondary metabolites from the tropical Brazilian brown alga *Dictyota menstrualis* on the amphipod *Parhyale hawaiensis. Mar. Ecol. Progr. Ser.* 205:95–100.

Phillips, J. A., and Clayton, M. N. (1993). Comparative flagellar morphology of spermatozoids of the Dictyotales (Pheophyceae). *Eur. J. Phycol*. 28:123–7.

Pohnert, G., and Boland, W. (2002). The oxylipin chemistry of attraction and defense in brown algae and diatoms. *Nat. Prod. Rep.* 19:108–22.

Potin, P., Bouarab, K., Kupper, F., and Kloareg, B. (1999). Oligosaccharide recognition signals and defense reactions in marine plant-microbe interactions. *Curr. Opin. Microbiol.* 2:276–83.

Price, I. R., and Ducker, S. C. (1966). The life history of the brown alga *Splachnidium rugosum. Phycologia* 5:261–73.

Pueschel, C. M., and Korb, R. E. (2001). Storage of nitrogen in the form of protein bodies in the kelp *Laminaria solidungula. Mar. Ecol. Progr. Ser.* 218:107–14.

Rawlence, D. J. (1973). Some aspects of the ultrastructure of *Ascophyllum nodosum* (L.) Le Jolis (Phaeophyceae, Fucales) including observations on cell plate formation. *Phycologia* 12:17–28.

Reed, D. C., Laur, D. R., and Ebeling, A. W. (1988). Variation in algal dispersal and recruitment: the importance of episodic events. *Ecol. Monogr*. 58:321–55.

Reed, R. H., Davison, I. R., Chudek, J. A., and Foster, R. (1985). The osmotic role of mannitol in the Phaeophyta: An appraisal. *Phycologia* 24:35–47.

Rousseau, F., Leclerc, M-C., and de Reviers, B. (1997). Molecular phylogeny of European Fucales (Phaeophyceae) based on partial large-subunit rDNA sequence comparisons. *Phycologia* 36:438–46.

Russell, G., and Fletcher, R. L. (1975). A numerical taxonomic study of the British Phaeophyta. *J. Mar. Biol. Assoc. UK* 55:763–83.

Russell, G., and Garbary, D. (1978). Generic circumscription in the family Ectocarpaceae (Phaeophyceae). *J. Mar. Biol. Assoc. UK* 58:517–25.

Sargent, M. C., and Lantrip, L. W. (1952). Photosynthesis, growth and translocation in giant kelp. *Am. J. Bot*. 39:99–107.

Saunders, G. W., and Druehl, L. D. (1992). Nucleotide sequences of the small-subunit ribosomal RNA genes from selected Laminariales (Phaeophyta). Implications for kelp evolution. *J. Phycol*. 28:544–9.

Savaugeau, C. (1899). Les Cutlériacées et leur alternance de générations. *Ann. Sci. Nat. Bot. Ser. 8* 10:265–62.

Savaugeau, C. (1900–14). Remarques sur les Sphacélariacées. Bordeaux. 634 pp. in *J. Bot*. 14–18.

Scagel, R. F. (1971). *Guide to Common Seaweeds of British Columbia*. Victoria: British Columbia Prov. Museum.

Schaffelke, B., and Lüning, K. (1994). A circannual rhythm controls seasonal growth in the kelps *Laminaria hyperborea* and *L. digitata* from Helgoland (North Sea). *Eur. J. Phycol*. 29:49–56.

Schloesser, R. E., and Blum, J. L. (1980). *Sphacelaria lacustris* sp. nov., a freshwater brown alga from Lake Michigan. *J. Phycol*. 16:201–7.

Schmitt, T. M., Lindquist, N., and Hay, M. E. (1998). Seaweed secondary metabolites as antifoulants: effects if *Dictyota* spp. diterpenes on survivorship, settlement, and development of marine invertebrate larvae. *Chemoecology* 8:125–31.

Schoenwaelder, M. E. A., and Clayton, M. N. (1999). The presence of phenolic compounds in isolated cell walls of brown algae. *Phycologia* 38:161–6.

Schoenwaelder, M. E. A., and Clayton, M. N. (2000). Physode formation in embryos of *Phyllospora comosa* and *Hormosira banksii* (Phaeophyceae). *Phycologia* 39:1–9.

Schreiber, E. (1932). Über die Entwicklungsgeschichte und die systematische Stellung der Desmarestiaceen. *Z. Bot*. 25:561–82.

Serrão, E. A., Pearson, G., Kautsky, M. L., and Brawley, S. H. (1996). Successful external fertilization in turbulent environments. *Proc. Natl. Acad. Sci., USA* 93:5286–90.

Shibata, T., Tamaguchi, K., Nagayama, K., Kawaguchi, S., and Nakamura, T. (2002). Inhibitory activity of brown algal phlorotannins against glycosidases from

the viscera of the turban shell *Turbo cornutus. Eur. J. Phycol.* 37:493–500.

Shih, M. L., Floch, J-Y., and Srivastava, L. M. (1983). Localization of ^{14}C-labeled assimilates in sieve elements of *Macrocystis integrifolia* by histoautoradiography. *Can. J. Bot.* 61:157–63.

Sideman, E. J., and Scheirer, D. C. (1977). Some fine structural observations on developing and mature sieve elements in the brown alga *Laminaria saccharina. Am. J. Bot.* 64:649–57.

Sjøtun, K., and Schoschina, E. V. (2002). Gametophytic development of *Laminaria* spp. (Laminariales, Phaeophyta) at low temperature. *Phycologia* 41:147–52.

Smith, G. M. (1955). *Cryptogamic Botany*, Vol. 1, 2nd edn. New York: McGraw-Hill.

Smith, G. M. (1969). *Marine Algae of the Monterey Peninsula, California*, 2nd edn. Stanford, Calif.: Stanford University Press.

Speransky, V. V., Speransky, S. S., and Brawley, S. H. (1999). Cryoanalytical studies of freezing damage and recovery in *Fucus vesiculosus* (Phaeophyceae). J. *Phycol.* 35:1264–75.

Speransky, V. V., Brawley, S. H., and McCully, M. E. (2001). Ion fluxes and modification of the extracellular matrix during gamete release in fucoid algae. *J. Phycol.* 37:555–73.

Stafford, C. J., Green, J. R., and Callow, J. A. (1992). Organization of glycoproteins into plasma membrane domains on *Fucus serratus* eggs. *J. Cell Sci.* 101:437–48.

Steen, H. (2003). Apical hair formation and growth of *Fucus evanescens* and *F. serratus* (Phaeophyceae) germlings under various nutrient and temperature regimes. *Phycologia* 42:26–30.

Sundene, O. (1962a). Growth in the sea of *Laminaria digitata* sporophytes from cultures. *Nytt Mag. Bot.* 9:5–24.

Sundene, O. (1962b). The implications of transplant and culture experiments on the growth and distribution of *Alaria esculenta. Nytt Mag. Bot.* 9:155–74.

Sundene, O. (1963). Reproduction and ecology of *Chorda tomentosa. Nytt Mag. Bot.* 10:159–71.

Tan, I. H., and Druehl, L. D. (1996). A ribosomal DNA phylogeny supports the close evolutionary relationships among the Sporochnales, Desmarestiales, and Laminariales (Phaeophyceae). *J. Phycol.* 32:112–18.

Targett, N. M., and Arnold, T. M. (1998). Predicting the effects of brown algal phlorotannins on marine herbivores in tropical and temperate oceans. *J. Phycol.* 34:195–205.

Tatewaki, M. (1966). Formation of a crustaceous sporophyte with unilocular sporangia in *Scytosiphon lomentaria. Phycologia* 6:62–6.

Taylor, W. R. (1957). *Marine Algae of the Northeastern Coast of North America*. Ann Arbor: University of Michigan Press.

Taylor, W. R. (1960). *Marine Algae of the Eastern Tropical and Subtropical Coasts of the Americas*. Ann Arbor: University of Michigan Press.

Terry, L. A., and Moss, B. L. (1980). The effect of photoperiod on receptacle initiation in *Ascophyllum nodosum* (Lo) Le Jol. *Br. Phycol. J.* 15:291–301.

Terry, L. A., and Moss, B. L. (1981). The effect of irradiance and temperature on the germination of four species of Fucales *Br. Phycol. J.* 16:143–51.

Thuret, G. (1854). Recherches sur la fécondation des Fucacées. *Ann. Sci. Nat. Bot. IV* 2:197–214.

Thuret, G., and Bornet, E. (1878). *Études Phycologiques*. Paris.

Tovey, D. J., and Moss, B. L. (1978). Attachment of the haptera of *Laminaria digitata* (Huds.) Lamour. *Phycologia* 17:17–22.

Tseng, C. K. (1981). Commercial cultivation. In *The Biology of Seaweeds*, ed. C. S. Lobban, and M. J. Wynne, pp. 680–725. Berkeley and Los Angeles: Univ. Calif. Press.

Vadas, R. L. (1972). Ecological implications of culture studies on *Nereocystis luetkeana. J. Phycol.* 8:196–203.

Van Alstyne, K. L., and Pelletreau, K. N. (2000). Effect of nutrient enrichment on growth and phlorotannin production in *Fucus gardneri* embryos. *Mar. Ecol. Progr. Ser.* 206:33–43.

van den Hoek, C. (1982). The distribution of benthic marine algae in relation to the temperature regulation of their life histories. *Biol. J. Linn. Soc.* 18:81–144.

van den Hoek, C., and Flinterman, A. (1968). The life history of *Sphacelaria furcigera* Kütz. (Phaeophyceae). *Blumea* 16:193–242.

Vreeland, V. (1972). Immunocytochemical localization of the extracellular polysaccharide alginic acid in the brown seaweed. *Fucus distichus. J. Histochem. Cytochem.* 20:358–67.

Vreeland, V., Waite, J. H., and Epstein, M. (1998). Polyphenols and oxidases in substratum adhesion by marine algae and mussels. *J. Phycol.* 34:1–8.

Walker, F. T. (1956). Periodicity of the Laminariaceae around Scotland. *Nature* 177:1246.

Williams, J. L. (1898). Reproduction in *Dictyota dichotoma. Ann. Bot.* 12:559–60.

Williams, J. L. (1904). Studies in the Dictyotaceae. I. The cytology of the gametophyte generation. *Ann. Bot.* 18:183–204.

Williams, J. L. (1905). Studies in the Dictyotaceae. II. The periodicity of sexual cells in *Dictyota dichotoma*. *Ann. Bot*. 19:531–60.

Wright, P. J., Callow, J. A., and Green, J. R. (1995a). The *Fucus* (Phaecophyceae) sperm receptor for eggs. II. Isolation of a binding protein which partially activates eggs. *J. Phycol.* 31:592–600.

Wright, P. J., Green, J. A., and Callow, J. A. (1995b). The *Fucus* (Phaeophyceae) sperm receptor for eggs. I. Development and characteristics of a binding assay. *J. Phycol*. 31:584–91.

Wynne, M. J. (1969). Life history and systematic studies of some Pacific North American Phaeophyceae (brown algae). *Univ. Calif. Publ. Bot*. 50:1–88.

Chapter 22

Prymnesiophyta

PRYMNESIOPHYCEAE

The Prymnesiophyta are a group of uninucleate flagellates characterized by the presence of a haptonema between two smooth flagella. The Prymnesiophyta have two membranes of chloroplast endoplasmic reticulum, as do the Cryptophyta and the Heterokontophyta, but differ in having flagella without mastigonemes. Molecular data also show that the Prymnesiophyta are distinct from the Cryptophyta and Heterokontophyta (Bhattacharya and Ehlting, 1995; Medlin et al., 1994). Until 1962, the organisms were considered part of the Chrysophyceae, at which time Christensen split them off into a separate class, the Haptophyceae (named after the presence of the haptonema). The name Haptophyceae was a descriptive name and not based on a genus in the class; thus the name was later changed to Prymnesiophyceae, based on the genus *Prymnesium* (Fig. 22.7) (Hibberd, 1976). The fossil record of the Prymnesiophyceae is known from the Carboniferous (approximately 300 000 000 years ago) (Faber and Preisig, 1994; Jordan and Chamberlain, 1997).

The cells are commonly covered with scales. In many cases, the scales are calcified, thereby producing coccoliths. The chloroplasts lack girdle lamellae and most contain chlorophylls *a* and c_1/c_2, β-carotene, diadinoxanthin, and diatoxanthin (Zapata et al., 2004). The storage product is chrysolaminarin (leucosin) in vesicles in the posterior end of the cell (Janse et al., 1996). The anterior end of the cell has a large Golgi apparatus and sometimes a contractile vacuole.

The Prymnesiophyceae are primarily marine organisms, although there are some freshwater representatives. They make up a major part of the marine nannoplankton and constitute about 45% of the total phytoplankton cells in the middle latitudes of the South Atlantic. They decrease in frequency toward the poles although some still occur in polar waters (Manton et al., 1977).

Cell structure

Flagella

Most of the Prymnesiophyceae have two smooth flagella of approximately the same length (Figs. 22.1, 22.3(*a*)). The Pavlovales is the exception, where one flagellum is longer than the other and is usually covered by small cylindrical to club-shaped hollow scales 70 nm long and 20 nm wide (Fig. 22.3(*b*)) (van der Veer, 1969; Green and Manton, 1970). Because the class is characterized by two more or less equal, smooth flagella, a number of genera, such as *Diacronema* (Fig. 22.4), *Isochrysis* (Fig. 22.18(*b*)), and *Dicrateria*, which have rudimentary or no haptonema, are grouped in the Prymnesiophyceae (Green and Pienaar, 1977). There is usually no flagellar swelling associated with an eyespot as occurs in many other golden-brown flagellates with two membranes of chloroplast E.R. (Hibberd, 1976), although there are exceptions (Green and Hibberd, 1977).

During swimming, the flagellar end of the cell can be forward with the flagella sweeping outward and backward down the sides of the body (Fig. 22.5(*a*)), or the flagellar end may be directed

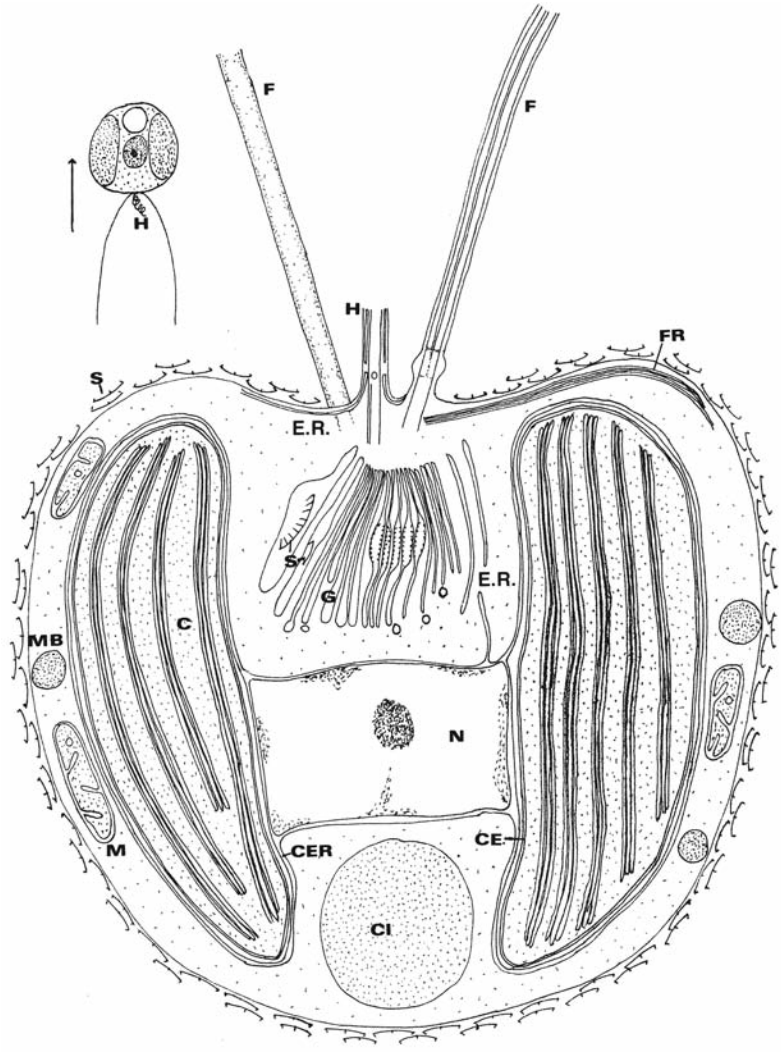


Fig. 22.1 A light and electron microscopical drawing of a cell of a typical member of the Prymnesiophyceae, *Chrysochromulina* sp. A rapidly swimming individual is shown, with the arrow indicating the direction of movement. (C) Chloroplast; (CE) chloroplast envelope; (CER) chloroplast endoplasmic reticulum; (CI) chrysolaminarin vesicle; (E.R.) endoplasmic reticulum; (F) flagellum; (FR) flagellar root; (G) Golgi body; (H) haptonema; (M) mitochondrion; (MB) muciferous body; (N) nucleus; (S) scale. (Adapted from Hibberd, 1976.)

backward (Fig. 22.5(*b*)). Movement is usually rapid, the cells swimming only for a short distance in one direction, after which they rapidly change the position of the flagella and move off in the opposite direction. In *Pavlova* (Fig. 22.3(*b*)), the flagellar action is a little different, with the longer flagellum directed forward and the shorter flagellum trailing or directed outward.

Haptonema

A **haptonema** is a filamentous appendage arising near the flagella but thinner and with different properties and structure. The haptonema ranges from a few profiles of E.R. that represent a reduced haptonema in *Imatonia rotunda* (Fig. 22.18(*c*), (*d*)) (Green and Pienaar, 1977) to a short bulbous structure in *Hymenomonas roseola* (Fig. 22.6(*a*)) to the 80-μm-long whip-like structure in *Chrysochromulina parva* (Fig. 22.6(*b*)) (Manton, 1967a). The haptonema of *Prymnesium parvum* has an internal structure similar to the haptonema of other Prymnesiophyceae and will be used as an example of haptonemal structure (Fig. 22.7) (Manton, 1964). In transverse section the haptonema is composed of three concentric membranes surrounding a core containing seven microtubules. The core is covered by the innermost of the three membranes so that there is no contact between the core microtubules and the outer portion of the haptonema. The space



Fig. 22.2 **Irene Manton** 1904–1988. Dr. Manton was a graduate of Cambridge University. She was a lecturer in botany at the University of Manchester from 1929 to 1945 and Professor of Botany at the University of Leeds from 1945 to 1969. Dr. Manton was one of the foremost cytologists during the 1950s and 1960s when the new science of electron microscopy was adding vast amounts of new information to the understanding of algae. The work of Dr. Manton and her colleagues led to the distinct features of the haptophytes and the recognition of these organisms as a distinct group of algae.

between the innermost and middle membranes is a vesicle continuous over the tip of the core. The haptonema is commonly covered with small body scales.

The microtubules in the haptonema slide, relative to one another, probably through the calcium-binding protein centrin (Lechtreck, 2004), to produce two basic movements, coiling and bending (Greyson et al., 1993):

1 **Coiling** is a sensory response to obstacles (Kawachi and Inouye, 1994). The haptonema coils instantly when forward-swimming cells encounter obstacles. The flagella are thrown backward and generate propulsive forces, resulting in backward swimming.
2 **Bending** by the haptonema occurs during food capture by the cells (Inouye and Kawachi, 1994; Kawachi et al., 1991). Prey particles adhere to the haptonema as the cells swim with the haptonema projecting ahead of the cell, and the flagella beating alongside. The adhering particles are transported down to a particular point on the haptonema, about 2 μm distal from the base, called the **particle-aggregating center** (Fig. 22.8). The particles accumulate at the particle-aggregating center, resulting in the production of a massive aggregate. In the aggregate, individual particles tightly adhere to one another, suggesting that some sort of cementing material is secreted. After reaching a certain size, the aggregate moves to the tip of the haptonema. The haptonema bends into a sigmoid shape and eventually delivers the aggregate to the posterior end of the cell, where the aggregate is injected into a food vacuole.

Chloroplasts

Usually there are two elongate discoid chloroplasts in each cell (Fig. 22.1). Each chloroplast is surrounded by four membranes: the two membranes of the chloroplast envelope, and outside of them the two membranes of the chloroplast E.R. The thylakoids are aggregated into bands of three. A girdle band of thylakoids is usually absent (Hibberd, 1976). A pyrenoid is commonly present in the center of the chloroplast or as a bulge to one side. Eyespots are not common in the Prymnesiophyceae although *Pavlova* has an eyespot, which consists of a group of lipid droplets inside the anterior end of a chloroplast (Green, 1973) (Fig. 22.21).

Other cytoplasmic structures

Two types of membrane-bounded vesicles are in the cytoplasm, the first containing lipids and the second the storage product. The storage product is usually stated as being chrysolaminarin (leucosin) (Janse et al., 1996), although in a study of *Pavlova mesolychnon* (Fig. 22.3(*b*)) it was found that one of

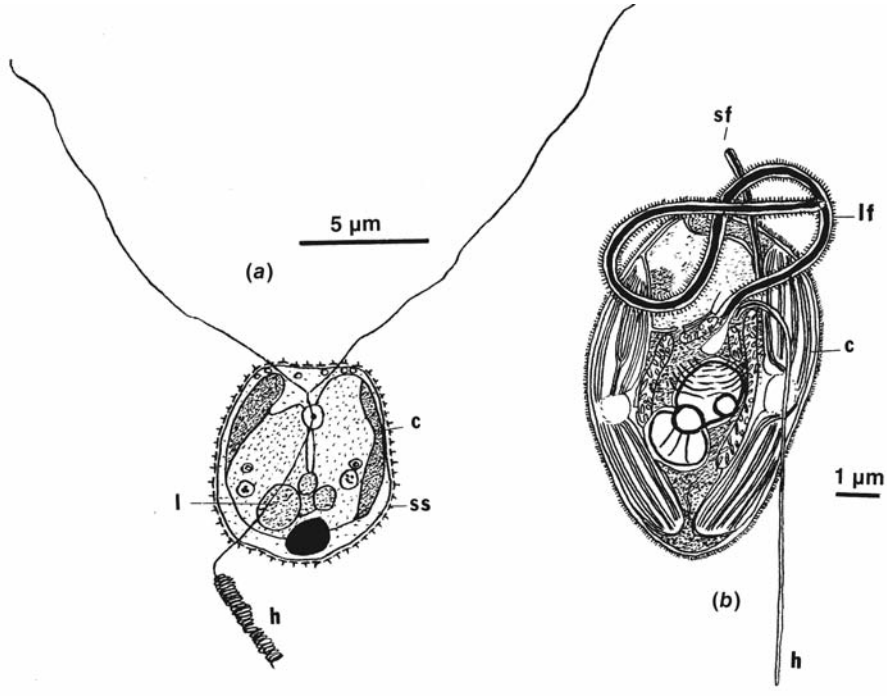


Fig. 22.3 (*a*) Ventral view of a saddle-shaped cell of *Chrysochromulina ephippum* with the haptonema loosely coiled. (*b*) *Pavlova mesolychnon*. (c) Chloroplast; (h) haptonema; (l) leucosin vesicle; (lf) long flagellum; (ss) spined scale; (sf) short flagellum. ((*a*) after Parke et al., 1956; (*b*) after van der Veer, 1969.)

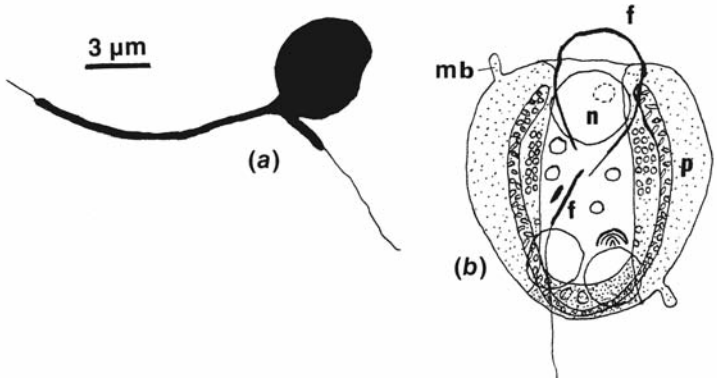


Fig. 22.4 (*a*) Drawing of a direct preparation of *Diacronema vlkianum* showing the hair points at the tip of the flagella and the absence of lateral hairs. (*b*) A resting cell of *D. vlkianum*. (f) Flagellum; (mb) muciferous body (discharged); (n) nucleus; (p) plastid. (After Fournier, 1969.)

the storage products present in the cells was a β-1,3 linked glucan similar to paramylon in the Euglenophyceae (Kreger and van der Veer, 1970).

In some of the Prymnesiophyceae and particularly the genus *Chrysochromulina*, muciferous bodies are under the plasma membrane (Figs. 22.1, 22.5(*a*), 22.10(*b*)). They have the same structure as the muciferous bodies in the Raphidophyceae, Dinophyceae, and Chrysophyceae, and consist of a single-membrane-bounded vesicle filled with semi-opaque contents. When they are discharged outside the cell, they appear as substantial cylinders of opaque material of uniform diameter. The function of muciferous bodies is not known.

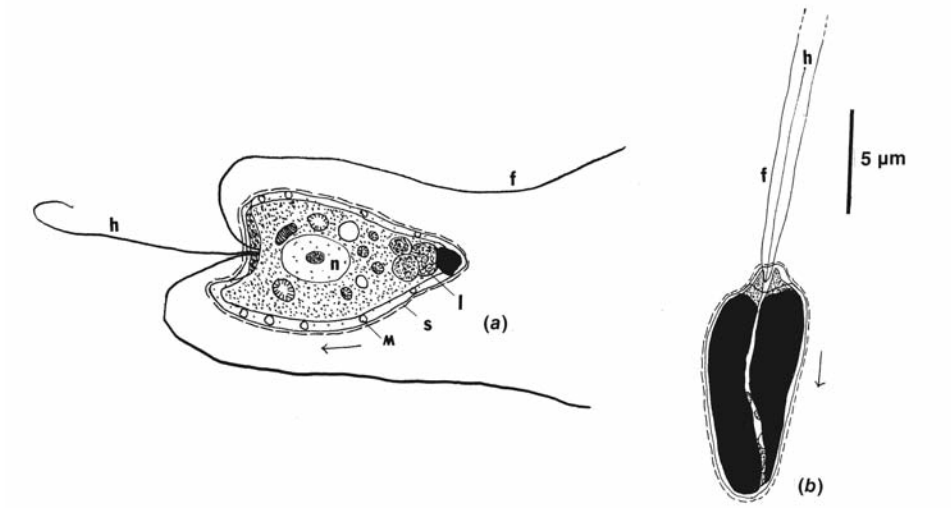


Fig. 22.5 *Chrysochromulina polylepis*. (*a*) Cell with flagella in position for swimming with flagellar pole forward. (*b*) Cell swimming with flagellar pole to the rear. (f) Flagellum; (h) haptonema; (l) leucosin vesicle; (m) muciferous body; (n) nucleus; (s) scale. (After Manton and Parke, 1962.)

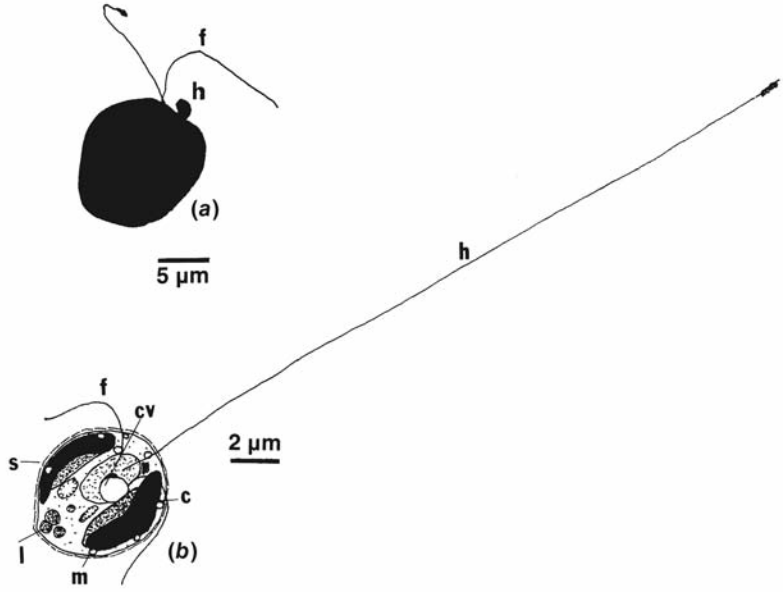


Fig. 22.6 (*a*) *Hymenomonas roseola*, a dried cell showing the flagella and the short bulbous haptonema (which actually arises between the two flagella). (*b*) A slowly gliding cell of *Chrysochromulina parva*. (c) Chloroplast; (cv) contractile vacuole; (f) flagellum; (h) haptonema; (l) leucosin; (m) muciferous body; (s) scale. ((*a*) after Manton and Peterfi, 1969; (*b*) after Parke et al., 1962.)

Phaeocystis globosa has vesicles that contain tightly-wound filaments of chitin (Chrétiennot-Dinet et al., 1997). Each vesicle contains five chitin filaments that attach near the base of another chitin filament (Fig. 22.9). The chitin filaments produce a five-sided star at their base when they are released from their vesicles.

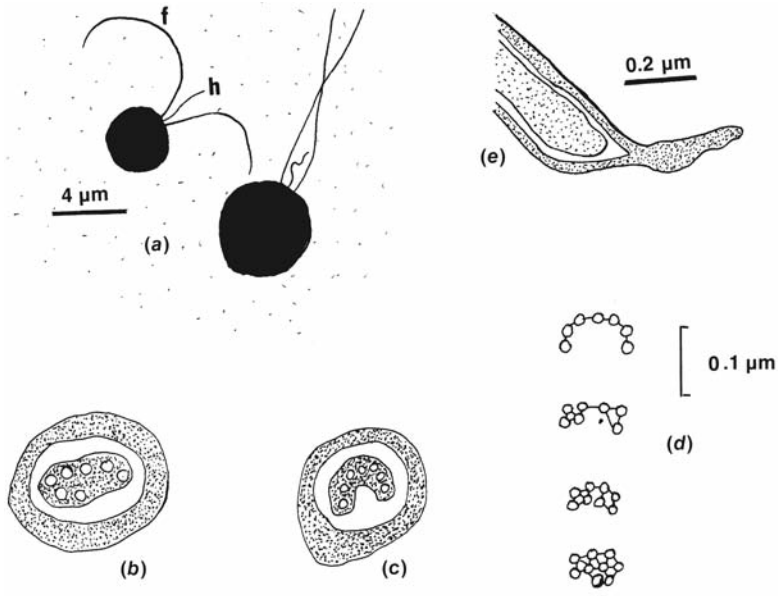


Fig. 22.7 *Prymnesium parvum.* (*a*) Drawing of two cells dried and shadow-cast showing the two smooth flagella (f) and the short haptonema (h) on each cell. (*b*) Transverse section of a haptonema showing the structure of the middle region of seven microtubules in the core surrounded by the membrane-bounded cavity and the haptonemal wall bounded by the plasmalemma externally. (*c*) Transverse section of a haptonema near the point of union with the cell showing the crescentric shape of the core characteristic of this region. (*d*) Progressive levels of haptonema tubules from immediately below the plasmalemma to the distal points of the microtubules. (e) Longitudinal section of a tip of a haptonema. ((*a*) after Manton, 1966; (*b*)–(e) after Manton, 1968.)

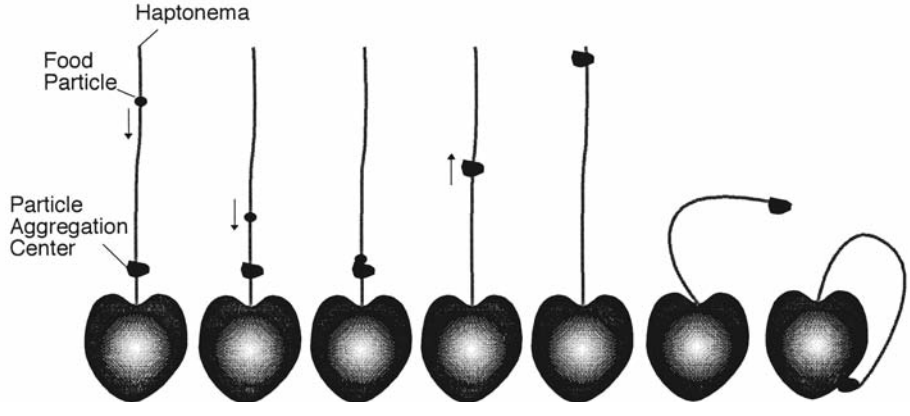


Fig. 22.8 The sequence of events by which food particles adhere to a haptonema and are moved toward the particle aggregation center. The mass of particles at the particle aggregation center then moves to the tip of the haptonema; the haptonema bends to deposit the mass of particles at the posterior end of the cell where the particles are taken up in food vacuoles. (Adapted from Kawachi et al., 1991.)

Surface protrusions containing cytoplasm are common in the Prymnesiophyceae; they are called **pseudopodia**. Also, cells can extrude slender trailing filaments from their surfaces, which can be straight or branched. These filaments, called **filopodia**, eventually become segmentally constricted and break up into droplets. Many of the organisms are phagocytic and consequently have food vesicles in the cytoplasm in which they digest bacteria and other small algae. They are not selective in taking up material into the food vesicles, and will take up indigestible detritus as rapidly as bacteria and other algae.

Like many of the other algal groups, the Prymnesiophyceae participate in symbiotic events. Invertebrate radiolaria can harbor prymnesiophyte algal symbionts (Anderson et al., 1983).

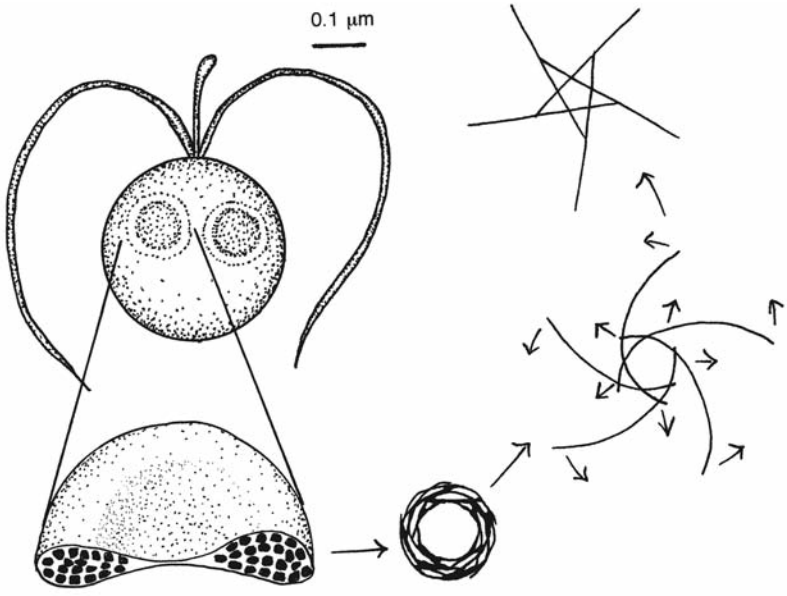


Fig. 22.9 *Phaeocystis globosa* showing a cell with two vesicles containing coiled filaments made of chitin. The coiled filaments unwind when they are discharged outside the cell, forming a 5-ray star structure. (After Chrétiennot-Dinet et al., 1997.)

The symbionts are held in the rhizopodial network surrounding the central capsule of the radiolarian. The algal symbionts fix carbon dioxide, and some of the photosynthate passes to the radiolarian.

Scales and coccoliths

Most of the members of the Prymnesiophyceae have a cell covering consisting of a number of elliptical scales (Figs. 22.1, 22.10). The elliptical scales are embedded in a mucilaginous substance, and in some organisms a layer of calcified coccoliths is outside the scales. The structure of the scales can vary considerably, but all of them appear to have an elliptical organic scale constituting either the whole structure of the scale or just the base plate on which the rest of the structure is based. The elliptical organic scale (plate scale) has radiating ridges extending to the edge (Fig. 22.10(*a*)) (Parke and Manton, 1962). *Chrysochromulina minor* (Fig. 22.10(*b*)) (Parke et al., 1955) and *Chrysochromulina parva* (Fig. 22.6(*b*)) (Parke et al., 1962) have a cell covering of only plate scales of the type just described. In other Prymnesiophyceae the rims of the elliptical base plate have become turned up to form a variety of different types of scales ranging from very shallow tub-shaped scales with the edges of the scales barely turned up, to very long spined structures with the spine being the very elongated upturned rim of the organic scale (Fig. 22.10(*c*)) (Manton, 1972). A number of different types of scales can be present on the same organism. *Chrysochromulina kappa* (Fig. 22.10(*d*)) has plate scales around most of the body with a few short-spined scales near the flagella (Parke et al., 1955). *Chrysochromulina ericina* (Fig. 22.10(*e*)) has a cell covering consisting of plate scales with about 30 long-spined scales intermixed with the plate scales (Parke et al., 1956). *Chrysochromulina pringsheimii* (Fig. 22.10(*f*)) has an even more complex cell covering consisting of four types of scales. Long-spined scales are at either end of the cell with small-spined scales covering the rest of the cell. Underneath this spined layer is a layer of plate scales, and, finally, near the base of the flagella are a number of small plate scales (Parke and Manton, 1962).

The organic scales originate in the Golgi apparatus (Figs. 22.1, 22.13) (Hawkins and Lee, 2001). A scale, when first formed in a Golgi vesicle, is closely enveloped by the vesicle membrane no matter how elaborate the shape of the scale is (long-spined, etc.); but immediately before the scale is liberated to the outside of the cell, this close contact is lost (Manton, 1967b).

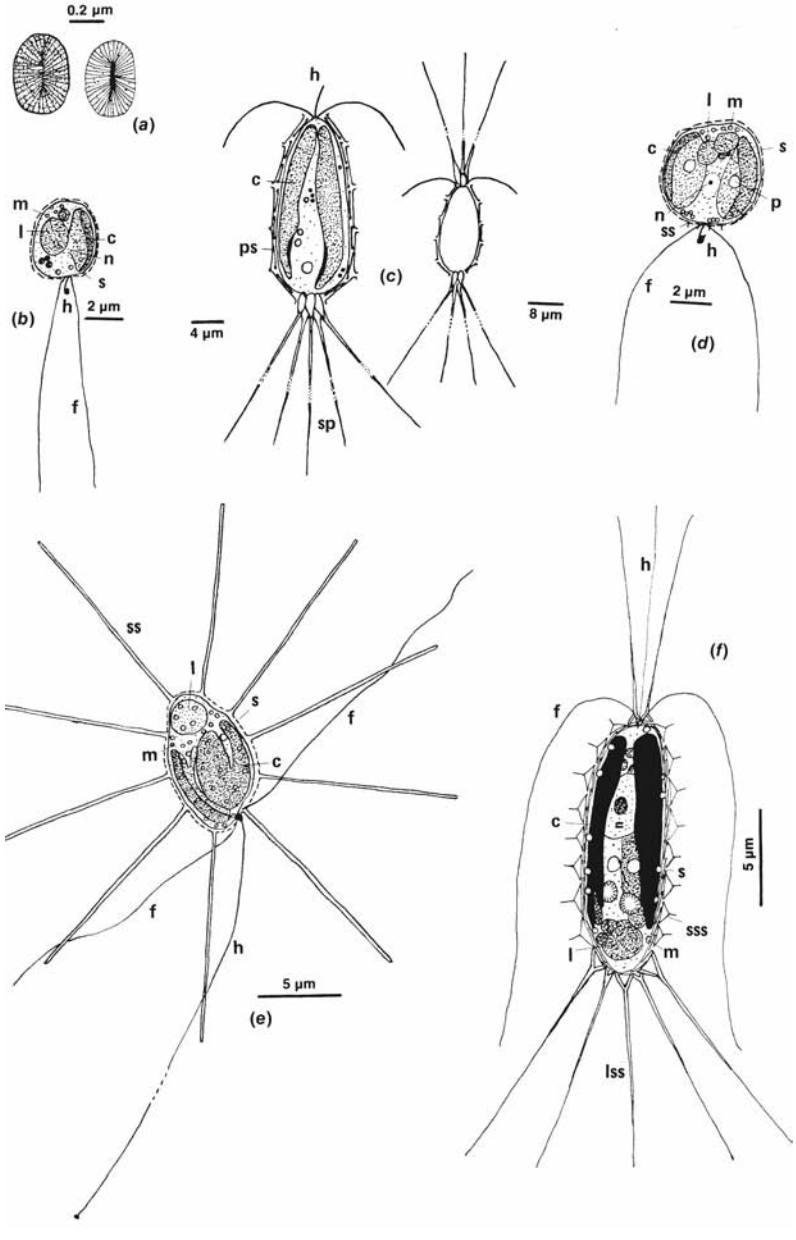


Fig. 22.10 (*a*) Small plate scales of *Chrysochromulina pringsheimii*, the upper face on the left and the lower face on the right. (*b*) *Chrysochromulina minor*, individual swimming with the flagella and haptonema behind the body in the position characteristic of the species during rigid swimming. (*c*) *Chrysochromulina parkae*, two forms. (*d*) *Chrysochromulina kappa*, swimming with the flagella and haptonema behind the body, the characteristic position of species during rapid swimming. (e) *Chrysochromulina ericina*, individual with dividing chloroplasts anchored by a haptonema which is partially extended; the flagella are in the characteristic position when the cells are stationary. (*f*) *Chrysochromulina pringsheimii*, individual swimming with the flagella and haptonema in front of the body, and the haptonema fully extended. (c) Chloroplast; (f) flagellum; (h) haptonema; (l) leucosin vesicle; (lss) long-spined scale; (m) muciferous body; (n) nucleus; (p) pyrenoid; (ps) plate scale; (s) scale; (sp) spine; (ss) spined scale; (sss) small-spined scale. ((*a*), (*f*) after Parke and Manton, 1962; (*b*), (*d*) after Parke et al., 1955; (*c*) after Green and Leadbeater, 1972; (e) after Parke et al., 1956.)

There is a diurnal rhythm in the production of scales. Manton and Parke (1962) showed that in *Chrysochromulina polylepis* the greatest production of scales is in the late afternoon with the least in the early morning hours. The time of nuclear division is the reverse, with the most mitotic figures appearing in the early morning.

Even in the non-motile filamentous stages of the Prymnesiophyceae, the cell wall is composed of scales embedded in a gelatinous matrix. In *Pleurochrysis scherffelii* (Fig. 22.11) the cells of the filamentous stage are covered in cellulosic scales produced by the single Golgi apparatus. By the use of the cinephotography, Brown (1969) showed that during wall formation the whole protoplast revolves so that the scale secretions of the Golgi apparatus are received more or less evenly by all portions of the cell wall.

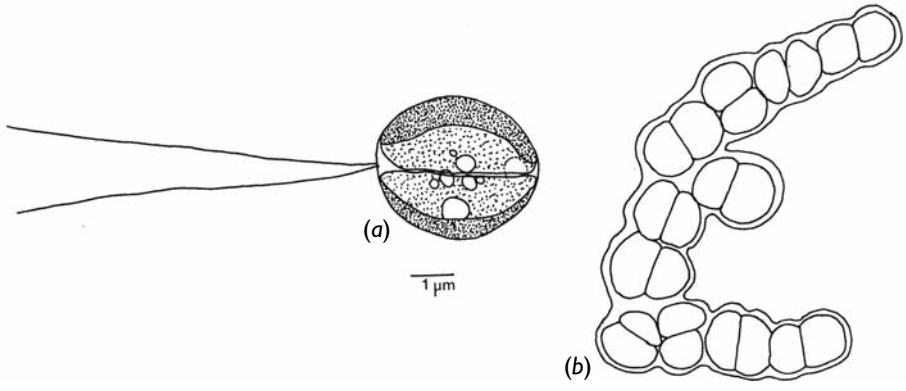


Fig. 22.11 *Pleurochrysis scherffelii.* (*a*) Motile cell. (*b*) Filamentous stage. (After Pringsheim, 1955.)

Coccoliths are calcified scales of the Prymnesiophyceae. They were originally described as minute carbonate discs in Cretaceous deposits and thought to be of inorganic origin (Marsh, 2004). Later they were in sea bottom oozes brought up by the first Atlantic cable survey in 1858. Their algal nature was not recognized until 1898. Coccoliths are basically organic scales that have calcium carbonate ($CaCO_3$) deposited on one surface in a characteristic pattern depending on the species of the alga. Under ordinary conditions anhydrous $CaCO_3$ exists in nature in two crystalline forms (Fig. 4.7), **calcite** (rhombohedral) and **aragonite** (orthorhombic), which differ in structure, hardness, specific gravity, and solubility. In coccoliths the form of $CaCO_3$ is usually calcite. The calcite is attached to the outer surface of a plate scale, which has a pattern of radiating ridges (Figs. 22.13, 22.24) whereas the inner side of the scale (toward the cell) is virtually patternless. The coccoliths of *Emiliania huxleyi* (Fig. 22.16(*b*)) are relatively simple and can serve as an example of coccolith structure although it should be realized that there is a multitude of different coccolith forms, some very complex (Fig. 22.16). The coccoliths of *E. huxleyi* (Figs. 22.12, 22.16(*b*)) are composed of a number of hollow crystals of calcite arranged around the periphery of a plate scale (Young et al., 1992). Each coccolith consists of an upper and lower shield joined by a tube. The tube and the shields are composed of subunits.

Coccolith formation begins with the production of an uncalcified organic plate-scale in the center of Golgi cisternae (Figs. 22.13, 22.14) (Marsh, 1996, 2004). Highly acidic polysaccharides are produced as 25 nm diameter spheres in the peripheral part of Golgi cisternae. The highly acidic polysaccharides are extremely negative polyanions that sequester large numbers of calcium ions. The 25 nm diameter spheres are pinched off the Golgi cisternae as vesicles, which eventually fuse with a vesicle containing an uncalcified organic plate-scale. The 25 nm diameter spheres aggregate on the scales in the area of future calcium deposition. Calcium is deposited in the area of the 25 nm diameter spheres to produce calcified coccoliths. The remaining material in the spheres is reorganized into an amorphous coat that surrounds the mature crystals of calcium carbonate that make up the coccoliths. The coccoliths are carried in the vesicles to the plasma membrane where the coccoliths are deposited outside the cell. Two to seven coccoliths are produced per day by *Emiliania huxleyi* (Balch et al., 1993; Linschooten et al., 1991).

Coccoliths are detached from cells in layers at the same time as other coccoliths are produced. During logarithmic growth, about the same number of coccoliths are detached as are produced. In stationary growth, however, the rate of coccolith detachment increases about threefold, while coccolith production drops off (Balch et al., 1993). Coccolithophorids have greater rates of calcification when nitrogen and phosphorus are limiting in the seawater (Corstjens and Gonzales, 2004).

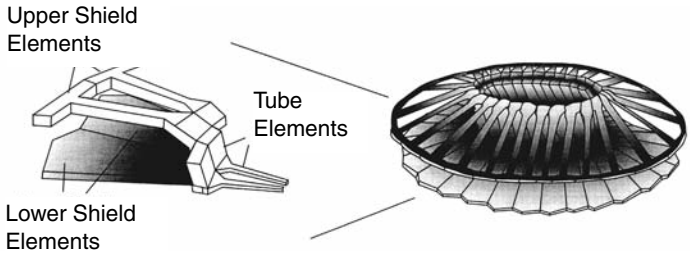


Fig. 22.12 Construction of a heterococcolith of *Emiliania huxleyi*. The heterococcolith is composed of a tube joining the upper and lower shields, each of which is composed of subunits. (Adapted from Young et al., 1992.)

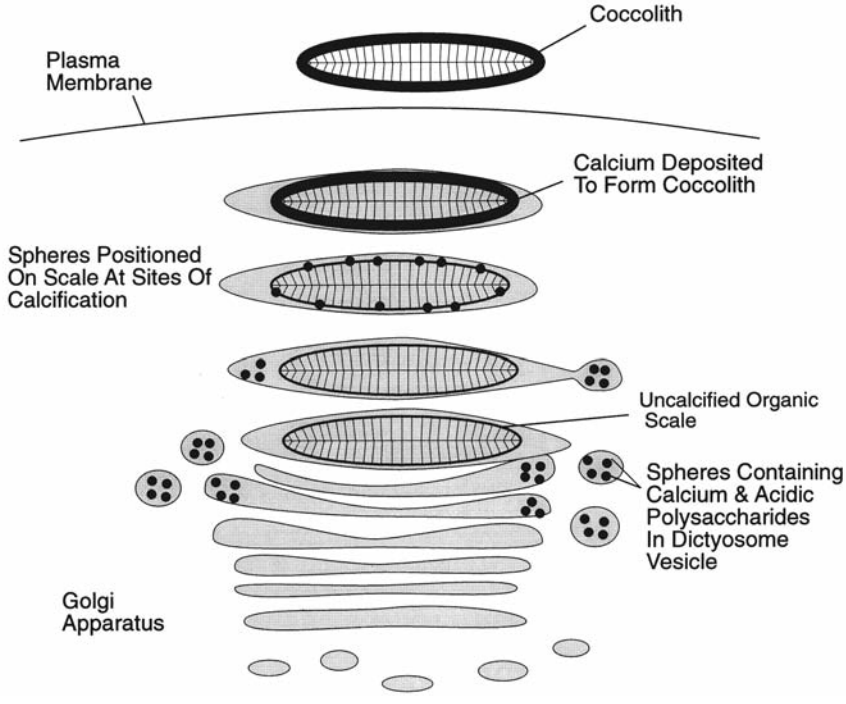


Fig. 22.13 Coccolith formation in *Pleurochrysis*. Spheres containing calcium bound to acidic polysaccharides are produced in vesicles by the Golgi apparatus. These vesicles fuse with Golgi vesicles containing uncalcified organic scales. The calcium-containing spheres become positioned on the scales at the sites of calcification and the calcium is released. The calcified scales are carried to the plasma membrane, releasing the coccoliths outside of the cell. (Adapted from Marsh, 1994.)

Coccoliths can have an outer covering of heterococcoliths that contain assemblages of morphologically complex and diverse $CaCO_3$ elements (Figs. 22.12, 22.14, 22.16), which are composed of similar (often rhombohedral) calcite crystals (Fig. 22.15). The two types of coccoliths can occur in the same organism with heterococcoliths on the diploid cells and holococcoliths on the haploid cells (Geisen et al., 2002). In *Coccolithus*, holococcoliths occur in the motile *Crystallolithus* stage (Fig. 22.15) whereas heterococcoliths occur in the non-motile stage. The base plates of heterococcoliths are produced in Golgi cisternae followed by calcification in the same cisternae. However, only the base plates of holococcoliths are produced in Golgi cisternae. These base plates are discharged outside the cell where calcification occurs within an outer vestment (Rowson et al., 1986).

The coccolithophorids (algae with coccoliths) (Fig. 22.16) are common in tropical waters because these warm waters have a low partial pressure of carbon dioxide and are usually saturated or supersaturated with calcium carbonate,

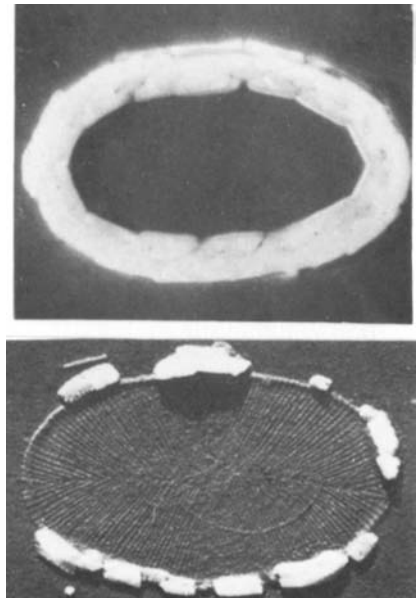


Fig. 22.14 *Top*: Intact heterococcolith of *Hymenomonas carterae*. *Bottom*: The calcium carbonate making up the heterococcolith is partially dissolved away, revealing the scale on which the calcium carbonate is deposited. (From Outka and Williams, 1971.)

the concentrations being especially high in the upper layers. Supersaturation of calcium carbonate is favorable for the formation of coccoliths, and the distribution of coccolithophorids shows a close correlation with the degree of saturation of seawater by calcium carbonate. In the seas of polar regions, the degree of saturation does not even reach 90%.

The calcification reaction is:

$$2\,HCO_3^- + Ca^{2+} \rightleftharpoons CaCO_3 + CO_2 + H_2O$$

Carbon dioxide is released in calcification, and this may make coccolithophorids more competitive by increasing the amount of CO_2 available for photosynthesis inside the cell (Nielsen, 1995). This may be particularly important in seawater where the pH of 8.2 results in a very low concentration of dissolved CO_2 of about 10 μM compared to a total dissolved carbonate (mostly HCO_3^-) of 2000 μM.

The membrane of the coccolith vesicle contains an H^{2-}ATPase that pumps H^+ out of the coccolith vesicle, removing protons produced during dehydration of bicarbonate and increasing the rate of calcification (Corstjens and Gonzales, 2004; Gonzales, 2004).

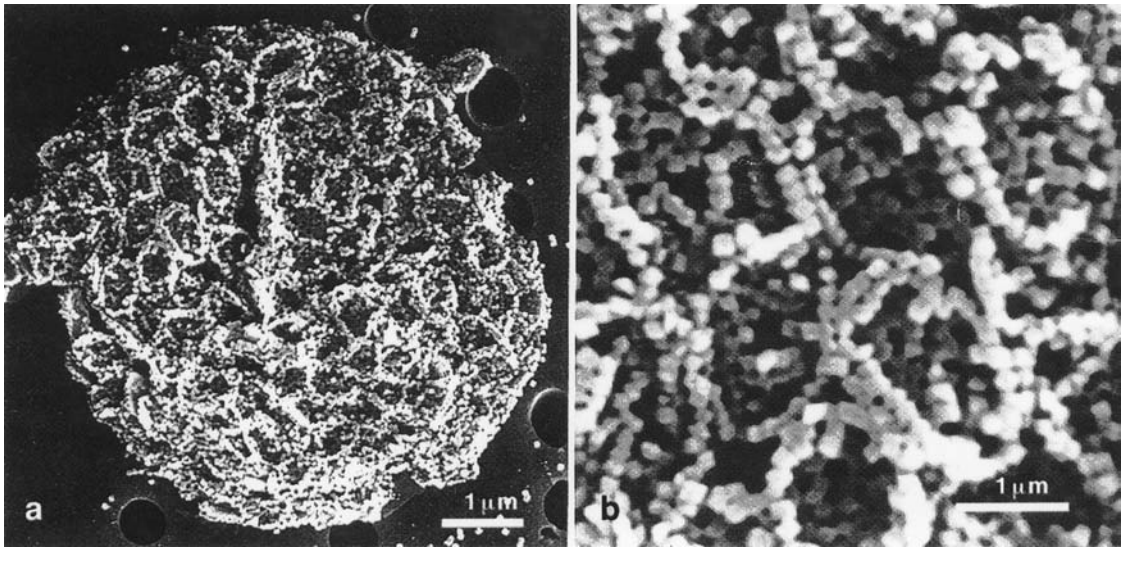


Fig. 22.15 Scanning electron micrograph of holococcoliths covering a cell of *Crystallolithus hyalinus*. (From Faber and Preisig, 1994.)

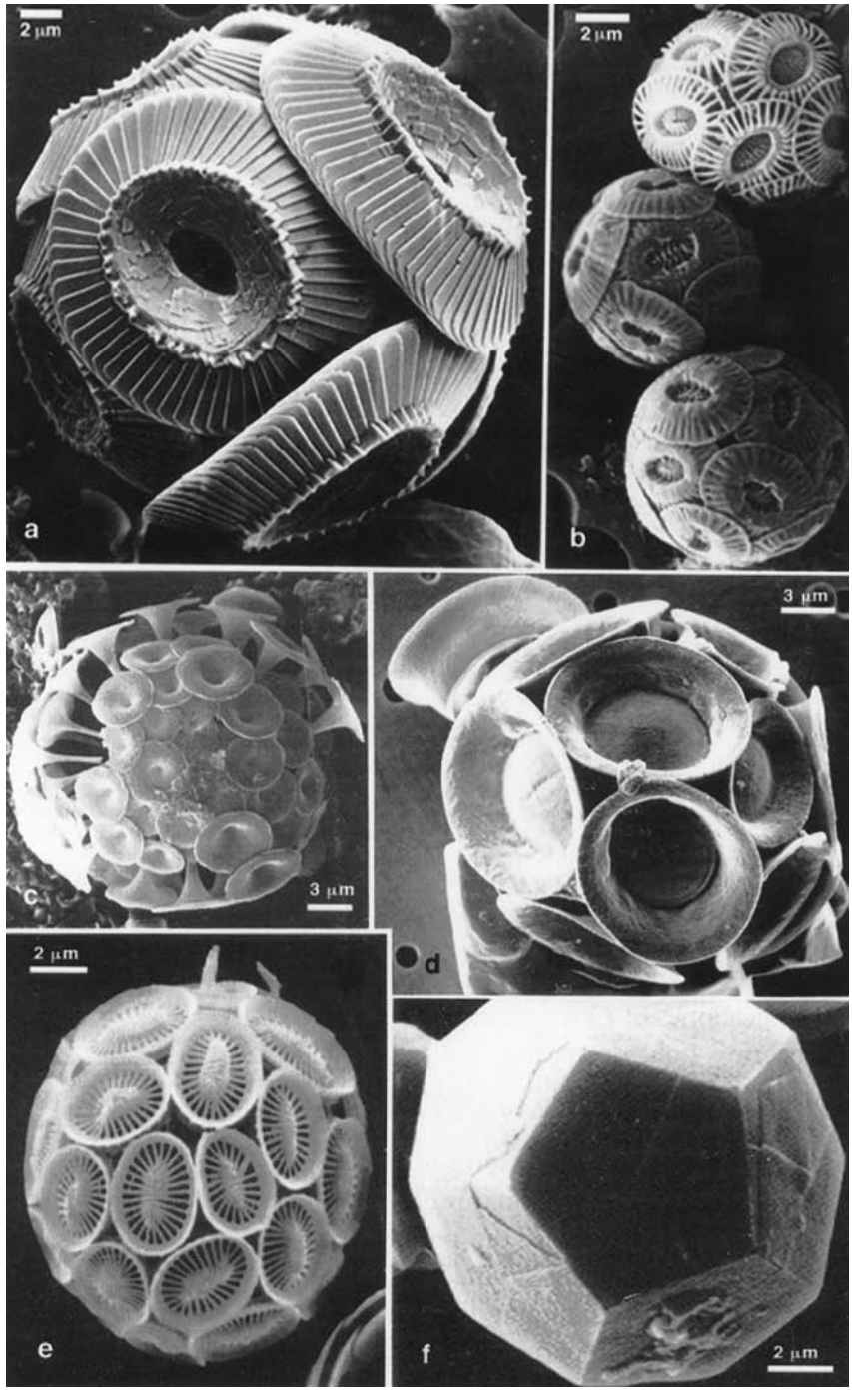


Fig. 22.16 Scanning electron micrographs of coccolithophorid cells. (*a*) *Coccolithus pelagicus*. (*b*) *Emiliania huxleyi*. (*c*) *Discosphaera tubifera*. (*d*) *Pontosphaera syracusana*. (*e*) *Syracosphaera nodosa*. (*f*) *Braarudosphaera bigelowii*. (From Faber and Preisig, 1994.)

The external coccoliths can be removed by lowering the pH of the culture medium. Cells of *Coccolithus huxleyi* decalcified in this manner may acquire a complete coccolith envelope (about 15 coccoliths) within 15 hours of their being transferred back to a normal medium in the light. Complete recalcification in *Cricosphaera* sp. may require 40 hours. In both instances, cell division is not a prerequisite for the formation of new coccoliths. If the organisms are grown in artificial seawater, the coccoliths dissolve if the product of the concentrations of calcium and carbonate is appreciably smaller than the solubility product of calcite. In *C. huxleyi*, coccoliths are still formed inside cells even when the calcium content of the medium is reduced to levels where external coccoliths dissolve, although coccolith production is retarded at calcium concentrations less than half that of normal seawater. A photochemical process is apparently directly associated with coccolith production because when light is turned off, there is a sharp drop in coccolith production.

Pleurochrysis carterae has biflagellate cells surrounded by a coccosphere consisting of a single layer of 100 to 200 coccoliths. The cells incorporate calcium into extracellular coccoliths at a more or less constant rate throughout a 16-hour light:8-hour dark cycle. The cells divide during the dark periods with a concomitant decrease in cell size during the dark period followed by an increase in cell size during the light period. The cells form coccoliths in the light as well as in the dark at a similar rate (van der Wal et al., 1987) (although *Emiliania huxleyi* (Fig. 22.16(*b*)) produces coccoliths only during the light period (Linschooten et al., 1991).

Although coccolithophorids constitute a minor part of recent calcareous oozes (bottom sediments composed of calcified remains of organisms) in the ocean, in the Cretaceous they dominated the calcareous nanoplankton (Tasch, 1973). This domination paralleled an increase in Ca^{2+} in seawater at the time (Brennan et al., 2004). Coccolithophorids provided the major constituent of Mesozoic (Jurassic and Cretaceous) and Tertiary chalks and marls. The abundance of coccolithophorids in these chalks can be demonstrated by taking a piece of ordinary blackboard chalk, pulverizing it, mixing it with distilled water in a test tube, and letting it stand for 20 minutes. Draw some of the solution into a pipette, dispose of the first four to five drops, and place the next few drops on a slide. Place a cover slip on the slide, and view it at a magnification of 400 to 500×. Many coccoliths and other remains will be seen.

Coccoliths in sedimentary rocks can be used as markers in the discovery and mode of deposition of oil deposits. For example, the oil shales of the Kimmeridge Clays in England are sandwiched between limestone bands that are composed mostly of coccoliths of one species, *Ellipsagelosphaera britannica* (Gallois, 1976). Other oil-bearing rocks have similar characteristic coccoliths. Therefore petroleum geologists know that when a drill core shows certain coccoliths that are associated with petroleum, there is a good chance of finding oil in that stratum of rock.

Toxins

The prymnesiophycean alga *Prymnesium parvum* (Fig. 22.7) secretes the potent exotoxin **prymnesin** (Fig. 22.17). The toxin causes fish mortalities by increasing cell membrane permeability and disturbing cellular ion balance (Fistarol et al., 2003). The toxin is most effective against aquatic gill-breathing animals, such as fish and molluscs. In Amphibia, only the gill-containing tadpole stage is sensitive to immersion in solutions containing the ichthytoxin. The rapidity of the action of *Prymnesium* toxin on immersed fish suggests that the immediate target must be an exposed organ, probably the gill. Experiments have shown that the toxins affect the permeability of the gill, resulting in the increased sensitivity of the fish. In fish removed promptly from such toxin solutions, the gill damage is repaired within hours. In Israel, Shilo (1967) has found that it is possible to control *P. parvum* in fish breeding ponds by adding small amounts of ammonium salt, which causes the algal cells to lyse.

Secretion of prymnesin by *Prymnesium parvum* immobilizes prey organisms and enables *P. parvum* to more easily seize its prey (Skovgaard and Hansen, 2003). *Prymnesium* produces higher quantities of toxin when phosphorus is limiting

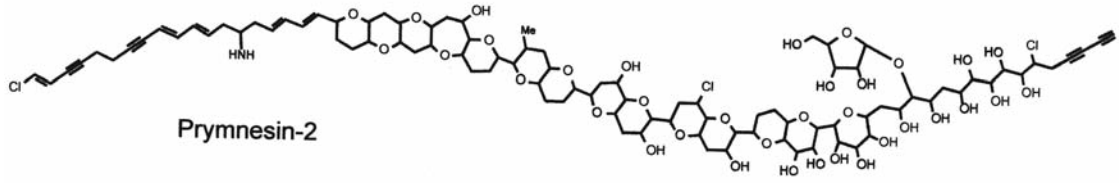


Fig. 22.17 The chemical structure of prymnesin-2. (After Igarashi et al., 1996.)

(Legrand et al., 2001). Secretion of the toxin results in greater kill of prey organisms which are subsequently ingested by the *Prymnesium* cells. The phosphorus in the prey organisms alleviates the phosphorus deficiency in the *Prymnesium* cells, resulting in decreased production of toxin.

Some species of *Chrysochromulina* produce toxins that kill fish, mussels, and ascidians (Hansen et al., 1995; Moestrup, 1994; Simonsen and Moestrup, 1997). The best documented fish kills have occurred off the coast of Norway and Sweden. The large blooms of *Chrysochromulina* causing the fish kills have been associated with a lack of predation by the normal ciliate grazers of *Chrysochromulina*. It appears that the long spines on the surface of the *Chrysochromulina* cells make them too large to be taken up by the ciliates (Hansen et al., 1995).

In the North Sea of Europe, and in the seas off Antarctica, blooms of the prymnesiophyte *Phaeocystis* (Figs. 22.4, 22.18(*a*)) occur as macroscopic lobed colonies or "bladders" in the spring and fall. *Phaeocystis* colonies are hollow, balloon-like structures with individual cells lying beneath a thin mucous skin (Hamm et al., 1999; Solomon et al., 2003). Grazing by invertebrates results in colonies of larger size, the larger size induced by chemicals released into the water by the grazing (Tang, 2003). Colony formation and enlargement is a defense mechanism that results in clogging of the filtration apparatus of the grazers (Haberman et al., 2002).

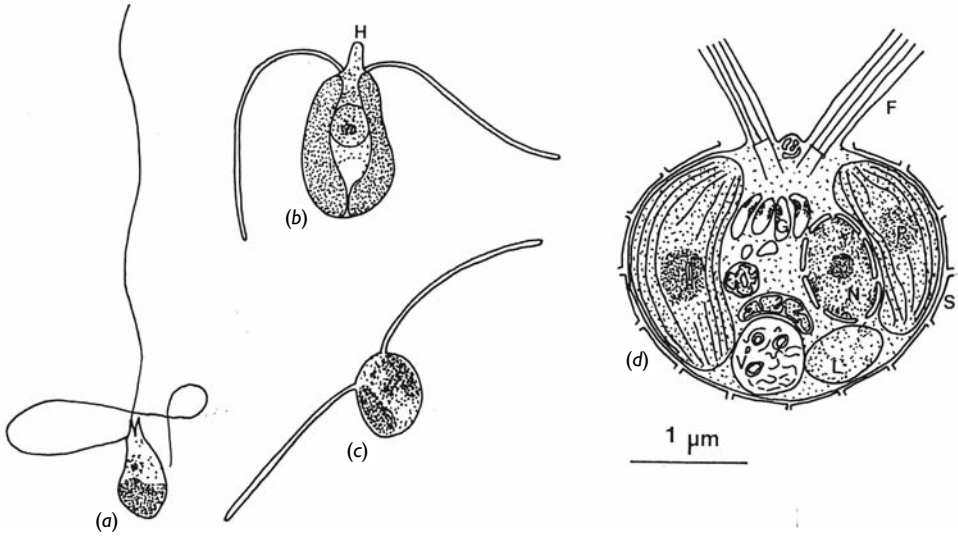


Fig. 22.18 (*a*) Motile cell of *Phaeocystis poucheti*. (*b*) *Isochrysis galbana*. (*c*), (*d*) *Imantonia rotunda*. (F) Flagellum; (H) haptonema; (L) leucosin vesicle; (N) nucleus; (P) pyrenoid; (S) scale. ((*d*) after Reynolds, 1974.)

In the North Sea, herring avoid the ocean areas where there are *Phaeocystis* blooms because of its unpalatability to the fish (Savage, 1930). Also, for a number of years biologists were puzzled by the near sterility of the intestines of certain Antarctic birds in regard to Protozoa and microorganisms. This condition was shown to be due to the large quantities of *Phaeocystis* in their diet, with *Phaeocystis* producing large amounts of acrylic acid which has a strong bactericidal action. *Phaeocystis* secretes 16% to 64% of the carbon assimilated in photosynthesis as polysaccharides of varying molecular weight. As much as 7 μg liter^{-1} of acrylic acid, and at least 0.3 mg liter^{-1} of polysaccharides, can be released in the formation of a dense bloom (Guillard and Hellebust, 1971; van Rijssel et al., 1997).

Classification

The Prymnesiophyceae can be divided into two orders (Edvardsen et al., 2000; Fujiwara et al., 2001):

Order 1 Prymnesiales: cells with two equal smooth flagella, no eyespot, scales commonly covering the cell body.

Order 2 Pavlovales: cells with two unequal flagella often covered with hairs and deposits, eyespots may be present.

Prymnesiales

Emiliania huxleyi (Fig. 22.16(*b*)) is typical of the order with motile cells that have two flagella. The life cycle of *E. huxleyi* (Fig. 22.19) probably involves a diploid, non-motile phase with coccoliths, which alternates with a haploid phase that has scales but no coccoliths (Paasche, 2002).

Every spring from 1978 to 1983, large areas (10 to 100 square miles) of water off the Atlantic Coast of France and southern England gave a strong reflectance of visible light to the Nimbus space satellite. Samples showed that the water contained mostly the coccolithophorid *Emiliania huxleyi* (Fig. 22.16(*b*)). The large coccoliths of *E. huxleyi* resulted in the high light reflectance which was picked up by the satellite (Holligan et al., 1983).

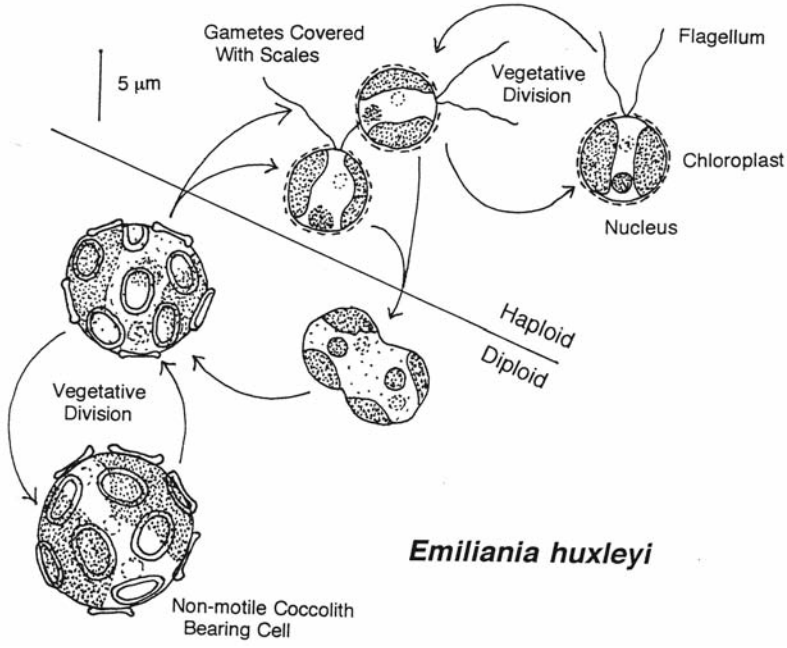


Fig. 22.19 The probable life history of *Emiliania huxleyi*. (Adapted from Green et al., 1996; Klaveness, 1972.)

The life cycle of the coccolithophorid *Hymenomonas carterae* is more complex (Fig. 22.20). *H. carterae* has a haploid *Apistonema* stage (21 ± 1 chromosomes) that consists of a filamentous branched system of spherical or elongate cells. Cells of the *Apistonema* stage can give rise either to asexual swarmers, which form new *Apistonema* thalli, or to motile gametes. Each asexual swarmer has two long flagella and a cup-shaped chloroplast, and the cell is covered with uncalcified scales. Gametes can be distinguished from asexual swarmers by their smaller size and the reduced number or absence of chloroplasts. After fusion of two gametes, the resulting zygote develops coccoliths. The diploid *Hymenomonas* stage (42 ± 1 chromosomes) has an outer layer of coccoliths under which are several layers of organic scales. A short haptonema is present between the flagella. The coccolith-bearing stage can perpetuate itself asexually by mitotic divisions. Under certain circumstances the protoplasts of *Hymenomonas* divide meiotically to produce four meiospores, which form haploid *Apistonema* thalli (von Stosch, 1967; Leadbeater, 1970; Parke, 1971).

The non-motile benthic stages of this order are resistant to fairly wide variations in the environment. The benthic stage of *Cricosphaera* sp. can survive temperatures of 35 to 40 °C for an hour or more as well as deep freezing for periods up 4 days. The same benthic phase is able to withstand a salinity up to the crystallization of the salt in solution. Normally benthic stages of *Cricosphaera* sp. grow near the high-water mark where they are presumably exposed to great variations in the

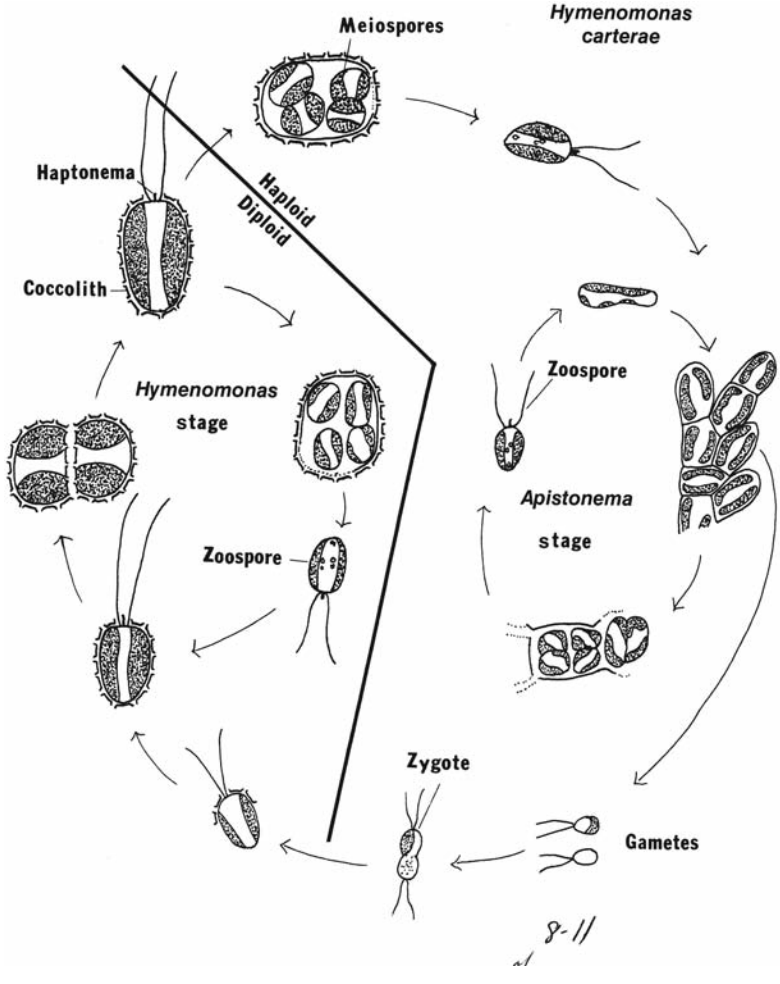


Fig. 22.20 The life history of *Hymenomonas carterae*.

environment. The motile phase of *Cricosphaera* sp. will tolerate salinities only as low as 0.4% to 0.8% salt and as high as 4.5% to 5.0% salt (see Paasche, 1968, for a review).

Pavlovales

The Pavlovales have cells with two unequal flagella with the haptonema arising between the flagella. In *Pavlova*, the two unequal flagella are attached some distance below the cell apex (Fig. 22.3(*b*)) (Green, 1967, 1976; van der Veer, 1969, 1976; Green and Manton, 1970). The longer flagellum is directed forward during swimming and is covered with fine hairs and dense bodies, whereas the short flagellum projects outward and can have fibrillar hairs on it. The flagella and haptonema are attached at the bottom of a depression (Green, 1973). A pit or canal passes from the bottom of the depression, under the base of the long flagellum, and terminates at the inner face of the eyespot (Fig. 22.21). The shape of the cells is variable, and there is a single two-lobed chloroplast with a pyrenoid. An eyespot is present inside the chloroplast. No sexual reproduction is known, and the cells propagate by longitudinal division in the motile state.

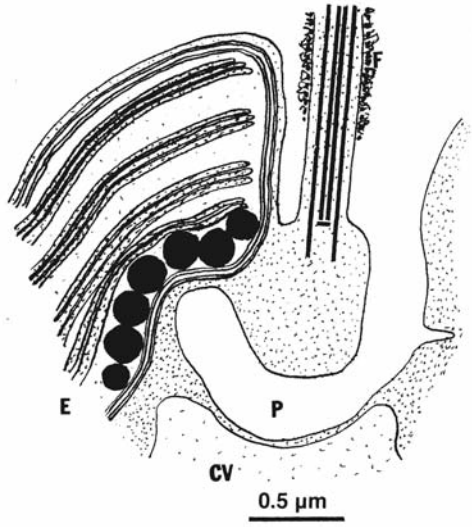


Fig. 22.21 A drawing of a section through the apical area of *Pavlova granifera* showing the contactile vacuole (CV), eyespot (E), long flagellum (F), and pit (P). (After Green, 1973.)

The algae in the Pavlovales have unusual sterols with two hydroxyl groups called pavlovals (Ghosh et al., 1998).

REFERENCES

Anderson, O. R., Swanberg, N. R., and Bennett, P. (1983). Fine structure of yellow-brown symbionts (Prymnesiida) in solitary radiolaria and their comparison with similar Acantharian symbionts. *J. Protozool*. 30:718–22.

Balch, W. M., Kilpatrick, K., Holligan, P. M., and Cucci, T. (1993). Coccolith production and detachment in *Emiliania huxleyi* (Prymnesiophyceae). *J. Phycol*. 29:566–75.

Bhattacharya, D., and Ehlting, J. (1995). Actin coding regions: gene family evolution and use as a phylogenetic marker. *Arch. Protistenk*. 145:155–64.

Brennan, S. L., Lowenstein, T. K., and Horita, J. (2004). Seawater chemistry and the advent of biocalcification. *Geology* 32:473–6.

Brown, R. M. (1969). Observations on the relationship of the Golgi apparatus to wall formation in the marine chrysophycean alga, *Pleurochrysis scherfferlii* Pringsheim. *J. Cell Biol*. 41:109–23.

Chrétiennot-Dinet, M-J., Giraud-Guille, M. M., Vaulot, D., Putaux, J-L., Saito, Y., and Chanzy, H. (1997). The chitinous nature of filaments ejected by *Phaeocystis* (Prymnesiophyceae). *J. Phycol*. 33:666–72.

Christensen, T. (1962). *Alger Botanik*, Vol. 2, No. 2. Copenhagen: Munksgaard.

Corstjens, P. L. A. M., and Gonzales, E. L. (2004). Effects of nitrogen and phosphorus availability on the expression of the coccolith V-ATPase (subunit *C*) of *Pleurochrysis* (Haptophyta). *J. Phycol*. 40:82–7.

Edvardsen, B., Eikrem, W., Green, J. C., Andersen, R. A., Moon-van der Stay, S. Y., and Medlin, L. K. (2000). Phylogenetic reconstructions of the Haptophyta inferred from 18S ribosomal DNA sequences and available morphological data. *Phycologia* 39:19–35.

Faber, W. W., and Preisig, H. R. (1994). Calcified structures and calcification in protists. *Protoplasma* 181:78–105.

Fistarol, G. O., Legrand, C., and Granéli, E. (2003). Allelopathic effect of *Prymnesium parvum* on a natural plankton community. *Mar. Ecol. Progr. Ser*. 255:115–25.

Fournier, R. O. (1969). Observations on the flagellate *Diacronema vlkianum* Prauser (Haptophyceae). *Br. Phycol. J*. 4:185–90.

Fujiwara, S., Tsuzuki, M., Kawachi, M., Minaka, N., and Inouye, I. (2001). Molecular phylogeny of the

Haptophyta based in the *rbc*L gene and sequence variation in the spacer region of the Rubisco operon. *J. Phycol*. 37:121–9.

Gallois, R. W. (1976). Coccolith blooms in the Kimmeridge Clay and origin of the North Sea Oil. *Nature* 259:473–5.

Geisen, M., Billard, C., Broerse, A. T. C., Cros, L., Probert, I., and Young, J. R. (2002). Life-cycle associations involving pairs of holococcolithophorid species: intraspecific variation or cryptic speciation? *Eur. J. Phycol*. 37:531–50.

Ghosh, P., Patterson, G. W., and Wikfors, G. H. (1998). Sterols of some marine Prymnesiophyceae. *J. Phycol*. 34:511–4.

Gonzales, E. L. (2004). The proton pump of the calcifying vesicle of the coccolithophore, *Pleurochrysis*. In *Biomineralization*, ed. E. Baeuerlein, pp. 217–8. Weinheim: Wiley-VCH.

Green, J. C. (1967). A new species of *Pavlova* from Madeira. *Br. Phycol. Bull*. 3:299–303.

Green, J. C. (1973). Studies in the fine structure and taxonomy of flagellates in the genus *Pavlova*. II. A freshwater representative, *Pavlova granifera* (Mack) comb. nov. *Br. Phycol. J*. 8:1–12.

Green, J. C. (1976). Notes on the flagellar apparatus and taxonomy of *Pavolva mesolychnon* van der Veer, and on the status of *Pavlova* Butcher and related genera within the Haptophyceae. *J. Mar. Biol. Assoc. UK* 56:595–602.

Green, J. C., and Hibberd, D. J. (1977). The ultrastructure and taxonomy of *Diacronema vlkianum* (Prymnesiophyceae) with special reference to the haptonema and flagellar apparatus. *J. Mar. Biol. Assoc. UK* 57:1125–36.

Green, J. C., and Leadbeater, B. S. C. (1972). *Chrysochromulina parkae* sp. nov. (Haptophyceae) a new species recorded from S.W. England and Norway. *J. Mar. Biol. Assoc. UK* 52:469–74.

Green, J. C., and Manton, I. (1970). Studies in the fine structure and taxonomy of flagellates in the genus *Pavlova*. I. A revision of *Pavlova gyrans*, the type species. *J. Mar. Biol. Assoc. UK* 50:1113–30.

Green, J. C., and Pienaar, R. N. (1977). The taxonomy of the order Isochrysidales (Prymnesiophyceae) with special reference to the genera *Isochrysis* Parke, *Dicrateria* Parke and *Imantonia* Reynolds. *J. Mar. Biol. Assoc. UK* 57:7–17.

Green, J. C., Course, P. A., and Tarran, G. A. (1996). The life-cycle of *Emiliania huxleyi*: A brief review and a study of relative ploidy levels analyzed by flow cytometry. *J. Marine Systems* 9:33–44.

Greyson, A. J., Green, J. C., and Leadbeater, B. S. C. (1993). Structure and physiology of the haptonema in *Chrysochromulina* (Prymnesiophyceae). II. Mechanisms of haptonemal coiling and the regeneration process. *J. Phycol*. 29:686–700.

Guillard, R. R. L., and Hellebust, J. A. (1971). Growth and production of extracellular substances by two strains of *Phaeocystis poucheti*. *J. Phycol*. 7:330–8.

Haberman, K. L., Ross, R. M., Quetin, L. B., Vernet, M., Nevitt, G. A., and Kozlowski, W. (2002). Grazing by Antarctic krill *Euphausia superba* on *Phaeocystis antarctica*: an immunochemical approach. *Mar. Ecol. Progr. Ser*. 241:139–49.

Hamm, C. E., Simson, D. A., Merkel, R., and Smetacek, V. (1999). Colonies of *Phaeocystis globosa* are protected by a thin but tough skin. *Mar. Ecol. Progr. Ser*. 187:101–11.

Hansen, P. J., Nielsen, T. G., and Kaas, H. (1995). Distribution and growth of protists and mesozooplankton during a bloom of *Chrysochromulina* spp. (Prymnesiophyceae, Prymnesiales). *Phycologia* 34:409–16.

Hawkins, E. K., and Lee, J. J. (2001). Architecture of the Golgi apparatus of a scale-forming alga biogenesis and transport of scales. *Protoplasma* 216:227–38.

Hibberd, D. J. (1976). The ultrastructure and taxonomy of the Chrysophyceae and Prymnesiophyceae (Haptophyceae): A survey with some new observations on the ultrastructure of the Chrysophyceae. *Bot. J. Linn. Soc*. 72:55–80.

Holligan, P. M., Viollier, M., Habour, D. S., Camus, P., and Champagne-Phillipe, M. (1983). Satellite and ship studies of coccolithophore production along a continental shelf. *Nature* 304:339–42.

Igarashi, T., Satake, M., and Yasumoto, T. (1996). Prymnesium-2: a potent ichthyotoxic and hemolytic glycoside isolated from the red tide alga *Prymnesium parvum*. *J. Am. Chem. Soc*. 118:479–80.

Inouye, I., and Kawachi, M. (1994). The haptonema. In *The Haptophyte Algae*, ed. J. C. Green, and B. S. C. Leadbeater, Systematics Assn. Special Vol. 51, pp. 73–89. Oxford: Clarendon Press.

Janse, I., van Rijssel, M., van Hall, P. J., Gerswig, G. J., Gottschel, J. C., and Prins, R. A. (1996). The storage glucan of *Phaeocystis globosa* (Prymnesiophyceae) cells. *J. Phycol*. 32:382–7.

Jordan, R. W., and Chamberlain, A. H. L. (1997). Biodiversity among haptophyte algae. *Biodiversity and Conservation* 6:131–52.

Kawachi, M., and Inouye, I. (1994). Ca^{2+} mediated induction of the coiling of the haptonema in

Chrysochromulina hirata (Prymnesiophyceae = Haptophyta). *Phycologia* 33:53–7.

Kawachi, W., Inouye, I., Maeda, O., and Chihara, M. (1991). The haptonema as a food-capturing device: observations on *Chrysochromulina hirata* (Prymnesiophyceae). *Phycologia* 30:563–73.

Klaveness, D. (1972). *Coccolithus huxleyi* (Lohm.) Kamptn. II. The flagellate cell, aberrant cell types, vegetative propagation and life cycles. *Br. Phycol. J.* 7:309–18.

Kreger, D. R., and van der Veer, J. (1970). Paramylon in a Chrysophyte. *Acta Bot. Neerl.* 19:401–2.

Leadbeater, B. S. C. (1970). Preliminary observations on differences of scale morphology at various stages in the life cycle of "*Apistonema-Syracosphaera*" *sensu* von Stosch. *Br. Phycol. J.* 5:57–69.

Lechtreck, K.-F. (2004). An immunofluorescence study of the haptonema of *Chrysochromulina parva* (Prymnesiophyceae). *Phycologia* 43:635–40.

Legrand, C., Johansson, N., Johnsen, G., Borsheim, K. Y., and Graneli, E. (2001). Phagotrophy and toxicity variation in the mixotrophic *Prymnesium patelliferum* (Haptophyceae). *Limnol. Oceanogr.* 46:1208–14.

Linschooten, C., van Bleijswijk, J. D. L., van Emburg, P., de Vrind, J. P. M., Kempers, E. S., Westbroek, P., and de Vrind-de Jong, E. W. (1991). Role of light-dark cycle and medium composition in the production of coccoliths by *Emiliania huxleyi* (Haptophyceae). *J. Phycol.* 27:82–6.

Manton, I. (1964). Further observations on the fine structure of the haptonema in *Prymnesium parvum*. *Arch. Mikrobiol.* 49:315–30.

Manton, I. (1966). Further observations on the fine structure of *Chrysochromulina chiton*, with special reference to the pyrenoid. *J. Cell Sci.* 1:187–92.

Manton, I. (1967a). Further observations on the fine structure of *Chrysochromulina chiton* with special reference to the haptonema, "peculiar" Golgi and aspects of scale production. *J. Cell Sci.* 2:265–72.

Manton, I. (1967b). Further observations on scale formation in *Chrysochromulina chiton*. *J. Cell Sci.* 2:411–18.

Manton, I. (1968). Further observations on the microanatomy of the haptonema in *Chrysochromulina chiton* and *Prymnesium parvum*. *Protoplasma* 66:35–53.

Manton, I. (1972). Preliminary observations on *Chrysochromulina mactra* sp. nov. *Br. Phycol. J.* 7:21–35.

Manton, I., and Parke, M. (1962). Preliminary observations on scales and their mode of origin in *Chrysochromulina polylepis* sp. nov. *J. Mar. Biol. Assoc. UK* 42:565–78.

Manton, I., and Peterfi, L. S. (1969). Observations on the fine structure of coccoliths, scales and the protoplast of a freshwater coccolithophorid. *Hymenomonas roseola* Stein, with supplementary observations on the protoplast of *Cricosphaera carterae*. *Proc. R. Soc. Lond.* [*B*] 172:1–15.

Manton, I., Sutherland, J., and Oates, K. (1977). Arctic coccolithophorids: *Wigwammia arctica* gen. et sp. nov. from Greenland and arctic Canada. *W. annulifera* sp. nov. from South Africa and S. Alaska and *Calciarcus alaskensis* gen. et sp. nov. from S. Alaska. *Proc. R. Soc. Lond.* [*B*] 197:145–68.

Marsh, M. E. (1994). Polyanion-mediated mineralization – assembly and reorganization of acidic polysachharides in the Golgi system of a coccolithophorid alga during mineral deposition. *Protoplasma* 177:108–22.

Marsh, M. E. (1996). Polyanion-mediated mineralization – a kinetic analysis of the calcium-carrier hypothesis in the phytoflagellate *Pleurochrysis carterae*. *Protoplasma* 190:181–8.

Marsh, M. E. (2004). Biomineralization in coccolithophores. In *Biomineralization*, ed. E. Baeuerlein, pp. 198–215. Weinheim: Wiley-VCH.

Medlin, L. K., Barker, G. L. A., Baumann, M., Hayes, P. K., and Lange, M. (1994). Molecular biology and systematics. In *The Haptophyte Algae*, ed. J. C. Green, and B. S. C. Leadbeater, Systematics Assn. Special Vol. 51, pp. 393–411. Oxford: Clarendon Press.

Moestrup, Ø. (1994). Economic aspects: "blooms", nuisance species, and toxins. In *The Haptophyte Algae*, ed. J. C. Green, and B. S. C. Leadbeater, Systematics Assn. Special Vol. 51, pp. 265–85. Oxford: Clarendon Press.

Nielsen, M. V. (1995). Photosynthetic characteristics of the coccolithophorid *Emiliania huxleyi* (Prymnesiophyceae) exposed to elevated concentrations of dissolved inorganic carbon. *J. Phycol.* 31:715–19.

Outka, D. E., and Williams, D. C. (1971). Sequential coccolith morphogenesis in *Hymenomonas carterae*. *J. Protozool.* 18:285–97.

Paasche, E. (1968). Biology and physiology of coccolithophorids. *Annu. Rev. Microbiol.* 22:71–86.

Paasche, E. (2002). A review of the coccolithophorid *Emiliania huxleyi* (Prymnesiophyceae), with particular reference to growth, coccolith formation and calcification-photosynthesis interactions. *Phycologia* 40:503–29.

Parke, M. (1971). The production of calcareous elements by benthic algae belonging to the class Haptophyceae (Chrysophyta). *Proc. II Plank. Conf.*, pp. 929–38.

Parke, M., and Manton, I. (1962). Studies on marine flagellates. VI. *Chrysochromulina pringsheimii* sp. nov. *J. Mar. Biol. Assoc. UK* 42:391–404.

Parke, M., Manton, I., and Clarke, B. (1955). Studies on marine flagellates. II. Three new species of *Chrysochromulina*. *J. Mar. Biol. Assoc. UK* 34:579–609.

Parke, M., Manton, I., and Clarke, B. (1956). Studies on marine flagellates. III. Three further species of *Chrysochromulina*. *J. Mar. Biol. Assoc. UK* 35:387–414.

Parke, M., Lund, J. W. G., and Manton, I. (1962). Observations on the biology and fine structure of the type species of *Chrysochromulina* (C. *parva* Lackey) in the English Lake District. *Arch. Mikrobiol*. 42:333–52.

Pringsheim, E. G. (1955). Kleine Mitteilungen über Flagellaten und Algen. I. Algenartige Chrysophyceen in Reinkultur. *Arch. Mikrobiol*. 21:401–10.

Reynolds, N. (1974). *Imantonia rotunda* gen. et sp. nov., a new member of the Haptophyceae. *Br. Phycol. J*. 9:429–34.

Rowson, J. D., Leadbeater, B. S. C., and Green, J. C. (1986). Calcium carbonate deposition in the motile (*Crystallolithus*) phase of *Coccolithus pelagicus*. *Br. J. Phycol*. 21:359–70.

Savage, R. E. (1930). The influence of *Phaeocystis* on the migration of the herring. *Fish. Invest., Lond., Ser. II* 12:5–14.

Shilo, M. (1967). Formation and mode of action of algal toxins. *Bacteriol. Rev.* 31:180–93.

Simonsen, S., and Moestrup, Ø. (1997). Toxicity tests in eight species of *Chrysochromulina* (Haptophyta). *Can. J. Bot*. 75:129–36.

Skovgaard, A., and Hansen, P. J. (2003). Food uptake in the harmful alga *Prymnesium parvum* mediated by excreted toxins. *Limnol. Oceanogr*. 48:1161–6.

Solomon, C. M., Lessard, E. J., Keil, R. G., and Foy, M. S. (2003). Characterization of extracellular polymers of *Phaeocystis globosa* and *P. antarctica*. *Mar. Ecol. Progr. Ser*. 250:81–9.

Tang, K. W. (2003). Grazing and colony size development in *Phaeocystis globosa* (Prymnesiophyceae): the role of the chemical signal. *J. Plankton Res*. 25:831–42.

Tasch, P. (1973). *Paleobiology of the Invertebrates*. New York: John Wiley.

van der Veer, J. (1969). *Pavlova mesolychnon* (Chrysophyta), a new species from the Tamar Estuary, Cornwall, *Acta Bot. Neerl*. 18:496–510.

van der Veer, J. (1976). *Pavlova calceolata* (Haptophyceae), a new species from the Tamar Estuary, Cornwall, England. *J. Mar. Biol. Assoc. UK* 56:21–30.

van der Wal, P., deVrind, J. P. M., deVrind-deJong, E. W., and Borman, A. H. (1987). Incompleteness of the coccosphere as a possible stimulus for coccolith formation in *Pleurochrysis carterae* (Prymnesiophyceae). *J. Phycol*. 23:218–21.

van Rijssel, M., Hamm, C. E., and Gieskes, W. W. C. (1997). *Phaeocystis globosa* (Prymnesiophyceae) colonies: hollow structures built with small amounts of polysaccharides. *Eur. J. Phycol*. 32:185–92.

von Stosch, H. A. (1967). Haptophyceae. In *Vegetative Forplanzung, Parthenogenese und Apogamie bie Algen*, ed. W. Ruhland, *Encyclopedia of Plant Physiology* 18:646–56.

Young, J. R., Didymus, J. M., Bown, P. R., Prins, B., and Mann, S. (1992). Crystal assembly and phylogenetic evolution in heterococcoliths. *Nature* 356:516–18.

Zapata, M., Jeffrey, S. W., Wright, S. W., Rodriguez, F., Garrido, J. L., and Clementson, L. (2004). Photosynthetic pigments in 37 species (65 strains) of Haptophyta: implications for oceanography and chemotaxonomy. *Mar. Ecol. Progr. Ser*. 270:83–102.

Chapter 23

Algae and the environment

It is possible to write whole books on the relationships between algae and the environment. In this chapter I have chosen a few subjects which have generated the most interest in the last decade.

Toxic algae

Algae can be harmful in two basic ways (Hallegraeff et al., 2003).

1 **Producing large populations in the aquatic environment** Large growths of some algae (e.g., the diatom *Chaetoceros* (Figs. 17.44, 17.45) or the prymnesiophyte *Chrysochromulina* (Fig. 23.1(*c*))) can clog the gills of fish and can be particularly a problem in aquaculture systems. Anoxic conditions, resulting in fish kills, can occur at the end of blooms of other algae (e.g., green algae) as the algae die and decompose.
2 **Production of toxins** Some algae produce toxins that sicken and kill other organisms that prey on these algae. Indeed, this probably was the reason that these algae were selected for in the evolutionary process since it reduced predation by grazers (Gilbert, 1996). Filter-feeding shellfish can accumulate large quantities of these toxins as they filter the algae out of the water. Consumption of the shellfish by man, birds, and animals results in sickness and death.

The algae that produce phycotoxins are:

***Cyanophyceae* (*cyanobacteria*)**

- **Neurotoxins** *anatoxin* (Fig. 23.2(*c*)) and *saxitoxin* (Fig. 23.2(*c*)) that block the transmission of signal from neuron to neuron. These alkaloids (nitrogen containing compounds) bind to voltage-activated Na^+-channels and block influx of Na^+, thereby preventing the generation of an action potential (Shimizu, 2000).
- **Hepatotoxins** *microcystin* (Fig. 23.2(*b*)) and *nodularin* (Fig. 23.2(*b*)) that are inhibitors of protein phosphatases 1 and 2A.

***Dinophyceae* (*dinoflagellates*)**

- **Diarrhetic shellfish poisoning** caused by *okadaic acid* (Fig. 23.3(*e*)), *macrolide toxins*, and *yessotoxins* (Fig. 23.4(*f*)). Okadaic acid and the related *dinophysistoxins* (Fig. 23.3(*e*)) are inhibitors of protein phosphatases, The free carboxyl groups bind to the catalytic site of the protein phosphatase. Yessotoxin may interfere with cyclic AMP in cells causing cytotoxicity (Cembella, 2003).
- **Ciguatera fish poisoning** caused by *ciguatoxin* (Fig. 23.4(*f*)), *maitotoxins* (Fig. 23.4(*f*)), and *brevetoxins* (Fig. 23.4(*f*)). All of these compounds are ion-channel disrupters, increasing the permeability of the cell membrane to positive ions and causing membrane depolarization. Brevetoxins require a lactone ring for activity. Ciguatoxin and brevetoxin bind voltage-sensitive channels, increasing the permeability of the cell membrane and causing membrane depolarization (Cembella, 2003). Maitotoxin initiates Ca^{2+}-channel activation, causing Ca^{2+}-influx and activation of calmodulin (Igarashi et al., 1999). This is followed by

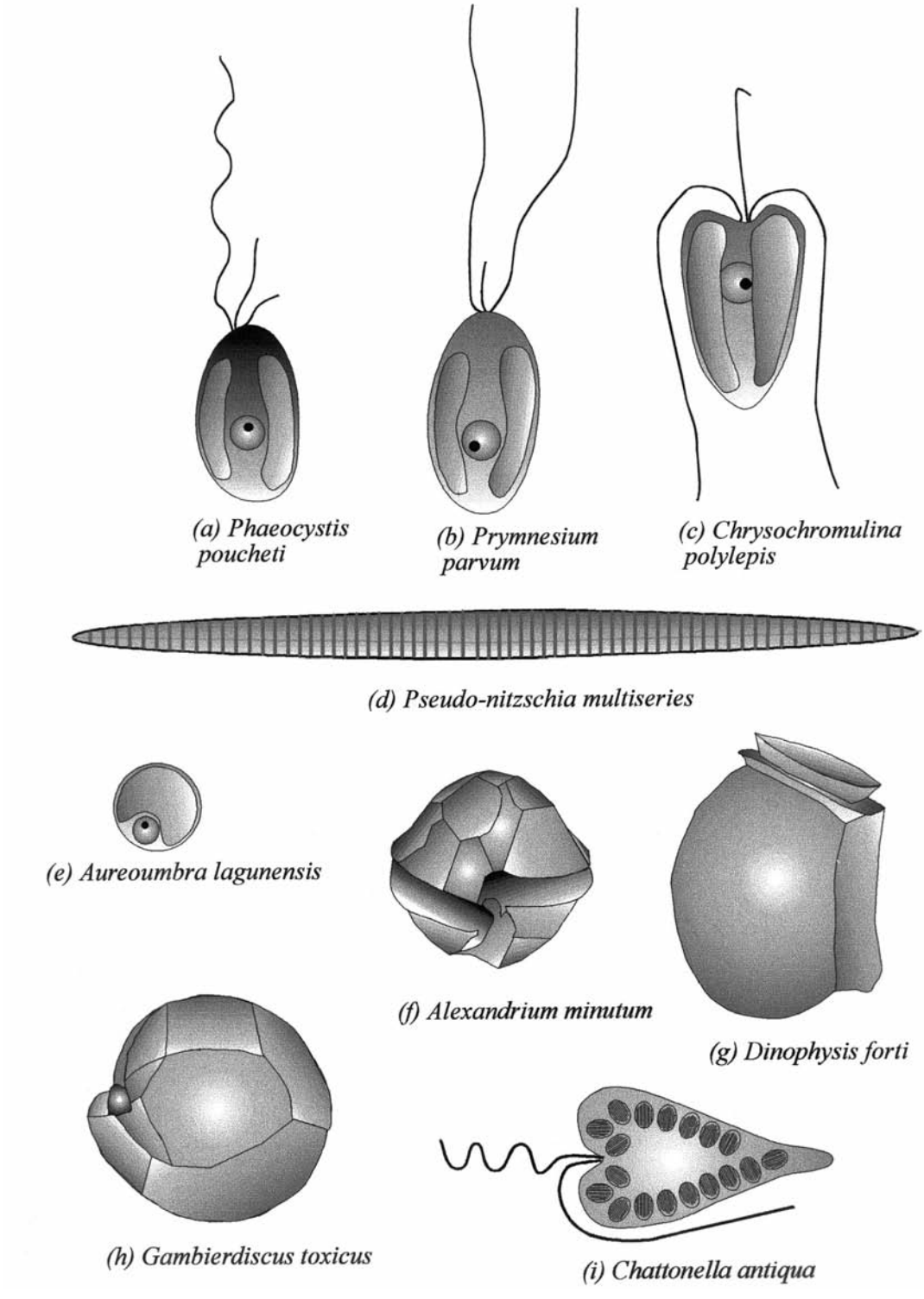
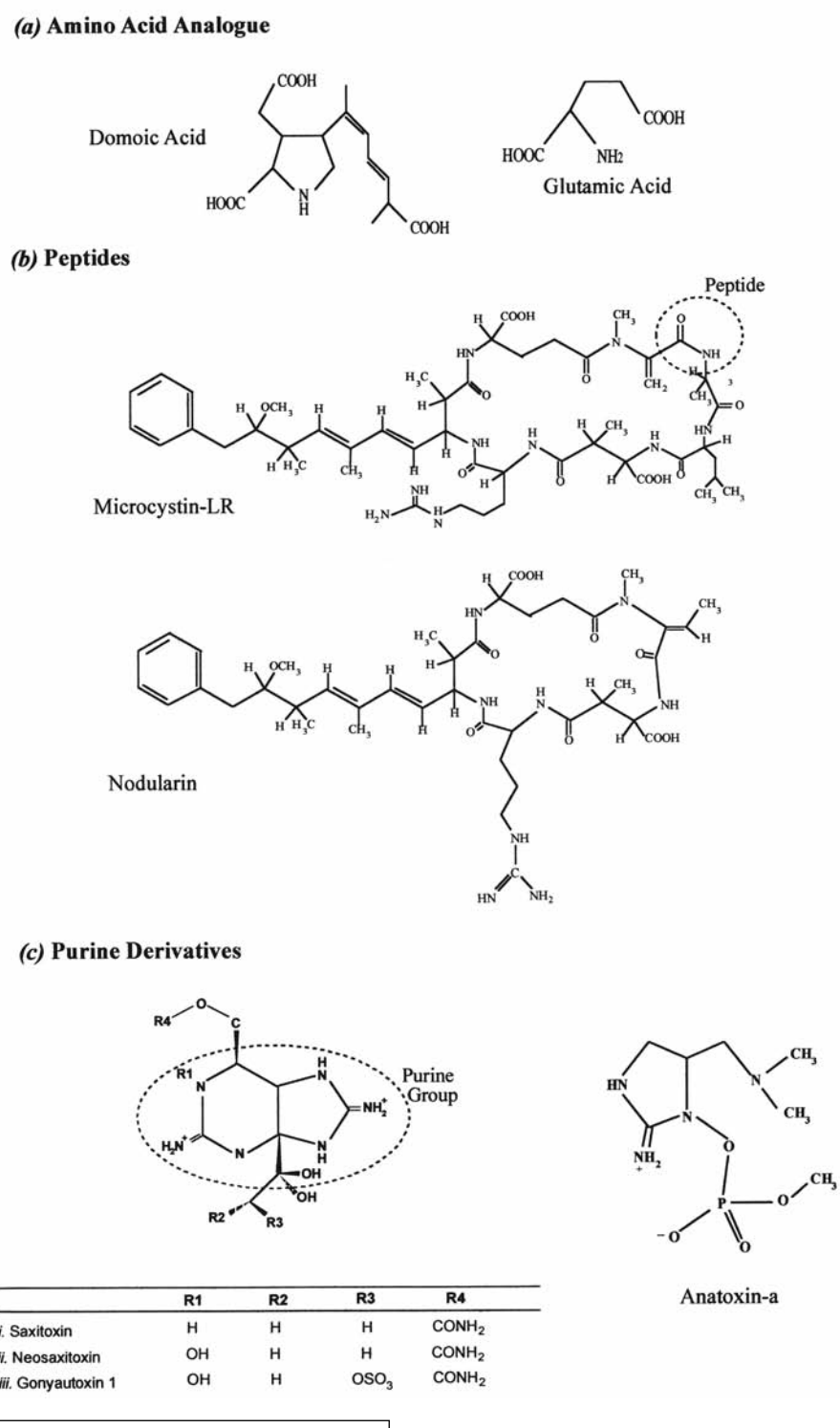


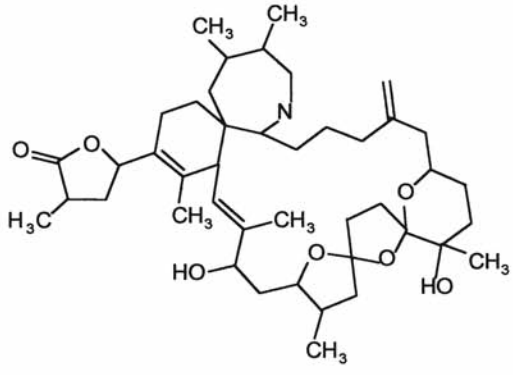
Fig. 23.1 Examples of toxic marine algae.



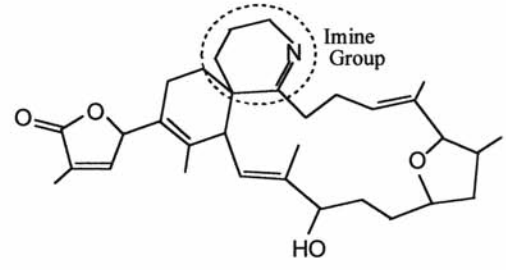
	R1	R2	R3	R4
i. Saxitoxin	H	H	H	$CONH_2$
ii. Neosaxitoxin	OH	H	H	$CONH_2$
iii. Gonyautoxin 1	OH	H	OSO_3	$CONH_2$

Fig. 23.2 Chemical structure of the phycotoxins composed of amino acid analogues, peptides, and purine derivatives.

***(d)* Cyclic Imines**



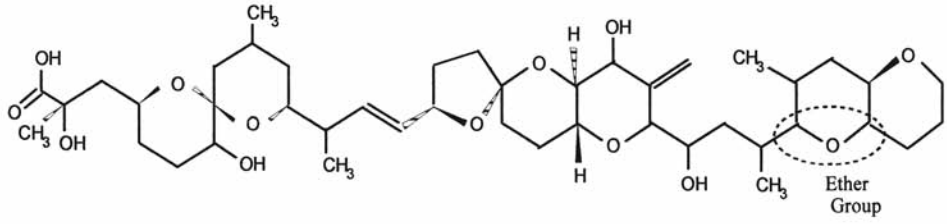
i. Spirolide D



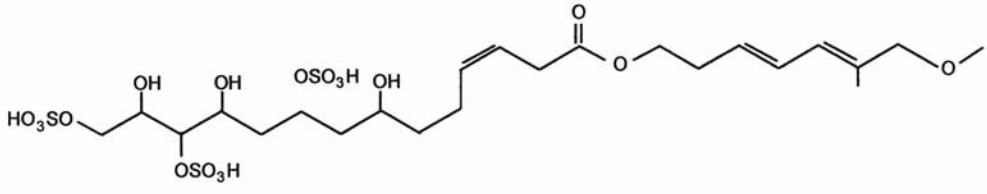
ii. Gymnodimine

***(e)* Non-nitrogen compounds containing linear and macrocyclic polyethers**

i. Okadaic Acid



ii. Dinophysistoxin-4



***iii.* Prymnesin-2**

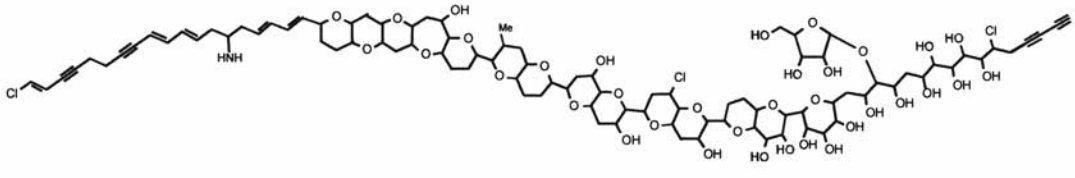


Fig. 23.3 Chemical structure of phycotoxins composed of cyclic imines and non-nitrogen compounds containing linear and macrocyclic polyethers.

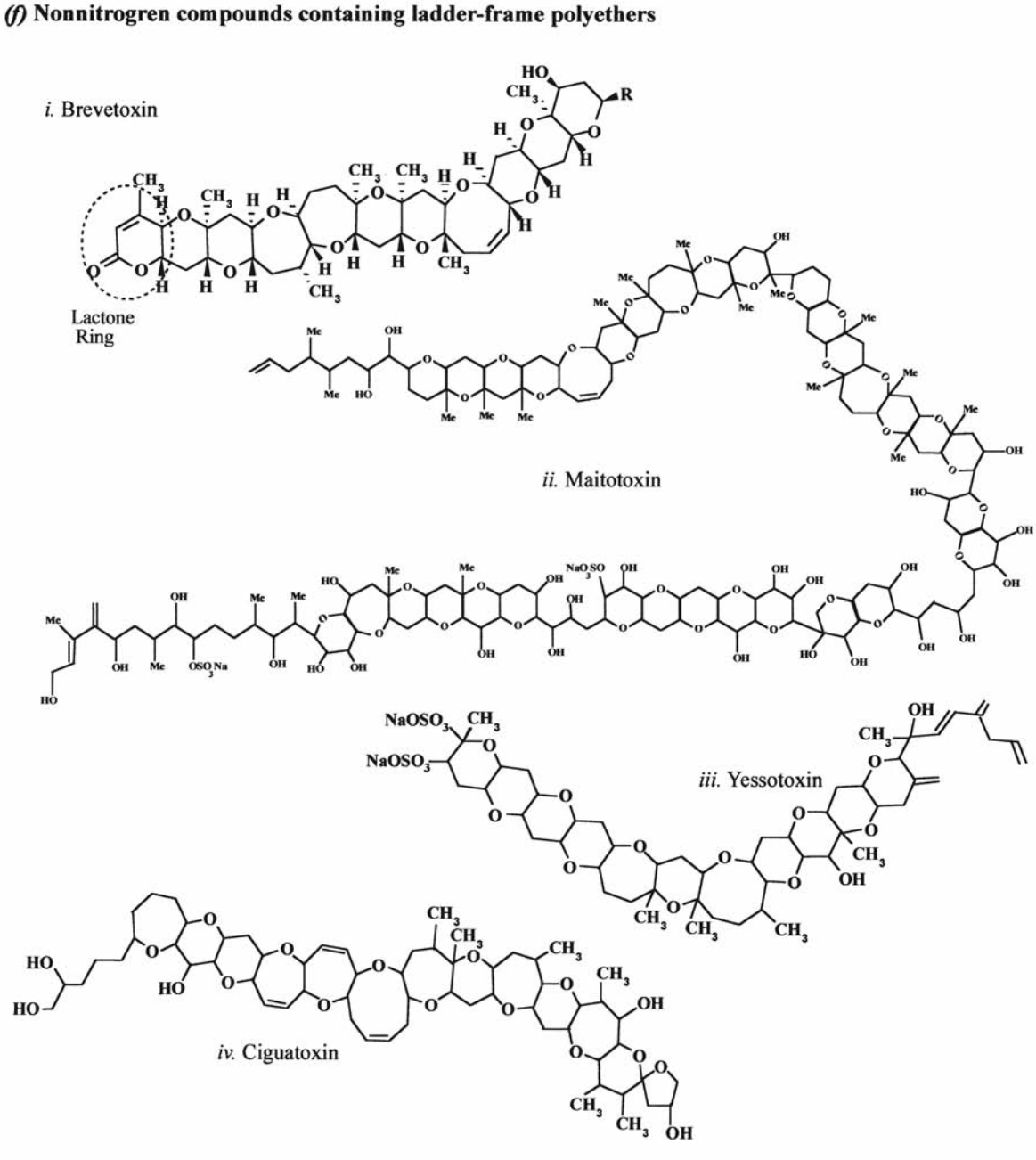


Fig. 23.4 Chemical structure of phycotoxins containing non-nitrogen compounds with ladder-frame polyethers.

promotion of phospholipase A2 activity and ultimately cell membrane disruption.
- **Paralytic shellfish poisoning** caused by *saxitoxin* (Fig. 23.2(*c*)) and approximately two dozen naturally occurring analogues (Fig. 23.2(*c*)). The saxitonins bind to voltage-activated Na^+-channels, blocking influx of Na^+ and preventing the generation of an action potential. Saxitoxins are retained primarily inside cells with very little excretion or leakage from cells. These highly water-soluble, but stable, compounds must be released during senescence or cell lysis, which coincides with the decline of a bloom (Cembella, 2003).
- **Spirolide poisoning**. This group of cyclic imines include the *spirolides* (Fig. 23.3(*d*)), *gymnodimine* (Fig. 23.3(*d*)), *pteriatoxin* and *pinnatoxins*. The imine ring gives the molecules their toxic properties. They are "fast-acting toxins", causing death of mice within minutes after oral application.

Bacillariophyceae (*diatoms*)
- **Amnesic shellfish poisoning** caused by the neurotoxin *domoic acid* (Fig. 23.2(*a*)). Domoic acid is an amino acid that functions as a *glutamate agonist* (compound that has an affinity for a cell receptor), and in humans causes extensive depolarization in areas rich in glutamate receptors (e.g., the hippocampus). The biosynthesis of domoic acid is inducible and sustained only under stress conditions (Pan et al., 1998).

Raphidophyceae (*chloromonads*)
- **"Red tide" poisoning**. Members of the Raphidophyceae produce *brevetoxins* (Fig. 23.4 (*f*)), neurotoxins that bind to voltage-activated Na^+-channels causing rapid influx of Na^+-ions and membrane depolarization.

Prymnesiophyceae (*haptophytes*)
- The phycotoxin *prymnesin* (Fig. 23.3(*e*)) produces hemolysis of red blood cells by disrupting the pores in the cell membrane, causing influx of positive ions and membrane depolarization.

Another way of classifying phycotoxins is by their chemical structure (Cembella, 2003):

1 *Amino acid analogues*. **Domoic acid** (Fig. 23.2(*a*)). This is a glutamate receptor agonist produced by the diatom *Pseudo-nitzchia* spp. (Figs. 17.27, 17.29, 23.1(*d*)).
2 *Peptides*. **Microcystins** (Figs. 23.2(*b*)) and **nodularin** (Fig. 23.2(*b*)). These phycotoxins are produced by cyanobacteria. Microcystin is formed by species of *Microcystis* (Figs. 2.48, 2.56(*b*)), *Anabaena* (Figs. 2.16, 2.18(*d*)), *Nostoc* (Figs. 2.46(*b*), (*c*), (*d*), 2.57(*a*)), *Nodularia* (Fig. 2.42(*a*)) and *Oscillatoria* (Figs. 2.19(*a*), (*b*), 2.34(*a*)), while nodularins are produced by species of *Nodularia* (Fig. 2.42(*a*)).
3 *Purine derivatives*. **Saxitoxins** (Fig. 23.2(*c*)), **gonyautoxins** (Fig. 23.2(*c*)), and **anatoxin** (Fig. 23.2(*c*)). There are about two dozen analogues of these molecules with their potency varying over several orders of magnitude. Saxitoxin has a LD_{50} of 10 $\mu g\ kg^{-1}$. The decarbamoyl derivates have intermediate toxicity (decarbamoyl saxitoxin has a LD_{50} of 20 $\mu g\ kg^{-1}$) while the *N*-sulphocarbamoyl forms have a low toxicity (*N*-sulphocarbamoyl (B-toxin)) has a LD_{50} of 163 $\mu g\ kg^{-1}$). Saxitoxins are produced by some cyanobacteria and by the dinoflagellates *Alexandrium* spp. (Figs. 7.35, 7.36, 23.1(*f*)), *Pyrodinium bahamense* (Fig. 7.34), and *Gymnodinium catenatum*. Anatoxin is produced by the cyanobacteria *Anabaena* (Figs. 2.16, 2.18(*d*)), *Aphanizomenon* (Fig. 2.18(*b*)), *Oscillatoria* (Figs. 2.19(*a*), (*b*), 2.34(*a*)), and *Trichodesmium* (Fig. 2.56(*g*)).
4 *Cyclic imines*. **Spirolides** (Fig. 23.3(*d*)) and **gymnodimine** (Fig. 23.3(*d*)). The spirolides are produced by the marine dinoflagellate *Alexandrium ostenfeldii* while gymnodimine is produced by the dinoflagellate *Karenia selliformis*.
5 *Non-nitrogen compounds containing linear and macrocyclic polyethers*. **Okadaic acid** (Fig. 23.3(*e*)), **dinophysistoxins** (Fig. 23.3(*e*)), and **prymnesium** (Fig. 23.3(*e*)). Okadaic acid and the related dinophysistoxins are produced by the benthic dinoflagellate *Prorocentrum* (Figs. 7.30(*c*), 7.55) and the planktonic forms of *Dinophysis* (Figs. 7.30(*a*), (*b*)). Prymnesium is formed by species of the haptophyte *Prymnesium* (Fig. 22.7).

6 *Non-nitrogren compounds containing ladder-frame polyethers*. **Brevetoxin** (Fig. 23.4(*f*)), **ciguatoxin** (Fig. 23.4(*f*)), and **yessotoxin** (Fig. 23.4(*f*)). Brevetoxins are formed by species of the dinoflagellate *Karenia* (*Gymnodinium*) (Figs. 7.19, 7.59) and by the raphidophytes *Chattonella* (Fig. 18.3) and *Heterosigma* (Fig. 18.1(*a*)). Ciguatoxins are produced by species of the tropical and subtropical benthic dinoflagellate *Gambierdiscus* (Figs. 7.6, 7.32). Yessotoxins are produced by the dinoflagellate *Prorocentrum*.

Toxic algae and the end-Permian extinction

All eukaryotic toxic algae contain chloroplast endoplasmic reticulum around the chloroplast and have evolved through a secondary endosymbiosis. Algae derived from secondary endosymbioses evolved during the middle to late Permian Period (Medlin et al., 1997).

There was extinction of approximately 90% of marine species during the late Permian (about 270 million years ago) (Sepkoski, 1984; Erwin, 1993) (Fig. 23.5). Before this extinction, the Paleozoic oceans were dominated by epifaunal (attached to a substrate in the adult form) invertebrates that were filter feeders, sieving food particles out of the water, or passive carnivores. The Permian Period is demarcated from the Triassic by the extinction of this fauna, and this boundary established the close of the Paleozoic era from the start of the Mesozoic era. The Mesozoic oceans comprise a different fauna with a much reduced number of filter feeders. The animals were more highly mobile with an expansion of predators and of a fauna that burrowed more deeply into the sediment.

Thus, the marine fauna that suffered the greatest extinction at the end of the Permian was attached to the seafloor in the adult form and filtered organic material from the water. In addition, those marine invertebrates with larvae that filtered plankton from the seawater had greater extinction rates than those invertebrates that did not feed on plankton (Christiansen and Fenchel, 1979; Jablonski and Lutz, 1983; Valentine and Jablonski, 1986). Filter feeding by sieving organic material from the seawater appears to be the one unifying characteristic of invertebrates that became extinct during the late Permian.

The evolution of toxic algae derived from secondary endosymbioses paralleled the decline of invertebrates during the end-Permian extinction. It appears that the attached filter-feeding invertebrates that characterized the Paleozoic seas were susceptible to the toxins produced by the newly evolved algae at the end of the Permian Period. This resulted in selective pressure that resulted in their decline and the evolution of a new fauna that was more mobile and less susceptible to the toxic algae in the marine environment.

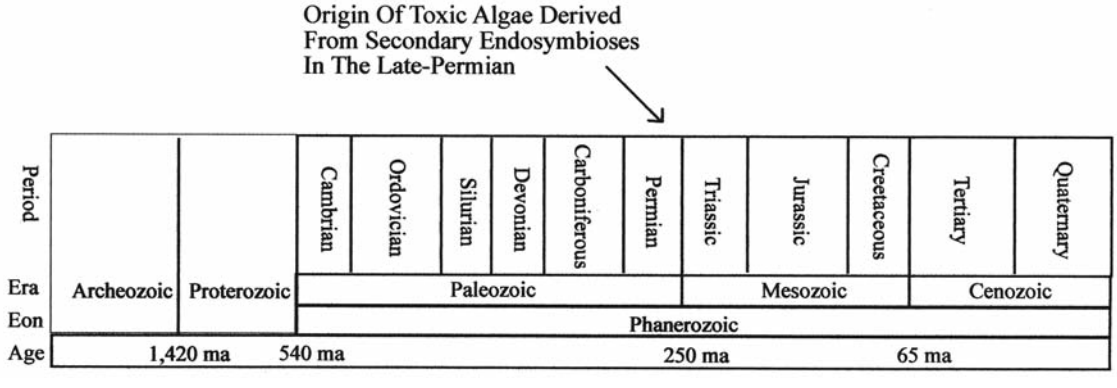


Fig. 23.5 Location of the end-Permian extinction in the geological time scale.

Cooling of the Earth, cloud condensation nuclei, and DMSP

Algae adjust to changes in external salt concentration by adjusting the osmolarity of the cell protoplasm through the production of glycerol in freshwater algae (Fisher et al., 1994) or dimethylsulfoniopriopionate (DMSP) in marine algae (Wolfe et al., 1997). The higher the external salt concentration, the greater the concentration of glycerol or DMSP in the protoplasm. DMSP and glycerol are used because they do not interfere with cellular function as do some organic salts (Keller and Korjeff-Bellows, 1996).

The production of DMSP by marine algae is an important factor in the formation of clouds and the temperature of the Earth's atmosphere. After a marine alga dies, DSMP is released into the ocean where it is broken down into the gas dimethyl sulfide (DMS) and propenoic acid (acrylic acid) (Fig. 23.6) (Liss et al., 1997). Dimethyl sulfide gas dissolves in the seawater and eventually some dimethyl sulfide escapes into the atmosphere. In the atmosphere, dimethyl sulfide is oxidized into methane sulfonic acid (MSA) and sulfuric acid. MSA and sulfuric acid have relatively low vapor pressures so they precipitate into atmospheric aerosols that produce cloud condensation nuclei. **Cloud condensation nuclei** are small particles of hygroscopic material on which liquid water condenses (Cox, 1997). This produces rain and cloud albedo. **Albedo** refers to the ability of clouds to reflect sunlight back out of the atmosphere. The more clouds the greater the reflectivity and albedo, and the less heating of the Earth (Charlson et al., 1987). This counters heating of the Earth by the greenhouse effect where anthropogenic (related to human activities) burning of fossil fuels has resulted in increased atmospheric carbon dioxide concentrations and heating of the Earth (Jones and Slingo, 1997).

Atmospheric sulfuric acid is also produced by burning of fossil fuels. Anthropogenic sulfuric acid in the atmosphere is mostly over land and in the Northern Hemisphere (Liss et al., 1997). In contrast, over the oceans, cloud condensation nuclei are produced mostly from dimethyl sulfide oxidation. Prymnesiophytes (haptophytes) and dinoflagellates produce more DMSP per cell than other marine algae (e.g., diatoms) and are the main contributors to the cloud condensation nuclei over oceans (Malin, 1996).

Marine flagellates may use DMSP (instead of glycerol) as an osmolyte because its degradation of DMSP produces propenoic (acrylic) acid. Acidifying seawater makes more carbon dioxide available for photosynthesis (see section on evolution of chloroplast endoplasmic reticulum). Although propenoic acid is metabolized by bacteria, the release of large quantities of propenoic acid from blooms of the prymensiophyte *Phaeocystis* appears to prevent growth of other microorganisms in the water for some time after the bloom (Savage, 1930).

Chemical defense mechanisms of algae

Herbivore grazing on macroalgae and predation by invertebrates on microalgae cause the greatest loss of algal biomass. Algae have evolved chemical defense mechanisms that can be defined as constitutive or inducible:

1 **Constitutive defense**. The chemicals involved in defense are present all of the time. An example is the toxic "red tide" dinoflagellates that have reduced grazing by copepods (Wolfe, 2000). Coccolithophorids are another example. *Emiliana huxleyi* has an increased amount of dimethylsulfonopropionate (DMSP) when it is grazed by invertebrates. DMSP lyase breaks down DMSP into dimethylsulfide and acrylate (Fig. 23.6). Water containing the latter compound is avoided by grazing protozoans (Strom et al., 2003).
2 **Inducible defense**. The chemicals that function in defense are only produced when the alga is under pressure from a consuming organism. Chemicals are costly for the alga to produce so it is more economical for the algal cells to produce the chemicals only when in danger of being consumed. Examples of inducible defense chemicals are the increased production of phlorotannins by brown algae,

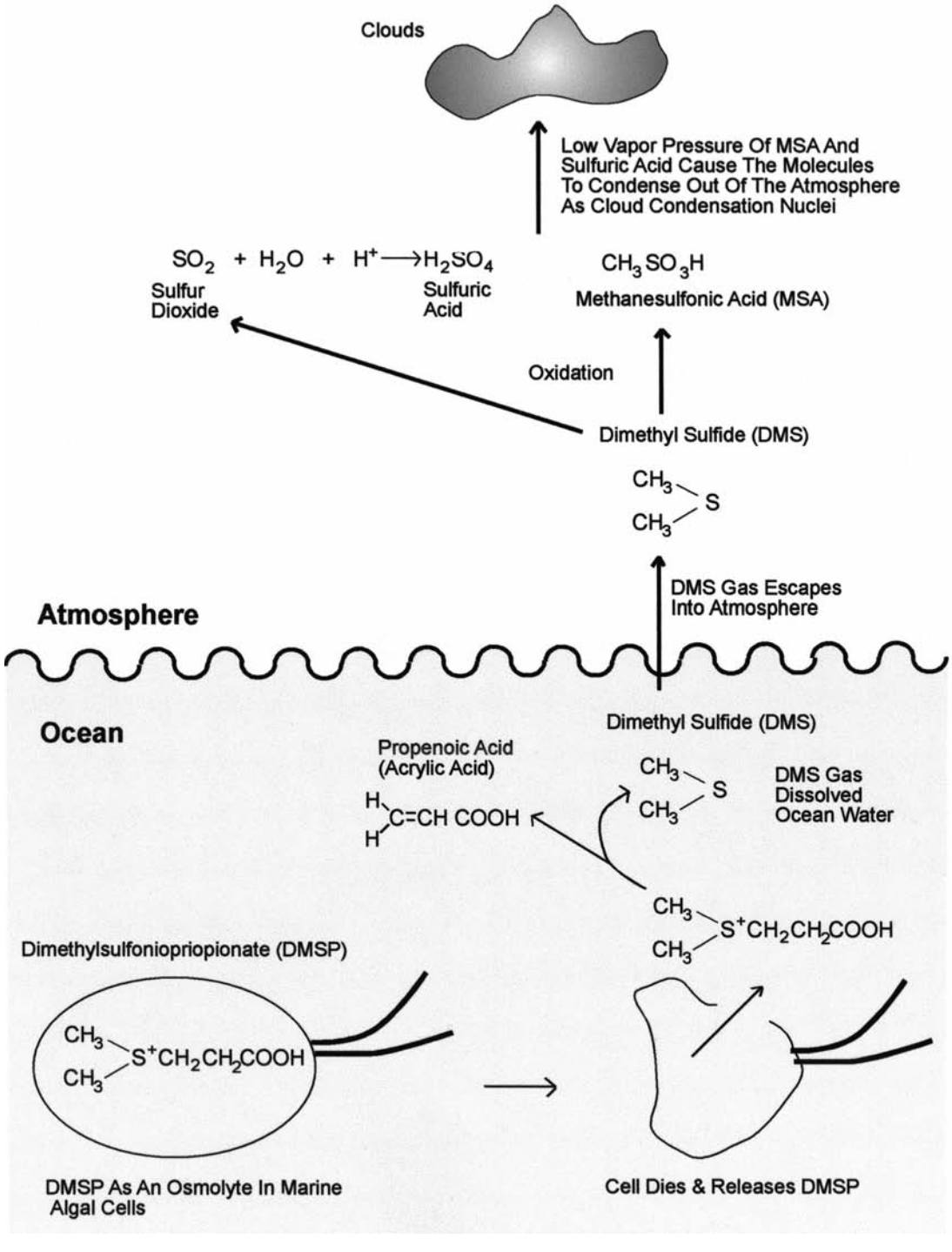


Fig. 23.6 The mechanism by which DMSP produces clouds and cooling in the atmosphere.

and the increased production of halogenated furones by red algae, on grazing by invertebrates (Pavia et al., 2003).

Defense chemicals can also be divided into:

- **seriochemicals**, which act between individuals of the same species. **Pheromones** that function in sexual reproduction are examples of seriochemicals.
- **allelochemicals**, which act between members of different species. Kairomones and synomones are examples of allelochemicals (Cembella, 2003).

Kairomones are chemicals secreted by a predator that induce changes in the behavior, morphology, or life history of the prey.

1 Kairomones can be noxious compounds produced by the prey to act as feeding deterrents via olfactory or gustatory responses of the predator at the preingestive stage. Such contact signals could be sequestered on the surface of the prey cells or released into the medium. Often their main purpose would not be to intoxicate the predator, but to discourage "tasting" or to initiate rapid release of the prey following physical handling and capture. For example, grazing experiments exposing the tintinnid *Favella ehrenbergi* to cells of the toxic dinoflagellate *Alexandrium* resulted in the ciliate swimming in retrograde (avoidance) manner once a threshold of dinoflagellate cells was reached (Hansen et al., 1992).
2 Kairomones can be toxic compounds released from ingested cells that result in physical incapacitation or mortality of the predator. The prymnesiophyte alga *Phaeocystis* contains large amounts of β-dimethylsulfoniopropionate (DMSP). Ingestion of the alga releases the intracellular DMSP resulting in reduced grazing by the heterotrophic dinoflagellates *Amphidinium*, *Gymnodinium*, *Oxyrrhis*, and the ciliate *Coxliella* (Strom et al., 2003).
3 Kairomones can be "stealth compounds" of low acute toxicity to adult predators that lead to postdigestive reduction in fecundity (ability to produce offspring). Postdigestive deterrence would obviously be ineffective for the protection of the individual ingested cell, but group defense would be maintained on a community basis. For example, the ingestion of high concentrations of diatoms by copepods results in the low viability of eggs of the nauplii (larvae) of the copepods (Paffenhofer, 2002; Ianora et al., 2003).

Synomones are produced by prey species to attract predators of their predators at the next level of the food web.

The Antarctic and Southern Ocean

The phytoplankton in the waters around Antarctica support a plethora of marine life. Easterly winds next to the Antarctic continent drive the **Antarctic Coastal Current** or **East Wind Drift** (Fig. 23.7). North of this, westerly winds drive one of the largest current systems of Earth, the **Antarctic Circumpolar Current** or **West Wind Drift** (Garrison and Siniff, 1986). This current flows unobstructed around Antarctica, transporting two to three times more water than the Gulf Stream. A region of upwelling occurs between the Antarctic Coastal Current and Antarctic Circumpolar Current. This area of upwelling pulls nutrient-rich deep water to the surface. This nutrient-rich water spills over all the Antarctic waters creating an environment for phytoplankton blooms. The **Southern Ocean**, comprising about 10% of the world ocean, occurs between the Antarctic continent and the outer edge of the Antarctic Circumpolar Current. There is an intense bloom of phytoplankton in the Southern Ocean during the austral (southern) summer that provides energy for marine food webs. Zooplankton, particularly the Antarctic krill (*Euphasia superba*), are abundant, providing a food source for vertebrate populations.

The sea ice surrounding the Antarctic continent can be divided into (1) **land-fast ice** that persists all year long and (2) **pack ice** that breaks up during the austral summer (December–March) (Fig. 23.7). There are two basic algal communities that exist in the ice in the Antarctic:

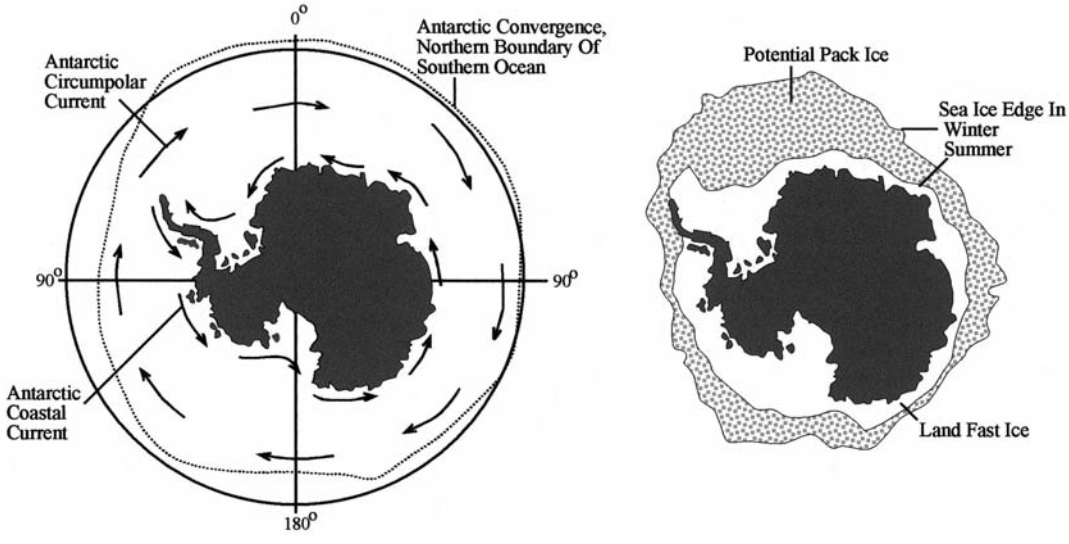


Fig. 23.7 Drawings of currents (*left*) and sea ice (*right*) in the Southern Ocean surrounding the Antarctic continent.

bottom-dwelling algae on the bottom of the ice, and algae growing in the ice itself.

1 The **bottom-dwelling algae** are mostly diatoms such as *Nitzschia stellata* and *Amphiprora* sp. These bottom-dwelling diatoms occur principally on the bottom of land-fast ice. Pack ice, though, does not have a well-developed community of bottom-dwelling diatoms. This is probably because the bottom of pack ice is extensively grazed by the krill (Garrison et al., 1986). Observers on ice-breaking ships have seen swarms of krill on upturned ice floes or in holes of decaying ice floes.
2 **Algae growing in the ice**. The algae growing in the ice depend on the conditions of the ice. Initially, salts are excluded from the ice as the salt water freezes during the austral fall and winter. This results in brine inclusions in the ice with salinities as high as 10%. The brine inclusions contain cryo- and halotolerant algae that are able to tolerate the cold and high salinity. Dinoflagellates, chrysophytes, and the green *Mantoniella* are common in these brine inclusions (Stoecker et al., 1998). These brine algae peak and form resting spores before the melting of the surface ice dilutes the brine and produces hyposaline conditions and a new population of algae. There is an abundance of nutrients available in the meltwater and diatoms such as *Nitzschia corta* proliferate. As pack ice melts, the algae in the ice are released to the water column where the algae form a seed population for the phytoplankton bloom that occurs during the austral summer (Smith and Nelson, 1986).

The grand experiment

Man's activities have resulted in an increase in CO_2 in the atmosphere and potential warming of the atmosphere of the earth due to the "greenhouse effect." This increase in CO_2 in the atmosphere can be addressed in one of two ways, either by a reduction in the burning of fossil fuels or by removing the CO_2 from the atmosphere.

John Martin of the Moss Landing Marine Laboratory in California put forth the hypothesis that iron availability limits phytoplankton production in nutrient-rich seas. He further suggested that it might be possible to fertilize the Southern Ocean (which has an abundance of unused nutrients) with iron, increase photosynthesis by plankton, and increase the flux of CO_2 from the atmosphere to the deep ocean, which contains 60 times more CO_2 than the atmosphere.

> I first said this more or less facetiously at a Journal Club lecture at Woods Hole Oceanographic Institute in July 1988. I estimated that with 300 000 tons of Fe, the Southern Ocean phytoplankton could bloom and remove two billion tons of carbon dioxide. Putting on my best Dr Strangelove accent, I suggested that with half a ship load of Fe, I could give you an ice age. Chisholm and Morel (1991)

Historically, there has been variation in the CO_2 concentration in the atmosphere. Man's activities have resulted in an increase in CO_2 concentration today to almost 350 parts per million (ppm). This is an increase from 200 ppm during the last ice age (glacial maximum, 18 000 years ago). The glacial minimum that preceded this, however, had an atmospheric concentration of 280 ppm, approximately the same as in 1900. The decrease in CO_2 concentration during the last glacial maximum is explained as follows. There was a fivefold increase in the arid areas of the earth, along with a 1.5 times increase in the winds. These two factors resulted in a 50-fold increase in the airborne dust particles. Since iron is the fourth most common element on Earth, the airborne dust contained a significant amount of iron, much of which was deposited in the oceans. This resulted in a threefold increase in photosynthesis and a decrease in CO_2 to around 200 ppm. This produced a decrease in the greenhouse effect, a cooling of the Earth, and an ice age (Martin, 1990).

The suggestion of adding iron to the Southern Ocean to reduce atmospheric CO_2 triggered a debate about whether we should engage in intentional large-scale intervention with the Earth's natural biogeochemical cycles. Martin put forward the following:

> One could argue that this really is not such a new or weighty issue. After all, we have already changed dramatically the landscape of terrestrial ecosystems, we have converted forests to croplands, croplands to deserts, rivers to lakes and deserts to greenbelts. So why is there such a big fuss about the prospect of spreading some iron around the ocean? If we are inadvertently, but knowly, changing the chemistry of the atmosphere through fossil fuel burning, why should we not change it purposely through iron fertilization or some other scheme? Chisholm and Morel (1991)

Ultimately it was decided to try a test of the hypothesis. John Martin orchestrated the scientific and logistical planning for a large-scale iron enrichment experiment in the open ocean, although his untimely death from cancer in 1993 prevented him from seeing the outcome. In mid-November 1993, the RV *Columbus Iselin* arrived 500 miles south of the Galapagos Islands with 480 kg of iron. The iron was pumped into the propellar wash as the vessel steamed to and fro across an 8 $\times$ 8 km field over 24 hours, raising the iron concentration from about 0.05 mM to about 4 mM. Water samples were taken and monitored for phytoplankton and nutrients, while a P-3 Orion airplane optically scanned the water for changes in phytoplankton pigments. The results showed that there was an increase in phytoplankton, although the increase was not as great as was predicted from laboratory cultures. This was probably due to increased grazing by zooplankton, which showed a 50% increase over the period (Wells, 1994). The experiment was repeated in 1995 (Coale et al., 1996) and again enrichment of photoplankton was obtained.

The experiment showed it is possible to remove 1000 to 100 000 tons of carbon from the atmosphere for each one ton of iron added to the Southern Ocean (Boyd, 2004; Dalton, 2002). The political realities of performing Fe enrichment in quantities high enough to significantly effect the atmospheric CO_2 concentration is on hold as the debate over the increase in CO_2 in the atmosphere, and global warming, continues.

Antarctic lakes as a model for life on the planet Mars or Jupiter's moon Europa

The McMurdo Dry Valleys in Antarctica (Fig. 23.8) have one of the driest and coldest deserts on Earth and house the only permanently ice-covered lakes on our planet (Pocock et al., 2004). The headquarters of Captain Robert F. Scott (who perished with his party returning from the South Pole) was across McMurdo Sound from the dry valleys. In December 1903, Scott wrote, "It is worthy to record, too, that we have seen no living thing, not even a moss or lichen; all that we did

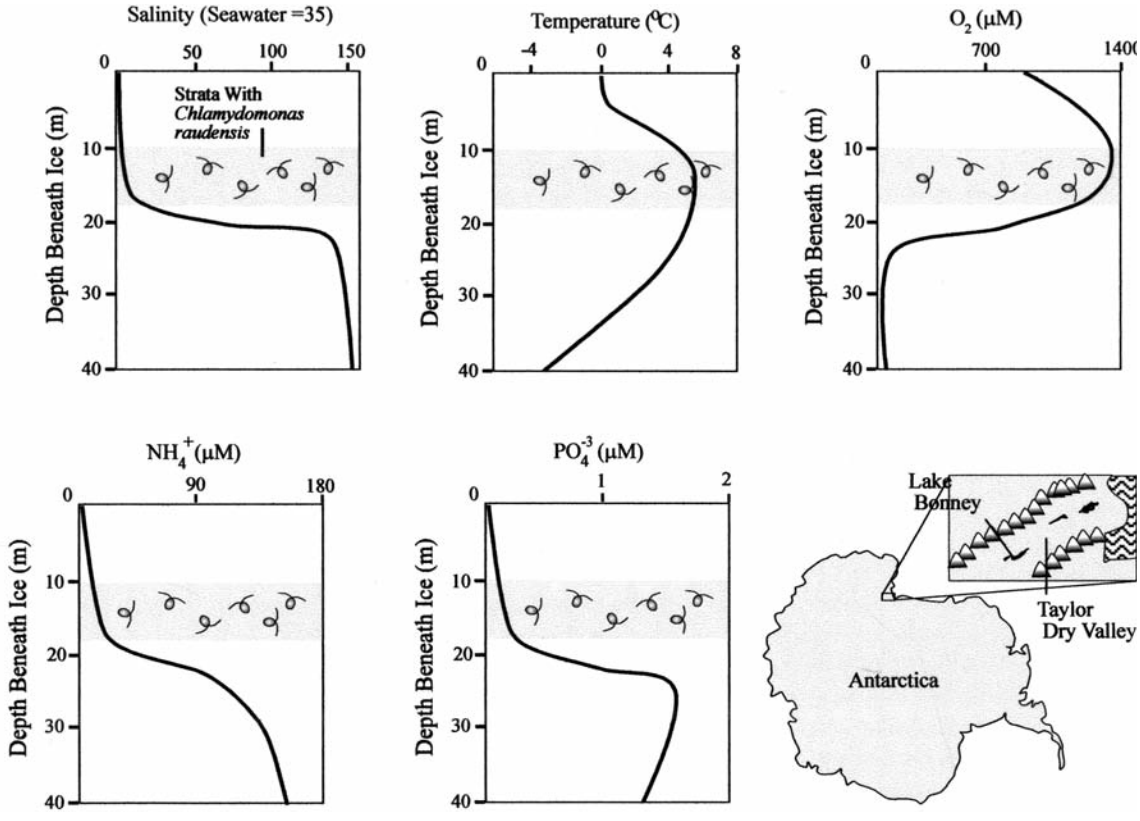


Fig. 23.8 Profiles of water conditions from Lake Bonney, Taylor Dry Valley, Antarctica. The dominant alga, *Chlamydomonas raudensis*, occurs primarily between 10 and 17 meters depth. (Modified from Spigel and Priscu, 1996.)

find, far inland among the moraine heaps, was the skeleton of a Weddell seal, and how that came there is beyond guessing. It is certainly a valley of the dead; even the great glacier which once pushed through it has withered away" (Priscu, 1999). Average annual precipitation in these dry valleys is less than 10 cm and average air temperature is about $-20°$ C. Lake Bonney is in the Taylor Valley and has a permanent ice cover that prevents wind mixing of the column, resulting in vertical mixing only on the molecular scale; vertical mixing time is approximately 50 000 years. Stratification in Lake Bonney is the result of strong salinity gradients. The salinity of the lake varies from freshwater at the surface (from melting glaciers in the austral (Southern Hemisphere) summer) to hypersaline brine more than five times seawater at the bottom. There are four months of darkness during the austral winter with algal cells generating energy from heterotrophy. During the austral summer the ice cover attenuates about 98% of light. Therefore, photosynthetic inhabitants of the water column below the ice are never exposed to saturating light levels and have adapted to a shade environment. *Chlamydomonas raudensis* is the dominant alga in this environment. This green alga is an obligate psychrophile because it does not grow above 16° C. *Chlamydomonas raudensis* lives in a discrete layer in the lake at depths of between 10 and 17 m, which is a transition zone between an oxygen-rich layer where O_2 production exceeds respiratory O_2 uptake and the deeper oxygen-deficient region (Fig. 23.8) (Pocock et al., 2004). The shade adaptation is reflected in its low chlorophyll *a*/*b* ratio (Morgan et al., 1998). Light above 680 nm is primarily absorbed by chlorophyll *a* while chlorophyll *b* absorbs shorter wavelengths (Fig. 1.13). Similarly there are low levels

of photosystem I to photosystem II; photosystem II utilizes light of wavelengths shorter than 680 nm while photosystem I utilizes light up to 700 nm wavelength. The permanent ice cover in these Antarctic lakes absorbs all light wavelengths above 600 nm (Pocock et al., 2004). The perennial ice overlying liquid water in these Antarctic lakes is similar to the situation on the moon Europa of Jupiter, and on Mars where permanently ice-covered lakes are thought to have existed between 3.1 and 3.8 billion years ago (Priscu et al., 1999).

Ultraviolet radiation, the ozone hole, and sunscreens produced by algae

Ultraviolet radiation in customarily divided into three spectral regions: UV-C (200–280 nm), UV-B (280–320 nm), and UV-A (320–400 nm) (Banaszak and Trench, 1999). UV-C, with the shortest wavelengths, is the most potentially damaging to cells but it is almost entirely absorbed by ozone and other atmospheric gases. Biological weighing functions, which estimate the effect of each wavelength on a biological process, indicate the affect of UV-B is most severe. This is because aromatic amino acids (e.g., tyrosine, phenylalanine, tryptophan) strongly absorb UV-B at 280 nm. Therefore, proteins containing these amino acids are highly susceptible to photodestruction, particularly to splitting of disulfide bridges between cysteine residues (which control the tertiary structure of proteins) (Bischof et al., 2000).

Recently there has been a depletion in the ozone layer, particularly in the polar regions, which has been at least partially attributed to chlorofluorocarbons. Springtime ozone reductions up to 60% compared with values 30 years ago have been recorded (Karsten et al., 1999). This has resulted in increased amounts of UV-B reaching the surface of the Earth.

The production of ultraviolet sunscreens by algae (especially those inhabiting shallow waters) is one mechanism the cells have evolved in dealing with damaging UV light. The most common of these UV-absorbing compounds are the mycosporine-like amino acids (MAAs) that absorb UV radiation between 310 and 360 nm (Karsten et al., 1999) (Fig. 23.9). Mycosporine is a generic term used to describe small, water-soluble, nitrogenous metabolites. The MAAs have amino groups conjugated to a cyclohexane chromophore (Fig. 23.9). The MAAs occur in many algal groups where they attenuate UV-B and reduce the harmful effects of the radiation on cells.

Hydrogen fuel cells and hydrogen gas production by algae

Hydrogen fuel cells are an attractive and clean energy source for motor cars. Electrolysis of water is the most commonly mentioned method for generating hydrogen gas. Algae can also be induced to produce hydrogen gas. Cyanobacteria produce hydrogen as a byproduct of nitrogen fixation (Fig. 23.10). The nitrogenase enzyme, however, has a low catalytic turnover and has a high energy requirement, leading most investigators to reject it as a source of hydrogen gas (Ghiradi et al., 2000). The production of hydrogen gas by hydrogenases in green algae has been more extensively investigated (Melis et al., 2000; Ghiradi et al., 2000). In the green algae, photons of light are captured in the chlorophyll *a* in a reaction center (P700) of photosystem I, driving the potential by 1 V. Excitation of P700 results in the transfer of an electron to a membrane-bound form of ferredoxin, a 11.6 kdal iron-sulfur protein of the Fe_4S_4 type. Hydrogenases in the green algae combine the electrons from ferredoxin with protons to produce hydrogen gas (Fig. 23.10). This is essentially an anaerobic reaction since the hydrogenase enzymes are inhibited by oxygen.

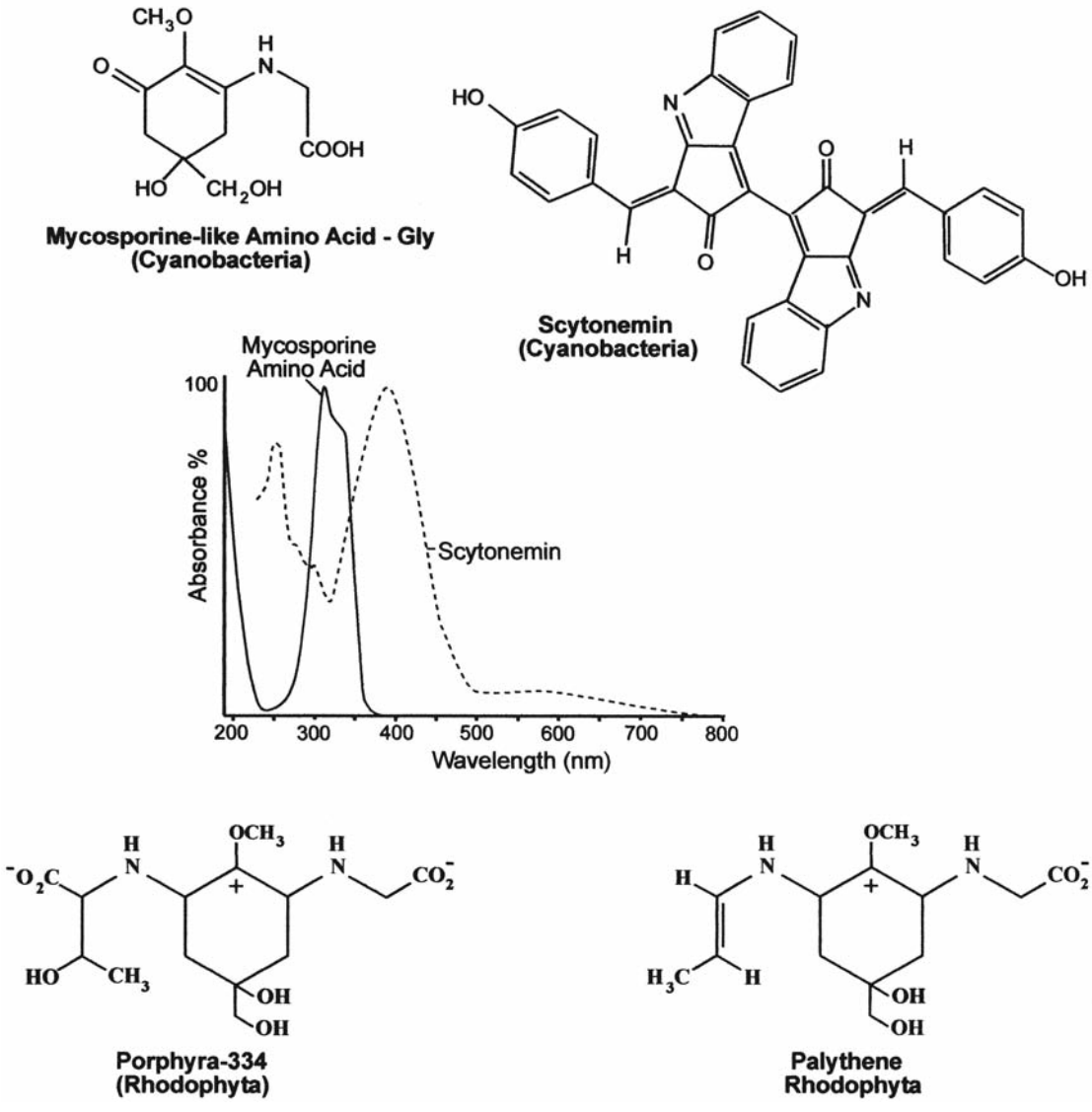


Fig. 23.9 Some UV-B absorbing compounds that occur in algae. The absorbance spectrum of scytonemin and mycosporine amino acid is also shown. (Modified from Ehling-Schulz and Scherer, 1999.)

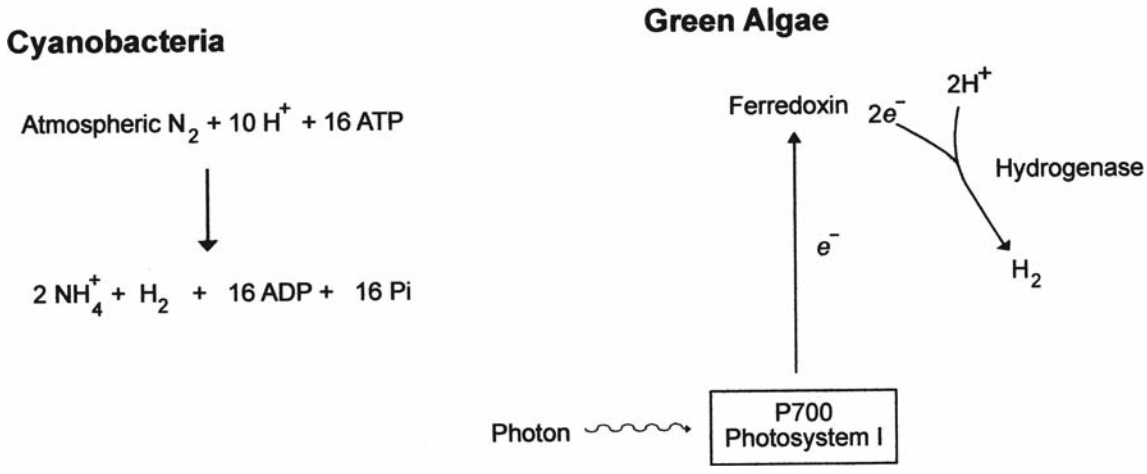


Fig. 23.10 The chemical reactions that result in the formation of hydrogen gas in the cyanobacteria and green algae.

REFERENCES

Banaszak, A., and Trench, R. K. (1999). Ultraviolet sunscreens in dinoflagellates. *Protist* 152:93–101.

Bischof, K., Hanelt, D., and Wiencke, C. (2000). Effects of ultraviolet radiation on photosynthesis and related enzyme reactions of marine macroalgae. *Planta* 211:555–62.

Boyd, P. (2004). Ironing out algal issues in the Southern Ocean. *Science* 304:396–7.

Cembella, A. D. (2003). Chemical ecology of eukaryotic microalgae in marine ecosystems. *Phycologia* 42:420–7.

Charlson, R. J., Lovelock, J. E., Andreae, M. O., and Warren, S. G. (1987). Oceanic phytoplankton, atmospheric sulphur, cloud albedo and climate. *Nature* 326:655–61.

Chisholm, S. W., and Morel, F. M. M. (1991). What controls phytoplankton production in nutrient-rich areas of the open sea? *Limnol. Oceanog*. 36:1507–970.

Christiansen, F. B. and Fenchel, T. M. (1979). Evolution of marine invertebrate reproductive patterns. *Theoret. Pop. Biol*. 16:267–82.

Coale, K. H., Johnson, K. S., Fitzwater, S. E., Gordon, R. M., Tanner, S., Chavez, F. P., Ferioli, L., Sakamoto, C., Rodgers, P., Millero, F., Steinberg, P., Nightingale, P., Cooper, D., Cochlan, W. P., Landry, M. R., Constantinou, J., Rollwagen, G., Trasvina, A., and Kudela, R. (1996). A massive phytoplankton bloom induced by an ecosystem-scale iron fertilization experiment in the equatorial Pacific Ocean. *Nature (Lond.)* 383:495–501.

Cox, R. A. (1997). Atmospheric sulphur and climate – what have we learned? *Phil. Trans. Royal Soc., Biol. Sci*. 352:251–4.

Dalton, R. (2002). Ocean tests raise doubts over use of algae as carbon sink. *Nature* 420:722.

Ehling-Schulz, M. A., and Scherer, S. (1999). UV protection in cyanobacteria. *Eur. J. Phycol*. 34:329–38.

Erwin, D. H. (1993). *The Great Paleozoic Crisis*. New York: Columbia University Press.

Fisher, M., Pick, U., and Zamir, A. (1994). A salt-induced 60-kilodalton plasma membrane protein plays a potential role in extreme halotolerence of the alga *Dunaliella. Plant Physiol*. 106:1359–65.

Garrison, D. L., and Siniff, D. B. (1986). An Antarctic perspective. *BioScience* 36:238–42.

Garrison, D. L., Sullivan, C. W., and Ackley, S. F. (1986). Sea ice microbial communities in Antarctica. *BioScience* 36:243–50.

Ghirardi, M. L., Zhang, L., Lee, J. W., et al. (2000). Microalgae: a green source of renewable H_2. *TIBTech*. 18:506–11.

Gilbert, J. J. (1996). Effect of food availability on the response of planktonic rotifers to a toxic strain of the cyanobacterium *Anabaena flos-aquae. Limnol. Oceanog*. 41:1565–72.

Hallegraeff, G. M., Andersen, D. M., and Cembella, A. D. (2003). *Manual on Harmful Marine Microalgae*. Paris: UNESCO Publishing.

Hansen, P. J., Cembella, A. D., and Moestrup, Ø. (1992). The marine dinoflagellate *Alexandrium ostenfeldii:* paralytic shellfish toxin content, composition and toxicity to a tintinnid ciliate. *J. Phycol*. 28:597–603.

Ianora, A., Poulet, S. A., and Miralto, A. (2003). The effects of diatoms on copepod reproduction: a review. *Phycologia* 42:351–63.

Igarashi, T., Aritake, S., and Yasumoto, T. (1999). Mechanisms underlying the hemolytic and ichthyotoxic activities of maitotoxin. *Nat. Toxins* 7:71–9.

Jablonski, D., and Lutz, R. A. (1983). Larval ecology of marine benthic invertebrates: paleobiological implications. *Biol. Rev*. 58:21–89.

Jones, A., and Slingo, A. (1997). Climate model studies of sulphate aerosols and clouds. *Phil. Trans. Royal Soc., Biol. Sci*. 352:221–7.

Karsten, U., Bischof, K., Hanelt, D., Tug, H., and Wiencke, C. (1999). The effect of ultraviolet radiation on photosynthesis and ultraviolet-absorbing substances in the endemic Arctic macroalgae *Devuleraea ramentacea* (Rhodophyta). *Physiol. Plantarum* 105:58–66.

Keller, M. D., and Korjeff-Bellows, W. (1996). Physiological aspects of the production of dimethylsulfoniopropionate (DMSP) by marine phytoplankton. In *Biological and Environmental Chemistry of DMSP and Related Sulfonium Compounds*, ed. R. P. Kiene, P. T. Visscher, M. D. Keller, and G. O. Kirst, pp. 131–42. New York: Plenum Press.

Liss, P. S., Hatton, A. D., Malin, G., Nightingale, P. D., and Turner, S. M. (1997). Marine sulphur emissions. *Phil. Trans. Royal Soc., Biol. Sci*. 352:159–67.

Malin, G. (1996). The role of DMSP and DMS in the global sulfur cycle and climate regulation. In *Biological and Environmental Chemistry of DMSP and Related Sulfonium Compounds*, ed. R. P. Kiene, P. T. Visscher, M. D. Keller, and G. O. Kirst, pp. 177–89. New York: Plenum Press.

Martin, J. H. (1990). Glacial–interglacial CO_2 change. The iron hypothesis. *Paleoceanography*. 5:1–13.

Medlin, L. K., Kooistra, W. H. C. F., Gersonde, R., Sims, P. A., and Wellbrock, U. (1997). Is the origin of diatoms related to the end-Permian mass extinction? *Nova Hedwigia* 65:1–11.

Melis, A., Zhang, L., Forestier, M., Ghirardi, M. L., and Siebert, M. (2000). Sustained photobiological hydrogen gas production upon reversible inactivation of oxygen evolution in the green alga *Chlamydomonas reinhardtii*. *Plant Physiol*. 122:127–36.

Morgan, R. M., Ivanov, A. G., Priscu, J. C., Maxwell, D. P., and Huner, N. P. A. (1998). Structure and composition of the photochemical apparatus of the Antarctic green alga *Chlamydomonas subcaudata*. *Photosynth. Res*. 56:303–14.

Paffenhofer, G.-A. (2002). An assessment of the effects of diatoms on planktonic copepods. *Mar. Ecol. Progr. Ser*. 227:305–10.

Pan, Y., Bates, S., and Cembella, A. D. (1998). Environmental stress and domoic acid production by *Pseudo-nitzschia:* a physiological perspective. *Nat. Toxins* 6:127–35.

Pavia, H., Toth, G. B., Lindgren, A., and Aberg, P. (2003). Intraspecific variation in the phlorotannin content of the brown alga *Ascophyllum nodosum. Phycologia* 42:378–83.

Pocock, T., Lachance, M.-A., Proschold, T., Priscu, J. C., Kim, S. S., and Huner, N. P. A. (2004). Identification of a psychrophilic green alga from Lake Bonney Antarctica *Chlamydomonas raudensis* Ettl. (UWO 241) Chlorophyceae. *J. Phycol*. 40:1138–48.

Priscu, J. C. (1999). Life in the valley of the "dead". *BioScience* 49:959.

Priscu, J. C., Wolf, C. F., Taakacs, C. D., et al. (1999). Carbon transformations in a perennially ice-covered Antarctic lake. *BioScience* 49:997–1008.

Savage, R. E. (1930). The influence of *Phaeocystis* on the migration of herring. *Fish. Investig., London, Ser. II* 12:5–14.

Sepkoski, J. J. (1984). A kinetic model of Phanerozoic taxonomic diversity. III. Post Paleozoic families and mass extinctions. *Paleobiology* 10:246–67.

Shimizu, Y. (2000). Chemistry and mechanism of action. In *Seafood and Freshwater Toxins: Pharmacology, Physiology and Detection*, ed. L. M. Botana, pp. 151–72. New York: Marcel Dekker.

Smith, W. O., and Nelson, D. M. (1986). Importance of ice edge phytoplankton production in the Southern Ocean. *BioScience* 36:251–7.

Spigel, R. H., and Priscu, J. C. (1996). Evolution of temperature and salt structure of Lake Bonney, a chemically stratified Antarctic lake. *Hydrobiologia* 321:177–90.

Stoecker, D. K., Gustafson, D. E., Black, M. M. D., and Baier, C. T. (1998). Population dynamics of microalgae in the upper land-fast sea ice at a snow-free location. *J. Phycol*. 34:60–9.

Strom, S., Wolfe, G., Slajer, A., Lambert, S., and Clough, J. (2003). Chemical defense in the microplankton. Inhibition of protist feeding by β-dimethylsulfoniopropionate (DMSP). *Limnol. Oceanogr*. 48:230–7.

Valentine, J. W., and Jablonski, D. (1986). Mass extinctions: sensitivity of marine larval types. *Proc. Natl. Acad. Sci., USA* 83:6912–14.

Wells, M. L. (1994). Pumping iron in the Pacific. *Nature (London)* 368:295–6.

Wolfe, G. V. (2000). The chemical defense ecology of marine unicellular plankton: constraints, mechanisms, and impacts. *Biol. Bull*. 198:235–44.

Wolfe, G. V., Steinke, M., and Kirst, G. O. (1997). Grazing-activated chemical defense in a unicellular alga. *Nature* 387:894–7.

Glossary

abaxial: located in a position away from the plant.
acronematic flagellum: a flagellum without hairs.
acropetal: toward the apex.
action spectrum: relative effectiveness of each stimulating light wave for the response rate.
adaxial: located on the side toward the main axis.
adelphoparasite: parasite that is closely related to the host.
aerobic: needing oxygen.
aeroplankton: air-borne microscopic organism.
agar: one or more polysaccharides containing sulfated galactose obtained from the walls of some red algae.
agarophyte: red algae used in the production of agar.
agglutin: chemical substance involved in the recognition of a gamete of the opposite strain.
agglutination: adherence of gametes of different mating types by their flagella tips.
akinete: thick-walled resting spore.
alginates: salts of polysaccharides composed of D-mannuronic and L-guluronic acids obtained from brown algae.
alkalinity: in water chemistry, the total quantity of base in equilibrium with carbonate or bicarbonate that can be determined by titration with strong acid. Alkaline waters have a high pH.
allelochemical: a chemical that functions between members of different species. Seriochemicals act between individuals of the same species.
allelopathy: injurious effects of one species on another.
allomone: a chemical excreted by a prey to avoid predation.
alloparasites: parasites not closely related to their host.
allophycocyanin: a blue biliprotein obtained from cyanobacteria and red algae.
alpha granule: protoplasmic structure containing myxophycean starch in the cyanobacteria.
alveoli: membrane-bounded flattened vesicles or sacs underlying the plasma membrane in certain algae, particularly the dinoflagellates.
amphiesma: the plasma membrane and underlying flattened vesicles of dinoflagellates which, in some species, contain plates.
amylopectin: the storage polysaccharide in the cyanobacteria, composed of α-1,4 glucoside linkages, with 1,6 linked side chains.
amyloplast: a colorless plastid containing starch.
amylum star: star-shaped aggregate of cells filled with starch that forms new plants in the stoneworts (Charales).
anaerobic: without oxygen.
androsporangium: sporangium that forms androspores.
androspore: spore that forms a dwarf male filament in the Oedogoniales (green algae).
anhydrobiotic: organisms that can withstand the removal of the bulk of their intracellular water for extended periods of time.
anisogamy: fusion of gametes that are unequal in size or physiology.
antapical: opposite from the apex.
anterior: the front end, forward.
antheridium: the sex organ in which the male gametes are formed.
antherozoid: male gamete.
anthropomorphic: related to man.
anticlinal: perpendicular to the circumference of the thallus.
apical growth: growth by means of an apical cell dividing to form the thallus beneath it.
aplanogamete: non-motile gamete.
aplanospore: non-motile spore.
apochlorotic: colorless.
aponin: Apparent Oceanic Naturally Occurring Cytolin. Chemicals that cause growth repression and mortality.
aragonite: orthorhombic crystals of calcium carbonate.
areolae: the chambers in the honeycomb arrangement of some diatom valves.
asexual: reproduction without the fusion of gametes.
autospore: aplanospore with the same shape as the parent cell.
autotroph: not needing an external source or organic compounds as an energy source. Energy is obtained from light or inorganic chemical reactions.
auxiliary cell: a cell that receives a nucleus from the zygote in the red algae.
auxospore: a resting cell in the diatoms that is commonly formed from the zygote.
axenic culture: a culture containing only one species.
axoneme: an axial array of (usually) nine outer doublet and two central microtubules.

bacteriocin: antibiotic secreted by cyanobacteria that kills related strains of cyanobacteria.
baeocyte: endospore produced by cyanobacteria.
basal apparatus: flagellar or ciliary apparatus exclusive of flagella/cilia.
basal body (kinetosome): cylindrical structure (*ca*. 0.2 μm diameter) found at the base of a flagellum/cilium consisting of a continuation of the nine outer axonemal doublets (A,B) but with the addition of a C-microtubules to form triplets.
basipetal: toward the base.
bathal zone: ocean water over continental slope.
benthic: pertaining to any part of a lake or ocean bottom.
benthos: organisms living on, and attached to, the bottom of aquatic habitats.
bilaterally symmetrical: a plane through an object divides it into mirror image halves.
biliprotein: a red or blue pigment and attached bile (linear tetrapyrrole) chromophore in the cyanobacteria, cryptophytes, and red algae.
biological carbon pump: trapping of carbon dioxide in the deep levels of the ocean.
bioluminescence: emission of light by a living organism.
biomass: the amount at any one time of living organisms in a habitat.
bisexual: both sexes produced on the same individual.
bisporangium: a sporangium forming two meiospores in the red algae.
bloom: heavy growth of planktonic algae in a body of water.
brackish: saline water with a salinity less than that of seawater.
budding: exospore formation in the cyanobacteria.
bulbil: small plant formed on rhizoids in the stoneworts (charophytes).
calcareous ooze: bottom sediment in oceans composed of calcified remains of organisms.
calcification: deposition of calcium carbonate, usually in association with smaller amounts of other carbonates.
calcite: rhombohedral crystals of calcium carbonate.
callose: polysaccharide associated with pores in sieve cells.
canal: rigid opening in some flagellates.
capsule: extracellular mucilage.
carotene: oxygen-free, unsaturated, hydrocarbon carotenoid.
carotenoid: yellow, orange, or red hydrocarbon fat-soluble pigment.
carpogonium: female gametangium in the red algae.
carposporangium: carpospore-producing sporangium derived directly, or indirectly, from the zygote in the red algae.
carpospore: usually diploid spore produced by the carposporangium in the red algae.
carposporophyte: usually diploid generation in the red algae derived from the zygote, it forms carpospores.
carrageenan: red algal polysaccharide (phycocolloid) similar to agar, but needing higher concentrations to form a gel.
cellulose: polysaccharide composed of β-1,4 linked glucose molecules that forms the main skeletal framework of most algal cells.
cell wall: a mostly rigid, often multilayered structure consisting of discrete microfibrillar polysaccharides embedded in an amorphous matrix composed of polysaccharides, lipids, and proteins, which together comprise an outermost layer of the cell proper.
centric: type of ornamentation arranged around a central point in the diatoms.
centriole: equivalent to a flagellar basal body.
chemical ecology: the relationship between the structure and function of metabolites and how these affect organisms in the environment, controlling the coexistence and coevolution of species.
chemoautotroph: an organism that obtains energy from oxidation of reduced inorganic compounds, and cell carbon primarily from carbon dioxide.
chemotaxis: the movement of a whole cell in response to a concentration gradient of a chemical substance. If it is toward higher concentration, it is positive; if away from a higher concentration, it is negative chemotaxis.
chitin: polysaccharide made up of repeating units of *N*-acetylglucosamine.
chlorophyll: fat-soluble, green, porphyrin-type pigment.
chloroplast: plastid with chlorophyll.
chloroplast endoplasmic reticulum (chloroplast E. R.): one or two membranes surrounding the chloroplast membrane.
chlorosis: degradation of photosynthetic pigments.
chromatic adaption: change in the proportions of different photosynthetic pigments enabling optimum absorption of the available wavelengths of light.
chromoplast or **chromatophore**: a chloroplast with some other color than green.
chrysolaminarin or **leucosin**: a liquid polysaccharide storage product composed principally of β-1,3 linked residues of glucose.

ciliary/flagellar matrix: the cytosol of the flagellum/cilium, often lacking structural detail.
cilium (flagellum): a long, cylindrical extension of a eukaryotic cell, bounded by the plasma membrane and containing an axoneme. A flagellum/cilium is a motility organelle that is mainly involved in cell movement by means of water propulsion, but can perform additional functions, such as feeding, mating, and sensory perception.
cingulum or **girdle**: transverse furrow in the dinoflagellates containing the transverse flagellum.
circadian rhythm: repeated sequence of events that occur about 24-hour intervals.
circein: female hormone secreted by oogonia in the green alga *Oedogonium*.
cirri: curled appendages on a zygote.
clone: the group of individuals derived from a single individual.
coccoid: spherical.
coccolith: calcareous scale or plate-like particle deposited on the surface membrane of some prymnesiophytes (the coccolithophorids), varying in complexity and surface decoration according to species.
coenobium: colony of algal cells in a specific arrangement and number that is fixed at the time of origin and is not subsequently augmented.
coenocyte: large multinucleate cell without cross walls, except where reproductive bodies are concerned.
colony: a group of unicells which cohere and remain together as a unit.
commensalism: a situation where one species benefits from an arrangement, while the other species does not benefit, nor does the second species suffer.
compensation depth: depth of water where there is sufficient light so photosynthesis equals respiration over a 24-hour period.
compensation point: light intensity at which respiration equals photosynthesis over a 24-hour period.
conceptacle: cavity in the thallus where gametangia are produced.
conjugation: fusion of two non-flagellated protoplasts.
connecting band: part of the girdle in diatoms.
contractile vacuole: vacuole fed by smaller vesicles that expels water and solutes rhythmically outside the cell.
coralline: reference to calcified algae.
cornuate process: horn-like wall extension.
corona: crown.
Corps de Maupas: a vesicular body in the cryptophytes used in digestion of unwanted cell components.
cortex: the outer portion or layer(s) of a protist cell, including the plasma membrane, but excluding secreted non-living structures that may lie outside the plasma membrane. The outer portion of an algal thallus.
cosmopolitan: occurring in many diverse places.
costa: an elongated, solid thickening of a diatom valve.
crenulate: wavy with small teeth or scallops.
cribellum: small sieve plate covering the pores in a cribrum in the diatoms.
cribrum: silicified plate with tiny pores covering the holes of the valve in the diatoms.
cross fertilization: the union of gamates from different thalli.
cruciate: cross-shaped.
cryoplankton: plankton of polar or cold regions.
cryptobiotic crust: accumulations of cyanobacteria, lichens, fungi, and/or mosses in desert soils.
cryptoendolith: organism that lives inside rocks.
cryptostomata or **cryptoblast**: flask-like opening in the thallus, with hairs.
cuticle: a thin hydrophobic layer deposited on the outside surface of the cell wall.
cyanelle: endosymbiotic cyanobacterium.
cyanobacterocin: an antibiotic produced by a cyanobacterium that inhibits growth of related cyanobacteria.
cyanoglobin: myogloblin-like molecule capable of scavenging oxygen in heterocysts of cyanobacteria.
cyanome: host cell containing a cyanelle.
cyanophage: virus in cells of the cyanobacteria.
cyanophycin granule: polypeptide storage granule in the cyanobacteria.
cyst: a non-motile, often dehydrated, resistant, inactive dormant stage in the life cycle.
cystocarp: in the red algae, the carposporophyte and surrounding gametophytic tissue (pericarp).
cytokinesis: division of the cytoplasm usually right after karyokinesis (nuclear division).
cytoskeleton: intracellular network of protein filaments that is insoluble in non-ionic detergents.
cytosome: cell opening used for ingestion of food particles.
dendricule: short protoplasmic extension with no organelles.
dendroid: a type of non-motile colony that produces mucilage in one area, usually forming a stalk.
detritus: particulate organic matter.
dexiotropic: clockwise when seen from the cell apex (the opposite is *leiotropic*).

diastole: filling of a contractile vacuole (*systole* is the emptying).
diatomaceous earth: a mineral consisting of the remains of the silicified frustules of diatoms.
diazocyte: cell capable of fixing nitrogen.
diazotroph: organism capable of fixing atmospheric N_2 into ammonium.
dichotomy: division of a thallus into two equal branches.
dictyosome: stack of vesicles in a Golgi apparatus.
diel: occurring over a 24-hour period.
diffuse growth: type of growth where most of the cells in a thallus are capable of division.
dioecious: an organism that has male and female gametes borne on separate plants.
diplobiontic: having two separate stages in the life cycle.
diplohaplont: an organism having a separate multicellular diploid and multicellular haploid stage.
diploid: possessing two sets of chromosomes.
diplont: an organism in which the haploid stage of the life cycle consists of only the gametes.
disc or **thylakoid**: membrane-bound sac in the chloroplast.
discobolocyst: type of projectile in the Chrysophyceae.
distichous: arranged in two equal rows.
distromatic: thallus that is two cells thick.
diurnal: daily.
dorsiventral: flattened in one plane.
dulse: a preparation of *Rhodymenia* (red alga) used as food.
ecad: a form of a plant species produced in response to a particular habitat, the modifications not being inheritable.
ecdysis: shedding of the theca in the dinoflagellates.
ecotype: a locally adapted variant.
ectoderm: outer protoplasm next to the plasma membrane in the Charales.
egg: large non-motile female gamete.
ejectisome: type of projectile found in green algae and cryptomonads.
electron-dense or **electron-opaque**: term used to describe a material that absorbs electrons and appears dark in electron micrographs.
electron-transparent: term used to describe a material that does not absorb electrons and appears light in electron micrographs.
eleutheroschisis: parent cell wall completely cast off and new daughter cell walls formed.
endemic: occurring in a specific area.
endochite: inner wall of the oogonium in the Fucales (Phaeophyceae).
endoderm: inner protoplasm next to the vacuole in the Charales, capable of cytoplasmic streaming.
endolithic: living inside rock.
endophyte: plant living inside another plant.
endosome: nucleus in the euglenoids.
endospore: asexual spore produced by some cyanobacteria.
endosymbiotic: term that describes an organism living inside a host in a symbiosis.
endozoic: living inside an animal.
enucleate: without a nucleus.
envelope: a general term used variously for such structures as plasma membranes, pellicles, walls, sheaths, and gelatinous coverings.
epicone: part of the cell above the girdle in the dinoflagellates.
epidermis: outer layer of cells.
epipelic: growing on mud.
epiphyte: one plant living on another plant.
epitheca: larger of the two halves of a diatom frustule.
epizoic: living on an animal.
epontic: living on the bottom of ice.
estuary: the mouth of a river where tidal effects are evident, and where freshwater and seawater mix.
euendolith: an organism that bores into rock.
eukaryotic or **eucaryotic**: cells with a membrane-bounded nucleus.
euphotic or **photic zone**: water above the compensation depth.
eurysaline (euryhaline): tolerant of a wide salinity range.
eurythermic: tolerant of a wide temperature range.
eutrophic: term that described a body of water that receives large amounts of nutrients, usually resulting in a large growth of algae.
exocite: outer wall of an oogonium of the Fucales (Phaeophyceae).
exotoxin: toxin secreted into the medium.
extant: living today.
extinct: not living today.
extracellular matrix: mucilaginous glycoproteins external to the plasma membrane.
eyespot: red to orange area in a cell, composed of lipid droplets.
facultative heterotroph or **autotroph**: organism that is able to live as a heterotroph or an autotroph.
facultative parasite or **saprophyte**: organism that is able to live as a parasite or a saprophyte.

false branching: in the cyanobacteria, breakage of a trichome through a sheath, giving the appearance of a branch.
fibulae: in diatoms, small nodules in rows on the inside of the valve.
filament: in the cyanobacteria, one or more trichomes enclosed in a sheath.
flagellar apparatus (kinetid): an organellar complex consisting of one or more basal bodies/kinetosomes that may bear flagella/cilia, may have microtubular and fibrous roots associated with their bases, and may function in locomotion, feeding, sensation, and reproduction.
flagellar/ciliary matrix: the cytosol of the flagellum/cilium, often lacking structural detail.
flagellar hairs: filamentous appendages usually arranged in one or more rows but not covering the entire surface of a flagellum/cilium. There are two types of flagellar hairs. (1) Tubular flagellar hairs consisting of at least a hollow shaft (>15 nm diameter), often with a cylindrical shaft and one or more terminal filaments. (2) Non-tubular flagellar hairs, assembled in the Golgi apparatus and consisting primarily of carbohydrates, forming two rows along the length of the flagellum, and attached through the flagellar membrane to specific outer doublets.
flagellar/ciliary roots: fibrous, microtubular or amorphous structures originating at or near basal bodies/kinetosomes and terminating somewhere else in the cell but not at nearby basal bodies/kinetosomes.
flagellar scales: organic structures of discrete size and shape, often covering the whole surface of the flagellum/cilium and generally assembled in the Golgi apparatus.
flagellate: a unicell having at least one flagellum.
flagellum (cilium): a long, cylindrical extension of a eukaryotic cell, bounded by the plasma membrane and containing an axoneme. A flagellum/cilium is a motility organelle that is mainly involved in cell movement by means of water propulsion, but can perform additional functions, such as feeding, mating, and sensory perception.
floridean starch: red algal storage product composed of α-1,4 and α-1,6 linked glucose residues.
floridoside: primary product of photosynthesis in the Rhodophyta.
foliose: leaf-like.
foramen: chamber or hole.
fragmentation: type of asexual reproduction where a thallus breaks into two or more parts, each of which forms a new thallus.
frustule: silicified cell wall in the diatoms.
fucoidin: polysaccharide in the cell wall and mucilage of the brown algae composed of sulfated fucose units.
fucosan or **phaeophycean tannin**: a colorless acidic fluid in brown algae, giving a characteristic red color with vanillin hydrochloride.
fucoserraten: a sex attractant secreted by the eggs of *Fucus* brown algae.
funori: a commercially produced phycocolloid of red algae used as a glue.
fusiform: spindle-shaped.
gametangium: structure forming gametes.
gamete: cell capable of fusion with another to form a zygote.
gametogenesis: the formation of gametes.
gametophyte: plant generation that forms the gametes, usually haploid.
gamone: a chemical involved in the attraction of one gamete to another.
gas vacuole: a collection of gas vesicles.
gas vesicle: hollow cylindrical gas-filled structures in the Cyanophyta.
generative auxiliary cell: cell in the Rhodophyta forming the gonimoblast filaments.
geotaxis: movement of a cell away (negative geotaxis) or toward (positive geotaxis) gravity.
girdle: the transverse groove containing the transverse flagellum in the Dinophyta.
girdle band: part of a diatom wall where the theca overlap; a band of thylakoids running parallel under the chloroplast envelope.
gliding: active movement of an organism in contact with a solid substrate where there is neither a visible organ responsible for the movement nor a distinct change in the shape of the organism.
globule: male reproductive structure in the Charales.
glycocalyx: sticky polysaccharide secreted by the zygote in the Fucales (Phaeophyceae).
glycogen: a storage polysaccharide related to amylopectin and stains red-purple with iodine.
glycopeptide or **glycoprotein**: polysaccharide composed of sugars and amino acids or peptides.
glycoside: a polysaccharide composed of glucose.
gonidium: a cell that divides to form a daughter colony.
gonimoblast: usually diploid cells that form the carposporangia in the Rhodophyta.
gonoid: type of ornamentation that is dominated by angles in the diatoms.

granum: stack of thylakoids in a chloroplast.
gullet: anterior of invagination in euglenoids and cryptomonads.
gyrogonite: fossilized nucule of the Charales.
hair: appendage on a flagellum; colorless elongate cell.
haplobiontic: having only one multicellular stage.
haploid: having one complete set of chromosomes.
haplont: an organism in which the only diploid stage is the zygote.
hapteron or **holdfast**: bottom part of an alga that attaches the plant to the substrate.
haptonema: appendage that arises between the flagella in the Prymnesiophyta.
heleoplankton: plankton that grow in marshy areas or in small ponds.
hematochrome: red or orange lipid bodies occurring outside the chloroplast.
hermaphroditic or **homothallic**: producing both male and female gametangia on the same thallus.
heterocyst: thick-walled, hollow-looking enlarged cell in the cyanobacteria.
heterokont: having flagella of unequal length.
heteromorphic alternation of generations: having haploid and diploid generations of different morphology.
heterothallic: producing male and female gametangia on different plants.
heterotrichous: term used to describe division of a plant into an erect and a prostrate part.
heterotrophic: needing an external source of organic compounds as an energy source.
histone: basic protein.
holdfast: part of an alga that attaches a plant to a substrate.
holophytic or **autotrophic**: needing only light and inorganic substances for growth.
holozoic or **phagocytic**: absorbing food particles whole into food vesicles for digestion.
homothallic: producing male and female plants on the same plant.
hormogonium: short pieces of a trichome in the cyanobacteria that become detached from the parent filament and move away by gliding, subsequently developing into new filaments.
hyaline: transparent.
hydrophilic: water-attracting.
hydrophobic: water-repelling.
hypersaline: greater than normal salinity.
hypha: long slender cell in the medulla of Laminariales (brown algae).
hypnospore: aplanospore with a greatly thickened cell wall.
hypocone: lower part of the cell in the Dinophyta, usually having a longitudinal sulcus.
hypogenous cells: in the Rhodophyta, those cells under the carpogonium.
hypolimnion: water beneath the thermocline in thermally stratified water bodies.
hypothallus: lower part of the thallus composed of large cells in the coralline reds.
hypotheca: smaller half of a diatom frustule.
hystrichospore or **hystrichosphaerid**: fossilized resting spore in the Dinophyta.
ichthytoxin: toxin that kills gill-bearing animals.
intercalary: in between two cells or tissues.
intercalary bands: bands between the valve and girdle band in the diatoms.
internode: part of axis between nodes.
interstitial water: that water trapped between particles of soil or mud.
intertidal: occurring between the low- and high-tide marks.
intraflagellar transport: the bidirectional movement of particles along the length of the flagellum between the axoneme and the flagellar membrane.
inversion: phenomenon in the green algae in which a colony turns itself inside out through a pore.
iridescence: the play of colors caused by refraction and interference of light waves at the surface.
isoagglutination: adhesion of flagella of the same sex when a mating-type substance of the opposite sex is added.
isoenzyme: enzymes having the same function but of a somewhat different structure.
isogamy: fusion of similar gametes.
isokont: cell with flagella of the same length.
isomorphic alternation of generations: generations that are morphologically alike.
isthmus: a passage connecting two bodies.
kairomone: a chemical that affects predator–prey interactions, inducing changes in prey behavior, morphology, or life history via compounds secreted by the predator.
karyogamy: fusion of two gamete nuclei.
karyokinesis: division of the nucleus.
keel: in pennate diatoms, an extension of the valve running lengthwise, similar to the keel of a ship.
kelp: a member of the Laminariales (brown algae); also used for the burnt ash of plants of the Laminariales.
kerogen: yellow-brown amorphous organic matter in sedimentary deposits.

kinesin: a mechanochemical protein capable of utilizing chemical energy from ATP hydrolysis to generate mechanical force.

kinetic movement: change in rate of movement. Ortho kinetic response is a decrease in swimming speed. Klino kinetic response is an increase in swimming speed.

kinetid (flagellar apparatus): an organellar complex consisting of one or more basal bodies/kinetosomes that may bear flagella/cilia, may have microtubular and fibrous roots associated with their bases, and may function in locomotion, feeding, sensation, and reproduction.

klino kinetic response: increase in swimming speed.

kleptoplasty: the capture of a chloroplast by a phagocytic organism.

kombu (**Japanese**): vegetable made from Laminariales (Phaeophyta).

labiate process: in diatoms, an appendage at the periphery of the valve through which mucilage may be secreted, functions in the movements of centric diatoms.

laminarin: food storage polysaccharide in the brown algae composed principally of β-1,3 linked glucose residues.

laminate: flat.

laver or **laver bread**: similar to Japanese *nori*, vegetable made from dried *Porphyra* (Rhodophyta).

leiotropic: counterclockwise when seen from the cell apex (opposite is dexiotropic).

lentic: related to a pond or lake.

lessepsian migration: migration of species through the Suez Canal. Derived from Ferdinand de Lesseps who designed the canal.

leucosin or **chrysolaminarin**: food storage polysaccharide of golden-brown algae composed mostly of β-1,3 linked glucose residues.

leucoplast: colorless plastid usually having a large number of starch grains and few thylakoids.

list: extension of the theca in the Dinophyta.

lithophyte: plant growing on rock.

lithotrophic or **autotrophic**: needing only light and/or inorganic compounds for growth.

littoral zone: zone from the water's edge to a water depth of about 6 m or the maximum depth of rooted vegetation, if any exists.

loculus: hexagonal chamber in the wall of diatoms.

log phase of growth: growth phase characterized by rapidly dividing cells.

lorica: an envelope around the protoplast, not attached to the protoplast as the wall is.

lotic: related to rivers or streams.

luciferase: enzyme that oxidizes luciferin.

luciferin: compound responsible for bioluminescence.

lysosome: single-membrane-bounded cytoplasmic particle containing destructive enzymes.

macrandous: species in the Oedogoniales (green algae) that do not produce dwarf male filaments.

macroplankton: plankton larger than 75 μm.

mäerl: coralline red algae applied to soil to increase the pH of the soil.

mannan: polysaccharide composed of mannose residues.

mannitol: sugar alcohol, $C_6H_{14}O_6$; primary product of photosynthesis in the brown algae.

mantle or **valve jacket**: part of a valve in the diatoms that is bent inward.

maerl: environment made up of coralline algae. Also refers to fertilizer manufactured by grinding up coralline algae.

marine snow: macroscopic organic aggregates (greater than 3 mm) in marine ecosystems produced by biological and chemical processes.

marl: deposits of calcium and magnesium carbonate.

mastigoneme or **hair**: filamentous appendage of a flagellum.

mating-type reaction: flagella adhesion between gametes of different sexes.

mating structure: a dense plate in the anterior part of the protoplasm of a gamete that determines its sex.

medulla: inner part of algal thallus, usually composed of packed colorless filaments.

meiocyte: a cell which undergoes meiosis.

meiosis: cell division in which the chromosome number is halved.

meiosporangium: structure in which spores are produced by meiosis.

meiospore: spore formed by meiosis.

meristem: dividing tissue that forms new cells.

meristoderm: dividing layer of cells in the brown algae.

mesochite: middle wall of an oogonium of the Fucales (brown algae).

metachromatic granule: protoplasmic body containing stored polyphosphate in the cyanobacteria.

microaerophilic: with small amounts of oxygen.

microfibril: crystalline anhydrous cellulose found in many algal cell walls.

microfilament: submicroscopic solid filament in protoplasm.

micrometer (μm): 10^{-6} m, 1 μm equals 1 micron.

microtubule: submicroscopic tubule in the protoplasm.
mitosis: nuclear division resulting in two daughter nuclei which are genetically identical to their parent.
mitosporangium: a sporangium in which spores are produced by mitosis.
mitospore: a spore produced as a direct result of mitosis.
mixotroph or **facultative heterotroph**: photosynthetic organism capable of using organic compounds in the medium.
monoecious or **homothallic**: having male and female gametangia borne on the same plant.
monopodial: having one main axis of growth.
monosporangium: a sporangium that forms a monospore in the Rhodophyta.
monospore: asexual spore that germinates to re-form the parent in the Rhodophyta.
monostromatic: a thallus only one cell thick.
muciferous body: a body, usually in the outer protoplasm of a cell, that discharges mucilage, usually explosively.
mucilage canal: canal present in some brown algae, composed of elongated cells in the cortex area that secrete mucilage.
mucopeptide: polysaccharide of the walls of the cyanobacteria, composed of sugars and amino acids.
multiaxial: having an axis with a number of apical cells that give rise to a number of nearly parallel filaments.
multicellular: composed of many cells.
multiseriate: with more than one row of cells.
mutualism: a situation where two organisms benefit equally.
myxophycean starch: storage polysaccharide of the cyanobacteria, similar to glycogen.
nannandrous: in the Oedogoniales (green algae), producing dwarf males.
nannoplankton or **nanoplankton**: plankton smaller than 75 μm but larger than 2 μm.
nanometer (nm): 10^{-9} meter, 1 nm equals 10 angstrom units.
necridium or **separation disc**: a cell that dies in a trichome of the cyanobacteria resulting in the formation of a hormogonium from part of the trichome.
nemathecium: wart-like surface elevation containing the reproductive structures in the Rhodophyta.
neritic region: ocean water over the bottom that extends from the high-tide mark to a depth of 200 m.
net plankton or **macroplankton**: plankton larger than 75 μm.
niche: the function of an organism within a community.
nitrogen fixation: the intracellular fixation of nitrogen gas from the atmosphere to ammonia in cyanobacteria.
node: part of the thallus that bears branches.
nori or **laver**: vegetable made from dried *Porphyra* (Rhodophyceae) in Japan, similar to laver bread.
nucule: female reproductive structure in the Charales.
oceanic region: open seas beyond 200-m bottom depth.
oligotrophic: term describing a body of water low in nutrients.
ooblast or **connecting filament**: a filament produced by the zygote that fuses with an auxiliary cell in the Rhodophyta.
oogamy: fusion of a large non-motile egg with a small motile sperm.
oogonium: single-celled female gametangium.
oospore or **zygospore**: thick-walled zygote with food reserves.
opsin: protein (apoprotein) part of a photoreceptor such as rhodopsin. The opsin is bound by a lysine group to the chromophore (colored compound) which is commonly retinal.
organelle: a membrane-bounded part of a cell.
ortho kinetic response: decrease in swimming speed.
osmotrophic: term describing a heterotrophic organism that absorbs organic molecules in a soluble form.
ostiole: an opening to the outside in a conceptacle.
overturn: phenomenon in a body of water in which the surface water becomes colder than the bottom water, causing the surface water to sink and resulting in a mixing of the water column.
ovoid: spherical (0.2–2 mm in diameter), concentrically laminated, carbonate grains that form by carbonate accretion in aggitated, shallow tropical marine environments.
ovum or **egg**: non-motile large female gamete.
palintomy: repeated binary fission of a cell without an intermediate stage of nutrition and growth.
pallium: a pseudopod projection used for feeding in thecate heterotrophic dinoflagellates.
palmelloid: term describing a colony of an indefinite number of single, non-motile cells in a mucilaginous matrix.
pantonematic or **tinsel flagellum**: flagellum with hairs attached to the surface.
papilla: a small rounded protuberance.

paraflagellar or **paracrystalline body**: photoreceptor in the Eugleophyta consisting of a crystalline swelling in one of the flagella.
paramylon: storage polysaccharide composed of β-1,3 linked glucose molecules.
paraphysis: sterile structure found with sporangia or gametangia.
parasite: heterotrophic organism that derives nutrients from a living host.
parasporangium: sporangium producing more than one asexual spore in the Rhodophyta.
paraxonemal body: proteinaceous structure restricted to a certain area along the flagellum/cilium.
paraxonemal rod: long cylindrical structure (solid or hollow) that extends nearly the entire length of a flagellum/cilium, located between the axoneme and flagellar membrane, and usually connected to the axoneme and flagellar membrane by specific links.
parenchyma: a tissue formed of thin-walled living cells produced by division in three planes.
parietal: peripheral.
parthenogenetic: germination of an egg without fertilization to form a new plant.
pedicel: supporting structure of a reproductive tissue.
peduncle: tail-like process with a central core of microtubules.
pelagic: living in the open ocean or oceanic region; in some definitions, living at or near the surface of the open sea.
pellicle: proteinaceous outer covering in the Euglenophyta.
pennate: term describing type of ornamentation arranged on either side of a central line in the diatoms (bilateral symmetry).
peptidoglycan: polysaccharide composed of sugars and amino acids in the walls of the cyanobacteria.
pericentral cell: a small cell formed around a central axis.
periclinal: parallel to the circumference of the surface.
peridinin: a xanthophyll in dinoflagellate cells.
periphyton: organism attached to submerged vegetation.
periplast: outer cell covering in the Cryptophyta.
perithallus: outer part of the thallus in the coralline Rhodophyta.
perizonium: siliceous wall of auxospore in diatoms, consisting of multiple overlapping bands.
phaeophycean tannin or **fucosan**: colorless, acidic fluid in physodes in the brown algae.
phagotrophic or **holozoic**: ingesting solid food particles into a food vesicle for digestion.
pheromone: compound that functions as a sexual attractant or acts as a trigger for reproductive behavior.
phialopore: hole in an inverted daughter colony in the Volvocales (Chlorophyta).
photic or **euphotic zone**: depth of water above the compensation depth.
photoautotrophic: term describing an autotrophic plant that obtains energy from photosynthesis.
photoheterotroph: organism capable of using organic compounds as a source of carbon in the light but not in the dark.
photokinesis: change in the rate of movement (swimming speed or frequency of change of direction).
photoperiodic time measurement: ability of plants and animals to sense the season of the year by measuring the duration of the day or night in the natural environment and respond appropriately so as to adapt to seasonal changes in the environment.
photophobic reaction: cessation of movement, followed by a change in swimming direction in response to an increase or decrease in photon irradiance.
photoreceptor: the part of the cell that receives the stimulus in phototaxis, usually a dense area in a flagellar swelling.
photosynthate: organic product of photosynthesis.
phototaxis: movement that is affected by the direction and intensity of the light.
phragmoplast: wall formation by the coalescence of Golgi vesicles between spindle microtubules.
phycobiliprotein or **phycobilin**: water-soluble blue-green or pink pigment in the cyanobacteria, Rhodophyta, and Cryptophyta.
phycobilisome: an aggregation of phycobiliproteins on the surface of a thylakoid.
phycobiont: algal partner in a lichen.
phycocolloid: polysaccharide colloid formed by an alga.
phycocyanin: blue-green-colored phycobiliprotein.
phycoerythrin: pink-colored phycobiliprotein.
phycomata: walled cyst produced by unicellular green algae.
phycophaein: black oxidized phaeophycean tannins.
phycoplast: type of cell division in which the mitotic spindle disperses after nuclear division with the two daughter nuclei coming close together, another set of microtubules arising perpendicular to the former position of the microtubules of the mitotic spindle, and the new cell wall forming along these microtubules.
physode: vesicle containing phaeophycean tannins in the brown algae.

phytochrome: photoperiod-regulating chemical.
phytoplankton: plants that float aimlessly or swim too feebly to maintain a constant position against a water current.
picoplankton: plankton that will pass through a filter with pores 2 μm in diameter but not through a filter with pores of 0.2 μm in diameter.
pili: proteinaceous appendages on the surface of cyanobacterial cells.
pit connection: a continuous area between two red algal cells consisting of an aperture in a cross wall, a plug, and a plug cap.
placoderm desmids: desmids which have two semicells joined by a narrow isthmus (contrasted to a saccoderm desmid without semicells).
plakea: flat plate of cells in the Volvocales (Chlorophyta).
plankton: organisms that float aimlessly or swim too feebly to maintain a constant position against a water current.
planogamete: motile gamete.
planospore: motile spore.
planozygote: motile zygote.
plasma membrane (plasmalemma): the outermost living membrane of a cell.
plasmodesma (plural **plasmodesmata)**: the minute cytoplasmic threads that extend through openings in cell walls and connect the protoplasts of adjacent living cells.
plasmogamy: fusion of protoplasm without fusion of nuclei (karyogamy).
plastid: double-membrane-bounded organelle usually containing the photosynthetic apparatus or some part of it.
pleomorphic: having more than one shape.
plesiomorphic: primitive evolutionary feature.
plethysmothallus: a stage composed of filaments or compacted filaments that can multiply itself by spores.
plurilocular sporangium: many-chambered sporangium in the brown algae, each chamber forming one swarmer.
pneumatocyst or **air bladder**: expanded part of thallus containing gases.
polar nodule: wall swelling near the end of a cell in diatoms.
polyglucan granule: protoplasmic structure containing the storage product in the cyanobacteria.
polyhedral body: protoplasmic structure in the cyanobacteria associated with DNA microfibrils; it may contain the carbon dioxide-fixing enzyme ribulose-1,5-bisphosphate carboxylase.
polymorphic: having more than one shape.
polyol: sugar alcohol.
polyphosphate body: protoplasmic structure containing stored phosphate in the cyanobacteria.
polysiphonous: term describing thallus made up of vertical files of parallel cells.
polystichous: a type of parenchymatous growth in the brown algae.
pore: a single hole.
pore membrane: part of wall over a loculus in diatoms.
poriod: pore occluded by a plate in diatoms.
practical salinity unit (PSU): conductivity of water relative to a standard KCl solution; seawater is about 35 PSU.
primary producer: photosynthetic plant.
proboscis: microtubules in the anterior part of a sperm, probably associated with the chemotactic response.
procarp: association of carpogonium and auxiliary cells in the Rhodophyta.
process: extension of a wall.
productivity: change in biomass per unit time.
profundal zone: part of a lake beneath the compensation depth.
prokaryotic cell: a type of cell lacking membrane-bounded organelles.
prolamellar body: a body composed of membrane-bounded connected tubules in dark-grown chloroplasts.
promeristem: a non-dividing apical cell controlling the division of a number of smaller promeristematic cells beneath it.
propagulum: branchlets that fall off and form new plants in the Sphacelariales (brown algae).
properizonium: secondary auxospore wall built of siliceous rings produced inside the primary scaly wall of diatoms.
proplastid: a small plastid that usually matures to a chloroplast or amyloplast.
pseudocilia: non-functional flagella.
pseudoparenchyma: densely packed filaments resembling parenchyma tissue.
pseudoraphe: unornamented area on a theca of diatoms where a raphe would occur.
psychrophile: organism able to grow at temperatures less than 15 °C.
psychrotroph: organism able to tolerate severe winter conditions and then grow in the warmer summer months.
puncta: opening in the frustule in diatoms, either a pore or a loculus.

pusule: a structure in the Dinophyta that is associated with the expulsion of excess protoplasmic water.
pyrenoid: proteinaceous area of the chloroplast associated with the formation of storage product.
pyriform: shaped like a pear.
radial: occurring around a central point.
radially symmetrical: when an object is cut in half, the two halves are superimposable by folding over at the plane of section.
ramulus: reproductive branch.
raphe: longitudinal slit in the valve of some diatoms.
receptacle: swollen tip of thallus containing conceptacles in the Fucales (brown algae).
red tide: water with a large number of dinoflagellates or other organisms that color the water red.
reservoir: large empty space at the bottom of a canal in some flagellates.
resting cell: cell with the same morphology as vegetative cells in diatoms, but with a large amount of lipid and reduced size of organelles.
resting spore: thick-walled cell resistant to unfavorable environmental conditions.
reticulate: net-like.
retinal: chromophore group (colored compound) that is bound by a lysine residue to the opsin (protein) part of a photoreceptor such as rhodopsin.
rhabdosome: an inclusion in dinoflagellates of the order Dinophysales that resembles a trichocyst but does not function as a projectile.
rhizoid: root-like filament without vascular tissue.
rhizoplast: flagellar root composed of microfibrils that are often contractile.
rhizopodium: long delicate cytoplasmic protrusion.
rhizostyle: flagellar root composed of microtubules and associated structures.
rodolith (maerl): bed of coralline algae that lack uncalcified joints.
rhodopsin: photoreceptor in many algal cells. Rhodopsin consists of the chromophore (colored compound) retinal bound to a protein (apoprotein).
rib: extension of the cell wall.
saccoderm desmid: a desmid without semicells (contrasted to a placcoderm desmid with semicells).
saprophyte: heterotrophic organism living off dead material.
scale: an organic or inorganic cell-surface element of variable geometry, distributed individually or arranged in a pattern sometimes forming an envelope around the cell.
scintillon: particle associated with bioluminescence.
scytonemin: pigment that accumulates in the sheaths of cyanobacteria acting as a sunscreen to reduce the amount of near ultraviolet (370–384 μm) reaching the protoplasm.
separation disc or **necridium:** a cell that dies in a trichome of the cyanobacteria, resulting in the separation of a hormogonium from part of the thallus.
septum: cross wall.
seriochemical: a chemical that acts between individuals of the same species. Allelochemicals function between members of different species.
serrate: toothed as in a saw.
sessile: lacking a stalk.
seta or **awn:** elongated hollow wall extension.
sheath: extracellular mucilage.
siderophore: secondary hydroxamate secreted by some cyanobacteria to solubilize external iron compounds.
sieve cell: cell in the medulla of the Laminariales (brown algae), involved in active transport of organic molecules.
sieve membrane: wall structure covering a loculus in diatoms.
sieve plate: end wall in a sieve cell with pores through which the cytoplasm is continuous (plasmodesmata).
silica deposition vesicle: vesicle in which silica is deposited.
silicalemma: membrane of a silica deposition vesicle.
sinus: the incision in the midregion of a desmid cell (green algae).
siphonaceous or **siphonous** or **coenocytic cells:** large multinucleate cells without cross walls except when reproductive bodies are formed.
sirenine: a sex attractant in *Ectocarpus* (brown algae).
skeleton: a hardened non-living, protective, or supportive structure, enclosed by, or attached to, cytoplasmic structures.
slime layer: extracellular mucilage.
somatic: vegetative.
sorus: cluster of reproductive bodies.
sperm: male gamete.
spermatangium: male gametangium forming one spermatium in the Rhodophyta.
spermatogenesis: formation of sperm.
spermocarp: zygote plus an enclosing layer of cells in *Coleochaete* (Chlorophyta).
spicule: a rod-like, spindle-shaped, stellate, or variously curved and ornamental structure, usually siliceous or calcareous, with blunt or tapered tips deposited individually on the cell surface, or distributed throughout the peripheral cytoplasm.

spine: a non-living, rod-like or tapered elongate structure attached to a scale, wall, or skeletal framework.
spinulax: very small wall extension.
sporangium: spore-producing structure.
spore: cell that germinates without fusing to form a new individual.
spore mother cell: a cell that divides to produce spores.
sporeling: young plant arising from a spore.
sporocyte: a cell that divides and gives rise to spores.
sporogenesis: the process of spore production.
sporont: free-living phase of parasitic dinoflagellates (compared with the parasitic or trophont state).
sporophyte: diploid plant that forms spores.
stalk: an elongate structure specifically formed to attach an organism to a substrate.
standing crop: the amount of biomass present at a specific time.
starch: storage polysaccharide composed of α-1,4 and α-1,6 linked glucose residues.
statospore or **cyst**: resting spore.
stellate: star-shaped.
stenohaline: able to tolerate only small changes in salinity.
stenothermic: able to tolerate only a small variation in temperature.
stephanokont: cell with a ring of flagella at one pole.
stichidia: specialized reproductive branches in *Polysiphonia* (red alga).
stigma or **eyespot**: group of pigmented lipid bodies that are associated with phototaxis.
stipe: organ between a holdfast and a blade.
streptophyte: refers to the grouping of stoneworts (Charales) and land plants (embryophytes).
stria: row of punctae (pores or loculi) in diatoms.
stroma: non-membranous part of a plastid.
stromatolite: rock-like deposition of carbonates and trapped sediments formed by cyanobacteria and diatoms.
stud process: short stubby wall extension.
sublittoral zone: in a lake the zone from the end of rooted vegetation (about 6 m) to the compensation depth; in the sea the zone from the lowest low-tide mark to 200-m depth.
suffultory cell: cell to which the dwarf male filament attaches in *Oedogonium* (Chlorophyta).
sulcus: longitudinal groove in the hypocone of Dinophyta.
supporting cell: a cell that bears the carpogonial branch in some Rhodophyta.
supralittoral zone: zone above the high-tide mark in the ocean and above the standing-water mark in lakes, which receives splash during windy periods.
suture: area of fusion of two adjacent structures.
swarmer: motile cell.
symbiosis or **reciprocal parasitism**: two organisms living together to the mutual benefit of each.
sympodial axis: axis formed from successive dichotomous branches in which one branch is shorter than the other, giving the appearance of a simple stem.
syncyanosis: the symbiotic association between a cyanome and a cyanelle.
syngamy: fusion of gametes.
synomone: a chemical produced by a prey species that attracts predators of their predators at the next level in the food web.
systole: contraction of a contractile vacuole (opposite is diastole).
tactic movement: directed movement.
taxon (plural **taxa**): a taxonomic group.
terrestrial: growing on soil.
test: a hardened cell covering typically secreted by the organism, or built up of particles gathered from the environment, forming a protective barrier around the cell.
tetrasporangium: a sporangium producing four tetraspores, usually by meiosis.
tetraspore: spore formed in a tetrasporangium, usually by meiosis.
tetrasporophyte: usually diploid plant forming tetraspores in the Rhodophyceae.
thallophyte: plant lacking roots, stem, and leaves.
theca: outer covering of the Dinophyceae and some Chlorophyceae.
thecal plate: a plate in a vesicle under the plasmalemma in the Dinophyceae.
thermal stratification: phenomenon in a body of water in which the water is progressively colder with depth, resulting in no interchange of water between the bottom and top.
thermocline: layer in a thermally stratified lake where the temperature changes suddenly with depth.
thermophiles: organisms that grow at high temperatures.
thermotaxis: movement away from lower temperature (positive thermotaxis) or higher temperature (negative thermotaxis).
thylakoid: membrane-bound sac in a plastid.
tinsel flagellum: flagellum with hairs.
trabeculae: wall ingrowths in some coenocytic green algae.
transitional region: the most proximal (basal) part of a flagellum/cilium adjacent to the basal body/

kinetosome, comprising matrix, axoneme, and flagellar/ciliary membrane.
trellisoid: type of uniformly arranged ornamentation without reference to a point or line in diatoms.
trichoblast: branching multicellular filament on a red alga.
trichocyst: projectile in the Dinophyceae and Raphidophyceae.
trichogyne: long colorless part of a carpognium that receives the spermatium in the Rhodophyceae.
trichome: a row of cells without the sheath in the cyanobacteria.
trichothallic: term describing intercalary meristem producing a hair in one direction and the thallus in the other direction.
trophocyte: vegetative cell.
trophont: parasitic stage of dinoflagellates (compared with the sporont or free-living phase).
trumpet hyphae: drawn-out sieve cells wider at the cross walls than in the middle of the cells (Laminariales).
uniaxial: having a main axis consisting of a single row of usually large cells.
unilocular sporangium: sporangium composed of a single cell producing zoospores usually by meiosis.
uniseriate: having a single row of cells.
unisexual: having only one type of gametangium formed on one plant.
upwelling: an area of the ocean where nutrient-rich bottom water rises to the surface.
uronic acid: a type of monosaccharide.
utricle: inflated branchlet.
valve: part of the cell wall in diatoms, a valve plus a connecting band making up a theca.
valve jacket or **mantle:** part of the valve in diatoms that is bent inward.
velum: wall extension over a loculus in diatoms.
volutin granule: protoplasmic body containing stored polyphosphate.
water column: a vertical section of a body of water.
whiplash flagellum: flagellum without hairs on its surface.
xanthophyll: a carotenoid composed of an oxygenated hydrocarbon.
xylan: polysaccharide composed of xylose sugar residues.
zoochlorellae: Chlorophyta living inside invertebrate animals.
zooplankton: animal plankton.
zoosporangium: sporangium that forms zoospores.
zoospore: flagellated planospore.
zoosporogenesis: formation of zoospores.
zooxanthellae: non-green algal cells, usually Dinophyta, living inside invertebrates.
zygospore: thick-walled resting spore.
zygote: product of the fusion of two gametes.

Index

The most important page references are in **bold**, and page references that contain figures are in *italics*.

abalone, 126
Acanthopeltis, 99
Acarychloris marina, 43, 90
accumulation body, 277, *297*
Acetabularia, 22, **175–8**; *acetabulum*, *177*; *calyculus*, 176; *crenulata*, *176*; *kilneri*, *176*; *mediterranea*, 176
acetate, 256
Achnanthes exigua, *393*, 395; *longipes*, 378, *379*; *lanceolata*, *395*
acidic water, 155–7, 197, 258
acritrachs, 277
Acrocarpia paniculata, 471
Acrochaetiales, 107, 108, **115–16**
Acrochaetium, 96, 115; *asparagopsis*, 106; *corymbiterum*, *102*
acronematic flagellum, 7
Acroseira, 448
acrylic acid (propenic acid), 498, 511–12
actin, 24, 156, 165, 195; chloroplast movement, 422; gliding, 380; *Fucus* zygote orientation, 470–11
Actiniscus pentasterias, 278, *279*
Actinocyclus subtilis, 380–*1*
adelphoparasite, **97**
aerolae, *371–3*
Aethiops vegetabilis, 460
agar, *10*, 90, **99–100**, 124–6
agaropectin, 10, 99
agarophytes, 99, 100, 124–6
agarose, *10*, 99
agglutination, 143, 193–4
agglutins, *Chlamydomonas*, 193–**4**
Aglaothamnion neglectum, 106
Aglaozonia, *438*, **439–42**
agricultural guild of diatoms, 394–**5**
Ahnfeltia, 99
air bladder, 464, *473–5*
akinete, cyanobacteria, 37, *41–2*, **45–9**, 72; Chlorophyta, 188, 208; Xanthophyceae, 416
Alaria, 451, 455, 464, 466; *esculenta*, *464*
Alariaceae, 453, **462**, **464**
Alexandrium, 282, *284*, 509, 513; *acatenella*, 281; *catenella*, *278*; *excavatum*, 281, *283*; *minutum*, *283*, 505; *ostenfeldii*, 509; *tamarensis*, 281
algal volatile compounds, *340*
algicide, 66, 387
alginic acid, *10*, 427–8, 458, **459**, 466, 470
algology, 3
alkadienes, *211*
alkaloids, 65
alkenes, *396*
allantoin, *115*
allelochemical, 66, 513
allelopathic interactions, **66**
alloparasite, 97
allophycocyanin, 17–18, 43, 90, 323
alveolus, *310*, **312**
ammonia, 26, 42–3, 47, 54, 72
amnesic shellfish poisoning, 387–8, **509**
AMP, cyclic, 37–8, 194, 504
Amphidinium, 513; *carteri*, 263, *270*, *cryophilum*, *295*; *klebsii*, 296–*7*
amphiesma, ***263***–5
Amphiprora, 514
Amphiroa rigida, *122*
Amphiscolops langerhansii, 296, *297*
Amphora, 379, 388, 403; *coffaeformis*, *382–3*; *perpusilla*, *395*
amylopectin, 20, 92; Chlorophyta, 140; Cryptophyta, 323; cyanobacteria, 41
amyloplast, 11, 140, 178–9, 184–6, 214
amylose, 140, 323
amylum stars, *Chara*, 165
Anabaena, 34–5, *37*, 47, *58*, 61, 65, 509; *azollae*, 57; *circinalis*, *72*; *crassa*, *41*; *cylindrica*, 62; *flos-aquae*, *42*, 45
Anacystis nidulans, *40*
anaerobe, 44
anatoxin, 65, 504, *506*, 509
ancestral green flagellate, 154
androsporangia, **224–6**
androspore, 225
anemones, symbiotic Dinophyta, 295–**6**
anhydrobiotic, **62**
anisogamy, 143
anisokont flagella, 9
Anomoeoneis, 398
Antarctic, **513–4**, Cryptophyta, 325; cyanobacteria, 61; Phaeophyta, 441, 464; Rhodophyceae, 89
Antarctic circumpolar current, 513–*14*
Antarctic coastal current, 513–*4*
Antarctic lakes, **515–6**
antheridium, Chlorophyta, 162, *163–6*; Rhodophyceae, 117–*18*, 125, *127*, 155
Anthophysa, 342; *vegetans*, 337, *341*
anthropogenic effects, 173, 189
antibiotics, 68
anticlinal division, 432, 446, 466
anti-herbivore chemicals, 66
Antithamnion, 95; *nipponicum*, *106*; *plumula*, *96*; vesicular cell, *97*
Apedinella, 359–60; *spinifera*, *360*
Aphanizomenon, 45, 61, 65, 509; *flos-aquae*, *42*, 67
Aphanocapsa thermalis, 62
Aphanothece sacrum, 67
Apicomplexa, 239, **310–23**
apicoplast, *310–2*
Apistonema,499
aplanogamete, 156
aplanospore, 143; Chlorophyta, *169*, *190*, 208, 210–1, 223; Phaeophyta, 434; Xanthophyceae, 415–16, 418
apoprotein, 141
apotosis, cyanobacteria, 48; Phaeophyceae, 128
aquaculture, 504
aragonite, **93–4**, 117; Chlorophyta, 184; Phaeophyta, 428; Prymnesiophyceae, 492
aragonite sea, 94–5
arctic, cyanobacteria, 61, Rhodophyceae, 89
Arthrobacteria, 99
Ascophyllum, 96–7, 472; *nodosum*, *97*, *473–4*; sperm, *8*
Astasia, 250; *klebsii*, *257*
astaxanthin, 139–*40*, 197
Asterionella, 379; *formosa*, 393–4, 398
Asterocytis, 101, *110*
atmosphere, ancient, 26, 44
ATP, 4; in nitrogen fixation, 49–51

ATPase in calcification, 494
Attheya, 350
Audouinella, 115
Aulosira fertilissima, *63–4*; *implexa*, *72*
Aureococcus anophagegefferens, 365–*6*
Aureodinium pigmentosum, 276
Aureoumbra lagunensis, 365–*6*, 505
autolysin, 194
autospore, 143, 217
autotrophy, 23
auxiliary cells, Rhodophyceae, **101–2**, 117, 120, 125, 127–*8*, 130
auxospore, 382, **383–6**, 388–*9*, 399, *400–1*, *403*
auxotroph, 23, 55
axoneme, **4**, **5**
Azolla, 56–*58*
Azotobacter, 181

babesiosis, 311
Bacillariales, **399**, **401–4**
Bacillariophyceae (diatoms), **369–407**, carotenoids, 17; chlorophyll, 16; chloroplast DNA, 14; chrysolaminarin, 21; evolution of, 368; glycolate dehydrogenase, 20; motile cell, *9*; sea ice, 514; scales, 336; silicification, 368; toxins, **509**
bacteria, 45; cell wall, 34; Rubisco, 12
bacteriocins, 68
baeocyte, 53–**5**
Bahamas, 69–70
Bangia, **113–4**; *atropurpurea*, *113*; cell wall, 90; fossil, 108; *fuscopurpurea*, 114; mucilage, 10
Bangiales, 90, 92, 107, 108, **110–15**
Bangiomorpha pubescens, 114
Bangiophycidae, 107
barium carbonate crystals, 160
barium sulphide statolith, 165
basal body of flagellum, 5
basidiomycete, 57
Batrachospermales, 107, **116–18**
Batrachospermum, 106, **117–18**
betaine and halotolerance, *64–5*
bicarbonate, 39, *40*; in calcium deposition, 94–5; in water, **239–42**
bicosoecids, 8
Biddulphiales, **398**–401
Bigelowiella natans, *318*
biocides, 99, 496
biofilms, 377
biological clock, **289–91**
biological oxygen demand, 216
bioluminescence, 96, **285–89**, 293
biosilicification, 376
bisporangia, **106**
bivalve, 285
block, polyspermy, 470, 474
blooms, **504–10**; control of, 387; cyanobacterial, 61; diatoms, 340; Dinophyta, **282**, 284–5; Pelagophyceae, 365; Prymnesiophyceae, 498
blue-green algae (cyanobacteria), **33–80**; chlorophylls, 16; endosymbiosis, **81–7**; fossils, 26; glycolate dehydrogenase, 20; phycobilisomes, 11–12, **16–19**; symbioses, 393; thyllakoids, *11–2*; toxins, 504, 509
Bodanella, 426
bodonids, 248, 252
Bolidomonas, *368*
Bolidophyceae, **368**; 398
Bonnemaisonia, 95–*6*
Botrydiales, 416, **418**
Botrydium, 418; granulatum, 416–18
botryococcene, *211*
Botryococcus brauni, *210–11*
Braarudosphaera bigelowii, *495*
Brachytrichia, 67
brevetoxin, 409–**10**, 504, *508–9*
brine algae, 514
bromine, 95
brown algae (Phaeophyceae), **426–83**; carotenoids, 17; chloroplasts, 11; evolution of, 346, 413; glycolate oxidase, 20; mucilages, *10*; storage product, 21–2
brown tides, 365
Bryopsis, 265–6; *plumosa*, 179, *182*
Bulbochaete gigantea, 222
Bumilleria, 14
buoyancy, cyanobacteria, **41–3**, 45; Bacillariophyceae, **391**, 393
butyric acid, 256

Cachonia niei, *264*
calcareous ooze, 496
Calcidinellum operosum, *278*
calcification, Chlorophyta, 164–7, 174, 198–9, 336; Chrysophyceae, 337; corals, 296; Dinophyta, **278**; Phaeophyceae, 427–8, 434; reaction, 494; Rhodophyceae, 93–5, **117–18**, **121**
calcite, **93–4**; Chlorophyta, 198–*9*; Prymnesiophyceae, 491–3, 496
calcite sea, 94–*5*; Chlorophyta, 164, 184–5
calcium, channels, 281, 504; euglenoid movement, 247; flagella beating, 142, 265, 267; in water, 160, 333; influx and blocks, 470; phototaxis, 13; Prymnesiophyceae, 484–5
calcium carbonate, 492–*4*; Chlorophyta, 164–5, 184; Dinophyta, 278; fossil cyanobacteria, **69**; Phaeophyta, 428; Rhodophyceae, **93–4**, 117
callose, 441, *451*
calmodulin, 504
Calothrix, 42, 59; *fusca*, *72*; *scopulorum*, *59*
Campylodiscus clypeus, *398*
canal, Euglenophyta, *246–7*; *256–8*; Dinophyta, *270*, *274*
capitulum, *164*, *166*
capsule, **37**–*8*
carbon, forms in water, **239–42**
carbon dioxide, and calcification, 494; in water, 43; in the atmosphere, 511, 514–15
carbon fixation, 12, 39, *40*
carbonic acid, 124
carbonic anhydrase, 39–40, 66, 240
carboxysome, **39**–*40*
carotene, 139–*40*; Bolidophyceae, 368; Cryptophyta, 322; Euglenophyta, 250; Eustigmatophyceae, 355; Pinguiophyceae, 358; Prymnesiophyceae, 484; Raphidophyceae, 410
carotenoids, **17**; Chlorophyta, 139, 197; cyanobacteria, 43; Dinophyta, 263, 269–71; Euglenophyta, 250; Raphidophyceae, 410
carpogonium, **101–3**, *111*, 115–*16*, *118–19*, *121*, 124–8, 130
carposporangium, **101–3**, *122*, 125–*7*, 130
carpospore, 91, **101–3**, 109, *112*, 117, *118–20*
carposporophyte, *98*, *116–17*, 124, *126–8*
carrageenan, 10, 90, **99–101**
catalase, *149*
Campylodiscus clypeus, *398*

Caulerpa, 140, 185; *floridana*, *182*; *microphysa*; *182*, *prolifera*, *182*; *taxifolia*, *186–7*
Caulerpaceae, 179, **185–7**
Caulerpales, 139, 168, **178–88**
caulerpenyene, 187
cell wall, **9–10**
cellulose, 9, 89; Chlorophyta, 139, 147, 153, 178; Dinophyta, 263; Phaeophyta, 427, 434, 458–9, 470; Prymnesiophyceae, 491; Rhodophyceae, 114; Xanthophyceae, 413
cellulose synthetase, *147*
Centrales, 399
centrin, 486
Ceramiales, 97, 107, **127–30**
Ceratium, 263, 298; *cornutum*, *300*; *fusus*, 287; *hirundinella*, 278; *horridum*, *301*
Chaetoceros, 383, 391, 504; *diadema*, 401–*2*; *laciniosus*, *403*; *peruvianus*, *392*
Chaetomorpha, 473; *aerea*, *173–4*; *microcladioides*, *173*
Chaetophora incrassata, *221*
Chaetophorales, 191, **221–2**
chalk, 496
Chamaesiphon, *63*; *incrustans*, 54
Chara, **163–7**, *corallina*, 164; *fibrosa*, *167*; *muelleri*, *167*; *vulgaris*, *167*
Charales, 148, 155, **163–8**
Charophyceae, **144**–50, 152, **154–68**
Chattonella, 409; *antigua*, *410–11*, *505*
chemical defense, 430–1
chemoheterotroph, 23, **55**
chemotaxis, Chlorophyta, 143, 225–6; cyanobacteria, 64; Cryptophyta, 325; Dinophyta, 295; Euglenophyta 257; Phaeophyta, 453, 462
chemotroph, 23
Chilomonas, 322, 324, 327; *paramecium*, 328
China, cyanobacteria as food, 67; fossils, *70*; *Porphyra*,114
chitin, Chrysophyceae, 336; Prymnesiophyceae, 488
Chlamydomonadaceae, **191–8**
Chlamydomonas, 172, 190, **191–8**; *allenworthii*, 196; *eugametos*, 193; flagella, 139; gamete, *8*; *moewusii*, *145*, *191–3*, 196; phototaxis, **13**, 141–3; *reinhardtii*, 141, 143, *195–6*; *rivalis*, 196
chlamydopsin, 141
chlamyrhodopsin, *13*
Chlorarachnion reprans, 317–*19*
Chlorarachniophyta, **317–19**
Chlorella, 141, 143, 213; *vulgaris*, *216*
Chlorellales, 191, 211, *212–18*
Chlorobotrys regularis, *354*
Chlorococcum, **212–4**; *echinozygotum*, 212; *humicola*, *214*
Chlorogloea fritschii, *56*
chloromonads, **409–12**
Chlorophyceae, **144**, *146–9*, 152, **189**
chlorophyll, **14–6**
Chlorophyta, chlorophylls, 15–16; chloroplast DNA, 14; endosymbiosis leading to, 81–2; eyespot, 14; glycolate enzymes, 20; mitochondria, 19; motile cell, *9*; mucilages, **9–10**; plastids, *11–12*; Rubisco, 12; starch, 21–2; sugars, 22
chloroplast division ring, 86
chloroplast endoplasmic reticulum, *11*, **239–43**, **315–17**
chloroplast movement, 156, 164, 421–*2*
Chlorosarcina, *220*
Chlorosarcinales, 191, **220**
Chlorosarcinopsis gelatinosa, 142
Chodatella, 214
cholesterol, *381*
Chondria, 96; *caerulescens*, *96*
Chondrus crispus, 100
Chorda, 432, 44–9, 453, **462**; *filum*, *462*
Chordaceae, 460, **462**
Choreocolax, 46; *polysiphonae*, 87–*8*
Choristocarpus tenellus, *433*
chromatic adaptation, **18**; Bacillariophyceae, 393; Cryptophyta, 323; cyanobacteria, 43; Dinophyta, 272
chromophore, **17–19**, 141
chromoplast, 10
Chromulina, 342; *conica*, *341*; *placentula*, 336; *psammobia*, 339
Chromulinales, **341–4**
Chroococcales, **71**
Chroomonadales, 327, **330**
Chroomonas, 330; *mesostigmatica*, *323–4*; *nordstedtii*, *328*; *oblonga*, *329*
Chroothece,110
Chrysoamoeba, *radians*, *360*
Chrysochromulina, *485*, 487, 497, 504; *ephippum*, *487*; *ericina*, 490–*1*; *kappa*, 490–*1*, *minor*, 342; 490–*1*; *parkae*, *491*; *polylepis*, *488*, *491*; *pringsheimii*, 490–*1*
Chrysocossus, 342; *rufescens*, *337*
chrysolaminarin (leucosin), **21**; Bacillariophyceae, 369, 381; Chrysophyceae, 33–4; *337–8*, *341–4*; Dictyochophyceae, *361*; Euglenophyta, 245, 255; Heterokontophyta, 317, 333; Synurophyceae, *349*, *352–3*; Prymnesiophyceae, 317, 484–*8*, *491*, *497*
Chrysomeridales, **341**, **344–5**
Chrysophaera, 343; *magna*, *344*
Chrysophyceae, **333–48**, 359, 365, 409, 484; carotenoids, 17; chloroplast DNA, 14; chlorophylls, 11,16; chrysolaminarin, 21; in ice, 514; osmoregulation, 22–3
ciguatera fish poisoning, **281**, 504
ciguatoxin, 281, 504, *508*
cilia, 4
ciliates, 294, 324, 326, 513
Ciliophrys, 359
cingulum, *262*
circadian rhythms, cyanobacteria, *51–2*; Dinophyta, **286–91**; Euglenophyta, 247, 252–3; Phaeophyta, 453; Rhodophyceae, **106**
circannual rhythm, 455
circein, 225
cirri, 218, *220*
Cladonia cristatella, 217–*18*
Cladophora, 173–4; *glomerata*, 169
Cladophorales, 168, **173–4**
Climaconeis colemaniae, *371*
Closterium moniliforma, *160*
cloud condensation nuclei, **511–12**
Cnidaria, 295
cnidocysts, *274*
coals, 210, **284–5**
coccoliths, 484, **490–6**, *499*
coccolithophorids, 284, 493–4, *495*, 511
Coccolithus, 493, *498*; *pelagicus*, *495*; *huxleyi*, 496
Cocconeis placentula, *395*

Codiaceae, **179–85**
Codiales, 179
Codium, **180–4**; *fragile*, 180–*1*
coenobia, 143, 191, 198
coenocytic algae, Chlorophyta, 175, 178, 184, 186–7, 190; Xanthophyceae, 416, 418, *419*, 422
Colacium, 247, *252*, 255; *libellae*, *258*–9; *vesiculosum*, *258*
Coleochaetales, 139, 148, 155, **162–3**, 221
Coleochaete, 143, *147*, **162**–*3*
Compsopogon, 93
conceptacle, Rhodophyceae, *98*, 117, *120–2*; Phaeophyta, 442, *448*, 464–8, 472, 475
Conchocelis, *107*, 113–15
conchosporangia, *111–13*
conchospore, *112*
Condylostoma magnum, 294
conjugation, Chlorophyta, 155–8, 160–*1*; Bacillariophyceae, 399
conjunctor cell, 98
conoid, 310
constitutive defense, **511**
contractile vacuole, **22–3**; Chlorophyta, 141; Chrysophyceae, 333–7, *341*; Dictychophyceae, *360–3*; Dinophyta, 335; Euglenophyta, *246*, 248, *256–7*; Phaeothamniophyceae, 424; Prymnesiophyceae, *488*, *500*; Raphidophyceae, *410*; Synurophyceae, *349*; Xanthophyceae, *413*, *416*
control of algae, 99, 387, 496
Convoluta, 152; *roscoffensis*, *153*
cooling of the Earth, **511**
copepod grazing, 282, 287, 390, 511
copper, inhibition of algal growth, 387
corals, Dinophyta, 295–6; endosymbiotic cyanobacteria, 58, 60; reefs, 124
Corallina, *122*
Corallinales, 93, 107, **118**, **120–4**
coralline algae, Rhodophyta, 93–95, 108, 117, **130–4**
Corethron, 350; *hystria*, *293*
corona, *Acetabularia*, 175–*8*
coronal cells, *Chara*, 166–7
Corps de Maupas, 277, *322*, **324**
Corynebacterium, 99
Coscinodiscus, 370, 383, 391; *linatus*, 372; *radiatus*, *397*; *wailesii*, *378*
Cosmarium botrytis, **160**–*1*
costa, 372
Coxiella, 513
cribum, 372
Cricosphaera, 496, 499
cryophilic algae, 514
cryptobiotic crust, 63
cryptoblast, 464, **467**
Cryptochlora perforens, *318*
Cryptomonadales, 326–**7**
Cryptomonas, 321, 325, 327, *329*; *erosa*, *328*; *rostella*, 323
Cryptophyta, **321–31**, 484; chlorophylls, 15; chloroplasts, 11–12; chloroplast DNA, 14; chloroplast endoplasmic reticulum, 317; Corps de Maupas, 277; contractile vacuole, **22–3**; eyespot, 14; mitochondria, 19; motile cell, *9*; phycobilisomes, 12, 16, **17–19**; starch, 21; symbioses, 268
cryptosporidosis, 311
cryptostomata, 462
Cryptothecodinium cohni, *264*, 275
Crystallolithus, 493; *hyalinus*, *494*
cuticle, Chlorophyta, 222; Phaeophyta, 440, 446, *465*–6; Rhodophyceae, 90, 96
Cutleria, 431, 433, 436; *multifida*, 432, *438*
Cutleriales, **433**
cyanelle, 12, 58, **85–88**
Cyanidales, 107–**9**
Cyanidioschyzon merolae, *108*
Cyanidium, 89; *caldarium*, *108*
cyanobacteria (blue-green algae), **33–80**; chlorophylls, 16; endosymbiosis, **81–7**; fossils, 26; glycolate dehydrogenase, 20; phycobilisomes, 11–12, **16–19**; symbioses, 393; thylakoids, *11–12*; toxins, 504, 509
cyanobacterin, 68
cyanoglobin, 50
cyanome, 58, **85**–9
cyanophages, **67**
Cyanophora paradoxa, *12*, **86–88**, 149
cyanophycin, 38–*9*, 45–*6*, 52
cyanotoxins, **65–7**, **509**
cycads, 57–*8*
Cyclotella antique, 396, *398*; *cryptica*, 387; *striata*, *375*
Cylindrocystis, 160; *brebissonii*, *156*
Cylindrospermum, *46*, 53; *majus*, 42; *raciborskii*, 46
Cymatiosphaera, 150
Cymatopleura, 396; *elliptica*, *398*
Cymbella, 403
cyst, Chlorophyta, 150, *176*, *178*, 225; Chrysophyceae, **337**, 342; Dinophyta, 265–6, **277–8**; Euglenophyta, 247–**8**; Raphidophyceae, 410, 412; Xanthophyceae, 416–18
cystocarp, *120*, 125, *127–30*
Cystophora, 464
cytokinesis, 144
Cytophaga, 170
cytoplasmic streaming, 165, 180
cytosome, 248, *252*, *257*, 291

damselfish, 130
damselfly, 258
Daphnia, 216; *pule*, *258*
Dasycladaceae, **175–8**
Dasycladales, 139, 168, **174–8**
Dasycladus, 175; *vermicularis*, *177*
defense mechanisms, **98–9**, **458**, **511**, **513**
Delisea pulchra, 99
Derbesia, 143, **179–80**; *tenuissima*, 179, *181*
Derbesiaceae, 179–80
Dermocarpa pacifica, 54
Dermocarpella gardneri, *55*
desiccation resistance, 473
desmarestene, 432, 441, 453
Desmarestia, 431, 439, *440*–1; *aculeata*, 432, *441–2*; *anceps*, 442; *menziesii*, 442
Desmarestiales, **434**, **439**
Desmidaceae, 156
desmids, **160–2**
Desmonema wrangelii, *73*
desmoschisis, 220
Diacronema, 484
diadinoxanthin, 415, 484
diarrhetic shellfish poisoning, **279–81**, 504
Diatoma vulgare, *395*
diatomaceous earth, 396–7, 464; ooze, 377

diatoms (Bacillariophyceae), **369–407**, carotenoids, 17; chlorophyll, 16; chloroplast DNA, 14; chrysolaminarin, 21; evolution of, 368; glycolate dehydrogenase, 20; motile cell, *9*; nutrient depletion, 284; sea ice, 514; scales, 336; silicification, 368; toxins, **509**
diatoxanthin, 322, 368, 484
diazocyte, 52
diazotroph, 49, 393
Dichotomosiphon, 178, 187; *pusillus*, 188; *tuberosus*, *188*
Dichotomosiphonaceae, 179, **187–9**
Dicrateria, 484
Dictyocales, **359–64**
Dictyocha, 360; *fibula*, 360, *363*; *speculum*, 361
Dictyochophyceae, **359–64**
Dictyosiphonaceae, 444, 462
Dictyosiphonales, 444, 462
Dictyosphaeria cavernosa, 189
Dictyota,170, 431; *dichotoma*, 432, **434–5**
Dictyotales, 429, **433–5**
dictyotene, *432*, 434
diel migration, 268, 325, 391
diffuse growth, 431
dimethyl sulfide, 511–*12*
dimethylsulfoniopriopionate and osmoregulation, 511–13
Dinobyron, 336, 339–40, 342–**3**; *cylindricum*, **342–3**
Dinophysales, 262, 296, **298**–9
Dinophysis, 279, 509; *acuminata*, *280*; *forti*, 280, *505*
dinophysistoxin, 279–81, 504, *507*, 509
Dinophyta, **262–313**; chlorophylls, 15–6; chloroplast, *11*–2, 239; chloroplast DNA, 14; DMSP production, 511; eyespot, 14; growth inhibition, 66; motile cell, *9*; Rubisco, 12; sea ice, 514; starch, 21; toxins, 504, 509
dinosporin, 279
dinosterol, *285*
dioecious, 467
Dioon spinulosum, *58*
Diplopsalis, 292
discobolocyst, **335**–*6*, *338*
Discosphaea tubifera, *495*
Dissodinium, 287
dissolved inorganic carbon and evolution of chloroplast E.R., **239–42**
Distigma, 288
Ditylum brightwelli, *382*, 391–*2*
diurnal rhythm in calcification, 185, 491, 496
DMSP and osmoregulation, 511–13
DNA, chloroplast, **12**, *14*, 428; cyanobacteria, 38–*9*; nucleotide sequencing, 24
domoic acid, *388*, *506*, 509
Draparnaldia glomerata, *221*
Dreissema polymorpha, *66*
dulcitol, *92*
Dumontia, 473
Dunaliella, 22, 139, *acidophila*, 197; *bioculata*, 198; *salina*, 197, *199*, *294*
Durvillea, 464
dynamin, 20
dynein, **4–5**

Earth cooling, 511
east coast fever, 311
ecad, 474
ecdysis, Dinophyta, 265–*6*
echineone, 43, 85, 250
Ecklonia, 458
Ectocarpaceae, **441–4**
Ectocarpales, 429, **434**, **442–9**, 462
ectocarpene, *432*, 436, 441, 443–4, 453
Ectocarpus fasciculatus, *431*; *siliculosus*, *427*, 432, **442–4**
ectoplasm, *Chara*, 165
eelgrass, 365
eicosanoic acid, 390
eicosapentaenoic acid, *357*, 390
ejectisome, Apicomplexa, *312*; Cryptophyceae, *322*, *324–5*, 327–*8*
eleutheroschisis, 425
Ellerbeckia anenaria, 385
Ellipsagelospaera britannica, 496
Ellipsoidion acuminatum, 355
Elysia, 183; *viridis*, 184
embryophyte, 144
Emiliania huxleyi, 492–*3*; *495*–6, **498**, 511
Encephalartos, *58*
endolith, **60**
endophyte, 115, 162, 220
endoplasm, *Chara*, 165
endosome, 248
endospore, 71; bacterial, 45; cyanobacteria, 55, *71*–2; Dinophyta, *302*–3
endosymbioses, primary, **81–2**; secondary, **239–42**; tertiary, 269, 361
Enteromorpha, 169–70, *172*, 473
Entosiphon, 246
envelope, 253
Eoentophysalis belcherensis, *70*
Eohyella dichotoma, *60*
epicone, *262–3*, *270*, 297–*9*, *302*
epilimnion, 42
epiphyte, Bacillariophyceae, 391, 394–5; Chlorophyta, 162, 179, 222; Rhodophyta, **96–8**, 99, 110, 115, 121
Epipyxia pulchra, *339*
epitheca, 369, *379*, *373–6*, 394
erogen, 342
Erythropsis cornuta, 273–*4*
ethanol, 256
Euastrum affine, 160
Eucheuma, 100
Eudorina unicocca, *200*
Euglena ascus, *248*; *gracilis*, 246, *249*, *251*, 253, 255, *257*; *obtusa*, 252; *proxima*, 252; *spirogyra*, 255; *stellata*, *244*; *terricola*, *250*
Euglenales, 246, **258–9**
Euglenamorpha, 245
euglenoid movement, 247, *251*
Euglenophyta, 239, **245–61**; chlorophylls, 15; chloroplast, *11*–12; eyespot, 14; glycolate dehydrogenase, 20; Rubisco, 12; storage product, **21–2**, 487
Eunotia, *370*, 398; *soleirolii*, 383
Euphasia superba, 513
euphotic zone, 60
euryhaline, 64, 409
eurythermic, 409
Eustigmatophyceae, **354–6**, 359, 409; chloroplast, *11*–12; eyespot, 14; motile cell, *9*
Eutreptia, 245, 250, 254, 258
Eutreptiales, 246, **256**, **258**
Eutreptiella, 245, 258; *gymnastica*, *254*–5; *marina*, *257*
eutrophic conditions, 43, 395
evolution of algal groups, **25–6**
exospore, cyanobacteria, *63*
extinction, end-Permian, **510**
extracellular polymeric substance (EPS), 37–8
extrusome, *318*
Exuviaella, 279

eyespot (stigma), Chlorophyta, *140*–5, *152–3*, 168–*9*, 172, 198; Chrysophyta, 333–*7*, *341*, *344*; Cryptophyta, 323–*4*; Dictyochophyceae, *360*; Dinophyta, **272–4**; Euglenophyta, *245–6*, **250**, 252; Eustigmatophyceae, *354–5*; Phaeophyta, *427–***8**, 440, *469*; Prymnesiophyceae, 484, *500*; Xanthophyceae, *413*, 415–*16*

facultative, heterotroph, 23; phototroph, 44
farmerfish, 130
Favella ehrenbergii, 513
feedback control, cyanobacteria, 56, 85
ferredoxin, 51
Fibrocapsa japonica, 409
filopodia, 489
fish kills, 210, 283, **295**, 410, 496–7, 504
flagellar structure, **4–9**; roots, **5–7**
flatworm symbioses, 152, 183, 296
flavins as photoreceptors, 421, 428
Flavobacterium, 99, 170
flavodoxin and salt stress, 65
flexibacteria, 61
floridean starch, **20**–1, 89, *91*–2
Florideophycidae, 107
florideoside, *21*–2, 91–*2*, 98
food algae, 67, 114–15, **173**, **216**, **459**, **460**
food vesicle in endosymbiosis, *81*, 85
fossil algae, **26**; Bacillariophyceae, **395**–8; Chlorophyta, 150, 167, 174–*5*, 184, *186*, 198; cyanobacteria, 33, *60*, *69*; Dictyochophyceae, 360, 364; Dinophyta, **279**, *280*, 298; Phaeophyceae, 433, 439, 449, 464; Prymnesiophyceae, 364, 484, 496
fouling, 99, 378, antifoulants, 436
Fragilaria virescens, *392*
fragmentation, 143, 157
Franceia, 214
Fritsch, Felix, 27
Fritschiella tuberosa, *221*
fructosan, 22
Frustula rhomboides, 398
frustule, 350, 369–**77**
frustulin, 376
Fucales, 429–30, 433–*4*, **464–75**
fucoidin, 10, 427, 452, 473
fucoserratene, *432*, 469
fucoxanthin, 16–*17*; Bacillariophyceae, 368; Bolidophyceae, 368; Chrysophyceae, 334; Dinophyta, 269–1; Heterokontophyta, 317, 333; Pinguiophyceae, 358; Phaeophyceae, 426, 429; Phaeothamniophyceae, 425; Prymnesiophyta, 317; Raphidophyceae, 409
Fucus, 431, 433, *437*, 464–*6*; 470–2; *serratus*, 433, *465*, *468*, 473; *spiralis*, 473; *vesiculosus*, *433*, 465, *467*–8, *473*
fuel cell, 517
furones, 99

galactans, 114
Galaxaura, 93, 117–18; *apiculata*, *120*
Galderia sulphuraria, 108
Gambierdiscus toxicus, *265–6*, *281*, *505*
gambieric acid, 281–*2*
gas vacuoles, **41–3**, 45, 52–3
gas vesicles, **465–6**, 473–4
Gastroclonium, 96
Gelidiales, 107, **124–5**
Gelidium, 99, **124–5**; *cartilagineum*, ***125–6***
gene sequencing, **24**
Geosiphon, 86
geosmin, *66*–7
geotaxis, 142–3, 165
germanium, 336, 349, 376, 387
Gigartina stellata, 100
Gigartinales, 97
Giraudyopsis stelliger, *345*
girdle, *262*, *273*, 298–*300*
girdle band, 369–*70*, *373*, *380*
gland cell, Rhodophyta, 96–*7*
Glaucocystis, 86; *nostochinearum*, **87**
Glaucophyta, **85–8**; glycolate oxidase, 20, 149
Glenodinium, 272–3; *foliaceum*, *273*
gliding, **13–14**; cyanobacteria, **33–5**, 53–4; Bacillariophyceae, 377–*9*, 386, 399; Chlorophyta, 142, 159; Euglenophyta, 246; Rhodophyta, **106**
globule, *Chara*, *164–6*
Gloeobacter violaceus, *42*–3, 71
Gloeothece, 37–8, 59; *magna*, *71*
Gloeotrichia, 61; *ghosei*, 41; *echinulata*, *42*
Glossomastix chrysoplasta, *358*
glucosylglycerol and halotolerance, *64*–5
glutamic acid, *388*, *506*, 509
glutamine, **47–9**
glycerol, *59*, 265; osmoregulation, 197, 511
glycine and halotolerance, *64*–5
glycocalyx, **263–4**, 470–*1*
glycogen, cyanobacteria, 33, 38–*9*; 43, 45
glycolate, 19, **149**, 256; dehydrogenase, 144–5, 190; oxidase, 144, 154, 162
glycoproteins, 139
Golgi body, 3,4
Gomphonema parvulum, *375*, *379*, *395*
gonidia, *Volvox*, **200–7**
gonimoblast filament, **101–3**, *116*–20, 125–*8*, 130
Gonimophyllum, 96
Goniomonadales, 327–**8**
Goniomonas, 321–2, 327–**8**; *truncata*, *328*
Goniotrichum, 106; *alsidii*, *110*
Gonium, 198, *200*
gonoid ornamentation, *370*, 383, 398–9
Gonyaulax grindleyi, *278*; *polyedra*, *287*
gonyautoxin, *506*, 509
Gonyostomum, 412; *semen*, *411*
Gracilaria, 100, *126–7*; *conferta*, 99; *verrucosa*, 98
Gracilariales, 107, **125–7**
gravity response, 142–3, 165
grazing, 216, 515; deterrent, 96, 162, 287, 325, 390, 394, 430, 434, 472, 497, 504, **511**, **513**
Great Barrier Reef, 61, 189
Great Salt Lake, 187
greenhouse effect, 514
gullet, 327
gymnodimine toxin, *507*, 509
Gymnodiniales, 297, *300*, *302*–**3**
Gymnodinium, *118*, 513; *brevis*, *272*; *catenatum*, *278*, 278, 509; *catenatus*, *283*; *fungiforme*, *294*; *galatheanum*, *283*; *mikimoto*, *272*; *neglectum*, *275*–6; *pseudopalustre*, 300, *302*; *sanguineum*, *268*
gyrogonite, 167
Gyrosigma, 396; *attenuatum*, *398*

haidai, 460
hair, 7–8; Bacillariophyceae, *368*; Bolidophyceae, *368*; Chlorophyta, 139, 151; cyanobacteria, 72; Dictychophyceae, *360–2*; Dinophyta, 265, 267; Eustigmatophyceae, *354–5*; Heterokontophyta, 317; Pelagophyceae, *366*; Phaeothamniophyceae, *424*; Phaeophyceae, 427–8, *469*; Pinguiophyceae, *351*; Raphidophyceae, **409–10**; Xanthophyceae, 413
Halicystis, 179–*80*
Halidrys, 472; *siliquosa*, 473–*4*
Halimeda, **184**, *185*; *discoidea*, *185*; *opuntia*, *185*
Haliotis, 126
halogens, Rhodophyceae, 95–6, 99, 511
halophilic algae, 64, 514, 197
Hantzschia amphioxys, *386*
haplostichous, 442
haptera, 447, 450, 456
haptonema, 484–**6**, *484–9*, *497*, *499*
Haptophyta (Prymnesiophyta), 269, 298, 315, 317, 361, **484–503**; carotenoids, 17; chloroplasts, *11*–12; DMSP production, 511; motile cell, *9*; scales, 336; storage product, **21–2**; toxins, **509–10**
Harveyella, 96
Haslea, 396; *nipkowii*, *372*
haustoria, 98, 219, 295
Hegnaria, 245
heliotrophic cyanobacteria, 67–70
hematochrome, 139
Hematococcus, 139, 141, 197, *199*
Hemiaulus, 393
hepatotoxins, 65, 504
Heribaudiella fluviatilis, *426*
Heterocapsa, 265; *artica*, *266*; *circularisquama*, *266*; *horiguchi*, *266*; *ildefina*, *266*; *niei*, *267*; *triquetra*, *266*
heterococcolith, 493–*4*
Heterococcus, 217
heterocyst, *38*–9, *41–2*; **46–52**, 57, 59, *62–3*, 71, *72–4*
heterokont, 9
Heterokontophyta, **333**, 484; chloroplast, *11*–12; chloroplast E.R., 315, 317; eyespot, 14; flagella, *9*
Heteronematales, **256–7**
Heterosigma carterae, 409–*10*
heterotrichy, cyanobacteria, 72
heterotrophy, 23, 73, 221, 256, **291–5**, 381, 387, 442
heteroxanthin, 415, 425
histones, 14, 38, 275
HIV virus, 101
Holmsella pachyderma, 96, 98
holococcolith, 493–*4*
holophyte, 23
holozoic, 23
hormogonia, 42, **53–4**, 72–4
Hormosira banksii, *430*
hot spring, Bacillariophyceae, 395; cyanobacteria, 61–2; Rhodophyceae, 108–9, 157
hydrocarbons, biocides, 99; *Botryococcus*, 210–*11*; Dinophyta, **284–5**
Hydrocoleus, *71–2*
Hydrodictyon reticulatum, ***212***, 215
hydrogen gas for fuel cells, 50, 517–*18*
hydrogen peroxide, 99, 149, 458
Hyella, *38*; *immanis*, *60*
Hymenomonas carterae, 494, *499*; *roseola*, 485; *488*
hypersaline, 64, 365
hyphae, 441, 448, *450*, *452*, 466
Hyphochytridomycetes, 8
Hypnea musciformis, *102*
hypnospore, Dinophyta, 281, *284*, *302–3*
hypnozygote, Dinophyta, *283*
hypocone, *262–3*, *270*, 297–*9*
hypogynous cell, 117, *119*
hypolimnion, 42
hypothallus, 120–*2*
hypotheca, 369–*70*, **373–6**, 379
hystrichosphaerids, **277–*8***

ice algae, 514
ichthytoxin, 496–7
Imatonia rotunda, 485, *497*
imine toxins, *507*, 509
inducible defense, **511**
infochemicals, 67, **216**, 497
infundibulum, 327–*8*
intercalary growth, 431, 434, 448–9, 452, 462
internode, 163, 165
inulin, 22
invasive algae, 180–1, 187
inversion, *Volvox*, *295–6*
invertebrate, fecundity, 390; grazing, 66
iodine, 95–6, 114, 446, 459
Iridaea, 96
iridescence, Rhodophyta, **96**
Irish moss, 100
iron, 42; cyst envelope, 254–5; growth, **514–5**; lorica, 336–7, 349; nitrogen fixation, 49; resting spore, 383; siderophores, **68**
Ischadites abbottae, *175*
Ischnura verticalis, *258*
isoagglutination, 143
Isochrysis, 484; *galbana*, *497*
isofloridoside, 22–3; and osmoregulation, 339
isogamy, 143, 155
isokont flagella, 9
isoprenoids, 396

Jania rubens, *122*
jasmonic acid, 431
Julescraneia grandicornis, 464
junctional pores, *34–5*

kai proteins, 52–*3*
kairomones, **513**
kappa particle, 324
Kappophycus, 100; *alvarezii*, 101
Karenia brevis, 269, *272*; *mikimotoi*, 269, *272*; *selliformis*, 509
Karlodinium veneficum, *264*, 269, *283*
karyolymph, 3
Katablepharis ovalis, *312*
Katagnymene, 51; *pelagica*, *52*; *spiralis*, *52*
kelp, 442, 459, 464; ash, 459
Kephyrion rubri claustri, 336
kerogen, 284
ketoglutarate, *47–9*, 55
Khawkinea, 245, 250
kieselguhr, 396
kinesin, 5; *Volvox* inversion, *206*
kinetochore, Dinophyta, 275–*6*
Kinetoplastida, 248, *252*, 256
Kirk, D., 208
Klamath Lake, 67
Klebsiella, 245
Klebsomormidales, **155**
Klebsormidium, 155
kleptoplastid, Dinophyta, 269
kombu, 460
Kraft, G., 131
krill, 513–14

Kylin, H., *131*
Kylinia, 106, 115; *rhipidandra*, *102*

labyrinthulids, 8
lagoon, 124, 185
Lake Kinnert, 66
Laminaria, 110, 428, 432, 450–1, 453, 458, 460–2; *cloustoni*, *452*; *digitata*, *455*, *457*; *groenlandica*, *457*; *hyperborea*, 449, 451, 455, *457*; *japonica*, *454*; *saccharina*, 451, *457–8*; *setchellii*, 110; *solidungula*, 455
Laminariaceae, 453, **460**, **462**
Laminariales, 429–30, 433–**4**, 436, 441–2, **448–64**
laminarin, **21**, 381, 426, 419, 458–9
laminin, 311
lamoxirene, *432–3*
Laurencia, 473; *spectabilis*, *121*; xylans, 10
laver, 114, 173
lectins, 104
lens, Dinophyta, *274*
Lepocincilis ovata, *248*
lessepsian species, 187
Lessonia, 442, 464; *nigrescens*, 462–*3*
Lessoniaceae, 453–**62**
leucoplast, 11, 322, 341–2
leucosin (chrysolaminarin), **21**; Bacillariophyceae, 369, 381; Chrysophyceae, 33–4; *337–8*, *341–4*; Dictyochophyceae, *361*; Euglenophyta, 245, 255; Heterokontophyta, 317, 333; Synurophyceae, *349*, *352–3*; Prymnesiophyceae, 317, 484–*8*, *491*, *497*
Liagora, 93; *viscida*, *102*
lichen, **57–9**, 62–3, 191, **217–***19*
Lichina, 59; *pygmea*, *57*
light-harvesting complex, **16**
light responses, **12–4**, *156*, **204–6**
Limnophycus paradoxa, 439
Lingulodinium polyedrum, 268, 275, *277*, 286–91
list, 298–*9*
lithophyte, 72, 121, 123, 474
Lithothamnion, 121; *glaciale*, *122*; *lenormandi*, *122*
lithotroph, 23
littoral zone, 59
loculus, 371–*2*, *378*
lorica, Euglenophyta, 247; Chrysophyceae, 198–*9*, **336**–*8*, 342–*3*
Lotharella globosa, 318
luciferase, **285–6**
luciferin, **285–7**
Lucina borealis, 285; *miniscula*, 285
luminescence, 96, 279, **285–89**, 293
lunar rhythms, *Derbesia*, 179; *Dictyota*, 434, *Ulva*, 170–*1*
lutein, 139–40, 410
lycopadiene, 211
lycopods, 162
Lyngbya, 61, 72; *aeruginosa*, 35; *birgei*, *71*; *majuscula*, *59*; *sordida*, *59*
lysosome, 255

macrandrous species of *Oedogonium*, **224–6**
Macrocystis, 432, 442, 452, 453, 459, 462; *pyrifera*, 447, *458*, 464; *integrifolia*, *452*
macrolide toxins, 279, 504
magnesium, 94, 110, 124; carbonate, 164
maitotoxin, 281–*2*; 504, *506*
malaria, 311
malic acid, 441
Mallomonas acaroids, *352*; *zellensis*, 350
maltose, 214
manganese, 254–5, 336–7
mangrove swamps, 175
mannan, 9, 104, 139, 178
mannitol, *21–2*, *57*, *92*, 98, 429, 451, 458, 459, 468
mantle, Bacillariophyceae, 369, *381*
Manton, I. *486*
Mantoniella, 152, 514; *squamata*, *191*
manubrium, **164–***6*
manure, 57, 460
marine snow, 377
marl, 124, 164, 496
Martin, John, 514–15
Mastigocladus laminosus, 61–*2*
mastigoneme, 7–8, 138; Bacillariophyceae, *368*; Bolidophyceae, *368*; Chlorophyta, 139, 151; Dictychophyceae, *360–2*; Dinophyta, 265, 267; Eustigmatophyceae, *354–5*; Heterokontophyta, 317; Pelagophyceae, *366*; Phaeothamniophyceae, *424*; Phaeophyceae, 427–8, *469*; Pinguiophyceae, *351*; Raphidophyceae, **409**–10; Xanthophyceae, 413
Mastogloia angulata, *373*; *grevillei*, *370*
mating structure, 6; *Chlamydomonas*, *195*
mating-type reaction, 143
Mattox, K., 144–*5*
McMurdo Dry Valleys, 325–*6*, **515–16**
medicinal uses, 459–60
Mehler reaction, 58–*9*
melatonin, 278, 291
Melkonian, M., 330
Melobesia lejolisii, *121*; *limitata*, *121*; *maginata*, *121*
Melosira, 383; *arenaria*, 396, *398*; *nummuloides*, *401*; *varians*, *395*, *399–400*
Mereschkowsky, K., 82–**3**, 85
meristoderm, 432, *441*, 449–*50*, *452*, *466*
Mesenchytraeus, 196
Mesodinium, 268
mesokaryotic nucleus, Euglenophyta, 245, **248–50**; Dinophyta, *263*, **275**
Mesophyllum, 121; *alternans*, *121*
Mesostigma,139; *viride*, *154*
Mesotaeniaceae, 156, **159–60**
Mesotaenium de greyi, *156*
metachromatic body, 40
methane, 26
methane sulfonic acid, 511–**12**
2–methylisoborneol, 66–*7*
Mg/Ca ratio, seawater, **94–5**, 123
MIB, *66–7*
Microasterias radiata, *160*
Microcoleus chthonoplastes, *59*, 64; *vaginatus*, 62–*3*
microcystin, 65–6, 504, *506*, 509
Microcystis, 61, *65*, 509; *aeruginosa*, 42, 66, *71*
Micromonadophyceae, 144, **150–4**
microneme, 310
Microspora, 218; *crassior*, *219*
migration in water column, **289**, 393, 410
Mischococcales, 416, **418**
Mischococcus, 418; *sphaerocephalus*, *413*
mitochondria, **19–20**
mixotroph, 23, 291, 325–6, 339, 359
molluscs and symbionts, 183
molybdenum in nitrogen fixation, 49
monoecious, 462
monosporangia, *102*, *106*, *113*, 115
monospore, 109–10, *112*, 115–*16*, *118*
Monostroma, 114, 169, 170; *cavernosa*, 58

Mougeotia, 155; *scalaris*, *156*
muciferous body, Chrysophyceae, *334–5*, *344*; Dictyochophyceae, 360; Euglenophyta, *246–7*, *253–4*
mucilage canals, 451–*2*
mucilages, **9–10**; Bacillariophyceae, 373, **377–80**; cyanobacteria, 61; Rhodophyceae, 90
mucocyst, Dinophyta, 264; Euglenophyta, *245–6*, *253*; Raphidophyceae, *409–10*, 412
mud algae, 64; Bacillariophyceae, 379, 386; Chrysophyceae, 339–40; Euglenophyta, 252–3
Muller, D. G., 432–*3*
multifidene, *432*, 439
multilayered structure (MLS), 144–**7**, 154, *162*, 190
mutualism, 130
mycobiont, 57, 217–*18*
mycosporine sunscreen, 517–*18*
myglobin, 50
myosin, 146
myxophycean starch, 21
myxoxanthophyll, 43, 85
myzocytosis, Dinophyta, 291

nannandrous species of *Oedogonium*, **224–6**
Nannoceratopsis, 298
nannoplankton, 484, 496
Navicula, *370*, *379*, 383, 396, 403; *cryptocephala*, *395*; *cuspidata*, *385*; *glaciei*, *393*; *pelliculosa*, *386–7*; *radiosa*, *395*
necridia, 54, 73
Nemaliales, 93, 107–8, **117–18**
Nemalion, **117**, **119**
Nemastoma laingii, 101
nemathecia, 120
nematocyst, 292
nematode, 67
Nematodinium armatum, 273–*4*
Neomeris, 175; *annulata*, *177*
Neoperidinium, 263
neosaxitoxin, *506*
Nereocystis, 451, 469, 462–*3*; *luetkeana*, 464
neurotoxin, **504–10**; cyanobacteria, **64**; Dinophyta, 281; Raphidophyceae, 408
Nitella, 164–5, 186
nitrate, 47, 72
nitrite, 47
nitrogen, algal growth, 340, 342; Bacillariophyceae symbiosis, 393; deficiency, 47, 255, 298, 393, 492; fixation, 43, **49–51**, 54, 57–8, 60, 62–4, 181, 517; induction of gametogenesis, 184, 196, 212, 214, 223–5; pollution, 395; resting spore formation, 383; storage, 18–*19*, 39
nitrogenase, 517; cyanobacterial, **47–52**
Nitzschia, 403; *corta*, 514; *palea*, 379, *386–7*, *395*; *putrida*, 379; *stellata*, 574
Noctiluca, 287, **291–***2*; *scintillans*, **296–***7*
node, *Chara*, 163, 165
Nodularia, 59, 65, 509; *spumigena*, *59*
nodularin, 65, 504, *506*
nori, 114–15
Nostoc, 45, 56, 65, 67, 509; *commune*, 62–*3*, 67; *linckia*, *72*; *punctiforme*, 54; *verrucosum*, *63*, 67
Nostocales, **71–3**
Notheia, 448
nucleoid, chloroplast, 14
nucleolus, 3
nucleomorph, 315–*16*, Chlorarachniophyta, 317–*18*; Cryptophyta, 321, *324*
nucule, *Chara*, *164–5*
nutrition, **230**
nutritive cell, Rhodophyceae, 124–5, *127*

ocellus, 274
Ochromonas, 333–*4*, 341; *danica*, 334–*5*; *malhamensis*, 23, 336, 339; *sociabilis*, 336; *sphaerocystis*, *338*; *tuberculatus*, 335–*6*; *338*
Octolaminaceae, 344
Oedocladium hazenii, *222*
Oedogoniales, 139, 144, 191, 218, 221–**6**
Oedogonium, 143, **222–6**; *cardiacum*, 225; *crassum*, *225*
ogonori poisoning, **126**
oil shales, 210, 284–5, 496
okadaic acid, 279–1, 504, *507*
omega-3 fatty acids, 358
ooblast, 120
ooid, **60**
Oomycetes, 8
Ophiocytium majus, *414–15*
opsin, 141
Opuntiella californica, *97*
organotroph, 23
Ornithocercus, 278; *magnificus*, *299*
Oscillatoria, 34, *37*, 53–4, 61, 65, 72, 509; *agardhii*, *42*; *limnetica*, *42*, 44; *princeps*, 35; *redekei*, 41; *terebriformis*, 61
Oscillatoriales, **71–2**
Oscillatoriopsis, *70*
oscillin, 33–*4*
osmoregulation, **22–3**, 511; Chlorophyta, 141, 197; Chrysophyceae, 339; cyanobacteria, 64–5; Euglenophyta, 248; Phaeophyta, 429; Rhodophyta, 91
osmotroph, 23, 256, 291
Ostreococcus tauri, *150*
Ovulites margaritula, 185–*6*
2–oxoglutarate, **47–9**, 55
oxygen, activated, 99; atmospheric, 26; radicals, 150
oxygenase, Dinophyta, 286
Oxyrrhis, 275, 277, 513: *marina*, 263, *267*
oxytoxin 2, *187*
oyster beds, *Codium* in, 181

pachydictyol, 434, *436*
Padina, 428, 434
Paleocodium, 185–6
Paleoconchocelis starmachii, *114*
Paleolynbya barghooriana, *70*
paleothermometer, 124
palium, Dinophyta, 291–**3**
Palmella miniata, *199*
Palmellaceae, **210**
Palmeria mollis, *93*
palythene, **518**
Pandorina, 198; *morum*, 200
pantonematic flagellum, 7
Paracentrotus lividus, 457
paraflagellar swelling, Euglenophyta, **246**, 250, 258–9
paralytic shellfish poisoning, **279–84**, **509**
Paramecium, 213
paramylon, **21–2**, *245–7*, **255**, *256*, 415, 487
paraphysis, 445–*7*, 453–4, 456, 465, 467
Paraphysomonas, 342, 336–*7*; *sigillifera*, *337*

parasitic algae, 23; Chlorophyta, 218; Euglenophyta, 245; Rhodophyceae, **96–8**
parasitophorus vacuole, 311
parasporangia, Rhodophyceae,106
paraxonemal rod of flagellum, **245**–*6*, *359*, 361
Parmales, 336, **341–4**, 369
parthenogenesis, 168, 176, 226, *438*–9
Pascher, A., 346
Patina pellucida, 455
Pavlova, 485–67, **500**; *granifera*, **500**; *mesolychnon*, 486–7
Pavlovales, **498**, **500**
PCU (practical salinity unit), 365
peat bogs, 160
pedicel, *Chara*, 164, *166*
Pedinella, 359–60; *hexacostata*, *361*; *squamata*, *362*
Pedinellales, **359–60**
Pedinomonas, *296*–7
peduncle, Dinophyta, 291, *294–5*
Pelagococcus subviridis, 365–*6*
Pelagomonas calceolata, 365–*6*
Pelagophyceae, 359, **365–7**
Pelagophycus, 462
pellicle, Apicomplexa, *310*; Euglenophyta, *246–51*, 253; Dinophyta, 263, 265–*66*
Pelvetia canaliculata, 473; *fastigata*, *472*
Penicillus, 180, 184–5; *capitatus*, *182*
pennate ornamentation, *370*, 383, 399, 403
Pentalamina, 345
Pentalaminaceae, 344
pentaster, *279*
pentose phosphate pathway, 55
peptidoglycan, cyanobacteria, 33–*5*
Peranema, 246, 248, *252*; *trichophorum*, *256*–7
Peridinium gatunense, 66
pericarp, 126
periclinal division, 432, 441, 446, 466
Peridiniales, 273, 297, **298–300**
peridinin, 263, 269–71; chlorophyll *a*-protein (PCP), 271–2
Peridinium, *263*; *cinctum*, *267*, *269*; *pentagonium*, 287; *westii*, 272
periplast, Cryptophyta, 317, 321–*2*, *329*
perithallus, *121–2*
perizonal auxospore, 383–*4*
perizonium, 383–***5***
Permian extinction, **510**
Permocalculus, 118
peroxisome, 19–20, 149
Petalonia, 431, 442, 444; *fascia*, 444, **446**–*7*
petroleum deposits, 210–11, **284–5**, 496
Pfiesteria piscicida, 294–**5**
Phacotus lenticularis, 198–*9*
Phacus, 255, *triqueter*, *248*, *257*
Phaeaster, 359; *pascheri*, *360*
Phaeocystis, ***497–8***, 511, 513; *globosa*, 488, *490*; *poucheti*, *497*, 505
Phaeodactylum tricornutum, *386*–7, *381*, 390
Phaeomonas parva, *357*
Phaeophyceae (brown algae), **426–83**; carotenoids, 17; chloroplasts, 11; evolution of, 346, 413; glycolate oxidase, 20; mucilages, *10*; storage product, 21–2
phaeophycin tannins (phloroglucinol), 426, **429–30**, 511
Phaeoschizochlamys mucosa, *425*
Phaeothamnion polychrysis, 424
Phaeothamniophyceae, **424–5**, 427
phagotrophy, 23; Apicomplexa, 312; Chrysophyceae, 339–40, 342; Cryptophyta, 325–6; Dictyochophyceae, 359–60; Dinophyta, *291–5*; Euglenophyta, 248, 256; evolution of chloroplast E.R., 240; Prymnesiophyceae, 489
pharmaceuticals from algae, 100–1
pheromone (sexual hormone, sirenine), 160, 196–*7*, 225–6; Phaeophyta, **432–3**, 436, 439, 441, 443, 462, 469, 513
phialopore, *Volvox*, *205–6*
phloroglucinol, *430*
phlorotannins (phaeophycin tannins), 426, **429–30**, 511
Phormidium, 59, 72; *autumnale*, *71*; *inundatum*, *42*; *uncinatum*, *34*, *36–7*
phosphoglycerate, 40, 149
phosphorescence, 96, 285
phosphorus, algal growth, 340, 459; deficiency, 45, 73, 298, 492; pollution, 375; marine snow, 278; resting spore induction, 383; storage, 40, 43
photoautotroph, 23, 255
photochemical reaction center, **16**
photoheterotroph, 23, 55
photoluminescence, 285
photoperiod, 110, 112, 169, 196, 455, 472
photophile, 106
photophobia (photoshock), **13**, 141–2, 250
photoreceptor, **141–3**; 349, 421, 426
photorespiration, 149
photosystem II, 17, 113
phototaxis, **12–13**; Bacillariophyceae, 386; Chlorophyta, **141–2**, 146, 158–*9*, 170, 172, 198, 202; Chrysophyceae, 340; Cryptophyta, 324–5; cyanobacteria, 54, 64; Dinophyta, **272–4**; Euglenophyta, 250, 252–3; Phaeophyta, **428**, 446, 449; Raphidophyceae, 412; Rhodophyceae, 109
phototroph, 55
phototropin, *194*
Phragmites communis, 394–*5*
phragmoplast, Chlorophyta, 144, *149*, 154, 162–3
phycobiliproteins, **17–18**, 27; cyanobacteria, 38, 43; Cryptophyta, 317, 321, **322–3**, 326–7; Rhodophyta, *90–1*
phycobiont, 57, 217–*18*
phycocyanin, 12, **17–19**, 43, 90–1, 322–3, 327, 330
phycoerythrin, 12, **17–19**, 43, 60, 90–1, 322–3, 326
phycomata, 150, *152*
phycophaein, 430
phycoplast, 144, *148*–**9**, 189, *218*, 221–2
phycotoxins, **504–10**; Dinophyta, **279–84**; Prymnesiophyta, **496–7**
Phymatolithon calcareum, *123*
physode, 425, *427*, *430*, 442
phytochrome, 113, 156, 194
Pickett-Heaps, J., preface, 144
picophytoplankton, **60**, 368
pili, cyanobacteria, **36**–*7*
Pinguiochrysis pyriformis, *358*
Pinguiococcus pyrenoidosus, *358*
Pinguiophyceae, **357–8**
pinnatoxin, 509
Pinnularia, *403*–4; *viridis*, *371*, *377*, *380*
pit connections, 89, **92–3**, 97–8, 102–3, 110, 115, 129–30
Placobranchus, 183
plakea, 196
planozygote, 281, *283*, 300–*1*, *352*

Plasmodium, 311
plastids, **10–12**
plastid division ring, **20**
plastoquinone, 196–*7*
plasmodermata, Chlorophyta, *148*, 155, 163, 191, 220; cyanobacteria, 49; Phaeophyceae, 428, 451–2
Platydorina, 199; *caudata*, *200*
Platymonas, 152
Plectonema notatum, 62
Pleodorina, *200*
pleomorphism, 386
Pleonosporium vancouverianum, *102*
plethysmothallus, 431
pleurilocular sporangia, *426*, *431*, 436–*8*, *442*–8
Pleurocapsa minor, *71*–2
Pleurochrysis carterae, 496; *scherffelii*, 491–*3*
Pleurochloris magna, *354*
Pleurocladia incustris, *426*
Pleurosigma, 396
Pleurotaenium nodosum, *160*
polyether toxins, *508*
polyglucan granule, cyanobacteria, 40
polyhedral body, *46*, 85
Polyhedriella helvetica, *354*
Polykrikos kofoides, *292*; *schwartzii*, *278*, *293*
polymorphism, desmids, 160; *Saccorhiza*, 455; *Scenedesmus*, *216*, *Ulva*, 179
polyphosphate body, **39–40**
Polysiphonia, 91, 98, **127–8**; *denudata*, 130, *fastigata*, 97; *lanosa*, 96–*7*; *nigrescens*, 95; *stricta*, *129*
polysiphonous structure, 127–8, 433, 436–*7*
polysporangia, Rhodophyceae, **106**
polystichous, 442
Pontosphaera syracusana, *495*
poroid, Bacillariophyceae, *372*, 388
Porolithon, 124
Porphyra, 91, **110–15**; cell wall, 90; *dioica*, *111*; *gardneri*, 110, *112*; mucilage, 10; *perforata*, 113
Porphyridiales, 92; 107–**10**
Porphyridium, *90*, 104, **109**
Porphyrosiphon notarissi, *62*
Postelsia palmeformis, 462–*3*
potassium, 189, 340, 395
Poterioochromonas malhamensis, 22–3
practical salinity unit (PCU), 365
Prasinocladus, **152**–*3*
Prasinophyceae, 139, **144**, 149–**54**, 255–6
Prasiola stipitata, 211–13
Prasiolales, 191, *211*–**13**
predation, 513; Bacillariophyceae, **390**; Dinophyta, 287; Euglenophyta, **256–7**
proboscis, *421*, 433, *469*
procarp, Rhodophyceae, 120, 125, 130
Prochlorococcus, 43, 40; *marinus*, 71
Prochloron, 43
Prochlorophyta, 33
Prochlorothrix, 43
projectiles, Chrysophyceae, 335; Dinophyta, **275–6**, 279
prokaryote, 3
promeristem, 433–4, **466**
propagule, 433, 436–*7*
propenic acid (acrylic acid), 498, 511, *512*
properizonal auxospores, 383–4
proplastid, 10, 90, 334, 381
Prorocentrales, **296–8**
Prorocentrum, 276, 279, 297, 509; *hoffmanianum*, *298*; *lima*, *280*; *mican*, *299*
prostaglandin E, 126–*7*
protein phosphatase and hepatatoxins, 65, 504
prothallus, 117–18
Protoperidinium, 292; *conicum*, *293*
Prototheca, 214, *216*
Prymnesiales, **498–500**
Prymnesiophyta (Haptophyta), 269, 298, 315, 317, 361, **484–503**; carotenoids, 17; chloroplasts, *11*–12; DMSP production, 511; motile cell, *9*; scales, 336; storage product, **21–2**; toxins, **509–10**
Prymnesium, 484, 496–*7*, *507*, 509; *parvum*, 485, *489*, 497, *505*
Pseudobumilleriopsis, 418; *pyrenoidosa*, 415–*16*
Pseudocharaciopsis texensis, *355*
pseudocilia, 191, *209*
Pseudokephyrion pseudospinale, 336
Pseudo-nitzschia, 383, 387–*8*, 409, 509; *multiseries*, *388*, 389, *404*, 509
pseudoparenchyma, 442
Pseudopedinella, 359
pseudopod, Chloroarachniophyta, 318; Dinophyta, 292–4; Prymnesiophyta, 489
pseudoraphe, *371*
Pseudotrebouxia, 217
psychrophile, 61, 365, 516
psychrotroph, 61
pteriatoxin, 509
Pteridomonas, 359
Pterocladia, 99
Pterosperma, 150; *cristatum*, *152*
Pterygophora californica, *449*
punctae, Bacillariophyceae, *372*
Punctariaceae, 444
purine toxins, 506
pusule, **268**, *270*, 278, 335, *361*
Pyramimonas 139; *obovata*, 150–*1*
pyrenoid, *11*–12, 21, 109
Pyrocystis fusiformia, 286–*7*; *lunula*, *293*; *noctiluca*, *293*
Pyrodinium bahamense, 281, 283, 287, 509

quartzite, **373**

radiolaria, 489–90
Ralfsia, 442, 444; *confusa*, *445*
Ralfsiaceae, **442**, **444**
raphe, *370*–*1*, 378–*80*, 399
ramuli, 124
Raphidiopsis curvata, 45; *mediterranea*, 45
Raphidonema nivale, 155
Raphidophyceae, **409–12**, 487; chloroplast DNA, 14; toxins, **503**
R-body, 324
receptacle, 464–*8*, *472*–*5*
Receptaculitaceae, **175**
red algae, **89–137**; endosymbiosis, 81–2; glycolate oxidase, 20; mitochondria, 19; mucilages, *10*; plastids, *11*; phycobilisomes, *11*–12, **17–19**; storage products, **20**–2
Red Sea, 61
red tides, Dinophyta, **279–84**, 511; Raphidophyceae, **410**
reef algae, Chlorophyta, 175, 185, 189; Dinophyta, 295; Rhodophyta, 123–**4**
reservoir, Eulenophyta, *246*–8, 250
resting spore, Bacillariophyceae, **382–3**, 401–*2*; Chrysophyceae, 337; Dinophyta, **277**–*8*, *284*; Xanthophyceae, 418
reticulopodia, 317, *319*
retinal, 141–*2*, 334

retinoid, *274*
R-fiber, flagellum, 265, *268*
Rhipocephalus, 185
Rhizochromulina, 359; *marina*, *360*
Rhizochromulinales, **359**
rhizoid, 96, 98, 110, 112, 128–9, 221, 416–17, 439–*40*, *465*, 470–*1*
rhizoplast, *5–7*; Chlorophyta, 144–**6**, *152*, 154, 171, 190
rhizopodia, Dictyochophyceae, 359–*60*
Rhizosolenia, 350, 391, 396; *castracanei*, *393*; *imbricate*, 393
Rhodella maculata, *109*
Rhodochaete, 93
Rhodochorton, *96*, **115–16**; *investiens*, **115**; *purpureum*, 106; xylans, 10
rhodolith, **94**
Rhodomonas lacustris, *328*
Rhodophyta (red algae), **89–137**; endosymbiosis, 81–2; glycolate oxidase, 20; mitochondria, 19; mucilages, *10*; plastids, *11*; phycobilisomes, *11*–12, **17–19** storage products, **20**–2
rhodopsin, 141–*2*, 334
Rhodosorus marinus, *109*
Rhodymenia, xylans, 10
Rhoicosphaera curvata, *395*
Rhopalodia gibba, *398*
rhoptry, 310
rhythms, Bacillariophyceae, **383**; bioluminescence, **286**; Chlorophyta, 150, 170, 184; cyanobacteria, **50–2**; Dinophyta, **287–91**; Euglenophyta, 247, 252–3; lunar, 170, 179; Rhodophyta, **106**; Phaeophyta, 434, 453, 455; Prymnesiophyta, 491, 496
rib, Bacillariophyceae, 372, 388
riboflavin, 422
ribosomes, 3–4, **24**; cyanobacteria, 38–*9*
ribulose 1,5-diphosphate, 149
ribulose-1,5–bisphosphate carboxylase/oxygenase (Rubisco), **12**, 24, 39–*40*, 55, 85–6, 240
rice paddies, 64
Rivularia, 59; *dura*, *72*
RNA nucleotide sequencing 24
RNA polymerase, 24
Rubisco (ribulose-1,5–bisphosphate carboxylase/oxygenase), **12**, 24, 39–*40*; 55, 85–6, 240
Saccorhiza, 436, 448, 453; *bulbosa*, 462; *polyschides*, *457*
salt marsh, 427
salt-stress protein, 65
salt tolerance, *Dunaliella*, 197
saprophyte, 23, 219
Sargasso Sea, 393, 427, **475**
Sargassum, *464*; *filiendula*, *476*; *longifolium*, *475*
Saunders, G. W., 131
saxitoxin, 65, 281, 504, 506, *509*
scales, Bacillariophyceae, *385*, *401*; Chlorophyta, 139, 145–**6**, 149–*51*, *154*–5, 162, 166, 168, 191; Chrysophyceae, 333, 336–*7*; Cryptophyta, 321–*2*; Dictyochophyceae, 360–*2*; Dinophyta, **265**–7; Prymnesiophyceae, 484–*8*, **490–7**; Synurophyceae, *349–50*, *352*
Scenedesmus, **214**; *armatus*, *216*; *obliquus*, *216*
Scherffelia dubis, 7
Schizothrix, 62, 69
Schoenoplectus lacustris, 394–*5*
scintillon, 280
Scrippsiella trochoidea, *262*, 277–*8*
Scytonema, 62, 63; *arcangelii*, *73*; *hofmanni*, *63*, 68; *myochrous*, *74*; **518**
Scytosiphon lomentaria, *429*, 442, 444, *446*
Scytosiphonaceae, **442**, **444–8**
sea ice, 513–14
sea lettuce communities, 5, **173**
sea otter, 457
sea palm, 462
sea sawdust, 61
sea urchin, 457
seas, ancient, 94–*5*
seawater, carbon dioxide, 494; density, 391; HCO_3, 494; pH 494; physical characteristics, 239–40; salinity, 365
secondary endosymbiosis, **239–43**, 315, 510
secretion, mucilage, 109, 141–2, 253; proteins, 56
secretory cells, Rhodophyta, **95**–*6*
segregative cell division, 188–*9*
separation disc, 54, 73
seriochemical, **513**
setae, 155, 162, *342*, 401–*2*, 391
sexual hormone (pheromone, sirenine), 160, 196–*7*, 225–6; Phaeophyta, **432–3**, 436, 439, 441, 443, 462, 469, 513
shade form, *Ceratium*, 298
sheath, cyanobacteria, **37–8**, 63
shellfish poisoning, **504–10**; Bacillariophyceae, **387–8**; Dinophyta, **279–84**
siderophores, cyanobacterial, **68**
sieve, cells, 451–*2*; filaments, 441, *463*, 466; membrane, *372*, 378; sieve plates, *451*, 466; pore, *372*
silaffins, **376–7**, 378
silica, Bacillariophyceae, 369, 373–4, 393; Dictyochophyceae, 359–60; Synurophyceae, 347
silica deposition vesicle, Bacillariophyceae, *375–6*, 378; Chrysophyceae, 336, *338*, 342–*3*, 349
silicalemma, Bacillariophyceae, *375*–6; Synurophyceae, 349
silicoflagellates, 360
silicon, 278–*9*, 342, 344–5, 367, 374
silting, adaption to, 64
sinus, desmids, 160
siphonaceous algae, Chlorophyta, 139–40, 175, 178, 184, 186–*7*, 190; Xanthophyceae, 416, 418, *419*, 422
Siphonales, 179
siphonein, 139, 168, 178, 188
Siphonocladales, 139, 168, **188–9**
Siphonocladus tropicus, *188*–9
siphonoxanthin, 139–*40*, 168, 179, 188
Skeletonema costatum, *374*, 387, *392*; *pseudocostatum*, 390
skotophile, 106
Skuja, H. L., *131*
slime secretion, cyanobacteria, **33–5**
Smith, M. S., 27
Smithora, 90
snow algae, *Chlamydomonas*, **196**
sodium, and osmoregulation, 197; channels, 281, 470, 474, 504, 509; silica uptake, 375
sorbitol, *92*
sorus, 434, 439, 446, 452, 454, 469
Southern Ocean, 513–15
spermatangia, Rhodophyta, **103–5**
spermine, 104–*5*
spermocarp, Chlorophyta, 163

Sphacelaria, 429, 431–2; *bipinnata*, 436–7; *cirrhosa*, *437*; *furcigera*, 436; *lacustris*, *426*
Sphacellariales, **433**
Sphaeroplea, 218; *annulina*, *218*; *fragilis*, *220*
Sphenomonas, 246; *laevis*, 255
spindle, 144–5, **148**–*9*; 162, 189
Spirogyra, **157–9**; *adnata*, 156
spirolide toxin, *507*, *509*
Spirotaenia, 160; *condensata*, *156*
Spirulina, *67*, 72; *major*, *71*
Splachnidiaceae, **442**, **448**
Splachnidium, *448*
Sphaeopleales, 191, **218–20**
Spondylosium moniliforme, *160*
spongiome, 22
Sporochnales, 439
sporophylls, 462, 464
sporopollenin, 193, 279
stalk, Euglenophyta, 247, 253, *258*
starch, Chlorophyta, *140*, *150–3*, *198*; Cryptophyta, 321–4; Dinophyta, *263*, *297*; Rhodophyta, *91*–2, 98
statoliths, *Chara*, 165
statospore, Chrysophyceae, 333, **337–8**, 342–*3*; Synurophyceae, 350, 352–*3*; Xanthophyceae, 416
Stauroastrum curvatum, *160*
Stegastes nigricans, 130
stephanokont flagella, 9, 179, 191, **222–6**
Stephanoon, 199; *askenasyi*, *200*
Stephanopyxis, 383; *broschi*, *397*; *turris*, 392–3, *397*
sterols, Dinophyta, **285**; Bacillariophyceae, 381
Stewart, K., 144–*5*
stichidia, 130
Stichococcus bacillaris, *155*
Stigeoclonium farctum, 221
stigma (eyespot), Chlorophyta, *140*–5, *152–3*, 168–*9*, 172, 198; Chrysophyta, 333–*7*, *341*, *344*; Cryptophyta, 323–*4*; Dictychophyceae, *360*; Dinophyta, **272–4**; Euglenophyta, *245–6*, **250**, 252; Eustigmatophyceae, *354–5*; Phaeophyta, *427*–**8**, 440, *469*; Prymnesiophyceae, 484, *500*; Xanthophyceae, *413*, 415–*16*
Stigonema, *mammilosum*, *74*; *ocellatum*, *74*; *turfaceus*, *73*
stoneworts, 164
storage products, **20–3**
stramenopile, 7–8
Streptophyta, 144
streptophyte, 163
striae, Bacillariophyceae, *370–2*
striated strand, flagellum, 265, *269*, *271*
stroma, 3, 11
stromatolite, *69*
stylet, 311
suffultory cell, *224*–**5**
sulcus, Dinophyta, *262*, *267*, *274*, 298–*300*
sulfated polysaccharides, Rhodophyta, 96
sulfur, cyanobacterial photosynthesis, 44
sulfuric acid in the atmosphere, 511–*12*
sunscreens, **517**; cyanobacteria, 63; Phaeophyta, 430
superoxide dismutase, Chlorophyta, **149–50**
supporting cell, Rhodophyta, 103, 124–*5*, *128*
suture, 297–8
Sweeney, B. M., *289*
swimming rate, Dinophyta, **268**–*9*; Euglenophyta, **246**
Symbiodinium microadriaticum, 276, 295
symbioses, Bacillariophyceae, 393; Chlorophyta, 152–3, 183–4, 213; Cryptophyta, 326–*7*; Dinophyta, 276–7, 287, **295–6**; Prymnesiophyceae, 489–90
syncyanosis, **85–8**
Syndinium, 275; *turbo*, *275*–6
Synechococcus, 50–*2*, 60–1, 71; *aeruginosus*, 42; *elongates*, 52–3; *lividus*, 61–*2*
Synechocystis, 36–*7*, 60, 71
syngamy, 144
synomone, 513
Synura, *349*; *echinulata*, *352*; *petersenii*, 350, *352*; *uvella*, *351*
Synurales, 350
Synurophyceae, **349–53**; scales, 336
Syracosphaera nodosa, *495*

Tabellaria, 398; *fenestrata*, *393*; *flocculosa*, 344, *393*, 395
tannins, 426, **429–30**
Tasmanites, 150
tentacle, Dictyochophyceae, 359, *361*; Dinophyta, *274*, *291–2*, *297*, *299*
terpenoids, water quality, 66; grazing deterrent, 434–*6*
tertiary endosymbiosis, 269, 361
Tessellaria volvocina, 350–*1*
Tetrachrysis minor, *425*
Tetraparma, *344*
Tetraselmis, 139, 146, 151–*3*
Tetraspora, 210; *gelatinosa*, *209*
Tetrasporaceae, **209–10**
Tetrasporales, 191, **208–11**
tetrasporangia, **105**, 117, *119–20*, 125–6, *128–9*
tetraspores, **101–3**, 109, *116–19*, *127–8*, 130, 434–*5*
tetrasporophyte, **101–3**, *116*, 118, 124, 126–*7*, 130
Tetrasporopsis fusescens, *425*
Texas cattle fever, 311
Thalassiosira gessneri, *374*; *lacustris*, *374*; *pseudonana*, 387; *wailesii*, *372*
thallophyte, 3
thallusin, *170*
theca, Chlorophyta, 145–**6**, *148*–50, *152*–3, 189; Dinophyta, 262, *264–6*, 273, 276, *277*–8
thecal plates, *262*, *264–6*, 273, 276–*7*, 297–8
Theileriosis, 311
thermophilic algae, 61, 108–9, 395
thraustochytrids, 8
thylakoid, *11*, 38–9, 43
Thysanocladia densa, 95
tidal rhythms, *Derbesia*, 179; *Dictyota*, 434, *Ulva*, 170–*1*
Tiffaniella snyderae, *106*
tinsel flagellum, 7–*8*
tintinnid grazing, 513
Tolypothrix, 42; *tenuis*, *73*
torbonite, 210
toxic algae, **504–10**; Dinophyta, **279–84**; Prymnesiophyta, **496–7**
Toxoplasma, 311
trabeculae, *Caulerpa*, 185
Trachelomonas, 247, 253, 255; *grandis*, *257*; *lefeveri*, *254*
Trailiella, *96*
translocation of nutrients, 441, 466
Trebouxia, 143, **217**; *erici*, **218**
Trebouxiales, 191, 211, **217–18**
trehalose, 22; and halotolerance, 64

trellisoid ornamentation, *370*, 383, 399, 403
Trentepholia, 217
Tribonema, 413, 415–16, 418; *bombycinum*, *414*; *regulare*, *414*; *utriculosum*, *414*; *viridae*, *414*
Tribonematales, 416, **418**
Tribophyceae, 413
tricarboxylic acid cycle, 55
Triceratium, *370*
Trichodesmium, 42, 51, **60–1**, 65, 72; *lacustre*, *52*, *71*
trichoblast, *128–30*
trichocyst, Dinophyta, 263, **275–7**, 324; Raphidophyceae, *410*, 412
Trichodesmium, 509
trichogyne, **102–4**, *113*, 115–*16*, *119*, 120–*1*, 124, *128*, 130
trichome, 33, 53
trichothallic growth, 431, 433–4, 436, 439, 441–2, 448, 472
Tridachia, 183
Triparma, 344–5; *laevis*, *345*; *stigmata*, *345*
Triticum, 275
trumpet hyphae, 441, *450*
trypanosomes, 245, 248
tubulin, 4
twitching, cyanobacteria, 36

Udotea, 180, 185; *conglutinata*, *182*
Ulothrix, 141, 143, 145, 155, **168–9**; *zonata*, *169*
Ulotrichales, 139, 144, **168–9**
ultraplankton, 365
ultraviolet radiation, 517
Ulva, *141*, **169–73**; *arasaki*, *171*; *intestinalis*, *171*; *lactuca*, *5*,*6*; *lobata*, 170; *mutabilis*, 170; *pertusa*, 170
Ulvales, **168–73**
Ulvophyceae, 144–*49*, **168–89**, 217
unilocular sporangia, 345, *426–7*, **431**, 434, 436–*8*, *440*, 442–*5*, 448, 452–4, 456
upwelling, 513
urea, 144, 149; amidolyase, 144–5, 149, 190
urease, 144–5, 149
Uroglena, 340, 342; *conradii*, *341*
Urospora, 473
utricles, *Codium*, 181; *Halimeda*, 184

Vacuolaria, 412; *virescens*, 410
Valonia, 188; *ventricosa*, *189–90*
valve, Bacillariophyceae, 369
Vaucheria, 413, 416, *418–19*, 422, 433; chloroplast DNA, 14; *dillwynii*, *419*; *sessilis*, *420*; *synandra*, *421*
Vaucheriales, 416, **418–22**
vaucheriaxanthin, 355, 415
velum, Bacillariophyceae, 372
Ventricaria ventricosa, *189–90*
Verrucaria, 57, 59
vesicular cells, Rhodophyta, *95*, *96–7*
vestibulum, Cryptophyta, 327
violaxanhin, 345, 355, 358
viridene, 441
Viridiplantae, 144
vitamins, 115, 255
volatile organic compounds, cyanobacteria, **66**
volutin granule, 40
Volvocaceae, 191, **198–208**
Volvocales, 22, 139, 143–4, 151–2, **191–208**
Volvox, *140*, **198–208**; *carteri*, 141, 143, *201–3*
volvoxopsin, 141
Volvulina, 199; *steinii*, 200
von Stosch, H. A., 303

Warnowiaceae, 273
water quality, Chrysophyceae, 340; cyanobacteria, **66**
water stress protein, 62
whiplash flagellum, 7–*8*
Woloszynskia coronata, 272; *tenuissima*, *273*; *tylota*, 276, 278
wound response, Chlorophyta, 174, 187

Xanthidium antilopaeum, *160*
Xanthophyceae, 57, 217–18, 354, 359, **413–23**; chloroplast, 14; paramylon, 21
xanthophylls, 16–17, 250, 322, 410
Xanthoria parietina, *217*
xylans, 10; Chlorophyta, 139, 178, 188; Rhodophyta, 90, 114

yessotoxin, 279, 504, *508*

Zanardina, 436
zeaxanthin, 358
zebra mussel, *66*
Zhao, J., *74*
zoospores, 143, 152–*3*
zooxanthellae, Dinophyta, 58, **295–6**; storage product, 22
Zostera marine, 365
Zygnemataceae, **156–8**
Zygnematales, 143–4, **155–62**
Zygogonium, 156
zygospore, Chlorophyta, 155, 157–*8*, *161*, *183*, *196*, *203*, 208, 215

HEAVY METALS POISONING IN ANIMALS

"Heavy Metals" are chemical elements with a specific gravity that is at least 5times the specific gravity of water.

e.g , arsenic, chromium, cobalt, copper, gallium, gold, iron, lead, mercury, nickel, platinum, silver, tellurium, thallium, aluminum, uranium, and beryllium .

In general heavy metals produce their toxicity by forming complexes or "Ligand" with organic compounds.

These modified biological molecules lose their ability to function properly ,and result in malfunction or death of the affected cells.

The most common groups involved in ligand formation are oxygen ,Sulfur, and nitrogen .

When metals bind to these groups they may inactive important enzyme systems ,or affect protein structure.

- 1-Arsenic Poisoning
- -Duration of exposure. Sources of poisoning: Poisoning occurs due to
- arsenic trioxide, arsenic pentoxide, sodium and potassium arsenite.
- Toxicokinnetics:-
- After absorption, arsenic is distributed throughout the body but tends to
- accumulate in the liver and kidneys.
- In domestic animals, arsenic does not stay in soft tissues for long period.
- It is rapidly excreted in bile, milk saliva, sweat and urine and faeces.
- After chronic exposure the poison stays in bones, skin and keratinized
- tissues. Such as hoof and hair .
- Arsenic does not cross the blood brain barrier.
- Milk that is poisoned by arsenic can be toxic to humans.

- Clinical Signs:
- Acute: diarrhea, severe colic, dehydration, weakness,
- depression, weak pulse, cardiovascular collapse.
- 2-Lead Poisoning
- In Veterinary Medicine, lead is one of the most common causes of
- metallic poisoning in dogs and cattle.
- Only 1-2% of the ingested lead may be absorbed. The organic form of
- lead could penetrate intact skin. Organic forms are tetraethyl lead and
- tetramethyl lead.
- Sources of poisoning:-
- Animals may ingest lead-based paints.
- Lead tetroxide, carbonate, or sulphate
- Engine oil and lead battery improperly disposed
- Animals feed agents sprayed with lead insecticides (lead
- arsenate

- Toxicokinetics;-
- Lead salts are sparingly soluble
- Absorption of lead from GIT is very limited (1-2%) and therefore about 98% of lead is eliminated in faeces.
- Clinical Signs:
- In cattle, GIT and nervous signs after 24hours of exposure to toxicity
- blindness, salivation, jaw champing, tremor convulsion.رعاش.

- **3-Mercury poisoning :**
- **Mercury can combine with a methyl group to become methyl mercury .**
- **this form found in environmental pollution and produce toxicities.**
- **1-Acute toxicity .**
- **2-Chronic toxicity .**
- **In acute toxicity: affect GIT , break down barriers in capillaries, and**
- **neurological toxicities .**
- **In chronic toxicity: CNS affect ,bone , jaw, teeth , liver and kidney.**
- **Treatment:-**
- **EDTA and Penicillamine.**

- 4-Cadmium poisoning :
- Mechanism of toxicity .
- Free cadmium binds to protein sulfhydryl groups ,disrupting the cellular redox cycle ,.
- Toxicokinetic .
- Concentrations of cadmium in liver and kidney but muscle ,and bone do not accumulate high concentrations of cadmium.
- Blood cadmium concentrations are indicators of recent exposure.
- Treatment:-
- Metal chelators and Zinc useful for protection.

- 5-Cooper poisoning :
- Acute poisoning and chronic poisoning .

- Acute poisoning:
- is usually seen after accidental administration and
- cause sever gastroenteritis characterized by abdominal pain ,diarrhea,
- dehydration and shock.
- Hemolysis and hemoglobinuria may develop after 3 days .
- Chronic poisoning :
- is most commonly in sheep when excessive amounts
- of copper ingested for prolonged period.
- Mechanism of toxicity:
- Blood copper concentrations increases suddenly ,causing lipid
- peroxidation and intravascular hemolysis .
- Liver enzymes including ALT and AST are usually increased

- Animal Toxins :
- 1- Snake venoms:
- Snake bites are one of the most common forms of poisoning by natural toxins worldwide. Many snake venoms are being mixtures of proteins or polypeptides. The proteins may be enzymes, especially hydrolytic enzymes. Some of the more important are proteinases, phospholipases, ribonucleases, deoxyribonucleases, phosphomonoesterases and phosphodiesterases, and ATPases.

- Venom characteristics: It is thought that neurotoxin consists of two active principles,
- 1--cause paralysis of the respiratory system and the other
- 2-----causes the failure of the cardiac movement. Mechanism of action: At least four toxic actions can result from snake venom. Different snakes have different combinations of toxins in their venom.

- The toxins consist:
- 1-necrotizing coagulant portions .
- 2-- neurotoxic and
- 3--hemolytic fractions.
- The effect of snake bite is dependent on the size and species of snakes, the size of bitten animal and the location of the bite particularly with reference to the thickness of the hair coat and the quality of subcutaneous fat.
- The neurotoxins cause initial stimulation of the CNS followed by paralysis. Effect of the other toxins cause local tissue necrosis, capillary damage and hemolysis.

- Clinical signs:
- a))
- Large animals: snake bites cause a local swelling, severe pain, excitement and anxiety. The bites in the head causes severe swelling that cause difficult respiration.
- Other symptoms include pupil dilatationتوسع حدقة العين, excessive salivation, hyperesthesia, tetany, depression leading to paralysis.
- Cobra bite causes excitement with convulsion and death due to asphyxia.
-

Treatment:

a) Local treatment: application of a tourniquet above the bite to restrict the venom but not the arterial circulation.

The bitten area should be removed through cut (0.5 inch length × 0.5 inch depth). The incised wound should be squeezed and suction applied for 10-30 minutes. The oral suction is not recommended.

b) Systemic treatment:

1) Antivenin: It is greatly reduces the tissue necrosis. It is best administered if diluted with 500-1000 ml of 5% dextrose solution i.v.

2) Antibiotic: Broad spectrum antibiotics are indicated to bacterial infections.

3) Antitoxin: Clostridial bacteria have isolated from the snake mouth. The dose of antitetanus serum 1500-3000 I.U. .

4) Anti-inflammatory: Cortisone is valuable drug and renders a protection against possible anaphylaxisالحساسية المفرطة after the treatment.

c) Supportive therapy:

- Fluids are indicated to combat shock and dehydration.
- Epinephrine is also effective in combating shock.
- Pethinidine may be used to alleviate pain or excitement.
- Vitamin C and calcium gluconate are useful in preventing haemolysis.
- Blood transfusion and hemodialysis.

- 2- Bee stings:
- Bee stings are multiple in nature and cause severe local swellings in
- animal. Bee sting in horses cause excitement due to pain and may also
- include diarrhea, hemoglobinuria, jaundice.
- Treatment:
- a) Local application of a week solution of ammonia or sodium
- bicarbonate.
- b) If prostration is severe nervous stimulants may be given.

- **3- Toads:**
- **Toads are not containing poisonous apparatus like snakes. However glands**
- **present in their head secretes various toxins e.g., steroids, bufogenine and**
- **butotoxin which act like digitalis.**
- **Symptoms:**
- **Dogs and cats hat generally attach toad show symptoms of distress and**
- **excessive salivation.**
- **Treatment:**
- **Treatment depends upon species of toads. In case of *Bufo valgaris* no**
- **specific treatment is essential and animal recover quietly.**
- **In case of *Bufo marinas* which cause convulsion and death within 15 minutes.**
- **The following treatment is adopted:**
- **a) Wash the mouth with fresh water.**
- **b) Atropine as a specific antidote s/c.**
- **c) Sodium pentobarbitone is given to control convulsions.**

- **e) Oxygen therapy may be given in severe cases**

Methods of collection of biological samples

The pre-analytical phase for samples collected for the analysis of therapeutic drugs and toxins is as critical as the analytical phase.

One of the most important aspects to this phase is the knowledge of the time at which the sample was collected and its relationship to the time of dosing or ingestion.

These information are necessary for interpretation of the results.

In addition, samples must be collected using the suitable devices and processed or stored under conditions that minimize alterations to the drug concentration.

- Whole blood, plasma (the fluid obtained on centrifugation of anticoagulated whole blood), or serum (the fluid remaining when blood has clotted) are widely used in clinical work.
- This is because not only is blood relatively easy to collect, but also a quantitative analysis can often give useful information as to the size of exposure and hence the severity of poisoning.
- Excretions (exhaled air, urine) or secretions (saliva, bile) are often less useful as regards understanding of quantitative data, but can be very useful in qualitative work.

Sample requirements for general analytical toxicology

Sample	notes
Whole blood *or*	10 mL (lithium heparin or EDTA tube – use fluoride/oxalate if ethanol suspected; plastic tube if paraquat suspected; glass or plastic tube with minimal headspace if carbon monoxide or other volatiles suspected)
Plasma/serum	5mL(send whole blood if volatiles, metals and some other compounds suspected
Urine	20–50 mL plain bottle, no preservative(مادة حافظة
Gastric contents	25–50 mL plain bottle, no preservative
Other samples	Vitreous humour (maximum available, collect separately from both eyes), bile (2 mL) or liver (about 5 g) can substitute for urine in postmortem work. Other tissues (brain, liver, kidney, lung, subcutaneous fat – 5 g) may also be valuable, especially if organic solvents or other volatile poisons are suspected

Documentation

- Information recorded on the sample container at the time the sample is collected should include the names (first and family or last name), patient/subject/animal number, the date and time of collection, collection site, and the sample type (including a note of any preservative), and any other suitable information.
- The date and time of receipt of all specimens by the laboratory should be recorded and a unique identifying number assigned in each case

CONTAINERS

- Most laboratories have also transitioned from glass tubes to plastic for safety reasons.
- All organ and tissue samples, and any tablet bottles or scene residues, should be placed in separate containers to avoid any chance of cross contamination.

- Plastic tubes are thus favored and are also less likely to shatter than glass, especially if frozen.
- On the other hand, if volatile solvents or anaesthetic gases, for example, are to be analyzed then glass is preferred if available
- This should be followed by gentle mixing to ensure contact with the anticoagulant if one is being used.
- Biological specimens should be stored at 4 ◦C before transport to the laboratory in general.
- Any residual specimen should be kept at −20◦C or below until investigation of the incident has been concluded.
- Exceptions to this include hair and nail, which are stable at room temperature.

Clinical sample types

Clinical samples can be divided into:

- blood and related fluids
- body fluids other than blood
- excretory fluids/residues
- other clinical specimens

Blood and related fluids .1

Arterial blood –

Venous blood –

Serum –

Plasma –

Blood cells –

- In analytical toxicology, plasma or serum is normally used for quantitative assays.
- However, some poisons such as carbon monoxide, cyanide and many other volatile organic compounds, lead and other heavy metals, and some drugs, such as chlortalidone, are found primarily in or associated with erythrocytes and thus haemolyzed whole blood should be used for such measurements.
- The space above the blood in the tube ('headspace') should be minimized if carbon monoxide, solvents, or other volatiles are suspected.

Clinical sample types

Serum

- When whole blood is allowed to stand (15 min, room temperature) in a plain tube (no anticoagulant) a clot forms that will retract sufficiently to allow serum to be collected.
- For many analyses serum is preferred to plasma because it produces less precipitate (of .fibrin) on freezing and thawing

Plasma

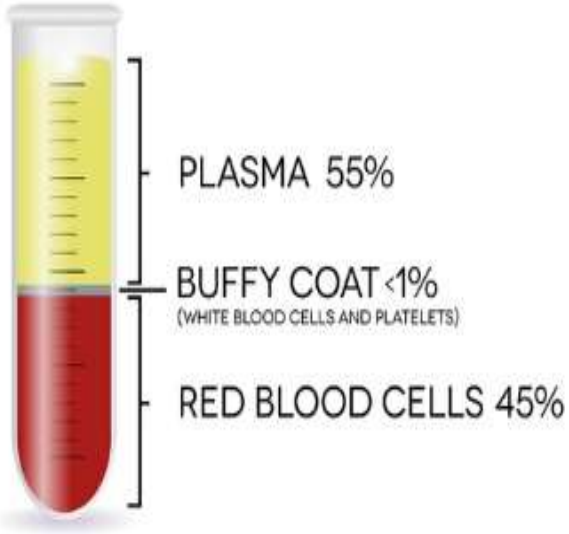
- The use of such tubes will invalidate many trace element analyses and may impair analyses for solvents and other volatiles.

سيؤدي استخدام هذه الأنابيب إلى إبطال العديد من تحليلات العناصر النزرة وقد يضعف تحليلات المذيبات والمواد المتطايرة الأخرى

Blood cells

- To collect erythrocytes, heparinized blood should be centrifuged (2000 *g*, 10 min), the plasma, buffy coat and top 10% of erythrocytes (mainly reticulocytes) removed, and the remaining erythrocytes carefully washed with isotonic,

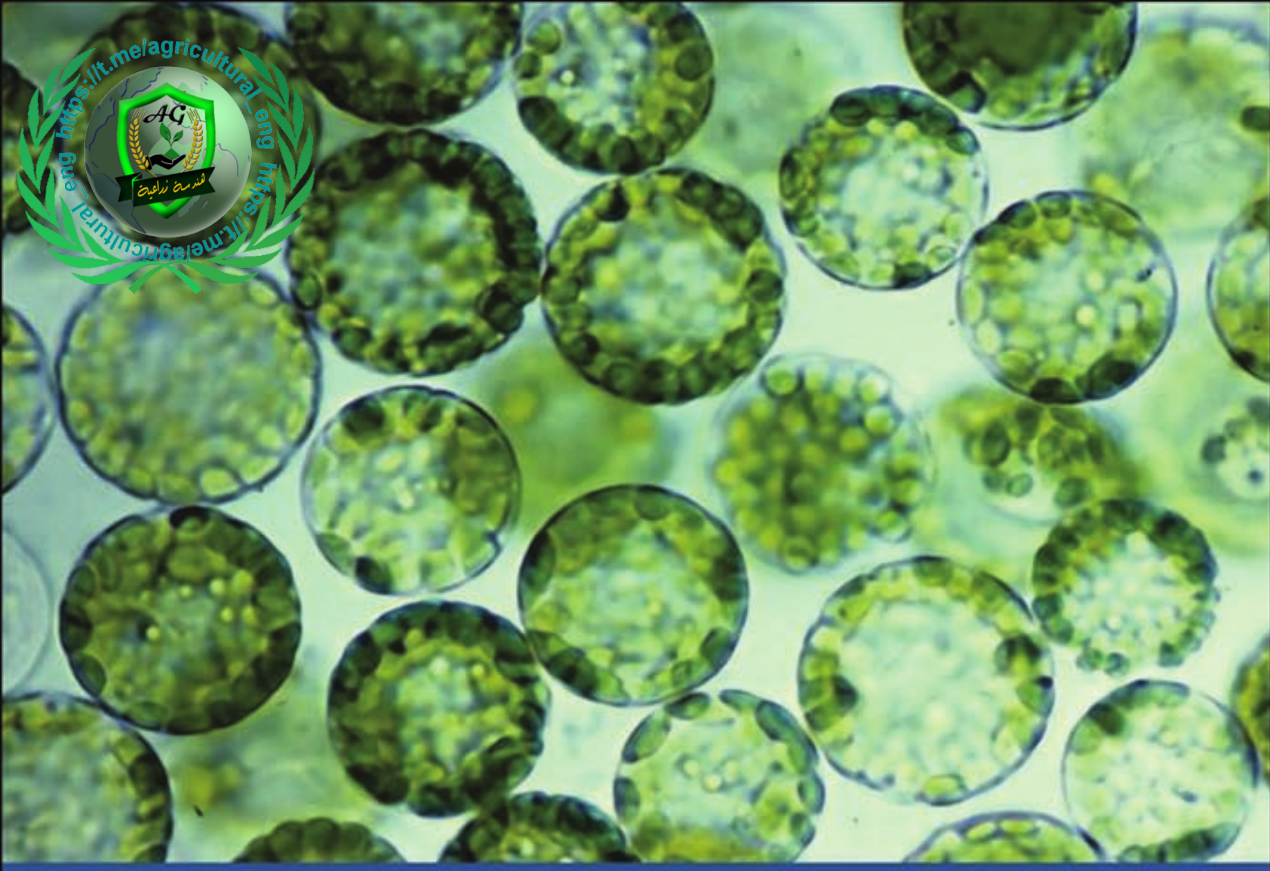
remove trapped plasma.



Urine.2

- Urine is useful for ‘poisons screening’ as it is often available in large volumes and may contain higher concentrations of drugs or other poisons, or metabolites, than blood.
- The presence of metabolites may sometimes assist identification of a poison if chromatographic techniques are used
- A 50mL specimen from an adult, collected in a sealed, sterile container, is sufficient for most purposes.

https://t.me/agricultural_eng



Plant Cell Culture

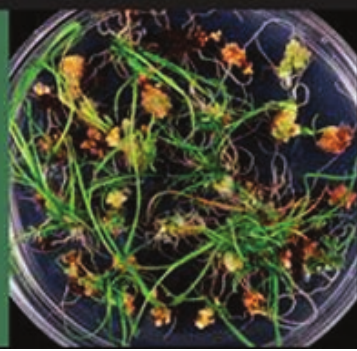
Essential Methods

Michael R. Davey and Paul Anthony

WILEY-BLACKWELL

https://t.me/agricultural_eng

@AGRICULTURAL_ENG



Plant Cell Culture

Essential Methods

Michael R. Davey and **Paul Anthony**

Plant and Crop Sciences Division
School of Biosciences
University of Nottingham
Sutton Bonington Campus
Loughborough, UK

WILEY-BLACKWELL
A John Wiley & Sons, Ltd., Publication

1
Plant Micropropagation

Ivan Iliev[1], Alena Gajdošová[2], Gabriela Libiaková[2] and Shri Mohan Jain[3]*

[1]*Faculty of Ecology and Landscape Architecture, University of Forestry, Sofia, Bulgaria*
[2]*Institute of Plant Genetics and Biotechnology SAS, Nitra, Slovakia*
[3]*Plant Breeding Unit, International Atomic Energy Agency, Laboratories Siebersdorf, Vienna, Austria*
**Current address – Department of Applied Biology, University of Helsinki, Helsinki, Finland*

1.1 Introduction

The technique of plant tissue culture is used for growing isolated plant cells, tissues and organs under axenic conditions (*in vitro*) to regenerate and propagate entire plants. 'Tissue culture' is commonly used as a blanket term to describe all types of plant cultures, namely callus, cell, protoplast, anther, meristem, embryo and organ cultures [1]. It relies on the phenomenon of cell totipotency, the latter being the ability of single cells to divide, to produce all the differentiated cells characteristic of organs, and to regenerate into a whole plant. The different techniques of culturing plant tissues may offer certain advantages over traditional methods of propagation. Growing plants *in vitro* in a controlled environment, with in-depth knowledge of the culture conditions and the nature of the plant material, ensures effective clonal propagation of genetically superior genotypes of economically important plants. Tissue cultures represent the major experimental systems used for plant genetic engineering, as well as for studying the regulation of growth and organized development through examination of structural, physiological, biochemical and molecular bases underlying developmental processes. Micropropagation has become an important part of the commercial propagation of many plants [2–6] because of its advantages as a multiplication system [7–9]. Several techniques for *in vitro* plant propagation have been devised, including the induction of axillary and adventitious shoots,

Plant Cell Culture Edited by Michael R. Davey and Paul Anthony
© 2010 John Wiley & Sons, Ltd.

the culture of isolated meristems and plant regeneration by organogenesis and/or somatic embryogenesis [10–12].

Fertile plants can be regenerated either by the growth and proliferation of existing axillary and apical meristems, or by the regeneration of adventitious shoots. Adventitious buds and shoots are formed *de novo*; meristems are initiated from explants, such as those of leaves, petioles, hypocotyls, floral organs and roots.

This chapter summarizes the application of the most commonly used *in vitro* propagation techniques for trees, shrubs and herbaceous species that can be implemented on a continuous basis throughout the year.

1.2 Methods and approaches

1.2.1 Explants and their surface disinfection

Small pieces of plants (explants) are used as source material to establish cells and tissues *in vitro*. All operations involving the handling of explants and their culture are carried out in an axenic (aseptic; sterile) environment under defined conditions, including a basal culture medium of known composition with specific types and concentrations of plant growth regulators, controlled light, temperature and relative humidity, in culture room(s) or growth cabinet(s). The disinfection of explants before culture is essential to remove surface contaminants such as bacteria and fungal spores. Surface disinfection must be efficient to remove contaminants, with minimal damage to plant cells. This chapter focuses on the general procedures for developing *in vitro* cultures, illustrated by protocols for specific plants and explants.

PROTOCOL 1.1 Surface Disinfection of Explants

Equipment and Reagents

- Autoclave
- Laminar flow cabinet
- Ultraviolet lamp
- Scalpels, forceps, scissors, rest for supporting axenic instruments (Duchefa), glass beakers (100 ml), glass Petri dishes (100 × 15 mm), white cotton gauze[a] (15 × 15 cm), magnetic mini-stirrer (ScienceLab) and stirring bars, filter paper (Whatman, Standard Grade; 10 mm diameter circles), aluminium foil, funnel and suction flask, glass beakers (100 ml–1 l in volume).
- Unifire Gasburner (Uniequip), glass bead sterilizer (Duchefa) or alcohol lamp
- Distilled water: 350 ml aliquots in 500 ml bottles
- Tween 20 (Sigma)
- Ethanol: 95 and 70% (v/v)
- NaClO or $Ca(ClO)_2$: 0.5–5% or 3–7% (w/v) aqueous solutions, respectively (Chemos GmbH)

- $HgCl_2$ (Sigma): 0.1–0.2% (w/v) aqueous solution[b]
- H_2SO_4: 96% (v/v) solution[c]
- Bacteriocidal soap
- Culture vessels with sterile culture medium (See Protocol 1.2 for preparation of culture medium).

Method

1 Place several filter papers into each of the glass Petri dishes. Wrap the Petri dishes, glass beakers, scissors, scalpels, forceps, funnel, white gauze and suction flask in aluminium foil.

2 Disinfect the material from Step 1 and bottles of distilled water in an autoclave at 120 °C, 118 kPa (1.18 bar) steam pressure for 20 min.

3 Disinfect the laminar flow cabinet by exposing the work bench to ultraviolet illumination for 3 h. Spray the work surface of the cabinet with 95% (v/v) ethanol; allow to dry.

4 Remove the epidermis from stem segments and scale leaves from buds of woody species[d].

5 Wash the explants under running tap water for 5 min.

6 Wash hands thoroughly with bacteriocidal soap before commencing work.

7 Disinfect the explants in the laminar flow cabinet. Place the explants in a beaker (autoclaved). Wash the explants (by stirring on magnetic mini-stirrer) in 70% (v/v) ethanol (2 min) and 5% (w/v) NaClO, containing 20 drops per litre of Tween 20 (15–30 min). After immersion in each solution, wash the explants 3 times with sterile distilled water for 3, 5 and 10 min; discard the washings

8 After surface disinfection, keep the plant material in distilled water in Petri dishes in the laminar flow cabinet to prevent drying.

9 Before preparing the explants, disinfect the forceps and scalpels using a glass bead sterilizer, Unifire Gasburner, or by flaming using the alcohol lamp for 10–15 s.

10 Remove the cut ends of the explants[e] (e.g. apical or axillary buds, leaves, petioles, flowers, seedling segments) with a sterile scalpel before placing the explants on the culture medium.

Notes

[a]Place small plant parts, such as tiny seeds or buds, into gauze bags to facilitate manipulation during disinfection.

[b]Mercuric chloride ($HgCl_2$) is a highly effective surface sterilant but is extremely toxic. Local regulations must be enforced with its use. The duration of surface disinfection in 0.1% (w/v) aqueous solution is 1–3 min for leaves and stems of herbaceous plants, 8–10 min for nodal and apical segments of woody plants, and 10–20 min for seeds.

[c]Use for 4–5 min to disinfect seeds with a hard testa.

[d]Removal of the epidermis from the stem segments and scale leaves from buds may increase the disinfection efficiency in woody species.

[e]Cut the ends of the explants in the laminar flow cabinet on sterile filter papers or on a sterile white tile.

1.2.2 Culture media and their preparation

Culture media contain macroelements, microelements, vitamins, other organic components (e.g. amino acids), plant growth regulators, gelling agents (if semisolid) and sucrose. Gelling agents are omitted for liquid media. The composition of the culture medium depends upon the plant species, the explants, and the aim of the experiments. In general, certain standard media are used for most plants, but some modifications may be required to achieve genotype-specific and stage-dependent optimizations, by manipulating the concentrations of growth regulators, or by the addition of specific components to the culture medium. Commercially available ready-made powdered medium or stock solutions can be used for the preparation of culture media. A range of culture media of different formulations, and plant growth regulators are supplied by companies such as Duchefa and Sigma-Aldrich. Murashige and Skoog medium (MS) is used most extensively [13]. A procedure for the preparation of MS medium supplemented with plant growth regulators for raspberry micropropagation [14] is given in Protocol 1.2.

PROTOCOL 1.2 Preparation of Culture Medium

Equipment and Reagents

- Culture vessels: 25 × 150 mm sterile plastic disposable culture tubes with screw-caps (Sigma-Aldrich), Full-Gas Microbox culture jars (jar and lid OS60 + ODS60; Combiness), Erlenmeyer 'Pyrex' flasks 125 ml capacity (Sigma-Aldrich) or Petri dishes (60 × 15 mm or 100 × 15 mm; Greiner Bio-One). Glass Petri dishes, if used, must be disinfected by autoclaving or dry heat treatment
- Autoclave
- Laminar flow cabinet
- Refrigerator/freezer
- Distilled water (water purification system)
- Electronic heated stirrer
- Analytical balances
- pH meter
- Microwave oven
- Pipettes and measuring cylinders

- Beakers, 100 ml and 1–2 l, 100 ml flasks, funnels, aluminium foil
- PP/PE syringes without needles, capacity 50 ml (Sigma-Aldrich)
- Acrodisc syringe membrane filters (25 mm, 0.2 μm pore size; Sigma-Aldrich)
- 1 M HCl and KOH
- MS packaged powdered medium, including macro and microelements and vitamins (Duchefa)
- Plant growth regulators for raspberry micropropagation: benzylaminopurine (BAP) and β-indolebutyric acid (IBA; Duchefa)
- Other plant growth regulators: auxins – naphthaleneacetic acid (NAA), indole-3-acetic acid (IAA), 2,4-dichlorophenoxyacetic acid (2,4-D); cytokinins – kinetin, zeatin, 6-γ-γ-(dimethylallylamino)-purine (2-iP), thidiazuron (TDZ); gibberellins – gibberellic acid (GA_3); abscisic acid (ABA); organic components – sucrose, plant agar, citric acid, ascorbic acid (Duchefa)
- Plant preservative mixture – PPM (Plant Cell Technology, Inc.).

Method

1 To prepare 1 l MS medium, dissolve 4.406 g powdered medium in 500 ml of double distilled water in a 2 l beaker.

2 Prepare separate stock solutions of each plant growth regulator.

3 Add heat stable supplements to the medium before autoclaving, such as 30 g sucrose, 8 g agar, the desired plant growth regulators in a specific volume of stock solution (e.g. 5 ml BAP and 5 ml IBA) to reach the required final concentrations (1 mg/l BAP and 0.1 mg/l IBA for raspberry micropropagation). Adjust the medium to the final volume (1 l) by adding double distilled water[a].

4 Adjust the pH of the medium to 5.6–5.8 with 1 M HCl or KOH[b] and heat in microwave oven until the gelling agent is dissolved.

5 Autoclave the medium at 1 kg/cm (15 psi) at 121 °C for 20 min[c].

6 Dispense the medium into the culture vessels (15 ml per culture tube, 50 ml per Erlenmeyer bank, 50 ml per Full-Gas Microbox culture jar, 30 ml per 9 cm Petri dish) in the laminar flow cabinet. Close the vessels.

Preparation of Stock Solutions

1 Prepare separate stock solution for each plant growth regulator. Weigh the plant growth regulators to obtain a quantity 20 times the quantity given in the formulation for the medium (e.g. 20 mg BAP and 2 mg IBA), and dissolve in 100 ml distilled water[d].

2 Dissolve auxins (NAA, IAA, IBA and 2,4-D) in 1 ml ethanol and make up to 100 ml with distilled water.

3 Dissolve cytokinins (kinetin, zeatin, BAP, 2-iP) and ABA in 1 ml 1 M NaOH or 1 M KOH; make up to 100 ml with distilled water.

4 Store the stock solutions in 100 ml flasks in a refrigerator (not frozen) for not more than 2 months[e].

Filter Sterilization of Heat Sensitive Compounds

1 Wrap a funnel and 100 ml flask in aluminum foil and autoclave.

2 Fill the PP/PE syringe with the solution of heat labile constituents (e.g. zeatin, 2-iP, IAA, GA_3, citric acid, ascorbic acid). Mount an Acrodisc syringe membrane filter on the syringe and filter the solution into the funnel and into a sterile flask. Dispense the filter sterilized solution into convenient aliquots (e.g. 10–20 ml) in sterile, screw-capped vessels. Perform this operation in a laminar flow cabinet. Store the filter sterilized solutions at −20 °C.

Notes

[a]Heat labile constituents, such as some growth regulators and organic compounds (e.g. zeatin, 2-iP, IAA, GA_3, citric acid, ascorbic acid), should not be autoclaved but filter sterilized before adding to the autoclaved culture medium after the medium has cooled to 40–50 °C in the laminar flow cabinet.

[b]The pH of the culture medium is usually adjusted to 5.6–5.8. For acid-loving species, a lower pH is required (4.5 or less).

[c]To minimize contamination by micro-organisms, a broad-spectrum biocide/fungicide for plant tissue culture [Plant Preservative Mixture (PPM); Plant Cell Technology, Inc.] may be added to the medium at a concentration of 2–20 ml/l, which effectively prevents or reduces microbial contamination. Some plant species are more sensitive to PPM than others. Rooting in less tolerant plant species may be partially inhibited. In this case, the explants should be exposed to PPM for only a limited time.

[d]Cytokinins (BAP, kinetin, 2-iP, zeatin) are added to the culture medium to induce axillary or adventitious shoots. Auxins (2,4-D, NAA, IAA) induce callus formation. IBA is generally used to induce adventitious roots. GA_3 or polyamines added to the medium will promote shoot elongation.

[e]Culture media should be used within 2 to 4 weeks of preparation and may be kept for 6 weeks before use, if refrigerated.

1.2.3 Stages of micropropagation

The following distinct stages are recognized for the micropropagation of most plants:

Stage I: Establishment of axenic cultures – introduction of the surface disinfected explants into culture, followed by initiation of shoot growth. The objective of this stage is to place selected explants into culture, avoiding contamination and providing an environment that promotes shoot production [15]. Depending on the type of explant, shoot formation may be initiated from apical and axillary buds

(pre-existing meristems), from adventitious meristems that originate on excised shoots, leaves, bulb scales, flower stems or cotyledons (direct organogenesis), or from callus that develops at the cut surfaces of explants (indirect organogenesis). Usually 4–6 weeks are required to complete this stage and to generate explants that are ready to be moved to Stage II [16]. Some woody plants may take up to 12 months to complete Stage I [15], termed 'stabilization'. A culture is stabilized when explants produce a constant number of normal shoots after subculture [16].

Stage II: Multiplication – shoot proliferation and multiple shoot production. At this stage, each explant has expanded into a cluster of small shoots. Multiple shoots are separated and transplanted to new culture medium [16]. Shoots are subcultured every 2–8 weeks. Material may be subcultured several times to new medium to maximise the quantity of shoots produced.

Stage III: Root formation – shoot elongation and rooting. The rooting stage prepares the regenerated plants for transplanting from *in vitro* to *ex vitro* conditions in controlled environment rooms, in the glasshouse and, later, to their ultimate location. This stage may involve not only rooting of shoots, but also conditioning of the plants to increase their potential for acclimatization and survival during transplanting. The induction of adventitious roots may be achieved either *in vitro* or *ex vitro* in the presence of auxins [17–19]. The main advantage of *ex vitro* compared to *in vitro* rooting is that root damage during transfer to soil is less likely to occur. The rates of root production are often greater and root quality is optimized when rooting occurs *ex vitro* [20–23].

Stage IV: Acclimatization – transfer of regenerated plants to soil under natural environmental conditions [16]. Transplantation of *in vitro*-derived plants to soil is often characterized by lower survival rates. Before transfer of soil-rooted plants to their final environment, they must be acclimatized in a controlled environment room or in the glasshouse [24, 25]. Plants transferred from *in vitro* to *ex vitro* conditions, undergo gradual modification of leaf anatomy and morphology, and their stomata begin to function (the stomata are usually open when the plants are in culture). Plants also form a protective epicuticular wax layer over the surface of their leaves. Regenerated plants gradually become adapted to survival in their new environment [26].

1.2.4 Techniques of micropropagation

Cultures of apical and axillary buds

Currently, the most frequently used micropropagation method for commercial mass production of plants utilizes axillary shoot proliferation from isolated apical or axillary buds under the influence of a relatively high concentration of cytokinin. In this procedure, the shoot apical or axillary buds contain several developing leaf primordia. Typically, the explants are 3–4 mm in diameter and 2 cm in length. Development *in vitro* is regulated to support the growth of shoots, without adventitious regeneration.

PROTOCOL 1.3 Propagation by Culture of Apical and Axillary Buds

Equipment and Reagents

- Culture facilities – culture room or plant growth cabinet with controlled temperature, light and humidity; culture vessels
- Laminar flow cabinet, ultraviolet lamp
- Scalpels, forceps, scissors, a rest for holding sterile tools (Duchefa), 50 ml beakers
- Unifire Gasburner (Uniequip), glass bead sterilizer (Duchefa) or glass alcohol lamp
- Ethanol 70% and 95% (v/v); Tween 20 (Sigma); NaClO (Chemos GmbH); $HgCl_2$ (Sigma)
- Bacteriocidal soap
- Murashige and Skoog medium (MS-Duchefa)
- Anderson's Rhododendron medium (AN-Duchefa)
- Plant growth regulators and organic components: BAP, 2-iP, zeatin, TDZ, adenine sulfate, NAA, IAA, IBA, sucrose, agar
- Distilled water
- Activated charcoal (Duchefa)
- Commercial plastic multi-pot containers (pot diam. 40 mm) with covers
- Peat, perlite, vermiculite

Method

Explant selection and disinfection:

1 Select the explants as single-node segments, preferentially from juvenile[a], rejuvenated plants[b,c], or *in vitro*-derived plants.

2 For commercial large-scale micropropagation, it is preferable to use pathogen-indexed stock plants as a source of explants.

3 See Protocol 1.1 for surface disinfection of explants.

Establishment of cultures:

1 Place isolated disinfection apical and axillary buds, from which the upper scale leaves have been removed, on culture medium (MS-based medium for *Lavandula dentata* L. and AN medium for *Vaccinium corymbosum* L.). See Protocol 1.2 for preparation of culture media. Carry out these operations in a laminar flow cabinet after UV and ethanol disinfection (See Protocol 1.1).

2 Add cytokinins to the medium to induce axillary shoots: BAP (0.01–5 mg/l), 2-iP (0.01–10 mg/l), zeatin (2–15 mg/l), TDZ (0.01–10 mg/l), adenine sulfate (40–120 mg/l). Add auxins (NAA, IAA, IBA) in low concentrations (0.01–0.1 mg/l) to

the medium to support shoot growth[d]. Optimize experimentally the cytokinin and auxin types and concentrations for each species[e].

3 Culture the explants for 4 weeks on cytokinin-containing medium in the growth cabinet at 23 ± 2 °C with a 16 h photoperiod (50 μmol/m^2/s; white fluorescent lamps).

Shoot multiplication:

1 Separate *in vitro* regenerated axillary shoots and transfer the shoots onto the appropriate culture medium (MS medium for *L. dentata* and AN medium for *V. corymbosum*) supplemented with the same or a reduced cytokinin concentration.

2 Cut the regenerated shoots into one-node segments and culture on cytokinin-supplemented medium to stimulate shoot proliferation.

3 Repeat the procedure depending on the number of shoots required. Some of the regenerated shoots *in vitro* can be retained for use to provide an axenic stock of explants for further multiplication.

Rooting of regenerated shoots:

Root the regenerated shoots by two approaches:

1 *Ex vitro* rooting by 'pulse treatment' – immerse the stem bases of 15–20 mm long regenerated shoots into an auxin solution (e.g. IBA at 1–10 mg/l) in 50 ml beakers for 3–7 days, followed by planting in commercial plastic multi-pot containers with soil or a mixture of peat, perlite and vermiculite (equal volumes). Cover the containers and shoots to maintain soil and air humidity.

2 *In vitro* rooting on culture medium supplemented with IBA at a concentration of 1 mg/l and activated charcoal at 1–10 g/l[f]. Reduction of the components of the culture medium to half strength, darkness during culture[g] and inoculation with mycorrhizal fungi[h], may stimulate rooting.

Examples

Micropropagation of *Lavandula dentata* by culture of apical and axillary buds (27).

1 Excise stem segments (each 2–3 cm in length) bearing apical or lateral axillary buds from 5-year-old plants between September and December.

2 Disinfect the stem segments by immersion in 70% (v/v) ethanol for 30 s, and sodium hypochlorite (NaClO) solution (1 g/l) containing 0.01% (v/v) Tween-20 for 20 min; rinse thoroughly with sterile distilled water.

3 Culture the dissected apical and lateral buds vertically on MS culture medium supplemented with sucrose (30 g/l), agar (6 g/l; Merck), cytokinin (BAP; 0.5 mg/l) and auxin (IBA; 0.5 mg/l) at pH 5.6–5.8.

4 Maintain the cultures in the growth cabinet at 25 ± 2 °C under a 16 h photoperiod (50 μmol/m^2/s; white fluorescent illumination).

5 Root the isolated shoots on MS medium supplemented with 0.5 mg/l NAA.

Micropropagation of *Vaccinium corymbosum* by culture of apical and axillary buds [17].

1 Harvest branches with dormant buds from mature donor plants during February and at the beginning of March; cut the branches into single-node segments.

2 Disinfect the segments with apical and axillary buds by washing under running tap water for 1 h, followed by immersion in 70% (v/v) ethanol for 2 min. Transfer the cuttings into 300 ml 0.1% (w/v) mercuric chloride with three drops of Tween for 6 min. Wash the explants thoroughly with sterile distilled water (three changes, each 15 min). Retain all the washings and discard according to local regulations for toxic chemicals.

3 Culture the isolated dormant apical and axillary buds, from which the upper scales are removed after disinfection, on AN medium supplemented with sucrose (30 g/l), Phytoagar (8 g/l) and zeatin (2 mg/l), at pH 4.5–5.0.

4 Maintain the cultures in the growth cabinet at $23 \pm 2\,^{\circ}C$ with a 16 h photoperiod ($50\,\mu mol/m^2/s$, white fluorescent illumination).

5 For further proliferation of *in vitro* regenerated axillary shoots, culture the shoots on the same medium with zeatin (0.5 mg/l) with subculture every 5 weeks.

6 Root the regenerated shoots (each 15–20 mm in height) *ex vitro* by dipping (2–3 min) into IBA solution (0.8 mg/l), followed by planting in commercial plastic multi-pot containers (pot diam. 40 mm) filled with peat-based compost, or *in vitro* on AN medium with IBA (0.8 mg/l) and activated charcoal (0.8 g/l).

Notes

[a]The branches from the basal part of the crown, near to the trunk and highest order of branching, are more juvenile than others in the crown of the plant. More juvenile are epicormics, shoots originating from spheroblasts, severely pruned trees, stump and root sprouts [28].

[b]Rejuvenation may be initiated by grafting scions from mature trees onto juvenile rootstocks. Use explants for culture from trees 1–3 years after grafting [29].

[c]Keeping the cut branches in the sterile liquid medium without growth regulators or in water, in a growth cabinet for 4–5 days, may force the plant material into growth.

[d]Synthetic auxins are more stable and most effective. They include IBA and NAA at 0.1–10 mg/l, 2,4-D at 0.05–0.5 mg/l and the natural auxin IAA (1–50 mg/l). IBA is the most effective auxin for adventitious root induction.

[e]Prepare the MS culture medium with several combinations of growth regulators and grow the same type of explant (dormant bud) for 5 weeks. During testing for the optimal culture medium, change only one factor at a time in the composition of the medium. In order to determine appropriate cytokinin type and concentration for shoot induction, combine different concentrations (0.5, 1, 2, 3 and 5 mg/l) of cytokinins with 0.05 mg/l auxin. Evaluate the number of regenerated shoots and select the most efficient cytokinin concentration. Use the most efficient cytokinin concentration in combination with different auxin concentrations (0.05, 0.1, 0.2, 0.5) to determine the optimal auxin concentration.

[f]For some plants, such as *Sequoiadendron giganteum* and *Fraxinus excelsior*, rooting is optimal by maintaining the shoots in auxin-supplemented medium (induction medium) for 1–5 days, followed by transfer to an auxin-free medium for root formation.

[g]Some plants form roots more rapidly in the dark during auxin treatment.

[h]Mycorrhizae are a close relationship between specialized soil fungi (mycorrhizal fungi) and plant roots. Mycorrhizae may stimulate the rooting of some species [30–34].

Meristem and single- or multiple-node cultures (shoot cultures)

Meristems are groups of undifferentiated cells that are established during plant embryogenesis [35]. Meristems continuously produce new cells which undergo differentiation into tissues and the initiation of new organs, providing the basic structure of the plant body [36]. Shoot meristem culture is a technique in which a dome-shaped portion of the meristematic region of the stem tip is dissected from a selected donor plant and incubated on culture medium [37]. Each dissected meristem comprises the apical dome with a limited number of the youngest leaf primordia[a], and excludes any differentiated provascular or vascular tissues. A major advantage of working with meristems is the high probability of excluding pathogenic organisms, present in the donor plant, from cultures[b]. The culture conditions are controlled to allow only organized outgrowth of the apex directly into a shoot, without the formation of any adventitious organs, ensuring the genetic stability of the regenerated plants.

The single-or multiple-node technique involves production of shoots from cultured stem segments, bearing one or more lateral buds, positioned horizontally or vertically on the culture medium[c]. Axillary shoot proliferation from the buds in the leaf axils is initiated by a relatively high cytokinin concentration[d]. Meristem and node cultures are the most reliable for micropropagation to produce true-to-type plants[e].

PROTOCOL 1.4 Propagation by Meristem and Nodal Cultures

Equipment and Reagents

- Culture facilities (culture room or plant growth cabinet) with automatically controlled temperature, light, and air humidity; sterile disposable Petri dishes (60 and 100 mm; Greiner Bio-One), Full-Gas Microbox culture jars (jar and lid OS60 + ODS60; Combiness)
- Laminar flow cabinet, ultraviolet lamp
- Stereomicroscope
- Unifire Gasburner (Uniequip), glass bead sterilizer (Duchefa) or glass alcohol lamp
- Scalpel, needles, fine tweezers, rest for holding sterile tools (Duchefa)
- Detergent Mistol (Henkel Ibérica, SA), ethanol 70% and 95% (v/v); Tween 20 (Sigma); NaClO (Chemos GmbH); $HgCl_2$ (Sigma)
- 'Keep Kleen' disposable vinyl gloves (Superior Glove Works Ltd.)

- Bacteriocidal soap
- Plant growth regulators and organic components: BAP, GA_3, IBA, myoinositol, sorbitol, thiamine, nicotinic acid, glycine, phloroglucinol, agar, sucrose, ribavirin (Duchefa)
- Double distilled water
- Activated charcoal (Duchefa)
- Quoirin and Lepoivre medium (QL; Duchefa)
- Driver and Kuniyuki medium (DKW; Duchefa)
- Filter paper bridges made from Whatman filter paper[f]

Method

Explant selection and disinfection:

1 Select the explants, single-or multiple-node segments, preferentially from juvenile, rejuvenated plants, *in vitro* derived plants, or branches with dormant buds in the case of woody species.

2 Disinfect the explants according to Protocol 1.1. *In vitro*-derived plants should already be axenic.

Meristem cultures:

1 Isolate the meristems under the stereomicroscope in the laminar hood. Remove the upper leaves from each bud. Hold shoot segments with each bud and carefully remove the remaining leaves and leaf primordia one by one using dissection instruments. Disinfect the equipment (needle, scalpel and tweezers) regularly during this procedure using the gasburner. Excise each meristem (0.1 mm in diam.; 0.2–0.5 mm high) with one to two leaf primordia and transfer to the surface of semi-solid QL culture medium [38].

2 Culture the isolated meristems on semi-solid QL medium, or in the same liquid medium by placing the meristems on semisubmerged filter paper bridges. Use a similar composition of growth regulators as for bud cultures. Determine the optimal types and concentrations of growth regulators for each species.

Nodal cultures:

1 Culture the nodal explants in a vertical or horizontal position on cytokinin-enriched medium (see Protocol 1.3).

2 Avoid inserting the explants too deeply into the medium and submerging the nodes.

3 Culture for 4 weeks on cytokinin-containing medium.

See Protocol 1.3 for shoot multiplication and rooting.

Examples

Micropropagation of *Prunus armeniaca* from cultured meristems [38].

1 Collect branches from adult apricot field-grown trees between January and March, when buds are starting to swell.

2 Cut the shoots into two- or three-nodal sections; wash with water and detergent (e.g. Mistol; Henkel Ibérica, SA), shake for 5 min in 70% (v/v) ethanol and 20 min in a 20% (v/v) solution of sodium hypochlorite (Chemos GmbH; 0.8% final concentration). Wash three times with sterile distilled water.

3 Dissect out buds and meristems from lateral and apical buds perform in a laminar flow cabinet using sterile disposable Petri dishes and steriler instruments. Wearing sterile 'Keep Kleen' disposable vinyl gloves, hold the basal end of the stem; disinfect the instruments frequently. Remove the bark surrounding each bud followed by the outer bud scales; continue until the meristematic dome and a few leaf primordia are exposed. Remove the meristem by cutting its base leaving an explant approx. 0.5–1 mm long with a wood portion that allows further manipulations and culture.

4 Prepare culture medium consisting of QL macro-and micronutrients and vitamins (38), supplemented with myoinositol (50 mg/l), 2% (w/v) sorbitol and semi-solidified with 0.6% (w/v) agar (Hispanlab); adjust the pH to 5.7. In order to induce development of the rosette of leaves, add 0.5–2.0 mg/l BAP. For elongation, add 2.0–4.0 mg/l GA and 0.5–1.0 mg/l BAP.

5 Subculture the meristems to new culture medium every 2 weeks and maintain the cultures in the growth chamber at $23 \pm 1\,^{\circ}C$ under a 16 h photoperiod (55 $\mu mol/m^2/s$, white fluorescent lamps).

6 For proliferation of elongated shoots, transfer the shoots to Full-Gas Microbox culture jars (jar and lid OS60 + ODS60) each containing 50 ml of proliferation medium with QL macronutrients, DKW (38) micronutrients (DKW; Duchefa), sucrose (30 g/l), thiamine (2 mg/l), nicotinic acid (1 mg/l), myoinositol (100 mg/l), glycine (2 mg/l) and the growth regulators 0.04 mg/l IBA and 0.40–0.70 mg/l BAP.

7 Root isolated shoots on medium containing half strength QL macronutrients, DKW micronutrients, sucrose (20 g/l), thiamine (2 mg/l), nicotinic acid (1 mg/l), myoinositol (100 mg/l), glycine (2 mg/l), plus 40 mg/l phloroglucinol and 0.20–0.60 mg/l IBA.

Micropropagation of *Prunus armeniaca* from cultured nodes [38].

1 Excise shoots from rapidly growing branches during spring; remove the expanded leaves.

2 Follow the procedure as described for meristem culture to surface disinfect the explants.

3 Cut nodal explants, each 2 cm long, and culture the explants vertically with the basal end of each node embedded a few mm into the culture medium.

4 For culture establishment, use the same proliferation medium as described for meristem cultures supplemented with BAP (0.4 mg/l) and IBA (0.04 mg/l).

5 Transfer sprouted and elongated shoots to Full-Gas Microbox culture jars (OS60 + ODS60) each containing 50 ml of the same proliferation medium but with 0.04 mg/l IBA and 0.40–0.70 mg/l BAP.

6 Root the isolated shoots in the same way as described for meristem cultures. The original protocols are described by Pérez-Tornero and Burgos [38].

Notes

[a]The size of the isolated explant (meristem only or meristem with leaf promordia) is crucial for survival and regeneration. Meristems alone have less chance of survival. However, obtaining virus-free plants is more probable with only meristems.

[b]To generate virus-free plants, thermotherapy (cultivation for 6 weeks at 35–38 °C) or chemotherapy (treatment with 40 mg/l ribavirin for several weeks) can be used during meristem culture.

[c]Sometimes one dormant bud develops and inhibits elongation of other shoots. In this case, the shoot may be excised and the base recultured. GA_3 at 0.1–10.0 mg/l [39] and activated charcoal at 1–10 g/l [40] is sometimes used to promote shoot elongation [16].

[d]High concentration of cytokinins may induce vitrification (pale and glassy appearance of cultures followed by growth reduction). Vitrification can be prevented by replacing BAP with 2-iP, by reducing chloride, ammonium and/or growth regulator concentrations in the culture medium [42]. Gelrite (Duchefa) should be avoided, but may be used in combination with agar at 3 : 1 (w : w). Vitrification can be prevented by subculture of the shoots from a semi-solid to a liquid medium, by incubating at low temperature (8–10 °C) for 1–2 months, or by increasing the concentration of agar to 0.8–1.0% (w/v) (if the concentration of agar increases, growth may be depressed because of increased osmotic pressure).

[e]During multiplication, off-type propagules sometimes appear, depending on the plant and method of regeneration. Restricting the multiplication phase to three subcultures is recommended to avoid development of off-type shoots in some plants, such as Boston fern (*Nephrolepis exaltata* 'Bostoniensis'). Exploiting procedures that decrease the potential for variability (e.g. reduce the growth regulator concentrations and avoiding callus formation that may result in adventitious shoots) [43]. Sometimes regenerated shoots deteriorate with time, lose their leaves and the potential to grow [44].

[f]Cut the Whatman filter paper into 1.5–2 cm strips and fold over.

Adventitious shoot formation

Adventitious shoot formation is one of the plant regeneration pathways *in vitro*, and is employed extensively in plant biotechnology for micropropagation and genetic transformation, as well as for studying plant development [45]. Adventitious meristems develop *de novo* and *in vitro* they may arise directly on stems, roots or leaf explants, often after wounding or under the influence of exogenous growth regulators (direct organogenesis). Cytokinins are often applied to stem, shoot or leaf

cuttings to promote adventitious bud and shoot formation [46]. Adventitious buds and shoots usually develop near existing vascular tissues enabling the connection with vascular tissue to be observed. Adventitious organs sometimes also originate in callus that forms at the cut surface of explants (indirect organogenesis). Somaclonal variation, which may be useful or detrimental, may occur during adventitious shoot regeneration.

PROTOCOL 1.5 Induction of Adventitious Buds and Shoots

Equipment and Reagents

- Culture facilities (culture room or plant growth cabinet) with automatically controlled temperature, light, and air humidity; sterile disposable Petri dishes (60 and 100 mm, Greiner Bio-One), Full-Gas Microbox culture jars (jar and lid OS60 + ODS60, Combiness)
- Laminar flow cabinet, ultraviolet lamp
- Unifire Gasburner (Uniequip), glass bead sterilizer (Duchefa) or glass alcohol lamp
- Scalpel, fine tweezers, rest for holding sterile tools (Duchefa)
- Plant growth regulators and organic components: zeatin, Plant agar, sucrose, (Duchefa)
- Anderson's Rhododendron medium (AN; Duchefa)

Method

Selection of explants:

1 Excise cotyledons, hypocotyls, petioles, segments of laminae, flower stems of immature inflorescences, or bulb scales, preferentially from *in vitro*-growing plants[a].

2 Disinfect explants according to Protocol 1.1.

Establishment of cultures:

1 Place explants on the AN medium for adventitious shoot regeneration in *Vaccinium corymbosum*. Wounding of the explants using a scalpel may improve adventitious bud regeneration.

2 For the induction of adventitious buds in many plant species, a high cytokinin concentration and low auxin concentration are required in the medium, as in the case for axillary bud induction (see Protocol 1.3). Cytokinins and their concentrations need to be optimized experimentally for each species.

3 Culture for 4 weeks on a cytokinin-rich medium; transfer to medium with a low cytokinin concentration to promote further shoot growth and elongation.

See Protocol 1.3 for shoot multiplication and rooting.

Example

Micropropagation of *Vaccinium corymbosum* by adventitious shoot regeneration [17]:

1 Excise the upper three to four leaves from *in vitro*-grown plants of *V. corymbosum* cv. Berkeley and wound each explant on the midrib using a scalpel held vertically. Place leaf explants with their adaxial surfaces on the culture medium in 60 or 100 mm diam. Petri dishes.

2 Use AN medium with sucrose (30 g/l), plant agar (8 g/l) and zeatin (0.5 mg/l), at pH 4.5–5.0, to induce adventitious buds.

3 After 5 weeks, transfer the explants to AN medium in Full-Gas Microbox culture jars. The medium should be of the same composition and cytokinin concentration as used for shoot regeneration and multiplication.

4 For long-term proliferation of *in vitro* regenerated shoots, maintain material on the same medium containing 0.5 mg/l zeatin and subculture every 4–5 weeks.

5 Increase shoot proliferation by excising regenerated shoots and cutting the shoots into segments, each with one node. Culture the explants on medium with 0.5 mg/l zeatin.

6 Maintain the cultures in the growth cabinet at $24 \pm 2\,^{\circ}C$ under a 16 h photoperiod ($50\,\mu mol/m^2/s$; white fluorescent illumination)[b,c].

7 Use the procedure described in Protocol 1.3 for *ex vitro* or *in vitro* rooting of isolated shoots.

Notes

[a]Juvenile or rejuvenated explants regenerate adventitious shoots more easily than older material.

[b]Light intensity and quality play important roles in adventitious shoot regeneration, mainly during the initiation phase. Keep the cultures in the light during the first 3–5 days to initiate adventitious buds.

[c]A higher temperature (24–25 °C) is favourable for adventitious shoot regeneration in many species.

[d]Rich culture medium (such as MS-based medium) with vitamins, has a stimulatory effect on adventitious shoot regeneration.

Somatic embryogenesis

Somatic embryogenesis was defined by Emons [47] as the development from somatic cells of structures that follow a histodifferentiation pattern which leads to a body pattern resembling that of zygotic embryos. This process occurs naturally in some plant species and can be also induced *in vitro* in others species. There is considerable information available on *in vitro* plant regeneration from somatic cells by somatic embryogenesis. Somatic embryogenesis may occur directly from cells or organized tissues in explants or indirectly through an intermediate callus stage [48, 49, 50].

It has been confirmed in many species that the auxins 2,4-D and NAA, in the correct concentrations, play a key role in the induction of somatic embryogenesis. Application of the cytokinins, BAP or kinetin, may enhance plant regeneration from

somatic embryos after the callus or somatic embryos have been induced by auxin treatment. However, in some species (such as *Abies alba*) cytokinins on their own induce somatic embryogenesis [51].

PROTOCOL 1.6 Induction of Somatic Embryogenesis

Equipment and Reagents

- Culture facilities (culture room or plant growth cabinet) with automatically controlled temperature, light, and air humidity; sterile disposable Petri dishes (60 and 100 mm, Greiner Bio-One), six-well Falcon Multiwell dishes, culture jars such as Full-Gas Microboxes (jar and lid OS60 + ODS60; Combiness)
- Laminar flow cabinet, ultraviolet lamp
- Gasburner Unifire (Uniequip), glass bead sterilizer (Duchefa) or glass alcohol lamp
- Stereomicroscope
- Glasshouse
- Scalpel, needles, fine tweezers, rest for holding sterile tools (Duchefa)
- Bacteriocidal soap
- 10% (v/v) H_2O_2 containing one drop of Silwet (Union Chemicals)
- Plant growth regulators and organic components: 2,4-D, NAA, BAP, ABA, Plant agar, Gelrite (Duchefa), sucrose, maltose, activated charcoal (Duchefa)
- PEG-4000
- Distilled water
- Initiation and maintenance medium (EDM6); embryo maturation media (EMM1 and EMM2); germination medium (BMG-2)
- Nylon cloth (30 μm pore size; Spectrum Laboratory Products, Inc.)
- Plastic food wrap; aluminium foil
- Peat and pumice
- Hyco V50 trays with plastic lids

Method

Selection of explants:

1 Cotyledons, hypocotyls, petioles and leaf segments, flower stems of immature inflorescences, bulb scales, mature and immature zygotic embryos (excise embryos from disinfected seeds under sterile conditions using the stereomicroscope), preferentially from juvenile *in vitro*-growing plants.

2 Disinfect the explants, if not from *in vitro*-grown plants, according to Protocol 1.1.

Induction of somatic embryogenesis and embryo development:

1 For many plant species (e.g. *Arachis hypogaea, Brassica napus*), culture the explants in sterile Petri dishes on medium supplemented with a high auxin concentration (2,4-D, NAA at 2–6 mg/l), but for some species (e.g. *Abies alba, Dendrobium* sp., *Corydalis yanhusuo*) on cytokinin-containing medium[a].

2 Proliferate embryogenic tissues by culture on new culture medium of the same composition.

3 Transfer the cultures to growth regulator-free medium for further somatic embryo development (pre-maturation). Embryos in globular, heart, torpedo and cotyledonary stages, the latter coinciding with the initiation of root primordia, should be visible on the surface of explants or in any induced callus [52]. In conifers, embryonal-suspensor masses are formed composed of small dense meristematic cells with long transparent suspensor cells.

4 In order to induce the maturation of somatic embryos (initiation of embryo growth and accumulation of storage products), transfer the embryogenic calli to medium supplemented with ABA (abscisic acid) with a decreased osmotic potential achieved by application of PEG-4000[b], or by increasing the carbohydrate content (maltose) for 8 weeks [53, 54].

5 Apply a desiccation treatment for embryo germination and conversion to plants. Isolate well-formed somatic embryos and transfer to unsealed 90 mm Petri dishes (six-well Falcon Multiwell dishes) placed in a sterile desiccator containing sterile distilled water for 2 weeks. Germinate the somatic embryos on hormone-free medium containing 1% (w/v) activated charcoal [55].

Example

Micropropagation of *Pinus radiata* by somatic embryogenesis [56]:

1 Collect cones approx. 8–10 weeks after fertilization. Remove the seeds from the cones, surface disinfect the seeds in 10% (v/v) H_2O_2 containing one drop of Silwet (Union Chemicals) for 10 min. Rinse two to three times in sterile water. Remove aseptically the seed coats.

2 Place whole megagametophytes containing immature embryos, at the torpedo to precotyledonary stages, onto initiation medium (EDM6) with sucrose (30 g/l), Gelrite (3 g/l), BAP (0.6 mg/l), auxin 2,4-D (1 mg/l), at pH 5.7 [56].

3 Maintain the cultures in the growth chamber at $24 \pm 1\,^{\circ}C$ under low illumination ($5\,\mu mol/m^2/s$).

4 After 2–6 weeks when the embryos are expelled from the megagametophytes onto the medium and embryogenic tissue reaches 10 mm in diameter, separate the tissue from the original explant and transfer to maintenance medium of the same composition as the initiation medium (EDM6). Maintain the cultures by serial transfer to new medium every 14 days.

5 To induce embryo maturation, take five portions (each 10 mm in diam.) of embryogenic tissue after 7 days of culture on EDM6 medium and place the tissues onto

Embryo Maturation Medium (EMM1) [56] supplemented with sucrose (30 g/l), Gelrite (6 g/l) and abscisic acid (15 mg/l). After 14 days, transfer onto the second maturation medium (EMM2) which has the same composition as EMM1 except for a lower concentration of Gelrite (4.5 g/l). Transfer to new EMM2 medium every 14 days until mature somatic embryos develop (6–8 weeks). Maintain the cultures at $24 \pm 1\,^{\circ}C$ under low intensity illumination (5 $\mu mol/m^2/s$).

6 To germinate the somatic embryos, harvest the white somatic embryos with well formed cotyledons and place them on nylon cloth contained in each of three wells of six-well Falcon Multiwell dishes (several embryos per week). Half fill the remaining three wells with sterile water. Seal the dishes with plastic food wrap. Wrap each dish in aluminium foil and store at $5\,^{\circ}C$ for at least 7 days. Transfer the nylon cloth containing the embryos to germination medium (BMG-2) and incubate for 7 days at $24\,^{\circ}C$ in the light and $20\,^{\circ}C$ in the dark (16 h photoperiod with 90 $\mu mol/m^2/s$, cool white fluorescent illumination). Remove the embryos from the nylon cloth and place the embryos horizontally on the germination medium. After 6–8 weeks, transplant germinating embryos into Hyco V50 trays containing a mixture of peat : pumice (2 : 1, v : v), and cover the trays with plastic lids. Gradually acclimatize the plants to glasshouse conditions by removing the lids for increasing periods.

7 Media formulations and additional procedure details are given in the original protocol.

Notes

[a]Stress-related stimuli, such as osmotic shock, the presence of heavy metals and auxin starvation induce somatic embryogenesis [57].

[b]PEG stimulates embryo maturation but induces alterations in somatic embryo morphology and anatomy that may lead to reduced germination and survival.

1.3 Troubleshooting

- Some explants placed on culture medium exude dark coloured compounds into the culture medium (phenols, pigments) that are released from the cut ends of the explants. This can cause browning of tissue and the medium, which is often connected with poor culture establishment and reduced regeneration ability. Minimize the wounding of explants during isolation and surface disinfection to reduce this response. Other approaches to prevent tissue browning include removal of these compounds by washing of explants in sterile water for 2–3 h, frequent subculture of explants to new medium with the excision of brown tissues, initial culture in liquid medium with subsequent transfer to semi-solid medium, culture on a porous substrate (paper bridges) and adsorption with activated charcoal (AC) or PVP (polyvinylpyrrolidone) by addition of these compounds to the culture medium. However, AC can also adsorb growth regulators or be toxic to some tissues. The use of antioxidants, such as ascorbic acid, citric acid, L-cysteine or mercaptoethanol, can also prevent browning of tissues in culture [58]. Excessive browning may cause serious problems in the different stages of shoot regeneration.

- Hyperhydricity (vitrification), i.e. the appearance of transparent and watery structures, is a physiological disorder occuring in plant tissue cultures [36, 59, 60]. Major problems are not encountered up to the weaning stage when it is limited in extent. Hyperhydricity can be caused by a high cytokinin concentration, high water retention capacity when the container is too tightly closed, or by a low concentration of gelling agent.

- Sometimes decline of vigour in culture with stagnacy in shoot growth and proliferation is observed which may be caused by several factors. These include unsuitable composition of the culture medium, lack of some nutrients, calcium deficiency in the apices, which causes necrosis, the presence of latent persistent microbial contaminants, cytokinin habituation (extensive proliferation of short shoots on cytokinin-free medium without elongation and rooting ability), loss of regeneration ability in long-term cultures (due to epigenetic variation) and culture aging, including transition from the juvenile to a mature stage.

- Somaclonal variation may arise during *in vitro* regeneration [61]. Chromosomal rearrangements are an important source of this variation [62]. Somaclonal variation is not restricted to, but is common in plants regenerated from callus. Variation can be genotypic or phenotypic which, in the later case, can be either genetic or epigenetic in origin [41]. Cytological, biochemical and molecular analyses are required to confirm clonal fidelity of vegetatively propagated plant material. Such analyses enable efficient and rapid testing of undesired genetic variability in comparison with traditional methods based on morphological and physiological assays.

- Detailed information on *in vitro* propagation techniques for a broad spectrum of plant species are available in Jain and Gupta [63], Rout *et al*. [64] and Jain and Häggman [65].

References

***1. George EF (1993) *Plant Propagation by Tissue Culture: The Technology*. Exegetics Ltd., Edington, UK.

Fundamental information on tissue culture methods.

2. Dirr MA, Heuser Jr CW (1987) *The Reference Manual of Woody Plant Propagation: From Seed to Tissue Culture*. Varsity Press, Athens, GA, USA.

3. George EF, Sherrington PD (1984) *Plant Propagation by Tissue Culture:Handbook and Directory of Commercial Laboratories*. Exegetics Ltd., Eversley, UK.

4. Zimmerman RH, Greisbach FA, Hammerschlag FA, Lawson RH (1986) (eds) *Tissue Culture as a Plant Production System for Horticultural Crops*. Martinus Nijhoff Publishers, Dordrecht, The Netherlands.

5. Stimart DP (1986) Commercial micropropagation of florist flower crops. In: *Tissue Culture as a Plant Production System for Horticultural Crops*. Edited by RH Zimmerman, FA

Greisbach, FA Hammerschlag and RH Lawson. Martinus Nijhoff Publishers, Dordrecht, The Netherlands, pp. 301–315.

6. Fiorino P, Loreti F (1987) *HortScience* **22**, 353–358.

7. Debergh PC (1987) In: *Plant Tissue and Cell Culture*. Edited by CE Green, DA Somers, WP Hacket and DD Biesboer. Alan R. Liss, New York, pp. 383–393.

8. Pierik RLM (1997) *In Vitro Culture of Higher Plants*, 4th edn. Kluwer Academic Publishers, Dordrecht, The Netherlands.

***9. Razdan MK (2003) *Introduction to Plant Tissue Culture*. Science Publishers Inc., Enfield, NH, USA.

Clearly written, well-documented introductory information on plant tissue culture methods.

10. Williams EG, Maheswaran G (1986) *Ann. Bot.* **57**, 443–462.

11. Gautheret RJ (1983) *Bot. Mag.* **96**, 393–410.

12. Gautheret RJ (1985) In: *Cell Culture and Somatic Cell Genetics of Plants*. Edited by IK Vasil. Academic Press, New York, USA. Vol. 2, pp. 1–59.

13. Murashige T, Skoog F (1962) *Physiol. Plant.* **15**, 473–497.

14. Gajdošová A, Ostrolucká MG, Libiaková G, Ondrušková E, Šimala D (2006) *J. Fruit Ornamental Plant Res.* **14**, 61–76.

15. McCown BH (1986) In: *Tissue Culture as a Plant Production System for Horticultural Crops*. Edited by RH Zimmeman, RJ Griesbach, FA Hammerschlag and RH Lawson. Martinus Nijhoff Publishers, Dordrecht, The Netherlands, pp. 333–342.

***16. Hartmann HT, Kester DE, Davies FT Jr., Geneve RL (2002) *Hartmann and Kester's Plant Propagation: Principles and Practices*, 7th edn. Prentice-Hall, Inc., Englewood Cliffs, NJ, USA

Volume covering all aspects of plant propagation.

17. Ostrolucká MG, Gajdošová A, Libiaková G, Hrubíková K, Bežo M (2007) In: *Protocols for Micropropagation of Woody Trees and Fruits*. Edited by SM Jain and H Häggman. Springer-Verlag, Berlin, Heidelberg, pp. 445–455.

18. Ostrolucká MG, Gajdošová A, Libiaková G (2007) In: *Protocols for Micropropagation of Woody Trees and Fruits*. Edited by SM Jain and H Häggman. Springer-Verlag, Berlin, Heidelberg, pp. 85–91.

19. Gajdošová A, Ostrolucká MG, Libiaková G, Ondrušková E (2007) In: *Protocols for Micropropagation of Woody Trees and Fruits*. Edited by SM Jain & H Häggman. Springer, Dordrecht, The Netherlands, pp. 447–464.

20. Bonga J, von Aderkas P (1992) *In vitro Culture of Trees*. Kluwer Academic Publishers, Dordrecht, The Netherlands.

21. De Klerk GJ, Van der Krieken W, De Jong JC (1999) *In Vitro Cell. Dev. Biol-Plant.* **35**, 189–199.

22. De Klerk GJ (2001) In: *Plant Roots: the Hidden Half*. Edited by Y Waisel, A Eshel and U Kafkafi. Marcel Dekker Publishers, New York, Basel, pp. 349–357.

23. De Klerk GJ., Arnold-Schmitt B, Lieberei R, Neumann KH (1997) *Bio. Plant.* **39**, 53–66.

24. Preece JE, Sutter EG (1991) In: *Micropropagation Technology and Application*. Edited by PC Debergh and RH Zimmerman. Martinus Nijhoff Publishers, Dordrecht, The Netherlands, pp. 71–93.

25. Rohr R, Iliev I, Scaltsoyiannes A, Tsoulpha P (2003) *Acta Hort.* **616**, 59–69.

26. Donelly D & Tisdall L (1993) In: *Micropropagation of Woody Plants*. Edited by MR Ahuja. Kluwer Academic Publishers, Dordrecht, Boston, London, pp. 153–166.

27. Echeverrigaray S, Basso R, Andrade LB (2005) *Biol. Plant.* **49**, 439–442.

*28. Bonga J (1982) In: *Tissue Culture in Forestry*. Edited by J Bonga and D Durzan. Martinus Nijhoff/Dr.W. Junk Publishers, Amsterdam, The Netherlands, pp. 387–412.

Application of tissue culture methods to woody plants.

29. Franklet A, Boulay M, Bekkaoui F, Fouret Y, Verschoore-Martouze B, Walker N (1987) In: *Cell and Tissue Culture in Forestry*. Edited by JM Bonga and DJ Durzan. Martinus Nijhoff Publishers, Dordrecht, The Netherlands, Vol. 1. pp. 232–248.

30. David A, Faye M, Rancillac M (1983) *Plant Soil* **71**, 501–505.

31. Stein A, Fortin JA (1990) *Can. J. Bot.* **68**, 492–498.

32. Piola F, Rohr R, von Aderkas P (1995) *Physiol. Plant.* **95**, 575–580.

33. Douds Jr DD, Bécard G, Pfeffer PE, Doner LW (1995) *HortScience* **30**, 133–134.

34. Grange O, Bärtschi H, Gay G (1997) *Trees*, **12**, 49–56.

35. Hay A, Tsiantis M (2005) *Development*, **132**, 2679–2684.

36. Castellano MM, Sablowski R (2005) *Curr. Opin. Plant Biol.* **8**, 26–31.

***37. Wang PJ, Charles A (1991) In: *Biotechnology in Agriculture and Forestry*. Vol. 17. *High-Tech and Micropropagation*. Edited by YPS Bajaj. Springer-Verlag, Heidelberg, pp. 32–53.

Basic information on micropropagation through meristem culture.

38. Pérez-Tornero O, Burgos L (2007) In: *Protocols for Micropropagation of Woody Trees and Fruits*. Edited by SM Jain and H Häggman. Springer-Verlag, Berlin, Heidelberg, pp. 267–278.

39. Aitken-Christie J, Jones C (1985) *Acta Hort.* **166**, 93–100.

40. Gaspar Th, Kevers C, DeBergh P, Maene L, Paques M, Boxus Ph. (1987) In: *Cell and Tissue Culture in Forestry*. Edited by JM Bonga and DJ Durzan. Martinus Nijhoff Publishers, Dordrecht, The Netherlands, Vol. 1, pp. 152–166.

41. Kitin P, Iliev I, Skaltsoyiannes A, Nellas Ch, Rubos A, Funada R (2005) *Plant Cell, Tiss. Org. Cult.* **82**, 141–150.

42. Dumas E, Monteuuis O (1995) *Plant Cell Tissue Org. Cult.* **40**, 231–235.

43. Anderson WC (1980) In: *Proceedings of the conference on nursery production of fruit plants through tissue culture. Applications and feasibility*. pp. 1–10. Edited by RH Zimmermann. US Department of Agricultural Science and Education Administration ARR-NE-11.

44. Geneve RL (1989) *Proc. Internatl. Plant Propagtors Soc.* **39**, 458–462.

45. Zhang S, Lemaux P (2004) *Critical Rev. Plant Sci.* **23**, 325–335.

46. Vooková B, Gajdošová A (1992) *Biol. Plant.* **34**, 23–29.

47. Emons AMC (1994) *Acta Bot. Neerl.* **43**, 1–14.

48. Williams EG, Maheswaran G (1986) *Ann. Bot.* **57**, 443–462.

49. Fehér A, Pasternak TP, Dudits D (2003) *Plant Cell Tissue Org. Cult.* **74**, 201–228.

50. Castellanos M, Power B, Davey M, (2008) *Propag. Ornam. Plants.* **8**, 173–185.

51. Vooková B, Gajdošová A, & Matúšová R (1998) *Biol. Plant.* **40**, 523–530.

*52. Dodeman VL, Ducreux G, Kreis M (1997) *J. Exp. Bot.* **313**, 1493–1509.

Identification of the mechanism underlying the developmental stages of somatic and zygotic embryogenesis.

***53. von Arnold S, Sabala I, Bozkhov P, Daychok J, Filonova L (2002) *Plant Cell Tiss. Organ Cult.* **69**, 233–249.

Factors regulating somatic embryogenesis.

54. Salaj T, Matúšová R, Salaj J (2004) *Biol. Cracoviensia Series Botanica*, **46**, 159–167.

55. Salajova T, Salaj J, Kormut'ák A (1999) *Plant Sci.* **145, 33–40.

Efficient protocol for conifer somatic embryogenesis.

56. Walter Ch, Find JI, Grace LJ (2005) In: *Protocols for Somatic Embryogenesis in Woody Plants*. Edited by SM Jain SM and PK Gupta. Springer-Verlag, Berlin, Heidelberg, pp. 11–24.

57. Quiroz-Figueroa FR, Rojas-Herrera R, Galas-Avalos RM, Loyola-Vargas VM (2006) *Plant Cell Tiss. Organ Cult.* **86**, 285–301.

***58. George EF (1996) *Plant Propagation by Tissue Culture: In Practice*. Exegetics Ltd., Edington, UK.

Fundamental information on tissue culture methods.

59. Ziv M (1991) In: *Micropropagation: Technology and Application*. Edited by PC Debergh and RH Zimmerman. Kluwer Academic Publishers, Dordrecht, The Netherlands, pp. 45–70.

60. Debergh P, Aitken-Christie J, Cohen D *et al.* (1992) *Plant Cell Tissue Org. Cult.* **30**, 135–140.

61. Jain SM (2001) *Euphytica* **118**, 153–166.

**62. Jain, SM, Brar DS, Ahloowalia BS (1998) *Somaclonal Variation and Induced Mutations in Crop Improvement*. Kluwer Academic Publishers, Dordrecht, The Netherlands.

Information on genetic variability arising during *in vitro* culture and its use in plant breeding.

**63. Jain SM, Gupta PK (2005) *Protocols for Somatic Embryogenesis in Woody Plants*. Springer-Verlag, Berlin, Heidelberg.

Detailed information on somatic embryogenesis in a broad spectrum of plant species.

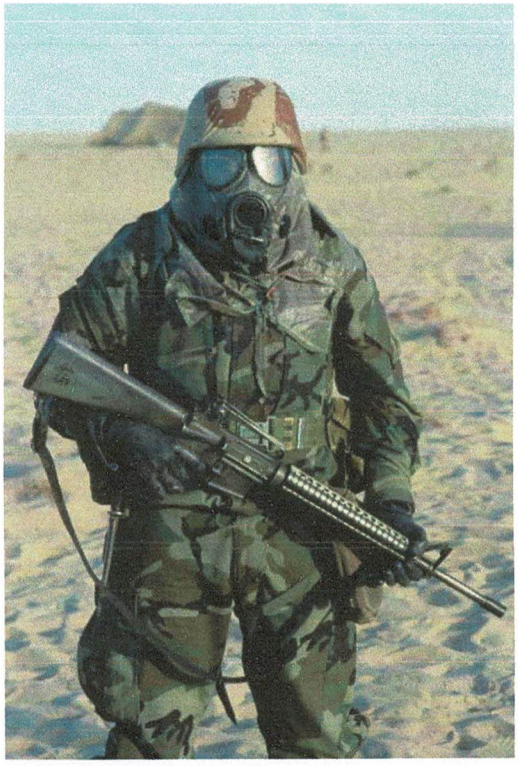
64. Rout GR, Mohapatra A, Jain SM (2006) *Biotechnol. Adv.* **24**, 531–560.

**65. Jain SM, Häggman H (2007) *Protocols for Micropropagation of Woody Trees and Fruits*. Springer-Verlag, Berlin, Heidelberg.

Detailed information on *in vitro* propagation techniques for a broad spectrum of plant species.

CHAPTER 4

The Structure and Function of the Plasma Membrane



SOURCE: © Peter Turnley / Corbis Images.

NERVE GAS

On March 20, 1995, during the morning rush hour in the Tokyo Subway system, one of the busiest in the world, a religious cult released a chemical called Sarin into the air. The attack was coordinated between multiple subway stations, and before long thousands of people were finding it difficult to breathe. Although only eight people died in the attack, hundreds were seriously injured. Sarin is a type of **nerve gas**—a chemical weapon produced by the Nazis that is designed to interfere with the nervous system. After World War II, both the United States and the Soviet Union produced massive stockpiles of sarin and other nerve gases, and while these weapons were not used on a global scale, nerve gas was used by Iraqi armed forces in an attack on the Kurdish city of Halabja in 1988, as well as in the Iran–Iraq war. The sarin molecule is small but deadly, and it works by poisoning an enzyme that degrades chemical signals used by nerves to activate muscle cells. Sarin victims die because the muscles used for breathing become paralyzed. In this chapter we will learn how proteins in the cell membrane convert chemical signals to electrical signals that are required for many physiological activities.

CHAPTER OUTLINE

4.1 Introduction to the Plasma Membrane
4.2 The Lipid Composition of Membranes
4.3 Membrane Carbohydrates
4.4 Membrane Proteins
4.5 Studying the Structure and Properties of Integral Membrane Proteins
4.6 Membrane Lipids and Membrane Fluidity
4.7 The Dynamic Nature of the Plasma Membrane
4.8 The Red Blood Cell: An Example of Plasma Membrane Structure
4.9 Solute Movement across Cell Membranes
4.10 Diffusion through the Lipid Bilayer
4.11 The Diffusion of Ions through Membranes
4.12 **EXPERIMENTAL PATHWAYS:** The Acetylcholine Receptor
4.13 Facilitated Diffusion
4.14 Active Transport
4.15 **THE HUMAN PERSPECTIVE:** Defects in Ion Channels and Transporters as a Cause of Inherited Disease
4.16 Membrane Potentials
4.17 Propagation of Action Potentials as an Impulse
4.18 Neurotransmission: Jumping the Synaptic Cleft

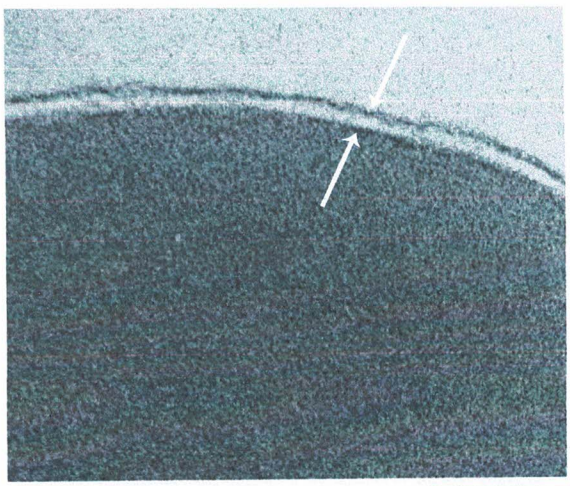
4.1 Introduction to the Plasma Membrane

The outer walls of a house or car provide a strong, inflexible barrier that protects its human inhabitants from an unpredictable and harsh external world. You might expect the outer boundary of a living cell to be constructed of an equally tough and impenetrable barrier because it must also protect its delicate internal contents from a nonliving, and often inhospitable, environment. Yet cells are separated from the external world by a thin, fragile structure called the **plasma membrane** that is only 5 to 10 nm wide. It would require about 5000 plasma membranes stacked one on top of the other to equal the thickness of a single page of this book.

Because it is so thin, no hint of the plasma membrane is detected when a section of a cell is examined under a light microscope. In fact, it wasn't until the late 1950s that techniques for preparing and staining tissue had progressed to the point where the plasma membrane could be resolved in the electron microscope. These early electron micrographs, such as those taken by J. D. Robertson of Duke University (FIGURE 4.1a), portrayed the plasma membrane as a three-layered structure, consisting of darkly staining inner and outer layers and lightly staining middle layer. All membranes that were examined closely—whether they were plasma, nuclear, or cytoplasmic membranes (Figure 4.1*b*), or taken from plants, animals, or microorganisms—showed this same ultrastructure. In addition to providing a visual image of this critically important cellular structure, these electron micrographs touched off a vigorous debate as to the molecular composition of the various layers of a membrane, an argument that went to the very heart of the subject of membrane structure and function. As we will see shortly, cell membranes contain a lipid bilayer, and the two dark-staining layers in the electron micrographs of Figure 4.1 correspond primarily to the inner and outer polar surfaces of the bilayer. We will return to the structure of membranes below, but first we will survey some of the major functions of membranes in the life of a cell (FIGURE 4.2).

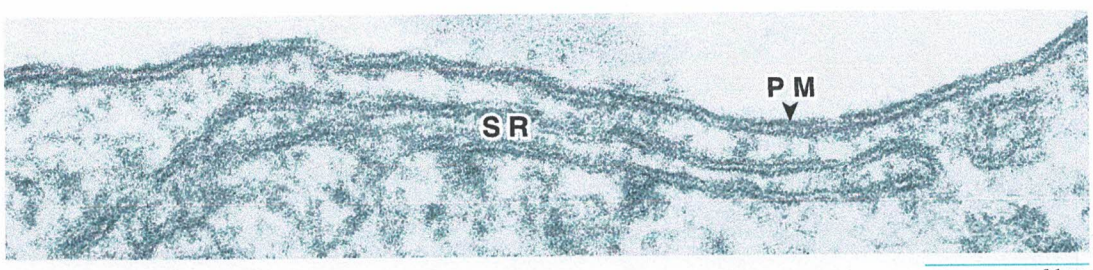
An Overview of Membrane Functions

1. ***Compartmentalization.*** Membranes are continuous, unbroken sheets and, as such, inevitably enclose compartments. The plasma membrane encloses the contents of the entire cell, whereas the nuclear and cytoplasmic membranes enclose diverse intracellular spaces. The various membrane-bounded compartments of a cell possess markedly different contents. Membrane compartmentalization allows specialized activities to proceed without external interference and enables cellular activities to be regulated independently of one another.
2. ***Scaffold for biochemical activities.*** Membranes not only enclose compartments but are also a distinct compartment themselves. For reactants floating around in solution, their interactions are dependent on random collisions. In contrast, components that are embedded in a membrane are no longer floating free and can be ordered for effective interaction.
3. ***Providing a selectively permeable barrier.*** Membranes prevent the unrestricted exchange of molecules from one side to the other. At the same time, membranes provide the means of communication between the compartments they separate. The plasma membrane, which encircles a cell, can be compared to a moat around a castle: Both serve as a general barrier, yet both have gated "bridges" that promote the movement of select elements into and out of the enclosed living space.



(*a*)

50 nm



(*b*)

0.1 μm

FIGURE 4.1 The trilaminar appearance of membranes. (*a*) Electron micrograph showing the three-layered (trilaminar) structure of the plasma membrane of an erythrocyte after staining the tissue with the heavy metal osmium. Osmium binds preferentially to the polar head groups of the lipid bilayer, producing the trilaminar pattern. The arrows denote the inner and outer edges of the membrane. (*b*) The outer edge of a differentiated muscle cell grown in culture showing the similar trilaminar structure of both the plasma membrane (PM) and the membrane of the sarcoplasmic reticulum (SR), a calcium-storing compartment of the cytoplasm.

SOURCE: (*a*) Courtesy of J. D. Robertson; (*b*) From Andrew R. Marks, et al., *J. Cell Biol.*, 114, 305, 1991. Reproduced with permission of the Rockefeller University Press.

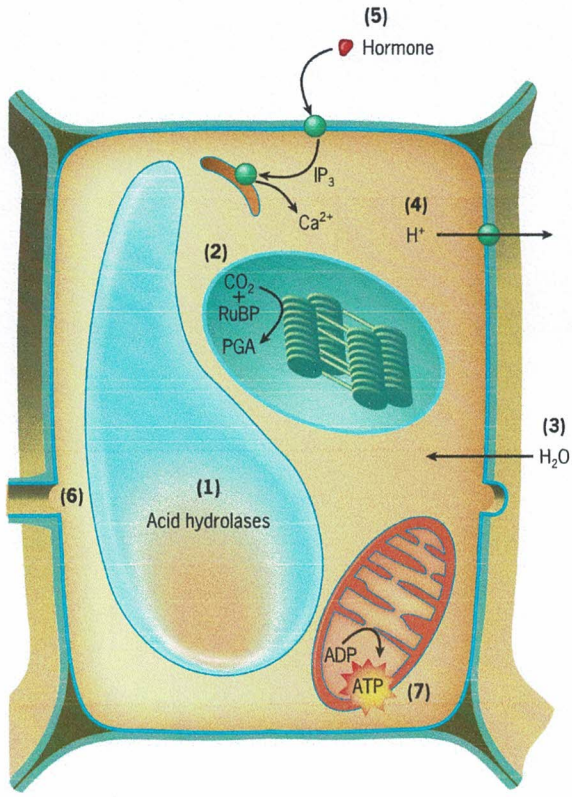


FIGURE 4.2 A summary of membrane functions in a plant cell. (1) An example of membrane compartmentalization in which hydrolytic enzymes (acid hydrolases) are sequestered within the membrane-bounded vacuole. (2) An example of the role of cytoplasmic membranes as a site of enzyme localization. The fixation of CO_2 by the plant cell is catalyzed by an enzyme that is associated with the outer surface of the thylakoid membranes of the chloroplasts. (3) An example of the role of membranes as a selectively permeable barrier. Water molecules are able to penetrate rapidly through the plasma membrane, causing the plant cell to fill out the available space and exert pressure against its cell wall. (4) An example of solute transport. Hydrogen ions, which are produced by various metabolic processes in the cytoplasm, are pumped out of plant cells into the extracellular space by a transport protein located in the plasma membrane. (5) An example of the involvement of a membrane in the transfer of information from one side to another (signal transduction). In this case, a hormone (e.g., abscisic acid) binds to the outer surface of the plasma membrane and triggers the release of a chemical message (such as IP_3) into the cytoplasm. In this case, IP_3 causes release of Ca^{2+} ions from a cytoplasmic warehouse. (6) An example of the role of membranes in cell–cell communication. Openings between adjoining plant cells, called plasmodesmata, allow materials to move directly from the cytoplasm of one cell into its neighbors. (7) An example of the role of membranes in energy transduction. The conversion of ADP to ATP occurs in close association with the inner membrane of the mitochondrion.

4. ***Transporting solutes.*** The plasma membrane contains the machinery for physically transporting substances from one side of the membrane to another, often from a region where the solute is present at low concentration into a region where that solute is present at much higher concentration. The membrane's transport machinery allows a cell to accumulate substances, such as sugars and amino acids, that are necessary to fuel its metabolism and build its macromolecules. The plasma membrane is also able to transport specific ions, thereby establishing ionic gradients across itself. This capability is especially critical for nerve and muscle cells.
5. ***Responding to external stimuli.*** The plasma membrane plays a critical role in the response of a cell to external stimuli, a process known as **signal transduction**. Membranes possess **receptors** that combine with specific molecules (**ligands**) or respond to other types of stimuli such as light or mechanical tension. Different types of cells have membranes with different receptors and are, therefore, capable of recognizing and responding to different environmental stimuli. The interaction of a plasma membrane receptor with an external stimulus may cause the membrane to generate a signal that stimulates or inhibits internal activities. For example, signals generated at the plasma membrane may tell a cell to manufacture more glycogen, to prepare for cell division, to move toward a higher concentration of a particular compound, to release calcium from internal stores, or possibly to commit suicide.
6. ***Intercellular interaction.*** Situated at the outer edge of every living cell, the plasma membrane of multicellular organisms mediates the interactions between a cell and its neighbors. The plasma membrane allows cells to recognize and signal one another, to adhere when appropriate, and to exchange materials and information. Proteins within the plasma membrane may also facilitate the interaction between extracellular materials and the intracellular cytoskeleton.
7. ***Energy transduction.*** Membranes are intimately involved in the processes by which one type of energy is converted to another type (energy transduction). The most fundamental energy transduction occurs during photosynthesis when energy in sunlight is absorbed by membrane-bound pigments, converted into chemical energy, and stored in carbohydrates. Membranes are also involved in the transfer of chemical energy from carbohydrates and fats to ATP. In eukaryotes, the machinery for these energy conversions is contained within membranes of chloroplasts and mitochondria.

We will concentrate in this chapter on the structure and functions of the plasma membrane, but remember that the principles discussed here are common to all cell membranes. Specialized aspects of the structure and functions of mitochondrial, chloroplast, cytoplasmic, and nuclear membranes will be discussed in Chapters 5, 6, 8, and 12, respectively.

A Brief History of Studies on Plasma Membrane Structure

The first insights into the chemical nature of the outer boundary layer of a cell were obtained by Ernst Overton of the University of Zürich during the 1890s. Overton knew that nonpolar solutes dissolved more readily in nonpolar solvents than in polar solvents, and that polar solutes had the opposite solubility. Overton reasoned that a substance entering a cell from the medium would first have to dissolve in the outer boundary layer of that cell. To test the permeability of the outer boundary layer, Overton placed plant root hairs into hundreds of different solutions containing a diverse array of solutes. He discovered that the more lipid-soluble the solute, the more rapidly it would enter the root hair cells. He concluded that the dissolving power of the outer boundary layer of the cell matched that of a fatty oil.

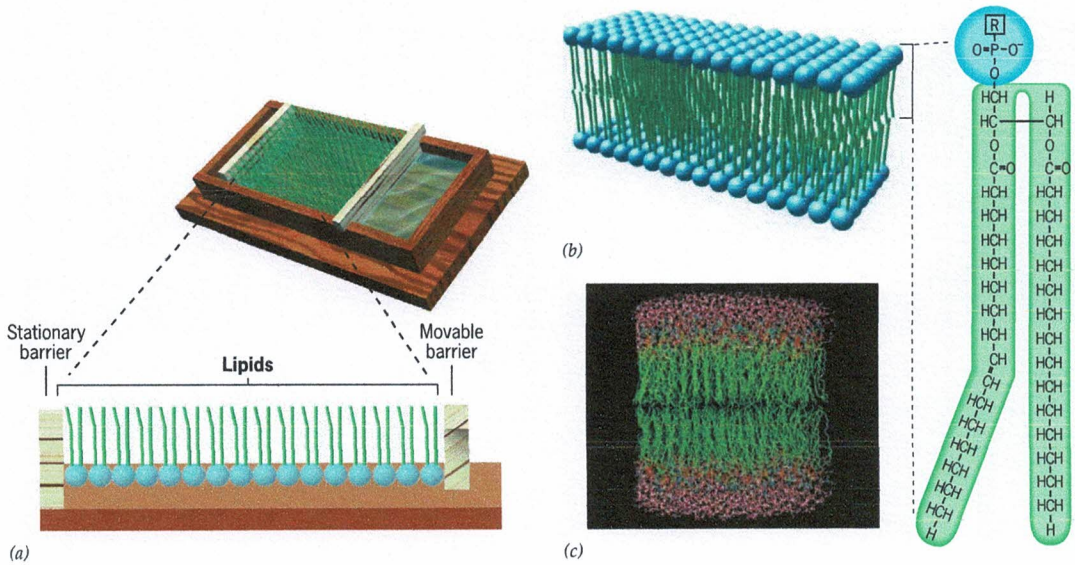


FIGURE 4.3 The plasma membrane contains a lipid bilayer. (*a*) Calculating the surface area of a lipid preparation. When a sample of phospholipids is dissolved in an organic solvent, such as hexane, and spread over an aqueous surface, the phospholipid molecules form a layer over the water that is a single molecule thick: a monomolecular layer. The molecules in the layer are oriented with their hydrophilic groups bonded to the surface of the water and their hydrophobic chains directed into the air. To estimate the surface area the lipids would cover if they were part of a membrane, the lipid molecules can be compressed into the smallest possible area by means of movable barriers. Using this type of apparatus, which is called a Langmuir trough after its inventor, Gorter and Grendel concluded that red blood cells contained enough lipid to form a layer over their surface that was two molecules thick: a bilayer. (*b*) As Gorter and Grendel first proposed, the core of a membrane contains a bimolecular layer of phospholipids oriented with their water-soluble head groups facing the outer surfaces and their hydrophobic fatty acid tails facing the interior. The structures of the head groups are given in Figure 4.6*a*. (*c*) Simulation of a fully hydrated lipid bilayer composed of the phospholipid phosphatidylcholine. Phospholipid head groups are purple, water molecules are blue, fatty acid chains are green.

SOURCE: (*c*) Simulation of a fully hydrated lipid bilayer. Phospholipid head groups are shown in blue and orange, water molecules in red and white, and fatty acid chains are green.

The first proposal that cellular membranes might contain a lipid bilayer was made in 1925 by two Dutch scientists, E. Gorter and F. Grendel. These researchers extracted the lipid from human red blood cells and measured the amount of surface area the lipid would cover when spread over the surface of water (FIGURE 4.3a). Because mature mammalian red blood cells lack both nuclei and cytoplasmic organelles, the plasma membrane is the only lipid-containing structure in the cell. Consequently, all of the lipids extracted from the cells can be assumed to have resided in the cells' plasma membranes. The ratio of the surface area of water covered by the extracted lipid to the surface area calculated for the red blood cells from which the lipid was extracted varied between 1.8 to 1 and 2.2 to 1. Gorter and Grendel speculated that the actual ratio was 2:1 and concluded that the plasma membrane contained a bimolecular layer of lipids, that is, a **lipid bilayer** (Figure 4.3*b*). They also suggested that the polar groups of each molecular layer (or *leaflet*) were directed outward toward the aqueous environment, as shown in Figure 4.3*b*,*c*. This would be the thermodynamically favored arrangement, because the polar head groups of the lipids could interact with surrounding water molecules, just as the hydrophobic fatty acyl chains would be protected from contact with the aqueous environment (Figure 4.3*c*). Thus, the polar head groups would face the cytoplasm on one edge and the blood plasma on the other. Even though Gorter and Grendel made several experimental errors (which fortuitously canceled one another out), they still arrived at the correct conclusion that membranes contain a lipid bilayer.

In the 1920s and 1930s, cell physiologists obtained evidence that there must be more to the structure of membranes than simply a lipid bilayer. It was found, for example, that lipid solubility was not the sole determining factor as to whether a substance could penetrate the plasma membrane. Similarly, the surface tensions of membranes were calculated to be much lower than those of pure lipid structures. This decrease in surface tension could be explained by the presence of protein in the membrane.

This protein is present in the form of individual protein molecules and protein complexes that penetrate a fluid lipid bilayer (FIGURE 4.4a) and extend out into the surrounding aqueous environment (Figure 4.4*b*). Because of the fluidity of the lipid bilayer, cellular membranes are dynamic structures in which the components are mobile and capable of coming together to engage in various types of transient or semipermanent interactions.

REVIEW

1. Describe some of the important roles of membranes in the life of a eukaryotic cell. What do you think might be the effect of a membrane that was incapable of performing one or another of these roles?
2. Summarize some of the major steps leading to the current model of membrane structure. How does each new model retain certain basic principles of earlier models?

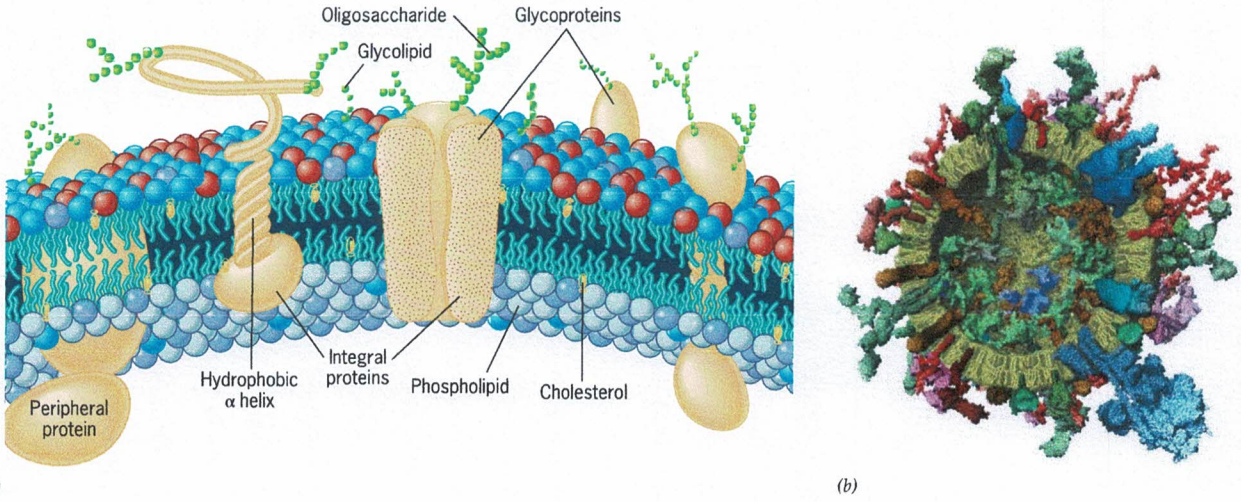


FIGURE 4.4 Plasma mebranes as lipid plus proteins. (*a*) A representation of the plasma membrane showing the organization of proteins embedded in the lipid bilayer. The external surface of most membrane proteins, as well as a small percentage of the phospholipids, contain short chains of sugars, making them glycoproteins and glycolipids. Those portions of the polypeptide chains that extend through the lipid bilayer typically occur as α helices composed of hydrophobic amino acids. The two leaflets of the bilayer contain different types of lipids as indicated by the differently colored head groups. (*b*) Molecular model of the membrane of a synaptic vesicle constructed using known structures of the various proteins along with information on their relative numbers obtained from the analysis of purified synaptic vesicles. The high protein density of the membrane is apparent. Most of the proteins in this membrane are required for the interaction of the vesicle with the plasma membrane. The large blue protein at the lower right pumps H^+ ions into the vesicle.

SOURCE: (*b*) From Shigeo Takamori, et al. Courtesy of Reinhard Jahn, *Cell*, 127:841, 2006, reprinted with permission from Elsevier.

4.2 The Lipid Composition of Membranes

Membranes are lipid–protein assemblies in which the components are held together in a thin sheet by noncovalent bonds. As noted on page 117, the core of the membrane consists of a sheet of lipids arranged in a bimolecular layer (Figure 4.3*b*,*c*). The lipid bilayer serves primarily as a structural backbone of the membrane and provides the barrier that prevents random movements of water-soluble materials into and out of the cell. The proteins of the membrane, on the other hand, carry out most of the specific functions summarized in Figure 4.2. Each type of differentiated cell contains a unique complement of membrane proteins that contributes to the specialized activities of that cell type (see Figure 4.32*d* for an example).

The ratio of lipid to protein in a membrane varies, depending on the type of cellular membrane (plasma vs. endoplasmic reticulum vs. Golgi), the type of organism (bacterium vs. plant vs. animal), and the type of cell (cartilage vs. muscle vs. liver). For example, the inner mitochondrial membrane has a very high ratio of protein/lipid in comparison to the red blood cell plasma membrane, which is high in comparison to the membranes of the myelin sheath that form a multilayered wrapping around a nerve cell (**FIGURE 4.5**). To a large degree, these differences can be correlated with the basic functions of these membranes. The inner mitochondrial membrane contains the protein carriers of the electron-transport chain, and relative to other membranes, lipid is diminished. In contrast, the myelin sheath acts primarily as electrical insulation for the nerve cell it encloses, a function that is best carried out by a thick lipid layer of high electrical resistance with a minimal content of protein. Membranes also contain carbohydrates, which are attached to the lipids and proteins as indicated in Figure 4.4*a*.

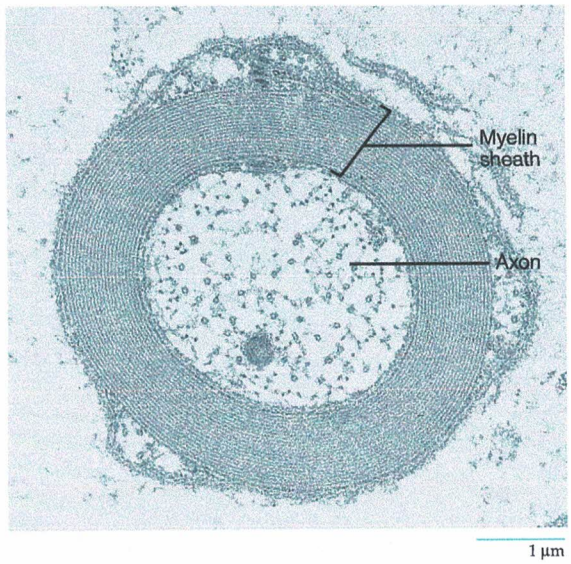


FIGURE 4.5 The myelin sheath. Electron micrograph of a nerve cell axon surrounded by a myelin sheath consisting of concentric layers of plasma membrane that have an extremely low protein/lipid ratio. The myelin sheath insulates the nerve cell from the surrounding environment, which increases the velocity at which impulses can travel along the axon (discussed on page 162). The perfect spacing between the layers is maintained by interlocking protein molecules (called P_0) that project from each membrane.

SOURCE: From Leonard Napolitano, Francis LeBaron, and Jospeh Scaletti, *J. Cell Biol.* 34:820, 1967. Reproduced with permission of the Rockefeller University Press.

Membrane Lipids

Membranes contain a wide diversity of lipids, all of which are **amphipathic**; that is, they contain both hydrophilic and hydrophobic regions. There are three main types of membrane lipids: phosphoglycerides, sphingolipids, and cholesterol.

PHOSPHOGLYCERIDES Most membrane lipids contain a phosphate group, which makes them **phospholipids**. Because most membrane phospholipids are built on a glycerol backbone, they are called **phosphoglycerides** (FIGURE 4.6a). Unlike triglycerides, which have three fatty acids (page 46) and are not amphipathic, membrane glycerides are *diglycerides*—only two of the hydroxyl groups of the glycerol are esterified to fatty acids; the third is esterified to a hydrophilic phosphate group. Without any additional substitutions beyond the phosphate and the two fatty acyl chains, the molecule is called *phosphatidic acid*, which is virtually absent in most membranes. Instead, membrane phosphoglycerides have an additional group linked to the phosphate, most commonly either choline (forming *phosphatidylcholine*, PC), ethanolamine (forming *phosphatidylethanolamine*, PE), serine (forming *phosphatidylserine*, PS), or inositol (forming *phosphatidylinositol*, PI). Each of these groups is small and hydrophilic and, together with the negatively charged phosphate to which it is attached, forms a highly water-soluble domain at one end of the molecule, called the **head group**. At physiologic pH, the head groups of PS and PI have an overall negative charge, whereas those of PC and PE are neutral. In contrast, the fatty acyl chains are hydrophobic, unbranched hydrocarbons approximately 16 to 22 carbons in length (Figure 4.6*a*). A membrane fatty acid may be fully saturated (i.e., lack double bonds), monounsaturated (i.e., possess one double bond), or polyunsaturated (i.e., possess more than one double bond). Phosphoglycerides often contain one unsaturated and one saturated fatty acyl chain. Recent interest has focused on the apparent health benefits of two highly unsaturated fatty acids (EPA and DHA) found at high concentration in fish oil. EPA and DHA contain five and six double bonds, respectively, and are incorporated primarily into PE and PC molecules of certain membranes, most notably in the brain and retina. EPA and DHA are described as omega-3 fatty acids because their last double bond is situated three carbons from the omega (CH_3) end of the fatty acyl chain. With fatty acid chains at one end of the molecule and a polar head group at the other end, all of the phosphoglycerides exhibit a distinct amphipathic character.

SPHINGOLIPIDS A less abundant class of membrane lipids, called **sphingolipids**, are derivatives of sphingosine, an amino alcohol that contains a long hydrocarbon chain (Figure 4.6*b*). Sphingolipids consist of sphingosine linked to a fatty acid (R of Figure 4.6*b*) by its amino group. This molecule is a *ceramide*. The various sphingosine-based lipids have additional groups esterified to the terminal alcohol of the sphingosine moiety. If the substitution is phosphorylcholine, the molecule is *sphingomyelin*, which is the only phospholipid of the membrane that is not built with a glycerol backbone. If the substitution is a carbohydrate, the molecule is a **glycolipid**. If the carbohydrate is a simple sugar, the glycolipid is called a *cerebroside*; if it is a small cluster of sugars that includes sialic acid, the glycolipid is called a *ganglioside*. Hundreds of different gangliosides have been identified by differences in their carbohydrate chains. Because all sphingolipids have two long, hydrophobic hydrocarbon chains at one end and a hydrophilic region at the other, they are also amphipathic and

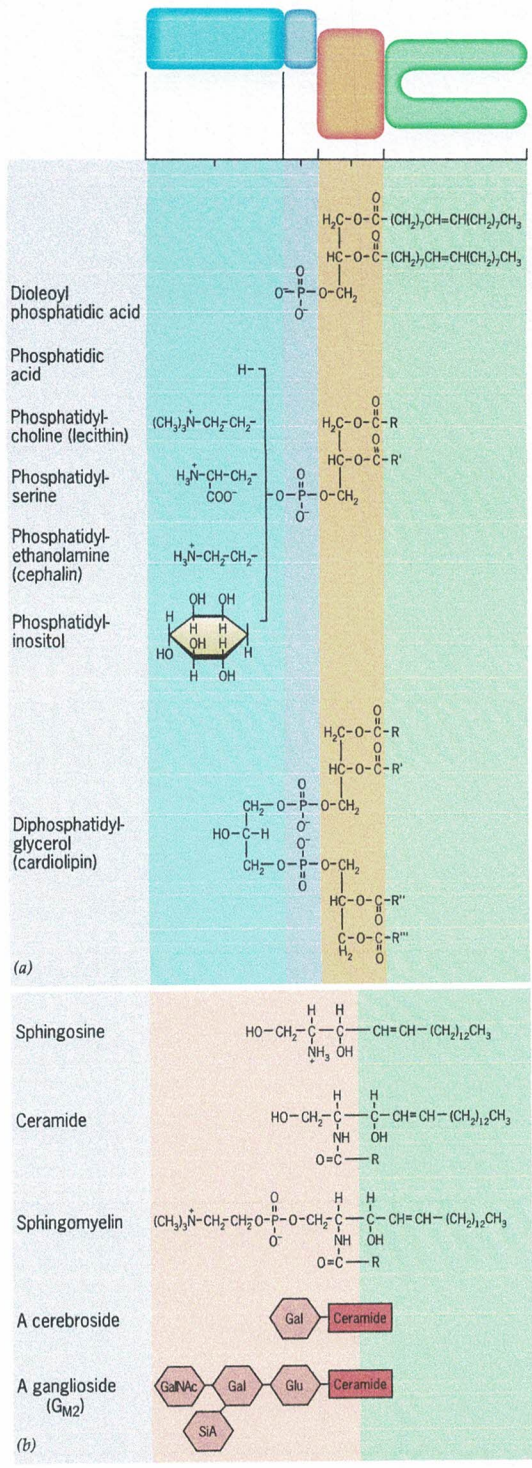


FIGURE 4.6 The chemical structures of membrane lipids. (*a*) The structures of phosphoglycerides (see also Figure 2.22). (*b*) The structures of sphingolipids. Sphingomyelin is a phospholipid; cerebrosides and gangliosides are glycolipids. A third membrane lipid is cholesterol, which is shown in the next figure. (R = fatty acyl chain). [The green portion of each lipid, which represents the hydrophobic tail(s) of the molecule, is actually much longer than the hydrophilic head group (see Figure 4.23).]

basically similar in overall structure to the phosphoglycerides. The fatty acyl chains of sphingolipids, however, tend to be longer and more highly saturated than those of phosphoglycerides.

Glycolipids are interesting membrane components. Relatively little is known about them, yet tantalizing hints have emerged to suggest they play crucial roles in cell function. The nervous system is particularly rich in glycolipids. The myelin sheath pictured in Figure 4.5 contains a high content of a particular glycolipid, called galactocerebroside (shown in Figure 4.6*b*), which is formed when a galactose is added to ceramide. Mice lacking the enzyme that carries out this reaction exhibit severe muscular tremors and eventual paralysis. Similarly, humans who are unable to synthesize a particular ganglioside (G_{M3}) suffer from a serious neurological disease characterized by severe seizures and blindness. Glycolipids also play a role in certain infectious diseases; the toxins that cause cholera and botulism both enter their target cell by first binding to cell-surface gangliosides, as does the influenza virus.

CHOLESTEROL Another lipid component of certain membranes is the sterol **cholesterol** (see Figure 2.21), which in certain animal cells may constitute up to 50 percent of the lipid molecules in the plasma membrane. Plant cells contain cholesterol-like sterols, but biologists disagree as to whether they completely lack cholesterol. Cholesterol molecules are oriented with their small hydrophilic hydroxyl group toward the membrane surface and the remainder of the molecule embedded in the lipid bilayer (**FIGURE 4.7**). The hydrophobic rings of a cholesterol molecule are flat and rigid, and they interfere with the movements of the fatty acid tails of the phospholipids (page 131).

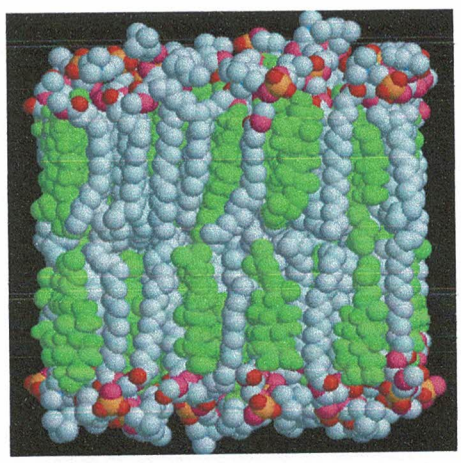


FIGURE 4.7 The cholesterol molecules (shown in green) of a lipid bilayer are oriented with their small hydrophilic end facing the external surface of the bilayer and the bulk of their structure packed in among the fatty acid tails of the phospholipids. The placement of cholesterol molecules interferes with the flexibility of the lipid hydrocarbon chains, which tends to stiffen the bilayer while maintaining its overall fluidity. Unlike other lipids of the membrane, cholesterol is often rather evenly distributed between the two layers (leaflets).

SOURCE: From H. L. Scott, *Curr. Opin. Struct. Biol.* 12:499, 2002, Figure 3. © 2002, with permission from Elsevier.

The Nature and Importance of the Lipid Bilayer

Each type of cellular membrane has its own characteristic lipid composition, differing from one another in the types of lipids, the nature of the head groups, and the particular species of fatty acyl chain(s). Because of this structural variability, it is estimated that some biological membranes contain hundreds of chemically distinct species of phospholipids, which can be catalogued by mass spectrometry. The biological significance of this remarkable diversity of lipid species remains the subject of interest and speculation.

The percentages of some of the major types of lipids of a variety of membranes are given in Table 4.1. The lipids of a membrane are more than simple structural elements; they can have important effects on the biological properties of a membrane. Lipid composition can determine the physical state of the membrane (page 131) and influence the activity of particular membrane proteins. Membrane lipids also provide the precursors for highly active chemical messengers that regulate cellular function (Section 15.6).

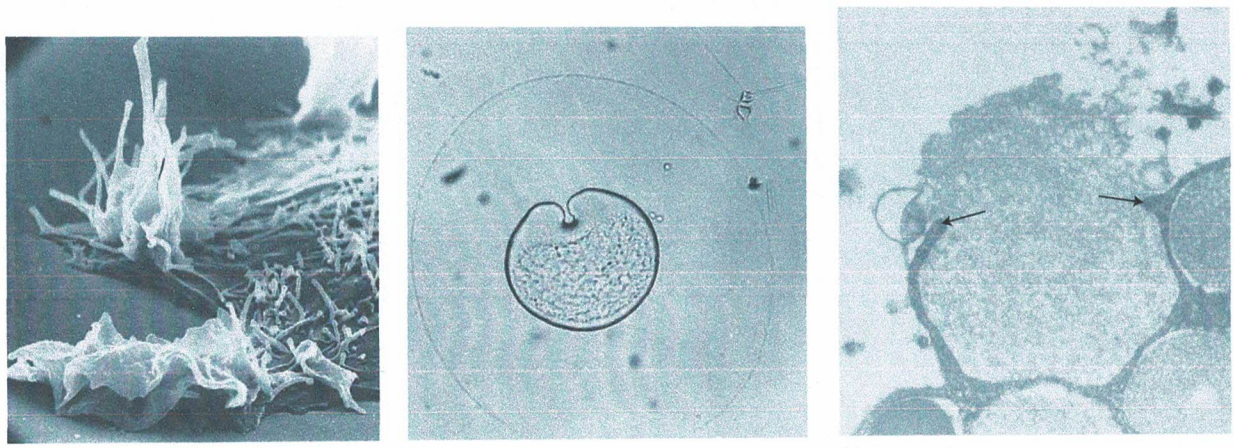
Various types of measurements indicate that the combined fatty acyl chains of both leaflets of the lipid bilayer span a width of about 30 Å and that each row of head groups (with its adjacent shell of water molecules) adds another 15 Å. Thus, the entire lipid bilayer is only about 60 Å (6 nm) thick. The presence in membranes of this thin film of amphipathic lipid molecules has remarkable consequences for cell structure and function. Because of thermodynamic considerations, the hydrocarbon chains of the lipid bilayer are never exposed to the surrounding aqueous solution. Consequently, membranes are never seen to have a free edge; they are always continuous, unbroken structures. As a result, membranes form extensive interconnected networks within the cell. Because of the flexibility of the lipid bilayer, membranes are deformable and their overall shape can change, as occurs during locomotion (**FIGURE 4.8a**) or cell division (Figure 4.8*b*). The lipid bilayer is thought to facilitate the regulated fusion or budding of membranes. For example, the events of secretion, in which cytoplasmic vesicles fuse to the plasma membrane (Figure 4.8*c*), or of fertilization, where two cells fuse to form a single cell, involve processes in which two separate membranes come together to become one continuous sheet (see Figure 8.32). The importance of the lipid bilayer in maintaining the proper internal composition of a cell, in separating electric charges across the plasma membrane, and in many other cellular activities will be apparent throughout this and subsequent chapters.

Another important feature of the lipid bilayer is its ability to self-assemble, which can be demonstrated more easily within a test tube than a living cell. If, for example, a small amount of phosphatidylcholine is dispersed in an aqueous solution, the phospholipid molecules assemble spontaneously to form the walls of fluid-filled spherical vesicles, called **liposomes**. The walls of these liposomes consist of a continuous lipid bilayer that is organized in the same manner as that of the lipid bilayer of a natural membrane. Liposomes have proven invaluable in membrane research. Membrane proteins can be inserted into liposomes and their function studied in a much simpler environment than that of a natural membrane. Liposomes have also been developed as vehicles to deliver drugs or DNA molecules within the body. The drugs or DNA can be linked to the wall of the liposome or contained at high concentration within its lumen (Figure 4.9). In these studies, the walls of the liposomes are constructed to contain specific proteins (such as antibodies or hormones) that allow the liposomes to bind selectively to the surfaces of

TABLE 4.1 Lipid Compositions of Some Biological Membranes*

Lipid	Human erythrocyte	Human myelin	Beef heart mitochondria	*E. coli*
Phosphatidic acid	1.5	0.5	0	0
Phosphatidylcholine	19	10	39	0
Phosphatidyl-ethanolamine	18	20	27	65
Phosphatidylgycerol	0	0	0	18
Phosphatidylserine	8.5	8.5	0.5	0
Cardiolipin	0	0	22.5	12
Sphingomyelin	17.5	8.5	0	0
Glycolipids	10	26	0	0
Cholesterol	25	26	3	0

*The values given are weight percent of total lipid.
Source: C. Tanford, *The Hydrophobic Effect*, p. 109, copyright 1980, John Wiley & Sons, Inc. Reprinted by permission of John Wiley & Sons, Inc.



(a) (b) (c)

FIGURE 4.8 The dynamic properties of the plasma membrane. (a) The leading edge of a moving cell often contains sites where the plasma membrane displays undulating ruffles. (b) Division of a cell is accompanied by the deformation of the plasma membrane as it is pulled toward the center of the cell. Unlike most dividing cells, the cleavage furrow of this dividing ctenophore egg begins at one pole and moves unidirectionally through the egg. (c) Membranes are capable of fusing with other membranes. This electron micrograph shows a secretory granule discharging its contents after fusion with the overlying plasma membrane (arrows).

SOURCE: (a) Courtesy of Jean Paul Revel; (b) Courtesy of Gary Freeman; (c) Courtesy of Susan Jo Burwen.

particular target cells where the drug or DNA is intended to go. Most of the early clinical studies with liposomes met with failure because the injected vesicles were rapidly removed by phagocytic cells of the immune system. This obstacle has been overcome with the development of so-called stealth liposomes that contain an outer coating of a synthetic polymer that protects the liposomes from immune destruction (FIGURE 4.9). One important example is Caelyx, a stealth liposome containing the chemotherapy drug doxorubicin. Caelyx is now an accepted therapy for treatment of metastatic breast cancer.

The Asymmetry of Membrane Lipids

The lipid bilayer consists of two distinct leaflets that have a distinctly different lipid composition. One line of experiments that has led to this conclusion takes advantage of the fact that lipid-digesting enzymes cannot penetrate the plasma membrane and, consequently, are only able to digest lipids that reside in the outer leaflet of the bilayer. If intact human red blood cells are treated with a lipid-digesting phospholipase, approximately 80 percent of the phosphatidylcholine (PC) of the membrane is hydrolyzed, but only about 20 percent of

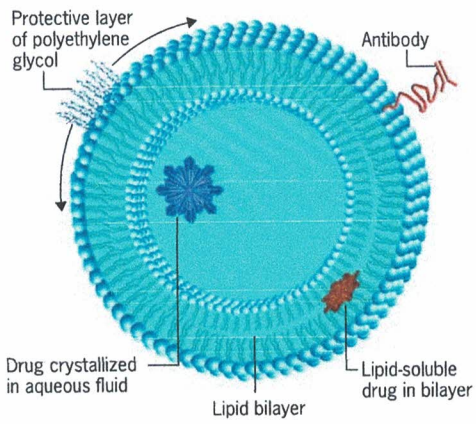


FIGURE 4.9 Liposomes. A schematic diagram of a stealth liposome containing a hydrophilic polymer (such as polyethylene glycol) to protect it from destruction by immune cells, antibody molecules that target it to specific body tissues, a water-soluble drug enclosed in the fluid-filled interior chamber, and a lipid-soluble drug in the bilayer.

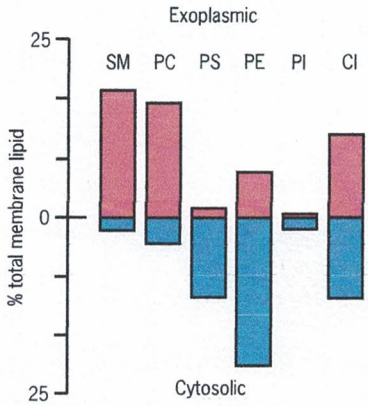


FIGURE 4.10 The asymmetric distribution of phospholipids (and cholesterol) in the plasma membrane of human erythrocytes. (SM, sphingomyelin; PC, phosphatidylcholine; PS, phosphatidylserine; PE, phosphatidylethanolamine; PI, phosphatidylinositol; CI, cholesterol.)

the membrane's phosphatidylethanolamine (PE) and less than 10 percent of its phosphatidylserine (PS) are attacked. These data indicate that, compared to the inner leaflet, the outer leaflet has a relatively high concentration of PC (and sphingomyelin) and a low concentration of PE and PS (**FIGURE 4.10**). It follows that the lipid bilayer can be thought of as composed of two more-or-less stable, independent monolayers having different physical and chemical properties.

The different classes of lipids in Figure 4.10 exhibit different properties. All the glycolipids of the plasma membrane are in the outer leaflet where they often serve as receptors for extracellular ligands. Phosphatidylethanolamine, which is concentrated in the inner leaflet, tends to promote the curvature of the membrane, which is important in membrane budding and fusion. Phosphatidylserine, which is concentrated in the inner leaflet, has a net negative charge at physiologic pH, which makes it a candidate for binding positively charged lysine and arginine residues, such as those adjacent to the membrane-spanning α helix of glycophorin A in Figure 4.18. The appearance of PS on the outer surface of aging lymphocytes marks the cells for destruction by macrophages, whereas its appearance on the outer surface of platelets leads to blood coagulation. Phosphatidylinositol (PI), which is concentrated in the inner leaflet, can be phosphorylated at different sites on the inositol ring, which converts the lipid into a phosphoinositide. As discussed in Chapter 15, phosphoinositides play a key role in the transfer of stimuli from the plasma membrane to the cytoplasm (Section 15.6) and the recruitment of proteins to the cytosolic face of the plasma membrane.

REVIEW

1. Draw the basic structure of the major types of lipids found in cellular membranes. How do sphingolipids differ from glycerolipids? Which lipids are phospholipids? Which are glycolipids? How are these lipids organized into a bilayer? How is the bilayer important for membrane activities?
2. What is a liposome? How are liposomes used in medical therapies?

4.3 Membrane Carbohydrates

The plasma membranes of eukaryotic cells also contain carbohydrate. Depending on the species and cell type, the carbohydrate content of the plasma membrane ranges between 2 and 10 percent by weight. More than 90 percent of the membrane's carbohydrate is covalently linked to proteins to form glycoproteins; the remaining carbohydrate is covalently linked to lipids to form glycolipids, which were discussed on page 119. As indicated in Figure 4.4*c*, all of the carbohydrate of the plasma membrane faces outward into the extracellular space.[1] The carbohydrate of internal cellular membranes also faces away from the cytosol (the basis for this orientation is illustrated in Figure 8.14).

The modification of proteins was discussed briefly on page 50. The addition of carbohydrate, or **glycosylation**, is the most complex of these modifications. The carbohydrate of glycoproteins is present as short, branched hydrophilic **oligosaccharides**, typically having fewer than about 15 sugars per chain. In contrast to most high-molecular-weight carbohydrates (such as glycogen, starch, or cellulose), which are polymers of a single sugar, the oligosaccharides attached to membrane proteins and lipids can display extensive variability in composition and structure. Even the same protein can display different chains of sugars in different cells and tissues. Oligosaccharides may be attached to several different amino acids by two major types of linkages (**FIGURE 4.11**). These carbohydrate projections play an important role in mediating the interactions of a cell with its environment (Chapter 7) and sorting of membrane proteins to different cellular compartments (Chapter 8). The carbohydrates of the glycolipids of the red blood cell plasma membrane determine whether a person's blood type is A, B, AB, or O (**FIGURE 4.12**). A person having blood type A has an enzyme that adds an *N*-acetylgalactosamine to the end of the chain, whereas a person with

[1]It can be noted that even though phosphatidylinositol contains a sugar group (Figure 4.6), it is not considered to be part of the carbohydrate portion of the membrane in this discussion.

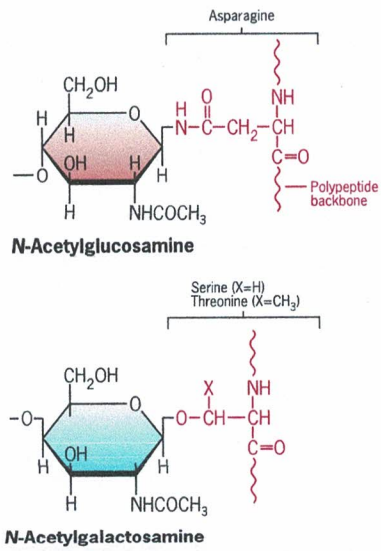


FIGURE 4.11 Two types of linkages that join sugars to a polypeptide chain. The *N*-glycosidic linkage between asparagine and *N*-acetylglucosamine is more common than the *O*-glycosidic linkage between serine or threonine and *N*-acetylgalactosamine.

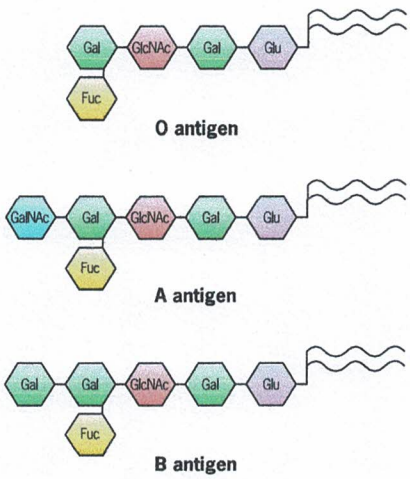


FIGURE 4.12 Blood-group antigens. Whether a person has type A, B, AB, or O blood is determined by a short chain of sugars covalently attached to membrane lipids and proteins of the red blood cell membrane. The oligosaccharides attached to membrane lipids (forming a ganglioside) that produce the A, B, and O blood types are shown here. A person with type AB blood has gangliosides with both the A and B structure. (Gal, galactose; GlcNAc, *N*-acetylglucosamine; Glu, glucose; Fuc, fucose; GalNAc, *N*-acetylgalactosamine.)

type B blood has an enzyme that adds galactose to the chain terminus. These two enzymes are encoded by alternate versions of the same gene, yet they recognize different substrates. People with AB blood type possess both enzymes, whereas people with O blood type lack enzymes capable of attaching either terminal sugar. The ABO carbohydrate modifications are found in many other tissues besides blood, and genetic variation in the AB gene is a strong predictor of risk for pancreatic cancer, heart disease, and viral infection, but the biochemical function of the ABO blood-group antigens remains a mystery.

REVIEW

1. What is an oligosaccharide? How are oligosaccharides linked to membrane proteins? How are they related to human blood types?

4.4 Membrane Proteins

Depending on the cell type and the particular organelle within that cell, a membrane may contain hundreds of different proteins. Each membrane protein has a defined orientation relative to the cytoplasm, so that the properties of one surface of a membrane are very different from those of the other surface (as in Figure 4.4*a*). This asymmetry is referred to as membrane "sidedness." In the plasma membrane, for example, those parts of membrane proteins that interact with other cells or with extracellular substances are exposed to the extracellular space, whereas those parts of membrane proteins that interact with cytoplasmic molecules are exposed to the cytosol. Membrane proteins can be grouped into three distinct classes distinguished by the intimacy of their relationship to the lipid bilayer (**FIGURE 4.13**). These are

1. **Integral proteins** (Figure 4.13*a*) that penetrate the lipid bilayer. Integral proteins are **transmembrane proteins**; that is, they

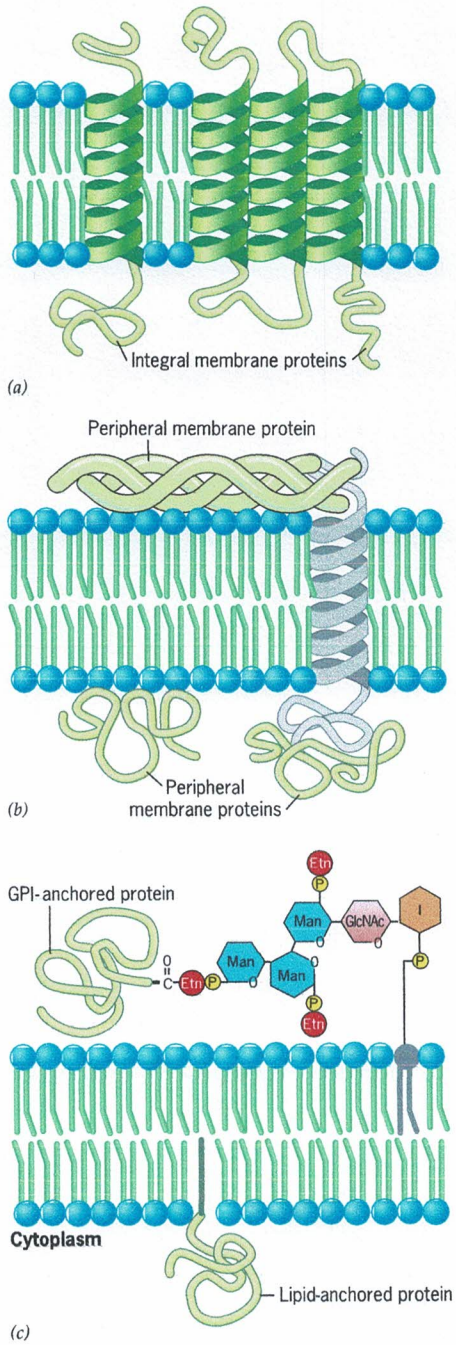


FIGURE 4.13 Three classes of membrane protein. (*a*) Integral proteins typically contain one or more transmembrane helices (see Figure 5.4 for an exception). (*b*) Peripheral proteins are noncovalently bonded to the polar head groups of the lipid bilayer and/or to an integral membrane protein. (*c*) Lipid-anchored proteins are covalently bonded to a lipid group that resides within the membrane. The lipid can be phosphatidylinositol, a fatty acid, or a prenyl group (a long-chain hydrocarbon built from five-carbon isoprenoid units). I, inositol; GlcNAc, *N*-acetylglucosamine; Man, mannose; Etn, ethanolamine; GPI, glycosylphosphatidylinositol.

pass entirely through the lipid bilayer and thus have domains that protrude from both the extracellular and cytoplasmic sides of the membrane. Some integral proteins have only one membrane-spanning segment, whereas others are multispanning. Genome-sequencing studies suggest that integral proteins constitute 25–30 percent of all encoded proteins and roughly 60 percent of all current drug targets.

2. **Peripheral proteins** (Figure 4.13*b*) that are located entirely outside of the lipid bilayer, on either the cytoplasmic or extracellular side, yet are associated with the surface of the membrane by noncovalent bonds.
3. **Lipid-anchored proteins** (Figure 4.13*c*) that are located outside the lipid bilayer, on either the extracellular or cytoplasmic surface, but are covalently linked to a lipid molecule that is situated within the bilayer.

Integral Membrane Proteins

Most integral membrane proteins function in the following capacities: as receptors that bind specific substances at the membrane surface, as channels or transporters involved in the movement of ions and solutes across the membrane, or as agents that transfer electrons during the processes of photosynthesis and respiration. Like the phospholipids of the bilayer, integral membrane proteins are also amphipathic, having both hydrophilic and hydrophobic portions. As discussed below, those portions of an integral membrane protein that reside within the lipid bilayer—the transmembrane domains—tend to have a hydrophobic character. Amino acid residues in transmembrane domains form van der Waals interactions with the fatty acyl chains of the bilayer, which seals the protein into the lipid "wall" of the membrane. As a result, the permeability barrier of the membrane is preserved, the protein is anchored within the bilayer, and the protein is brought into direct contact with surrounding lipid molecules (**FIGURE 4.14a**). According to current consensus, most of the lipid molecules that make contact with a transmembrane domain, such as those shown in Figure 4.14*a*, are simply passive bystanders and are rapidly exchanged with other lipid molecules in the bilayer. There is increasing evidence, however, that certain sites on the surface of many membrane proteins do form important functional interactions with specific lipid molecules. An example of this is shown in Figure 14.4*b*, where anionic lipid molecules are seen to bind in the crevice at the interfaces between the subunits of a tetrameric KcsA K^+ channel. The channel does not open normally in a bilayer that lacks these specific lipid molecules.

Those portions of an integral membrane protein that project into either the cytoplasm or extracellular space tend to be more like the globular proteins discussed in Section 2.10. These nonembedded domains tend to have hydrophilic surfaces that interact with water-soluble substances (low-molecular-weight substrates, hormones, and other proteins) at the edge of the membrane. In some membrane proteins, the transmembrane domains are essentially devoid of water molecules, whereas others allow the aqueous solvent to penetrate deep into the protein's membrane-embedded regions. Several large families of membrane proteins contain an interior channel that provides an aqueous passageway through the lipid bilayer. The linings of these channels typically contain key hydrophilic residues at strategic locations. As will be discussed later, integral proteins need not be fixed structures but may be able to move laterally within the membrane.

The concept that proteins penetrate through membranes, rather than simply remaining external to the bilayer, was derived primarily from the results of a technique called **freeze-fracture replication**

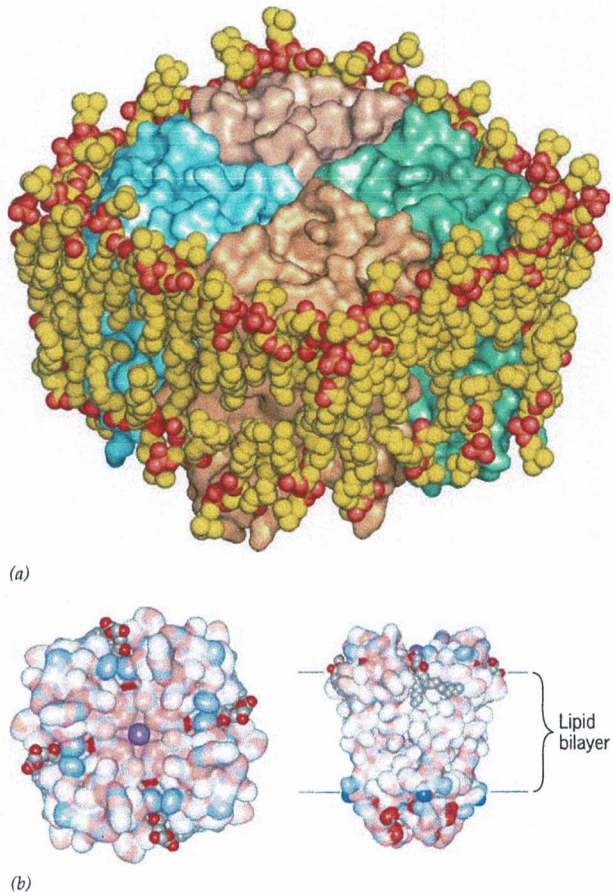
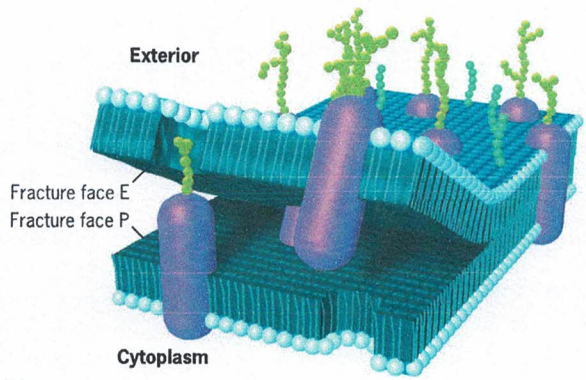


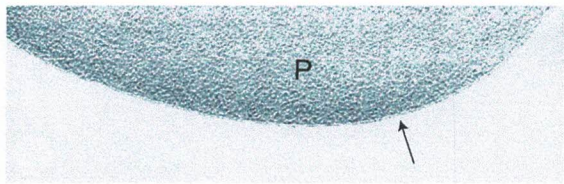
FIGURE 4.14 The interactions between membrane proteins and lipids. (a) Aquaporin is a membrane protein containing four subunits (colored differently in the illustration) with each subunit containing an aqueous channel. Analysis of the protein's structure revealed the presence of a surrounding layer of bound lipid molecules. In this case, these lipid molecules are not likely to play a role in the function of aquaporin because the protein retains its function as a water channel in bilayers containing nonnative lipids. (*b*) Two views of another tetrameric membrane protein, in this case the bacterial K^+ channel, KcsA. Anionic phosphatidylglycerol molecules (red/gray) are seen in each crevice between the subunits and are thought to be required for normal channel function. A K^+ ion (purple sphere) is seen in transit through the pore.

SOURCE: (*a*) From Carola Hunte and Sebastian Richers, *Curr. Opin. Struct. Biol.* 18:407, © 2008, with permission from Elsevier Science; (*b*) From Anthony G. Lee, *Trends Biochem. Sci.* 36:497, © 2011, with permission from Elsevier Science.

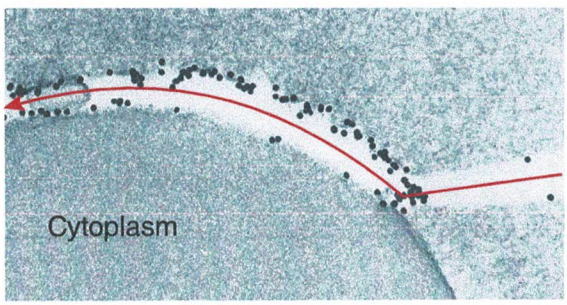
(see Section 18.5). In this procedure, tissue is frozen solid and then struck with a knife blade, which fractures the block into two pieces. As this occurs, the fracture plane often takes a path between the two leaflets of the lipid bilayer (**FIGURE 4.15a**). Once the membranes are split in this manner, metals are deposited on their exposed surfaces to form a shadowed *replica*, which is viewed in the electron microscope (see Figure 18.20). As shown in Figure 4.15*b*, the replica resembles a road strewn with pebbles, which are called *membrane-associated particles*. Because the fracture plane passes through the center of the bilayer, most of these particles correspond to integral membrane proteins that extend at least halfway through the lipid core. When the fracture plane reaches a given particle, it goes around it rather



(a)



(b) 0.2 μm



(c) 0.3 μm

FIGURE 4.15 Freeze fracture: a technique for investigating cell membrane structure. (*a*) When a block of frozen tissue is struck by a knife blade, a fracture plane runs through the tissue, often following a path that leads it through the middle of the lipid bilayer. The fracture plane goes around the proteins rather than cracking them in half, and they segregate with one of the two halves of the bilayer. The exposed faces within the center of the bilayer can then be covered with a metal deposit to form a metallic replica. These exposed faces are referred to as the E, or ectoplasmic face, and the P, or protoplasmic face. (*b*) Replica of a freeze-fractured human erythrocyte. The P fracture face is seen to be covered with particles approximately 8 nm in diameter. A small ridge (arrow) marks the junction of the particulate face with the surrounding ice. (*c*) This micrograph shows the surface of an erythrocyte that was frozen and then fractured, but rather than preparing a replica, the cell was thawed, fixed, and labeled with a marker for the carbohydrate groups that project from the external surface of the integral protein glycophorin (Figure 4.18). Thin sections of the labeled, fractured cell reveal that glycophorin molecules (black particles) have preferentially segregated with the outer half of the membrane. The red line shows the path of the fracture plane.

SOURCE: (*b*) From Thomas W. Tillack and Vincent T. Marchesi, *J. Cell Biol.* 45:649, 1970, Reproduced with permission of The Rockefeller University Press; (*c*) From Pedro Pinto Da Silva and Maria R. Torrisi, *J. Cell Biol.* 93:467, 1982, Reproduced with permission of The Rockefeller University Press.

than cracking it in half. Consequently, each protein (particle) separates with one half of the plasma membrane (Figure 4.15*c*), leaving a corresponding pit in the other half (see Figure 7.27*c*). One of the great values of the freeze-fracturing technique is that it allows an investigation of the microheterogeneity of the membrane. Localized differences in parts of the membrane stand out in these replicas and can be identified (as illustrated by the replica of a gap junction shown in Figure 7.30*d*). Biochemical analyses, in contrast, average out such differences.

Peripheral Membrane Proteins

Peripheral proteins are associated with the membrane by weak electrostatic bonds (refer to Figure 4.13*b*). Peripheral proteins can usually be solubilized by extraction with high-concentration salt solutions that weaken the electrostatic bonds holding peripheral proteins to a membrane. In actual fact, the distinction between integral and peripheral proteins is blurred because many integral membrane proteins consist of several polypeptides, some that penetrate the lipid bilayer and others that remain on the periphery.

The best studied peripheral proteins are located on the internal (cytosolic) surface of the plasma membrane, where they form a fibrillar network that acts as a membrane "skeleton" (see Figure 4.32*d*). These proteins provide mechanical support for the membrane and function as an anchor for integral membrane proteins. Other peripheral proteins on the internal plasma membrane surface function as enzymes, specialized coats (see Figure 8.24), or factors that transmit transmembrane signals (see Figure 15.19). Peripheral proteins typically have a dynamic relationship with the membrane, being recruited to the membrane or released from the membrane depending on prevailing conditions.

Lipid-Anchored Membrane Proteins

Several types of lipid-anchored membrane proteins can be distinguished. Numerous proteins present on the external face of the plasma membrane are bound to the membrane by a small, complex oligosaccharide linked to a molecule of phosphatidylinositol that is embedded in the outer leaflet of the lipid bilayer (refer to Figure 4.13*c*). Peripheral membrane proteins containing this type of glycosylphosphatidylinositol linkage are called **GPI-anchored proteins**. They were discovered when it was shown that certain membrane proteins could be released by a phospholipase that specifically recognized and cleaved inositol-containing phospholipids. The normal cellular prion protein PrP^C (page 63) is a GPI-linked molecule, as are various receptors, enzymes, and cell-adhesion proteins. A rare type of anemia, paroxysmal nocturnal hemoglobinuria, results from a deficiency in GPI synthesis that makes red blood cells susceptible to lysis.

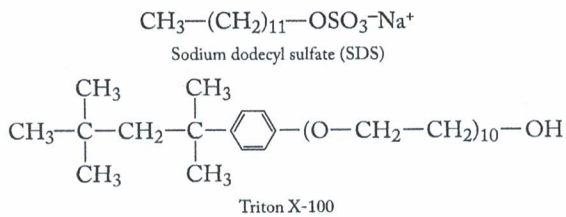
Another group of proteins present on the *cytoplasmic* side of the plasma membrane is anchored to the membrane by one or more long hydrocarbon chains embedded in the inner leaflet of the lipid bilayer (refer to Figure 4.13*c* and accompanying legend). At least two proteins associated with the plasma membrane in this way (Src and Ras) have been implicated in the transformation of a normal cell to a malignant state.

REVIEW

1. What is meant by the statement that the proteins of a membrane are distributed asymmetrically? Is this also true of the membrane's carbohydrate?
2. Describe the properties of the three classes of membrane proteins (integral, peripheral, and lipid-anchored), how they differ from one another, and how they vary among themselves.

4.5 Studying the Structure and Properties of Integral Membrane Proteins

Because of their hydrophobic transmembrane domains, integral membrane proteins are difficult to isolate in a soluble form. Removal of these proteins from the membrane normally requires the use of a detergent, such as the ionic (charged) detergent SDS (which denatures proteins) or the nonionic (uncharged) detergent Triton X-100 (which generally does not alter a protein's tertiary structure)



Like membrane lipids, detergents are amphipathic, being composed of a polar end and a nonpolar hydrocarbon chain (see Figure 2.20). As a consequence of their structure, detergents can substitute for phospholipids in stabilizing integral proteins while rendering them soluble in aqueous solution (**FIGURE 4.16**). Once the proteins have been solubilized by the detergent, various analyses can be carried out to determine the protein's amino acid composition, molecular mass, amino acid sequence, and so forth.

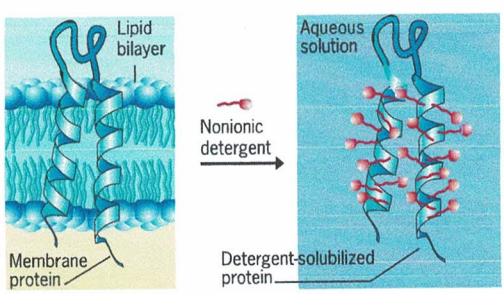
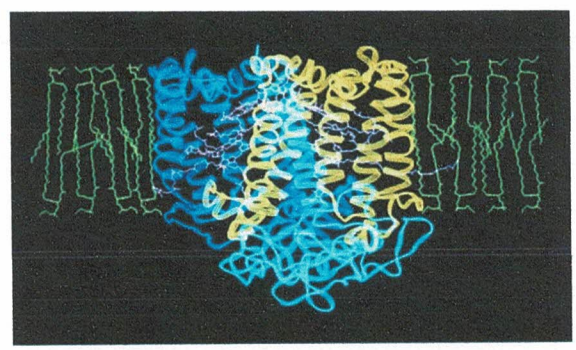


FIGURE 4.16 Solubilization of membrane proteins with detergents. The nonpolar ends of the detergent molecules associate with the nonpolar residues of the protein that had previously been in contact with the fatty acyl chains of the lipid bilayer. In contrast, the polar ends of the detergent molecules interact with the surrounding water molecules, keeping the protein in solution. Nonionic detergents, as shown here, solubilize membrane proteins without disrupting their structure.

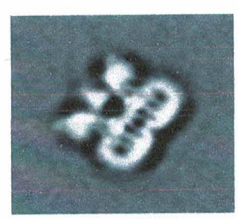
Researchers have had great difficulty obtaining crystals of most integral membrane proteins for use in X-ray crystallography. In fact, fewer than 1 percent of the known high-resolution protein structures represent integral membrane proteins.[2] Furthermore, most of these structures represent prokaryotic versions of a particular protein, which are often smaller than their eukaryotic homologues and easier to obtain in large quantity. Once the structure of one member of a membrane protein family is determined, researchers can usually apply a strategy called *homology modeling* to learn about the structure and activity of other members of the family. For example, solution of the structure of the bacterial K^+ channel KcsA (shown in Figure 4.39) provided a wealth of data that could be applied to the structure and mechanism of action of the much more complex eukaryotic K^+ channels (Figure 4.42).

One of the first membrane proteins whose entire three-dimensional structure was determined by X-ray crystallography is shown in **FIGURE 4.17a**. This protein—the bacterial photosynthetic reaction center—consists of three subunits containing 11 membrane-spanning α helices. Most membrane proteins have not been as amenable to crystallization as the photosynthetic reaction center.

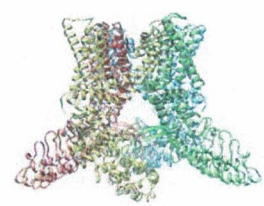
[2]Many integral membrane proteins have a substantial portion that is present in the cytoplasm or extracellular space. In many cases, this soluble portion has been cleaved from its transmembrane domain, crystallized, and its tertiary structure determined. While this approach provides valuable data about the protein, it fails to provide information about the protein's orientation within the membrane.



(a)



(b)



(c)

FIGURE 4.17 Structure of integral proteins. (a) Tertiary structure of the photosynthetic reaction center of a bacterium as determined by X-ray crystallography. The protein contains three different membrane-spanning polypeptides, shown in yellow, light blue, and dark blue. The helical nature of each of the transmembrane segments is evident. (b) High resolution electron microscopy images of the TRPV ion channel reconstructed by averaging many individual electron micrographs of proteins frozen in ice at low temperatures (Cryo-electron microscopy). (c) Structure of the TRPV channel determined by electron microscopy.

SOURCE: (a) From G. Feher, J. P. Allen, M. Y. Okamura, and D. C. Rees, *Nature* 339:113, © 1989; Reprinted by permission from Macmillan Publishers Ltd.; (b, c) From Maofu Liao et al., *Nature* 504:107. 2013.

Among the obstacles, many membrane proteins (1) are present at low numbers per cell, (2) are unstable in the detergent-containing solutions required for their extraction, (3) are prone to aggregation, and (4) are heavily modified by glycosylation and cannot be expressed as recombinant proteins in other types of cells. Some of the technical difficulties in preparing membrane protein crystals have been overcome using new methodologies and laborious efforts. In one study, for example researchers were able to obtain high-quality crystals of a bacterial transporter after testing and refining more than 95,000 different conditions for crystallization. In some cases, mutant versions of a membrane protein are found to be better suited to forming the ordered arrays of molecules that make up a crystal lattice. In many other cases, crystallization has been achieved by covalently linking the membrane protein to other molecules, often small soluble proteins. Recent developments in electron microscopy technology have allowed membrane protein structure to be determined at high resolution by imaging large numbers of identical proteins at very low temperatures to reduce imaging noise, then averaging their images together (Figure 4.17*b*). Because the microscopy is done at very low temperatures it is known as cyro-electron microscopy **(See the Experimental Walkthrough Video: Solving protein structures using cryo-EM for this chapter).** Using this approach, it is now possible to see individual amino acid side chains and reconstruct a molecular structure entirely from electron microscopy information (Figure 4.17*c*).

Despite increasing success in protein crystallization and rapid advances in cryo-electron microscopy, researchers still rely largely on indirect approaches for determining the three-dimensional organization of most membrane proteins. We will examine some of these approaches in the following paragraphs.

Identifying Transmembrane Domains

A great deal can be learned about the structure of a membrane protein and its orientation within the lipid bilayer from a computer-based (computational) analysis of its amino acid sequence, which is readily deduced from the nucleotide sequence of an isolated gene. The first question one might ask is: Which segments of the polypeptide chain are actually embedded in the lipid bilayer? Those segments of a protein embedded within the membrane, which are described as the **transmembrane domains**, have a simple structure; they consist of a string of about 20 predominantly nonpolar amino acids that span the core of the lipid bilayer as an a helix.[3] The chemical structure of a single transmembrane helix is shown in **FIGURE 4.18**, which depicts the two-dimensional structure of glycophorin A, the major integral protein of the erythrocyte plasma membrane. Of the 20 amino acids that make up the lone α helix of a glycophorin monomer (amino acids 73 to 92 of Figure 4.18), all but three have hydrophobic side chains (or an H atom in the case of the glycine residues). The exceptions are serine and threonine, which are noncharged, polar residues (Figure 2.26). **FIGURE 4.19a** shows a portion of a transmembrane helix with a threonine residue, not unlike those of glycophorin A. The hydroxyl group of the residue's side chain can form a hydrogen bond with one of the oxygen atoms of the peptide backbone. Fully charged residues may also appear in transmembrane helices, but they tend to be near one of the ends of the helix and to be accommodated in ways that allow them to fit into their hydrophobic environment. This is illustrated in the model transmembrane helices shown in Figures 4.19*b* and *c*. Each of the helices in these figures contains a pair of charged residues whose side chains are able to reach out and interact with the innermost polar regions of the membrane, even if it requires distorting the helix to do so. Figure 4.19*d* shows two tyrosine residues with their hydrophobic aromatic side chains; each aromatic ring is oriented parallel with the hydrocarbon chains of the bilayer with which it has become integrated.

Knowing the amino acid sequence of an integral membrane protein, we can usually identify the transmembrane segments using

[3]It was noted on page 54 that the α helix is a favored conformation because it allows for a maximum number of hydrogen bonds to be formed between atoms of the polypeptide backbone, thereby creating a highly stable (low-energy) configuration. This is particularly important for a membrane-spanning polypeptide that is surrounded by fatty acyl chains and, thus, cannot form hydrogen bonds with an aqueous solvent. Transmembrane helices are at least 20 amino acids in length, because this is the minimum stretch of polypeptide capable of spanning the hydrocarbon core of a lipid bilayer of 30 Å width. A few integral membrane proteins have been found to contain loops or helices that penetrate but do not span the bilayer. An example is the P helix in Figure 4.39.

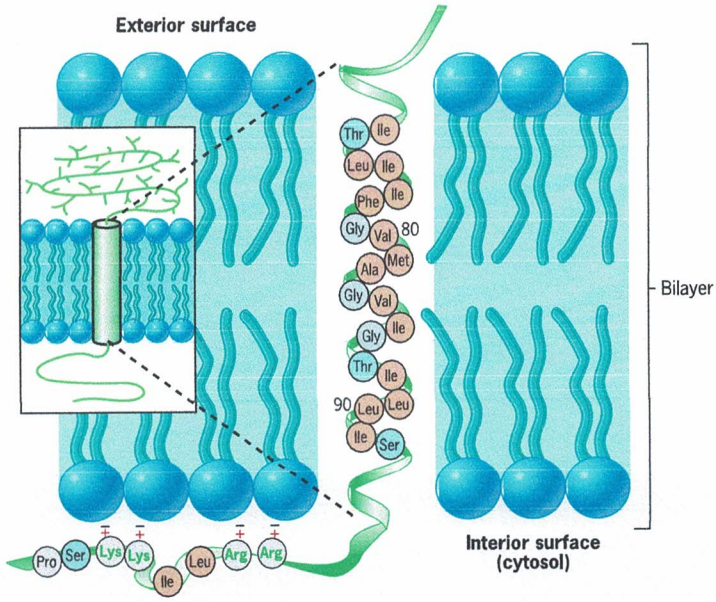


FIGURE 4.18 Glycophorin A, an integral protein with a single transmembrane domain. The single α helix that passes through the membrane consists predominantly of hydrophobic residues (brown-colored circles). The four positively charged amino acid residues of the cytoplasmic domain of the membrane protein form ionic bonds with negatively charged lipid head groups. Carbohydrates are attached to a number of amino acid residues on the outer surface of the protein (shown in the inset). All but one of the 16 oligosaccharides are small *O*-linked chains (the exception is a larger oligosaccharide linked to the asparagine residue at position 26). Glycophorin molecules are present as homodimers within the erythrocyte membrane (Figure 4.32*d*). The two helices of the dimer cross over one another in the region between residues 79 and 83. This Gly-X-X-X-Gly sequence is commonly found where transmembrane helices come into close proximity.

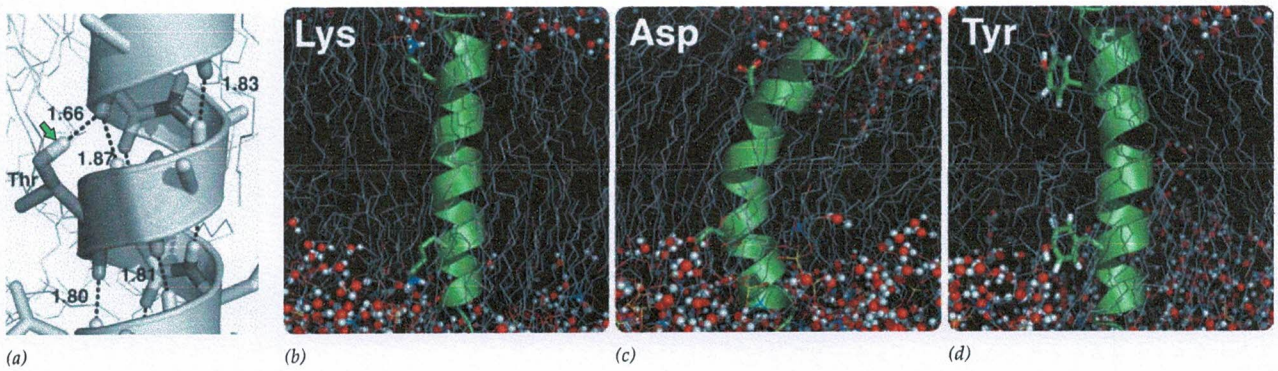


FIGURE 4.19 Accommodating various amino acid residues within transmembrane helices. (a) In this portrait of a small portion of a transmembrane helix, the hydroxyl group of the threonine side chain (arrow) is able to form a (shared) hydrogen bond with a backbone oxygen within the lipid bilayer. Hydrogen bonds are indicated by the dashed lines and their distances are shown in angstroms. (*b*) The side chains of the two lysine residues of this transmembrane helix are sufficiently long and flexible to form bonds with the head groups and water molecules of the polar face of the lipid bilayer. (*c*) The side chains of the two aspartic acid residues of this transmembrane helix can also reach the polar face of the bilayer but introduce distortion in the helix to do so. (*d*) The aromatic side chains of the two tyrosine residues of this transmembrane helix are oriented perpendicular to the axis of the membrane and parallel to the fatty acyl chains with which they interact.

SOURCE: (*a–d*) From Anna C. V. Johansson and Erik Lindahl, *Biophys. J.* 91:4459, 4453, 2006, © 2006, with permission from Elsevier.

a *hydropathy plot*, in which each site along a polypeptide is assigned a value that provides a measure of the *hydrophobicity* of the amino acid at that site as well as that of its neighbors. This approach provides a "running average" of the hydrophobicity of short sections of the polypeptide and guarantees that one or a few polar amino acids in a sequence do not alter the profile of the entire stretch. Hydrophobicity of amino acids can be determined using various criteria, such as their lipid solubility or the energy that would be required to transfer them from a nonpolar medium into an aqueous medium. A hydropathy plot for glycophorin A is shown in **FIGURE 4.20**. Transmembrane segments are usually identified as a jagged peak that extends well into the hydrophobic side of the spectrum. A reliable prediction concerning the orientation of the transmembrane segment within the bilayer can usually be made by examining the flanking amino acid residues. In most cases, as illustrated by glycophorin in Figure 4.18, those parts of the polypeptide at the cytoplasmic flank of a transmembrane segment tend to be more positively charged than those at the extracellular flank.

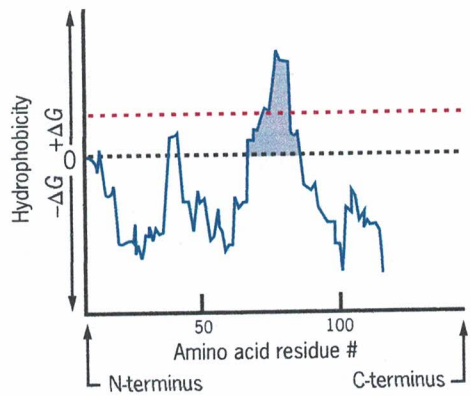


FIGURE 4.20 Hydropathy plot for glycophorin A, a single membrane-spanning protein. Hydrophobicity is measured by the free energy required to transfer each segment of the polypeptide from a nonpolar solvent to an aqueous medium. Values above the 0 line are energy-requiring (+ΔGs), indicating predominantly nonpolar side chains. Peaks that project above the red-colored line indicate continuous stretches of mostly nonpolar amino acids, and are interpreted as transmembrane domains.

Not all integral membrane proteins contain transmembrane α helices. A number of membrane proteins contain a relatively large channel positioned within a circle of membrane-spanning β strands organized into a barrel as illustrated in Figure 5.4. To date, aqueous channels constructed of β barrels have only been found in the outer membranes of bacteria, mitochondria, and chloroplasts.

Experimental Approaches to Identifying Conformational Changes within an Integral Membrane Protein

Suppose you have isolated a gene for an integral membrane protein and, based on its nucleotide sequence, determined that it contains 12 apparent membrane-spanning α helices. You might want to know which sites within these transmembrane domains are accessible to the aqueous environment and how this changes as the protein carries out its function. This type of information is particularly important when working with a membrane channel or transporter that functions in the movement of hydrophilic substances across the membrane. Although these determinations are difficult to make without detailed structural models, considerable insight can be gained by site-directed mutagenesis, that is, by introducing specific changes into the gene that encodes the protein (Section 18.25). An experiment of this type, which was conducted on lactose permease, a sugar-transporting protein in bacterial cell membranes, is shown in **FIGURE 4.21**. In this experiment, researchers prepared different versions of the permease in which nearly all of the individual amino acids of the protein were replaced, one at a time, by a cysteine residue. Each mutated membrane protein was then incubated with a water-soluble reagent (NEM) that is capable of adding an alkyl group to the cysteine side chain—as long as it has access to that side chain. The incubations with NEM were carried out under two different

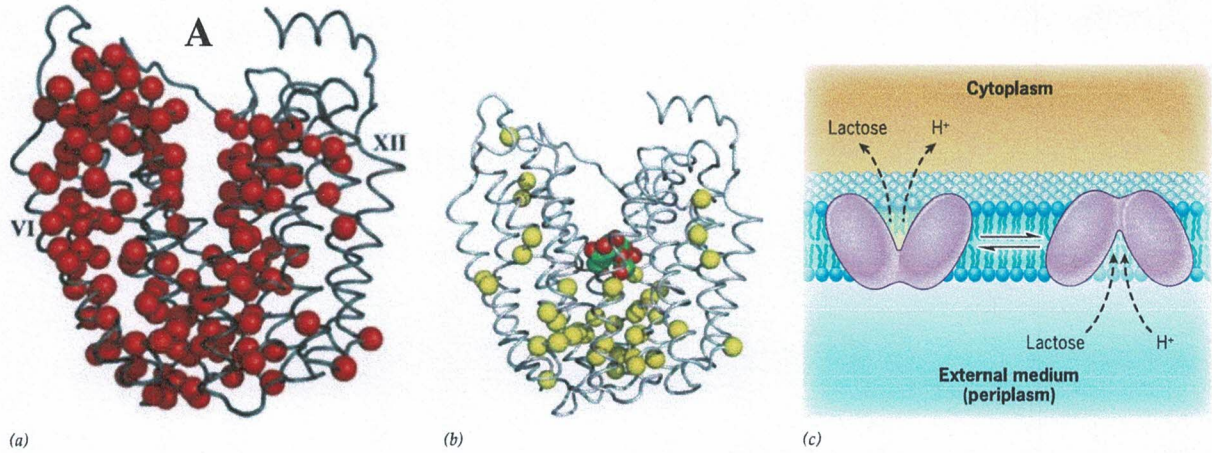


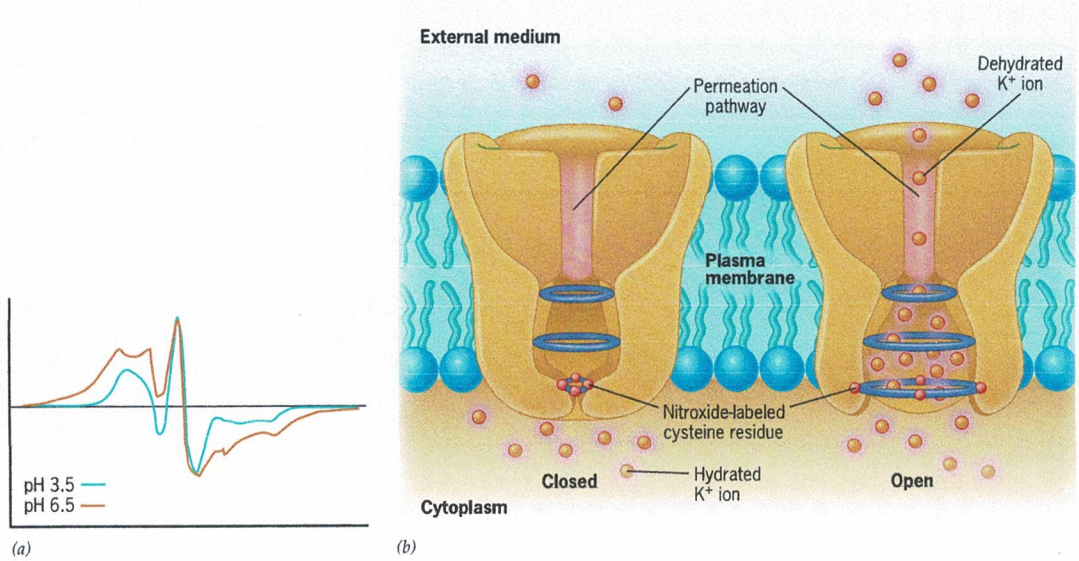
FIGURE 4.21 An experiment employing site-directed mutagenesis to learn about dynamic changes in the conformation of a membrane protein as it carries out its activity. The experimental strategy of the experiment and its results are discussed in the text. The cytoplasmic surface of the protein (lactose permease) is at the top. (*a*) The red spheres indicate the residues of the membrane protein that reacted with the alkylating agent NEM in the absence of a sugar to be transported. (*b*) The gold spheres denote the residues that are much more accessible to the alkylating agent when the protein is incubated with the sugar. The gold spheres in *b* are seen to cluster in a portion of the protein near the external medium (the periplasm in bacteria). The authors concluded that the gold spheres correspond to residues that line an outward-facing cavity, i.e., one that is open to the external medium. The results support a model of alternating access to the medium as depicted in part *c*. (Note the structure that is depicted in parts *a*–*b* is that of the inward-facing conformation as determined by X-ray crystallography.)

SOURCE: (*a*, *b*) From H. Ronald Kaback, et al., *PNAS* 104:492, 2007, © 2007 National Academy of Sciences, U.S.A.; (*c*) Reprinted from *Current Opinion in Structural Biology* 14:414, 2004 Fig. 1 by H. R. Kaback, with permission from Elsevier.

conditions: either in the presence of the sugar to be transported or in its absence. The image in Figure 4.21*a* shows those residues (depicted as red spheres) of the protein that become alkylated by NEM *in the absence of the sugar*. Many of these accessible residues are thought to line an inward-facing hydrophilic cavity in the permease that is open to the cytoplasm. Those cysteine residues that are not labeled, most notably on helices VI and XII, are presumed to either face the fatty acyl chains of the phospholipids or to be located in tightly packed regions of the molecule, thus making them inaccessible to NEM.

The image in Figure 4.21*b* shows those residues (depicted as gold spheres) that show a significant *increase* in reactivity to NEM when the permease is incubated with the sugar to be transported. The difference in NEM reactivity of the residues between the protein in the absence of the sugar (*a*) and the presence of the sugar (*b*) indicates that different parts of the protein are accessible to the aqueous medium under these two conditions. The results, in other words, suggest that addition of the sugar induces a conformational change in the permease. Careful analysis of the positions of the residues that become labeled in these two conformations supports the model shown in Figure 4.21*c*. According to this model of alternating access, the sugar-binding site is open to the cytoplasm of the bacterial cell in one conformation and is open to the extracellular space in the other conformation. Alternation between the two conformations brings about transport of the sugar across the membrane. This type of ion-driven transport system is discussed further on page 155.

Determining spatial relationships between specific amino acids in a membrane protein is another approach to learning about dynamic events that occur as a protein carries out its function. One way to learn about the distance between selected residues in a protein is to introduce chemical groups whose properties are sensitive to the distance that separates them. *Nitroxides* are chemical groups that contain an unpaired electron, which produces a characteristic spectrum when monitored by a technique called *electron paramagnetic resonance (EPR) spectroscopy*. A nitroxide group can be introduced at any site in a protein by first mutating that site to a cysteine and then attaching the nitroxide to the —SH group of the cysteine residue. **FIGURE 4.22** shows how this technique was used to discover the conformational changes that occur in a membrane protein as its channel is opened in response to changes in the pH of the medium. The protein in question, a bacterial K^+ channel, is a tetramer composed of four identical subunits. The cytoplasmic opening to the channel is bounded by four transmembrane helices, one from each subunit of the protein. Figure 4.22*a* shows the EPR spectra that were obtained when a nitroxide was introduced near the cytoplasmic end of each transmembrane helix. The red line shows the spectrum obtained at pH 6.5 when the channel is in the closed state, and the blue line shows the spectrum at pH 3.5 when the channel is open. The shape of each line depends on the proximity of the nitroxides to one another. The spectrum is broader at pH 6.5 because the nitroxide groups on the four subunits are closer together at this pH, which decreases the intensity of their EPR signals. These results indicate that the activation of the channel is accompanied by an increased separation between the labeled residues of the four subunits (Figure 4.22*b*). An increase in diameter of the channel opening allows ions in the cytoplasm to reach the actual permeation pathway (shown in red) within the channel, which allows only the passage of K^+ ions (discussed on page 144). An alternate technique, called FRET, that can also be used to measure changes in the distance between labeled groups within a protein, is illustrated in Figure 18.8. As discussed in Chapter 2, NMR spectroscopy is another technique that provides information about distances between atoms in a protein structure, and recently NMR has become increasingly the method of choice for studying dynamics of membrane proteins.



(a) (b)

FIGURE 4.22 Use of EPR spectroscopy to monitor changes in conformation of a bacterial K^+ ion channel as it opens and closes. (*a*) EPR spectra from nitroxides that have been attached to cysteine residues near the cytoplasmic end of the four transmembrane helices that line the channel. The cysteine residue in each helix replaces a glycine residue that is normally at that position. The shapes of the spectra depend on the distances between unpaired electrons in the nitroxides on different subunits. (Nitroxides are described as "spin-labels," and this technique is known as site-directed spin labeling.) (*b*) A highly schematic model of the ion channel in the open and closed states based on the data from part *a*. Opening of the channel is accompanied by the movement of the four nitroxide groups apart from one another.

SOURCE: (*a*) Reprinted by permission from Macmillan Publishers Ltd: From E. Perozo et al., *Nature Struct. Biol.* 5:468, 1998.

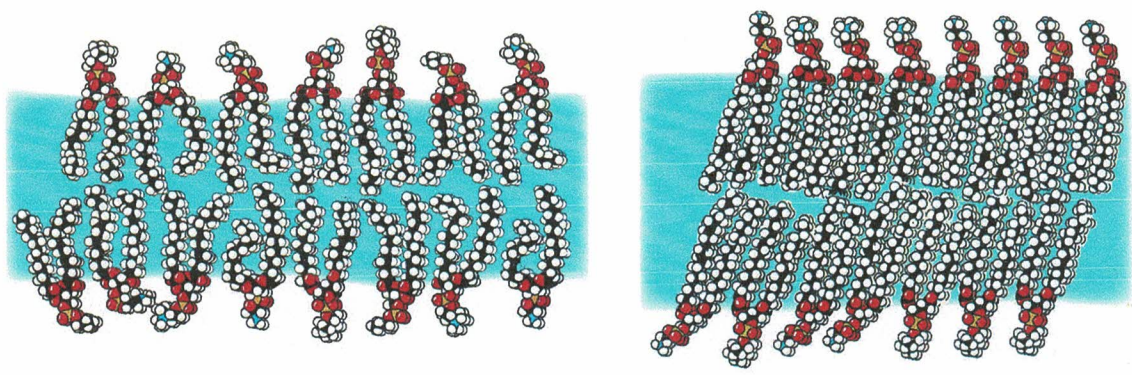
REVIEW

1. Why are detergents necessary to solubilize membrane proteins? How might one determine the diversity of integral proteins that reside in a purified membrane fraction?
2. How can one determine: (1) the location of transmembrane segments in the amino acid sequence or (2) the relative locations of transmembrane helices with access to the external medium?

4.6 Membrane Lipids and Membrane Fluidity

The physical state of the lipid of a membrane is described by its fluidity (or viscosity).[4] Consider a simple artificial bilayer composed of phosphatidylcholine and phosphatidylethanolamine, whose fatty acids are largely unsaturated. If the temperature of the bilayer is kept relatively warm (e.g., 37°C), the lipid exists in a relatively fluid state (**FIGURE 4.23a**).

[4]Fluidity and viscosity are inversely related; fluidity is a measure of the ease of flow, and viscosity is a measure of the resistance to flow.



(a) (b)

FIGURE 4.23 The structure of the lipid bilayer depends on the temperature. The bilayer shown here is composed of two phospholipids: phosphatidylcholine and phosphatidylethanolamine. (*a*) Above the transition temperature, the lipid molecules and their hydrophobic tails are free to move in certain directions, even though they retain a considerable degree of order. (*b*) Below the transition temperature, the movement of the molecules is greatly restricted, and the entire bilayer can be described as a crystalline gel.

SOURCE: (*a*, *b*) R. N. Robertson, *The Lively Membranes*, Cambridge Univ. Press, 1983, reprinted with permission of Cambridge Univ. Press.

At this temperature, the lipid bilayer is best described as a two-dimensional liquid crystal. As in a crystal, the molecules still retain a specified orientation; in this case, the long axes of the molecules tend toward a parallel arrangement, yet individual phospholipids can rotate around their axis or move laterally within the plane of the bilayer. If the temperature is slowly lowered, a point is reached where the bilayer distinctly changes (Figure 4.23*b*). The lipid is converted from a liquid crystalline phase to a frozen crystalline gel in which the movement of the phospholipid fatty acid chains is greatly restricted. The temperature at which this change occurs is called the **transition temperature**.

The transition temperature of a particular bilayer depends on the ability of the lipid molecules to be packed together, which depends in turn on the particular lipids of which it is constructed. Saturated fatty acids have the shape of a straight, flexible rod. *Cis*-unsaturated fatty acids, on the other hand, have crooks in the chain at the sites of a double bond (Figures 2.19 and 4.23). Consequently, phospholipids with saturated chains pack together more tightly than those containing unsaturated chains. The greater the degree of unsaturation of the fatty acids of the bilayer, the *lower* the temperature before the bilayer gels. The introduction of one double bond in a molecule of stearic acid lowers the melting temperature almost 60°C (Table 4.2).[5] Another factor that influences bilayer fluidity is fatty acid chain length. The shorter the fatty acyl chains of a phospholipid, the lower its melting temperature. The physical state of the membrane is also affected by cholesterol. Because of their orientation within the bilayer (Figure 4.7), cholesterol molecules disrupt the close packing of fatty acyl chains and interfere with their mobility. The presence of cholesterol tends to abolish sharp transition temperatures and creates a condition of intermediate fluidity. In physiologic terms, cholesterol tends to increase the durability while decreasing the permeability of a membrane.

The Importance of Membrane Fluidity

What effect does the physical state of the lipid bilayer have on the biological properties of the membrane? Membrane fluidity provides a perfect compromise between a rigid, ordered structure in which mobility would be absent and a completely fluid, nonviscous liquid in which the components of the membrane could not be oriented and structural organization and mechanical support would be lacking. In addition, fluidity allows for interactions to take place within the membrane. For example, membrane fluidity makes it possible for clusters of membrane proteins to assemble at particular sites within the membrane and form specialized structures, such as intercellular junctions, light-capturing photosynthetic complexes, and synapses. Because of membrane fluidity, molecules that interact can come together, carry out the necessary reaction, and move apart.

[5]The effect of fatty acid saturation on melting temperature is illustrated by familiar food products. Vegetable oils remain a liquid in the refrigerator, whereas margarine is a solid. Vegetable oils contain polyunsaturated fatty acids, whereas the fatty acids of margarine have been saturated by a chemical process that hydrogenates the double bonds of the vegetable oils used as the starting material.

TABLE 4.2 Melting Points of the Common 18-Carbon Fatty Acids

Fatty acid	*cis* Double bonds	M.p. (°C)
Stearic acid	0	70
Oleic acid	1	13
Linoleic acid	2	−9
Linolenic acid	3	−17
Eicosapentanoic acid (EPA)*	5	−54

*EPA has 20 carbons.

Fluidity also plays a key role in membrane assembly, a subject discussed in Chapter 8. Membranes arise only from preexisting membranes, and their growth is accomplished by the insertion of lipids and proteins into the fluid matrix of the membranous sheet. Many of the most basic cellular processes, including cell movement, cell growth, cell division, formation of intercellular junctions, secretion, and endocytosis, depend on the movement of membrane components and would probably not be possible if membranes were rigid, nonfluid structures.

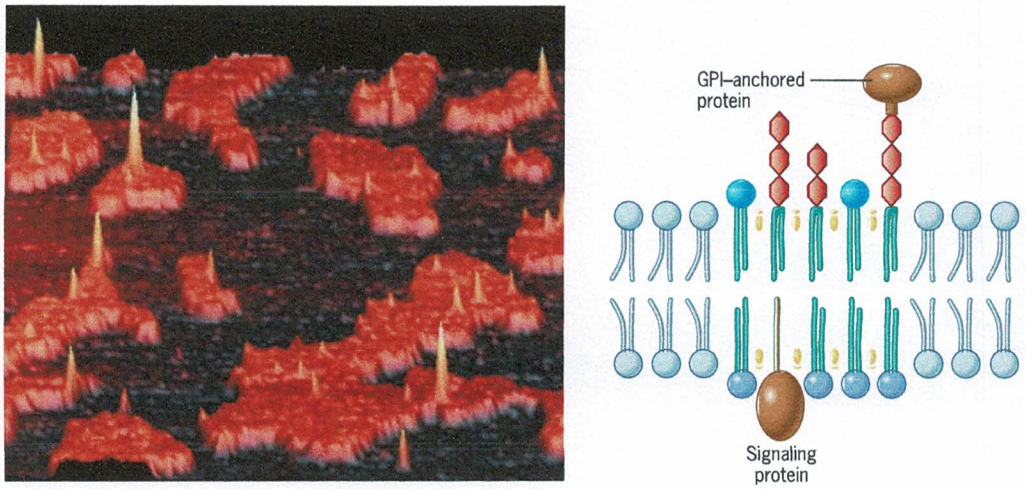
Maintaining Membrane Fluidity

The internal temperature of most organisms (other than birds and mammals) fluctuates with the temperature of the external environment. Because it is essential for many activities that the membranes of a cell remain in a fluid state, cells respond to changing conditions by altering the types of phospholipids of which they are made. Maintenance of membrane fluidity is an example of homeostasis at the cellular level and can be demonstrated in various ways. For example, if the temperature of a culture of cells is lowered, the cells respond metabolically. The initial "emergency" response is mediated by enzymes that remodel membranes, making the cell more cold resistant. Remodeling is accomplished by (1) desaturating single bonds in fatty acyl chains to form double bonds, and (2) reshuffling the chains between different phospholipid molecules to produce ones that contain two unsaturated fatty acids, which greatly lowers the melting temperature of the bilayer. Desaturation of single bonds to form double bonds is catalyzed by enzymes called *desaturases*. Reshuffling is accomplished by *phospholipases*, which split the fatty acid from the glycerol backbone, and *acyltransferases*, which transfer fatty acids between phospholipids. In addition, the cell changes the types of phospholipids being synthesized in favor of ones containing more unsaturated fatty acids. As a result of the activities of these various enzymes, the physical properties of a cell's membranes are matched to the prevailing environmental conditions. Maintenance of fluid membranes by adjustments in fatty acyl composition has been demonstrated in a variety of organisms, including hibernating mammals, pond-dwelling fish whose body temperature changes markedly from day to night, cold-resistant plants, and bacteria living in hot springs. Prokaryotic cells that live at very high temperatures have plasma membranes that contain highly unusual lipids.

Lipid Rafts

Every so often an issue emerges that splits the community of cell biologists into believers and nonbelievers. The issue of lipid rafts falls into this category. When membrane lipids are extracted from cells and used to prepare *artificial* lipid bilayers, cholesterol and sphingolipids tend to self-assemble into microdomains that are more gelated and highly ordered than surrounding regions consisting primarily of phosphoglycerides. Because of their distinctive physical properties, such microdomains tend to float within the more fluid and disordered environment of the artificial bilayer (FIGURE 4.24a). As a result, these patches of cholesterol and sphingolipid are referred to as **lipid rafts**. When added to these artificial bilayers, certain proteins tend to become concentrated in the lipid rafts, whereas others tend to remain outside their boundaries. GPI-anchored proteins show a particular fondness for the ordered regions of the bilayer (Figure 4.24*a*).

The controversy arises over whether similar types of sphingolipid- and cholesterol-rich lipid rafts, such as that illustrated in Figure 4.24*b*, exist within living cells. Most of the evidence in favor of lipid rafts is derived from studies that employ unnatural treatments, such as



(a) (b)

FIGURE 4.24 Lipid rafts. (a) Image of the upper surface of an artificial lipid bilayer containing phosphatidylcholine, which appears as the black background, and sphingomyelin molecules, which organize themselves spontaneously into the orange-colored rafts. The yellow peaks show the positions of a GPI-anchored protein, which is almost exclusively raft-associated. This image is provided by an atomic force microscope, which measures the height of various parts of the specimen at the molecular level. (b) Schematic model of a lipid raft within a cell. The outer leaflet of the raft consists primarily of cholesterol (yellow) and sphingolipids (red head groups). Phosphatidylcholine molecules (blue head groups) with long saturated fatty acids also tend to concentrate in this region. GPI-anchored proteins are thought to become concentrated in lipid rafts. The lipids in the outer leaflet of the raft have an organizing effect on the lipids of the inner leaflet. As a result, the inner-leaflet raft lipids consist primarily of cholesterol and glycerophospholipids with long saturated fatty acyl tails. The inner leaflet tends to concentrate lipid-anchored proteins, such as Src kinase, that are involved in cell signaling. (The controversy over the existence of lipid rafts is discussed in *Nature Revs. Mol. Cell Biol.* 11:688, 2010 and *Science* 334:1046, 2011.)

SOURCE: (a) From D. E. Saslowsky, et al., *J. Biol. Chem.* 277, cover of #30, July 26, 2002; (b) Courtesy of J. Michael Edwardson © 2002 The American Society for Biochemistry and Molecular Biology.

detergent extraction, cholesterol depletion, or crosslinking of membrane proteins. The artificial nature of these treatments makes the results difficult to interpret. Attempts to demonstrate the presence of lipid rafts in living cells have generally been unsuccessful, which can either mean that such rafts do not exist or they are so small (5 to 25 nm diameter) and short-lived as to be difficult to detect with current techniques. The concept of lipid rafts is very appealing because it provides a means to introduce order into a seemingly random sea of lipid molecules. Lipid rafts are postulated to serve as floating platforms that concentrate particular proteins, thereby organizing the membrane into functional compartments (Figure 4.24*b*). For example, lipid rafts are thought to provide a favorable local environment for cell-surface receptors to interact with other membrane proteins that transmit signals from the extracellular space to the cell interior.

REVIEW

1. What is the importance of fatty acid unsaturation for membrane fluidity? Of enzymes that are able to desaturate fatty acids?
2. What is meant by a membrane's transition temperature, and how is it affected by the degree of saturation or length of fatty acyl chains? How are these properties important in the formation of lipid rafts?
3. Why is membrane fluidity important to a cell?
4. How can the two sides of a lipid bilayer have different ionic charges?

4.7 The Dynamic Nature of the Plasma Membrane

It is apparent from the previous discussion that the lipid bilayer can exist in a relatively fluid state. As a result, a phospholipid can move laterally within the same leaflet with considerable ease. The mobility of individual lipid molecules within the bilayer of the plasma membrane can be directly observed under the microscope by linking the polar heads of the lipids to gold particles or fluorescent compounds (see Figure 4.29). It is estimated that a phospholipid can diffuse from one end of a bacterium to the other end in a second or two. In contrast, it takes a phospholipid molecule a matter of hours to days to move across to the other leaflet. Thus, of all the possible motions that a phospholipid can make, its flip-flop to the other side of the membrane is the most restricted (**FIGURE 4.25**). This finding is not surprising. For flip-flop to occur, the hydrophilic head group of the lipid must pass through the internal hydrophobic sheet of the membrane, which is thermodynamically unfavorable. However, cells contain enzymes that actively move certain phospholipids from one leaflet to the other. These enzymes, known as *flippases*, play a role in establishing lipid asymmetry.

Because lipids provide the matrix in which integral proteins of a membrane are embedded, the physical state of the lipid is an important determinant of the mobility of integral proteins. The demonstration that integral proteins can move within the plane of the membrane was a cornerstone in the formulation of the fluid-mosaic model. The dynamic properties of membrane proteins have been revealed in several ways.

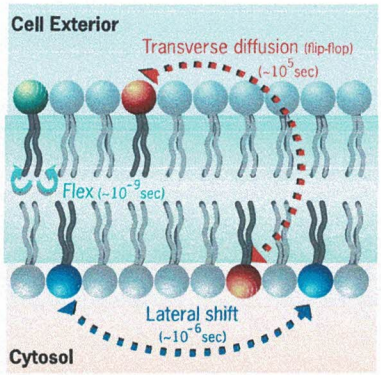


FIGURE 4.25 The possible movements of phospholipids in a membrane. The types of movements in which membrane phospholipids can engage and the approximate time scales over which they occur. Whereas phospholipids move from one leaflet to another at a very slow rate, they diffuse laterally within a leaflet rapidly. Lipids lacking polar groups, such as cholesterol, can move across the bilayer quite rapidly.

The Diffusion of Membrane Proteins after Cell Fusion

Cell fusion is a technique whereby two different types of cells, or cells from two different species, can be fused to produce one cell with a common cytoplasm and a single, continuous plasma membrane. Cells are induced to fuse with one another by making the outer surface of the cells "sticky" so that their plasma membranes adhere to one another. Cells can be induced to fuse by addition of certain inactivated viruses that attach to the surface membrane, by adding the compound polyethylene glycol, or by a mild electric shock. Cell fusion has played an important role in cell biology and is currently used in an invaluable technique to prepare specific antibodies (Section 18.26).

The first experiments to demonstrate that membrane proteins could move within the plane of the membrane utilized cell fusion, and they were reported in 1970 by Larry Frye and Michael Edidin of Johns Hopkins University. In their experiments, mouse and human cells were fused, and the locations of specific proteins of the plasma membrane were followed once the two membranes had become continuous. To follow the distribution of either the mouse membrane proteins or the human membrane proteins at various times after fusion, antibodies against one or the other type of protein were prepared and covalently linked to fluorescent dyes. The antibodies against the mouse proteins were complexed with a dye that fluoresces green and the antibodies against human proteins with one that fluoresces red. When the antibodies were added to fused cells, they bound to the human or mouse proteins and could be located under a fluorescence light microscope (FIGURE 4.26a). At the time of fusion, the plasma membrane appeared half human and half mouse; that is, the two protein types remained segregated in their own hemisphere (step 3, Figure 4.26*a*,*b*). As the time after fusion increased, the membrane proteins were seen to move laterally within the membrane into the opposite hemisphere. By about 40 minutes, each species' proteins were uniformly distributed around the entire hybrid cell membrane (step 4, Figure 4.26*a*). If the same experiment was performed at lower temperature, the viscosity of the lipid bilayer increased, and the mobility of the membrane proteins decreased. These early cell fusion experiments gave the impression that integral membrane proteins were capable of virtually unrestricted movements. As we will see shortly, subsequent studies made it apparent that membrane dynamics was a much more complex subject than first envisioned.

Restrictions on Protein and Lipid Mobility

Several techniques allow researchers to follow the movements of molecules in the membranes of living cells using the light microscope. In a technique called **fluorescence recovery after photobleaching (FRAP)**, which is illustrated in FIGURE 4.27a, integral membrane components in cultured cells are first labeled by linkage to a fluorescent dye. A particular membrane protein can be labeled using a specific probe, such as a fluorescent antibody. Once labeled, cells are placed under the microscope and irradiated by a sharply focused laser beam that bleaches the fluorescent molecules in its path, leaving a circular spot (typically about 1 μm diameter) on the surface of the cell that is largely devoid of fluorescence. If the labeled

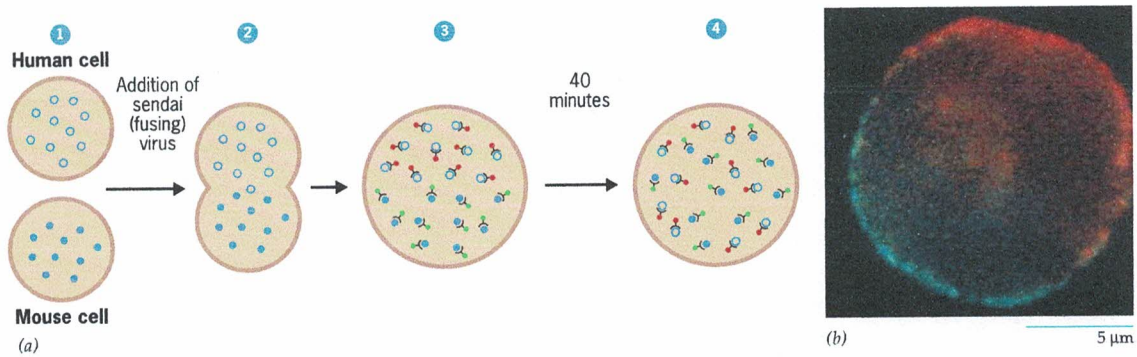


FIGURE 4.26 The use of cell fusion to reveal mobility of membrane proteins. (*a*) Outline of the experiment in which human and mouse cells were fused (steps 1–2) and the distribution of the proteins on the surface of each cell were followed in the hybrids over time (steps 3–4). Mouse membrane proteins are indicated by solid circles, human membrane proteins by open circles. Locations of human and mouse proteins in the plasma membranes of the hybrid cells were monitored by interaction with fluorescent red and fluorescent green antibodies, respectively. (*b*) Micrograph showing a fused cell in which mouse and human proteins are still in their respective hemispheres (equivalent to the hybrid in step 3 of part *a*).

SOURCE: (*b*) From L. D. Frye and Michael Edidin, *J. Cell Science* 7:328, 334, 1970, By Permission of The Company of Biologists, Ltd. Courtesy of Michael Edidin, Johns Hopkins University.http://jcs.biologists.org/content/7/2/319 full.pdf+html?sid=d93ae648-abca-4f5d-90a6- a6d9726d7d30.

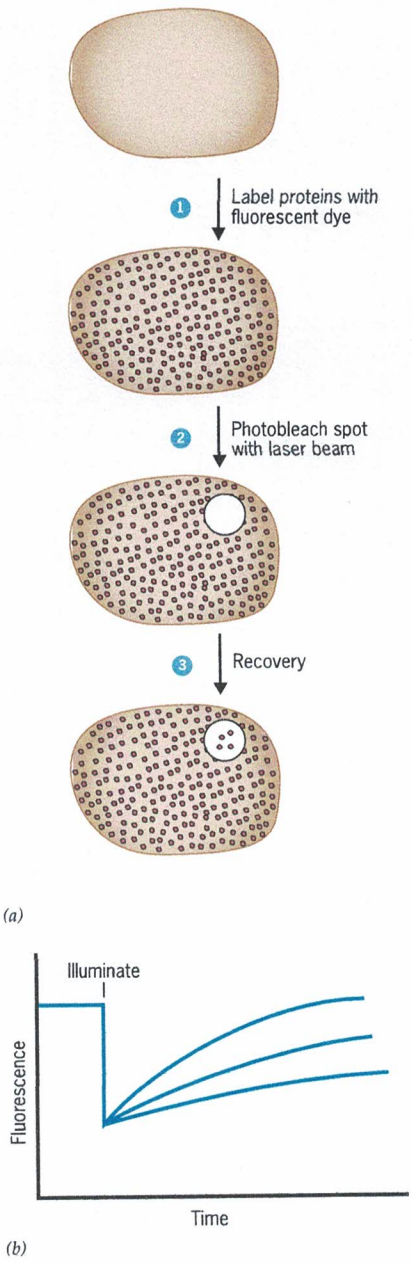


FIGURE 4.27 Measuring the diffusion rates of membrane proteins by fluorescence recovery after photobleaching (FRAP). (*a*) In this technique, a particular component of the membrane is first labeled with a fluorescent dye (step 1). A small region of the surface is then irradiated to bleach the dye molecules (step 2), and the recovery of fluorescence in the bleached region is followed over time (step 3). (*b*) The rate of fluorescence recovery within the illuminated spot can vary depending on the protein(s) being followed. The rate of recovery is related to the diffusion coefficient of the fluorescently labeled protein.

proteins in the membrane are mobile, then the random movements of these molecules should produce a gradual reappearance of fluorescence in the irradiated circle. The rate of fluorescence recovery (Figure 4.27*b*) provides a direct measure of the rate of diffusion (expressed as a diffusion coefficient, *D*) of the mobile molecules. The extent of fluorescence recovery (expressed as a percentage of the original intensity) provides a measure of the percentage of the labeled molecules that are free to diffuse.

Early studies utilizing FRAP suggested that (1) membrane proteins moved much more slowly in the plasma membrane of living cells than they would in a pure lipid bilayer and (2) a significant fraction of membrane proteins (30 to 70 percent) were not free to diffuse back into the irradiated circle. But the FRAP technique has its drawbacks. FRAP can only follow the average movement of a relatively large number of labeled molecules (hundreds to thousands) as they diffuse over a relatively large distance (e.g., 1 μm). As a result, researchers using FRAP cannot distinguish between proteins that are truly immobile and ones that can only diffuse over a limited distance in the time allowed. To get around these limitations, alternate techniques have been developed that allow researchers to observe the movements of individual protein molecules over very short distances and to determine how they might be restrained.

In **single-particle tracking (SPT)**, individual membrane protein molecules are labeled, usually with fluorescent molecular tags that emit light under a microscope. The movements of the labeled molecules are then followed by a type of microscopy known as TIRF (Total Internal Reflection Fluorescence) that is specialized for imaging fluorescent molecules at the surface of cells. The results of these studies often depend on the particular protein being investigated. For example,

- Some membrane proteins move randomly throughout the membrane (Figure 4.28, protein A), although generally at rates considerably less than would be measured in an artificial lipid bilayer. (If protein mobility were based strictly on physical parameters such as lipid viscosity and protein size, one would expect proteins to migrate with diffusion coefficients of approximately 10^{-8} to 10^{-9} cm^2/sec rather than 10^{-10} to 10^{-12} cm^2/sec, as is observed for molecules of this group.) The reasons for the reduced diffusion coefficient have been debated.
- Some membrane proteins fail to move and are considered to be immobilized (Figure 4.28, protein B).
- In some cases, a protein is found to move in a highly directed (i.e., nonrandom) manner toward one part of the cell or another (Figure 4.28, protein C). For example, a particular membrane protein may tend to move toward the leading or the trailing edge of a moving cell.
- In most studies, the largest fraction of protein species exhibit random (Brownian) movement within the membrane at rates consistent with free diffusion (diffusion coefficients about 5×10^{-9} cm^2/sec), but the molecules are unable to migrate freely more than a few tenths of a micrometer. Long-range diffusion occurs but at slower rates, apparently because of the presence of a system of barriers. These barriers are discussed in the following sections.

CONTROL OF MEMBRANE PROTEIN MOBILITY It is apparent that plasma membrane proteins are not totally free to drift around randomly on the lipid "sea." Instead, this class of proteins is subjected to various influences that affect their mobility and, in doing so, promote intramembrane organization. Some membranes are crowded with proteins, so that the random movements of one molecule can be impeded by its neighbors (FIGURE 4.28, protein D).

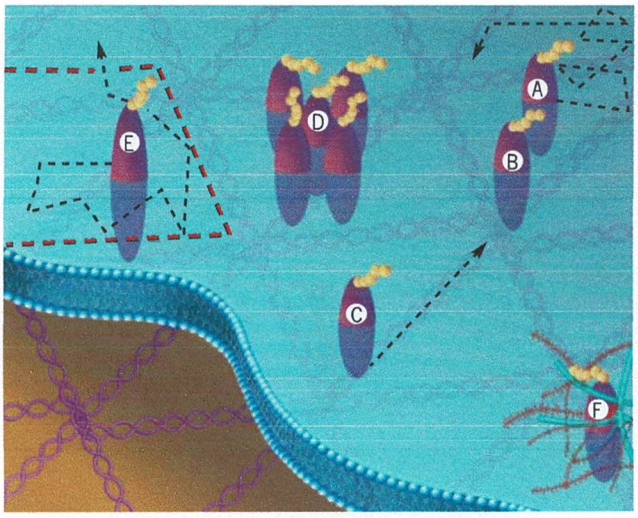


FIGURE 4.28 Patterns of movement of integral membrane proteins. Depending on the cell type and the conditions, integral membrane proteins can exhibit several different types of mobility. Protein A is capable of diffusing randomly throughout the membrane, though its rate of movement may be limited; protein B is immobilized as the result of its interaction with the underlying membrane skeleton; protein C is being moved in a particular direction as the result of its interaction with a motor protein at the cytoplasmic surface of the membrane; movement of protein D is restricted by other integral proteins of the membrane; movement of protein E is restricted by fences formed by proteins of the membrane skeleton, but it can hop into adjacent compartments through transient openings in a fence; movement of protein F is restrained by extracellular materials.

The strongest influences on an integral membrane protein are thought to be exerted from just beneath the membrane on its cytoplasmic face. The plasma membranes of many cells possess a fibrillar network, or "membrane skeleton," consisting of peripheral proteins situated on the cytoplasmic surface of the membrane. A certain proportion of a membrane's integral protein molecules are either tethered to the membrane skeleton (Figure 4.28, protein B) or otherwise restricted by it.

Information concerning the presence of membrane barriers has been obtained using an innovative technique that allows investigators to trap integral proteins and drag them through the plasma membrane with a known force. This technique, which uses an apparatus referred to as *optical tweezers*, takes advantage of the tiny optical forces that are generated by a focused laser beam. The integral proteins to be studied are tagged with antibody-coated beads, which serve as handles that can be gripped by the laser beam. It is generally found that optical tweezers can drag an integral protein for a limited distance before the protein encounters a barrier that causes it to be released from the laser's grip. As it is released, the protein typically springs backward, suggesting that the barriers are elastic structures.

One approach to studying factors that affect membrane protein mobility is to genetically modify cells so that they produce altered membrane proteins. Integral proteins whose cytoplasmic portions have been genetically deleted often move much greater *distances* than their intact counterparts, indicating that barriers reside on the cytoplasmic side of the membrane. These findings suggest that the membrane's underlying skeleton forms a network of "fences" around portions of the membrane, creating compartments that restrict the distance an integral protein can travel (Figure 4.28, protein E). Proteins move across the boundaries from one compartment to another through breaks in the fences. Such openings are thought to appear and disappear along with the dynamic disassembly and reassembly of parts of the meshwork. Membrane compartments may keep specific combinations of proteins in close enough proximity to facilitate their interaction.

Integral proteins lacking that portion that would normally project into the extracellular space typically move at a much faster *rate* than the wild-type version of the protein. This finding suggests that the movement of a transmembrane protein through the bilayer is slowed by extracellular materials that can entangle the external portion of the protein molecule (Figure 4.28, protein F).

MEMBRANE LIPID MOBILITY Proteins are huge molecules, so it isn't surprising that their movement within the lipid bilayer might be restricted. Phospholipids, by comparison, are small molecules that make up the very fabric of the lipid bilayer. One might expect their movements to be completely unfettered, yet a number of studies have suggested that phospholipid diffusion is also restricted. When individual phospholipid molecules of a plasma membrane are tagged and followed under the microscope using ultra-high-speed cameras, they are seen to be confined for very brief periods and then hop from one confined area to another. **FIGURE 4.29a** shows the path taken by an individual phospholipid within the

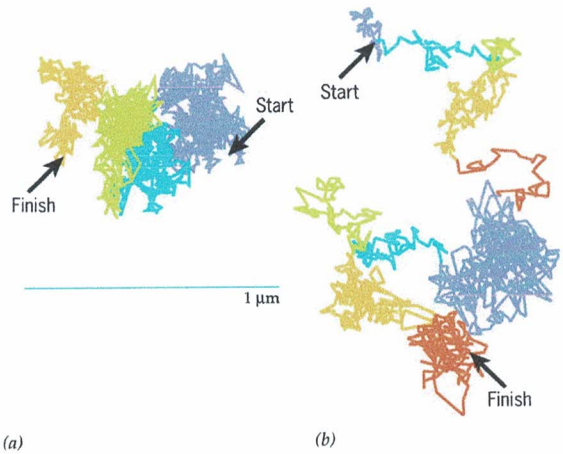


FIGURE 4.29 Experimental demonstration that diffusion of phospholipids within the plasma membrane is confined. (a) The track of a single labeled unsaturated phospholipid is followed for 56 ms as it diffuses within the plasma membrane of a rat fibroblast. Phospholipids diffuse freely within a confined compartment before hopping into a neighboring compartment. The rate of diffusion within a compartment is as rapid as that expected by unhindered Brownian movement. However, the overall rate of diffusion of the phospholipid appears slowed because the molecule must hop a barrier to continue its movement. The movement of the phospholipid within each compartment is represented by a single color. (*b*) The same experiment shown in *a* is carried out for 33 ms in an artificial bilayer, which lacks the "picket fences" present in a cellular membrane. The much more open, extended trajectory of the phospholipid can now be explained by simple, unconfined Brownian movement. For the sake of comparison, fake compartments were assigned in *b* and indicated by different colors.

SOURCE: From Takahiro Fujiwara et al., Courtesy of Akihiro Kusumi, Nagoya, *J. Cell Biol.* 157:1073, 2002; Reproduced with permission of The Rockefeller University Press.

plasma membrane over a period of 56 milliseconds. Computer analysis indicates that the phospholipid diffuses freely within one compartment (shaded in purple) before it jumps the "fence" into a neighboring compartment (shaded in blue) and then over another fence into an adjacent compartment (shaded in green), and so forth. Treatment of the membrane with agents that disrupt the underlying membrane skeleton removes some of the fences that restrict phospholipid diffusion. But if the membrane skeleton lies beneath the lipid bilayer, how can it interfere with phospholipid movement? The authors of these studies speculate that the fences are constructed of rows of integral membrane proteins whose cytoplasmic domains are attached to the membrane skeleton. This is not unlike the confinement of horses or cows by a picket fence whose posts are embedded in the underlying soil.

MEMBRANE DOMAINS AND CELL POLARITY For the most part, studies of membrane dynamics, such as those discussed above, are carried out on the relatively homogeneous plasma membrane situated at the upper or lower surface of a cell residing on a culture dish. Most membranes, however, exhibit distinct variations in protein composition and mobility, especially in cells whose various surfaces display distinct functions. For example, the epithelial cells that line the intestinal wall or make up the microscopic tubules of the kidney are highly polarized cells whose different surfaces carry out different functions (FIGURE 4.30). Studies indicate that the apical plasma membrane, which selectively absorbs substances from the lumen, possesses different enzymes than the lateral plasma membrane, which interacts with neighboring epithelial cells, or the basal membrane, which adheres to an underlying extracellular substrate (a *basement membrane*). In other examples, the receptors for neurotransmitter substances are concentrated into regions of the plasma membrane located within synapses (see Figure 4.57), and receptors for low-density lipoproteins are concentrated into patches of the plasma membrane specialized to facilitate their internalization (see Figure 8.38).

Of all the various types of mammalian cells, sperm may have the most highly differentiated structure. A mature sperm can be divided into head, midpiece, and tail, each having its own specialized functions. Although divided into a number of distinct parts, a sperm is covered by a *continuous* plasma membrane which, as revealed by numerous techniques, consists of a mosaic of different types of localized domains. For example, when sperm are treated with a variety of antibodies, each antibody combines with the surface of the cell in a unique topographic pattern that reflects the distribution within the plasma membrane of the particular protein antigen recognized by that antibody (FIGURE 4.31).

REVIEW

1. Describe two techniques to measure the rates of diffusion of a specific membrane protein.
2. Compare and contrast the types of protein mobility depicted in Figure 4.28.
3. Compare the rate of lateral diffusion of a lipid with that of flip-flop. What is the reason for the difference?

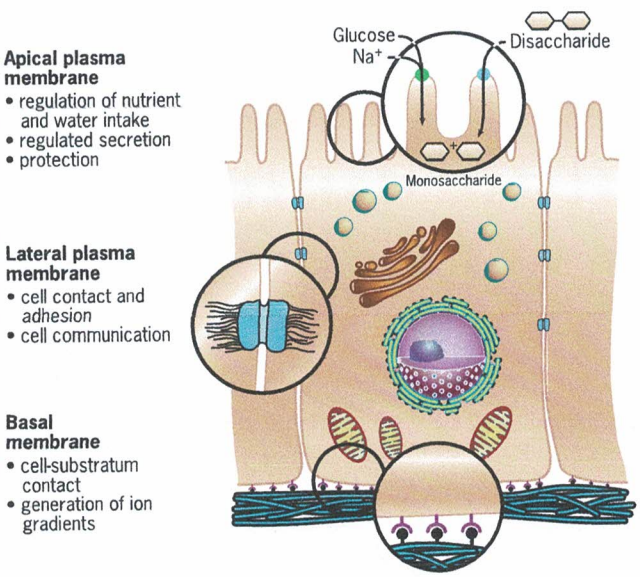


FIGURE 4.30 Differentiated functions of the plasma membrane of an epithelial cell. The apical surface of this intestinal epithelial cell contains integral proteins that function in ion transport and hydrolysis of disaccharides, such as sucrose and lactose; the lateral surface contains integral proteins that function in intercellular interaction; and the basal surface contains integral proteins that function in the association of the cell with the underlying basement membrane.

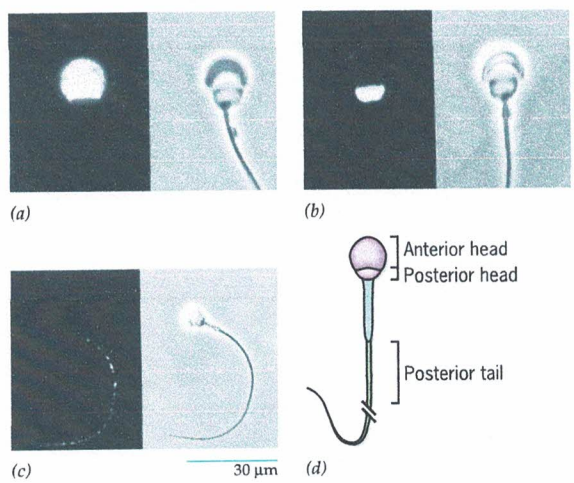


FIGURE 4.31 Differentiation of the mammalian sperm plasma membrane as revealed by fluorescent antibodies. (a–c) Three pairs of micrographs, each showing the distribution of a particular protein at the cell surface as revealed by a bound fluorescent antibody. The three proteins are localized in different parts of the continuous sperm membrane. Each pair of photographs shows the fluoresence pattern of the bound antibody and a phase contrast micrograph of the same cell. (*d*) Diagram summarizing the distribution of the proteins.

SOURCE: (a–c) From Diana G. Myles, Paul Primakoff, and Anthony R. Bellvé, *Cell* 23:434,1981 © with permission from Elsevier.

4.8 The Red Blood Cell: An Example of Plasma Membrane Structure

Of all the diverse types of membranes, the plasma membrane of the human erythrocyte (red blood cell) is the most studied and best understood (**FIGURE 4.32a**). There are several reasons for the popularity of this membrane. The cells are inexpensive to obtain and readily available in huge numbers from whole blood. They are already present as single cells and need not be dissociated from a complex tissue. The cells are simple by comparison with other cell types, lacking nuclear and cytoplasmic membranes that inevitably contaminate plasma membrane preparations from other cells. In addition, purified, *intact* erythrocyte plasma membranes can be obtained simply by placing the cells in a dilute (hypotonic) salt solution. The cells respond to this osmotic shock by taking up water and swelling, a phenomenon termed *hemolysis*. As the surface area of each cell increases, the cell becomes leaky, and the contents, composed almost totally of dissolved hemoglobin, flow out of the cell leaving behind a plasma membrane "ghost" (Figure 4.32*b*).

Once erythrocyte plasma membranes are isolated, the proteins can be solubilized and separated from one another (fractionated), providing a better idea of the diversity of proteins within the membrane. Fractionation of membrane proteins can be accomplished using polyacrylamide gel electrophoresis (PAGE) in the presence of the ionic detergent sodium dodecyl sulfate (SDS). (The technique of SDS–PAGE is discussed in Section 18.13.) The SDS keeps the integral proteins soluble and, in addition, adds a large number of negative charges to the proteins with which it associates. Because the number of charged SDS molecules per unit weight of protein tends to be relatively constant, the molecules separate from one another according to their molecular weight. The largest proteins move most slowly through the molecular sieve of the gel. The major proteins of the erythrocyte membrane are separated into about a dozen conspicuous bands by SDS–PAGE (Figure 4.32*c*). Among the proteins are a variety of enzymes (including glyceraldehyde 3-phosphate dehydrogenase, one of the enzymes of glycolysis), transport proteins (for ions and sugars), and skeletal proteins (e.g., spectrin).

Integral Proteins of the Erythrocyte Membrane

A model of the erythrocyte plasma membrane showing its major proteins is seen in Figure 4.32*d*. The most abundant integral proteins of this membrane are a pair of carbohydrate-containing, membrane-spanning proteins called band 3 and glycophorin A. The high density of these proteins within the membrane is evident in the freeze-fracture micrographs of Figure 4.15. Band 3, which gets its name from its position in an electrophoretic gel (Figure 4.32*c*), is present as a dimer composed of two identical subunits (a *homodimer*). Each subunit spans the membrane at least a dozen times and contains a relatively small amount of carbohydrate (6–8 percent of the molecule's weight). Band 3 protein serves as a channel for the passive exchange of anions across the membrane. As blood circulates through the tissues, carbon dioxide becomes dissolved in the fluid of the bloodstream (the plasma) and undergoes the following reaction:

$$H_2O + CO_2 \rightarrow H_2CO_3 \rightarrow HCO_3^- + H^+$$

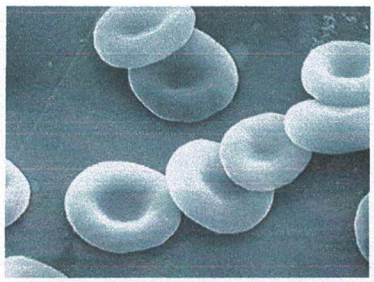
The bicarbonate ions (HCO_3^-) enter the erythrocyte in exchange for chloride ions, which leave the cell. In the lungs, where carbon dioxide is released, the reaction is reversed and bicarbonate ions leave the erythrocyte in exchange for chloride ions. The reciprocal movement of HCO_3^- and Cl^- occurs through a channel in the center of each band 3 dimer.

Glycophorin A was the first membrane protein to have its amino acid sequence determined. The arrangement of the polypeptide chain of glycophorin A within the plasma membrane is shown in Figure 4.18. (Other related glycophorins, B, C, D, and E, are also present in the membrane at much lower concentrations.) Like band 3, glycophorin A is also present in the membrane as a dimer. Unlike band 3, each glycophorin A subunit spans the membrane only once, and it contains a bushy carbohydrate cover consisting of 16 oligosaccharide chains that together make up about 60 percent of the molecule's weight. It is thought that the primary function of glycophorin derives from the large number of negative charges borne on sialic acid, the sugar residue at the end of each carbohydrate chain. Because of these charges, red blood cells repel each other, which prevents the cells from clumping as they circulate through the body's tiny vessels. It is noteworthy that persons who lack both glycophorin A and B in their red blood cells show no ill effects from their absence. At the same time, the band 3 proteins in these individuals are more heavily glycosylated, which apparently compensates for the otherwise missing negative charges required to prevent cell–cell interaction. Glycophorin also happens to be the receptor utilized by the protozoan that causes malaria, providing a path for entry into the blood cell. Consequently, individuals whose erythrocytes lack glycophorin A and B are thought to be protected from acquiring malaria.

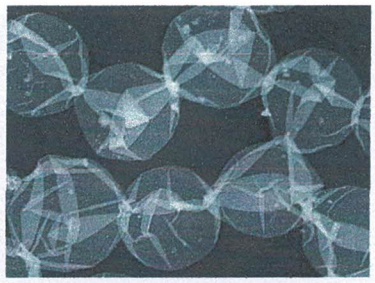
The Erythrocyte Membrane Skeleton

The erythrocyte plasma membrane is supported by a fibrillar skeleton composed of peripheral membrane proteins (Figure 4.32*d*,*e*) that plays a major role in determining the biconcave shape of the erythrocyte. As discussed on page 135, the membrane skeleton can establish domains within the membrane that enclose particular groups of membrane proteins and may greatly restrict the movement of these proteins. The major component of the skeleton is an elongated fibrous protein, called *spectrin*. Spectrin is a heterodimer approximately 100 nm long, consisting of an a and b subunit that curl around one another. Two such dimeric molecules are linked at their head ends to form a 200-nm-long filament that is both flexible and elastic. Spectrin is attached to the internal surface of the membrane by means of noncovalent bonds to another peripheral protein, *ankyrin* (the green spheres of Figure 4.32), which in turn is linked noncovalently to the cytoplasmic domain of a band 3 molecule. As is evident in Figures 4.32*d* and *e*, spectrin filaments are organized into hexagonal or pentagonal arrays. This two-dimensional network is constructed by linking both ends of each spectrin filament to a cluster of proteins that include a short filament of *actin* and *tropomyosin*, proteins typically involved in contractile activities (see Chapter 9). A number of genetic diseases (*hemolytic anemias*) characterized by fragile, abnormally shaped erythrocytes have been traced to mutations in ankyrin or spectrin.

If the peripheral proteins are removed from erythrocyte ghosts, the membrane becomes fragmented into small vesicles, indicating that the inner protein network is required to maintain the integrity of the membrane. Erythrocytes are circulating cells that are squeezed under pressure through microscopic capillaries whose diameter is considerably less than that of the erythrocytes themselves. To



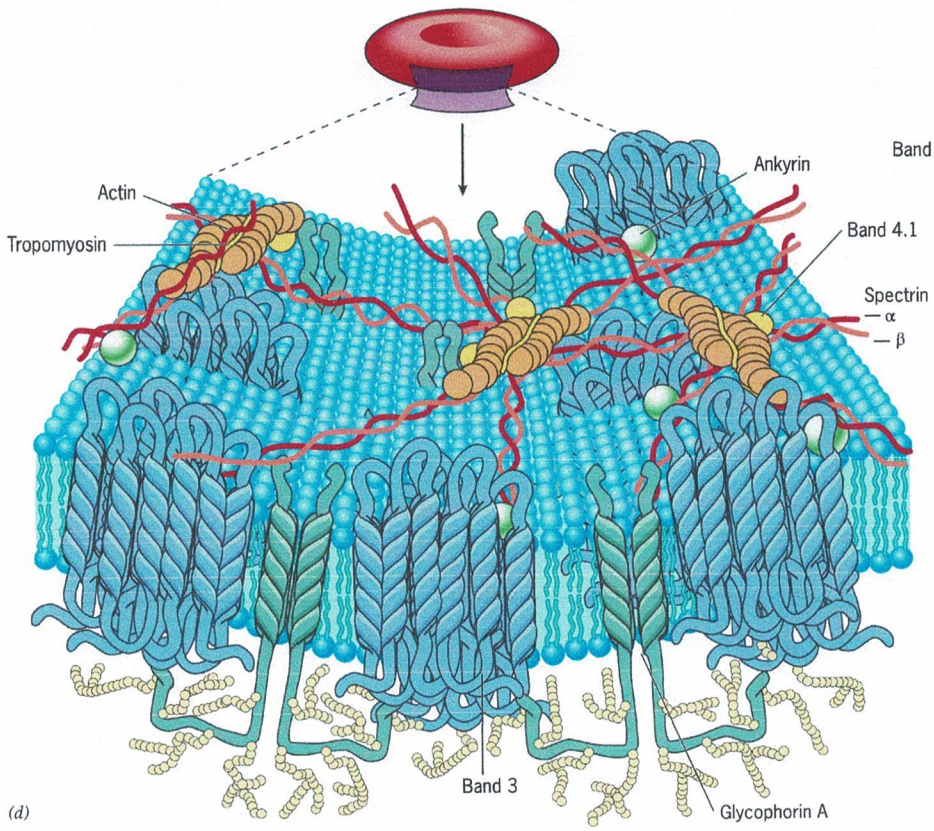
(a) 7 μm



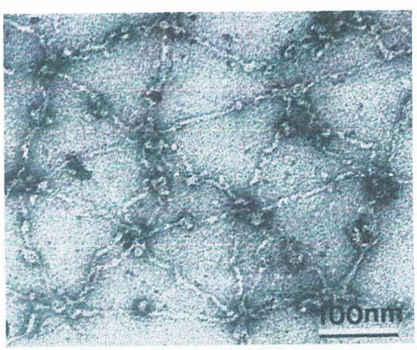
(b)



(c)



(d)



(e)

FIGURE 4.32 The plasma membrane of the human erythrocyte. (*a*) Scanning electron micrograph of human erythrocytes. (*b*) Micrograph showing plasma membrane ghosts, which were isolated by allowing erythrocytes to swell and hemolyze as described in the text. (*c*) The results of SDS–polyacrylamide gel electrophoresis (SDS–PAGE) used to fractionate the proteins of the erythrocyte membrane, which are identified at the sides of the gel. (*d*) A model of the erythrocyte plasma membrane as viewed from the internal surface, showing the integral proteins embedded in the lipid bilayer and the arrangement of peripheral proteins that make up the membrane's internal skeleton. The band 3 dimer shown here is simplified. The band 4.1 protein stabilizes actin–spectrin complexes. (*e*) Electron micrograph showing the arrangement of the proteins of the inner membrane skeleton.

SOURCE: (*a*) Courtesy François M. M. Morel, Richard F. Baker, and Harold Wayland, Reproduced with permission of The Rockefeller University Press; (*b*) Courtesy of Joseph F. Hoffman; (*c*) From V. T. Marchesi, H. Furthmayr, and M. Tomita, *Annu. Rev. Biochem.* vol. 45; © 1976 by Annual Reviews Inc.; (*d*) After D. Voet and J. G. Voet, *Biochemistry*, 2d ed.; Copyright © 1995, John Wiley & Sons, Inc.; (e) From Shih-Chun Liu, Laura H. Derick, and Jiri Palek, *J. Cell Biol.* 104:527, 1987, Reproduced with permission of The Rockefeller University Press.

traverse these narrow passageways, and to do so day after day, the red blood cell must be highly deformable, durable, and capable of withstanding shearing forces that tend to pull it apart. The spectrin–actin network gives the cell the strength, elasticity, and pliability necessary to carry out its demanding function.

When first discovered, the membrane skeleton of the erythrocyte was thought to be a unique structure suited to the unique shape and mechanical needs of this cell type. However, as other cells were examined, similar types of membrane skeletons containing members of the spectrin and ankyrin families have been revealed, indicating that inner membrane skeletons are widespread. Dystrophin, for example, is a member of the spectrin family that is found in the membrane skeleton of muscle cells. Mutations in dystrophin are responsible for causing muscular dystrophy, a devastating disease that cripples and kills children. The most debilitating mutations are ones that lead to a complete absence of the protein in the cell. The plasma membranes of muscle cells lacking dystrophin are apparently destroyed as a consequence of the mechanical stress exerted on them as the muscle contracts. As a result, the muscle cells die and eventually are no longer replaced.

REVIEW

1. Discuss two major functions of the integral and peripheral proteins of the erythrocyte membrane.

4.9 Solute Movement across Cell Membranes

Because the contents of a cell are completely surrounded by its plasma membrane, all communication between the cell and the extracellular medium must be mediated by this structure. The plasma membrane is a barrier that retains the dissolved materials of the cell so that they do not simply leak out into the environment, yet it must allow the necessary exchange of materials into and out of the cell. The lipid bilayer of the membrane is ideally suited to prevent the loss of charged and polar solutes from a cell. Consequently, some special provision must be made to allow the movement of nutrients, ions, waste products, and other compounds in and out of the cell. There are basically two means for the movement of substances through a membrane: passively by diffusion or actively by an energy-coupled transport process. Both types of movements lead to the net flux of a particular ion or compound. The term *net flux* indicates that the movement of the substance into the cell (*influx*) and out of the cell (*efflux*) is not balanced, but that one exceeds the other.

Four different processes are known by which substances move across membranes: simple diffusion through the lipid bilayer; simple diffusion through an aqueous, protein-lined channel; diffusion that is facilitated by a protein transporter; and active transport, which requires an energy-driven protein "pump" capable of moving substances against a concentration gradient (**FIGURE 4.33**). We will consider each in turn, but first we will discuss the energetics of solute movement.

The Energetics of Solute Movement

Diffusion is a spontaneous process in which a substance moves from a region of high concentration to a region of low concentration, eventually eliminating the concentration difference between the two

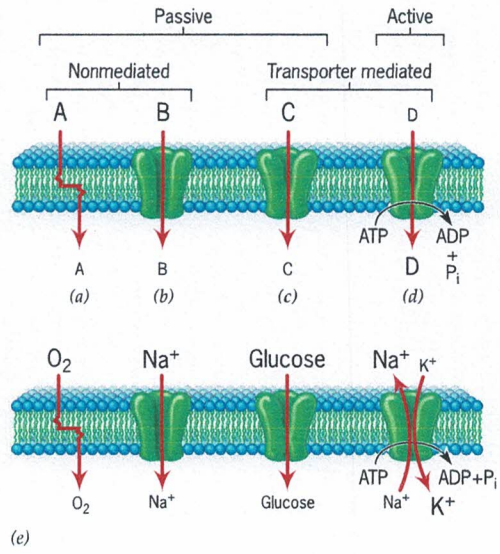


FIGURE 4.33 Four basic mechanisms by which solute molecules move across membranes. The relative sizes of the letters indicate the directions of the concentration gradients. (*a*) Simple diffusion through the bilayer, which always proceeds from high to low concentration. (*b*) Simple diffusion through an aqueous channel formed within an integral membrane protein or a cluster of such proteins. As in *a*, movement is always down a concentration gradient. (*c*) Facilitated diffusion in which solute molecules bind specifially to a membrane protein carrier (a facilitative transporter). As in *a* and *b*, movement is always from high to low concentration. (*d*) Active transport by means of a protein transporter with a specific binding site that undergoes change in affiniy driven with energy released by an exergonic process, such as ATP hydrolysis. Movement occurs against a concentration gradient. (*e*) Examples of each type of mechanism as it occurs in the membrane of an erythrocyte.

regions. As discussed in Chapter 3, diffusion depends on the random thermal motion of solutes and is an exergonic process driven by an increase in entropy. Individual diffusing molecules do not "know" which way to move—an individual molecule will be equally likely to move into a region of higher or lower concentration. But because there are more molecules in a given volume of a high concentration region than in a low concentration region, on average more molecules will move from higher concentration regions to lower concentration regions than vice versa. We will restrict the following discussion to diffusion of substances across membranes.

To understand the energetics of diffusion, we recall that ΔG depends on how far away a state is from equilibrium. In diffusion, equilibrium occurs when the concentration is equal on both sides of the membrane. The free-energy change when an uncharged solute (a nonelectrolyte) diffuses across a membrane thus depends on how different the concentration is on the two sides of the membrane. This difference is known as the concentration gradient. The following relationship describes the movement of a nonelectrolyte *into* the cell:

$$\Delta G = RT \ln \frac{[C_i]}{[C_o]}$$

$$\Delta G = 2.303\ RT \log_{10} \frac{[C_i]}{[C_o]}$$

where ΔG is the free-energy change (Section 3.2), R is the gas constant, T is the absolute temperature, and $[C_i]/[C_o]$ is the ratio of the

concentration of the solute on the inside (i) and outside (o) surfaces of the membrane. At 25°C,

$$\Delta G = 1.4 \text{ kcal/mol} \cdot \log_{10} \frac{[C_i]}{[C_o]}$$

Clearly, if the concentrations inside and outside are equal, $\Delta G = 0$, thus the system is at equilibrium. If the ratio of $[C_i]/[C_o]$ is less than 1.0, then the log of the ratio is negative, ΔG is negative, and the net influx of solute is thermodynamically favored (exergonic). If, for example, the external concentration of solute is 10 times the internal concentration, $\Delta G = -1.4$ kcal/mole. Thus, the maintenance of a tenfold concentration gradient represents a storage of 1.4 kcal/mol. As solute moves into the cell, the concentration gradient decreases, the stored energy is dissipated, and ΔG decreases until, at equilibrium, ΔG is zero. (To calculate ΔG for movement of a solute out of the cell, the term for concentration ratios becomes $[C_o]/[C_i]$).

Formation of an Electrochemical Gradient

If the solute is an electrolyte (a charged species), the overall charge difference between the two compartments must also be considered. As a result of the mutual repulsion of ions of like charges, it is thermodynamically unfavorable for an electrolyte to move across a membrane from one compartment into another compartment having a net charge of the same sign. Conversely, if the charge of the electrolyte is opposite in sign to the compartment into which it is moving, the process is thermodynamically favored. The greater the difference in charge (the potential difference or voltage) between the two compartments, the greater the difference in free energy. Thus, the tendency of an electrolyte to diffuse between two compartments depends on two gradients: a chemical gradient, determined by the concentration difference of the substance between the two compartments, and the electric potential gradient, determined by the difference in charge. Together these differences are combined to form an **electrochemical gradient**. The free-energy change for the diffusion of an electrolyte into the cell is

$$\Delta G = RT \ln \frac{[C_i]}{[C_o]} + zF\Delta E_m$$

where z is the charge of the solute, F is the Faraday constant (23.06 kcal/V · equivalent, where an equivalent is the amount of the electrolyte having one mole of charge), and ΔE_m is the potential difference (in volts) between the two compartments. We saw in the previous example that a tenfold difference in concentration of a nonelectrolyte across a membrane at 25°C generates a ΔG of −1.4 kcal/mol. Suppose the concentration gradient consisted of Na^+ ions, which were present at tenfold higher concentration outside the cell than in the cytoplasm. Because the voltage across the membrane of a cell is typically about −70 mV (page 159), the free-energy change for the movement of a mole of Na^+ ions into the cell under these conditions would be

$$\Delta G = -1.4 \text{ kcal/mol} + zF\Delta E_m$$
$$\Delta G = -1.4 \text{ kcal/mol} + (1)(23.06 \text{ kcal/V} \cdot \text{mol})(-0.07 \text{V})$$
$$= -3.1 \text{ kcal/mol}$$

Thus under these conditions, the concentration difference and the electric potential make similar contributions to the storage of free energy across the membrane.

The interplay between concentration and potential differences is seen in the diffusion of potassium ions (K^+) out of a cell. The efflux of the ion is favored by the K^+ concentration gradient, which has a higher K^+ concentration inside the cell, but hindered by the electrical gradient that its diffusion creates, which leaves a higher negative charge inside the cell. We will discuss this subject further when we consider the topic of membrane potentials and nerve impulses in Section 4.16.

REVIEW

1. Compare and contrast the four basically different ways that a substance can move across the plasma membrane (as indicated in Figure 4.33).
2. Contrast the energetic difference between the diffusion of an electrolyte versus a nonelectrolyte across the membrane.

4.10 Diffusion through the Lipid Bilayer

The plasma membrane is a selectively permeable barrier that allows solute passage by several mechanisms, including simple diffusion through the lipid bilayer. Diffusion is an energy-independent process in which a solute moves down an electrochemical gradient, dissipating the free energy stored in the gradient. Small inorganic solutes, such as O_2, CO_2, and H_2O, penetrate the lipid bilayer readily, as do solutes with high lipid solubility. Ions and polar organic solutes, such as sugars and amino acids, require special transporters to enter or leave the cell.

Diffusion of Substances through Membranes

Two qualifications must be met before a nonelectrolyte can diffuse passively across a plasma membrane. The substance must be present at higher concentration on one side of the membrane than the other, and the membrane must be permeable to the substance. A membrane may be permeable to a given solute either (1) because that solute can pass directly through the lipid bilayer, or (2) because that solute can traverse an aqueous pore that spans the membrane. Let us begin by considering the former route in which a substance must dissolve in the lipid bilayer on its way through the membrane.

Discussion of simple diffusion leads us to consider the polarity of a solute. One simple measure of the polarity (or nonpolarity) of a substance is its **partition coefficient**, which is the ratio of its solubility in a nonpolar solvent, such as octanol or a vegetable oil, to that in water under conditions where the nonpolar solvent and water are mixed together. **FIGURE 4.34** shows the relationship between partition coefficient and membrane permeability of a variety of chemicals

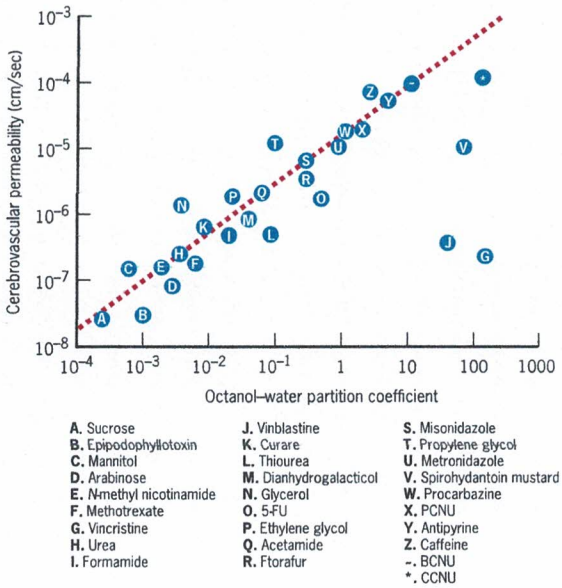


FIGURE 4.34 The relationship between partition coefficient and membrane permeability. In this case, measurements were made of the penetration of a variety of chemicals and drugs across the plasma membranes of the cells that line the capillaries of the brain. Substances penetrate by passage through the lipid bilayer of these cells. The partition coefficient is expressed as the ratio of solubility of a solute in octanol to its solubility in water. Permeability is expressed as penetrance (P) in cm/sec. For all but a few compounds, such as vinblastine and vincristine, penetrance is directly proportional to lipid solubility.

SOURCE: From N. J. Abbott and I. A. Romero, *Molec. Med.* Today, 2:110, 1996; Copyright 1996, with permission from Elsevier Science.

and drugs. It is evident that the greater the lipid solubility, the faster the penetration.

Another factor determining the rate of penetration of a compound through a membrane is its size. If two molecules have approximately equivalent partition coefficients, the smaller molecule tends to penetrate the lipid bilayer of a membrane more rapidly than the larger one. Very small, uncharged molecules penetrate very rapidly through cellular membranes. Consequently, membranes are highly permeable to small inorganic molecules, such as O_2, CO_2, NO, and H_2O, which are thought to slip between adjacent phospholipids. In contrast, larger polar molecules, such as sugars, amino acids, and phosphorylated intermediates, exhibit poor membrane penetrability. As a result, the lipid bilayer of the plasma membrane provides an effective barrier that keeps these essential metabolites from diffusing out of the cell. Some of these molecules (e.g., sugars and amino acids) must enter cells from the bloodstream, but they cannot do so by simple diffusion. Instead, special mechanisms must be available to mediate their penetration through the plasma membrane. The use of such mechanisms allows a cell to regulate the movement of substances across its surface barrier. We will return to this feature of membranes later.

The Diffusion of Water through Membranes

Water molecules move much more rapidly through a cell membrane than do dissolved ions or small polar organic solutes, which are essentially nonpenetrating. Because of this difference in the penetrability of water versus solutes, membranes are said to be **semipermeable**. Water moves readily through a semipermeable membrane from a region of lower *solute* concentration to a region of higher *solute* concentration. This process is called **osmosis**, and it is readily demonstrated by placing a cell into a solution containing a nonpenetrating solute at a concentration different than that present within the cell itself.

When two compartments of different solute concentration are separated by a semipermeable membrane, the compartment of higher solute concentration is said to be **hypertonic** (or **hyperosmotic**) relative to the compartment of lower solute concentration, which is described as being **hypotonic** (or **hypoosmotic**). When a cell is placed into a hypotonic solution, the cell rapidly gains water by

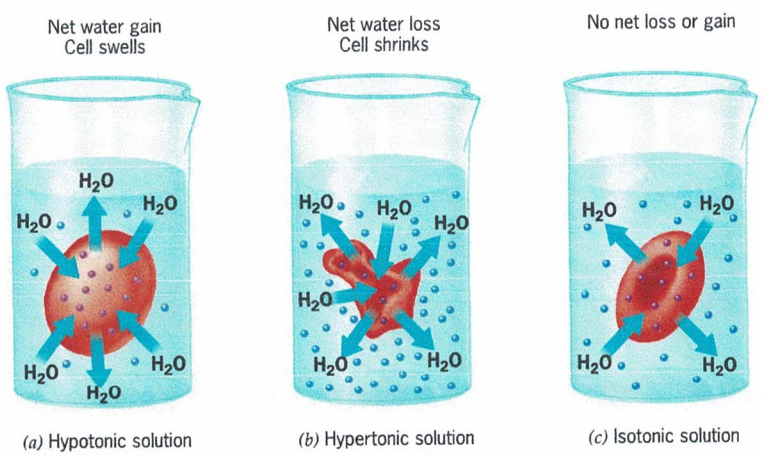


FIGURE 4.35 The effects of differences in the concentration of solutes on opposite sides of the plasma membrane. (a) A cell placed in a hypotonic solution (one having a lower solute concentration than the cell) swells because of a net gain of water by osmosis. (b) A cell in a hypertonic solution shrinks because of a net loss of water by osmosis. (c) A cell placed in an isotonic solution maintains a constant volume because the inward flux of water is equal to the outward flux.

osmosis and swells (FIGURE 4.35a). Conversely, a cell placed into a hypertonic solution rapidly loses water by osmosis and shrinks (Figure 4.35*b*). These simple observations show that a cell's volume is controlled by the difference between the solute concentration inside the cell and that in the extracellular medium. The swelling and shrinking of cells in slightly hypotonic and hypertonic media are usually only temporary events. Within a few minutes, the cells recover and return to their original volume. In a hypotonic medium, recovery occurs as the cells lose ions, thereby reducing their internal osmotic pressure. In a hypertonic medium, recovery occurs as the cells gain ions from the medium. Once the internal solute concentration (which includes a high concentration of dissolved proteins) equals the external solute concentration, the internal and external fluids are **isotonic** (or **isosmotic**), and no net movement of water into or out of the cells occurs (Figure 4.35*c*).

Osmosis is an important factor in a multitude of bodily functions. Your digestive tract, for example, secretes several liters of fluid daily, which is reabsorbed osmotically by the cells that line your intestine. If this fluid weren't reabsorbed, as happens in cases of extreme diarrhea, you would face the prospect of rapid dehydration. Indeed, the bacterial disease cholera kills over 100,000 people every year, mostly because of water loss into the intestines, driven by osmosis. Plants utilize osmosis in different ways. Unlike animal cells, which are generally isotonic with the medium in which they are bathed, plant cells are generally hypertonic compared to their fluid environment. As a result, there is a tendency for water to enter the cell, causing it to develop an internal (*turgor*) pressure that pushes against its surrounding wall (FIGURE 4.36a). Turgor pressure provides support for nonwoody plants and for the nonwoody parts of trees, such as the leaves. If a plant cell is placed into a hypertonic medium, its volume shrinks as the plasma membrane pulls away from the surrounding cell wall, a process called **plasmolysis** (Figure 4.36*b*). The loss of water due to plasmolysis causes plants to lose their support and wilt.

Not all cells are equally permeable to water. In fact, many cells are much more permeable to water than can be explained by simple diffusion through the lipid bilayer. A family of small integral proteins, called *aquaporins*, allow the passive movement of water from one side of the plasma membrane to the other. Each aquaporin subunit (in the four-subunit protein) contains a central channel that is lined primarily by hydrophobic amino acid residues and is highly specific for water molecules. A billion or so water molecules can pass—in single file—through each channel every second. At the same time, H^+ ions, which normally hop along a chain of water molecules, are not able to penetrate these open pores. The apparent mechanism by which these channels are able to exclude protons has been suggested by a combination of X-ray crystallographic studies, which has revealed the structure of the protein, and molecular dynamics simulations (page 58), which has put this protein structure into operation. A model based on such simulations is shown in FIGURE 4.37a. Very near its narrowest point, the wall of an aquaporin channel contains a pair of precisely positioned positive charges (residues N203 and N68 in Figure 4.37*b*) that attract the oxygen atom of each water molecule as it speeds through the constriction in the protein. This interaction reorients the central water molecule in a position that prevents it from maintaining the hydrogen bonds that normally link it to its neighboring water molecules. This removes the bridge that would normally allow protons to move from one water molecule to the next.

Aquaporins are particularly prominent in cells, such as those of a kidney tubule or plant root, where the passage of water plays a crucial role in the tissue's physiologic activities. The hormone vasopressin, which stimulates water retention by the collecting ducts of the kidney, acts by way of one of these proteins (AQP2). Some cases of the inherited disorder *congenital nephrogenic diabetes insipidus* arise from mutations in this aquaporin channel. Persons suffering from this disease excrete large quantities of urine because their kidneys do not respond to vasopressin.

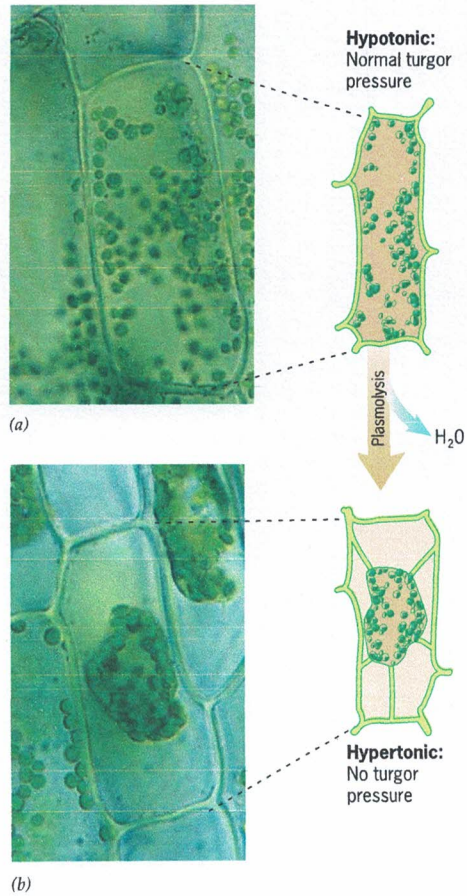
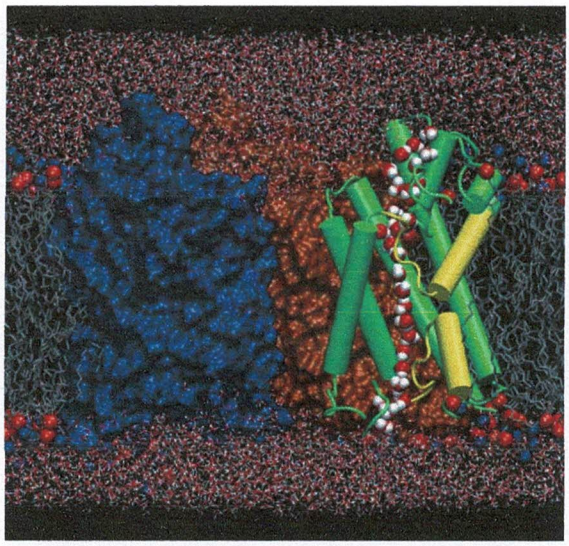


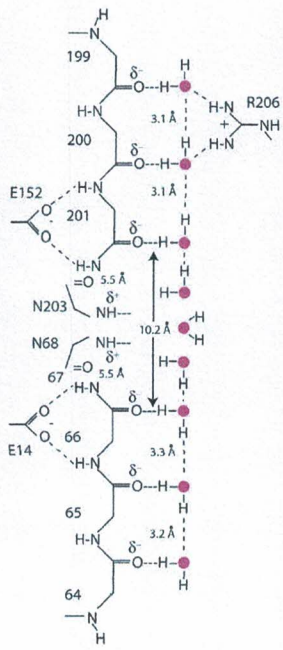
FIGURE 4.36 The effects of osmosis on a plant cell. (*a*) Aquatic plants living in freshwater are surrounded by a hypotonic environment. Water therefore tends to flow into the cells, creating turgor pressure. (*b*) If the plant is placed in a hypertonic solution, such as seawater, the cell loses water, and the plasma membrane pulls away from the cell wall.
SOURCE: Ed Reschke.

REVIEW

1. Describe the relationship between partition coefficient and molecular size with regard to membrane permeability.
2. Explain the effects of putting a cell into a hypotonic, hypertonic, or isotonic medium.



(a)



(b)

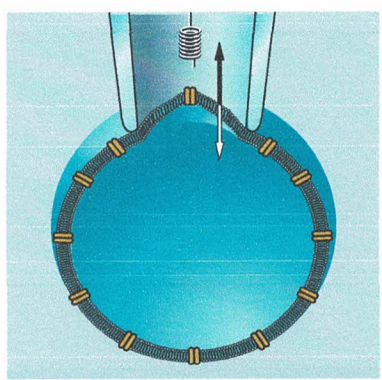
FIGURE 4.37 Passage of water molecules through an aquaporin channel. (*a*) Snapshot from a molecular dynamics simulation of a stream of water molecules (red and white spheres) passing in single file through the channel in one of the subunits of an aquaporin molecule residing within a membrane. (*b*) A model describing the mechanism by which water molecules pass through an aquaporin channel with the simultaneous exclusion of protons. Nine water molecules are shown to be lined up in single file along the wall of the channel. Each water molecule is depicted as a red circular O atom with two associated Hs. In this model, the four water molecules at the top and bottom of the channel are oriented, as the result of their interaction with the carbonyl (C=O) groups of the protein backbone (page 49), with their H atoms pointed away from the center of the channel. These water molecules are able to form hydrogen bonds (dashed lines) with their neighbors. In contrast, the single water molecule in the center of the channel is oriented in a position that prevents it from forming hydrogen bonds with other water molecules, which has the effect of interrupting the flow of protons through the channel. Animations of aquaporin channels can be found at www.nobelprize.org/nobel_prizes/chemistry/laureates/2003/animations.html

SOURCE: (*a*) From Benoit Roux and Klaus Schulten, *Structure* 12:1344, 2004, with permission from Elsevier; (*b*) From R. M. Stroud et al., *Curr. Opin. Struct. Biol.* 13:428, © 2003, with permission from Elsevier.

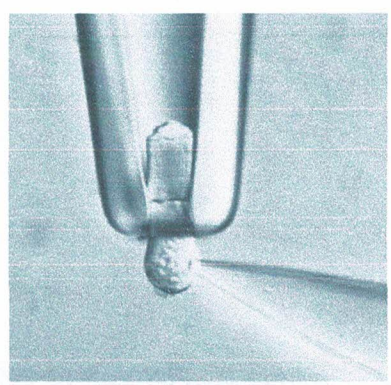
4.11 The Diffusion of Ions through Membranes

The lipid bilayer that constitutes the core of biological membranes is highly impermeable to charged substances, including small ions such as Na^+, K^+, Ca^{2+}, and Cl^-. Yet the rapid movement (**conductance**) of these ions across membranes plays a critical role in a multitude of cellular activities, including formation and propagation of a nerve impulse, secretion of substances into the extracellular space, muscle contraction, regulation of cell volume, and the opening of stomatal pores on plant leaves.

In 1955, Alan Hodgkin and Richard Keynes of Cambridge University first proposed that cell membranes contain **ion channels**, that is, openings in the membrane that are permeable to specific ions. Direct proof of the existence of ion channels emerged through the work of Bert Sakmann and Erwin Neher at the Max-Planck Institute in Germany in the late 1970s and early 1980s who developed techniques to monitor the ionic current passing through a single ion channel. This is accomplished using very fine micropipette-electrodes made of polished glass that are placed on the outer cell surface and sealed to the membrane by suction. The voltage across the membrane can be maintained (*clamped*) at any particular value, and the current originating in the small patch of membrane surrounded by the pipette can be measured (FIGURE 4.38). These landmark studies marked the first successful investigations into the activities of individual protein molecules. Today, biologists have identified a bewildering variety of



(a)



(b)

FIGURE 4.38 Measuring ion channel conductance by patch-clamp recording. (*a*) In this technique, a highly polished glass micropipette is placed against a portion of the outer surface of a cell, and suction is applied to seal the rim of the pipette against the plasma membrane. Because the pipette is wired as an electrode (a *microelectrode*), a voltage can be applied across the patch of membrane enclosed by the pipette, and the responding flow of ions through the membrane channels can be measured. As indicated in the figure, the micropipette can enclose a patch of membrane containing a single ion channel, which allows investigators to monitor the opening and closing of a single gated channel, as well as its conductance at different applied voltages. (*b*) The micrograph shows patch-clamp recordings being made from a single photoreceptor cell of the retina of a salamander. One portion of the cell is drawn into a glass micropipette by suction, while a second micropipette-electrode (lower right) is sealed against a small patch of the plasma membrane on another portion of the cell.

SOURCE: (*b*) From T. D. Lamb, H. R. Matthews, and V. Torre, *J. Physiology* 372:319, 1986. © 1986, reproduced with permission of John Wiley & Sons.

ion channels, each formed by integral membrane proteins that enclose a central aqueous pore. As might be predicted, mutations in the genes encoding ion channels can lead to many serious diseases (see Table 1 of the Human Perspective, page 158).

Most ion channels are highly selective in allowing only one particular type of ion to pass through the pore. As with the passive diffusion of other types of solutes across membranes, the diffusion of ions through a channel is always downhill, that is, from a state of higher energy to a state of lower energy. Most of the ion channels that have been identified can exist in either an open or a closed conformation; such channels are said to be **gated**. The opening and closing of the gates are subject to complex physiologic regulation and can be induced by a variety of factors depending on the particular channel. Three major categories of gated channels are distinguished:

1. **Voltage-gated channels** whose conformational state depends on the difference in ionic charge on the two sides of the membrane.
2. **Ligand-gated channels** whose conformational state depends on the binding of a specific molecule (the ligand), which is usually not the solute that passes through the channel. Some ligand-gated channels are opened (or closed) following the binding of a molecule to the outer surface of the channel; others are opened (or closed) following the binding of a ligand to the inner surface of the channel. For example, neurotransmitters, such as acetylcholine, act on the outer surface of certain cation channels, whereas? cyclic nucleotides, such as cAMP, act on the inner surface of certain calcium ion channels.
3. **Mechano-gated channels** whose conformational state depends on mechanical forces (e.g., stretch tension) that are applied to the membrane. Members of one family of cation channels, for example, are opened by the movements of stereocilia (see Figure 9.46) on the hair cells of the inner ear in response to sound or motions of the head.

We will focus in the following discussion on the structure and function of voltage-gated potassium ion channels because these are the best understood.

In 1998, Roderick MacKinnon and his colleagues at Rockefeller University provided the first atomic-resolution image of an ion channel protein, in this case, a bacterial K^+ ion channel called KcsA. The relationship between structure and function is evident everywhere in the biological world, but it would be difficult to find a better example than that of the K^+ ion channel depicted in **FIGURE 4.39**. As we will see shortly, the formulation of this structure led directly to an understanding of the mechanism by which these remarkable molecular machines are able to select overwhelmingly for K^+ ions over Na^+ ions, yet at the same time allow an incredibly rapid conductance of K^+ ions through the membrane. We will also see that the mechanisms of ion selectivity and conductance in this bacterial channel are virtually identical to those operating in the much larger mammalian channels. Evidently, the basic challenges in operating an ion channel were solved relatively early in evolution, although many refinements appeared over the following one or two billion years.

The KcsA channel consists of four subunits, two of which are shown in Figure 4.39. Each subunit of Figure 4.39 is seen to contain two membrane-spanning helices (M1 and M2) and a pore region (P) at the extracellular end of the channel. P consists of a short pore helix that extends approximately one-third the width of the channel and a nonhelical loop (colored light brown in Figure 4.39) that forms the lining of a narrow *selectivity filter*, so named because of its role in allowing only the passage of K^+ ions.

The lining of the selectivity filter contains a highly conserved pentapeptide—Gly-Tyr-Gly-Val-Thr (or GYGVT in single-letter nomenclature). The X-ray crystal structure of the KcsA channel shows that the backbone carbonyl (C═O) groups from the conserved pentapeptide (see the backbone structure on page 49) create five successive rings of oxygen atoms (four rings are made up of carbonyl oxygens from the polypeptide backbone, and one ring consists of oxygen atoms from the threonine side chain). Each ring contains four oxygen atoms (one from each subunit) and has a diameter of approximately 3 Å, which is slightly larger than the 2.7 Å diameter of a K^+ ion that

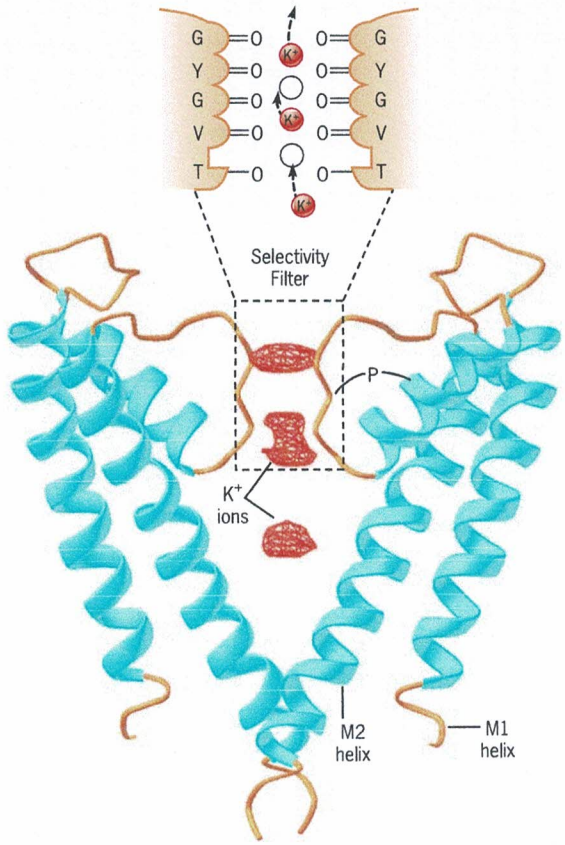


FIGURE 4.39 Three-dimensional structure of the bacterial KcsA channel and the selection of K^+ ions. This K^+ ion channel consists of four subunits, two of which are shown here. Each subunit is comprised of M1 and M2 helices joined by a P (pore) segment consisting of a short helix and a nonhelical portion that lines the channel through which the ions pass. A portion of each P segment contains a conserved pentapeptide (GYGVT) whose residues line the selectivity filter that screens for K^+ ions. The oxygen atoms of the carbonyl groups of these residues project into the channel where they can interact selectively with K^+ ions (indicated by the red mesh objects) within the filter. As indicated in the top inset, the selectivity filter contains four rings of carbonyl O atoms and one ring of threonyl O atoms; each of these five rings contains four O atoms, one donated by each subunit. The diameter of the rings is just large enough so that eight O atoms can coordinate a single K^+ ion, replacing its normal water of hydration. Although four K^+ binding sites are shown, only two are occupied at one time.

SOURCE: From Roderick MacKinnon, *Nature Med.* 5:1108, © 1999, reprinted by permission from Macmillan Publishers Ltd.

has lost its normal shell of hydration. Consequently, the electronegative O atoms that line the selectivity filter can substitute for the shell of water molecules that are displaced as each K^+ ion enters the pore. In this model, the selectivity filter contains four potential K^+ ion binding sites. As indicated in the top inset of Figure 4.39, a K^+ ion bound at any of these four sites would occupy the center of a "box" having four O atoms in a plane above the ion and four O atoms in a plane below the atom. As a result, each K^+ ion in one of these sites could coordinate with eight O atoms of the selectivity filter. Whereas the selectivity filter is a precise fit for a dehydrated K^+ ion, it is much larger than the diameter of a dehydrated Na^+ ion (1.9 Å). Consequently, a Na^+ ion cannot interact optimally with the eight oxygen atoms necessary to stabilize it in the pore. As a result, the smaller Na^+ ions cannot overcome the higher energy barrier required to penetrate the pore.

Although there are four potential K^+ ion binding sites, only two are occupied at any given time. Potassium ions are thought to move, two at a time—from sites 1 and 3 to sites 2 and 4—as indicated in the top inset of Figure 4.39. The entry of a third K^+ ion into the selectivity filter creates an electrostatic repulsion that ejects the ion bound at the opposite end of the line. Studies indicate that there is virtually no energy barrier for an ion to move from one binding site to the next, which accounts for the extremely rapid flow of ions across the membrane. Taken together, these conclusions concerning K^+ ion selectivity and conductance provide a superb example of how much can be learned about biological function through an understanding of molecular structure.

The KcsA channel depicted in Figure 4.39 has a gate, just like eukaryotic channels. The opening of the gate of the KcsA channel in response to very low pH was illustrated in Figure 4.22. The structure of KcsA shown in Figure 4.39 is actually the closed conformation of the protein (despite the fact that it contains ions in its channel). Comparison of the open and closed structures of KcsA strongly suggests that gating of these molecules is accomplished by conformational changes of the cytoplasmic ends of the inner (M2) helices. In the closed conformation, as seen in Figure 4.39 and **FIGURE 4.40** in blue, the M2 helices are straight and cross over one another to form a "helix bundle" that seals the cytoplasmic face of the pore. In the model shown in Figure 4.40, the channel opens when the M2 helices bend at a specific hinge point where a glycine residue is located.

Now that we have seen how these prokaryotic K^+ channels operate, we are in a better position to understand the structure and function of the more complex eukaryotic versions, which are thought to perform in a similar manner. Genes that encode a variety of distinct voltage-gated K^+ (or Kv) channels have been isolated and the molecular anatomy of their proteins scrutinized. The Kv channels of plants play an important role in salt and water balance and in regulation of cell volume. The Kv channels of animals are best known for their role in muscle and nerve function, which is explored at the end of the chapter. Eukaryotic Kv channel subunits contain six membrane-associated helices, named S1–S6, which are shown two-dimensionally in Figure 4.41. These six helices can be grouped into two functionally distinct domains:

1. A **pore domain**, which has the same basic architecture as that of the entire bacterial channel illustrated in Figure 4.39 and contains the selectivity filter that permits the selective passage of K^+ ions. Helices M1 and M2 and the P segment of the KcsA channel of Figure 4.39 are homologous to helices S5 and S6 and the P segment of the voltage-gated eukaryotic channel illustrated in **FIGURE 4.41**. Like the four M2 helices of KcsA, the four S6 helices line much of the pore, and their configuration determines whether the gate to the channel is open or closed.

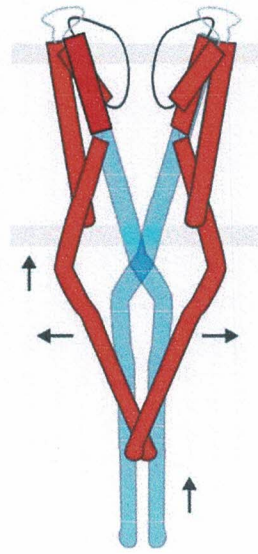


FIGURE 4.40 Schematic illustration of the hinge-bending model for the opening of the KcsA channel. The M2 helices from each subunit bend outward at a specific glycine residue, which opens the gate at the intracellular end of the channel to K^+ ions.

SOURCE: Serdar Uysal, et al. 2011. Mechanism of activation gating in the full-ength KcsA K^+ channel. *Proc. Natl. Acad. Sci. U.S.A.* 108, 11896–9.

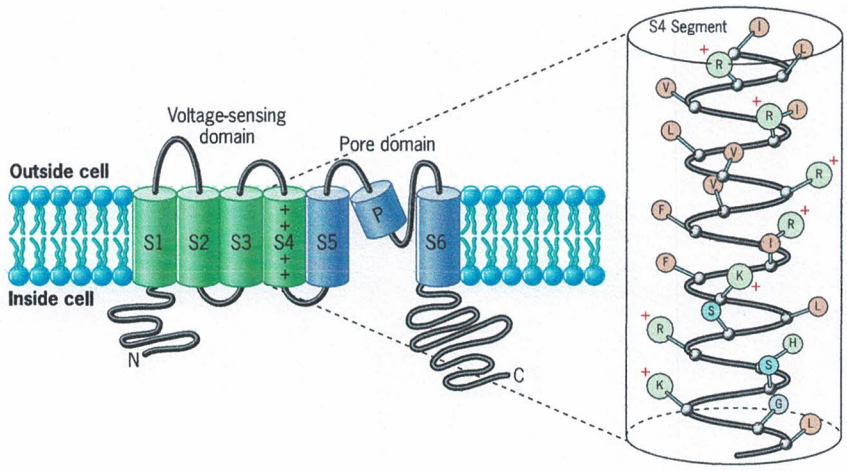
2. A **voltage-sensing domain** consisting of helices S1–S4 that senses the voltage across the plasma membrane (as discussed below).

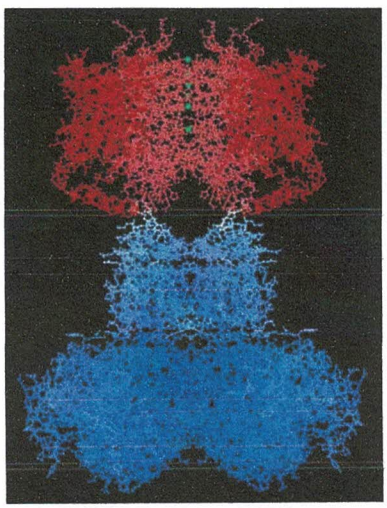
The three-dimensional crystal structure of a complete eukaryotic Kv channel purified from rat brain is shown in **FIGURE 4.42a**. Determination of this structure was made possible by use of a mixture of detergent and lipid throughout the purification and crystallization process. The presence of negatively charged phospholipids is thought to be important in maintaining the native structure of the membrane protein and promoting its function as a voltage-gated channel. Like the KcsA channel, a single eukaryotic Kv channel consists of four homologous subunits arranged symmetrically around the central ion-conducting pore (Figure 4.42*b*). The selectivity filter, and thus the presumed mechanism of K^+ ion selection, is virtually identical in the prokaryotic KcsA and eukaryotic Kv proteins. The gate leading into a Kv channel is formed by the inner ends of the S6 helices and is thought to open and close in a manner roughly similar to that of the M2 helices of the bacterial channel (shown in Figure 4.40). The protein depicted in Figure 4.42 represents the open state of the channel.[6]

The S4 helix, which contains several positively charged amino acid residues spaced along the polypeptide chain (inset of Figure 4.41), acts as the key element of the voltage sensor. The voltage-sensing domain is seen to be connected to the pore domain by a short linker helix denoted as S4–S5 in the model in Figure 4.42*b*. Under resting conditions, the negative potential across the membrane (page 159) keeps the gate closed. A change in the potential to a more positive value (a depolarization, page 160) exerts an electric force on the S4 helix. This force is thought to cause the transmembrane S4 helix to

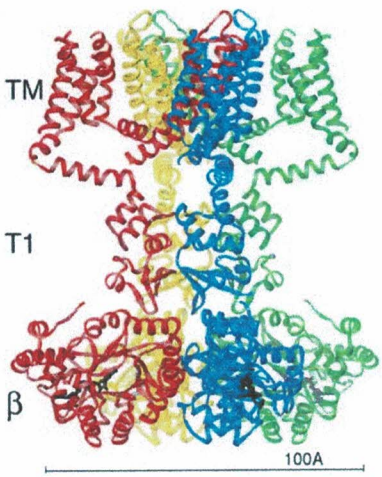
[6]Other studies strongly suggest that K^+ channels are gated by two distinct mechanisms: one involving the opening and closing of the inner helix bundle as described here and another involving the selectivity filter, which is not discussed (see *PNAS* 107:7623, 2010 and *Nature* 466:203, 2010).

FIGURE 4.41 The structure of one subunit of a eukaryotic, voltage-gated K^+ channel. A two-dimensional portrait of a K^+ channel subunit showing its six transmembrane helices and a portion of the polypeptide (called the pore helix or P) that dips into the protein to form part of the channel's wall. The inset shows the sequence of amino acids of the positively charged S4 helix of the *Drosophila* K^+ *Shaker* ion channel, which serves as a voltage sensor. The positively charged side chains are situated at every third residue along the otherwise hydrophobic helix. This member of the Kv family is called a *Shaker* channel because flies with certain mutations in the protein shake vigorously when anesthesized with ether. The *Shaker* channel was the first K^+ channel to be identified and cloned in 1987.

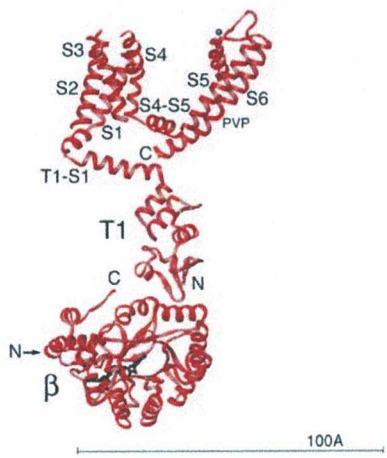




(a)



(b)



(c)

FIGURE 4.42 Three-dimensional structure of a voltage-gated mammalian K^+ channel. (*a*) The crystal structure of the entire tetrameric Kv1.2 channel, a member of the *Shaker* family of K^+ ion channels found in nerve cells of the brain. The transmembrane portion is shown in red, and the cytoplasmic portion in blue. The potassium ion binding sites are indicated in green. (*b*) Ribbon drawing of the same channel shown in *a*, with the four subunits that make up the channel shown in different colors. If you focus on the red subunit, you can see (1) the spatial separation between the voltage-sensing and pore domains of the subunit and (2) the manner in which the voltage-sensing domain from each subunit is present on the outer edge of the pore domain of a neighboring subunit. The cytoplasmic portion of this particular channel consists of a T1 domain, which is part of the channel polypeptide itself, and a separate β polypeptide. (*c*) Ribbon drawing of a single subunit showing the spatial orientation of the six membrane-spanning helices (S1–S6) and also the presence of the S4–S5 linker helix, which connects the voltage-sensing and pore domains. This linker transmits the signal from the S4 voltage sensor that opens the channel. The inner surface of the channel below the pore domain is lined by the S6 helix (roughly similar to the M2 helix of the bacterial channel shown in Figure 4.39). The channel shown here is present in the open configuration with the S6 helices curved outward (compare to Figure 4.40) at the site marked PVP (standing for Pro-Val-Pro, which is likely the amino acid sequence of the "hinge").

SOURCE: (*a–c*) From Stephen B. Long et al., *Science* 309:867, 899, 2005, courtesy of Roderick Mackinnon; © 2005, reprinted with permission from AAAS.

move in such a way that its positively charged residues shift from a position where they were exposed to the cytoplasm to a new position where they are exposed to the outside of the cell. Voltage sensing is a dynamic process whose mechanism cannot be resolved by a single static view of the protein such as that shown in Figure 4.42. In fact, several competing models describing the mechanism of action of the voltage sensor are currently debated. However it occurs, the movement of the S4 helix in response to membrane depolarization initiates a series of conformational changes within the protein that opens the gate at the cytoplasmic end of the channel.

Once opened, more than 10 million potassium ions can pass through the channel per second, which is nearly the rate that would occur by free diffusion in solution. Because of the large ion flux, the opening of a relatively small number of K^+ channels has significant impact on the electrical properties of the membrane. After the channel is open for a few milliseconds, the movement of K^+ ions is "automatically"

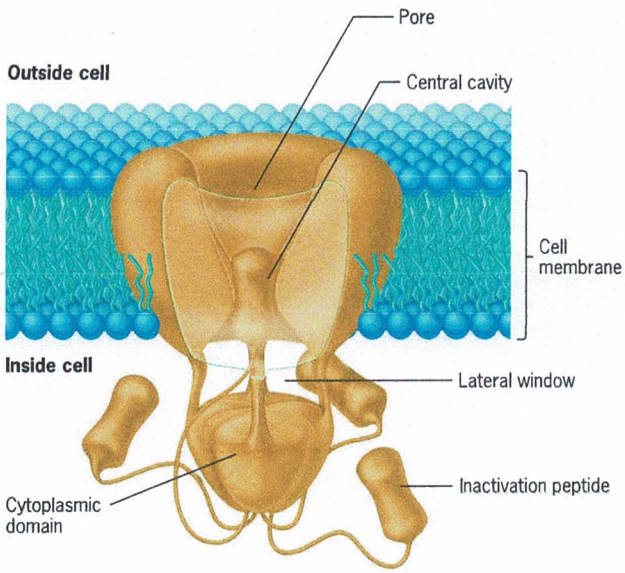


FIGURE 4.43 Conformational states of a voltage-gated K^+ ion channel. (*a*) Three-dimensional model of a eukaryotic K^+ ion channel. Inactivation of channel activity occurs as one of the inactivation peptides, which dangle from the cytoplasmic portion of the complex, fits into the cytoplasmic opening of the channel. (*b*) Schematic representation of a view into a K^+ ion channel, perpendicular to the membrane from the cytoplasmic side, showing the channel in the closed (resting), open, and inactivated state.

SOURCE: (*b*) Reprinted from *Neuron*, vol. 20, C. M. Armstrong and B. Hille, Voltage-Gated Ion Channels and Electrical Escitability, p. 377; copyright 1998, with permission from Elsevier Science.

stopped by a process known as inactivation. To understand channel inactivation, we have to consider an additional portion of a Kv channel besides the two transmembrane domains discussed above.

Eukaryotic Kv channels typically contain a large cytoplasmic structure whose composition varies among different channels. As indicated in **FIGURE 4.43a**, inactivation of the channel is accomplished by movement of a small inactivation peptide that dangles from the cytoplasmic portion of the protein. The inactivation peptide is thought to gain access to the cytoplasmic mouth of the pore by snaking its way through one of four "side windows" indicated in the figure. When one of these dangling peptides moves up into the mouth of the pore (Figure 4.43*a*), the passage of ions is blocked, and the channel is inactivated. At a subsequent stage of the cycle, the inactivation peptide is released, and the gate to the channel is closed. It follows from this discussion that the potassium channel can exist in three different states—open, inactivated, and closed—which are illustrated schematically in Figure 4.43*b*.

Potassium channels come in many different varieties. It is remarkable that *C. elegans*, a nematode worm whose body consists of only about 1000 cells, contains approximately 80 different genes that encode K^+ channels. It is evident that a single cell—whether in a nematode, human, or plant—is likely to possess a variety of different K^+ channels that open and close in response to different voltages. In addition, the voltage required to open or close a particular K^+ channel can vary depending on whether the channel protein is phosphorylated, which in turn is regulated by hormones and other factors. It is apparent that ion channel function is under the control of a diverse and complex set of regulatory agents. The structure and function of a very different type of ion channel, the ligand-gated nicotinic acetylcholine receptor, is the subject of the Experimental Pathways section.

REVIEW

1. What are three different types of gated channels?
2. Describe how a potassium channel can allow potassium ions to flow but prevent sodium ions from flowing.

4.12 EXPERIMENTAL PATHWAYS

The Acetylcholine Receptor

The discovery of the acetylcholine receptor illustrates the important roles that natural toxins and unusual organisms can play in dissecting a fundamental biochemical process with central importance to health and medicine. The story begins in 1843, when the pharmacist and aspiring playwright Claude Bernard moved from a small French town to Paris, where he planned to pursue his literary career. Instead, Bernard enrolled in medical school and went on to become the foremost physiologist of the nineteenth century. Among his many interests was the mechanism by which nerves stimulate the contraction of skeletal muscles. His studies included the use of curare, a highly toxic drug isolated from tropical plants and utilized for centuries by native South American hunters to make poisonous darts. Bernard found that curare paralyzed a skeletal muscle without interfering with either the ability of nerves to carry impulses to that muscle or the ability of the muscle to contract on direct stimulation. Bernard concluded that curare somehow acted on the region of contact between the nerve and muscle.

This conclusion was confirmed and extended by John Langley, a physiologist at Cambridge University. Langley was

continued

studying the ability of nicotine, another substance derived from plants, to stimulate the contraction of isolated frog skeletal muscles and the effect of curare in inhibiting nicotine action. In 1906, Langley concluded that "the nervous impulse should not pass from nerve to muscle by an electric discharge, but by the secretion of a special substance on the end of the nerve."[1] Langley proposed that this "chemical transmitter" was binding to a "receptive substance" on the surface of the muscle cells, the same site that bound nicotine and curare. These proved to be farsighted proposals.

Langley's suggestion that the stimulus from nerve to muscle was transmitted by a chemical substance was confirmed in 1921 in an ingenious experiment by the Austrian-born physiologist, Otto Loewi, the design of which came to Loewi during a dream. The heart rate of a vertebrate is regulated by input from two opposing (antagonistic) nerves. Loewi isolated a frog's heart with both nerves intact. When he stimulated the inhibitory (*vagus*) nerve, a chemical was released from the heart preparation into a salt solution, which was allowed to drain into the medium bathing a second isolated heart. The rate of the second heart slowed dramatically, as though its own inhibitory nerve had been activated.[2] Loewi called the substance responsible for inhibiting the frog's heart "Vagusstoff." Within a few years, Loewi had shown that the chemical and physiologic properties of Vagusstoff were identical to acetylcholine, and he concluded that acetylcholine (ACh) was the substance released by the tips of the nerve cells that made up the vagus nerve.

In 1937, David Nachmansohn, a neurophysiologist at the Sorbonne, was visiting the World's Fair in Paris where he observed several living electric fish of the species *Torpedo marmarota* that were on display. These rays have electric organs that deliver strong shocks (40–60 volts) capable of killing potential prey. At the time, Nachmansohn was studying the enzyme acetylcholinesterase, which acts to destroy ACh after its release from the tips of motor nerves. Nachmansohn was aware that the electric organs of these fish were derived from modified skeletal muscle tissue (**FIGURE 1**), and he asked if he could have a couple of the fish for study once the fair had ended. The results of the first test showed the electric organ was an extraordinarily rich source of acetylcholinesterase.[3] It was also a very rich source of the nicotinic acetylcholine receptor (nAChR),* the receptor present on the postsynaptic membranes of skeletal muscle cells that binds ACh molecules released from the tips of a motor nerve. Finding an ideal system can prove invaluable in the study of a particular aspect of cell structure or function. As will be evident from this discussion, the electric organs of fish have been virtually the sole source of material for the study of the nAChR.

The nAChR is an integral membrane protein, and it wasn't until the 1970s that techniques were developed for the isolation of such proteins. As discussed in Chapter 18, the purification of a particular protein requires a suitable assay to determine the amount of that protein present in any particular fraction. The ideal assay for nAChR was a compound that bound selectively

*The receptor is described as nicotinic because it can be activated by nicotine as well as by acetylcholine. This contrasts with muscarinic acetylcholine receptors of the parasympathetic nerve synapses, which can be activated by muscarine, but not nicotine, and are inhibited by atropine, but not curare. Smokers' bodies become accustomed to high levels of nicotine, and they experience symptoms of withdrawal when they stop smoking because the postsynaptic neurons that possess nAChRs are no longer stimulated at their usual level. The drug Chantix, which is marketed as an aid to stop smoking, acts by binding to the most common version of brain nAChR (one with $\alpha 4\beta 2$ subunits). Once bound, the Chantix molecule partially stimulates the receptor while preventing binding of nicotine.

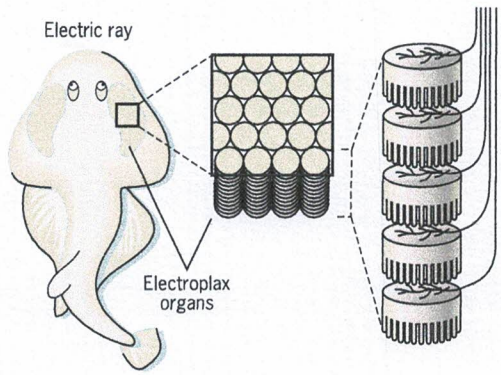


FIGURE 1 The electric organs of Torpedo consist of stacks of modified neuromuscular junctions located on each side of the body.
SOURCE: From Z. W. Hall, *An Introduction to Neurobiology*, Sinauer Associates, Inc., Sunderland, MA © 1992.

and tightly to this particular protein. Such a compound was discovered in 1963 by Chen-Yuan Lee and his colleagues of the National Taiwan University. The compound was α-bungarotoxin, a substance present in the venom of a Taiwanese snake. The α-bungarotoxin causes paralysis by binding tightly to the nAChRs on the postsynaptic membrane of skeletal muscle cells, blocking the response of the muscle to ACh.[4]

Equipped with labeled α-bungarotoxin to use in an assay, electric organs as a source, and a detergent capable of solubilizing membrane proteins, a number of investigators were able to isolate the acetylcholine receptors in the early 1970s. In one of these studies,[5] the membranes containing the nAChR were isolated by homogenizing the electric organs in a blender and centrifuging the suspension to pellet the membrane fragments. Membrane proteins were extracted from the membrane fragments using Triton X-100 (page 126), and the mixture was passed through a column containing tiny beads coated with a synthetic compound whose end bears a structural resemblance to ACh (**FIGURE 2a**). As the mixture of dissolved proteins passed through the column, two proteins that have binding sites for acetylcholine, nAChR and acetylcholinesterase (AChE), stuck to the beads. The remaining 90 percent of the protein in the extract failed to bind to the beads and simply passed through the column and was collected (Figure 2*b*). Once this group of proteins had passed through, a solution of 10^{-3} M flaxedil was passed through the column, which selectively removed the nAChR from the beads, leaving the AChE behind. Using this procedure, the acetylcholine receptor as measured by bungarotoxin binding was purified by more than 150-fold in a single step. This type of procedure is known as *affinity chromatography*, and its general use is discussed in Section 18.11.

The next step was to determine something about the structure of the acetylcholine receptor. Studies in the laboratory of Arthur Karlin at Columbia University determined that the nAChR was a pentamer, a protein consisting of five subunits. Each receptor contained two copies of a subunit called α, and one copy each of three other subunits. The subunits could be distinguished by extracting membrane proteins in Triton X-100, purifying the nAChR by affinity chromatography, and then subjecting the purified protein to electrophoresis through a polyacrylamide gel (SDS–PAGE, as discussed in Section 18.13), which separates the individual polypeptides according to size (**FIGURE 3**).[6] The four different subunits proved to be homologous to one another, each subunit containing four homologous transmembrane helices (M1–M4).

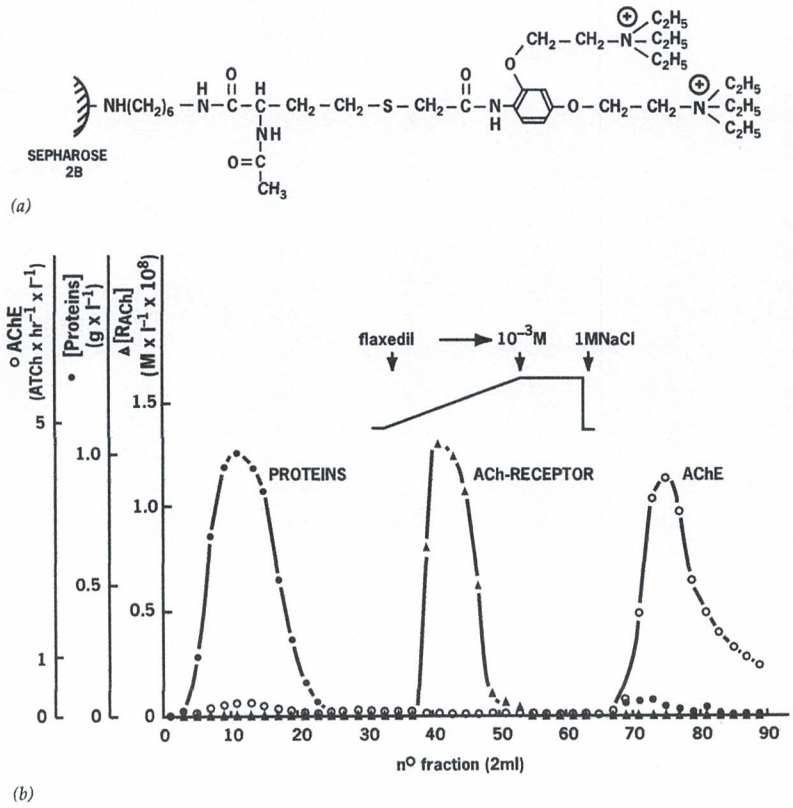


FIGURE 2 Steps used in the isolation of the nAChR. (*a*) Structure of a synthetic compound, CT5263, that was attached to sepharose beads to form an affinity column. The ends of the compound projecting from the beads resemble acetylcholine, causing both acetylcholinesterase (AChE) and the nicotinic acetylcholine receptor (nAChR) to bind to the beads. (*b*) When the Triton X-100 extract was passed through the column, both of the acetylcholine-binding proteins stuck to the beads, while the remaining dissolved protein (about 90 percent of the total protein in the extract) passed directly through the column. Subsequent passage of a solution of 10^{-3} M flaxedil through the column released the bound nAChR, without disturbing the bound AChE (which was subsequently eluted with 1 M NaCl).
SOURCE: (*a*) From R. W. Olsen, J.-C. Meunier, and J.-P. Changeux, *FEBS Lett.* 28:99, 1972. © 1972, with permission of Elsevier.

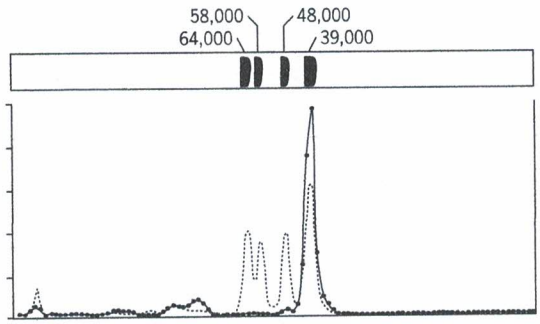


FIGURE 3 The top portion of the figure shows an SDS–polyacrylamide gel following electrophoresis of a preparation of the purified nAChR. The receptor consists of four different subunits whose molecular weights are indicated. Prior to electrophoresis, the purified receptor preparation was incubated with a radioactive compound (^{3}H-MBTA) that resembles acetylcholine and binds to the acetylcholine-binding site of the nAChR. Following electrophoresis, the gel was sliced into 1-mm sections and the radioactivity of each slice determined. All of the radioactivity was bound to the 39,000 dalton subunit, indicating this subunit contains the ACh-binding site. The dotted line indicates the light absorbance of each fraction, which provides a measure of the total amount of protein present in that fraction. The heights of the peaks provide a measure of the relative amounts of each of the subunits in the protein. All of the subunits are present in equal numbers except the smallest subunit (the α subunit, which contains the ACh-binding site), which is present in twice the number of copies.
SOURCE: From C. L. Weill, M. G. McNamee, and A. Karlin, *Biochem. Biophys. Res. Commun.* 61:1002, 1974, Reproduced with permission of Elsevier.

Another important milestone in the study of the nAChR was the demonstration that the purified receptor acted as both a site for binding ACh and a channel for the passage of cations. It had been postulated years earlier by Jean-Pierre Changeux of the Pasteur Institute in Paris that the binding of ACh to the receptor caused a conformational change that opened an ion channel within the protein. The inward flux of Na^+ ions through the channel could then lead to a depolarization of the membrane and the activation of the muscle cell. During the last half of the 1970s, Changeux and his colleagues succeeded in incorporating purified nAChR molecules into artificial lipid vesicles.[7] Using vesicles containing various concentrations of labeled sodium and potassium ions, they demonstrated that binding of ACh to the receptors in the lipid bilayer initiated a flux of cations through the "membrane." It was evident that "the pure protein does indeed contain all the structural elements needed for the chemical transmission of an electrical signal—namely, an acetylcholine binding site, an ion channel and a mechanism for coupling their activity." A personal narrative of the early work on nAChR can be found in Reference 8.

Since that time, researchers have focused on determining the structure of the nAChR and the mechanism by which binding of acetylcholine induces the opening of the ion gate. Analysis of the structure has taken several different paths. In one approach, scientists have used purified genes, determination of amino acid sequences, and site-directed mutagenesis to determine the specific parts of the polypeptides that span the membrane, or bind the neurotransmitter, or form the ion channel. These noncrystallographic studies on the molecular anatomy of a protein are similar in principle to those described in Section 4.5.

Another approach employed the electron microscope. The first glimpses of the nAChR were seen in electron micrographs of the membranes of the electric organs (**FIGURE 4**).[9] The receptors

continued

appeared to be ring shaped, with a diameter of 8 nm and a central channel of 2-nm diameter, and protruded out from the lipid bilayer into the external space. An increasingly detailed model of the nAChR has been developed by Nigel Unwin and his colleagues of the Medical Research Council of England.[10–14] These researchers employed the technique of electron crystallography (Section 18.16), which involves a mathematical analysis of large numbers of electron micrographs of frozen membranes containing the proteins being studied. Electric organs are well suited for electron crystallography because they contain highly ordered (crystalline) arrays of the nAChR within the plane of the lipid bilayer. As a result, Unwin was able to analyze the structure of the nAChR as it exists in its native lipid environment. He described the arrangement of the five subunits around a central channel (**FIGURE 5**). The ion channel consists of a narrow pore lined by a wall composed of five inner (M2) α helices, one from each of the surrounding subunits. The gate to the pore lies near the middle of the membrane, where each of the M2 α helices bends inward (at the apex of the V-shaped bars in Figure 5a) to form a kink in the unactivated receptor. The side chain of a leucine residue projects inward from each kink. In this model, the leucine residues from the five inner helices form a tight hydrophobic ring that prevents the ions from crossing the membrane. The gate opens following the binding of two ACh molecules, one per α subunit. Each ACh binds to a site located within a pocket of an α subunit (Figure 5b).

To study the changes in the nAChR during channel opening, Unwin carried out the following experiment.[12] Preparations of nAChR-rich membranes were applied to a support grid that was allowed to fall into a bath of liquid nitrogen-cooled ethane, which freezes the membranes. Approximately 5 msec before they reached the surface of the freezing bath, the grids were sprayed with a solution of ACh, which bound to the receptors and triggered the conformational change required to open the channel. By comparing electron micrographs of nAChRs trapped in the open versus closed state, Unwin found that ACh binding triggers a small conformational change in the extracellular domains of the receptor subunits near the two ACh binding sites. This conformational change is then propagated down the protein, causing the M2 helices that line the ion-conduction pore to straighten out (**FIGURE 6**), widening the channel and exposing more hydrophilic residues, thus allowing Na^+ ions to enter the cell.[13,14] Other models for channel opening have been proposed

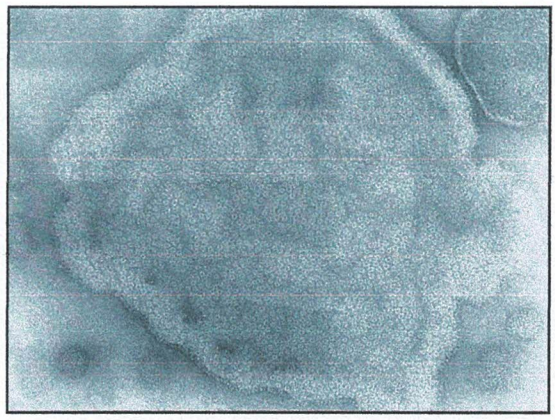
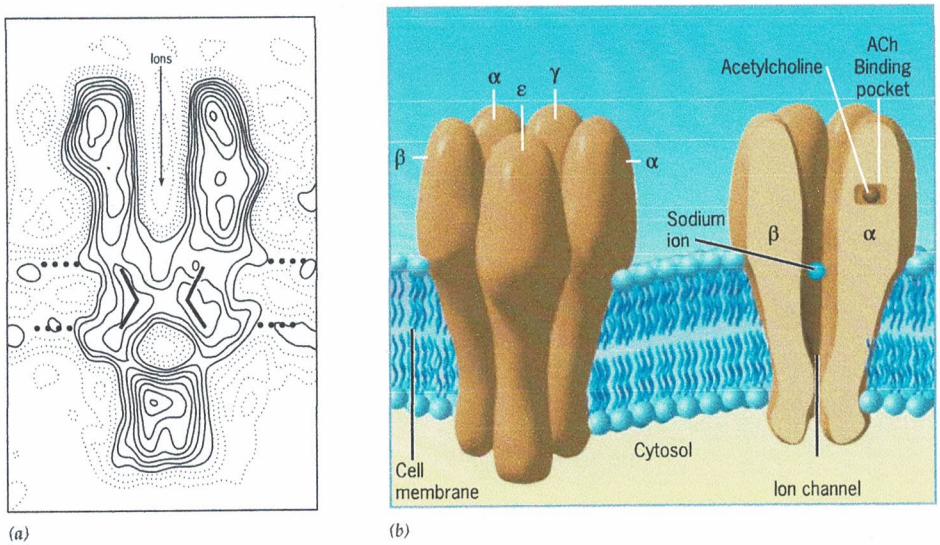


FIGURE 4 Electron micrograph of negatively stained, receptor-rich membranes from the electric organ of an electric fish showing the dense array of nAChR molecules. Each receptor molecule is seen as a small whitish circle with a tiny black dot in its center; the dot corresponds to the central channel, which has collected electron-dense stain.
SOURCE: From Werner Schiebler and Ferdinand Hucho, *Eur. J. Biochem.* 85:58, 1978, reprinted with permission John Wiley & Sons.



(a) (b)

FIGURE 5 (a) An electron density map of a slice through the nAChR obtained by analyzing electron micrographs of tubular crystals of *Torpedo* membranes embedded in ice. These analyses have allowed researchers to reconstruct the three-dimensional appearance of a single nAChR protein as it resides within the membrane. The continuous contours indicate lines of similar density greater than that of water. The two dark, bar-shaped lines represent the α helices that line the channel at its narrowest point. (b) Schematic diagram of the nAChR showing the arrangement of the subunits and a cross-sectional representation of the protein. Each of the five subunits contains four membrane-spanning helices (M1–M4). Of these, only the inner helix (M2) lines the pore, and is the subject of the remainder of the discussion.
SOURCE: From N. Unwin, *J. Mol. Biol.* 229:1118, 1993; © 1993, with permission of Elsevier.

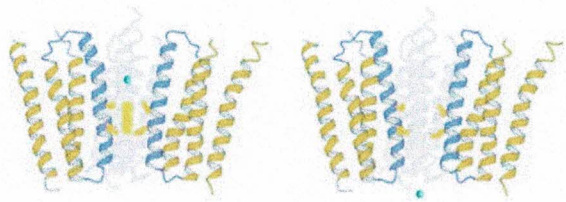


FIGURE 6 Ribbon drawings illustrating the changes that occur within the nAChR conducting channel upon binding of acetylcholine. Only the two alpha subunits of the receptor are shown. In the closed state (left) the pore is blocked (yellow patch) by the close apposition of a ring of hydrophobic residues. The diameter of the pore at its narrowest point is about 6 Å, which is not sufficient for a hydrated Na^+ ion to pass. This constriction arises because the inner transmembrane helices are slightly bent. Although it is wide enough for passage of a dehydrated Na^+ ion (blue sphere), the wall of the channel lacks the polar groups that would be required to substitute for the displaced shell of water molecules (as occurs in the selectivity filter of the K^+ channel, Figure 4.39). Following binding of ligand, a conformational change in the ligand-binding domain of the alpha subunits (not shown), causes the inner transmembrane helices of the subunits (blue) to straighten out, expanding the diameter of the pore, which allows the flow of Na^+ ions through the open channel (right).

SOURCE: From N. Unwin, Quart Rev Biophys 46:283, 2013.

by other laboratories, and a more definitive statement about the mechanism of gating will probably require a high-resolution X-ray crystal structure of the protein in both the open and closed states. Discussion of various models and the bases for them can be found in References 15–17.

References

1. Langley, J. N. 1906. On nerve endings and on special excitable substances in cells. *Proc. R. Soc. London B Biol. Sci.* 78:170–194.
2. Loewi, O. 1921. Uber humorale ubertragbarkeit der herznervenwirkung. *Pfluger's Arch.* 214:239–242. (A review of Loewi's work written by him in English can be found in *Harvey Lect.* 28:218–233, 1933.)
3. Marnay, A. 1937. Cholinesterase dans l'organe électrique de la torpille. *Compte Rend.* 126:573–574. (A review of Nachmansohn's work written in English can be found in his book, *Chemical and Molecular Basis of Nerve Action*, 2nd ed., Academic Press, 1975.)
4. Chang, C. C. & Lee, C.-Y. 1963. Isolation of the neurotoxins from the venom of Bungarus multicinctus and their modes of neuromuscular blocking action. *Arch. Int. Pharmacodyn. Ther.* 144:241–257.
5. Olsen, R. W., Meunier, J. C., & Changeux, J. P. 1972. Progress in the purification of the cholinergic receptor protein from Electrophorus electricus by affinity chromatography. *FEBS Lett.* 28:96–100.
6. Weill, C. L., Mcnamee, M. G., & Karlin, A. 1974. Affinity-labeling of purified acetylcholine receptor *from Torpedo californica. Biochem. Biophys. Res. Commun.* 61:997–1003.
7. Popot, J. L., Cartaud, J., & Changeux, J.-P. 1981. Reconstitution of a functional acetylcholine receptor. *Eur. J. Biochem.* 118:203–214.
8. Changeux, J. P. 2010. Allosteric receptors: From electric organ to cognition. *Ann. Rev. Pharmacol. Toxicol.* 50:1–38.
9. Schiebler, W. & Hucho, F. 1978. Membranes rich in acetylcholine receptor: Characterization and reconstitution to excitable membranes from exogenous lipids. *Eur. J. Biochem.* 85:55–63.
10. Brisson, A. & Unwin, N. 1984.Tubular crystals of acetylcholine receptor. *J. Cell Biol.* 99:1202–1211.
11. Unwin, N. 1993. Acetylcholine receptor at 9 Å resolution. *J. Mol. Biol.* 229:1101–1124.
12. Unwin, N. 1995. Acetylcholine receptor channel imaged in the open state. *Nature* 373:37–43.
13. Miyazawa, A., Fujiyoshi, Y. & Unwin, N. 2003. Structure and gating mechanism of the acetylcholine receptor pore. *Nature* 423:949–955.
14. Unwin, N. 2005. Refined structure of the nicotinic acetylcholine receptor at 4.0 Å resolution. *J. Mol. Biol.* 346:967–989.
15. Corry, B. 2006. An energy-efficient gating mechanism in the acetylcholine receptor channel suggested by molecular and brownian dynamics. *Biophys. J.* 90:799–810.
16. Cymes, G. D. & Grosman, C. 2008. Pore-opening mechanism of the nicotinic acetylcholine receptor evinced by proton transfer. *Nature Struct. Mol. Biol.* 15:389–396.
17. Taly, A., et al. 2009. Nicotinic receptors: Allosteric transitions and therapeutic targets in the nervous system. Nature Revs. Drug Disc. 8: 733–750.

4.13 Facilitated Diffusion

Substances always diffuse across a membrane from a region of higher concentration on one side to a region of lower concentration on the other side, but they do not always diffuse through the lipid bilayer or through a channel. In many cases, the diffusing substance first binds selectively to a membrane-spanning protein, called a **facilitative transporter**, that facilitates the diffusion process. The binding of the solute to the facilitative transporter on one side of the membrane is thought to trigger a conformational change in the protein, exposing the solute to the other surface of the membrane, from where it can diffuse down its concentration gradient. This mechanism is illustrated in FIGURE 4.44. Because they operate passively, that is, without being coupled to an energy-releasing system, facilitated transporters can mediate the movement of solutes equally well in both directions. The direction of net flux depends on the relative concentration of the substance on the two sides of the membrane.

Facilitated diffusion, as this process is called, is similar in many ways to an enzyme-catalyzed reaction. Like enzymes, facilitative transporters are specific for the molecules they transport, discriminating, for example, between D and L stereoisomers (page 43). In addition, both enzymes and transporters exhibit **saturation**-type kinetics (FIGURE 4.45). Unlike ion channels, which can conduct millions of ions per second, most facilitative transporters can move only hundreds to thousands of solute molecules per second across the membrane, so once the concentration of ions becomes very large, the transport rate levels off to this maximum value, and the transporters are said to be saturated. Another important feature of facilitative transporters is that, like enzymes and ion channels, their activity can be regulated. Facilitated diffusion is particularly important in mediating the entry and exit of polar solutes, such as sugars and amino acids, that do not penetrate the lipid bilayer. This is illustrated in the following section.

The glucose transporter is an example of facilitated diffusion. Glucose is the body's primary source of direct energy, and most mammalian cells contain a membrane protein that facilitates the diffusion of glucose from the bloodstream into the cell (as depicted in Figures 4.44 and 4.49). A gradient favoring the continued diffusion of glucose into the cell is maintained by phosphorylating the sugar after it enters the cytoplasm, thus lowering the intracellular glucose

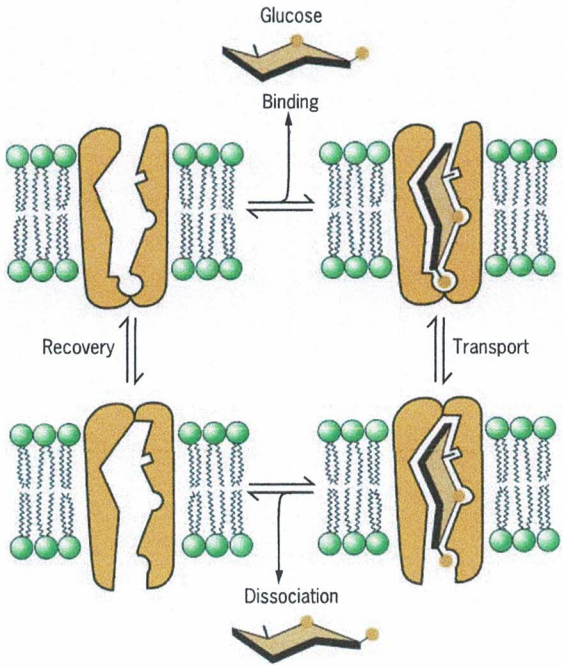


FIGURE 4.44 Facilitated diffusion. *A schematic model for the facilitated diffusion of glucose depicts the alternating conformation of a carrier that exposes the glucose binding site to either the inside or outside of the membrane.*

SOURCE: Reprinted from S. A. Baldwin and G. E. Lienhard, *Trends Biochem. Sci.* 6:210, 1981. Used with permission from Elsevier, Ltd.

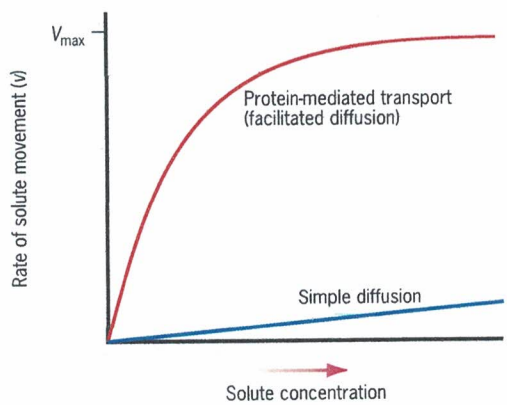


FIGURE 4.45 The kinetics of facilitated diffusion as compared to that of simple physical diffusion.

concentration. Humans have at least five related proteins (isoforms) that act as facilitative glucose transporters. These isoforms, termed GLUT1 to GLUT5, are distinguished by the tissues in which they are located, as well as their kinetic and regulatory characteristics.

Insulin is a hormone produced by endocrine cells of the pancreas that plays a key role in maintaining proper blood sugar levels. An increase in blood glucose levels triggers the secretion of insulin, which stimulates the uptake of glucose into various target cells, most notably skeletal muscle and fat cells (adipocytes). Insulin-responsive cells share a common isoform of the facilitative glucose transporter, specifically GLUT4. When insulin levels are low, these cells contain relatively few glucose transporters on their plasma membrane. Instead, the transporters are present within the membranes of cytoplasmic vesicles. Rising insulin levels act on target cells to stimulate the fusion of the cytoplasmic vesicles to the plasma membrane, which moves transporters to the cell surface where they can bring glucose into the cell (see Figure 15.26).

REVIEW

1. Compare and contrast facilitative transporters with channels.
2. Discuss why enzymes and transporters show saturation kinetics.

4.14 Active Transport

Life cannot exist under equilibrium conditions (section 3.4). Nowhere is this more apparent than in the imbalance of ions across the plasma membrane. The differences in concentration of the major ions between the outside and inside of a typical mammalian cell are shown in Table 4.3. The ability of a cell to generate such steep concentration gradients across its plasma membrane cannot occur by either simple or facilitated diffusion. Rather, these gradients must be generated by **active transport**.

Like facilitated diffusion, active transport depends on integral membrane proteins that selectively bind a particular solute and move it across the membrane in a process driven by changes in the protein's conformation. Unlike facilitated diffusion, however, movement of a solute against a gradient requires the coupled input of energy. Consequently, the endergonic movement of ions or other solutes across the membrane against a concentration gradient is coupled to an exergonic process, such as the hydrolysis of ATP, the absorbance of light, the transport of electrons, or the flow of other substances down their gradients. Proteins that carry out active transport are often referred to as "pumps."

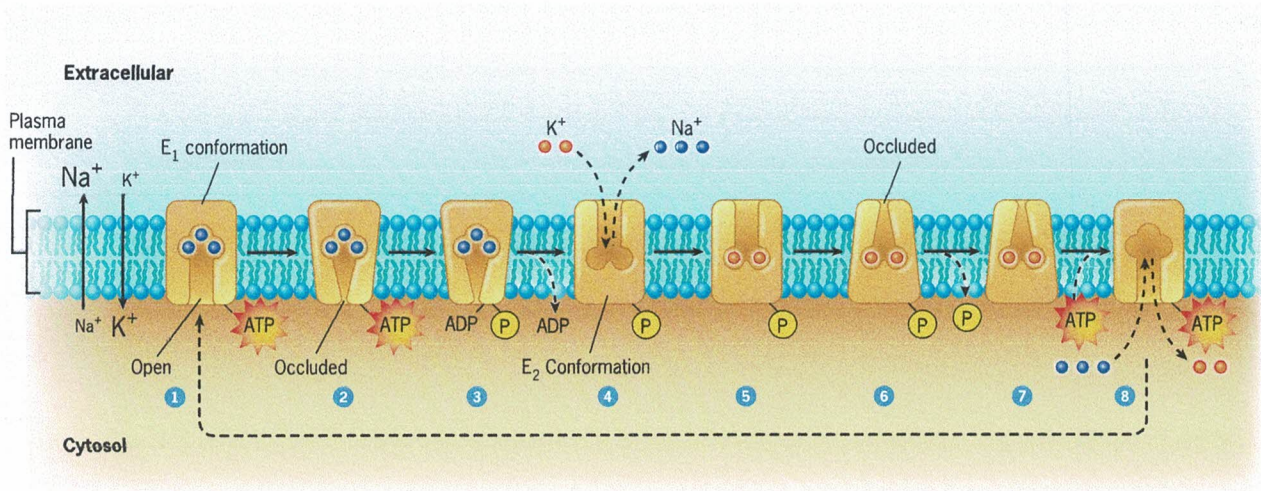
Primary Active Transport: Coupling Transport to ATP Hydrolysis

In 1957, Jens Skou, a Danish physiologist, discovered an ATP-hydrolyzing enzyme in the nerve cells of a crab that was only active in the presence of both Na^+ and K^+ ions. Skou proposed, and correctly so, that this enzyme, which was responsible for ATP hydrolysis, was the

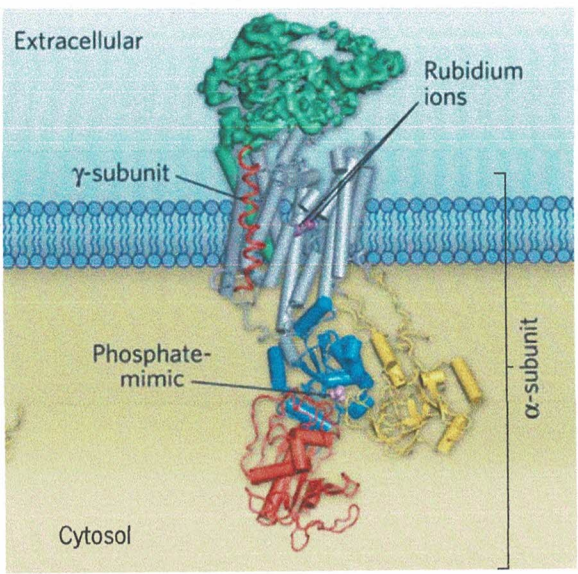
TABLE 4.3 Ion Concentrations Inside and Outside of a Typical Mammalian Cell

	Extracellular concentration	Intracellular concentration	Ionic gradient
Na^+	150 mM	10 mM	15×
K^+	5 mM	140 mM	28×
Cl^-	120 mM	10 mM	12×
Ca^{2+}	10^{-3} M	10^{-7} M	10,000×
H^+	$10^{-7.4}$ M (pH of 7.4)	$10^{-7.2}$ M (pH of 7.2)	Nearly 2×

The ion concentrations for the squid axon are given on page 167.



(a)



(b)

FIGURE 4.46 The Na^+/K^+-ATPase. *(a)* Simplified schematic model of the transport cycle as described in the text. Note that the actual Na^+/K^+-ATPase is composed of at least two different membrane-spanning subunits: a larger α subunit, which carries out the transport activity, and a smaller β subunit, which functions primarily in the maturation and assembly of the pump within the membrane. A third (γ) subunit may also be present. *(b)* A model of the E_2 conformation of the protein based on an X-ray crystallographic study. The cation binding sites are located deep within the transmembrane domain, which consists of 10 membrane-spanning helices. The two rubidium ions are located where the potassium ions would normally be bound.

SOURCE: *(b)* From Ayako Takeuchi, courtesy of David C. Gadsby, *Nature* 450: 958, 2007, © 2007 reprinted by permission from Macmillan Publishers Ltd.

same protein that was active in transporting the two ions; the enzyme was called the Na^+/K^+-ATPase, or the *sodium–potassium pump*.

Unlike the protein-mediated movement of a facilitated diffusion system, which will carry the substance equally well in either direction, active transport drives the movement of ions in only one direction. It is the Na^+/K^+-ATPase that is responsible for the large excess of Na^+ ions outside of the cell and the large excess of K^+ ions inside the cell. The positive charges carried by these two cations are balanced by negative charges carried by various anions so that the extracellular and intracellular compartments are, for the most part, electrically neutral. Cl^- ions are present at greater concentration outside of cells, where they balance the extracellular Na^+ ions. The abundance of intracellular K^+ ions is balanced primarily by excess negative charges carried by proteins and nucleic acids.

The ratio of Na^+:K^+ pumped by the Na^+/K^+-ATPase is not 1:1, but 3:2 (see **FIGURE 4.46**). In other words, for each ATP hydrolyzed, three sodium ions are pumped out as two potassium ions are pumped in. Because of this pumping ratio, the Na^+/K^+-ATPase is *electrogenic*, which means that it contributes directly to the separation of charge across the membrane. The Na^+/K^+-ATPase is an example of a *P-type* ion pump. The "P" stands for phosphorylation, indicating that, during the pumping cycle, the hydrolysis of ATP leads to the transfer of the released phosphate group to an aspartic acid residue of the transport protein. As denoted by the name of the protein, this reaction is catalyzed by the pump itself.

Consider the activity of the protein. It must pick up sodium or potassium ions from a region of low concentration, which means that the protein must have a relatively high affinity for the ions. Then the protein must release the ions on the other side of the membrane into a much greater concentration of each ion. To do this, the affinity of the protein for that ion must decrease. Thus, the affinity for each ion on the two sides of the membrane must be different. This is achieved by ATP hydrolysis and the subsequent release of ADP, which induces a large conformational change within the protein molecule. The change in protein structure—between the E_1 and E_2 conformations—also serves to alternately expose the ion binding sites to the opposite side of the membrane, as discussed in the following paragraph.

A proposed scheme for the pumping cycle of the Na^+/K^+-ATPase is shown in Figure 4.46*a*, which is based on X-ray crystallographic structures of P-type ion pumps. In step 1, Figure 4.46*a*, the pump is in the E_1 conformation, and the ion binding sites are accessible to the inside of the cell. In this step, the protein has bound three Na^+ ions

and an ATP. In step 2, a gate within the protein has closed, shifting the pump into an occluded E_1 state in which the Na^+ ions can no longer flow back into the cytosol. Hydrolysis of the bound ATP (step 2→3) and release of ADP (step 3→4) cause the change from the E_1 to the E_2 conformation. In doing so, the binding site becomes accessible to the extracellular compartment, and the protein loses its affinity for Na^+ ions, which are then released outside the cell. Once the three Na^+ ions have been released, the protein picks up two K^+ions (step 5). The closing of another gate within the protein shifts the pump into an occluded state (step 6), preventing back flow of the K^+ ions into the extracellular space. Occlusion is followed by dephosphorylation (step 6→7) and ATP binding (step 8), which induces the return of the protein to the original E_1 conformation. In this state, the binding site is open to the internal surface of the membrane and has lost its affinity for K^+ ions, leading to the release of these ions into the cell. The cycle is then repeated. A model of the crystal structure of the Na^+/K^+-ATPase structure is shown in Figure 4.46*b*. Because they require complex conformational changes, these active transport pumps move ions across membranes at rates that are several orders of magnitude lower than their flow through ion channels.

The sodium–potassium pump is found only in animal cells. This protein is thought to have evolved in primitive animals as the primary means to maintain cell volume and as the mechanism to generate the steep Na^+ and K^+ gradients that play such a key role in the formation of impulses in nerve and muscle cells. These same ionic gradients are used in nonexcitable cells to power the movement of other solutes as discussed below. The importance of the sodium–potassium pump becomes evident when one considers that it consumes approximately one-third of the energy produced by most animal cells and two-thirds of the energy produced by nerve cells. Digitalis, a steroid obtained from the foxglove plant that has been used for 200 years as a treatment for congestive heart disease, binds to the Na^+/K^+-ATPase. Digitalis strengthens the heart's contraction by inhibiting the Na^+/K^+ pump, which leads to a chain of events that increases Ca^{2+} availability inside the muscle cells of the heart.

Other Primary Ion Transport Systems

The best studied P-type pump is the Ca^{2+}-ATPase whose three-dimensional structure has been determined at several stages of the pumping cycle. The calcium pump is present in the membranes of the endoplasmic reticulum, where it actively transports calcium ions out of the cytosol into the lumen of this organelle. Plant cells have a H^+-transporting, P-type, plasma membrane pump. In plants, this proton pump plays a key role in the secondary transport of solutes (discussed later), in the control of cytosolic pH, and possibly in control of cell growth by means of acidification of the plant cell wall.

The epithelial lining of the stomach also contains a P-type pump, the H^+/K^+-ATPase, which secretes a solution of concentrated acid (up to 0.16 N HCl) into the stomach chamber. In the resting state, these pump molecules are situated in cytoplasmic membranes of the parietal cells of the stomach lining and are nonfunctional (**FIGURE 4.47**). When food enters the stomach, a hormonal message is transmitted to the parietal cells that causes the pump-containing membranes to move to the apical cell surface, where they fuse with the plasma membrane and begin secreting acid (Figure 4.47). In addition to functioning in digestion, stomach acid can also lead to heartburn. Prilosec and related drugs are widely used to prevent heartburn by inhibiting the stomach's H^+/K^+-ATPase. Other acid-blocking heartburn medications (e.g., Zantac, Pepcid, and Tagamet) do not inhibit the H^+/K^+-ATPase directly, but block a receptor on the surface of the parietal cells, thereby stopping the cells from becoming activated by the hormone.

Unlike P-type pumps, *V-type* pumps utilize the energy of ATP without forming a phosphorylated protein intermediate. V-type pumps actively transport hydrogen ions across the walls of cytoplasmic organelles and vacuoles (hence the designation V-type). They occur in the membranes that line lysosomes, secretory granules, and plant cell vacuoles where they maintain the low pH of the contents. V-type pumps have also been found in the plasma membranes of a variety of cells. For example, a V-type pump in the plasma membranes

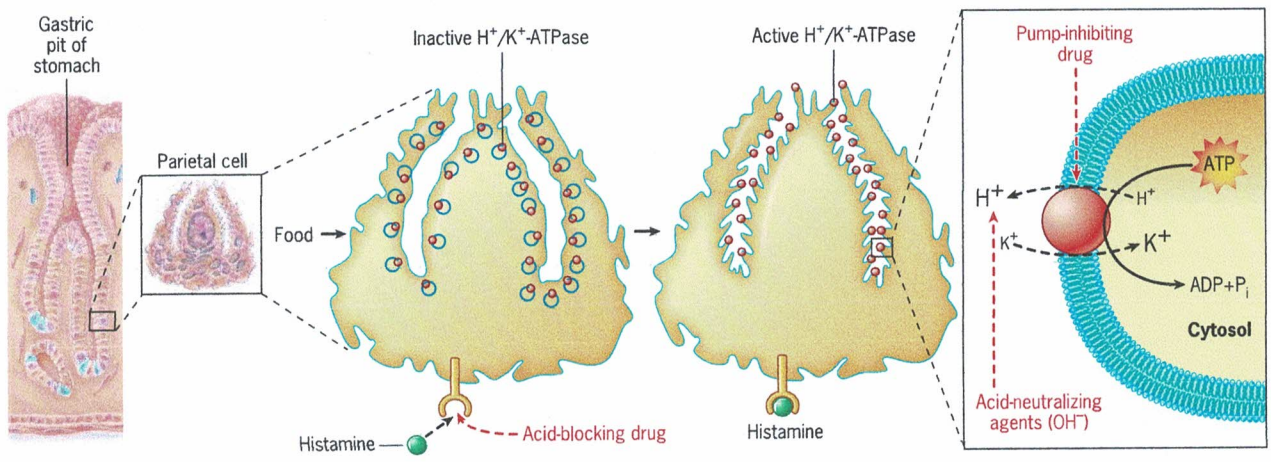


FIGURE 4.47 Control of acid secretion in the stomach. In the resting state, the H^+/K^+-ATPase molecules are present in the walls of cytoplasmic vesicles. Food entering the stomach triggers a cascade of hormone-stimulated reactions in the stomach wall leading to the release of histamine, which binds to a receptor on the surface of the acid-secreting parietal cells. Binding of histamine to its receptor stimulates a response that causes the H^+/K^+-ATPase-containing vesicles to fuse to the plasma membrane, forming deep folds, or canaliculi. Once at the surface, the transport protein is activated and pumps protons into the stomach cavity against a concentration gradient (indicated by the size of the letters). The heartburn drugs Prilosec, Nexium, and Prevacid block acid secretion by directly inhibiting the H^+/K^+-ATPase, whereas several other acid-blocking medications interfere with activation of the parietal cells. Acid-neutralizing medications provide basic anions that combine with the secreted protons.

of kidney tubules helps maintain the body's acid–base balance by secreting protons into the forming urine. V-type pumps are large multi-subunit complexes (shown in Figure 4.4*d*) and similar in structure to that of the ATP synthase shown in Figure 5.23.

Another diverse group of proteins that actively transport ions is the *ATP-binding cassette* (*ABC*) *transporters*, so called because all of the members of this superfamily share a homologous ATP-binding domain. The best studied ABC transporter is described in the accompanying Human Perspective.

Using Light Energy to Actively Transport Ions

Halobacterium salinarium (or *H. halobium*) is an archaebacterium that lives in extremely salty environments, such as that found in the Great Salt Lake. When grown under anaerobic conditions, the plasma membranes of these prokaryotes take on a purple color due to the presence of one particular protein, *bacteriorhodopsin*, which acts as a light-driven proton pump. As shown in **FIGURE 4.48**, bacteriorhodopsin contains retinal, the same prosthetic group present in rhodopsin, the light-absorbing protein of the rods of the vertebrate retina. The absorption of light energy by the retinal group induces a series of conformational changes in the protein that cause a proton to move from the retinal group, through a channel in the protein, to the cell exterior (Figure 4.48). The proton donated by the photo-excited retinal is replaced by another proton transferred to the protein from the cytoplasm. In effect, this process results in the translocation of protons from the cytoplasm to the external environment, thereby generating a steep H^+ gradient across the plasma membrane. This gradient is subsequently used by an ATP-synthesizing enzyme to phosphorylate ADP, as described in the next chapter.

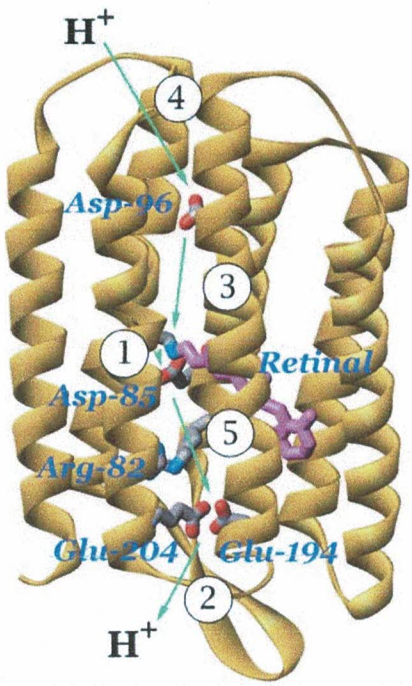


FIGURE 4.48 Bacteriorhodopsin: a light-driven proton pump. The protein contains seven membrane-spanning helices and a centrally located retinal group (shown in purple), which serves as the light-absorbing element (chromophore). Absorption of a photon of light causes a change in the electronic structure of retinal, leading to the transfer of a proton from the $—NH^+$ group to a closely associated, negatively charged aspartic acid residue (#85) (step 1). The proton is then released to the extracellular side of the membrane (step 2) by a relay system consisting of several amino acid residues (Asp82, Glu204, and Glu194). The spaces between these residues are filled with hydrogen-bonded water molecules that help shuttle protons along the pathway. The deprotonated retinal is returned to its original state (step 3) when it accepts a proton from an undissociated aspartic acid residue (Asp96) located near the cytoplasmic side of the membrane. Asp96 is then reprotonated by a H^+ from the cytoplasm (step 4). Asp85 is deprotonated (step 5) prior to receiving a proton from retinal in the next pumping cycle. As a result of these events, protons move from the cytoplasm to the cell exterior through a central channel in the protein.

SOURCE: From Hartmut Luecke et al., courtesy of Janos K. Lanyi, *Science* 286:255, 1999; © 1999, reprinted with permission from AAAS.

Secondary Active Transport (or Cotransport): Coupling Transport to Existing Ion Gradients

The establishment of concentration gradients, such as those of Na^+, K^+, and H^+, provides a means by which free energy can be stored in a cell. The potential energy stored in ionic gradients is utilized by a cell in various ways to perform work, including the transport of other solutes. Consider the physiologic activity of the intestine. Within its lumen, enzymes hydrolyze high-molecular-weight polysaccharides into simple sugars, which are absorbed by the epithelial cells that line the intestine. The movement of glucose across the apical plasma membrane of the epithelial cells, against a concentration gradient, occurs by **cotransport** with sodium ions, as illustrated in **FIGURE 4.49**. The Na^+ concentration is kept very low within the cells by the action of a *primary* active transport system (the Na^+/K^+-ATPase), located in the basal and lateral plasma membrane, which pumps sodium ions out of the cell against a concentration gradient. The tendency for sodium ions to diffuse back across the apical plasma membrane down their concentration gradient is "tapped" by the epithelial cells to drive the cotransport of glucose molecules into the cell *against* a concentration gradient. The glucose molecules are said to be driven by *secondary active transport*. In this case, the transport protein, called a *Na^+/glucose cotransporter*, moves two sodium ions and one glucose molecule with each cycle. Once inside, the glucose molecules diffuse through the cell and are moved across the basal membrane by facilitated diffusion (page 152).

To appreciate the power of an ion gradient in accumulating other types of solutes in cells, we can briefly consider the energetics of the Na^+/glucose cotransporter. Recall from page 140 that the free-energy change for the movement of a mole of Na^+ ions into the cell is equal to −3.1 kcal/mol, and thus 6.2 kcal for two moles of Na^+ ions, which would be available to transport one mole of glucose uphill into the cell. Recall also from page 139 that the equation for the movement of a nonelectrolyte, such as glucose, across the membrane is

$$\Delta G = RT \ln \frac{[C_i]}{[C_o]}$$

$$\Delta G = 2.303\ RT \log_{10} \frac{[C_i]}{[C_o]}$$

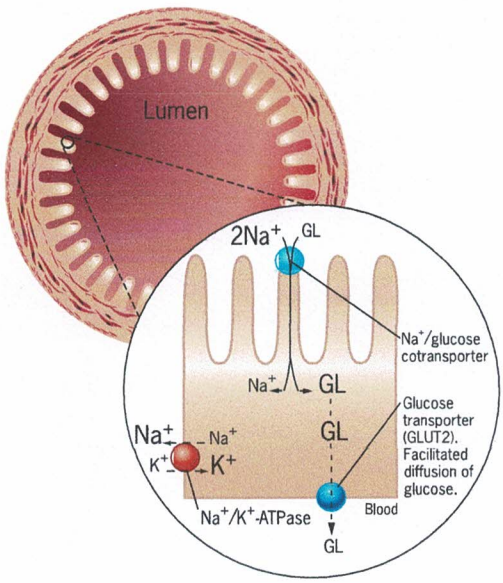


FIGURE 4.49 Secondary transport: the use of energy stored in an ionic gradient. The Na^+/K^+-ATPase residing in the plasma membrane of the lateral surface maintains a very low cytosolic concentration of Na^+. The Na^+ gradient across the plasma membrane represents a storage of energy that can be tapped to accomplish work, such as the transport of glucose by a Na^+/glucose cotransporter located in the apical plasma membrane. Once transported across the apical surface into the cell, the glucose molecules diffuse to the basal surface where they are carried by a glucose facilitative transporter out of the cell and into the bloodstream. The relative size of the letters indicates the directions of the respective concentration gradients. Two Na^+ ions are transported for each glucose molecule; the 2:1 Na^+/glucose provides a much greater driving force for moving glucose into the cell than a 1:1 ratio.

Using this equation, we can calculate how steep a concentration gradient of glucose (X) that this cotransporter can generate. At 25°C,

$$-6.2 \text{ kcal/mol} = 1.4 \text{ kcal/mol} \cdot \log_{10} X$$

$$\log_{10} X = -4.43$$

$$X = \frac{1}{23{,}000}$$

This calculation indicates that the Na^+/glucose cotransporter is capable of transporting glucose into a cell against a concentration gradient greater than 20,000-fold.

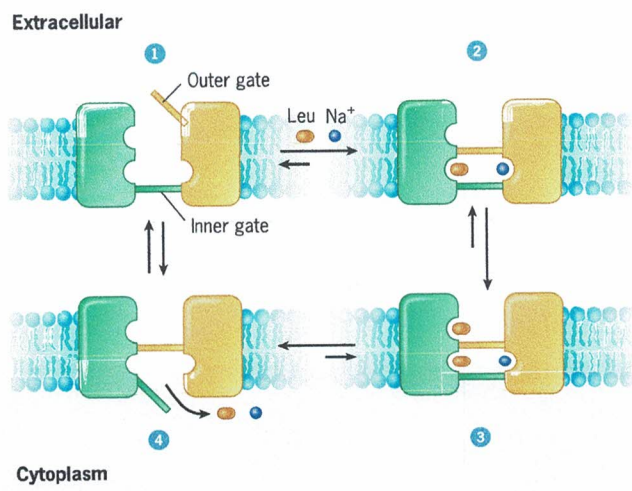
FIGURE 4.50 A schematic model of the transport cycle of a secondary transporter. Four different conformational states during the transport cycle of a bacterial symporter of the LeuT family are shown. The protein actively transports the amino acid leucine into the cell using the established Na^+ ion gradient as its source of energy. In step 1, the outer gate in the protein is open, whch allows both Na^+ and leucine to reach their binding sites from the extracellular space. In step, 2, the outer gate closes, occluding the substrates within the protein. In step 3, a second leucine molecule binds to another site just outside the outer gate. In step 4, the inner gate opens and the substrates are released into the cytoplasm. The protein returns to its original state when the inner gate is closed and the outer gate is opened.

SOURCE: Reprinted by permission from Macmillan Publishers Ltd: *Nature*, 465: 171, 2010 by N. K. Karpowich and Da-Neng Wang (NYU School of Medicine).

Plant cells rely on secondary active transport systems to take up a variety of nutrients, including sucrose, amino acids, and nitrate. In plants, uptake of these compounds is coupled to the downhill, inward movement of H^+ ions rather than Na^+ ions. The secondary active transport of glucose into the epithelial cells of the intestine and the transport of sucrose into a plant cell are examples of *symport*, in which the two transported species (Na^+ and glucose or H^+ and sucrose) move in the same direction. Numerous cotransporters have been isolated that engage in ***antiport***, in which the two transported species move in opposite directions. For example, cells often maintain a proper cytoplasmic pH by coupling the inward, downhill movement of Na^+ with the outward movement of H^+. Cotransporters that mediate antiport are usually called *exchangers*. The three-dimensional structures of a number of secondary transporters have been solved in recent years, and, like the Na^+/K^+-ATPase, they exhibit a transport cycle in which the protein's binding sites gain alternating access to the cytoplasm and the extracellular space. A proposed model of the transport cycle of one of the major families of secondary transporters is shown in **FIGURE 4.50**.

REVIEW

1. Describe two ways in which energy is utilized to move ions and solutes against a concentration gradient.
2. How does the Na^+/K^+-ATPase illustrate the asymmetry of the plasma membrane?
3. What is the role of phosphorylation in the mechanism of action of the Na^+/K^+-ATPase?
4. What is the structural relation between the parts of the prokaryotic KcsA K^+ channel and the eukaryotic voltage-regulated K^+ channel? Which part of the channel is involved in ion selectivity, which part in channel gating, and which part in channel inactivation? How does each of these processes (ion selectivity, gating, and inactivation) occur?
5. Because of its smaller size, one would expect Na^+ ions to be able to penetrate any pore large enough for a K^+ ion. How does the K^+ channel select for this specific ion?



4.15 THE HUMAN PERSPECTIVE

Defects in Ion Channels and Transporters as a Cause of Inherited Disease

Several severe, inherited disorders have been traced to mutations in genes that encode ion channel proteins (Table 1). Most of the disorders listed in Table 1 affect the movement of ions across the plasma membranes of excitable cells (i.e., muscle, nerve, and sensory cells), reducing the ability of these cells to develop or transmit impulses (page 160). In contrast, cystic fibrosis, the best studied and most common inherited ion channel disorder, results from a defect in the ion channels of epithelial cells.

On average, 1 out of every 25 persons of Northern European descent carries one copy of the mutant gene that can cause cystic fibrosis. Because they show no symptoms of the mutant gene, most heterozygotes are unaware that they are carriers. Consequently, approximately 1 out of every 2500 infants in this Caucasian population (1/25 × 1/25 × 1/4) is homozygous recessive at this locus and born with cystic fibrosis (CF). Although cystic fibrosis affects various organs, including the intestine, pancreas, sweat glands, and reproductive tract, the respiratory tract usually exhibits the most severe effects. Victims of CF produce a thickened, sticky mucus that is very hard to propel out of the airways. Afflicted individuals typically suffer from chronic lung infections and inflammation, which progressively destroy pulmonary function.

The gene responsible for cystic fibrosis was isolated in 1989. Once the sequence of the CF gene was determined and the amino acid sequence of the corresponding polypeptide was deduced, it was apparent that the polypeptide was a member of the ABC transporter superfamily. The protein was named *cystic fibrosis transmembrane conductance regulator* (*CFTR*), an ambiguous term that reflected the fact that researchers weren't sure of its precise function. The question was thought to be answered after the protein was purified, incorporated into artificial lipid bilayers, and shown to act as a cyclic AMP-regulated chloride channel, not a transporter. But subsequent studies have added numerous complications to the story as it has been shown that, in addition to functioning as a chloride channel, CFTR also (1) conducts bicarbonate (HCO_3^-) ions, (2) suppresses the activity of an epithelial Na^+ ion channel (ENaC), and (3) stimulates the activity of a family of epithelial chloride/bicarbonate exchangers. As the role of CFTR has become more complex, it has become difficult to establish precisely how a defect in this protein leads to the development of chronic lung infections. While there is considerable debate, many researchers would agree with the following statements.

Because the movement of water out of epithelial cells by osmosis follows the movement of salts, abnormalities in the flux of Cl^-, HCO_3^-, and/or Na^+ caused by CFTR deficiency leads to a decrease in the fluid that bathes the epithelial cells of the airways (**FIGURE 1**). A reduction in volume of the surface liquid, and a resulting increase in viscosity of the secreted mucus, impair the function of the cilia that push mucus and bacteria out of the respiratory tract. Many CF patients are helped by inhaling a mist of hypertonic saline, which helps to draw more water into the airways and reduce the viscosity of the mucus. Clinical trials are also being carried out on compounds that have the potential to increase the volume of surface fluid by altering the movements of ions in and out of the epithelial cells (Figure 1). One such compound is the ENaC Na^+-channel inhibitor named GS-9411, which was hoped to help treat CF by reducing Na^+ ion absorption from the airway fluid into the epithelium. Unfortunately, this drug caused elevated potassium in the blood, and the clinical trials had to be terminated, illustrating the challenges of treating a disease by targeting ion channels with broad roles in physiology. It was therefore hoped that better understanding of the genetics of CF might lead to development of more precisely targeted drugs that could treat CF without causing wide-ranging alterations in body chemistry.

In the past decade, researchers have identified more than 1000 different mutations that give rise to cystic fibrosis. However, approximately 70 percent of the alleles responsible for cystic fibrosis in the United States contain the same genetic alteration (designated ΔF508)—they are all missing three base pairs of DNA that encode a phenylalanine at position 508,

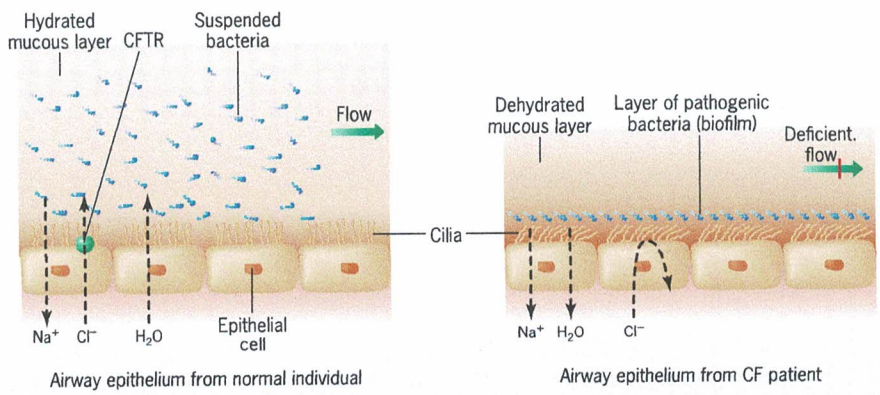


FIGURE 1 An explanation for the debilitating effects on lung function from the absence of the *CFTR* protein. In the airway epithelium of a normal individual, water flows out of the epithelial cells in response to the outward movement of ions, thus hydrating the surface mucous layer. The hydrated mucous layer, with its trapped bacteria, is readily moved out of the airways. In the airway epithelium of a person with cystic fibrosis, the abnormal movement of ions causes water to flow in the opposite direction, thus dehydrating the mucous layer. As a result, trapped bacteria cannot be moved out of the airways, which allows them to proliferate as a biofilm (page 13) and cause chronic infections.

TABLE 1

Inherited disorder	Type of channel	Gene	Clinical consequences
Familial hemiplegic migraine (FHM)	Ca^{2+}	*CACNL1A4*	Migraine headaches
Episodic ataxia type-2 (EA-2)	Ca^{2+}	*CACNL1A4*	Ataxia (lack of balance and coordination)
Hypokalemic periodic paralysis	Ca^{2+}	*CACNL1A3*	Periodic myotonia (muscle stiffness) and paralysis
Episodic ataxia type-1	K^+	*KCNA1*	Ataxia
Benign familial neonatal convulsions	K^+	*KCNQ2*	Epileptic convulsions
Nonsyndromic dominant deafness	K^+	*KCNQ4*	Deafness
Long QT syndrome	K^+	*HERG*	Dizziness, sudden death from ventricular fibrillation
	Na^+	*KCNQ1, or SCN5A*	
Hyperkalemic periodic paralysis	Na^+	*SCN4A*	Periodic myotonia and paralysis
Liddle Syndrome	Na^+	*B-ENaC*	Hypertension (high blood pressure)
Myasthenia gravis	Na^+	*nAChR*	Muscle weakness
Dent's disease	Cl^-	*CLCN5*	Kidney stones
Myotonia congenita	Cl^-	*CLC-1*	Periodic myotonia
Bartter's syndrome type IV	Cl^-	*CLC-Kb*	Kidney dysfunction, deafness
Cystic fibrosis	Cl^-	*CFTR*	Lung congestion and infections
Cardiac arrhythmias	Na^+ K^+ Ca^{2+}	many different genes	Irregular or rapid heartbeat

See *Nature Cell Biol.* 6:1040, 2004, or *Nature* 440:444, 2006, for a more complete list.

within one of the cytoplasmic domains of the CFTR polypeptide. Subsequent research has revealed that CFTR polypeptides lacking this particular amino acid fail to be processed normally within the membranes of the endoplasmic reticulum and, in fact, never reach the surface of epithelial cells. As a result, CF patients who are homozygous for the ΔF508 allele completely lack the CFTR channel in their plasma membranes and have a severe form of the disease. When cells from these patients are grown in culture at lower temperature, the mutant protein is transported to the plasma membrane where it functions quite well. This finding has prompted a number of drug companies to screen for small molecules that can bind to these mutant CFTR molecules, preventing their destruction in the cytoplasm and allowing them to reach the cell surface. One of these candidate drugs, VX-809, failed to show improvements in patient outcome in clinical trials. Another drug named Kalydeco (also known as ivacaftor), binds to CFTR and keeps the ion channel open. This drug is clinically approved for treatment of CF in patients who carry the G551D amino acid substitution, which doesn't prevent CFTR from reaching the surface but instead reduces the ability of the channel to open. Kalydeco overcomes this defect. Unfortunately only 4 percent of CF patients carry the G551D mutation. However, clinical trials suggest that Kalydeco in combination with VX-809 can be used to treat patients with the ΔF508 allele, presumably by helping those channels that do reach the surface to stay open longer.

According to one estimate, the ΔF508 mutation had to have originated more than 50,000 years ago to have reached such a high frequency in the population. The fact that the CF gene has reached this frequency suggests that heterozygotes may receive some selective advantage over those lacking a copy of the defective gene. It has been proposed that CF heterozygotes may be protected from the effects of cholera. One difficulty with this proposal is that there is no record of cholera epidemics in Europe until the 1820s. An alternate proposal suggests that heterozygotes are protected from typhoid fever because the bacterium responsible for this disease adheres poorly to the wall of an intestine having a reduced number of CFTR molecules.

Ever since the isolation of the gene responsible for CF, the development of a cure by gene therapy—that is, by replacement of the defective gene with a normal version—has been a major goal of CF researchers. Cystic fibrosis is a good candidate for gene therapy because the worst symptoms of the disease result from the defective activities of epithelial cells that line the airways and, therefore, are accessible to agents that can be delivered by inhalation of an aerosol. Clinical trials have been conducted using several different types of delivery systems. In one group of trials, the normal *CFTR* gene was incorporated into the DNA of a defective adenovirus, a type of virus that normally causes upper respiratory tract infections. The recombinant virus particles were then allowed to infect the cells of the airway, delivering the normal gene to the genetically deficient cells. The primary disadvantage in using adenovirus is that the viral DNA (along with the normal *CFTR* gene) does not become integrated into the chromosomes of the infected host cell so that the virus must be readministered frequently. As a result, the procedure often induces an immune response within the patient that eliminates the virus and leads to lung inflammation. Researchers are hesitant to employ viruses that integrate their genomes for fear of initiating the formation of cancers. In other trials, the DNA encoding the normal *CFTR* gene has been linked to positively charged liposomes (page 121) that can fuse with the plasma membranes of the airway cells, delivering their DNA contents into the cytoplasm. Lipid-based delivery has an advantage over viruses in being less likely to stimulate a destructive immune response following repeated treatments, but has the disadvantage of being less effective in achieving genetic modification of target cells. To date, none of the clinical trials of gene therapy has resulted in significant improvement of either physiologic processes or disease symptoms. The development of more effective DNA delivery systems, which are capable of genetically altering a greater percentage of airway cells, will be required if a treatment for CF based on gene therapy is to be achieved.

4.16 Membrane Potentials

All organisms respond to external stimulation, a property referred to as *irritability*. Even a single-celled amoeba, if poked with a fine glass needle, responds by withdrawing its pseudopodia, rounding up, and moving off in another direction. Irritability in an amoeba depends on the same basic properties of membranes that lead to the formation and propagation of nerve impulses, which is the subject of the remainder of the chapter.

Nerve cells (or *neurons*) are specialized for the collection, conduction, and transmission of information, which is coded in the form of fast-moving electrical impulses. The basic parts of a typical neuron are illustrated in **FIGURE 4.51a**. The nucleus of the neuron is located within an expanded region called the *cell body*, which is the metabolic center of the cell and the site where most of its material contents are manufactured. Extending from the cell bodies of most neurons are a number of fine extensions, called **dendrites**, which receive *incoming* information from external sources, typically other neurons. Also emerging from the cell body is a single, more prominent extension, the **axon**, which conducts *outgoing* impulses away from the cell body and toward the target cell(s). Although some axons may be only a few micrometers in length, others extend over much longer distances (Figure 4.51*b*) and in the body of a large vertebrate, such as a giraffe or whale, axons can be many meters long. Most axons split near their ends into smaller processes, each ending in a *terminal knob*—a specialized site where impulses are transmitted from neuron to target cell. Many neurons in the brain end in thousands of terminal knobs, allowing these brain cells to communicate with thousands of potential targets. As discussed on page 118, most neurons in the vertebrate body are wrapped in a lipid-rich **myelin sheath**, whose function is described below.

The Resting Potential

A voltage (or electric potential difference) between two points, such as the inside and outside of the plasma membrane, results when there is an excess of positive ions at one point and an excess of negative ions at the other point. Voltages across plasma membranes can be measured by inserting one fine glass electrode (or *microelectrode*) into the cytoplasm of a cell, placing another electrode in the extracellular fluid outside the cell, and connecting the electrodes to a voltmeter, an instrument that measures a difference in charge between two points (**FIGURE 4.52**). When this experiment was first carried out on a giant axon of the squid, a potential difference of approximately 70 millivolts (mV) was recorded, the inside being negative with respect to the outside (indicated with a minus sign, –70 mV). The presence of a **membrane potential** is not unique to nerve cells; such potentials are present in all types of cells, the magnitude varying between about –15 and –100 mV. When a nerve or muscle cell is in an unexcited state, the membrane potential is referred to as the **resting potential** because it is subject to dramatic change, as discussed in the following section.

The magnitude and direction of the voltage across the plasma membrane are determined by the differences in concentrations of ions on either side of the membrane and their relative permeabilities. As described earlier in the chapter, the Na^+/K^+-ATPase pumps Na^+ out of the cell and K^+ into the cell, thereby establishing steep gradients of these two ions across the plasma membrane. Because of these gradients, you might expect that potassium ions would leak out of the cell and sodium ions would leak inward through their respective ion channels. However, the vast majority of the ion channels in the plasma membrane of a *resting* nerve cell are closed. Those that are open are selective for K^+; they are often referred to as *K^+ leak channels*. K^+ leak channels are members of the K2P family of K^+ channels, which lack the S4 voltage sensor (page 145) and fail to respond to changes in voltage.

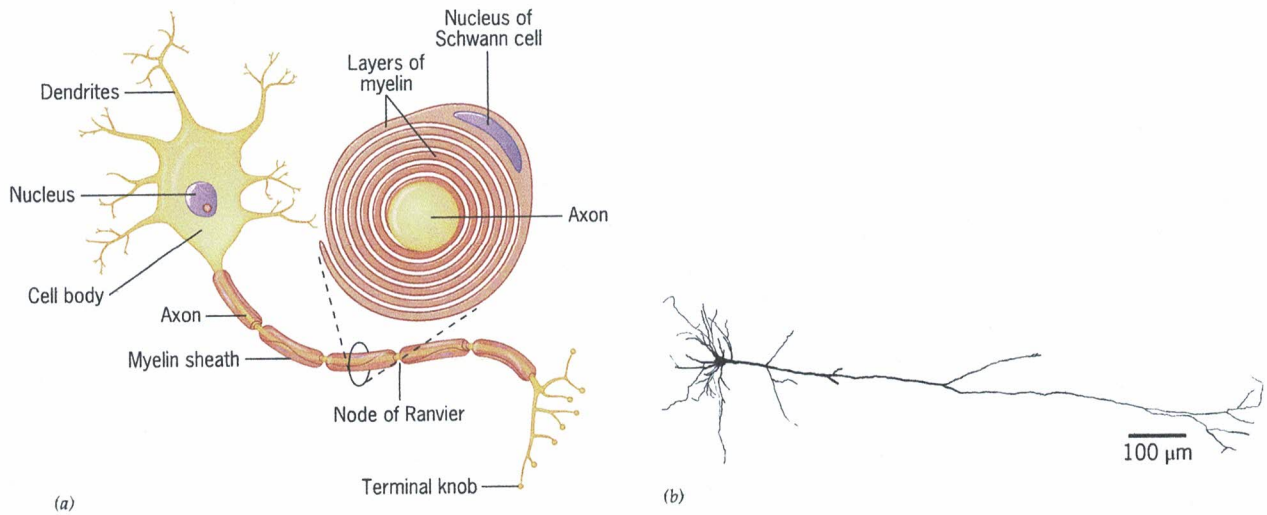


FIGURE 4.51 The structure of a nerve cell. (*a*) Schematic drawing of a simple neuron with a myelinated axon. As the inset shows, the myelin sheath comprises individual Schwann cells that have wrapped themselves around the axon. The sites where the axon lacks myelin wrapping are called nodes of Ranvier. (*Note:* Myelin-forming cells within the central nervous system are called oligodendrocytes rather than Schwann cells.) (*b*) A composite micrograph of a single rat hippocampal neuron with cell body and dendrites (purple) and an axon 1 cm in length (red). Motor nerve cells in larger mammals can be 100 times this length.

SOURCE: (*b*) From Carlos F. Ibáñez, *Trends Cell Biol.* 17:520, 2007, © 2007, with permission from Elsevier.

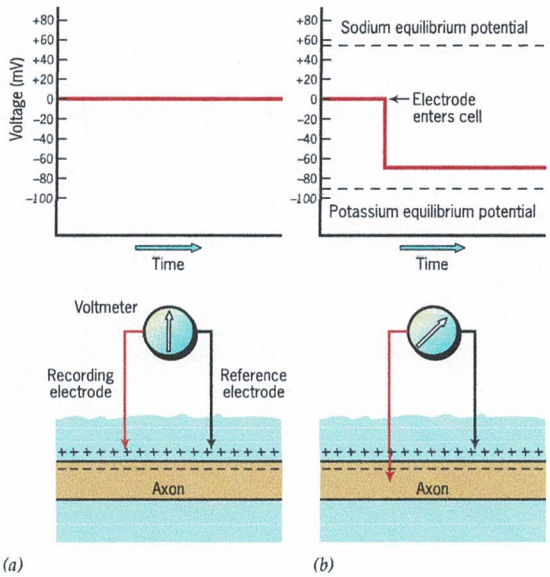


FIGURE 4.52 Measuring a membrane's resting potential. A potential is measured when a difference in charge is detected between the reference and recording electrodes. In (a), both electrodes are on the outside of the cell, and no potential difference (voltage) is measured. As one electrode penetrates the plasma membrane of the axon in (b), the potential immediately drops to −70 mV (inside negative), which approaches the equilibrium potential for potassium ions, that is, the potential that would result if the membrane were impermeable to all ions except potassium.

Because K^+ ions are the only charged species with significant permeability in a resting nerve cell, their outflow through the membrane leaves an excess of negative charges on the cytoplasmic side of the membrane. Although the concentration gradient across the membrane favors continued efflux of K^+, the electrical gradient resulting from the excess negative charge on the inside of the membrane favors the retention of K^+ ions inside the cell. When these two opposing forces are balanced, the system is at equilibrium, and there is no further *net* movement of K^+ ions across the membrane. Using the following equation, which is called the Nernst equation, one can calculate the membrane potential (V_m) that would be measured at equilibrium if the plasma membrane of a nerve cell were permeable only to K^+ ions.[7] In this case, V_m would be equal to the potassium equilibrium potential (E_K):

$$E_K = 2.303\frac{RF}{zF}\cdot\log_{10}\frac{[K_o^+]}{[K_i^+]}$$

For a squid giant axon, the internal $[K_i^+]$ is approximately 350 mM, while the external $[K_o^+]$ is approximately 10 mM; thus at 25°C (298 K) and $z = +1$ (for the univalent K^+ ion),

$$E_K = 59\log_{10}0.028 = -91\text{ mV}$$

A similar calculation of the Na^+ equilibrium potential (E_{Na}) would produce a value of approximately +55 mV. Because measurements of the voltage across the resting nerve membrane are similar in sign and magnitude (−70 mV) to the potassium equilibrium potential just calculated, the movement of potassium ions across the membrane is considered the most important factor in determining the resting potential. The difference between the calculated K^+ equilibrium potential (−91 mV) and the measured resting potential (−70 mV, Figure 4.52) is due to a slight permeability of the membrane to Na^+ through a recently described Na^+ leak channel.

[7]The Nernst equation is derived from the equation provided on page 140, by setting ΔG at zero, which is the case when the movement of the ions is at equilibrium.

The Action Potential

Our present understanding of membrane potentials and nerve impulses rests on a body of research carried out on the giant axons of the squid in the late 1940s and early 1950s by a group of British physiologists, most notably Alan Hodgkin, Andrew Huxley, and Bernard Katz. These axons, which are approximately 1 mm in diameter, carry impulses at high speeds, enabling the squid to escape rapidly from predators. The large size of these axons also made it easier to measure their electrical activity, compared to the microscopic axons of mammalian neurons. If the membrane of a resting squid axon is stimulated by poking it with a fine needle or jolting it with a very small electric current, some of its sodium channels open, allowing a limited number of sodium ions to diffuse into the cell. This opportunity for positively charged ions to move into the cell reduces the membrane potential, making it less negative. Because the positive change in membrane voltage causes a *decrease* in the polarity between the two sides of the membrane, it is called a **depolarization**.

If the stimulus causes the membrane to depolarize by only a few millivolts, say from −70 to −60 mV, the membrane rapidly returns to its resting potential as soon as the stimulus has ceased (**FIGURE 4.53a**, left box). If, however, the stimulus depolarizes the membrane beyond a certain point, called the **threshold**, which occurs at about −50 mV, then a new series of events is launched. The change in voltage causes the voltage-gated sodium channels to open. As a result, sodium ions diffuse freely into the cell (Figure 4.53*a*, middle box) down both their concentration and electric gradients. The increased permeability of the membrane to Na^+ ions and the corresponding movement of positive charge into the cell causes the membrane to reverse potential briefly (Figure 4.53*b*), becoming positive at about +40 mV, which approaches the equilibrium potential for Na^+ (Figure 4.52).

After approximately 1 msec, the sodium channels spontaneously inactivate, blocking further influx of Na^+ ions. According to the prevailing view, inactivation results from the random diffusion of an inactivation peptide into the opening of the channel pore in a manner similar to that described for K^+ channels on page 147. Meanwhile, the change in membrane potential caused by Na^+ influx triggers the opening of the voltage-gated potassium channels (Figure 4.53*a*, right box) discussed on page 145. As a result, potassium ions diffuse freely out of the cell down their steep concentration gradient. The decreased permeability of the membrane to Na^+ and the increased permeability to K^+ cause the membrane potential to swing back to a negative value of about −80 mV, approaching that of the K^+ equilibrium potential (Figure 4.52). The large negative membrane potential causes the voltage-gated potassium channels to close (see Figure 4.43*b*), which returns the membrane to its resting state. Collectively, these changes in membrane potential are called an **action potential** (Figure 4.53*b*). The entire series of changes during an action potential takes only about 5 msec in the squid axon and less than 1 msec in a myelinated mammalian nerve cell. Following an action potential, the membrane enters a brief *refractory period*

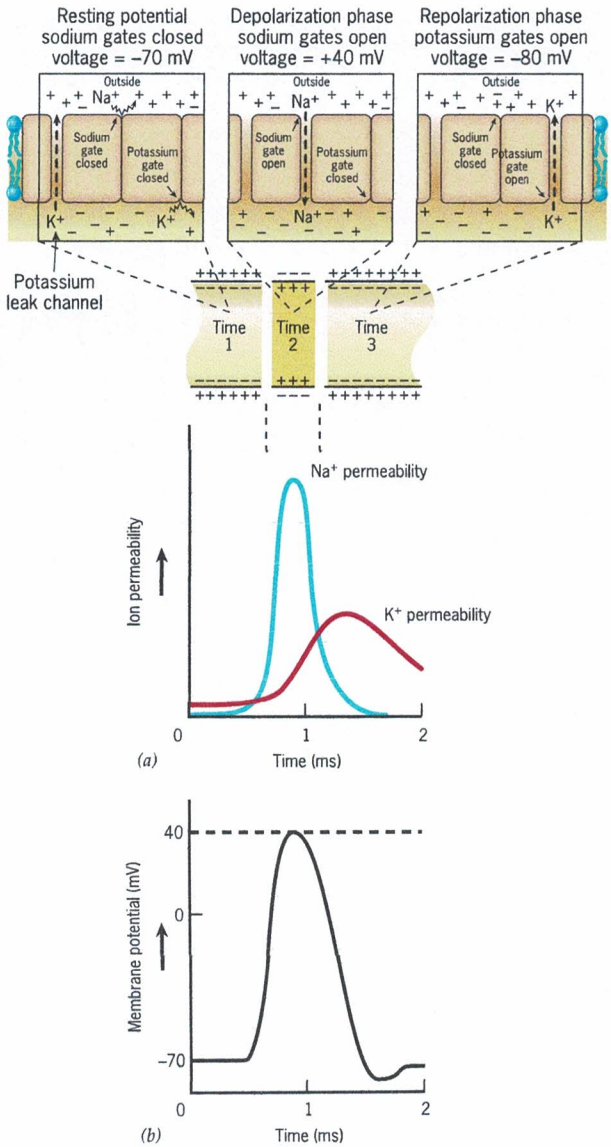


FIGURE 4.53 Formation of an action potential. (*a*) Time 1, upper left box: *The membrane in this region of the nerve cell exhibits the resting* potential, in which only the K^+ leak channels are open and the membrane voltage is approximately −70 mV. Time 2, upper middle box, shows the depolarization phase: The membrane has depolarized beyond the threshold value, opening the voltage-regulated sodium gates, leading to an influx of Na^+ ions (indicated in the permeability change in the lower graph). The increased Na^+ permeability causes the membrane voltage to temporarily reverse itself, reaching a value of approximately +40 mV in the squid giant axon (time 2). It is this reversal of membrane potential that constitutes the action potential. Time 3, upper right box, shows the repolarization phase: Within a tiny fraction of a second, the sodium gates are inactivated and the potassium gates open, allowing potassium ions to diffuse across the membrane (lower part of the drawing) and establish an even more negative potential at that location (−80 mV) than that of the resting potential. Almost as soon as they open, the potassium gates close, leaving the potassium leak channels as the primary path of ion movement across the membrane and reestablishing the resting potential. (*b*) A summary of the voltage changes that occur during an action potential, as described in part *a*.

during which it cannot be restimulated. The refractory period occurs because the sodium channels that were inactivated during the initial stage of the action potential must close before they can be reopened in response to another stimulus. As depicted in Figure 4.43, the transformation of the ion channel from the inactivated to the closed conformation can only occur after the inactivating peptide has swung out of the opening of the pore.

Although the action potential changes membrane voltage dramatically, only a minute percentage of the ions on the two sides of the membrane are involved in any given action potential. The striking changes in membrane potential seen in Figure 4.53*b* are not caused by changes in Na^+ and K^+ ion *concentrations* on the two sides of the membrane (such changes are insignificant). Rather, they are caused by the movements of charge in one direction or the other that result from the fleeting changes in permeability to these ions. Those Na^+ and K^+ ions that do change places across the membrane during an action potential are eventually pumped back by the Na^+/K^+-ATPase. Even if the Na^+/K^+-ATPase is inhibited, a neuron can often continue to fire thousands of impulses before the ionic gradients established by the pump's activity are dissipated.

Once the membrane of a neuron is depolarized to the threshold value, a full-blown action potential is triggered without further stimulation. This feature of nerve cell function is known as the *all-or-none law.* There is no in-between; subthreshold depolarization is incapable of triggering an action potential, whereas threshold depolarization automatically elicits a maximum response. The energy required to create an action potential is stored ahead of time by the Na^+/K^+-ATPase, which generates steep ionic gradients across the plasma membrane. Once that is accomplished, the various ions are poised to flow through the membrane down their respective electrochemical gradients as soon as their ion channels are opened, just like water flowing from a dam once the flood-gates are released.

The movements of ions across the plasma membrane of nerve cells form the basis for neural communication. Certain *local* anesthetics, such as procaine and novocaine, act by closing ion channels in the membranes of sensory cells and neurons. As long as these ion channels remain closed, the affected cells are unable to generate action potentials and thus unable to inform the brain of events occurring at the skin or teeth.

REVIEW

1. What is a resting potential? How is it established as a result of ion flow?
2. What is an action potential? What are the steps that lead to its various phases?

4.17 Propagation of Action Potentials as an Impulse

Up to this point, we have restricted the discussion to events occurring at a particular site on the nerve cell membrane where experimental depolarization has triggered an action potential. Once an action potential has been initiated, it does not remain localized at a particular site but is *propagated* as a **nerve impulse** down the length of the cell to the nerve terminals.

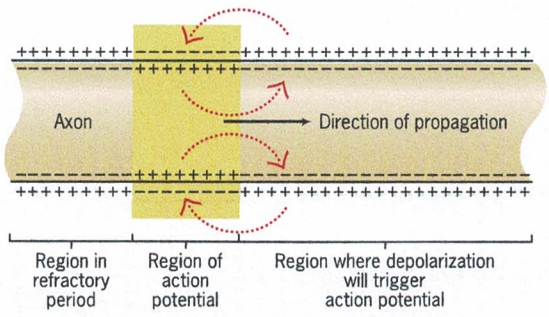


FIGURE 4.54 Propagation of an impulse results from the local flow of ions. An action potential at one site on the membrane depolarizes an adjacent region of the membrane, triggering an action potential at the second site. The action potential can only flow in the forward direction because the portion of the membrane that has just experienced an action potential remains in a refractory period.

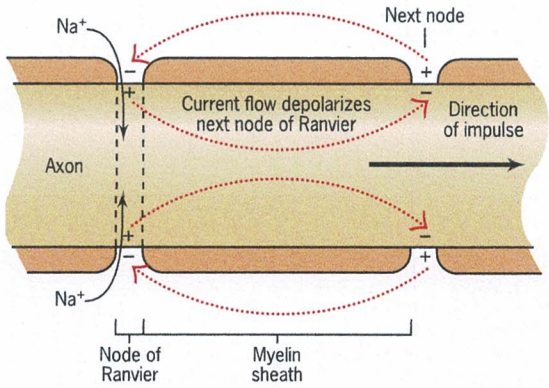


FIGURE 4.55 Saltatory conduction. During saltatory conduction, only the membrane in the nodal region of the axon becomes depolarized and capable of forming an action potential. This is accomplished as current flows directly from an activated node to the next resting node along the axon.

Nerve impulses are propagated along a membrane because an action potential at one site has an effect on the adjacent site. The large depolarization that accompanies an action potential creates a difference in charge along the inner and outer surfaces of the plasma membrane (FIGURE 4.54). As a result, positive ions move toward the site of depolarization on the outer surface of the membrane and away from that site on the inner surface (Figure 4.54). This local flow of current causes the membrane in the region just ahead of the action potential to become depolarized. Because the depolarization accompanying the action potential is very large, the membrane in the adjacent region is readily depolarized to a level greater than the threshold value, which opens the sodium channels in this adjacent region, generating another action potential. Thus, once triggered, a succession of action potentials passes down the entire length of the neuron without any loss of intensity, arriving at its target cell with the same strength it had at its point of origin.

Because all impulses traveling along a neuron exhibit the same strength, stronger stimuli cannot produce "bigger" impulses than weaker stimuli. Yet, we are clearly capable of detecting differences in the strength of a stimulus. The ability to make sensory discriminations depends on several factors. For example, a stronger stimulus such as scalding water activates more nerve cells than does a weaker stimulus such as warm water. It also activates "high-threshold" neurons that would remain at rest if the stimulus were weaker. Stimulus strength is also encoded in the pattern and frequency by which action potentials are launched down a particular neuron. In most cases, the stronger the stimulus, the greater the number of impulses generated.

The greater the diameter of an axon, the less the resistance to local current flow and the more rapidly an action potential at one site can activate adjacent regions of the membrane. Some invertebrates, such as squid and tube worms, have evolved giant axons that facilitate the animal's escape from danger. There is, however, a limit to this evolutionary approach. Because the speed of conduction increases with the square root of the increase in diameter, an axon that is 480 μm in diameter can conduct an action potential only four times faster than one that is 30 μm in diameter.

During the evolution of vertebrates, an increase in conduction velocity was achieved when the axon became wrapped in a myelin sheath (see Figures 4.5 and 4.51). Because it is composed of many layers of lipid-containing membranes, the myelin sheath is ideally suited to prevent the passage of ions across the plasma membrane. In addition, nearly all of the Na^+ ion channels of a myelinated neuron reside in the unwrapped gaps, or *nodes of Ranvier*, between adjacent Schwann cells or oligodendrocytes that make up the sheath (see *Figure 4.51*). Consequently, the nodes of Ranvier are the only sites where action potentials can be generated. An action potential at one node triggers an action potential at the next node (FIGURE 4.55), causing the impulse to jump from node to node without having to activate the intervening membrane. Propagation of an impulse by this mechanism is called **saltatory conduction**. Impulses are conducted along a myelinated axon at speeds up to 120 meters per second, which is more than 20 times faster than the speed that impulses travel in an unmyelinated neuron of the same diameter.

The importance of myelination is dramatically illustrated by multiple sclerosis (MS), a disease associated with deterioration of the myelin sheath that surrounds axons in various parts of the nervous system. Manifestations of the disease usually begin in young adulthood; patients experience weakness in their hands, difficulty in walking, and problems with their vision.

REVIEW

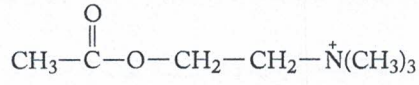
1. How is an action potential propagated along an axon? What is saltatory conduction, and how does such a process occur?
2. What is the role of the myelin sheath in conduction of an impulse?

4.18 Neurotransmission: Jumping the Synaptic Cleft

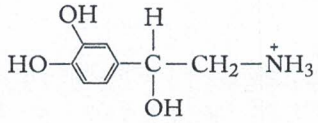
Neurons are linked with their target cells at specialized junctions called **synapses**. Careful examination of a synapse reveals that the two cells do not make direct contact but are separated from each

other by a narrow gap of about 20 to 50 nm. This gap is called the **synaptic cleft**. A **presynaptic cell** (a receptor cell or a neuron) conducts impulses toward a synapse, and a **postsynaptic cell** (a neuron, muscle, or gland cell) always lies on the receiving side of a synapse. FIGURE 4.56 shows a number of synapses between the terminal branches of an axon and a skeletal muscle cell; synapses of this type are called **neuromuscular junctions**.

How does an impulse in a presynaptic neuron jump across the synaptic cleft and affect the postsynaptic cell? Studies carried out decades ago indicated that a chemical substance is involved in the transmission of an impulse from one cell to another (page 148). The very tips (terminal knobs) of the branches of an axon appear in the electron microscope to contain large numbers of **synaptic vesicles** (Figure 4.56, left inset) that serve as storage sites for the chemical transmitters that act on postsynaptic cells. Two of the best studied **neurotransmitters** are acetylcholine and norepinephrine,



Acetylcholine (ACh)



Norepinephrine

which transmit impulses to the body's skeletal and cardiac muscles.

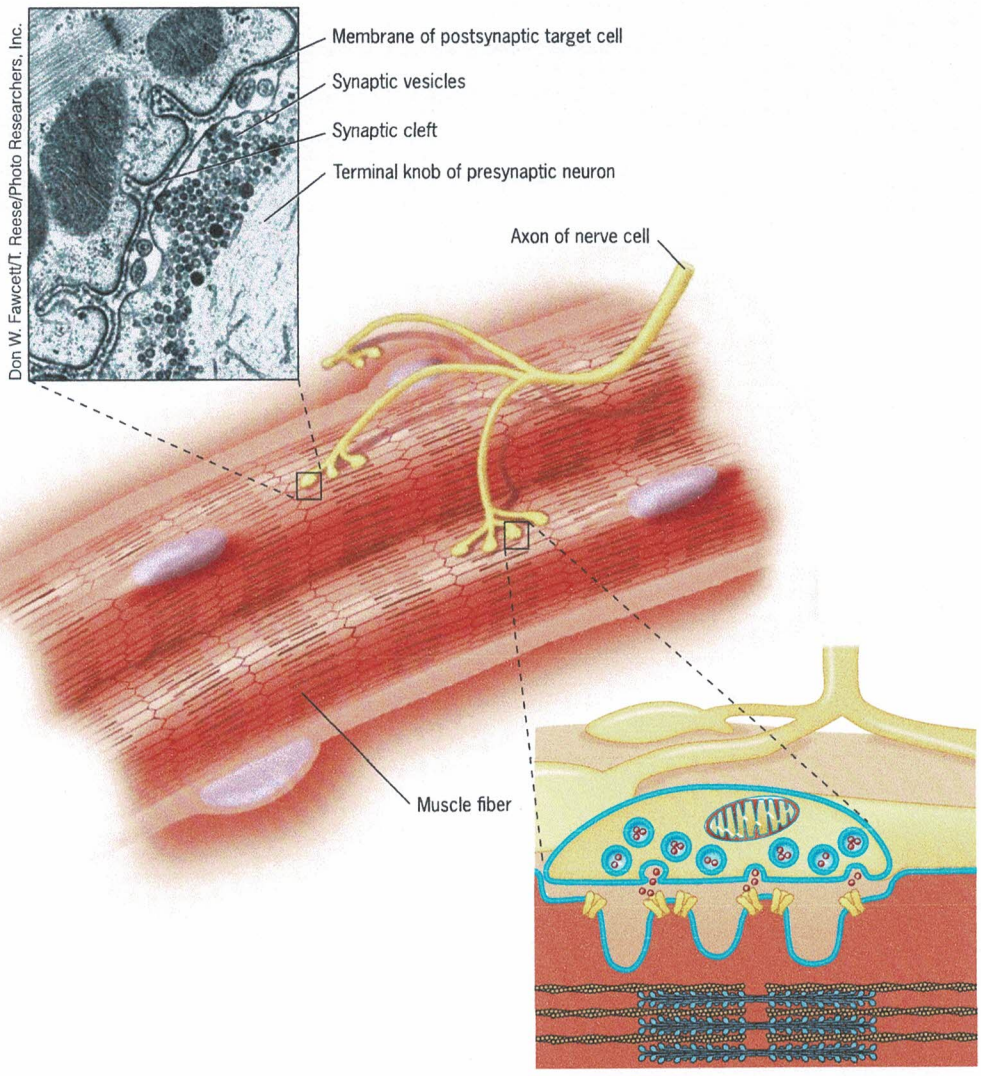


FIGURE 4.56 The neuromuscular junction is the site where branches from a motor axon form synapses with the muscle fibers of a skeletal muscle. The left inset shows the synaptic vesicles residing within the terminal knob of the axon and the narrow synaptic cleft between the terminal knob and the postsynaptic target cell. The right inset shows the terminal knob pressed closely against the muscle cell plasma membrane. Neurotransmitter molecules (red) released from synaptic vesicles of the presynaptic neuron are binding to receptors (yellow) on the surface of the muscle cell (blue).

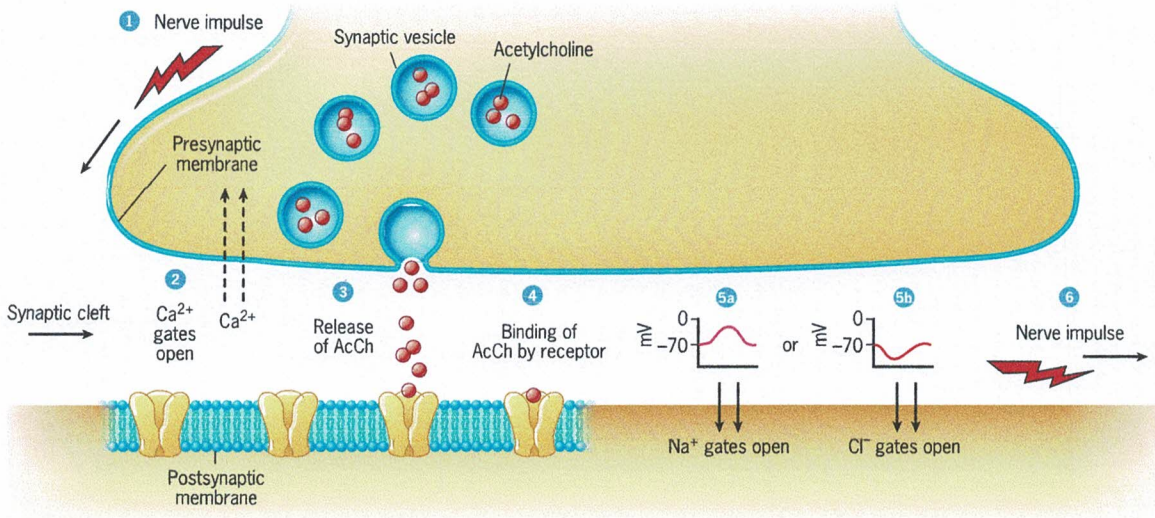


FIGURE 4.57 The sequence of events during synaptic transmission with acetylcholine as the neurotransmitter. During steps 1–4, a nerve impulse reaches the terminal knob of the axon, calcium gates open leading to an influx of Ca^{2+}, and acetylcholine is released from synaptic vesicles and binds to receptors on the postsynaptic membrane. If the binding of the neurotransmitter molecules causes a depolarization of the postsynaptic membrane (as in 5a), a nerve impulse may be generated there (6). If, however, the binding of neurotransmitter causes a hyperpolarization of the postsynaptic membrane (5b), the target cell is inhibited, making it more difficult for an impulse to be generated in the target cell by other excitatory stimulation. The breakdown of the neurotransmitter by acetylcholinesterase is not shown.

The sequence of events during synaptic transmission can be summarized as follows (FIGURE 4.57). When an impulse reaches a terminal knob (step 1, Figure 4.57), the accompanying depolarization induces the opening of a number of voltage-gated Ca^{2+} channels in the plasma membrane of this part of the presynaptic nerve cell (step 2, Figure 4.57). Calcium ions are normally present at very low concentration within the neuron (about 100 nM), as in all cells. When the gates open, calcium ions diffuse from the extracellular fluid into the terminal knob of the neuron, causing the $[Ca^{2+}]$ to rise more than a thousandfold within localized microdomains near the channels. The elevated $[Ca^{2+}]$ triggers the rapid fusion of one or a few nearby synaptic vesicles with the plasma membrane, causing the release of neurotransmitter molecules into the synaptic cleft (step 3, Figure 4.57).

Once released from the synaptic vesicles, the neurotransmitter molecules diffuse across the narrow gap and bind selectively to receptor molecules that are concentrated directly across the cleft in the postsynaptic plasma membrane (step 4, Figure 4.57). A neurotransmitter molecule can have one of two opposite effects depending on the type of receptor on the target cell membrane to which it binds:[8]

1. The bound transmitter can trigger the opening of cation-selective channels in the membrane, leading primarily to an influx of sodium ions and a less negative (more positive) membrane potential. This depolarization of the postsynaptic membrane *excites* the cell, making the cell more likely to respond to this or subsequent stimuli by generating an action potential of its own (Figure 4.57, steps 5a and 6).
2. The bound transmitter can trigger the opening of anion-selective channels, leading mainly to an influx of chloride ions, and a more negative (hyperpolarized) membrane potential. Hyperpolarization of the postsynaptic membrane makes it less likely the cell will generate an action potential because greater sodium influx is subsequently required to reach the membrane's threshold (Figure 4.57, step 5b).

Most nerve cells in the brain receive both excitatory and inhibitory signals from many different presynaptic neurons. It is the summation of these opposing influences that determine whether or not an impulse will be generated in the postsynaptic neuron.

All terminal knobs of a given neuron release the same neurotransmitter(s). However, a given neurotransmitter may have a stimulatory effect on one particular postsynaptic membrane and an inhibitory effect on another. Acetylcholine, for example, inhibits contractility of the heart but stimulates contractility of skeletal muscle. Within the brain, glutamate serves as the primary excitatory neurotransmitter and gamma-aminobutyric acid (GABA) as the primary inhibitory neurotransmitter. A number of general anesthetics, as well as Valium and its derivatives, act by binding to the GABA receptor and enhancing the activity of the brain's primary "off" switch. As will be evident in the following section, many different drugs affecting disorders, such as anxiety, depression, insomnia, and schizophrenia, exert their action at the synapse.

[8]It is important to note that this discussion ignores an important class of neurotransmitter receptors that are not ion channels and thus do not *directly* affect membrane voltage. This other group of receptors are members of a class of proteins called GPCRs, which are discussed at length in Section 15.3. When a neurotransmitter binds to one of these receptors, it can initiate a variety of responses, which often includes the opening of ion channels by an indirect mechanism.

Actions of Drugs on Synapses

It is important that a neurotransmitter has only a short half-life following its release from a presynaptic neuron; otherwise, the effect of the neurotransmitter would be extended, and the postsynaptic neuron would not recover. A neurotransmitter is eliminated from the synapse in two ways: by enzymes that destroy neurotransmitter molecules in the synaptic cleft and by proteins that transport neurotransmitter molecules back to the presynaptic terminals—a process called *reuptake*. Because of the destruction or reuptake of neurotransmitter molecules, the effect of each impulse lasts no more than a few milliseconds.

Interfering with the destruction or reuptake of neurotransmitters can have dramatic physiologic and behavioral effects. Acetylcholinesterase is an enzyme localized within the synaptic cleft that hydrolyzes acetylcholine. We began this chapter describing the horrific effects of the nerve gas sarin, which works by inhibiting acetylcholinesterase. When this enzyme is inhibited by exposure to sarin, the subsequent buildup of acetylcholine in the neuromuscular junctions throughout the body causes overstimulation of the adjoining postsynaptic muscle fibers. As a result, the skeletal muscles of the body, including those required for breathing, undergo violent contraction followed by muscle weakness and paralysis. Milder inhibitors of acetylcholinesterase are used to treat the symptoms of Alzheimer's disease, which is characterized by the loss of acetylcholine-releasing neurons.

Many drugs act by inhibiting the transporters that sweep neurotransmitters out of the synaptic cleft. A number of widely prescribed antidepressants, including Prozac and Zoloft, inhibit the reuptake of serotonin, a neurotransmitter implicated in mood disorders. Cocaine, on the other hand, interferes with the reuptake of the neurotransmitter dopamine that is released by certain nerve cells in a portion of the brain known as the limbic system. The limbic system contains the brain's "pleasure" or "reward" centers. The sustained presence of dopamine in the synaptic clefts of the limbic system produces a short-lived feeling of euphoria, as well as a strong desire to repeat the activity. Mice that have been genetically engineered to lack the dopamine transporter (DAT)—the protein responsible for dopamine reuptake—show behavior similar to that of normal mice that have been given cocaine or amphetamines. Administration of cocaine or amphetamines has no additional behavioral effects on animals lacking the *DAT* gene. Numerous other drugs act on presynaptic dopamine-releasing or postsynaptic dopamine-responding neurons. Amphetamines are thought to stimulate the excessive release of dopamine from presynaptic terminals and also interfere with the reuptake of the neurotransmitter molecules from the synaptic cleft. A number of antipsychotic drugs bind to certain subtypes of the dopamine receptor on postsynaptic neurons and block their stimulation by dopamine.

The active compound in marijuana (Δ^9-tetrahydrocannabinol) acts by a totally different mechanism. It binds to cannabinoid (CB1) receptors located on the *presynaptic* terminals of certain neurons of the brain, which reduces the likelihood that these neurons will release neurotransmitters. CB1 receptors normally interact with compounds produced in the body called *endocannabinoids*. Endocannabinoids are produced by postsynaptic neurons following depolarization. These substances diffuse "backwards" across the synaptic cleft to the presynaptic membrane, where they bind to CB1 receptors, suppressing synaptic transmission. CB1 receptors are located in many areas of the brain, including the hippocampus, cerebellum, and hypothalamus, which explains the effects of marijuana on memory, motor coordination, and appetite, respectively. If marijuana increases appetite by binding to CB1 receptors, it follows that blocking these receptors might decrease appetite. This line of reasoning led to the development of a CB1-blocking weight-loss drug called Acomplia, which has been pulled from the market because of side effects.

Synaptic Plasticity

Synapses are more than simply connecting sites between adjacent neurons; they are key determinants in the routing of impulses through the nervous system. The human brain is thought to contain at least one hundred trillion synapses. These synapses act like gates stationed along the various pathways, allowing some pieces of information to pass from one neuron to another, while holding back other pieces or rerouting them in another direction. While synapses are often perceived as fixed, unchanging structures, they can display a remarkable dynamic quality known as "synaptic plasticity." Synaptic plasticity is particularly important during infancy and childhood, when the neuronal circuitry of the brain achieves its mature configuration.

Synaptic plasticity is most readily observed in studies on neurons from the hippocampus, a portion of the brain that is vitally important in learning and short-term memory. When hippocampal neurons are repeatedly stimulated over a short period of time, the synapses that connect these neurons to their neighbors become "strengthened" by a process known as long-term potentiation (LTP), which may last for days, weeks, or even longer. Research into LTP has focused on the NMDA receptor, which is one of several receptor types that bind the excitatory neurotransmitter glutamate. When glutamate binds to a postsynaptic NMDA receptor, it opens an internal cation channel within the receptor that allows the influx of Ca^{2+} ions into the postsynaptic neuron, triggering a cascade of biochemical changes that lead to synaptic strengthening. Synapses that have undergone LTP are able to transmit weaker stimuli and evoke stronger responses in postsynaptic cells. These changes are thought to play a major role as newly learned information or memories are encoded in the neural circuits of the brain. When laboratory animals are treated with drugs that inhibit LTP, such as those that interfere with the activity of the NMDA receptor, their ability to learn new information is greatly reduced.

There are numerous other reasons the study of synapses is so important. For example, a number of diseases of the nervous system, including myasthenia gravis, Parkinson's disease, schizophrenia, and even depression, are thought to have their roots in synaptic dysfunction.

REVIEW

1. Describe the steps between the time an impulse reaches the terminal knob of a presynaptic neuron and an action potential is initiated in a postsynaptic cell.
2. Contrast the roles of ion pumps and channels in establishing and using ion gradients, particularly as it applies to nerve cells.

Analytic Questions

1. What types of integral proteins would you expect to reside in the plasma membrane of an epithelial cell that might be absent from that of an erythrocyte? How do such differences relate to the activities of these cells?
2. *Many different types of cells possess receptors that bind steroid* hormones, which are lipid-soluble molecules. Where in the cell do you think such receptors might reside? Where in the cell would you expect the insulin receptor to reside? Why?
3. We calculated on page 140 that when a solute is 10 times more concentrated outside a cell than inside, the free energy for moving the solute into the cell is –1.4 kcal/mol. What would the free energy change be for moving the solute into the cell if the external concentration (outside the cell) was a thousand times more concentrated than the internal concentration (inside the cell)? How many times higher would the external concentration have to be compared to the internal concentration for the free energy of moving the solute into the cell to be –2.8 kcal/mol? If instead the free energy for moving solute into the cell was +2.8 kcal/mol, what would that tell you about the external concentration relative to the internal concentration? **(See Quantitative Tutorial Video).**
4. Suppose you were planning to use liposomes in an attempt to deliver drugs to a particular type of cell in the body, for example, a fat or muscle cell. Is there any way you might be able to construct the liposome to increase its target specificity?
5. How is it that, unlike polysaccharides such as starch and glycogen, the oligosaccharides on the surface of the plasma membrane can be involved in specific interactions? How is this feature illustrated by determining a person's blood type prior to receiving a transfusion?
6. Trypsin is an enzyme that can digest the hydrophilic portions of membrane proteins, but it is unable to penetrate the lipid bilayer and enter a cell. Because of these properties, trypsin has been used in conjunction with SDS–PAGE to determine which proteins have an extracellular domain. Describe an experiment using trypsin to determine the sidedness of proteins of the erythrocyte membrane.
7. Look at the scanning electron micrograph of erythrocytes in Figure 4.32a. These cells, which are flattened and have circular depressions on each side, are said to have a biconcave shape. What is the physiologic advantage of a biconcave erythocyte over a spherical cell with respect to O_2 uptake?
8. Suppose you were culturing a population of bacteria at 15°C and then raised the temperature of the culture to 37°C. What effect do you think this might have on the fatty acid composition of the membrane? on the transition temperature of the lipid bilayer? on the activity of membrane desaturases?
9. Looking at Figure 4.6, which lipids would you expect to have the greatest rate of flip-flop? which the least? Why? If you determined experimentally that phosphatidylcholine actually exhibited the greatest rate of flip-flop, how might you explain this finding? How would you expect the rate of phospholipid flip-flop to compare with that of an integral protein? Why?
10. What is the difference between a two-dimensional and a three-dimensional representation of a membrane protein? How are the different types of profiles obtained, and which is more useful? Why do you think there are so many more proteins whose two-dimensional structure is known?
11. If you were to inject a squid giant axon with a tiny volume of solution containing 0.1 M NaCl and 0.1 M KCl in which both the Na^+ and K^+ ions were radioactively labeled, which of the radioactively labeled ions would you expect to appear most rapidly within the seawater medium while the neuron remained at rest? After the neuron had been stimulated to conduct a number of action potentials?
12. *It has been difficult to isolate proteins containing water chan*nels (i.e., aquaporins) due to the high rate of diffusion of water through the lipid bilayer. Why would this make aquaporin isolation difficult? Is there any way you might be able to distinguish diffusion of water through the lipid bilayer versus that through aquaporins? The best approach to studying aquaporin behavior has been to express the aquaporin genes in frog oocytes. Is there any reason why the oocytes of a pond-dwelling amphibian might be particularly well suited for such studies?
13. How is it that diffusion coefficients measured for lipids within membranes tend to be closer to that expected for free diffusion than those measured for integral proteins in the same membranes?
14. Assume that the plasma membrane of a cell was suddenly permeable to the same degree to both Na^+ and K^+ and that both ions were present at a concentration gradient of the same magnitude. Would you expect these two ions to move across the membrane at the same rates? Why or why not?
15. Most marine invertebrates show no loss or gain of water by osmosis, whereas most marine vertebrates experience continual water loss in their high-salt environment. Speculate on the basis for this difference and how it might reflect different pathways of evolution of the two groups.
16. How would you expect the concentrations of solute inside a plant cell to compare to that of its extracellular fluids? Would you expect the same to be true of the cells of an animal?
17. What would be the consequence for impulse conduction if the Na^+ channels were able to reopen immediately after they had closed during an action potential?
18. What would be the value of the potassium equilibrium potential if the external K^+ concentration was 200 mM and the internal concentration was 10 mM at 25°C? at 37°C?
19. As discussed on page 155, the Na^+/glucose cotransporter transports two Na^+ ions for each glucose molecule. What if this ratio were 1:1 rather than 2:1; how would this affect the glucose concentration that the transporter could work against?
20. A transmembrane protein usually has the following features: (1) the portion that transits the membrane bilayer is at least 20 amino acids in length, which are largely or exclusively nonpolar residues; (2) the portion that anchors the protein on the external face has two or more consecutive acidic residues; and (3) the portion that anchors the protein on the cytoplasmic face has two or more consecutive basic residues. Consider the transmembrane protein with the following sequence:

    NH_2-MLSTGVKRKGAVLLILLFPWMVAGGPLFWLAADESTYKGS-COOH

    Draw this protein as it would reside in the plasma membrane. Make sure you label the N- and C-termini and the external and cytoplasmic faces of the membrane. (Single-letter code for amino acids is given in Figure 2.26.)
21. Many marine invertebrates, such as squid, have extracellular fluids that resemble seawater and therefore have much higher intracellular ion concentrations than mammals. For a squid neuron, the ionic concentrations are roughly

ion	*intracellular concentration*	*extracellular concentration*
K^+	350 mM	10 mM
Na^+	40 mM	440 mM
Cl^-	100 mM	560 mM
Ca^{2+}	2×10^{-4} mM	10 mM
pH	7.6	8.0

If the resting potential of the plasma membrane, V_m, is −70 mV, are any of the ions at equilibrium? How far out of equilibrium, in mV, is each ion? What is the direction of net movement of each ion through an open channel permeable to that ion?

22. The membrane potential V_m of a cell is determined by the relative permeability of the membrane to various ions. When acetylcholine binds to its receptors on the postsynaptic muscle membrane, it causes a massive opening of channels that are equally permeable to sodium and potassium ions. Under these conditions,

$$V_m = (V_{k^+} + V_{Na^+})/2$$

If $[K^+_{in}]$ = 140 mM and $[Na^+_{in}]$ = 10 mM for the muscle cell, and $[Na^+_{out}]$ = 150 mM and $[K^+_{out}]$ = 5 mM, what is the membrane potential of the neuromuscular junction of an acetylcholine-stimulated muscle?

23. Transmembrane domains consist of individual α helices or a β sheet formed into a barrel. Looking at Figures 2.30 and 2.31, why is a single α helix more suited to spanning the bilayer than a single β strand?

24. Knowing how the K^+ channel selects for K^+ ions, suggest a mechanism by which the Na^+ channel is able to select for its ion.

25. How would you compare the rate of movement of ions passing through a channel versus those transported actively by a P-type pump? Why?

Protection ,support ,and movement

The integument

- The integument(L. Integumentum, cover)
- Is the external covering of animal. It protects the animal from mechanical and chemical injury and invasion by microorganism. It function : regulation of body temperature; excretion of waste materials; conversion of sunlight into vitamin D;reception of environmental stimuli; such as,temperature, and pressure;locomotion;and movement;and movement of nutrients and gases.

The integumentary system of invertebrates

- in protozoa , the plasma membrane has a large surface area relative to body volume, so that gas exchange and the removal of soluble wastes occur by simple diffusin. This large surface area also faciliates the uptake of dissolved nutrients from surrounding fluids.
- Most multicellular invertebrates have an integument consisting of a single layer of columnar epithelial cells .this outer layer ,the epidermis,rests on a basement membrane.
- Some invertebrates possess cuticales that are highly variable in structure . Such cuticles consist of chitin and potien that in rigid plates that a flexible membrane links togather . Animal have difficulty growing within cuticle . As result, someof these invertebrates shed the old outgrown cuticalein proee called molting or ecdysis.

The integumentary system of vertebrates

The skin of cartilaginous fishes

- The skin of cartilaginous fishes is multilayered and contains mucous and sensory cells.The dermis contains bone in the form of small placoid scalescalled denticales(little teeth)

The skin of Bony fishes

- The skin of bony fishes contains scales .a thin layer of dermal tissue overlaid by the superfaicial epidermis normally covers scales. Because scales are not shed,they grow at the margins and over the lower surface.
- The skin of bony fishes is permeable and function in gas exchange
- The epidermis also contains many mucous glands. Mucous production helps prevent bacterial and fungal infections

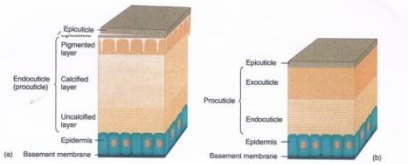


FIGURE 23.2
Cuticles. The cuticles of (*a*) a crustacean and (*b*) an insect. The underlying epidermis secretes the cuticles of both groups of animals. From: "A LIFE OF INVERTEBRATES" © 1979 W. D. Russell-Hunter.

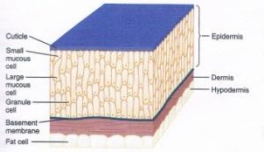


FIGURE 23.3
Skin of Jawless Fishes. The skin of an adult lamprey has a multilayered epidermis with glandular cells and fat storage cells in the hypodermis.

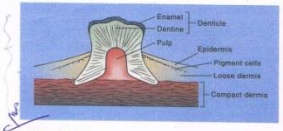


FIGURE 23.4
Skin of Cartilaginous Fishes. Shark skin contains toothlike denticles that become exposed through loss of the epidermal covering. The skin is otherwise fishlike in structure.

The Skin of Amphibians

Amphibian skin consists of a stratified epidermis and a dermis containing mucous and serous glands plus pigmentation cells (figure 23.6). *Phylogenetically, amphibians are transitional between aquatic and terrestrial vertebrates. The earliest amphibians were covered by dermal bone scales like their fish ancestors.* Three problems associated with terrestrial environments are desiccation, the damaging effects of ultraviolet light, and physical abrasion. During amphibian evolution, keratin production increased in the outer layer of skin cells. (Keratin is a tough, impermeable protein that protects the skin in the physically abrasive, rigorous terrestrial environment.) The increased keratin in the skin also protects the cells, especially their nuclear material, from ultraviolet light. The mucus that mucous glands produce helps prevent desiccation, facilitates gas exchange when the skin is used as a respiratory organ, and makes the body slimy, which facilitates escape from predators.

Within the dermis of some amphibians are poison glands that produce an unpleasant-tasting or toxic fluid that acts as a predator deterrent. Sensory nerves penetrate the epidermis as free nerve endings. Interestingly, the "warts" of toads seem to be specialized sensory structures, since they contain many sensory cells.

The Skin of Reptiles

The skin of reptiles reflects their greater commitment to a terrestrial existence. The outer layer of the epidermis (stratum corneum) is thick (figure 23.7), lacks glands, and is modified into keratinized scales, scutes (thick scales) in snakes and turtles, beaks in turtles, rattles on snakes, and claws, plaques, and spiny crests on most other reptiles. This thick, keratinized layer resists abrasion, inhibits dehydration, and protects like a suit of armor. During shedding or molting of the skin of many reptiles (e.g., snakes and lizards), the old outer layer separates from newly formed epidermis. Diffusion of fluid between the layers aids this separation.

The skin of Amphibians

- Amphibain skinconsists of a stratified epidermis and a dermis containing mucous and serous glands plus pigmentation cells.
- Amphibains are transitional between aquatic and terrestrial vertebrates
- The mucus that mucous glands produce helps prevent desication, facilitates gas exchange when the skin is used as a respiratort organ, and makes the body slimy , which facilitates escape from predators.

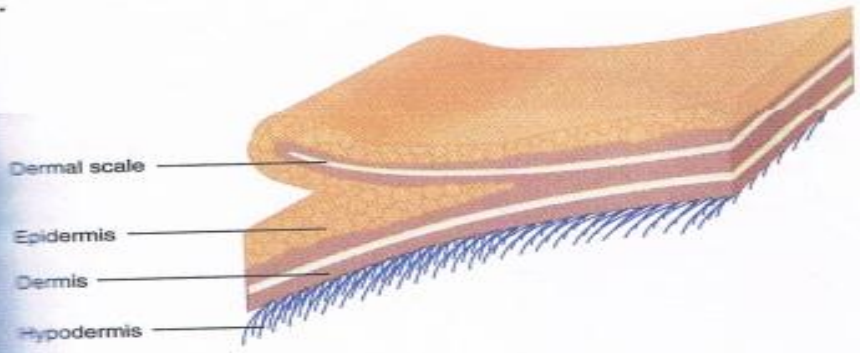


FIGURE 23.5
Skin of Bony Fishes. The skin of a typical bony fish has overlapping scales (two are shown here). The scales are layers of collagenous fibers covered by a thin, flexible layer of bone.

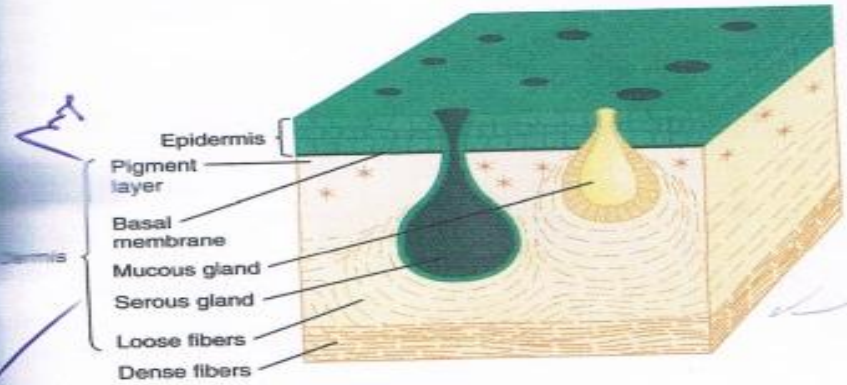


FIGURE 23.6
Skin of Amphibians. Frog skin has a stratified epidermis and several types of glands in the dermis. Notice the pigment layer in the upper part of the dermis.

The Skin of Birds

The skin of birds shows many typically reptilian features with no epidermal glands (the only epidermal gland of birds is the uropygial or preen gland). Over most of the bird's body, the epidermis is usually thin and only two or three cell layers thick (figure 23.8). Indeed, the term "thin skinned," sometimes applied figuratively to

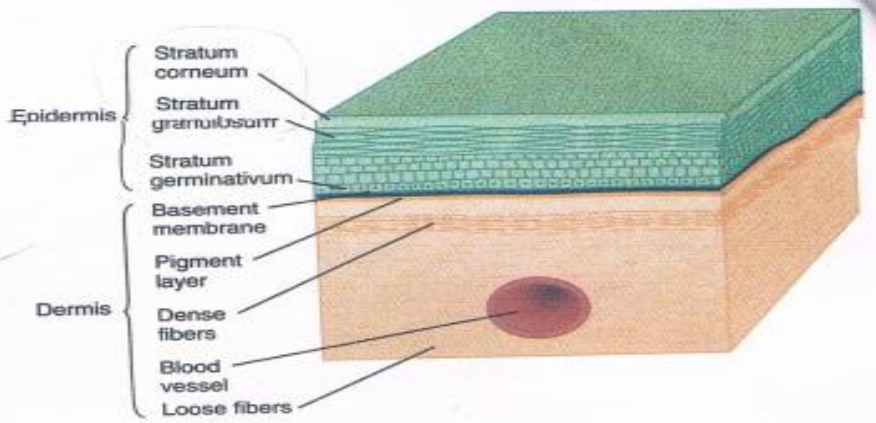


FIGURE 23.7
Skin of Reptiles. Lizard skin has the heavily keratinized outer epidermis (scales) characteristic of reptiles. Notice the absence of integumentary glands, making reptilian skin exceptionally dry.

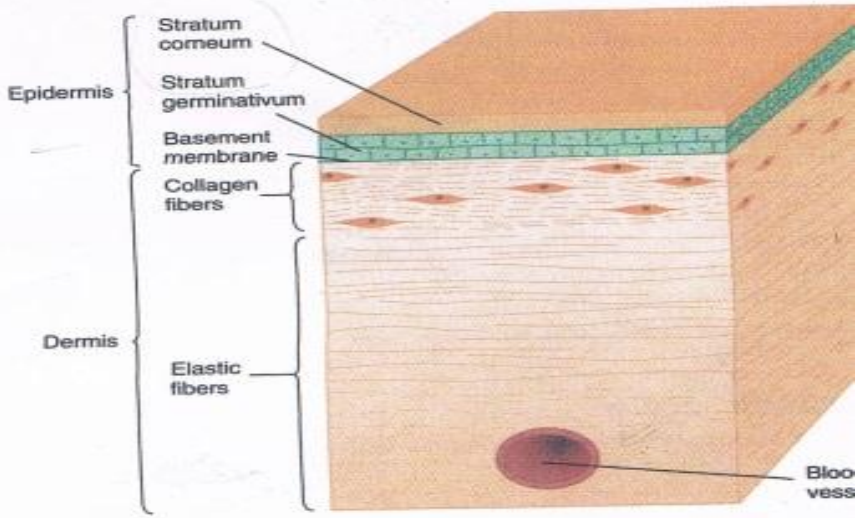


FIGURE 23.8
Skin of Birds. Bird skin has a relatively soft and thin epidermis with no epidermal glands.

The skin of mammals

- The notable features of mammals skin are 1-hair.2 –a greater variety of epidermal glands than in any other vertebrate class;3-a highly stratified epidermis
- The epidermis of mammalian skin is composed of stratified squamous epithelium and consists of several layers of a variety of cells

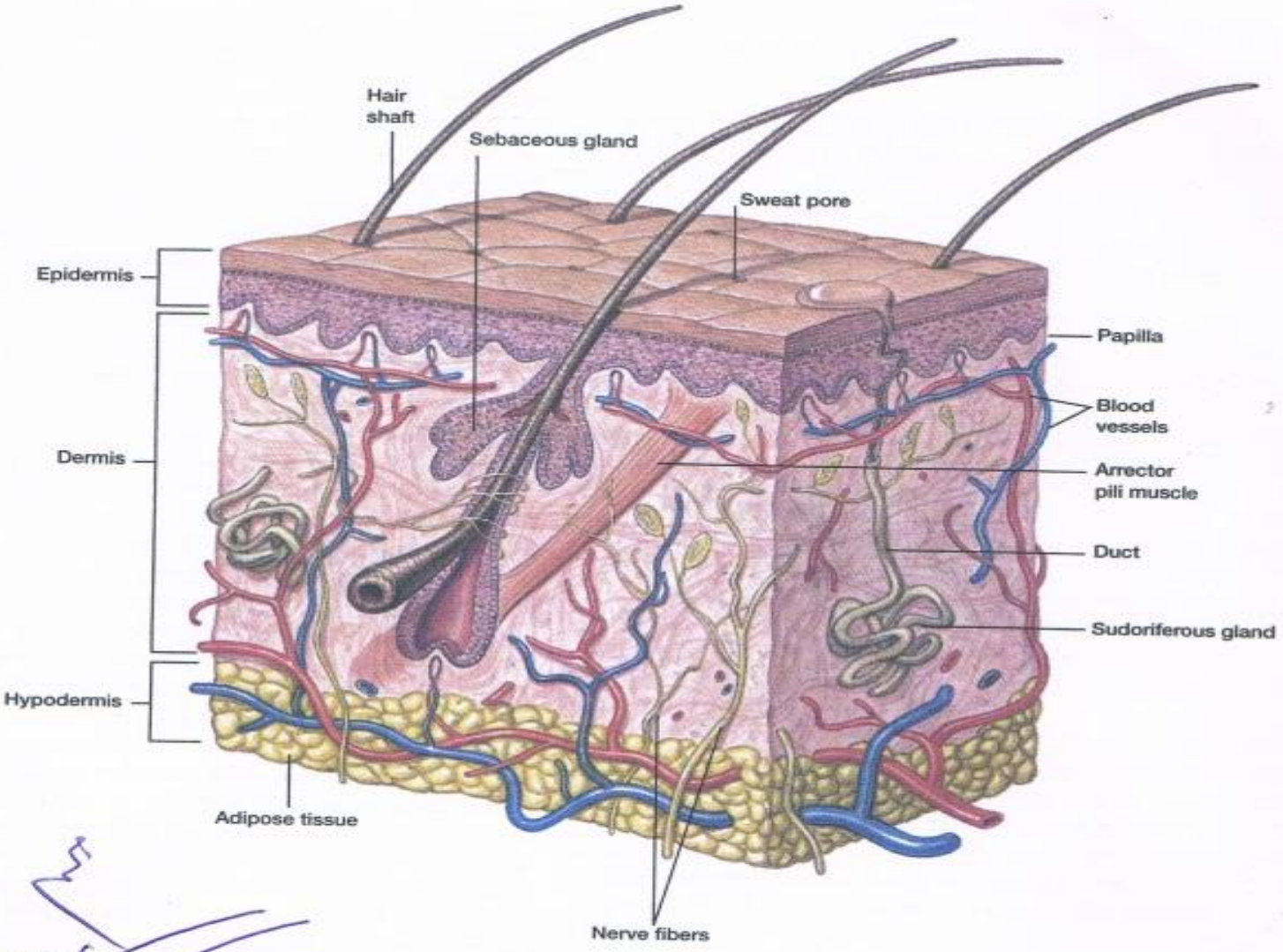


FIGURE 23.9
Skin of Mammals. Notice the various structures in the dermis of human skin.

- In humans and a few other animals (horses)
- The skin regulates body temperature by opening and closing sweat pores and perspiring or sweating

The skeletal system of invertebrates

- There are three types os skeletal system
- Hydroststic skeletons
- The hydrostatic skeleton is a core of liquid srrounding by a tension –resistant sheath of longitudinal and /or circular muscles.
- It is similar to a water filled balloon because the force exerted against the incopressible fluid in one region can be transmitted

- Exoskeletons
- Rigid exoskeletons also have locomotor function because they provide sites for muscle attachment and counterforces for muscle movements
- Exoskeleton also suport and protect the body ,but these are secondary function
- In arthropods the epidermis of the body wall secretes a thich hard cuticle that waterproofs the body .the cuticle also protects and supports the animals soft internalorgans.in crustaceans the exoskeleton contaian calcium carbonate crystals that make it hard and inflexible except at the joints

endoskeletons

- Like the term implies ,other body tissues enclose endoskeletons for example ,the endoskeletons of sponges consist of mineral spicules and fibers of spongin that keep the body from collasping

The skeletal system of vertebrates

The vertebrate skeletal system is an endoskeleton enclosed by other body tissues. This endoskeleton consists of two main types of supportive tissue :cartilage and bone.

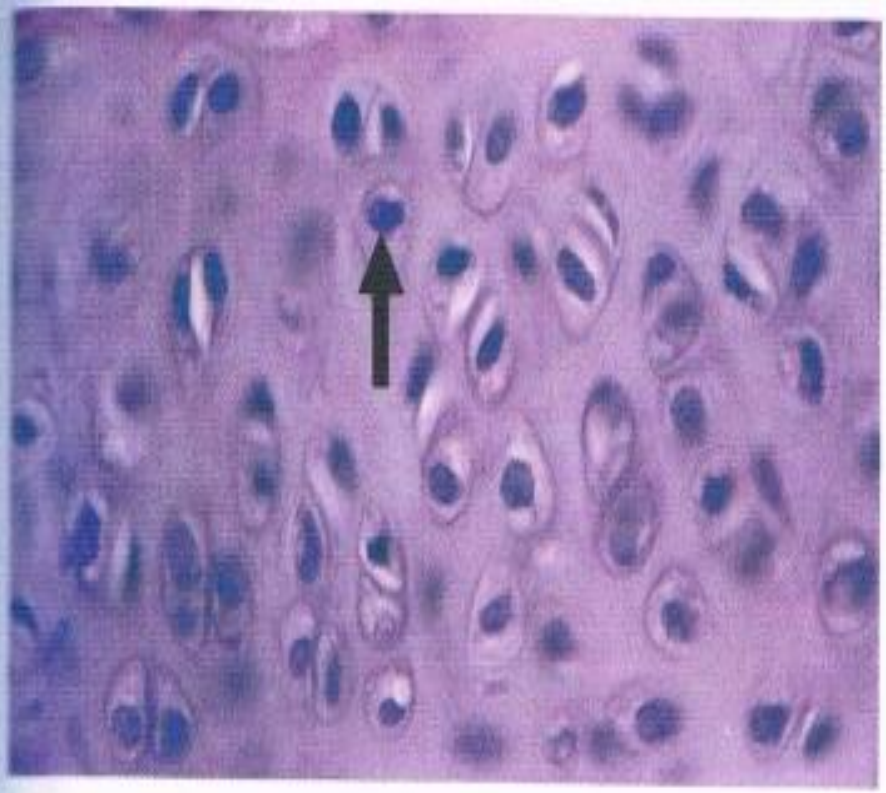
Cartilage

Is a specialized type of connective tissue that provides a site for muscle attachment,aids in movement at joints and provides support ,like other connective tissues it consists of cells ,fibers and cellular matrix.

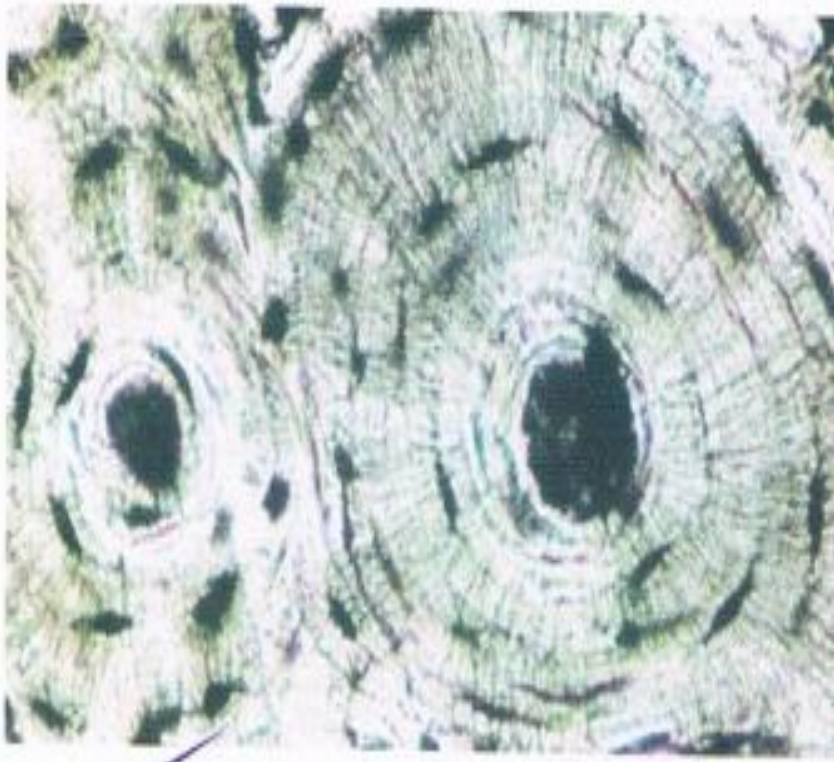
Bone or osseous tissue

- Bone (osseous)tissue is a speciallized tissue that provides a point of attachment for muscles transmits the force of nuscular contraction from one part of the body to another during movement.in addition ,bone of the skeleton support the internal organs of many animals ,store reserve calcium and phosphate, and manufacture red blood cells and some white blood cells.

- Bone tissue is more rigid than other connective tissues because its homogeneous organic ground substance also contains inorganic salts – mainly calcium phosphate and calcium carbonate.
- Bone cells (osteocytes) are in minute chambers called lacunae which are arrenged in concentric rings around osteonic canals (harversain system). These cells communicate with nearby cells by means of cellular processes passing through small channels called canaliculi.



(j) **Hyaline cartilage** cells are located in lacunae (arrow) surrounded by intercellular material containing fine collagenous fibers (LM ×250). **Location:** Forms embryonic skeleton; covers ends of long bones; and forms cartilage of nose, trachea, and larynx. **Function:** Support and reinforcement.



(l) **Bone (osseous) tissue.** Bone matrix is deposited in concentric lay around osteonic canals (LM ×160). **Location:** Bones. **Function:** Sup ports, protects, provides lever system for muscles to act on, stores cal cium and fat, and forms blood cells.

An introduction to animal muscles

- Muscular tissue is the driving force
- The power behind movement in most invertebrates and vertebrates in addetion muscle tissue has three other important properties 1- excitabelity (or irritability), the capacity to receive and respond to a stimulus
- 2- extensibility, the ability to be streched and 3- elasticity, the ability to return to its orginal shap after being streched or contracted .

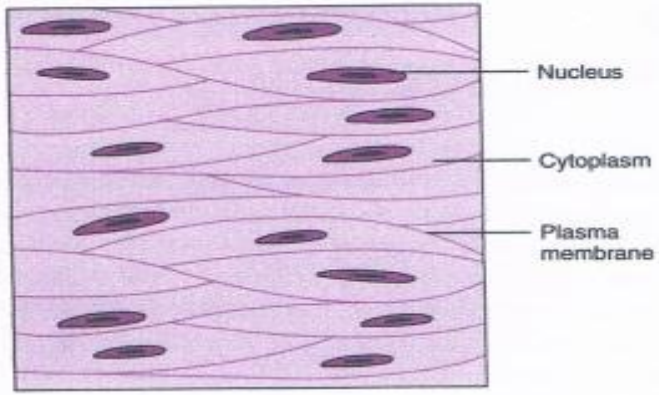
- Animals may have one or more of the following types of muscles tissues are called muscle fibers .
- Smooth muscle is also called involentary muscle because higher brain center do not control its contraction , smooth muscle fibers have a single nucleus , are spindle shaped . It contracts slowly , but it can sustain prolonged contaraction and dose not fatigue(tire)easly.

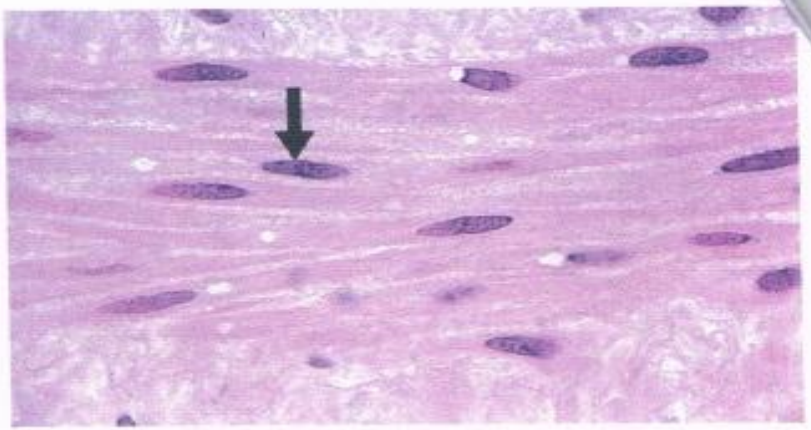
- Cardiac muscle fibers are involuntary , have a single nucleus are striated (have dark and light bands) and are branched .
- Hearts dont fatigue because cardiac fibers relax complitly between contraction .
- Skeletal muscles , also straited muscles , is a volontary muscles because the nervous system consciously controls its contractions .skeletals muscles fibers are multinucleated and straited .skeletal muscles attach to skeleton .when skeleton muscles contract they shorten .

Skeletal muscle contraction

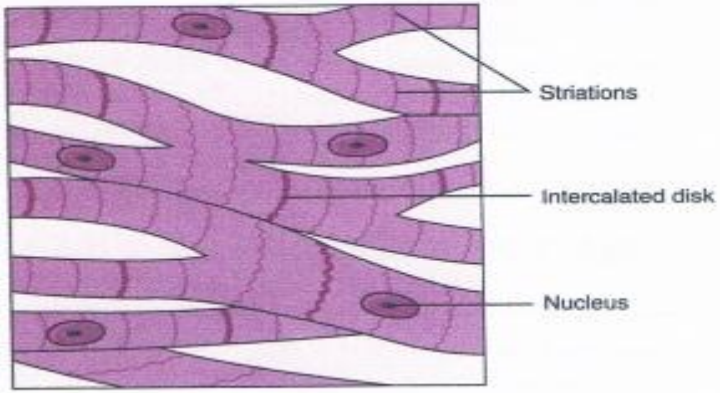
- When observed with the light microscope , each skeletal muscle fiber (cell) has a pattern of alternate dark and light bands . The striation of whole fibers arises from the alternating dark and light bands of many smaller , threadlike myofibers in each muscle fiber . Electron microscpy and biochemical analysis show that these bands are due to the placement of the muscle protiens actin and myosin within the myofibriles . Myosin occurs as thich filaments and actin as thin filamemts . The lightest region of a myofibrils (I band) contains both actin and myosin .)

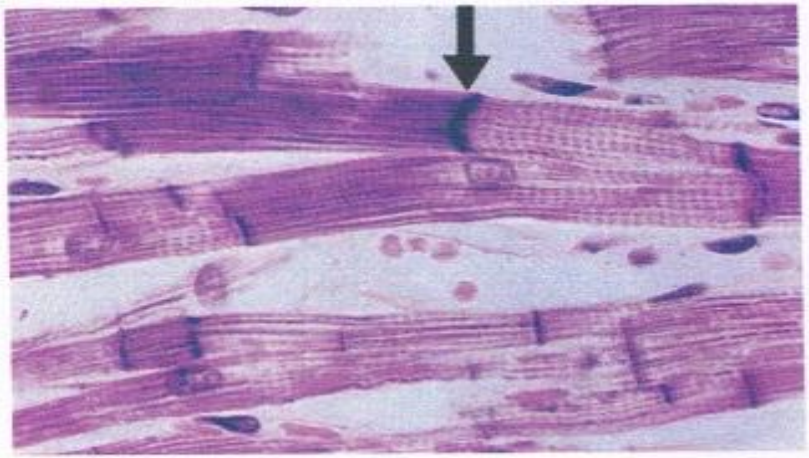
- The funcional (contalile) unit of myofibrel is the sarcomer , each of which extends from z line to another z line . Notice that the actin filaments attach to the z lines , where as myosin filaments do not .when a sarcomers contracts , the actin filament slide past the myosin filaments as they approach one another . They prosses shorten the sarcome is called the sliding filament model of muscle contraction .





(*p*) **Smooth muscle tissue** is formed of spindle-shaped cells, each containing a single nucleus (arrow) (LM ×250). Cells are arranged closely to form sheets. Smooth muscle tissue is not striated. **Location:** Mostly in the walls of hollow organs. **Function:** Moves substances or objects (foodstuffs, urine, baby) along internal passageways; involuntary control.





(*q*) **Cardiac muscle tissue** consists of striated cells, each containing a single nucleus and specialized cell junctions called intercalated disks (arrow) th allow ions (action potentials) to move quickly from cell to cell (LM ×400). **Location:** The walls of the heart. **Function:** As the walls of the heart co tract, cardiac muscle tissue propels blood into the circulation; involuntary control.

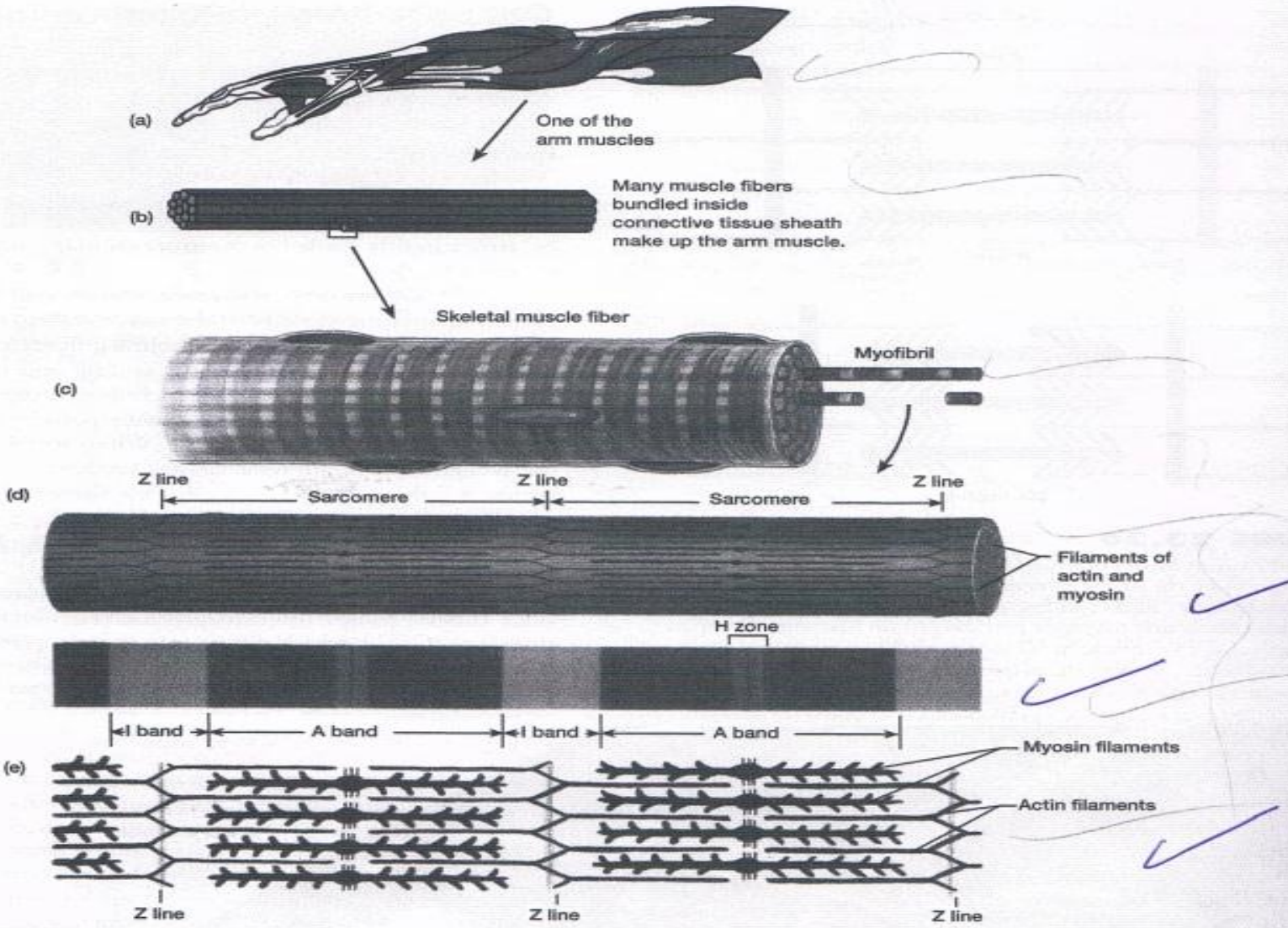


FIGURE 23.25

Structure of Skeletal Muscle Tissue. *(a)* A skeletal muscle in the forearm consists of many muscle fibers (cells) *(b)* bundled inside a connective tissue sheath. *(c)* A skeletal muscle fiber contains many myofibrils, each consisting of *(d)* functional units called sarcomeres. *(e)* The characteristic striations of a sarcomere are due to the arrangement of actin and myosin filaments.

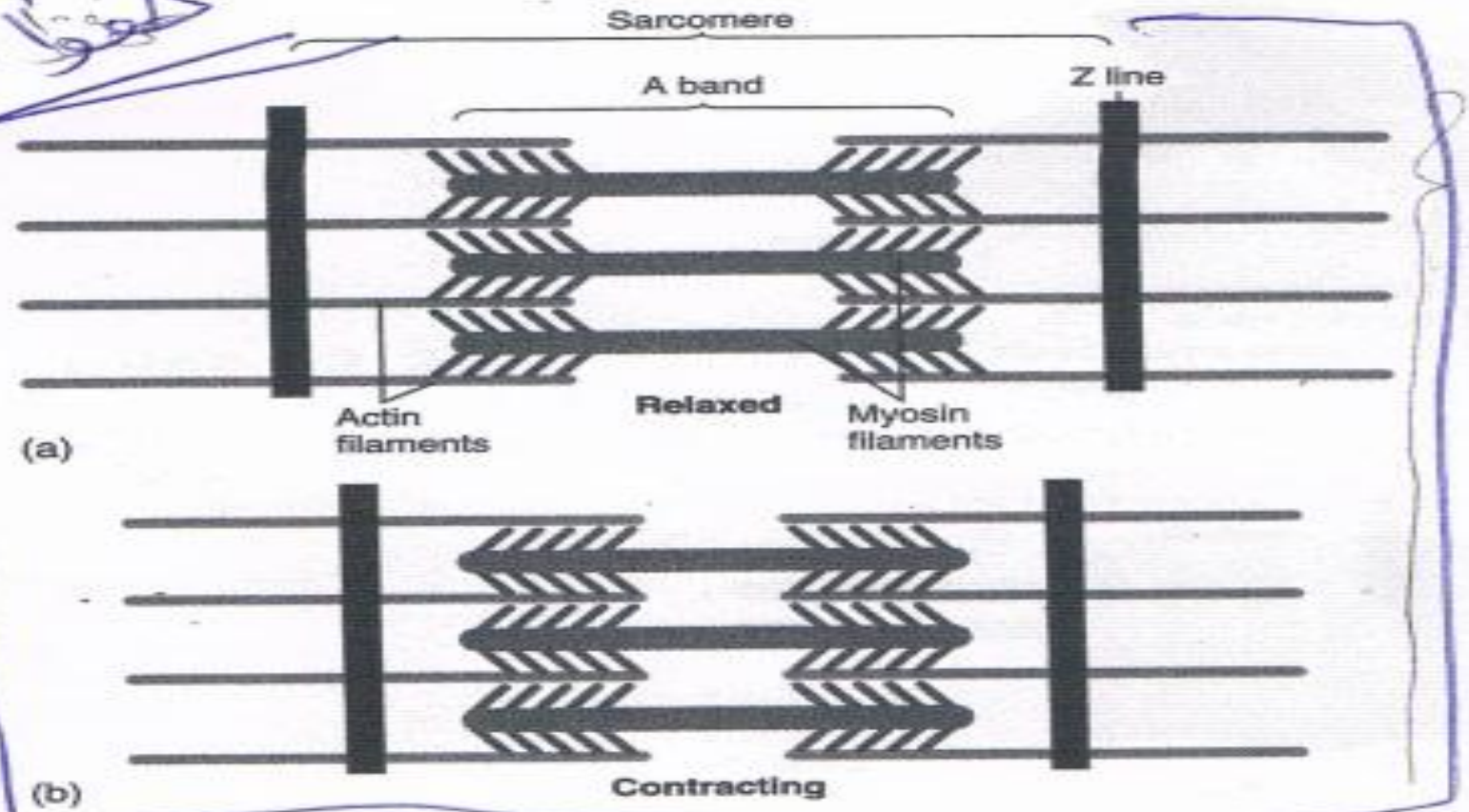


FIGURE 23.26

Sliding-Filament Model of Muscle Contraction. *(a)* A sarcomere in a relaxed position. *(b)* As the sarcomere contracts, the myosin filaments form attachments called cross-bridges to the actin filaments and pull the actin filaments so that they slide past the myosin filaments. Compare the length of the sarcomere in *(a)* to that in *(b)*.

ResearchGate

See discussions, stats, and author profiles for this publication at: https://www.researchgate.net/publication/300772196

Overview of Real-Time PCR Principles

Chapter · May 2012

DOI: 10.5772/39220

CITATIONS
2

READS
8,689

8 authors, including:



Morteza Seifi
University of Alberta
53 PUBLICATIONS **443** CITATIONS
SEE PROFILE



Siamak Heidarzadeh
Zanjan University of Medical Sciences
17 PUBLICATIONS **90** CITATIONS
SEE PROFILE



Mahmood Khosravi
Arak University of Medical Sciences
8 PUBLICATIONS **8** CITATIONS
SEE PROFILE



Atefeh Nami-Pashaki
Monash University (Australia)
6 PUBLICATIONS **72** CITATIONS
SEE PROFILE

Some of the authors of this publication are also working on these related projects:

Neuroscience View project

Cleft lip and palate genetics View project

All content following this page was uploaded by Mahmood Khosravi on 12 October 2017.

The user has requested enhancement of the downloaded file.

19

Overview of Real-Time PCR Principles

Morteza Seifi[1,*], Asghar Ghasemi[1], Siamak Heidarzadeh[2], Mahmood Khosravi[3], Atefeh Namipashaki[4], Vahid Mehri Soofiany[5], Ali Alizadeh Khosroshahi[6] and Nasim Danaei[7]

[1]*Laboratory of Genetics, Legal Medicine Organization of Tabriz, Tabriz,*
[2]*Division of Microbiology, School of Public Health, Tehran University of Medical Sciences, Tehran,*
[3]*Hematology Department of Medicine Faculty, Guilan University of Medical Sciences, Rasht,*
[4]*Department of Biotechnology, School of Allied Medical Sciences, Tehran University of Medical Sciences, Tehran,*
[5]*Faculty of Medicine, Shahid Behesti University of Medical Sciences, Tehran,*
[6]*Jarrah Pasha Medicine Faculty of Istanbul, Istanbul,*
[7]*Department of Health and Nutrition, Tabriz University of Medical Sciences, Tabriz*
[1,2,3,4,5,7]*Iran*
[6]*Turkey*

1. Introduction

Real-time PCR is based on the revolutionary method of PCR, developed by Kary Mullis in the 1980s, which allows researchers to amplify specific pieces of DNA more than a billion-fold (Saiki, Scharf et al. 1985; Mullis and Faloona 1987; Mullis 1990). PCR-based strategies have propelled molecular biology forward by enabling researchers to manipulate DNA more easily, thereby facilitating both common procedures, such as cloning, and huge endeavors such as the Human Genome Project (Olson, Hood et al. 1989; Ausubel, Brent et al. 2005). Real-time PCR represents yet another technological leap forward that has opened up new and powerful applications for researchers throughout the world. This is in part because the enormous sensitivity of PCR has been coupled to the precision afforded by "real-time" monitoring of PCR products as they are generated (Valasek and Repa 2005).

Higuchi and co-workers (Higuchi, Dollinger et al. 1992; Higuchi, Fockler et al. 1993) at Roche Molecular Systems and Chiron accomplished the first demonstration of real-time PCR. By including a common fluorescent dye called ethidium bromide (EtBr) in the PCR and running the reaction under ultraviolet light, which causes EtBr to fluoresce, they could visualize and record the accumulation of DNA with a video camera. It has been known since 1966 that EtBr increases its fluorescence upon binding of nucleic acids (Le Pecq and Paoletti 1966), but only by combining this fluorescent chemistry with PCR and real-time videography could real-time PCR be born as it was in the early 1990s. Subsequently, this

* Corresponding Author

technology quickly matured into a competitive market, becoming commercially widespread and scientifically influential (Valasek and Repa 2005).

Real-time PCR instrumentation was first made commercially available by Applied Biosystems in 1996, after which several other companies added new machines to the market. Presently, Applied Biosystems, BioGene, Bioneer, Bio-Rad, Cepheid, Corbett Research, Idaho Technology, MJ Research, Roche Applied Science, and Stratagene all offer instrumentation lines for real-time PCR (BioInformatics 2003).

Widespread use has also resulted in a multiplicity of names for the technology, each with a different shade of meaning. Real-time PCR simply refers to amplification of DNA (by PCR) that ismonitored while the amplification is occurring. The benefit of this real-time capability is that it allows the researcher to better determine the amount of starting DNA in the sample before the amplification by PCR. Present day real-time methods generally involve fluorogenic probes that "light up" to show the amount of DNA present at each cycle of PCR. "Kinetic PCR" refers to this process as well. "Quantitative PCR" refers to the ability to quantify the starting amount of a specific sequence of DNA. This term predates real-time PCR because it can refer to any PCR procedure, including earlier gel-based end-point assays, that attempts to quantify the starting amount of nucleic acid. Rarely, one might see the term "quantitative fluorescent PCR" to designate that the quantification was accomplished via measuring output from a fluorogenic probe, although this is redundant because all of the present chemistries for real-time PCR are fluorescent. In addition, if reverse transcriptase enzymes are used before PCR amplification in any of the above situations, then "RT-PCR" replaces "PCR" in the term. Today, the two most common terms, real-time and quantitative, are often used interchangeably or in combination, because real-time PCR is quickly becoming the method of choice to quantify nucleic acids (Valasek and Repa 2005).

The basic goal of real-time PCR is to precisely distinguish and measure specific nucleic acid sequences in a sample even if there is only a very small quantity. Real-time PCR amplifies a specific target sequence ina sample then monitors theamplification progress using fluorescent technology. During amplification, how quickly the fluorescent signal reaches a threshold level correlates with the amount of original target sequence, thereby enabling quantification. In addition, the final product can be further characterized by subjecting it to increasing temperatures to determine when the double-stranded product "melts." This melting point is a unique property dependent on product length and nucleotide composition. To accomplish these tasks, conventional PCR has been coupled to state-of-the-art fluorescent chemistries and instrumentation to becomereal-time PCR (Valasek and Repa 2005).

2. The chemistries of real-time PCR

Today fluorescence is exclusively used as the detection method in real-time PCR. Both sequence specific probes and non-specific labels are available as reporters. In his initial work Higuchi used the common nucleic acid stain ethidium bromide, which becomes fluorescent upon intercalating into DNA (Higuchi, Dollinger et al. 1992). Classical intercalators, however, interfere with the polymerase reaction, and asymmetric cyanine dyes such as SYBR Green I and BEBO have become more popular (Bengtsson, Karlsson et al. 2003; Zipper, Brunner et al. 2004). Asymmetric cyanines have two aromatic systems containing nitrogen, one of which is positively charged, connected by amethine bridge. These dyes have virtually no fluorescence when they are free in solution due to vibrations engaging

both aromatic systems, which convert electronic excitation energy into heat that dissipates to the surrounding solvent. On the other hand the dyes become brightly fluorescent when they bind to DNA, presumably to the minor groove, and rotation around the methine bond is restricted (Nygren, Svanvik et al. 1998). In PCR the fluorescence of these dyes increases with the amount of double stranded product formed, though not strictly in proportion because the dye fluorescence depends on the dye: base binding ratio, which decreases during the course of the reaction. The dye fluorescence depends also to some degree on the DNA sequence. But a certain amount of a particular double-stranded DNA target, in the absence of significant amounts of other double-stranded DNAs, gives rise to the same fluorescence every time. Hence, the dyes are excellent for quantitative real-time PCR when samples are compared at the same level of fluorescence in absence of interfering DNA. Although minor groove binding dyes show preference for runs of AT base-pairs (Jansen, Norde´n et al. 1993), asymmetric cyanines are considered sequence non-specific reporters in real-time PCR. They give rise to fluorescence signal in the presence of any double stranded DNA including undesired primer–dimer products. Primer–dimer formation interferes with the formation of specific products because of competition of the two reactions for reagents and may lead to erroneous readouts. It is therefore good practice to control for primer–dimer formation. This can be done by melting curve analysis after completing the PCR. The temperature is then gradually increased and the fluorescence is measured as function of temperature. The fluorescence decreases gradually with increasing temperature because of increased thermal motion which allows for more internal rotation in the bound dye (Nygren, Svanvik et al. 1998). However, when the temperature is reached at which the double stranded DNA strand separates the dye comes off and the fluorescence drops abruptly (Ririe, Rasmussen et al. 1997). This temperature, referred to as the melting temperature, Tm, is easiest determined as the maximum of the negative first derivative of the melting curve. Since primer–dimer products typically are shorter than the targeted product, they melt at a lower temperature and their presence is easily recognized by melting curve analysis (Kubista, Andrade et al. 2006).

Labeled primers and probes are based on nucleic acids or some of their synthetic analogues such as the peptide nucleic acids (PNA) (Egholm, Buchardt et al. 1992) and the locked nucleic acids (LNA) (Costa, Ernault et al. 2004). The dye labels are of two kinds: (i) fluorophores with intrinsically strong fluorescence, such as fluorescein and rhodamine derivatives (Sjöback, Nygren et al. 1995), which through structural design are brought into contact with a quencher molecule, and (ii) fluorophores that change their fluorescence properties upon binding nucleic acids. Examples of probes with two dyes are the hydrolysis probes, popularly called Taqman probes (Holland, Abramson et al. 1991), which can be based either on regular oligonucleotides or on LNA (Braasch and Corey 2001), Molecular Beacons (Tyagi and Kramer 1996; Tyagi, Bratu et al. 1998), Hybridization probes (Caplin, Rasmussen et al. 1999), and the Lion probes (http://www.biotools.net). The dyes form a donor–acceptor pair, where the donor dye is excited and transfers its energy to the acceptor molecule if it is in proximity. Originally the acceptor molecule was also a dye, but today quencher molecules are more popular (Wilson and Johansson 2003). Energy transfer and quenching are distance dependent and structural rearrangement of the probe, or, in the case of hydrolysis probes, degradation, change the distance between the donor and acceptor and, hence, the fluorescence of the system (Kubista, Andrade et al. 2006).

Probes based on a single dye, whose fluorescence changes upon binding target DNA include the LightUp probes (Svanvik, Westman et al. 2000), AllGlo probes

(http://www.allelogic.com), Displacement probes (Li, Qingge et al. 2002), and the Simple probes (http://www.idahotech.com/itbiochem/simpleprobes.html).

Chemical modifications and alterations of the oligonucleotide backbone are employed in some probes to improve the binding properties to the target template. This makes it possible to use shorter probes, which is advantageous for the detection of targets with short conserved regions such as retroviruses. LightUp probes have a neutral peptide nucleic acid (PNA) backbone that binds to DNA with greater affinity than normal oligonucleotides (Kubista, Andrade et al. 2006).

The LightUp probes are 10–12 bases, which is short compared to normal oligonucleotide probes that are usually at least 25 bases (http://www.lightup.se). LNA-probes make use of modified nucleotides to enhance binding affinity. MGBprobes are hydrolysis probes with a minor groove binding molecule attached to the end of the probe to increase affinity for DNA, which makes it possible to use shorter probes (Kutyavin, Afonina et al. 2000). Examples of modified primers include: Scorpion primers (Whitcombe, Theaker et al. 1999), LUX primers (Nazarenko, Lowe et al. 2002), Ampliflour primers (Uehara, Nardone et al. 1999), and the QZyme system (BD QZymeTM Assays for Quantitative PCR, 2003). As long as a single target is detected per sample there is not much of a difference in using a dye or a probe. Assay specificity is in both cases determined by the primers. Probes do not detect primer–dimer products, but using non-optimized probe assays is hiding the problem under the rug. If primer–dimers form they cause problems whether they are seen or not. In probe based assays, particularly when high CT values are obtained, one should verify the absence of competing primer–dimer products (Kubista, Andrade et al. 2006). The traditional way is by gel electrophoresis. Recently, an alternative approach was proposed based on the BOXTO dye. BOXTO is a sequence non-specific doublestranded DNA binding dye that has distinct spectral characteristics to fluorescein and can be used in combination with FAM based probes. The BOXTO and the probe signals are detected in different channels of the real-time PCR instrument. While the probe reflects formation of the targeted product as usual, the BOXTO dye also reports the presence of any competing primer–dimer products, which can be identified by melting curve analysis (Lind, Stahlberg et al. 2006). The great advantage of probes is for multiplexing, where several products are amplified in the same tube and detected in parallel (Wittwer, Herrmann et al. 2001). Today multiplexing is mainly used to relate expression of reporter genes to that of an exogenous control gene in diagnostic applications (Mackya 2004), and for single nucleotide polymorphism (SNP) and mutation detection studies (Mhlanga and Malmberg 2001; Mattarucchi, Marsoni et al. 2005). Multiplex assays are more difficult to design because when products accumulate the parallel PCR reactions compete for reagents. To minimize competition limiting amounts of primers must be used. Also, primer design is harder, because complementarity must be avoided between all the primers. Multiplex assays can be based either on probes or on labeled primers, where labeled primers usually give rise to signal from primer–dimer products, while probes do not. The different probing technologies have their advantages and limitations. Dyes are cheaper than probes but they do not distinguish between products. Hairpin forming probes have the highest specificity, because the formation of the hairpin competes with the binding to mismatched targets. This makes them most suitable for SNP and multi-site variation (MSV) analysis (Bonnet, Tyagi et al. 1999). Hydrolysis probes require two-step PCR to function properly, which is not optimal for the polymerase reaction, and short amplicons are

necessary to obtain reasonable amplification efficiencies. But they are easier to design than hairpin forming probes and an 80% success rate was recently reported (Kubista 2004).

In summary, a 'good'probe, independent of chemistry, should have low background fluorescence, high fluorescence upon target formation (high signal to noise ratio), and high target specificity. The dyes'excitation and emission spectra are important parameters to consider when designing multiplex reactions. Spectral overlap in excitation and emission should be minimized to keep cross-talk to a minimum (Kubista, Andrade et al. 2006).

2.1 SYBR green I

SYBR green I binds to the minor groove of dsDNA, emitting 1,000-fold greater fluorescence than when it is free in solution (Wittwer, Herrmann et al. 1997). Therefore, the greater the amount of dsDNA present in the reaction tube, the greater the amount of DNA binding and fluorescent signal from SYBR green I. Thus any amplification of DNA in the reaction tube is measured (Valasek and Repa 2005).

2.2 BEBO

The minor groove binding asymmetric cyanine dye BEBO is tested as sequence nonspecific label in real-time PCR. The Fluorescence intensity of BEBO increases upon binding to double-stranded DNA allowing emission to be measured at the end of the elongation phase in the PCR cycle. BEBO concentrations between 0.1 and 0.4 mM generated sufficient Fluorescence signal without inhibiting the PCR. A comparison with the commonly used reporter dye SYBR Green I shows that the two dyes behave similarly in all important aspects. The dye has absorbance and emission wavelengths that can be detected on the FAM channel on most common real-time PCR platforms, and shows a strong fluorescence increase when bound to dsDNA. BEBO can be used as an unspecific dye for real-time PCR applications or other applications where staining of dsDNA is wanted (Bengtsson, Karlsson et al. 2003).

2.3 BOXTO

The unsymmetrical cyanine dyes BOXTO and its positive divalent derivative BOXTO-PRO were studied as real-time PCR reporting fluorescent dyes and compared to SYBR GREEN I (SG). Unmodified BOXTO showed no inhibitory effects on real-time PCR, while BOXTO-PRO showed complete inhibition, sufficient fluorescent signal was acquired when 0.5–1.0 μM BOXTO was used with RotorGene and iCycler platforms. Statistical analysis showed that there is no significant difference between the efficiency and dynamic range of BOXTO and SG (Ahmad 2007).

2.4 5' nuclease (TaqMan) probes

Hydrolysis probes (also called 5′-nuclease probes because the 5′-exonuclease activity of DNA polymerase cleaves the probe) offer an alternative approach to the problem of specificity. These are likely the most widely used fluorogenic probe format (Mackay 2004) and are exemplified by TaqMan probes. In terms of structure, hydrolysis probes are sequence- specific dually fluorophore-labeled DNA oligonucleotides (Valasek and Repa 2005). One fluorophore is termed the quencher and the other is the reporter. When the quencher and reporter are in close proximity, that is, they are both attached to the same

short oligonucleotide; the quencher absorbs the signal from the reporter (Valasek and Repa 2005). This is an example of fluorescence resonance energy transfer (also called Forster transfer) in which energy is transferred from a "donor" (the reporter) to an "acceptor" (the quencher) fluorophore. During amplification, the oligonucleotide is broken apart by the action of DNA polymerase (5/-nuclease activity) and the reporter and quencher separate, allowing the reporter's energy and fluorescent signal to be liberated. Thus destruction or hydrolysis of the oligonucleotide results in an increase of reporter signal and corresponds with the specific amplification of DNA (Valasek and Repa 2005). Examples of common quencher fluorophores include TAMRA, DABCYL, and BHQ, whereas reporters are more numerous (e.g., FAM, VIC, NED, etc). Hydrolysis probes afford similar precision as SYBR green I (Wilhelm, Pingoud et al. 2003), but they give greater insurance regarding the specificity because only sequence-specific amplification is measured. In addition, hydrolysis probes allow for simple identification of point mutations within the amplicon using melting curve analysis (Valasek and Repa 2005).

2.5 Molecular beacons

Molecular beacons are similar to TaqMan probes but are not designed to be cleaved by the 5' nuclease activity of Taq polymerase. These probes have a fluorescent dye on the 5' end and a quencher dye on the 3' end of the oligonucleotide probe. A region at each end of the molecular beacon probe is designed to be complementary to itself, so at low temperatures, the ends anneal, creating a hairpin structure. This integral annealing property positions the two dyes in close proximity, quenching the fluorescence from the reporter dye (Espy, Uhl et al. 2006). The central region of the probe is designed to be complementary to a region of the PCR amplification product. At high temperatures, both the PCR amplification product and probe are single stranded. As the temperature of the PCR is lowered, the central region of the molecular beacon probe binds to the PCR product and forces the separation of the fluorescent reporter dye from the quenching dye. The effects of the quencher dye are obviated and a light signal from the reporter dye can be detected. If no PCR amplification product is available for binding, the probe reanneals to itself, forcing the reporter dye and quencher dye together, preventing fluorescent signal (Espy, Uhl et al. 2006). Typically, a single molecular beacon is used for detection of a PCR amplification product and multiple beacon probes with different reporter dyes are used for single nucleotide polymorphism detection. By selection of appropriate PCR temperatures and/or extension of the probe length, molecular beacons will bind to the target PCR product when an unknown nucleotide polymorphism is present but at a slight cost of reduced specificity. There is not a specific temperature thermocycling requirement for molecular beacons, so temperature optimization of the PCR is simplified (Espy, Uhl et al. 2006).

2.6 FRET hybridization probes

FRET hybridization probes, also referred to as LightCyclerprobes; represent a third type of probe detection format commonly used with real-time PCR testing platforms. FRET hybridization probes are two DNA probes designed to anneal next to each other in a head-to-tail configuration on the PCR product. The upstream probe has a fluorescent dye on the 3' end and the downstream probe has an acceptor dye on the 5' end. If both probes anneal to the target PCR product, fluorescence from the 3' dye is absorbed by the adjacent acceptor dye on the 5' end of the second probe. The second dye is excited and emits light at a third

wavelength and this third wavelength is detected. If the two dyes do not align together because there is no specific DNA for them to bind, then FRET does not occur between the two dyes because the distances between the dyes are too great. A design detail of FRET hybridization probes is the 3' end of the second (downstream) probe is phosphorylated to prevent it from being used as a primer by Taq during PCR amplification. The two probes encompass a region of 40 to 50 DNA base pairs, providing exquisite specificity (Espy, Uhl et al. 2006). FRET hybridization probe technology permits melting curve analysis of the amplification product. If the temperature is slowly raised, eventually the probes will no longer be able to anneal to the target PCR product and the FRET signal will be lost. The temperature at which half the FRET signal is lost is referred to as the melting temperature of the probe system (Espy, Uhl et al. 2006). The Tm depends on the guanine plus cytosine content and oligonucleotide length. In contrast to TaqMan probes, a single nucleotide polymorphism in the target DNA under a hybridization FRET probe will still generate a signal, but the melting curve will display a lower Tm. The lowered Tm can be characteristic for a specific polymorphism underneath the probes; however, a lowered Tm can also be the result of any sequence difference under the probes. The target PCR product is detected and the altered Tm informs the user there is a difference in the sequence being detected. Generally, more than three base pair differences under a FRET hybridization probe prevent hybridization at typical annealing temperatures and are not detected (Espy, Uhl et al. 2006). This trait of FRET hybridization probes is advantageous in cases where the genome of the organism is known to mutate at a high frequency, such as with viruses. When a single or limited number (<3) of known polymorphisms occur between two similar targets, FRET hybridization probes can also be used for discriminating strains of organisms (Espy, Uhl et al. 2006). Like molecular beacons, there is not a specific thermocycling temperature requirement for FRET hybridization probes. Molecular beacons and FRET hybridization probes, unlike TaqMan probes, are both recycled (conserved) in each round of PCR temperature cycle. Also, for Molecular beacons and FRET hybridization probes, unlike TaqMan probes, fluorescent signal does not accumulate as PCR product accumulates after each PCR cycle (Espy, Uhl et al. 2006).

2.7 Scorpions

Scorpions combine the detection probe with the upstream PCR primer (Whitcombe, Theaker et al. 1999) and consist of a fluorophore on the 5′ end, followed by a complementary stem-loop structure (also containing the specific probe sequence), quencher dye, DNA polymerase blocker (a nonamplifiable monomer that prevents DNA polymerase extension), and finally a PCR primer on the 3′ end. The probe sequence contained within the hairpin allows the scorpion to anneal to the template strand, which separates the quencher for the fluorophore and results in increased fluorescence. Because sequence-specific priming and probing is a unimolecular event, scorpions perform better than bimolecular methods under conditions of rapid cycling such as the LightCycler (Thelwell, Millington et al. 2000). Cycling is performed at a temperature optimal for DNA polymerase activity instead of the reduced temperature necessary for the 5′ nuclease assay. Scorpions are specific enough for allele discrimination and may be multiplexed easily (Thelwell, Millington et al. 2000). The scorpion chemistry has been improved with the creation of duplex scorpions in which the reporter dye/probe and quencher fragment are on separate, complementary molecules (Solinas, Brown et al. 2001). The duplex scorpions still bind in a unimolecular event, but because the reporter and quenchers are on separate molecules, they yield greater signal

intensity because the reporter and quencher can separate completely (Wong and Medrano 2005).

2.8 Sunrise™ primers

Created by Oncor (Gaithersburg, MD, USA), Sunrise primers are similar to scorpions in that they combine both the PCR primer and detection mechanism in the same molecule (Nazarenko, Bhatnagar et al. 1997). These probes consist of a dual-labeled (reporter and quencher fluorophores) hairpin loop on the 5′ end, with the 3′ end acting as the PCR primer. When unbound, the hairpin is intact, causing reporter quenching via FRET. Upon integration into the newly formed PCR product, the reporter and quencher are held far enough apart to allow reporter emission (Wong and Medrano 2005).

2.9 LUX™ fluorogenic primers

Light upon extension (LUX) primers (Invitrogen, Carlsbad, CA, USA) are self-quenched single-fluorophore labeled primers almost identical to Sunrise primers. However, rather than using a quencher fluorophore, the secondary structure of the 3′ end reduces initial fluorescence to a minimal amount (Nazarenko, Lowe et al. 2002). Because this chemistry does not require a quencher dye, it is much less expensive than dual-labeled probes. While this system relies on only two oligonucleotides for specificity, unlike the SYBR Green I platform in which a dissociation curve is used to detect erroneous amplification, no such convenient detection exists for the LUX platform. Agarose gels must be run to ensure the presence of a single PCR product, a step that is extremely important not only for the LUX primers but also for the Sunrise primers and scorpions because PCR priming and probe binding are not independent in these chemistries (Wong and Medrano 2005).

2.10 Light-up probes

Light-up probes are peptide nucleic acids (PNAs) that use thiazole orange as the fluorophor. Upon hybridisation with DNA, duplex or triplex structures are formed with increased fluorescence intensity of the fluorophor. A quencher is not required. This technique is limited by unspecific fluorescence, which increases during PCR and therefore restricts the achievable sensitivity (Isacsson, Cao et al. 2000; Svanvik, Stahlberg et al. 2000;Svanvik, Westman et al. 2000). Some other formats use the increasing quench as indicator for product accumulation (Crockett and Wittwer 2001; Kurata, Kanagawa et al. 2001). In this case, the fluorescence is quenched by a guanine residue of the PCR product. These probes are comparatively inexpensive and easy to construct; however, measurement of the decrease of a signal is problematic, especially during the early exponential phase in which only very few probes are quenched (Wilhelm and Pingoud 2003).

2.11 Eclipse probe

qPCR assays using an Eclipse probe employ two primers and a sequence-specific oligonucleotide probe. The probe is complementary to a sequence within the amplicon and contains a fluorescent reporter at the 3' end, a quencher at the 5' end, and a minor groove binder (Bio-Rad Laboratories 2006). The unhybridized probe adopts a conformation that brings the reporter and quencher together, quenching the reporter. During the annealing

step of PCR, the probe hybridizes to the target with the help of the minor groove binder. The probe thus becomes linearized, separating the reporter and quencher and allowing the reporter to fluoresce. The resulting fluorescent signal is proportional to the amount of amplified product in the sample (Bio-Rad Laboratories 2006).

2.12 Amplifluor primer

qPCR assays using Amplifluor chemistry employ two target-specific primers and one universal primer called the UniPrimer. The first target-specific primer contains a 5' extension sequence called the Z-sequence that is also found at the 3' end of the UniPrimer. The UniPrimer forms a hairpin structure (Bio-Rad Laboratories 2006). A fluorescent reporter and a quencher are attached at the 5' and the 3' ends of the stem structure, respectively. In the hairpin conformation, the reporter fluorescence is quenched due to its proximity to the quencher. During the first amplification cycle, the first target-specific primer (with the Z-sequence) hybridizes to the template and is extended. During the second amplification cycle, the second target-specific primer is used to synthesize a new target template that contains a sequence complementary to the Z-sequence. The product from the second amplification cycle can then serve as the template for the UniPrimer. In the third amplification cycle, the extended UniPrimer serves as a template for the next amplification cycle (Bio-Rad Laboratories 2006). In the fourth cycle, extension of the template through the hairpin region of the UniPrimer causes the UniPrimer to open up and adopt a linear configuration, which allows the reporter to fluoresce. Exponential amplification using the second target-specific primer and the UniPrimer occurs in subsequent amplification cycles. The resulting fluorescent signal is proportional to the amount of amplified product in the sample (Bio-Rad Laboratories 2006).

2.13 BD QZyme primer

qPCR assays using BD QZyme primers employ a target-specific zymogene primer, a target-specific reverse primer, and a universal oligonucleotide substrate. The oligonucleotide contains a fluorescent reporter on the 5' end and a quencher on the 3' end. When oligonucleotide substrate is intact, the fluorescence of the reporter is quenched by the quencher due to their proximity (Bio-Rad Laboratories 2006). The zymogene primer contains a sequence that encodes a catalytic DNA. During the first amplification cycle, the zymogene primer is extended. In the second cycle, the product of the first cycle is used as the template by the target-specific reverse primer, which is extended to create a new target sequence containing a catalytic DNA region. In the subsequent annealing step, the fluorescently labeled oligonucleotide substrate hybridizes to the catalytic DNA sequence and is cleaved. This cleavage separates the reporter from the quencher, resulting in a fluorescent signal that is proportional to the amount of amplified product in the sample (Bio-Rad Laboratories 2006).

3. Design and optimization of SYBR Green I reactions

A SYBR Green I assay uses a pair of PCR primers that amplifies a specific region within the target sequence of interest and includes SYBR Green 1 for detecting the amplified product. The steps for developing a SYBR Green I assay are:

1. Primer design and amplicon design

2. Assay validation and optimization

A) Primer and Amplicon Design:

A successful real-time PCR reaction requires efficient and specific amplification of the product. Both primers and target sequence can affect this efficiency. Therefore, care must be taken when choosing a target sequence and designing primers. A number of free and commercially available software programs are available for this purpose. One popular web-based program for primer design is Primer3 (http://frodo.wi.mit.edu/cgi-bin/primer3/primer3_www.cgi). A commercially available program such as Beacon Designer software performs both primer design and amplicon selection (Bio-Rad Laboratories 2006).

B) Guidelines of amplicon design:

1. Design amplicon to be 75–200 bp.Shorteramplicons are typically amplified with higher efficiency. An amplicon should be at least 75 bp to easily distinguish it from any primer-dimers that might form
2. Avoid secondary structure if possible. Use programs such as mfold http://www.bioinfo.rpi.edu/applications/mfold/) to predict whether an amplicon will form any secondary structure at annealing temperature. See Real-Time PCR: General Considerations (Bio-Rad bulletin 2593) for more details
3. Avoid templates with long (>4) repeats of single bases
4. Maintain a GC content of 50–60%

C) Parameters of primer design:

1. Design primers with a GC content of 50–60%
2. Maintain a melting temperature (T_m) between 50°C and 65°C. We calculate T_m values using the nearest-neighbor method with values of 50 mM for salt concentration and 300 nM for oligonucleotide concentration
3. Avoid secondary structure; adjust primer locations outside of the target sequence secondary structure if required
4. Avoid repeats of Gs or Cs longer than three bases
5. Place Gs and Cs on ends of primers
6. Check sequence of forward and reverse primers to ensure no 3' complementarity (avoid primer-dimer formation)
7. Verify specificity using tools such as the Basic Local Alignment Search Tool (http://www.ncbi.nlm.nih.gov/blast/)

D) Assay Validation and Optimization:

Components a SYBR Green I qPCR reaction:

1. PCR master mix with SYBR Green I
2. Template
3. Primers

Preformulated real-time PCR master mixes containing buffer, DNA polymerase, dNTPs, and SYBR Green I dye are available from several vendors.

Optimized SYBR Green I qPCR reactions should be sensitive and specific and should exhibit good amplification efficiency over a broad dynamic range (Bio-Rad Laboratories 2006).

Steps of to determine the performance of your SYBR Green I qPCR assay:

a. Identify the optimal annealing temperature for your assay
b. Construct a standard curve to evaluate assay performance

E) Annealing Temperature Optimization:

The optimal annealing temperature can easily be assessed on qPCR instruments that have a temperature gradient feature, such as the MiniOpticon™, MyiQ™, DNA Engine Opticon®, Opticon™ 2, iCycleriQ®, Chromo4™, and iQ™5 systems.

A gradient feature allows you to test a range of annealing temperatures simultaneously, so optimization reactions can be performed in a single experiment.

To find the optimal annealing temperature for reaction, recommend testing a range of annealing temperatures above and below the calculated T_m of the primers.

Because SYBR Green I binds to all dsDNA, it is necessary to check the specificity of your qPCR assay by analyzing the reaction product(s). To do this, use the melt-curve function on your real-time instrument and also run products on an agarose gel. An optimized SYBR Green I qPCR reaction should have a single peak in the melt curve, corresponding to the single band on the agarose gel.

Nonspecific products that may have been co-amplified with the specific product can be identified by melt-curve analysis. In this example, the specific product is the peak with a T_m of 89°C and corresponds to the upper band on the gel. The nonspecific product is the peak with a T_m of 78°C and corresponds to the lower band in the gel. By comparing the gel image with the melt curve, you can identify peaks in the melt curve that correspond to specific product, additional nonspecific bands, and primer-dimers. If nonspecific products such as primer-dimers are detected by melt-curve analysis, recommend that redesign primers (Bio-Rad Laboratories 2006).

F) Assay Performance Evaluation Using Standard Curves:

The efficiency, reproducibility, and dynamic range of a SYBR Green I assay can be determined by constructing a standard curve using serial dilutions of a known template. The efficiency of the assay should be 90–105%, the R^2 of the standard curve should be >0.980 or $r > |-0.990|$, and the C_T values of the replicates should be similar.

It is important to note that the range of template concentrations used for the standard curve must encompass the entire range of template concentration of the test samples to show that results from the test samples are within the linear dynamic range of the assay. If the test samples give results outside of the range of the standard curves, one of the following must be performed:

1. Construct a wider standard curve covering the test sample concentrations and perform analysis to ensure that the assay is linear in that new range
2. If the test samples give a lower C_T than the highest concentration of standards used in the standard curve, repeat the assay using diluted test samples
3. If the test samples give a higher C_T than the lowest concentration of standards used in the standard curve, repeat the assay using larger amounts of the test samples

4. Design and optimization of TaqManProbe reactions

A TaqMan assay uses a pair of PCR primers and a dual-labeled target-specific fluorescent probe. The steps for developing a TaqMan assay are:

a. Primer and probe design
b. Assay validation and optimization

A. Primer and Probe Design:

As with any qPCR reaction, TaqMan-based assays require efficient and specific amplification of the product. Typically, the primers are designed to have an annealing temperature between 55 and 60°C. We recommend using software such as Beacon Designer for designing your TaqMan primers and TaqMan probe.. Because the dual-labeled probe is the most costly component of a TaqMan assay, suggested that order the two primers and validate their performance using SYBR Green I before ordering the dual-labeled probe.

The TaqMan probe should have a T_m 5–10°C higher than that of the primers. In most cases, the probe should be <30 nucleotides and must not contain a G at its 5' end because this could quench the fluorescent signal even after hydrolysis. Choose a sequence within the target that has a GC content of 30–80%, and design the probe to anneal to the strand that has more Gs than Cs (so the probe contains more Cs than Gs).

An important aspect of designing a TaqMan probe is reporter and quencher selection. We recommend using FAM-labeled probes when designing singleplex reactions, because they are inexpensive and readily available, perform well, and can be detected by all instruments currently on the market.

Another important consideration for obtaining accurate real-time qPCR data is probe quality. Even a perfectly designed probe can fail if the probe is improperly synthesized or purified. Improper removal of uncoupled fluorescent label, inefficient coupling, and/or poor quenching can produce high fluorescent background or noise. A low signal-to-noise ratio results in decreased sensitivity and a smaller linear dynamic range. Two probes with identical sequences and identical fluorophore labels can be measurably different when synthesized by different suppliers or even at different times by the same supplier.

B. Assay Validation and Optimization:

A TaqMan probe-based qPCR reaction contains the following components:

1. PCR master mix
2. Template
3. Primers
4. Probe(s)

Preformulated PCR master mixes containing buffer, DNA polymerase, and dNTPs are commercially available from several vendors. For TaqMan assays, we recommend using iQ™ supermix with 300 nM of each of the two primers and 200 nM of probe(s). TaqMan assays require careful attention to temperature conditions. A typical TaqMan protocol contains a denaturation step followed by a combined annealing and extension step at 55–60°C, instead of the traditional three-step PCR cycle of denaturation, annealing, and extension. This is to ensure that the probe remains bound to its target during primer

extension. Typical TaqMan probes for nucleic acid quantification are designed to have a T_m of 60–70°C. An optimized TaqMan assay should be sensitive and specific, and should exhibit good amplification efficiency over a broad dynamic range.

In short, construct a standard curve using dilutions of a known template and use this curve to determine the efficiency of the assay along with R^2 or r of the regression line. The efficiency of the reaction should be between 90 and 105%, the R^2 should be >0.980 or r > |–0.990|, and the replicates should give similar C_T values. If the assay performs within these specifications, you are ready to start your experiment. If the assay performs outside these specifications, we suggest that you redesign your primers and TaqMan probe. It is important to note that the range of template concentrations used for the standard curve must encompass the entire range of template concentrations of the test samples to demonstrate that results from the test samples are within the dynamic range of the assay (Bio-Rad Laboratories 2006). If test samples give results outside the range of the standard curve, one of the three following steps must be performed:

1. Construct a wider standard curve covering the test sample concentrations and perform analysis to ensure that the assay is linear in that new range
2. If the test samples give a lower C_T than the highest concentration of standards used in the standard curve, repeat the assay using diluted test samples
3. If the test samples give a higher C_T than the lowest concentration of standards used in the standard curve, repeat the assay using larger amounts of the test samples

5. The instrumentation of real-time PCR

A critical requirement for real-time PCR technology is the ability to detect the fluorescent signal and record the progress of the PCR. Because fluorescent chemistries require both a specific input of energy for excitation and a detection of a particular emission wavelength, the instrumentation must be able to do both simultaneously and at the desired wavelengths. Thus the chemistries and instrumentation are intimately linked (Valasek and Repa 2005).

At present, there are three basic ways in which real-time instrumentation can supply the excitation energy for fluorophores: by lamp, light-emitting diode (LED), or laser. Lamps are classified as broad-spectrum emission devices, whereas LEDs and lasers are narrow spectrum. Instruments that utilize lamps (tungsten halogen or quartz tungsten halogen) may also include filters to restrict the emitted light to specific excitation wavelengths. Instruments using lamps include Applied Biosystem's ABI Prism 7000, Stratagene's Mx4000 and Mx3000P, and Bio-Rad's iCycleriQ. LED systems include Roche's LightCycler, Cepheid's SmartCycler, Corbett's Rotor-Gene, and MJ Research's DNA Engine Opticon 2. The ABI Prism 7900HT is the sole machine to use a laser for excitation (Valasek and Repa 2005). To collect data, the emission energies must also be detected at the appropriate wavelengths. Detectors include charge-coupled device cameras, photomultiplier tubes, or other types of photodetectors. Narrow wavelength filters or channels are generally employed to allow only the desired wavelength(s) to pass to the photodetector to be measured. Usually, multiple discrete wavelengths can be measured at once, which allows for multiplexing, i.e., running multiple assays in a single reaction tube (Valasek and Repa 2005). Another portion of the instrumentation consists of a thermocycler to carry out PCR. Of particular importance for real-time PCR is the ability of the thermocycler to maintain a

consistent temperature among all sample wells, as any differences in temperature could lead to different PCR amplification efficiencies. This is accomplished by using a heating block (Peltier based or resistive), heated air, or a combination of the two. As one might expect, heating blocks generally change temperature more slowly than heated air, resulting in longer thermocycling times. For example, Roche's LightCycler models utilizing heated air can perform 40 cycles in 30 min, whereas Applied Biosystem's ABI Prism 7900HT utilizing a Peltier-based heating block take s 1 h 45 min (Valasek and Repa 2005). Real-time instrumentation certainly would not be complete without appropriate computer hardware and data-acquisition and analysis software. Software platforms try to simplify analysis of real-time PCR data by offering graphical output of assay results including amplification and dissociation (melting point) curves. The amplification curve gives data regarding the kinetics of amplification of the target sequence, whereas the dissociation curve reveals the characteristics of the final amplified product (Valasek and Repa 2005).

5.1 Comparison of the different systems

Essentially, each real time PCR instrument consists of a computer-controlled thermocycler integrated with fluorescent detection system and dedicated software to analyze the result. Some systems can detect four different wave lengths (I-cycler, Mx4000 [stratagene] and Smart Cycler®, Version 2.0 Light Cycler®) whereas others can detect two different wavelengths (Light Cycler®). The Light Cycler® and Smart Cycler® are capable of performing rapid-cycle real time PCR because the reaction is set-up in capillaries or especially designated tubes. Both have optimized heating- cooling characteristic. A complete amplification protocol can be performed in 30-45 minutes (Myi ; Giulietti, Overbergh et al. 2001; Soheili and Samiei 2005). The Smart Cycler® is a combination of 16 individual, one tube real time PCR units. It is capable of performing a different PCR program on each of 16 reaction tubes. This is very useful for a rapid optimization of the assay as many variables can be tested at the same time. The Bio-Rad I-cycler IQ® instrument can perform real time amplification with a temperature gradient for specific PCR steps, allowing the optimization of real time PCR assay. The spectrofluorometers in the thermal cycler have a number of differences. Laser-based systems are tuned to excite each fluorophore at a specific wavelength and provide maximum efficiency. Lamp-based systems provide a broad excitation range that can be filtered to work with a number of fluorophores. The laser source not only gives brighter illumination to the fluorophore signal, but also produces less background noise(Myi ; Giulietti, Overbergh et al. 2001; Soheili and Samiei 2005).

In conclusion, real time PCR is a powerful advancement of the basic PCR technique. The important steps in deciding which particular assay format to use are related to the type of data required. The requirement for a research laboratory is quite distinct from those of a diagnostic laboratory. For the latter, probe confirmation of the PCR product is an essential part of the assay, whereas SYBR green detection may be sufficient for many other applications such as quantifying expression of a gene. All of the real-time PCR machines analyzed are capable of detecting PCR product in real time and a specific assay can be made optionally on every system. However, there are some decisions to be made when selecting among different formats. The choice of system is dependent on individual laboratory needs (Myi ; Giulietti, Overbergh et al. 2001; Soheili and Samiei 2005). Considering diagnostic applications, the Light Cycler® or Smart Cycler® may obtain faster results for urgent assays.

This could reduce the time of analysis to result from 3-4 hours to 1.5 hours. On the other hand, if sensitivity is the most important issue, these machines, with their smaller reaction volume and consequently lower sensitivity, wouldn't be the first choice. The ABI 7700 and Bio-Rad -I-Cycler IQ® have a 96 well format, enabling higher throughput than other systems. The 384-well plates, as designed by ABI for use in the 7900 HT system, can further enhance through put. For diagnostic application, internal control of nucleic acid isolation and PCR inhibition, it is essential to obtain valid results. This can be achieved using the system that enables multi-color detection, such as the I-Cycler IQ® and the Smart Cycler®. Recently, a multi-color format of the Light Cycler® is also present in market. Multiplex real-time PCRs can be developed for three different targets and an internal control by using the four detection wavelengths possible in multicolor detection. As a matter of fact, the choice of which real time system to use depends on the range of application required. To achieve meaningful results, each assay must be validated and optimized for the particular system chosen (Myi ; Giulietti, Overbergh et al. 2001; Soheili and Samiei 2005).

6. Advantages of real-time PCR quantitation

There are many methods in molecular biology for measuring quantities of target nucleic acid sequences. However, most of these methods exhibit one or more of the following shortcomings: they are time consuming, labor intensive, insufficiently sensitive, non-quantitative, require the use of radioactivity, or have a substantial probability of cross contamination (Reischl, Wittwer et al. 2002). These methods include but are not limited to Northern and Southern hybridizations, HPLC, scintillation proximity assay, PCR-ELISA, RNase protection assay, in situ hybridization, and various gel electrophoresis PCR end-point systems (Valasek and Repa 2005). Real-time PCR has distinct advantages over these earlier methods for several reasons. Perhaps the most important is its ability to quantify nucleic acids over an extraordinarily wide dynamic range (at least 5 log units). This is coupled to extreme sensitivity, allowing the detection of less than five copies (perhaps only one copy in some cases) of a target sequence, making it possible to analyze small samples like clinical biopsies or miniscule lysates from laser capture microdissection. With appropriate internal standards and calculations, mean variation coefficients are 1–2%, allowing reproducible analysis of subtle gene expression changes even at low levels of expression (Klein 2002; Luu-The, Paquet et al. 2005). In addition, all real-time platforms are relatively quick, with some affording high-throughput automation. Finally, real-time PCR is performed in a closed reaction vessel that requires no post-PCR manipulations, thereby minimizing the chances for cross contamination in the laboratory (Valasek and Repa 2005).

7. Limitations of real-time PCR quantitation

There are several limitations to real-time PCR methods. The majority of these are present in all PCR or RT-PCR-based techniques. Real-time PCR is susceptible to PCR inhibition bycompounds present in certain biological samples. For example, clinical and forensic uses for real-timePCR may be affected by inhibitors found in certain body fluidssuch as hemoglobin or urea (Wilson 1997). Food microbiological applications may encounter organic and phenolic inhibitors (Wilson 1997). To circumvent this problem, alternative DNA polymerases (e.g., Tfl, Pwo, Tth, etc.) that are resistant to particular inhibitors can be used. Other limitations primarily concern real-time PCR- based analysis of gene expression

(Bustin 2000; Bustin 2002;Bustin and Nolan 2004). Because of the necessary use of RNA in an extra enzymatic step, more problems have the opportunity to occur. RNA itself is extremely labile compared with DNA, and therefore isolation must be carefully performed to ensure both the integrity of the RNA itself and the removal of contaminating nucleases, genomic DNA, and RT or PCR inhibitors. This can be a problem with any sample source, but clinical samples are of special concern because inconsistencies in sample size, collection, storage, and transport can lead to a variable quality of RNA templates. Conversion of RNA to cDNA during the RT reaction is also subject to variability because multiple reverse transcriptase enzymes with different characteristics exist, and different classes of oligonucleotides (e.g., random, poly-dT, or gene specific primers) can be used to prime RT (Valasek and Repa 2005). Probably the largest present limitation of real-time PCR, however, is not inherent in the technology but rather resides in human error: improper assay development, incorrect data analysis, or unwarranted conclusions. In our experience using real-time PCR for gene expression analysis, real-time PCR primer sets must be designed and validated by stringent criteria to ensure specificity and accuracy of the results. For microbiology, false positives or negatives must be considered when designing an assay to detect pathogens. Amplification and melting curves must be visually inspected while independent calculations based on these curves should be double-checked for accuracy. Real-time PCR gene expression analysis measures mRNA levels and, therefore, only suggests possible changes in protein levels or function rather than demonstrating them. And although there is a tight connection between gene expression and gene product function (Brown and Botstein 1999)(8), this is certainly not always the case, and formal demonstration may be needed for a given research project. Of course, conclusions based on data derived from real-time PCR are best utilized when the biological context is well understood (Bustin 2002).

8. Types of real-time quantification

1. Absolute Quantitation

Absolute quantitation uses serially diluted standards of known concentrations to generate a standard curve. The standard curve produces a linear relationship between Ct and initial amounts of total RNA or cDNA, allowing the determination of the concentration of unknowns based on their Ct values (Heid, Stevens et al. 1996). This method assumes all standards and samples have approximately equal amplification efficiencies (Souaze, Ntodou-Thome et al. 1996). In addition, the concentration of serial dilutions should encompass the levels in the experimental samples and stay within the range of accurately quantifiable and detectable levels specific for both the real-time PCR machine and assay.The PCR standard is a fragment of double-stranded DNA (dsDNA), single-stranded DNA (ssDNA), or cRNA bearing the target sequence (Wong and Medrano 2005). A simple protocol for constructing a cRNA standard for one-step PCR can be found in Fronhoffs et al. (Fronhoffs, Totzke et al. 2002), while a DNA standard for two-step real-time PCR can be synthesized by cloning the target sequence into a plasmid (Gerard, Olsson et al. 1998), purifying a conventional PCR product (Liss 2002), or directly synthesizing the target nucleic acid. The standard used must be a pure species. DNA standards have been shown to have a larger quantification range and greater sensitivity, reproducibility, and stability than RNA standards (Pfaffl, Tichopad et al. 2004). However, a DNA standard cannot be used for a one-step real-time RT-PCR due to the absence of a control for the reverse transcription efficiency (Giulietti, Overbergh et al. 2001).

2. Relative quantitation

During relative quantitation, changes in sample gene expression are measured based on either an external standard or a reference sample, also known as a calibrator (Livak and Schmittgen 2001). When using a calibrator, the results are expressed as a target/reference ratio. There are numerous mathematical models available to calculate the mean normalized gene expression from relative quantitationassays. Depending onthe method employed, these can yield different results and thus discrepant measures of standard error (Liu and Saint 2002; Muller, Janovjak et al. 2002). Table 1 shows a comparison of the different methods, with an explanation of each method to follow (Wong and Medrano 2005).

9. Quantitative analyses

For quantitative analysis, the amplification curves are evaluated. The amplification process is monitored either through the fluorescence of dsDNA-specific dyes (like SYBR Green I) or ofsequence-specific probes. Each curve consists of at least three distinct phases: 1) an initial lag phase in which no product accumulation can be measured, 2) an exponential phase, and 3) a plateau phase (Wilhelm and Pingoud 2003). The exponential phase in principle could be extrapolated to the start of the reaction (Cycle 0) to calculate the template copy number, but the error would be too high. The template copy number can be estimated with greater precision from the number of cycles needed for the signal to reach an arbitrary threshold. The threshold must intersect the signal curve in its exponential phase, in which the signal increase correlates with product accumulation. The intersection point is the so-called threshold value (C_T) or crossing point (C_P). This point may be between two successive cycles (i.e. it may be a fractional number). For exact quantifications, the efficiency of the amplification reaction must be known. It is crucial that the amplification efficiencies of standards and unknowns are identical (Wilhelm and Pingoud 2003). The efficiency can be estimated from the C_T values of samples with known template concentrations ('standards') as described below (Wilhelm and Pingoud 2003).

During the exponential phase, the signal *S*can be described by Equation 1:

$$S = pN_0\varepsilon^c \tag{1}$$

where*p*is a proportionality factor to relate PCR product concentration and signal intensity, $N_0$is the amount of template, $\varepsilon$is the amplification efficiency ($1 \le \varepsilon \le 2$; $\varepsilon = 2$ means 100% efficiency) and *c*is the cycle number.

Solving for c results in Equation 2:

$$c = -(\log\varepsilon)^{-1}(\log N_0 + \log p - \log S) \tag{2}$$

With $m = -(\log\varepsilon)^{-1}$ and $b = -(\log\varepsilon)^{-1}(\log p - \log S)$, Equation 2 simplifies to Equation 3:

$$c = m\log N_0 + b \tag{3}$$

This equation describes the linear relationship between the $C_T$values determined and the log of the template concentration (N_0). The parameters *m*and *b*can be determined by a regression analysis of the C_T values of the standards. When solved for N_0, this equation serves as a calibration curve for the calculation of the unknowns according to Equation 4:

$$N_0 = 10^{(C_T - b)/m} \tag{4}$$

Methods (Reference)	Amplification Efficiency Correction	Amplification Efficiency Calculation	Amplification Efficiency Assumptions	Automated Excel-Based Program
Standard Curve (31)	no	standard curve	no experimental sample variation	no
Comparative C_t ($2^{-\Delta\Delta Ct}$) (21)	yes	standard curve	reference = target	no
Pfaffl et al. (26)	yes	standard curve	sample = control	REST[a]
Q-Gene (23)	yes	standard curve	sample = control	Q-Gene[b]
Gentle et al. (7)	yes	raw data	researcher defines log-linear phase	no
Liu and Saint (22)	yes	raw data	reference and target genes can have different efficiencies	no
DART-PCR (30)	yes	raw data	statistically defined log-linear phase	DART-PCR[c]

C_t, cycle threshold, DART-PCR, data analysis for real-time PCR; REST, relative expression software tool.

[a]www.gene-quantification.info
[b]www.BioTechniques.com
[c]nar.oupjournals.org/cgi/content/full/31/14/e73/DC1

Table 1. Characteristics of Relative Quantitation Methods

Detection Chemistries	Specificity	Multiplex Capability	Specific Oligonucleotide Required	Allelic Discrimination	Cost
DNA Binding Dyes	two PCR primers	No	No	No	$
Hybridization Probe Four Oligonucleotide Method	two PCR primers; two specific probes	Yes	Yes	Yes	$$$
Hybridization Probe Three Oligonucleotide Method	two PCR primers; one specific probe	Yes	Yes	Yes	$$$
Hydrolysis Probes	two PCR primers; one specific probe	Yes	Yes	Yes	$$$
Molecular Beacons	two PCR primers; one specific probe	Yes	Yes	Yes	$$$
Scorpions	one PCR primer; one primer/probe	Yes	Yes	Yes	$$$
Sunrise Primers	two PCR primers	Yes	Yes	Yes	$$$
LUX Primers	two PCR primers	Yes	Yes	No	$$

$$$, very expensive; $$, moderately expensive; $, inexpensive. LUX, light upon extension.

Table 2. Characteristics of Detection Chemistries

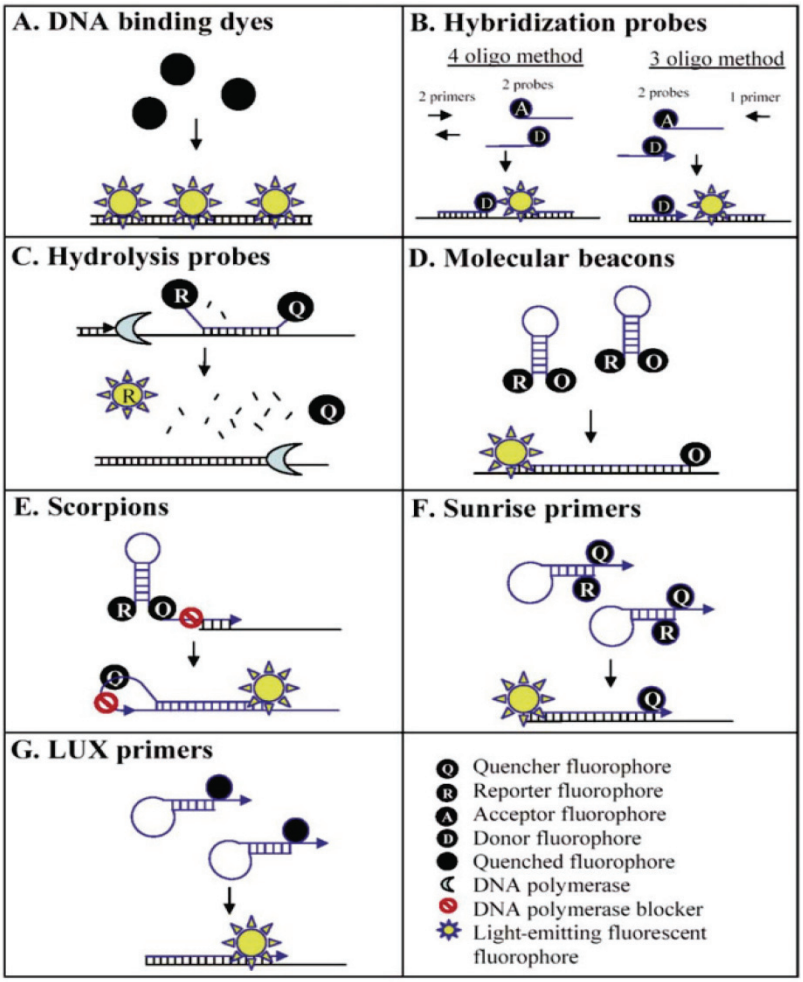


Fig. 1. Real-time PCR detection chemistries. Probe sequences are shown in blue while target DNA sequences are shown in black. Primers are indicated by horizontal arrowheads. Not all unlabeled PCR primers are shown. Oligo, oligonucleotide.

The efficiency can be calculated from the parameter m by using Equation 5:

$$\varepsilon = 10^{-1/m} \tag{5}$$

By inserting ε back into Equation 4, one obtains Equation 6:

$$N_0 = \varepsilon^{(b-C_T)} \tag{6}$$

The maximum value for ε is 2.0 (i.e. the amount of product is doubled in each cycle). The experimental value for ε usually varies between 1.5 and 1.9. Lower efficiencies limit the sensitivity of the assay but allow quantifications with higher precisions. Therefore, reactions

should be optimized for high efficiency. The effect of the efficiency on the precision, however, is not pronounced.

With more than six orders of magnitude, the dynamic range of this procedure is extraordinarily high (Marcucci, Livak et al. 1998; Verhagen, Willemse et al. 2000;Sails, Fox et al. 2003). The accuracy of this technique is limited by the precision of the determination of the C_T values. The error of the C_T values results from the signal noise and the C_T calculation method. In highly optimized assays, standard errors of less than ± 0.2 cycles can be achieved. By assuming an amplification efficiency of 2 (i.e. 100 %), this implies that the minimum relative error for the quantification is about 10- 20%. The effects of different analysis and calculation methods and the effects of amplification-independent signal trends on the accuracy and precision of quantifications by realtime PCR are described in detail in papers by Lui et al. and Wilhelm et al (Liu and Saint 2002; Wilhelm, Pingoud et al. 2003).

Quantification is relative to the standard used. Only when the absolute concentration of the template molecules in the standard sample is known can the results be absolute. However, in most cases, determination of absolute concentrations is not required. That real-time PCR allows absolute quantification is demonstrated in principle by the reported determination of genome sizes (Wilhelm, Pingoud et al. 2003).

All quantifications by PCR are relative, either to a standard or to a reference gene. Interestingly, Equation 6 nicely illustrates the relative character of the quantifications using a dilution series of a standard; the meaning of the parameter b is the expected C_T value of a sample with 'one' copy (or any other unit as defined by the operator). The difference of this value minus the C_T value determined for the unknown sample ($\Delta C_T = b - C_T$) is a direct measure for the relative difference in template concentrations of the unknown and standard (Wilhelm and Pingoud 2003).

To analyse relative changes in transcript levels, the chosen standard is usually a reference transcript, for example from a housekeeping gene, itself with unknown template concentration. The calculation of ΔC_T values between reference and sample transcript in a reference and a test sample then provides a simple tool to estimate relative changes. The derivation, assumptions and applications of the so-called $2^{\Delta\Delta CT}$ method are described elsewhere by Livak et al (Livak and Schmittgen 2001). The results of this method are only semiquantitative because the efficiency ε is assumed to be 2.0 in all experiments and for all templates, which is at best an optimistic estimate. More precise results are obtained with a procedure introduced by Pfaffl et al., which includes a measured value for ε (Pfaffl 2001; Wilhelm and Pingoud 2003).

In general, care must also be taken for accurate quantifications with external standardization, especially with respect to polymerase inhibitors, which may be present in differentconcentrations in the unknowns and standards. This problem is circumvented by internal standardization. Here, an analytically distinguishable standard template ('competitor') is added to the sample and co-amplified in the same reaction (Gilliland, Perrin et al. 1990; Goerke, Bayer et al. 2001). The direct and simultaneous quantitative analysis of both products in realtime PCR also poses problems. These difficulties are mostly due to the fact that different fluorophors have to be used to distinguish the sequences of competitor and sample. As a result of different FRET and quantum efficiencies, the C_T values obtained for competitor and sample are not directly comparable.

The problem of where to set the threshold makes relativequantifications difficult if not impossible. However, a simple trickcan be used to combine the advantages of both methods: thereaction mixtures are prepared in duplicate (Gibson, Heid et al. 1996). To one of thesemixtures, the probe specific for the competitor sequence isadded, whereas the probe specific for the sample sequence isadded to the other mixture. This process is carried out for a seriesof reactions with different amounts of competitor added. Withthis procedure, two calibration lines are obtained and theintersection of the two lines is the equivalence point (Wilhelm and Pingoud 2003).

10. Melting curve analyses

Melting curves represent the temperature dependence of the fluorescence. They are recorded subsequent to the amplification of the target sequence by PCR. The detection can be performed either with dsDNA-specific dyes like SYBR Green I or with sequence-specific probes such as the molecular beacons and the hybridisation probes (scorpion and sunrise primers cannot be used for melting curve analysis because they are integrated into the PCR products; TaqMan probes cannot be used for melting curve analyses either, since their signal generation depends on the hydrolysis of the probe). Melting curves of sequence-specific probes are used for genotyping, resolving single base mismatches between target sequence and probe (Lay and Wittwer 1997; Whitcombe, Brownie et al. 1998), whereas SYBR Green I is used most frequently for product characterization (Ririe, Rasmussen et al. 1997). It has been reported that melting curves measured with SYBR Green I can also be utilized for genotyping of insertion/deletion polymorphisms and of single nucleotide polymorphisms (SNPs) (Akey, Sosnoski et al. 2001; Lin, Tseng et al. 2001).

In melting curves, the signal decreases gradually as a result of a temperature-dependent quench and more abruptly at a certain temperature because of the melting of the products

(dsDNA or ssDNA/probe hybrid). The melting temperature (T_m) of a product is defined as the temperature at which the steepest decrease of signal occurs. This can be identified conveniently as the peak value(s) (global or local maxima) in the negative derivative of the melting curve. Additionally, the area under the curve (AUC) of the peaks is proportional to the amount of product. Therefore, melting curve analysis may be used for quantifications with internal standardization when the T_m values of sample and competitor products are significantly different (Al-Robaiy, Rupf et al. 2001). However, well-performed normalization is required to reduce the systematic error due to the temperature dependent quench. This quench also limits the sensitivity of melting curve analyses. At present, there is only one software package available that can remove the quench effects from the data (Wilhelm, Pingoud et al. 2003).

With SYBR Green I, the amplification of the correct target sequence can be confirmed. In most cases, nonspecific products have different lengths and therefore deviating melting temperatures (Ririe, Rasmussen et al. 1997).Hybridisation probes, molecular beacons and TaqMan probes are used for mutation detection (Lay and Wittwer 1997; Bernard, Ajioka et al. 1998; Bernard and Wittwer 2000), genotyping (Whitcombe, Brownie et al. 1998; Ulvik and Ueland 2001; Grant, Steinlicht et al. 2002; Randen, Sørensen et al. 2003) and SNP screening (Sasvari-Szekely, Gerstner et al. 2000; Mhlanga and Malmberg 2001).

11. Applications

Real-time PCR is used for absolute and relative quantifications of DNA and RNA template molecules and for genotyping in a variety of applications (Wilhelm and Pingoud 2003).

Quantitative real-time PCR is used to determine viral loads (Mackay, Arden et al. 2002),gene expression (Bustin 2000; Goerke, Bayer et al. 2001), titers of germs and contaminations (infood, blood, other body fluids and tissues) (Locatelli, Urso et al. 2000; Hernandez, Rio et al. 2001; Norton 2002), allele imbalances (Ruiz-Ponte, Loidi et al. 2000) and the degrees of amplification and deletion ofgenes (Chiang, Wei et al. 1999; Nigro, Takahashi et al. 2001).

Real-time PCR is also becoming increasingly important in thediagnosis of tumors, such as for the detection and monitoringof minimal residual diseases (Marcucci, Livak et al. 1998; Elmaagacli, Beelen et al. 2000; Amabile, Giannini et al. 2001; Krauter, Heil et al. 2001; Krauter, Hoellge et al. 2001), the identification of micrometastases in colorectal cancer (Bustin, Gyselman et al. 1999), neuroblastoma (Cheung and Cheung 2001) and prostate cancer (Gelmini, Tricarico et al. 2001). It has been used to quantify amplifications of oncogenes (Bieche, Laurendeau et al. 1999; Lehmann, Glöckner et al. 2000; Lyon, Millson et al. 2001; Konigshoff, Wilhelm et al. 2003) as well as deletions of tumor suppressor genes in tumor samples (Wilhelm and Pingoud 2003). Also, the response of human cancer to drugs has been studied (Au, Chim et al. 2002; Miyoshi, Ando et al. 2002;Reimer, Koczan et al. 2002). Other clinically relevant applications are cytokine mRNA profiling in immune response (Hempel, Smith et al. 2002; Stordeur, Poulin et al. 2002) and tissue-specific gene expression analysis (Bustin 2002; Poola 2003; Prieto-Alamo, Cabrera-Luque et al. 2003).

Also, the results of DNA chip experiments are validated by real-time PCR quantifications (Miyazato, Ueno et al. 2001; Rickman, Bobek et al. 2001;Crnogorac-Jurcevic, Efthimiou et al. 2002).

Chimerism analysis is possible when sequence-specific probes are utilized to differentiate and quantify alleles. High dynamic ranges can be achieved with allele-specific real-time PCR (Shively, Chang et al. 2003). Robust chimerism analyses with extremely large dynamic ranges based on insertion/deletion polymorphisms and on SNPs are also possible (Wilhelm, Reuter et al. 2002; Maas, Schaap et al. 2003). Genetic chimerisms have been monitored by Y-chromosome-specific real-time PCR for sex-mismatched transplantations (Fehse, Chukhlovin et al. 2001; Byrne, Huang et al. 2002; Elmaagacli 2002) and by allele-specific real-time PCR (Maas, Schaap et al. 2003; Shively, Chang et al. 2003). This combination of allele-specific amplification with real-time PCR has been shown to reveal detection limits of down to 0.01% for SNPs (Maas, Schaap et al. 2003). Real-time PCR is increasingly used in forensic analyses (Andreasson, Gyllensten et al. 2002; von Wurmb-Schwark, Higuchi et al. 2002; Ye, Parra et al. 2002), but also to monitor disease- or age-related accumulation of deletions in the mitochondrial genome (Mehmet, Ahmed et al. 2001; He, Chinnery et al. 2002).

Melting curve analyses are used for real-time competitive PCR (Al-Robaiy, Rupf et al. 2001; Lyon, Millson et al. 2001), gene dosage tests (Ruiz-Ponte, Loidi et al. 2000) and genotyping and SNP detection (Bullock, Bruns et al. 2002; Burian, Grosch et al. 2002; Randen, Sørensen et al. 2003). These applications will have a particularly strong impact on pharmacogenetics (Palladino, Kay et al. 2003). Profiling of DNA methylation is also possible by melting curve

analysis (Worm, Aggerholm et al. 2001; Akey, Akey et al. 2002), which simplifies the analysis of epigenetic variations of the genome and developmental processes.

In brief, the advantages of real-time PCR are exploited in clinical diagnosis and the monitoring of infectious diseases and tumors. The technique is applied for the analysis of age dependent diseases, cytokine and tissue-specific expression, forensic samples, epigenetic factors like DNA methylation and for food monitoring. The field of applications is still growing rapidly, which suggests that real-time PCR will become one of the most important techniques in molecular life sciences and medicine (Wilhelm and Pingoud 2003).

12. Normalization

Gene expression analysis at the messenger RNA (mRNA) level has become increasingly important in biological research. Generally we detect RNAs to determine if differences protein expression could be explained at the transcriptional level. In particular, measurement of mRNA is needed in situations where quantification of the protein is difficult or cumbersome. Most recently, mRNA expression analysis is being used to provide insight into complex regulatory networks and to identify genes relevant to new biological processes or implicated in diseases (Hendriks-Balk, Michel et al. 2007).Common methods for RNA detection include: Northern blotting, in situ hybridization, qualitative RTPCR, RNase protection assay, competitive RT-PCR, microarray analysis, and quantitative real-time PCR. The specificity, wide dynamic range , ease-of-use , requiring a minimal amount of RNA, no post-PCR handling and avoiding the use of radioactivity, has made the real-time quantitative reverse transcription polymerase chain reaction (qRT-PCR) the method of choice for quantitating RNA levels (Radonic, Thulke et al. 2004). The technique has two main steps: CDNA synthesis by reverse transcription of mRNA and subsequent quantification of specific CDNAs by real-time PCR. It is in many cases the only method for measuring mRNA levels of vivo low copy number targets of interest for which alternative assays either do not exist or lack the required sensitivity so these specification has led to made it the "gold standard" for mRNA quantification (Huggett, Dheda et al. 2005). Most gene expression assays are based on the comparison of two or more samples and require uniform sampling conditions for this comparison to be valid. Unfortunately, many factors can contribute to variability in the analysis of samples, making the results difficult to reproduce between experiments. During the preparation of CDNA for real-time PCR analysis there is significant potential for small errors to accumulate. For example, differences in sample size, RNA extraction efficiency, pippetting accuracy and reverse transcription efficiency will all add variability to your samples (Huggett, Dheda et al. 2005). Not only can the quantity and quality of RNA extracted from multiple samples vary, but even replicates can vary dramatically due to factors such as sample degradation, extraction efficiency, and contamination. On the other hand, since many biological samples contain inhibitors of the RT and/or the PCR step, it is crucial to assess the presence of any inhibitors of polymerase activity in RT and PCR. so it is clear that we need to incorporate some normalization method to control for errors. The identification of a valid reference for data normalisation remains the most stubborn of problems and none of the solutions proposed are ideal. Normalization methods range from ensuring that a similar sample size is chosen to using an internal housekeeping or reference gene (Table 3) (Huggett, Dheda et al. 2005).

Normalisation strategy	*Pros*	*Cons*	*Note*
Similar sample size/tissue volume	Relatively easy	Sample size/tissue volume may be difficult to estimate and/or may not be biological representative	Simple first step to reduce experimental error
Total RNA	Ensures similar reverse transcriptase input. May provide information on the integrity (depending on technique used)	Does not control for error introduced at the reverse transcription or PCR stages. Assumes no variation in rRNA/mRNA ratio	Requires a good method of assessing quality and quantity
Genomic DNA	Give an idea of the cellular sample size.	May vary in copy number per cell. Difficult to extract with RNA	Rarely used. Can be measured optically or by real time PCR
Reference genes ribosomal RNAs (rRNA)	Internal control that is subject to the same conditions as the RNA of interest. Also measured by real time RT-PCR	Must be validated using the same experimental samples. Resolution of assay is defined by the error of the reference gene	Oligo dt priming of RNA for reverse transcription will not work well with rRNA as no polyA tail is present. Usually in high abundance
Reference genes messenger RNAs (mRNA)	Internal control that is subject to the same conditions as the mRNA of interest. Also measured by real time RT-PCR	Must be validated using the same experimental samples. Resolution of assay is defined by the error of the reference gene	Most, but not all, of mRNAs contain polyA tails and can be primed with oligo dt for reverse transcription
Alien molecules	Internal control that is subject to most of the conditions as the mRNA of interest. Is without the biological variability of a reference gene	Must be identified and cloned or synthesised. Unlike the RNA of interest, is not extracted from the within the cells	Requires more characterisation and to be made available commercially

There is good correlation between the RNA concentration used and the real time PCR estimation of the different amounts of HuPO cDNA (using omniscript reverse transcriptase).

(Huggett, Dheda et al. 2005)

Table 3. Comparison of the actual amount of RNA used in different reverse transcription reactions with the respective amount of HuPO

Comparison of the actual amount of RNA used in different reverse transcription reactions with the respective amount of HuPO

cDNA measured by real-time RT-PCR

12.1 Methods of normalization

1. Standardizing Sample size

The most basic method of normalization ensures that an experiment compares similar sample sizes and this is achieved by measuring tissue weight, volume or cell number. This method can reduce the experimental error of first stage of qRT-PCR. It seems to be straightforward, but we can't ensure that equal volume of different samples contain the same cellular material. Real-time RT-PCR experiments that rely on the extraction of RNA from complex tissue samples are averaging the data from numerous, variable subpopulations of cells of different lineage at different stages of differentiation (Bustin, Benes et al. 2005). This can be misleading, as is illustrated when sampling a similar volume of blood from HIV +ve patients. Patients with HIV that have less advanced immunosupression (CD4 counts X200 cells/ml) will yield a higher amount RNA than patients with CD4 counts p200 cells/ml. This is simply because there are fewer cells per

milliliter of blood in the latter group. Even cellular subpopulations of the same pathological origin can be highly heterogeneous. Tumor biopsies, in particular, are made up not just of normal and cancer epithelial cells, but there may be several subclones of epithelial cancer cells together with stromal, immune and vascular components (Vandesompele, De Preter et al. 2002; Bustin, Benes et al. 2005). This variability can give us misleading or meaningless result to solve this we can use laser capture microdissection to normalize against the dissected area which can report the target mRNA levels conveniently as copies per area or cell dissected. In in vitro cell culture, due to different morphologies or clumping up of cells, it's hard to determine sample size (cell number) .we can treat them with buffers and/or enzymes till they could be counted, however these treatments surely could affect gene expression. This approach could not be applied for solid tumors for which the amount of cells cannot be determined accurately. To work around this problem, it was suggested to standardize the RT-qPCR data between samples using the amount of genomic DNA as an indicator reflecting the number of cells in each sample. However, these approaches do not account for the degradation of RNA or the efficiency of RT and PCR. So, while ensuring a similar sample size is important it clearly is not sufficient on its own (Huggett, Dheda et al. 2005).

2. Normalization with genomic DNA

Another method for normalization is measuring the amount of genomic DNA (gDNA). This appears to be an ideal method as it does not require reverse transcription for detection by real-time PCR (Bustin 2002). However, this approach do not account for the degradation of RNA or the efficiency of RT and PCR. .Moreover, in the case of normalization with genomic DNA, the fact of working with tumor cells can present additional problems because they tend to have abnormal karyotype. Therefore, the ratio between the amount of DNA and cell number is variable (Huggett, Dheda et al. 2005). Another major problem with using this strategy is that RNA extraction procedures are usually not designed to purify DNA, so the extraction rate may vary between different samples, with DNA yields often being low. In conclude Normalization against genomic DNA is rarely used since it is difficult to coextract with RNA and it may vary in copy number per cell (Huggett, Dheda et al. 2005).

3. Normalization with total RNA

The normalization of RT-qPCR results can be compared to the amount of total RNA used in the reverse transcription step. Not only does this facilitates normalization but circumvents problems associated with the linearity of the reverse transcriptase step. There are several methods for quantifying RNA; the most common is to measure the absorbance at 260 nm (A_{260}) with a UV spectrophotometer. The major advantage of this spectrometer, whose sensitivity is estimated at 5 ng/uL, is that it requires only 1 microL of sample, placed in direct contact with the optical system (Huggett, Dheda et al. 2005; Hendriks-Balk, Michel et al. 2007). However, contaminants absorbing at 260 nm, such as proteins, phenol or genomic DNA, can lead to overestimated results. Another optical system is flourimetry in which intercalating fluorescent nucleic acid is used, the kit RiboGreen ® Molecular Probes based on this principle. This is a more sensitive technique but does not discriminate RNA from DNA, and contaminants such as phenol can produce variable results (Huggett, Dheda et al. 2005). Since it is generally assumed that OD260 analysis is less accurate than the RiboGreen assay, we have compared RNA quantification data obtained using the RiboGreen assay with

OD260 analysis using a Genequant II (Pharmacia). The results (Fig. 2) suggest that both methods generate comparable results when the RNA concentration is not less than 100 ng/µl, with RiboGreen measurements lower than those obtained using the spectrophotometer. OD260 analysis becomes less reliable at lower RNA concentrations (Bustin 2002).

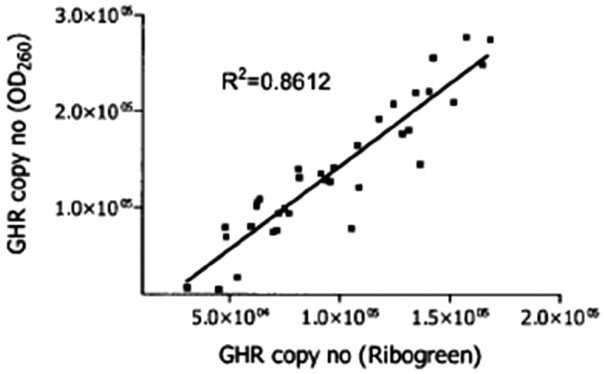


Fig. 2. Comparison of RNA quantification using the Genequant II and the RiboGreen fluorescent assay. RNA from 34 normal colon biopsies was quantitated using a standard Genequant II protocol which measures the absorbance at 260 nm. The same samples were then quantitated using a standard RiboGreen fluorescent assay. RT-PCR assays targeting the GHR were carried out and Ct normalised against the respective concentrations determined by the two methods. The scatterplot shows a good correlation between the two methods (*r*2=0·8612) (Bustin 2002).

What is also important, but often overlooked, is the need to assess the quality of RNA because degraded RNAs may adversely affect results. The opportune development of Agilent's 2100 Bioanalyser and LabChip technology has provided a new standard of RNA quality control as well as permitting concomitant quantification of RNA. The analysis is not influenced by contamination of phenol or proteins, against the presence of genomic DNA requires a correction of the measurement of the concentration of RNA (Bustin, Benes et al. 2005). This is particularly important when the RNA has been extracted from 'dirty' tissue such as the colon (Vandesompele, De Preter et al. 2002). This technique allows characterizing the RNA in a concentration between 5 and 500 ng/uL. For each sample, the software determines the ratio 28S/18S and assigns a RIN (RNA Integrity Number) which takes into account the entire electropherogram. The value of RIN ranges from 1 to 10, with 1 being totally degraded RNA, and 10 to a high-quality RNA. In addition to being fast and allow high throughput, this technique requires only 1 microL of sample. It is the simplest method and objective qualitative analysis of RNA, its use is recommended (Schmittgen and Zakrajsek 2000; Bustin 2002). Similar in concept, but requiring an additional RT-PCR assay, is normalization against one of the rRNAs. rRNA levels may vary less under conditions that affect the expression of mRNAs and the use of rRNA has been claimed to be more reliable than that of several reference genes in rat livers and human skin fibroblasts (Bustin 2002; Huggett, Dheda et al. 2005). But, a drawback is that it primarily measures ribosomal RNA (rRNA) whereas real-time PCR aims to determine mRNA expression and normalization for

total RNA assumes that the rRNA:mRNA ratio is the same in all groups, which might not always be the case. Moreover, rRNA is not present in purified mRNA and the high abundance of rRNA compared to mRNA makes it difficult to subtract the baseline value in realtime PCR analysis. Thus, markers of rRNA such as 18S or 28S rRNA might also be suboptimal as normalization factors in many settings (Hendriks-Balk, Michel et al. 2007). Also, it has been reported that rRNA transcription is affected by biological factors and drugs. An important parameter to consider when normalized relative to the RNA is the quality of it. Differences in the quality of the samples strongly depend on the extraction step and are the source of the most common variations in RT-qPCR. It is therefore important to use the same method of extraction for all samples analyzed (Vandesompele, De Preter et al. 2002). The quality of RNA is defined by both its purity (no contamination) and integrity (non-degraded RNA). Its purity was determined by measuring the absorbance at 230 (organic contaminants) and 280 nm (specific proteins), RNA is considered pure ratios A_{260}/A_{230} and $A_{260} / A_{280} > 1.8$. With regard to the integrity, the traditional method was to visualize the bands of 28S and 18S ribosomal RNA on a gel electrophoresis. Indeed, it is difficult to analyze directly the mRNA; they represent only 1% to 3% of total RNA. We must therefore consider that the degradation of ribosomal RNA, the majority, reflecting the degradation of mRNA. Thus, the 18S/28S ratio assesses the integrity of RNA; a ratio close to 2 is considered an indicator of RNA with little or no gradient. However, this method requires a large amount of RNA (0.5-2 mg), and is not sensitive enough to detect slight damage. Normalizing a sample against total RNA has the drawback of not controlling for variation inherent in the reverse transcription or PCR reactions and it ignores the efficiency of converting RNA into CDNA. Also rRNA cannot be used for normalization when quantifying targets from polyA-enriched samples (Huggett, Dheda et al. 2005). A final drawback when using total RNA for normalization is the lack of internal control for RT or PCR inhibitors. All quantitative methods assume that the RNA targets are reverse transcribed and subsequently amplified with similar efficiency but the reaction is extremely sensitive to the presence of inhibitors, which can be reagents used in the extraction step (salts, alcohols, phenols), or components copurification organic (urea, heme, heparin, immunoglobulin G). These compounds can also inhibit the PCR reaction. Thus, two reactions with an equal amount of RNA, but the efficiencies of RT and / or PCR are different, will yield results that cannot be compared. Different methods exist to assess the presence of inhibitors in biological samples. First, it is possible to compare the efficacy of PCR for different dilutions (1/20 and 1/80 for example) of a sample. An alternative is to add a defined amount of a synthetic single-stranded amplicon CDNA samples, and comparing its amplification compared to a control without CDNA. However, these methods are limited to verify the absence of PCR inhibitors, and do not evaluate the effectiveness of the reverse transcription step (Bustin 2002).

4. Normalization with an artificial molecule (spike)

An interesting solution to control the two enzymatic reactions (RT and PCR) is added to RNA extracted an exogenous RNA, which will compare the amplification between the different samples. This sequence control should show no similarity to the target RNA, we will use such a specific mRNA from a plant when studying gene expression in humans. The main criticism of using spikes is that, while they can be introduced prior to extraction, unlike the cellular RNAs they are not extracted from within the tissue. Consequently, there

may be situations (e.g. if the samples differ histologically) when the spike may not be a good control for the extraction procedure. The stages required to generate the alien molecule may also not be feasible for small laboratories wanting to perform limited amounts of real-time RTPCR (Schmittgen and Zakrajsek 2000; Argyropoulos, Psallida et al. 2006).

5. Normalization with reference genes

Reference genes represent the by far most common method for normalizing qRT-PCR data. Reference genes are often referred to as housekeeping genes assuming that those genes are expressed at a constant level in various tissues at all stages of development and are unaffected by the experimental treatment (Hendriks-Balk, Michel et al. 2007; Balogh, Paragh et al. 2008). Use of this endogenous control theory allows controlling all stages of the experimental protocol; its expression reflects not only the quantity and quality of RNA used, but the efficiencies of the RT and PCR. An advantage of reference genes as compared to total or rRNA is that the reference gene is subject to the same conditions as the mRNA of interest (Hendriks-Balk, Michel et al. 2007). The most commonly used reference genes include β-actin (ACTB), (GAPDH), (HPRT) and 18S rRNA. The other commonly used reference genes would be PGK1, B2M, GAPD, HMBS, HPRT1, RPL13A, SDHA, TBP, UBC and YWHAZ (Vandesompele, De Preter et al. 2002). The initial concentration of a target is usually derived from the C_T (cycle threshold), which is the number of amplification cycles where the amplification curve crosses the threshold line. This line is placed at the exponential phase, so as to be clearly distinguishable from background noise. For each sample, the C_T obtained for the genes of interest and reference must be converted to normalized expression ratio. For this, various options are available, they are integrated in the software provided with the various qPCR instruments or described in the literature. The relative standard curve method requires the construction, for the target gene and reference gene, a range made from a series of dilutions of a reference sample. These ranges to obtain standard curves, obtained by expressing the C_T as a function of log of the initial concentration of cDNA. Concentration values for each point of the range can be set arbitrarily in accordance with the dilution factors. Therefore, the relative amount of a target is determined by the C_T by interpolation with the standard curve. The standard expression of a gene of interest is determined by the following formula:

$$R = \frac{Relative\ amount\ of\ the\ gene\ of\ intrest}{Relative\ amount\ of\ the\ refrence\ gene}$$

In addition, a calibrator is typically used. This is a sample used as a basis for comparing results. The normalized ratio of each sample is divided by the normalized ratio of the calibrator. Thus, the calibrator becomes the reference 1x, and all other samples are expressed as a ratio relative to the calibrator. The method of $\Delta\Delta C_T$ uses a mathematical formule to calculate the ratio of expression of a target gene between two samples, normalized with reference gene. First, the differences ΔC_T between the values of C_T target gene and reference gene were determined for the test sample and control.

$$\Delta C_{T\,(sample)} = C_T \text{ (target sample)} - C_T \text{ (reference sample)}$$

$$\Delta C_{t\,(control)} = C_T \text{ (target control)} - C_T \text{ (reference control)}$$

Next, the $\Delta\Delta C_T$ between control and the sample is calculated:

$$\Delta\Delta C_T \Delta C_{T\,(\text{control})} - \Delta C_{T\,(\text{sample})}$$

Finally, the normalized ratio of expression of a target gene is determined by the formula: $2^{-\Delta\Delta CT}$.

Unlike the relative standard curve method, where the amplification efficiency (E) target genes and reference is directly taken into account when building ranges, the method of $\Delta\Delta C_T$ is assumed that the efficiencies of the two genes are equal to 100% (E = 2, with each cycle of the exponential phase, the concentration of PCR products is doubled). However, a difference in PCR efficiency of 3% ($\Delta E = 0.03$) between the two genes results in an error of 47% for the ratio of expression if $E_{target} < E_{ref}$ and 209% if $E_{target} > E_{ref}$ after 25 cycles. In addition, the error increases exponentially with larger variations of efficiency and a greater number of cycles. New models have been developed taking into account the efficiency of PCR target gene and reference gene. The most common is the model of Pfaffl, where the relative expression ratio (R) of a target gene between a sample and control is determined by the following formula:

$$R = \frac{(E_{\text{target}})^{\Delta C\,T\text{target}(\text{control}\,-\text{sample})}}{(E_{\text{reference}})^{\Delta C\,T\text{reference}(\text{control}\,-\text{sample})}}$$

In this model of Pfaffl, the efficiency of PCR for a given gene is calculated from the construction of a calibration curve using the following formula: $E = 10^{[-1/\ \text{gradient}]}$. This method gives a good estimate of effectiveness, although it is possible that it is overestimated. However, this approach assumes that the amplification efficiencies between the diluted samples are identical, creating a linear relationship between C_T and amount of CDNA in the beginning. Therefore, some authors such as Liu and Saint have developed models that take into account standards of efficiency for each sample, the latter being determined by the kinetics of the amplification curve. However, with this kind of approach, the slightest error in the measurement of effectiveness is amplified and passed exponentially on the expression ratio calculated. The different models of normalization with reference genes therefore have all the advantages and disadvantages. At present, there is no time-honored method for the treatment of the results of RT-qPCR. Normalization to a reference gene is a simple method and frequently used because it can control many variables. An advantage of reference genes as compared to total or rRNA is that the reference gene is subject to the same conditions as the mRNA of interest (Bustin, Benes et al. 2005; Hendriks-Balk, Michel et al. 2007). What has become apparent over recent years is that there is no single reference gene for all experimental systems. Quantified errors related to the use of a single reference gene as more than three-fold in 25% and more than six-fold in 10% of samples. Today it is clear that reference genes must be carefully validated for each experimental situation and those new experimental conditions or different tissue samples require re-validation of the chosen reference genes (Balogh, Paragh et al. 2008). If inappropriate reference genes are used for normalization, the experimental results obtained can differ greatly from those using a validated reference gene. Validation of a reference gene requires removal of any non-specific variation in expression. This can be done using a

recently introduced program called geNorm (freely available at http://medgen.ugent.be/~jvdesomp/genorm/) that mathematically identifies the most suitable reference gene for a given experimental condition. Because of the inherent variation in the expression of reference genes the use of multiple reference genes rather than one reference gene is recommended to ensure reliable normalization of real-time PCR. Several statistical programs can help to determine the most appropriate reference gene or set of genes (Hendriks-Balk, Michel et al. 2007; Borges, Ferreira et al. 2010).

13. Abbreviation

ACTB: Beta actin
B2M: Beta-2-microglobulin
C_T: Threshold Cycle
FRET: Fluorescence Resonance Energy Transfer
GAPD: Glyceraldehyde-3- phosphate dehydrogenase
HMBS: Hydroxymethyl-bilane synthase
HPRT: hypoxanthine ribosyltransferase
HPRT1: Hypoxanthine phosphoribosyl-transferase 1
HRM: High Resolution Melting
KPCR: Kinetic Polymerase Chain Reaction
LNA: Locked Nucleic Acid
LUX: Light Upon Extension
PCR: Polymerase Chain Reaction
PGK1: phosphoglycerokinase 1
PNA: Peptide Nucleic Acid
Q-PCR (QRT-PCR): Quantitative Real-Time Polymerase Chain Reaction
RPL13A: Ribosomal protein L13a
RT PCR: Reverse transcription PCR
SDHA: Succinate dehydrogenase complex, subunit A
TBP: TATA box binding protein
T_m: Melting Point
UBC: Ubiquitin C
YWHAZ: Tyrosine 3-monooxygenase/ tryptophan 5-monooxygenase activation protein, zeta polypeptide

14. References

Ahmad, A. I. (2007). "BOXTO as a real-time thermal cycling reporter dye." *Journal of Biosciences*32(2): 229-239.

Akey, D. T., J. M. Akey, et al. (2002). "Assaying DNA methylation based on high-throughput melting curve approaches." *Genomics*80(4): 376-384.

Akey, J., D. Sosnoski, et al. (2001). "Research Report Melting Curve Analysis of SNPs (McSNP®): A Gel-Free and Inexpensive Approach for SNP Genotyping." *Biotechniques*30(2): 358-367.

Al-Robaiy, S., S. Rupf, et al. (2001). "Research Report Rapid Competitive PCR Using Melting Curve Analysis for DNA Quantification." *Biotechniques*31(6): 1382-1388.

Amabile, M., B. Giannini, et al. (2001). "Real-time quantification of different types of bcr-abl transcript in chronic myeloid leukemia." *Haematologica*86(3): 252-259.

Andreasson, H., U. Gyllensten, et al. (2002). "Real-time DNA quantification of nuclear and mitochondrial DNA in forensic analysis." *Biotechniques*33(2): 402-411.

Au, W. Y., C. S. Chim, et al. (2002). "Real-time quantification of multidrug resistance-1 gene expression in relapsed acute promyelocytic leukemia treated with arsenic trioxide." *Haematologica*87(10): 1109-1111.

Ausubel, F. M., R. Brent, et al. (2005). "Current Protocols in Molecular Biology." *Hoboken, NJ: Wiley*.

Bengtsson, M., H. J. Karlsson, et al. (2003). "A new minor groove binding asymmetric cyanine reporter dye for real-time PCR." *Nucleic Acids Res*31(8): e45.

Bernard, P. S., R. S. Ajioka, et al. (1998). "Homogeneous multiplex genotyping of hemochromatosis mutations with fluorescent hybridization probes." *The American journal of pathology*153(4): 1055-1061.

Bernard, P. S. and C. T. Wittwer (2000). "Homogeneous amplification and variant detection by fluorescent hybridization probes." *Clinical chemistry*46(2): 147-148.

Bieche, I., I. Laurendeau, et al. (1999). "Quantitation of MYC gene expression in sporadic breast tumors with a real-time reverse transcription-PCR assay." *Cancer Res*59(12): 2759-2765.

Bio-Rad Laboratories, I. n. c. (2006). "Real-Time PCR Applications Guide."

BioInformatics (2003). "The Market for Real-Time PCR Reagents & Instrumentation." *Arlington VA: BioInformatics*.

Bonnet, G., S. Tyagi, et al. (1999). "Thermodynamic basis of the enhanced specificity of structured DNA probes." *Proc Natl Acad Sci*USA 96(5): 6171-6176.

Braasch, D. A. and D. R. Corey (2001). "Locked nucleic acid (LNA): fine-tuning the recognition of DNA and RNA." *Chem Biol*8(1): 1-7.

Brown, P. O. and D. Botstein (1999). "Exploring the new world of the genome with DNA microarrays." *Nat Genet*21: 33-37.

Bullock, G. C., D. E. Bruns, et al. (2002). "Hepatitis C genotype determination by melting curve analysis with a single set of fluorescence resonance energy transfer probes." *Clinical chemistry*48(12): 2147-2154.

Burian, M., S. Grosch, et al. (2002). "Validation of a new fluorogenic real-time PCR assay for detection of CYP2C9 allelic variants and CYP2C9 allelic distribution in a German population." *Br J Clin Pharmaco*l54(5): 518-521.

Bustin, S., V. Gyselman, et al. (1999). "Detection of cytokeratins 19/20 and guanylyl cyclase C in peripheral blood of colorectal cancer patients." *British Journal of Cancer*79(11/12): 1813-1820.

Bustin, S. A. (2000). "Absolute quantification of mRNA using real-time reverse transcription polymerase chain reaction assays." *J Mol Endocrinol* 25: 169-193.

Bustin, S. A. (2002). "Quantification of mRNA using real-time reverse transcription PCR (RT-PCR): trends and problems." *J Mol Endocrinol*29(1): 23-39.

Bustin, S. A. and T. Nolan (2004). "Pitfalls of quantitative real-time reverse-trasncription polymerase chain reaction." *J Biomol Tech*15: 155-166.

Byrne, P., W. Huang, et al. (2002). "Chimerism analysis in sex-mismatched murine transplantation using quantitative real-time PCR." *Biotechniques*32(2): 279-286.

Caplin, B. E., R. P. Rasmussen, et al. (1999). "LightCyclerTM hybridization probes- the most direct way to monitor PCR amplification and mutation detection." *Biochemica*1: 5-8.

Cheung, I. Y. and N. K. Cheung (2001). "Quantitation of marrow disease in neuroblastoma by real-time reverse transcription-PCR." *Clin Cancer Res*7(6): 1698-1705.

Chiang, P. W., W. L. Wei, et al. (1999). "A fluorescent quantitative PCR approach to map gene deletions in the Drosophila genome." *Genetics*153(3): 1313-1316.

Costa, J. M., P. Ernault, et al. (2004). "Chimeric LNA/DNA probes as a detection system for real-time PCR." *Clin Biochem*37(10): 930-932.

Crnogorac-Jurcevic, T., E. Efthimiou, et al. (2002). "Expression profiling of microdissected pancreatic adenocarcinomas." *Oncogene*21(29): 4587-4594.

Crockett, A. O. and C. T. Wittwer (2001). "Fluorescein-labeled oligonucleotides for real-time pcr: using the inherent quenching of deoxyguanosine nucleotides." *Anal Biochem*290(1): 89-97.

Egholm, M., O. Buchardt, et al. (1992). "Peptide nucleic acids (PNA). Oligonucleotide analogs with an achiral peptide backbone." *J Am Chem Soc*114: 1895-1897.

Elmaagacli, A., D. Beelen, et al. (2000). "The amount of BCR-ABL fusion transcripts detected by the real-time quantitative polymerase chain reaction method in patients with Philadelphia chromosome positive chronic myeloid leukemia correlates with the disease stage." *Annals of hematology*79(8): 424-431.

Elmaagacli, A. H. (2002). "Real-time PCR for monitoring minimal residual disease and chimerism in patients after allogeneic transplantation." *Int J Hematol*76 Suppl 2: 204-205.

Espy, M. J., J. R. Uhl, et al. (2006). "Real-time PCR in clinical microbiology: applications for routine laboratory testing." *Clin Microbiol Rev*19(1): 165-256.

Fehse, B., A. Chukhlovin, et al. (2001). "Real-time quantitative Y chromosome-specific PCR (QYCS-PCR) for monitoring hematopoietic chimerism after sex-mismatched allogeneic stem cell transplantation." *J Hematother Stem Cell Res*10(3): 419-425.

Fronhoffs, S., G. Totzke, et al. (2002). "A method for the rapid construction of cRNA standard curves in quantitative real-time reverse transcription polymerase chain reaction." *Molecular and cellular probes*16(2): 99-110.

Gelmini, S., C. Tricarico, et al. (2001). "Real-Time quantitative reverse transcriptase-polymerase chain reaction (RT-PCR) for the measurement of prostate-specific antigen mRNA in the peripheral blood of patients with prostate carcinoma using the taqman detection system." *Clin Chem Lab Med*39(5): 385-391.

Gerard, C. J., K. Olsson, et al. (1998). "Improved quantitation of minimal residual disease in multiple myeloma using real-time polymerase chain reaction and plasmid-DNA complementarity determining region III standards." *Cancer research*58(17): 3957-3964.

Gibson, U. E., C. A. Heid, et al. (1996). "A novel method for real time quantitative RT-PCR." *Genome Res*6(10): 995-1001.

Gilliland, G., S. Perrin, et al. (1990). "Analysis of cytokine mRNA and DNA: detection and quantitation by competitive polymerase chain reaction." *Proceedings of the National Academy of Sciences*87(7): 2725-2729.

Giulietti, A., L. Overbergh, et al. (2001). "An overview of real-time quantitative PCR: applications to quantify cytokine gene expression." *Methods*25(4): 386-401.

Goerke, C., M. G. Bayer, et al. (2001). "Quantification of bacterial transcripts during infection using competitive reverse transcription-PCR (RT-PCR) and LightCycler RT-PCR." *Clinical and Vaccine Immunology*8(2): 279-282.

Grant, S. F. A., S. Steinlicht, et al. (2002). "SNP genotyping on a genome-wide amplified DOP-PCR template." *Nucleic Acids Research*30(22): e125-e125.

He, L., P. F. Chinnery, et al. (2002). "Detection and quantification of mitochondrial DNA deletions in individual cells by real-time PCR." *Nucleic Acids Res*30(14): e68.

Heid, C. A., J. Stevens, et al. (1996). "Real time quantitative PCR." *Genome Res*6(10): 986-994.

Hempel, D. M., K. A. Smith, et al. (2002). "Analysis of cellular immune responses in the peripheral blood of mice using real-time RT-PCR." *J Immunol Methods*259(1-2): 129-138.

Hernandez, M., A. Rio, et al. (2001). "A rapeseed-specific gene, acetyl-CoA carboxylase, can be used as a reference for qualitative and real-time quantitative PCR detection of transgenes from mixed food samples." *J Agric Food Chem*49(8): 3622-3627.

Higuchi, R., G. Dollinger, et al. (1992). "Simultaneous amplification and detection of specific DNA sequences." *Biotechnology*10: 413-417.

Higuchi, R., C. Fockler, et al. (1993). "Kinetic PCR analysis: real-time monitoring of DNA amplification reactions." *Biotechnology (N Y)*11(9): 1026-1030.

Holland, P. M., R. D. Abramson, et al. (1991). "Detection of specific polymerase chain reaction product by utilizing the 5´ → 3´ exonuclease activity of Thermus aquaticus DNA polymerase." *Proc Natl Acad Sci*USA 88(16): 7276-7280.

Isacsson, J., H. Cao, et al. (2000). "Rapid and specific detection of PCR products using light-up probes." *Molecular and cellular probes*14(5): 321-328.

Jansen, K., B. Norde´n, et al. (1993). "Sequence dependence of 40,6-diamidino-2-phenylindole (DAPI)-DNA interactions." *J Am Chem Soc*115: 10527-10530.

Klein, D. (2002). "Quantification using real-time PCR technology: applications and limitations." *Trends Mol Med*8(6): 257-260.

Konigshoff, M., J. Wilhelm, et al. (2003). "HER-2/neu gene copy number quantified by real-time PCR: comparison of gene amplification, heterozygosity, and immunohistochemical status in breast cancer tissue." *Clin Chem*49(2): 219-229.

Krauter, J., G. Heil, et al. (2001). "The AML1/MTG8 Fusion Transcript in t (8; 21) Positive AML and its Implication for the Detection of Minimal Residual Disease; Malignancy." *Hematology (Amsterdam, Netherlands)*5(5): 369-381.

Krauter, J., W. Hoellge, et al. (2001). "Detection and quantification of CBFB/MYH11 fusion transcripts in patients with inv(16)-positive acute myeloblastic leukemia by real-time RT-PCR." *Genes Chromosomes Cancer*30(4): 342-348.

Kubista, M. (2004). "Nucleic acid-based technologies: application amplified." *Pharmacogenomics*5(6): 767-773.

Kubista, M., J. M. Andrade, et al. (2006). "The real-time polymerase chain reaction." *Molecular Aspects of Medicine*27 95-125.

Kurata, S., T. Kanagawa, et al. (2001). "Fluorescent quenching-based quantitative detection of specific DNA/RNA using a BODIPY® FL-labeled probe or primer." *Nucleic Acids Research*29(6): e34.

Kutyavin, I. V., I. A. Afonina, et al. (2000). "3´-Minor groove binder-DNA probes increase sequence specificity at PCR extension temperatures." *Nucleic Acids Res*28(2): 655-661.

Lay, M. J. and C. T. Wittwer (1997). "Real-time fluorescence genotyping of factor V Leiden during rapid-cycle PCR." *Clin Chem*43(12): 2262-2267.

Le Pecq, J. B. and C. Paoletti (1966). "A new fluorometric method for RNA and DNA determination." *Anal Biochem*17: 100-107.

Lehmann, U., S. Glöckner, et al. (2000). "Detection of gene amplification in archival breast cancer specimens by laser-assisted microdissection and quantitative real-time polymerase chain reaction." *Am J Pathol*156(6): 1855-1864.

Li, Qingge, et al. (2002). "A new class of homogeneous nucleic acid probes based on specific displacement hybridization." *Nucleic Acids Res*30: e5.

Lin, M. H., C. H. Tseng, et al. (2001). "Real-time PCR for rapid genotyping of angiotensin-converting enzyme insertion/deletion polymorphism1." *Clinical biochemistry*34(8): 661-666.

Lind, K., A. Stahlberg, et al. (2006). "Combining sequence-specific probes and DNA binding dyes in real-time PCR for specific nucleic acid quantification and melting curve analysis." *Biotechniques*40(3): 315-319.

Liss, B. (2002). "Improved quantitative real-time RT-PCR for expression profiling of individual cells." *Nucleic Acids Res*30(17): e89.

Liu, W. and D. A. Saint (2002). "A new quantitative method of real time reverse transcription polymerase chain reaction assay based on simulation of polymerase chain reaction kinetics." *Analytical Biochemistry*302(1): 52-59.

Liu, W. and D. A. Saint (2002). "Validation of a quantitative method for real time PCR kinetics." *Biochem Biophys Res Commun*294(2): 347-353.

Livak, K. J. and T. D. Schmittgen (2001). "Analysis of relative gene expression data using real-time quantitative PCR and the 2(-Delta Delta C(T)) Method." *Methods*25(4): 402-408.

Locatelli, G., V. Urso, et al. (2000). "Quantitative analysis of GMO food contaminations using real time PCR." *Ital J Biochem*49(3-4): 61-63.

Luu-The, V., N. Paquet, et al. (2005). "Improved real-time RT-PCR method for high-throughput measurements using second derivative calculation and double correction." *Biotechniques*38(2): 287-293.

Lyon, E., A. Millson, et al. (2001). "Quantification of HER2/neu gene amplification by competitive PCR using fluorescent melting curve analysis." *Clinical chemistry*47(5): 844-851.

Maas, F., N. Schaap, et al. (2003). "Quantification of donor and recipient hemopoietic cells by real-time PCR of single nucleotide polymorphisms." *Leukemia*17(3): 621-629.

Mackay, I. M. (2004). "Real-time PCR in the microbiology laboratory." *Clin Microbiol Infect*10(3): 190-212.

Mackay, I. M., K. E. Arden, et al. (2002). "Real-time PCR in virology." *Nucleic Acids Res*30(6): 1292-1305.

Mackya, I. M. (2004). "Real-time PCR in the microbiology laboratory." *Clin Microbiol Infect*10: 190-212.

Marcucci, G., K. Livak, et al. (1998). "Detection of minimal residual disease in patients with AML1/ETO-associated acute myeloid leukemia using a novel quantitative reverse transcription polymerase chain reaction assay." *Leukemia: official journal of the Leukemia Society of America, Leukemia Research Fund, UK*12(9): 1482-1489.

Mattarucchi, E., M. Marsoni, et al. (2005). "Different real time PCR approaches for the fine quantification of SNP's alleles in DNA pools: assays development, characterization and pre-validation." *J Biochem Mol Bio*l38(5): 555-562.

Mehmet, D., F. Ahmed, et al. (2001). "Quantification of the common deletion in human testicular mitochondrial DNA by competitive PCR assay using a chimaeric competitor." *Molecular human reproduction*7(3): 301-306.

Mhlanga, M. M. and L. Malmberg (2001). "Using molecular beacons to detect single-nucleotide polymorphisms with real-time PCR." *Methods*25(4): 463-471.

Miyazato, A., S. Ueno, et al. (2001). "Identification of myelodysplastic syndrome–specific genes by DNA microarray analysis with purified hematopoietic stem cell fraction." *Blood*98(2): 422-427.

Miyoshi, Y., A. Ando, et al. (2002). "Prediction of response to docetaxel by CYP3A4 mRNA expression in breast cancer tissues." *International Journal of Cancer*97(1): 129-132.

Muller, P. Y., H. Janovjak, et al. (2002). "Processing of gene expression data generated by quantitative real-time RT-PCR." *Biotechniques*32(6): 1372-1379.

Mullis, K. B. (1990). "The unusual origin of the polymerase chain reaction." *Sci Am*262: 56-61.

Mullis, K. B. and F. A. Faloona (1987). "Specific synthesis of DNA in vitro via a polymerase-catalyzed chain reaction." *Methods Enzymol*155: 335-350.

Myi, Q. "single-color real-time PCR instruction manual Biorad Company."

Nazarenko, I., B. Lowe, et al. (2002). "Multiplex quantitative PCR using self-quenched primers labelled with a single fluorophore." *Nucleic Acids Res*30(9): e37.

Nazarenko, I. A., S. Bhatnagar, et al. (1997). "A closed tube format for amplification and detection of DNA based on energy transfer." *Nucleic Acids Research*25(12): 2516-2521.

Nigro, J. M., M. A. Takahashi, et al. (2001). "Detection of 1p and 19q loss in oligodendroglioma by quantitative microsatellite analysis, a real-time quantitative polymerase chain reaction assay." *The American journal of pathology*158(4): 1253-1262.

Norton, D. M. (2002). "Polymerase chain reaction-based methods for detection of Listeria monocytogenes: toward real-time screening for food and environmental samples." *Journal of AOAC International*85(2): 505-515.

Nygren, J., N. Svanvik, et al. (1998). "The interaction between the fluorescent dye thiazole orange and DNA." *Biopolymers*46: 39-51.

Olson, M., L. Hood, et al. (1989). "A common language for physical mapping of the human genome." *Science*245: 1434-1435.

Palladino, S., I. D. Kay, et al. (2003). "Real-time PCR for the rapid detection of vanA and vanB genes." *Diagn Microbiol Infect Dis*45(1): 81-84.

Pfaffl, M. W. (2001). "A new mathematical model for relative quantification in real-time RT-PCR." *Nucleic Acids Res*29(9): e45.

Pfaffl, M. W., A. Tichopad, et al. (2004). "Determination of stable housekeeping genes, differentially regulated target genes and sample integrity: BestKeeper–Excel-based tool using pair-wise correlations." *Biotechnology letters*26(6): 509-515.

Poola, I. (2003). "Molecular assay to generate expression profile of eight estrogen receptor alpha isoform mRNA copy numbers in picogram amounts of total RNA from breast cancer tissues." *Analytical Biochemistry*314(2): 217-226.

Prieto-Alamo, M. J., J. M. Cabrera-Luque, et al. (2003). "Absolute quantitation of normal and ROS-induced patterns of gene expression: an in vivo real-time PCR study in mice." *Gene Expr*11(1): 23-34.

Randen, I., K. Sørensen, et al. (2003). "Rapid and reliable genotyping of human platelet antigen (HPA)-1,-2,-3,-4, and-5 a/b and Gov a/b by melting curve analysis." *Transfusion*43(4): 445-450.

Reimer, T., D. Koczan, et al. (2002). "Tumour Fas ligand: Fas ratio greater than 1 is an independent marker of relative resistance to tamoxifen therapy in hormone receptor positive breast cancer." *Breast Cancer Research*4(5): R9.

Reischl, U., C. T. Wittwer, et al. (2002). "Rapid Cycle Real-time PCR: Methods and Applications; Microbiology and Food Analysis." *New York: Springer-Verlag*.

Rickman, D. S., M. P. Bobek, et al. (2001). "Distinctive molecular profiles of high-grade and low-grade gliomas based on oligonucleotide microarray analysis." *Cancer research*61(18): 6885-6891.

Ririe, K. M., R. P. Rasmussen, et al. (1997). "Product differentiation by analysis of DNA melting curves during the polymerase chain reaction." *Anal Biochem*245(2): 154-160.

Ruiz-Ponte, C., L. Loidi, et al. (2000). "Rapid real-time fluorescent PCR gene dosage test for the diagnosis of DNA duplications and deletions." *Clin Chem*46(10): 1574-1582.

Saiki, R. K., S. Scharf, et al. (1985). "Enzymatic amplification of beta-globin genomic sequences and restriction site analysis for diagnosis of sickle cell anemia." *Science*230: 1350-1354.

Sails, A. D., A. J. Fox, et al. (2003). "A real-time PCR assay for the detection of Campylobacter jejuni in foods after enrichment culture." *Appl Environ Microbiol*69(3): 1383-1390.

Sasvari-Szekely, M., A. Gerstner, et al. (2000). "Rapid genotyping of factor V Leiden mutation using single-tube bidirectional allele-specific amplification and automated ultrathin-layer agarose gel electrophoresis." *Electrophoresis*21(4): 816-821.

Shively, L., L. Chang, et al. (2003). "Real-time PCR assay for quantitative mismatch detection." *Biotechniques*34(3): 498-502, 504.

Sjöback, R., J. Nygren, et al. (1995). "Absorption and fluorescence properties of fluorescein Spetrochim." *Acta Part*A 51: L7-L21.

Soheili, Z. and S. Samiei (2005). "Real Time PCR: Principles and Application." *Hepatitis*5(3): 83-87.

Solinas, A., L. J. Brown, et al. (2001). "Duplex Scorpion primers in SNP analysis and FRET applications." *Nucleic Acids Research*29(20): e96-e96.

Souaze, F., A. Ntodou-Thome, et al. (1996). "Quantitative RT-PCR: limits and accuracy." *Biotechniques*21(2): 280-285.

Stordeur, P., L. F. Poulin, et al. (2002). "Cytokine mRNA quantification by real-time PCR." *J Immunol Methods*259(1-2): 55-64.

Svanvik, N., A. Stahlberg, et al. (2000). "Detection of PCR products in real time using light-up probes." *Anal Biochem*287(1): 179-182.

Svanvik, N., G. Westman, et al. (2000). "Light-up probes: thiazole orange-conjugated peptide nucleic acid for detection of target nucleic acid in homogenous solution." *Anal Biochem*281: 26-35.

Thelwell, N., S. Millington, et al. (2000). "Mode of action and application of Scorpion primers to mutation detection." *Nucleic Acids Research*28(19): 3752-3761.

Tyagi, S., D. P. Bratu, et al. (1998). "Multicolor molecular beacons for allele discrimination." *Nat Biotechnol*16(1): 49-53.

Tyagi, S. and F. R. Kramer (1996). "Molecular Beacons: probes that fluorescence upon hybridization." *Nat Biotechnol*14(3): 303-308.

Uehara, H., G. Nardone, et al. (1999). "Detection of telomerase activity utilizing energy transfer primers: comparison with gel- and ELISA-based detection." *Biotechniques*26(3): 552-558.

Ulvik, A. and P. M. Ueland (2001). "Single nucleotide polymorphism (SNP) genotyping in unprocessed whole blood and serum by real-time PCR: application to SNPs affecting homocysteine and folate metabolism." *Clin Chem*47(11): 2050-2053.

Valasek, M. A. and J. J. Repa (2005). "The power of real-time PCR." *Adv Physiol Educ*29(3): 151-159.

Verhagen, O. J., M. J. Willemse, et al. (2000). "Application of germline IGH probes in real-time quantitative PCR for the detection of minimal residual disease in acute lymphoblastic leukemia." *Leukemia*14(8): 1426-1435.

von Wurmb-Schwark, N., R. Higuchi, et al. (2002). "Quantification of human mitochondrial DNA in a real time PCR." *Forensic Sci Int*126(1): 34-39.

Whitcombe, D., J. Brownie, et al. (1998). "A homogeneous fluorescence assay for PCR amplicons: its application to real-time, single-tube genotyping." *Clin Chem*44(5): 918-923.

Whitcombe, D., J. Theaker, et al. (1999). "Detection of PCR products using self-probing amplicons and fluorescence." *Nat Biotechnol*17(8): 804-807.

Wilhelm, J. and A. Pingoud (2003). "Real-time polymerase chain reaction." *Chembiochem*4(11): 1120-1128.

Wilhelm, J., A. Pingoud, et al. (2003). "Real-time PCR-based method for the estimation of genome sizes." *Nucleic Acids Res*31(10): e56.

Wilhelm, J., A. Pingoud, et al. (2003). "SoFAR: software for fully automatic evaluation of real-time PCR data." *Biotechniques*34(2): 324-332.

Wilhelm, J., H. Reuter, et al. (2002). "Detection and quantification of insertion/deletion variations by allele-specific real-time PCR: application for genotyping and chimerism analysis." *Biol Chem*383(9): 1423-1433.

Wilson, I. G. (1997). "Inhibition and facilitation of nucleic acid amplification." *Appl Environ Microbiol*63: 3741-3751.

Wilson, R. and M. K. Johansson (2003). "Photoluminescence and electrochemiluminescence of a Ru(II) (bpy)3- quencher dual-labeled oligonucleotide probe." *Chem Commun*21: 2710-2711.

Wittwer, C. T., M. G. Herrmann, et al. (2001). "Real-time multiplex PCR assays." *Methods*25(4): 430-442.

Wittwer, C. T., M. G. Herrmann, et al. (1997). "Continuous fluorescence monitoring of rapid cycle DNA amplification." *Biotechniques*22: 130-138.

Wong, M. L. and J. F. Medrano (2005). "Real-time PCR for mRNA quantitation." *Biotechniques*39(1): 75-85.

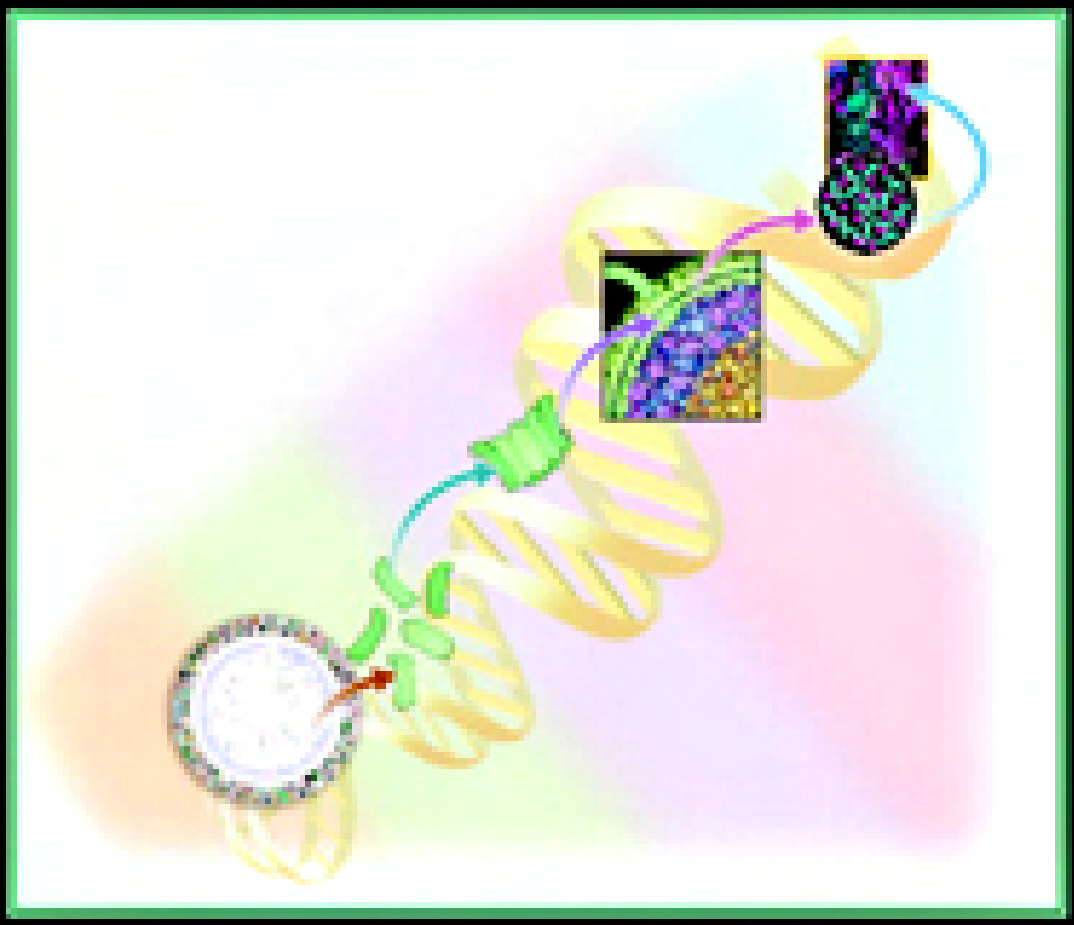
Worm, J., A. Aggerholm, et al. (2001). "In-tube DNA methylation profiling by fluorescence melting curve analysis." *Clinical chemistry*47(7): 1183 -1189.

Ye, J., E. J. Parra, et al. (2002). "Melting Curve SNP (McSNP) Genotying: a Useful Approach for Diallelic Genotyping in Forensic Science." *Journal of forensic sciences*47(3): 593-600.

Zipper, H., H. Brunner, et al. (2004). "Investigations on DNA intercalation and surface binding by SYBR Green I, its structure determination and methodological implications." *Nucleic Acids Res*32(12): e103.

View publication stats

Alexander N. Glazer • Hiroshi Nikaido



MICROBIAL BIOTECHNOLOGY

FUNDAMENTALS OF APPLIED MICROBIOLOGY

Second Edition

CAMBRIDGE www.cambridge.org/9780521842105

MICROBIAL BIOTECHNOLOGY

Fundamentals of Applied Microbiology, Second Edition

Alexander N. Glazer

University of California, Berkeley

Hiroshi Nikaido

University of California, Berkeley

CAMBRIDGE UNIVERSITY PRESS

CAMBRIDGE UNIVERSITY PRESS
Cambridge, New York, Melbourne, Madrid, Cape Town, Singapore, São Paulo

Cambridge University Press
The Edinburgh Building, Cambridge CB2 8RU, UK
Published in the United States of America by Cambridge University Press, New York
www.cambridge.org
Information on this title: www.cambridge.org/9780521842105

© Alexander N. Glazer and Hiroshi Nikaido 2007

This publication is in copyright. Subject to statutory exception and to the provision of relevant collective licensing agreements, no reproduction of any part may take place without the written permission of Cambridge University Press.

First published in print format 2007

ISBN-13 978-0-511-34136-6 eBook (EBL)
ISBN-10 0-511-34136-9 eBook (EBL)

ISBN-13 978-0-521-84210-5 hardback
ISBN-10 0-521-84210-7 hardback

Cambridge University Press has no responsibility for the persistence or accuracy of urls for external or third-party internet websites referred to in this publication, and does not guarantee that any content on such websites is, or will remain, accurate or appropriate.

NINE

Primary Metabolites: Organic Acids and Amino Acids

Microorganisms can function as efficient factories for the industrial scale production of the primary metabolites. Among these, ethanol will be discussed in Chapter 13. Other important primary metabolites currently produced by fermentation are listed in Table 9.1. Some organic acids and amino acids are seen to be the most important products in this category (excluding ethanol, of course).

CITRIC ACID

About 1 billion pounds of citric acid are produced worldwide (Table 9.1) by fermentation with the wild-type strains of a fungus, *Aspergillus niger*. Citric acid is used, for example, as a flavoring agent in food and drinks and to prevent oxidation and rancidity of fats and oils. In the very efficient fermentation process, up to 80% of the source sugar is converted into citric acid. Because this process, in operation since 1916, has been studied "probably more than any other process in mold metabolism," according to one review, and could serve as a model for primary metabolite fermentation processes including glutamate fermentation (discussed later), we will examine this process in some detail.

Citric acid, unlike ethanol, is not one of the typical waste products of energy metabolism, and is usually degraded completely into CO_2 and water through the operation of the citric acid cycle. Thus, the efficient conversion of sugars, such as glucose and sucrose, into citric acid by *A. niger* is rather unexpected, especially because mitochondria of *A. niger* contain all the enzymes of the citric acid cycle. The citric acid production occurs predominantly in the stationary phase, and indeed requires several unusual conditions. (1) The medium should be strongly acidic, with the pH value between 1.6 and 2.2. (2) The sugar concentration should be very high (120 to 250 g/L). (3) The medium should be deficient in Mn^{2+}. (4) The medium should contain a high concentration of NH_4^+ ions.

Extensive studies showed that under these conditions, glucose is fermented rapidly by the glycolytic pathway. Normally, the key controlling step,

TABLE 9.1 Estimated annual production of important primary metabolites of microorganisms worldwide

Metabolite	Production (tons)	Market value (million dollars)
AMINO ACIDS		
L-Glutamate	1,000,000	3000
L-Lysine	800,000	915
L-Threonine	20,000	100
L-Aspartate	13,000	198
L-Isoleucine	400	43
NUCLEOTIDES		
5′-IMP + 5′-GMP	2500	350
ORGANIC ACIDS		
Citric acid	400,000	1400
VITAMINS		
B_{12}	3	100
C[a]	60,000	71
Riboflavin	2000	60

[a] Partially synthetic.
IMP, inosine monophosphate; GMP, guanosine monophosphate.
Based mainly on Demain, A. L. (2000). Small bugs, big business: the economic power of the microbe. *Biotechnology Advances*, 18, 499–514.

phosphofructokinase (PFK1), would be inhibited by citrate, to which the glycolytic product, pyruvate, is converted. However, this citrate inhibition is abolished by the presence of high concentrations of NH_4^+. Furthermore, very high concentrations of sugars lead to the increased level of fructose-2,6-bisphosphate, the most powerful activator of PFK1. These factors presumably contribute to increased flux through the glycolytic pathway, culminating in the runaway production of pyruvate.

Some of the pyruvate molecules enter mitochondria and are converted into acetyl-CoA by the normal process catalyzed by pyruvate dehydrogenase. Acetyl-CoA then condenses with oxaloacetate to produce citrate. However, the flux is far higher than what can be handled by the rest of the citric acid cycle, especially because the isocitrate dehydrogenase is inhibited by glycerol, which is generated as a part of the hyperosmotic response (see Box 9.1) to the high concentration of sugars. Thus, citrate is exported out of mitochondria via citrate/malate antiporter, concomitantly with the influx of malate, which is converted to oxaloacetate for the next round of citrate synthesis. The remainder of the pyruvate molecules generated through glycolysis is converted into oxaloacetate by pyruvate carboxylase, which is located in the cytosol in this group of fungi. The cytosolic oxaloacetate is then reduced to malate by cytosolic malate dehydrogenase, and malate enters mitochondria as described above. The conversion of pyruvate to malate ensures the continuous operation of the glycolytic pathway, at least partially, by regenerating adenosine diphosphate (ADP) and NAD^+ from ATP and NADH, which were generated during the conversion of sugars to pyruvate.

Until recently, however, there was almost nothing known about one area of this proposed scheme. That is the exit of citrate from the cytosol into the medium. Citrate, with its three negative charges, cannot cross membranes spontaneously, and its export into the medium is likely to be catalyzed by a transporter protein. Furthermore, intracellular concentration of citrate is several millimolars, and the "uphill" export into the medium, which could contain more than 0.5 M of citrate, is likely to be catalyzed by an active,

Hyperosmotic and Hypoosmotic Responses of Microorganisms

The cytosolic osmolarity of microorganisms must be maintained slightly above that of the environment so that the cytoplasm does not collapse and a small turgor pressure is constantly applied to the rigid cell wall. Thus, a microbial cell is like a balloon in a small cage. When the environment becomes hyperosmotic, microorganisms must respond by increasing the solute concentration in the cytoplasm in order to maintain the small difference in osmolarity. Large increases in mineral salt concentration, however, are often deleterious to the proper function of proteins and organelles. Thus in such situations, they accumulate "compatible solutes," which are less toxic to proteins. They include proline, betaine, trehalose, and glycerol. When the environment suddenly becomes hypoosmotic, small cytosolic solutes are released into the medium through the opening of stretch-activated channels and the activation of other transporters. Amino acid exporters in *Corynebacterium glutamicum*, described later in this chapter, apparently play this role when large amounts of peptides are taken up and their hydrolysis in cytoplasm suddenly increases the osmolarity of cytoplasm.

BOX 9.1

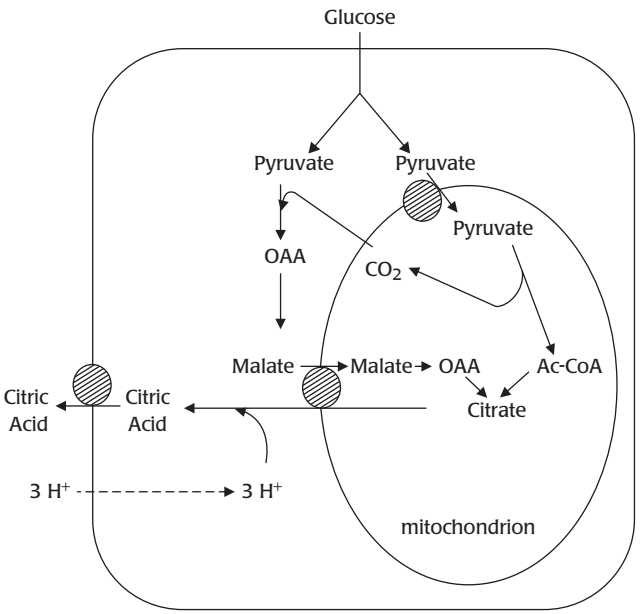


FIGURE 9.1

Metabolic pathways involved in the production of citric acid by *A. niger*. *Shaded circles* represent specific transport proteins. Thus, one of the pyruvate molecules generated from glucose via glycolysis enters the mitochondrion through the ubiquitous pyruvate/H^+ symporter and is converted into acetyl-CoA by pyruvate dehydrogenase. The other pyruvate molecule is converted into oxaloacetate (OAA) by the cytosolic pyruvate carboxylase. However, because there is no OAA transporter in the mitochondrion, OAA must be reduced to malate and then must enter the mitochondrion through a specific carrier, and OAA is regenerated inside the mitochondrion. The malate carrier is known to catalyze the exchange of malate with α-ketoglutarate, but in this case it may well catalyze the exchange of malate with citrate generated within the mitochondrion. Citric acid leaves the cell via a specific carrier. It seems plausible that the carrier catalyzes the export of the protonated citric acid, thereby preventing the acidification of the cytosol from the protons that have leaked into the cytosol from a highly acidic medium. However, this part of the pathway is still a speculation, and a possibility exists that citrate^{3-}, for example, is exported without using any energy input (see text).

energy-consuming process. Indeed, export of citrate from *A. niger* was shown in 1997 to be inhibited by sodium azide and a proton conductor, carbonyl cyanide (*m*-chlorophenyl)hydrazone (CCCP), a result consistent with the presence of an active exporter protein. (Interestingly, cultivation of *A. niger* in Mn^{2+}-poor medium was necessary to activate this process, and this may be the major reason for the inhibitory effect of Mn^{2+} for citrate production). If the export substrate is the protonated form, citric acid, perhaps its extrusion may decrease the proton concentration in the cytoplasm and thereby help the survival of *A. niger* in the strongly acidic environment, in which proton leakage from the medium will produce the acidification of the cytoplasm. In this speculative scheme (Figure 9.1), the production of citrate by this organism under strongly acidic conditions will therefore be a process that is physiologically significant. Alternatively, if the transporter catalyzes the flux of citrate^{3-}, the accumulation of citric acid in the medium can be explained as the result of conversion of most of citrate^{3-} into uncharged citric acid; this flux might be facilitated by the outside-positive membrane potential, if such a potential exists.

AMINO ACID: L-GLUTAMATE

OVERVIEW

The industrial production of an amino acid, L-glutamate, dates back to 1908, when the Japanese agricultural chemist K. Ikeda discovered that L-glutamate was responsible for the characteristic taste, much appreciated in Japan, of foods cooked with dried kelp (konbu). For the first 50 years, monosodium L-glutamate (MSG) was manufactured by expensive chemical processes, based

largely on the acid hydrolysis of proteins. This hydrolysis process was costly because glutamate had to be separated from all other amino acids in the hydrolyzate. Significant amounts of MSG were also made by chemical synthesis. This process was expensive too, because it produced a mixture of D- and L-glutamate that had to be resolved to eliminate the D-isomer, which is tasteless.

A revolutionary change was introduced in 1957, when scientists at Kyowa Hakko Co. discovered a soil bacterium that excreted large amounts of L-glutamate into the medium. Similar bacteria were soon isolated by several other companies, ushering in a new industrial technology: amino acid fermentation, the production of amino acids by microorganisms. Except for ethanol, some other organic solvents, and a few vitamins, glutamate was the first organic compound produced on an industrial scale by a microbial fermentation technique.

MSG is used as a flavor enhancer in very large amounts (Table 9.1). It was also the first amino acid to be produced by the fermentation process, using wild-type strains. Because amino acids are building blocks for the assembly of proteins, their biosynthesis is usually regulated tightly so that energy and carbon are not wasted for the synthesis of needless excesses of these compounds. Thus, the overproduction of glutamate by wild-type bacteria is surprising, and the mechanism, despite much study, is not yet totally clear.

MSG overproduction (or fermentation) requires *Corynebacterium glutamicum*. Various companies isolated glutamate-producing organisms named, for example, *Brevibacterium* and *Arthrobacter*, but it now appears that all these strains are close relatives of *C. glutamicum*. One striking observation made in the early days of development of glutamate fermentation technology was that all these strains were naturally auxotrophic for (requiring as growth factors) biotin, and the production of glutamate required starvation for biotin (Figure 9.2).

NEED FOR BIOTIN STARVATION

Why is biotin starvation necessary for the excretion of glutamic acid? The major function of biotin is to serve as a prosthetic group in acetyl-CoA carboxylase, the first enzyme of fatty acid synthesis, so it was hypothesized that the excretion might be related to an increased general permeability of the cell membrane, caused by an insufficiency of fatty acids. This notion appeared to be supported by the finding that other treatments affecting the integrity of the cell membrane – for example, adding to the medium a detergent, Tween 60, or a low concentration of β-lactam antibiotics (the latter treatment strains the cell membrane by weakening the peptidoglycan cell wall) or limiting the amount of exogenously fed oleic acid in unsaturated fatty acid auxotrophs – also led to glutamic acid production, even in the presence of excess biotin.

These observations were also of practical importance because they suggested ways to stimulate glutamic acid excretion while feeding the bacteria with inexpensive carbon sources (such as molasses) that happen to be rich

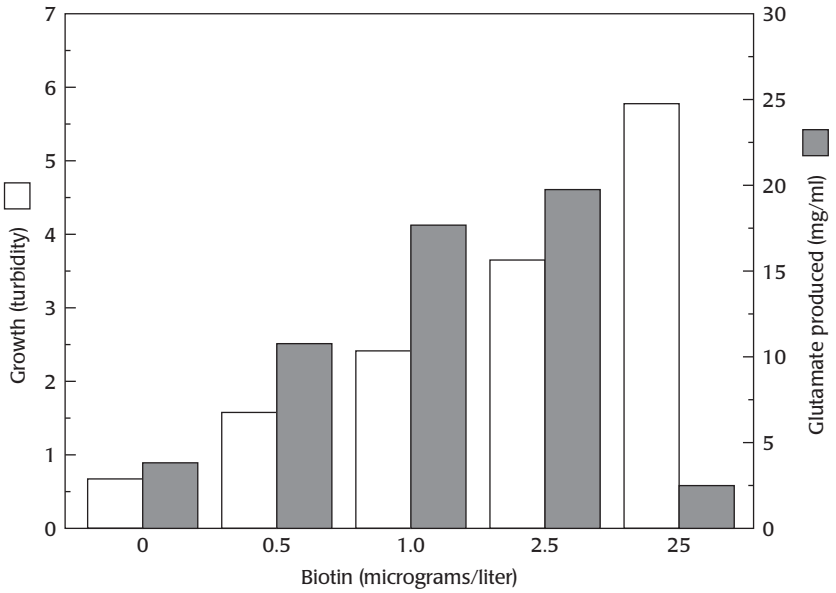


FIGURE 9.2

Influence of biotin concentration on the production of glutamic acid by *C. glutamicum*. Based on Tanaka, K., Iwasaki, T., and Kinoshita, S. (1960), Nihon Nogei Kagakukai Zasshi, 34, 593–600.

Redrawn based on artwork from the first edition (1995), published by W.H. Freeman.

in biotin. During the period when petroleum was inexpensive, petroleum hydrocarbons were also tried as a carbon source. When scientists found that unsaturated fatty acid auxotrophs do not produce glutamic acid when petroleum hydrocarbons are present (presumably because they are easily converted to unsaturated fatty acids by the organism), they tried an alternative way of weakening the cell membrane: They constructed conditional auxotrophs for glycerophosphate so that the synthesis of phospholipids from glycerophosphate became deficient under certain conditions. Such mutants also excreted glutamate when the supply of glycerophosphate became limiting.

The results described above seemed to support the hypothesis that a leaky cell membrane is responsible for the excretion of glutamic acid. Several important questions remained, however. Principally, how do the cells remain alive if the membrane becomes so leaky? In other words, what prevents the leakage of essential metabolites and ions? And why is this treatment needed only for the production of glutamic acid and not for that of other amino acids, described later in this chapter?

In the early 1990s, it was shown that *C. glutamicum* and its relatives produce specific exporters that function solely to excrete amino acids, such as lysine, that they also overproduce (see below). These "efflux transporters" are thought to be useful when the cytoplasm becomes flooded with amino acids, possibly as a consequence of the rapid uptake and intracellular hydrolysis of peptides from the medium. The intracellular glutamate concentration is unusually high among amino acids, around 200 mM, in contrast to those of other amino acids, which are usually around a few millimolars or less. The involvement of a specific glutamate efflux transporter presumably explains the export of only glutamate, if its activity is activated by alterations leading to the straining of the cell membrane. However, this glutamate exporter

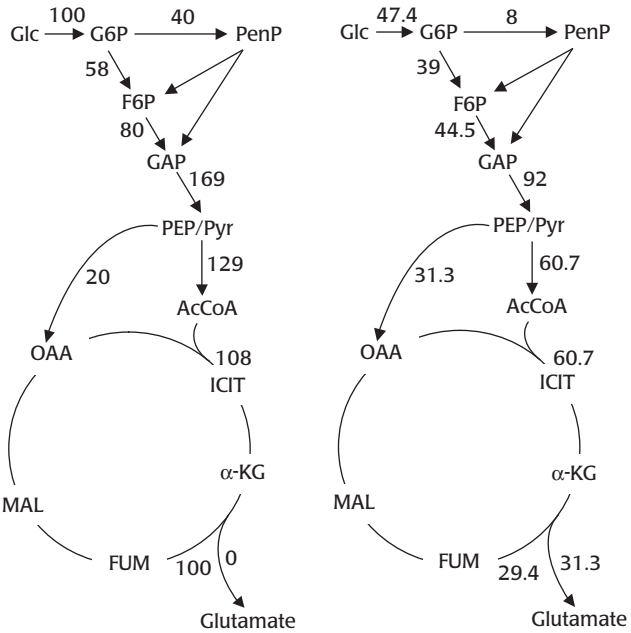


FIGURE 9.3

Carbon metabolism in *C. glutamicum*. In an older model, the citric acid cycle was thought to be truncated, with low or nonexistent α-ketoglutarate dehydrogenase activity. However, more recent studies in which metabolic balancing was combined with ^{13}C-NMR shows that the α-ketoglutarate dehydrogenase remains quite active. (**A**) Flux values in *C. glutamicum* growing in biotin-rich medium and therefore not excreting glutamate. (**B**) Flux values in *C. glutamicum* growing in biotin-limited medium and excreting glutamate into the medium. The net flux values (in molar units) are shown as percentages of the flux of glucose in non–glutamate-excreting cells, here taken as 100. In glutamate-excreting cells, the growth is slowed (the influx of glucose is less than half that seen in the exponentially growing cells), the contribution of the pentose phosphate pathway is minimized, the production of oxaloacetate from pyruvate/PEP is greatly increased, and about half the α-ketoglutarate is siphoned off as glutamate, producing a yield of 0.66 mole of glutamate per one mole of glucose taken up. At some steps, there are large bidirectional (exchange) fluxes, but they are not shown here for simplicity. In both cases, the contribution of the glyoxylate cycle was negligible. Abbreviations: G6P, glucose 6-phosphate; F6P, fructose 6-phosphate; PenP, pentose phosphate; GAP, glyceraldehyde 3-phosphate; PEP, phospho*enol*pyruvate; Pyr, pyruvate; AcCoA, acetyl-CoA; OAA, oxaloacetate; ICIT, isocitrate; α-KG, α-ketoglutarate, FUM, fumarate; MAL, malate. Flux values are based on Sonntag K., et al. (1995). *Applied Microbiology and Biotechnology*, 44, 489–495.

Redrawn based on artwork from the first edition (1995), published by W.H. Freeman.

still remains unidentified in spite of the knowledge of the complete genome sequence of *C. glutamicum*.

IS THE CITRIC ACID CYCLE TRUNCATED?

Another factor that was thought to be important in the early days of glutamate fermentation was the presence of a truncated citric acid cycle. It was felt that the secretion of very large amounts of glutamate must involve unusual features in metabolic pathways, which lead to its extensive accumulation. The metabolic precursor of glutamic acid is α-ketoglutaric acid, an intermediate in the citric acid cycle (Figure 9.3A). When the enzymes of the citric acid cycle were first examined, glutamic acid producers were reported to contain all the enzymes of the cycle except α-ketoglutarate dehydrogenase. More recently, α-ketoglutarate dehydrogenase was shown to be present. However, it is difficult to decide, from enzyme activities determined *in vitro*, how much substrate flux the enzyme is catalyzing in intact cells. In this connection, it is important that recent elucidation of detailed substrate flux (Box 9.2), determined by growing the organism with 1-^{13}C-glucose followed by the NMR-based determination of the labeling pattern of products, showed that the section of the cycle after the α-ketoglutarate dehydrogenase step had full activity in nonsecreting cells (Figure 9.3A), and even in glutamate-secreting cells it still had about half the activity of the flux of the section preceding α-ketoglutarate (Figure 9.3B); that is, the citric acid cycle is not truncated in *C. glutamicum*, and the change in the flow of substrates through the citric acid cycle, observed during glutamate secretion, may be a result, rather than the cause, of this process.

Metabolic Flux Analysis

Quantitative determination of metabolite flux through each step of the central metabolic pathway is essential in order to understand processes such as amino acid production and to design rational improvements for such processes (see Box 9.3). However, such a determination is difficult in intact cells. Earlier, activities of the enzymes and their kinetic properties, measured in cell extracts, were used to build models. However, often the enzymes are labile, and their activities measured *in vitro* have only a remote relation to the activities in intact cells. Another approach is Metabolic Control Analysis (MCA).[1] In this elegant mathematical approach, flux alterations caused by alterations in the amount of an enzyme are measured, and the determination of these "flux control coefficients" leads to the quantitative, dynamic model of the pathway. Because amplification of a gene is easily accomplished by cloning on plasmid vectors, this approach has been strongly advocated by some scientists. This method works when the segment of the pathway does not contain an enzyme that is regulated by the intermediate or product of the pathway. However, practically all important metabolic pathways contain such feedback-regulated enzymes, and in such cases, this approach fails, as shown by a simple computer simulation,[2] presumably because the mathematics involves the simple integration of partial derivatives. This problem has not been dealt with properly by the advocates of MCA, and the situation makes any MCA-derived models rather suspect.

The most reliable and useful models are generated, in the authors' view, by starting from Metabolite Balancing Analysis. Here one measures the consumption of the carbon and energy source – say, glucose – and the excretion and accumulation of products such as lactate, acetate, and amino acids in the proteins synthesized. One then tries to balance the uptake of glucose into the cell with the synthesis of all these products, using the knowledge of the central catabolic and anabolic pathways. However, presence of parallel pathways and bidirectional flow in many parts of metabolism make this simple analysis impossible. Thus, one combines the balancing analysis with the isotopic labeling patterns of various products by growing cells on, say, 1–^{13}C-glucose. For example, with regard to the parallel pathways, C-3 of pyruvate generated by glycolysis will be labeled with ^{13}C at the 50% level, but C-3 of pyruvate coming from the pentose phosphate pathway will contain no ^{13}C. The position and the degree of enrichment in ^{13}C can be determined by NMR or mass spectroscopy, and the patterns in isotopic labeling in various products can then be simulated by using a computer. The final result is a model with precise flux figures for each step of the metabolism.[3,4]

1 Fell D. (1997). *Understanding the Control of Metabolism*, London: Portland Press.

2 Atkinson, D. E. (1990). An experimentalist's view of control analysis. In *Control of Metabolic Processes*, A. Cornish-Bowden and M. L. Cárdenas (eds.), pp. 413–429, New York: Plenum Press.

3 Sahm H., Eggeling, L., and de Graaf, A. A. (2000). Pathway analysis and metabolic engineering in *Corynebacterium glutamicum*. *Biological Chemistry*, 381, 899–910.

4 Weigert, W. (2001). ^{13}C metabolic flux analysis. *Metabolic Engineering*, 3, 195–206.

BOX 9.2

In the simplest hypothesis, we may assume that the trigger of the whole process is the activation of the glutamate exporter by straining of the membrane. This will lower the cytosolic concentration of glutamate as discussed in the next section, shifting the steady-state fluxes around α-ketoglutarate in the citric acid cycle. When only insufficient amounts of oxaloacetate are generated at the end of the cycle because of the siphoning off of a large amount of α-ketoglutarate (Figure 9.3B), the replenishing (or anaplerotic) reactions, generating C4 compounds from C3 compounds (pyruvate and phospho*enol*pyruvate) become important. Indeed, the overproduction of pyruvate carboxylase, which catalyzes this reaction, was reported to improve the yield of glutamic acid.

Regardless of the nature of the trigger, glutamate fermentation results in the consumption of NADPH (generated by the isocitrate dehydrogenase step) by glutamate dehydrogenase (Figure 9.3A). In fact, glutamate fermentation is known to require oxygen but not very high concentrations of dissolved oxygen, which tend to favor the excretion of α-ketoglutarate rather than

Metabolic Engineering

Metabolic engineering means in a narrow sense the application of recombinant DNA methods in order to alter the flow of metabolites in the cell, usually in order to increase the yield of a desired end product or to produce a novel product. Such approaches often require knowledge of the carbon flow in the central metabolic pathway (see Box 9.2), especially when the synthesis of the product consumes a large fraction of the cellular resources.

BOX 9.3

glutamate. It is also obvious that the process demands high concentrations of NH_3. Oxygen tension and ammonia concentration are controlled precisely in the industrial process.

POSSIBLE PHYSIOLOGICAL ROLE OF THE GLUTAMATE PRODUCTION

Scientists used to assume that citric acid or glutamate fermentation occurred because of a complete block at relevant steps in general metabolism. Metabolic flux studies now show that such blocks are unlikely to exist and that massive excretion of primary metabolites may occur as a result of modest adjustments in the central metabolic pathway, as described already. This new knowledge of the immense flexibility of the major metabolic pathways is extremely important in the emerging field of metabolic engineering (see Box 9.3), which deals with the alterations of the fluxes of the major pathways, often required for the production of not only the usual primary metabolites but also novel products.

The processes leading to the production of primary metabolites, especially those involving fungi (such as citric acid fermentation), used to be – and sometimes still are – explained as "overflow metabolism." This is an old idea in which microbial cells are thought to consume excess carbon sources (the "overflow") when cell growth is limited by another nutrient – for example, by the paucity of divalent cations in the *A. niger* citric acid fermentation process. We now know, however, that catabolism is linked tightly to anabolism through many regulatory processes. Thus, the overproduction of metabolites is not simply an overflow phenomenon but must have physiological and ecological relevance. Such a physiological "purpose" of the glutamate excretion response is difficult to assess. However, *C. glutamicum* and its relatives, being natural biotin auxotrophs, are likely to become starved for biotin in their habitat, presumably soil. Blocked synthesis of membrane lipids will then cause mechanical strains in the cytoplasmic membrane because the intracellular osmotic pressure is usually much higher than the osmotic pressure of the extracellular medium. Perhaps the important point here is that the intracellular concentration of glutamate is about two, sometimes three, orders of magnitude higher than those of other amino acids. Efflux of glutamate, thus a major anionic component of the cytosol, can then be seen as a response designed to reduce the strain in the membrane by decreasing the osmotic pressure difference across the membrane (see Box 9.1). The realignment of metabolic fluxes caused by the excretion of glutamate and the decrease in growth rate will then lead to the characteristic flux pattern seen in Figure 9.3B. For *C. glutamicum*, in addition to relieving the membrane stress through the export of glutamate, the glutamate production process produces additional ATP through the oxidation of pyruvate to acetyl-CoA and in addition produces a much less acidic product (0.66 mole of glutamate per one mole of glucose) in comparison with pure fermentation (two moles of lactate per one mole of glucose), thus keeping the environment closer to the neutral pH.

The operation of the glutamate production system as a shifted yet balanced and interconnected central metabolic response is illustrated in the example of an ATP synthase mutant of *C. glutamicum*. In this strain that showed only 25% activity of ATP synthase (or H^+-ATPase), secretion of glutamic acid was totally abolished, when the biotin starvation conditions were moderate; instead, a large amount of lactic acid was excreted. It appears that with low ATP synthase activity, not enough ATP can be made from the NADH obtained in the altered flow through the citric acid cycle, so glycolysis (which generates ATP directly) becomes enhanced instead, resulting in the excretion of lactate.

It thus appears that *C. glutamicum* produces glutamate as a waste product of catabolism under a specific set of environmental conditions. This suggests that the enzyme responsible for the process, glutamate dehydrogenase, may not be regulated as tightly as are the obligatorily biosynthetic enzymes. Evidence that this is indeed the case is described below.

REGULATION OF THE ENZYMES INVOLVED IN GLUTAMATE SYNTHESIS

In most microorganisms, the major pathway for glutamate synthesis is the GS-GOGAT pathway:

(1) L-Glutamate + NH_3 + ATP → L-glutamine + ADP + P_i

(GS: glutamine synthetase)

(2) L-Glutamine + α-ketoglutarate + NADPH + H^+ → 2 L-glutamate + $NADP^+$

(GOGAT: glutamine oxoglutarate aminotransferase)

Sum (1) + (2):

α-ketoglutarate + NH_3 + ATP + NADPH + H^+ → L-glutamate + ADP + P_i + $NADP^+$.

Although this pathway consumes one ATP for every molecule of L-glutamate synthesized, it is preferred over the alternative pathway described below because it has a low Michaelis constant (K_m; much lower than 1 mM) for NH_3 and thus can efficiently utilize ammonia.

The second pathway is the glutamate dehydrogenase pathway:

α-Ketoglutarate + NH_3 + NAD(P)H + H^+ → L-glutamate + $NAD(P)^+$ + H_2O.

Because of the rather high K_m value (usually around 1 mM) for NH_3, this pathway becomes significant only when NH_3 concentrations are high. In most organisms, mutational inactivation of this enzyme does not make the mutants auxotrophic for glutamate, a finding that confirms the relatively minor role of this pathway for glutamate synthesis in most species. Because

the GS-GOGAT pathway is so much more important, its enzymes are strongly regulated, as is typical of obligatorily biosynthetic enzymes; on the other hand, regulation of the glutamate dehydrogenase activity tends to be rather loose.

In *C. glutamicum*, the regulation of glutamate dehydrogenase is exceptionally loose; 50% inhibition of the enzyme requires the addition of 0.2 M glutamate to the cell extract, whereas similar inhibition of *Alkaligenes eutrophus* glutamate dehydrogenase requires only 20 mM.

These considerations suggest that the overproduction of glutamic acid in *C. glutamicum* is the result of a fortuitous combination of several factors. Over evolutionary time, the organisms of this group have developed a peculiar combination of enzymes, presumably equipping them to deal with ecological conditions perhaps related to those described above. It appears that the fermentation conditions used in the laboratory and in industry are precisely those that led to stimulation of the synthesis, and excretion, of glutamic acid.

AMINO ACIDS OTHER THAN GLUTAMATE

NEED FOR AMINO ACIDS OTHER THAN GLUTAMATE

Glutamate, as we have seen, is used widely as a flavor enhancer. But other amino acids are also needed in large amounts worldwide. The most important use of some of these amino acids is as an additive to human food and animal feed. This is because humans and most higher animals cannot synthesize lysine, threonine, tryptophan, phenylalanine, isoleucine, leucine, valine, methionine, and histidine – the "essential amino acids" – but must obtain them from the proteins in their diet. However, the less expensive, more abundant sources of food proteins, the seeds of crop plants (the main source of proteins for humans, especially in developing countries), are rather deficient in some of the essential amino acids, particularly lysine, methionine, and tryptophan (Table 9.2). The demand for such amino acids is particularly high in growing children and young animals. Yet the lysine content in wheat flour and corn proteins is only 21% and 27%, respectively, of that in pork protein (Table 9.2). The nutritional value of these cereal proteins can be increased significantly if seeds can be fortified with the deficient amino acid. Lysine is now produced at the rate of about 800,000 tons/year by fermentation, and its production is increasing at the rate of almost 10% per year. Lysine is added to both human food and animal feed. Similarly, L-threonine is produced by fermentation at the rate of 20,000 tons/year, and used mainly as a feed additive. Nutritionists evaluate food proteins by calculating the ratio between the weight the animal gains and the weight of the protein it is fed: the *protein efficiency ratio (PER)*. Corn proteins, because of their low lysine and tryptophan content (see Table 9.2), have a low PER of 0.85, but this value can be increased about threefold, to 2.55, by adding 0.4% lysine and 0.07% tryptophan to corn.

TABLE 9.2 Levels of some essential amino acids in cereal and animal meat proteins[a]

	Cereal proteins			Meat proteins	
	Maize	Wheat flour	Sorghum	Beef	Pork
Lysine	167	130	126	556	625
Threonine	225	168	189	287	319
Tryptophan	44	67	76	70	85
Methionine	120	91	145	169	188

[a] Amino acid content is expressed as milligrams per gram of protein nitrogen.
Source: Food and Agriculture Organization of the United Nations (1970). *Amino-Acid Content of Foods and Biological Data on Proteins. FAO Nutritional Study No. 24,* Rome, Italy: FAO.

FERMENTATION WITH MUTANT STRAINS IS NEEDED FOR AMINO ACIDS OTHER THAN GLUTAMATE

Except glutamate, which is produced as an end product of an incomplete oxidation process in biotin-limited *C. glutamicum* as described above, other amino acids are end products of biosynthetic pathways. These amino acids are synthesized – at a net expense of energy – as building blocks of proteins. It is to the cells' advantage not to waste energy by producing more amino acids than they need. Consequently, amino acid production is usually effectively regulated.

Our understanding of such regulatory processes has come primarily through studies of *Escherichia coli*, which lives in the intestinal tract of higher vertebrates and thus leads a life of "feast or famine." It can predict neither the nature of the amino acids that will become available in its environment nor when they will arrive. Consequently, the regulatory mechanisms of *E. coli* are much more sophisticated than those of many soil microorganisms – for example, those whose environments are less complex and more stable.

In *E. coli*, the biosynthesis of most amino acids is regulated at two different levels: (1) by control of the *activity of preexisting enzymes*, and (2) by control of the *synthesis of new enzyme molecules*. The former governs the response of *E. coli* to the sudden appearance of amino acids in the environment. The biosynthesis of amino acids consumes a large amount of chemical energy. Thus, when a supply of exogenous amino acids becomes available, it is advantageous for the bacterium to shut down its own biosynthetic pathway and start utilizing the prefabricated amino acids. However, the cells already contain a full complement of the enzymes that participate in the formation of amino acids. Under these circumstances, the best response for the cell is to lower the activity of preexisting enzymes. This is usually achieved by *feedback inhibition*, a process in which an excess of end product, in this case an amino acid, inhibits the activity of the first enzyme of the biosynthetic pathway via an allosteric mechanism (Figure 9.4).

Feedback inhibition is an ideal mechanism for coping with rapid fluctuations in the supply of amino acids in the environment, but it is inefficient

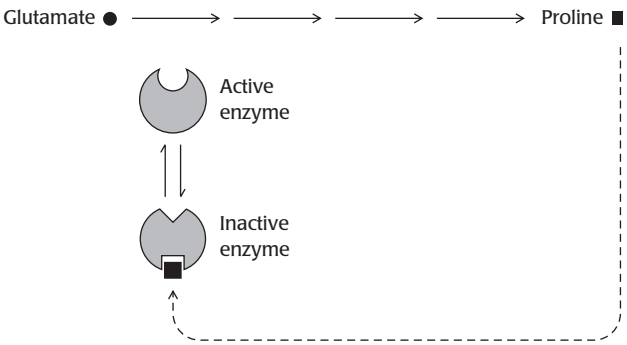


FIGURE 9.4

Regulation of proline biosynthesis by feedback inhibition. In this example, the biosynthesis of the amino acid proline is regulated by altering the activity of the first enzyme of the pathway, glutamate kinase. This enzyme is an allosteric enzyme, with a binding site for the substrate, glutamate, as well as a separate binding site for the inhibitor, proline. Whenever excess proline is present, it binds to the regulatory site of glutamate kinase, thereby converting the enzyme into an inactive form. This shuts down the endogenous proline synthesis instantaneously.

Redrawn based on artwork from the first edition (1995), published by W.H. Freeman.

for long-term adaptation. If a population of bacteria continues to live in an environment in which tryptophan, for example, is always available at high concentrations, it makes no sense for the bacteria to synthesize all the enzymes needed for tryptophan biosynthesis, using much energy in the process, and then to keep all of these enzymes from functioning by a system of feedback inhibition. It is much more economical to shut down the synthesis of the unneeded enzymes. Thus, regulation at the level of enzyme synthesis is also important, although it does not help the organism adjust to sudden changes in its environment.

Enzyme synthesis can be regulated by one of two mechanisms. In *repression*, the amino acid end product of the pathway binds to a specific repressor protein as a *corepressor*, altering its conformation. The unliganded repressor has no effect on enzyme synthesis, but the corepressor–repressor complex binds to an upstream sequence of the genes and operons coding for the biosynthesis of that particular amino acid, preventing transcription of the mRNA (Figure 9.5). *Attenuation*, the other mechanism, works by controlling the frequency of RNA chain termination during mRNA transcription. In this mechanism, the 5′-end of the mRNA can form one of the two alternative stem-loop (or hairpin) structures (Figure 9.6). When segments 3 and 4 form a hydrogen-bonded stem loop, that structure acts as a rho-independent termination signal for RNA polymerase (see Box 3.6), because its GC-rich stem

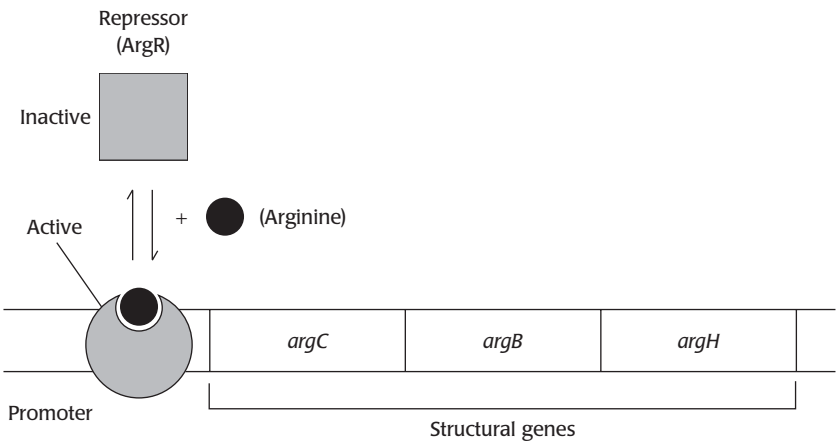


FIGURE 9.5

Regulation of amino acid biosynthesis by repression. In *E. coli* K-12, the transcription by RNA polymerase of genes for arginine biosynthesis (here *argC*, *argB*, and *argH*, which form an operon) is regulated by the repressor protein (ArgR). When no free arginine is present in the cytoplasm, ArgR does not bind to the upstream region of the operon, and transcription occurs. When arginine is present, it binds to ArgR and the liganded form of ArgR binds to the region of DNA just behind the promoter, presumably preventing the RNA polymerase from initiating the transcription process. Note that repression affects the synthesis of *all* the enzymes of the pathway (other genes of arginine synthesis are located elsewhere on the chromosome but are similarly regulated by ArgR). In contrast, feedback inhibition usually affects the activity of only the first enzyme of the pathway (or of the branch in a branched pathway).

Redrawn based on artwork from the first edition (1995), published by W.H. Freeman.

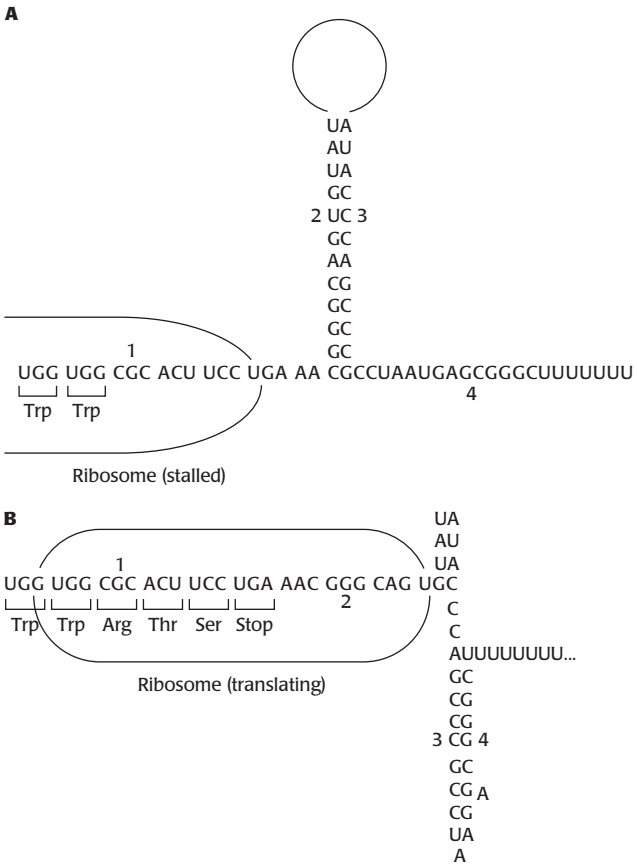


FIGURE 9.6

Regulation of amino acid biosynthesis by attenuation. In *E. coli* K-12, the levels of the enzymes responsible for tryptophan biosynthesis are regulated predominantly by attenuation. The 5′-terminal part of the mRNA for the *trp* operon can form two alternative looped structures, (**A**) one involving the pairing of regions 2 and 3, and (**B**) one involving the pairing of regions 3 and 4. Close to the beginning of this stretch of mRNA, there are two consecutive codons for tryptophan. When tryptophan (and therefore tryptophanyl-tRNA) is scarce, translation is stalled at the position of the tryptophan codons. In this state (**A**), region 1 is entirely covered by the ribosome, the 2-3 stem loop is formed, and transcription continues. When tryptophan is readily available, the ribosome moves past the tryptophan codons, inhibiting formation of the 2-3 stem loop, and structure (**B**) forms instead. The stem-loop structure created by the pairing of regions 3 and 4 is a typical rho-independent terminator, with a loop followed by stretches of U (see Box 3.6). In its presence, mRNA transcription is terminated, and tryptophan biosynthetic enzymes are not produced. [Yanofsky, C. (1981). Attenuation in the control of expression of bacterial operons. *Nature*, 289, 751–758.]

is followed by a continuous stretch of U residues. However, the stem loop formed when segment 2 becomes aligned with segment 3 does not act as a termination signal, because there is no stretch of U right after this hairpin. Attenuation works because segment 1 contains multiple codons for the particular amino acid whose synthesis is to be regulated – for example, tryptophan. If no tryptophanyl-tRNA molecules are present, then translation becomes stalled in segment 1. Segment 2 then forms a hairpin structure with segment 3, and transcription continues. In contrast, if tryptophanyl-tRNA is abundant, the continued translation inhibits the formation of a stem structure between segments 2 and 3, and the chain-terminating hairpin between 3 and 4 is formed instead, halting production of the enzymes needed to synthesize tryptophan.

In *E. coli*, the biosynthesis of many amino acids is regulated at the level of enzyme synthesis by both the repression and the attenuation mechanisms. This redundancy apparently expands the range of amino acid concentrations to which *E. coli* can respond. There is evidence that repression plays the predominant regulatory role when the amino acid concentrations in the medium are rather high and that attenuation becomes more important when the amino acids are scarce.

PRODUCTION BY THE USE OF AUXOTROPHIC MUTANTS

The foregoing discussion of the multiple regulatory mechanisms in *E. coli* may give the impression that to create mutant strains that overproduce amino acids is a hopelessly complex task. This is true to a certain extent, as we will see. Much more practicable, however, is the creation of strains that overproduce biosynthetic intermediates of amino acids. All regulatory mechanisms – feedback inhibition, repression, and attenuation – require the end product in order to function. If one of the steps in amino acid biosynthesis is blocked, none of the regulatory machineries will work, and the cell will overproduce the intermediate that lies just before the blocked step. This type of mutant is termed *auxotrophic* (requiring growth factors, such as amino acids, purines, pyrimidines, or vitamins, for nutrition) because it cannot survive without the amino acid whose biosynthesis is blocked. These auxotrophic mutants are useful if the intermediate itself is a useful commodity or if it can be converted easily into the desired amino acid by a chemical process.

To isolate mutants that are defective in amino acid biosynthesis, one must create an environment in which they have the survival advantage. A classical technique is *penicillin selection*. Assume that the parent strain can synthesize all of the amino acids; that is, it is "prototrophic" and can grow in a mineral medium containing a single organic compound as its major source of cellular carbon and energy. In order to isolate mutants that are unable to synthesize L-arginine ("arginine auxotrophs"), one usually exposes the population of wild-type cells to mutagens so that the frequency of mutants will increase. Then the bacteria are grown in the same mineral medium with the carbon source, but this time it is fortified with L-arginine as well. When the population has reached a suitable density, the cells are harvested, washed, and transferred to a medium exactly like the last one except that it lacks L-arginine. When penicillin is added to this culture, only arginine auxotrophs survive. Penicillin kills growing bacteria because it inhibits the cross-linking of the newly synthesized cell walls and eventually causes lysis of the cells. However, it is totally without effect on nongrowing bacteria, which do not possess new peptidoglycan material. The prototrophic cells are killed because they are capable of growth in the arginine-free medium. The mutant cells, which are incapable of growth, survive. The arginine auxotrophs can then be recovered by plating the mixture on a medium containing L-arginine but no penicillin.

L-Ornithine, which has medicinal applications, is an example of a useful biosynthetic intermediate. Because L-arginine is made from L-citrulline, which in turn is derived from L-ornithine, L-ornithine is overproduced by mutants that are blocked in the arginine biosynthetic pathway at the step converting L-ornithine to L-citrulline. Mutants blocked at earlier or later steps are useless. To find L-ornithine–producing mutants, researchers isolated arginine auxotrophs and then selected those that were able to grow after the addition of citrulline to the medium but were unable to grow after the addition of ornithine. Such mutants are defective in ornithine transcarbamylase, which catalyzes the conversion of ornithine to citrulline, and they

accumulate large amounts of ornithine because there is no arginine present to trigger negative regulation. During 1957, the first year of the modern era of amino acid fermentation, researchers isolated such a mutant belonging to the newly discovered glutamate producer, *C. glutamicum*, described earlier.

Auxotrophic mutations are also useful in the production of certain amino acids that are synthesized by branched pathways. If several amino acids – say, A, B, C, and D – are produced as end products of a branched pathway, the effect, in some organisms, of cutting off the branches leading to B, C, and D is often an increase in the production of A. This is primarily because the negative regulatory effects of B, C, and D are eliminated and secondarily because the flow of carbon to the cut-off branches is decreased. These cases will be considered in more detail in our discussion of regulatory mutants of branched pathways.

A major drawback to the use of auxotrophic mutants is that the amino acid that the auxotrophic strain cannot synthesize must be added to the medium. If too much is added, the excess exerts negative regulatory effects on the biosynthetic pathway, the very effect the mutant was designed to avoid. Thus, the mutant strains must be grown in a defined medium (such media tend to be expensive), and the required amino acids must be added in carefully controlled amounts (this process is called fed-batch fermentation). As a result, auxotrophic mutants are usually not the ideal strains for amino acid production.

PRODUCTION OF AMINO ACIDS BY REGULATORY MUTANTS OF UNBRANCHED PATHWAYS

Mutants that are defective in the negative regulation of amino acid biosynthesis overproduce the amino acid. Unlike auxotrophic mutants, these regulatory mutants can be grown in inexpensive, complex media, and they do not require careful control of growth conditions.

In almost all cases, these regulatory mutants are isolated through the use of amino acid analogs that inhibit the growth of the parent strain in a minimal medium. It has been known for many years that some analogs of amino acids are toxic. Earlier, the prevailing view was that these analogs inhibited growth by becoming misincorporated into proteins, thereby producing nonfunctional proteins. This may well occur in some instances, but in a vast majority of cases, the major cause of inhibition appears to be that the analogs mimic the way the amino acid regulates its own production. Thus, an analog may bind to the allosteric site of the first enzyme of the synthetic pathway or may bind effectively to the repressor, in either case shutting off the synthesis of that particular amino acid. Growth is inhibited because the cells now become starved of that amino acid. Researchers take advantage of this phenomenon to select for regulatory mutants by synthesizing a wide variety of analogs of an amino acid, selecting those analogs that effectively inhibit growth of the wild-type strain in a minimal medium, and then selecting for mutants that are able to grow in the presence of these analogs. In many such

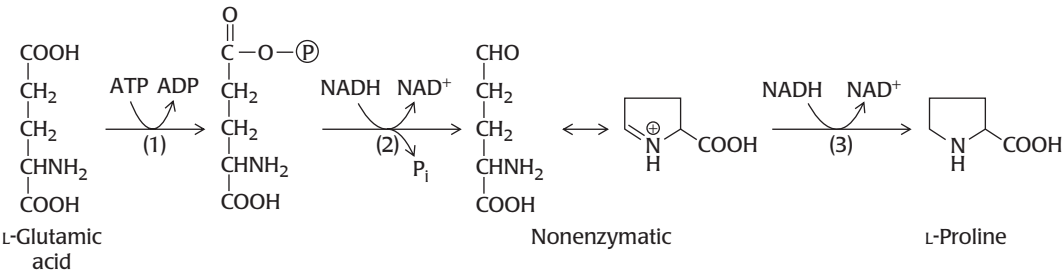


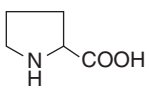
FIGURE 9.7

Proline biosynthesis pathway. The enzymes are (1) glutamate kinase, (2) glutamic γ-semialdehyde dehydrogenase, and (3) Δ^1-pyrroline 5-carboxylate reductase.

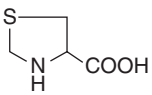
mutants, either the repressor or the first enzyme of the pathway is altered, which is why the amino acid synthesis proceeds even in the presence of the analog and will do so in the presence of the amino acid itself.

This approach does not work well when a biosynthetic pathway is regulated at more than one level. Mutation is a rare event, so the probability of isolating a strain that has simultaneously acquired two desirable mutations is miniscule. This is a major concern because in *E. coli*, many pathways are regulated at *three* levels: feedback inhibition, repression, and attenuation. Fortunately, many aquatic and soil microorganisms regulate amino acid biosynthesis more simply than does *E. coli*, presumably because, unlike *E. coli*, they live in a more or less constant environment that is always poor in amino acids. In these organisms, the major function of the regulation of amino acid biosynthesis is not to enable the organism to adjust to a varying supply of the amino acids in the environment but to control the rate of amino acid biosynthesis so that it will meet the demands of the cell's protein synthesis machinery.

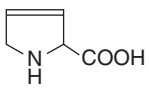
The foregoing points are well illustrated by certain mutant strains of a water and soil inhabitant, *Serratia marcescens*, that overproduce proline. Proline is the end product of an unbranched pathway (Figure 9.7). In *S. marcescens*, its synthesis is controlled almost entirely by feedback inhibition, making the system ideally suited to the use of amino acid analogs. A few of the proline analogs tested, such as thiazolidine-4-carboxylic acid and 3,4-dehydroproline (Figure 9.8), selected mutants in which the first enzyme of the pathway, glutamate kinase, was altered in such a way that it was no longer susceptible to feedback inhibition by proline. These mutants overproduced proline, as expected, but maximizing the production required the introduction of two additional changes. First, many wild-type strains of *S. marcescens* produce an enzyme that degrades proline. This enzyme enables the organism to use proline as a source of carbon and nitrogen and, in so doing, decreases the yield of proline by breaking some of it down after it has been synthesized. Thus, it was necessary to inactivate the gene coding for this enzyme, proline oxidase. Second, proline functions as an osmoprotectant solute. When bacterial cells are forced to grow in a high-osmolarity medium, they try to avoid the injurious effect of high salt concentration in the cytoplasm by accumulating proline (see Box 9.1), both by overproducing it and by transporting it from the medium. Because of this additional regulatory mechanism, the yield of proline increases when the bacteria are grown in high-salt media. With these two improvements, yields of 60 to 70 g/L of



Proline



Thiazolidine-4-carboxylic acid



3,4-Dehydroproline

FIGURE 9.8

L-Proline and two toxic analogs.

TABLE 9.3 Histidine biosynthesis in *Serratia* strains[a]

	1	2	3
	Extent of Repression (specific activity of histidinol dehydrogenase, units/mg protein)	Extent of Feedback Inhibition of the First Enzyme (inhibition of PRPP adenyltransferase by 10 mM histidine, %)	Histidine Production (g/L)
Sr41 (wild type)	1.1	100	0
Hd-16 (histidase$^-$)	0.9	100	0
581 (2MH^r)	1.6	0	0.8
142 (TRA^r)	12.4	94	1.3
2604 (142 × 581)	14.7	0	12.9

[a] This table shows the effectiveness of the two regulatory mechanisms of histidine biosynthesis in various strains of *S. marcescens*. In column **1**, the specific activity of one of the enzymes of the pathway is shown. The activity is low in the strains in which repression is inhibiting the expression of the genes, but it becomes higher in strains in which this regulatory mechanism has been altered. In column **2**, the efficiency of feedback control is indicated. In the wild-type strain, the first enzyme of the pathway, phosphoribosylpyrophosphate (PRPP) adenyltransferase, is completely inhibited by the end product, histidine, but in mutant 581 this regulatory mechanism is practically eliminated.
2MH, 2-methylhistidine; TRA, 1,2,4-triazole-3-alanine.
Source: Kisumi, M., Komatsubara, S., Sugiura, M., and Takagi, T. (1987). Transductional construction of amino-acid hyperproducing strains of *Serratia marcescens*. *Critical Reviews in Biotechnology*, 6, 233–252.

L-proline could be achieved. It is estimated that about 350 tons of L-proline are produced worldwide by fermentation each year.

When a pathway is regulated at more than one level, a production strain must contain a mutation at each level. Mutants selected with an analog are usually altered in only one of the regulatory mechanisms. However, mutations can be combined via the classical methods of bacterial genetics, especially in organisms such as *Serratia* that are phylogenetically related to *E. coli*. This principle is illustrated by the construction of a histidine-producing mutant of *S. marcescens*. Because *Serratia* uses histidine as a source of carbon and nitrogen, the first step was to create mutants in which the degradative enzyme, histidase, had been inactivated. Starting from this mutant, investigators then selected strains capable of growing in the presence of the toxic histidine analogs 2-methylhistidine and 1,2,4-triazole-3-alanine (Figure 9.9), respectively. As summarized in Table 9.3, one of the triazole-3-alanine (TRA)-resistant mutants, 142, overproduced enzymes of the histidine biosynthetic pathway (Figure 9.10), here exemplified by the much higher specific activity of one such enzyme, histidinol dehydrogenase, but the first enzyme of the pathway, phosphoribosyl phosphate adenyltransferase, was unaltered in its susceptibility to the feedback inhibition. In contrast, one of the 2-methylhistidine (2MH)-resistant mutants, 581, produced an adenyltransferase that is remarkably resistant to feedback inhibition by histidine. Because each mutant was altered in only one regulatory mechanism, neither mutant produced large amounts of histidine (see column 3 of Table 9.3). However, scientists at Tanabe, a pharmaceutical company in Japan, were able to combine the two regulatory mutations by using transduction. The transductant, 2604 (see Table 9.3), was desensitized in both

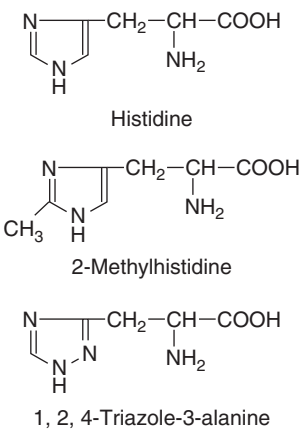


FIGURE 9.9
L-Histidine and two toxic analogs.

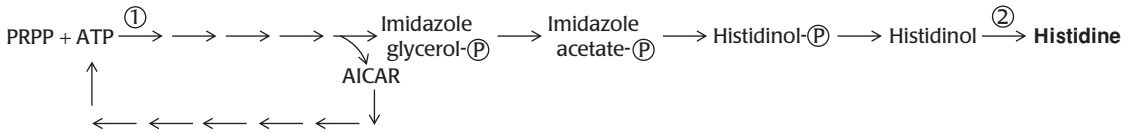


FIGURE 9.10

Histidine biosynthetic pathway. Steps 1 and 2 are catalyzed by PRPP adenyltransferase and histidinol dehydrogenase, respectively. Abbreviations: PRPP, 5-phosphoribosyl pyrophosphate; AICAR, 5-aminoimidazole-4-carboxamide ribonucleotide.

Redrawn based on artwork from the first edition (1995), published by W.H. Freeman.

repression and feedback inhibition processes, and, as expected, it produced large amounts of histidine.

Creating a system that overproduces metabolites is usually more complicated than creating one that overproduces primary gene products. The increased flux through metabolic pathways may become limited in unexpected ways. This is one of the reasons why straightforward applications of recombinant DNA technology have not always produced spectacular results in this field. In the foregoing example, strain 2604 and similar histidine-production strains developed adenine deficiency that is presumably related to the consumption of ATP in the first step of the histidine pathway. Although an adenine moiety is expected to be regenerated from 5-aminoimidazole-4-carboxamide ribonucleotide (AICAR; see Figure 9.10), this process probably cannot keep pace with the extremely rapid rate of histidine biosynthesis. Tanabe scientists solved the problem by putting the mutant strain through yet another selection cycle, this time using a toxic adenine analog, 6-methylpurine. The result was a resistant strain that overproduces adenine and hence is able to produce histidine at an increased level (23 g/L) without requiring the addition of adenine to the medium. Histidine is now produced at the rate of about 400 tons/year worldwide, by fermentation processes.

PRODUCTION OF AMINO ACIDS BY REGULATORY MUTANTS OF BRANCHED PATHWAYS

Proline and histidine, which we have described, are the products of unbranched biosynthetic pathways, but many other amino acids are produced by branched pathways. Members of the aspartate family of amino acids (lysine, methionine, threonine, and isoleucine – all essential amino acids) are produced by one branched pathway, those of the pyruvate family (valine and leucine) by another branched pathway, and those belonging to the aromatic family (tryptophan, phenylalanine, and tyrosine) by still another. The regulation of these pathways is much more complex, because it requires a system in which an excess of one product does not accidentally shut off the entire pathway. The regulatory mechanisms in the branched pathways of *E. coli* are very complicated indeed. For example, in the aspartate pathway (Figure 9.11), each product inhibits and/or represses the first enzyme of the common pathway, aspartate kinase. However, so that one product does not shut down all of the kinase activity, three different isozymes (different enzymes that catalyze the same chemical reaction) of aspartate kinase are produced: one sensitive to lysine inhibition, one sensitive to threonine inhibition, and one repressed mainly by an excess of methionine. In addition, *E. coli* is able to adjust to the presence of an unbalanced mixture of the products of the pathway. For example, if it encounters an excess

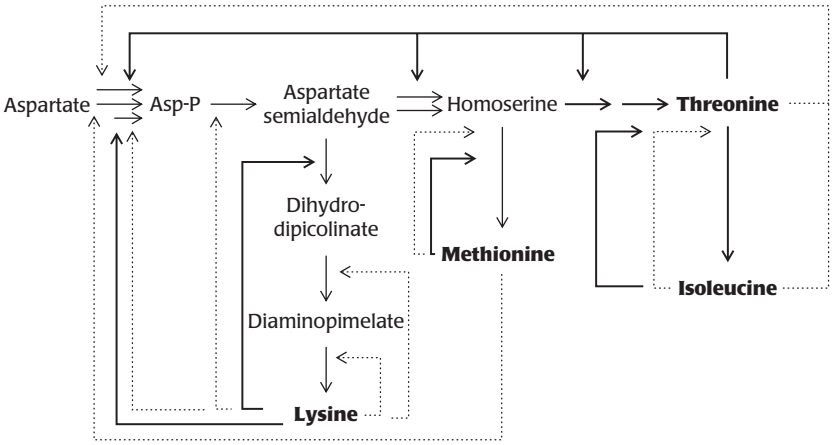


FIGURE 9.11

Regulation of synthesis of the aspartate family amino acids in *E. coli*. The pathways are shown in abbreviated form; for example, a *single arrow* from threonine to isoleucine represents five consecutive enzyme-catalyzed steps. *Continuous thick arrows* indicate regulation by feedback inhibition, and *dotted arrows* represent repression or attenuation regulation. Repression and attenuation affect all enzymes of a branch, but here only the effect on the first enzyme of the branch is shown. Step 1 is catalyzed by three isozymes of aspartate kinase. [Modified from Tosaka, O., and Takinami, K. (1986). Lysine. In *Biotechnology of Amino Acid Production*, Aida, K., et al. (eds.), pp. 152–172, Tokyo: Kodansha.]

of methionine but low levels of the other products (lysine, isoleucine, and threonine), regulating the aspartate kinase alone will not lead to the proper ratio of methionine to the other three amino acids. Thus, each amino acid usually controls the first enzyme of its own particular branch. Methionine and isoleucine regulate the pathway through both feedback inhibition and repression mechanisms, whereas lysine and threonine participate in more complex regulatory patterns.

Eliminating various types of controls in a system like this is a major endeavor. However, it is not impossible, especially given the highly developed state of techniques in bacterial genetics and in recombinant DNA manipulations when applied to *E. coli*. Indeed, an *E. coli* strain containing at least nine mutations and producing threonine almost at the level of 100 g/L has been reported.

An easier approach, however, would be the use of microorganisms that have much simpler regulatory mechanisms. Presumably these organisms do not often encounter mixtures of amino acids, sometimes of unbalanced composition, in their environment. If the organism usually lives in an environment that is poor in amino acids, the major function of the regulation of amino acid biosynthesis is to adjust its rate in response to the growth rate of the organism. Thus, there is no need to adjust the ratios of the various amino acids produced. When such an organism is producing excess lysine (e.g., because its growth has slowed), it is also likely to be producing excess methionine, threonine, and isoleucine. The major regulation of the branched pathway can then be achieved by a system in which only one or a few of the products inhibit the first common enzyme. This type of simple regulatory scheme is indeed found in the soil bacterium *C. glutamicum* and its relatives (Figure 9.12).

Lysine production was extensively studied in these organisms, because lysine is one of the amino acids that occur only in small amounts in cereal proteins, as mentioned earlier. The simplicity of the regulatory system in *C. glutamicum* makes it possible to obtain a relatively large amount of lysine simply by cutting off the branches leading to other amino acids. For example, a yield of 34 g lysine per liter of medium was obtained from a mutant that

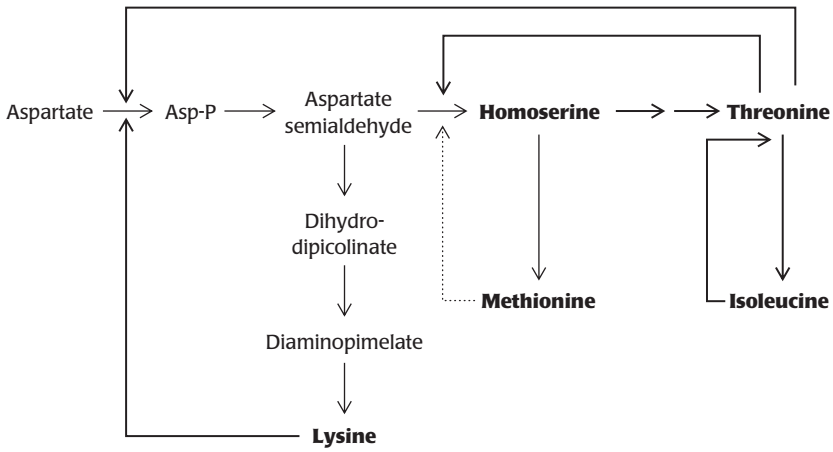


FIGURE 9.12

Regulation of synthesis of the aspartate family amino acids in *C. glutamicum*. *Thick continuous arrows* show regulation by feedback inhibition, and *dotted arrows* represent repression control. [After Tosaka, O., and Takinami, K. (1986). Lysine. In *Biotechnology of Amino Acid Production*, Aida, K., et al. (eds.), pp. 152–172, Tokyo: Kodansha.]

was defective in the branches leading to methionine and to threonine and isoleucine. The diversion of metabolites that would normally go to create those other amino acids contributed to the overproduction of lysine, but the primary reason it occurred is that efficient feedback inhibition of aspartate kinase requires both lysine and threonine (see Figure 9.12). However, lysine-producing auxotrophic mutants of this type must be fed methionine, threonine, and isoleucine continuously and in carefully measured amounts so that they are never present in large excess. Consequently, such mutants are not the desirable type for the commercial production of lysine.

Regulatory mutants of *C. glutamicum*, better suited for commercial production, were obtained by using the lysine analog *S*-aminoethylcysteine (AEC) (Figure 9.13). Like lysine, this analog inhibits the activity of aspartate kinase and hence inhibits the growth of wild-type bacteria. Thus, AEC-resistant mutants are likely to have an alteration in their aspartate kinase such that the altered allosteric, regulatory site of the enzyme has a lower affinity for AEC. These mutant enzymes are also likely to bind lysine with lower affinity and to be defective in the feedback regulation of lysine synthesis. A yield of 32 g lysine per liter was reported for such a mutant; additional fine-tuning that presumably modified the minor regulatory mechanisms increased the yield to 60 g/L. In such fermentation processes, more than 0.3 mole of lysine is obtained from one mole of glucose consumed.

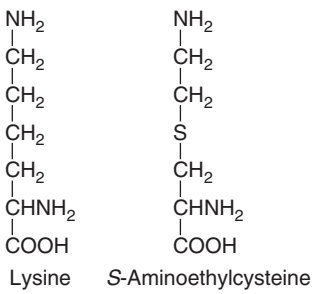


FIGURE 9.13

Structures of lysine and *S*-aminoethylcysteine.

The pathway for lysine synthesis in *C. glutamicum* has been studied in depth in recent years, and the flux of intermediates was determined by several methods, notably by combining metabolic flux balancing with the fate of 1-^{13}C carbon in glucose, analyzed by ^{13}C-NMR (see Box 9.2). Another important finding is that lysine is exported into the medium by a specific export transporter, LysE. The sequencing of the *C. glutamicum* genome also supplied additional pieces of information. Because a large fraction of the central metabolic flux is diverted into the synthesis and excretion of lysine, many scientists feel that the best approach is the metabolic engineering method (see Box 9.3), in which one would apply recombinant DNA methods based on the detailed information on the metabolic flux. It was found that expanding an isolated step of the terminal pathway without regard to its effect on other

parts of metabolism may have unexpected effects. For example, increasing the level of the first enzyme, aspartate kinase, by the amplification of the *lysC* gene, inhibited the growth of the organism presumably because so much of the flux of central metabolites was now siphoned off into the aspartate pathway, and this did not lead to the greatly increased production rate for lysine (Table 9.4). In contrast, *lysC* amplification combined with amplification of the genes coding for the first and the second enzymes in the lysine-specific branch (Figure 9.12) (*dapA* and *dapB*), significantly increased the lysine production (Table 9.4). Lysine synthesis starts from aspartate, which is made by the amination of oxaloacetate. Thus, increasing the production of oxaloacetate in the cell, by amplification of the pyruvate carboxylase gene (*pyc*) was attempted, and was indeed found to increase the final concentration of lysine in the medium by about 50%.

TABLE 9.4 Effect of gene amplification on lysine production in *C. glutamicum*

Strain and the genes introduced on plasmids[a]	Lysine produced (g/L)		Growth (OD_{562})
	at 40 hrs	at 72 hrs	
AJ11082	22.0	29.8	0.450
+*lysC*^{fbr}	16.8	34.5	0.398
+*lysC*^{fbr} *dapA*	19.7	36.5	0.360
+*lysC*^{fbr} *dapB*	23.3	35.0	0.440
+*lysC*^{fbr} *dapA dapB*	23.0	45.0	0.425

[a] Strain AJ11082 is an AEC-resistant mutant of *C. glutamicum* and produces feedback-resistant LysC protein (aspartate kinase). The feedback-resistant *lysC* gene (*lysC*^{fbr}) was cloned from this strain in a multicopy plasmid, and the plasmid was added to the strain in the row "+*lysC*^{fbr}." Similarly, the strains contained multicopy plasmids containing additional genes in other rows. OD_{562}, optical density at 562 nm.
Data from Otsuna, S., et al., patent WO 96/40934.

In the exploratory experiments discussed above, gene amplification was achieved by using recombinant plasmids. Such a strategy is not suitable for the industrial production of amino acids because the addition of antibiotics needed for the maintenance of plasmids is expensive and because the presence of antibiotic resistance genes is undesirable for the products used as food and feed additives. Use of amino acid/purine/pyrimidine biosynthesis genes as selective markers, as done for yeast plasmids (see Chapter 3), is not practical either because the inexpensive carbon source material used in the growth medium may contain such nutrients. A recent innovation is the use of *dlr* mutant host, defective in alanine racemase, and plasmid vectors containing the *dlr* gene as the selective marker. Here only plasmid-containing cells can synthesize D-alanine, needed for the construction of peptidoglycan cell wall, and therefore can survive. In this way, the use of antibiotic selection can be avoided.

In another approach, recombinant plasmids are used only to create alterations in the bacterial chromosome. Lysine-overproducing strains have been improved by the successive isolation of mutants with better properties. Since some of the mutants were isolated after generalized, non-specific mutagenesis, these multiple steps resulted in the inadvertent introduction of undesirable mutations that affected the "vigor" of the producing strain. Now that the complete genome of *C. glutamicum* is available, it became possible to introduce, into a vigorous wild-type parent, only the desired mutations that increase lysine production, such as those in aspartokinase (*lysC*), homoserine dehydrogenase (*hom*, catalyzing the first step in the threonine branch), and pyruvate carboxylase (*pyc*), generating a strain

with the highest lysine-producing capacity. Improving the regeneration of a cofactor, NADPH, through the introduction of a mutant allele of the 6-phosphogluconate dehydrogenase gene resulted in further enhancement of the yield of lysine.

AMINO ACID PRODUCTION WITH ENZYMES

Although many amino acids are produced by fermentation processes, it is sometimes advantageous to use an enzymatic process instead. A good example is the production of L-aspartic acid, which is used as a starting material for the chemical synthesis of the sweetener aspartame. L-Aspartic acid has been produced in Japan since 1969, primarily by exploiting the *E. coli* enzyme aspartase, which catalyzes the conversion of L-aspartate into fumarate and NH_3:

$$\text{L-aspartic acid} \rightarrow \text{fumaric acid} + NH_3.$$

Aspartase is a catabolic enzyme used by *E. coli* to degrade exogenous aspartic acid into readily utilizable sources of carbon and nitrogen for growth. Under physiological conditions, the reaction equilibrium lies far toward the right. More precisely, because the equilibrium constant (K_{eq}) is 20 mM, if the initial concentration of aspartate is 1 mM, almost 95% of it will be converted into fumarate and NH_3. Thus, at first the enzyme appears to be a poor choice for *synthesizing* aspartate. However, the law of mass action favors aspartate synthesis when the reactant concentrations are high – that is, under conditions that would be used for industrial production of an amino acid. Based on the K_{eq} value cited above, we can calculate that if we start from 2 M fumarate and 2 M NH_3, the reaction will proceed far toward the left and will come to equilibrium when 90% of the reactants are converted into L-aspartate. Thus, aspartase, although it is a degradative enzyme, is ideal for the industrial synthesis of aspartate. In contrast, most enzymes that catalyze biosynthetic reactions in intact cells are not suitable for the industrial production of amino acids, either because they use complex, expensive substrates or because they require an expensive cofactor, such as NADPH or ATP.

When amino acids *can* be produced by a simple enzyme reaction, such a process has many advantages.

1. The amino acids are produced in high concentrations (in the case of aspartate, about 1 M), making their recovery easy.

2. Because the solution contains only a few reactants, purification of the product is simple. In contrast, the supernatant in a fermentation run always contains some of the growth medium, the ingredients of which are usually quite complex and difficult to eliminate.

3. Compared with fermentation processes, the rate of production per unit volume is much higher. Fermentation requires huge tanks and much material for growth media, whereas enzymatic production can be done in a small space. Consequently, the required capital investment is much smaller.

TEN

Secondary Metabolites: Antibiotics and More

The preceding chapter described the industrial production of some primary metabolites, including citric acid and amino acids. In contrast to these compounds, which are present in most living organisms and are produced by the ubiquitous major metabolic pathways, secondary metabolites are produced only by special groups of organisms through specialized pathways. Their chemical structure tends to be complex, and they are often produced only during the special growth phase, most often during the stationary phase. The most important of these secondary metabolites are the antibiotics.

Many science historians argue that among the many scientific discoveries of the twentieth century, that of the first antibiotic, penicillin (Figure 10.1), by Alexander Fleming (reported in 1928) is the discovery that had the largest impact on human life. The story is well known. Fleming is supposed to have kept a rather untidy laboratory and to have discovered, after returning from his vacation, that the bacterial colonies neighboring a contaminating mold colony were lysed on one of the Petri plates left on his bench. This story is often cited as an example of the importance of serendipity in science. This view, however, totally disregards the fact that Fleming dedicated his entire career to the search for natural products that lyse bacterial cells, in an effort to find agents that could be used in the treatment of bacterial infections. He had, in fact, discovered the enzyme lysozyme several years earlier but was disappointed that most human pathogens were intrinsically resistant to its lytic action. (Pathogenic bacteria presumably have been subjected to evolutionary selection for such resistance because lysozyme is present in most tissues and body fluids of higher animals.) Another important aspect of Fleming's discovery of penicillin is that he tried to isolate the active substance and to use it in the treatment of infections. Dozens of scientists before Fleming had published reports of either lysis or growth inhibition of bacteria caused by products of molds and other microorganisms. Yet nothing came out of these findings because the authors operated as classical "naturalists" reporting "curious" phenomena. The ultimate industrial-scale production and the clinical application of penicillin required, more than a decade later, great efforts by many outstanding chemists and a wartime collaboration

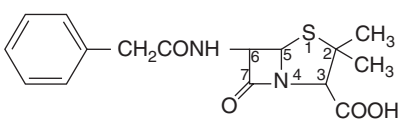
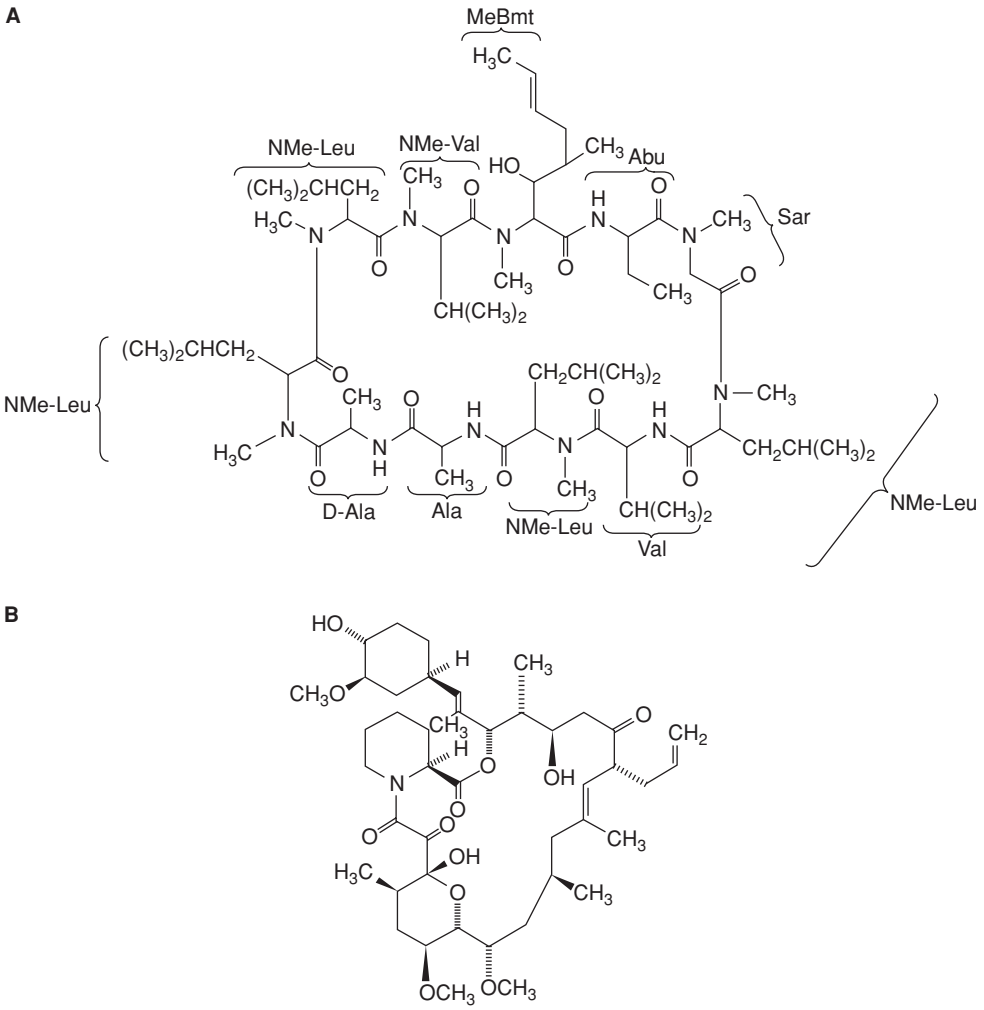


FIGURE 10.1
Penicillin G.



apparently because its outer leaflet is composed exclusively of an unusual lipid molecule, the lipopolysaccharide (LPS). Consequently, the larger and more lipophilic antibiotics tend to have significant activity against Gram-positive bacteria only.

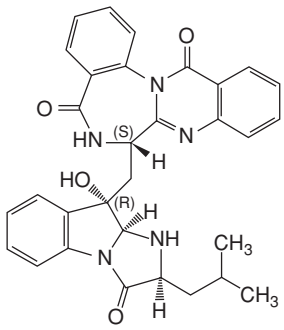
FIGURE 10.14

(**A**) Cyclosporin A. The new amino acid, MeBmt, is apparently essential for the biological activity as is the presence of numerous *N*-methyl groups, which inhibit hydrogen bonding between backbone residues and presumably help cyclosporin assume a particular conformation. (**B**) FK-506 (tacrolimus). Abbreviations: NMe, *N*-methyl; Sar, sarcosine; Abu, 2-aminobutyric acid; MeBmt, 4-(2-butenyl)-4,*N*-dimethyl-L-threonine.

β-Lactams

Penicillin (benzylpenicillin, penicillin G) (Figure 10.1) is the classical example of a β-lactam antibiotic. The β-lactams inhibit the synthesis of the eubacterial cell wall, which is composed of a polymer unique to the bacterial world, called peptidoglycan. Peptidoglycan is a network of polysaccharide (or glycan) chains composed of alternating *N*-acetylglucosamine and *N*-acetylmuramic acid residues (see also Figure 1.1). The polysaccharide chains are cross-linked to each other via short peptide chains, which include some D-amino acids and are attached to the *N*-acetylmuramic acid residues (Figure 10.16). This structure gives peptidoglycan exceptional chemical stability, mechanical strength, and rigidity.

A



B

Lys—Ala—Pro—Ser—Gly—Arg—Met—Ser—Ile—Val—
Lys—Asn—Leu—Gln—Asn—Leu—Asp—Pro—Ser—His—
Arg—Ile—Ser—Asp—Arg—Asp—Tyr (SO_3H) —Met—Gly—Trp— Met—Asp—Phe—NH_2

FIGURE 10.15

(**A**) Asperlicin. (**B**) Human cholecystokinin.

The addition of new glycan chains to the cell wall in growing cells takes place by the cross-linking of the peptide side chain of a new unit to the preexisting peptidoglycan structure (Figure 10.17). The cross-linking reaction is catalyzed by a DD-transpeptidase. This enzyme cleaves the peptide bond between the two D-alanine residues in the side chain of a newly made glycan chain and transfers the glycan–peptidyl complex to the free amino group of the diamino acid residue in the side chain of the preexisting peptidoglycan, thereby cross-linking different chains. As first pointed out by Tipper and Strominger, the β-lactam ring system structurally resembles the D-alanyl-D-alanine of the nascent side chain (Figure 10.18). They demonstrated that the interaction between transpeptidase and penicillin generates a covalent penicilloyl enzyme, resulting in the irreversible inactivation of the enzyme. Thus, a β-lactam is an example of a "suicide inhibitor" because it interacts with its target enzyme like a substrate and then undergoes chemical reaction with the enzyme, thereby causing its permanent inactivation. Suicide

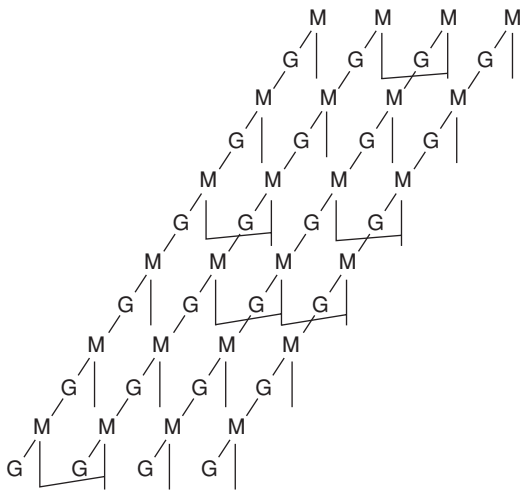
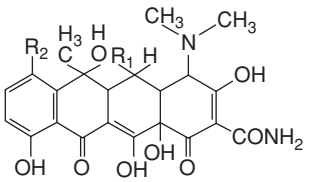


FIGURE 10.16

Structure of peptidoglycan from Gram-negative bacteria. Polysaccharide chains are made of alternating *N*-acetylmuramic acid units (M) and *N*-acetylglucosamine units (G). Short peptides (*vertical lines*) are attached to the *N*-acetylmuramic acid residues, and the polysaccharide chains are connected via peptide cross-links (*nearly horizontal lines*).

Chloramphenicol

Chloramphenicol (Figure 10.22) was originally isolated from the filtrate of *Streptomyces venezuelae* cultures. However, because it is a small molecule with a simple structure, it is more economical to produce by chemical synthesis than by fermentation. Chloramphenicol inhibits prokaryotic protein synthesis. It penetrates through the outer membrane porin channels of Gram-negative bacteria easily because of its small size and is therefore another broad-spectrum antibiotic. However, chloramphenicol can enter eukaryotic cells and inhibit mitochondrial protein synthesis. Thus, use of chloramphenicol may prevent growth of rapidly proliferating cells and this may be related to at least one of its side effects, the suppression of bone marrow cells. Because of this and other side effects, chloramphenicol is not widely used today, except in the treatment of diseases in which the pathogen survives within human cells, such as infection by *Salmonella typhi* (typhoid fever).



	R_1	R_2
Tetracycline	H	H
Chlortetracycline	H	Cl
Oxytetracycline	OH	H

FIGURE 10.21
The structure of tetracyclines.

Peptide Antibiotics

Several peptide antibiotics (Figure 10.23) are now in commercial production. Many of these are produced by *Bacillus* species. These peptides contain unusual amino acids, such as D-amino acids, ornithine, and diaminobutyric acid, and have significant toxicity to humans when injected, and are thus useful only for topical applications. Some of these agents are used in Europe as feed additives because they are not used in human therapy (see the discussion above on tetracycline).

Many of these antibiotics are too bulky and hydrophobic to cross the outer membrane barrier of Gram-negative bacteria, and their efficacy is therefore limited to Gram-positive bacteria. An interesting exception is polymyxin, which has a two-step mode of attack on Gram-negative bacteria. This polycationic antibiotic apparently binds to the highly negatively charged LPS molecules in the outer membrane of many Gram-negative bacteria and disrupts the molecular organization of the outer membrane bilayer. Once the integrity of the outer membrane is destroyed, polymyxin can bind to and insert into the cytoplasmic membrane through its hydrophobic tail, thereby killing the bacterial cell by permeabilizing the plasma membrane. Polymyxin shows strong activity against organisms like *Pseudomonas aeruginosa*, which is resistant to almost all other antibiotics because of the unusually low permeability of its outer membrane. Hence, polymyxin still has its place in the treatment of life-threatening infections by *P. aeruginosa*, in spite of its significant toxicity.

Vancomycin, a glycopeptide antibiotic of 1449 daltons (Figure 10.24), acts only on Gram-positive bacteria through an unusual mechanism of binding to the D-Ala-D-Ala moiety of the peptidoglycan precursor. This has become an important drug for the treatment of infection caused by methicillin-resistant *Staphylococcus aureus* (MRSA). Daptomycin, a lipopeptide antibiotic (Figure 10.25), inserts into the cell membrane of Gram-positive bacteria (including MRSA) in the presence of Ca^{2+}, and kills them by producing leakage of

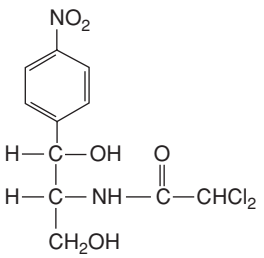


FIGURE 10.22
The structure of chloramphenicol.

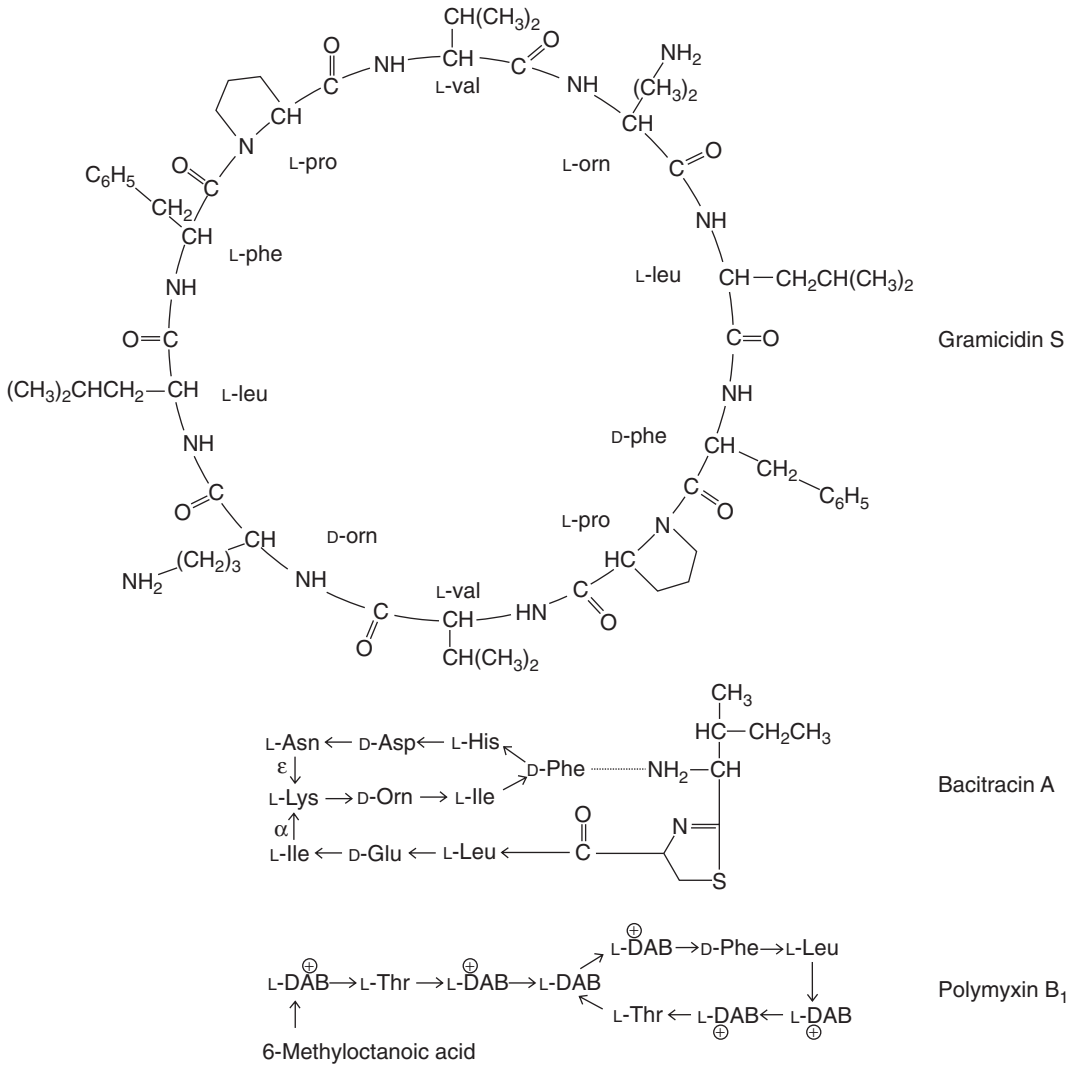


FIGURE 10.23

Some examples of peptide antibiotics. The *arrows* indicate the direction of peptide bonds (–CO→NH–). In the structure of polymyxin, DAB indicates 2,4-diaminobutyric acid. The positive charge due to the free 4-amino group of this residue is also indicated.

cytosolic ions. It is remarkable that this compound is tolerated by humans; the plasma membrane of higher animals does not contain much anionic lipids in its outer leaflet, and perhaps this prevents the Ca^{2+}-bridged interaction between the drug and the membrane.

Aminoglycosides (Aminocyclitols)

Aminoglycosides, which are discussed in detail later in this chapter, consist of an aminocyclitol moiety (streptidine in streptomycin, 2-deoxystreptamine in many other aminoglycosides; see Figure 10.26) to which amino sugars are attached in various ways. All of these compounds are produced by the prokaryotes of the actinomycete line (*Streptomyces* in most cases, *Micromonospora* for gentamicin). These antibiotics are inhibitors of prokaryotic protein synthesis. Because they are quite hydrophilic and sufficiently small, aminoglycosides can cross the Gram-negative outer

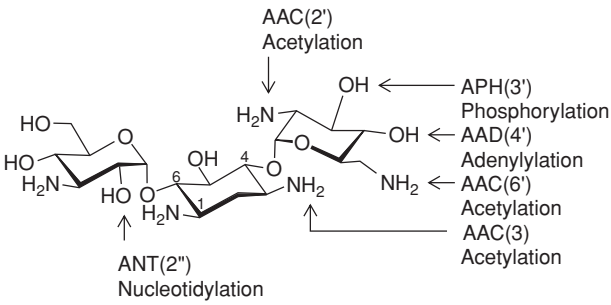


FIGURE 10.31

Kanamycin B can be inactivated in many different ways. The name of the enzyme and the nature of the modification reaction are shown. Note that the atoms in the sugar linked to the 4-position of the aminocyclitol (at the right end of the molecule) are numbered with primes and that the atoms on the 6-substituent sugar (at the left end of the molecule) are numbered with double primes. The enzymes include all those listed in Table 10.1 as being capable of inactivating kanamycin A, plus AAC(2′), which inactivates kanamycin B but not kanamycin A (because the latter lacks the 2′-amino group).

of gastrointestinal infections, especially in developing countries. Unfortunately, this use may have contributed heavily to the selection and dissemination of R plasmids.

3. Currently, the most important use of aminoglycosides is in the treatment of systemic infections caused by species of Gram-negative bacteria that are intrinsically resistant to most other antibiotics. Under these circumstances, we tolerate the inherent toxicity of these antibiotics because we do not have many other choices and because we are treating life-threatening infections. Aminoglycosides can cross even outer membranes of very low permeability, possibly because these polycations can bind to the anionic surface of the outer membrane, disorganize it, and thereby destroy the permeability barrier in a manner reminiscent of the action of polymyxin (page 335). The presence of inactivating enzymes, however, can make the drug totally ineffective, so one major thrust of the research in aminoglycoside development has been the search for compounds that are not inactivated significantly by commonly encountered enzymes.

STREPTOMYCIN

Streptomycin (Figure 10.32) was discovered by Selman A. Waksman, a soil microbiologist interested in the antagonism between different groups of soil organisms. Waksman and coworkers were examining the products of *Streptomyces* species, a typical inhabitant of soil, and were looking for agents that were active against Gram-negative bacteria, for most of which penicillin G, the only commercially produced antibiotic at that time, was totally ineffective. (*Neisseria* spp. are susceptible to penicillin G, possibly because their porin channel favors anionic solutes, and thus constitute an exception among Gram-negative bacteria.) Their short note published in 1944 describing the discovery of streptomycin is impressive because they described not only the activity of streptomycin against both Gram-positive and

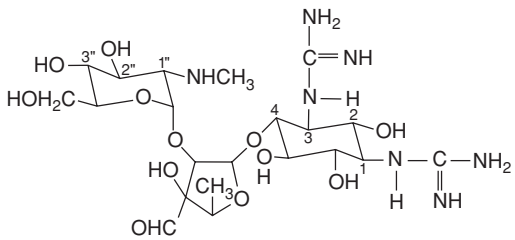


FIGURE 10.32

Streptomycin.

Gram-negative bacteria but also its bactericidal property and the fact that its production is affected greatly by the nature of the growth medium and the growth phase.

Although the toxicity of the compound prevented it from becoming the "penicillin for Gram-negative infections," the discovery of its activity against *M. tuberculosis* made this antibiotic extremely important. As mentioned earlier, streptomycin is no longer a first-line drug for the treatment of tuberculosis. However, because *M. tuberculosis* can develop resistance to first-line drugs such as rifampicin, streptomycin still remains an important agent for the treatment of cases caused by such resistant organisms.

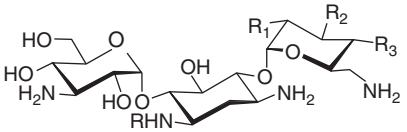
DEVELOPMENT OF NEWER AMINOGLYCOSIDES

Kanamycin

Kanamycin (Figure 10.33), the second commercially produced aminoglycoside, was discovered by Hamao Umezawa and coworkers in 1957 from the culture filtrate of another *Streptomyces* species. This was a timely discovery because kanamycin proved to be active on enteric bacteria that produce streptomycin-inactivating enzymes. When studies of plasmid-coded resistance to streptomycin showed that the antibiotic is inactivated through adenylylation or phosphorylation of its 3″-hydroxyl group, it became clear why the kanamycins remain fully active against strains that contain the streptomycin resistance plasmids. In streptomycin, the amino sugar is connected via another sugar to the 4-position of the aminocyclitol streptamine, but in kanamycins, the amino sugar is connected directly to the corresponding position of the aminocyclitol. Thus, in kanamycins, there is no group that corresponds to the 3″-hydroxyl group of streptomycin.

As mentioned earlier (see Figure 10.30), the aminocyclitol in kanamycin, 2-deoxystreptamine, is different from the one found in streptomycin, streptamine. 2-Deoxystreptamine is the aminocyclitol found in most other aminoglycosides either isolated or synthesized since the discovery of kanamycin. In kanamycin and most other compounds, 2-deoxystreptamine is substituted by amino sugars at both the 4- and 6-positions, although exceptions such as neomycin, ribostamycin, and butirosin (Figure 10.34), which are substituted at the 4- and 5-positions, exist.

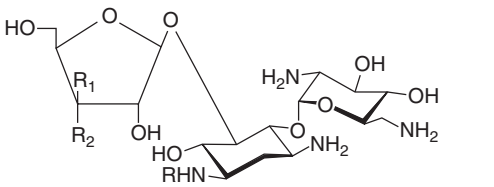
Kanamycin proved to be significantly more active against most Gram-negative bacteria than streptomycin. However, it had poor activity against *P. aeruginosa*, partly because many strains of this organism contain enzymes, sometimes coded for by a chromosomal gene, that inactivate kanamycin.



Antibiotic	R	R_1	R_2	R_3
Kanamycin A	H	OH	OH	OH
Kanamycin B	H	NH_2	OH	OH
Tobramycin	H	NH_2	H	OH
Dibekacin	H	NH_2	H	H
Amikacin	HABA	OH	OH	OH

FIGURE 10.33

Kanamycin A and its relatives. The molecule is drawn in such a way as to roughly represent its three-dimensional structure as determined by x-ray crystallography of the free drugs as well as the drug-16S rRNA complexes. Abbreviation: HABA, 2-hydroxy-4-aminobutyryl. [See for example, Bau, R., and Tsyba, I. (1999). Crystal structure of amikacin. *Tetrahedron* 55, 14839–14846 and Vicens, Q., and Westhof, E. (2002) Crystal Structure of a complex between the aminoglycoside tobramycin and an oligonucleotide containing the ribosomal decoding A site. *Chemistry & Biology* 9, 747–755.]



	R	R_1	R_2
Ribostamycin	H	OH	H
Butirosin A	NH_2—$(CH_2)_2$—CHOH—CO	H	OH

FIGURE 10.34

Ribostamycin and butirosin A.

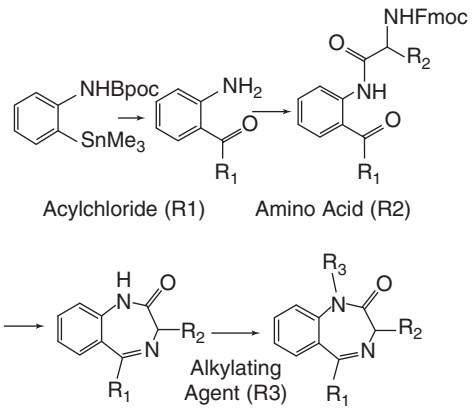


FIGURE 10.76

An example of a combinatorial chemistry process. This version, developed by J. A. Ellman's group, starts with acylation using acylchloride (R1; *first arrow*). The amino group, deprotected after the first reaction, is then acylated using an amino acid ester R2 (*second arrow*). After cyclization to produce 1,4-benzodiazepine (*third arrow*), the NH group is modified by an alkylating agent (R3). If one uses a set of 50 different reagents at each step, one may end up synthesizing 125,000 different compounds after only three steps. Although not shown in the figure, the starting material is anchored on a solid support, so isolation of intermediates becomes trivial. Bpoc and Fmoc are protective groups for $-NH_2$. [Based on Bunin, B. A., Plunkett, M. J., and Ellman, J. A. (1996). Synthesis and evaluation of 1,4-benzodiazepine libraries. *Methods in Enzymology*, 267, 448–465.]

protein. Any phage expressing a peptide that binds tightly to the target protein will become adsorbed to this affinity matrix. The peptide produced by these phages thus will give us a clue as to the shape of the "peptidomimetic" inhibitors to be synthesized. As we have already seen, we can combine genes from different sources to achieve "combinatorial" biosynthesis of antibiotics, although the range of compounds generated will be much more limited. It is encouraging that innovative methods such as these are being developed in response to the challenge of countering drug resistance among pathogenic microorganisms.

SUMMARY

Antibiotics are secondary metabolites of microorganisms and are usually produced in the stationary phase of growth. The majority of antibiotics come from eukaryotic fungi or from streptomycetes, a prokaryotic group with a complex life cycle reminiscent of that of fungi; a few are produced by unicellular bacteria not known to have developmental cycles. Many of the genes of antibiotic biosynthesis have been cloned and sequenced. In many cases, they occur as a cluster. This arrangement explains the apparent occurrence of the horizontal transfer of these genes, during evolution, between distantly related organisms. The gene sequence also explains (e.g., with the producers of polyketide antibiotics) why a single antibiotic producer often secretes many related antibiotics that are different from one another in minor details. Cloning of production genes is opening up ways to produce novel antibiotics by the combination of defined genes.

Antibiotics have been extremely effective in our battle against bacterial infections and they have drastically changed the ecological balance between humans and various pathogenic microorganisms. Yet every introduction of a new antibiotic into clinical practice has been followed by the emergence of resistant organisms. Very often these organisms have harbored R plasmids that have contained resistance genes specifying the degradation, inactivation, or pumping out of the antibiotic molecules. Sometimes